Theory of Water-Proton Spin Relaxation in Complex Biological Systems

Zhiwei Chang

LUND
UNIVERSITY

Doctoral Thesis

by due permission of the Faculty of Engineering LTH, Lund University, Sweden.
The thesis will be publicly defended on the June 16th 2017 at 9.15 in lecture hall G, Kemicentrum, Getingvägen 60, Lund

Faculty opponent

Professor Emeritus Jozef Kowalewski
Department of Materials and Environmental Chemistry, Stockholm University

Organization
LUND UNIVERSITY

Biophysical Chemistry
Center for Molecular Protein Science

Document name
DOCTORAL DISSERTATION

Date of issue
2017-05-23

Sponsoring organization

Author(s)
Zhiwei Chang

Title and subtitle

Theory of water-proton spin relaxation in complex biological systems

Abstract

In complex biological systems (e.g. gels, cross-linked proteins and biological tissues), the longitudinal spin relaxation of water protons is primarily induced by exchange-mediated orientational randomization (EMOR) of intra- and intermolecular magnetic dipole-dipole couplings. The chemical exchange processes that dominate the magnetic relaxation dispersion (MRD) typically occur on a time scale of microseconds or longer, where the conventional perturbation theory of spin relaxation breaks down. In this thesis, we have systematically studied water proton MRD in different immobilized model spin systems corresponding to different exchange cases. In the study of a dipole-coupled spin-1/2 pair which exchanges with bulk water proton spins, we presented the first treatment of dipolar MRD outside the motional-narrowing regime based on the stochastic Liouville equation for the EMOR mechanism. Moreover, we obtained simple analytical expressions which generalize the well-known Solomon equations. Then we studied the asymmetric exchange case for the two-spin system, when the spin system is fragmented by the exchange. Some new and unexpected phenomena showed up in this case. Notably, the anisotropic dipole couplings of non-exchanging spins break the axial symmetry in spin Liouville space, thereby opening up new relaxation channels in the locally anisotropic sites, including longitudinal-transverse cross relaxation. Such cross-mode relaxation operates only at low fields; at higher fields it becomes nonsecular, leading to an unusual inverted relaxation dispersion that splits the extreme-narrowing regime into two sub-regimes. Then we extended our studies to a macromolecule-bound three-spin system, where one, two, or all three spins exchange with the bulk solution phase. In contrast to the previously studied two-spin system with a single dipole coupling, there are now three dipole couplings so relaxation is affected by distinct correlations as well as by self-correlations. Moreover, relaxation can now couple the magnetizations with three-spin modes and, in the presence of a static dipole coupling, with two-spin modes. In another study of the three-spin system in which the relaxation is induced by rotational diffusion, we calculated longitudinal relaxation rate of this model system in arbitrary geometry and with arbitrary rotational dynamics. In this study, we found that the odd-valued spectral density function influences longitudinal relaxation, which is at variance with conventional wisdom. Based on these studies, we have constructed a multi-spin dipolar EMOR relaxation theory based on stochastic Redfield equations with generalizations. This theory yields a quantitative molecular description of tissue-water relaxation and thus provides a rigorous link between relaxation-based magnetic resonance image contrast and molecular parameters.

Key words: spin relaxation theory, immobilized macromolecules, magnetic relaxation dispersion, integral longitudinal relaxation rate, stochastic Liouville equations, multi-spin systems, cross-mode relaxation, spectral density functions

Classification system and/or index termes (if any):

Supplementary bibliographical information:

Language
English

ISSN and key title:

ISBN
978-91-7422-531-0

Recipient's notes

Number of pages
378

Price

Security classification

Distribution by (name and address) Zhiwei Chang, Division of Biophysical Chemistry, Kemicentrum

I, the undersigned, being the copyright owner of the abstract of the above-mentioned dissertation, hereby grant to all reference sources permission to publish and disseminate the abstract of the above-mentioned dissertation.

Signature 常志伟 Date 2017-05-09

Theory of Water-Proton Spin Relaxation in Complex Biological Systems

Zhiwei Chang

LUND
UNIVERSITY

Front cover: (photo) Water proton exchange in protein solutions.
by Filip Persson, Paula Leckius, and Zhiwei Chang
(title language): English and Chinese

Supervisor: Professor Bertil Halle
Co-supervisor: Professor Mikael Akke

Examination committee:

Professor Juha Vaara
Department of Physics, NMR Spectroscopy Unit
University of Oulu

Associate Professor Giacomo Parigi
Department of Chemistry "Ugo Schiff" and Magnetic Resonance Center (CERM)
University of Florence

Professor Daniel Topgaard
Division of Physical Chemistry, Department of Chemistry
Lund University

Doctoral Thesis

Biophysical Chemistry
Center for Molecular Protein Science
Lund University
P.O. Box 124
SE-221 00 Lund
Sweden

ISBN 978-91-7422-531-0 (print)
ISBN 978-91-7422-532-7 (digital)

Printed by Media-Tryck, Lund University, Lund

Dedicated to my families

献给我的家人

学而时习之，不亦说乎？

To learn something and practice it often, isn't it pleasant?

—— 孔子《论语》

Confucius "The Analects"

List of Papers

This thesis is based on the following papers, which will be referred to in the text by their Roman numerals. The papers are appended at the end of the thesis.

I Nuclear magnetic relaxation induced by exchange-mediated orientational randomization: Longitudinal relaxation dispersion for a dipole-coupled spin-1/2 pair.

Z. Chang and B. Halle
J. Chem. Phys. 139, 144203:1-11 (2013).

II Nuclear magnetic relaxation by the dipolar EMOR mechanism: General theory with applications to two-spin systems.

Z. Chang and B. Halle
J. Chem. Phys. 144, 084202:1-16 (2016).

III Nuclear magnetic relaxation by the dipolar EMOR mechanism: Three-spin systems.

Z. Chang and B. Halle
J. Chem. Phys. 145, 034202:1-18 (2016).

IV Nuclear magnetic relaxation by the dipolar EMOR mechanism: Multi-spin systems.

Z. Chang and B. Halle
Manuscript.

V Longitudinal relaxation in dipole-coupled homonuclear three-spin systems: Distinct correlations and odd spectral densities.

Z. Chang and B. Halle
J. Chem. Phys. 143, 234201:1-22 (2015).

My Contribution to the papers

I I performed derivations and calculations of the SLE theory for the two-spin symmetric exchange case, and derived the approximate analytical expressions for the generalized auto- and cross-relaxation rates.

II I performed derivations and calculations of SLE theory for the two-spin asymmetric case, and worked on part of formulating the general formalism. I also repeated and checked all the SRE derivations and calculations in the paper.

III I performed derivations and calculations of SLE theory for the three-spin systems as well as SRE theory for one asymmetric exchange case (*ISP–IS*). I also calculated the coefficient matrices used in the SRE calculations for *ISP–I*, and checked all the derivations and calculations in the paper.

IV I performed derivations and calculations of SLE theory for the four-spin systems, and worked on part of the GSRE derivations. I also computed the coefficient matrices used in the multi-spin GSRE theory and did some calculations.

V I performed derivations and calculations of the SLE theory for the three-spin system and worked on part of symmetry definitions used in the paper. I also repeated and checked all the BWR derivations and calculations in the paper.

For paper I – V, I also participated in the paper writing and review process.

科普性简介

我们目所能及的宏观物质世界都是由微观的原子所构成的。原子的成分包括原子核和电子。电子和很多原子核都具有内在的磁矩，所以它们在磁场中表现的像条形磁铁或者指南针的小磁针一样。如果这些小的带有磁性的粒子被放置在一个外磁场（用$\boldsymbol{B}_0$来表示）中，那么这些原子核和电子的磁矩就会同外磁场相互作用，从而让这些磁矩指向外磁场$\boldsymbol{B}_0$的方向。这种类型的磁相互作用被称之为塞曼相互作用。但是与条形磁铁或者指南针的小磁针不同：电子和原子核同时还具有我们称之为自旋的内禀角动量（可以简单理解为这些粒子能够自转），从而这些粒子的磁矩方向会偏离外磁场的方向并且会绕着外磁场的方向旋转（就如同陀螺停下来之前，中心轴绕着重力场方向进动一样）。这个过程叫做拉莫进动，相应的进动频率被称之为拉莫频率。除了外磁场$\boldsymbol{B}_0$之外，如果我们再对这些粒子施加一个与$\boldsymbol{B}_0$垂直的磁场$\boldsymbol{B}_1$，那么这些粒子的磁矩就会在绕着$\boldsymbol{B}_0$进动的同时绕着$\boldsymbol{B}_1$进动。我们可以控制这个磁脉冲$\boldsymbol{B}_1$的强度和施加时间，让这些粒子所形成的宏观磁矩$\boldsymbol{M}$刚好指向探测器的方向（$\boldsymbol{M} \to \boldsymbol{M}'$）从而能够被探测到。从量子力学的角度来看，这个过程的发生是由于塞曼相互作用的能量是量子化的（对应的是这些粒子的磁矩只能指向有限的几个方向）。如果施加的电磁场辐射频率刚好等于塞曼能级两个能级差所对应的频率（即达到了共振），那这些被探测的原子核就会吸收或者辐射具有微波频率的光子。这种物理现象就被称之为核磁共振。

除了上文提到的能够产生共振现象的磁场$\boldsymbol{B}_0$和$\boldsymbol{B}_1$外，这些被探测的原子核的磁矩还受到周围原子核和电子所产生的微磁场的影响。这些产生微磁场的原子核和电子伴随着携带着它们的分子做着极快的无规则的运动（在室温下的蛋白质溶液当中，蛋白质分子的无规则运动能够达到纳秒（10^{-9}秒）的量级），从而这些微磁场的磁场强度和方向也以极快的速度做着无规则的变化。这些快速变化的微磁场尽管强度非常小，但经过足够长的时间，它们就能影响我们用$\boldsymbol{B}_0$和$\boldsymbol{B}_1$所产生的非平衡态的磁矩$\boldsymbol{M}'$，让其向只存在$\boldsymbol{B}_0$磁场时的平衡态磁矩$\boldsymbol{M}$转化。这种$\boldsymbol{M}' \to \boldsymbol{M}$的转化是不可逆的，我们把这个过程叫做核自旋弛豫。

从表面上看，弛豫现象是核磁共振实验的制约因素之一，因为它决定了一个实验结束而另一个实验开始的等待时间。而且通常这种等待时间会很长（测量两个数据点的时间间隔有时候能达到几分钟）。但任何事物都具有两面性，核自旋弛豫也是如此。由于弛豫过程完成的时间对于产生导致弛豫现象的微磁场的原子及分子的运动非常敏感，所以我们可以把某一类原子核作为“间谍”，通过探索该原子核的自旋弛豫过程来研究导致其产生的周围分子的动力学。核自旋弛豫更重要的应用领域是飞速发展的磁共振成像技术。这项革命性的诊断工具在医学上能够绘制人体软组织的结构图像，而自旋弛豫率则被用于关键的对比度成像参数。

水是地球上维持生命存在最重要的化学物质。水分子中的氢原子核（质子）是与生物相关的最普通以及核磁共振最敏感的原子核。从核磁共振现象发现到现在的几十年来，人们进行了大量的关于水分子质子的核磁共振理论和实验的研究。大量的水分子质子通过磁偶极相互作用关联在一起。在核磁共振实验中，这种磁偶极相互作用的大小取决于质子之间的距离和质子间矢量（从一个质子指向另一个质子）与外磁场$\boldsymbol{B}_0$方向的夹角。质子的弛豫现象则是通过磁偶极相互作用的不断变化而产生。在一杯普通的水中，水分子质子间的磁偶极相互作用由于极快的水分子热运动（皮秒（10^{-12}秒）量级）而趋于零，从而质子的弛豫过程非常缓慢（可以达到若干秒）。二十世纪六十年代，在实验上发现了水分子质子的弛豫过程在蛋白质溶液中被大大

加快。产生该现象的原因是由于部分质子的运动由于携带水分子和蛋白质分子的相互作用而减缓。相应的，这些水分子质子之间的磁偶极相互作用的变化被减缓，从而这些溶液中的蛋白质分子就作为弛豫源而存在。

随着核磁共振技术的发展，纵向弛豫率R_1（描述$\boldsymbol{B}_0$方向的纵向磁矩的弛豫快慢）在一段较宽的磁场（$\boldsymbol{B}_0$）范围内的变化能够利用快变式的核磁共振仪来测量。这种R_1随$\boldsymbol{B}_0$变化的函数关系被称之为磁弛豫色散（MRD）。尽管磁弛豫色散曲线很容易被测量，但是由于缺乏分子层面上对于水分子质子如何"感受"到蛋白质分子运动的理解，从MRD数据中提取水分子和蛋白质分子相互作用的动力学信息就变得非常困难。若干个相关的分子模型被提出，但是在过去的二十年中对于这个生物物理学问题的争议从来没有停止。通过本小组的研究，现在我们清楚这种水分子质子在蛋白质溶液中的弛豫现象是由于存在一些中间态的质子，包括在特定的蛋白质支链上短暂停留的质子以及嵌在蛋白质分子内部的水分子质子。蛋白质分子在溶液中不停的转动会使得这些中间态质子的质子间矢量与外磁场方向的夹角不断变化，从而与这些中间态质子相关的磁偶极相互作用会随之变化而导致弛豫。

水分子质子的弛豫现象在构成生物组织的蛋白质系统中会变得更加复杂。由于具有生物大分子结构，蛋白质分子在软组织（例如大脑，肝脏，肾脏等等）中可以相互接触，所以相较在溶液环境它们的自由运动被抑制。研究水分子质子在运动被抑制的蛋白质系统中的弛豫现象不但对于生物物理学研究具有重要的基础意义，同时还对探测健康及病理组织的磁共振成像技术具有潜在的应用价值。实验和理论研究发现，在弱场环境下纵向弛豫率R_1在运动被抑制的蛋白质系统中被极大的增强。为了在磁共振成像的定量诊断中利用这个效应，我们需要在分子层面上理解质子在运动被抑制的生物系统中的弛豫机制。在磁共振成像领域，这种机制通常用一种唯象的模型来描述，所以并不能提供微观层面上对弛豫机制的理解，因而该模型没有理论的预言能力。而有些微观模型涉及到一些错误的假设，因而在实验研究中已经被否定。

解决这个问题的关键是理解所谓的化学交换在质子弛豫过程中扮演的角色。化学交换是一种动力学过程，指的是一个特定的原子核从一种磁场环境中转移到另一种磁场环境，同时有可能伴随着化学键的断裂和形成。前文所提到的中间态的质子通过化学交换不断的在蛋白质分子和周围水分子之间变换位置。如果蛋白质分子在溶液中能够自由的运动，那化学交换仅仅使得质子的磁矩在蛋白质分子和水溶液中转移，并不能提供比蛋白质转动更慢的一些运动的信息。但是当蛋白质分子的自由运动被抑制（例如在生物组织中）时，化学交换过程比蛋白质的转动要快得多。在这种情况下，化学交换不但起到转移质子磁矩的作用，同时也诱导了弛豫过程的发生。因为此时非各向同性的磁偶极相互作用变化快慢取决于化学交换过程的快慢。因此在构成生物组织的蛋白质系统中，这种以交换为媒介的非各向同性的原子核磁相互作用的各向平均化（EMOR）就成为主要的弛豫机制。

到目前为止，EMOR弛豫机制在定量解释类生物组织系统中弱场的磁弛豫色散曲线（MRD）方面被证实。相关的理论和实验主要利用自旋量子数大于1的原子核（比如^{2}H，^{17}O）通过研究该类原子核的电四极弛豫过程来实现。这种电四极弛豫机制仅涉及到单一的原子核，在理论上处理起来较为简单。但是就临床诊断而言，利用EMOR模型来分析类生物组织系统中通过测量水分子质子的磁偶极弛豫而得到的MRD数据则更为关键。在本论文中，作者从量子统计力学的第一性原理出发，系统的建立了一个多自旋体系的磁偶极EMOR弛豫理论。该理论完整的处理了类生物组织系统中质子弛豫复杂的物理过程，例如由于质子间相互耦合所引起的多体效应，不同交换情况的物理机制等等。本论文提出了一种非微扰的理论框架，从而克服了传统的弛豫理论在微扰条件下仅允许研究极快化学交换的限制。同时该理论也是第一个可以研究慢交换动力学所导致的磁偶极弛豫现象从而能够定量解释类生物组织系统中质子弛豫现象的严格理论。更重要的是，该理论为快变场磁共振成像技术提供了解释软组织成像对比度的物理模型和数学工具。

Popular science summary

Electrons and many atomic nuclei possess intrinsic magnetic moments which behave like bar magnets or compass needles in the magnetic field. If these small magnetic particles are placed in an external magnetic field $\boldsymbol{B}_0$, then the interactions between nuclear or electron magnetization and the applied magnetic field $\boldsymbol{B}_0$ will generate a magnetic torque which tends to line up the magnetization vector $\boldsymbol{M}$ with $\boldsymbol{B}_0$. This type of magnetic interactions is called Zeeman interaction. But unlike bar magnets or compass needles, electron or magnetic nucleus also has intrinsic angular momentum called *spin* which make $\boldsymbol{M}$ being tipped away from the direction of $\boldsymbol{B}_0$ so that $\boldsymbol{M}$ rotates about $\boldsymbol{B}_0$ (like a spinning top precessing about the direction of gravitational field). This process is named Larmor precession and the corresponding frequency is termed Larmor frequency. In addition to the external field $\boldsymbol{B}_0$, we also apply another $\boldsymbol{B}_1$ field which is perpendicular to $\boldsymbol{B}_0$ to rotate $\boldsymbol{M}$ out of alignment with $\boldsymbol{B}_0$ ($\boldsymbol{M} \rightarrow \boldsymbol{M'}$), so that Larmor precession of $\boldsymbol{M'}$ in $\boldsymbol{B}_0$ can be detected. From the spectroscopic point of view, this process occurs because of the quantisation of the Zeeman energy (nuclear magnetic moment only has a few permitted orientations). If the applied electromagnetic radiation frequency matches the difference between two Zeeman energy levels (in resonance), the detected nucleus will absorb or emit radio-frequency photons and this phenomenon is called nuclear magnetic resonance (NMR).

Apart from $\boldsymbol{B}_0$ and $\boldsymbol{B}_1$ fields that give rise to resonance phenomenon, the nuclei also experiences internal magnetic field generated by the magnetic moments of nearby nuclei and electrons which also fluctuates rapidly due to the thermal motions of their carrier molecules. Although the fluctuating field is pretty weak, it causes generated non-equilibrium magnetization returns to its previous equilibrium value ($\boldsymbol{M'} \rightarrow \boldsymbol{M}$) and we call this irreversible process as nuclear spin relaxation.

At a first glance, the relaxation phenomenon seems a drawback in NMR experiments because it determines the waiting time for repeating another experiment and it is usually very slow (sometimes it could take minutes). But every cloud has a silver lining — the relaxation time is very sensitive to the surroundings of nuclei and the molecular motions which generate the fluctuating internal field. Therefore, nuclear spin relaxation can be used as a very informative source to probe the molecular dynamics which causes relaxation. Moreover, the relaxation rates are used as contrast generating parameters in the clinical magnetic resonance imaging (MRI) — a rapidly developing diagnostic technique allowing soft-tissue morphology to be imaged.

Water is the most important chemical substance for the sustaining of the life on earth. Water proton (^{1}H), as the most common and NMR-sensitive nucleus, naturally has been studied in NMR both theoretically and experimentally for several decades. The protons are mutually connected via direct magnetic dipole-dipole interactions which depend on the distances between nuclei and orientations of internuclear vectors (pointing from one proton to another) with respect to the external $\boldsymbol{B}_0$ field. Therefore, the proton relaxation is mainly induced by the modulation of these diplole-dipole couplings. In bulk water, the dipole-dipole couplings are quickly averaged to zero

by unrestricted thermal motions of water molecules. The proton relaxation is thus pretty slow (in the order of seconds). In 1960s, it was found in experiment that the relaxation is much more efficient in protein solutions. The reason is that the proton motions are somehow slowed down by water-protein interactions. Consequently, the dipolar interactions among these protons are modulated relatively slowly and the protein molecules serve as relaxation sink in solutions.

With the development of NMR techniques, the longitudinal relaxation rate R_1 (describing the decay of longitudinal magnetization) now can be measured over a wide field $\boldsymbol{B}_0$ range by using field-cycling NMR spectrometers. The dependence of R_1 on $\boldsymbol{B}_0$ is called magnetic relaxation dispersion (MRD). However, it is very difficult to extract dynamical information about water–protein interactions from the observed proton MRD data due to the lack of the molecular understanding of how protons sense the protein motions. Several microscopic molecular models were brought up and this issue had been controversial for over 20 years. Now it is clear that the relaxation is produced by some intermediary protons which temporarily reside in certain protein side-chains and internal water molecules buried inside the protein molecules. The intra- and intermolecular dipole couplings involving these intermediary protons are modulated by the rotational diffusion (tumbling) of the protein molecules.

Water proton relaxation in tissue-like protein systems is more complicated. Due to their supramolecular structures, the protein molecules in soft tissues (such as brain, liver, kidney, etc.) experience direct protein-protein contact so that they can not move freely as in bulk water. These proteins are thus effectively immobilized. To study the proton relaxation in immobilized protein systems is not only of academic interest in biophysics, but also has the potential usage in the detection of healthy and diseased tissues by using MRI. Particularly, it was found that the longitudinal relaxation rate R_1 in the low external field will be enhanced enormously by protein immobilisation. To employ this effect for quantitative diagnostics, we need to understand the proton relaxation mechanism in such immobilized systems at the molecular level. In MRI field, the tissue water proton relaxation is often described by a phenomenological model which does not provide much microscopic understanding of relaxation and thus has no predictive power. Other microscopic models involve some questionable assumptions and have already been refuted in experiments.

The key to solve this problem is to understand the role of chemical exchange on relaxation. Chemical exchange is a dynamic process that a given nucleus is transferred from one magnetic environment to another different one which may or may not involve breaking/making chemical bonds. The intermediary protons always change positions between protein molecules and bulk water via chemical exchange. As mentioned before, if the protein tumble freely, then the exchange merely transfers proton magnetizations between proteins and bulk water, and can not report protein motions slower than the tumbling. However, when the free motion of protein molecules is inhibited (e.g. in immobilized systems), the exchange process is much faster than the protein tumbling. Now the exchange does not only transfer magnetizations, it also induces relaxation as now the anisotropic dipole couplings are mainly modulated by exchange of intermediary protons. In the tissue-like immobilized protein systems, the principal relaxation mechanism is therefore the exchange-mediated orientational randomization (EMOR) of the anisotropic nuclear couplings.

So far, the EMOR relaxation mechanism which accounts quantitatively for the low-field MRD has been tested and validated in the the tissue-like model protein systems. Theoretical and experimental studies have been performed mainly by using spin $I \geqslant 1$ nuclei governed by quadrupolar relaxation which only involves single spin. However, in purpose of clinical diagnosis, it is crucial to apply EMOR model to the water ^{1}H MRD in immobilized systems governed by dipolar relaxation. In this thesis, I have formulated a multi-spin dipolar EMOR relaxation theory from first principles of quantum statistical mechanics. This theory incorporates many intrinsic physical features of the proton relaxation in immobilized protein systems (such as many-body

effects arising from mutual dipole couplings of protons, complications for different exchange cases, etc.). Moreover, it is a non-perturbative approach which overcomes the limitation of the traditional relaxation theory that only allows the fast relaxation-inducing motions to be studied. This theory is the first treatment of dipolar relaxation that enables the studies of slow exchange cases, which is applicable for the interpretation of the experimental ^{1}H MRD data from the tissue-like immobilized protein systems. More importantly, it can provide a quantitative formalism for the interpretation of the soft-tissue contrast in field-cycled MRI.

Contents

Abbreviations

3SM three-spin mode approximation. 24, 33

BPP initials of Bloembergen, Purcell, and Pound. 2

BPTI bovine pancreatic trypsin inhibitor. 5

BWR initials of Bloch, Wangsness, and Redfield. 6, 11, 18, 19, 28–30, 36, 37

CSA chemical shift anisotropy. 1

EMOR exchange-mediated orientational randomisation. iv, 5–8, 11, 14, 16, 19, 22, 23, 25, 28, 30–33, 39

EN extreme-narrowing. 30, 36

ESE extended Solomon equations. 33

GSDF generalised spectral density function. 24

GSRE relaxation theory based on stochastic Redfield equation with generalisations. 12, 24, 33, 34

ILRR integral longitudinal relaxation rate. 9, 18, 22, 23, 25, 27, 28, 31, 32, 36

ISTO irreducible spherical tensor operator. 14, 19–23

LF low-field. 3, 5, 25, 27, 28, 31

MN motional-narrowing. 3, 5, 6, 11, 25, 27, 28, 30–33, 36, 37

MRD magnetic relaxation dispersion. iv, v, 2–6, 8, 11, 34, 39

MRI magnetic resonance imaging. iii–v, 1, 3, 39

NMR nuclear magnetic resonance. iii, iv, 1, 2, 4, 8

OSDF odd (imaginary) parts of the complex spectral density functions. 36, 37

OSIC odd parity under spin inversion conjugation. 22, 28, 36

RMN restricted motional-narrowing. 11, 18, 19, 23, 24, 33, 34

SBM initials of Solomon, Bloembergenl, and Morgan. 2, 5

SDC static dipole coupling. 6, 18, 19, 23, 31–34, 39

SDF spectral density function. 22, 24

SLE stochastic Liouville equation. 11, 12, 16, 19, 21–25, 29, 30, 32, 36, 37

SND suppression of nonsecular decoupling. 24, 34

SRE stochastic Redfield equation. 11, 12, 19, 21–24, 29, 32, 33

USM ultraslow-motion. 31–33

ZF zero-field. 28, 30, 31, 33

Chapter 1

Introduction

1.1 Spin and NMR

In 1925, when Uhlenbeck and Goudsmit discovered that electron has a fourth degree of freedom – spin, they asked Lorentz for his advice about their idea "a charge that rotates". Lorentz replied "Yes, that is very difficult because it causes the self-energy of the electron to be wrong". Then Uhlenbeck got panicked and went to their supervisor Ehrenfest to withdraw their paper but Ehrenfest had already sent it off for publication. Later Ehrenfest told Goudsmit that "Well, that is a nice idea, though it may be wrong, But you don't yet have a reputation, so you have nothing to lose".[1]

Now we know that spin is one of the intrinsic physical properties possessed by elementary particles and atomic nuclei.[2] The internal spin structures of nuclei are very complicated. Even for the "simplest" nucleus – proton, people have spent over 30 years figuring out how is the proton's spin constructed by orbital motions and spins of its composing quarks and gluons and there is still no consensus about this issue.[3,4] Like other counterintuitive phenomena in quantum world, there is no classical analogue to spin and its physical origin is still unknown. But these issues do not bother us here and we are satisfied with the "superficial" knowledge that spin behaves exactly like angular momentum so that it can be described by the rotational symmetry in quantum mechanics. The magnetic moment resulted from the spin angular momentum of magnetic atomic nuclei and electrons lays the foundations of nuclear magnetic resonance (NMR) — a physical phenomenon discovered by Bloch *et al*[5] and Purcell *et al*[6] in condensed matter in 1946. From spectroscopic point of view, NMR is a physical process that the nuclei absorb or emit radio-frequency photons in the presence of magnetic field.[7,8] The NMR spectroscopy has been widely used in physics, chemistry, biology, material science, medicine, and has a very broad range of applications from quantum computing[9–11] to the magnetic resonance imaging (MRI).[12–14]

1.2 Nuclear spin relaxation

One fundamental aspect of NMR is relaxation. Magnetic or spin relaxation is the irreversible process that a non-equilibrium magnetization returns to its equilibrium value (prescribed by Curie's law) due to the coupling of the spin system to the thermal motion of the surrounding molecules (historically called lattice).[15] Various physical interactions which stochastically modulate the spin Hamiltonian will induce relaxation. In diamagnetic macromolecules, the main relaxation-mediating interactions are quadrupolar, dipolar, scalar couplings and chemical shift anisotropy (CSA).[16] Compared to the first two interactions, the scalar coupling is several orders of magnitude weaker and usually is neglected. Moreover, the relaxation due to CSA is manifested

either in the heteronuclear spin systems with large chemical shifts, or homonuclear systems in the strong external field, which are not concerned in this work. Here we only briefly introduce the first two interactions which are of significant importance for the relaxation mechanism discussed in this thesis.

Quadrupolar coupling refers to the interactions between electric quadrupole of the nucleus and the electric field gradient produced by the surrounding molecules. The orientation of the nuclear electric quadrupole tensor and that of the nuclear magnetic moment are tied to each other. If the molecules carrying the charges which produce electric field gradient undergo thermal motions, it modulates the electrostatic interaction and causes spin relaxation.[7,15] The quadrupolar relaxation only involves single spins, and is the dominant relaxation mechanism for magnetic nuclei with spin quantum number $I \geqslant 1$ due to the large magnitude of quadrupole coupling constant (typically in the range of 0.1 – 10 MHz).

Dipolar coupling is the magnetic dipole-dipole coupling between the magnetic nuclei. There are two types of modulation of the dipolar interactions. For a dipole-dipole coupled two-spin system, either the distance between the two nuclei is fixed and the angle specifying the orientation of the internuclear vector relative to the external magnetic field B_0 fluctuates, or both the distance and angle fluctuate. The former case normally occurs when the two nuclei belong to the same rotating molecule and therefore referred to as intramolecular dipolar relaxation. The latter case is called intermolecular dipolar relaxation as the two nuclei belong to different molecules which undergo translational diffusion.[15,16] The dipolar relaxation is usually the main relaxation mechanism for the nuclei with $I = 1/2$. Compare to quadurupolar relaxation, the dipolar relaxation is less efficient ($\sim$10 KHz) but it is a multi-spin effect (involving at least two spins) and therefore more difficult to deal with.

1.3 Water ^{1}H relaxation in simple solutions

Nuclear spin relaxation is a powerful and versatile tool of studying the molecular dynamics in solids and liquids.[15] Among all the nuclei, proton is the most common magnetic nucleus of biological relevance and also the most sensitive NMR nucleus due to the largest gyromagnetic ratio. Water is the most abundant carrier of protons on earth and also the most vital chemical substance for the evolution of life. The water ^{1}H relaxation has been studied over 70 years in various systems, from bulk phase to protein solutions.

Bloembergen, Purcell, and Pound first described relaxation rate in terms of correlation time (known as BPP theory) and obtained the spin-lattice relaxation time T_1 of protons in bulk water at room temperature.[17] Then Solomon extended their work by analysing intramolecular dipolar relaxation of a dipole-dipole coupled heternuclear two-spin system in which the dipolar cross relaxation was described.[18] Later, Solomon's work was further extended to describe the water ^{1}H relaxation in the presence of paramagnetic ions in solution, which is known as Solomon-Bloembergen-Morgan (SBM) theory.[19] The pioneer study of water ^{1}H relaxation in protein solutions was done by Daszkiewicz *et al* in 1963 in which they found that the ovalbumin (hen egg protein) dissolved in water increases the proton relaxation rate.[20] They attributed this effect to the increasing of the water correlation time due to the exchange of water molecules rigidly bound to the proteins with bulk water.

With the aid of the field-cycling technique,[21,22] the magnetic relaxation dispersion (MRD) which is the dependence of longitudinal relaxation rate R_1 on the strength of applied magnetic field B_0, can be measured over a wide field range. The interpretation of these MRD data minimises the ambiguity of the model-dependent analysis of single-field spin relaxation data and opens up a new window to quantitatively study protein hydration dynamics and conformational changes in solutions. Such studies have been of fundamental interest in biophysics and still re-

maining an active field. Very soon, this technique was applied to protein-hydration problems. The first protein (demetallated (apo) transferrin) proton MRDMRD profile was published by Koenig *et al* in 1969.[23] However, the interpretation of water MRD data in terms of relaxation-inducing motions in protein solutions was controversial during the following 25 years. Koenig *et al* proposed a long-range hydrodynamic interaction model that relaxation of hydration water nuclei in protein solutions was induced by a component of the motion of the water molecules that mimics the protein motion.[24] Kimmich *et al* advocated another model that water relaxation in protein systems was caused by the long-lived water molecules remaining "locked" within the hydration shells which nevertheless are able to diffuse along the rugged protein surface.[25] However, these two models were both refuted by the ^{17}O MRD studies in several protein solutions, which demonstrated that the ^{17}O relaxation dispersion is due to a small number of internal water molecules buried inside the protein which exchange with bulk water.[26,27] A combined ^{1}H, ^{2}H, and ^{17}O MRD study also showed that the water ^{1}H relaxation in protein solutions can be quantitatively accounted for in terms of exchanging internal water molecules, labile protons, and intermolecular auto-spin relaxation of the protein protons which contributes additively.[28] Moreover, this study also confirmed that the effect of cross-relaxation which is the coupling between the longitudinal magnetizations of different spins is negligible for the water ^{1}H relaxation in protein solutions.

1.4 Water ^{1}H relaxation in immobilized biological systems

Water ^{1}H relaxation in the tissue-like immobilized systems is not only of academic interest but also has the potential usage in the detection of healthy and diseased tissues by using MRI. In most tissues, the tumbling of most protein molecules is slowed down due to supramolecular structures so that they are effectively immobilized. Moreover, in some diseased tissues the protein molecules may be immobilized by the pathological aggregation processes (for example, the amyloid fibrils formed by Aβ40 which is the primary suspect causing the Alzheimer disease[29,30]). Due to protein immobilisation, the longitudinal relaxation rate R_1 in the LF will be greatly enhanced (several orders of magnitudes).[31,32] The traditional MRI technology only measures relaxation in the field far above the region where this large MRD occurs. However, field-cycling technique allows R_1 to be measured in the LF with the spatial resolution which enables us to detect the immobilized proteins in vivo. The field-cycling MRI technology which may realise this aim is being developed in several labs.[33–40] In order to employ this protein-immobilisation effect for quantitative diagnostics, the molecular mechanistic understanding of water ^{1}H relaxation in immobilized protein systems is crucial. Unfortunately, there is still no consensus on this issue in the MRI field.[41]

Most MRI researchers employ a phenomenological description of tissue water ^{1}H relaxation — the so-called "two-pool" model.[41,42] In this model, the proton magnetization are exchanged between the water (free pool) and polymer (bound pool) phases with different intrinsic longitudinal relaxation rates. However, this model does not provide understanding of relaxation mechanism at molecular level and thus has no predictive power. Koenig *et al* proposed a molecular theory of water ^{1}H relaxation in immobilized protein systems by postulating that the observed MRD profile can be accounted for by the existence of a class of long-lived, temperature-independent water in the first hydration shell, which can form four hydrogen bonds to protein surface atoms.[43,44] However, this model fails because: (i) it does not correctly identify the role of intermediary protons (protons from labile groups and internal water molecules) on the relaxation; (ii) MRD data are interpreted based on Solomon equations which is only valid in the motional-narrowing (MN) condition; (iii) the multi-spin effect is not treated. Another group of workers suggested a microscopic model of tissue-water relaxation — the "spin fracton" model, which attributes

the water ^{1}H relaxation to the small-amplitude localized longitudinal and librational collective motions of the protein backbone.[45–47] This model predicts that the longitudinal relaxation rate decays with Larmor frequencies as a power law: $R_1 \sim A\,\omega^{-b}$, and especially $b = 1/3$ for ω from 10^4 to 10^8 Hz. However, both experimental[48] and theoretical[49] studies of the vibrational energy transfer in proteins show a classic ω^2 scaling up to $\sim 10^{12}$ Hz. Moreover, this model can not explain the strong pH dependence of MRD profiles in the high-field.[31,50] Furthermore, a H→D substitution MRD study showed that the spin-fracton model fails to predict the isotope effects on the relaxation.[32]

1.5 Chemical exchange on ^{1}H relaxation

It is well known that NMR spectroscopy is affected by chemical exchange — a dynamic process that a given nucleus is transferred from one magnetic environment to another different one which may or may not involve breaking/making chemical bonds.[7,51] This process does not affect the macroscopic equilibrium of the sample since when individual nucleus moves to a different environment, it is always replaced by another so that the equilibrium is maintained. The effect of chemical exchange on proton relaxation was realised several decades ago.

McConnell added first order kinetics terms to the Bloch equations (known as Bloch-McConnell equations) to study a model system in which a single spin-1/2 is transferred back and forth between two or more magnetic environments by kinetic molecular processes. The exchange was assumed to be much slower than the (rotational) motions inducing relaxation so that the relaxation rate in each environment is independent of exchange rate.[52] About the same time, Zimmerman et al studied the relaxation phenomena of water protons when water molecules were adsorbed on the surface of silica gel.[53] They developed a stochastic relaxation theory based on phenomenological rate law in which relaxation rate was treated as a stochastic variable. In this theory, water molecules interchange between two adsorbing phases with different intrinsic relaxation rates (assumed independent of the exchange rate). The exchange was modelled as stationary Markoff process. From the analysis of this two-phase model system, they discovered that the longitudinal magnetization decays exponentially under fast exchange limit ($\tau_{\rm ex} \ll 1/R_{1,\rm A(B)}$)

$$\Delta M_z(t) \;=\; \Delta M_z(0)\exp\left(-R_{1,\rm av}\,t\right) \tag{1.5.1}$$

where the average relaxation rate $R_{1,\rm av}$ is

$$R_{1,\rm av} \;=\; P_{\rm A}\,R_{1,\rm A} + P_{\rm B}\,R_{1,\rm B} \tag{1.5.2}$$

and bi-exponentially under slow exchange limit ($\tau_{\rm ex} \gg 1/R_{1,\rm A(B)}$)

$$\Delta M_z(t) \;=\; \Delta M_z(0)\left[P_{\rm A}\exp\left(-R_{1,\rm A}\,t\right) + P_{\rm B}\exp\left(-R_{1,\rm B}\,t\right)\right] \tag{1.5.3}$$

where ΔM_z is the observed longitudinal magnetization; $P_{\rm A}$ and $P_{\rm B}$ are populations of water molecules in phase A and phase B ($P_{\rm A} + P_{\rm B} = 1$), and $R_{1,\rm A}$ and $R_{1,\rm B}$ are the corresponding intrinsic relaxation rates, respectively.

Luz and Meiboom studied the relaxation of the hydroxyl and methyl protons in methanol solutions containing low concentration of paramagnetic ions at different temperatures.[54] In this sample solutions, the methanol molecules exchange between the coordination sphere of the paramagnetic ions (phase A) and the bulk methanol (phase B). In this two-phase relaxation model, the ^{1}H relaxation in phase A is much more efficient than that in phase B ($R_{1,\rm A} \gg R_{1,\rm B}$) due to the presence of paramagnetic ions, while the population of protons in phase A is much smaller than that in phase B ($P_{\rm A} \ll P_{\rm B}$, dilute regime). In addition, the motions that induce

relaxation (with correlation time τ_c) are much faster than the exchange (i.e., $\tau_c \ll \tau_A$), so that the intrinsic relaxation rate $R_{1,A}$ is independent of τ_A. Under these three conditions, they derived an expression of longitudinal relaxation rate based on Bloch-McConnell equations

$$R_1 = \frac{P_A}{\tau_A + \frac{1}{R_{1,A}}} \tag{1.5.4}$$

where τ_A is the residence time of methanol molecules in phase A. This expression is also only valid under MN condition ($\tau_c \ll 1/R_{1,A}$).

The role of exchange on the ^{1}H relaxation in the protein solutions is more complicated. In protein solutions, generally there are three types of relaxation-inducing motions need to be considered: (i) over-all tumbling of the protein molecule; (ii) chemical exchange of the intermediary protons with bulk water protons;[55] (iii) internal motion (vibrations, librations, rotate/flip about the molecular symmetry axis, etc.). Here we only consider the relaxation caused by the first two motions. The internal motions (in the order of picoseconds) are usually much faster than the tumblings or chemical exchange and therefore it makes small contributions to the observed R_1 and can be easily incorporated via order parameters.[50,56]

The correlation time that enters into the expressions of longitudinal relaxation rate can be written as[55,57]

$$\frac{1}{\tau_c} = \frac{1}{\tau_R} + \frac{1}{\tau_{ex}} \tag{1.5.5}$$

where τ_R is the protein tumbling time, and τ_{ex} is the exchange time of the intermediary protons. This expression also appears in the SBM theory,[57] with the addition of a third term describing electron spin relaxation. In solutions, the dipolar interactions are averaged to zero by the protein rotational motion (typically in the order of nanoseconds[58]) which is much faster than exchange (typically, in the range of microseconds to milliseconds[59]). Therefore, Eq. (1.5.5) shows that the correlation time τ_c characterising the modulation of dipolar Hamiltonian is the protein tumbling time τ_R ($\tau_c = \tau_R$) since $\tau_R \ll \tau_{ex}$. In this case, the exchange merely transfers proton magnetizations between the proton residence sites on proteins and bulk region, and can not report any motions slower than the protein tumbling.

However, when the free motion of protein molecules is inhibited by chemical cross-linking or direct protein-protein contact, the exchange process between orientationally confined protein sites and isotropic sites in bulk region is much slower than the protein tumbling ($\tau_R \gg \tau_{ex}$). In this case, the exchange does not only transfer magnetizations, it also induces relaxation as now the correlation time for the modulation of the anisotropic spin couplings is the exchange (residence) time of intermediary protons on proteins ($\tau_c = \tau_{ex}$).[59–62] In the tissue-like immobilized protein systems, therefore the principal relaxation mechanism is the exchange-mediated orientational randomization (EMOR) of the anisotropic nuclear couplings.[50,59–61]

1.6 Aim and challenges

So far, the EMOR relaxation mechanism which accounts quantitatively for the LF MRD has been tested and validated in the the tissue-like model protein systems. Theoretical and experimental studies have been performed mainly by using spin $I \geqslant 1$ nuclei governed by quadrupolar relaxation. For example, a ^{2}H and ^{17}O MRD study has been performed to investigate the hydration and conformational dynamics of the chemically cross-linked bovine pancreatic trypsin inhibitor (BPTI) and ubiquitin proteins in the $D_2O/H_2{}^{17}O$ solvent.[59] This study confirms that the MRD is produced by a small fraction of long-lived internal water molecules and labile protein deuterons. However, in purpose of clinical diagnosis, it is crucial to apply EMOR model to the

water ^{1}H MRD in immobilized systems governed by dipolar relaxation. The first attempt made use of the extended Solomon equations with invoking several approximations.[50,61] Although this approach is not rigorous and some of the approximations are *ad hoc*, it provides useful physical insights on the dipolar EMOR mechanism.

The primary goal of the work presented in this thesis is to develop a rigorous water ^{1}H dipolar EMOR relaxation theory in complex biological systems. However, there are three main challenges in developing such a theory from first principles:

1. Compared to dipolar relaxation, the quadrupolar relaxation is relatively simpler to deal with because it is a single-spin mechanism and thus can be treated exactly within the low-dimensional Hilbert or Liouville spin space. The rigorous theory of quadrupolar relaxation based on this model is now available.[56,60] In contrast, the dipolar relaxation involves multi-spin network and therefore the dimension of the Liouville space needed to describe the spin system grows exponentially with the number of spins. Normally there are hundreds or thousands of protons in one protein molecule. Considering a "simple" spin $I = 1/2$ system consisting of 10 spins, the dimension of the spin Liouville space is 1048576 and it is impractical to generate all the corresponding matrix elements of the Zeeman and dipolar Liouvillians, not even mention to invert these huge matrices and isotropically average them with different orientations.

2. Conventionally, the relaxation behaviour of the dipole-dipole coupled spin systems was studied by using the Bloch-Wangsness-Redfield (BWR) theory.[15,63] This second-order perturbation theory requires the molecular motion which induces the relaxation is much faster than the coherent evolution of the magnetization under dipolar interactions ($\omega_{\mathrm{D}}\,\tau_{\mathrm{A}} \ll 1$), which is usually the case in liquids. However, this so-called motional narrowing condition is violated in the immobilized protein systems. Therefore, we need to use more general, non-perturbative theoretical framework to describe the spin dynamics beyond the MN limit.

3. The immobilized biological systems have both solid-like and liquid-like features. On one hand, nonlabile protons reside permanently in the immobilized protein molecules which is solid-like; on the other hand, the exchange of the intermediary protons transiently associated with the protein molecules with the bulk region averages out the associated nuclear couplings which is thus liquid-like. The anisotropy of the spin system, the exchange between anisotropic sites and isotropic bulk region, and the presence of both fluctuating and static dipole couplings (SDCs) must all be accounted for in a rigorous relaxation theory.

In this thesis, I have addressed these problems and formulated a multi-spin dipolar relaxation theory based on the EMOR mechanism, which can be used for the interpretation of the experimental ^{1}H MRD data from the tissue-like immobilized protein systems. Moreover, it can provide a quantitative formalism for the interpretation of the soft-tissue contrast in field-cycled MRI.

Chapter 2

Model

In this chapter, we first briefly describe the model of the spin systems based on dipolar EMOR relaxation mechanism. Then we introduce the integral longitudinal relaxation rate which is suitable to characterise the longitudinal relaxation in the dilute regime where the longitudinal magnetization decays exponentially. These contents have been described in section II, paper II, where more details can be found.

2.1 Spin systems

In the aqueous protein systems, there are three types of proton: (i) bulk water protons; (ii) nonlabile protons that reside on protein molecules permanently; and (iii) intermediary protons comprising the labile protons residing in certain side-chains (hydroxyl, carboxyl, amino, etc.) and internal water molecules buried inside the protein molecules which exchange with the bulk region.[50] Dipolar couplings among bulk water protons are averaged to zero by unrestricted water motions (on the picosecond scale). The second and third types of protons form a multi-spin network through mutual dipole-dipole couplings in the protein molecules. Dipolar interactions between protons from different protein molecules are neglected due to the fast decay over the distances ($\sim 1/r^3$).

We consider an ensemble of such mutually non-interacting $I = 1/2$ spin systems where each spin is subject to a Zeeman coupling with the external magnetic field B_0 and experiences mutual magnetic dipole-dipole couplings. In the spin system, some or all of the spins exchange between the liquid-like bulk (B) state and the solid-like anisotropic (A) state. In state B, all dipole couplings are assumed to be averaged to zero (the very small relaxation contribution from the fast modulation of dipole couplings can be added, if necessary), leaving only the Zeeman coupling; in state A, the spins experience both Zeeman and dipole couplings. The state A consists of a large number (N) of protein molecules distinguished by different orientations, which are labeled with the index $\alpha = 1, 2, ..., N$ ($\alpha = 0$ refers to the B state for notational convenience). As a good approximation, we assume that the orientations of these N macromolecules sample an isotropic distribution. Suppose each of N molecules hosts a spin system comprising $m_{\rm A}$ ($m_{\rm A} \geqslant 2$) spins of which $m_{\rm B}$ ($1 \leqslant m_{\rm B} \leqslant m_{\rm A}$) spins exchange with the B state, we refer to the case $m_{\rm B} = m_{\rm A}$ when all spins exchange as symmetric exchange, and $m_{\rm B} < m_{\rm A}$ as asymmetric exchange when only some of them exchange. The $m_{\rm B}$ exchanging spins are referred to as labile spins, and the $m_{\rm A} - m_{\rm B}$ nonexchanging spins as nonlabile spins.

We identify different exchange cases using the notation "(spins in state A) – (spins in state B)". For example, *IS–I* and *ISP–I* are asymmetric exchange cases with one labile proton for two- and three-spin systems, respectively; *IS–IS* denotes a symmetric exchange case for a two-spin

system with both protons labile. Here we are primarily interested in two asymmetric exchange cases: (i) one labile (hydroxyl, carboxyl, etc.) proton spin which is dipole-coupled to the rest protein proton spins undergoes exchange; (ii) two labile proton spins exchange as an intact unit, which would be the two proton spins of a water molecule temporarily residing in a protein cavity and dipole-coupled to the rest of protein proton spins. These two cases are denoted as IP_m–I and ISP_m–IS, with P symbolising nonlabile spins and m indicating the number of nonlabile protein proton spins ($m = m_\mathrm{A} - m_\mathrm{B}$). In both cases (for $m > 0$), the spin systems are fragmented by exchange, and the orientations of dipole couplings involving at least one labile spin are assumed to be instantaneously randomized by exchange, which induces relaxation (see more details in section 3.1.4). The theory dealing with these two cases can also be extended to variant cases that several labile spins or spin pairs exchange independently (e.g. ISP_m–I/S).

Let P_A be the population of labile spins residing in state A, and $P_\mathrm{B} = 1 - P_\mathrm{A}$ be that in state B. In the special case with $P_\mathrm{A} = 1$, the EMOR model reduces to the random phase approximation or strong collision model, which assumes that the new state to which the spin Hamiltonian jumps is completely uncorrelated to the old states.[64] The general dipolar EMOR theory developed here is valid without restrictions on P_A, but we will focus on the dilute regime where $P_\mathrm{A} \ll 1$, which is more relevant in experiments and applications.

For simplicity, hereafter we mainly focus on exchange case IP_m–I, and the final results can be easily generalised to ISP_m–IS case. Moreover, these $m+1$ spins are treated as isochronous if not specified since the chemical shift for protein protons rarely exceeds 10 ppm.

2.2 Integral longitudinal relaxation rate

The initial non-equilibrium proton magnetizations need to be prepared for the measurement of ^{1}H MRD profiles in the aqueous proteins gels. In conventional relaxation experiments, the labile proton spins can be excited selectively by using a soft radio frequency pulse if the nonlabile protons have a much wider NMR. Alternatively, all proton spins can be excited non-selectively in the field-cycling experiments by rapidly changing the magnitude of the B_0 field.

Macroscopic spin observables (like the longitudinal magnetization for the observed spins) are related to a density operator[65] summed over all sites,

$$\langle \sigma(t) \rangle \equiv \sum_{\alpha=0}^{N} \sigma^\alpha(t) = \sigma^\mathrm{B}(t) + \sigma^\mathrm{A}(t) \tag{2.2.1}$$

where $\sigma^\alpha(t)$ is the spin density operator for a particular site α (see more details in section 3.1.3), and $\sigma^\mathrm{B}(t) \equiv \sigma^0(t)$ as defined in section 2.1.

The intitial density operator $\sigma^\alpha(0)$ is proportional to the relative population P_α. We express this as

$$\sigma^\alpha(0) = \begin{cases} P_\mathrm{B}\, \eta^\mathrm{B} & \text{for } \alpha = 0 \\ \dfrac{P_\mathrm{A}}{N}\, \eta^\mathrm{A} & \text{for } \alpha \geq 1 \end{cases} \tag{2.2.2}$$

so that Eq. (2.2.1) yields

$$\langle \sigma(0) \rangle = \sigma^\mathrm{B}(0) + \sigma^\mathrm{A}(0) = P_\mathrm{B}\, \eta^\mathrm{B} + P_\mathrm{A}\, \eta^\mathrm{A} \tag{2.2.3}$$

Here the η^A and η^B are spin operators that depend on the initial condition of the spin system.

Specifically, for nonselective excitation

$$\eta_n^{\mathrm{A}} \;=\; \sum_{i=1}^{m_{\mathrm{A}}} \delta_{n,i} \tag{2.2.4a}$$

$$\eta_n^{\mathrm{B}} \;=\; \delta_{n,1} \tag{2.2.4b}$$

where δ is the Dirac delta function, subscript n denotes the basis operator indices corresponding to the longitudinal magnetization of the observed spins (we adopt the convention that the longitudinal magnetization modes are always indexed before the other spin modes, and the first one is the longitudinal mode for exchanging spin I). For I-selective excitation, we have instead

$$\eta_n^{\mathrm{A}} \;=\; \eta_n^{\mathrm{B}} \;=\; \delta_{n,1} \tag{2.2.5}$$

As discussed in section 1.5 that the longitudinal magnetization decays exponentially in dilute regime under general conditions (fast or slow exchange). The longitudinal relaxation rate of the observed spins can then be identified as the inverse of the time integral of the observed longitudinal magnetization, normalised by its initial value. The integral longitudinal relaxation rate (ILRR) can be expressed as[56,60]

$$\widehat{R}_1 \;\equiv\; \left[\int_0^\infty \mathrm{d}t\; \frac{\sigma_L(t)}{\sigma_L(0)}\right]^{-1} \;=\; \frac{\sigma_L(0)}{\widetilde{\sigma}_L(0)} \tag{2.2.6}$$

where the subscript L represents the observed longitudinal spin modes. Laplace transform

$$\widetilde{\sigma}_L(s) \;\equiv\; \int_0^\infty \mathrm{d}t\; \exp(-st)\, \sigma_L(t) \tag{2.2.7}$$

was used in the second step. Then we set $s = 0$ according to the definition of ILRR.

Substitution of Eqs. (2.2.1) – (2.2.5) into Eq. (2.2.6) yields

$$\widehat{R}_1 \;\equiv\; \left[\int_0^\infty \mathrm{d}t\; \frac{\sum_{n_{\mathrm{B}}} \sigma_{n_{\mathrm{B}}}^{\mathrm{B}}(t) + \sum_{n_{\mathrm{A}}} \sigma_{n_{\mathrm{A}}}^{\mathrm{A}}(t)}{\sum_{n_{\mathrm{B}}} \sigma_{n_{\mathrm{B}}}^{\mathrm{B}}(0) + \sum_{n_{\mathrm{A}}} \sigma_{n_{\mathrm{A}}}^{\mathrm{A}}(0)}\right]^{-1} \;=\; \frac{P_{\mathrm{B}} \sum_{n_{\mathrm{B}}} \eta_{n_{\mathrm{B}}}^{\mathrm{B}} + P_{\mathrm{A}} \sum_{n_{\mathrm{A}}} \eta_{n_{\mathrm{A}}}^{\mathrm{A}}}{\sum_{n_{\mathrm{B}}} \widetilde{\sigma}_{n_{\mathrm{B}}}^{\mathrm{B}}(0) + \sum_{n_{\mathrm{A}}} \widetilde{\sigma}_{n_{\mathrm{A}}}^{\mathrm{A}}(0)} \tag{2.2.8}$$

where the sums run over the modes (or basis operators) corresponding to the longitudinal magnetization of the observed spin(s). As seen from Eq. (2.2.6) that if longitudinal magnetization decays exponentially $\sigma_L(t) = \sigma_L(0) \exp(-R_1\, t)$, then $\widehat{R}_1$ is identical to the longitudinal relaxation rate R_1. However, if longitudinal magnetization deviates significantly from single-exponential decay, then the integral rate $\widehat{R}_1$ only provides some "reduced" information. But we can still extract some model parameters by fitting the measured or calculated $\widehat{R}_1$.[56]

Chapter 3

Theory

In this chapter, we sketch essential scheme of the multi-spin dipolar EMOR theory. This theory deals with the spin-dynamical problem for a system of exchanging dipolar nuclei described in section 2.1 and is constructed based on a two-fold approach: stochastic Liouville equation (SLE) and stochastic Redfield equation (SRE).

SLE theory was first developed by Anderson[66] and Kubo[67] for the analysis of spectral line shape when the frequencies were modulated randomly — known as Kubo-Anderson process. It is a very general and non-perturbative theoretical framework which is capable of describing the EMOR relaxation mechanism over full range of exchange rates and spin coupling strengths. This theory is valid for the systems comprising arbitrary number of spins, and for both symmetric and asymmetric exchange cases. The exact EMOR SLE theory was first developed for quadrupolar relaxation for nuclei with $I = 1$,[56,60] and then extended to dipolar relaxation for spin-1/2 systems in general form (in section II, paper II). For small-sized spin systems that can be described within low-dimensional Liouville spin spaces (e.g. quadruplar relaxation with $I = 1$ or dipolar relaxation with $m_{\mathrm{A}} \leqslant 4$ spin-1/2 systems), the SLE approach is simpler in terms of formalism compared to SRE. However, there are two drawbacks with this approach: (i) as mentioned in section 1.6 that in order to implement the multi-spin SLE theory, we need to evaluate all matrix elements of Zeeman and dipolar Liouvillians in the $(4^{m_{\mathrm{A}}} - 1)$-dimensional Liouville space (neglect the redundant identity superoperator), and then invert and isotropically average these matrices, which is a formidable task for multi-spin systems (in paper IV, the SLE version of the dipolar EMOR theory has been implemented for $m_{\mathrm{A}} = 4$, where the 65025 matrix elements were generated analytically). It is also not clear how to construct a computationally efficient yet reasonably accurate multi-spin dipolar EMOR theory within the framework of SLE; (ii) the SLE approach is more of a "black box" which does not provide much physical understanding of the complex relaxation behaviour exhibited in different EMOR cases.

SRE approach is the restricted second-order perturbative BWR theory which also incorporates the exchange kinetics. Similar to Bloch-McConnell equations[52] and extended Solomon equations,[50] the SRE theory is only valid in the restricted motional-narrowing (RMN) regime where the exchange is much faster than the coherent evolution of the magnetization under both fluctuating and static dipolar interactions. Compared to SLE, the SRE enables us to directly explore the physical origins of the peculiar features displayed on MRD profiles (most of them appear in asymmetric exchange cases) despite of its complicated forms and restrictions. Similar to the SLE results, the exact solutions for spin systems with $m_{\mathrm{A}} \leqslant 4$ have been obtained in paper II – IV. Besides providing physical insights, more importantly, it is possible to systematically formulate a multi-spin EMOR theory within the SRE framework by invoking a few physically reasonable approximations, which is also valid beyond the MN limit. The validity of these ap-

proximations can be tested by comparing with the exact SLE results available for small-sized spin systems. This generalised multi-spin SRE theory (GSRE) is applicable to experimental ^{1}H relaxation data from aqueous protein gels.

3.1 Stochastic Liouville approach

Spin Hamiltonians

The spin Hamiltonians for the two states B and A discussed in section 2.1 are

$$H_{\mathrm{B}} = H_{\mathrm{Z}} \tag{3.1.1a}$$

$$H_{\mathrm{A}} = H_{\mathrm{Z}} + \sum_{\alpha=1}^{N} H_{\mathrm{D}}^{\alpha} \tag{3.1.1b}$$

Before writing down the explicit forms of Zeeman and dipolar Hamiltonian, it is useful to first distinguish different reference frames that have been used to describe nuclear interactions.[57,68] We define a Cartesian lab-fixed (L) frame in which the z-axis is set along the external B_0 field. Then we define a molecular (M) frame which is another Cartesian frame bound to the rigid molecules. The axes of M frame are normally chosen based on the molecular symmetry for small molecules. But for macromolecules with irregular geometries (e.g. proteins), the M frame can be defined arbitrarily. Finally, we define a particular M frame — principal (P) frame in which the spin Hamiltonian can be described by a diagonal tensor. The P frame depends on the type of interactions. For the dipolar interactions concerned here, the z-axis of P frame is set along the internuclear vector.

The Zeeman Hamiltonian for the IP_m system in the L frame is

$$H_{\mathrm{Z}} = \omega_L \left(I_z + \sum_{i=1}^{m} P_{iz} \right) \tag{3.1.2}$$

where ω_L is the static Larmor frequency, I_z and P_{iz} represents the z-component of the spin angular momentum of spin I and P_i, respectively.

The dipolar Hamiltonian for a particular site α in A state can be written as a sum of that for each of the $\frac{m\,(m+1)}{2}$ spin pairs (denoted as X)

$$H_{\mathrm{D}}^{\alpha} = \sum_{X} H_{\mathrm{D},X}^{\alpha} \tag{3.1.3}$$

where the explicit form of $H_{\mathrm{D},X}^{\alpha}$ is[15,57,68–70]

$$H_{\mathrm{D},X}^{\alpha} = c\,\omega_{\mathrm{D},X} \sum_{M=-2}^{2} T_M^2(X)\, D_{M0}^{2*}(\Omega_X^{\alpha}) \tag{3.1.4}$$

Here, if the spin pair X related to fluctuating dipole coupling (involving labile spin I) or static dipole coupling consists two spins i and j which are separated by distance r_{ij}, the dipolar coupling constant $\omega_{\mathrm{D},X}$ is (in rad s^{-1})

$$\omega_{\mathrm{D},X} \equiv \frac{3\mu_0}{8\pi} \frac{|\gamma_i\,\gamma_j|\,\hbar}{r_{ij}^3} \tag{3.1.5}$$

where γ_i and γ_j are the gyromagnetic ratios for spin i and j, respectively. $T_M^2(X)$ are orthonormal $(m+1)$-spin irreducible spherical tensor operators[71] (see details in section 3.1.2) acting only on

the spin variables, c is the constant related to $D^2_{M0}(0)$ and the normalisation of $T^2_M(X)$ (e.g. for $m = 1, 2, 3$, c $= -\frac{\sqrt{6}}{3}, -\frac{2\sqrt{3}}{3}$, and $-\frac{2\sqrt{6}}{3}$, respectively), $D^2_{M0}(\Omega^\alpha_X)$ are rank-2 Wigner functions indicating transformations from L frame to P^α_X frame.

The rotation of the z-axis of L frame to that of P^α_X frame (orientation of internuclear vector $\boldsymbol{r}^\alpha_X$) can be achieved by three successive coordinate frame rotations. For the L frame with axes (x, y, z), first rotate the frame by angle ψ about the z axis, then rotate the new frame by angle ϑ about the y' axis. Finally, this intermediate frame is again rotated by angle φ about the z' axis. Now the original L frame with (x, y, z) has been transformed to a new frame (x', y', z'). The L$\rightarrow$P$^\alpha_X$ transformation can be done with the same procedure by assigning these angles to specify the orientation of the internuclear vector r_X in site α which is the z-axis of P_α frame, with respect to the L frame. These three angles defined above are known as Euler angles ($\psi, \vartheta, \varphi \equiv \Omega$). The operator corresponding to this three-step passive rotation is[71]

$$D(\Omega) \;=\; \exp(-i\,\varphi\,I_z)\exp(-i\,\vartheta\,I_y)\exp(-i\,\psi\,I_z) \tag{3.1.6}$$

which can also be represented as a matrix form in a Hilbert space expanded by the $2I+1$ common eigenvectors of angular momentum I^2 and I_z

$$D^I_{MN}(\Omega) \;=\; \langle IM\,|\exp(-i\,\varphi\,I_z)\exp(-i\,\vartheta\,I_y)\exp(-i\,\psi\,I_z)|\,IN\rangle \tag{3.1.7}$$

This type of functions is known as Wigner function named after Hungarian-American theoretical physicist Eugene P. Wigner. This expression can be further simplified by using the fact that $I_z|\,IM\rangle = M\,|\,IM\rangle$

$$\begin{aligned} D^I_{MN}(\Omega) \;&=\; \langle IN\,|\exp(-i\,\varphi\,I_z)\exp(-i\,\vartheta\,I_y)\exp(-i\,\psi\,I_z)|\,IM\rangle \\ &=\; \exp(-i\,M\,\psi)\;\langle IM\,|\exp(-i\,\vartheta\,I_y)\,|\,IN\rangle\exp(-i\,N\,\varphi) \\ &=\; \exp(-i\,M\,\psi)\,d^I_{MN}(\vartheta)\exp(-i\,N\,\varphi) \end{aligned} \tag{3.1.8}$$

where $d^I_{MN}(\vartheta)$ is the reduced Wigner function and its analytical forms have been calculated for different angular momenta I.[71]

Compared to the quadrupolar interactions which require asymmetry parameters to specify the EFG tensors,[56,60] the dipolar interactions have the cylindrical symmetry and the alignment of z axis is all we need. For the two-spin systems, we therefore only need two Euler angles, ψ and ϑ, to specify the dipolar vectors and the third redundant angle φ can be chosen to zero. For the three-spin systems, however, the φ is not redundant anymore and it serves as a dihedral angle to indicate the orientation of the plane formed by the three spins. The internuclear geometry is set up by first setting one dipolar vector as the z-axis in the M frame and the Wigner functions of the other two vectors were transformed in two steps L$\rightarrow$M$\rightarrow$P by using the formula[71]

$$D^2_{M0}(\Omega^\alpha_X) \;=\; \sum_{N=-2}^{2} D^2_{MN}(\Omega^\alpha_{LM})\,D^2_{N0}(\Omega_{MP}) \tag{3.1.9}$$

For the multi-spin system IP_m ($m \geqslant 3$), the z-axis of the M frame is chosen to be the internuclear vector pointing from spin I to its nearest nonlabile spin P_1. The details of specifying the internuclear geometry of multi-spin system are given in paper IV.

Spin operator basis

In quantum mechanics, a state of spin system is usually described in the Hilbert space which is spanned by a complete set of orthonormal basis vectors. The relaxation problem in isotropic sys-

tems can often be simplified by making use of extensive symmetries based on group theory.[69,72,73] However, in order to better employ these symmetry arguments, it is necessary to develop the relaxation theory in the so-called Liouville representation of quantum mechanics[73,74] which also gives compact notations while avoiding the cumbersome multiple commutators. Here we adapt this representation and develop the dipolar EMOR relaxation theory in the Liouville space, which is spanned by a complete basis set of orthonormal spin operators. These spin operators are irreducible spherical tensor operators (ISTOs) with respect to rotations in the Liouville space. For two such spin operators T_m and T_n, the orthonormality is expressed by

$$(T_m \,|\, T_n) = \mathrm{Tr}\,\{T_m^\dagger\, T_n\} = \delta_{mn} \tag{3.1.10}$$

The $(m+1)$-spin ISTOs are constructed by consecutive couplings of the set of orthonormal single-spin ISTOs for each spin. e.g.,

$$T_0^0(I) \;=\; \frac{1}{\sqrt{2}}\, E_I \;; \quad T_0^1(I) \;=\; \sqrt{2}\, I_z \;; \quad T_{\pm 1}^1(I) \;=\; \mp\, I_\pm \tag{3.1.11}$$

Here we give an example of constructing the ISTOs for a four-spin (IP_3) system, in which the three nonlabile spins are denoted as S, P, and U.

For a four-spin *ISPU* system, 255 ISTOs are needed to span the complete Liouville space. These ISTOs are denoted by $T_Q^K\left(\left[k_I k_S\left(\bar{K}\right) k_P\right]\{\bar{\bar{K}}\} k_U\right)$, constructed by three consecutive couplings of the set of four orthonormal single-spin ISTOs[71] $T_{q_I}^{k_I}(I)$, $T_{q_S}^{k_S}(S)$, $T_{q_P}^{k_P}(P)$, and $T_{q_U}^{k_U}(U)$ to obtain

$$\begin{aligned}
&T_Q^K\left(\left[k_I k_S\left(\bar{K}\right) k_P\right]\{\bar{\bar{K}}\} k_U\right) \\
&= (-1)^{k_I - k_S - k_P - k_U + \bar{K} + \bar{\bar{K}} + Q}\,(2K+1)^{1/2}(2\bar{K}+1)^{1/2}(2\bar{\bar{K}}+1)^{1/2} \\
&\times \sum_{\bar{Q}=-\bar{\bar{K}}}^{\bar{\bar{K}}} \sum_{\bar{Q}=-\bar{K}}^{\bar{K}} \sum_{q_I=-k_I}^{k_I} \begin{pmatrix} \bar{\bar{K}} & k_U & K \\ \bar{\bar{Q}} & Q-\bar{\bar{Q}} & -Q \end{pmatrix} \begin{pmatrix} \bar{K} & k_P & \bar{\bar{K}} \\ \bar{Q} & \bar{\bar{Q}}-\bar{Q} & -\bar{\bar{Q}} \end{pmatrix} \begin{pmatrix} k_I & k_S & \bar{K} \\ q_I & \bar{Q}-q_I & -\bar{Q} \end{pmatrix} \\
&\times\, T_{q_I}^{k_I}(I)\; T_{\bar{Q}-q_I}^{k_S}(S)\; T_{\bar{\bar{Q}}-\bar{Q}}^{k_P}(P)\; T_{Q-\bar{\bar{Q}}}^{k_U}(U)
\end{aligned} \tag{3.1.12}$$

where $\bar{K}$ is the rank of the intermediate tensor operator obtained by first coupling spins I and S, and $\bar{\bar{K}}$ is that by consecutively coupling spin P, and K is the total rank by further coupling spin U. $\bar{Q}$, $\bar{\bar{Q}}$, and Q are the corresponding projection quantum numbers, respectively. All the operators obtained from Eq. (3.1.12) are orthonormal in the same four-spin Liouville space in the sense

$$\begin{aligned}
&\left(T_Q^K\left(\left[k_I k_S\left(\bar{K}\right) k_P\right]\{\bar{\bar{K}}\} k_U\right) \,|\, T_{Q'}^{K'}\left(\left[k_I' k_S'\left(\bar{K}'\right) k_P'\right]\{\bar{\bar{K}}'\} k_U'\right)\right) \\
&= \delta_{KK'}\,\delta_{QQ'}\,\delta_{\bar{\bar{K}}\bar{\bar{K}}'}\,\delta_{\bar{K}\bar{K}'}\,\delta_{k_I k_I'}\,\delta_{k_S k_S'}\,\delta_{k_P k_P'}\delta_{k_U k_U'}
\end{aligned} \tag{3.1.13}$$

Composite Liouville space

For the spin system IP_m defined in section 2.1, the total spin density operator for the sample is the direct product of the spin density operators for the $N+1$ different sites

$$\sigma \;=\; \sigma^0 \otimes \sigma^1 \otimes \sigma^2 \otimes \cdots \otimes \sigma^N \tag{3.1.14}$$

where σ^α is the ensemble averaged spin density operator of sites α (here the σ^α is interpreted as the deviation from its equilibrium value). The $N+1$ sites can be expressed as a $(N+1)$-dimensional site operator space $\{|\,\alpha\,\rangle\}$. These basis site operators also satisfy the orthogonal relation $\langle\alpha|\beta\rangle = \delta_{\alpha\beta}$ and the completeness relation $\sum_\alpha |\alpha\rangle\langle\alpha| = 1$. In this representation σ^α can be formally written as

$$\sigma^\alpha \;=\; \langle\alpha|\sigma\rangle \tag{3.1.15}$$

Without exchange, the evolution of σ^α is given by Liouville-von Neumann equation[15,75]

$$\frac{\mathrm{d}}{\mathrm{d}t}\,\sigma^\alpha(t) \;=\; -\,i\,\mathcal{L}^\alpha\,\sigma^\alpha(t) \tag{3.1.16}$$

where $\mathcal{L}^\alpha$ is Liouvillian, a superoperator acting on the spin Liouville space (see details in section 3.1.2) which is defined as

$$\mathcal{L}^\alpha\,\sigma^\alpha(t) \;=\; [H^\alpha,\,\sigma^\alpha(t)] \tag{3.1.17}$$

where H^α is the spin Hamiltonian for site α.

In spin Liouville space, σ^α is expressed as a column vector of dimension $D_\alpha = 2^{2\,m_\alpha} - 1$, where m_α ($= m_\mathrm{A}$ or m_B) is number of spins-1/2 in site α and the -1 comes from omitting the superfluous identity operator. For example, for exchange case IP_3–I, there is one 1-spin system in state B ($\alpha = 0$), so $D_0 = 2^2 - 1 = 3$. In A-α site, there is a four-spin system so that $D_\alpha = 255$ ($\alpha \geqslant 1$). It is convenient to write the $N+1$ decoupled Liouville equations (3.1.16) in matrix form by constructing a composite (site + spin) Liouville space of dimension $D = D_\mathrm{B} + D_\mathrm{A}\,N$ and a composite spin density operator

$$\boldsymbol{\sigma} \;=\; \begin{bmatrix} \boldsymbol{\sigma}^0 \\ \boldsymbol{\sigma}^1 \\ \vdots \\ \boldsymbol{\sigma}^N \end{bmatrix} \qquad \text{where} \qquad \boldsymbol{\sigma}^\alpha \;=\; \begin{bmatrix} \sigma^\alpha_1 \\ \vdots \\ \sigma^\alpha_{D_\alpha} \end{bmatrix} \tag{3.1.18}$$

In this notation, the $N+1$ independent Liouville equation (3.1.16) can be expressed as

$$\frac{\mathrm{d}}{\mathrm{d}t}\,\boldsymbol{\sigma}(t) \;=\; -\,i\,\mathbf{L}\,\boldsymbol{\sigma}(t) \tag{3.1.19}$$

An element of the D-dimensional column vector $\boldsymbol{\sigma}$ can then be expressed in the following equivalent ways

$$\begin{aligned} \sigma^\alpha_{n_\alpha} \;&=\; (n_\alpha\,|\sigma^\alpha) \;=\{B^\dagger_{n_\alpha}\sigma_\alpha\} \;=\{B^\dagger_{n_\alpha}\langle\alpha|\sigma\rangle\} \\ &=\; \langle\alpha|\sigma_{n_\alpha}\rangle \;=\; \langle\alpha|(n_\alpha\,|\sigma)\rangle \;=\; \{\alpha, n_\alpha\,|\sigma\} \end{aligned} \tag{3.1.20}$$

where B_{n_α} is a member of spin basis operators defined in section 3.1.2. The Liouvillian $\mathbf{L}$ is block-diagonal in the composite space

$$\mathbf{L} \;=\; \begin{bmatrix} \mathbf{L}_0 & \mathbf{0} & \mathbf{0} & \cdots & \mathbf{0} \\ \mathbf{0} & \mathbf{L}_1 & \mathbf{0} & \cdots & \mathbf{0} \\ \mathbf{0} & \mathbf{0} & \mathbf{L}_2 & \cdots & \mathbf{0} \\ \vdots & \vdots & \vdots & \ddots & \vdots \\ \mathbf{0} & \mathbf{0} & \mathbf{0} & \cdots & \mathbf{L}_N \end{bmatrix} \tag{3.1.21}$$

where $\mathbf{L}_\alpha$ is a $D_\alpha \times D_\alpha$ matrix with elements $L^\alpha_{n_\alpha p_\alpha}$ and $\mathbf{0}$ is the $D_\alpha \times D_\beta$ null matrix.

Stochastic Liouville equation

If the exchange process is included, then the Liouvillian $\mathcal{L}^\alpha$ is time-dependent and Eq. (3.1.16) becomes

$$\frac{\mathrm{d}}{\mathrm{d}t}\,\sigma^\alpha(t) \;=\; -\,i\,\mathcal{L}^\alpha(t)\,\sigma^\alpha(t) \tag{3.1.22}$$

The random modulation of $\mathcal{L}^\alpha$ can be regarded as a stationary Markov process. According to Eq. (3.1.19), the composite spin density operator $\sigma(t)$ now becomes a function of the spin state and stochastic variable. In the composite Liouville space, the time evolution of the spin state follows Liouville-von Neumann equation (Eq. (3.1.16)), and the stochastic variable can be represented by a propagator $P(t)$, which follows a master equation[76]

$$\frac{\mathrm{d}}{\mathrm{d}t}\,P(t) \;=\; W\,P(t) \tag{3.1.23}$$

with the initial condition $P(0) = 1$. In site space, $\langle\,\alpha\,|P(t)\,|\,\beta\,\rangle$ represents the conditional probability of finding spin at site α at time t, given the spin was initially at site β. W is the stationary rate operator describing the exchange kinetics, which only acts on site space.

The composite spin density operator evolves according to the Stochastic Liouville equation (SLE)[77,78] obtained from Eqs. (3.1.19), (3.1.22) and (3.1.23)

$$\frac{\mathrm{d}}{\mathrm{d}t}\,\sigma(t) \;=\; (\mathcal{W} -\, i\,\mathcal{L})\;\sigma(t) \tag{3.1.24}$$

where the Liouvillian $\mathcal{L}$ is time-independent and its matrix representation is given by Eq. (3.1.21). $\mathcal{W}$ is the exchange superoperator describing the transfer of one or more spins from one site to another.

An exchange from site α to site β can have two distinct effects. One effect is to instantaneously change the spin Hamiltonian from H^α to H^β. If this stochastic modulation (of the dipole coupling) is sufficiently frequent, it produces relaxation. The other effect only occurs in asymmetric exchange cases, in which the spin systems are fragmented by the exchange (e.g. IP_m–I with $m \geqslant 1$). Then all multispin correlations within the spin system that have developed as a result of the dipole coupling with the exchanging spin(s) are lost.[79] In contrast, for symmetric exchange, where the whole spin system exchanges as an intact unit, then all multi-spin correlations are retained even though the couplings are modulated. Both of these effects can be described by the exchange superoperator $\mathcal{W}$

$$\mathcal{W} \;=\; \mathcal{T}_\mathrm{m} \otimes \mathcal{T}_\mathrm{s} \;-\; \mathcal{K}_\mathrm{m} \otimes \mathcal{K}_\mathrm{s} \tag{3.1.25}$$

The superoperators $\mathcal{T}_\mathrm{m}$ and $\mathcal{K}_\mathrm{m}$ act on site operators only, so their direct product matrix representations are block-diagonal with respect to the spin operators. These operators contain all the kinetic information (exchange rates or mean survival times). The superoperators $\mathcal{T}_\mathrm{s}$ and $\mathcal{K}_\mathrm{s}$ act on spin operators only, so (like $\mathcal{L}$ expressed in Eq. (3.1.21)) their direct product matrix representations are block-diagonal with respect to the site operators. These operators account for the decorrelation of multispin modes by exchange fragmentation of the spin system. (see section II - C in paper II for more details).

Formal solution of SLE in site space

The SLE (3.1.24) is a stochastic differential equation involving superoperators acting in the composite Liouville space. The EMOR model allows the exact analytical solution of SLE in site space, leaving the spin-dynamical problem in a finite-dimensional spin Liouville space. Here we

only present the essential results of the partial solutions for further discussion. More details can be found in section II-D in paper II. Full derivation of solution was also given in paper II, appendix B.

Eq. (3.1.24) can be converted to an algebraic equation by using Laplace transform (Eq. (2.2.7)) so that

$$\widetilde{\sigma}(s) \;=\; (s\,\mathcal{E} - \mathcal{W} + i\,\mathcal{L})^{-1}\,\sigma(0) \;=\; \widetilde{\mathcal{U}}(s)\,\sigma(0) \tag{3.1.26}$$

where $\mathcal{E}$ is the identity operator and $\widetilde{\mathcal{U}}(s)$ is referred to as resolvent superoperator.

Substituting Eqs. (2.2.1) – (2.2.3) and (3.1.25) into Eq. (3.1.26) we may obtain

$$\langle\widetilde{\sigma}(s)\rangle \;=\; \sum_{\alpha=0}^{N}\sum_{\beta=0}^{N}\langle\alpha|\,\widetilde{\mathcal{U}}(s)|\beta\rangle\,P_\beta\,\eta^\beta \tag{3.1.27}$$

where η^β equals η^{B} for $\beta = 0$ and η^{A} for $\beta \geq 1$ and P_β equals P_{B} for $\beta = 0$ and P_{A}/N for $\beta \geq 1$.

For asymmetric exchange case IP_m–I, where we need to use different spin operator bases for states B and A, it is convenient to express the spin operator basis representation of Eq. (3.1.26) in terms of partitioned matrices:

$$\begin{bmatrix} \widetilde{\boldsymbol{\sigma}}^{\mathrm{B}}(s) \\ \widetilde{\boldsymbol{\sigma}}^{\mathrm{A}}(s) \end{bmatrix} \;=\; \begin{bmatrix} \widetilde{\mathbf{U}}^{\mathrm{BB}}(s) & \widetilde{\mathbf{U}}^{\mathrm{BA}}(s) \\ \widetilde{\mathbf{U}}^{\mathrm{AB}}(s) & \widetilde{\mathbf{U}}^{\mathrm{AA}}(s) \end{bmatrix} \begin{bmatrix} \boldsymbol{\eta}^{\mathrm{B}} \\ \boldsymbol{\eta}^{\mathrm{A}} \end{bmatrix} \tag{3.1.28}$$

Here the site-averaged density operator column vector has been partitioned into

$$\widetilde{\boldsymbol{\sigma}}^{\mathrm{B}} \;=\; \begin{bmatrix} \widetilde{\sigma}_1^{\mathrm{B}}(s) \\ \vdots \\ \widetilde{\sigma}_{D_{\mathrm{B}}}^{\mathrm{B}}(s) \end{bmatrix} \quad \text{and} \quad \widetilde{\boldsymbol{\sigma}}^{\mathrm{A}} \;=\; \begin{bmatrix} \widetilde{\sigma}_1^{\mathrm{A}}(s) \\ \vdots \\ \widetilde{\sigma}_{D_{\mathrm{A}}}^{\mathrm{A}}(s) \end{bmatrix} \tag{3.1.29}$$

where $D_{\mathrm{B}} = 3$. Furthermore, $\boldsymbol{\eta}^{\mathrm{B}} = [\eta_1^{\mathrm{B}}\ \ldots\ \eta_{D_{\mathrm{B}}}^{\mathrm{B}}]^{\mathrm{T}}$ and $\boldsymbol{\eta}^{\mathrm{A}} = [\eta_1^{\mathrm{A}}\ \ldots\ \eta_{D_{\mathrm{A}}}^{\mathrm{A}}]^{\mathrm{T}}$. Finally, $\widetilde{\mathbf{U}}^{\mathrm{BB}}(s)$, $\widetilde{\mathbf{U}}^{\mathrm{BA}}(s)$, $\widetilde{\mathbf{U}}^{\mathrm{AB}}(s)$ and $\widetilde{\mathbf{U}}^{\mathrm{AA}}(s)$ are, respectively, (3×3), $(3 \times D_{\mathrm{A}})$, $(D_{\mathrm{A}} \times 3)$ and $(D_{\mathrm{A}} \times D_{\mathrm{A}})$ submatrices of the spin basis representation of the site-averaged spin superoperator

$$\langle\widetilde{\mathcal{U}}(s)\rangle \;=\; \sum_{\alpha=0}^{N}\sum_{\beta=0}^{N}\langle\alpha|\,\widetilde{\mathcal{U}}(s)|\beta\rangle\,P_\beta \tag{3.1.30}$$

with the explicit form

$$\widetilde{\mathbf{U}}^{\mathrm{BB}}(s) \;=\; \tau_{\mathrm{B}}\,P_{\mathrm{B}}\left[\mathbf{1}^{\mathrm{B}} - \mathbf{G}^{\mathrm{B}}(s)\,\mathbf{T}\,\mathbf{G}^{\mathrm{A}}(s)\,\mathbf{T}'\right]^{-1}\mathbf{G}^{\mathrm{B}}(s) \tag{3.1.31a}$$

$$\widetilde{\mathbf{U}}^{\mathrm{BA}}(s) \;=\; \tau_{\mathrm{B}}\,P_{\mathrm{A}}\left[\mathbf{1}^{\mathrm{B}} - \mathbf{G}^{\mathrm{B}}(s)\,\mathbf{T}\,\mathbf{G}^{\mathrm{A}}(s)\,\mathbf{T}'\right]^{-1}\mathbf{G}^{\mathrm{B}}(s)\,\mathbf{T}\,\mathbf{G}^{\mathrm{A}}(s) \tag{3.1.31b}$$

$$\widetilde{\mathbf{U}}^{\mathrm{AB}}(s) \;=\; \tau_{\mathrm{A}}\,P_{\mathrm{B}}\left[\mathbf{1}^{\mathrm{A}} - \mathbf{G}^{\mathrm{A}}(s)\,\mathbf{T}'\,\mathbf{G}^{\mathrm{B}}(s)\,\mathbf{T}\right]^{-1}\mathbf{G}^{\mathrm{A}}(s)\,\mathbf{T}'\,\mathbf{G}^{\mathrm{B}}(s) \tag{3.1.31c}$$

$$\widetilde{\mathbf{U}}^{\mathrm{AA}}(s) \;=\; \tau_{\mathrm{A}}\,P_{\mathrm{A}}\left[\mathbf{1}^{\mathrm{A}} - \mathbf{G}^{\mathrm{A}}(s)\,\mathbf{T}'\,\mathbf{G}^{\mathrm{B}}(s)\,\mathbf{T}\right]^{-1}\mathbf{G}^{\mathrm{A}}(s) \tag{3.1.31d}$$

where

$$\mathbf{G}^{\mathrm{B}}(s) \;=\; \left[(1 + s\tau_{\mathrm{B}})\,\mathbf{1}^{\mathrm{B}} \;+\; i\,\mathbf{L}_{\mathrm{B}}\,\tau_{\mathrm{B}}\right]^{-1} \tag{3.1.32}$$

and

$$\mathbf{G}^{\mathrm{A}}(s) \;=\; \frac{1}{8\pi^2}\int \mathrm{d}\Omega\,[s\,\tau_{\mathrm{A}}\,\mathbf{1}^{\mathrm{A}} \;+\; \mathbf{K} \;+\; i\,\mathbf{L}_{\mathrm{A}}(\Omega)\,\tau_{\mathrm{A}}]^{-1} \tag{3.1.33}$$

Here, $\mathbf{1}^{\mathrm{B}}$ and $\mathbf{1}^{\mathrm{A}}$ are the (3×3) and $(D_{\mathrm{A}}\times D_{\mathrm{A}})$ identity matrices; $\mathbf{T}$ and $\mathbf{K}$ are the $(3\times D_{\mathrm{A}})$ and $(D_{\mathrm{A}}\times D_{\mathrm{A}})$ matrices representing $\mathcal{T}_{\mathrm{s}}$ and $\mathcal{K}_{\mathrm{s}}$; $\mathbf{L}_{\mathrm{B}}$ and $\mathbf{L}_{\mathrm{A}}$ are the Liouvillian supermatrices corresponding to H_{B} and H_{A} (Eq. (3.1.1)), respectively. In the following, the matrix elements in Eq. (3.1.31) and (3.1.33) with $s=0$ will be abbreviated as

$$U_{np}^{\mathrm{XY}} \;\equiv\; (n|\widetilde{\mathbf{U}}^{\mathrm{XY}}(0)|p) \tag{3.1.34}$$

and

$$g_{np} \;\equiv\; (n|\mathbf{G}^{\mathrm{A}}(0)|p) \tag{3.1.35}$$

In the *dilute regime*, where $P_{\mathrm{A}}\ll 1$ and $P_{\mathrm{B}}\approx 1$, the detailed balance relation $P_{\mathrm{A}}\,\tau_{\mathrm{B}} = P_{\mathrm{B}}\,\tau_{\mathrm{A}}$ and Eq. (3.1.31) show that the matrix elements U_{np}^{XY} are of the following relative magnitudes

$$U_{np}^{\mathrm{BB}} \;\sim\; 1 \tag{3.1.36a}$$
$$U_{np}^{\mathrm{BA}} \;\sim\; P_{\mathrm{A}} \tag{3.1.36b}$$
$$U_{np}^{\mathrm{AB}} \;\sim\; P_{\mathrm{A}} \tag{3.1.36c}$$
$$U_{np}^{\mathrm{AA}} \;\sim\; P_{\mathrm{A}}^2 \tag{3.1.36d}$$

so that

$$\widetilde{\mathbf{U}}^{\mathrm{BB}}(0) \;=\; \frac{\tau_{\mathrm{A}}}{P_{\mathrm{A}}}\left[\mathbf{1} \;+\; i\,\mathbf{L}_{\mathrm{Z}}\,\tau_{\mathrm{B}} - \mathbf{T}\,\mathbf{G}^{\mathrm{A}}(0)\,\mathbf{T}'\right]^{-1} \tag{3.1.37}$$

Combination of Eqs. (2.2.4), (2.2.5), (3.1.28) – (3.1.37) yields the simple exact expression of ILRR for asymmetric exchange case IP_m–I

$$\widehat{R}_{1,I}^{\mathrm{dil}}(IP_m\text{–}I) \;=\; [U_{11}^{\mathrm{BB}}]^{-1} \;=\; \frac{P_{\mathrm{A}}}{\tau_{\mathrm{A}}}\,(1-g_{11}) \tag{3.1.38}$$

3.2 Stochastic Redfield approach

Stochastic Redfield equation

In the absence of exchange and in the RMN regime, where $\omega_{\mathrm{D}}\,\tau_{\mathrm{A}}\ll 1$, the Liouville-von Neumann equation (3.1.16) can be replaced by BWR master equation[15]

$$\frac{\mathrm{d}}{\mathrm{d}t}\,\widehat{\sigma}^{\alpha}(t) \;=\; -i\widehat{\Delta}^{\alpha}(t)\,\widehat{\sigma}^{\alpha}(t) - \int_0^{\infty}\mathrm{d}\tau\,\left\langle \widehat{\mathcal{L}}_{\mathrm{D}}^{\alpha}(t)\,\widehat{\mathcal{L}}_{\mathrm{D}}^{\alpha}(t-\tau)\right\rangle_{\alpha}\,\widehat{\sigma}^{\alpha}(t) \tag{3.2.1}$$

where the angular brackets with subscript α denote an equilibrium ensemble average over the molecular degrees of freedom in site α. The spin density operator in site α, $\sigma^{\alpha}(t)$ is expressed in interaction representation

$$\widehat{\sigma}^{\alpha}(t) \;=\; \exp(i\,H_{\mathrm{Z}}\,t)\,\sigma^{\alpha}(t)\,\exp(-i\,H_{\mathrm{Z}}\,t) \;=\; \exp(i\,\mathcal{L}_{\mathrm{Z}}\,t)\,\sigma^{\alpha}(t) \tag{3.2.2}$$

and similar for the dipolar Liouvillians corresponding to fluctuating dipole couplings

$$\widehat{\mathcal{L}}_{\mathrm{D}}^{\alpha}(t) = \exp(i\,\mathcal{L}_{\mathrm{Z}}\,t)\,\mathcal{L}_{\mathrm{D}}^{\alpha}(t)\,\exp(-i\,\mathcal{L}_{\mathrm{Z}}\,t) \tag{3.2.3}$$

and SDCs

$$\widehat{\Delta}^{\alpha}(t) = \exp(i\,\mathcal{L}_{\mathrm{Z}}\,t)\,\Delta^{\alpha}(t)\,\exp(-i\,\mathcal{L}_{\mathrm{Z}}\,t) \tag{3.2.4}$$

For a rigorous BWR treatment of asymmetric exchange cases, the transformation of $\sigma(t)$ or $\mathcal{L}_{\mathrm{D}}^{\alpha}(t)$ from Schrödinger representation to the interaction representation should involve the total static Liouvillian $\mathcal{L}_{\mathrm{Z}} + \Delta^{\alpha}(t)$. The first term in Eq. (3.2.1) would then be absent, but the following analytical development would be complicated by the fact that the ISTOs T_Q^K are only eigenoperators of $\mathcal{L}_{\mathrm{Z}}$, but not of the total static Liouvillian. To avoid this complication, the BWR theory for EMOR model was developed under RMN condition, $\omega_{\mathrm{D},I\mu}\,\tau_{\mathrm{A}} \ll 1$ and $\omega_{\mathrm{D},\mu\nu}\,\tau_{\mathrm{A}} \ll 1$ (μ and ν denote the nonlabile spins), and the spin density operator and dipolar Liouvillians were transformed to an intermediate interaction representation as in Eqs. (3.2.1) – (3.2.4).

Defining a relaxation superoperator $\mathcal{R}$

$$\mathcal{R}^{\alpha} \;\equiv\; \int_0^{\infty} \mathrm{d}\tau \,\big\langle \mathcal{L}_{\mathrm{D}}^{\alpha}(0)\, \widehat{\mathcal{L}}_{\mathrm{D}}^{\alpha}(-\tau) \big\rangle \tag{3.2.5}$$

which is block-diagonal in the composite space (like $\mathcal{L}$ expressed in Eq. (3.1.21)) and introducing the exchange superoperator $\mathcal{W}$ which is the same as in the SLE (3.1.25), we obtain the stochastic Redfield equation (SRE)

$$\frac{\mathrm{d}}{\mathrm{d}t}\,\sigma(t) \;=\; (\mathcal{W} - i\,\mathcal{L}_{\mathrm{Z}} - i\,\Delta - \mathcal{R})\,\sigma(t) \tag{3.2.6}$$

where $\sigma(t)$ is the composite spin density operator in Eq. (3.1.24). The relaxation supermatrix $\mathbf{R}^{\alpha}$ is given by

$$\mathbf{R}^{\alpha} \;=\; \frac{2}{3} \sum_X \sum_Y \omega_{\mathrm{D},X}\, \omega_{\mathrm{D},Y} \sum_{M=-2}^{2} \sum_{M'=-2}^{2} F_{MM'}(\Omega_X^{\alpha}, \Omega_Y^{\alpha})\, J(-M'\omega_0)\, \mathbf{C}_{MM'}^{XY} \tag{3.2.7}$$

where $F_{MM'}(\Omega_X^{\alpha}, \Omega_Y^{\alpha})$ is the angular function formed by a product of two Wigner functions. $J(-M'\omega_0)$ is the generalised spectral density function and its explicit form is given in section 3.2.4. $\mathbf{C}_{MM'}^{XY}$ is the coefficient matrix involving double commutators (explicit form is given in section 3.2.2). The coherent mode transfer supermatrix $\mathbf{\Delta}^{\alpha}$, which is present for the cases IP_m–I and ISP_m–IS if $m \geqslant 2$, is given by

$$\mathbf{\Delta}^{\alpha} \;=\; -\,\frac{2}{\sqrt{6}} \sum_X \omega_{\mathrm{D},X} \sum_{M=-2}^{2} D_{M0}^{2\,*}(\Omega_X^{\alpha})\, \mathbf{D}_M^X \tag{3.2.8}$$

where $\mathbf{D}_M^X$ is the coefficient matrix involving single commutator. In Eq. (3.2.7), X and Y refer to dipole couplings that involve at least one labile spin, so they are randomized by the exchange. In Eq. (3.2.8), X refers to SDCs between pairs of nonlabile spins.

In the EMOR model, exchange plays a dual role: it transfers magnetization between the A and B states and it induces relaxation in the A sites. In the SLE, both of these roles are played by the exchange superoperator $\mathcal{W}$. In the SRE approach, in contrast, the exchange enters the theory in two ways: (1) via the local (orientation-dependent) relaxation rate described by $\mathcal{R}^{\alpha}$, reflecting the effect of orientational randomization of dipole vectors in site α, and (2) via the exchange superoperator $\mathcal{W}$, describing the exchange-mediated transfer (or destruction) of localized (site-based) spin modes $\sigma_n^{\alpha}(t)$ between the A and B sites. This exchange also brings about isotropic averaging of the orientation-dependent local (site-specific) relaxation rate.

Symmetry and selection rules

As we mentioned in section 3.1.2 that various symmetries can be employed in the study of relaxation problems, which are only well defined in Liouville representation. Here we introduce three different symmetries that have been extensively used in the present work. We also briefly discuss how the selection rules deduced from these symmetries simplify the relaxation problem. In addition, we introduce another set of selection rules deduced from the evaluation of single and double commutators which appear in the static and relaxation superoperators.

Rotational symmetry

We first introduce the Wigner-Eckart theorem[71,72] which allows the quick determination of selection rules for the systems with rotational symmetry. Moreover, it also greatly simplifies the calculation of matrix elements of a tensor operator with respect to the basis operators.

We consider the matrix element of an ISTO T_q^k with rank k and projection quantum number q. Suppose the basis operators $|IM\rangle$ are the eigenoperators of I^2 and I_z, then both T_q^k and $|IM\rangle$ are transformed in the same rotation group. In this case, Wigner-Eckart theorem states that the matrix element of T_q^k in this eigenoperator basis can be factorised into two parts

$$\langle JN \,|\, T_q^k \,|\, IM \rangle = (-1)^{2k} \left\langle J \,||\, T^k \,||\, I \right\rangle \langle JN \,|\, IkMq \,\rangle \tag{3.2.9}$$

where $\left\langle J \,||\, T^k \,||\, I \right\rangle$ is called reduced matrix element which depends on the physical properties of spin systems. $\langle JN \,|\, IkMq \,\rangle$ is the Clebsch-Gordan coefficient which indicates the geometric dependence of the system on the spin quantum numbers. These coefficients can be expressed in terms of Wigner 3-j symbols

$$\langle JN \,|\, IkMq \,\rangle = (-1)^{N+q} \begin{pmatrix} I & J & k \\ -M & N & q \end{pmatrix} \tag{3.2.10}$$

and evaluated separately. From the properties of Wigner 3-j symbols and combining Eqs. (3.2.9) and (3.2.10), we obtain the selection rule that $\langle JN \,|\, T_q^k \,|\, IM \rangle = 0$ unless

$$M = q + N \tag{3.2.11}$$

and the triangle condition

$$|J - I| \leqslant k \leqslant |J + I| \tag{3.2.12}$$

is satisfied.

As stated in section 2.1, we assume that the number N of A sites is sufficiently large that the Euler angles Ω_α indicating the orientations of these N sites can be treated as a continuous variable Ω with a distribution function $f(\Omega)$. Furthermore, we assume that this distribution is isotropic

$$f(\Omega) = \frac{1}{8\,\pi^2} \tag{3.2.13}$$

Eq. (3.2.13) implies that any site-averaged superoperator derived from the Liouvillian $\mathcal{L}$, such as the resolvent superoperator $\langle \widetilde{\mathcal{U}}(s) \rangle$, must share the cylindrical symmetry of the B_0 field. Eq. (3.2.11) then implies that all such superoperators are block diagonal $Q = Q'$ in the ISTO representation. For example,

$$\left(T_Q^K \,|\, \langle \widetilde{\mathcal{U}}(s) \rangle \,|\, T_{Q'}^{K'} \right) = \delta_{QQ'} \left(T_Q^K \,|\, \langle \widetilde{\mathcal{U}}(s) \rangle \,|\, T_Q^{K'} \right) \tag{3.2.14}$$

In addition, if the external B_0 field is absent, then the macroscopic system is rotationally invari-

ant. Eqs. (3.2.11) and (3.2.12) then imply that the matrix elements of these superoperators are not only block-diagonal in projection number Q but also in rank K. For example,

$$\left(T_Q^K \,|\, \langle\widetilde{\mathcal{U}}(s)\rangle \,|\, T_{Q'}^{K'}\right) = \delta_{KK'}\delta_{QQ'}\left(T_Q^K \,|\, \langle\widetilde{\mathcal{U}}(s)\rangle \,|\, T_Q^K\right) \tag{3.2.15}$$

Selection rules (3.2.14) and (3.2.15) are valid in both SLE and SRE approaches.

Spin inversion conjugation symmetry

Here we consider the effect of spin inversion, spin conjugation, and spin inversion conjugation operations[69,73] on superoperators and operators, respectively.

The spin inversion superoperator acting on I-spin operators is defined as[69,73]

$$\mathcal{Y}_I \;\equiv\; \exp(i\,\pi\,\mathcal{I}_y) \tag{3.2.16}$$

with $\mathcal{I}_y = [I_y, ...]$, so that

$$\mathcal{Y}_I\, I_z = -I_z \tag{3.2.17a}$$
$$\mathcal{Y}_I\, I_+ = -I_- \tag{3.2.17b}$$
$$\mathcal{Y}_I\, I_- = -I_+ \tag{3.2.17c}$$

The spin conjugation superoperator is defined in terms of its action on the shift operators[69,73]

$$\mathcal{V}_I\,|Im\rangle\langle In| \;\equiv\; (|Im\rangle\langle In|)^\dagger \;=\; (|In\rangle\langle Im|) \tag{3.2.18}$$

so that

$$\mathcal{V}_I\, I_z = I_z \tag{3.2.19a}$$
$$\mathcal{V}_I\, I_+ = I_- \tag{3.2.19b}$$
$$\mathcal{V}_I\, I_- = I_+ \tag{3.2.19c}$$

Now the spin inversion conjugation (SIC) operation is simply the combination of the first two operations $\mathcal{W} = \mathcal{V}\mathcal{Y}$,[69,73] and

$$\mathcal{W}_I\, I_z = -I_z \tag{3.2.20a}$$
$$\mathcal{W}_I\, I_+ = -I_+ \tag{3.2.20b}$$
$$\mathcal{W}_I\, I_- = -I_- \tag{3.2.20c}$$

The transformations of the relaxation superoperator $\mathcal{R}$ under these three operations are

$$\mathcal{Y}\,\mathcal{R}\,\mathcal{Y} = \mathcal{R}^\dagger \tag{3.2.21a}$$
$$\mathcal{V}\,\mathcal{R}\,\mathcal{V} = \mathcal{R}^\dagger \tag{3.2.21b}$$
$$\mathcal{W}\,\mathcal{R}\,\mathcal{W} = \mathcal{R} \tag{3.2.21c}$$

From Eq. (3.2.21c) we see that $\mathcal{R}$ is invariant under SIC operation. Moreover, the transformation of basis ISTOs under SIC operation is

$$\mathcal{W}\,T_Q^K \;=\; (-1)^{N_\mathrm{s}}\,T_Q^K \tag{3.2.22}$$

where $N_\mathrm{s} = \sum_{i=1}^{m_\mathrm{A}} k_i$ is the number of single-spin operators (not counting identity operators) involved in the basis operator.

According to the basic orthogonality theorem of group theory, the matrix representation of $\mathcal{R}$ in the ISTO basis can have nonzero elements only between basis operators of the same parity (that is, belonging to the same irreducible representation of symmetry group).[80] The longitudinal spin modes have the odd parity under SIC operations (OSIC). Consequently, relaxation superoperator $\mathcal{R}$ can have nonzero matrix elements only between OSIC basis operators.

Nuclear permutation symmetry

In the SRE approach, nuclear permutation symmetry refers to the spectral density functions.[69,73] For the isochronous multi-spin system, the relaxation superoperator $\mathcal{R}$ is invariant under permutation (or interchange) of two nuclei if these nuclei are related by a symmetry operation of the molecular point group (geometric symmetry) and if the dipole couplings between each of these nuclei and any other nucleus are modulated in the same way by the molecular motion (dynamic symmetry). These two requirements can be concisely expressed in terms of the spectral density functions (SDFs). For example, in ISP_m–IS case, we consider a SDF $J_{XY}(\omega)$ where X and Y denote two dipole couplings shared by one common spin. Then $\mathcal{R}$ is invariant under $I \leftrightarrow S$ interchange if $J_{IP_i,IP_i}(\omega) = J_{SP_i,SP_i}(\omega)$ and $J_{IS,IP_i}(\omega) = J_{IS,SP_i}(\omega)$.

If the relaxation is induced by isotropic motion, such as spherical-top rotational diffusion, all dipole couplings are modulated in the same way (full dynamic symmetry). Now the geometric equivalence implies nuclear permutation symmetry. This symmetry could be quite useful in some special cases. For example, for a three-spin system in which three spin reside at the vertices of an equilateral triangle (referred to as A_3 system), the relaxation behaviour of this model system can be fully described within the small liouville space spanned by only three symmetry-adapt basis operators.[81] More applications of nuclear permutation symmetry can be found in paper V.

In the EMOR model, all labile spins are affected in the same way since all dipole couplings involving labile spins are randomized in orientation by exchange. Nuclear permutation symmetry is evident also in ILRR (for both SLE and SRE) which is solely determined by the internuclear geometry. Consequently, the ILRR is invariant under any permutation of the observed labile spins. Similar conclusions can be drawn for nonlabile spins, e.g. the ILRR for a specific labile spin is invariant under any permutation of the nonlabile spins.

Additional selection rules

As seen from Eq. (3.2.7) and (3.2.8) that evaluation of $\mathbf{R}^\alpha$ and $\mathbf{\Delta}^\alpha$ involves calculating the real-valued elements for the two coefficient matrices

$$C^{XY}_{MM',np} = \left\{ \left[B_n^\dagger,\, T^2_M(X) \right] \left[T^2_{M'}(Y),\, B_p \right] \right\} \tag{3.2.23}$$

$$D^X_{M,np} = \left\{ B_n^\dagger \left[T^2_M(X),\, B_p \right] \right\} = \left\{ \left[B_n^\dagger,\, T^2_M(X) \right] B_p \right\} \tag{3.2.24}$$

where the last step follows from the cyclic permutation invariance of the trace. The ISTOs $T^2_M(X)$ are taken to be normalised in the two-spin Liouville space corresponding to the two spins involved in the dipole coupling X. The basis operators B_n are normalised in the multi-spin Liouville space as expressed in Eq. (3.1.10).

Several additional selection rules are derived from Eqs. (3.2.23) and (3.2.24) by making use of two general results. First, because two operators associated with different spins (such as I_z and S_+) necessarily commute, it follows that the commutator of two operators, each of which is a product of single-spin operators associated with distinct spins, vanishes if the two product operators have no spin in common. Second, since $\mathrm{Tr}_I\{I_z\} = \mathrm{Tr}_I\{I_+\} = \mathrm{Tr}_I\{I_-\} = 0$, it follows that the multi-spin trace of a product operator vanishes if the product operator contains at

least one lone operator, that is, if any spin occurs only once in the product operator. These selection rules are presented in details in paper IV, which play important role in simplifying the development of the multi-spin SRE theory.

Framework of multi-spin SRE theory

For the EMOR model, the SRE (3.2.6) can be solved in site space in the same manner as the SLE (3.1.24). Specifically, Eqs. (3.1.28)–(3.1.37) remain valid, but Eq. (3.1.33) is replaced by

$$\mathbf{G}^{\mathrm{A}}(s) \;=\; \frac{1}{8\pi^2}\int \mathrm{d}\Omega\,[s\,\tau_{\mathrm{A}}\,\mathbf{1}^{\mathrm{A}} \;+\; \mathbf{K} \;+\; i\,\mathbf{L}_{\mathrm{Z}}^{\mathrm{A}}\,\tau_{\mathrm{A}} \;+\; i\,\boldsymbol{\Delta}^{\alpha}\,\tau_{\mathrm{A}} \;+\; \mathbf{R}^{\alpha}\,\tau_{\mathrm{A}}]^{-1} \tag{3.2.25}$$

where $\mathbf{R}^{\alpha}$ is the orientation-dependent relaxation supermatrix for site α. We may rewrite Eq. (3.2.25) (setting $s = 0$) as

$$\mathbf{G}^{\mathrm{A}}(0) \;=\; \left\langle (\boldsymbol{\Lambda}^{\alpha})^{-1} \right\rangle \tag{3.2.26}$$

where the angular brackets indicate an isotropic orientation average shown in Eq. (3.2.23). The supermatrix $\boldsymbol{\Lambda}^{\alpha}$ associated with a particular site α is

$$\boldsymbol{\Lambda}^{\alpha} \;=\; \mathbf{K} + \mathbf{R}^{\alpha}\,\tau_{\mathrm{A}} + i\,\boldsymbol{\Delta}^{\alpha}\,\tau_{\mathrm{A}} + i\,\mathbf{L}_{\mathrm{Z}}\,\tau_{\mathrm{A}} \tag{3.2.27}$$

Just as in SLE theory, the dimension of the supermatrix $\boldsymbol{\Lambda}^{\alpha}$ is $(4^{m_{\mathrm{A}}} - 1)$, which is prohibitively large for realistic spin systems. However, by using the SIC symmetry of $\mathbf{R}^{\alpha}$ and $\boldsymbol{\Delta}^{\alpha}$, as well as the symmetry rules derived from Eqs. (3.2.23) and (3.2.24), the SRE theory can be greatly simplified.

If the multi-spin ISTO basis for state A is ordered with the odd-parity operators before the even-parity operators, the relaxation supermatrix $\mathbf{R}^{\alpha}$ is block-diagonal whereas the SDC supermatrix $\boldsymbol{\Delta}^{\alpha}$ is anti-block-diagonal. Furthermore, $\mathbf{K}$ and $\mathbf{L}_{\mathrm{Z}}$ (for isochronous spins) are diagonal. We can therefore partition $\boldsymbol{\Lambda}^{\alpha}$ in Eq. (3.2.27) into blocks associated with the anti-symmetric ($\mathbb{A}$) and symmetric ($\mathbb{S}$) subspaces:

$$\boldsymbol{\Lambda}^{\alpha} \;=\; \begin{bmatrix} (\mathbf{K}_{\mathbb{A}\mathbb{A}} + \mathbf{R}^{\alpha}_{\mathbb{A}\mathbb{A}}\,\tau_{\mathrm{A}} + i\,\mathbf{L}_{\mathrm{Z},\,\mathbb{A}\mathbb{A}}\,\tau_{\mathrm{A}}) & i\,\boldsymbol{\Delta}^{\alpha}_{\mathbb{A}\mathbb{S}}\,\tau_{\mathrm{A}} \\ i\,\boldsymbol{\Delta}^{\alpha}_{\mathbb{S}\mathbb{A}}\,\tau_{\mathrm{A}} & (\mathbf{K}_{\mathbb{S}\mathbb{S}} + \mathbf{R}^{\alpha}_{\mathbb{S}\mathbb{S}}\,\tau_{\mathrm{A}} + i\,\mathbf{L}_{\mathrm{Z},\,\mathbb{S}\mathbb{S}}\,\tau_{\mathrm{A}}) \end{bmatrix} \tag{3.2.28}$$

To calculate the ILRR from Eq. (3.1.38), we only need matrix elements from the $\mathbb{A}\mathbb{A}$ block of the inverse $(\boldsymbol{\Lambda}^{\alpha})^{-1}$, which is

$$(\boldsymbol{\Lambda}^{\alpha})^{-1}_{\mathbb{A}\mathbb{A}} \;=\; [\mathbf{K}_{\mathbb{A}\mathbb{A}} + (\mathbf{R}^{\alpha}_{\mathbb{A}\mathbb{A}} + \mathbf{X}^{\alpha}_{\mathbb{A}\mathbb{A}} + i\,\mathbf{L}_{\mathrm{Z},\,\mathbb{A}\mathbb{A}})\,\tau_{\mathrm{A}}]^{-1} \tag{3.2.29}$$

with

$$\mathbf{X}^{\alpha}_{\mathbb{A}\mathbb{A}} \;\equiv\; \boldsymbol{\Delta}^{\alpha}_{\mathbb{A}\mathbb{S}}\,(\mathbf{K}_{\mathbb{S}\mathbb{S}}/\tau_{\mathrm{A}} + \mathbf{R}^{\alpha}_{\mathbb{S}\mathbb{S}} + i\,\mathbf{L}_{\mathrm{Z},\,\mathbb{S}\mathbb{S}})^{-1}\boldsymbol{\Delta}^{\alpha}_{\mathbb{S}\mathbb{A}} \tag{3.2.30}$$

By further decomposing the anti-symmetric subspace and implementing the RMN approximation, we may obtain

$$\mathbf{G}^{\mathrm{A}}_{\mathbb{L}\mathbb{Z},\mathbb{L}\mathbb{Z}}(0) \;=\; \mathbf{1} \;-\; \left\langle \mathbf{R}^{\alpha}_{\mathbb{L}\mathbb{Z},\mathbb{L}\mathbb{Z}} \right\rangle \tau_{\mathrm{A}} \;+\; \left\langle \boldsymbol{\Gamma}^{\alpha}_{\mathbb{L}\mathbb{Z},\mathbb{L}\mathbb{Z}} \right\rangle \tau_{\mathrm{A}} \tag{3.2.31}$$

where

$$\boldsymbol{\Gamma}^{\alpha}_{\mathbb{L}\mathbb{Z},\mathbb{L}\mathbb{Z}} \;=\; \mathbf{R}^{\alpha}_{\mathbb{L}\mathbb{Z},\mathbb{N}_1}\left(\mathbf{R}^{\alpha}_{\mathbb{N}_1\mathbb{N}_1} + \mathbf{W}^{\alpha}_{\mathbb{N}_1\mathbb{N}_1} + i\,\mathbf{L}_{\mathrm{Z},\,\mathbb{N}_1\mathbb{N}_1}\right)^{-1}\mathbf{R}^{\alpha}_{\mathbb{N}_1,\mathbb{L}\mathbb{Z}} \tag{3.2.32}$$

with

$$\mathbf{W}^{\alpha}_{\mathbb{N}_1\mathbb{N}_1} \;\equiv\; \mathbf{X}^{\alpha}_{\mathbb{N}_1\mathbb{N}_1} - \mathbf{Y}^{\alpha}_{\mathbb{N}_1\mathbb{N}_1} \tag{3.2.33}$$

Here, $\mathbb{L}\mathbb{Z}$ denotes one- or two-dimensional subspace spanned by basis operators proportional to I_z or S_z, and $\mathbb{N}_1$ denotes the subspace spanned by single-spin basis operators involving only nonlabile spins, respectively. The supermatrix $\mathbf{W}^{\alpha}_{\mathbb{N}_1\mathbb{N}_1}$ describes coherent transfer among single-spin modes associated with different nonlabile spins. This transfer proceeds via two-spin modes

(described by $\mathbf{X}^{\alpha}_{\mathbb{N}_1\mathbb{N}_1}$) and three-spin and higher (up to m-spin) modes (described by $\mathbf{Y}^{\alpha}_{\mathbb{N}_1\mathbb{N}_1}$), which simultaneously undergo relaxation induced by the fluctuating dipole couplings between the associated nonlabile spins and the labile spin(s). Explicit expressions of the supermatrices appearing in Eqs. (3.2.31) – (3.2.33) are presented in paper IV.

Developing exact multi-spin SRE theory which includes all spin modes is unattainable for the spin systems with large m. Fortunately, the mathematical structure of the multi-spin SRE theory allows us to systematically construct approximate theories by neglecting high-order spin modes (or basis operators). Specifically, we have developed the three-spin mode (3SM) approximation to SRE theory, which includes single-spin, two-spin and three-spin modes, but neglects four-spin and higher modes. The SRE-3SM theory is exact (in the RMN regime) for exchange cases comprising four or fewer spins, including $IP_3{-}I$ and $ISP_2{-}IS$, and it can be expressed fully in terms of the generic matrix elements needed for these four-spin cases.

Generalisations in GSRE theory

The validity of the SRE-3SM theory can be extended beyond the RMN regime by introducing three generalisations. For the $IP_m{-}I$ ($m \geqslant 3$) case, we first replace all spectral density functions (SDFs) in SRE-3SM theory by the generalised form (GSDF)

$$\widehat{J}(n\,\omega_0) \;=\; \frac{\tau_{\mathrm{A}}}{1 \;+\; \zeta_I\,(\omega_{\mathrm{D},I}\,\tau_{\mathrm{A}})^2 \;+\; (n\,\omega_0\,\tau_{\mathrm{A}})^2} \tag{3.2.34}$$

where $\omega_{\mathrm{D},I}$ is the effective fluctuating dipole coupling

$$\omega_{\mathrm{D},I} \;=\; \left[\sum_{\mu=1}^{m} \omega_{\mathrm{D},I\mu}^2\right]^{1/2} \tag{3.2.35}$$

and the coefficient ζ_I is

$$\zeta_I \;\equiv\; \left[\frac{10 + \omega_{\mathrm{D},I}\,\tau_{\mathrm{A}}}{4 + \omega_{\mathrm{D},I}\,\tau_{\mathrm{A}}}\right]\frac{2}{15} \tag{3.2.36}$$

obtained from minimising the deviation between the exact $\widehat{R}^{\mathrm{dil}}_{1,I}(0)$ computed from the SLE theory for $m = 3$ without static dipole couplings (SDCs) and the $\widehat{R}^{\mathrm{dil}}_{1,I}(0)$ computed from the GSRE theory.

Second, we implement a modification to the frequency term $\omega_0\,\mathbf{Q}_1$ appearing in the explicit form of $\mathbf{\Gamma}^{\alpha}_{\mathbb{LZ},\mathbb{LZ}}$ in Eq. (3.2.32) which gives rise to an artificial inverted relaxation step in the GSRE profiles even outside the RMN regime. Such modification is referred to as suppression of nonsecular decoupling (SND), consisting of the substitution

$$\omega_0 \;\rightarrow\; \widehat{\omega}_0 \;\equiv\; \frac{\omega_0}{(1 + 2\,\omega_{\mathrm{D},I}\,\tau_{\mathrm{A}})} \tag{3.2.37}$$

which eliminates the spurious feature in the GSRE profiles that is not present in the exact SLE results.

Finally, each individual SDC $\omega_{\mathrm{D},\mu\nu}$ appearing in the coherent mode transfer matrix Eq. (3.2.33) is replaced by the corresponding renormalized SDC

$$\widehat{\omega}_{\mathrm{D},\mu\nu} \;\equiv\; \frac{\omega_{\mathrm{D},\mu\nu}}{(1 + c\,\omega_{\mathrm{D},\mu\nu}\,\tau_{\mathrm{A}})^2} \tag{3.2.38}$$

where the numerical factor $c = 4/3$ resulted from a rough optimization.

The generalisations in the SRE-3SM theory for the $ISP_m{-}IS$ ($m \geqslant 2$) case is pretty similar as that for $IP_m{-}I$ ($m \geqslant 3$) case, which only slightly modifies the GSDF and SND.

Chapter 4

Results

In this chapter, we briefly discuss and summarise the results presented in appended five papers. The equations and figures referred to in these papers are denoted by prefixes I – V.

4.1 Paper I: Two-spin symmetric exchange case

In this paper, we studied the longitudinal relaxation of a dipole-dipole coupled spin-1/2 pair (denoted I and S, repectively) induced by EMOR mechanism. This two-spin symmetric exchange case (*IS–IS*) is treated by using SLE approach and the gyromagnetic ratios (γ) for the two spins are allowed to be different.

The two spins I and S are referred to as "like spins" if the difference of their Larmor frequencies satisfies the inequality (Eq. I–2.6)

$$[(\omega_I - \omega_S)\,\tau_{\rm A}]^2 \;\ll\; 1 + (\omega_{\rm D}\,\tau_{\rm A})^2 \tag{4.1.1}$$

where $\tau_{\rm A}$ is the mean survival time of the spin pair in an A site. The like-spin case applies to homonuclear ($\gamma_I = \gamma_S$) spin pairs, in particular when both I and S are proton spins. If the inequality (4.1.1) is not satisfied, we refer to the spins as "unlike". In practice, this case applies to all heteronuclear ($\gamma_I \neq \gamma_S$) spin pairs.

For the unlike spins, if the spin pair was excited selectively when only the observed I spin has a nonzero nonequilibrium longitudinal magnetization at $t = 0$, the ILRR is given by (Eq. I–4.2)

$$\widehat{R}_1^{\rm US} \;=\; \frac{1}{(1\,|\langle\widetilde{\mathcal{U}}(0)\rangle|\,1)} \tag{4.1.2}$$

where the superscript US refers to unlike spins and selective excitation. If the spin pair was excited non-selectively which applies generally to field-cycling experiments with the initial nonequilibrium state prepared by rapidly changing the magnitude of the $\boldsymbol{B}_0$ field, the ILRR is (Eq. I–4.4)

$$\widehat{R}_1^{\rm UN} \;=\; \frac{1}{(1\,|\langle\widetilde{\mathcal{U}}(0)\rangle|\,1) \;+\; \kappa\,(1\,|\langle\widetilde{\mathcal{U}}(0)\rangle|\,2)} \tag{4.1.3}$$

where $\kappa \equiv \gamma_S/\gamma_I$. The labels 1 and 2 in these two expressions represent the longitudinal magnetization of spin I and S, respectively.

For the two-spin system, the ILRR in Eq. (4.1.2) and (4.1.3) can be obtained numerically with modest computational effort. To gain conceptual insight, we also derived analytical results for these two expressions in the dilute regime ($P_{\rm A} \ll 1$), which are exact in both the LF and MN

limits (Eqs. (I–4.12) and (I–4.13))

$$\widehat{R}_1^{\mathrm{US}} \;=\; \rho_I \;-\; \frac{\sigma_{IS}\,\sigma_{SI}}{\rho_S} \tag{4.1.4}$$

$$\widehat{R}_1^{\mathrm{UN}} \;=\; \frac{\rho_I\,\rho_S \;-\; \sigma_{IS}\,\sigma_{SI}}{\rho_S \;-\; \kappa\,\sigma_{IS}} \tag{4.1.5}$$

where ρ and σ are generalised auto- and cross-relaxation rates expressed on the following simple analytical forms (Eqs. (I–4.14) and (I–4.15))

$$\begin{aligned}\rho_I \;=\; P_{\mathrm{A}}\,\chi_{\mathrm{D}}^2 \Bigg\{ & \frac{0.1\,\tau_{\mathrm{A}}}{1+(\omega_{\mathrm{D}}\tau_{\mathrm{A}})^2\,\eta_D/3+\left[(\omega_{\mathrm{I}}-\omega_{\mathrm{S}})\tau_{\mathrm{A}}\right]^2} \;+\; \frac{0.15\,\tau_{\mathrm{A}}}{1+(\omega_{\mathrm{D}}\tau_{\mathrm{A}})^2\,\eta_D/3+(\omega_{\mathrm{I}}\tau_{\mathrm{A}})^2} \\ & +\; \frac{0.15\,\tau_{\mathrm{A}}}{1+(\omega_{\mathrm{D}}\tau_{\mathrm{A}})^2+(\omega_{\mathrm{I}}\,\tau_{\mathrm{A}})^2} \;+\; \frac{0.6\,\tau_{\mathrm{A}}}{1+(\omega_{\mathrm{D}}\tau_{\mathrm{A}})^2+\left[(\omega_{\mathrm{I}}+\omega_{\mathrm{S}})\,\tau_{\mathrm{A}}\right]^2}\Bigg\}\end{aligned} \tag{4.1.6}$$

$$\begin{aligned}\sigma_{IS} \;=\; P_{\mathrm{A}}\,\chi_{\mathrm{D}}^2 \Bigg\{ & -\frac{0.1\,\tau_{\mathrm{A}}}{1+(\omega_{\mathrm{D}}\tau_{\mathrm{A}})^2\,\eta_D/3+\left[(\omega_{\mathrm{I}}-\omega_{\mathrm{S}})\tau_{\mathrm{A}}\right]^2} \;-\; \frac{0.15\,\tau_{\mathrm{A}}}{1+(\omega_{\mathrm{D}}\tau_{\mathrm{A}})^2\,\eta_D/3+(\omega_{\mathrm{I}}\tau_{\mathrm{A}})^2} \\ & +\; \frac{0.15\,\tau_{\mathrm{A}}}{1+(\omega_{\mathrm{D}}\tau_{\mathrm{A}})^2+(\omega_{\mathrm{I}}\,\tau_{\mathrm{A}})^2} \;+\; \frac{0.6\,\tau_{\mathrm{A}}}{1+(\omega_{\mathrm{D}}\tau_{\mathrm{A}})^2+\left[(\omega_{\mathrm{I}}+\omega_{\mathrm{S}})\tau_{\mathrm{A}}\right]^2}\Bigg\}\end{aligned} \tag{4.1.7}$$

where (Eqs. (I–4.16) and (I–2.4))

$$\eta_D \;\equiv\; \frac{1+(\chi_{\mathrm{D}}\tau_{\mathrm{A}})^2/3}{1+(\chi_{\mathrm{D}}\tau_{\mathrm{A}})^2/2} \tag{4.1.8}$$

$$\chi_{\mathrm{D}} \;\equiv\; \frac{2}{3}\,\omega_{\mathrm{D}} \tag{4.1.9}$$

The rates ρ_S and σ_{SI} are obtained by interchanging ω_I and ω_S everywhere in Eqs. (4.1.6) and (4.1.7).

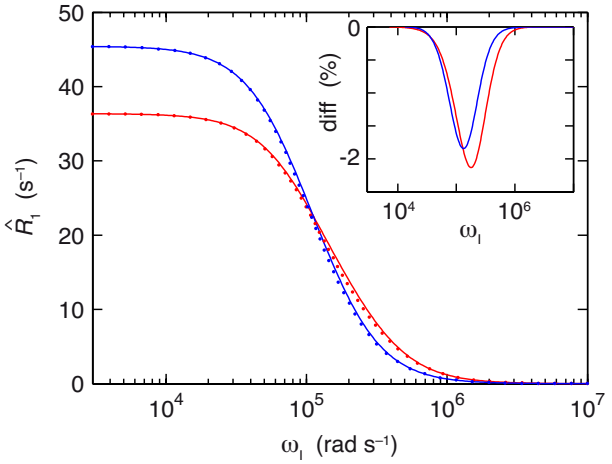

Figure 4.1: Dispersion of the unlike-spin integral relaxation rates $\widehat{R}_1^{\mathrm{US}}$ (red) and $\widehat{R}_1^{\mathrm{UN}}$ (blue), computed exactly (solid curves) and in the dilute approximation (dots) for $P_{\mathrm{A}} = 10^{-2}$, $\tau_{\mathrm{A}} = 10$ µs, $\chi_{\mathrm{D}} = 10^5$ rad s^{-1} and $\kappa = 0.9412$ (as for a ^{1}H–^{19}F spin pair). The inset shows the relative error of the dilute approximation, defined as $[R_1^{\mathrm{dilute}}(\omega_I) - R_1^{\mathrm{exact}}(\omega_I)]/R_1^{\mathrm{exact}}(0)$.

Fig. 4.1 (I–2) compares the approximate analytical rates given by Eqs. (4.1.4) – (4.1.9) with that given by Eqs. (4.1.2) and (4.1.3) in dilute regime ($P_{\mathrm{A}} = 10^{-3}$). The approximate analytical

rates coincide with the exact rates at the high-frequency end of the dispersion, where the MN condition is satisfied, and also at the low-frequency end, where the LF condition is satisfied. Even at intermediate frequencies, where neither condition is satisfied, the analytical expressions remain quite accurate.

For the like-spin case, we mainly consider the nonselective excitation which applies generally to field-cycling experiments, the integral longitudinal relaxation rate of the total magnetization of the spin pair is (Eq. (I–5.1))

$$\begin{aligned} \widehat{R}_1 &= \frac{2}{(1\,|\langle\widetilde{\mathcal{U}}(0)\rangle|\,1) + (1\,|\langle\widetilde{\mathcal{U}}(0)\rangle|\,2) + (2\,|\langle\widetilde{\mathcal{U}}(0)\rangle|\,1) + (2\,|\langle\widetilde{\mathcal{U}}(0)\rangle|\,2)} \\ &= \frac{1}{(1\,|\langle\widetilde{\mathcal{U}}(0)\rangle|\,1) + (1\,|\langle\widetilde{\mathcal{U}}(0)\rangle|\,2)} \end{aligned} \tag{4.1.10}$$

which indicates $\widehat{R}_1$ is the same irrespective of whether one observes both spins or only spin I. In the dilute regime, the analytical approximation of ILRR is $\widehat{R}_1 = \rho + \sigma$ where ρ and σ are taken from Eqs. (4.1.6) and (4.1.7) with $\omega_I = \omega_S$ (Eq. (I–5.2))

$$\widehat{R}_1 = \frac{3}{2} P_{\mathrm{A}}\, \chi_{\mathrm{D}}^2\, (0.2\, J_1 + 0.8\, J_2) \tag{4.1.11}$$

with the generalized spectral density (Eq. (I–5.3))

$$J_n \equiv \frac{\tau_{\mathrm{A}}}{1 + (\omega_{\mathrm{D}}\,\tau_{\mathrm{A}})^2 + (n\,\omega_I\,\tau_{\mathrm{A}})^2} \tag{4.1.12}$$

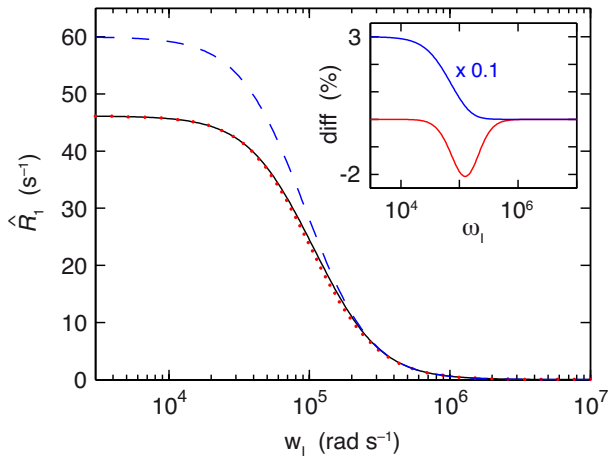

Figure 4.2: Dispersion of the like-spin integral relaxation rate $\widehat{R}_1$ in the dilute regime, computed numerically (black solid curve), from the analytical approximation (red dots) and from the nonrigorous approximation[50] (blue dashed) for $P_{\mathrm{A}} = 10^{-3}$, $\tau_{\mathrm{A}} = 10$ µs and $\chi_{\mathrm{D}} = 10^5$ rad s^{-1}. The inset shows the relative error of the approximations, defined as $[R_1^{\mathrm{approx}}(\omega_I) - R_1^{\mathrm{exact}}(\omega_I)]/R_1^{\mathrm{exact}}(0)$. For the nonrigorous approximation (blue curve), the error has been divided by a factor 10.

Fig. 4.2 (I–6) compares the approximate analytical rate given by Eqs. (4.1.11) and (4.1.12) with that given by Eqs. (4.1.10). Similarly, the analytical approximations agree with the exact results both in the MN and LF limits. At intermediate frequencies, the analytical expressions remain quite accurate with a maximum error of ~ -2 %. Figure 4.2 also shows the relaxation dispersion profile predicted by the nonrigorous analytical expression given in ref. 50. Here, the error is much larger, reaching 30 % at low frequencies. The maximum error in $\widehat{R}_1$ varies from

0.7 % to 50 % when τ_{A} increases from 1 to 100 μs at $\chi_{\mathrm{D}} = 10^5$ rad s^{-1}.

In this paper, we also demonstrated the quantitative breakdown of the previously used non-rigorous extension of the Solomon equations outside the MN regime. Moreover, the basic EMOR model was generalised by including the effects of fast internal motions in the macromolecular and solvent phases as well as the effect of kinetic heterogeneity. Please note that in this paper we did not realise the effect of fragmentation of the spin system in asymmetric exchange cases, so we argued that *IS–I* case has the same effect as *IS–IS*. This error has been corrected in paper II.

4.2 Paper II: Two-spin asymmetric exchange case

In this paper, we presented the general framework of the dipolar EMOR theory, which is illustrated by a detailed analysis of the asymmetric two-spin case (*IS–I*). For the *IS–I* case, we calculated ILRR in the dilute regime and the corresponding expression for the exchanging spin I is given by Eqs. (3.1.38). Unlike the *IS–IS* case treated in paper I, the LF and zero-field (ZF) regimes are distinct in asymmetric exchange cases.

In the MN regime, according to SIC symmetry described in section 3.2 that the relaxation superoperator $\mathcal{R}$ only has nonzero elements between six OSIC basis operators, which are ordered as $\{I_z,\, S_z,\, I_+,\, S_+,\, I_-,\, S_-\}$. Without exchange, the BWR master equation (3.2.1) can be written in interaction representation as (Eq. (II–E. 27))

$$\frac{\mathrm{d}}{\mathrm{d}t}\begin{bmatrix} I_z^\alpha(t) \\ S_z^\alpha(t) \\ \widehat{I}_+^\alpha(t) \\ \widehat{S}_+^\alpha(t) \\ \widehat{I}_-^\alpha(t) \\ \widehat{S}_-^\alpha(t) \end{bmatrix} = -\widehat{\mathbf{R}}^\alpha(t)\begin{bmatrix} I_z^\alpha(t) \\ S_z^\alpha(t) \\ \widehat{I}_+^\alpha(t) \\ \widehat{S}_+^\alpha(t) \\ \widehat{I}_-^\alpha(t) \\ \widehat{S}_-^\alpha(t) \end{bmatrix} \tag{4.2.1}$$

where, for clarity, we have represented the six spin density operator elements by the corresponding basis operators. The time-dependent relaxation supermatrix is (Eq. (II–E. 28))

$$\widehat{\mathbf{R}}^\alpha(t) = \begin{bmatrix} R_{zz}^{II} & R_{zz}^{IS} & e^{-i\omega_I t}\,R_{z+}^{II} & e^{-i\omega_S t}\,R_{z+}^{IS} & e^{i\omega_I t}\,R_{z-}^{II} & e^{i\omega_S t}\,R_{z-}^{IS} \\ R_{zz}^{SI} & R_{zz}^{SS} & e^{-i\omega_I t}\,R_{z+}^{SI} & e^{-i\omega_S t}\,R_{z+}^{SS} & e^{i\omega_I t}\,R_{z-}^{SI} & e^{i\omega_S t}\,R_{z-}^{SS} \\ e^{i\omega_I t}\,R_{+z}^{II} & e^{i\omega_I t}\,R_{+z}^{IS} & R_{++}^{II} & e^{i\Delta t}\,R_{++}^{IS} & e^{i2\omega_I t}\,R_{+-}^{II} & e^{i\Sigma t}\,R_{+-}^{IS} \\ e^{i\omega_S t}\,R_{+z}^{SI} & e^{i\omega_S t}\,R_{+z}^{SS} & e^{-i\Delta t}\,R_{++}^{SI} & R_{++}^{SS} & e^{i\Sigma t}\,R_{+-}^{SI} & e^{i2\omega_S t}\,R_{+-}^{SS} \\ e^{-i\omega_I t}\,R_{-z}^{II} & e^{-i\omega_I t}\,R_{-z}^{IS} & e^{-i2\omega_I t}\,R_{-+}^{II} & e^{-i\Sigma t}\,R_{-+}^{IS} & R_{--}^{II} & e^{-i\Delta t}\,R_{--}^{IS} \\ e^{-i\omega_S t}\,R_{-z}^{SI} & e^{-i\omega_S t}\,R_{-z}^{SS} & e^{-i\Sigma t}\,R_{-+}^{SI} & e^{-i2\omega_S t}\,R_{-+}^{SS} & e^{i\Delta t}\,R_{--}^{SI} & R_{--}^{SS} \end{bmatrix} \tag{4.2.2}$$

where

$$\Sigma \equiv \omega_I + \omega_S \tag{4.2.3a}$$

$$\Delta \equiv \omega_I - \omega_S \tag{4.2.3b}$$

In the ZF regime, where the frequencies ω_I, ω_S and $\omega_I \pm \omega_S$ are much smaller than the relaxation rates (of order $\omega_{\mathrm{D}}^2\,\tau_{\mathrm{A}}$), the complex exponential factors in Eq. (E.28) can all be replaced by unity.

The cross-mode relaxation rates then come into play, coupling the evolution of the longitudinal and transverse magnetization components. This happens in the asymmetric IS–I case because the I–S dipole coupling is not isotropically averaged. At higher fields, where $\omega_I,\ \omega_S \gg \omega_{\mathrm{D}}^2\,\tau_{\mathrm{A}}$, the oscillating factors cancel all relaxation supermatrix elements, except possibly those involving the difference frequency $\omega_I - \omega_S$ (for a homonuclear spin pair). The relaxation supermatrix then becomes block-diagonal,

$$\widehat{\mathbf{R}}^{\alpha}(t) \;=\; \begin{bmatrix} R_{zz}^{II} & R_{zz}^{IS} & 0 & 0 & 0 & 0 \\ R_{zz}^{SI} & R_{zz}^{SS} & 0 & 0 & 0 & 0 \\ 0 & 0 & R_{++}^{II} & e^{i\Delta t}\,R_{++}^{IS} & 0 & 0 \\ 0 & 0 & e^{-i\Delta t}\,R_{++}^{SI} & R_{++}^{SS} & 0 & 0 \\ 0 & 0 & 0 & 0 & R_{--}^{II} & e^{-i\Delta t}\,R_{--}^{IS} \\ 0 & 0 & 0 & 0 & e^{i\Delta t}\,R_{--}^{SI} & R_{--}^{SS} \end{bmatrix} \tag{4.2.4}$$

Nonsecular decoupling thus cancels all cross-mode rates so the longitudinal modes (I_z and S_z) evolve independently from the transverse modes ($I_\pm$ and $S_\pm$).

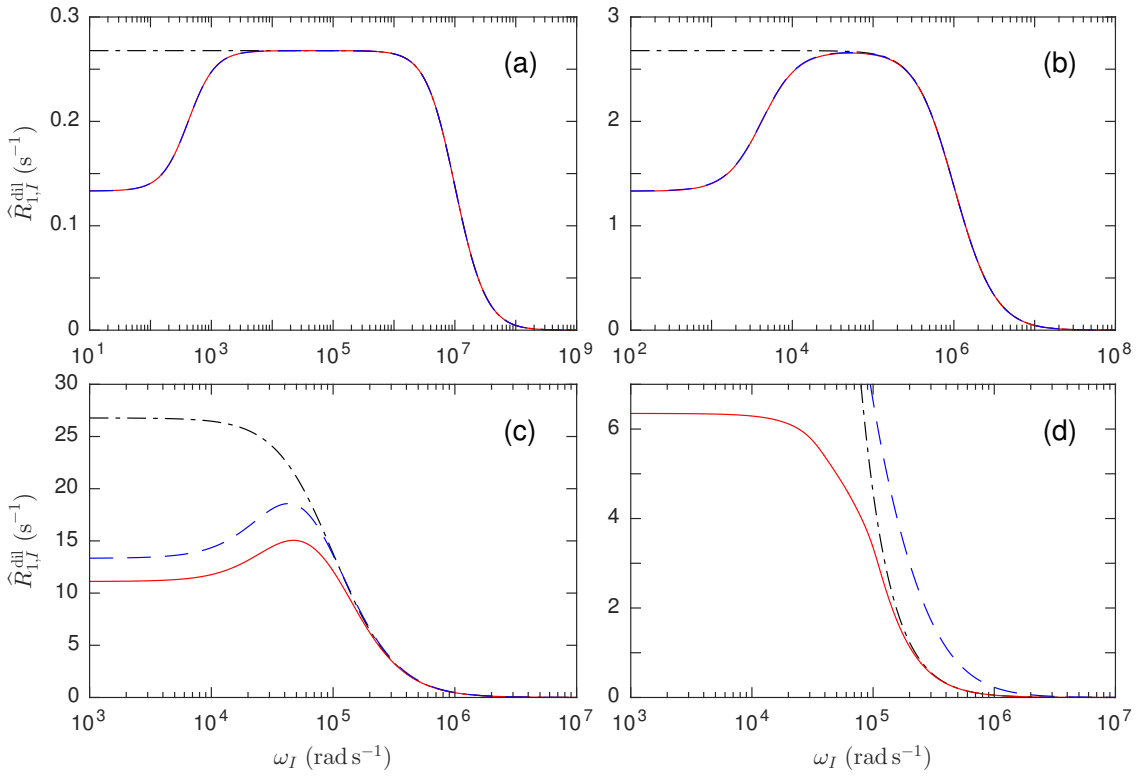

Figure 4.3: Dispersion of the integral longitudinal relaxation rate of spin I for exchange case $IS{-}I$. Parameter values: $P_{\mathrm{A}} = 10^{-3}$, $\omega_S = \omega_I$, $\omega_{\mathrm{D}} = 10^5$ rad s^{-1} and $\tau_{\mathrm{A}} = 10^{-7}$ s (a), 10^{-6} s (b), 10^{-5} s (c) or 10^{-4} s (d). The three dispersion profiles show $\widehat{R}_{1,I}^{\mathrm{dil}}$ computed from the SLE (red solid curves), SRE (blue dashed curves), and the secular SRE result (black dash-dotted curves).

Figure 4.3 (II–2) shows dispersion profiles $\widehat{R}_{1,I}^{\mathrm{dil}}(\omega_I)$ for the integral longitudinal relaxation rate of spin I in the dilute regime for four different values of the mean survival time τ_{A} in the A sites. As expected, the SLE and BWR results coincide in panels a and b, where $(\omega_{\mathrm{D}}\,\tau_{\mathrm{A}})^2 \ll 1$.

In panel c, where $\omega_D \tau_A = 1$, the approximate BWR rate exceeds the exact SLE rate by 20% in the ZF limit. In panel d, where $(\omega_D \tau_A)^2 = 100$, the corresponding discrepancy is a factor ~ 21. The inverted and normal dispersion steps in panels a and b are centered at the frequencies $\omega_I = \omega_D^2 \tau_A$ and $\omega_I = 1/\tau_A$, respectively, corresponding to the red and blue curves, respectively, in Fig. 4.3. The slower relaxation in the ZF regime is a consequence of longitudinal-transverse cross-mode relaxation in the anisotropic A sites (as seen from Eqs.(4.2.2) and (4.2.4)). In the LF regime (and above), cross-mode relaxation is abolished by nonsecular decoupling.

For the symmetric *IS*–*IS* case in the MN regime, the same IS spin pair samples all anisotropic A sites on a time scale that is short compared to the relaxation in each site because, when the exchange time is also the correlation time (as in the EMOR model), the MN regime coincides with the fast-exchange regime. The relaxation behavior is then governed by the isotropic average of the relaxation supermatrix in Eq. (4.2.4)), which becomes

$$\langle \widehat{\mathbf{R}}^{\alpha}(t) \rangle = \begin{bmatrix} \langle R_{zz}^{II} \rangle & \langle R_{zz}^{IS} \rangle & 0 & 0 & 0 & 0 \\ \langle R_{zz}^{SI} \rangle & \langle R_{zz}^{SS} \rangle & 0 & 0 & 0 & 0 \\ 0 & 0 & \langle R_{++}^{II} \rangle & e^{i\Delta t} \langle R_{++}^{IS} \rangle & 0 & 0 \\ 0 & 0 & e^{-i\Delta t} \langle R_{++}^{SI} \rangle & \langle R_{++}^{SS} \rangle & 0 & 0 \\ 0 & 0 & 0 & 0 & \langle R_{--}^{II} \rangle & e^{-i\Delta t} \langle R_{--}^{IS} \rangle \\ 0 & 0 & 0 & 0 & e^{i\Delta t} \langle R_{--}^{SI} \rangle & \langle R_{--}^{SS} \rangle \end{bmatrix} \tag{4.2.5}$$

since all cross-mode rates vanish when isotropically averaged. This result, including the familiar Solomon equations, is usually derived from BWR theory by invoking the secular approximation. Fundamentally, however, the decoupling of the longitudinal and transverse magnetizations is a consequence of isotropic averaging. Cross-mode coupling is therefore absent also at zero field, which is not obvious if the secular approximation is invoked.

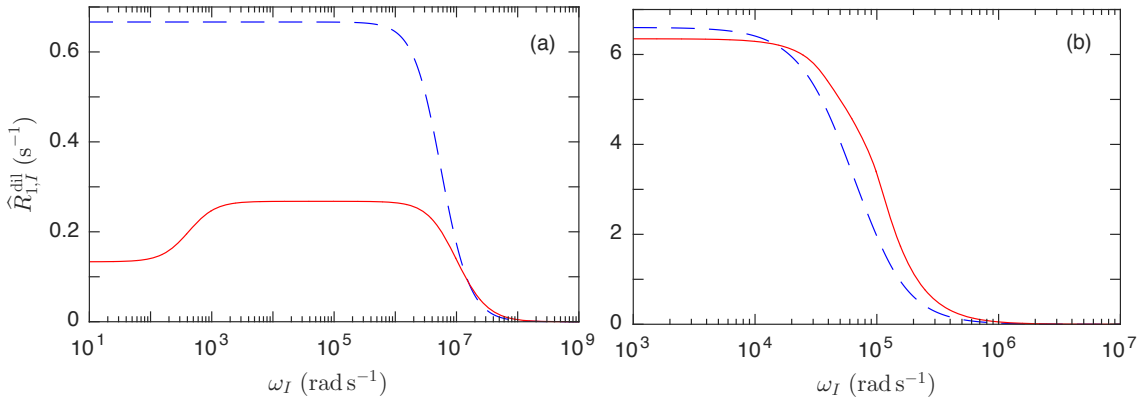

Figure 4.4: Dispersion of the integral longitudinal relaxation rate of spin I for exchange case *IS*–*I* computed from the SLE result (red solid curves, same as in Figs. 4.3) and for exchange case *IS*–*IS* computed from the corresponding SLE result in paper I (blue dashed curves). Parameter values as in Figs. 4.3 but with $\tau_A = 10^{-7}$ s (a), 10^{-4} s (b).

In Fig. 4.4 (II–4), we compare the dispersion profiles for the *IS*–*I* and *IS*–*IS* cases with the same parameter values as in Figs. 4.3(a) and 4.3(d). The red *IS*–*I* profiles are thus the same in Figs. 4.3(a) and 4.3(d). Because of isotropic averaging, there is no cross-mode relaxation in the A sites for the symmetric case so the integral relaxation rate is constant throughout the extreme-narrowing (EN) regime (no inverted dispersion at the boundary between the ZF and

LF regimes). In addition, the dispersion midpoint occurs at a lower frequency for the symmetric case. In the MN regime (panel a), the ratio $\widehat{R}^{\rm dil}_{1,I}(IS{-}IS)/\widehat{R}^{\rm dil}_{1,I}(IS{-}I)$ is thus 5 in the ZF regime, while it is ~ 2.5 in the LF regime. In the ultraslow-motion (USM) regime $(\omega_{\rm D}\,\tau_{\rm A})^2 \gg 1$ (panel b), the ZF rates for the symmetric and asymmetric exchange cases converge to the same value, $\widehat{R}^{\rm dil}_{1,I}(0) = (2/3)\,P_{\rm A}/\tau_{\rm A}$, but the dispersion for the asymmetric case is upshifted in frequency and deviates more from "Lorentzian" shape.

In this paper, we also presented a detailed analysis of the time evolution of the spin modes in the ZF regime. The total I-spin longitudinal magnetization was found to be very nearly exponential in the dilute regime.

4.3 Paper III: Three-spin EMOR cases

In this paper, we implemented the general dipolar EMOR theory for a three-spin (*ISP*) system, where one (*ISP–I*), two (*ISP–IS*), or all three spins (*ISP–ISP*) exchange with the bulk solutions. In contrast to the two-spin systems studied in paper I and II, there are now three dipole couplings, so relaxation is affected by both self- and distinct-correlations (see more details in section 4.5). Moreover, relaxation can now couple the magnetizations with three-spin modes and, in the presence of a SDC, with two-spin modes for the *ISP–I* case.

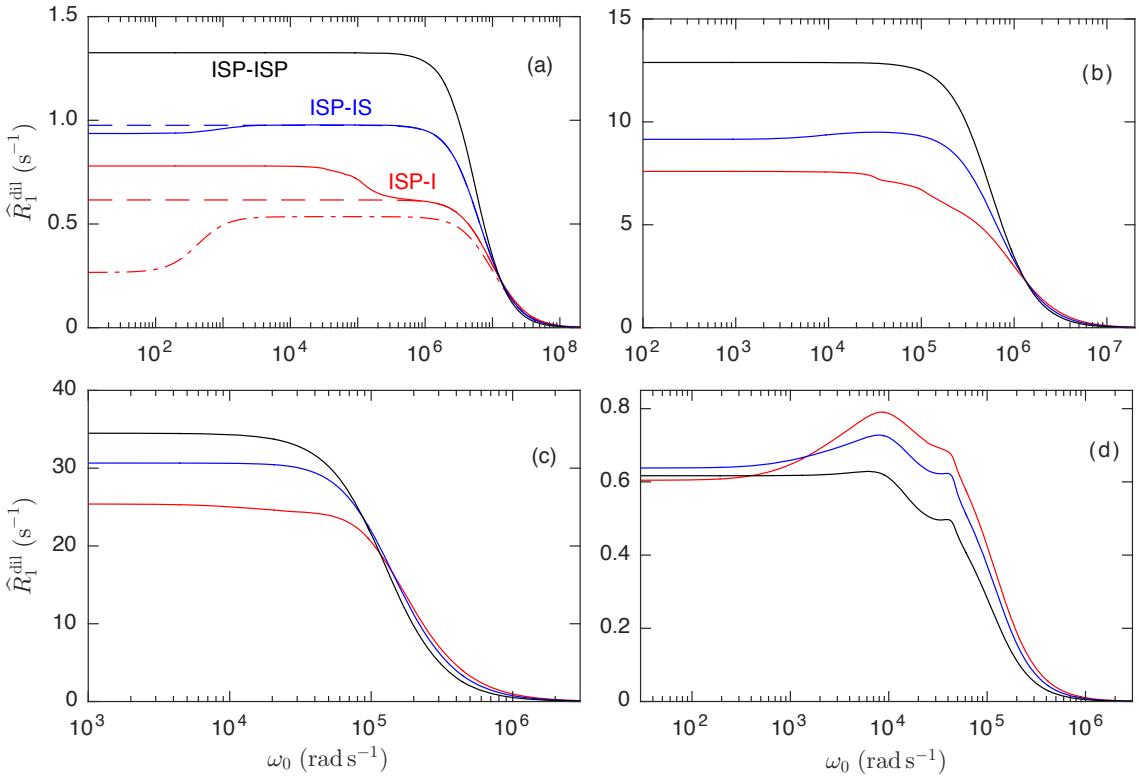

Figure 4.5: ILRR dispersion profiles for the three-spin cases. Color coding of exchange cases as in panel (a). Parameter values: $P_{\rm A} = 10^{-3}$, $\omega_{\rm D} = 10^5$ rad s^{-1}, $\beta_I = \beta_S = 60°$, and $\tau_{\rm A} = 10^{-7}$ s (a), 10^{-6} s (b), 10^{-5} s (c), or 10^{-3} s (d).

In Fig. 4.5 (III–2), we present the complete dispersion profiles of $\widehat{R}^{\rm dil}_{1,I}(ISP{-}I)$, $\widehat{R}^{\rm dil}_{1,IS}(ISP{-}IS)$ and $\widehat{R}^{\rm dil}_{1,ISP}(ISP-ISP)$ at four values of the mean survival time $\tau_{\rm A}$, ranging from the MN regime with $\omega_{\rm D}\,\tau_{\rm A} = 0.01$ to the USM regime with $\omega_{\rm D}\,\tau_{\rm A} = 100$. Here we also assume an equilateral triangle geometry ($\beta_I = \beta_S = 60°$) so all three dipole couplings have the same magnitude, taken to be $\omega_{\rm D} = 1 \times 10^5$ rad s^{-1}, which corresponds to an internuclear separation

of $r_{IS} = 2.245$ Å for two protons. The profiles with solid lines are computed from SLE theory and those with dashed lines are computed from SRE theory.

In Fig. 4.5(a), with $\tau_A = 100$ ns and $\omega_D \tau_A = 0.01$, we are squarely in the MN regime, where the SRE results apply. For the symmetric exchange case *ISP–ISP* where the spin system exchanges as an intact unit, we may expect that $\widehat{R}^{dil}_{1,ISP}(ISP-ISP)$ to be precisely a factor 2 larger than $\widehat{R}^{dil}_{1,IS}(IS-IS)$ since each spin is involved in two equally strong dipole couplings. This is true as long as we only take self-correlations into account. However, correlations between distinct dipole couplings also contribute negatively to $\widehat{R}^{dil}_{1,ISP}(ISP-ISP)$ which happens to be small for the equilateral triangle case (see more details in section 4.5).

Consider now the asymmetric exchange case *ISP–IS* with one nonlabile spin P. In the MN regime, which is also the fast-exchange regime for the EMOR model, relaxation rates that couple labile-spin (IS) modes are isotropically averaged, as in Eq. (4.2.5). In contrast, relaxation rates involving one or two nonlabile-spin modes are not exchange averaged; cf. Eq. (4.2.2). The local relaxation matrix (not exchange-averaged) has lower axial symmetry and relaxation can therefore couple local spin modes with different quantum order Q, which we refer to as cross-mode relaxation (see more details in section 4.2). If, as is the case here, the exchanging spin system contains one spin and the invariant odd-parity subspace only contains single-spin modes. The only available cross-mode relaxation channel is therefore between the longitudinal and transverse magnetizations of the same or different spins, at least one of which is nonlabile. The dispersion profile (blue solid curve) exhibits an inverted secondary dispersion step at $\omega_0 \approx \omega_D^2 \tau_A$, in addition to the primary dispersion step at $\omega_0 \approx 1/\tau_A$. The blue-dashed dispersion profiles in Fig. 4.5(a) were computed from the SRE results in the secular approximation, where cross-mode relaxation is neglected. The secular approximation is evidently not valid in the ZF regime.

Finally, we consider the asymmetric exchange case *ISP–I* with a static dipole coupling (SP). Like the $ISP-IS$ profile, the $ISP-I$ profile in Fig. 4.5(a) exhibits a secondary dispersion in addition to the primary dispersion at $\omega_0 \approx 1/\tau_A$. However, the secondary dispersion step now appears at $\omega_0 \approx \omega_D$ (rather than at $\omega_0 \approx \omega_D^2 \tau_A$) and it is not inverted. The origin of the secondary dispersion step in the $ISP-I$ profile is the SDC between the nonlabile spins S and P. If we set $\omega_{D,SP} = 0$ without altering the other two (equal) dipole couplings, then this secondary dispersion step disappears and instead an inverted dispersion step at $\omega_0 \approx \omega_D^2 \tau_A$ appears (the dash-dotted curve in Fig. 4.5(a)). In fact, for $\omega_{D,SP} = 0$ we have $\widehat{R}^{dil}_{1,I}(ISP-I) = 2\,\widehat{R}^{dil}_{1,I}(IS-I)$. The effect of static SP coupling is the singular nature of the matrix $\mathbf{X}$ in Eq. (3.2.33). More details can be found in Appendix H in paper III.

Increasing τ_A, thereby moving from the MN regime to the USM regime, has two principal effects on the dispersion profile, as described in Papers I and II for the two-spin system. First, the position of the primary dispersion step at $\omega_0 \approx 1/\tau_A$ is down-shifted in frequency until τ_A becomes comparable to $1/\omega_D$ ($= 10^{-5}$ s, here) and eventually stops at $\omega_0 \approx \omega_D$ when the USM limit is reached. Second, the ILRR in the ZF regime first increases and then decreases, with a maximum near $\omega_D \tau_A \approx 1$. As seen from Fig. 4.5(a)-(d), this is true for all three exchange cases. In addition, the USM profiles are no longer "Lorentzian" but exhibit a "fine-structure" that is particularly striking for the three-spin cases, with two distinct maxima (or "bumps") for the equilateral triangle geometry (Fig. 4.5(d)).

In this paper, we also examined the dependence of ILRR on the internuclear geometry which is specified by the relative orientation of the internuclear vectors as well as their lengths. Furthermore, we found that in contrast to the two-spin system, longitudinal relaxation for the symmetric exchange case *ISP–ISP* can be significantly affected by chemical shifts and by the odd-valued ("imaginary") part of the spectral density function.

4.4 Paper IV: Multi-spin EMOR cases

In this paper, we constructed a multi-spin dipolar EMOR theory which is valid beyond the RMN limit based on the SRE-3SM framework. This theory mainly deals with the two EMOR cases: IP_m–I ($m \geqslant 3$) and ISP_m–IS ($m \geqslant 2$), which correspond to one labile proton spin I or two internal-water proton spins I and S coupled to m nonlabile protein protons and exchanging with bulk water protons, respectively. In the dilute regime, we may compare the GSRE results for these two cases with: (i) the exact SLE theory available for the spin systems containing up to four spins; (ii) multi-spin dipolar EMOR theory based on extended Solomon equations[50] (ESE) which ignores both cross-mode relaxation and all SDC effects.

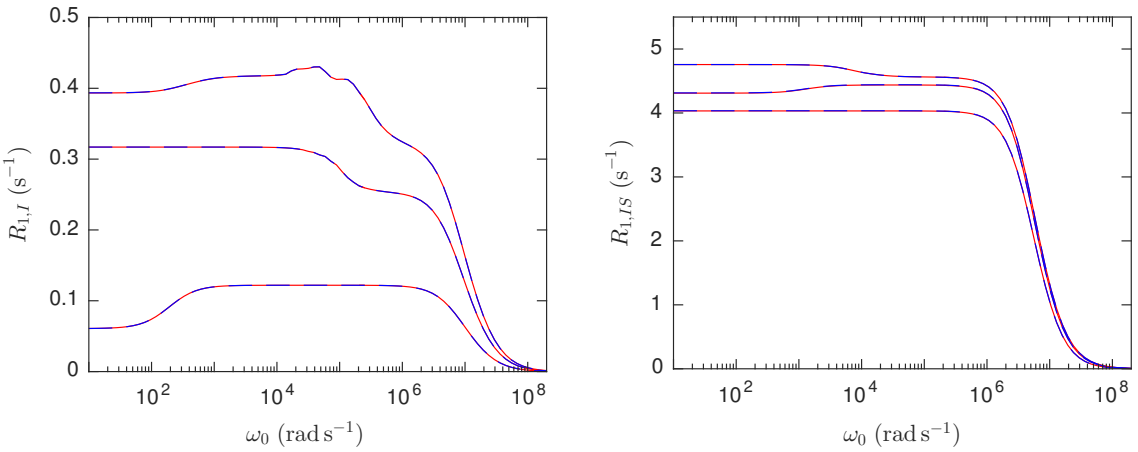

Figure 4.6: (left) Dispersion of $\widehat{R}^{\rm dil}_{1,I}(\omega_0)$ for the labile hydroxyl proton Thr-22 in ubiquitin coupled to $m = 1$, 2 or 3 nonlabile ptorons. (right) Dispersion of $\widehat{R}^{\rm dil}_{1,IS}(\omega_0)$ for the protons of internal water W122 in BPTI, coupled to $m = 0$, 1 or 2 nonlabile protons. In both panels, m increases from the lower to the upper profile and the dispersion profiles were computed from SLE (red solid) and SRE (blue dash) theory with $\tau_{\rm A} = 10^{-7}$s (in the RMN regime).

The multi-spin SRE theory is exact in the RMN regime for IP_m–I ($m \leqslant 3$) and ISP_m–IS ($m \leqslant 2$). As seen from Fig. 4.6 (IV–2) that it agrees with SLE theories quantitatively in the RMN regime, as expected. Fig. 4.7 shows $\widehat{R}^{\rm dil}_{1,I}(\omega_0)$ profiles for Thr-22 in ubiquitin with 1 – 10 nonlabile protons, computed from the SRE-3SM theory. Two secondary dispersion steps are present for all $m \geqslant 3$. In the frequency range between these steps, the profile becomes more smooth with increasing m. We may expect $\widehat{R}^{\rm dil}_{1,I}(\omega_0)$ to increase monotonically with m as more fluctuating dipole couplings are included. This is true above the inverted dispersion step at $\omega_0 \approx \omega^2_{{\rm D},I}\,\tau_{\rm A}$, but not in the ZF regime below this frequency. For ISP_m–IS ($m \geqslant 2$) case, the ILRR is dominated by the strong intramolecular I–S coupling. Consequently, the SRE-3SM profile never deviates much from the ESE profile, and the variation with m of ILRR converges much faster than that for IP_m–I case.

Outside the MN regime, the slow-motion effect is incorporated in the SRE-3SM theory by introducing the three generalisations discussed in section 3.2 (Eqs.(3.2.34) – (3.2.38)). For IP_m–I case, the GSRE theory predicts that $\widehat{R}^{\rm dil}_{1,I}(0) = P_{\rm A}/\tau_{\rm A}$ for any $m \geqslant 3$ in the USM limit, which indicates that the magnetization is randomised on the time scale $\tau_{\rm A}$ and $1/\tau_{\rm A}$ can be regarded as the local relaxation rate in the ZF USM limit, independent of the SDCs. SLE ($m = 3$) and ESE also give the same result or very nearly so. In slow-motion regime ($\tau_{\rm A} = 10^{-4}$ s), the GSRE theory predicts a too small $\widehat{R}^{\rm dil}_{1,I}(0)$ for most residues, by as much as 10 – 15 % in some cases. However, the ESE theory overestimates $\widehat{R}^{\rm dil}_{1,I}(0)$ even more. Figure 4.8 (IV–4) illustrates the effect of the different modifications in the GSRE theory. At $\tau_{\rm A} = 10^{-6}$ s, close to the

RMN regime, the SDCs have a large effect that is well captured by the GSRE theory. Well outside the RMN regime, the SDCs have a much smaller effect, but the SND in Eq. (3.2.37) and the SDC renormalization in Eq. (3.2.38) are both essential in making the GSRE profile agree (approximately) with the exact SLE profile. More MRD profiles (including 20 labile protons in ubiquitin and 5 internal water molecules in BPTI and ubiquitin) can be found in paper IV.

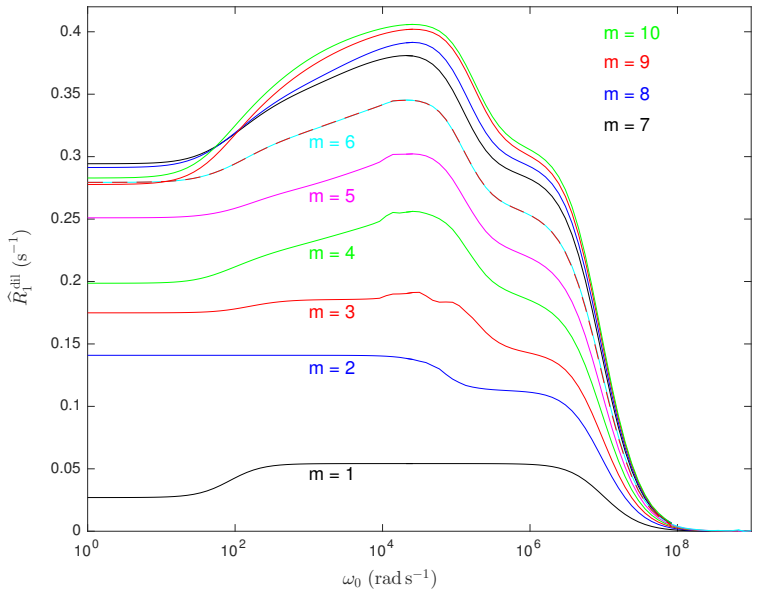

Figure 4.7: Dispersion of $\widehat{R}^{\rm dil}_{1,I}(\omega_0)$ for the labile hydroxyl proton Thr-22 in ubiquitin coupled to $m = 1 - 10$ nonlabile protons computed from SRE theory with $\tau_{\rm A} = 10^{-7}$s.

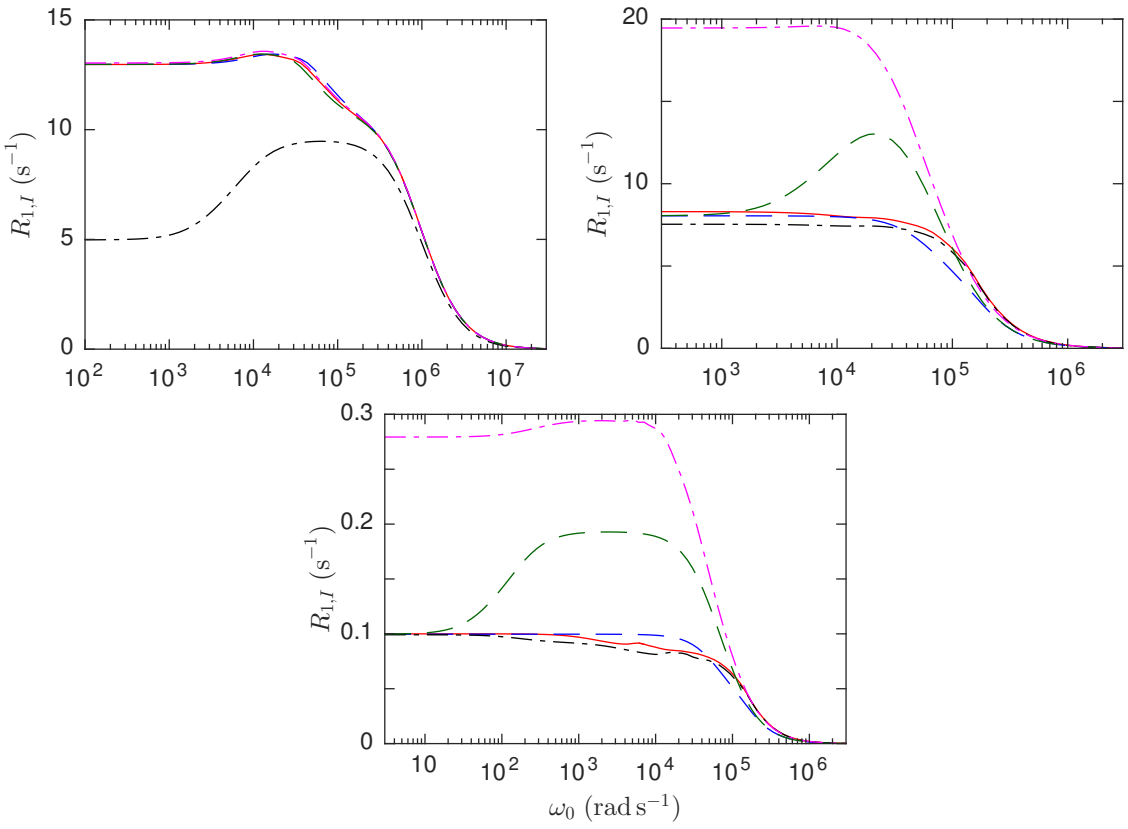

Figure 4.8: $\widehat{R}^{\rm dil}_{1,I}(\omega_0)$ dispersion with $\tau_{\rm A} = 10^{-6}$ s (top left), 10^{-4} s (top right) and 10^{-2} s (bottom) for labile protons in Thr-7 side-chains in ubiquitin coupled to three nonlabile protons, computed from the SLE theory with SDCs (red solid) and without SDCs (black dash-dot) and from the full GSRE theory (blue dash) and from GSRE theory without SND (green dash) or without SND and without SDC renormalization (magenta dash-dot).

4.5 Paper V: Imaginary part of the spectral density functions

In this paper, we studied the longitudinal relaxation of a system of three dipole-coupled spins (*ISP*) induced by rotational diffusion. This three-spin system was treated in arbitrary geometry and with arbitrary rotational dynamics. Three possible types of geometric symmetry or equivalence for this system were investigated. In the A_3 system, the three nuclei reside at the vertices of an equilateral triangle and are therefore geometrically equivalent. In the A_2A' system, the nuclei define an isosceles triangle. If spin P is at the apex then spins I and S are geometrically equivalent. Finally, in the $AA'A''$ system, all three internuclear vectors have different lengths so there is no geometrical equivalence.

The dimension of spin operator subspace required to describe the longitudinal relaxation of the three-spin system can be reduced by systematically using the symmetries and associated selection rules introduced in section 3.2. For isotropic dynamic models, such as spherical-top rotational diffusion, Wigner-Eckart theorem implies that the longitudinal relaxation can be fully described within the subspace of the ten zero-quantum OSIC operators, corresponding to the three longitudinal magnetizations and seven zero-quantum coherences. In these ten OSIC operators, seven of them are odd-rank and Hermitian whereas the rest three are even-rank and anti-Hermitian. Therefore, the 10×10 relaxation supermatrix that governs longitudinal relaxation has 7×7 and 3×3 real symmetric blocks along the diagonal and 7×3 and 3×7 purely imaginary "off-diagonal" blocks. The effect of the odd spectral density functions (OSDFs) is to couple odd-rank and even-rank spin modes. If the OSDF is neglected, this coupling disappears and the longitudinal relaxation is then fully described by the real symmetric 7×7 block associated with the odd-rank basis operators. This is the case in the EN regime, where, in addition, the selection rule (3.2.15) holds so that only the six rank-1 modes of this subspace can couple. For A_2A' or A_3 systems with geometrical symmetries, the number of required basis operators can be further reduced.

A relaxation supermatrix element R_{np} with $n \neq p$ describes cross relaxation between spin modes n and p. Both auto relaxation rates R_{nn} and cross relaxation rates R_{np} $(n \neq p)$ may have contributions from self correlations (correlations from the same dipole coupling) and from distinct correlations (correlations from different dipole couplings). Fig. 4.6 (V–8) shows the dispersion profiles of the total ($\widehat{R}_1$) and self ($\widehat{R}_1^{\text{self}}$) integral relaxation rates and of the initial relaxation rate (R_1^0) (defined as $R_1^0 \equiv -\frac{\mathrm{d}}{\mathrm{d}t}\left[\frac{\sigma_z(t)}{\sigma_z(0)}\right]\Big|_{t=0}$) for an A_2A' system with $\beta_P = 120°$. As seen that distinct correlations have a large effect in this A_2A' system, reducing $\widehat{R}_1$ by as much as 36 % (in the EN regime) as compared to R_1^0, which is unaffected by distinct correlations.

Fig. 4.6 also shows that the OSDF increases $\widehat{R}_1$ by up to 1.5 % in the dispersive regime, which is at variance with conventional wisdom. This conclusion has been confirmed by comparing the ILRR computed from SLE theory which implicitly incorporate any effect of the OSDF with that from BWR with and without OSDFs. The reason we can make this comparison is that within the MN regime ($\omega_D \tau_c \ll 1$), the spherical-top rotational diffusion and strong-collision models produce the same relaxation behavior. As shown in Fig. 4.7 (V–18) that the OSDF effect for the A_2A' system with $\beta_P = 108°$ is 2.6 %.

In this paper, we also analysed the time evolution of the total longitudinal magnetization via decomposition of eigenmodes. The number of exponential components are computed for different geometries, frequency regimes, and isotropic/anisotropic motions. We find that longitudinal relaxation in the A_3 geometry can involve up to six exponential components. From SLE theory, we found that the chemical shifts break the nuclear permutation symmetry, thereby increasing the number of relaxation components. An inverted relaxation dispersion step is predicted at the frequency where the differential precession rate matches the relaxation rate. Above this fre-

quency, nonsecular decoupling preferentially eliminates contributions from distinct correlations, thereby increasing the integral relaxation rate. The effect of chemical shifts disappears when the nonsecular decoupling frequency exceeds the main dispersion frequency, as is always the case for homonuclear spin systems outside the MN regime.

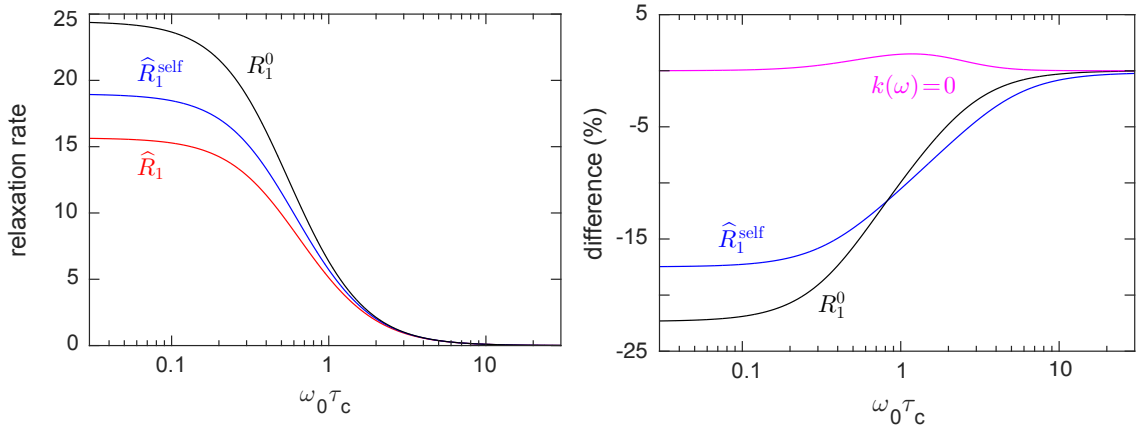

Figure 4.9: Dispersion of the integral relaxation rate $\widehat{R}_1$, its self-correlation part $\widehat{R}_1^{\rm self}$ and the initial relaxation rate R_1^0 (all three in units of $\omega_{{\rm D},IS}^2\,\tau_{\rm c}$) for an A_2A' spin system with $\beta_P = 120°$ and isotropic motion. The right panel shows the relative differences between $\widehat{R}_1$ and $\widehat{R}_1^{\rm self}$ (blue), between $\widehat{R}_1^{\rm self}$ and R_1^0 (black), and between $\widehat{R}_1$ with and without the OSDF (magenta).

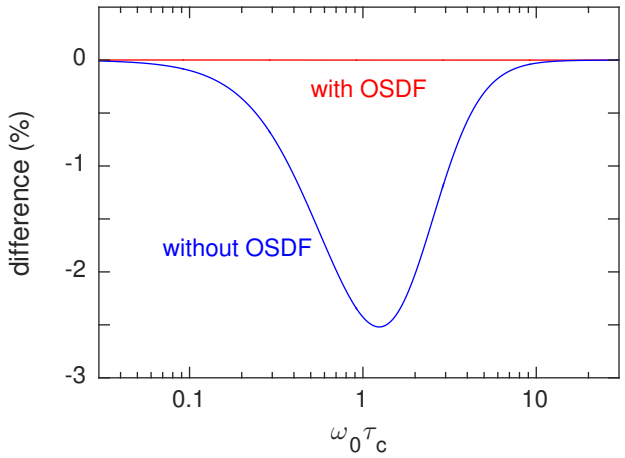

Figure 4.10: Relative difference $(\widehat{R}_1^{\rm BWR} - \widehat{R}_1^{\rm SLE})/\widehat{R}_1^{\rm SLE}$ of integral relaxation rates computed with BWR and SLE theories, the former with or without inclusion of the OSDF, for an isochronous A_2A' system with $\beta_P = 108°$, $\omega_{{\rm D},IS} = 10^4$ rad s^{-1}, $\tau_{\rm c} = 10^{-7}$ s and isotropic motion.

Outlook

In papers I to IV, we have systematically studied water ^{1}H MRD in different immobilised model spin systems corresponding to different exchange cases. The complications accompanied by the increase of the spin system size (e.g. distinct correlations, SDCs) were investigated in details. Based on these studies, we have formulated a multi-spin dipolar EMOR relaxation theory which yields a quantitative molecular description of tissue-water relaxation. In the near future, this theory can be applied to the clinical field-cycled MRI for the soft-tissue imaging. However, as one might notice that even for the spin system with 10 nonlaibile protons, the computations are still quite time-consuming with present-day computers. We hope that the computation efficiency could be improved with the further development of computation power.

References

[1] S. A. Goudsmit, "The discovery of the electron spin," *Nederlands Tijdschrift voor Natuurkunde*, vol. 37, p. 386, 1971.

[2] D. J. Griffiths, *Introduction to quantum mechanics*. Pearson Education India, 2005.

[3] C. A. Aidala, S. D. Bass, D. Hasch, and G. K. Mallot, "The spin structure of the nucleon," *Reviews of Modern Physics*, vol. 85, no. 2, p. 655, 2013.

[4] Y.-B. Yang, R. S. Sufian, A. Alexandru, T. Draper, M. J. Glatzmaier, K.-F. Liu, and Y. Zhao, "Glue spin and helicity in the proton from lattice qcd," *Phys. Rev. Lett.*, vol. 118, p. 102001, 2017.

[5] F. Bloch, "Nuclear induction," *Physical review*, vol. 70, no. 7-8, p. 460, 1946.

[6] E. M. Purcell, H. Torrey, and R. V. Pound, "Resonance absorption by nuclear magnetic moments in a solid," *Physical review*, vol. 69, no. 1-2, p. 37, 1946.

[7] P. Hore, *Nuclear magnetic resonance*. Oxford University Press, USA, 2015.

[8] J. Keeler, *Understanding NMR spectroscopy*. John Wiley & Sons, 2011.

[9] W. S. Warren, "The usefulness of nmr quantum computing," *Science*, vol. 277, no. 5332, pp. 1688–1690, 1997.

[10] D. G. Cory, A. F. Fahmy, and T. F. Havel, "Ensemble quantum computing by nmr spectroscopy," *Proceedings of the National Academy of Sciences*, vol. 94, no. 5, pp. 1634–1639, 1997.

[11] N. A. Gershenfeld and I. L. Chuang, "Bulk spin-resonance quantum computation," *Science*, vol. 275, no. 5298, pp. 350–356, 1997.

[12] R. R. Edelman and S. Warach, "Magnetic resonance imaging," *New England Journal of Medicine*, vol. 328, no. 10, pp. 708–716, 1993.

[13] Z.-P. Liang and P. C. Lauterbur, *Principles of magnetic resonance imaging: a signal processing perspective*. The Institute of Electrical and Electronics Engineers Press, 2000.

[14] R. W. Brown, Y.-C. N. Cheng, E. M. Haacke, M. R. Thompson, and R. Venkatesan, *Magnetic resonance imaging: physical principles and sequence design*. John Wiley & Sons, 2014.

[15] A. Abragam, *Principles of nuclear magnetism*. Clarendon Press, Oxford, 1961.

[16] J. Cavanagh, W. J. Fairbrother, A. G. Palmer III, and N. J. Skelton, *Protein NMR spectroscopy: principles and practice*. Academic Press, 1995.

[17] N. Bloembergen, E. M. Purcell, and R. V. Pound, "Relaxation effects in nuclear magnetic resonance absorption," *Physical review*, vol. 73, no. 7, p. 679, 1948.

[18] I. Solomon, "Relaxation processes in a system of two spins," *Physical Review*, vol. 99, no. 2, p. 559, 1955.

[19] N. Bloembergen and L. Morgan, "Proton relaxation times in paramagnetic solutions. effects of electron spin relaxation," *The Journal of Chemical Physics*, vol. 34, no. 3, pp. 842–850, 1961.

[20] O.K.-Daszkiewicz, J. Hennel, B. Lubas, and T. Szczepkowski, "Proton magnetic relaxation and protein hydration," *Nature*, vol. 200, no. 4910, pp. 1006–1007, 1963.

[21] F. Noack, "NMR field-cycling spectroscopy: principles and applications," *Progress in nuclear magnetic resonance Spectroscopy*, vol. 18, no. 3, pp. 171–276, 1986.

[22] R. Kimmich and E. Anoardo, "Field-cycling NMR relaxometry," *Progress in Nuclear Magnetic Resonance Spectroscopy*, vol. 44, no. 3-4, pp. 257–320, 2004.

[23] S. H. Koenig and W. E. Schillinger, "Nuclear magnetic relaxation dispersion in protein solutions i. apotransferrin," *Journal of Biological Chemistry*, vol. 244, no. 12, pp. 3283–3289, 1969.

[24] S. H. Koenig, K. Hallenga, and M. Shporer, "Protein-water interaction studied by solvent ^{1}H, ^{2}H, and ^{17}O magnetic relaxation," *Proceedings of the National Academy of Sciences*, vol. 72, no. 7, pp. 2667–2671, 1975.

[25] R. Kimmich, T. Gneiting, K. Kotitschke, and G. Schnur, "Fluctuations, exchange processes, and water diffusion in aqueous protein systems: A study of bovine serum albumin by diverse nmr techniques," *Biophysical journal*, vol. 58, no. 5, pp. 1183–1197, 1990.

[26] V. P. Denisov and B. Halle, "Dynamics of the internal and external hydration of globular proteins," *Journal of the American Chemical Society*, vol. 116, no. 22, pp. 10324–10325, 1994.

[27] V. P. Denisov and B. Halle, "Protein hydration dynamics in aqueous solution," *Faraday Discussions*, vol. 103, pp. 227–244, 1996.

[28] K. Venu, V. P. Denisov, and B. Halle, "Water ^{1}H magnetic relaxation dispersion in protein solutions. a quantitative assessment of internal hydration, proton exchange, and cross-relaxation," *Journal of the American Chemical Society*, vol. 119, no. 13, pp. 3122–3134, 1997.

[29] C. Nilsberth, A. Westlind-Danielsson, C. B. Eckman, M. M. Condron, K. Axelman, C. Forsell, C. Stenh, J. Luthman, D. B. Teplow, and S. G. Younkin, "The 'arctic' app mutation (e693g) causes alzheimer's disease by enhanced aβ protofibril formation," *Nature neuroscience*, vol. 4, no. 9, pp. 887–893, 2001.

[30] C. Haass and D. J. Selkoe, "Soluble protein oligomers in neurodegeneration: lessons from the alzheimer's amyloid β-peptide," *Nature reviews Molecular cell biology*, vol. 8, no. 2, pp. 101–112, 2007.

[31] F. V. Chávez and B. Halle, "Molecular basis of water proton relaxation in gels and tissue," *Magnetic resonance in medicine*, vol. 56, no. 1, pp. 73–81, 2006.

[32] E. P. Sunde and B. Halle, "Slow internal protein dynamics from water ^{1}H magnetic relaxation dispersion," *Journal of the American Chemical Society*, vol. 131, no. 51, pp. 18214–18215, 2009.

[33] D. J. Lurie, M. A. Foster, D. Yeung, and J. M. Hutchison, "Design, construction and use of a large-sample field-cycled PEDRI imager," *Physics in medicine and biology*, vol. 43, no. 7, p. 1877, 1998.

[34] S. K. Lee, M. Möble, W. Myers, N. Kelso, A. H. Trabesinger, A. Pines, and J. Clarke, "Squid-detected MRI at 132 μt with t1-weighted contrast established at 10 μt–300 mt," *Magnetic resonance in medicine*, vol. 53, no. 1, pp. 9–14, 2005.

[35] N. I. Matter, G. C. Scott, R. D. Venook, S. E. Ungersma, T. Grafendorfer, A. Macovski, and S. M. Conolly, "Three-dimensional prepolarized magnetic resonance imaging using rapid acquisition with relaxation enhancement," *Magnetic resonance in medicine*, vol. 56, no. 5, pp. 1085–1095, 2006.

[36] S. E. Ungersma, N. I. Matter, J. W. Hardy, R. D. Venook, A. Macovski, S. M. Conolly, and G. C. Scott, "Magnetic resonance imaging with T1 dispersion contrast," *Magnetic resonance in medicine*, vol. 55, no. 6, pp. 1362–1371, 2006.

[37] K. Gilbert, W. Handler, T. Scholl, J. Odegaard, and B. Chronik, "Design of field-cycled magnetic resonance systems for small animal imaging," *Physics in medicine and biology*, vol. 51, no. 11, p. 2825, 2006.

[38] C. Kegler, H. Seton, and J. Hutchison, "Prepolarized fast spin-echo pulse sequence for low-field MRI," *Magnetic resonance in medicine*, vol. 57, no. 6, pp. 1180–1184, 2007.

[39] J. K. Alford, T. J. Scholl, W. B. Handler, and B. A. Chronik, "Design and construction of a prototype high-power b0 insert coil for field-cycled imaging in superconducting mri systems," *Concepts in Magnetic Resonance Part B: Magnetic Resonance Engineering*, vol. 35, no. 1, pp. 1–10, 2009.

[40] K. J. Pine, G. R. Davies, and D. J. Lurie, "Field-cycling NMR relaxometry with spatial selection," *Magnetic resonance in medicine*, vol. 63, no. 6, pp. 1698–1702, 2010.

[41] L. Calucci and C. Forte, "Proton longitudinal relaxation coupling in dynamically heterogeneous soft systems," *Progress in Nuclear Magnetic Resonance Spectroscopy*, vol. 55, no. 4, pp. 296–323, 2009.

[42] R. G. Bryant, D. A. Mendelson, and C. C. Lester, "The magnetic field dependence of proton spin relaxation in tissues," *Magnetic resonance in medicine*, vol. 21, no. 1, pp. 117–126, 1991.

[43] S. H. Koenig, R. D. Brown, and R. Ugolini, "A unified view of relaxation in protein solutions and tissue, including hydration and magnetization transfer," *Magnetic resonance in medicine*, vol. 29, no. 1, pp. 77–83, 1993.

[44] S. H. Koenig and R. D. Brown III, "A molecular theory of relaxation and magnetization transfer: Application to cross-linked bsa, a model for tissue," *Magnetic resonance in medicine*, vol. 30, no. 6, pp. 685–695, 1993.

[45] J.-P. Korb and R. G. Bryant, "The physical basis for the magnetic field dependence of proton spin-lattice relaxation rates in proteins," *The Journal of Chemical Physics*, vol. 115, no. 23, pp. 10964–10974, 2001.

[46] J.-P. Korb and R. G. Bryant, "Magnetic field dependence of proton spin-lattice relaxation times," *Magnetic resonance in medicine*, vol. 48, no. 1, pp. 21–26, 2002.

[47] Y. A. Goddard, J.-P. Korb, and R. G. Bryant, "Water molecule contributions to proton spin–lattice relaxation in rotationally immobilized proteins," *Journal of Magnetic Resonance*, vol. 199, no. 1, pp. 68–74, 2009.

[48] S. Lushnikov, A. Svanidze, and I. Sashin, "Vibrational density of states of hen egg white lysozyme," *JETP Letters*, vol. 82, no. 1, pp. 30–33, 2005.

[49] X. Yu and D. M. Leitner, "Heat flow in proteins: computation of thermal transport coefficients," *The Journal of chemical physics*, vol. 122, no. 5, p. 054902, 2005.

[50] B. Halle, "Molecular theory of field-dependent proton spin-lattice relaxation in tissue," *Magnetic resonance in medicine*, vol. 56, no. 1, pp. 60–72, 2006.

[51] A. D. Bain, "Chemical exchange in nmr," *Progress in nuclear magnetic resonance spectroscopy*, vol. 43, no. 3, pp. 63–103, 2003.

[52] H. M. McConnell, "Reaction rates by nuclear magnetic resonance," *The Journal of Chemical Physics*, vol. 28, no. 3, pp. 430–431, 1958.

[53] J. Zimmerman and W. Brittin, "Nuclear magnetic resonance studies in multiple phase systems: lifetime of a water molecule in an adsorbing phase on silica gel," *J. phys. Chem*, vol. 61, no. 10, pp. 1328–1333, 1957.

[54] Z. Luz and S. Meiboom, "Proton relaxation in dilute solutions of cobalt (II) and nickel (II) ions in methanol and the rate of methanol exchange of the solvation sphere," *The Journal of Chemical Physics*, vol. 40, no. 9, pp. 2686–2692, 1964.

[55] B. Halle, V. P. Denisov, and K. Venu, "Multinuclear relaxation dispersion studies of protein hydration," *Biological magnetic resonance*, pp. 419–484, 2002.

[56] T. Nilsson and B. Halle, "Nuclear magnetic relaxation induced by exchange-mediated orientational randomization: Longitudinal relaxation dispersion for spin $I = 1$," *The Journal of chemical physics*, vol. 137, no. 5, p. 054503, 2012.

[57] J. Kowalewski and L. Maler, *Nuclear spin relaxation in liquids: theory, experiments, and applications*. CRC press, 2006.

[58] V. A. Jarymowycz and M. J. Stone, "Fast time scale dynamics of protein backbones: NMR relaxation methods, applications, and functional consequences," *Chemical reviews*, vol. 106, no. 5, pp. 1624–1671, 2006.

[59] E. Persson and B. Halle, "Nanosecond to microsecond protein dynamics probed by magnetic relaxation dispersion of buried water molecules," *Journal of the American Chemical Society*, vol. 130, no. 5, pp. 1774–1787, 2008.

[60] B. Halle, "Spin dynamics of exchanging quadrupolar nuclei in locally anisotropic systems," *Progress in Nuclear Magnetic Resonance Spectroscopy*, vol. 28, no. 2, pp. 137–159, 1996.

[61] F. Vaca Chávez, E. Persson, and B. Halle, "Internal water molecules and magnetic relaxation in agarose gels," *Journal of the American Chemical Society*, vol. 128, no. 14, pp. 4902–4910, 2006.

[62] F. V. Chávez, E. Hellstrand, B. Halle, *et al.*, "Hydrogen exchange and hydration dynamics in gelatin gels," *Journal of Physical Chemistry B*, vol. 110, no. 43, p. 21551, 2006.

[63] M. Goldman, "Formal theory of spin–lattice relaxation," *Journal of Magnetic Resonance*, vol. 149, no. 2, pp. 160–187, 2001.

[64] S. Dattagupta and M. Blume, "Stochastic theory of line shape. I. nonsecular effects in the strong-collision model," *Physical Review B*, vol. 10, no. 11, p. 4540, 1974.

[65] U. Fano, "Description of states in quantum mechanics by density matrix and operator techniques," *Reviews of Modern Physics*, vol. 29, no. 1, p. 74, 1957.

[66] P. W. Anderson, "A mathematical model for the narrowing of spectral lines by exchange or motion," *Journal of the Physical Society of Japan*, vol. 9, no. 3, pp. 316–339, 1954.

[67] R. Kubo, "Note on the stochastic theory of resonance absorption," *Journal of the Physical Society of Japan*, vol. 9, no. 6, pp. 935–944, 1954.

[68] M. H. Levitt, *Spin dynamics: basics of nuclear magnetic resonance*. John Wiley & Sons, 2001.

[69] N. Pyper, "Theory of symmetry in nuclear magnetic relaxation including applications to high resolution NMR line shapes," *Molecular Physics*, vol. 21, no. 1, pp. 1–33, 1971.

[70] S. A. Smith, W. E. Palke, and J. Gerig, "The Hamiltonians of NMR. part II," *Concepts in magnetic resonance*, vol. 4, no. 3, pp. 181–204, 1992.

[71] D. M. Brink and G. R. Satchler, *Angular momentum*. Clarendon Press, 1968.

[72] N. Pyper, "Theory of symmetry in nuclear magnetic relaxation: Part II," *Molecular Physics*, vol. 22, no. 3, pp. 433–458, 1971.

[73] S. Szymanski, A. M. Gryff-Keller, and G. Binsch, "A liouville space formulation of wangsness-bloch-redfield theory of nuclear spin relaxation suitable for machine computation. I. fundamental aspects," *Journal of Magnetic Resonance*, vol. 68, no. 3, pp. 399–432, 1986.

[74] U. Fano, *Liouville representation of quantum mechanics with application to relaxation processes*, vol. 2. Academic Press: New York, 1964.

[75] R. R. Ernst, G. Bodenhausen, and A. Wokaun, *Principles of nuclear magnetic resonance in one and two dimensions*, vol. 14. Clarendon Press Oxford, 1987.

[76] N. G. van Kampen, *Stochastic processes in physics and chemistry*. North-Holland, Amsterdam, 1981.

[77] R. Kubo, "Stochastic liouville equations," *Journal of Mathematical Physics*, vol. 4, no. 2, pp. 174–183, 1963.

[78] R. Kubo, "A stochastic theory of line shape," *Stochastic Processes in Chemical Physics*, vol. 15, pp. 101–127, 1969.

[79] N. Skrynnikov and R. Ernst, "Detection of intermolecular chemical exchange through decorrelation of two-spin order," *Journal of Magnetic Resonance*, vol. 137, no. 1, pp. 276–280, 1999.

[80] M. Tinkham, *Group Theory and Quantum Mechanics*. Courier Corporation, 2003.

[81] L. Werbelow and D. Grant, "Intramolecular dipolar relaxation in multispin systems," *Adv. Magn. Reson*, vol. 9, no. 182-299, p. 34, 1977.

Acknowledgements

Finally, it comes to this part, and almost the very end of this six-year long journey. My memories now are fresh and vivid that I still remembered the complicated feelings when I first boarded the plane from Beijing to Copenhagen on August 25, 2011 — a bit afraid and panicked of the unfamiliar environment in another country and numerous potential challenges ahead of me, but more was the excitement of the first experience in abroad and getting the opportunity of doing cutting-edge research. Now when I look back this period of my lifetime, there are so many people I want to say thanks. But I have to apologise in advance if I forgot to mention someone's name here that also makes this work possible.

First of all, I want to express my deepest gratitude to my supervisor **Bertil**. Thank you for offering me this valuable PhD position in your group. This thesis would have never been possible without your intensive guidances and deep involvement. There were so many times that I desperately faced some seemingly unsolvable problems, and you just found solutions like a magician. I still remembered six years ago, when you picked me up at the Copenhagen airport and on the way back to Lund, you told me that I was going to learn so many things not just research and science. Now I think I understand what you meant. Apart from specific knowledge of relaxation theory and protein science, you taught me how to think and work as a physicist. I am impressed not only by your master skills of problem solving and paper writing but also, more importantly, by your determination, faith, and almost endless patience on finding the perfect solution for a specific scientific problem, no matter how hard it is and how much work it will take. These invaluable spiritual wealth I got from you together with the one to one relaxation course, midnight emails, available-at-any-time discussions as well as your broad interests and special sense of humour will keep shedding the light and inspiring me for the rest of my scientific career.

I also want to thank my co-supervisor **Mikael** for advices on my studies during the regular meetings and giving the wonderful NMR course. The positive feedback you gave to me after my first seminar here was also very encouraging. **Bengt** for helping me with preparing the lab tutoring and fixing the little "woodpecker" for the student lab "thermodynamic smörgåsbord". As a respected professor, you helped me with carrying those heavy nitrogen tanks which was really a cultural shock to me as a student from China. **Kristofer** for the discussions and "private tutoring" before each exercise session when I was your teaching assistant for the thermodynamics course. I must say that I learnt more on this subject during teaching than being a student actually taking the course. From the nice Matlab script you wrote for the data analysis for the student lab "chemical equilibrium", I also learnt one needs constant improving to be a dedicated teacher. **Pär** for the nice chatting during the department excursion. **Magnus** for the interesting coffee-break talks and always keeping the Toshiba machine functioning. **Adine** for ordering the chemicals for the student lab. **Susanna** for the administrative work.

My previous group members **Johan Q** for showing me basics of Matlab when I was a complete

"noob". Thank you for the comfort chatting when I felt stressed at the beginning of my PhD studies, and also inviting me for dinner. **Shuji** for seriously answering my all kinds of naive questions about NMR and protein science. Moreover, thank you for the nice lunch talks, tasty handmade pizza in Möllevångsvägen corridor, and being a nice company at conference in Torino. The CMPS members **Olga** for being a cool office mate and giving me the priority of taking your desk after you leave, the very nice next-to-window spot which I have been sitting for almost five years. **Gleb** for being my first office mate here and always making the office atmosphere pleasant. **Uli** for being the most responsible coffee-break organiser ever and reminding us at 10 am and 3 pm, respectively, for every day. I am glad to hear that you have introduced this tradition to your own group in Germany. **Risto** for being my lab partner during the NMR course, although I ruined everything by accidentally tuning that bronze knob of solid-state NMR spectrometer we were told not to, which I still have no clue what the function of that knob is. Thank you for pushing me to play football with you in a department game which I could only play goalkeeper. Thanks a ton also for being a reliable consultant of car issues. **Ashhar** for sharing a lot of interesting stories in India and cooking me nice Indian food. **Henry** for the swimming teaching and delicious spicy food in your apartment. **Erik**, **Andreas**, **Anders B** for playing badminton together in my first two years. **Karin**, **Tanja**, **Kalyani**, **Dev**, **Stefan**, **Marwin**, **Birgitta**, **Tina**, **Mattias**, **Thom**, **Ingemar** for nice casual chatting during the coffee break.

To the BPC tennis group. **Filip**, it is lucky to have you in the same research group. As a Matlab omnipotent, your suggestions on mex files compiling saved my life. It was also a lot of good memories in Gothenburg when we were taking the statistical mechanics course. Many thanks again for helping me with many other things including so much time you spent on this beautiful cover for my thesis. **Bhakat** for always being a nice buddy in the office. Although as a Barça fan, I disagree with you (a C Ronaldo fan) in many aspects about football, we still have so many interests in common, e.g, weekly badminton practice, chatting on various topics, drinking in your apartment and pubs, etc., you really make my KC life colourful. **Olof** for being my best tennis partner so we two NMR people could always beat the two simulation guys mentioned above. Thank you for taking the responsibility of coffee-break organiser after Uli and recommending me several TV-shows for leisure time. Thank you also for showing me the pingpong table in NMR corridor so I could have some fun with my Chinese friends. You guys deserve a separate paragraph here and many thanks again!

Now to the other BPC friends. **Johan W** for always being a good listener and active organiser of department events. Your "mini-library" also proves to be very handy when I could not find some books on my desk. **Sven** for many interesting conversations and always helping me with documents in Swedish. It was fun to perform the "apple burning" experiments for the safety course with both of you guys. **Kristine** for sharing the experiences in raising kids. **Anders R**, **Santosh**, **Eric**, **Magdalena**, **Emil** for many interesting chatting.

I would like to thank **Paula** for the hard work on the printing issues of this thesis (e.g. adjusting the format, margins, etc.) and very helpful suggestions on the cover design.

A special thanks here is dedicated to **Art**, my oral English teacher when I was a master student in China, who spent countless hours helping me practising my English. The office hours you spent with me and your encouragement is very important to me. Wish all the best to you and your families in the US.

The following are the acknowledgements to my families and Chinese friends:

首先感谢我的爸爸妈妈对我三十年的培养和教育。感谢你们不辞辛苦，不远万里来到异国他乡帮我们照看孩子和照顾我们的生活。你们永远是我在外拼搏最坚强的后盾。感谢我在家乡的亲人们，每次回国你们都能让我感受到家的温暖。 感谢我在隆德的中国朋友们：吕游，你是我在这里认识的第一个中国朋友，感谢你在我刚来隆德时对我生活上的帮助；晓婷，维珉，

知非，得朋，我们几乎同时来到隆德，你们是我结识的第一批朋友，当然还有Aiew。怀念我们那时候一起聊天，看电影，聚餐，玩真心话大冒险的那种单纯的快乐。希望我们的友谊不会随着距离的增加和时间的流逝而褪色；感谢余斌，张璇的热情好客，无数次在你们家的聚餐和游戏，还有你们和忆翥，樊星，飞哥组织的德国啤酒节之旅；感谢忆翥和飞哥，在我生病的时候帮忙照顾亮亮，送我去医院；感谢陈领，那一段经常互相蹭饭的岁月，而且总是邀请我去参加教会的活动；感谢飞飞和宏多组织的聚餐和牌局；感谢王健和芮羽经常组织聚餐并且送亮亮礼物；感谢海强，虽然你在隆德停留的时间很短，但你绝对是我最好的朋友之一；感谢我们的DOTA小组：余斌，王健，王冀，维珉，宇盼，怀念我们一起度过的无数个疯狂的夜晚；感谢宇盼组织的滑雪，还有邀请我去你家聚餐；感谢哲成和郭晨组织的周日羽毛球，还有积极参加活动的刘成，宇盼，魏来，周波，陈路，方圆，在球场上挥汗如雨总是件非常痛快的事；感谢我们的乒乓球小组：美娜，黎黎，海亮，振东，周末打球是写论文最好的调剂；感谢哲明，孟芹，邵栋，芮瑜组织的亲子活动；感谢哲成，谢非，统昌，张卡，宝中，赵倩组织的聚餐及小朋友们的活动；感谢师博，泽鹏在阿姆斯特丹的盛情款待；感谢冀光，潘凡一起的聚餐和斯德哥尔摩之旅。最后感谢我的妻子姜虹，为了支持我的学业和照顾家庭而牺牲了自己在国内的事业来到国外，在这边对我的日常生活照顾的无微不至，让我能够心无旁骛的投入研究和本论文的写作；还有我们的儿子常思，感谢那些陪伴你成长时，你带给我们的无数快乐时光。

ERRATA

Paper I

Page 8: The plus sign between the first and second terms in Eq. (4.24) should be a minus sign.

Page 9: on line -5, left column, "single-quantum" should be "zero-quantum".

Figure 6: the symbol on the abscissa should be ω_I.

Appendix E: in Eq. (E.3c), the plus sign should be a minus sign.

Appendix F: in Eq. (F.1), the second plus sign should be a minus sign.

Paper III

Table S1 D: Basis operator 56 should be $(I_z S_- - I_- S_z)P_-$.

Table S1 D: Basis operator 57 should be $-\frac{1}{\sqrt{3}}[2I_- S_- P_z - (I_z S_- + I_- S_z)P_-]$.

Appendix H: the line between Eqs. (H.18) and (H.19) should read "and, since $\mathbf{U}^{-1} = \mathbf{U}^\dagger$,".

Paper I

THE JOURNAL OF CHEMICAL PHYSICS **139**, 144203 (2013)

Nuclear magnetic relaxation induced by exchange-mediated orientational randomization: Longitudinal relaxation dispersion for a dipole-coupled spin-1/2 pair

Zhiwei Chang and Bertil Halle[a)]
Biophysical Chemistry, Lund University, POB 124, SE-22100 Lund, Sweden

(Received 8 July 2013; accepted 17 September 2013; published online 10 October 2013)

In complex biological or colloidal samples, magnetic relaxation dispersion (MRD) experiments using the field-cycling technique can characterize molecular motions on time scales ranging from nanoseconds to microseconds, provided that a rigorous theory of nuclear spin relaxation is available. In gels, cross-linked proteins, and biological tissues, where an immobilized macromolecular component coexists with a mobile solvent phase, nuclear spins residing in solvent (or cosolvent) species relax predominantly via exchange-mediated orientational randomization (EMOR) of anisotropic nuclear (electric quadrupole or magnetic dipole) couplings. The physical or chemical exchange processes that dominate the MRD typically occur on a time scale of microseconds or longer, where the conventional perturbation theory of spin relaxation breaks down. There is thus a need for a more general relaxation theory. Such a theory, based on the stochastic Liouville equation (SLE) for the EMOR mechanism, is available for a single quadrupolar spin $I = 1$. Here, we present the corresponding theory for a dipole-coupled spin-1/2 pair. To our knowledge, this is the first treatment of dipolar MRD outside the motional-narrowing regime. Based on an analytical solution of the spatial part of the SLE, we show how the integral longitudinal relaxation rate can be computed efficiently. Both like and unlike spins, with selective or non-selective excitation, are treated. For the experimentally important dilute regime, where only a small fraction of the spin pairs are immobilized, we obtain simple analytical expressions for the auto-relaxation and cross-relaxation rates which generalize the well-known Solomon equations. These generalized results will be useful in biophysical studies, e.g., of intermittent protein dynamics. In addition, they represent a first step towards a rigorous theory of water ^{1}H relaxation in biological tissues, which is a prerequisite for unravelling the molecular basis of soft-tissue contrast in clinical magnetic resonance imaging. [http://dx.doi.org/10.1063/1.4824105]

I. INTRODUCTION

Nuclear spin relaxation is among the most powerful and versatile techniques available for studying molecular motions in liquids and solids.[1] However, in complex biological or colloidal samples, where motions occur on multiple time scales, the interpretation of single-field spin relaxation data tends to be model-dependent. This ambiguity can be minimized by measuring, with the aid of the field-cycling technique,[2–4] the longitudinal relaxation rate R_1 over a correspondingly wide field/frequency range. For a quantitative analysis of such magnetic relaxation dispersion (MRD) data, a rigorous theoretical link between R_1 and the molecular parameters is needed.

Typically, this link is provided by the Bloch-Wangsness-Redfield (BWR) theory of nuclear spin relaxation.[1,5] This perturbation theory is valid when the molecular motion is fast compared to the nuclear interaction (in frequency units) that it modulates, as is usually the case in liquids. But MRD experiments are increasingly performed on samples where this so-called motional-narrowing condition may be violated. For example, this is the case in samples containing immobilized macromolecules immersed in a mobile solvent, e.g, polymer hydrogels, cross-linked proteins, or more complex biological samples like cells and tissues.

From a nuclear magnetic resonance (NMR) point of view, such samples have both solid-like and liquid-like features. Nuclear spins residing permanently in the immobilized macromolecules give rise to wide NMR spectra typical of solids. However, for spins that are only transiently associated with the macromolecules and exchange chemically or physically with the solvent phase, the NMR properties are liquid-like provided that the immobilized macromolecules are isotropically distributed so that anisotropic nuclear spin couplings are averaged out. In such samples, the need to go beyond the conventional BWR theory arises whenever the mean survival time of the macromolecule-bound spin is comparable to, or longer than, the inverse of the anisotropic nuclear spin coupling that it experiences in the bound state.

In samples of this kind, exchange plays a dual role. On the one hand, exchange transfers magnetization between the macromolecule and the solvent. On the other hand, exchange randomizes the orientation of the anisotropic nuclear spin interaction tensor and thereby induces spin relaxation. For

a)Author to whom correspondence should be addressed. Electronic mail: bertil.halle@bpc.lu.se.

this relaxation mechanism, known as exchange-mediated orientational randomization (EMOR),[6] the motional-narrowing regime coincides with the fast-exchange regime. We have recently presented a general theory of nuclear spin relaxation by the EMOR mechanism for the case of a single spin $I = 1$ with an asymmetric quadrupole coupling.[6] This non-perturbative theory is based on the stochastic Liouville equation[7,8] and it is valid for arbitrary values of the exchange time, quadrupole coupling, and Larmor frequency.

Here, we present the corresponding theory for a dipole-coupled spin-1/2 pair. While the BWR theory of dipolar relaxation of a spin-1/2 pair is well established,[1,5,9,10] only a few studies have considered dipolar relaxation outside the motional-narrowing regime. The stochastic Liouville equation has been solved numerically to obtain lineshapes for an intramolecular dipole coupling modulated by rotational diffusion[11] or for an intermolecular dipole coupling (with the nonsecular parts neglected) modulated by translational diffusion.[12] Another numerical study of this kind considered longitudinal intramolecular dipolar relaxation in the presence of a fast internal motion, but only in the high-field limit.[13]

Here, we present numerical as well as analytical results for longitudinal relaxation of like and unlike spin-1/2 pairs with a dipole coupling (including the nonsecular parts) modulated by the EMOR mechanism. Special attention is devoted to the experimentally important dilute regime, where only a small fraction of the spins are associated with immobilized macromolecules. For this regime, we obtain highly accurate analytical approximations that generalize the well-known BWR results for the auto-relaxation and cross-relaxation rates.[1,14]

A major motivation for the present work is the need for a rigorous theory of the water ^{1}H MRD from gels and biological tissues. The spin-1/2 pair may then be identified with either the two protons in a water molecule or with a labile macromolecular proton and another (labile or nonlabile) proton. In the past, such data have been interpreted[15–17] with semi-phenomenological models involving dubious assumptions about the relaxation-inducing motions.[18,19] Previous water ^{1}H MRD studies of biopolymer gels from this laboratory[19,20] made use of a nonrigorous extension of the multi-spin Solomon equations to conditions outside the motional-narrowing regime. For a two-spin system, this approach[18] is closely related to a well-known result[21] for two-phase relaxation in the dilute regime. With the rigorous results presented here, the accuracy of this approximation can be assessed. The results presented here may also be seen as the first step towards a rigorous theoretical foundation of relaxation contrast in magnetic resonance imaging of soft tissues, in particular, in conjunction with field cycling.[22]

The outline of this paper is as follows. Section II summarizes the salient features of the dipolar EMOR model. Further details can be found in the preceding EMOR publications.[6,23] An overview is presented of the three exchange scenarios treated here, where the two spins exchange together, where only one of them exchanges or where they exchange independently. In Sec. III, we treat the stochastic Liouville equation and its analytical solution. This section closely parallels the corresponding development for the spin $I = 1$ case, except that the spin Liouville space is now spanned by 16 (rather than 9) spin operators.

In Sec. IV, we calculate the MRD for unlike (heteronuclear) spin pairs with selective or non-selective excitation. Rather than computing the time evolution of the magnetization and extracting R_1 from an exponential fit,[13] we focus on the integral relaxation rate $\widehat{R}_1$, defined as the inverse of the time integral of the normalized magnetization. This quantity can be obtained more directly and, moreover, it is well-defined (and measurable) whether relaxation is exponential or not. For samples with an abundant solvent phase (i.e., in the dilute regime), relaxation is usually found to be exponential within experimental accuracy. The integral rate $\widehat{R}_1$ can then be identified with the usual longitudinal relaxation rate R_1. We derive analytical approximations for the auto-relaxation and cross-relaxation rates that make up $\widehat{R}_1$ and we show that these simple results are highly accurate. We also consider various limiting cases of the general theory and we delineate the quantitative breakdown of the previously used nonrigorous extension of the Solomon equations.[18–20]

In Sec. V, we calculate the MRD for like (homonuclear) spin pairs, e.g., two protons, along the same lines as in Sec. IV. Finally, in Sec. VI, we generalize the basic EMOR model by including the effects of fast internal motions in the macromolecular and solvent phases as well as the effect of kinetic heterogeneity. Lengthy derivations are relegated to Appendices A–F of the supplementary material.[24]

II. MODEL

A. Spin Hamiltonian

We consider an ensemble of "isolated" nuclear spin pairs with $I = S = 1/2$. Each spin is subject to a Zeeman (Z) coupling with the external magnetic field $\boldsymbol{B}_0$ and the two spins experience a mutual magnetic dipole (D) coupling. The molecular system is spatially heterogeneous and this is modeled by assigning each spin pair to either of two states. In the isotropic bulk (B) state, the dipole coupling is averaged to zero, leaving only the Zeeman coupling. (Previously,[6] the B state was denoted by I.) In the anisotropic (A) state, the spin pair experiences, in addition to the Zeeman coupling, a (residual) dipole coupling.

The relative equilibrium population of spin pairs in the two states is denoted by P_A and $P_\mathrm{B} = 1 - P_\mathrm{A}$. The A and B state populations are chemically homogeneous, but each of the N_A spin pairs in the A state is distinguished by the orientation Ω_α of the internuclear vector $\boldsymbol{r}_{IS}$ relative to the $\boldsymbol{B}_0$ field. We refer to these distinguishable members of the A state as sites and label them with the index $\alpha = 1, 2, \ldots, N_\mathrm{A}$. For notational convenience, we use the site label $\alpha = 0$ to refer to the B state. It follows then that *site* populations P_α are related to *state* populations as follows: $P_\alpha = P_\mathrm{B}$ for $\alpha = 0$ and $P_\alpha = P_\mathrm{A}/N_\mathrm{A}$ for $\alpha \geq 1$.

The spin Hamiltonians for the two states are

$$\mathcal{H}_\mathrm{B} = \mathcal{H}_\mathrm{Z}, \tag{2.1a}$$

$$\mathcal{H}_{\mathrm{A}\alpha} = \mathcal{H}_\mathrm{Z} + \mathcal{H}_{\mathrm{D}\alpha}. \tag{2.1b}$$

The Zeeman Hamiltonian is

$$\mathcal{H}_{\rm Z} = \omega_{\rm I}\, I_z + \omega_{\rm S}\, S_z, \tag{2.2}$$

where $\omega_{\rm I}$ and $\omega_{\rm S}$ are the static Larmor frequencies of the two spins averaged over all sites. The fluctuating part of $\mathcal{H}_{\rm Z}$, due to exchange among sites with different chemical shift, does not affect the longitudinal relaxation of spin I since $[\mathcal{H}_{\rm Z}, I_z] = 0$.

The dipole Hamiltonian may be expressed as[1]

$$\mathcal{H}_{{\rm D}\alpha} = -\frac{\sqrt{6}}{3}\,\omega_{\rm D} \sum_{m=-2}^{2} T_m^2(11)\, C_{2,m}(\Omega_\alpha), \tag{2.3}$$

where the $T_m^2(11)$ are two-spin irreducible spherical tensor operators (Sec. III A), the $C_{2,\,m}(\Omega_\alpha)$ are (unnormalized) rank-2 spherical harmonics,[25] and $\Omega_\alpha \equiv (\theta_\alpha, \varphi_\alpha)$ are the spherical polar angles that specify the orientation of the internuclear vector $\boldsymbol{r}_{IS}$ in site α with respect to the lab-fixed frame (with the z axis along the $\boldsymbol{B}_0$ field). To simplify the analytical results, we define the dipole frequency $\omega_{\rm D}$ as

$$\omega_{\rm D} \equiv \frac{3}{2}\,\chi_{\rm D}, \tag{2.4}$$

with the dipole coupling constant $\chi_{\rm D}$ (in rad s^{-1}) given by

$$\chi_{\rm D} = \frac{\mu_0}{4\pi}\,\frac{|\gamma_I\,\gamma_S|\,\hbar}{r_{IS}^3}. \tag{2.5}$$

The dipole frequency $\omega_{\rm D}$ is taken to be the same in all A sites (this restriction is lifted in Sec. VI), which then differ only in the orientation Ω_α.

The electron-mediated scalar coupling between spins I and S can be ignored here since it is generally much weaker than the dipole coupling ($2\pi\,|J_{IS}| \ll \omega_{\rm D}$). The scalar coupling therefore does not contribute significantly to longitudinal relaxation by the EMOR mechanism, where both couplings are modulated by the same exchange process. Were it not for this exchange averaging, the scalar coupling should have been incorporated into the time-independent Hamiltonian along with $\mathcal{H}_{\rm Z}$. A homonuclear spin pair would then be strongly coupled at low field and weakly coupled at high field.[26,27] In the two-spin EMOR model, a homonuclear spin pair is always strongly coupled due to the large dipole coupling.

B. Like and unlike spins

We refer to spins I and S as "like" if

$$[(\omega_I - \omega_S)\,\tau_{\rm A}]^2 \ll 1 + (\omega_{\rm D}\,\tau_{\rm A})^2\,, \tag{2.6}$$

where $\tau_{\rm A}$ is the mean survival time of the spin pair in an A site (Sec. II C). If this inequality is satisfied, we can set $\omega_I = \omega_S$ and only the magnetic triplet state of the spin pair is relevant. The relaxation behavior of the dipole-coupled spin-1/2 pair is then analogous to that of a single spin $I = 1$ with a uniaxial quadrupole coupling,[6] except that the quadruple frequency $\omega_{\rm Q}$ is replaced by the dipole frequency $\omega_{\rm D}$. In practice, the like-spin case applies to homonuclear ($\gamma_I = \gamma_S$) spin pairs, in particular when both I and S are proton spins. If the inequality (2.6) is not satisfied, we refer to the spins as "unlike." In practice, this case applies to all heteronuclear ($\gamma_I \neq \gamma_S$) spin pairs. Results for the unlike-spin case are presented in Sec. IV, whereas the simpler like-spin case is considered in Sec. V.

C. Exchange scenarios

In the basic version of the EMOR model, relaxation is induced exclusively by the physical or chemical exchange of spins or spin pairs among sites. (In Sec. VI, we generalize the EMOR model to include effects of internal motions.) We distinguish three exchange cases: *IS* exchange, *I* exchange, and *I*/*S* exchange.

For *IS* exchange the intact spin pair exchanges physically without any covalent bond breaking. Like-spin *IS* exchange is best exemplified by the protons of a water molecule exchanging between the bulk solvent (B state) and an internal hydration site (A state) in a sample of immobilized macromolecules. In general, the two water protons are not magnetically equivalent in an internal hydration site, but the inequality (2.6) is satisfied so we can set $\omega_I = \omega_S$. An example of unlike-spin *IS* exchange is ^{1}H–^{19}F in the HF molecule or in partially fluorinated ethanol or acetate.

From a spin-dynamical point of view, *IS* exchange of a dipole-coupled spin pair is equivalent to exchange of a quadrupole-coupled single spin.[6] In both cases, exchange randomizes the orientation of the interaction tensor effectively instantaneously because, in the B state, the molecule rotates on a time scale that is short compared to the mean survival time $\tau_{\rm A}$ in an A site.[6,28] The spin dynamics can then be described by a stochastic Liouville equation involving an exchange operator W with the nonzero matrix elements in the site basis given by[6]

$$\langle 0|W|\alpha\rangle = \frac{1}{\tau_{\rm A}}, \tag{2.7a}$$

$$\langle \alpha|W|0\rangle = \frac{1}{N_{\rm A}\,\tau_{\rm B}}, \tag{2.7b}$$

$$\langle \alpha|W|\alpha\rangle = -\frac{1}{\tau_{\rm A}}, \tag{2.7c}$$

$$\langle 0|W|0\rangle = -\frac{1}{\tau_B}, \tag{2.7d}$$

where $\alpha \geq 1$ refers to an A site. Furthermore, the populations and mean survival times in the two states are linked by the equilibrium condition[6]

$$P_{\rm A}\,\tau_{\rm B} = P_{\rm B}\,\tau_{\rm A}. \tag{2.8}$$

An example of like-spin *I* exchange is a labile proton (*I*), such as a hydroxyl proton in a serine side-chain, dipole-coupled to a nearby nonlabile proton (*S*), such as a methylene proton next to the serine hydroxyl group. In this case, only the *I* spin undergoes exchange, e.g., between an immobilized hydroxyl group and bulk H_2O. *I* exchange modulates both the length and orientation of the internuclear vector $\boldsymbol{r}_{IS}$. Moreover, the orientational randomization is slower than for *IS* exchange (typically, nanoseconds rather than picoseconds) because it involves translational diffusion of the *I* spin (typically on a nanometer length scale). Nevertheless, because of its r_{IS}^{-3} dependence, the dipole coupling is strongly attenuated

once the I spin has exchanged. Moreover, the time scale for diffusional averaging of the tiny residual dipole coupling is typically short compared to τ_A. Therefore, also for I exchange, we can regard the EMOR process as effectively instantaneous.

An example of unlike-spin I exchange is a labile proton (I) covalently attached to a nitrogen atom (S), e.g., in a lysine, arginine, or histidine side-chain. The results presented in Sec. IV are valid for ^{15}N ($S = 1/2$), as in an isotope-labeled immobilized protein, but not for ^{14}N ($S = 1$). In the latter case, the dipole coupling is expected to be averaged out by fast (microsecond) quadrupolar ^{14}N relaxation rather than by proton exchange, which typically is much slower.[29] Because the I spin then undergoes "dipolar relaxation of the second kind," the mean survival time τ_A does not play the role of correlation time, as it does in the EMOR mechanism. For amide protons, τ_A is too long for this process to contribute significantly to I-spin relaxation. On the other hand, a more rapidly exchanging nearby proton, dipole-coupled to the amide proton, might mediate resonant cross-relaxation at the discrete MHz frequencies that correspond to transitions between the three nondegenerate eigenstates of the static ^{14}N spin Hamiltonian.[29]

Finally, I/S exchange refers to the case where both spins exchange independently, as when both I and S are labile protons. The dipole coupling is then averaged to zero by exchange of either spin. Again, we can use the same kinetic model as for IS exchange, but the correlation time is now shorter than the mean survival time of either spin: $\tau_A = (1/\tau_{A,1} + 1/\tau_{A,2})^{-1}$.

In summary, the same kinetic model can be used to describe EMOR relaxation in all three exchange scenarios. In each case, the I–S dipole coupling is spatially averaged to zero by the exchange process.

III. STOCHASTIC LIOUVILLE THEORY

A. Spin operator basis

In the direct-product space constructed from the 16-dimensional spin Liouville space (see below) and the (N_A + 1)-dimensional site space, the composite spin + site density operator $\sigma(t)$ evolves according to the stochastic Liouville equation,[7,8] which we express in operator notation (see Appendix A of the supplementary material[24]) as

$$\frac{\mathrm{d}}{\mathrm{d}t}\,\sigma(t) = (\mathcal{W} - i\,\mathcal{L})\,\sigma(t). \tag{3.1}$$

The Liouvillian $\mathcal{L} = \sum_\alpha |\alpha\rangle\mathcal{L}_\alpha\langle\alpha|$ is a superoperator in the direct-product space and it is trivially diagonal in the site basis. The superoperator $\mathcal{L}_\alpha \equiv [\mathcal{H}_\alpha, \dots]$ acts in spin Liouville space, which we represent by the spherical multipole basis, consisting of two-spin irreducible spherical tensor operators[25] $T^K_Q(k_I, k_S) \equiv |K\,Q\,k_I k_S)$ of rank $K = 0$, 1, or 2 and quantum order $Q = -K, -K+1, \dots, K-1, K$, formed as linear combinations of products of single-spin operators of ranks k_I and k_S (see Appendix B of the supplementary material[24]). The set of 16 such operators constitutes a complete orthonormal basis for a spin-1/2 pair:[30]

$$(K\,Q\,k_I k_S \,|\, K'Q'\,k'_I k'_S) = \delta_{KK'}\,\delta_{QQ'}\,\delta_{k_I k'_I}\,\delta_{k_S k'_S}. \tag{3.2}$$

TABLE I. Basis operators A_n with $Q = 0$.

n	Explicit form	Description
1	$I_z E_S$	Longitudinal I-spin magnetization
2	$E_I S_z$	Longitudinal S-spin magnetization
3	$2 I_z S_z$	Longitudinal two-spin order
4	$\frac{1}{\sqrt{2}}(I_- S_+ - I_+ S_-)$	Odd-rank zero-quantum coherence
5	$\frac{-1}{\sqrt{2}}(I_- S_+ + I_+ S_-)$	Even-rank zero-quantum coherence

For numerical work, we use a basis of 15 spin operators (the identity operator can be omitted), for brevity denoted by A_n with $n = 1, 2, \dots, 15$. The explicit form and ordering of the spin operators can be found in Appendix B of the supplementary material.[24] The operators A_1–A_5 with total projection quantum number $Q = 0$ are also given in Table I. Two of these operators (A_3 and A_5) are actually linear combinations of $T^K_0(k_I, k_S)$ operators (Appendix B of the supplementary material).[24]

The spin observables are related to a reduced density operator $\langle\sigma(t)\rangle$, obtained by averaging over the molecular degrees of freedom,[6,23]

$$\langle\sigma(t)\rangle = \sum_{\alpha=0}^{N_A}\sum_{\beta=0}^{N_A}\langle\alpha|\sigma(t)|\beta\rangle\,P_\beta, \tag{3.3}$$

where $\langle\alpha|\sigma(t)|\beta\rangle$ is the density operator for a sub-ensemble where the spin starts out ($t = 0$) in site β, with equilibrium population P_β, and ends up (at time t) in site α (see Appendix A of the supplementary material[24]). The projections of the reduced density operator on the basis operators are the so-called state multipoles,[30]

$$\sigma_Q^{K(k_I k_S)}(t) \equiv (K\,Q\,k_I k_S\,|\langle\sigma(t)\rangle). \tag{3.4}$$

Our focus here is on $\sigma_0^{1(10)}(t)$ and $\sigma_0^{1(01)}(t)$, which are proportional to the non-equilibrium longitudinal magnetizations, $I_z(t) - I_0$ and $S_z(t) - S_0$, respectively.

Laplace transforming the stochastic Liouville equation (3.1) and averaging over sites as in Eq. (3.3), we obtain[6]

$$\langle\widetilde{\sigma}(s)\rangle = \langle\widetilde{\mathcal{U}}(s)\rangle\,\sigma(0), \tag{3.5}$$

where we have introduced the site-averaged resolvent superoperator

$$\langle\widetilde{\mathcal{U}}(s)\rangle = \langle(s - \mathcal{W} + i\,\mathcal{L})^{-1}\rangle. \tag{3.6}$$

As before,[6] we assume that the number N_A of A sites is sufficiently large that Ω_α can be treated as a continuous variable Ω with a distribution function $f(\Omega)$. Furthermore, we assume that this distribution is isotropic,

$$f(\Omega) = \frac{1}{4\pi}. \tag{3.7}$$

Because of the rotational invariance implied by Eq. (3.7), any site-averaged superoperator derived from the Liouvillian $\mathcal{L}$, such as the resolvent superoperator $\langle\widetilde{\mathcal{U}}(s)\rangle$, must share the cylindrical symmetry of the $\boldsymbol{B}_0$ field. The Liouville-space Wigner-Eckart theorem then implies that all such

superoperators are block-diagonal ($Q = Q'$) in the multipole representation.[31] For example,

$$(K\,Q\,k_I k_S\,|\langle\widetilde{\mathcal{U}}(s)\rangle|\,K'Q'\,k'_I k'_S) = \delta_{QQ'}\,(K\,Q\,k_I k_S\,|\langle\widetilde{\mathcal{U}}(s)\rangle|\,K'\,Q\,k'_I k'_S). \tag{3.8}$$

Combination of Eqs. (3.4), (3.5), and (3.8) now yields for the Laplace transformed I-spin longitudinal magnetization

$$\widetilde{\sigma}_0^{1(10)}(s) = \sum_K \sum_{k_I} \sum_{k_S} (10\,10\,|\langle\widetilde{\mathcal{U}}(s)\rangle|\,K0\,k_I k_S)\sigma_0^{K(k_I k_S)}(0). \tag{3.9}$$

B. Formal solution

To compute the integral relaxation rate, defined in Sec. IV A, we need not compute the full time dependence of the reduced density operator $\langle\sigma(t)\rangle$. It is sufficient to obtain the time integral, that is, the Laplace transform at $s = 0$: $\int_0^\infty \mathrm{d}t\ \langle\sigma(t)\rangle = \langle\widetilde{\sigma}(0)\rangle$. Consequently, we need the site-averaged resolvent superoperator $\langle\widetilde{\mathcal{U}}(s=0)\rangle$, which, for the kinetic model considered here, takes the form[6]

$$\langle\widetilde{\mathcal{U}}(0)\rangle = \tau_\mathrm{A}\left[i\,\mathcal{L}_\mathrm{Z}\,\tau_\mathrm{A} + \frac{P_\mathrm{A}}{P_\mathrm{B}}\,(1-\mathcal{B})\right]^{-1} \times \left[P_\mathrm{B} + P_\mathrm{A}\left(2 + \frac{P_\mathrm{A}}{P_\mathrm{B}} + i\,\mathcal{L}_\mathrm{Z}\,\tau_\mathrm{A}\right)\mathcal{B}\right]. \tag{3.10}$$

Here, we have introduced the superoperator

$$\mathcal{B} \equiv \frac{1}{4\pi}\int \mathrm{d}\Omega\,[1 + i\,\mathcal{L}_\mathrm{Z}\,\tau_\mathrm{A} + i\,\mathcal{L}_\mathrm{D}(\Omega)\,\tau_\mathrm{A}]^{-1}, \tag{3.11}$$

where $\mathrm{d}\Omega = \mathrm{d}\varphi\,\mathrm{d}\theta\sin\theta$ is the element of solid angle. Further, $\mathcal{L}_\mathrm{Z} = [H_\mathrm{Z},\ ]$ and $\mathcal{L}_\mathrm{D}(\Omega) = [H_\mathrm{D}(\Omega),\ ]$ are the Liouvillians formed from the Hamiltonians in Eqs. (2.2) and (2.3), respectively. As discussed in Appendix C of the supplementary material,[24] Eq. (3.10) is exact only for the longitudinal 3×3 block ($n = 1, 2, 3$) of $\langle\widetilde{\mathcal{U}}(0)\rangle$, which is the only part that is needed here (Sec. IV). The matrix representations of the superoperators $\mathcal{L}_\mathrm{Z}$ and $\mathcal{L}_\mathrm{D}(\Omega)$ in the spherical multipole basis are given in Appendix D of the supplementary material.[24] The angular average in Eq. (3.11) was computed by Lebedev quadrature of order 131, corresponding to 5810 points on the unit sphere.[32,33]

IV. UNLIKE-SPIN RELAXATION DISPERSION

A. Integral relaxation rate

In the unlike-spin case, only one of the two spins, say I, is observed. Our objective is to describe the relaxation of the longitudinal I-spin magnetization under general conditions, including the slow-motion regime where the conventional BWR theory of spin relaxation fails. Under the conditions ($P_\mathrm{A} \ll 1$) of primary interest here, the longitudinal relaxation is generally observed to be exponential. The longitudinal relaxation time can then be identified with the time integral of the normalized non-equilibrium longitudinal magnetization, so the longitudinal relaxation rate can be expressed as

$$\widehat{R}_1 \equiv \left[\int_0^\infty \mathrm{d}t\,\frac{\sigma_1(t)}{\sigma_1(0)}\right]^{-1} = \frac{\sigma_1(0)}{\widetilde{\sigma}_1(0)}, \tag{4.1}$$

where $\widetilde{\sigma}_1(0) = \int_0^\infty \mathrm{d}t\ \sigma_1(t)$ is obtained from Eq. (3.9). Here, and in the following, we use the simplified n label (Table I) to specify components of the spin density matrix and elements of the resolvent supermatrix. The relaxation rate obtained from Eq. (4.1) is referred to as the integral relaxation rate, $\widehat{R}_1$. When relaxation is exponential, $\sigma_1(t) = \sigma_1(0)\exp(-R_1\,t)$, then $\widehat{R}_1$ is identical to the longitudinal relaxation rate R_1. But the integral rate $\widehat{R}_1$ can be computed and measured even when relaxation is non-exponential. We therefore use a notation that distinguishes (with a caret) the more general integral relaxation rate.

In the case of selective excitation of the unlike spin pair, when only the observed I spin has a nonzero nonequilibrium longitudinal magnetization at $t = 0$, we obtain from Eqs. (3.9) and (4.1):

$$\widehat{R}_1^\mathrm{US} = \frac{1}{(1\,|\langle\widetilde{\mathcal{U}}(0)\rangle|\,1)}, \tag{4.2}$$

where the superscript US refers to unlike spins and selective excitation. (Selective excitation of the S spin is not considered here, since the integral relaxation rate is not useful in this case.)

In the case of nonselective excitation, which applies generally to field-cycling experiments with the initial nonequilibrium state prepared by rapidly changing the magnitude of the $\boldsymbol{B}_0$ field, Eq. (3.9) yields

$$\widetilde{\sigma}_1(0) = (1\,|\langle\widetilde{\mathcal{U}}(0)\rangle|\,1)\,\sigma_1(0) + (1\,|\langle\widetilde{\mathcal{U}}(0)\rangle|\,2)\,\sigma_2(0). \tag{4.3}$$

For a heteronuclear spin pair, we have $\sigma_2(0) = \kappa\,\sigma_1(0)$, with $\kappa \equiv \gamma_S/\gamma_I$, so that Eqs. (4.1) and (4.3) yield

$$\widehat{R}_1^\mathrm{UN} = \frac{1}{(1\,|\langle\widetilde{\mathcal{U}}(0)\rangle|\,1) + \kappa\,(1\,|\langle\widetilde{\mathcal{U}}(0)\rangle|\,2)}. \tag{4.4}$$

B. Dilute regime

In the dilute regime, where only a small fraction of the nuclei reside in state A so that $P_\mathrm{A} \ll 1$ and $P_\mathrm{B} \approx 1$, the resolvent superoperator in Eq. (3.10) simplifies to

$$\langle\widetilde{\mathcal{U}}(0)\rangle = (\,\Gamma + i\,\mathcal{L}_\mathrm{Z}\,)^{-1}, \tag{4.5}$$

with

$$\Gamma \equiv \frac{P_\mathrm{A}}{\tau_\mathrm{A}}\,(1-\mathcal{B}). \tag{4.6}$$

In the like-spin case (Sec. V), as well as for a single spin $I = 1$,[6] we can simply drop $\mathcal{L}_\mathrm{Z}$ in Eq. (4.5) because the $Q = 0$ block of $\mathcal{L}_\mathrm{Z}$ is then a null matrix. In the unlike-spin case, we cannot omit $\mathcal{L}_\mathrm{Z}$ since the $Q = 0$ block of $\mathcal{L}_\mathrm{Z}$ has off-diagonal elements, proportional to $\omega_I - \omega_S$, linking the two zero-quantum coherences ($n = 4$ and 5 in Table I and Appendix D of the supplementary material[24]). However, the longitudinal 3×3 block of $\langle\widetilde{\mathcal{U}}(0)\rangle$ is equal to the inverse of the corresponding block of Γ (but differs from the longitudinal block of Γ^{-1}). Therefore, the integral relaxation rates

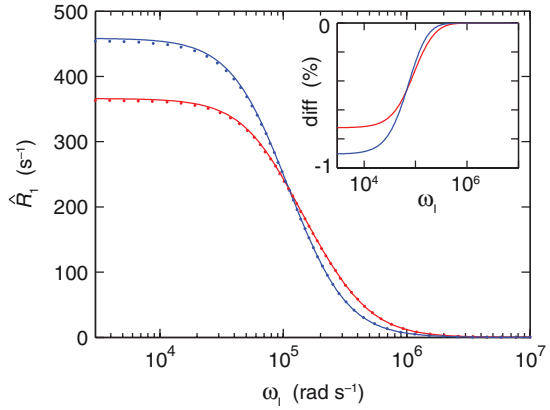

FIG. 1. Dispersion of the unlike-spin integral relaxation rates $\widehat{R}_1^{\rm US}$ (red) and $\widehat{R}_1^{\rm UN}$ (blue), computed exactly (solid curves) and in the dilute approximation (dots) for $P_{\rm A} = 10^{-2}$, $\tau_{\rm A} = 10$ μs, $\chi_{\rm D} = 10^5$ rad s^{-1}, and $\kappa = 0.9412$ (as for a ^{1}H–^{19}F spin pair). The inset shows the relative error of the dilute approximation, defined as $[R_1^{\rm dilute}(\omega_I) - R_1^{\rm exact}(\omega_I)]/R_1^{\rm exact}(0)$.

$\widehat{R}_1^{\rm US}$ and $\widehat{R}_1^{\rm UN}$ are rigorously proportional to $P_{\rm A}$ in the dilute regime, despite the $\mathcal{L}_{\rm Z}$ term in Eq. (4.5).

Figure 1 shows the dispersions of the two integral relaxation rates obtained from Eqs. (4.2) and (4.4) with the resolvent matrix elements computed either from the exact Eq. (3.10) or from the dilute-regime approximation in Eq. (4.5). Even for $P_{\rm A} = 0.01$, the approximate results differ by less than 1% from the exact results. The maximum error in $\widehat{R}_1^{\rm US}$ ($\widehat{R}_1^{\rm UN}$) varies from −0.02 (−0.03)% to −1.6 (−1.3)% when $\tau_{\rm A}$ increases from 1 to 100 μs at $\chi_{\rm D} = 10^5$ rad s^{-1}. In most applications,[15,16,19,20,34] $P_{\rm A} < 10^{-3}$ and Eq. (4.5) is highly accurate (maximum error −0.2%).

C. Analytical approximations

Even though the integral relaxation rates can be obtained numerically with modest computational effort, closed-form analytical approximations offer conceptual insight. Analytical results are readily obtained in two limiting regimes. In the motional-narrowing regime, here defined as

$$(\omega_{\rm D}\,\tau_{\rm A})^2 \ll 1 + [(|\omega_I| - |\omega_S|)\,\tau_{\rm A}]^2\,, \tag{4.7}$$

the relaxation behavior of a spin-1/2 pair is well-known.[1,14] For the EMOR model, analytical results can also be obtained, as previously shown for the quadrupolar case,[6,23] in the low-field limit, here defined as

$$[(|\omega_I| + |\omega_S|)\,\tau_{\rm A}]^2 \ll 1 + (\omega_{\rm D}\,\tau_{\rm A})^2\,. \tag{4.8}$$

In the following, we present analytical results for the dilute regime ($P_{\rm A} \ll 1$) that are exact in the both of these limits, and, for many purposes, remain sufficiently accurate for all values of $\tau_{\rm A}$, $\omega_{\rm D}$, $\omega_{\rm I}$, and $\omega_{\rm S}$.

The starting point is Eq. (3.5) with $s = 0$. Operating with $\langle\widetilde{\mathcal{U}}(0)\rangle^{-1}$ on both members and making use of Eq. (4.5), valid in the dilute regime, we obtain

$$\sum_p \big[\,(n\,|\Gamma|\,p) + i\,(n\,|\mathcal{L}_{\rm Z}|\,p)\,\big]\,\widetilde{\sigma}_p(0) = \sigma_n(0). \tag{4.9}$$

The second term within brackets can be dropped since $(n\,|\mathcal{L}_{\rm Z}|\,p) = 0$ for $n = 1$ or 2 (Appendix D of the supplementary material[24]). Furthermore, in the motional-narrowing and low-field regimes, the $Q = 0$ block of the block-diagonal $\mathbf{\Gamma}$ supermatrix is itself block-diagonal with a decoupled 2×2 magnetization block ($n, p = 1, 2$). In the motional-narrowing regime, this simplification corresponds to the well-known[9,10] fact that the magnetizations evolve independently from the longitudinal two-spin order because the corresponding spin operators have different symmetry with respect to total spin inversion.[31] The approximation made here corresponds to neglecting the dynamical coupling between the magnetizations and the two-spin order under all conditions, not just in the motional-narrowing and low-field regimes. In the like-spin case (Sec. V), this amounts to neglecting the dynamical coupling between the (total) magnetization ($T_0^1 \sim I_z$) and the rank-2 polarization ($T_0^2 \sim 3I_z^2 - 1$). In the spin $I = 1$ case, this was referred to as the exponential approximation.[6]

From Eq. (4.9), we thus obtain a closed system of two equations, with solution

$$\widetilde{\sigma}_1(0) = \frac{\rho_S\,\sigma_1(0) - \sigma_{IS}\,\sigma_2(0)}{\rho_I\,\rho_S - \sigma_{IS}\,\sigma_{SI}}, \tag{4.10}$$

where we have defined the generalized auto-relaxation and cross-relaxation rates

$$\rho_I \equiv (1\,|\Gamma|\,1) = P_{\rm A}\,\frac{1 - (1\,|\mathcal{B}|\,1)}{\tau_{\rm A}}, \tag{4.11a}$$

$$\rho_S \equiv (2\,|\Gamma|\,2) = P_{\rm A}\,\frac{1 - (2\,|\mathcal{B}|\,2)}{\tau_{\rm A}}, \tag{4.11b}$$

$$\sigma_{IS} \equiv (1\,|\Gamma|\,2) = -\,P_{\rm A}\,\frac{(1\,|\mathcal{B}|\,2)}{\tau_{\rm A}}, \tag{4.11c}$$

$$\sigma_{SI} \equiv (2\,|\Gamma|\,1) = -\,P_{\rm A}\,\frac{(2\,|\mathcal{B}|\,1)}{\tau_{\rm A}}. \tag{4.11d}$$

Combination of Eqs. (4.1) and (4.10) yields for the integral relaxation rates

$$\widehat{R}_1^{\rm US} = \rho_I - \frac{\sigma_{IS}\,\sigma_{SI}}{\rho_S}, \tag{4.12}$$

$$\widehat{R}_1^{\rm UN} = \frac{\rho_I\,\rho_S - \sigma_{IS}\,\sigma_{SI}}{\rho_S - \kappa\,\sigma_{IS}}. \tag{4.13}$$

By introducing a further approximation, where we neglect cross terms of order $[(\omega_I\tau_{\rm A})(\omega_D\tau_{\rm A})]^n$ and $[(\omega_S\tau_{\rm A})(\omega_D\tau_{\rm A})]^n$ with $n \geq 2$, we show in Appendices E and F of the supplementary material[24] that the generalized auto-relaxation and cross-relaxation rates in Eqs. (4.11a)–(4.11d) can be expressed on the following simple analytical forms,

$$\begin{aligned}\rho_I = P_{\rm A}\,\chi_{\rm D}^2 \Bigg\{ &\frac{0.1\,\tau_{\rm A}}{1 + (\omega_{\rm D}\tau_{\rm A})^2\,\eta_D/3 + [(\omega_{\rm I} - \omega_{\rm S})\tau_{\rm A}]^2} \\ &+ \frac{0.15\,\tau_{\rm A}}{1 + (\omega_{\rm D}\tau_{\rm A})^2\,\eta_D/3 + (\omega_{\rm I}\tau_{\rm A})^2} \\ &+ \frac{0.15\,\tau_{\rm A}}{1 + (\omega_{\rm D}\tau_{\rm A})^2 + (\omega_{\rm I}\,\tau_{\rm A})^2} \\ &+ \frac{0.6\,\tau_{\rm A}}{1 + (\omega_{\rm D}\tau_{\rm A})^2 + [(\omega_{\rm I} + \omega_{\rm S})\,\tau_{\rm A}]^2} \Bigg\},\end{aligned} \tag{4.14}$$

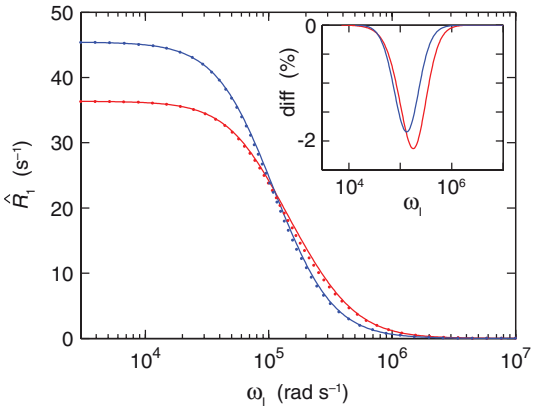

FIG. 2. Dispersion of the unlike-spin integral relaxation rates $\widehat{R}_1^{\rm US}$ (red) and $\widehat{R}_1^{\rm UN}$ (blue) in the dilute regime, computed numerically (solid curves) and from analytical approximations (dots) for $P_{\rm A} = 10^{-3}$, $\tau_{\rm A} = 10$ μs, $\chi_{\rm D} = 10^5$ rad s^{-1}, and $\kappa = 0.9412$. The inset shows the relative error of the approximation, defined as $[R_1^{\rm approx}(\omega_I) - R_1^{\rm exact}(\omega_I)]/R_1^{\rm exact}(0)$.

$$\sigma_{IS} = P_{\rm A}\,\chi_{\rm D}^2\left\{-\frac{0.1\,\tau_{\rm A}}{1+(\omega_{\rm D}\tau_{\rm A})^2\,\eta_D/3+[(\omega_{\rm I}-\omega_{\rm S})\tau_{\rm A}]^2}\right.$$
$$-\frac{0.15\,\tau_{\rm A}}{1+(\omega_{\rm D}\tau_{\rm A})^2\,\eta_D/3+(\omega_{\rm I}\tau_{\rm A})^2}$$
$$+\frac{0.15\,\tau_{\rm A}}{1+(\omega_{\rm D}\tau_{\rm A})^2+(\omega_{\rm I}\,\tau_{\rm A})^2}$$
$$\left.+\frac{0.6\,\tau_{\rm A}}{1+(\omega_{\rm D}\tau_{\rm A})^2+[(\omega_{\rm I}+\omega_{\rm S})\tau_{\rm A}]^2}\right\}, \tag{4.15}$$

where

$$\eta_D \equiv \frac{1+(\chi_{\rm D}\tau_{\rm A})^2/3}{1+(\chi_{\rm D}\tau_{\rm A})^2/2}. \tag{4.16}$$

The rates ρ_S and σ_{SI} are obtained by interchanging ω_I and ω_S everywhere in Eqs. (4.14) and (4.15).

In Fig. 2, we compare the approximate analytical rates given by Eqs. (4.12)–(4.16) with the corresponding rates computed numerically using Eq. (4.5), which is virtually exact at $P_{\rm A} = 10^{-3}$. The approximate analytical rates coincide with the exact rates at the high-frequency end of the dispersion, where the motional-narrowing condition (4.7) is satisfied, and also at the low-frequency end, where the low-field condition (4.8) is satisfied. Even at intermediate frequencies, where neither condition is satisfied, the analytical expressions remain quite accurate with a maximum error of ∼−2% for the parameter values used in Fig. 2. The maximum error in $\widehat{R}_1^{\rm US}$ ($\widehat{R}_1^{\rm UN}$) varies from −0.03 (−0.03)% to −10.0 (−5.6)% when $\tau_{\rm A}$ increases from 1 to 100 μs at $\chi_{\rm D} = 10^5$ rad s^{-1}.

D. Limiting forms

In the motional-narrowing regime, where the inequality (4.7) holds, Eqs. (4.14) and (4.15) reduce to the familiar[1,14] forms

$$\rho_I = P_{\rm A}\,\chi_{\rm D}^2\left\{\frac{0.1\,\tau_{\rm A}}{1+[(\omega_{\rm I}-\omega_{\rm S})\tau_{\rm A}]^2}\right.$$
$$\left.+\frac{0.3\,\tau_{\rm A}}{1+(\omega_{\rm I}\tau_{\rm A})^2}+\frac{0.6\,\tau_{\rm A}}{1+[(\omega_{\rm I}+\omega_{\rm S})\,\tau_{\rm A}]^2}\right\}, \tag{4.17}$$

$$\sigma_{IS} = \sigma_{SI} = P_{\rm A}\,\chi_{\rm D}^2\left\{-\frac{0.1\,\tau_{\rm A}}{1+[(\omega_{\rm I}-\omega_{\rm S})\tau_{\rm A}]^2}\right.$$
$$\left.+\frac{0.6\,\tau_{\rm A}}{1+[(\omega_{\rm I}+\omega_{\rm S})\tau_{\rm A}]^2}\right\}. \tag{4.18}$$

In the low-field regime, where the inequality (4.8) holds, Eqs. (4.14) and (4.15) and the analogous expressions for ρ_S and σ_{SI} reduce to

$$\rho_I = \rho_S = P_{\rm A}\,\chi_{\rm D}^2\left\{\frac{0.75\,\tau_{\rm A}}{1+(\omega_{\rm D}\tau_{\rm A})^2}+\frac{0.25\,\tau_{\rm A}}{1+(\omega_{\rm D}\tau_{\rm A})^2\,\eta_D/3}\right\}, \tag{4.19}$$

$$\sigma_{IS} = \sigma_{SI} = P_{\rm A}\,\chi_{\rm D}^2\left\{\frac{0.75\,\tau_{\rm A}}{1+(\omega_{\rm D}\tau_{\rm A})^2}-\frac{0.25\,\tau_{\rm A}}{1+(\omega_{\rm D}\tau_{\rm A})^2\,\eta_D/3}\right\}. \tag{4.20}$$

Equation (4.20) implies that, in the low-field regime, $\sigma_{IS} = \sigma_{SI} = 0$ for $\omega_{\rm D}\tau_{\rm A} = 3$. For this special case, $\widehat{R}_1^{\rm US} = \widehat{R}_1^{\rm UN} = \rho_I$, as expected.

Combination of Eqs. (4.12), (4.13), (4.19), and (4.20) yields for the zero-frequency limit of the integral relaxation rates in the dilute regime

$$\widehat{R}_1^{\rm US}(0) = \frac{3}{4}\,P_{\rm A}\,\chi_{\rm D}^2\,\frac{\tau_{\rm A}}{1+(\omega_{\rm D}\tau_{\rm A})^2\,(1+\eta_{\rm D})/4}, \tag{4.21}$$

$$\widehat{R}_1^{\rm UN}(0) = \frac{3}{4}\,P_{\rm A}\,\chi_{\rm D}^2\,\frac{\tau_{\rm A}}{1-\kappa/2+(\omega_{\rm D}\tau_{\rm A})^2\,[1+\eta_{\rm D}+\kappa\,(1-\eta_{\rm D})]/4}. \tag{4.22}$$

Note that these two expressions are exact in the dilute regime. Figure 3 shows the variation of $\widehat{R}_1^{\rm US}(0)$ and $\widehat{R}_1^{\rm UN}(0)$ with $\tau_{\rm A}$. The maximum relaxation rate occurs at $\tau_{\rm A} \approx 1/\chi_{\rm D}$ for $\widehat{R}_1^{\rm US}(0)$ and at $\tau_{\rm A} \approx (1-\kappa/2)^{1/2}/\chi_{\rm D}$ for $\widehat{R}_1^{\rm UN}(0)$. This maximum is reminiscent of the transition from fast to slow exchange in a two-state exchange model with a sparsely populated high-relaxivity state.[21,35] However, in the EMOR model, the survival time is also the correlation time for the high-relaxivity state so "fast exchange" corresponds to the motional-narrowing regime. The maximum in $\widehat{R}_1(0)$ thus signals the breakdown of the motional-narrowing approximation.

Figure 4 shows normalized dispersions $\widehat{R}_1^{\rm US}(\omega_I)/\widehat{R}_1^{\rm US}(0)$ and $\widehat{R}_1^{\rm UN}(\omega_I)/\widehat{R}_1^{\rm UN}(0)$ for different values of the mean survival time $\tau_{\rm A}$. As expected, the dispersion shifts to lower frequency as site exchange is slowed down (making $\tau_{\rm A}$ longer). However, when $\tau_{\rm A}$ becomes longer than $1/\omega_{\rm D}$ (10 μs in Fig. 4), the position of the profile is less affected and in the ultraslow-motion limit, where $(\omega_{\rm D}\tau_{\rm A})^2 \gg 1$, the profile remains fixed on the $\omega_{\rm I}$ axis but decreases in amplitude on further increase of $\tau_{\rm A}$. In the ultraslow-motion limit, Eqs. (4.14) and (4.15)

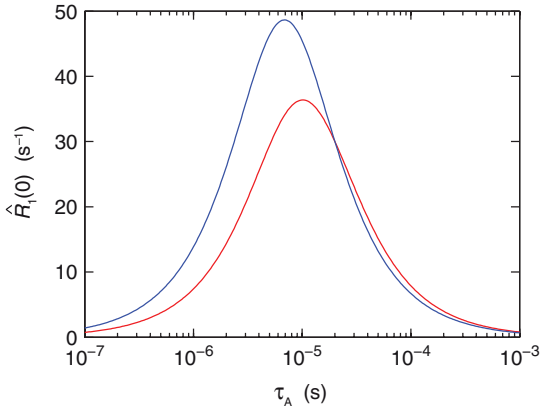

FIG. 3. Low-frequency limit of the unlike-spin integral relaxation rates $\widehat{R}_1^{\mathrm{US}}$ (red) and $\widehat{R}_1^{\mathrm{UN}}$ (blue) versus mean survival time τ_{A} for $P_{\mathrm{A}} = 10^{-3}$, $\chi_{\mathrm{D}} = 10^5$ rad s^{-1}, and $\kappa = 0.9412$ (only affects $\widehat{R}_1^{\mathrm{UN}}$).

yield

$$\rho_I = \frac{4}{9}\frac{P_{\mathrm{A}}}{\tau_{\mathrm{A}}}\left\{\frac{0.1}{\eta_{\mathrm{D}}/3 + [(\omega_{\mathrm{I}} - \omega_{\mathrm{S}})/\omega_{\mathrm{D}}]^2} + \frac{0.15}{\eta_{\mathrm{D}}/3 + (\omega_{\mathrm{I}}/\omega_{\mathrm{D}})^2} + \frac{0.15}{1 + (\omega_{\mathrm{I}}/\omega_{\mathrm{D}})^2} + \frac{0.6}{1 + [(\omega_{\mathrm{I}} + \omega_{\mathrm{S}})/\omega_{\mathrm{D}}]^2}\right\}, \tag{4.23}$$

$$\sigma_{IS} = \frac{4}{9}\frac{P_{\mathrm{A}}}{\tau_{\mathrm{A}}}\left\{-\frac{0.1}{\eta_{\mathrm{D}}/3 + [(\omega_{\mathrm{I}} - \omega_{\mathrm{S}})/\omega_{\mathrm{D}}]^2} + \frac{0.15}{\eta_{\mathrm{D}}/3 + (\omega_{\mathrm{I}}/\omega_{\mathrm{D}})^2} + \frac{0.15}{1 + (\omega_{\mathrm{I}}/\omega_{\mathrm{D}})^2} + \frac{0.6}{1 + [(\omega_{\mathrm{I}} + \omega_{\mathrm{S}})/\omega_{\mathrm{D}}]^2}\right\}, \tag{4.24}$$

showing that the effective correlation time is $\sim 1/\omega_{\mathrm{D}}$. In this limit, information about site exchange kinetics is contained in the zero-frequency rate, but not in the position (and shape) of the dispersion profile on the frequency axis. As seen from Fig. 4, while the analytical expressions based on Eqs. (4.14) and (4.15) are highly accurate in the slow-motion regime (and exact in the motional-narrowing regime), they are less accurate in the ultraslow-motion limit, particularly for $\widehat{R}_1^{\mathrm{US}}(\omega_I)$.

As the ultraslow-motion limit is approached, the dispersion profile becomes steeper. This feature, which is most pronounced for $\widehat{R}_1^{\mathrm{US}}(\omega_I)$, is not captured by the analytical approximations based on Eqs. (4.23) and (4.24). Because the dispersion changes shape, the low-frequency part of the dispersion actually shifts to higher frequency with increasing τ_{A} close to the ultraslow-motion limit (Fig. 4(a)).

In the ultraslow-motion limit, the dispersion profile has a characteristic temperature dependence: the amplitude grows with increasing temperature, while the shape and position on the ω_{I} axis are invariant. This follows since the dipole frequency ω_{D} is essentially independent of temperature.

E. Breakdown of the motional-narrowing approximation

In the motional-narrowing regime, the integral relaxation rates $\widehat{R}_1^{\mathrm{US}}$ and $\widehat{R}_1^{\mathrm{UN}}$ for the dilute regime are obtained by substituting Eqs. (4.17) and (4.18) into Eqs. (4.12) and (4.13). Within the context of a two-state exchange model, this result

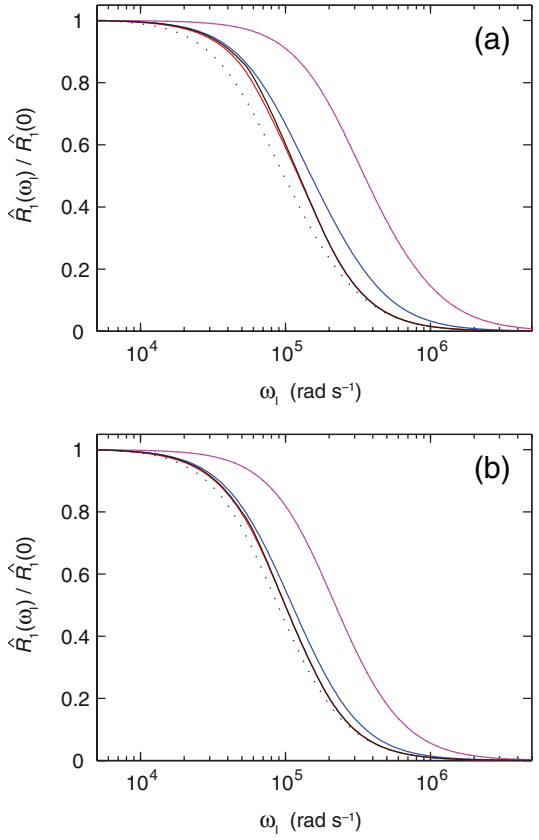

FIG. 4. Normalized dispersion of the dilute-regime integral relaxation rates **(a)** $\widehat{R}_1^{\mathrm{US}}$ and **(b)** $\widehat{R}_1^{\mathrm{UN}}$ for $P_{\mathrm{A}} = 10^{-3}$, $\chi_{\mathrm{D}} = 10^5$ rad s^{-1}, $\kappa = 0.9412$, and different τ_{A}: 3 μs (magenta), 10 μs (blue), 0.1 ms (red), and 1 ms (black). The dispersion profiles were computed numerically (solid curves) and, for the shortest and longest τ_{A}, also from analytical approximations (dots).

corresponds to the fast-exchange limit. However, when $\omega_{\mathrm{D}}\,\tau_{\mathrm{A}}$ is sufficiently large to violate the inequality (4.7), these fast-exchange (or motional-narrowing) expressions greatly overestimate the exact integral relaxation rates, as computed with Eqs. (4.2), (4.4), and (4.5).

A plausible but nonrigorous extension of the fast-exchange result has been suggested,[18] where

$$\widehat{R}_1 = \frac{P_{\mathrm{A}}}{\tau_{\mathrm{A}} + 1/\widehat{R}_{1,\mathrm{A}}}, \tag{4.25}$$

and with the intrinsic integral relaxation rate $\widehat{R}_{1,\mathrm{A}}$ in state A given by expressions like Eqs. (4.12) and (4.13), but with intrinsic auto-relaxation and cross-relaxation rates obtained from Eqs. (4.17) and (4.18) after setting $P_{\mathrm{A}} = 1$. The expression (4.25) is of the same form as a well-known result[21] for the dilute regime, derived from the extended Bloch equations[35] (which do not take dipolar cross-relaxation into account). Equation (4.25) is the two-spin version of an approximate result previously derived for a homonuclear multispin system.[18]

In Fig. 5, we compare Eq. (4.25) with the exact dilute-regime result based on Eq. (4.5). As expected, the two results agree at high frequencies, where the motional-narrowing condition (4.7) is obeyed, but diverge substantially at lower frequencies. The maximum error in $\widehat{R}_1^{\mathrm{US}}$ ($\widehat{R}_1^{\mathrm{UN}}$) varies from 0.4

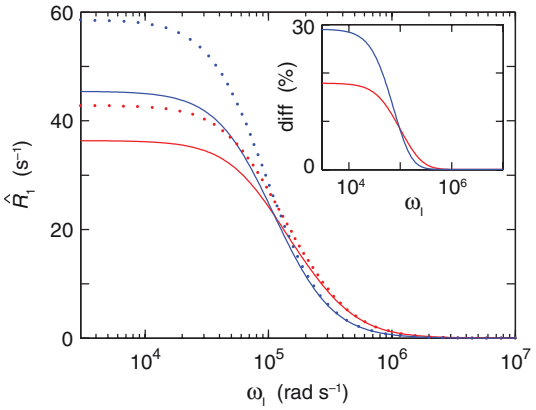

FIG. 5. Dispersion of the unlike-spin integral relaxation rates $\widehat{R}_1^{\mathrm{US}}$ (red) and $\widehat{R}_1^{\mathrm{UN}}$ (blue) in the dilute regime, computed numerically (solid curves) and from the nonrigorous approximation based on Eq. (4.25) (dots) for $P_{\mathrm{A}} = 10^{-3}$, $\tau_{\mathrm{A}} = 10$ μs, $\chi_{\mathrm{D}} = 10^5$ rad s^{-1}, and $\kappa = 0.9412$. The inset shows the relative error of the approximation, defined as $[R_1^{\mathrm{approx}}(\omega_I) - R_1^{\mathrm{exact}}(\omega_I)]/R_1^{\mathrm{exact}}(0)$.

(0.7)% to 25 (48)% when τ_{A} increases from 1 to 100 μs at $\chi_{\mathrm{D}} = 10^5$ rad s^{-1}.

In contrast to Eq. (4.25), the stochastic Liouville approach adopted here introduces site exchange in a rigorous way and without any restrictions on the mean survival time τ_{A}. In the dilute regime, the *measured* R_1 is not in the "slow-motion" regime; as seen from Figs. 1–3 and 5, $1/\widehat{R}_1$ is then always much longer than τ_{A}. The stochastic Liouville approach is needed because the *intrinsic* relaxation rate (which does not appear explicitly in our treatment) violates the motional-narrowing condition unless the condition (4.7) is satisfied.

V. LIKE-SPIN RELAXATION DISPERSION

A. Homonuclear spin pair

If the spins I and S are both protons, their Larmor frequencies are not likely to differ by more than ∼10 ppm. Since the EMOR dispersion generally occurs below $\omega_I \approx 10^7$ rad s^{-1}, we therefore expect that $|\omega_I - \omega_S| < 10^2$ rad s^{-1}, which is much less than ω_{D}. For a proton pair, or a homonuclear ($\gamma_I = \gamma_S$) spin pair in general, the inequality (2.6) is thus satisfied and we can set $\omega_I = \omega_S$ throughout.

For pedagogical reasons and to keep the general notation already introduced, we shall obtain the like-spin results as a special case of the unlike-spin problem addressed in Sec. IV. However, it is possible, and computationally preferable, to obtain the like-spin results more directly by recognizing that we now have a I_2 triplet state and that the problem is isomorphic with that of a single quadrupolar spin-1.[6] The dimension of the spin Liouville space is then reduced from 16 to 9 (or from 15 to 8 after excluding the identity operator). There are no single-quantum coherences and the longitudinal $Q = 0$ block then only involves the magnetization (basis operator T_0^1) and rank-2 (quadrupolar) alignment (T_0^2). All results for the quadrupolar spin-1 case can thus be taken over directly by replacing the quadrupole frequency ω_{Q} by the dipole frequency ω_{D} and setting the asymmetry parameter to zero (since the magnetic dipole-dipole interaction is uniaxial).[6]

Assuming nonselective excitation ($\sigma_1(0) = \sigma_2(0)$), which applies generally to field-cycling experiments, the integral longitudinal relaxation rate of the total magnetization of the spin pair is

$$\widehat{R}_1 = \frac{2}{(1\,|\langle\widetilde{\mathcal{U}}(0)\rangle|\,1)+(1\,|\langle\widetilde{\mathcal{U}}(0)\rangle|\,2)+(2\,|\langle\widetilde{\mathcal{U}}(0)\rangle|\,1)+(2\,|\langle\widetilde{\mathcal{U}}(0)\rangle|\,2)}, \\ = \frac{1}{(1\,|\langle\widetilde{\mathcal{U}}(0)\rangle|\,1)+(1\,|\langle\widetilde{\mathcal{U}}(0)\rangle|\,2)}, \tag{5.1}$$

where the matrix elements refer to the 15-dimensional two-spin basis (Appendix B of the supplementary material[24]), and the equality of the two forms follows since the two like spins must have the same relaxation properties. In other words, $\widehat{R}_1$ is the same irrespective of whether one observes both spins or only spin I. (Selective observation of spin I would be possible, for example, if spin S had a static dipole coupling to a third spin. But here we only consider an isolated spin pair.)

B. Dilute regime

For numerical calculation of $\widehat{R}_1$ in the dilute regime, we can drop the $\mathcal{L}_{\mathrm{Z}}$ superoperator in Eq. (4.5), because the $Q = 0$ block is now a null matrix. As in the unlike-spin case (Sec. IV), we can obtain approximate analytical results for $\widehat{R}_1$ by neglecting the dynamical coupling between magnetizations and two-spin order. Equation (4.10) reduces to $\widetilde{\sigma}_1(0) = \sigma_1(0)/(\rho + \sigma)$, since $\rho_I = \rho_S \equiv \rho$ and $\sigma_{IS} = \sigma_{SI} \equiv \sigma$ in the like-spin case and $\sigma_1(0) = \sigma_2(0)$ for nonselective excitation. Equation (4.1) then yields $\widehat{R}_1 = \rho + \sigma$. The desired analytical approximation is obtained by taking ρ and σ from Eqs. (4.14) and (4.15) with $\omega_I = \omega_S$, with the result

$$\widehat{R}_1 = \frac{3}{2} P_{\mathrm{A}} \chi_{\mathrm{D}}^2 \,(0.2\, J_1 + 0.8\, J_2)\,, \tag{5.2}$$

with the generalized spectral density

$$J_n \equiv \frac{\tau_{\mathrm{A}}}{1 + (\omega_{\mathrm{D}}\,\tau_{\mathrm{A}})^2 + (n\,\omega_I\,\tau_{\mathrm{A}})^2}. \tag{5.3}$$

This approximate result coincides with the exact result in the low-field and motional-narrowing regimes and, as expected, it is of the same form as the corresponding result for a single spin $I = 1$ with a uniaxial quadrupole coupling.[6]

In Fig. 6, we compare the approximate analytical rate given by Eqs. (5.2) and (5.3) with the essentially exact rate computed numerically from Eqs. (5.1) and (4.5) (with $\mathcal{L}_{\mathrm{Z}}$ omitted). The approximate analytical rates coincide with the exact rates at the high-frequency end of the dispersion, where the motional-narrowing condition $(\omega_{\mathrm{D}}\,\tau_{\mathrm{A}})^2 \ll 1 + (\omega_I\,\tau_{\mathrm{A}})^2$ is satisfied, and also at the low-frequency end, where the low-field condition $(\omega_I\,\tau_{\mathrm{A}})^2 \ll 1 + (\omega_{\mathrm{D}}\,\tau_{\mathrm{A}})^2$ is satisfied. Even at intermediate frequencies, where neither condition is satisfied, the analytical expressions remain quite accurate with a maximum error of ∼−2% for the parameter values used in Fig. 5. The maximum error in $\widehat{R}_1$ varies from −0.04% to −5.5% when τ_{A} increases from 1 to 100 μs at $\chi_{\mathrm{D}} = 10^5$ rad s^{-1}.

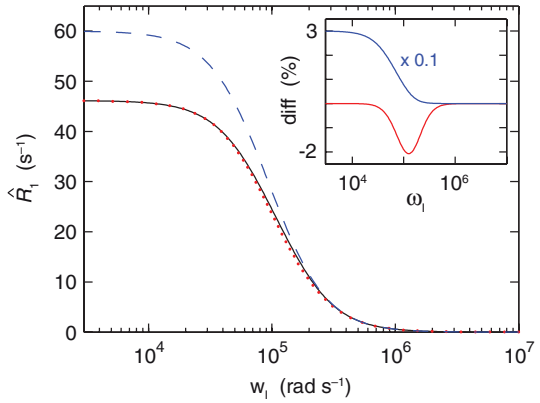

FIG. 6. Dispersion of the like-spin integral relaxation rate $\widehat{R}_1$ in the dilute regime, computed numerically (black solid curve), from the analytical approximation (red dots) and from the nonrigorous approximation based on Eq. (4.25) (blue dashed) for $P_A = 10^{-3}$, $\tau_A = 10$ μs, and $\chi_D = 10^5$ rad s^{-1}. The inset shows the relative error of the approximations, defined as $[R_1^{approx}(\omega_I) - R_1^{exact}(\omega_I)]/R_1^{exact}(0)$. For the nonrigorous approximation (blue curve), the error has been divided by a factor 10.

Figure 6 also shows the relaxation dispersion profile predicted by the nonrigorous analytical expression (4.25) with the intrinsic relaxation rate $\widehat{R}_{1,A} = \widehat{R}_1/P_A$ obtained from Eq. (5.2) after setting $\omega_D = 0$ (as in the motional-narrowing regime) in Eq. (5.3). Here, the error is much larger, reaching 30% at low frequencies. The maximum error in $\widehat{R}_1$ varies from 0.7% to 50% when τ_A increases from 1 to 100 μs at $\chi_D = 10^5$ rad s^{-1}.

VI. GENERALIZATIONS

Several generalizations of the basic EMOR model were considered in connection with the previous EMOR treatment of the quadrupolar spin $I = 1$ case.[6] With obvious modifications, those generalizations are applicable also to the dipolar two-spin case treated here. For simplicity, we shall only show how the approximate analytical results for the dilute regime are modified when the EMOR model is generalized. (As seen from Figs. 2 and 6, those results are likely to be sufficiently accurate for most purposes.)

We are thus concerned with the generalization of Eqs. (4.14)–(4.16) (unlike spins) or Eqs. (5.2) and (5.3) (like spins) when the EMOR model comprises, not one, but n_A anisotropic states, each represented by an isotropic distribution of sites with mean survival time τ_ν and fast anisotropic internal motions described by intrinsic auto-relaxation and cross-relaxation rates and an orientational order parameter $S_\nu = \omega_{D,\nu}/\omega_D^0$. In addition, a fast isotropic motion is associated with the isotropic bulk state (B).

For unlike spins, the generalized auto-relaxation rate is

$$\rho_I = P_B\,\rho_{I,B} + P_A \sum_{\nu=1}^{n_A} x_\nu\,\rho_{I,\nu}^{int} + \sum_{\nu=1}^{n_A} x_\nu\,\rho_{I,\nu}^{EMOR}(\tau_\nu, S_\nu), \quad (6.1)$$

where x_ν is the fraction of all A sites that belong to state ν, and $\rho_{I,\nu}^{EMOR}(\tau_\nu, S_\nu)$ is the EMOR contribution to the auto-relaxation rate from state ν as given by Eq. (4.14) with τ_A replaced by τ_ν, and χ_D and ω_D multiplied by the order parameter S_ν. Similarly, the generalized cross-relaxation rate is

$$\sigma_{IS} = P_B\,\sigma_{IS,B} + P_A \sum_{\nu=1}^{n_A} x_\nu\,\sigma_{IS,\nu}^{int} + \sum_{\nu=1}^{n_A} x_\nu\,\sigma_{IS,\nu}^{EMOR}(\tau_\nu, S_\nu). \quad (6.2)$$

For like spins, the integral relaxation rate in Eq. (5.2) is generalized to

$$\widehat{R}_1 = P_B\,R_{1,B} + P_A \sum_{\nu=1}^{n_A} x_\nu\,R_{1,\nu}^{int} + \sum_{\nu=1}^{n_A} x_\nu\,R_{1,\nu}^{EMOR}(\tau_\nu, S_\nu). \quad (6.3)$$

These generalizations are rigorously valid only under certain conditions. Notably, the internal motion is assumed to be sufficiently fast that $\tau_\nu^{int} \ll \tau_\nu$, $(1 - S_\nu^2)(\omega_D\,\tau_\nu^{int})^2 \ll 1$, and $\rho_{I,\nu}^{int}\,\tau_\nu \ll 1$ (and similarly for $\sigma_{IS,\nu}^{int}$ and $R_{1,\nu}^{int}$). Here, τ_ν^{int} is the correlation time for the internal motion in state ν. Furthermore, the internal motion is assumed to modulate the orientation (but not the length) of the internuclear vector $\boldsymbol{r}_{IS}$ and to exhibit at least 3-fold symmetry, so that $S_\nu = 1 - (3/2)\langle \sin^2\theta \rangle_\nu$.

VII. CONCLUSIONS

We have presented a non-perturbative theoretical treatment of longitudinal relaxation induced by EMOR of the magnetic dipole coupling of a spin-1/2 pair. To our knowledge, this is the first treatment of dipolar relaxation dispersion outside the motional-narrowing regime. For the experimentally important dilute regime, we have obtained simple analytical results that remain accurate to better than a few percent over practically the entire parameter space. (The somewhat lower accuracy in the ultraslow-motion regime is of little consequence, since the R_1 contribution from such sites, being proportional to $1/\tau_A$, tends to be negligibly small.) These analytical results provide conceptual insight and they can readily be incorporated in nonlinear optimization protocols for MRD data analysis.

So far, the main application of the EMOR theory for spin $I = 1$ has been to water ^{2}H MRD studies of cross-linked protein gels.[34] Such studies provide unique insights into intermittent structural dynamics and transient solvent penetration of globular proteins.[28,34] Corresponding water ^{1}H MRD studies are less useful for extracting clear-cut biophysical information, since the smaller coupling constant (ω_D is an order of magnitude smaller than ω_Q) allows more labile protons to contribute to R_1 in addition to well-defined internal hydration sites. Nevertheless, ^{1}H MRD can sometimes be a useful complement to water ^{2}H MRD measurements[20] and, in addition, can be used to study cosolvent interactions with proteins or other macromolecules.

Arguably, the most important application of the present results is to water ^{1}H relaxation in biological tissues, which is the primary determinant of contrast in magnetic resonance imaging. Despite several decades of work, there is still no consensus on the mechanism of water ^{1}H relaxation in biological tissues. We believe that the EMOR mechanism is the dominant source of water ^{1}H MRD in tissues and the present

work represents a first step towards a rigorous and quantitative theory. We are currently extending the theory to larger spin systems, including the effects of coherent processes involving nonlabile protons with static dipole couplings.

ACKNOWLEDGMENTS

This work was financially supported by the Swedish Research Council.

[1]A. Abragam, *The Principles of Nuclear Magnetism* (Clarendon Press, Oxford, 1961).
[2]F. Noack, Prog. Nucl. Magn. Reson. Spectrosc. **18**, 171 (1986).
[3]R. Kimmich and E. Anoardo, Prog. Nucl. Magn. Reson. Spectrosc. **44**, 257 (2004).
[4]G. Ferrante and S. Sykora, Adv. Inorg. Chem. **57**, 405 (2005).
[5]M. Goldman, J. Magn. Reson. **149**, 160 (2001).
[6]T. Nilsson and B. Halle, J. Chem. Phys. **137**, 054503 (2012).
[7]R. Kubo, J. Math. Phys. **4**, 174 (1963).
[8]R. Kubo, Adv. Chem. Phys. **15**, 101 (1969).
[9]L. G. Werbelow and D. M. Grant, Adv. Magn. Reson. **9**, 189 (1977).
[10]D. Canet, Prog. Nucl. Magn. Reson. Spectrosc. **21**, 237 (1989).
[11]N. P. Benetis, D. J. Schneider, and J. H. Freed, J. Magn. Reson. **85**, 275 (1989).
[12]A. A. Nevzorov and J. H. Freed, J. Chem. Phys. **112**, 1413 (2000).
[13]L.-P. Hwang, Mol. Phys. **49**, 1341 (1983).
[14]I. Solomon, Phys. Rev. **99**, 559 (1955).
[15]S. H. Koenig and R. D. Brown, Prog. Nucl. Magn. Reson. Spectrosc. **22**, 487 (1990).
[16]S. H. Koenig and R. D. Brown, Magn. Reson. Med. **30**, 685 (1993).
[17]J. P. Korb and R. G. Bryant, J. Chem. Phys. **115**, 10964 (2001).
[18]B. Halle, Magn. Reson. Med. **56**, 60 (2006).
[19]E. P. Sunde and B. Halle, J. Am. Chem. Soc. **131**, 18214 (2009).
[20]F. V. Chávez and B. Halle, Magn. Reson. Med. **56**, 73 (2006).
[21]Z. Luz and S. Meiboom, J. Chem. Phys. **40**, 2686 (1964).
[22]K. J. Pine, G. R. Davies, and D. J. Lurie, Magn. Reson. Med. **63**, 1698 (2010).
[23]B. Halle, Prog. Nucl. Magn. Reson. Spectrosc. **28**, 137 (1996).
[24]See supplementary material at http://dx.doi.org/10.1063/1.4824105 for further details on the notation (Appendix A); spin operator basis (Appendix B); the exact formal solution of the EMOR model (Appendix C); matrix representations of the Zeeman and dipole Liouvillians (Appendix D); approximate analytical solution for the dilute regime (Appendix E); and the minors of the **M** matrix (Appendix F).
[25]D. M. Brink and G. R. Satchler, *Angular Momentum*, 2nd ed. (Clarendon Press, Oxford, 1968).
[26]K. Ivanaov, A. Yurkovskaya, and H.-M. Vieth, J. Chem. Phys. **129**, 234513 (2008).
[27]A. N. Pravdivtsev, K. L. Ivanov, R. Kaptein, and A. V. Yurkovskaya, Appl. Magn. Reson. **44**, 23 (2013).
[28]F. Persson and B. Halle, J. Am. Chem. Soc. **135**, 8735 (2013).
[29]E. P. Sunde and B. Halle, J. Magn. Reson. **203**, 257 (2010).
[30]K. Blum, *Density Matrix Theory and Applications* (Plenum Press, New York, 1981).
[31]N. C. Pyper, Mol. Phys. **22**, 433 (1971).
[32]V. I. Lebedev and D. N. Laikov, Dokl. Math. **59**, 477 (1999).
[33]X.-G. Wang and T. Carrington, J. Theor. Comput. Chem. **2**, 599 (2003).
[34]E. Persson and B. Halle, J. Am. Chem. Soc. **130**, 1774 (2008).
[35]H. M. McConnell, J. Chem. Phys. **28**, 430 (1958).

Supplemental Material

Nuclear magnetic relaxation induced by exchange-mediated orientational randomization: Longitudinal relaxation dispersion for a dipole-coupled spin-1/2 pair

Zhiwei Chang and Bertil Halle
Division of Biophysical Chemistry, Department of Chemistry, Lund University, POB 124, SE-22100 Lund, Sweden

APPENDIX A: NOTATION

Here we elaborate on the notation introduced in Sec. III of the main text. Site exchange is modeled as a stationary Markov process, specified by an operator $P(t)$ obeying the operator master equation[1]

$$\frac{\mathrm{d}}{\mathrm{d}t} P(t) \;=\; W\, P(t)\,, \tag{A.1}$$

with the initial condition $P(0) = \mathit{1}$. The sites are represented by an orthonormal basis $\{|\alpha\rangle\}$ with the formal mathematical properties of a linear vector space, such as orthonormality and closure:

$$\langle\alpha|\beta\rangle \;=\; \delta_{\alpha\beta}\,, \tag{A.2}$$

$$\sum_{\alpha} |\alpha\rangle\langle\alpha| \;=\; \mathit{1}\,. \tag{A.3}$$

Taking matrix elements of Eq. (A.1) and using the closure relation, one recovers the usual form of the master equation:

$$\frac{\mathrm{d}}{\mathrm{d}t}\, \langle\alpha|\, P(t)\, |\beta\rangle \;=\; \sum_{\gamma} \langle\alpha|\, W\, |\gamma\rangle\; \langle\gamma|\, P(t)\, |\beta\rangle\;, \tag{A.4}$$

where the propagator $\langle\alpha|\, P(t)\, |\beta\rangle$, more commonly written as $P(\alpha, t|\beta)$, is the conditional probability that a particular spin is in site α at time t given that it was in site β at time $t = 0$. The $\{|\alpha\rangle\}$ basis matrix representation of the operator equation (A.1) thus involves a square jump matrix with elements $\langle\alpha|\, W\, |\gamma\rangle$ and a column vector propagator with elements $\langle\alpha|\, P(t)\, |\beta\rangle$ *for a given initial site* β.

The probability that a particular spin is in site α at time t regardless of its initial location is given by the partially averaged propagator

$$P_\alpha(t) \;\equiv\; \sum_{\beta} \langle\alpha|\, P(t)\, |\beta\rangle\; P_\beta\,, \tag{A.5}$$

where P_β is the equilibrium population in site β. It is clear that $P_\alpha(t)$ satisfies the same master equation as the conditional probability $P(\alpha, t|\beta)$.

The density operator $\sigma(t)$, featuring in the stochastic Liouville equation (SLE) (3.1), describes the state of the IS two-spin system *and* the state of the relevant molecular degrees of freedom, specified by the site index α. We can therefore regard $\sigma(t)$ as a vector in a composite space formed as the direct product $\{|KQ\, k_I k_S)\} \otimes \{|\alpha\rangle\}$ of the spin Liouville space and the site space. In this direct-product space, the Liouvillian can be formally expressed as

$$\mathcal{L} \;=\; \sum_{\alpha} |\alpha\rangle\, \mathcal{L}_\alpha\, \langle\alpha|\;. \tag{A.6}$$

From the orthonormality (A.2), it follows that $\mathcal{L}$ is diagonal in the site basis:

$$\langle\alpha|\, \mathcal{L}\, |\beta\rangle \;=\; \delta_{\alpha\beta}\, \mathcal{L}_\alpha \;=\; \delta_{\alpha\beta}\, [\mathcal{H}_\alpha, \ldots]\;. \tag{A.7}$$

Formally, the exchange superoperator $\mathcal{W}$ in the operator SLE (3.1) is related to the jump operator W in the master equation (A.1) as

$$\mathcal{W} \;=\; W \otimes E_{IS}\,, \tag{A.8}$$

where E_{IS} is the identity operator in the two-spin Liouville space. Consequently, $\mathcal{W}$ is diagonal in the spin basis.

There is a close analogy between the density operator $\sigma(t)$ and the site operator $P(t)$. We can thus define the conditional density operator $\langle\alpha|\,\sigma(t)\,|\beta\rangle$ as the density operator for the sub-ensemble of all site trajectories that start out (at $t = 0$) in site β and occupy site α at time t. By taking matrix elements in the operator SLE (3.1) and using Eqs. (A.3), (A.7) and (A.8), we find, in analogy with Eq. (A.4),

$$\frac{\mathrm{d}}{\mathrm{d}t}\,\langle\alpha|\,\sigma(t)\,|\beta\rangle \;=\; -\,i\,\mathcal{L}_\alpha\,\langle\alpha|\,\sigma(t)\,|\beta\rangle \;+\; \sum_\gamma \langle\alpha|\,\mathcal{W}\,|\gamma\rangle\,\langle\gamma|\,\sigma(t)\,|\beta\rangle\;. \tag{A.9}$$

In analogy with Eq. (A.5), we can define a partially averaged propagator,

$$\sigma_\alpha(t) \;\equiv\; \sum_\beta \langle\alpha|\,\sigma(t)\,|\beta\rangle\; P_\beta\,, \tag{A.10}$$

which satisfies the SLE

$$\frac{\mathrm{d}}{\mathrm{d}t}\,\sigma_\alpha(t) \;=\; -\,i\,\mathcal{L}_\alpha\,\sigma_\alpha(t) \;+\; \sum_\gamma \langle\alpha|\,\mathcal{W}\,|\gamma\rangle\,\sigma_\gamma(t)\,. \tag{A.11}$$

The reduced density operator $\langle\sigma(t)\rangle$, introduced in Sec. III of the main text, is the density operator averaged over all site trajectories, that is,

$$\langle\sigma(t)\rangle \;\equiv\; \sum_\alpha \sigma_\alpha(t)\,. \tag{A.12}$$

This Appendix is dedicated to an anonymous reviewer.

APPENDIX B: SPIN OPERATOR BASIS

The irreducible spherical tensor operators (ISTOs) $T^K_Q(k_I, k_S)$ that span the Liouville space of the spin-1/2 pair are formed as linear combinations of products of the single-spin ISTOs $T^{k_I}_{q_I}(I)$ and $T^{k_S}_{q_S}(S)$ according to[2]

$$T^K_Q(k_I, k_S) \;=\; (-1)^{k_I - k_S + Q}(2K+1)^{1/2} \sum_{q_I=-k_I}^{k_I} \begin{pmatrix} k_I & k_S & K \\ q_I & Q-q_I & -Q \end{pmatrix} T^{k_I}_{q_I}(I)\, T^{k_S}_{Q-q_I}(S)\,. \tag{B.1}$$

For notational simplicity, we denote these operators by $A_n \equiv T^K_Q(k_I k_S)$, where the subscript n indicates the basis ordering. The operators are grouped according to the total projection quantum number Q. Within the $Q = 0$ manifold, we define A_3 and A_5 as linear combinations of $T^0_0(11)$ and $T^2_0(11)$ in order to facilitate the physical interpretation. A_1 and A_2 correspond to the longitudinal magnetizations of spin I and S, respectively, A_3 corresponds to longitudinal two-spin order, and A_4 and A_5 correspond to the odd-rank and even-rank, respectively, zero-quantum coherence.

Table S1: Order and explicit form of basis operators.[a]

n	$A_n \equiv T^K_Q(k_I k_S)$	explicit form
1	$T^1_0(10)$	$I_z\, E_S$
2	$T^1_0(01)$	$E_I\, S_z$
3	$-a\, T^0_0(11) \;+\; b\, T^2_0(11)$	$2\, I_z\, S_z$
4	$T^1_0(11)$	$\frac{1}{\sqrt{2}}\,(I_-\, S_+ - I_+\, S_-)$
5	$b\, T^0_0(11) \;+\; a\, T^2_0(11)$	$\frac{-1}{\sqrt{2}}\,(I_-\, S_+ + I_+\, S_-)$
6	$T^1_1(10)$	$\frac{-1}{\sqrt{2}}\, I_+\, E_S$
7	$T^1_1(01)$	$\frac{-1}{\sqrt{2}}\, E_I\, S_+$
8	$T^1_1(11)$	$I_z\, S_+ - I_+\, S_z$
9	$T^2_1(11)$	$-(I_z\, S_+ + I_+\, S_z)$
10	$T^1_{-1}(10)$	$\frac{1}{\sqrt{2}}\, I_-\, E_S$
11	$T^1_{-1}(01)$	$\frac{1}{\sqrt{2}}\, E_I\, S_-$
12	$T^1_{-1}(11)$	$I_z\, S_- - I_-\, S_z$
13	$T^2_{-1}(11)$	$I_z\, S_- + I_-\, S_z$
14	$T^2_2(11)$	$I_+\, S_+$
15	$T^2_{-2}(11)$	$I_-\, S_-$

[a] The coefficients in A_3 and A_5 are $a = 1/\sqrt{3}$ and $b = \sqrt{2/3}$.

APPENDIX C: FORMAL SOLUTION

For the kinetic model considered here, the exact result for the site-averaged resolvent superoperator is[3]

$$\begin{aligned}\left\langle \widetilde{\mathcal{U}}(s)\right\rangle \;=\; & \tau_{\mathrm{A}}\,[1-\mathcal{B}_{\mathrm{A}}(s)\,\mathcal{B}_{\mathrm{B}}(s)]^{-1}\,\mathcal{B}_{\mathrm{A}}(s)\,[P_{\mathrm{A}}+P_{\mathrm{B}}\,\mathcal{B}_{\mathrm{B}}(s)] \\ & +\;\tau_{\mathrm{B}}\,[1-\mathcal{B}_{\mathrm{B}}(s)\,\mathcal{B}_{\mathrm{A}}(s)]^{-1}\,\mathcal{B}_{\mathrm{B}}(s)\,[P_{\mathrm{B}}+P_{\mathrm{A}}\,\mathcal{B}_{\mathrm{A}}(s)]\;,\end{aligned} \tag{C.1}$$

where

$$\mathcal{B}_{\mathrm{B}}(s)\;\equiv\;(1\;+\;s\,\tau_{\mathrm{B}}\;+\;i\,\mathcal{L}_{\mathrm{Z}}\,\tau_{\mathrm{B}})^{-1}\;, \tag{C.2}$$

$$\mathcal{B}_{\mathrm{A}}(s)\;\equiv\;\frac{1}{4\,\pi}\int \mathrm{d}\Omega\,[1\;+\;s\,\tau_{\mathrm{A}}\;+\;i\,\mathcal{L}_{\mathrm{Z}}\,\tau_{\mathrm{A}}\;+\;i\,\mathcal{L}_{\mathrm{D}}(\Omega)\,\tau_{\mathrm{A}}]^{-1}\;. \tag{C.3}$$

Like $\langle\widetilde{\mathcal{U}}(s)\rangle$, the site-averaged supermatrices $\mathcal{B}_{\mathrm{B}}(s)$ and $\mathcal{B}_{\mathrm{A}}(s)$ are block-diagonal in Q. Therefore, $\mathcal{B}_{\mathrm{B}}(s)$ and $\mathcal{B}_{\mathrm{A}}(s)$ commute if the individual Q-blocks commute. This is the case for like spins ($\omega_I = \omega_S$) and for a single spin $I = 1$,[3] since the Q-blocks of $\mathcal{B}_{\mathrm{B}}(s)$ are then diagonal and proportional to the identity matrix. This is not the case for unlike spins ($\omega_I \neq \omega_S$). However, the $Q = 0$ block of $\mathcal{B}_{\mathrm{B}}(s)$ is itself block-diagonal, with a longitudinal 3×3 block ($n = 1, 2, 3$) that is proportional to the identity matrix and a non-diagonal zero-quantum coherence block ($n = 4, 5$). The longitudinal 3×3 block of $\mathcal{B}_{\mathrm{B}}(s)$ therefore commutes with the corresponding block of $\mathcal{B}_{\mathrm{A}}(s)$. As long as we are only concerned with the longitudinal 3×3 block of $\langle\widetilde{\mathcal{U}}(s)\rangle$, we can therefore proceed as if $\mathcal{B}_{\mathrm{B}}(s)$ and $\mathcal{B}_{\mathrm{A}}(s)$ commute. Equation (C.1) can thus be simplified and, after setting $s = 0$, we recover Eq. (3.10) of the main text.

APPENDIX D: MATRIX REPRESENTATION

To evaluate Eq. (3.11), we need the supermatrix elements of the Zeeman and dipole Liouvillians. Using Eq. (2.2) and the commutation relations

$$[I_z, T_{q_I}^{k_I}(I)] \;=\; q_I\, T_{q_I}^{k_I}(I) \tag{D.1a}$$

$$[S_z, T_{q_S}^{k_S}(S)] \;=\; q_S\, T_{q_S}^{k_S}(S) \tag{D.1b}$$

we obtain

$$\left(T_Q^K(k_I k_S)\,|\,\mathcal{L}_{\rm Z}\,|\,T_{Q'}^{K'}(k_I' k_S')\right) \;=\; c_I\,\omega_{\rm I} \;+\; c_S\,\omega_{\rm S} \tag{D.2}$$

where the numerical values of c_I and c_S are evident from Eq. (D.8).

The matrix elements of $\mathcal{L}_{\rm D}(\Omega)$ are obtained from Eq. (2.3) and the Liouville space Wigner-Eckart theorem.[4] For $K' \geq K$,

$$\begin{aligned}\left(T_Q^K(k_I k_S)\,|\mathcal{L}_{\rm D}(\Omega)|\,T_{Q'}^{K'}(k_I' k_S')\right) \;=\; &\sqrt{30}\,\omega_D\, C_{2,Q-Q'}(\Omega)(-1)^{K-Q}\left[(-1)^{k_I+k_S} - (-1)^{k_I'+k_S'}\right] \\ &\times\left[(2K+1)(2K'+1)(2k_I+1)(2k_I'+1)(2k_S+1)(2k_S'+1)\right]^{1/2} \\ \times \begin{pmatrix} K & 2 & K' \\ -Q & Q-Q' & Q' \end{pmatrix} &\begin{Bmatrix} k_I & 1 & k_I' \\ 1/2 & 1/2 & 1/2 \end{Bmatrix}\begin{Bmatrix} k_S & 1 & k_S' \\ 1/2 & 1/2 & 1/2 \end{Bmatrix}\begin{Bmatrix} K & K' & 2 \\ k_I & k_I' & 1 \\ k_S & k_S' & 1 \end{Bmatrix}\end{aligned} \tag{D.3}$$

Since $\mathcal{H}_{\rm D}(\Omega)$ is Hermitian, matrix elements with $K' < K$ can be obtained from the symmetry relation

$$\left(T_Q^K(k_I k_S)\,|\,\mathcal{L}_{\rm D}(\Omega)\,|\,T_{Q'}^{K'}(k_I' k_S')\right) \;=\; \left(T_{Q'}^{K'}(k_I' k_S')\,|\,\mathcal{L}_{\rm D}(\Omega)\,|\,T_Q^K(k_I k_S)\right)^* \tag{D.4}$$

In general, the matrix elements in Eq. (D.3) depend on two angles $\Omega = (\theta, \varphi)$. The angle φ describes a rotation about the $\boldsymbol{B}_0$ field axis and θ is the angle between the $\boldsymbol{B}_0$ field and the internuclear $I - S$ vector.

The explicit matrix representation $\mathbf{M}$, in the spherical multipole basis, of the superoperator

$$\mathcal{M}(\Omega) \;\equiv\; 1 \;+\; i\,\mathcal{L}_{\rm Z}\,\tau_{\rm A} \;+\; i\,\mathcal{L}_{\rm D}(\Omega)\,\tau_{\rm A}\,, \tag{D.5}$$

the inverse of which appears in the integrand of Eq. (3.11), can now be obtained from Eqs. (D.2) – (D.4) after evaluating the $3j$, $6j$, and $9j$ symbols and substituting trigonometric expressions for the Wigner functions in Eq. (D.3). The Zeeman and dipole couplings involve the dimensionless quantities

$$L_I \;\equiv\; \omega_{\rm I}\,\tau_{\rm A} \tag{D.6a}$$

$$L_S \;\equiv\; \omega_{\rm S}\,\tau_{\rm A} \tag{D.6b}$$

$$D \;\equiv\; \omega_{\rm D}\,\tau_{\rm A} \tag{D.6c}$$

The nonzero off-diagonal elements can all be expressed in terms of three quantities:

$$a \equiv \frac{i\,D}{2} \cos\theta\, \sin\theta \exp(i\,\varphi) \tag{D.7a}$$

$$b \equiv \frac{i\,D}{2\sqrt{2}} \sin^2\theta\, \exp(i\,2\varphi) \tag{D.7b}$$

$$c \equiv \frac{i\,D}{2\sqrt{2}} \left(3\cos^2\theta - 1\right) \tag{D.7c}$$

The complete $\mathbf{M}$ matrix is given in Eq. (D.8) with the basis operators ordered as in Table S1. Here, $L_\Delta \equiv L_I - L_S$ and $L_\Sigma \equiv L_I + L_S$.

$$
\mathbf{M} = \begin{bmatrix}
 & |1) & |2) & |3) & |4) & |5) & |6) & |7) & |8) & |9) & |10) & |11) & |12) & |13) & |14) & |15) \\
(1| & 1 & 0 & 0 & \frac{2}{3}c & 0 & 0 & 0 & a^* & a^* & 0 & 0 & a & -a & -\sqrt{2}\,b^* & -\sqrt{2}\,b \\
(2| & 0 & 1 & 0 & -\frac{2}{3}c & 0 & 0 & 0 & -a^* & a^* & 0 & 0 & -a & -a & -\sqrt{2}\,b^* & -\sqrt{2}\,b \\
(3| & 0 & 0 & 1 & 0 & 0 & \sqrt{2}\,a^* & \sqrt{2}\,a^* & 0 & 0 & -\sqrt{2}\,a & -\sqrt{2}\,a & 0 & 0 & 0 & 0 \\
(4| & \frac{2}{3}c & -\frac{2}{3}c & 0 & 1 & iL_\Delta & a^* & -a^* & 0 & 0 & a & -a & 0 & 0 & 0 & 0 \\
(5| & 0 & 0 & 0 & iL_\Delta & 1 & a^* & a^* & 0 & 0 & -a & -a & 0 & 0 & 0 & 0 \\
(6| & 0 & 0 & -\sqrt{2}\,a & -a & -a & 1{+}iL_I & 0 & -\frac{1}{3}c & -c & 0 & 0 & -b & -b & -\sqrt{2}\,a^* & 0 \\
(7| & 0 & 0 & -\sqrt{2}\,a & a & -a & 0 & 1{+}iL_S & \frac{1}{3}c & -c & 0 & 0 & b & -b & -\sqrt{2}\,a^* & 0 \\
(8| & -a & a & 0 & 0 & 0 & -\frac{1}{3}c & \frac{1}{3}c & 1{+}\frac{i}{2}L_\Sigma & \frac{i}{2}L_\Delta & -b & b & 0 & 0 & 0 & 0 \\
(9| & -a & -a & 0 & 0 & 0 & -c & -c & \frac{i}{2}L_\Delta & 1{+}\frac{i}{2}L_\Sigma & b & b & 0 & 0 & 0 & 0 \\
(10| & 0 & 0 & \sqrt{2}\,a^* & -a^* & a^* & 0 & 0 & b^* & -b^* & 1{-}iL_I & 0 & -\frac{1}{3}c & c & 0 & \sqrt{2}\,a \\
(11| & 0 & 0 & \sqrt{2}\,a^* & a^* & a^* & 0 & 0 & -b^* & -b^* & 0 & 1{-}iL_S & \frac{1}{3}c & c & 0 & \sqrt{2}\,a \\
(12| & -a^* & a^* & 0 & 0 & 0 & b^* & -b^* & 0 & 0 & -\frac{1}{3}c & \frac{1}{3}c & 1{-}\frac{i}{2}L_\Sigma & \frac{i}{2}L_\Delta & 0 & 0 \\
(13| & a^* & a^* & 0 & 0 & 0 & b^* & b^* & 0 & 0 & c & c & \frac{i}{2}L_\Delta & 1{-}\frac{i}{2}L_\Sigma & 0 & 0 \\
(14| & \sqrt{2}\,b & \sqrt{2}\,b & 0 & 0 & 0 & \sqrt{2}\,a & \sqrt{2}\,a & 0 & 0 & 0 & 0 & 0 & 0 & 1{+}iL_\Sigma & 0 \\
(15| & \sqrt{2}\,b^* & \sqrt{2}\,b^* & 0 & 0 & 0 & 0 & 0 & 0 & 0 & -\sqrt{2}\,a^* & -\sqrt{2}\,a^* & 0 & 0 & 0 & 1{-}iL_\Sigma
\end{bmatrix} \tag{D.8}
$$

APPENDIX E: ANALYTICAL APPROXIMATION

Here, we derive approximate analytical expressions for the generalized auto-relaxation and cross-relaxation rates defined in Eq. (4.11), starting with ρ_I. Using the superoperator identity $1 - \mathcal{M}^{-1} = (\mathcal{M} - 1)\,\mathcal{M}^{-1}$, we can express Eq. (4.11a) as

$$\rho_I \;=\; \frac{P_\mathrm{A}}{\tau_\mathrm{A}} \sum_n \left\langle (1\,|(\mathcal{M}-1)|\,n)\,(n\,|\mathcal{M}^{-1}|\,1) \right\rangle \,, \tag{E.1}$$

where the superoperator $\mathcal{M}$ was defined in Eq. (D.5) and the angular brackets indicate the isotropic average in Eq. (3.11). From the structure of the $\mathbf{M}$ supermatrix in Eq. (D.8) it is clear that only the 7 terms with $n = 4$, 8, 9, 12, 13, 14 or 15 contribute to the sum in Eq. (E.1). Noting that $(n\,|\mathcal{M}^{-1}|\,1) = (-1)^{n+1}\,(1\,|\Delta|\,n)/\Delta$, where $\Delta = \det \mathbf{M}$ is the determinant of $\mathbf{M}$ and the minor $(1\,|\Delta|\,n)$ is the determinant of the matrix obtained be deleting row $(1\,|$ and column $|\,n)$ from $\mathbf{M}$, we can cast Eq. (E.1) on the form

$$\rho_I \;=\; P_\mathrm{A}\,\chi_\mathrm{D}^2\,\tau_\mathrm{A} \left[\left\langle \frac{H_0^1}{\Delta} \right\rangle + \left\langle \frac{H_1^1}{\Delta} \right\rangle + \left\langle \frac{H_1^2}{\Delta} \right\rangle + \left\langle \frac{H_2^2}{\Delta} \right\rangle \right] , \tag{E.2}$$

where we have defined the real-valued quantities

$$H_0^1 \;\equiv\; -\frac{3\,c}{2\,D^2}\,(1\,|\Delta|\,4)\,, \tag{E.3a}$$

$$H_1^1 \;\equiv\; -\frac{9}{4\,D^2}\,[\,a^*\,(1\,|\Delta|\,8) \;+\; a\,(1\,|\Delta|\,12)]\,, \tag{E.3b}$$

$$H_1^2 \;\equiv\; \frac{9}{4\,D^2}\,[\,a^*\,(1\,|\Delta|\,9) \;+\; a\,(1\,|\Delta|\,13)]\,, \tag{E.3c}$$

$$H_2^2 \;\equiv\; \frac{9\sqrt{2}}{4\,D^2}\,[\,b^*\,(1\,|\Delta|\,14) \;-\; b\,(1\,|\Delta|\,15)]\,. \tag{E.3d}$$

Here and in the following, we make use of the dimensionless quantities a, b and c, defined in Eq. (D.7), and L_I, L_S and D, defined in Eq. (D.6). The quantities Δ and H_Q^K are polynomials in $L_I^n\,L_S^p\,D^m$ with n, p, $m = 0$, 2, 4 or 6, $n+p+m \leq 6$, and with coefficients that depend on the angle θ, but not on φ.

We seek an analytical expression for ρ_I that reduces to the known exact results in the low-field and motional-narrowing regimes and that is sufficiently accurate to be quantitatively useful for any values of L_I, L_S and D. To reproduce those limits exactly, we must retain all pure terms in Δ and H_Q^K, that is, terms proportional to L_I^n, L_S^p or D^m. We thus derive the approximate expression for ρ_I by discarding all mixed terms in the full expressions for Δ and H_Q^K (Appendix F). These truncated expressions are then rearranged (without further approximations) into forms that directly reduce to the known results in the low-field and motional-narrowing limits.

The truncated determinant is expressed as

$$\Delta(L_I, L_S, D) \;=\; \Delta_L(L_I, L_S) \;+\; \Delta_D(D) \;-\; 1\,, \tag{E.4}$$

where $\Delta_D(D) = 1$ in the motional-narrowing regime and $\Delta_L(L_I, L_S) = 1$ in the low-field regime. These parts are given by

$$\Delta_L(L_I, L_S) \;=\; (1 + L_I^2)^2\,(1 + L_S^2)^2\left[1 + (L_I + L_S)^2\right]\left[1 + (L_I - L_S)^2\right]\,, \tag{E.5}$$

$$\Delta_D(D) \;=\; \left[1 + \frac{D^2}{9}\right]^2\left[1 + \frac{4\,D^2}{9}\right]\left[1 + D^2\right]^2\,, \tag{E.6}$$

Since the truncated determinant $\Delta(L_I, L_S, D)$ does not depend on the Euler angles, we only need to average the quantities H_Q^K in Eq. (E.2).

The truncated H_Q^K polynomials are derived in Appendix F. After isotropic averaging over the angle θ, they can be expressed as

$$\left\langle H_Q^K \right\rangle \;=\; c_Q^K\left[g_Q^K(L_I, L_S) \;+\; h_Q^K(D) \;-\; 1\right]\,, \tag{E.7}$$

where $g_Q^K(L_I, L_S)$ is a polynomial in L_I and L_S and $h_Q^K(D)$ is a polynomial in D and the coefficients c_Q^K are the numerical prefactors outside the curly brackets in Eqs. (F.7) – (F.10). Combining Eqs. (E.2), (E.4) and (E.7), we can now write

$$\rho_I \;=\; P_{\mathrm{A}}\,\chi_{\mathrm{D}}^2\left[\,0.1\,J_0^1 \;+\; 0.15\,J_1^1 \;+\; 0.15\,J_1^2 \;+\; 0.6\,J_2^2\,\right]\,, \tag{E.8}$$

where we have introduced the generalized spectral densities

$$J_Q^K \;\equiv\; \tau_{\mathrm{A}}\,\frac{g_Q^K(L_I, L_S) + h_Q^K(D) - 1}{\Delta_L(L_I, L_S) + \Delta_D(D) - 1} \;=\; \frac{\tau_{\mathrm{A}}}{1 \;+\; \Lambda_Q^K}\,, \tag{E.9}$$

with

$$\begin{aligned}\Lambda_Q^K \;&=\; \frac{\Delta_L(L_I, L_S) - g_Q^K(L_I, L_S) + \Delta_D(D) - h_Q^K(D)}{g_Q^K(L_I, L_S) + h_Q^K(D) - 1} \\ &=\; W_Q^K(L_I, L_S) \;+\; \Gamma_Q^K(D) \;+\; \mathcal{O}(L^2 D^2)\,.\end{aligned} \tag{E.10}$$

To be consistent with the preceding treatment, we discard the mixed terms, of order $L_I^2\,D^2$, $L_S^2\,D^2$ or higher. The first two terms in Eq. (E.10) are obtained by taking the limits $D \to 0$ and $L_I, L_S \to 0$, respectively, of Λ_Q^K. We thus obtain,

$$W_0^1 \;=\; (L_I - L_S)^2\,, \tag{E.11a}$$

$$W_1^1 \;=\; W_1^2 \;=\; L_I^2\,, \tag{E.11b}$$

$$W_2^2 \;=\; (L_I + L_S)^2\,, \tag{E.11c}$$

and

$$\Gamma_0^1 \;=\; \Gamma_1^1 \;=\; \frac{D^2\,(1 + 4\,D^2/27)}{3\,(1 + 2\,D^2/9)}\,, \tag{E.12a}$$

$$\Gamma_1^2 \;=\; \Gamma_2^2 \;=\; D^2\,. \tag{E.12b}$$

Finally, combining Eqs. (E.8) – (E.12), we obtain the desired analytical approximation

$$\begin{aligned}\rho_I \;=\; P_{\rm A}\,\chi_{\rm D}^2\Bigg[&\frac{0.1\,\tau_{\rm A}}{1+(L_I-L_S)^2+D^2\,\eta_{\rm D}/3}\;+\;\frac{0.15\,\tau_{\rm A}}{1+L_I^2+D^2\,\eta_{\rm D}/3}\\&+\frac{0.15\,\tau_{\rm A}}{1+L_I^2+D^2}\;+\;\frac{0.6\,\tau_{\rm A}}{1+(L_I+L_S)^2+D^2}\Bigg]\,,\end{aligned} \tag{E.13}$$

with

$$\eta_{\rm D} \;\equiv\; \frac{1+4\,D^2/27}{1+2\,D^2/9}\,. \tag{E.14}$$

Equations (E.13) and (E.14) correspond to Eqs. (4.14) and (4.16) of the main text. It follows from the symmetry of the problem that the auto-relaxation rate ρ_S is given by an expression identical to Eq. (E.13), except that L_I and L_S are interchanged throughout.

We now consider the cross-relaxation rate σ_{IS} in Eq. (4.11c). Because the operator basis is orthonormal, we can replace the superoperator $\mathcal{B}$ by $1-\mathcal{B}$ in the off-diagonal element in Eq. (4.11c). We can then proceed in the same way as for the auto-relaxation rate ρ_I, obtaining

$$\sigma_{IS} \;=\; \frac{P_{\rm A}}{\tau_{\rm A}}\,\sum_n (-1)^n \left\langle (1\,|(\mathcal{M}-1)|\,n)\,\frac{(2\,|\Delta|\,n)}{\Delta}\right\rangle\,. \tag{E.15}$$

This result differs in two ways from the corresponding result for ρ_I. First, because of the sign of the cofactors, all terms have the opposite explicit sign compared to the case of ρ_I. Second, the minors $(2\,|\Delta|\,n)$ now involve row 2 rather than row 1. Inspection of the $\mathbf{M}$ supermatrix in Eq. (D.8) shows that the first and second rows are identical except for a sign reversal in columns 4, 8 and 12. As a result, we obtain in place of Eq. (E.2)

$$\sigma_{IS} \;=\; P_{\rm A}\,\chi_{\rm D}^2\,\tau_{\rm A}\left[-\left\langle\frac{H_0^1}{\Delta}\right\rangle\;-\;\left\langle\frac{H_1^1}{\Delta}\right\rangle\;+\;\left\langle\frac{H_1^2}{\Delta}\right\rangle\;+\;\left\langle\frac{H_2^2}{\Delta}\right\rangle\right]\,, \tag{E.16}$$

with the quantities H_0^1 still given by Eq. (E.3). Consequently, the desired analytical expression for σ_{IS} is identical to the expression for ρ_I in Eq. (E.13) except for a sign reversal in the first two terms, as in Eq. (4.15) of the main text. Finally, the cross-relaxation rate σ_{SI} is obtained from the expression for σ_{IS} by interchanging L_I and L_S everywhere.

APPENDIX F: TRUNCATED H_Q^K POLYNOMIALS

The polynomials H_Q^K are obtained from the minors of the $\mathbf{M}$ matrix according to Eq. (E.3). We truncate these polynomials by expressing them on the form

$$H_Q^K \;=\; \left\{H_Q^K\right\}_{\rm L} \,+\, \left\{H_Q^K\right\}_{\rm D} \,+\, \left\{H_Q^K\right\}_{\rm LD} \,, \tag{F.1}$$

where

$$\left\{H_Q^K\right\}_{\rm L} \;\equiv\; \lim_{D\to 0} H_Q^K \,, \tag{F.2a}$$

$$\left\{H_Q^K\right\}_{\rm D} \;\equiv\; \lim_{L_I,L_S\to 0} H_Q^K \,, \tag{F.2b}$$

$$\left\{H_Q^K\right\}_{\rm LD} \;\equiv\; \lim_{L_I,L_S,D\to 0} H_Q^K \,. \tag{F.2c}$$

We thus obtain, with $x \equiv \cos\theta$,

$$\left\{H_0^1\right\}_{\rm L} \;=\; \frac{1}{8}\left[1+L_I^2\right]^2\left[1+L_S^2\right]^2\left[1+(L_I+L_S)^2\right](3\,x^2-1)^2 \,, \tag{F.3a}$$

$$\left\{H_0^1\right\}_{\rm D} \;=\; \frac{1}{8}\left[1+\frac{D^2}{9}\right]\left[1+D^2\right]^2(3\,x^2-1)\left[(3\,x^2-1)+\frac{2\,(3\,x^2-2)D^2}{9}\right] \,, \tag{F.3b}$$

$$\left\{H_0^1\right\}_{\rm LD} \;=\; \frac{1}{8}\,(3\,x^2-1)^2 \,. \tag{F.3c}$$

$$\left\{H_1^1\right\}_{\rm L} \;=\; \frac{9}{8}\left[1+L_I^2\right]\left[1+L_S^2\right]^2\left[1+(L_I+L_S)^2\right]\left[1+(L_I-L_S)^2\right]x^2\,(1-x^2) \,, \tag{F.4a}$$

$$\left\{H_1^1\right\}_{\rm D} \;=\; \frac{9}{8}\left[1+\frac{D^2}{9}\right]\left[1+\frac{2\,D^2}{9}\right]\left[1+D^2\right]^2 x^2\,(1-x^2) \,, \tag{F.4b}$$

$$\left\{H_1^1\right\}_{\rm LD} \;=\; \frac{9}{8}\,x^2\,(1-x^2) \,. \tag{F.4c}$$

$$\left\{H_1^2\right\}_{\rm L} \;=\; \left\{H_1^1\right\}_{\rm L} \,, \tag{F.5a}$$

$$\left\{H_1^2\right\}_{\rm D} \;=\; \frac{9}{8}\left[1+\frac{D^2}{9}\right]^2\left[1+\frac{4\,D^2}{9}\right]\left[1+D^2\right]x^2\,(1-x^2) \,, \tag{F.5b}$$

$$\left\{H_1^2\right\}_{\rm LD} \;=\; \left\{H_1^1\right\}_{\rm LD} \,. \tag{F.5c}$$

$$\left\{H_2^2\right\}_{\rm L} \;=\; \frac{9}{8}\left[1+L_I^2\right]^2\left[1+L_S^2\right]^2\left[1+(L_I-L_S)^2\right](1-x^2)^2 \,, \tag{F.6a}$$

$$\left\{H_2^2\right\}_{\rm D} \;=\; \frac{9}{8}\left[1+\frac{D^2}{9}\right]^2\left[1+\frac{4\,D^2}{9}\right]\left[1+D^2\right](1-x^2)^2 \,, \tag{F.6b}$$

$$\left\{H_2^2\right\}_{\rm LD} \;=\; \frac{9}{8}\,(1-x^2)^2 \,. \tag{F.6c}$$

Isotropic averaging and substitution of these results into Eq. (F.1) yields

$$\begin{aligned}\left\langle H_0^1 \right\rangle \;=\; & \frac{1}{10}\Bigg\{\left[1+\frac{D^2}{9}\right]\left[1+\frac{2\,D^2}{9}\right]\left[1+D^2\right]^2 \\ & +\;\left[1+L_I^2\right]^2\left[1+L_S^2\right]^2\left[1+(L_I+L_S)^2\right]-1\Bigg\},\end{aligned} \tag{F.7}$$

$$\begin{aligned}\left\langle H_1^1 \right\rangle \;=\; & \frac{3}{20}\Bigg\{\left[1+\frac{D^2}{9}\right]\left[1+\frac{2\,D^2}{9}\right]\left[1+D^2\right]^2 \\ & +\;\left[1+L_I^2\right]\left[1+L_S^2\right]^2\left[1+(L_I+L_S)^2\right]\left[1+(L_I-L_S)^2\right]-1\Bigg\},\end{aligned} \tag{F.8}$$

$$\begin{aligned}\left\langle H_1^2 \right\rangle \;=\; & \frac{3}{20}\Bigg\{\left[1+\frac{D^2}{9}\right]^2\left[1+\frac{4\,D^2}{9}\right]\left[1+D^2\right] \\ & +\;\left[1+L_I^2\right]\left[1+L_S^2\right]^2\left[1+(L_I+L_S)^2\right]\left[1+(L_I-L_S)^2\right]-1\Bigg\},\end{aligned} \tag{F.9}$$

$$\begin{aligned}\left\langle H_2^2 \right\rangle \;=\; & \frac{3}{5}\Bigg\{\left[1+\frac{D^2}{9}\right]^2\left[1+\frac{4\,D^2}{9}\right]\left[1+D^2\right] \\ & +\;\left[1+L_I^2\right]^2\left[1+L_S^2\right]^2\left[1+(L_I-L_S)^2\right]-1\Bigg\},\end{aligned} \tag{F.10}$$

References

[1] S. Dattagupta, *Relaxation Phenomena in Condensed Matter Physics* (Academic Press, Orlando, FL, 1987).

[2] D. M. Brink and G. R. Satchler, *Angular Momentum*, 2nd ed. (Clarendon Press, Oxford, 1968).

[3] T. Nilsson and B. Halle, J. Chem. Phys. **137**, 054503 (2012).

[4] N. C. Pyper, Mol. Phys. **22**, 433 (1971).

Paper II

THE JOURNAL OF CHEMICAL PHYSICS **144**, 084202 (2016)

Nuclear magnetic relaxation by the dipolar EMOR mechanism: General theory with applications to two-spin systems

Zhiwei Chang and Bertil Halle[a)]
Division of Biophysical Chemistry, Department of Chemistry, Lund University, P.O. Box 124, SE-22100 Lund, Sweden

(Received 6 January 2016; accepted 3 February 2016; published online 25 February 2016)

In aqueous systems with immobilized macromolecules, including biological tissue, the longitudinal spin relaxation of water protons is primarily induced by exchange-mediated orientational randomization (EMOR) of intra- and intermolecular magnetic dipole-dipole couplings. We have embarked on a systematic program to develop, from the stochastic Liouville equation, a general and rigorous theory that can describe relaxation by the dipolar EMOR mechanism over the full range of exchange rates, dipole coupling strengths, and Larmor frequencies. Here, we present a general theoretical framework applicable to spin systems of arbitrary size with symmetric or asymmetric exchange. So far, the dipolar EMOR theory is only available for a two-spin system with symmetric exchange. Asymmetric exchange, when the spin system is fragmented by the exchange, introduces new and unexpected phenomena. Notably, the anisotropic dipole couplings of non-exchanging spins break the axial symmetry in spin Liouville space, thereby opening up new relaxation channels in the locally anisotropic sites, including longitudinal-transverse cross relaxation. Such cross-mode relaxation operates only at low fields; at higher fields it becomes nonsecular, leading to an unusual inverted relaxation dispersion that splits the extreme-narrowing regime into two sub-regimes. The general dipolar EMOR theory is illustrated here by a detailed analysis of the asymmetric two-spin case, for which we present relaxation dispersion profiles over a wide range of conditions as well as analytical results for integral relaxation rates and time-dependent spin modes in the zero-field and motional-narrowing regimes. The general theoretical framework presented here will enable a quantitative analysis of frequency-dependent water-proton longitudinal relaxation in model systems with immobilized macromolecules and, ultimately, will provide a rigorous link between relaxation-based magnetic resonance image contrast and molecular parameters. [http://dx.doi.org/10.1063/1.4942026]

I. INTRODUCTION

Soft-tissue contrast in clinical magnetic resonance imaging derives largely from spatial variations in the relaxation behavior of water protons. Yet, a rigorous theory relating the water ^{1}H relaxation rate to microscopic parameters is still not available. The lack of theoretical underpinning is also a limitation in biophysical studies of, for example, water-protein interactions and intermittent protein dynamics by field-cycling measurements of the water ^{1}H magnetic relaxation dispersion (MRD) in protein gels. Previously, such data have been interpreted with semi-phenomenological models[1–3] involving questionable assumptions about the relaxation-inducing motions.[4,5] Earlier water ^{1}H MRD studies of biopolymer gels from this laboratory[5,6] made use of a nonrigorous extension of the multi-spin Solomon equations to conditions outside the motional-narrowing regime.

Nuclear spins residing permanently in immobilized macromolecules give rise to solid-state type NMR spectra, whereas spins that are only transiently associated with the macromolecules, because they exchange chemically or physically with the solvent phase, exhibit liquid-state NMR properties provided that the immobilized macromolecules are isotropically distributed so that anisotropic nuclear spin couplings are averaged to zero. In such locally anisotropic samples, exchange plays a dual role. On the one hand, exchange transfers magnetizations and coherences between macromolecule-bound spins and solvent spins. On the other hand, exchange randomizes the orientation of anisotropic nuclear interaction tensors, thereby inducing spin relaxation. For this relaxation mechanism, known as exchange-mediated orientational randomization (EMOR), the motional-narrowing regime coincides with the fast-exchange regime. For the EMOR mechanism, the conventional Bloch-Wangsness-Redfield (BWR) perturbation theory of nuclear spin relaxation[7] breaks down when, as is frequently the case, the mean survival time of the macromolecule-bound spin is comparable to, or longer than, the inverse of the anisotropic nuclear spin coupling that it experiences in the bound state. We have therefore embarked on a program to develop a general non-perturbative theory, based on the stochastic Liouville equation (SLE),[8,9] that can describe relaxation by the EMOR mechanism over the full range of exchange rates and spin coupling strengths.

a)bertil.halle@bpc.lu.se

The EMOR SLE theory was first developed for quadrupolar relaxation[10,11] and it has been extensively applied to water ^{2}H MRD studies of colloidal silica,[12] polymer gels,[13,14] cross-linked proteins,[15–18] and cells.[19] As compared to quadrupolar relaxation, which only involves single spins, dipolar relaxation is theoretically more challenging. The EMOR SLE theory for dipolar relaxation of a homonuclear spin pair exchanging as a unit[20] is isomorphic with the corresponding theory for quadrupolar relaxation of a single spin-1,[11] but for heteronuclear spins, multispin (>2) systems and/or fragmentation of the spin system by exchange, qualitatively new phenomena appear in the dipolar relaxation. In a previous report,[20] hereafter referred to as Paper I, we developed the EMOR SLE theory for a (homonuclear or heteronuclear) spin pair that exchanges as an intact unit, a situation that we now refer to as symmetric exchange. Contrary to our earlier expectations,[20] the case of asymmetric exchange, where only one of the two dipole-coupled spins undergoes exchange, differs fundamentally from the symmetric case. In particular, since the non-exchanging spins are not isotropically averaged, the longitudinal and transverse magnetizations are dynamically coupled in the anisotropic sites. Such cross-mode relaxation, distinct from the cross-spin relaxation familiar from the Solomon equations,[21] gives rise to an inverted relaxation dispersion at low field.

Here, we develop the general dipolar EMOR SLE theory, valid for spin systems of arbitrary size and for symmetric as well as asymmetric exchange. To illustrate the general theory, we present explicit results for the asymmetric two-spin case, which is contrasted with the previously treated symmetric two-spin case.[20] These results are directly applicable to, for example, a macromolecular hydroxyl proton in chemical exchange with water protons (asymmetric case) or to an internal water molecule in physical exchange with bulk water (symmetric case).

This paper is organized as follows. In Sec. II, we present the dipolar EMOR formalism for an arbitrary spin system, with general and two-spin results in separate subsections. As compared to Paper I, the formalism has been modified and extended in order to accommodate asymmetric exchange. In Sec. III, we discuss the zero-field regime, which is of special significance for asymmetric exchange, and the motional-narrowing regime, where we obtain explicit results for the asymmetric two-spin case that serve to rationalize the unexpected inverted relaxation dispersion. In Sec. IV, we illustrate the theory by numerical results for the two-spin case, emphasizing the new phenomena that emerge for asymmetric exchange. Further physical insight is provided by an analysis of the time evolution of the relevant spin modes. Lengthy derivations and tables are relegated to six appendices.[22]

II. DIPOLAR EMOR THEORY

A. Spin systems and exchange cases

1. General case

We consider a system of spin-1/2 nuclei, some or all of which exchange between a solid-like anisotropic (A) state and a liquid-like bulk (B) state. The spins need not be isochronous (or even homonuclear), but the Zeeman coupling is taken to be the same in states A and B. (In any case, longitudinal relaxation is not affected by exchange-modulation of the Zeeman coupling.) The A state comprises a large number, N, of sites distinguished by their fixed orientations. Collectively, the N site orientations approximate an isotropic distribution. Each A site hosts a spin system with $m_A \geq 2$ mutually dipole-coupled spins. A subset (or fragment) of this spin system, comprising m_B spins (with $1 \leq m_B \leq m_A$), exchanges with the B state. The exchange is said to be symmetric if $m_B = m_A$ and asymmetric if $m_B < m_A$. We refer to the m_B exchanging spins as labile spins and the $m_A - m_B$ nonexchanging spins as nonlabile. The general theory developed here is valid without further restrictions on m_A and m_B.

To identify different exchange cases, we use the notation "(spins in state A)–(spins in state B)." For example, IS–I is a two-spin system with one labile spin and ISP–IS is a three-spin system with two labile spins. The IS–I case might refer to a macromolecular hydroxyl proton (I) dipole-coupled to a nearby aliphatic proton (S). The ISP–IS case might refer to the two protons (IS) of a water molecule temporarily trapped in a protein cavity, where the water protons are dipole-coupled to a nearby aliphatic proton (P). Note that both of these cases involve asymmetric exchange since the spin system is fragmented, even though no covalent bonds are broken in the latter case. We shall only consider cases where a single type of spin system is present in each state, but we note that it is straightforward to extend the theory to cases where more than one subset of spins exchange independently, possibly at different rates.

The orientations of all internuclear vectors involving at least one labile spin are taken to be instantaneously randomized upon exchange, thereby inducing dipolar relaxation. This assumption in the EMOR model is justified if the mean survival time of the labile spin(s) in the A sites is long compared to the time required for orientational randomization when the labile spin(s) has been transferred to state B. This is the case, for example, for chemical exchange of labile macromolecular protons with bulk water and for physical exchange of trapped (internal) water molecules with bulk water.[20,23] We can then ignore all dipole couplings among the labile spins in state B. If so desired, the small and frequency-independent relaxation contribution from fast modulation of dipole couplings in state B can be added to the final expression for the overall relaxation rate.[20]

At any time, a fraction P_A of the labile spins reside in state A, while a fraction $P_B = 1 - P_A$ reside in state B. The nonlabile spins are only present in state A. The general dipolar EMOR theory developed here is valid without restrictions on P_A. However, some of our results are only valid in the dilute regime, where $P_A \ll 1$. In most applications of interest, this inequality is satisfied with a wide margin.[4–6]

2. Two-spin case

In Paper I, we analyzed the symmetric exchange case IS–IS. Here, we consider the more complicated and interesting asymmetric exchange case IS–I. In a typical application, spin I is a labile proton, e.g., in a hydroxyl

group, exchanging with bulk water protons. This is actually an IS–I_2 case, but since the I–I dipole coupling in state B plays no role (see above), the results are the same as for the IS–I case. The only difference between the IS–I and IS–I_2 cases lies in the interpretation of the I-spin fraction: $P_A(IS\text{–}I_2) = P_A(IS\text{–}I)/[2 - P_A(IS\text{–}I)]$.

The Zeeman (H_Z) and dipolar (H_D) Hamiltonians for the two-spin system are given by Eqs. (2.2) and (2.3) of Paper I, with the dipole frequency ω_D defined as 3/2 times the usual dipole coupling constant, i.e., $\omega_D \equiv (3/2)\,[\mu_0/(4\pi)]\,\gamma_I\gamma_S\,\hbar/r_{IS}^3$.

B. Composite Liouville space

1. General case

Formally, we can regard the total system as a mixture of $N+1$ species, labeled by $\alpha = 0, 1, 2, \ldots, N$, with $\alpha = 0$ referring to state B and $\alpha \geq 1$ to site α in state A. Thus, $P_0 = P_B$ and $P_\alpha = P_A/N$ for $\alpha \geq 1$. All spin systems belonging to a given species α have the same spin Hamiltonian H^α, with $H^0 = H_Z$ for $\alpha = 0$ and $H^\alpha = H_Z + H_D^\alpha$ for $\alpha \geq 1$.

To an excellent approximation, the individual spin systems can be regarded as mutually noninteracting and uncorrelated. The spin density operator of the total system then reduces to a direct sum of species spin density operators σ^α, each of which represents an ensemble of spin systems in site α.[24–26] In the absence of exchange, the spin systems associated with the $N+1$ species evolve independently according to the Liouville equation

$$\frac{\mathrm{d}}{\mathrm{d}t}\,\sigma^\alpha(t) = -\,i\,\mathcal{L}^\alpha\,\sigma^\alpha(t). \tag{1}$$

The Liouville-space representation $\boldsymbol{\sigma}^\alpha$ of the species density operator σ^α is a column vector of dimension $D_\alpha = 2^{2\,m_\alpha} - 1$, where m_α ($= m_A$ or m_B) is the number of spins in species α and -1 comes from omitting the superfluous identity basis operator.

The spin density operator of the total system is represented as a column vector in a composite Liouville space[24,25] of dimension $D = D_B + D_A N$, formed as the direct sum of the spin operator spaces of the $N+1$ species. Thus,

$$\boldsymbol{\sigma} = \begin{bmatrix} \boldsymbol{\sigma}^0 \\ \boldsymbol{\sigma}^1 \\ \vdots \\ \boldsymbol{\sigma}^N \end{bmatrix} \quad \text{and} \quad \boldsymbol{\sigma}^\alpha = \begin{bmatrix} \sigma_1^\alpha \\ \vdots \\ \sigma_{D_\alpha}^\alpha \end{bmatrix}. \tag{2}$$

An element of the D-dimensional column vector $\boldsymbol{\sigma}$ can be expressed in the following equivalent ways:

$$\begin{aligned} \sigma_{n_\alpha}^\alpha &= (n_\alpha\,|\sigma^\alpha) = \mathrm{Tr}\{B_{n_\alpha}^\dagger \sigma^\alpha\} = \mathrm{Tr}\{B_{n_\alpha}^\dagger\,\langle\alpha|\sigma\rangle\} \\ &= \langle\alpha|\sigma_{n_\alpha}\rangle = \langle\alpha|(n_\alpha\,|\sigma)\rangle = \{\alpha, n_\alpha\,|\sigma\}, \end{aligned} \tag{3}$$

where B_{n_α} is a member of a complete set of orthonormal spin basis operators for species α,

$$(B_{n_\alpha}|B_{p_\alpha}) = \mathrm{Tr}\{B_{n_\alpha}^\dagger B_{p_\alpha}\} = \delta_{n_\alpha p_\alpha}. \tag{4}$$

To make full use of symmetry, we represent spin Liouville space in a basis of irreducible spherical tensor operators (ISTOs) $T_Q^K(\lambda)$ of rank K, quantum order Q, and additional quantum numbers λ.[27]

In the composite space, the $N+1$ independent Liouville equations (1) can be expressed as

$$\frac{\mathrm{d}}{\mathrm{d}t}\,\boldsymbol{\sigma}(t) = -\,i\,\mathbf{L}\,\boldsymbol{\sigma}(t) \tag{5}$$

with a block-diagonal Liouvillian supermatrix,

$$\mathbf{L} = \begin{bmatrix} \mathbf{L}^0 & \mathbf{0} & \mathbf{0} & \cdots & \mathbf{0} \\ \mathbf{0} & \mathbf{L}^1 & \mathbf{0} & \cdots & \mathbf{0} \\ \mathbf{0} & \mathbf{0} & \mathbf{L}^2 & \cdots & \mathbf{0} \\ \vdots & \vdots & \vdots & \ddots & \vdots \\ \mathbf{0} & \mathbf{0} & \mathbf{0} & \cdots & \mathbf{L}^N \end{bmatrix}, \tag{6}$$

where $\mathbf{L}^\alpha$ is a $D_\alpha \times D_\alpha$ matrix with elements $L^\alpha_{n_\alpha p_\alpha}$ and $\mathbf{0}$ is the $D_\alpha \times D_\beta$ null matrix.

2. Two-spin case

Whereas $D_A = D_B = 15$ for the symmetric IS–IS case,[20] we have $D_A = 15$ and $D_B = 3$ for the asymmetric IS–I case. The one-spin (state B) and two-spin (state A) ISTOs are given in Appendix A of the supplementary material.[22] For the IS–I case, n_B refers to one of the three B-state basis operators, while n_A refers to one of the 15 A-state basis operators. All these operators are normalized in the same two-spin (IS) space according to Eq. (4).

C. Exchange superoperator

1. General case

In the presence of exchange, the composite spin density operator evolves according to the SLE

$$\frac{\mathrm{d}}{\mathrm{d}t}\,\sigma(t) = (\mathcal{W} - i\,\mathcal{L})\,\sigma(t). \tag{7}$$

The exchange superoperator $\mathcal{W}$ describes the transfer of one or more spins from one site to another.[24,25] An exchange from site α to site β instantaneously switches the spin Hamiltonian from H^α to H^β. If this stochastic modulation is sufficiently frequent, it induces relaxation. For asymmetric exchange, which breaks up the spin system into fragments, A → B exchange has an additional effect: all multispin correlations within the spin system that have developed as a result of dipole couplings between labile and nonlabile spins in state A are lost.[28] For symmetric exchange, where the whole spin system exchanges as an intact unit, all multispin correlations are retained even though the dipole couplings are modulated.

To describe both of these effects, we decompose the exchange superoperator as

$$\mathcal{W} = \mathcal{T}_m \otimes \mathcal{T}_s - \mathcal{K}_m \otimes \mathcal{K}_s. \tag{8}$$

The "molecular" operators $\mathcal{T}_m$ and $\mathcal{K}_m$ act on the site kets $|\alpha\rangle$, so their composite-space supermatrix representations are block-diagonal with respect to the spin operators. These operators define the kinetic model (site-to-site transition probabilities), regardless of whether the spin system is

fragmented or not. The superoperators $\mathcal{T}_s$ and $\mathcal{K}_s$ act on spin operators, so (as for $\mathcal{L}$) their composite-space supermatrix representations are block-diagonal in the site basis. These superoperators distinguish labile from nonlabile spins and they account for decorrelation of multispin modes by exchange fragmentation of the spin system.[28] The composite-space supermatrix representation of $\mathcal{W}$ factorizes as

$$\{\alpha, n_\alpha\,|\mathcal{W}\,|\,\beta, p_\beta\} = \langle\alpha|\,\mathcal{T}_m\,|\beta\rangle\,(n_\alpha|\mathcal{T}_s|\,p_\beta) - \langle\alpha|\,\mathcal{K}_m\,|\beta\rangle\,(n_\alpha|\mathcal{K}_s|\,p_\beta). \tag{9}$$

The first term in Eq. (9) describes the exchange-mediated transfer of mode p_β in site β into mode n_α in site α. Conversely, the second term represents transfer of mode n_α in site α into mode p_β in site β.

The matrix representation of the transition rate operator $\mathcal{T}_m$ in the site basis is

$$\langle\alpha|\,\mathcal{T}_m\,|\beta\rangle = \frac{\pi_{\alpha\beta}}{\tau_\beta} = \frac{1}{\tau_\beta}\left[\delta_{\alpha 0}(1-\delta_{\beta 0}) + \frac{1}{N}(1-\delta_{\alpha 0})\delta_{\beta 0}\right] = \frac{1}{\tau_\beta}\left(1-\delta_{\alpha\beta}\right)\left(\delta_{\alpha 0} + \frac{\delta_{\beta 0}}{N}\right), \tag{10}$$

where $\pi_{\alpha\beta}$ is the transfer probability from site β to site α. The second step in Eq. (10) follows from the model assumption[10,20] that direct exchange between sites belonging to state A is not allowed, so that all $\pi_{\alpha\beta} = 0$ except $\pi_{0,\beta\geq 1} = 1$ and $\pi_{\alpha\geq 1,0} = 1/N$. The form of the site operator $\mathcal{K}_m$ then follows from probability conservation as[29]

$$\langle\alpha|\,\mathcal{K}_m\,|\beta\rangle = \delta_{\alpha\beta}\sum_{\gamma=0}^{N}\langle\gamma|\,\mathcal{T}_m\,|\alpha\rangle = \frac{\delta_{\alpha\beta}}{\tau_\alpha}. \tag{11}$$

Combination of Eqs. (9)–(11) yields for the four types of matrix element

$$\{n_B\,|\mathcal{W}\,|\,p_B\} = -\frac{1}{\tau_B}\,(n_B|\mathcal{K}_s|\,p_B), \tag{12a}$$

$$\{\alpha, n_A\,|\mathcal{W}\,|\,\beta, p_A\} = -\frac{1}{\tau_A}\,\delta_{\alpha\beta}\,(n_A|\mathcal{K}_s|\,p_A), \tag{12b}$$

$$\{n_B\,|\mathcal{W}\,|\,\alpha, p_A\} = \frac{1}{\tau_A}\,(n_B|\mathcal{T}_s|\,p_A), \tag{12c}$$

$$\{\alpha, p_A\,|\mathcal{W}\,|\,n_B\} = \frac{1}{N\,\tau_B}\,(p_A|\mathcal{T}_s|\,n_B), \tag{12d}$$

where we have suppressed the superfluous 0 site index for state B.

The spin supermatrix elements $(n_\alpha|\mathcal{T}_s|\,p_\beta)$ and $(n_\alpha|\mathcal{K}_s|\,p_\beta)$ in Eq. (9) can be regarded as selection rules; their values are either 0 or 1. The element $(n_B|\mathcal{T}_s|\,p_A)$ in Eq. (12c) equals 1 if A → B exchange converts spin mode p_A into spin mode n_B; otherwise it equals 0. In other words, $(n_B|\mathcal{T}_s|\,p_A) = 1$ only if the mode with sequence number n_B in the B-state operator basis is the same as the mode with sequence number p_A in the A-state operator basis, and if the exchange transfers all spins that are involved in this mode. Thus,

$$(n_B|\mathcal{T}_s|\,p_A) = (p_A|\mathcal{T}_s|\,n_B) \equiv \Delta_T(n_B, p_A) = \begin{cases} 1\,, & \text{if A} \leftrightarrow \text{B exchange interconverts modes } p_A \text{ and } n_B, \\ 0\,, & \text{otherwise,} \end{cases} \tag{13}$$

where $\Delta_T(n_B, p_A)$ is a sum of products of Kronecker deltas for the exchange-linked modes.

The elements $(n_B|\mathcal{K}_s|\,p_B)$ and $(n_A|\mathcal{K}_s|\,p_A)$ in Eqs. (12a) and (12b) are selection rules for the spin modes that leave state B or A, respectively. Like $\langle\alpha|\,\mathcal{K}_m\,|\beta\rangle$ in Eq. (11), these matrices are diagonal. Since only labile spins can exist in state B, it follows that $(n_B|\mathcal{K}_s|\,n_B) = 1$. However, state A may contain modes that only involve nonlabile spins. For such modes, $(n_A|\mathcal{K}_s|\,n_A) = 0$. Thus,

$$(n_B|\mathcal{K}_s|\,p_B) = \delta_{n_B,p_B}, \tag{14a}$$

$$(n_A|\mathcal{K}_s|\,p_A) = \delta_{n_A,p_A}\left[1-\Delta_K(n_A)\right], \tag{14b}$$

where $\Delta_K(n_A)$ is a sum of Kronecker deltas over non-exchanging modes, composed exclusively of operators associated with nonlabile spins. In view of Eqs. (12)–(14), the exchange supermatrix in the composite space can be expressed as

$$\mathbf{W} = \begin{bmatrix} -\frac{1}{\tau_B}\mathbf{1}^B & \frac{1}{\tau_A}\mathbf{T} & \frac{1}{\tau_A}\mathbf{T} & \cdots & \frac{1}{\tau_A}\mathbf{T} \\ \frac{1}{N\tau_B}\mathbf{T}' & -\frac{1}{\tau_A}\mathbf{K} & \mathbf{0} & \cdots & \mathbf{0} \\ \frac{1}{N\tau_B}\mathbf{T}' & \mathbf{0} & -\frac{1}{\tau_A}\mathbf{K} & \cdots & \mathbf{0} \\ \vdots & \vdots & \vdots & \ddots & \vdots \\ \frac{1}{N\tau_B}\mathbf{T}' & \mathbf{0} & \mathbf{0} & \cdots & -\frac{1}{\tau_A}\mathbf{K} \end{bmatrix}, \tag{15}$$

where τ_A and τ_B are the mean survival times[30] in the two states. Furthermore, $\mathbf{1}^B$ is the $D_B \times D_B$ identity matrix, $\mathbf{T}$ is the $D_B \times D_A$ matrix with elements $T_{n_B p_A} = (n_B|\mathcal{T}_s|\,p_A)$ given by Eq. (13), $\mathbf{T}'$ is the $D_A \times D_B$ matrix transpose of $\mathbf{T}$, and $\mathbf{K}$ is a diagonal $D_A \times D_A$ matrix with elements $K_{n_A p_A} = (n_A|\mathcal{K}_s|\,p_A)$ given by Eq. (14b). The elements of the matrices $\mathbf{T}$ and $\mathbf{K}$ are thus either 0 or 1. The nonzero elements of $\mathbf{T}$ connect labile-spin modes that are interconverted by exchange, and the vanishing diagonal elements of $\mathbf{K}$ correspond to A-state modes that only involve nonlabile spins. For symmetric exchange, $\mathcal{T}_s = \mathcal{K}_s = \mathcal{E}$ so $\mathbf{T} = \mathbf{K} = \mathbf{1}$.

2. Two-spin case

For the symmetric *IS–IS* case,[20] all spins are labile so there is no exchange fragmentation. Consequently, $\mathbf{T} = \mathbf{K} = \mathbf{1}$, the 15×15 identity matrix.

For the asymmetric *IS–I* case, exchange interconverts the three one-spin modes in state B, $n_B = 1$, 2, and 3 (Table S2), and the corresponding three one-spin modes in state A, $p_A = 1$, 6, and 10 (Table S1).[22] Consequently,

$$T_{n_B p_A} = \delta_{n_B,1}\,\delta_{p_A,1} + \delta_{n_B,2}\,\delta_{p_A,6} + \delta_{n_B,3}\,\delta_{p_A,10}. \tag{16}$$

The three one-spin modes in state A that do not involve the labile *I* spin are $n_A = 2$, 7, and 11 (Table S1),[22] so

$$K_{n_A p_A} = \delta_{n_A p_A}[1 - \delta_{n_A,2} - \delta_{n_A,7} - \delta_{n_A,11}]. \tag{17}$$

Therefore, $\mathbf{K}$ differs from the 15×15 identity matrix only in that $K_{22} = K_{77} = K_{11,11} = 0$.

D. Partial solution of the SLE

1. General case

The SLE (7) is a differential equation involving superoperators acting in the composite Liouville space. As previously shown for quadrupolar spins[10,11] and for the symmetric dipolar IS–IS case,[20] the SLE for the EMOR model admits an exact analytical solution that only involves spin superoperators, without explicit reference to site operators. Because we now develop the general dipolar EMOR theory using a somewhat modified formalism, the full derivation of the analytical SLE solution is presented in Appendix B.[22] In this subsection, we merely display the definitions that are needed for the following development.

A Laplace transform,

$$\widetilde{\sigma}(s) \equiv \int_0^\infty \mathrm{d}t \exp(-st)\, \sigma(t), \tag{18}$$

converts the SLE (7) into an algebraic equation with formal solution

$$\widetilde{\sigma}(s) = (s\,\mathcal{E} - \mathcal{W} + i\,\mathcal{L})^{-1}\sigma(0) \equiv \widetilde{\mathcal{U}}(s)\,\sigma(0), \tag{19}$$

where $\mathcal{E}$ is the identity superoperator in composite space and $\widetilde{\mathcal{U}}(s)$ is referred to as the resolvent superoperator.

Macroscopic spin observables are related to a density operator summed over all sites,

$$\langle\sigma(t)\rangle \equiv \sum_{\alpha=0}^{N} \sigma^\alpha(t) = \sigma^{\mathrm{B}}(t) + \sigma^{\mathrm{A}}(t), \tag{20}$$

where $\sigma^\alpha(t) = \langle\alpha|\sigma(t)\rangle$ and $\sigma^{\mathrm{B}}(t) \equiv \sigma^0(t)$. Combination of Eqs. (19) and (20) yields

$$\langle\widetilde{\sigma}(s)\rangle = \sum_{\alpha=0}^{N}\sum_{\beta=0}^{N} \langle\alpha|\,\widetilde{\mathcal{U}}(s)\,|\beta\rangle\,\sigma^\beta(0). \tag{21}$$

In Paper I, $\sigma(t)$ referred to a single spin system and to obtain $\langle\sigma(t)\rangle$ we then had to weight with the relative population, P_α, of spin systems in different sites α. Now, this relative weight is subsumed into $\sigma(t)$ so that $\langle\sigma(t)\rangle$ is simply a sum over sites, as in Eq. (20), without the need to account explicitly for the fact that the macroscopic sample contains different numbers of spin systems in A and B sites. According to this new convention, the initial density operator $\sigma^\alpha(0)$ is proportional to the relative population, P_α, for excitation under high-field conditions or by a fast field switch.[10] We express this as

$$\sigma^\alpha(0) = \begin{cases} P_{\mathrm{B}}\,\eta^{\mathrm{B}}, & \text{for } \alpha = 0 \\ \dfrac{P_{\mathrm{A}}}{N}\,\eta^{\mathrm{A}}, & \text{for } \alpha \geq 1 \end{cases} \tag{22}$$

so that Eq. (20) yields

$$\langle\sigma(0)\rangle = \sigma^{\mathrm{B}}(0) + \sigma^{\mathrm{A}}(0) = P_{\mathrm{B}}\,\eta^{\mathrm{B}} + P_{\mathrm{A}}\,\eta^{\mathrm{A}}. \tag{23}$$

Here, η^{A} and η^{B} are spin operators that depend on the initial condition of the spin system (selective or nonselective excitation) and, for heteronuclear spin systems, on the relative magnetogyric ratios (Sec. II D 2).

Combination of Eqs. (21) and (22) yields

$$\langle\widetilde{\sigma}(s)\rangle = \sum_{\alpha=0}^{N}\sum_{\beta=0}^{N} \langle\alpha|\,\widetilde{\mathcal{U}}(s)\,|\beta\rangle\,P_\beta\,\eta^\beta, \tag{24}$$

where η^β equals η^{B} for $\beta = 0$ and η^{A} for $\beta \geq 1$ and P_β equals P_{B} for $\beta = 0$ and P_{A}/N for $\beta \geq 1$. For asymmetric exchange, when different spin operator bases are used for states A and B, it is convenient to express the spin operator basis representation of Eq. (24) in terms of partitioned matrices,

$$\begin{bmatrix} \widetilde{\boldsymbol{\sigma}}^{\mathrm{B}}(s) \\ \widetilde{\boldsymbol{\sigma}}^{\mathrm{A}}(s) \end{bmatrix} = \begin{bmatrix} \widetilde{\mathbf{U}}^{\mathrm{BB}}(s) & \widetilde{\mathbf{U}}^{\mathrm{BA}}(s) \\ \widetilde{\mathbf{U}}^{\mathrm{AB}}(s) & \widetilde{\mathbf{U}}^{\mathrm{AA}}(s) \end{bmatrix} \begin{bmatrix} \boldsymbol{\eta}^{\mathrm{B}} \\ \boldsymbol{\eta}^{\mathrm{A}} \end{bmatrix}, \tag{25}$$

with the column vectors $\boldsymbol{\eta}^{\mathrm{B}} = [\eta_1^{\mathrm{B}} \ldots \eta_{D_{\mathrm{B}}}^{\mathrm{B}}]'$ and $\boldsymbol{\eta}^{\mathrm{A}} = [\eta_1^{\mathrm{A}} \ldots \eta_{D_{\mathrm{A}}}^{\mathrm{A}}]'$ (the prime denotes transposition). In Eq. (25), the site-averaged density operator column vector has been partitioned into (for notational simplicity, we omit the angular brackets)

$$\widetilde{\boldsymbol{\sigma}}^{\mathrm{B}} = \begin{bmatrix} \widetilde{\sigma}_1^{\mathrm{B}}(s) \\ \vdots \\ \widetilde{\sigma}_{D_{\mathrm{B}}}^{\mathrm{B}}(s) \end{bmatrix} \quad \text{and} \quad \widetilde{\boldsymbol{\sigma}}^{\mathrm{A}} = \begin{bmatrix} \widetilde{\sigma}_1^{\mathrm{A}}(s) \\ \vdots \\ \widetilde{\sigma}_{D_{\mathrm{A}}}^{\mathrm{A}}(s) \end{bmatrix}. \tag{26}$$

Furthermore, $\widetilde{\mathbf{U}}^{\mathrm{BB}}(s)$, $\widetilde{\mathbf{U}}^{\mathrm{BA}}(s)$, $\widetilde{\mathbf{U}}^{\mathrm{AB}}(s)$, and $\widetilde{\mathbf{U}}^{\mathrm{AA}}(s)$ are, respectively, $D_{\mathrm{B}} \times D_{\mathrm{B}}$, $D_{\mathrm{B}} \times D_{\mathrm{A}}$, $D_{\mathrm{A}} \times D_{\mathrm{B}}$, and $D_{\mathrm{A}} \times D_{\mathrm{A}}$ submatrices of the spin basis representation of the site-averaged resolvent superoperator

$$\langle\widetilde{\mathcal{U}}(s)\rangle \equiv \sum_{\alpha=0}^{N}\sum_{\beta=0}^{N} \langle\alpha|\,\widetilde{\mathcal{U}}(s)\,|\beta\rangle\,P_\beta. \tag{27}$$

Without further approximations, we show in Appendix B[22] that

$$\widetilde{\mathbf{U}}^{\mathrm{BB}}(s) = \tau_{\mathrm{B}}\,P_{\mathrm{B}}\big[\mathbf{1}^{\mathrm{B}} - \mathbf{G}^{\mathrm{B}}(s)\,\mathbf{T}\,\mathbf{G}^{\mathrm{A}}(s)\,\mathbf{T}'\big]^{-1}\mathbf{G}^{\mathrm{B}}(s), \tag{28a}$$

$$\widetilde{\mathbf{U}}^{\mathrm{BA}}(s) = \tau_{\mathrm{B}}\,P_{\mathrm{A}}\big[\mathbf{1}^{\mathrm{B}} - \mathbf{G}^{\mathrm{B}}(s)\,\mathbf{T}\,\mathbf{G}^{\mathrm{A}}(s)\,\mathbf{T}'\big]^{-1}\mathbf{G}^{\mathrm{B}}(s)\,\mathbf{T}\,\mathbf{G}^{\mathrm{A}}(s), \tag{28b}$$

$$\widetilde{\mathbf{U}}^{\mathrm{AB}}(s) = \tau_{\mathrm{A}}\,P_{\mathrm{B}}\big[\mathbf{1}^{\mathrm{A}} - \mathbf{G}^{\mathrm{A}}(s)\,\mathbf{T}'\,\mathbf{G}^{\mathrm{B}}(s)\,\mathbf{T}\big]^{-1}\mathbf{G}^{\mathrm{A}}(s)\,\mathbf{T}'\,\mathbf{G}^{\mathrm{B}}(s), \tag{28c}$$

$$\widetilde{\mathbf{U}}^{\mathrm{AA}}(s) = \tau_{\mathrm{A}}\,P_{\mathrm{A}}\big[\mathbf{1}^{\mathrm{A}} - \mathbf{G}^{\mathrm{A}}(s)\,\mathbf{T}'\,\mathbf{G}^{\mathrm{B}}(s)\,\mathbf{T}\big]^{-1}\mathbf{G}^{\mathrm{A}}(s), \tag{28d}$$

where

$$\mathbf{G}^{\mathrm{B}}(s) \equiv \big[(1 + s\tau_{\mathrm{B}})\,\mathbf{1}^{\mathrm{B}} + i\,\mathbf{L}_Z\,\tau_{\mathrm{B}}\big]^{-1} \tag{29}$$

and

$$\begin{aligned}\mathbf{G}^{\mathrm{A}}(s) &\equiv \frac{1}{4\pi}\int \mathrm{d}\Omega\,\big[s\,\tau_{\mathrm{A}}\,\mathbf{1}^{\mathrm{A}} + \mathbf{K} + i\,\mathbf{L}_Z\,\tau_{\mathrm{A}} + i\,\mathbf{L}_{\mathrm{D}}(\Omega)\,\tau_{\mathrm{A}}\big]^{-1} \\ &\equiv \big\langle\big[s\,\tau_{\mathrm{A}}\,\mathbf{1}^{\mathrm{A}} + \mathbf{K} + i\,\mathbf{L}_Z\,\tau_{\mathrm{A}} + i\,\mathbf{L}_{\mathrm{D}}(\Omega)\,\tau_{\mathrm{A}}\big]^{-1}\big\rangle\,.\end{aligned} \tag{30}$$

Here $\mathbf{L}_Z$ and $\mathbf{L}_{\mathrm{D}}(\Omega)$ are the Liouvillian supermatrices (in the appropriate spin basis) corresponding to the Zeeman and dipolar Hamiltonians, respectively. Because $\mathbf{G}^{\mathrm{A}}$ is isotropically averaged, it must reflect the axial symmetry of the spin system in the external magnetic field. For a basis of ISTOs $T_Q^K(\lambda)$, it then follows from the Wigner-Eckart theorem[27] that $\mathbf{G}^{\mathrm{A}}$ and the resolvent submatrices in Eq. (28) are block-diagonal in the projection index Q. (For asymmetric

exchange, where $D_B < D_A$ so that the matrices $\widetilde{\mathbf{U}}^{BA}$ and $\widetilde{\mathbf{U}}^{AB}$ are rectangular, also the "Q-blocks" are rectangular.) Longitudinal relaxation can therefore be fully described within the zero-quantum subspace. The dimension of this subspace is 5 for two spins and 19 for three spins. However, in the individual sites, the zero-quantum modes do not evolve independently of the remaining modes. The matrix within square brackets in Eq. (30) is not block-diagonal in Q so it must be evaluated in the full D_A-dimensional spin Liouville space of state A.

2. Two-spin case

With the spin operators indexed as in Tables S1 and S2 for the IS–I case,[22] the elements of the initial-condition vectors $\boldsymbol{\eta}^B$ and $\boldsymbol{\eta}^A$ in Eq. (25) are for nonselective excitation

$$\eta_n^A = \delta_{n1} + \kappa\,\delta_{n2}, \tag{31a}$$

$$\eta_n^B = \delta_{n1}. \tag{31b}$$

For I-selective excitation, we have instead

$$\eta_n^A = \eta_n^B = \delta_{n1}, \tag{32}$$

while for S-selective excitation

$$\eta_n^A = \kappa\,\delta_{n2}, \tag{33a}$$

$$\eta_n^B = 0. \tag{33b}$$

Here, $\kappa \equiv \gamma_S/\gamma_I$, the ratio of the magnetogyric ratios. For the IS–IS case, η_n^A is the same as for the IS–I case and $\eta_n^B = \eta_n^A$ for all three excitation modes. In Paper I, we used a slightly different notation.

E. Integral relaxation rate

1. General case

The integral longitudinal relaxation rate is defined as the inverse of the time integral of the reduced longitudinal magnetization and it may be expressed in terms of spin density operator components as

$$\widehat{R}_1 \equiv \left[\int_0^\infty \mathrm{d}t\,\frac{\sum_{n_B}\sigma_{n_B}^B(t) + \sum_{n_A}\sigma_{n_A}^A(t)}{\sum_{n_B}\sigma_{n_B}^B(0) + \sum_{n_A}\sigma_{n_A}^A(0)}\right]^{-1} = \frac{P_B\sum_{n_B}\eta_{n_B}^B + P_A\sum_{n_A}\eta_{n_A}^A}{\sum_{n_B}\widetilde{\sigma}_{n_B}^B(0) + \sum_{n_A}\widetilde{\sigma}_{n_A}^A(0)}, \tag{34}$$

where the sums run over spin modes (or basis operators) corresponding to the longitudinal magnetization of the observed spin(s) and Eq. (23) was used to obtain the last form. In the following, we specify the observed spin by a subscript, e.g., $\widehat{R}_{1,I}$. According to Eq. (25),

$$\widetilde{\sigma}_{n_B}^B(0) = \sum_{p_B=1}^{D_B} U_{n_B p_B}^{BB}\,\eta_{p_B}^B + \sum_{p_A=1}^{D_A} U_{n_B p_A}^{BA}\,\eta_{p_A}^A, \tag{35a}$$

$$\widetilde{\sigma}_{n_A}^A(0) = \sum_{p_B=1}^{D_B} U_{n_A p_B}^{AB}\,\eta_{p_B}^B + \sum_{p_A=1}^{D_A} U_{n_A p_A}^{AA}\,\eta_{p_A}^A, \tag{35b}$$

where we have introduced the shorthand notation

$$U_{np}^{XY} \equiv (n|\widetilde{\mathbf{U}}^{XY}(0)|p). \tag{36}$$

The values of $\eta_{p_B}^B$ and $\eta_{p_A}^A$ depend on the initial conditions for the relaxation experiment, as exemplified by Eqs. (31)–(33) for the two-spin case. In field-cycling experiments, excitation is always nonselective. In conventional relaxation experiments, selective excitation of the labile spins can be accomplished with a soft RF pulse if the nonlabile spins have a much wider NMR spectrum than the labile spins. For selective excitation, we only consider the case where the excited spin is also observed. The excitation mode is indicated by a superscript, e.g., $\widehat{R}_{1,I}^{non}$ or $\widehat{R}_{1,I}^{sel}$.

In the dilute regime, where $P_A \ll 1$, the detailed balance condition[11] $P_A\,\tau_B = P_B\,\tau_A$ and Eq. (28) show that the matrix elements U_{np}^{XY} are of the following orders of magnitude:

$$U_{np}^{BB} \sim P_A^{-1}, \tag{37a}$$

$$U_{np}^{BA} \sim 1, \tag{37b}$$

$$U_{np}^{AB} \sim 1, \tag{37c}$$

$$U_{np}^{AA} \sim P_A. \tag{37d}$$

In the dilute regime, we only need to retain the matrix elements of leading order in P_A in the denominator of Eq. (34). The condition $P_A \ll 1$ is specified by a superscript, e.g., $\widehat{R}_{1,I}^{dil}$.

2. Two-spin case

For the IS–I case, with the spin modes indexed as in Tables S1 and S2,[22] Eq. (34) yields

$$\widehat{R}_{1,I} = \frac{P_B\,\eta_1^B + P_A\,\eta_1^A}{\widetilde{\sigma}_1^B(0) + \widetilde{\sigma}_1^A(0)}, \tag{38a}$$

$$\widehat{R}_{1,S} = \frac{P_A\,\eta_2^A}{\widetilde{\sigma}_2^A(0)}. \tag{38b}$$

Using Eqs. (31)–(33), (35), and (38) and noting that $P_A + P_B = 1$, we obtain for nonselective excitation

$$\widehat{R}_{1,I}^{non} = [U_{11}^{BB} + U_{11}^{BA} + U_{11}^{AB} + U_{11}^{AA} + \kappa\,(U_{12}^{BA} + U_{12}^{AA})]^{-1}, \tag{39a}$$

$$\widehat{R}_{1,S}^{non} = \kappa\,P_A\,[U_{21}^{AB} + U_{21}^{AA} + \kappa\,U_{22}^{AA}]^{-1}, \tag{39b}$$

and for selective excitation

$$\widehat{R}_{1,I}^{sel} = [U_{11}^{BB} + U_{11}^{BA} + U_{11}^{AB} + U_{11}^{AA}]^{-1}, \tag{40a}$$

$$\widehat{R}_{1,S}^{sel} = P_A\,[U_{22}^{AA}]^{-1}. \tag{40b}$$

In the dilute regime, Eq. (37) allows us to reduce these expressions to

$$\widehat{R}_{1,I}^{dil} = [U_{11}^{BB}]^{-1}, \tag{41a}$$

$$\widehat{R}_{1,S}^{dil/non} = \kappa\,P_A\,[U_{21}^{AB}]^{-1}. \tag{41b}$$

In Eq. (41a), we only display the superscript "dil" since $\widehat{R}_{1,I}^{dil/non} = \widehat{R}_{1,I}^{dil/sel}$.

The foregoing expressions for the integral relaxation rate can be further simplified by expressing the matrix elements U_{np}^{XY} in terms of elements of the $\mathbf{G}^A(0)$ matrix, defined by

Eq. (30). This reduction is outlined in Appendix C 1;[22] here we merely quote the results for the rates in Eqs. (40b) and (41),

$$\widehat{R}^{\rm dil}_{1,I} = \frac{P_{\rm A}}{\tau_{\rm A}}\,(1 - g_{11})\,, \tag{42a}$$

$$\widehat{R}^{\rm dil/non}_{1,S} = \frac{P_{\rm A}}{\tau_{\rm A}}\,\frac{\kappa\,(1 - g_{11})}{g_{21}}, \tag{42b}$$

$$\widehat{R}^{\rm sel}_{1,S} = \frac{1}{\tau_{\rm A}}\,\frac{(1 - g_{11})}{(1 - g_{11})\,g_{22} + g_{12}\,g_{21}}, \tag{42c}$$

with the shorthand notation

$$g_{np} \equiv (n|\mathbf{G}^{\rm A}(0)|p). \tag{43}$$

As expected, $\widehat{R}^{\rm sel}_{1,S}$ is independent of $P_{\rm A}$, whereas in the dilute regime, the nonselective rates $\widehat{R}^{\rm dil}_{1,I}$ and $\widehat{R}^{\rm dil/non}_{1,S}$ are rigorously proportional to $P_{\rm A}$.

The corresponding expressions for the integral relaxation rate in the IS–IS case, most of which are given in Paper I, are readily obtained in the same manner. For convenience, these expressions are collected in Appendix C 2[22] with the same notation as used here for the IS–I case.

III. LIMITING CASES

A. Zero-field regime

1. General case

In the absence of an external magnetic field, the macroscopic system is rotationally invariant (isotropic). The Wigner-Eckart theorem[27] then implies that supermatrices that are averaged over the A sites are block-diagonal in the rank index K as well as in the projection index Q if they are represented in the ISTO basis $T^K_Q(\lambda) \equiv B_n$. Furthermore, the nonzero matrix elements do not depend on Q. For example,

$$\begin{aligned}&\left(T^K_Q(\lambda)\,|\,\mathcal{G}^{\rm A}\,|\,T^{K'}_{Q'}(\lambda')\right)\\ &\quad = \delta_{KK'}\delta_{QQ'}\left(T^K_0(\lambda)\,|\,\mathcal{G}^{\rm A}\,|\,T^K_0(\lambda')\right).\end{aligned} \tag{44}$$

We refer to the conditions under which this selection rule is valid as the zero-field (ZF) regime. In the ZF regime, the Larmor frequencies are much smaller than the rate of evolution induced by the dipole coupling, so we can set $\mathcal{L}_{\rm Z} \equiv 0$.

In Paper I, we defined a low-field (LF) regime through the inequality

$$(\omega_I\,\tau_{\rm A})^2 \ll 1 + (\omega_{\rm D}\,\tau_{\rm A})^2, \tag{45}$$

where $\omega_{\rm D}$ is the dipole coupling frequency, as defined in Sec. II A 2, and ω_I is the Larmor frequency. In the ultraslow-motion regime, where $(\omega_{\rm D}\,\tau_{\rm A})^2 \gg 1$, inequality (45) implies that $\omega_I^2 \ll \omega_{\rm D}^2$, that is, the Larmor precession is much slower than the coherent dipolar evolution. In the motional-narrowing (MN) regime, where $(\omega_{\rm D}\,\tau_{\rm A})^2 \ll 1$, inequality (45) implies that $(\omega_I\,\tau_{\rm A})^2 \ll 1$, which is the so-called extreme-narrowing condition. Physically, extreme narrowing corresponds to a situation where the local field (produced by the dipole coupling) is randomized by exchange (on the time scale $\tau_{\rm A}$) before any significant Larmor precession has taken place.

For symmetric exchange, such as the IS–IS case treated in Paper I, the LF condition (45) also defines the ZF regime. In other words, the integral relaxation rate is independent of ω_I in the frequency range defined by inequality (45). In contrast, for asymmetric exchange, such as the IS–I case, the Zeeman coupling can be neglected only if the Larmor precession is slow compared to the cross-mode relaxation in the A sites (Sec. III B 2). For asymmetric exchange, the ZF regime is therefore defined by the more restrictive inequality

$$|\omega_I|\,\tau_{\rm A} \ll \frac{(\omega_{\rm D}\,\tau_{\rm A})^2}{1 + (\omega_{\rm D}\,\tau_{\rm A})^2 + (\omega_I\,\tau_{\rm A})^2}. \tag{46}$$

Figure 1 depicts the LF and ZF regimes for the case of asymmetric exchange, as defined by inequalities (45) and (46). In the MN regime (the lower half of Fig. 1), the ZF regime corresponds to $|\omega_I| \ll \omega_{\rm D}^2\,\tau_{\rm A}$ and the LF regime to $\omega_{\rm D}^2\,\tau_{\rm A} \ll |\omega_I| \ll 1/\tau_{\rm A}$. In the ultraslow-motion regime (the upper half of Fig. 1), the ZF regime corresponds to $|\omega_I| \ll 1/\tau_{\rm A}$ and the LF regime to $1/\tau_{\rm A} \ll |\omega_I| \ll |\omega_{\rm D}|$. The blue curve in Fig. 1, at the boundary between the LF and adiabatic regimes, indicates the frequency of the main dispersion step for the integral longitudinal relaxation rate. The red curve, at the boundary between the ZF and LF regimes, indicates the frequency of an inverted dispersion step that only appears for asymmetric exchange (Sec. III B 2).

In the ZF regime, selection rule (44) implies that $\mathbf{G}^{\rm A}$ and other site-averaged supermatrices consist of $(m_{\rm A} + 1)^2$ blocks. For a given rank K, the $2K + 1$ blocks corresponding to different values of the projection index Q are identical. Furthermore, all blocks are symmetric. In the ZF regime, the evolution of the longitudinal magnetizations can therefore be fully described within the rank-1 zero-quantum subspace.

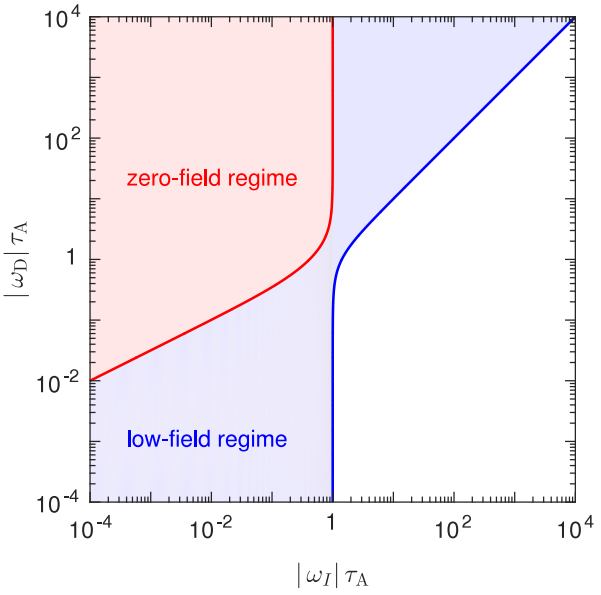

FIG. 1. For asymmetric exchange, the LF and ZF regimes are distinct, as shown here. For symmetric exchange, the coincident LF and ZF regimes both extend up to the blue boundary.

2. Two-spin case

For two-spin (IS) systems in the ZF regime, selection rule (44) implies that $\mathbf{G}^{\mathrm{A}}$ has one diagonal element corresponding to the rank-0 singlet operator $T_0^0(11)$, three identical 3×3 rank-1 blocks spanned by the operators $T_0^1(k_I k_S)$, $T_1^1(k_I k_S)$, and $T_{-1}^1(k_I k_S)$, respectively, with $(k_I k_S) = (10)$, (01) or (11), and five identical rank-2 diagonal elements corresponding to $T_Q^2(11)$. Since the matrix is symmetric, there are only 9 unique elements. The evolution of the longitudinal magnetizations in state A is fully described by the $T_0^1(k_I k_S)$ block, spanned by the basis operators (Table S1)[22]

$$B_1 \equiv T_0^1(10) = I_z, \tag{47a}$$

$$B_2 \equiv T_0^1(01) = S_z, \tag{47b}$$

$$B_4 \equiv T_0^1(11) = \frac{1}{\sqrt{2}}\,(I_-\,S_+ - I_+\,S_-) = i\,\sqrt{2}\,(I_x\,S_y - I_y\,S_x)\,. \tag{47c}$$

Since longitudinal relaxation in the ZF regime can be fully described within the rank-1 zero-quantum subspace, many results can be obtained in analytical form. For example, in Appendix D,[22] we derive, for the IS–I case, closed-form expressions for $\widetilde{\sigma}_1^{\mathrm{A}}(s)$, $\widetilde{\sigma}_2^{\mathrm{A}}(s)$, and $\widetilde{\sigma}_4^{\mathrm{A}}(s)$, from which the time evolution of these spin modes can be obtained by an inverse Laplace transformation. In Appendix D,[22] we also derive expressions for the integral relaxation rate in Eqs. (39) and (40). For example,

$$\widehat{R}_{1,I}^{\mathrm{dil}}(0) = \frac{2}{3}\,P_{\mathrm{A}}\,\frac{\omega_{\mathrm{D}}^2\,\tau_{\mathrm{A}}}{5+(\omega_{\mathrm{D}}\,\tau_{\mathrm{A}})^2}, \tag{48a}$$

$$\widehat{R}_{1,S}^{\mathrm{sel}}(0) = \frac{2\,\omega_{\mathrm{D}}^2\,\tau_{\mathrm{A}}}{6+(\omega_{\mathrm{D}}\,\tau_{\mathrm{A}})^2}. \tag{48b}$$

In the MN regime, Eq. (48a) can be written as $\widehat{R}_{1,I}^{\mathrm{dil}}(0) = P_{\mathrm{A}}\,R_1^{\mathrm{A}}(0)$, with an intrinsic A-state relaxation rate $R_1^{\mathrm{A}}(0) = (2/15)\,\omega_{\mathrm{D}}^2\,\tau_{\mathrm{A}}$. This is as expected, because, for the EMOR model, the MN regime is also the fast-exchange regime. If relaxation in the A-sites were governed by an internal motion independent of the exchange kinetics, then the Luz-Meiboom equation, $R_1 = P_{\mathrm{A}}/(\tau_{\mathrm{A}} + 1/R_1^{\mathrm{A}})$, should hold in the dilute + MN regime.[31] However, if Eq. (48a) is cast on this form, we find that $R_1^{\mathrm{A}}(0) = (2/3)\,\omega_{\mathrm{D}}^2\,\tau_{\mathrm{A}}/[5+(\omega_{\mathrm{D}}\,\tau_{\mathrm{A}})^2/3]$, which agrees with the foregoing expression only in the MN (fast-exchange) regime. This inconsistency arises because the Luz-Meiboom equation is not valid for the EMOR model, where the intrinsic relaxation is induced by the exchange itself so that the MN condition $(\omega_{\mathrm{D}}\,\tau_{\mathrm{A}})^2 \ll 1$ is automatically violated as soon as we leave the fast-exchange regime.

B. Motional-narrowing regime

1. General case

In the MN regime, where $(\omega_{\mathrm{D}}\,\tau_{\mathrm{A}})^2 \ll 1$, the composite spin density operator evolves according to the "stochastic Redfield equation" (SRE)

$$\frac{\mathrm{d}}{\mathrm{d}t}\,\sigma(t) = (\mathcal{W} - i\,\mathcal{L}_0 - \mathcal{R})\,\sigma(t), \tag{49}$$

where $\mathcal{W}$ is same exchange superoperator (8) as in SLE (7) and $\mathcal{R}$ is the relaxation superoperator prescribed by the BWR perturbation theory.[7] The Liouvillian $\mathcal{L}_0$ is associated with the time-independent part of the spin Hamiltonian that is unaffected by the exchange process. For symmetric exchange in general and for asymmetric exchange with only one nonlabile spin ($m_{\mathrm{A}} = m_{\mathrm{B}} + 1$), the static Hamiltonian only contains the Zeeman coupling so $\mathcal{L}_0 = \mathcal{L}_{\mathrm{Z}}$. For example, this is true for the IS–IS and IS–I cases. However, for asymmetric exchange with $m_{\mathrm{A}} \geq m_{\mathrm{B}} + 2$ (e.g., ISP–I), so the A sites contain at least two nonlabile spins, $\mathcal{L}_0$ includes the static dipole coupling(s) besides the Zeeman coupling.

Like SLE (7), SRE (49) can be solved in site space, in full analogy with the treatment in Appendix B.[22] Specifically, Eqs. (25) and (28) remain valid, but Eq. (30) is replaced by

$$\mathbf{G}^{\mathrm{A}}(s) = \left\langle [s\,\tau_{\mathrm{A}}\,\mathbf{1}^{\mathrm{A}} + \mathbf{K} + i\,\mathbf{L}_0^{\alpha}\,\tau_{\mathrm{A}} + \mathbf{R}^{\alpha}\tau_{\mathrm{A}}]^{-1}\right\rangle, \tag{50}$$

where the angular brackets indicate the same isotropic orientational average as in Eq. (30) and $\mathbf{R}^{\alpha}$ is the orientation-dependent relaxation supermatrix for site α. As noted in Sec. II D 1, the isotropically averaged supermatrix $\mathbf{G}^{\mathrm{A}}(s)$ is block-diagonal in the projection index Q. To determine the integral longitudinal relaxation rate, as described in Sec. II E, we only need the $Q = 0$ block of the supermatrix

$$\mathbf{G}^{\mathrm{A}}(0) = \left\langle (\mathbf{\Lambda}^{\alpha})^{-1}\right\rangle, \tag{51}$$

with

$$\mathbf{\Lambda}^{\alpha} \equiv \mathbf{K} + i\,\mathbf{L}_0^{\alpha}\,\tau_{\mathrm{A}} + \mathbf{R}^{\alpha}\tau_{\mathrm{A}}. \tag{52}$$

In the EMOR model, exchange plays two roles: it transfers spin modes between the A and B states and it induces relaxation by randomizing the orientation of the dipole vector(s) in the A sites. In SLE (7), both of these roles are played by the exchange superoperator $\mathcal{W}$. In the SRE (49), on the other hand, the first role is played by the exchange superoperator $\mathcal{W}$, which describes the transfer (or decorrelation) of local spin modes $\sigma_n^{\alpha}(t)$, while the second role is played by the orientation-dependent relaxation superoperator $\mathcal{R}^{\alpha}$, which describes relaxation induced by orientational randomization of the dipole vector(s) in site α. Because of the dual role played by exchange in the EMOR model, the MN condition $(\omega_{\mathrm{D}}\,\tau_{\mathrm{A}})^2 \ll 1$ not only ensures that the BWR theory is valid, but it also corresponds to the fast-exchange limit of the SRE because $R^{\alpha}\,\tau_{\mathrm{A}} \approx (\omega_{\mathrm{D}}\,\tau_{\mathrm{A}})^2 \ll 1$. To derive the integral relaxation rate in the MN regime from SRE (49), we must therefore implement the MN condition twice: first in obtaining the relaxation supermatrix $\mathbf{R}^{\alpha}$ from the BWR theory[7] and then in implementing the fast-exchange limit by expanding the matrix inverse $(\mathbf{\Lambda}^{\alpha})^{-1}$ to first order in $\|\mathbf{R}^{\alpha}\|\,\tau_{\mathrm{A}}$, that is, to second order in $\omega_{\mathrm{D}}\,\tau_{\mathrm{A}}$.

The theoretical analysis of relaxation in the MN regime is greatly simplified by making full use of symmetry.[32–34] As noted above, rotational symmetry ensures that we only need to consider the $Q = 0$ block of the isotropically averaged supermatrix $\mathbf{G}^{\mathrm{A}}(0)$. In contrast, the relaxation supermatrix $\mathbf{R}^{\alpha}$ in Eq. (52) pertains to a site α with a particular orientation so it is not block-diagonal in Q. However, in the MN regime, the relaxation problem can be further simplified by exploiting spin inversion conjugation (SIC) symmetry.[32–34] The ISTOs have definite SIC parity (either odd or even) and the superoperators $i\,\mathcal{L}_{\mathrm{Z}}$ and $\mathcal{R}^{\alpha}$ both have even SIC parity.[32–34] According

to the basic orthogonality theorem of group theory,[35] the supermatrices $i\,\mathbf{L}_Z$ and $\mathbf{R}^\alpha$ in the ISTO basis can then have nonzero elements only between basis operators of the same parity. If we order the basis operators so that the odd operators (including the single-spin longitudinal operators) precede the even operators, then the supermatrices $i\,\mathbf{L}_Z$ and $\mathbf{R}^\alpha$ are block-diagonal. For exchange cases with less than two nonlabile spins, so that $\mathbf{L}_0^\alpha = \mathbf{L}_Z$, it then follows (since matrix inversion does not alter the block structure and since $\mathbf{K}$ is diagonal) that also the supermatrix $\mathbf{\Lambda}^\alpha$ in Eq. (52) is block-diagonal. As long as we are concerned with longitudinal relaxation, we therefore need to consider only the odd-parity zero-quantum subblock of the $\mathbf{G}^{\mathrm{A}}(0)$ supermatrix. This partitioning of the $Q = 0$ subspace on the basis of SIC parity is helpful also for exchange cases with two or more nonlabile spins, even though the odd and even subblocks are then coupled because the superoperator $i\,\mathcal{L}_{\mathrm{D}}$ associated with the static dipole coupling(s) has odd SIC parity.[34]

2. Two-spin case

If we reorder the 15 basis operators in Table S1[22] so that the six odd-parity (single-spin) operators (including I_z and S_z) precede the nine even-parity (two-spin) operators, the supermatrix $\mathbf{\Lambda}^\alpha$ in Eq. (52) is block-diagonal. Longitudinal relaxation is fully described by the odd 6×6 block. Ordering the odd basis operators as $\{I_z, I_+, I_-, S_z, S_+, S_-\}$, we can then partition $\mathbf{\Lambda}^\alpha$ into 3×3 submatrices as

$$\mathbf{\Lambda}^\alpha = \begin{bmatrix} \mathbf{\Lambda}^\alpha_{II} & \mathbf{\Lambda}^\alpha_{IS} \\ \mathbf{\Lambda}^\alpha_{SI} & \mathbf{\Lambda}^\alpha_{SS} \end{bmatrix}, \tag{53}$$

where, for the IS–I case,

$$\mathbf{\Lambda}^\alpha_{II} = \mathbf{1} + \tau_{\mathrm{A}}(\mathbf{R}^\alpha_{II} + i\,\omega_I\,\mathbf{Q}), \tag{54a}$$
$$\mathbf{\Lambda}^\alpha_{IS} = \tau_{\mathrm{A}}\,\mathbf{R}^\alpha_{IS}, \tag{54b}$$
$$\mathbf{\Lambda}^\alpha_{SI} = \tau_{\mathrm{A}}\,\mathbf{R}^\alpha_{SI}, \tag{54c}$$
$$\mathbf{\Lambda}^\alpha_{SS} = \tau_{\mathrm{A}}(\mathbf{R}^\alpha_{SS} + i\,\omega_S\,\mathbf{Q}). \tag{54d}$$

Here, $\mathbf{1}$ is the 3×3 identity matrix and $\mathbf{Q}$ is a diagonal matrix with diagonal elements $[0, 1, -1]$. To obtain Eq. (54), we also noted that, according to Eq. (17), $\mathbf{K}_{II} = \mathbf{1}$ and $\mathbf{K}_{IS} = \mathbf{K}_{SI} = \mathbf{K}_{SS} = \mathbf{0}$.

For the elements of the four relaxation submatrices, given explicitly in Appendix E,[22] we use a notation where, e.g., $R^{IS}_{z+} = (T^1_0(10)\,|\mathbf{R}^\alpha_{IS}|\,T^1_1(01)) = -2^{-1/2}\,(I_z\,|\mathbf{R}^\alpha_{IS}|\,S_+)$. These local (orientation-dependent) relaxation rates are of four kinds. First, there are longitudinal (R^{II}_{zz} and R^{SS}_{zz}) and transverse ($R^{II}_{\pm\pm}$ and $R^{SS}_{\pm\pm}$) auto-spin auto-mode rates. Second, there are longitudinal (R^{IS}_{zz} and R^{SI}_{zz}) and transverse ($R^{IS}_{\pm\pm}$ and $R^{SI}_{\pm\pm}$) cross-spin auto-mode rates. Auto-spin and cross-spin rates also occur in the two-spin Solomon equations,[7] but they are then isotropically averaged. Third, there are the auto-spin cross-mode rates $R^{II}_{z\pm}$, $R^{II}_{\pm z}$, and $R^{II}_{\pm\mp}$, and the corresponding rates for spin S. Finally, there are cross-spin cross-mode rates, like $R^{IS}_{z\pm}$. All these rates pertain to a particular site α and they therefore depend on the orientation of the dipole vector in that site as detailed in Appendix E.[22]

The cross-mode rates couple the longitudinal and transverse magnetizations of the same or different spins. This coupling is a consequence of the spatial anisotropy of the A sites. Indeed, we show in Appendix E[22] that all cross-mode rates vanish after isotropic averaging. As shown below, such averaging occurs in the symmetric IS–IS case, where the same I–S pair exchanges rapidly among the A sites (via the B site), but not in the asymmetric IS–I case, where the two spins are no longer correlated after the exchange. As shown explicitly in Appendix E,[22] the cross-mode rates are only effective in the ZF regime, as defined by Eq. (46). At higher fields, they become nonsecular, that is, the longitudinal and transverse magnetizations are decoupled by the Larmor precession, which then is much faster than the (local) cross-mode relaxation.

All the local relaxation rates, except for the longitudinal auto-mode rates R^{II}_{zz}, R^{SS}_{zz}, and $R^{IS}_{zz} = R^{SI}_{zz}$, involve both the even (real) and the odd (imaginary) parts of the complex spectral density function (Appendix E[22]). However, the odd spectral density function (OSDF) has no effect on longitudinal relaxation in the two-spin cases. In the IS–IS case, isotropic averaging cancels the cross-mode rates so only the longitudinal auto-mode rates are relevant. In the IS–I case, the cross-mode rates are only effective in the ZF regime, where the OSDF is negligibly small compared to the real part. So, in either case, the OSDF only affects the evolution of the transverse spin modes, giving rise to the well-known second-order dynamic frequency shift.[36] However, for larger spin systems, the OSDF can also affect the longitudinal modes, e.g., in the ISP–ISP case.[34]

Returning now to the derivation of the integral relaxation rate for the IS–I case, we invert the partitioned matrix in Eq. (53), obtaining for the II block

$$\begin{aligned}[(\mathbf{\Lambda}^\alpha)^{-1}]_{II} &= \left[\mathbf{\Lambda}^\alpha_{II} - \mathbf{\Lambda}^\alpha_{IS}\,(\mathbf{\Lambda}^\alpha_{SS})^{-1}\mathbf{\Lambda}^\alpha_{SI}\right]^{-1} \\ &= \left[\,\mathbf{Z} + \tau_{\mathrm{A}}(\mathbf{R}^\alpha_{II} - \mathbf{\Gamma}^\alpha_{II})\,\right]^{-1},\end{aligned} \tag{55}$$

where Eq. (54) was used in the second step. Here we have also defined the diagonal matrix

$$\mathbf{Z} \equiv \mathbf{1} + i\,\omega_I\,\tau_{\mathrm{A}}\,\mathbf{Q}, \tag{56}$$

and the "cross relaxation" matrix

$$\mathbf{\Gamma}^\alpha_{II} \equiv \mathbf{R}^\alpha_{IS}(\mathbf{R}^\alpha_{SS} + i\,\omega_S\,\mathbf{Q})^{-1}\mathbf{R}^\alpha_{SI}. \tag{57}$$

We now expand the inverse in Eq. (55) to second order in $\omega_{\mathrm{D}}\,\tau_{\mathrm{A}}$ and perform the isotropic site average, to obtain

$$\left\langle[(\mathbf{\Lambda}^\alpha)^{-1}]_{II}\right\rangle = \mathbf{Z}^{-1} - \tau_{\mathrm{A}}\,\mathbf{Z}^{-1}\left[\left\langle\mathbf{R}^\alpha_{II}\right\rangle - \left\langle\mathbf{\Gamma}^\alpha_{II}\right\rangle\right]\mathbf{Z}^{-1}. \tag{58}$$

We are primarily interested in the I-spin integral relaxation rate in the dilute regime. This rate only involves the matrix element

$$g_{11} = (1\,|\mathbf{G}^{\mathrm{A}}(0)|\,1) = (1\,|\,\left\langle[(\mathbf{\Lambda}^\alpha)^{-1}]_{II}\right\rangle\,|\,1). \tag{59}$$

Combination of Eqs. (42a) and (56)–(59) yields

$$\widehat{R}^{\mathrm{dil}}_{1,I} = P_{\mathrm{A}}\left[\left\langle R^{II}_{zz}\right\rangle - \left\langle\Gamma^{II}_{zz}\right\rangle\right], \tag{60}$$

where $R^{II}_{zz} \equiv (1\,|\mathbf{R}^\alpha_{II}|\,1)$ and $\Gamma^{II}_{zz} \equiv (1\,|\mathbf{\Gamma}^\alpha_{II}|\,1)$. The first term within square brackets in Eq. (60) is the well-known[7,21] longitudinal auto-spin relaxation rate, averaged over the isotropic distribution of A sites (Appendix E[22]),

$$\langle R^{II}_{zz}\rangle = \frac{2}{45}\,\omega_{\rm D}^2\,[\,j(\omega_I-\omega_S)+3\,j(\omega_I)+6\,j(\omega_I+\omega_S)\,], \tag{61}$$

with the reduced spectral density function given by

$$j(\omega) = \frac{\tau_{\rm A}}{1+(\omega\,\tau_{\rm A})^2}. \tag{62}$$

The second term in Eq. (60) accounts for cross-spin as well as cross-mode relaxation. Cross-mode relaxation only comes into play in the ZF regime, where all relaxation channels are secular, meaning that all oscillating factors in Eq. (E.28)[22] can be replaced by unity. According to Eq. (57), the cross relaxation matrix element $\Gamma^{II}_{zz} = (1\,|\mathbf{\Gamma}^{\alpha}_{II}|\,1)$ only has contributions from the first row of $\mathbf{R}^{\alpha}_{IS}$ and from the first column of $\mathbf{R}^{\alpha}_{SI}$. The four off-diagonal elements in this group of six elements involve the cross-spin cross-mode rates $R^{IS}_{z\pm}$ and $R^{SI}_{\pm z}$, all of which are multiplied by oscillating factors $\exp(\pm i\,\omega_S\,t)$ in Eq. (E.28).[22] Two conclusions follow. First, the longitudinal-transverse cross-mode relaxation contribution to $\widehat{R}^{\rm dil}_{1,I}$ in the zero-field regime involves the four cross-spin cross-mode rates $R^{IS}_{z\pm}$ and $R^{SI}_{\pm z}$ and the four auto-spin-S cross-mode rates $R^{SS}_{z\pm}$ and $R^{SS}_{\pm z}$, but it does not involve the four auto-spin-I cross-mode rates $R^{II}_{z\pm}$ and $R^{II}_{\pm z}$. Second, for a heteronuclear spin pair, with $\omega_S \neq \omega_I$, the entire cross-mode contribution to $\widehat{R}^{\rm dil}_{1,I}$ disappears when $|\omega_S| \gg \omega_{\rm D}^2\,\tau_{\rm A}$ (Sec. IV B).

Outside the ZF regime, cross-mode relaxation is nonsecular and can therefore be neglected. The four relaxation submatrices are then diagonal so Eqs. (57) and (60) yield

$$\widehat{R}^{\rm dil}_{1,I} = P_{\rm A}\left[\langle R^{II}_{zz}\rangle - \left\langle\frac{(R^{IS}_{zz})^2}{R^{SS}_{zz}}\right\rangle\right], \tag{63}$$

where the orientation-dependent auto-spin and cross-spin rates in the second term are given in Appendix E.[22] In the LF + MN regime, which is also the extreme-narrowing regime (Sec. III A 1), these rates are given by Eqs. (E.35a) and (E.35b).[22] Substitution into Eq. (63) yields after isotropic averaging

$$\widehat{R}^{\rm dil}_{1,I} = c\,P_{\rm A}\,\omega_{\rm D}^2\,\tau_{\rm A}, \tag{64}$$

with the numerical constant

$$c \equiv \int_0^1 {\rm d}x\,\frac{(1-x^2)(1+3\,x^2)}{(5-3\,x^2)} = 0.267\,779\ldots. \tag{65}$$

Result (63) is not valid in the ZF regime, where there is cross-mode coupling. In the ZF + MN regime, Eq. (48a) reduces to

$$\widehat{R}^{\rm dil}_{1,I}(0) = \frac{2}{15}\,P_{\rm A}\,\omega_{\rm D}^2\,\tau_{\rm A}, \tag{66}$$

which is a factor 2.008 343 ... smaller than the result in Eq. (64). It is clear, therefore, that longitudinal-transverse cross-mode coupling slows down the longitudinal relaxation of the labile I-spin. As the Larmor frequency increases from below $\omega_{\rm D}^2\,\tau_{\rm A}$ to above this value, the integral relaxation rate $\widehat{R}^{\rm dil}_{1,I}$ thus exhibits an inverted dispersion step. The locus of this dispersion step is indicated by the red curve in Fig. 1 (the boundary between the ZF and LF regimes).

It is instructive to contrast these results for the asymmetric IS–I case with the corresponding results for the symmetric IS–IS case.[20] For the symmetric case, Eq. (41a) is replaced by (Appendix C 2[22])

$$\widehat{R}^{\rm dil/non}_{1,I} = \left[U^{\rm BB}_{11} + \kappa\,U^{\rm BB}_{12}\right]^{-1}, \tag{67a}$$

$$\widehat{R}^{\rm dil/non}_{1,IS} = (1+\kappa)\left[U^{\rm BB}_{11} + U^{\rm BB}_{21} + \kappa\,(U^{\rm BB}_{12} + U^{\rm BB}_{22})\right]^{-1}, \tag{67b}$$

depending on whether we observe spin I only or both spins. Spin Liouville space is now spanned by the same 15 basis operators (Table S1)[22] for both states A and B. Furthermore, $\mathbf{T} = \mathbf{K} = \mathbf{1}$ and Eqs. (28a) and (50) yield (in the dilute regime)

$$\widetilde{\mathbf{U}}^{\rm BB}(0) = \frac{\tau_{\rm A}}{P_{\rm A}}[\mathbf{1} + i\,\mathbf{L}_{\rm Z}\,\tau_{\rm B} - \mathbf{G}_{\rm A}(0)]^{-1} \tag{68}$$

and

$$\mathbf{G}_{\rm A}(0) = \left\langle[\mathbf{1} + i\,\mathbf{L}_{\rm Z}\,\tau_{\rm A} + \mathbf{R}^{\alpha}\,\tau_{\rm A}]^{-1}\right\rangle$$
$$= [\mathbf{1} + i\,\mathbf{L}_{\rm Z}\,\tau_{\rm A}]^{-1} - [\mathbf{1} + i\,\mathbf{L}_{\rm Z}\,\tau_{\rm A}]^{-1}\,\tau_{\rm A}\,\langle\mathbf{R}^{\alpha}\rangle\,[\mathbf{1} + i\,\mathbf{L}_{\rm Z}\,\tau_{\rm A}]^{-1}, \tag{69}$$

where we have invoked the MN approximation by expanding $\mathbf{G}_{\rm A}(0)$ to second order in $\omega_{\rm D}\,\tau_{\rm A}$. In contrast to the asymmetric exchange case, relaxation now enters only via the isotropically averaged relaxation supermatrix $\langle\mathbf{R}^{\alpha}\rangle$. This has two important consequences. First, all cross-mode relaxation rates vanish (Appendix E[22]). Second, because the relaxation supermatrix is now isotropically averaged, we can invoke the Wigner-Eckart theorem to establish that $\langle\mathbf{R}^{\alpha}\rangle$ is block-diagonal in Q. To describe longitudinal relaxation, we therefore only need to consider the 5×5 $Q = 0$ block. Moreover, because $\mathbf{R}^{\alpha}$ is invariant under SIC, this block decomposes into an odd-parity 2×2 block (spanned by I_z and S_z) and an even-parity 3×3 block (spanned by the basis operators B_3, B_4, and B_5 in Table S1).[22] Although the $Q = 0$ block of $\mathbf{L}_{\rm Z}$ is not diagonal for $\omega_I \neq \omega_S$, we only need the odd-parity sub-block, which is the 2×2 null matrix. We thus obtain from Eqs. (68) and (69),

$$\widetilde{\mathbf{U}}^{\rm BB}(0) = \frac{\langle\mathbf{R}^{\alpha}\rangle^{-1}}{P_{\rm A}} = \frac{1}{P_{\rm A}}\begin{bmatrix}\rho_I & \sigma\\ \sigma & \rho_S\end{bmatrix}^{-1}, \tag{70}$$

where the familiar expressions for the longitudinal auto-spin rates $\rho_I \equiv \langle R^{II}_{zz}\rangle$ and $\rho_S \equiv \langle R^{SS}_{zz}\rangle$ and cross-spin rate $\sigma \equiv \langle R^{IS}_{zz}\rangle = \langle R^{SI}_{zz}\rangle$ are given in Eq. (E.32) of Appendix E.[22] Combination of Eqs. (67) and (70) then yields

$$\widehat{R}^{\rm dil/non}_{1,I} = P_{\rm A}\frac{(\rho_I\,\rho_S - \sigma^2)}{(\rho_S - \kappa\,\sigma)}, \tag{71a}$$

$$\widehat{R}^{\rm dil/non}_{1,IS} = P_{\rm A}\frac{(1+\kappa)(\rho_I\,\rho_S - \sigma^2)}{(\rho_S - \sigma) + \kappa\,(\rho_I - \sigma)}, \tag{71b}$$

in agreement with the results (using a slightly different notation) of Paper I. In particular, for symmetric exchange of a pair of homonuclear ($\kappa = \gamma_S/\gamma_I = 1$) and isochronous ($\omega_I = \omega_S$) spins, both rates in Eq. (71) reduce to the familiar form

$$\widehat{R}^{\rm dil/non}_{1,I} = \widehat{R}^{\rm dil/non}_{1,IS} = P_{\rm A}\,(\rho+\sigma)$$
$$= \frac{2}{15}\,P_{\rm A}\,\omega_{\rm D}^2\,[\,j(\omega_I) + 4\,j(2\,\omega_I)\,]. \tag{72}$$

In the MN regime, rotational and SIC symmetries ensure that longitudinal relaxation can be fully described within

the two-dimensional zero-quantum odd-parity subspace corresponding to the longitudinal spin modes I_z and S_z. This is true for symmetric as well as for asymmetric exchange. The crucial difference between these exchange cases in the MN regime is that the intrinsic relaxation rates in the A sites are isotropically averaged only for the symmetric IS–IS case. For the asymmetric IS–I case, the orientation-dependent relaxation in the A sites must, in general, be described in the six-dimensional odd-parity subspace corresponding to the single-spin longitudinal and transverse local modes. However, outside the ZF regime, the longitudinal local spin modes I_z^α and S_z^α are decoupled from the transverse local spin modes $I_\pm^\alpha$ and $S_\pm^\alpha$.

IV. NUMERICAL RESULTS FOR TWO-SPIN SYSTEMS

In this section, we illustrate the theoretical results obtained in Secs. II and III by numerical calculations. Except in Sec. IV B, we consider a homonuclear and effectively isochronous ($\omega_S = \omega_I$) spin pair. The dipole coupling frequency is set to $\omega_D = 1 \times 10^5$ rad s^{-1}, corresponding to an internuclear separation of $r_{IS} = 2.245$ Å for two protons, and the fraction bound I spins is $P_A = 10^{-3}$, corresponding to the dilute regime. Following the standard convention, we take ω_I to be positive. We focus on the asymmetric IS–I case, highlighting differences compared to the symmetric IS–IS case.

A. Cross-mode relaxation

Figure 2 shows dispersion profiles $\widehat{R}_{1,I}^{\rm dil}(\omega_I)$ for the integral longitudinal relaxation rate of spin I in the dilute regime for four different values of the mean survival time τ_A in the A sites. As expected, the SLE and BWR results, computed from Eqs. (42a) and (60), respectively, coincide in panels (a) and (b), where $(\omega_D\,\tau_A)^2 \ll 1$. In panel (c), where $\omega_D\,\tau_A = 1$, the approximate BWR rate exceeds the exact SLE rate by 20% in the ZF limit. In panel (d), where $(\omega_D\,\tau_A)^2 = 100$, the corresponding discrepancy is a factor of ∼21.

The inverted and normal dispersion steps in panels (a) and (b) are centered at the frequencies $\omega_I = \omega_D^2\,\tau_A$ and $\omega_I = 1/\tau_A$, respectively, corresponding to the red and blue curves, respectively, in Fig. 1. The slower relaxation in the ZF regime is a consequence of longitudinal-transverse cross-mode relaxation in the anisotropic A sites (Sec. III B 2). In the LF regime (and above), cross-mode relaxation is abolished by nonsecular decoupling. The ZF drop in $\widehat{R}_{1,I}^{\rm dil}(\omega_I)$ is close to 50% in the MN regime (Sec. III B 2), but it becomes less pronounced in the slow-motion regime. The ZF rate $\widehat{R}_{1,I}^{\rm dil}(0)$ agrees with Eq. (48a) at all τ_A values and in panel (d) it is already within 5% of the ultraslow-motion limit $\widehat{R}_{1,I}^{\rm dil}(0) = (2/3)\,P_A/\tau_A$. In accordance with the frequency-dependent MN condition $(\omega_D\,\tau_A)^2 \ll 1 + (\omega_I\,\tau_A)^2$ for isochronous spins, the BWR and SLE results coincide in the high-frequency part of the main dispersion in panels (c) and (d). As seen from panel (d), the SLE profile merges with secular BWR result (63), without cross-mode relaxation, at high frequency. (In panels (c) and (d), the BWR and secular BWR profiles cross over just below the main dispersion.) In the slow-motion regime, the effect of cross-mode coupling on the exact SLE profile is only evident as a distortion of the main dispersion shape. As τ_A is increased further, $\widehat{R}_{1,I}^{\rm dil}(0)$ decreases as $1/\tau_A$ in accordance with Eq. (48a), but the locus of the main

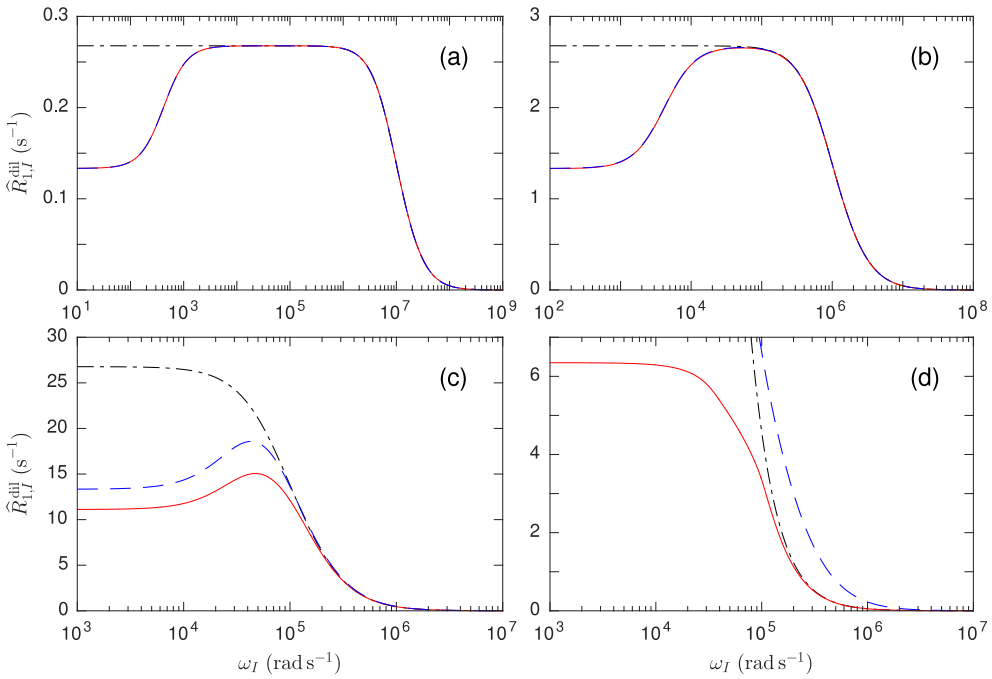

FIG. 2. Dispersion of the integral longitudinal relaxation rate of spin I for exchange case IS–I. Parameter values: $P_A = 10^{-3}$, $\omega_S = \omega_I$, $\omega_D = 10^5$ rad s^{-1} and $\tau_A = 10^{-7}$ s (a), 10^{-6} s (b), 10^{-5} s (c), or 10^{-4} s (d). The three dispersion profiles show $\widehat{R}_{1,I}^{\rm dil}$ computed from the SLE result in Eq. (42a) (red solid curves), from the BWR result in Eq. (60) (blue dashed curves), and from the secular BWR result in Eq. (63) (black dashed-dotted curves).

dispersion remains at $\omega_I \approx \omega_D$, as demonstrated in Paper I for the symmetric IS–IS case.

B. Heteronuclear spins

Although our focus is on homonuclear spin systems, all results in Secs. II and III are valid also for heteronuclear spin systems. To illustrate the different relaxation behaviors of homonuclear and heteronuclear spin systems, we shall compare, for the IS–I case, the dispersion of the integral relaxation rate $\widehat{R}^{\rm dil}_{1,I}(\omega_I)$ for a homonuclear spin pair ($\omega_S = \omega_I$) with that for a heteronuclear spin pair with $\omega_S = -0.1014\,\omega_I$. The homonuclear case might represent a serine side-chain with the I spin in the labile hydroxyl proton and the S spin in one of the adjacent methylene protons (chemical shifts have no significant effect). The heteronuclear case might represent an ^{15}N-labeled lysine side-chain, with the I spin in one of the labile amino protons and the S spin in the directly bonded nitrogen atom so that $\kappa = \gamma_S/\gamma_I = -0.1014$. In both cases, we excite nonselectively but observe only the I spin. For simplicity, the dipole coupling ω_D is taken to be the same for the two cases.

In Fig. 3, the homonuclear dispersion profiles (red) are compared with the heteronuclear profiles (blue) for the same parameter values as in Fig. 2. The red profiles are thus the same in the two figures. In the MN regime (panels (a) and (b)), the principal difference between the two profiles is that the inverted dispersion occurs at a 10-fold higher frequency in the heteronuclear profile. This observation is consistent with our earlier conclusion (Sec. III B 2) that the effect of cross-mode relaxation vanishes when ω_S exceeds $\omega_D^2\,\tau_A$, that is, when $\omega_I \gtrsim 10\,\omega_D^2\,\tau_A$. Consequently, the inverted dispersion in the heteronuclear profile has only one step (that is, there is no dispersion step at $\omega_I \approx \omega_D^2\,\tau_A$) and it has the same shape as in the homonuclear profile. In addition to the shift of the inverted dispersion, there is also a small difference in the main (normal) dispersion step, where differences in the spectral densities $j(\omega_S)$, $j(\omega_I - \omega_S)$, and $j(\omega_I + \omega_S)$ result in a slightly steeper dispersion in the heteronuclear profile. As a result, the heteronuclear profile lies ∼15% below the homonuclear profile at the high-frequency end of the main dispersion (but this is not visible on the scale of Fig. 3).

Outside the MN regime (panels (c) and (d)), the effects of having $\omega_S \neq \omega_I$ are more complicated. For $\omega_D\,\tau_A = 1$ (panel (c)), the prominent maximum in the homonuclear profile is replaced by a small shoulder in the heteronuclear profile. For $\omega_D\,\tau_A = 10$ (panel (d)), the heteronuclear profile has a down-shifted and more nearly "Lorentzian" main dispersion and a distinct high-frequency dispersion step. In all four panels, the heteronuclear profile lies ∼15% below the homonuclear profile at the high-frequency end of the dispersion profile.

In Fig. 3, we also examine the effect of the relative sign of the magnetogyric ratios γ_I and γ_S by comparing dispersion profiles for $\gamma_S = -0.1014\,\gamma_I$ (blue solid curves), corresponding to ^{1}H–^{15}N, and $\gamma_S = +0.1014\,\gamma_I$ (magenta dashed curves). The sign of γ_S can affect the spin dynamics in three ways: via the Larmor frequency $\omega_S = -\gamma_S B_0$, via the dipole coupling frequency $\omega_D \propto \gamma_I\,\gamma_S$, and via the factor $\kappa = \gamma_S/\gamma_I$ in the initial condition, reflecting the equilibrium magnetization. Following standard practice, we regard ω_I as positive, even though $\gamma_I > 0$ in the most relevant situation, where I refers to the proton spin.

The dispersion profiles in Fig. 3 pertain to the dilute regime and nonselective excitation, so the initial

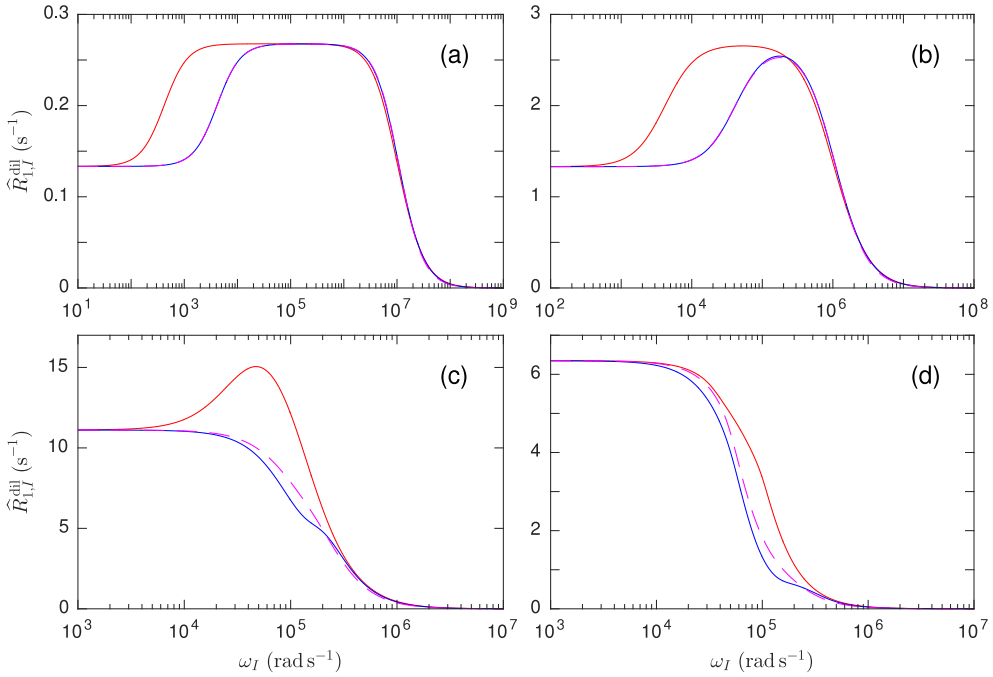

FIG. 3. Dispersion of the integral longitudinal relaxation rate of spin I for exchange case IS–I and homonuclear spins with $\omega_S = \omega_I$ (red solid curves, same as in Fig. 2) and heteronuclear spins with $\omega_S = -0.1014\,\omega_I$ (blue solid curves) or $\omega_S = 0.1014\,\omega_I$ (magenta dashed curves). Other parameter values as in Fig. 2. All dispersion profiles were computed from the SLE result in Eq. (42a).

I-spin magnetization is strongly dominated by the equilibrium magnetization in state B. Consequently (the sign of) κ has no significant effect on the dispersion profiles.

In the MN regime (panels (a) and (b)), the spin dynamics only depend on the square of ω_D so the only effect of reversing sign of γ_S is to interchange the spectral densities $j(\omega_I - \omega_S)$ and $j(\omega_I + \omega_S)$.[37] As seen from panels (a) and (b), this effect is rather small; the maximum effect (barely visible in Fig. 3) occurs in the adiabatic regime ($\omega_I \tau_A \gg 1$), where $\widehat{R}^{\rm dil}_{1,I}(\omega_I)$ is ~14% smaller for $\gamma_S = +0.1014\,\gamma_I$ than for $\gamma_S = -0.1014\,\gamma_I$.

Outside the MN regime (panels (c) and (d)), a sign reversal in γ_S makes the dispersion profile more smooth, without any pronounced shoulder. As in the MN regime, this effect is entirely due to the sign reversal of ω_S. Although the evolution of some spin modes depends on the sign of ω_D (for example, see Eqs. (D.9f) and (D.18)[22]), the evolution of the longitudinal magnetizations only involves even powers of ω_D. As in the MN regime, $\widehat{R}^{\rm dil}_{1,I}(\omega_I)$ is ~14% smaller for $\gamma_S = +0.1014\,\gamma_I$ than for $\gamma_S = -0.1014\,\gamma_I$ at the high-frequency end of the dispersion profile.

C. Symmetric versus asymmetric exchange

In Fig. 4, we compare the dispersion profiles for the IS–I and IS–IS cases with the same parameter values as in Figs. 2 and 3. The red IS–I profiles are thus the same in Figs. 2–4. Because of isotropic averaging (Appendix E[22]), there is no cross-mode relaxation in the A sites for the symmetric case so the integral relaxation rate is constant throughout the extreme-narrowing regime (no inverted dispersion at the boundary between the ZF and LF regimes). In addition, the dispersion midpoint occurs at a lower frequency for the symmetric case.

The numerical calculations confirm the analytical prediction, based on Eq. (48a) and Eqs. (5.2) and (5.3) of Paper I, that the ZF rate $\widehat{R}^{\rm dil}_{1,I}(0)$ is a factor $[5 + (\omega_D\tau_A)^2]/[1 + (\omega_D\tau_A)^2]$ larger for the IS–IS case than for the IS–I case. In the MN regime (panel (a)), the ratio $\widehat{R}^{\rm dil}_{1,I}(IS\text{–}IS)/\widehat{R}^{\rm dil}_{1,I}(IS\text{–}I)$ is thus 5 in the ZF regime, while it is ~2.5 in the LF regime. In the ultraslow-motion regime ($\omega_D\,\tau_A)^2 \gg 1$ (panel (d)), the ZF rates for the symmetric and asymmetric exchange cases converge to the same value, $\widehat{R}^{\rm dil}_{1,I}(0) = (2/3)\,P_A/\tau_A$, but the dispersion for the asymmetric case is upshifted in frequency and deviates more from "Lorentzian" shape.

For the comparison in Fig. 4, we use the same P_A value for the two exchange cases. If we want to compare the contributions to the observed bulk water proton relaxation rate from a single labile proton (I) and from the two protons in an internal water molecule (I_2), we should compare the exchange cases IS–I_2 and I_2 – I_2. As noted in Sec. II A 2, we should then (in the dilute regime) divide P_A by a factor 2 for the asymmetric IS–I_2 case. Consequently, in the MN regime, an internal water molecule contributes 10-fold more than a labile proton to $\widehat{R}^{\rm dil}_{1,I}(0)$ and ~5-fold more in the LF regime, other things (notably, τ_A and ω_D) being equal. However, the mean survival time τ_A is typically longer for labile protons than for internal water molecules.[16] Figure 5 compares the ZF rates for the asymmetric and symmetric cases as functions of the mean survival time τ_A. The maximum occurs at $\tau_A = 1/\omega_D$ for the symmetric case and at $\tau_A = \sqrt{5}/\omega_D$ for the asymmetric case. In practice, the shift of the maximum $\widehat{R}^{\rm dil}_{1,I}(0)$

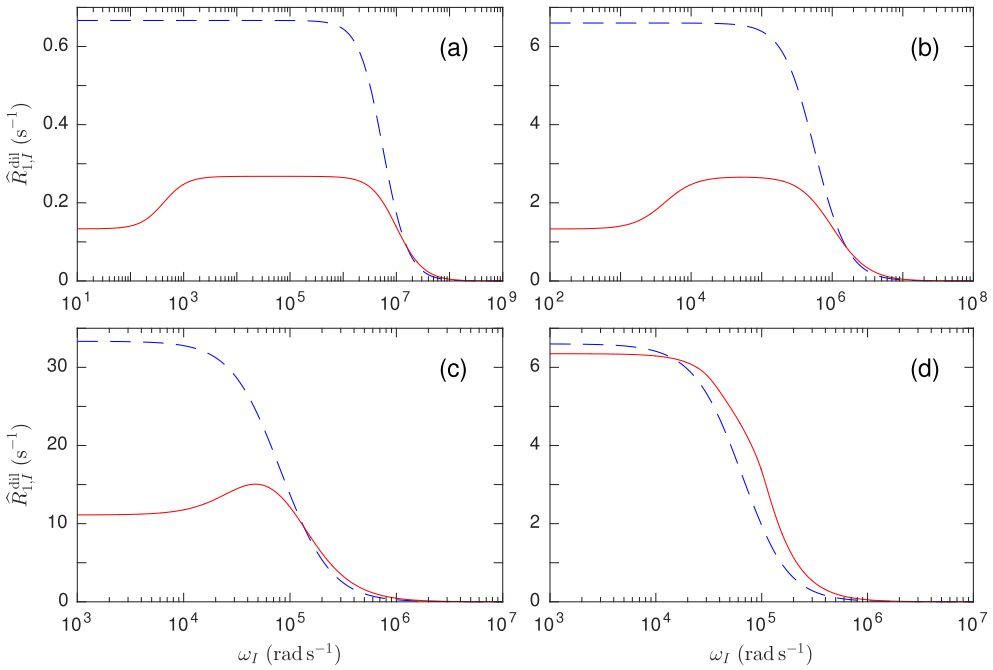

FIG. 4. Dispersion of the integral longitudinal relaxation rate of spin I for exchange case IS–I computed from the SLE result in Eq. (42a) (red solid curves, same as in Figs. 2 and 3) and for exchange case IS–IS computed from the corresponding SLE result in Paper I (blue dashed curves). Parameter values as in Figs. 2 and 3.

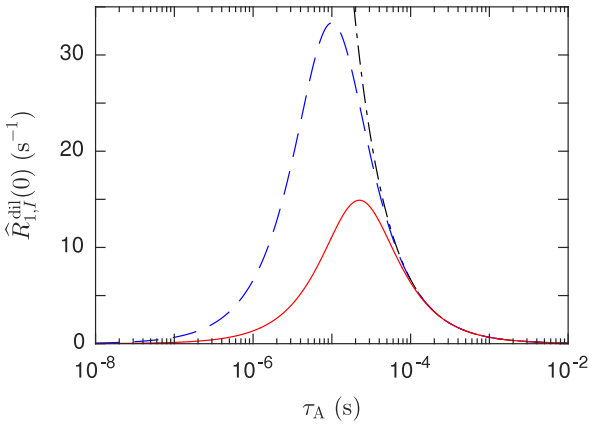

FIG. 5. Zero-field limit of the integral longitudinal relaxation rate of spin I for exchange case IS–I computed from Eq. (48a) (red solid curve) and for exchange case IS–IS computed from Eqs. (5.2) and (5.3) of Paper I (blue dashed curve). Parameter values: $P_{\rm A} = 10^{-3}$, $\omega_S = \omega_I$, and $\omega_{\rm D} = 10^5$ rad s^{-1}.

to larger $\tau_{\rm A}$ will be more pronounced because $\omega_{\rm D}$ is generally smaller for a labile proton in a macromolecule than for the water protons. In the ultraslow-motion regime, $(\omega_{\rm D}\,\tau_{\rm A})^2 \gg 1$, the symmetric and asymmetric cases yield the same ZF rate, $\widehat{R}^{\rm dil}_{1,I}(0) = (2/3)\,P_{\rm A}/\tau_{\rm A}$ (black dashed-dotted curve in Fig. 5).

D. Time evolution of spin modes

Further physical insight can be obtained by analyzing the evolution in time of the longitudinal magnetization and other spin modes. We shall perform such an analysis for the ZF regime, where longitudinal relaxation can be fully described in terms of the four rank-1 zero-quantum spin modes $\sigma^{\rm B}_1(t) = I^{\rm B}_z(t)$, $\sigma^{\rm A}_1 = I^{\rm A}_z(t)$, $\sigma^{\rm A}_2 = S^{\rm A}_z(t)$, and $\sigma^{\rm A}_4(t)$ (Sec. III A 2). Here we use a simplified notation where, for example, $I^{\rm B}_z(t) \equiv {\rm Tr}\{I_z\,\sigma^{\rm B}(t)\}$. Using Eqs. (D.9) and (D.18)[22] and performing the inverse Laplace transform, we obtain the results shown in Fig. 6 for the IS–I case with nonselective excitation. As before, we use $P_{\rm A} = 10^{-3}$ so we are in the dilute regime, where $I_z = I^{\rm A}_z + I^{\rm B}_z \approx I^{\rm B}_z$. As seen from Fig. 6, to an excellent approximation,

$$I^{\rm B}_z(t) = P_{\rm B}\,\exp[-\widehat{R}^{\rm dil}_{1,I}(0)\,t], \tag{73}$$

with the integral relaxation rate $\widehat{R}^{\rm dil}_{1,I}(0)$ given by Eq. (48a). The total I-spin longitudinal magnetization is thus very nearly exponential even outside the MN regime. Consequently, very little information is lost in charactering the decay of $I_z(t)$ by the integral relaxation rate $\widehat{R}^{\rm dil}_{1,I}(0)$.

Figure 6(a), with $(\omega_{\rm D}\,\tau_{\rm A})^2 = 10^{-4}$, pertains to the MN regime, where the longitudinal magnetizations are decoupled from modes with even SIC parity so $\sigma^{\rm A}_4(t) \equiv 0$. Because the MN regime is also the fast-exchange regime, the ratio of the longitudinal magnetizations in the two states is maintained at the initial value throughout the relaxation process,

$$\frac{I^{\rm A}_z(t)}{I^{\rm B}_z(t)} = \frac{I^{\rm A}_z(0)}{I^{\rm B}_z(0)} = \frac{P_{\rm A}}{P_{\rm B}}. \tag{74}$$

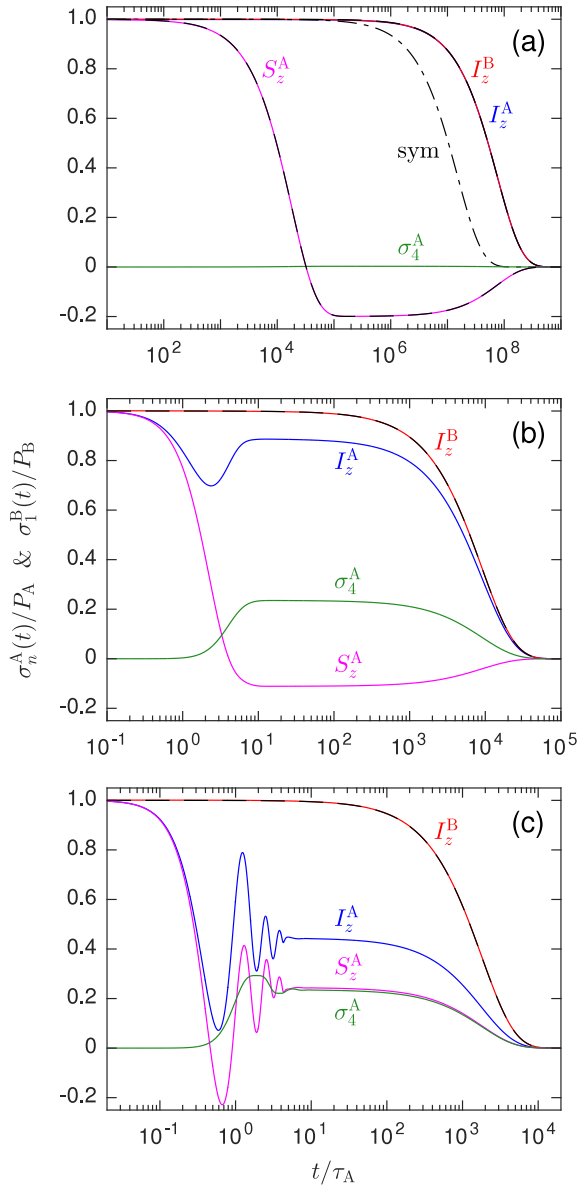

FIG. 6. Time evolution of the normalized spin modes $I^{\rm B}_z(t)/P_{\rm B}$ (red solid curve), $I^{\rm A}_z(t)/P_{\rm A}$ (blue), $S^{\rm A}_z(t)/P_{\rm A}$ (magenta), and $\sigma^{\rm A}_4(t)/P_{\rm A}$ (green) for the IS–I case in the zero-field regime and with nonselective excitation. The black dashed curve coinciding with $I^{\rm B}_z(t)/P_{\rm B}$ in all three panels is the exponential decay in Eq. (73) and the black dashed curve coinciding with $S^{\rm A}_z(t)/P_{\rm A}$ in panel (a) is the biexponential function in Eq. (77b). The black dashed-dotted curve in panel (a) is the exponential decay of $I^{\rm B}_z(t)/P_{\rm B} = S^{\rm A}_z(t)/P_{\rm A}$ for the symmetric IS–IS case. Parameter values: $P_{\rm A} = 10^{-3}$ and $\omega_{\rm D}\,\tau_{\rm A} = 0.01$ (a), 1 (b), or 5 (c).

The time evolution of the longitudinal modes can then be described by two coupled equations (Appendix F[22])

$$\frac{\rm d}{{\rm d}t}\,I_z(t) = -P_{\rm A}\,\rho_I\,I_z(t) - \sigma_{IS}\,S^{\rm A}_z(t), \tag{75a}$$

$$\frac{\rm d}{{\rm d}t}\,S^{\rm A}_z(t) = -P_{\rm A}\,\sigma_{SI}\,I_z(t) - \rho_S\,S^{\rm A}_z(t). \tag{75b}$$

For $P_{\rm A} = 1$, Eq. (75) is of the same form as the two-spin Solomon equations.[7,21] However, whereas $\rho_I = \rho_S$ and $\sigma_{IS} = \sigma_{SI}$ in the Solomon equations in the ZF regime, this symmetry is broken in the asymmetric IS–I model.

In Appendix F,[22] we show that

$$\rho_I = \frac{2}{9}\,\omega_D^2\,\tau_A, \tag{76a}$$

$$\rho_S = \frac{5}{9}\,\omega_D^2\,\tau_A, \tag{76b}$$

$$\sigma_{IS} = \frac{4}{9}\,\omega_D^2\,\tau_A, \tag{76c}$$

$$\sigma_{SI} = \frac{1}{9}\,\omega_D^2\,\tau_A. \tag{76d}$$

The solution to Eq. (75) subject to nonselective initial conditions, $I_z(0) = 1$ and $S_z^A(0) = P_A$, is then (Appendix F[22])

$$I_z(t) = \exp[-\widehat{R}_{1,I}^{dil}(0)\,t], \tag{77a}$$

$$S_z^A(t) = P_A\left[\frac{6}{5}\,\exp(-\rho_S\,t) - \frac{1}{5}\,\exp[-\widehat{R}_{1,I}^{dil}(0)\,t]\right], \tag{77b}$$

with $\widehat{R}_{1,I}^{dil}(0)$ given by Eq. (48a). The validity of this analytical result is numerically verified in Fig. 6(a).

With the aid of these analytical results, the time evolution in Fig. 6(a) can be understood in detail. On a short time scale, of order $(\omega_D^2\,\tau_A)^{-1}$, the total I_z magnetization hardly changes since only a tiny fraction $P_A \ll 1$ of the labile I spins is relaxed by dipole coupling to an S spin. Meanwhile, the S_z^A magnetization of the nonlabile S spin relaxes at a rate ρ_S, but, because of cross relaxation with spin I, it does not approach its equilibrium value (which, by our convention, is zero) but a non-equilibrium steady-state value (corresponding to a negative spin temperature). The steady-state magnetization is obtained from Eq. (75b) by setting $I_z(t) = 1$ and $dS_z^A(t)/dt = 0$, whereby $S_z^A(t)/S_z^A(0) = -\sigma_{SI}/\rho_S = -1/5$.

On a longer time scale, of order $(P_A\,\omega_D^2\,\tau_A)^{-1}$, the I-spin and S-spin magnetizations relax to their (zero) equilibrium values at a common rate $\widehat{R}_{1,I}^{dil}(0)$. By inserting the steady-state S_z^A magnetization, $-(1/5)\,P_A\,I_z(t)$, in Eq. (75a), we see that this rate is given by $P_A\,(\rho_I - \sigma_{IS}/5) = P_A\,[(2/9) - (4/45)]\,\omega_D^2\,\tau_A = (2/15)\,P_A\,\omega_D^2\,\tau_A$, consistent with Eqs. (48a), (76a), and (76c). The net magnetization flux due to cross relaxation is thus from the S spin to the I spin, thereby retarding I-spin relaxation. In contrast, for the symmetric IS–IS case, a similar analysis shows that the I-spin and S-spin magnetizations relax at a common rate $P_A\,(\rho_I + \sigma_{IS}) = P_A\,[(4/9) + (2/9)]\,\omega_D^2\,\tau_A = (2/3)\,P_A\,\omega_D^2\,\tau_A$. The 5-fold slower I-spin relaxation in the ZF + MN regime for asymmetric exchange as compared to symmetric exchange (Fig. 4(a)) is thus seen to be a consequence of a smaller auto-spin rate ρ_I (because of longitudinal-transverse cross-mode relaxation in the A sites) and a reversed magnetization flow from the negative steady-state S_z^A magnetization. The latter effect should operate also outside the ZF regime, when local cross-mode relaxation does not occur.

The inverse of the S-spin integral relaxation rate $\widehat{R}_{1,S}^{non}(0)$ equals the time integral of the expression within brackets in Eq. (77b). Noting that $\rho_S \gg \widehat{R}_{1,I}^{dil}(0)$ in the dilute regime, we thus obtain

$$\widehat{R}_{1,S}^{non}(0) = \frac{5\,\widehat{R}_{1,I}^{dil}(0)\,\rho_S}{6\,\widehat{R}_{1,I}^{dil}(0) - \rho_S} \approx -5\,\widehat{R}_{1,I}^{dil}(0)$$

$$= -\frac{2}{3}\,P_A\,\omega_D^2\,\tau_A, \tag{78}$$

in agreement with Eq. (D.22b).[22]

Outside the MN regime (Figs. 6(b) and 6(c)), when the mean survival time τ_A in an A site is no longer short compared to the time scale $1/\omega_D$ of coherent dipolar evolution, all three A-state modes show oscillatory features superimposed on the initial decay, which occurs on the time scale of τ_A when $(\omega_D\,\tau_A)^2 \gg 1$. However, as long as we are in the dilute regime, the I_z^B magnetization still relaxes exponentially as in Eq. (73). Because the SIC parity selection rule does not apply outside the MN regime, the odd-parity longitudinal magnetizations couple with the even-parity zero-quantum coherence $\sigma_4^A(t)$, which builds up when I_z^A and S_z^A start to decay and ultimately decays on the same time scale as I_z^B. As seen from Eq. (47c) or Eqs. (D.9d) and (D.18),[22] $\sigma_4^A(t)$ is purely imaginary so Fig. 6 shows $\mathrm{Im}\{\sigma_4^A(t)\}$.

V. CONCLUSIONS

The non-perturbative stochastic theory of longitudinal relaxation by the dipolar EMOR mechanism, based on an analytical partial solution of the SLE, was first developed for the symmetric IS–IS case.[20] Here, we have substantially generalized the theoretical framework to spin systems of arbitrary size with symmetric or asymmetric exchange. The asymmetric case, where the spin system is fragmented by the exchange, is of considerable interest since it applies to chemical exchange of labile macromolecular protons as well as to physical exchange of internal water molecules involved in intermolecular dipole couplings. Of course, the distinction between symmetric and asymmetric exchange is irrelevant for the single-spin quadrupolar EMOR mechanism.[10,11]

From a theoretical point of view, asymmetric exchange has two important consequences: (1) a decorrelation of spin modes involving both labile and nonlabile spins and (2) a lowering of the rotational symmetry of the local relaxation matrix. Both of these effects contribute to making the relaxation of a labile spin less efficient when its dipole-coupled partner is nonlabile. The effect of local symmetry reduction is most readily appreciated and most clearly manifested in the MN regime, where exchange is much faster than relaxation in the individual A sites. In the symmetric case, the local relaxation matrix is exchange-averaged over the isotropic distribution of A sites and it therefore exhibits the axial symmetry of the applied magnetic field. As a direct consequence of this axial symmetry, relaxation can only couple spin modes of the same quantum order. Longitudinal relaxation therefore only involves longitudinal magnetizations and zero-quantum coherences of odd parity under spin inversion conjugation (of which there are none for a two-spin system). In the asymmetric case, because the nonlabile spins are not exchange-averaged, local relaxation can couple local spin modes of the same parity but of different quantum order.

In particular, the observed longitudinal relaxation is affected by local longitudinal-transverse cross-mode relaxation in the A sites. To the best of our knowledge, such cross-mode relaxation phenomena have not previously been described in the literature.

As an illustration of the general dipolar EMOR theory and, in particular, of the previously unrecognized[20] effects of asymmetric exchange, we presented here a detailed analysis of the asymmetric two-spin case IS–I. A variety of analytical results were obtained for the ZF and MN regimes and numerical results were presented under more general conditions, including the case of a heteronuclear spin pair. We demonstrated how local longitudinal-transverse cross-mode relaxation slows down the observed relaxation of the labile I spin in the ZF regime and that an unusual inverted dispersion step occurs at higher fields, where the cross-mode relaxation channel becomes nonsecular. This inverted dispersion splits the extreme-narrowing regime into two sub-regimes, referred to here as the zero-field and low-field regimes. We also presented a detailed analysis of the time evolution of the spin modes in the ZF regime.

The general theoretical framework developed here will enable a quantitative analysis of frequency-dependent water-proton longitudinal relaxation in model systems with immobilized macromolecules and, ultimately, will provide a rigorous link between relaxation-based magnetic resonance image contrast and the molecular-level properties of the tissue. In a forthcoming report, we apply this framework to a three-spin system ISP, analyzing in detail the ISP–I, ISP–IS, and ISP–ISP exchange cases.

ACKNOWLEDGMENTS

This work was financially supported by the Swedish Research Council.

[1]S. H. Koenig and R. D. Brown, Prog. Nucl. Magn. Reson. Spectrosc. **22**, 487 (1990).
[2]S. H. Koenig and R. D. Brown, Magn. Reson. Med. **30**, 685 (1993).
[3]J. P. Korb and R. G. Bryant, J. Chem. Phys. **115**, 10964 (2001).
[4]B. Halle, Magn. Reson. Med. **56**, 60 (2006).
[5]E. P. Sunde and B. Halle, J. Am. Chem. Soc. **131**, 18214 (2009).
[6]F. V. Chávez and B. Halle, Magn. Reson. Med. **56**, 73 (2006).
[7]A. Abragam, *The Principles of Nuclear Magnetism* (Clarendon Press, Oxford, 1961).
[8]R. Kubo, J. Math. Phys. **4**, 174 (1963).
[9]R. Kubo, in *Advances in Chemical Physics*, edited by K. E. Shuler (Wiley, New York, 1969), Vol. 15, p. 101.
[10]B. Halle, Prog. Nucl. Magn. Reson. Spectrosc. **28**, 137 (1996).
[11]T. Nilsson and B. Halle, J. Chem. Phys. **137**, 054503 (2012).
[12]P. Roose, H. Bauwin, and B. Halle, J. Phys. Chem. B **103**, 5167 (1999).
[13]F. V. Chávez, E. Persson, and B. Halle, J. Am. Chem. Soc. **128**, 4902 (2006).
[14]F. V. Chávez, E. Hellstrand, and B. Halle, J. Phys. Chem. B **110**, 21551 (2006).
[15]B. Halle and V. P. Denisov, Biophys. J. **69**, 242 (1995).
[16]E. Persson and B. Halle, J. Am. Chem. Soc. **130**, 1774 (2008).
[17]S. Kaieda and B. Halle, J. Phys. Chem. B **117**, 14676 (2013).
[18]S. Kaieda and B. Halle, J. Phys. Chem. B **119**, 7957 (2015).
[19]E. Persson and B. Halle, Proc. Natl. Acad. Sci. U. S. A. **105**, 6266 (2008).
[20]Z. Chang and B. Halle, J. Chem. Phys. **139**, 144203 (2013).
[21]I. Solomon, Phys. Rev. **99**, 559 (1955).
[22]See supplementary material at http://dx.doi.org/10.1063/1.4942026 for lists of ISTO basis operators (Appendix A); partial solution of the SLE (Appendix B); expressions for integral relaxation rates (Appendix C); analytical results for the ZF (Appendix D) and MN (Appendix E) regimes; and time evolution of I_z and S_z (Appendix F).
[23]F. Persson and B. Halle, J. Am. Chem. Soc. **135**, 8735 (2013).
[24]G. Binsch, J. Am. Chem. Soc. **91**, 1304 (1969).
[25]R. R. Ernst, G. Bodenhausen, and A. Wokaun, *Principles of Nuclear Magnetic Resonance in One and Two Dimensions* (Clarendon Press, Oxford, 1987).
[26]N. R. Skrynnikov, T. N. Khazanovich, and B. C. Sanctuary, Mol. Phys. **91**, 977 (1997).
[27]D. M. Brink and G. R. Satchler, *Angular Momentum*, 3rd ed. (Clarendon Press, Oxford, 1994).
[28]N. R. Skrynnikov and R. R. Ernst, J. Magn. Reson. **137**, 276 (1999).
[29]N. G. van Kampen, *Stochastic Processes in Physics and Chemistry*, 3rd ed. (North-Holland, Amsterdam, 2007).
[30]F. Persson and B. Halle, J. Chem. Theory Comp. **9**, 2838 (2013).
[31]Z. Luz and S. Meiboom, J. Chem. Phys. **40**, 2686 (1964).
[32]N. C. Pyper, Mol. Phys. **21**, 1 (1971).
[33]S. Szymanski, A. M. Gryff-Keller, and G. Binsch, J. Magn. Reson. **68**, 399 (1986).
[34]Z. Chang and B. Halle, J. Chem. Phys. **143**, 234201 (2015).
[35]M. Tinkham, *Group Theory and Quantum Mechanics* (McGraw-Hill, New York, 1964).
[36]L. G. Werbelow, *Encyclopedia of NMR* (Wiley, New York, 1996), p. 1776.
[37]L. G. Werbelow, J. Chem. Soc., Faraday Trans. 2 **83**, 897 (1987).

Supplemental Material

Nuclear magnetic relaxation by the dipolar EMOR mechanism: General theory with applications to two-spin systems

Zhiwei Chang and Bertil Halle
Division of Biophysical Chemistry, Department of Chemistry, Lund University, POB 124, SE-22100 Lund, Sweden

APPENDIX A: BASIS OPERATORS

Here we list the 15 irreducible spin tensor operators (ISTOs)[1] $T^K_Q(k_I k_S)$ that constitute a complete (together with the identity operator) orthonormal basis for the spin Liouville space of two spins I and S. For the symmetric IS–IS case, the same two-spin basis (Table S1) is used for the A and B states. For the asymmetric $IS-I$ case, the single-spin basis in Table S2 is used for state B. All the operators in Tables S1 and S2 are normalized in the same two-spin Liouville space. For example, $(I_z|I_z) = \mathrm{Tr}\{I_z^2\} = \mathrm{Tr}_I\{I_z^2\} \times \mathrm{Tr}_S\{\mathcal{E}\} = \frac{1}{2} \times 2 = 1$. The two-spin basis used in paper I[2] differs from that in Table S1 in that the basis operators B_3 and B_5 were taken to be linear combinations of the ISTOs $T^0_0(11)$ and $T^2_0(11)$.

TABLE S1. Spin basis operators $B_n = T^K_Q(k_I k_S)$ for two spins IS.

n	Q	K	k_I	k_S	parity [a]	B_n [b]
1	0	1	1	0	−	I_z
2	0	1	0	1	−	S_z
3	0	0	1	1	+	$-\frac{2}{\sqrt{3}}\,\boldsymbol{I}\cdot\boldsymbol{S}$
4	0	1	1	1	+	$\frac{1}{\sqrt{2}}\,(I_-\,S_+ - I_+\,S_-)$
5	0	2	1	1	+	$\frac{2}{\sqrt{6}}\,(3\,I_z\,S_z - \boldsymbol{I}\cdot\boldsymbol{S})$
6	1	1	1	0	−	$-\frac{1}{\sqrt{2}}\,I_+$
7	1	1	0	1	−	$-\frac{1}{\sqrt{2}}\,S_+$
8	1	1	1	1	+	$I_z\,S_+ - I_+\,S_z$
9	1	2	1	1	+	$-\,(I_z\,S_+ + I_+\,S_z)$
10	−1	1	1	0	−	$\frac{1}{\sqrt{2}}\,I_-$
11	−1	1	0	1	−	$\frac{1}{\sqrt{2}}\,S_-$
12	−1	1	1	1	+	$I_z\,S_- - I_-\,S_z$
13	−1	2	1	1	+	$I_z\,S_- + I_-\,S_z$
14	2	2	1	1	+	$I_+\,S_+$
15	−2	2	1	1	+	$I_-\,S_-$

[a] Parity of B_n under spin inversion conjugation.
[b] Identity operators have been omitted.

TABLE S2. Spin basis operators $B_n = T^K_Q$ for a single spin I.

n	Q	K	B_n [a,b]
1	0	1	I_z
2	1	1	$-\frac{1}{\sqrt{2}}\,I_+$
3	−1	1	$\frac{1}{\sqrt{2}}\,I_-$

[a] Identity operators have been omitted.
[b] The operators B_n are normalized in the two-spin Liouville space.

APPENDIX B: PARTIAL SOLUTION OF THE SLE

Here we provide the details of the exact solution of the stochastic Liouville equation (7) in site space. Combination of Eqs. (8) and (19) yields

$$\widetilde{\mathcal{U}}(s) \;=\; (s\,\mathcal{E} - \mathcal{T}_{\rm m}\otimes\mathcal{T}_{\rm s} + \mathcal{K}_{\rm m}\otimes\mathcal{K}_{\rm s} + i\,\mathcal{L})^{-1} \;, \tag{B.1}$$

which may be rearranged into

$$\widetilde{\mathcal{U}}(s) \;=\; \widetilde{\mathcal{U}}_{\rm K}(s)\Big[\mathcal{E} \;+\; \mathcal{T}_{\rm m}\otimes\mathcal{T}_{\rm s}\,\widetilde{\mathcal{U}}(s)\Big] \;, \tag{B.2}$$

with

$$\widetilde{\mathcal{U}}_{\rm K}(s) \;\equiv\; (s\,\mathcal{E} + \mathcal{K}_{\rm m}\otimes\mathcal{K}_{\rm s} + i\,\mathcal{L})^{-1} \;. \tag{B.3}$$

Using Eq. (B.2) and noting that $\widetilde{\mathcal{U}}_{\rm K}(s)$ is diagonal in the site basis, we obtain

$$\widetilde{\mathcal{U}}^{\alpha}(s) \;\equiv\; \sum_{\beta=0}^{N} \langle\alpha|\,\widetilde{\mathcal{U}}(s)\,|\beta\rangle\; P_\beta \;=\; \langle\alpha|\,\widetilde{\mathcal{U}}_{\rm K}(s)|\alpha\rangle \left[P_\alpha\,\mathcal{E} \;+\; \sum_{\beta=0}^{N} \langle\alpha|\,\mathcal{T}_{\rm m}\,|\beta\rangle\,\mathcal{T}_{\rm s}\,\widetilde{\mathcal{U}}_\beta(s)\right] \;. \tag{B.4}$$

Summing Eq. (B.4) over the A sites and noting that $\langle\alpha|\,\mathcal{T}_{\rm m}\,|\beta\rangle = \delta_{\beta 0}/(N\tau_{\rm B})$ for $\alpha \geq 1$ according to Eq. (10), we obtain

$$\widetilde{\mathcal{U}}^{\rm A}(s) \;\equiv\; \sum_{\alpha=1}^{N} \widetilde{\mathcal{U}}^{\alpha}(s) \;=\; \tau_{\rm A}\,\mathcal{G}^{\rm A}(s)\left[P_{\rm A}\,\mathcal{E} \;+\; \frac{1}{\tau_{\rm B}}\,\mathcal{T}_{\rm s}\,\widetilde{\mathcal{U}}^{\rm B}(s)\right] \;, \tag{B.5}$$

with $\widetilde{\mathcal{U}}^{\rm B}(s) = \widetilde{\mathcal{U}}^{0}(s)$, $P_{\rm A} = N\,P_\alpha$ and

$$\mathcal{G}^{\rm A}(s) \;\equiv\; \frac{1}{N}\sum_{\alpha=1}^{N} (s\,\tau_{\rm A}\,\mathcal{E} \;+\; \mathcal{K}_{\rm s} \;+\; i\,\mathcal{L}^{\alpha}\,\tau_{\rm A})^{-1} \;, \tag{B.6}$$

where $\mathcal{E}$ now is the identity superoperator in spin space only. The spin superoperators in this expression are to be evaluated in the spin operator basis of state A, where the matrix elements of $\mathcal{K}_{\rm s}$ are given by Eq. (14b). If $N \gg 1$ and the A sites are isotropically distributed, we can replace the site average in Eq. (B.6) by an isotropic angular average and substitute $\mathcal{L}^{\alpha}$ by $\mathcal{L}^{\rm A}(\Omega) = \mathcal{L}_{\rm Z} + \mathcal{L}_{\rm D}(\Omega)$. Consequently,

$$\mathcal{G}^{\rm A}(s) \;=\; \frac{1}{4\pi}\int {\rm d}\Omega\;\left[s\,\tau_{\rm A}\,\mathcal{E} \;+\; \mathcal{K}_{\rm s} \;+\; i\,\mathcal{L}^{\rm A}(\Omega)\,\tau_{\rm A}\right]^{-1} \;. \tag{B.7}$$

Setting $\alpha = 0$ in Eq. (B.4) and using Eq. (10), we obtain, in analogy with Eq. (B.5),

$$\widetilde{\mathcal{U}}^{\rm B}(s) \;=\; \tau_{\rm B}\,\mathcal{G}^{\rm B}(s)\left[P_{\rm B}\,\mathcal{E} \;+\; \frac{1}{\tau_{\rm A}}\,\mathcal{T}_{\rm s}\,\widetilde{\mathcal{U}}^{\rm A}(s)\right] \;, \tag{B.8}$$

where

$$\mathcal{G}^{\rm B}(s) \;\equiv\; \left[(1 + s\,\tau_{\rm B})\,\mathcal{E} \;+\; i\,\mathcal{L}^{\rm B}\tau_{\rm B}\right]^{-1} \;. \tag{B.9}$$

Equations (B.5) and (B.8) can now be solved for the two unknowns, with the result

$$\widetilde{\mathcal{U}}^{\rm A}(s) \;=\; \tau_{\rm A}\left[\mathcal{E} - \mathcal{G}^{\rm A}(s)\,\mathcal{T}_{\rm s}\,\mathcal{G}^{\rm B}(s)\,\mathcal{T}_{\rm s}\right]^{-1}\mathcal{G}^{\rm A}(s)\left[P_{\rm A}\,\mathcal{E} + P_{\rm B}\,\mathcal{T}_{\rm s}\,\mathcal{G}^{\rm B}(s)\right] \;, \tag{B.10a}$$

$$\widetilde{\mathcal{U}}^{\rm B}(s) \;=\; \tau_{\rm B}\left[\mathcal{E} - \mathcal{G}^{\rm B}(s)\,\mathcal{T}_{\rm s}\,\mathcal{G}^{\rm A}(s)\,\mathcal{T}_{\rm s}\right]^{-1}\mathcal{G}^{\rm B}(s)\left[P_{\rm B}\,\mathcal{E} + P_{\rm A}\,\mathcal{T}_{\rm s}\,\mathcal{G}^{\rm A}(s)\right] \;. \tag{B.10b}$$

which allows us to obtain the site-averaged resolvent as

$$\langle\widetilde{\mathcal{U}}(s)\rangle \;=\; \widetilde{\mathcal{U}}^{\mathrm{A}}(s) \;+\; \widetilde{\mathcal{U}}^{\mathrm{B}}(s)\,. \tag{B.11}$$

The superoperator $\langle\widetilde{\mathcal{U}}(s)\rangle$ acts in a composite spin Liouville space of dimension $D = D_{\mathrm{B}} + D_{\mathrm{A}}$. In Eq. (25), we partitioned the $D \times D$ supermatrix representations of $\langle\widetilde{\mathcal{U}}(s)\rangle$ into four blocks. To express Eq. (B.10) in terms of partitioned matrices, we partition the identity matrix as

$$\mathcal{E} \;\to\; \begin{bmatrix} \mathbf{1}^{\mathrm{B}} & \mathbf{0} \\ \mathbf{0} & \mathbf{1}^{\mathrm{A}} \end{bmatrix}\,, \tag{B.12}$$

where $\mathbf{1}^{\mathrm{B}}$ and $\mathbf{1}^{\mathrm{A}}$ are $D_{\mathrm{B}} \times D_{\mathrm{B}}$ and $D_{\mathrm{A}} \times D_{\mathrm{A}}$ identity matrices, respectively, and $\mathbf{0}$ is a $D_{\mathrm{B}} \times D_{\mathrm{A}}$ or $D_{\mathrm{A}} \times D_{\mathrm{B}}$ null matrix. According to Eq. (13),

$$\mathcal{T}_{\mathrm{s}} \;\to\; \begin{bmatrix} \mathbf{0} & \mathbf{T} \\ \mathbf{T'} & \mathbf{0} \end{bmatrix}\,, \tag{B.13}$$

where the $D_{\mathrm{B}} \times D_{\mathrm{A}}$ matrix $\mathbf{T}$ (and its transpose $\mathbf{T'}$) was defined in connection with Eq. (15). Furthermore,

$$\mathcal{G}^{\mathrm{B}}(s) \;\to\; \begin{bmatrix} \mathbf{G}^{\mathrm{B}}(s) & \mathbf{0} \\ \mathbf{0} & \mathbf{0} \end{bmatrix}\,, \tag{B.14}$$

where, according to Eq. (B.9),

$$\mathbf{G}^{\mathrm{B}}(s) \;=\; \left[(1 + s\,\tau_{\mathrm{B}})\,\mathbf{1}^{\mathrm{B}} \;+\; i\,\mathbf{L}^{\mathrm{B}}\tau_{\mathrm{B}}\right]^{-1}\,. \tag{B.15}$$

Finally,

$$\mathcal{G}^{\mathrm{A}}(s) \;\to\; \begin{bmatrix} \mathbf{0} & \mathbf{0} \\ \mathbf{0} & \mathbf{G}^{\mathrm{A}}(s) \end{bmatrix}\,, \tag{B.16}$$

where, according to Eq. (B.7),

$$\mathbf{G}^{\mathrm{A}}(s) \;=\; \frac{1}{4\pi}\int \mathrm{d}\Omega\;\left[s\,\tau_{\mathrm{A}}\,\mathbf{1}^{\mathrm{A}} \;+\; \mathbf{K} \;+\; i\,\mathbf{L}^{\mathrm{A}}(\Omega)\,\tau_{\mathrm{A}}\right]^{-1}\,, \tag{B.17}$$

and the $D_{\mathrm{A}} \times D_{\mathrm{A}}$ matrix $\mathbf{K}$ is diagonal with elements $[1 - \Delta_{\mathrm{K}}(n_{\mathrm{A}})]$.

Substituting these partitioned matrices into Eq. (B.10) and using Eq. (B.11), we can express $\langle\widetilde{\mathcal{U}}(s)\rangle$ on the block form introduced in Eq. (25),

$$\langle\widetilde{\mathcal{U}}(s)\rangle \;=\; \begin{bmatrix} \widetilde{\mathbf{U}}^{\mathrm{BB}}(s) & \widetilde{\mathbf{U}}^{\mathrm{BA}}(s) \\ \widetilde{\mathbf{U}}^{\mathrm{AB}}(s) & \widetilde{\mathbf{U}}^{\mathrm{AA}}(s) \end{bmatrix}\,, \tag{B.18}$$

with the submatrices given by Eq. (28) of the main text.

APPENDIX C: INTEGRAL RELAXATION RATE

1. Asymmetric exchange

Here we simplify the expressions for the integral relaxation rate for the $IS-I$ case by expressing the matrix elements $U_{np}^{\rm XY} \equiv (n|\widetilde{\mathbf{U}}^{\rm XY}(0)|p)$ appearing in Eqs. (39) – (41) in terms of the elements $g_{np} \equiv (n|\mathbf{G}^{\rm A}(0)|p)$ of the supermatrix $\mathbf{G}^{\rm A}(0)$ in Eq. (30).

We consider first the submatrix $\widetilde{\mathbf{U}}^{\rm BB}(0)$. Combining Eqs. (28a) and (29) and the detailed balance relation $P_{\rm B}\tau_{\rm A} = P_{\rm A}\tau_{\rm B}$, we obtain

$$\widetilde{\mathbf{U}}^{\rm BB}(0) \;=\; \frac{P_{\rm B}^2\,\tau_{\rm A}}{P_{\rm A}}\left[\mathbf{1}^{\rm B} \;+\; i\,\mathbf{L}^{\rm B}\,\tau_{\rm B} - \mathbf{T}\,\mathbf{G}^{\rm A}(0)\,\mathbf{T'}\right]^{-1} \;. \tag{C.1}$$

Because the matrix $\mathbf{G}^{\rm A}(0)$ is isotropically averaged, it must reflect the axial symmetry of the spin system in the external magnetic field. According to the Wigner-Eckart theorem,[1] $\mathbf{G}^{\rm A}(0)$ must then be block-diagonal in the ISTO basis of Table S1, with one 5×5 block ($Q=0$), two 4×4 blocks ($Q=\pm 1$) and two 1×1 blocks ($Q=\pm 2$). Pre and post-multiplication by the matrix $\mathbf{T}$ in Eq. (16) picks out the first diagonal element in each of the first three blocks ($Q=0,\,\pm 1$) to give

$$\mathbf{T}\,\mathbf{G}^{\rm A}(0)\,\mathbf{T'} \;=\; \begin{bmatrix} g_{11} & 0 & 0 \\ 0 & g_{66} & 0 \\ 0 & 0 & g_{10,10} \end{bmatrix} \;. \tag{C.2}$$

The Liouvillian for the B state, with only a Zeeman coupling, is

$$\mathbf{L}^{\rm B} \;=\; \omega_I \begin{bmatrix} 0 & 0 & 0 \\ 0 & 1 & 0 \\ 0 & 0 & -1 \end{bmatrix} \;. \tag{C.3}$$

Combination of Eqs. (C.1) – (C.3) yields

$$\widetilde{\mathbf{U}}^{\rm BB}(0) \;=\; \frac{P_{\rm B}^2\,\tau_{\rm A}}{P_{\rm A}} \begin{bmatrix} (1-g_{11})^{-1} & 0 & 0 \\ 0 & (1-g_{66}+i\,\omega_I\tau_{\rm B})^{-1} & 0 \\ 0 & 0 & (1-g_{10,10}-i\,\omega_I\tau_{\rm B})^{-1} \end{bmatrix} , \tag{C.4}$$

so that

$$U_{11}^{\rm BB} \;=\; \frac{P_{\rm B}^2\,\tau_{\rm A}}{P_{\rm A}(1-g_{11})} \,. \tag{C.5}$$

Comparison of Eqs. (28a) and (28b) shows that

$$\widetilde{\mathbf{U}}^{\mathrm{BA}}(0) \;=\; \frac{P_{\mathrm{A}}}{P_{\mathrm{B}}}\,\widetilde{\mathbf{U}}^{\mathrm{BB}}(0)\,\mathbf{T}\,\mathbf{G}^{\mathrm{A}}(0)\,. \tag{C.6}$$

Using Eqs. (16) and (C.4), we thus obtain

$$U_{11}^{\mathrm{BA}} \;=\; \frac{P_{\mathrm{A}}}{P_{\mathrm{B}}}\,U_{11}^{\mathrm{BB}}\,g_{11} \;=\; \frac{P_{\mathrm{B}}\,\tau_{\mathrm{A}}\,g_{11}}{1-g_{11}}\,, \tag{C.7a}$$

$$U_{12}^{\mathrm{BA}} \;=\; \frac{P_{\mathrm{A}}}{P_{\mathrm{B}}}\,U_{11}^{\mathrm{BB}}\,g_{12} \;=\; \frac{P_{\mathrm{B}}\,\tau_{\mathrm{A}}\,g_{12}}{1-g_{11}}\,. \tag{C.7b}$$

Next, we consider the submatrix $\widetilde{\mathbf{U}}^{\mathrm{AA}}(0)$ in Eq. (28d). Like $\mathbf{G}^{\mathrm{A}}(0)$ it is block-diagonal, so we need only retain the $Q = 0$ block. From Eqs. (16), (29) and (C.3), it follows that in the $Q = 0$ block of the matrix $\mathbf{T'}\,\mathbf{G}^{\mathrm{B}}(0)\,\mathbf{T}$ all elements are 0, except the (11) element which is 1. Consequently,

$$[\mathbf{G}^{\mathrm{A}}(0)\,\mathbf{T'}\,\mathbf{G}^{\mathrm{B}}(0)\,\mathbf{T}]_{Q=0} \;=\; \begin{bmatrix} g_{11} & 0 & 0 & 0 & 0 \\ g_{21} & 0 & 0 & 0 & 0 \\ g_{31} & 0 & 0 & 0 & 0 \\ g_{41} & 0 & 0 & 0 & 0 \\ g_{51} & 0 & 0 & 0 & 0 \end{bmatrix}\,, \tag{C.8}$$

and

$$[\mathbf{1}^{\mathrm{A}} - \mathbf{G}^{\mathrm{A}}(0)\,\mathbf{T'}\,\mathbf{G}^{\mathrm{B}}(0)\,\mathbf{T}]^{-1}_{Q=0} \;=\; \begin{bmatrix} 1-g_{11} & 0 & 0 & 0 & 0 \\ -g_{21} & 1 & 0 & 0 & 0 \\ -g_{31} & 0 & 1 & 0 & 0 \\ -g_{41} & 0 & 0 & 1 & 0 \\ -g_{51} & 0 & 0 & 0 & 1 \end{bmatrix}^{-1} \;=\; \begin{bmatrix} \frac{1}{1-g_{11}} & 0 & 0 & 0 & 0 \\ \frac{g_{21}}{1-g_{11}} & 1 & 0 & 0 & 0 \\ \frac{g_{31}}{1-g_{11}} & 0 & 1 & 0 & 0 \\ \frac{g_{41}}{1-g_{11}} & 0 & 0 & 1 & 0 \\ \frac{g_{51}}{1-g_{11}} & 0 & 0 & 0 & 1 \end{bmatrix}\,. \tag{C.9}$$

Combination of Eqs. (28d) and (C.9) now yields

$$U_{11}^{\mathrm{AA}} \;=\; P_{\mathrm{A}}\,\tau_{\mathrm{A}}\,\frac{g_{11}}{1-g_{11}}\,, \tag{C.10a}$$

$$U_{12}^{\mathrm{AA}} \;=\; P_{\mathrm{A}}\,\tau_{\mathrm{A}}\,\frac{g_{12}}{1-g_{11}}\,, \tag{C.10b}$$

$$U_{21}^{\mathrm{AA}} \;=\; P_{\mathrm{A}}\,\tau_{\mathrm{A}}\,\frac{g_{21}}{1-g_{11}}\,, \tag{C.10c}$$

$$U_{22}^{\mathrm{AA}} \;=\; P_{\mathrm{A}}\,\tau_{\mathrm{A}}\left[\frac{g_{12}\,g_{21}}{1-g_{11}} \;+\; g_{22}\right]\,. \tag{C.10d}$$

Finally, comparison of Eqs. (28c) and (28d) shows that

$$\widetilde{\mathbf{U}}^{\mathrm{AB}}(0) \;=\; \frac{P_{\mathrm{B}}}{P_{\mathrm{A}}}\,\widetilde{\mathbf{U}}^{\mathrm{AA}}(0)\,\mathbf{T'}\,\mathbf{G}^{\mathrm{B}}(0)\,. \tag{C.11}$$

It follows from Eqs. (16), (29) and (C.3) that the first column of the 15×3 matrix $\mathbf{T}'\,\mathbf{G}^{\mathrm{B}}(0)$ has the first element equal to 1 and all others equal to 0. We then obtain from Eqs. (C.10) and (C.11),

$$U_{11}^{\mathrm{AB}} \;=\; \frac{P_{\mathrm{B}}}{P_{\mathrm{A}}}\, U_{11}^{\mathrm{AA}} \;=\; P_{\mathrm{B}}\, \tau_{\mathrm{A}}\, \frac{g_{11}}{1-g_{11}}\,, \tag{C.12a}$$

$$U_{21}^{\mathrm{AB}} \;=\; \frac{P_{\mathrm{B}}}{P_{\mathrm{A}}}\, U_{21}^{\mathrm{AA}} \;=\; P_{\mathrm{B}}\, \tau_{\mathrm{A}}\, \frac{g_{21}}{1-g_{11}}\,. \tag{C.12b}$$

With the aid of Eqs. (C.5), (C.7), (C.10) and (C.12), we can now express the integral relaxation rate in Eqs. (39) and (40) in terms of the matrix elements g_{np}. Noting that $P_{\mathrm{B}} + P_{\mathrm{A}} = 1$, we obtain

$$\widehat{R}_{1,I}^{\,\mathrm{non}} \;=\; \frac{P_{\mathrm{A}}}{\tau_{\mathrm{A}}}\, \frac{(1-g_{11})}{P_{\mathrm{B}}^2 + P_{\mathrm{A}}[(1+P_{\mathrm{B}})\, g_{11} + \kappa\, g_{12}]}\,, \tag{C.13a}$$

$$\widehat{R}_{1,S}^{\,\mathrm{non}} \;=\; \frac{P_{\mathrm{A}}}{\tau_{\mathrm{A}}}\, \frac{\kappa\,(1-g_{11})}{g_{21} + \kappa\, P_{\mathrm{A}}[(1-g_{11})\, g_{22} + g_{12}\, g_{21}]}\,, \tag{C.13b}$$

and

$$\widehat{R}_{1,I}^{\,\mathrm{sel}} \;=\; \frac{P_{\mathrm{A}}}{\tau_{\mathrm{A}}}\, \frac{(1-g_{11})}{P_{\mathrm{B}}^2 + P_{\mathrm{A}}(1+P_{\mathrm{B}})\, g_{11}}\,, \tag{C.14a}$$

$$\widehat{R}_{1,S}^{\,\mathrm{sel}} \;=\; \frac{1}{\tau_{\mathrm{A}}}\, \frac{(1-g_{11})}{(1-g_{11})\, g_{22} + g_{12}\, g_{21}}\,. \tag{C.14b}$$

In the dilute regime, where $P_{\mathrm{A}} \ll 1$ and $P_{\mathrm{B}} \approx 1$, the integral relaxation rate in Eqs. (C.13) and (C.14a) reduce to

$$\widehat{R}_{1,I}^{\,\mathrm{dil/non}} \;=\; \widehat{R}_{1,I}^{\,\mathrm{dil/sel}} \;=\; \frac{P_{\mathrm{A}}}{\tau_{\mathrm{A}}}\,(1-g_{11})\,, \tag{C.15}$$

and

$$\widehat{R}_{1,S}^{\,\mathrm{dil/non}} \;=\; \frac{P_{\mathrm{A}}}{\tau_{\mathrm{A}}}\, \frac{\kappa\,(1-g_{11})}{g_{21}}\,. \tag{C.16}$$

2. Symmetric exchange

For convenience, we collect here expressions for the integral relaxation rates analogous to those given in Sec. II E.2, but for the symmetric $IS{-}IS$ case. Most of these expressions were presented in paper I using a somewhat different notation.

With the spin modes indexed according to Table S1, Eq. (34) yields

$$\widehat{R}_{1,I} \;=\; \frac{P_{\mathrm{B}}\,\eta_1^{\mathrm{B}} + P_{\mathrm{A}}\,\eta_1^{\mathrm{A}}}{\widetilde{\sigma}_1^{\mathrm{B}}(0) + \widetilde{\sigma}_1^{\mathrm{A}}(0)}\,, \tag{C.17a}$$

$$\widehat{R}_{1,S} \;=\; \frac{P_{\mathrm{B}}\,\eta_2^{\mathrm{B}} + P_{\mathrm{A}}\,\eta_2^{\mathrm{A}}}{\widetilde{\sigma}_2^{\mathrm{B}}(0) + \widetilde{\sigma}_2^{\mathrm{A}}(0)}\,. \tag{C.17b}$$

$$\widehat{R}_{1,IS} \;=\; \frac{P_{\mathrm{B}}(\eta_1^{\mathrm{B}} + \eta_2^{\mathrm{B}}) + P_{\mathrm{A}}(\eta_1^{\mathrm{A}} + \eta_2^{\mathrm{A}})}{\widetilde{\sigma}_1^{\mathrm{B}}(0) + \widetilde{\sigma}_2^{\mathrm{B}}(0) + \widetilde{\sigma}_1^{\mathrm{A}}(0) + \widetilde{\sigma}_2^{\mathrm{A}}(0)}\,, \tag{C.17c}$$

where $\widehat{R}_{1,IS}$ is the integral relaxation rate associated with the total longitudinal magnetization of the two spins (in practice, relevant only for homonuclear spins).

For nonselective excitation, the initial conditions are

$$\eta_n^{\mathrm{A}} \;=\; \eta_n^{\mathrm{B}} \;=\; \delta_{n1} + \kappa\,\delta_{n2}\,, \tag{C.18}$$

so Eqs. (C.17) and (35) yield

$$\widehat{R}_{1,I}^{\mathrm{non}} \;=\; [U_{11}^{\mathrm{BB}} + U_{11}^{\mathrm{BA}} + U_{11}^{\mathrm{AB}} + U_{11}^{\mathrm{AA}} + \kappa\,(U_{12}^{\mathrm{BB}} + U_{12}^{\mathrm{BA}} + U_{12}^{\mathrm{AB}} + U_{12}^{\mathrm{AA}})]^{-1}\,, \tag{C.19a}$$

$$\widehat{R}_{1,S}^{\mathrm{non}} \;=\; \kappa\,[U_{21}^{\mathrm{BB}} + U_{21}^{\mathrm{BA}} + U_{21}^{\mathrm{AB}} + U_{21}^{\mathrm{AA}} + \kappa\,(U_{22}^{\mathrm{BB}} + U_{22}^{\mathrm{BA}} + U_{22}^{\mathrm{AB}} + U_{22}^{\mathrm{AA}})]^{-1}\,, \tag{C.19b}$$

$$\begin{aligned}\widehat{R}_{1,IS}^{\mathrm{non}} \;=\; (1+\kappa)\,[&U_{11}^{\mathrm{BB}} + U_{21}^{\mathrm{BB}} + U_{11}^{\mathrm{BA}} + U_{21}^{\mathrm{BA}} + U_{11}^{\mathrm{AB}} + U_{21}^{\mathrm{AB}} + U_{11}^{\mathrm{AA}} + U_{21}^{\mathrm{AA}} \\ &+\; \kappa\,(U_{12}^{\mathrm{BB}} + U_{22}^{\mathrm{BB}} + U_{12}^{\mathrm{BA}} + U_{22}^{\mathrm{BA}} + U_{12}^{\mathrm{AB}} + U_{22}^{\mathrm{AB}} + U_{12}^{\mathrm{AA}} + U_{22}^{\mathrm{AA}})]^{-1}\,.\end{aligned} \tag{C.19c}$$

In the dilute regime, Eq. (37) allows us to simplify Eq. (C.19) to

$$\widehat{R}_{1,I}^{\mathrm{dil/non}} \;=\; \frac{1}{U_{11}^{\mathrm{BB}} + \kappa\,U_{12}^{\mathrm{BB}}}\,, \tag{C.20a}$$

$$\widehat{R}_{1,S}^{\mathrm{dil/non}} \;=\; \frac{\kappa}{U_{21}^{\mathrm{BB}} + \kappa\,U_{22}^{\mathrm{BB}}}\,, \tag{C.20b}$$

$$\widehat{R}_{1,IS}^{\mathrm{dil/non}} \;=\; \frac{(1+\kappa)}{U_{11}^{\mathrm{BB}} + U_{21}^{\mathrm{BB}} + \kappa\,(U_{12}^{\mathrm{BB}} + U_{22}^{\mathrm{BB}})}\,. \tag{C.20c}$$

For selective excitation of spin I, the initial conditions are

$$\eta_n^{\mathrm{A}} \;=\; \eta_n^{\mathrm{B}} \;=\; \delta_{n1}\,, \tag{C.21}$$

so Eqs. (C.17a) and (35) yield

$$\widehat{R}_{1,I}^{\mathrm{sel}} \;=\; [U_{11}^{\mathrm{BB}} + U_{11}^{\mathrm{BA}} + U_{11}^{\mathrm{AB}} + U_{11}^{\mathrm{AA}}]^{-1}\,, \tag{C.22}$$

reducing in the dilute regime to

$$\widehat{R}_{1,I}^{\mathrm{dil/sel}} \;=\; \frac{1}{U_{11}^{\mathrm{BB}}}\,. \tag{C.23}$$

For selective excitation of spin S, the initial conditions are

$$\eta_n^{\mathrm{A}} \;=\; \eta_n^{\mathrm{B}} \;=\; \kappa\,\delta_{n2}\,, \tag{C.24}$$

so Eqs. (C.17b) and (35) yield

$$\widehat{R}_{1,S}^{\mathrm{sel}} \;=\; [U_{22}^{\mathrm{BB}} + U_{22}^{\mathrm{BA}} + U_{22}^{\mathrm{AB}} + U_{22}^{\mathrm{AA}}]^{-1}\,, \tag{C.25}$$

reducing in the dilute regime to

$$\widehat{R}_{1,S}^{\mathrm{dil/sel}} \;=\; \frac{1}{U_{22}^{\mathrm{BB}}}\,. \tag{C.26}$$

APPENDIX D: ZERO-FIELD REGIME

Here we derive analytical expressions, valid for the $IS-I$ case in the zero-field (ZF) regime, for the Laplace transform of the spin modes $\sigma_1^{\mathrm{A}}(t)$, $\sigma_2^{\mathrm{A}}(t)$, $\sigma_4^{\mathrm{A}}(t)$ and $\sigma_1^{\mathrm{B}}(t)$, with the subscripts referring to the basis operators in Tables S1 and S2. We also obtain analytical expressions, valid in the ZF regime, for the integral relaxation rates in Eqs. (C.13) and (C.14).

In the ZF regime, state A can be described in the subspace spanned by the rank-1 zero-quantum operators B_1, B_2 and B_4 in Table S1, so Eq. (25) can be written as

$$\begin{bmatrix} \widetilde{\sigma}_1^{\mathrm{B}}(s) \\ \widetilde{\sigma}_1^{\mathrm{A}}(s) \\ \widetilde{\sigma}_2^{\mathrm{A}}(s) \\ \widetilde{\sigma}_4^{\mathrm{A}}(s) \end{bmatrix} = \begin{bmatrix} \widetilde{U}^{\mathrm{BB}}(s) & \widetilde{\mathbf{U}}^{\mathrm{BA}}(s) \\ \widetilde{\mathbf{U}}^{\mathrm{AB}}(s) & \widetilde{\mathbf{U}}^{\mathrm{AA}}(s) \end{bmatrix} \begin{bmatrix} \eta_1^{\mathrm{B}} \\ \eta_1^{\mathrm{A}} \\ \eta_2^{\mathrm{A}} \\ \eta_4^{\mathrm{A}} \end{bmatrix}, \tag{D.1}$$

with the resolvent submatrices given by Eq. (28), where $\mathbf{G}^{\mathrm{A}}$ now is a 3×3 matrix. Furthermore, in the ZF regime, Eq. (29) reduces to

$$\mathbf{G}^{\mathrm{B}} = (1 + s\,\tau_{\mathrm{B}})^{-1}\,\mathbf{1}^{\mathrm{B}}, \tag{D.2}$$

with $\mathbf{1}^{\mathrm{B}}$ the 3×3 identity matrix, and Eq. (16) yields

$$\mathbf{T} = \begin{bmatrix} 1 & 0 & 0 \\ 0 & 0 & 0 \\ 0 & 0 & 0 \end{bmatrix}. \tag{D.3}$$

Combining these results with Eq. (28), we obtain

$$\widetilde{U}^{\mathrm{BB}}(s) = \frac{P_{\mathrm{B}}\,\tau_{\mathrm{B}}}{(1 - g_{11} + s\,\tau_{\mathrm{B}})}, \tag{D.4}$$

$$\widetilde{\mathbf{U}}^{\mathrm{BA}}(s) = \frac{P_{\mathrm{A}}\,\tau_{\mathrm{B}}}{(1 - g_{11} + s\,\tau_{\mathrm{B}})} \begin{bmatrix} g_{11} & g_{12} & g_{14} \end{bmatrix}, \tag{D.5}$$

$$\widetilde{\mathbf{U}}^{\mathrm{AA}}(s) = P_{\mathrm{A}}\,\tau_{\mathrm{A}}\,\frac{(1 + s\,\tau_{\mathrm{B}})}{(1 - g_{11} + s\,\tau_{\mathrm{B}})} \begin{bmatrix} g_{11} & g_{12} & g_{14} \\ g_{21} & G_{22} & G_{24} \\ g_{41} & G_{42} & G_{44} \end{bmatrix}, \tag{D.6}$$

$$\widetilde{\mathbf{U}}^{\mathrm{AB}}(s) = \frac{P_{\mathrm{B}}\,\tau_{\mathrm{A}}}{(1 - g_{11} + s\,\tau_{\mathrm{B}})} \begin{bmatrix} g_{11} \\ g_{21} \\ g_{41} \end{bmatrix}, \tag{D.7}$$

where now $g_{np} \equiv (n\,|\,\mathcal{G}_{\mathrm{A}}(s)\,|\,p)$ (for simplicity, the argument s is suppressed) and

$$G_{22} \;=\; g_{22} \;-\; \frac{(g_{11}\,g_{22} - g_{12}\,g_{21})}{(1 + s\,\tau_{\mathrm{B}})}\,, \tag{D.8a}$$

$$G_{24} \;=\; g_{24} \;-\; \frac{(g_{11}\,g_{24} - g_{14}\,g_{21})}{(1 + s\,\tau_{\mathrm{B}})}\,, \tag{D.8b}$$

$$G_{42} \;=\; g_{42} \;-\; \frac{(g_{11}\,g_{42} - g_{12}\,g_{41})}{(1 + s\,\tau_{\mathrm{B}})}\,, \tag{D.8c}$$

$$G_{44} \;=\; g_{44} \;-\; \frac{(g_{11}\,g_{44} - g_{14}\,g_{41})}{(1 + s\,\tau_{\mathrm{B}})}\,. \tag{D.8d}$$

Combination of Eqs. (31), (D.1) and (D.4) – (D.8) yields for nonselective excitation

$$\widetilde{\sigma}_1^{\mathrm{B}}(s) \;=\; \tau_{\mathrm{B}}\,\frac{[P_{\mathrm{B}} \;+\; P_{\mathrm{A}}\,(g_{11} + \kappa\,g_{12})]}{(1 - g_{11} + s\,\tau_{\mathrm{B}})}\,, \tag{D.9a}$$

$$\widetilde{\sigma}_1^{\mathrm{A}}(s) \;=\; \tau_{\mathrm{A}}\,\frac{[P_{\mathrm{B}}\,g_{11} \;+\; P_{\mathrm{A}}\,(g_{11} + \kappa\,g_{12})\,(1 + s\,\tau_{\mathrm{B}})]}{(1 - g_{11} + s\,\tau_{\mathrm{B}})}\,, \tag{D.9b}$$

$$\widetilde{\sigma}_2^{\mathrm{A}}(s) \;=\; \tau_{\mathrm{A}}\,\frac{\{P_{\mathrm{B}}\,g_{21} \;+\; P_{\mathrm{A}}\,[(g_{21} + \kappa\,g_{22})\,(1 + s\,\tau_{\mathrm{B}}) - \kappa\,(g_{11}\,g_{22} - g_{12}\,g_{21})]\}}{(1 - g_{11} + s\,\tau_{\mathrm{B}})}\,, \tag{D.9c}$$

$$\widetilde{\sigma}_4^{\mathrm{A}}(s) \;=\; \tau_{\mathrm{A}}\,\frac{\{P_{\mathrm{B}}\,g_{41} \;+\; P_{\mathrm{A}}\,[(g_{41} + \kappa\,g_{42})\,(1 + s\,\tau_{\mathrm{B}}) - \kappa\,(g_{11}\,g_{42} - g_{12}\,g_{41})]\}}{(1 - g_{11} + s\,\tau_{\mathrm{B}})}\,. \tag{D.9d}$$

The corresponding results for I-selective excitation follow by setting $\kappa = 0$ in Eq. (D.9).

The s-dependent quantities g_{np} used here are given by Eq. (B.7) as

$$g_{np}(s) \;\equiv\; (n\,|\,\mathcal{G}^{\mathrm{A}}(s)\,|\,p) \;=\; \frac{1}{4\pi}\int \mathrm{d}\Omega\,(n\,|\,\mathcal{M}^{-1}(s;\Omega)\,|\,p)\,, \tag{D.10}$$

with

$$\begin{aligned}\mathcal{M}(s;\Omega) \;&=\; s\,\tau_{\mathrm{A}}\,\mathcal{E}^{\mathrm{A}} \;+\; \mathcal{K}_{\mathrm{s}} \;+\; i\,\mathcal{L}_{\mathrm{D}}(\Omega)\,\tau_{\mathrm{A}} \\ &=\; s\,\tau_{\mathrm{A}}\,\mathcal{E}^{\mathrm{A}} \;+\; \mathcal{K}_{\mathrm{s}} \;+\; i\,\mathcal{D}^{\dagger}(\Omega)\,\mathcal{L}_{\mathrm{D}}(0)\,\mathcal{D}(\Omega)\,\tau_{\mathrm{A}} \\ &=\; \mathcal{D}^{\dagger}(\Omega)\,\mathcal{M}_0(s)\,\mathcal{D}(\Omega)\,,\end{aligned} \tag{D.11}$$

where $\mathcal{D}(\Omega)$ is the unitary ($\mathcal{D}^{\dagger} = \mathcal{D}^{-1}$) rotation superoperator and

$$\mathcal{M}_0(s) \;\equiv\; s\,\tau_{\mathrm{A}}\,\mathcal{E}^{\mathrm{A}} \;+\; \mathcal{K}_{\mathrm{s}} \;+\; i\,\mathcal{L}_{\mathrm{D}}(0)\,\tau_{\mathrm{A}}\,. \tag{D.12}$$

In the last step of Eq. (D.11), we noted that $\mathcal{D}(\Omega)\,\mathcal{K}_{\mathrm{s}}\,\mathcal{D}^{\dagger}(\Omega) = \mathcal{K}_{\mathrm{s}}$ since $\mathcal{K}_{\mathrm{s}}$ is rotationally invariant. Note that the full 15×15 $\mathbf{M}_0$ matrix must be used here, since the Wigner-Eckart theorem only applies after isotropic orientational averaging.

Identifying the basis operators B_n with the ISTOs $T_Q^K(k_1k_2)$ in Table S1 and using the transformation rules[1]

$$\mathcal{D}(\Omega)\,T_{Q'}^{K'} \;=\; \sum_{P'=-K}^{K} D_{P'Q'}^{K'}(\Omega)\,T_{P'}^{K'}\,, \tag{D.13a}$$

$$T_Q^K\,\mathcal{D}^{\dagger}(\Omega) \;=\; \sum_{P=-K}^{K} D_{PQ}^{K*}(\Omega)\,T_P^K\,, \tag{D.13b}$$

and the orthonormality of the Wigner functions,[1] we obtain from Eqs. (D.10) – (D.13)

$$
\begin{aligned}
g_{np}(s) \;&=\; \frac{1}{4\pi} \int \mathrm{d}\Omega \left(T^K_Q(k_1 k_2)\, \mathcal{D}^\dagger(\Omega) \,|\, \mathcal{M}_0^{-1}(s) \,|\, \mathcal{D}(\Omega)\, T^{K'}_{Q'}(k'_1 k'_2) \right) \\
&=\; \sum_{P=-K}^{K} \sum_{P'=-K'}^{K'} \left(T^K_P(k_1 k_2) \,|\, \mathcal{M}_0^{-1}(s) \,|\, T^{K'}_{P'}(k'_1 k'_2) \right) \frac{1}{4\pi} \int \mathrm{d}\Omega\; D^{K*}_{PQ}(\Omega)\, D^{K'}_{P'Q'}(\Omega) \qquad \text{(D.14)} \\
&=\; \delta_{KK'}\, \delta_{QQ'}\, \frac{1}{(2K+1)} \sum_{P=-K}^{K} \left(T^K_P(k_1 k_2) \,|\, \mathcal{M}_0^{-1}(s) \,|\, T^K_P(k'_1 k'_2) \right) \,.
\end{aligned}
$$

Equation (D.14) yields for the six matrix elements occurring in Eq. (D.9),

$$g_{11} \;=\; \frac{1}{3} \sum_{Q=-1}^{1} \left(T^1_Q(10) \,|\, \mathcal{M}_0^{-1}(s) \,|\, T^1_Q(10) \right) \,, \qquad \text{(D.15a)}$$

$$g_{12} \;=\; \frac{1}{3} \sum_{Q=-1}^{1} \left(T^1_Q(10) \,|\, \mathcal{M}_0^{-1}(s) \,|\, T^1_Q(01) \right) \,, \qquad \text{(D.15b)}$$

$$g_{21} \;=\; \frac{1}{3} \sum_{Q=-1}^{1} \left(T^1_Q(01) \,|\, \mathcal{M}_0^{-1}(s) \,|\, T^1_Q(10) \right) \,, \qquad \text{(D.15c)}$$

$$g_{22} \;=\; \frac{1}{3} \sum_{Q=-1}^{1} \left(T^1_Q(01) \,|\, \mathcal{M}_0^{-1}(s) \,|\, T^1_Q(01) \right) \,, \qquad \text{(D.15d)}$$

$$g_{41} \;=\; \frac{1}{3} \sum_{Q=-1}^{1} \left(T^1_Q(11) \,|\, \mathcal{M}_0^{-1}(s) \,|\, T^1_Q(10) \right) \,, \qquad \text{(D.15e)}$$

$$g_{42} \;=\; \frac{1}{3} \sum_{Q=-1}^{1} \left(T^1_Q(11) \,|\, \mathcal{M}_0^{-1}(s) \,|\, T^1_Q(01) \right) \,. \qquad \text{(D.15f)}$$

The matrix representation of $\mathcal{M}_0(s;\Omega)$ in the ISTO basis of Table S1 is

$$\begin{bmatrix}
1+x & 0 & 0 & \frac{2c}{3} & 0 & 0 & 0 & 0 & 0 & 0 & 0 & 0 & 0 & 0 & 0 \\
0 & x & 0 & \frac{-2c}{3} & 0 & 0 & 0 & 0 & 0 & 0 & 0 & 0 & 0 & 0 & 0 \\
0 & 0 & 1+x & 0 & 0 & 0 & 0 & 0 & 0 & 0 & 0 & 0 & 0 & 0 & 0 \\
\frac{2c}{3} & \frac{-2c}{3} & 0 & 1+x & 0 & 0 & 0 & 0 & 0 & 0 & 0 & 0 & 0 & 0 & 0 \\
0 & 0 & 0 & 0 & 1+x & 0 & 0 & 0 & 0 & 0 & 0 & 0 & 0 & 0 & 0 \\
0 & 0 & 0 & 0 & 0 & 1+x & 0 & \frac{-c}{3} & -c & 0 & 0 & 0 & 0 & 0 & 0 \\
0 & 0 & 0 & 0 & 0 & 0 & x & \frac{c}{3} & -c & 0 & 0 & 0 & 0 & 0 & 0 \\
0 & 0 & 0 & 0 & 0 & \frac{-c}{3} & \frac{c}{3} & 1+x & 0 & 0 & 0 & 0 & 0 & 0 & 0 \\
0 & 0 & 0 & 0 & 0 & -c & -c & 0 & 1+x & 0 & 0 & 0 & 0 & 0 & 0 \\
0 & 0 & 0 & 0 & 0 & 0 & 0 & 0 & 0 & 1+x & 0 & \frac{-c}{3} & c & 0 & 0 \\
0 & 0 & 0 & 0 & 0 & 0 & 0 & 0 & 0 & 0 & x & \frac{c}{3} & c & 0 & 0 \\
0 & 0 & 0 & 0 & 0 & 0 & 0 & 0 & 0 & \frac{-c}{3} & \frac{c}{3} & 1+x & 0 & 0 & 0 \\
0 & 0 & 0 & 0 & 0 & 0 & 0 & 0 & 0 & c & c & 0 & 1+x & 0 & 0 \\
0 & 0 & 0 & 0 & 0 & 0 & 0 & 0 & 0 & 0 & 0 & 0 & 0 & 1+x & 0 \\
0 & 0 & 0 & 0 & 0 & 0 & 0 & 0 & 0 & 0 & 0 & 0 & 0 & 0 & 1+x
\end{bmatrix}, \tag{D.16}$$

where we have defined

$$x \equiv s\,\tau_{\mathrm{A}}\,, \tag{D.17a}$$

$$c \equiv \frac{i}{\sqrt{2}}\,\omega_{\mathrm{D}}\,\tau_{\mathrm{A}}\,. \tag{D.17b}$$

Inverting the block-diagonal matrix $\mathbf{M}_0$ in Eq. (D.16) and inserting the results into Eq. (D.15), we obtain

$$g_{11} = \frac{1}{3}\left\{\frac{9x(1+x)+2D^2}{f_0} + \frac{2(1+x)[9x(1+x)+5D^2]}{f_1}\right\}, \tag{D.18a}$$

$$g_{12} = \frac{2D^2}{3}\left\{\frac{1}{f_0} - \frac{4(1+x)}{f_1}\right\}, \tag{D.18b}$$

$$g_{21} = g_{12}\,, \tag{D.18c}$$

$$g_{22} = \frac{1}{3}\left\{\frac{9(1+x)^2+2D^2}{f_0} + \frac{2(1+x)[9(1+x)^2+5D^2]}{f_1}\right\}, \tag{D.18d}$$

$$g_{41} = i\sqrt{2}\,D\left\{-\frac{x}{f_0} + \frac{[x(1+x)+D^2]}{f_1}\right\}, \tag{D.18e}$$

$$g_{42} = i\sqrt{2}\,D\left\{\frac{1+x}{f_0} - \frac{[(1+x)^2+D^2]}{f_1}\right\}, \tag{D.18f}$$

where we have defined

$$f_0 \equiv 9x(1+x)^2 + 2(1+2x)D^2\,, \tag{D.19a}$$

$$f_1 \equiv (1+x)[9x(1+x)^2 + 5(1+2x)D^2] + D^4\,, \tag{D.19b}$$

$$D \equiv \omega_{\mathrm{D}}\,\tau_{\mathrm{A}}\,. \tag{D.20}$$

The time evolution of the four rank-1 zero-quantum spin modes can now be obtained by inserting the matrix elements $g_{np}(s)$ from Eq. (D.18) into Eq. (D.9) (or the analogous expressions for selective excitation) and performing the inverse Laplace transform numerically.

Next we consider the integral relaxation rate in Eqs. (C.13) and (C.14) in the ZF regime. Here, we need the matrix elements $g_{np}(s = 0)$. Combining Eqs. (D.18) and (D.19) and then setting $x = 0$, we obtain (for $D \neq 0$)

$$g_{11} = \frac{5 + \frac{1}{3}D^2}{5 + D^2}\,, \tag{D.21a}$$

$$g_{12} = g_{21} = \frac{-1 + \frac{1}{3}D^2}{5 + D^2}\,, \tag{D.21b}$$

$$g_{22} = \frac{81 + 39D^2 + 2D^4}{6D^2(5 + D^2)}\,, \tag{D.21c}$$

$$g_{41} = \frac{i\sqrt{2}\,D}{5 + D^2}\,, \tag{D.21d}$$

$$g_{42} = \frac{i\,(3 - D^2)}{\sqrt{2}\,D\,(5 + D^2)}\,. \tag{D.21e}$$

Inserting these results into Eqs. (C.13) and (C.14), we obtain

$$\widehat{R}^{\mathrm{non}}_{1,I}(0) = \frac{2\,P_{\mathrm{A}}\,\omega_{\mathrm{D}}^2\,\tau_{\mathrm{A}}}{15 + 3\,P_{\mathrm{B}}^2 D^2 - P_{\mathrm{A}}[3\,\kappa - (1 + \kappa + P_{\mathrm{B}})D^2]}\,, \tag{D.22a}$$

$$\widehat{R}^{\mathrm{non}}_{1,S}(0) = \frac{2\,\kappa\,P_{\mathrm{A}}\,\omega_{\mathrm{D}}^2\,\tau_{\mathrm{A}}}{-3 + D^2 + \kappa\,P_{\mathrm{A}}(6 + D^2)}\,, \tag{D.22b}$$

and

$$\widehat{R}^{\mathrm{sel}}_{1,I}(0) = \frac{2\,P_{\mathrm{A}}\,\omega_{\mathrm{D}}^2\,\tau_{\mathrm{A}}}{15 + 3\,P_{\mathrm{B}}^2 D^2 + P_{\mathrm{A}}(1 + P_{\mathrm{B}})D^2}\,, \tag{D.23a}$$

$$\widehat{R}^{\mathrm{sel}}_{1,S}(0) = \frac{2\,\omega_{\mathrm{D}}^2\,\tau_{\mathrm{A}}}{6 + D^2}\,. \tag{D.23b}$$

In the dilute regime ($P_{\mathrm{A}} \ll 1$), Eqs. (D.22a) and (D.23a) reduce to

$$\widehat{R}^{\mathrm{dil}}_{1,I}(0) = \frac{2}{3}\,P_{\mathrm{A}}\,\frac{\omega_{\mathrm{D}}^2\,\tau_{\mathrm{A}}}{5 + (\omega_{\mathrm{D}}\,\tau_{\mathrm{A}})^2}\,. \tag{D.24}$$

APPENDIX E: MOTIONAL-NARROWING REGIME

Here we obtain the elements of the four orientation-dependent relaxation submatrices $\mathbf{R}^{\alpha}_{II}$, $\mathbf{R}^{\alpha}_{IS}$, $\mathbf{R}^{\alpha}_{SI}$ and $\mathbf{R}^{\alpha}_{SS}$, appearing in Sec. III B 2. We start from the semi-classical Bloch-Wangsness-Redfield (BWR) master equation[3]

$$\frac{\mathrm{d}}{\mathrm{d}t}\,\widehat{\sigma}^{\alpha}(t) \;=\; -\int_0^{\infty}\mathrm{d}\tau\,\big\langle\widehat{\mathcal{L}}^{\alpha}_{\mathrm{D}}(t)\,\widehat{\mathcal{L}}^{\alpha}_{\mathrm{D}}(t-\tau)\big\rangle_{\alpha}\,\widehat{\sigma}^{\alpha}(t)\,, \tag{E.1}$$

where $\widehat{\sigma}^{\alpha}(t) = \exp(i\,\mathcal{L}_{\mathrm{Z}}\,t)\,\sigma^{\alpha}(t)$ and $\widehat{\mathcal{L}}^{\alpha}_{\mathrm{D}}(t) = \exp(i\,\mathcal{L}_{\mathrm{Z}}\,t)\,\mathcal{L}^{\alpha}_{\mathrm{D}}(t)\,\exp(-i\,\mathcal{L}_{\mathrm{Z}}\,t)$ are the spin density operator and the dipolar Liouvillian for site α, both in the interaction representation. The Liouvillians are the usual derivation superoperators $\mathcal{L}_{\mathrm{Z}} \equiv [H_{\mathrm{Z}},\,\ldots]$ and $\mathcal{L}^{\alpha}_{\mathrm{D}}(t) \equiv [H^{\alpha}_{\mathrm{D}}(t),\,\ldots]$, with $H_{\mathrm{Z}} = \omega_I\,I_z + \omega_S\,S_z$ and the dipolar Hamiltonian $H^{\alpha}_{\mathrm{D}}(t)$ as given by Eq. (2.3) of paper I.[2] The angular brackets with subscript α denote an equilibrium ensemble average over the molecular degrees of freedom in site α.

The ISTOs $T^2_M(11)$ appearing in $H^{\alpha}_{\mathrm{D}}(t)$ are decomposed into eigenoperators $A_{M\lambda}$ (Table S3) of $\mathcal{L}_{\mathrm{Z}}$, such that

$$T^2_M(11) \;=\; \sum_{\lambda} A_{M\lambda}\,, \tag{E.2}$$

and

$$\mathcal{L}_{\mathrm{Z}}\,A_{M\lambda} \;=\; \Omega_{M\lambda}\,A_{M\lambda}\,, \tag{E.3}$$

where the eigenvalues $\Omega_{M\lambda}$ are linear combinations of ω_I and ω_S (Table S3). It then follows that

$$\widehat{A}_{M\lambda}(t) \;\equiv\; \exp(i\,\mathcal{L}_{\mathrm{Z}}\,t)\,A_{M\lambda} \;=\; \exp(i\,\Omega_{M\lambda}\,t)\,A_{M\lambda}\,, \tag{E.4}$$

so that

$$\widehat{\mathcal{L}}^{\alpha}_{\mathrm{D}}(t) \;=\; -\,\frac{\sqrt{6}}{3}\,\omega_{\mathrm{D}}\sum_{M}\sum_{\lambda}\exp(i\,\Omega_{M\lambda}\,t)\,\mathcal{A}_{M\lambda}\,C^2_M(\Omega_{\alpha}(t))\,, \tag{E.5}$$

where $\mathcal{A}_{M\lambda} \equiv [A_{M\lambda},\,\ldots]$.

Combination of Eqs. (E.1) and (E.5) yields

$$\begin{aligned}\frac{\mathrm{d}}{\mathrm{d}t}\,\widehat{\sigma}^{\alpha}(t) \;=\; -\;\frac{2}{3}\,\omega^2_{\mathrm{D}}\sum_{M}\sum_{M'}\sum_{\lambda}\sum_{\lambda'}\exp[i\,(\Omega_{M\lambda}+\Omega_{M'\lambda'})\,t] \\ \times\int_0^{\infty}\mathrm{d}\tau\;\exp(-i\,\Omega_{M'\lambda'}\,\tau)\,G^{\alpha}_{MM'}(\tau)\,\mathcal{A}_{M\lambda}\,\mathcal{A}_{M'\lambda'}\,\widehat{\sigma}^{\alpha}(t)\,,\end{aligned} \tag{E.6}$$

with the time correlation function

TABLE S3. Eigenoperators and eigenvalues of $\mathcal{L}_{\mathrm{Z}}$.

M	λ	$A_{M\lambda}$	$\Omega_{M\lambda}$
0	1	$\frac{4}{\sqrt{6}}\, I_z\, S_z$	0
0	2	$-\frac{1}{\sqrt{6}}\, I_-\, S_+$	$\omega_S - \omega_I$
0	3	$-\frac{1}{\sqrt{6}}\, I_+\, S_-$	$\omega_I - \omega_S$
1	1	$-\, I_z\, S_+$	ω_S
1	2	$-\, I_+\, S_z$	ω_I
-1	1	$I_z\, S_-$	$-\,\omega_S$
-1	2	$I_-\, S_z$	$-\,\omega_I$
2	1	$I_+\, S_+$	$\omega_I + \omega_S$
-2	1	$I_-\, S_-$	$-\,\omega_I - \omega_S$

$$
\begin{aligned}
G^{\alpha}_{MM'}(\tau) \;&\equiv\; \left\langle C^2_M(\Omega_\alpha(0))\, C^2_{M'}(\Omega_\alpha(\tau))\right\rangle_\alpha \\
&=\; C^2_M(\Omega_\alpha(0)) \int \mathrm{d}\Omega_\alpha(\tau)\, f(\Omega_\alpha(\tau)\,|\,\Omega_\alpha(0))\, C^2_{M'}(\Omega_\alpha(\tau))\,,
\end{aligned}
\tag{E.7}
$$

where the dipole vector orientation $\Omega_\alpha(\tau)$ is modeled as a stationary random process. Note that the time correlation function is not averaged over the initial orientation $\Omega_\alpha(0)$, which is fixed by the nuclear geometry in site α. In the EMOR model, the orientation of the dipole vector is randomized upon exchange, as expressed by the propagator

$$
f(\Omega_\alpha(\tau)\,|\,\Omega_\alpha(0)) \;=\; \frac{1}{4\pi} \;+\; \left[\delta(\Omega_\alpha(\tau) - \Omega_\alpha(0)) \;-\; \frac{1}{4\pi}\right] \exp(-\tau/\tau_{\mathrm{A}})\,, \tag{E.8}
$$

where τ_{A} is the mean survival time in the site. Combining Eqs. (E.7) and (E.8) and making use of the orthogonality of the spherical harmonics $C^2_M(\Omega_\alpha)$,[1] we find

$$
G^{\alpha}_{MM'}(\tau) \;=\; F_{MM'}(\Omega_\alpha)\, \exp(-\tau/\tau_{\mathrm{A}})\,, \tag{E.9}
$$

with

$$
F_{MM'}(\Omega_\alpha) \;\equiv\; C^2_M(\Omega_\alpha)\, C^2_{M'}(\Omega_\alpha) \;=\; d^2_{M0}(\beta)\, d^2_{M'0}(\beta)\, \exp[i(M+M')\alpha]\,. \tag{E.10}
$$

With the time correlation function (E.9), we can write the master equation (E.6) as

$$
\frac{\mathrm{d}}{\mathrm{d}t}\, \widehat{\sigma}^{\alpha}(t) \;=\; -\,\widehat{\mathcal{R}}^{\alpha}(t)\, \widehat{\sigma}^{\alpha}(t)\,. \tag{E.11}
$$

The time-dependent relaxation superoperator is given by

$$
\begin{aligned}
\widehat{\mathcal{R}}^{\alpha}(t) \;&=\; \frac{2}{3}\,\omega^2_{\mathrm{D}} \sum_{M} \sum_{M'} \sum_{\lambda} \sum_{\lambda'} \exp[i\,(\Omega_{M\lambda} + \Omega_{M'\lambda'})\, t] \\
&\times\; F_{MM'}(\Omega_\alpha)\, J(-\Omega_{M'\lambda'})\, \mathcal{A}_{M\lambda}\, \mathcal{A}_{M'\lambda'}\,,
\end{aligned}
\tag{E.12}
$$

with a complex-valued reduced spectral density function

$$J(\omega) \equiv j(\omega) + i\,k(\omega) \equiv \int_0^\infty \mathrm{d}\tau\, \exp(i\,\omega\tau)\,\frac{G^\alpha_{MM'}(\tau)}{G^\alpha_{MM'}(0)} = \frac{\tau_\mathrm{A}}{1+(\omega\,\tau_\mathrm{A})^2}\,(1+i\,\omega\,\tau_\mathrm{A})\,. \quad \text{(E.13)}$$

Our development is more general than the standard treatment in two respects. First, we retain the imaginary part, $k(\omega)$, of the spectral density, which, contrary to conventional wisdom,[3] can affect longitudinal relaxation under certain conditions.[4] Because $k(-\omega) = -\,k(\omega)$, we refer to $k(\omega)$ as the odd spectral density function (OSDF). Second, we do not invoke the secular approximation to eliminate terms with oscillating factors in Eq. (E.12), since we want to describe relaxation over the full frequency range.

The integral relaxation rate is most conveniently obtained from a time-independent relaxation superoperator. For this purpose, we transform the master equation (E.11) to the Schrödinger representation as

$$\frac{\mathrm{d}}{\mathrm{d}t}\,\sigma^\alpha(t) = -\,i\,\mathcal{L}_\mathrm{Z}\,\sigma^\alpha(t) - \exp(-i\,\mathcal{L}_\mathrm{Z}\,t)\,\widehat{\mathcal{R}}^\alpha(t)\exp(i\,\mathcal{L}_\mathrm{Z}\,t)\,\sigma^\alpha(t)\,, \quad \text{(E.14)}$$

The two superoperators $i\,\mathcal{L}_\mathrm{Z}$ and $\widehat{\mathcal{R}}^\alpha(t)$ appearing in Eq. (E.14) are invariant under spin inversion conjugation and can therefore have nonzero supermatrix elements only between ISTO basis operators B_n of the same parity.[4–6] In the motional-narrowing regime, longitudinal relaxation can therefore be fully described within the subspace of the six single-spin basis operators in Table S1. These operators have odd parity with respect to spin inversion conjugation, whereas the remaining nine two-spin operators have even parity. The supermatrix representation of the operator master equation (E.14) in the subspace of the six single-spin basis operators B_n takes the form

$$\frac{\mathrm{d}}{\mathrm{d}t}\,\boldsymbol{\sigma}^\alpha(t) = -\,i\,\mathbf{L}_\mathrm{Z}\,\boldsymbol{\sigma}^\alpha(t) - \mathbf{R}^\alpha\,\boldsymbol{\sigma}^\alpha(t)\,, \quad \text{(E.15)}$$

where $\boldsymbol{\sigma}^\alpha(t)$ is the column vector of the six single-spin modes $\sigma^\alpha_n(t) = (B_n\,|\,\sigma^\alpha(t)) = \mathrm{Tr}\{B_n^\dagger\,\sigma^\alpha(t)\}$ and the time-independent relaxation supermatrix $\mathbf{R}^\alpha$ is given by

$$\mathbf{R}^\alpha = \frac{2}{3}\,\omega_\mathrm{D}^2 \sum_M \sum_{M'} \sum_\lambda \sum_{\lambda'} F_{MM'}(\Omega_\alpha)\,J(-\Omega_{M'\lambda'})\,\mathbf{C}_{MM'\lambda\lambda'}\,, \quad \text{(E.16)}$$

where we have defined a coefficient supermatrix $\mathbf{C}_{MM'\lambda\lambda'}$ with real-valued elements

$$C_{MM'\lambda\lambda',np} \equiv (n\,|\mathcal{A}_{M\lambda}\,\mathcal{A}_{M'\lambda'}|\,p) = \mathrm{Tr}\{[B_n^\dagger, A_{M\lambda}]\,[A_{M'\lambda'}, B_p]\}\,. \quad \text{(E.17)}$$

The oscillating factors in Eq. (E.12) are absent from Eq. (E.16) because the single-spin basis operators are eigenoperators of the Zeeman Liouvillian

$$\mathcal{L}_\mathrm{Z}\,B_n = \Omega_n\,B_n\,, \quad \text{(E.18)}$$

and $\Omega_{M\lambda} + \Omega_{M'\lambda'} = \Omega_n - \Omega_p$ for all nonzero values of $C_{MM'\lambda\lambda',np}$.

Ordering the basis operators for the single-spin subspace as $\{I_z,\, I_+,\, I_-,\, S_z,\, S_+,\, S_-\}$, we can write the supermatrix $\mathbf{L}_\mathrm{Z}$ in Eq. (E.15) as

$$\mathbf{L}_\mathrm{Z} \;=\; \begin{bmatrix} \omega_I\,\mathbf{Q} & \mathbf{0} \\ \mathbf{0} & \omega_S\,\mathbf{Q} \end{bmatrix}, \tag{E.19}$$

where $\mathbf{0}$ is the 3×3 null matrix, and

$$\mathbf{Q} \;\equiv\; \begin{bmatrix} 0 & 0 & 0 \\ 0 & 1 & 0 \\ 0 & 0 & -1 \end{bmatrix}. \tag{E.20}$$

Similarly, we partition the relaxation supermatrix as

$$\mathbf{R}^\alpha \;=\; \begin{bmatrix} \mathbf{R}^\alpha_{II} & \mathbf{R}^\alpha_{IS} \\ \mathbf{R}^\alpha_{SI} & \mathbf{R}^\alpha_{SS} \end{bmatrix}. \tag{E.21}$$

The elements of the relaxation submatrices are obtained from Eqs. (E.10), (E.16) and (E.17), with spin operators and eigenfrequencies from Tables S1 and S3. Thus,

$$R^{II}_{zz} \;=\; \tfrac{2}{9}\,\omega_\mathrm{D}^2\left[(d_0)^2 j_- + 3\,(d_1)^2 j_I + 6\,(d_2)^2 j_+\right], \tag{E.22a}$$

$$\begin{aligned} R^{II}_{\pm\pm} \;=\; \tfrac{1}{9}\,\omega_\mathrm{D}^2\big\{&4\,(d_0)^2 j_0 + (d_0)^2 j_- + 3\,(d_1)^2 j_I + 6\,(d_1)^2 j_S + 6\,(d_2)^2 j_+ \\ &\pm\, i\left[(d_0)^2 k_- + 3\,(d_1)^2 k_I + 6\,(d_2)^2 k_+\right]\big\}, \end{aligned} \tag{E.22b}$$

$$R^{II}_{z\pm} \;=\; \pm\kappa\, e^{\mp i\alpha}\left[2\,d_0\, j_0 + (3\,\sin^2\beta - 1)\, j_S \;\mp\; i\, k_S\right], \tag{E.22c}$$

$$\begin{aligned} R^{II}_{\pm z} \;=\; \pm\kappa\, e^{\pm i\alpha}\big\{&-d_0\, j_- + 2\,d_0\, j_I + \tfrac{3}{2}\,\sin^2\beta\, j_+ \\ &\mp\, i\left[-d_0\, k_- + 2\,d_0\, k_I + \tfrac{3}{2}\,\sin^2\beta\, k_+\right]\big\}, \end{aligned} \tag{E.22d}$$

$$\begin{aligned} R^{II}_{\pm\mp} \;=\; \eta\, e^{\pm i2\alpha}\big\{&d_0\, j_- - 3\,\cos^2\beta\, j_I + d_0\, j_+ \\ &\mp\, i\left[d_0\, k_- - 3\,\cos^2\beta\, k_I + d_0\, k_+\right]\big\}, \end{aligned} \tag{E.22e}$$

and

$$R^{IS}_{zz} \;=\; \tfrac{2}{9}\,\omega_\mathrm{D}^2\left[-(d_0)^2 j_- + 6\,(d_2)^2 j_+\right], \tag{E.23a}$$

$$\begin{aligned} R^{IS}_{\pm\pm} \;=\; \tfrac{1}{9}\,\omega_\mathrm{D}^2\big\{&2\,(d_0)^2\,(j_0 + j_-) + 3\,(d_1)^2 (j_I + j_S) \\ &\mp\, i\left[2\,(d_0)^2\, k_- + 3\,(d_1)^2 (k_I - k_S)\right]\big\}, \end{aligned} \tag{E.23b}$$

$$\begin{aligned} R^{IS}_{z\pm} \;=\; \pm\kappa\, e^{\mp i\alpha}\big\{&d_0\, j_- + j_I + \tfrac{3}{2}\,\sin^2\beta\, j_+ \\ &\mp\, i\left[d_0\, k_- + (3\sin^2\beta - 1)\, k_I - \tfrac{3}{2}\,\sin^2\beta\, k_+\right]\big\}, \end{aligned} \tag{E.23c}$$

$$\begin{aligned} R^{IS}_{\pm z} \;=\; \pm\kappa\, e^{\pm i\alpha}\big\{&d_0\, j_- + j_S + \tfrac{3}{2}\,\sin^2\beta\, j_+ \\ &\mp\, i\left[d_0\, k_- - (3\sin^2\beta - 1)\, k_S + \tfrac{3}{2}\,\sin^2\beta\, k_+\right]\big\}, \end{aligned} \tag{E.23d}$$

$$\begin{aligned} R^{IS}_{\pm\mp} \;=\; \eta\, e^{\pm i2\alpha}\big\{&2\,d_0\, j_0 - 3\,\cos^2\beta\,(j_I + j_S) + 2\,d_0\, j_+ \\ &\pm\, i\left[3\,\cos^2\beta\,(k_I + k_S) - 2\,d_0\, k_+\right]\big\}. \end{aligned} \tag{E.23e}$$

The symbols in Eqs. (E.22) and (E.23) have the following meaning

$$j_0 \equiv j(0) = \tau_{\rm A} \,, \tag{E.24a}$$

$$j_I \equiv j(\omega_I) = \frac{\tau_{\rm A}}{1+(\omega_I\,\tau_{\rm A})^2} \,, \tag{E.24b}$$

$$j_S \equiv j(\omega_S) = \frac{\tau_{\rm A}}{1+(\omega_S\,\tau_{\rm A})^2} \,, \tag{E.24c}$$

$$j_\pm \equiv j(\omega_I \pm \omega_S) = \frac{\tau_{\rm A}}{1+[(\omega_I \pm \omega_S)\,\tau_{\rm A}]^2} \,, \tag{E.24d}$$

$$k_I \equiv k(\omega_I) = \frac{\omega_I\,\tau_{\rm A}^2}{1+(\omega_I\,\tau_{\rm A})^2} \,, \tag{E.25a}$$

$$k_S \equiv k(\omega_S) = \frac{\omega_S\,\tau_{\rm A}^2}{1+(\omega_S\,\tau_{\rm A})^2} \,, \tag{E.25b}$$

$$k_\pm \equiv k(\omega_I \pm \omega_S) = \frac{(\omega_I \pm \omega_S)\,\tau_{\rm A}^2}{1+[(\omega_I \pm \omega_S)\,\tau_{\rm A}]^2} \,, \tag{E.25c}$$

and

$$d_m \equiv d^2_{m0}(\beta) \,, \tag{E.26a}$$

$$\kappa \equiv -\frac{\sqrt{3}}{9}\,\omega_{\rm D}^2\,d_1 \,, \tag{E.26b}$$

$$\eta \equiv -\frac{\sqrt{6}}{9}\,\omega_{\rm D}^2\,d_2 \,. \tag{E.26c}$$

The elements of the submatrices $\mathbf{R}^\alpha_{SS}$ and $\mathbf{R}^\alpha_{SI}$ are obtained from the corresponding elements of $\mathbf{R}^\alpha_{II}$ and $\mathbf{R}^\alpha_{IS}$, respectively, by interchanging I and S everywhere, which amounts to the following three substitutions: $j_I \leftrightarrow j_S$, $k_I \leftrightarrow k_S$ and $k_- \leftrightarrow -k_-$. We note that the OSDF affects all rates, except the longitudinal auto-mode rates R^{II}_{zz}, R^{SS}_{zz} and $R^{IS}_{zz} = R^{SI}_{zz}$.

Whereas the master equation (E.15) in the Schrödinger representation is most convenient for obtaining the integral relaxation rate, the effect of nonsecular decoupling is more apparent in the interaction representation. For this purpose, it is more convenient to order the basis operators in the relevant subspace as $\{I_z,\, S_z,\, I_+,\, S_+,\, I_-,\, ,S_-\}$. In this subspace, the supermatrix representation of master equation (E.11) becomes

$$\frac{\rm d}{{\rm d}t}\begin{bmatrix} I^\alpha_z(t) \\ S^\alpha_z(t) \\ \widehat{I}^\alpha_+(t) \\ \widehat{S}^\alpha_+(t) \\ \widehat{I}^\alpha_-(t) \\ \widehat{S}^\alpha_-(t) \end{bmatrix} = -\,\widehat{\mathbf{R}}^\alpha(t)\begin{bmatrix} I^\alpha_z(t) \\ S^\alpha_z(t) \\ \widehat{I}^\alpha_+(t) \\ \widehat{S}^\alpha_+(t) \\ \widehat{I}^\alpha_-(t) \\ \widehat{S}^\alpha_-(t) \end{bmatrix} \,, \tag{E.27}$$

where, for clarity, we have represented the six spin density operator elements by the

corresponding basis operators. The time-dependent relaxation supermatrix is

$$\widehat{\mathbf{R}}^{\alpha}(t) \;=\; \begin{bmatrix} R^{II}_{zz} & R^{IS}_{zz} & e^{-i\omega_I t}\,R^{II}_{z+} & e^{-i\omega_S t}\,R^{IS}_{z+} & e^{i\omega_I t}\,R^{II}_{z-} & e^{i\omega_S t}\,R^{IS}_{z-} \\ R^{SI}_{zz} & R^{SS}_{zz} & e^{-i\omega_I t}\,R^{SI}_{z+} & e^{-i\omega_S t}\,R^{SS}_{z+} & e^{i\omega_I t}\,R^{SI}_{z-} & e^{i\omega_S t}\,R^{SS}_{z-} \\ e^{i\omega_I t}\,R^{II}_{+z} & e^{i\omega_I t}\,R^{IS}_{+z} & R^{II}_{++} & e^{i\Delta t}\,R^{IS}_{++} & e^{i2\omega_I t}\,R^{II}_{+-} & e^{i\Sigma t}\,R^{IS}_{+-} \\ e^{i\omega_S t}\,R^{SI}_{+z} & e^{i\omega_S t}\,R^{SS}_{+z} & e^{-i\Delta t}\,R^{SI}_{++} & R^{SS}_{++} & e^{i\Sigma t}\,R^{SI}_{+-} & e^{i2\omega_S t}\,R^{SS}_{+-} \\ e^{-i\omega_I t}\,R^{II}_{-z} & e^{-i\omega_I t}\,R^{IS}_{-z} & e^{-i2\omega_I t}\,R^{II}_{-+} & e^{-i\Sigma t}\,R^{IS}_{-+} & R^{II}_{--} & e^{-i\Delta t}\,R^{IS}_{--} \\ e^{-i\omega_S t}\,R^{SI}_{-z} & e^{-i\omega_S t}\,R^{SS}_{-z} & e^{-i\Sigma t}\,R^{SI}_{-+} & e^{-i2\omega_S t}\,R^{SS}_{-+} & e^{i\Delta t}\,R^{SI}_{--} & R^{SS}_{--} \end{bmatrix}, \tag{E.28}$$

where

$$\Sigma \;\equiv\; \omega_I + \omega_S\,, \tag{E.29a}$$

$$\Delta \;\equiv\; \omega_I - \omega_S\,. \tag{E.29b}$$

In the ZF regime (Sec. III A), where the frequencies ω_I, ω_S and $\omega_I \pm \omega_S$ are much smaller than the relaxation rates (of order $\omega_{\mathrm{D}}^2\,\tau_{\mathrm{A}}$), the complex exponential factors in Eq. (E.28) can all be replaced by unity. The cross-mode relaxation rates then come into play, coupling the evolution of the longitudinal and transverse magnetization components. This happens in the asymmetric IS–I case because the I–S dipole coupling is not isotropically averaged. At higher fields, where $\omega_I,\ \omega_S \gg \omega_{\mathrm{D}}^2\,\tau_{\mathrm{A}}$, the oscillating factors cancel all relaxation supermatrix elements, except possibly those involving the difference frequency $\omega_I - \omega_S$ (for a homonuclear spin pair). The relaxation supermatrix then becomes block-diagonal,

$$\widehat{\mathbf{R}}^{\alpha}(t) \;=\; \begin{bmatrix} R^{II}_{zz} & R^{IS}_{zz} & 0 & 0 & 0 & 0 \\ R^{SI}_{zz} & R^{SS}_{zz} & 0 & 0 & 0 & 0 \\ 0 & 0 & R^{II}_{++} & e^{i\Delta t}\,R^{IS}_{++} & 0 & 0 \\ 0 & 0 & e^{-i\Delta t}\,R^{SI}_{++} & R^{SS}_{++} & 0 & 0 \\ 0 & 0 & 0 & 0 & R^{II}_{--} & e^{-i\Delta t}\,R^{IS}_{--} \\ 0 & 0 & 0 & 0 & e^{i\Delta t}\,R^{SI}_{--} & R^{SS}_{--} \end{bmatrix}. \tag{E.30}$$

Nonsecular decoupling thus cancels all cross-mode rates so the longitudinal modes (I_z and S_z) evolve independently from the transverse modes ($I_\pm$ and $S_\pm$).

For the symmetric IS–IS case in the motional-narrowing regime, the same IS spin pair samples all anisotropic A sites on a time scale that is short compared to the relaxation in each site because, when the exchange time is also the correlation time (as in the EMOR model), the motional-narrowing regime coincides with the fast-exchange regime. The relaxation behavior is then governed by the isotropic average of the relaxation supermatrix

in Eq. (E.28), which becomes

$$\langle \widehat{\mathbf{R}}^{\alpha}(t) \rangle \;=\; \begin{bmatrix} \langle R^{II}_{zz} \rangle & \langle R^{IS}_{zz} \rangle & 0 & 0 & 0 & 0 \\ \langle R^{SI}_{zz} \rangle & \langle R^{SS}_{zz} \rangle & 0 & 0 & 0 & 0 \\ 0 & 0 & \langle R^{II}_{++} \rangle & e^{i\Delta t} \langle R^{IS}_{++} \rangle & 0 & 0 \\ 0 & 0 & e^{-i\Delta t} \langle R^{SI}_{++} \rangle & \langle R^{SS}_{++} \rangle & 0 & 0 \\ 0 & 0 & 0 & 0 & \langle R^{II}_{--} \rangle & e^{-i\Delta t} \langle R^{IS}_{--} \rangle \\ 0 & 0 & 0 & 0 & e^{i\Delta t} \langle R^{SI}_{--} \rangle & \langle R^{SS}_{--} \rangle \end{bmatrix} , \tag{E.31}$$

since all cross-mode rates vanish when isotropically averaged, as is evident from their dependence on the azimuthal angle α in Eqs. (E.22) and (E.23). This result, including the familiar Solomon equations, is usually derived from BWR theory by invoking the secular approximation. Fundamentally, however, the decoupling of the longitudinal and transverse magnetizations is a consequence of isotropic averaging. Cross-mode coupling is therefore absent also at zero field, which is not obvious if the secular approximation is invoked. The same result can be obtained from the time-independent relaxation supermatrix $\mathbf{R}^{\alpha}$ in Eq. (E.21) (with a different basis ordering). As a consequence of the vanishing of all cross-mode rates upon isotropic averaging, the four submatrices in Eq. (E.21) become diagonal. It is then evident from Eq. (E.15) that the longitudinal and transverse modes are decoupled.

The isotropically averaged auto-mode rates coincide with the familiar longitudinal and transverse auto-spin and cross-spin relaxation rates for a two-spin system,[3,7]

$$\langle R^{II}_{zz} \rangle \;=\; \frac{2}{45}\,\omega_{\mathrm{D}}^2\,(j_- + 3\,j_I + 6\,j_+) \;, \tag{E.32a}$$

$$\langle R^{SS}_{zz} \rangle \;=\; \frac{2}{45}\,\omega_{\mathrm{D}}^2\,(j_- + 3\,j_S + 6\,j_+) \;, \tag{E.32b}$$

$$\langle R^{IS}_{zz} \rangle \;=\; \langle R^{SI}_{zz} \rangle \;=\; \frac{2}{45}\,\omega_{\mathrm{D}}^2\,(-\,j_- + 6\,j_+) \;, \tag{E.32c}$$

$$\langle R^{II}_{\pm\pm} \rangle \;=\; \frac{1}{45}\,\omega_{\mathrm{D}}^2\,[4\,j_0 + j_- + 3\,j_I + 6\,j_S + 6\,j_+ \;\pm\; i\,(k_- + 3\,k_I + 6\,k_+)] \;, \tag{E.32d}$$

$$\langle R^{SS}_{\pm\pm} \rangle \;=\; \frac{1}{45}\,\omega_{\mathrm{D}}^2\,[4\,j_0 + j_- + 3\,j_S + 6\,j_I + 6\,j_+ \;\pm\; i\,(-k_- + 3\,k_S + 6\,k_+)] \;, \tag{E.32e}$$

$$\langle R^{IS}_{\pm\pm} \rangle \;=\; \frac{1}{45}\,\omega_{\mathrm{D}}^2\,[2\,j_0 + 2\,j_- + 3\,j_I + 3\,j_S \;\mp\; i\,(2\,k_- + 3\,k_I - 3\,k_S)] \;, \tag{E.32f}$$

$$\langle R^{SI}_{\pm\pm} \rangle \;=\; \frac{1}{45}\,\omega_{\mathrm{D}}^2\,[2\,j_0 + 2\,j_- + 3\,j_I + 3\,j_S \;\pm\; i\,(2\,k_- + 3\,k_I - 3\,k_S)] \;. \tag{E.32g}$$

In the extreme-narrowing regime, where $\omega_I, \omega_S \ll 1/\tau_{\mathrm{A}}$, all the even spectral densities in Eq. (E.24) are equal to τ_{A} and all the odd spectral densities in Eq. (E.25) can be neglected. The relaxation submatrices then take the form

$$\mathbf{R}^{\alpha}_{II} \;=\; \mathbf{R}^{\alpha}_{SS} \;=\; \begin{bmatrix} R_{1\mathrm{a}} & R^*_{\kappa} & -R_{\kappa} \\ R_{\kappa} & R_{2\mathrm{a}} & R_{\eta} \\ -R^*_{\kappa} & R^*_{\eta} & R_{2\mathrm{a}} \end{bmatrix} , \tag{E.33}$$

$$\mathbf{R}^{\alpha}_{IS} \;=\; \mathbf{R}^{\alpha}_{SI} \;=\; 2 \begin{bmatrix} R_{1\mathrm{c}} & R^{*}_{\kappa} & -R_{\kappa} \\ R_{\kappa} & R_{2\mathrm{c}} & R_{\eta} \\ -R^{*}_{\kappa} & R^{*}_{\eta} & R_{2\mathrm{c}} \end{bmatrix} , \tag{E.34}$$

where

$$R_{1\mathrm{a}} \;\equiv\; \tfrac{1}{9} \left(3 \, \sin^2\!\beta + 2\right) \omega_{\mathrm{D}}^2 \, \tau_{\mathrm{A}} \, , \tag{E.35a}$$

$$R_{1\mathrm{c}} \;\equiv\; \tfrac{2}{9} \left(3 \, \sin^2\!\beta - 1\right) \omega_{\mathrm{D}}^2 \, \tau_{\mathrm{A}} \, , \tag{E.35b}$$

$$R_{2\mathrm{a}} \;\equiv\; \tfrac{1}{18} \left(10 - 3 \, \sin^2\!\beta\right) \omega_{\mathrm{D}}^2 \, \tau_{\mathrm{A}} \, , \tag{E.35c}$$

$$R_{2\mathrm{c}} \;\equiv\; \tfrac{1}{9} \left(3 \, \cos^2\!\beta + 1\right) \omega_{\mathrm{D}}^2 \, \tau_{\mathrm{A}} \, , \tag{E.35d}$$

$$R_{\kappa} \;\equiv\; \tfrac{\sqrt{2}}{6} \, \sin\beta \, \cos\beta \, \exp(i\alpha) \, \omega_{\mathrm{D}}^2 \, \tau_{\mathrm{A}} \, , \tag{E.35e}$$

$$R_{\eta} \;\equiv\; \tfrac{1}{6} \, \sin^2\!\beta \, \exp(i2\alpha) \, \omega_{\mathrm{D}}^2 \, \tau_{\mathrm{A}} \, . \tag{E.35f}$$

APPENDIX F: TIME EVOLUTION OF I_z AND S_z

Here we derive analytical results for the time evolution of the longitudinal magnetizations in the ZF + MN regime, where only the spin modes $\sigma_1^{\mathrm{A}} = I_z$ and $\sigma_2^{\mathrm{A}} = S_z$ are coupled in state A. It must then be possible to describe the evolution of the longitudinal magnetizations in the A and B states by three coupled equations:

$$\frac{\mathrm{d}}{\mathrm{d}t} I_z^{\mathrm{B}}(t) \;=\; -\,\frac{1}{\tau_{\mathrm{B}}}\, I_z^{\mathrm{B}}(t) \;+\; \frac{1}{\tau_{\mathrm{A}}}\, I_z^{\mathrm{A}}(t)\,, \tag{F.1a}$$

$$\frac{\mathrm{d}}{\mathrm{d}t} I_z^{\mathrm{A}}(t) \;=\; \frac{1}{\tau_{\mathrm{B}}}\, I_z^{\mathrm{B}}(t) \;-\; \left(\rho_I + \frac{1}{\tau_{\mathrm{A}}}\right) I_z^{\mathrm{A}}(t) \;-\; \sigma_{IS}\, S_z^{\mathrm{A}}(t)\,, \tag{F.1b}$$

$$\frac{\mathrm{d}}{\mathrm{d}t} S_z^{\mathrm{A}}(t) \;=\; -\,\sigma_{SI}\, I_z^{\mathrm{A}}(t) \;-\; \rho_S\, S_z^{\mathrm{A}}(t)\,, \tag{F.1c}$$

where, without loss of generality, we have set the equilibrium magnetizations to zero. Apart from the exchange terms, Eqs. (F.1b) and (F1.c) have the same form as the two-spin Solomon equations,[3,8] but the four relaxation rates are not the same for the $IS-I$ EMOR model as for an isolated spin pair in isotropic solution. In the ZF regime, $\rho_I = \rho_S$ and $\sigma_{IS} = \sigma_{SI}$ in the Solomon equations,[3,8] but this symmetry is broken in the $IS-I$ EMOR model since only spin I can exchange with state B. For nonselective excitation, Eq. (F.1) is to be solved subject to the initial conditions

$$I_z^{\mathrm{B}}(0) \;=\; P_{\mathrm{B}}\,, \quad I_z^{\mathrm{A}}(0) \;=\; S_z^{\mathrm{A}}(0) \;=\; P_{\mathrm{A}}\,. \tag{F.2}$$

The MN regime is also the fast-exchange regime, so $1/\tau_{\mathrm{A}} \gg \rho_I,\, \rho_S,\, \sigma_{IS},\, \sigma_{SI}$. Because exchange is much faster than auto-spin and cross-spin relaxation, the ratio of the I_z magnetizations in states A and B remains at the initial value,

$$\frac{I_z^{\mathrm{A}}(t)}{I_z^{\mathrm{B}}(t)} \;=\; \frac{I_z^{\mathrm{A}}(0)}{I_z^{\mathrm{B}}(0)} \;=\; \frac{P_{\mathrm{A}}}{P_{\mathrm{B}}}\,. \tag{F.3}$$

When $I_z^{\mathrm{A}}(t)$ relaxes to the lattice (directly and via spin S), it is 'immediately' replenished with magnetization from state B. Consequently, the total I-spin magnetization, $I_z(t) = I_z^{\mathrm{A}}(t) + I_z^{\mathrm{B}}(t)$, relaxes slowly with an effective rate that is proportional to $P_{\mathrm{A}}\,\omega_{\mathrm{D}}^2\,\tau_{\mathrm{A}}$. Summing Eqs. (F.1a) and (F.1b), we obtain

$$\frac{\mathrm{d}}{\mathrm{d}t} I_z(t) \;=\; -\,\rho_I\, I_z^{\mathrm{A}}(t) \;-\; \sigma_{IS}\, S_z^{\mathrm{A}}(t)\,. \tag{F.4}$$

Substituting $I_z^{\mathrm{A}}(t) = P_{\mathrm{A}}\, I_z(t)$ from Eq. (F.3) into Eqs. (F.4) and (F.1c), we find

$$\frac{\mathrm{d}}{\mathrm{d}t} I_z(t) \;=\; -\,P_{\mathrm{A}}\,\rho_I\, I_z(t) \;-\; \sigma_{IS}\, S_z^{\mathrm{A}}(t)\,, \tag{F.5a}$$

$$\frac{\mathrm{d}}{\mathrm{d}t} S_z^{\mathrm{A}}(t) \;=\; -\,P_{\mathrm{A}}\,\sigma_{SI}\, I_z(t) \;-\; \rho_S\, S_z^{\mathrm{A}}(t)\,. \tag{F.5b}$$

We shall consider Eq. (F.5) in two different time regimes. At short times, such that $t \ll 1/(P_{\mathrm{A}}\,\omega_{\mathrm{D}}^2\,\tau_{\mathrm{A}})$, the I and S spins are decoupled because the I spin has not yet relaxed. We can then set $I_z(t) = I_z(0) = 1$ in Eq. (F.5b), whereby

$$\frac{\mathrm{d}}{\mathrm{d}t} S_z^{\mathrm{A}}(t) \;=\; -\,\sigma_{SI}\, P_{\mathrm{A}} \;-\; \rho_S\, S_z^{\mathrm{A}}(t) \;=\; -\,\rho_S \left[S_z^{\mathrm{A}}(t) + P_{\mathrm{A}}\, \frac{\sigma_{SI}}{\rho_S} \right]\,. \tag{F.6}$$

With $S_z^{\rm A}(0) = P_{\rm A}$ from Eq. (F.2), the solution to Eq. (F.6) is

$$S_z^{\rm A}(t) \;=\; P_{\rm A}\left[\left(1+\frac{\sigma_{SI}}{\rho_S}\right)\exp(-\rho_S\,t) \;-\; \frac{\sigma_{SI}}{\rho_S}\right] . \tag{F.7}$$

The S-spin magnetization thus relaxes to a (negative) steady-state value, $-P_{\rm A}\,\sigma_{SI}/\rho_S$, rather then to its zero equilibrium value.

After $S_z^{\rm A}(t)$ has reached its steady-state value while $I_z(t)$ remains essentially constant, both magnetizations relax together to zero at the same rate. This coupled evolution, on the time scale $t \gg 1/\rho_S$, is obtained by solving Eq. (F.5) subject to the initial conditions

$$I_z(0) \;=\; 1\,, \quad S_z^{\rm A}(0) \;=\; -\,P_{\rm A}\,\frac{\sigma_{SI}}{\rho_S}\,. \tag{F.8}$$

The solution is

$$\begin{aligned} I_z(t) \;=\; \frac{1}{(\lambda_+ - \lambda_-)}\Big\{ & \left[(\rho_S-\lambda_-)\,I_z(0) - \sigma_{IS}\,S_z^{\rm A}(0)\right]\exp(-\lambda_-\,t) \\ & -\;\left[(\rho_S-\lambda_+)\,I_z(0) - \sigma_{IS}\,S_z^{\rm A}(0)\right]\exp(-\lambda_+\,t)\Big\}\,, \end{aligned} \tag{F.9a}$$

$$\begin{aligned} S_z^{\rm A}(t) \;=\; \frac{1}{(\lambda_+ - \lambda_-)}\Big\{ & \left[(P_{\rm A}\,\rho_I-\lambda_-)\,S_z^{\rm A}(0) - P_{\rm A}\,\sigma_{SI}\,I_z(0)\right]\exp(-\lambda_-\,t) \\ & -\;\left[(P_{\rm A}\,\rho_I-\lambda_+)\,S_z^{\rm A}(0) - P_{\rm A}\,\sigma_{SI}\,I_z(0)\right]\exp(-\lambda_+\,t)\Big\}\,, \end{aligned} \tag{F.9b}$$

where

$$\lambda_\pm \;\equiv\; \tfrac{1}{2}\,(\rho_S + P_{\rm A}\,\rho_I) \;\pm\; \tfrac{1}{2}\left[(\rho_S - P_{\rm A}\,\rho_I)^2 + 4\,P_{\rm A}\,\sigma_{IS}\,\sigma_{SI}\right]^{1/2} . \tag{F.10}$$

In the dilute regime, we can expand these rates as

$$\lambda_+ \;=\; \rho_S \;+\; P_{\rm A}\,\frac{\sigma_{IS}\,\sigma_{SI}}{\rho_S} \;+\; \mathcal{O}(P_{\rm A}^2)\,, \tag{F.11a}$$

$$\lambda_- \;=\; P_{\rm A}\left(\rho_I - \frac{\sigma_{IS}\,\sigma_{SI}}{\rho_S}\right) \;+\; \mathcal{O}(P_{\rm A}^2)\,. \tag{F.11b}$$

Substitution from Eqs. (F.8) and (F.11) into Eq. (F.9) yields

$$I_z(t) \;=\; \left[1-\mathcal{O}(P_{\rm A}^2)\right]\exp(-\lambda_-\,t) \;+\; \mathcal{O}(P_{\rm A}^2)\,\exp(-\lambda_+\,t)\,, \tag{F.12a}$$

$$S_z^{\rm A}(t) \;=\; \left[-\,P_{\rm A}\,\frac{\sigma_{SI}}{\rho_S} + \mathcal{O}(P_{\rm A}^2)\right]\exp(-\lambda_-\,t) \;+\; \mathcal{O}(P_{\rm A}^2)\,\exp(-\lambda_+\,t)\,. \tag{F.12b}$$

Neglecting terms of second and higher order in $P_{\rm A}$, we thus obtain

$$I_z(t) \;=\; \exp(-R_{\rm slow}\,t)\,, \tag{F.13a}$$

$$S_z^{\rm A}(t) \;=\; -\,P_{\rm A}\,\frac{\sigma_{SI}}{\rho_S}\,\exp(-R_{\rm slow}\,t)\,, \tag{F.13b}$$

with

$$R_{\rm slow} \;\equiv\; P_{\rm A}\left(\rho_I - \frac{\sigma_{IS}\,\sigma_{SI}}{\rho_S}\right) . \tag{F.14}$$

Combination of Eqs. (F.3), (F.7) and (F.13) finally yields

$$I_z^{\mathrm{B}}(t) \;=\; P_{\mathrm{B}}\,\exp(-R_{\mathrm{slow}}\,t)\,, \tag{F.15a}$$

$$I_z^{\mathrm{A}}(t) \;=\; P_{\mathrm{A}}\,\exp(-R_{\mathrm{slow}}\,t)\,, \tag{F.15b}$$

$$S_z^{\mathrm{A}}(t) \;=\; P_{\mathrm{A}}\left[\left(1+\frac{\sigma_{SI}}{\rho_S}\right)\exp(-\rho_S\,t)\;-\;\frac{\sigma_{SI}}{\rho_S}\,\exp(-R_{\mathrm{slow}}\,t)\right]\,. \tag{F.15c}$$

In the ZF + MN regime, the auto-spin and cross-spin relaxation rates ρ_I, ρ_S, σ_{IS} and σ_{SI} are all proportional to $\omega_{\mathrm{D}}^2\,\tau_{\mathrm{A}}$, but they differ from the 'Solomon values' $\rho_I = \rho_S = (4/9)\,\omega_{\mathrm{D}}^2\,\tau_{\mathrm{A}}$ and $\sigma_{IS} = \sigma_{SI} = (2/9)\,\omega_{\mathrm{D}}^2\,\tau_{\mathrm{A}}$ because, in the $IS{-}I$ EMOR model, cross-mode relaxation occurs in the A sites. However, as we shall see, $\rho_I{+}\sigma_{IS} = \rho_S{+}\sigma_{SI} = (2/3)\,\omega_{\mathrm{D}}^2\,\tau_{\mathrm{A}}$ in both cases.

To obtain the numerical coefficients in front of $\omega_{\mathrm{D}}^2\,\tau_{\mathrm{A}}$ in ρ_I, ρ_S, σ_{IS} and σ_{SI}, we need four relations involving these rates. Such relations can be obtained in several ways, making use of the ZF results in Appendix D and then taking the MN and dilute limits. Three relations can be obtained from integral relaxation rates. Using Eqs. (F.2) and (F.15), we find for nonselective excitation in the dilute ZF + MN regime

$$\widehat{R}_{1,I}^{\mathrm{dil}}(0) \;=\; \frac{I_z(0)}{\widetilde{I}_z(0)} \;=\; R_{\mathrm{slow}} \;=\; P_{\mathrm{A}}\left(\rho_I - \frac{\sigma_{IS}\,\sigma_{SI}}{\rho_S}\right)\,, \tag{F.16a}$$

$$\widehat{R}_{1,S}^{\mathrm{dil/non}}(0) \;=\; \frac{S_z^{\mathrm{A}}(0)}{\widetilde{S}_z^{\mathrm{A}}(0)} \;=\; -\,\frac{\rho_S}{\sigma_{SI}}\,R_{\mathrm{slow}} + \mathcal{O}(P_{\mathrm{A}}^2) \;=\; -\,\frac{\rho_S}{\sigma_{SI}}\,R_{\mathrm{slow}}\,. \tag{F.16b}$$

A third relation can be obtained from $\widehat{R}_{1,S}^{\mathrm{sel}}(0)$. To this end, we integrate Eq. (F.5) from $t = 0$ to $t = \infty$ and apply the initial conditions for S-selective excitation, $I_z(0) = 0$ and $S_z^{\mathrm{A}}(0) = P_{\mathrm{A}}$, to obtain

$$0 \;=\; P_{\mathrm{A}}\,\rho_I\,\widetilde{I}_z(0) \;+\; \sigma_{IS}\,\widetilde{S}_z^{\mathrm{A}}(0)\,, \tag{F.17a}$$

$$P_{\mathrm{A}} \;=\; P_{\mathrm{A}}\,\sigma_{SI}\,\widetilde{I}_z(0) \;+\; \rho_S\,\widetilde{S}_z^{\mathrm{A}}(0)\,. \tag{F.17b}$$

Eliminating $\widetilde{I}_z(0)$, we find

$$\widetilde{S}_z^{\mathrm{A}}(0) \;=\; P_{\mathrm{A}}\left(\rho_S - \frac{\sigma_{IS}\,\sigma_{SI}}{\rho_I}\right)^{-1}\,, \tag{F.18}$$

so that

$$\widehat{R}_{1,S}^{\mathrm{sel}}(0) \;=\; \frac{S_z^{\mathrm{A}}(0)}{\widetilde{S}_z^{\mathrm{A}}(0)} \;=\; \rho_S - \frac{\sigma_{IS}\,\sigma_{SI}}{\rho_I}\,. \tag{F.19}$$

The three expressions in Eqs. (F.16) and (F.19) must be identical with the dilute MN limit of the corresponding expressions in Eqs. (D.22) and (D.23), that is,

$$\widehat{R}_{1,I}^{\mathrm{dil}}(0) \;=\; \frac{2}{15}\,P_{\mathrm{A}}\,\omega_{\mathrm{D}}^2\,\tau_{\mathrm{A}}\,, \tag{F.20a}$$

$$\widehat{R}_{1,S}^{\mathrm{dil/non}}(0) \;=\; -\,\frac{2}{3}\,P_{\mathrm{A}}\,\omega_{\mathrm{D}}^2\,\tau_{\mathrm{A}}\,. \tag{F.20b}$$

$$\widehat{R}_{1,S}^{\mathrm{sel}}(0) \;=\; \frac{1}{3}\,\omega_{\mathrm{D}}^2\,\tau_{\mathrm{A}}\,. \tag{F.20c}$$

For the fourth relation, we choose the S-spin initial relaxation rate with nonselective excitation

$$R_{1,S}^{0,\mathrm{non}}(0) \;\equiv\; -\,\frac{1}{S_z^{\mathrm{A}}(0)}\,\frac{\mathrm{d}\,S_z^{\mathrm{A}}(t)}{\mathrm{d}t}\bigg|_{t=0} \;=\; \lim_{t\to 0}\,\mathcal{L}^{-1}\left[1-\frac{s\,\widetilde{S}_z^{\mathrm{A}}(s)}{S_z^{\mathrm{A}}(0)}\right]\,, \tag{F.21}$$

where $\mathcal{L}^{-1}$ denotes the inverse Laplace transform. The initial time derivative in Eq. (F.21) is obtained directly from Eq. (F.1c) and the nonselective initial condition (F.2),

$$\frac{\mathrm{d}\,S_z^{\mathrm{A}}(t)}{\mathrm{d}t}\bigg|_{t=0} \;=\; -\,\sigma_{SI}\,I_z^{\mathrm{A}}(0) \;-\; \rho_S\,S_z^{\mathrm{A}}(0) \;=\; -\,P_{\mathrm{A}}\,(\rho_S+\sigma_{SI})\,, \tag{F.22}$$

so that

$$R_{1,S}^{0,\mathrm{non}}(0) \;=\; \rho_S+\sigma_{SI}\,. \tag{F.23}$$

It remains to obtain an expression for $R_{1,S}^{0,\mathrm{non}}(0)$ from Appendix D. From the ZF result in Eq. (D.9c), we have for nonselective excitation ($\kappa = 1$) and in the dilute regime ($P_{\mathrm{A}} \ll 1$),

$$\frac{1}{P_{\mathrm{A}}\,\tau_{\mathrm{A}}}\,\widetilde{S}_z^{\mathrm{A}}(s) \;=\; \frac{g_{21}+(g_{21}+g_{22})\,x}{P_{\mathrm{A}}\,(1-g_{11})+x}\,, \tag{F.24}$$

where we have noted that $P_{\mathrm{A}}\,s\,\tau_{\mathrm{B}} = P_{\mathrm{B}}\,s\,\tau_{\mathrm{A}} \approx s\,\tau_{\mathrm{A}} \equiv x$ in the dilute regime. With g_{11}, g_{21} and g_{22} from Eqs. (D.18) – (D.20), we obtain

$$\frac{1}{P_{\mathrm{A}}\,\tau_{\mathrm{A}}}\,\widetilde{S}_z^{\mathrm{A}}(s) \;=\; \frac{U}{V}\,, \tag{F.25}$$

with

$$\begin{aligned} U \;\equiv\;& 81\,x^7+405\,x^6+18\,(45+4\,D^2)\,x^5+45\,(18+5\,D^2)\,x^4 \\ &+(405+243\,D^2+19\,D^4)\,x^3+(81+99\,D^2+26\,D^4)\,x^2 \\ &+\tfrac{1}{3}\,D^2\,(27+15\,D^2+4\,D^4)\,x+\tfrac{2}{3}\,D^4\,(D^2-3)\,, \end{aligned} \tag{F.26}$$

and

$$\begin{aligned} V \;\equiv\;& 81\,x^8+27\,(15+3\,P_{\mathrm{A}})\,x^7+18\,(45+7\,D^2+18\,P_{\mathrm{A}})\,x^6 \\ &+9\,[90+54\,P_{\mathrm{A}}+(49+14\,P_{\mathrm{A}})\,D^2)]\,x^5 \\ &+[405+324\,P_{\mathrm{A}}+(567+351\,P_{\mathrm{A}})\,D^2+49\,D^4)\,x^4 \\ &+[81\,(1+P_{\mathrm{A}})+(315+324\,P_{\mathrm{A}})\,D^2+49\,(2+P_{\mathrm{A}})\,D^4]\,x^3 \\ &+D^2\,[63+99\,P_{\mathrm{A}}+(59+75\,P_{\mathrm{A}})\,D^2+4\,D^4]\,x^2 \\ &+D^4\,[10+26\,P_{\mathrm{A}}+(2+4\,P_{\mathrm{A}})\,D^2]\,x+\tfrac{4}{3}\,P_{\mathrm{A}}\,D^6\,. \end{aligned} \tag{F.27}$$

The MN approximation is valid on time scales much longer than the correlation time, that is, for $t \gg \tau_{\mathrm{A}}$. We can therefore neglect the higher powers of $x = s\,\tau_{\mathrm{A}}$ in Eqs. (F.27) and (F.28). Specifically, we retain terms up x^2 in U and up to x^3 in V. Moreover, in each term, we only retain the leading power of D (since $D^2 \ll 1$ in the MN regime). We also implement the dilute regime approximation ($P_{\mathrm{A}} \ll 1$). We thus obtain

$$\frac{1}{P_{\mathrm{A}}\,\tau_{\mathrm{A}}}\,\widetilde{S}_z^{\mathrm{A}}(s) \;=\; \frac{81\,x^2+9\,D^2\,x-2\,D^4}{81\,x^3+63\,D^2\,x^2+10\,D^4\,x}\,, \tag{F.28}$$

and

$$F(s) \;\equiv\; 1 \;-\; \frac{s\,\widetilde{S}_z^{\mathrm{A}}(s)}{S_z^{\mathrm{A}}(0)} \;=\; \frac{6D^2(9\,x+2D^2)}{81\,x^2+63\,D^2\,x+10\,D^4} \;=\; \frac{\frac{2}{3}\,\omega_{\mathrm{D}}^2\,\tau_{\mathrm{A}}}{s+\frac{5}{9}\,\omega_{\mathrm{D}}^2\,\tau_{\mathrm{A}}}\,. \tag{F.29}$$

Combination of Eqs. (F.21) and (F.29) then yields

$$\begin{aligned} R_{1,S}^{0,\mathrm{non}}(0) \;&=\; \lim_{t\to 0}\,\mathcal{L}^{-1}F(s) \;=\; \frac{2}{3}\,\omega_{\mathrm{D}}^2\,\tau_{\mathrm{A}}\,\lim_{t\to 0}\,\mathcal{L}^{-1}\biggl[\frac{1}{s+\frac{5}{9}\,\omega_{\mathrm{D}}^2\,\tau_{\mathrm{A}}}\biggr] \\ &=\; \frac{2}{3}\,\omega_{\mathrm{D}}^2\,\tau_{\mathrm{A}}\,\lim_{t\to 0}\,\exp\bigl(-\tfrac{5}{9}\,\omega_{\mathrm{D}}^2\,t\bigr) \;=\; \frac{2}{3}\,\omega_{\mathrm{D}}^2\,\tau_{\mathrm{A}}\,. \end{aligned} \tag{F.30}$$

The four desired relations can now be obtained by identifying Eqs. (F.16) and (F.19) with Eq. (F.20) and Eq. (F.23) with Eq. (F.30). This yields

$$\rho_I - \frac{\sigma_{IS}\,\sigma_{SI}}{\rho_S} \;=\; \frac{2}{15}\,\omega_{\mathrm{D}}^2\,\tau_{\mathrm{A}}\,, \tag{F.31a}$$

$$\sigma_{IS} - \frac{\rho_I\,\rho_S}{\sigma_{SI}} \;=\; -\,\frac{2}{3}\,\omega_{\mathrm{D}}^2\,\tau_{\mathrm{A}}\,, \tag{F.31b}$$

$$\rho_S - \frac{\sigma_{IS}\,\sigma_{SI}}{\rho_I} \;=\; \frac{1}{3}\,\omega_{\mathrm{D}}^2\,\tau_{\mathrm{A}}\,, \tag{F.31c}$$

$$\rho_S + \sigma_{SI} \;=\; \frac{2}{3}\,\omega_{\mathrm{D}}^2\,\tau_{\mathrm{A}}\,. \tag{F.31d}$$

Solving for the four rates, we find

$$\rho_I \;=\; \frac{2}{9}\,\omega_{\mathrm{D}}^2\,\tau_{\mathrm{A}}\,, \tag{F.32a}$$

$$\rho_S \;=\; \frac{5}{9}\,\omega_{\mathrm{D}}^2\,\tau_{\mathrm{A}}\,, \tag{F.32b}$$

$$\sigma_{IS} \;=\; \frac{4}{9}\,\omega_{\mathrm{D}}^2\,\tau_{\mathrm{A}}\,, \tag{F.32c}$$

$$\sigma_{SI} \;=\; \frac{1}{9}\,\omega_{\mathrm{D}}^2\,\tau_{\mathrm{A}}\,. \tag{F.32d}$$

Inserting ρ_S and σ_{SI} into Eq. (F.15c), we finally obtain

$$S_z^{\mathrm{A}}(t) \;=\; P_{\mathrm{A}}\left[\frac{6}{5}\,\exp(-\rho_S\,t) \;-\; \frac{1}{5}\,\exp[-\widehat{R}_{1,I}^{\mathrm{dil}}(0)\,t]\right]\,, \tag{F.33}$$

with ρ_S given by Eq. (F.32b) and $\widehat{R}_{1,I}^{\mathrm{dil}}(0)$ by Eq. (F.20a).

References

[1] D. M. Brink and G. R. Satchler, *Angular Momentum*, 3rd ed. (Clarendon Press, Oxford, 1994).

[2] Z. Chang and B. Halle, J. Chem. Phys. **139**, 144203 (2013).

[3] A. Abragam, *The Principles of Nuclear Magnetism* (Clarendon Press, Oxford, 1961).

[4] Z. Chang and B. Halle, J. Chem. Phys. **143**, 234201 (2015).

[5] N. C. Pyper, Molec. Phys. **21**, 1 (1971).

[6] S. Szymanski, A. M. Gryff-Keller and G. Binsch, J. Magn. Reson. **68**, 399 (1986).

[7] L. G. Werbelow and D. M. Grant, Advan. Magn. Reson. **9**, 189 (1977).

[8] I. Solomon, Phys. Rev. **99**, 559 (1955).

Paper III

THE JOURNAL OF CHEMICAL PHYSICS **145**, 034202 (2016)

Nuclear magnetic relaxation by the dipolar EMOR mechanism: Three-spin systems

Zhiwei Chang and Bertil Halle[a)]
Division of Biophysical Chemistry, Department of Chemistry, Lund University, P.O. Box 124, SE-22100 Lund, Sweden

(Received 29 February 2016; accepted 24 June 2016; published online 18 July 2016)

In aqueous systems with immobilized macromolecules, including biological tissue, the longitudinal spin relaxation of water protons is primarily induced by exchange-mediated orientational randomization (EMOR) of intra- and intermolecular magnetic dipole-dipole couplings. Starting from the stochastic Liouville equation, we have developed a non-perturbative theory that can describe relaxation by the dipolar EMOR mechanism over the full range of exchange rates, dipole couplings, and Larmor frequencies. Here, we implement the general dipolar EMOR theory for a macromolecule-bound three-spin system, where one, two, or all three spins exchange with the bulk solution phase. In contrast to the previously studied two-spin system with a single dipole coupling, there are now three dipole couplings, so relaxation is affected by distinct correlations as well as by self-correlations. Moreover, relaxation can now couple the magnetizations with three-spin modes and, in the presence of a static dipole coupling, with two-spin modes. As a result of this complexity, three secondary dispersion steps with different physical origins can appear in the longitudinal relaxation dispersion profile, in addition to the primary dispersion step at the Larmor frequency matching the exchange rate. Furthermore, and in contrast to the two-spin system, longitudinal relaxation can be significantly affected by chemical shifts and by the odd-valued ("imaginary") part of the spectral density function. We anticipate that the detailed studies of two-spin and three-spin systems that have now been completed will provide the foundation for developing an approximate multi-spin dipolar EMOR theory sufficiently accurate and computationally efficient to allow quantitative molecular-level interpretation of frequency-dependent water-proton longitudinal relaxation data from biophysical model systems and soft biological tissue. [http://dx.doi.org/10.1063/1.4955423]

I. INTRODUCTION

For many years, the absence of a rigorous molecular theory of nuclear magnetic relaxation induced by magnetic dipole couplings in aqueous systems with immobilized macromolecules has prevented a reliable quantitative analysis of water-proton NMR (or MRI) relaxation data in terms of structure and dynamics of soft biological tissue or biophysical model systems, such as cross-linked protein gels. In such systems, protons exchange on a wide range of time scales between the bulk aqueous solution phase and the locally anisotropic macromolecular sites. This exchange affects proton relaxation by transferring magnetizations and coherences between the two environments. In addition, by randomizing the orientation of internuclear vectors, the exchange is also the motion that induces spin relaxation in the macromolecular sites. For this relaxation mechanism, known as exchange-mediated orientational randomization (EMOR), the motional-narrowing regime coincides with the fast-exchange regime. The conventional Bloch-Wangsness-Redfield (BWR) perturbation theory of nuclear spin relaxation[1] therefore breaks down when, as is frequently the case, fast-exchange conditions do not prevail. Starting from the stochastic Liouville equation (SLE),[2,3] we have therefore developed a non-perturbative theory of relaxation induced by EMOR modulation of magnetic dipole-dipole couplings, valid without restrictions on exchange rate, dipole couplings, and Larmor frequencies.[4,5]

In the dipolar EMOR theory, we consider a system of $m_A \geq 2$ mutually dipole-coupled spin-1/2 nuclei in the anisotropic (A) sites. This spin system comprises m_B labile spins, which exchange with the isotropic bulk (B) phase, and $m_A - m_B$ nonlabile spins, which reside permanently in the A site. We distinguish two scenarios: symmetric exchange ($m_B = m_A$), where the spin system exchanges as an intact unit, and asymmetric exchange ($m_B < m_A$), where the spin system is fragmented by exchange. In asymmetric exchange, all multi-spin correlations that have developed as a result of dipole couplings between labile and nonlabile spins in the A site are lost,[5,6] leading to a qualitatively different relaxation behavior as compared to symmetric exchange. To identify different exchange cases, we use the notation "(spins in state A)–(spins in state B)." In previous reports in this series of papers, we have examined the symmetric case *IS–IS* (Paper I[4]) and the asymmetric case *IS–I* (Paper II[5]).

a)bertil.halle@bpc.lu.se

Here, we implement the general dipolar EMOR theory, presented in Paper II, for a three-spin system, examining the symmetric exchange case *ISP–ISP* and the asymmetric cases *ISP–IS* and *ISP–I*. The exchanging entity in these cases might be a hydronium ion binding to a specific site in a protein (*ISP–ISP*), a water molecule temporarily occupying an internal cavity in the protein (*ISP–IS*), or a labile hydroxyl proton in an amino acid side-chain (*ISP–I*). As compared to the previously analyzed two-spin system, several new features emerge for the three-spin system. Because there are now three dipole couplings rather than one, relaxation is affected by distinct correlations (as well as self-correlations) and the magnetizations are dynamically coupled to two-spin and three-spin modes. Furthermore, in the *ISP–I* case, one of the three dipole couplings is static. As a result of these complications, three secondary dispersion steps (some of them inverted) with different physical origins can appear, under different conditions, in the longitudinal relaxation dispersion profile, in addition to the primary dispersion step where the Larmor frequency matches the exchange rate. Furthermore, and in contrast to the two-spin system, the longitudinal relaxation can be significantly affected by chemical shifts and by the odd-valued ("imaginary") part of the spectral density function.[7]

The outline of this paper is as follows. In Sec. II, we develop the general dipolar EMOR theory for a three-spin system. Once the matrix elements of the Zeeman and dipolar Liouvillians in the 63-dimensional three-spin Liouville space have been calculated, it is straightforward to implement the general dipolar EMOR theory of Paper II. In Sec. III, we develop a limiting form of the dipolar EMOR theory, based on the BWR master equation, and valid in the motional-narrowing regime. The semi-analytical results obtained here are used to rationalize the rich variety of relaxation behavior exhibited by the three-spin system. In Sec. IV, we illustrate the theory developed in Secs. II and III by numerical results, emphasizing the new features that emerge at the three-spin level. Lengthy derivations and tables are relegated to eight appendices.[8]

II. GENERAL RESULTS

A. System, model, and solution

We consider a system of three mutually dipole-coupled spin-1/2 nuclei, denoted I, S, and P, some or all of which exchange between a solid-like anisotropic (A) state and a liquid-like bulk (B) state. The spins may be homonuclear or heteronuclear and the chemical shifts may differ between states A and B. State A comprises an isotropic distribution of sites, labelled $\alpha = 1, 2, \ldots$, each of which has a fixed orientation. At any time, a fraction P_A of the labile spins reside in state A, while a fraction $P_\mathrm{B} = 1 - P_\mathrm{A}$ reside in state B. In most applications of interest,[9–11] $P_\mathrm{A} \ll 1$, a condition that we refer to as the dilute regime. We consider three exchange cases.

In the symmetric case, denoted *ISP–ISP*, the three spins exchange as an intact unit, for example, the three protons in a hydronium ion, H_3O^+, or in an acetate ion, CH_3COO^-.

In the asymmetric *ISP–I* case, the labile spin I exchanges with state B, whereas the nonlabile spins S and P remain in state A so their mutual dipole coupling is static. An example of this case is a serine side-chain, with spin I identified as the labile hydroxyl proton and spins S and P identified as the adjacent nonlabile methylene protons.

In the asymmetric *ISP–IS* case, the labile spins I and S exchange as a unit, leaving the nonlabile spin P (without any dipole couplings) in state A. An example of this case is an internal water molecule, where, in the A sites, the two water protons I and S are also dipole-coupled to a nonlabile protein proton P.

In the EMOR model, the orientations of all internuclear vectors involving at least one labile spin are instantaneously randomized upon exchange, thereby inducing dipolar relaxation. This assumption is justified if the mean survival time of the labile spin(s) in the A sites is long compared to the time required for orientational randomization when the labile spin(s) has been transferred to state B. We can then ignore all dipole couplings among the labile spins in state B. If so desired, the small and frequency-independent relaxation contribution from fast modulation of dipole couplings in state B can be added to the final expression for the overall relaxation rate, as described in Paper I.

The Zeeman Hamiltonian in state A is

$$\begin{aligned} H_\mathrm{Z}^\mathrm{A} &= \omega_I^\mathrm{A} I_z + \omega_S^\mathrm{A} S_z + \omega_P^\mathrm{A} P_z \\ &= \omega_I^\mathrm{A} \left[I_z + (1 + \delta_S^\mathrm{A}) S_z + (1 + \delta_P^\mathrm{A}) P_z \right], \end{aligned} \tag{1}$$

and similarly for state B. The "chemical shifts" are defined with reference to spin I so $\delta_I^\mathrm{A} \equiv 0$ and $\delta_X^\mathrm{A} \equiv (\omega_X^\mathrm{A} - \omega_I^\mathrm{A})/\omega_I^\mathrm{A}$ for $X = S$ or P. As noted in Paper I, scalar couplings among non-isochronous spins in state A are neglected here because they are invariably much smaller than the corresponding dipole couplings. For the *ISP–ISP* and *ISP–IS* cases, scalar couplings among non-isochronous spins in state B would affect the relaxation behavior, but, for the applications that we have in mind (see above), molecular symmetry ensures that the proton spins are isochronous in state B.

The dipolar Hamiltonian for A-site α is

$$H_\mathrm{D}^\alpha = H_{\mathrm{D},IS}^\alpha + H_{\mathrm{D},IP}^\alpha + H_{\mathrm{D},SP}^\alpha, \tag{2}$$

with (X denotes either of the three spin pairs IS, IP, or SP)

$$H_{\mathrm{D},X}^\alpha = -\frac{2}{\sqrt{3}}\, \omega_{\mathrm{D},X} \sum_{M=-2}^{2} T_M^2(X)\, D_{M0}^{2\,*}(\Omega_X^\alpha). \tag{3}$$

Here, $T_M^2(X)$ are orthonormal three-spin irreducible spherical tensor operators (see below), $D_{M0}^2(\Omega_X^\alpha)$ are rank-2 Wigner functions,[12] and Ω_X^α are the Euler angles that specify the orientation of the internuclear vector $\boldsymbol{r}_X$ in site α with respect to the lab-fixed frame.

Rather than using the three sets of Euler angles Ω_X^α, it is more convenient to specify the internuclear geometry by the three interior angles β_I, β_S, and β_P of the *ISP* triangle (Fig. 1) and then specify the orientation of this triangle with respect to the lab-fixed frame by the Euler angles $\Omega^\alpha \equiv (\psi^\alpha, \vartheta^\alpha, \varphi^\alpha)$. We adopt the following convention: ψ^α is the angle of rotation of the vector $\boldsymbol{r}_{IS}^\alpha$ about the lab-fixed z_L axis (parallel to the $\boldsymbol{B}_0$ field), ϑ^α is the angle between the positive z_L axis and $\boldsymbol{r}_{IS}^\alpha$, and φ^α is the angle of rotation of the triangle plane about the

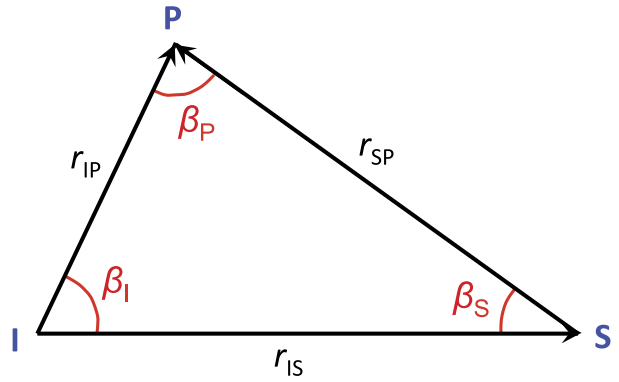

FIG. 1. Internuclear geometry of the three-spin system.

vector $\boldsymbol{r}^{\alpha}_{IS}$. Then

$$D^{2\,*}_{M0}(\Omega^{\alpha}_{IS}) = \exp(iM\psi^{\alpha})\, d^{2}_{M0}(\vartheta^{\alpha}), \tag{4a}$$

$$D^{2\,*}_{M0}(\Omega^{\alpha}_{IP}) = \exp(iM\psi^{\alpha}) \sum_{N=-2}^{2} d^{2}_{MN}(\vartheta^{\alpha}) \times \exp(iN\varphi^{\alpha})\, d^{2}_{N0}(\beta_I), \tag{4b}$$

$$D^{2\,*}_{M0}(\Omega^{\alpha}_{SP}) = \exp(iM\psi^{\alpha}) \sum_{N=-2}^{2} (-1)^{N} d^{2}_{MN}(\vartheta^{\alpha}) \times \exp(iN\varphi^{\alpha})\, d^{2}_{N0}(\beta_S). \tag{4c}$$

The internuclear geometry, which is the same in all sites α, is fully determined by specifying two of the three interior angles (which sum up to 180°) and one of the three dipole coupling frequencies $\omega_{\mathrm{D},IS}$, $\omega_{\mathrm{D},IP}$, and $\omega_{\mathrm{D},SP}$ (which depend on the internuclear separations r_X). If we specify

$$\omega_{\mathrm{D},IS} \equiv \frac{3}{2}\left(\frac{\mu_0}{4\pi}\right)\frac{\gamma_I\,\gamma_S\,\hbar}{r^3_{IS}}, \tag{5}$$

then the remaining two dipole couplings are given by

$$\omega_{\mathrm{D},IP} = \left[\frac{\sin(\beta_I+\beta_S)}{\sin\beta_S}\right]^3 \omega_{\mathrm{D},IS}, \tag{6a}$$

$$\omega_{\mathrm{D},SP} = \left[\frac{\sin(\beta_I+\beta_S)}{\sin\beta_I}\right]^3 \omega_{\mathrm{D},IS}. \tag{6b}$$

In the general case of a non-degenerate triangle ($\beta_I \neq \beta_S \neq \beta_P$), the three dipole couplings are all different. In the special case of an isosceles triangle with $\beta_I = \beta_S$ (so spin P is at the apex), Eq. (6) reduces to $\omega_{\mathrm{D},IP} = \omega_{\mathrm{D},SP} = 8\sin^3(\beta_P/2)\omega_{\mathrm{D},IS}$. For an equilateral triangle ($\beta_I = \beta_S = \beta_P = 60°$), of course, all three dipole couplings are equal.

The composite spin density operator $\sigma(t)$ evolves according to the stochastic Liouville equation (SLE)[2,3,5]

$$\frac{\mathrm{d}}{\mathrm{d}t}\,\sigma(t) = (\mathcal{W} - i\,\mathcal{L})\,\sigma(t), \tag{7}$$

where the Liouvillian $\mathcal{L} \equiv [H,\ldots]$ is the derivation superoperator corresponding to the Hamiltonian in each site: H^{B}_{Z} in state B and $H^{\mathrm{A}}_{Z} + H^{\alpha}_{\mathrm{D}}$ in A-site α. The exchange superoperator $\mathcal{W}$ describes the transfer of labile spins from state B to A-site α or vice versa (direct exchange between A-sites is not allowed in the EMOR model[5]) and the consequent instantaneous switching of the spin Hamiltonian. For the asymmetric cases *ISP–I* and *ISP–IS*, the spin system is fragmented by the exchange. Consequently, all multi-spin correlations that have developed as a result of dipole couplings between labile and nonlabile spins in state A are lost.[5,6] To describe both of these effects, we decompose the exchange superoperator as[5]

$$\mathcal{W} = \mathcal{T}_{\mathrm{m}} \otimes \mathcal{T}_{\mathrm{s}} - \mathcal{K}_{\mathrm{m}} \otimes \mathcal{K}_{\mathrm{s}}. \tag{8}$$

The "molecular" operators $\mathcal{T}_{\mathrm{m}}$ and $\mathcal{K}_{\mathrm{m}}$ act on the site kets $|\alpha\rangle$, so their composite-space supermatrix representations are block-diagonal with respect to the spin operators. These operators define the kinetic model (site-to-site transition probabilities), regardless of whether the spin system is fragmented or not. The superoperators $\mathcal{T}_{\mathrm{s}}$ and $\mathcal{K}_{\mathrm{s}}$ act on spin operators, so (as for $\mathcal{L}$) their composite-space supermatrix representations are block-diagonal in the site basis. These superoperators distinguish labile from nonlabile spins and they account for decorrelation of multi-spin modes by exchange fragmentation of the spin system.[5,6]

Macroscopic spin observables are related to a density operator summed over all sites,

$$\langle\sigma(t)\rangle \equiv \sum_{\alpha=0}^{N}\sigma^{\alpha}(t) = \sigma^{\mathrm{B}}(t) + \sigma^{\mathrm{A}}(t), \tag{9}$$

with the initial value

$$\langle\sigma(0)\rangle = P_{\mathrm{B}}\,\eta^{\mathrm{B}} + P_{\mathrm{A}}\,\eta^{\mathrm{A}}. \tag{10}$$

The operators η^{A} and η^{B}, which act in spin Liouville space, depend on the initial condition of the spin system (selective or nonselective excitation) and, for heteronuclear spin systems, on the relative magnetogyric ratios.

The Laplace-transformed density operator $\langle\widetilde{\sigma}(s)\rangle$, represented in spin Liouville space as a partitioned column vector, can be computed from the (exact) supermatrix equation[5]

$$\begin{bmatrix}\widetilde{\boldsymbol{\sigma}}^{\mathrm{B}}(s)\\ \widetilde{\boldsymbol{\sigma}}^{\mathrm{A}}(s)\end{bmatrix} = \begin{bmatrix}\widetilde{\mathbf{U}}^{\mathrm{BB}}(s) & \widetilde{\mathbf{U}}^{\mathrm{BA}}(s)\\ \widetilde{\mathbf{U}}^{\mathrm{AB}}(s) & \widetilde{\mathbf{U}}^{\mathrm{AA}}(s)\end{bmatrix}\begin{bmatrix}\boldsymbol{\eta}^{\mathrm{B}}\\ \boldsymbol{\eta}^{\mathrm{A}}\end{bmatrix}, \tag{11}$$

with the Laplace-transformed site-averaged resolvent matrices given by[5]

$$\widetilde{\mathbf{U}}^{\mathrm{BB}}(s) = \tau_{\mathrm{B}}\,P_{\mathrm{B}}\big[\mathbf{G}^{\mathrm{B}}(s)^{-1} - \mathbf{T}\,\mathbf{G}^{\mathrm{A}}(s)\,\mathbf{T}'\big]^{-1}, \tag{12a}$$

$$\widetilde{\mathbf{U}}^{\mathrm{AA}}(s) = \tau_{\mathrm{A}}\,P_{\mathrm{A}}\big[\mathbf{G}^{\mathrm{A}}(s)^{-1} - \mathbf{T}'\,\mathbf{G}^{\mathrm{B}}(s)\,\mathbf{T}\big]^{-1}, \tag{12b}$$

$$\widetilde{\mathbf{U}}^{\mathrm{BA}}(s) = \frac{P_{\mathrm{A}}}{P_{\mathrm{B}}}\,\widetilde{\mathbf{U}}^{\mathrm{BB}}(s)\,\mathbf{T}\,\mathbf{G}^{\mathrm{A}}(s), \tag{12c}$$

$$\widetilde{\mathbf{U}}^{\mathrm{AB}}(s) = \frac{P_{\mathrm{B}}}{P_{\mathrm{A}}}\,\widetilde{\mathbf{U}}^{\mathrm{AA}}(s)\,\mathbf{T}'\,\mathbf{G}^{\mathrm{B}}(s). \tag{12d}$$

Here, τ_{A} and τ_{B} are the mean survival times in the two states, related by the detailed balance condition $P_{\mathrm{A}}\,\tau_{\mathrm{B}} = P_{\mathrm{B}}\,\tau_{\mathrm{A}}$. The dimensions of the spin Liouville subspaces, excluding the physically irrelevant identity operator, are for state A $D_{\mathrm{A}} = 63$ and for state B $D_{\mathrm{B}} = 3$ (*ISP–I* case), $D_{\mathrm{B}} = 15$ (*ISP–IS*), or $D_{\mathrm{B}} = 63$ (*ISP–ISP*). In Eq. (12), we have also introduced the supermatrices

$$\mathbf{G}^{\mathrm{B}}(s) \equiv \big[(1+s\tau_{\mathrm{B}})\,\mathbf{1}^{\mathrm{B}} + i\,\mathbf{L}^{\mathrm{B}}_{Z}\,\tau_{\mathrm{B}}\big]^{-1} \tag{13}$$

and

$$\mathbf{G}^{\mathrm{A}}(s) \equiv \big\langle[s\,\tau_{\mathrm{A}}\,\mathbf{1}^{\mathrm{A}} + \mathbf{K} + i\,\mathbf{L}^{\mathrm{A}}_{Z}\,\tau_{\mathrm{A}} + i\,\mathbf{L}_{\mathrm{D}}(\Omega)\,\tau_{\mathrm{A}}]^{-1}\big\rangle, \tag{14}$$

where $\mathbf{L}_Z$ and $\mathbf{L}_D(\Omega)$ are the Liouvillian supermatrices corresponding to the Zeeman and dipolar Hamiltonians, respectively, and the angular brackets indicate an isotropic orientational average.

To make full use of symmetry, we represent spin Liouville space in a basis of irreducible spherical tensor operators (ISTOs) $B_n \equiv T_Q^K(\lambda)$ of rank K, quantum order Q, and additional quantum numbers λ.[12] The explicit form of the ISTOs in the three bases (of dimension 3, 15 and 63) used here is given in Appendix A of the supplementary material.[8] All of these operators are normalized in three-spin Liouville space. Explicit expressions for the elements of the Zeeman and dipolar Liouvillian supermatrices $\mathbf{L}_Z$ and $\mathbf{L}_D$ are derived in Appendices B and C,[8] respectively.

In Eqs. (12) and (14), $\mathbf{T}$ and $\mathbf{K}$ are the supermatrix representations of the spin superoperators $\mathcal{T}_s$ and $\mathcal{K}_s$ in Eq. (8). For the symmetric *ISP–ISP* case, all spins are labile so there is no exchange fragmentation. Consequently, $\mathbf{T} = \mathbf{K} = \mathbf{1}$, the 63×63 identity matrix.

For the asymmetric *ISP–I* case, exchange interconverts the three one-spin modes in state B, $n_B = 1$, 2, and 3 (Table S3) and the corresponding three one-spin modes in state A, $p_A = 1$, 20, and 35 (Table S1).[8] Consequently,

$$T_{n_B p_A} = \delta_{n_B,1}\,\delta_{p_A,1} + \delta_{n_B,2}\,\delta_{p_A,20} + \delta_{n_B,3}\,\delta_{p_A,35}. \quad (15)$$

Identifying the 15 one- and two-spin modes in state A that do not involve the labile I spin (Table S1),[8] we obtain

$$\begin{aligned} K_{n_A p_A} = \delta_{n_A p_A}[1 &- \delta_{n_A,2} - \delta_{n_A,3} - \delta_{n_A,13} - \delta_{n_A,16} \\ &- \delta_{n_A,19} - \delta_{n_A,21} - \delta_{n_A,22} \\ &- \delta_{n_A,31} - \delta_{n_A,34} - \delta_{n_A,36} - \delta_{n_A,37} - \delta_{n_A,46} \\ &- \delta_{n_A,49} - \delta_{n_A,55} - \delta_{n_A,61}]. \end{aligned} \quad (16)$$

For the asymmetric *ISP–IS* case, exchange interconverts the 15 modes in state B (Table S2) and the corresponding one- and two-spin modes in state A (Table S1).[8] Consequently,

$$\begin{aligned} T_{n_B p_A} = {} & \delta_{n_B,1}\,\delta_{p_A,1} + \delta_{n_B,2}\,\delta_{p_A,2} + \delta_{n_B,3}\,\delta_{p_A,11} + \delta_{n_B,4}\,\delta_{p_A,17} + \delta_{n_B,5}\,\delta_{p_A,14} \\ & + \delta_{n_B,6}\,\delta_{p_A,20} + \delta_{n_B,7}\,\delta_{p_A,21} + \delta_{n_B,8}\,\delta_{p_A,29} + \delta_{n_B,9}\,\delta_{p_A,32} + \delta_{n_B,10}\,\delta_{p_A,35} \\ & + \delta_{n_B,11}\,\delta_{p_A,36} + \delta_{n_B,12}\,\delta_{p_A,44} + \delta_{n_B,13}\,\delta_{p_A,47} + \delta_{n_B,14}\,\delta_{p_A,53} + \delta_{n_B,15}\,\delta_{p_A,59}. \end{aligned} \quad (17)$$

The three one-spin modes in state A that do not involve either of the labile spins I and S are $n_A = 3$, 22, and 37 (Table S1),[8] so

$$K_{n_A p_A} = \delta_{n_A p_A}[1 - \delta_{n_A,3} - \delta_{n_A,22} - \delta_{n_A,37}]. \quad (18)$$

The angular brackets in Eq. (14) signify an average over the isotropic distribution of site orientations, $f(\Omega) = 1/(8\pi^2)$. Because $\mathbf{G}^A$ is isotropically averaged, it must reflect the axial symmetry in spin Liouville space, imposed by the external magnetic field. For a basis of ISTOs $T_Q^K(\lambda)$, it then follows from the Wigner-Eckart theorem[12] that $\mathbf{G}^A$ and the resolvent matrices in Eq. (12) are block-diagonal in the projection index Q. Longitudinal relaxation can therefore be fully described within the 19-dimensional zero-quantum subspace. However, this does not mean that the zero-quantum modes evolve independently of the remaining modes. The matrix within square brackets in Eq. (14) is not block-diagonal in Q, so it must be evaluated in the full 63-dimensional spin Liouville basis of state A. The matrix elements of $\mathbf{L}_Z$ and $\mathbf{L}_D(\Omega)$ in this basis are given in Appendices B and C,[8] respectively.

B. Integral relaxation rate

The integral longitudinal relaxation rate (ILRR) is defined as the inverse of the time integral of the observed longitudinal magnetization, normalized by its initial value.[4] The ILRR may be expressed in terms of spin density operator components as[5]

$$\widehat{R}_1 = \frac{P_B \sum'_{n_B} \eta^B_{n_B} + P_A \sum'_{n_A} \eta^A_{n_A}}{\sum_{p_B}\left[\sum'_{n_B} U^{BB}_{n_B p_B} + \sum'_{n_A} U^{AB}_{n_A p_B}\right]\eta^B_{p_B} + \sum_{p_A}\left[\sum'_{n_B} U^{BA}_{n_B p_A} + \sum'_{n_A} U^{AA}_{n_A p_A}\right]\eta^A_{p_A}}, \quad (19)$$

where we have made use of Eqs. (10) and (11) and introduced the shorthand notation $U^{XY}_{np} \equiv (n|\widetilde{\mathbf{U}}^{XY}(0)|p)$. The primed sums in Eq. (19) run over spin modes (or basis operators) corresponding to the longitudinal magnetization of the observed spin(s). In the following, we specify the observed spin(s) by a subscript, e.g., $\widehat{R}_{1,IS}$.

The elements of the vectors $\boldsymbol{\eta}^B$ and $\boldsymbol{\eta}^A$ depend on the initial conditions for the relaxation experiment. For nonselective excitation, which always applies to field-cycling experiments,

$$\eta^A_n = \delta_{n,1} + \kappa_S\,\delta_{n,2} + \kappa_P\,\delta_{n,3}, \quad (20a)$$

$$\eta^B_n = \begin{cases} \delta_{n,1} & (ISP\text{–}I), \\ \delta_{n,1} + \kappa_S\,\delta_{n,2} & (ISP\text{–}IS), \\ \delta_{n,1} + \kappa_S\,\delta_{n,2} + \kappa_P\,\delta_{n,3} & (ISP\text{–}ISP). \end{cases} \quad (20b)$$

Here, the relative magnetogyric ratios $\kappa_S \equiv \gamma_S/\gamma_I$ and $\kappa_P \equiv \gamma_P/\gamma_I$ account for the relative magnitude and sign

of the equilibrium spin density operator components in the high-temperature approximation.[1] For selective excitation of the labile spin(s), $\eta_n^{\rm A} = \eta_n^{\rm B}$ with $\eta_n^{\rm B}$ as in Eq. (20b). These two initial conditions will be indicated by a superscript, e.g., $\widehat{R}_{1,I}^{\rm non}$ and $\widehat{R}_{1,IS}^{\rm sel}$. Explicit expressions for the ILRR, based on Eq. (19), are given in Appendix D[8] for the various combinations of excited, observed, and labile spin(s).

In the dilute regime, where $P_{\rm A} \ll 1$, all matrix elements in the denominator of Eq. (19) except $U^{\rm BB}_{n_{\rm B}p_{\rm B}}$ can be neglected if the observed magnetization includes at least one labile spin. Furthermore, in the numerator, the second term (proportional to $P_{\rm A}$) can then be neglected. The ILRR is then the same for nonselective excitation as for selective excitation of the labile spin(s). We therefore use the superscript "dil" without specifying the excitation mode. For the ISP–I case, we obtain

$$\widehat{R}_{1,I}^{\rm dil} = \widehat{R}_{1,IS}^{\rm dil} = \widehat{R}_{1,ISP}^{\rm dil} = [U_{11}^{\rm BB}]^{-1}. \tag{21}$$

Similarly, for the ISP–IS case,

$$\widehat{R}_{1,I}^{\rm dil} = [U_{11}^{\rm BB} + \kappa_S\, U_{12}^{\rm BB}]^{-1}, \tag{22a}$$

$$\widehat{R}_{1,IS}^{\rm dil} = \widehat{R}_{1,ISP}^{\rm dil} = (1+\kappa_S) \times [U_{11}^{\rm BB} + U_{21}^{\rm BB} + \kappa_S\,(U_{12}^{\rm BB} + U_{22}^{\rm BB})]^{-1}, \tag{22b}$$

and for the ISP–ISP case,

$$\widehat{R}_{1,I}^{\rm dil} = [U_{11}^{\rm BB} + \kappa_S\, U_{12}^{\rm BB} + \kappa_P\, U_{13}^{\rm BB}]^{-1}, \tag{23a}$$

$$\widehat{R}_{1,IS}^{\rm dil} = (1+\kappa_S)\,[U_{11}^{\rm BB} + U_{21}^{\rm BB} + \kappa_S\,(U_{12}^{\rm BB} + U_{22}^{\rm BB}) + \kappa_P\,(U_{13}^{\rm BB} + U_{23}^{\rm BB})]^{-1}, \tag{23b}$$

$$\widehat{R}_{1,ISP}^{\rm dil} = (1+\kappa_S+\kappa_P)\,[U_{11}^{\rm BB} + U_{21}^{\rm BB} + U_{31}^{\rm BB} + \kappa_S\,(U_{12}^{\rm BB} + U_{22}^{\rm BB} + U_{32}^{\rm BB}) + \kappa_P\,(U_{13}^{\rm BB} + U_{23}^{\rm BB} + U_{33}^{\rm BB})]^{-1}. \tag{23c}$$

According to Eq. (12a), $U_{np}^{\rm BB} \propto 1/P_{\rm A}$ in the dilute regime. It then follows from Eqs. (21)–(23) that the ILRR is strictly proportional to $P_{\rm A}$. For the ISP–I case, the 3×3 matrix $\mathbf{U}^{\rm BB}(0)$ is diagonal and, as shown in Appendix D,[8] Eq. (21) yields

$$\widehat{R}_{1,I}^{\rm dil} = \widehat{R}_{1,IS}^{\rm dil} = \widehat{R}_{1,ISP}^{\rm dil} = \frac{P_{\rm A}}{\tau_{\rm A}}\,(1 - g_{11}), \tag{24}$$

with the shorthand notation $g_{np} \equiv (n|\mathbf{G}^{\rm A}(0)|p)$. This result is of the same form as for the asymmetric two-spin case IS–I considered in Paper II.

C. Nuclear permutation symmetry

In the EMOR model, all labile spins are affected in the same way by the relaxation-inducing dynamics, since all dipole couplings involving labile spins are completely randomized in orientation by the exchange. The symmetry of the ILRR under nuclear permutation is therefore determined solely by the internuclear geometry, that is, the lengths of the internuclear vectors and the angles between them (Fig. 1). Consequently, the ILRR is invariant under any permutation of the observed labile spins. This is generally true for the dipolar EMOR model, even for non-dilute conditions and for multi-spin systems. For the three-spin system considered here, $\widehat{R}_{1,ISP}(ISP\text{–}ISP)$ is invariant under any permutation of the three spins I, S, and P, whereas $\widehat{R}_{1,IS}(ISP\text{–}ISP)$ and $\widehat{R}_{1,IS}(ISP\text{–}IS)$ are invariant under $I \leftrightarrow S$ interchange.

III. MOTIONAL-NARROWING REGIME

The results of Sec. II allow us to calculate the ILRR $\widehat{R}_1$ for any combination of excited, observed, and labile spin(s). With modest effort, we can compute the complete relaxation dispersion profile $\widehat{R}_1(\omega_0)$ for arbitrary values of the mean survival time $\tau_{\rm A}$, dipole coupling constant $\omega_{{\rm D},IS}$, internuclear geometry β_I and β_S, and chemical shifts in the A and B states. The main virtues of the SLE-based approach are its generality and computational efficiency, but it does not necessarily provide an understanding of the physical basis of the computed relaxation behavior. In this section, we shall therefore obtain the ILRR by a different approach, based on the semi-classical BWR perturbation theory.[1] Although restricted to the motional-narrowing (MN) regime, where $\omega_{\rm D}\,\tau_{\rm A} \ll 1$, the BWR approach is more physically transparent. (As discussed in Appendix E,[8] we assume that all three dipole couplings satisfy this inequality, including the static SP coupling in the ISP–I case.) In addition, the requirement that the SLE- and BWR-based results coincide in the MN regime provides a valuable check.

In the MN regime, the composite spin density operator evolves according to the "stochastic Redfield equation" (SRE)

$$\frac{\rm d}{{\rm d}t}\,\sigma(t) = [\mathcal{W} - i\,\mathcal{L}_{\rm Z} - i\,\Delta - \mathcal{R}]\,\sigma(t), \tag{25}$$

where $\mathcal{W}$ is the same exchange superoperator (8) as in the SLE (7), $\mathcal{L}_{\rm Z}$ is the Zeeman Liouvillian, and $\mathcal{R}$ is the relaxation superoperator prescribed by BWR theory.[1] The superoperator $\Delta \equiv \mathcal{L}_{{\rm D},SP}$ is associated with the time-independent dipolar coupling between spins S and P in the ISP–I case. For the other two exchange cases, this term is absent. For the EMOR model, the SRE (25) can be solved in site space in the same manner as the SLE (7).[5] Specifically, Eqs. (11) and (12) remain valid, but Eq. (14) is replaced by

$$\mathbf{G}^{\mathrm{A}}(s) = \left\langle [s\,\tau_{\mathrm{A}}\,\mathbf{1}^{\mathrm{A}} + \mathbf{K} + i\,\mathbf{L}_{\mathrm{Z}}^{\mathrm{A}}\,\tau_{\mathrm{A}} + i\,\boldsymbol{\Delta}^{\alpha}\,\tau_{\mathrm{A}} + \mathbf{R}^{\alpha}\,\tau_{\mathrm{A}}]^{-1} \right\rangle, \tag{26}$$

where $\mathbf{R}^{\alpha}$ is the orientation-dependent relaxation supermatrix for site α (Appendix E[8]).

We use the same notation as in Paper II for relaxation supermatrix elements between basis operators that involve a single spin. For example, $R_{z+}^{IP} = (1\,|\mathbf{R}^{\alpha}|\,22) = -2^{-3/2}\,(I_z\,|\mathbf{R}^{\alpha}|\,P_+)$, with the basis operators numbered as in Table S1.[8] These local relaxation rates are of four kinds. First, there are longitudinal (R_{zz}^{II}, R_{zz}^{SS} and R_{zz}^{PP}) and transverse ($R_{\pm\pm}^{II}$, $R_{\pm\pm}^{SS}$ and $R_{\pm\pm}^{PP}$) auto-spin auto-mode rates. Second, there are longitudinal (e.g., R_{zz}^{IS} and R_{zz}^{SP}) and transverse (e.g., $R_{\pm\pm}^{IS}$ and $R_{\pm\pm}^{SP}$) cross-spin auto-mode rates. Third, there are the auto-spin cross-mode rates $R_{z\pm}^{II}$, $R_{\pm z}^{II}$, and $R_{\pm\mp}^{II}$, and the corresponding rates for spin S and spin P. Finally, there are cross-spin cross-mode rates, like $R_{z\pm}^{IP}$. All these rates pertain to a particular site α and they therefore depend on the orientation of the dipole vectors in that site as detailed in Appendix E.[8]

In addition to these single-spin-mode rates, $\mathbf{R}^{\alpha}$ contains local relaxation rates connecting modes involving two or three spins. The two-spin modes have even parity under spin inversion conjugation (SIC),[7,13,14] whereas the single-spin and three-spin modes have odd parity. The relaxation supermatrix $\mathbf{R}^{\alpha}$ in the ISTO basis is therefore block-diagonal; that is, it does not couple modes of different parity (Appendix E[8]). The longitudinal relaxation behavior (and the ILRR) is therefore affected by local relaxation rates involving two-spin modes only in the *ISP–I* case, where $\boldsymbol{\Delta}^{\alpha}$ couples the odd and even blocks of $\mathbf{R}^{\alpha}$ (Appendix E[8]). The three-spin modes are destroyed by fragmentation of the spin system in the asymmetric exchange cases so the ILRR is affected by relaxation rates involving three-spin modes only in the symmetric *ISP–ISP* case. To sum up, the local relaxation rates that affect the ILRR are of types (1-spin|$\mathbf{R}^{\alpha}$|1-spin) and (2-spin|$\mathbf{R}^{\alpha}$|2-spin) for the *ISP–I* case; of type (1-spin|$\mathbf{R}^{\alpha}$|1-spin) only for the *ISP–IS* case; and of types (1-spin|$\mathbf{R}^{\alpha}$|1-spin), (1-spin|$\mathbf{R}^{\alpha}$|3-spin), and (3-spin|$\mathbf{R}^{\alpha}$|3-spin) for the *ISP–ISP* case.

We shall carry out the BWR treatment for three homonuclear spins in the dilute regime, which are also the conditions of primary interest for applications. Consequently, we have $\kappa_S = \kappa_P = 1$ and $P_{\mathrm{A}} \ll 1$. The ILRR in the dilute regime, given by Eqs. (21)–(24) for the different exchange cases, only involves elements of the supermatrix $\widetilde{\mathbf{U}}^{\mathrm{BB}}(0)$. Combining Eqs. (12a) and (13) and the detailed balance relation $P_{\mathrm{A}}\tau_{\mathrm{B}} = P_{\mathrm{B}}\tau_{\mathrm{A}} \approx \tau_{\mathrm{A}}$, we obtain

$$\widetilde{\mathbf{U}}^{\mathrm{BB}}(0) = \frac{\tau_{\mathrm{A}}}{P_{\mathrm{A}}}\left[\mathbf{1}^{\mathrm{B}} + i\,\mathbf{L}_{\mathrm{Z}}^{\mathrm{B}}\,\tau_{\mathrm{B}} - \mathbf{T}\,\mathbf{G}^{\mathrm{A}}(0)\,\mathbf{T}'\right]^{-1}, \tag{27}$$

with $\mathbf{G}^{\mathrm{A}}(0)$ given by Eq. (26). Because the supermatrix $\mathbf{G}^{\mathrm{A}}(0)$ is isotropically averaged, it must reflect the axial symmetry in spin Liouville space. According to the Wigner-Eckart theorem,[12] $\mathbf{G}^{\mathrm{A}}(0)$ must then be block-diagonal in the projection index Q of the ISTO basis of state A (Table S1).[8] The supermatrix $\mathbf{T}$ connects spin modes in states A and B that are transferred by exchange. It is clear, therefore, that the supermatrix $\mathbf{T}\,\mathbf{G}^{\mathrm{A}}(0)\,\mathbf{T}'$ is block-diagonal in the projection index Q of the ISTO basis of state B (Appendix A[8]), as is $\mathbf{L}_{\mathrm{Z}}^{\mathrm{B}}$. Because the ILRR is determined by elements from the $Q = 0$ block of $\widetilde{\mathbf{U}}^{\mathrm{BB}}(0)$ and since the block-diagonal structure is maintained under inversion, we need only retain the $Q = 0$ block of the matrices in Eq. (27). The dimension of this block is 1, 5, and 19 for exchange case *ISP–I*, *ISP–IS*, and *ISP–ISP*, respectively (Appendix A). Further simplification can be achieved by considering the SIC parity[7,13,14] of the supermatrix $\mathbf{G}^{\mathrm{A}}(0)$. We now consider the ILRR in the MN regime for the three exchange cases, in order of increasing complexity. For exchange cases *ISP–IS* and *ISP–I*, we only sketch the derivation, which is fully reproduced in Appendix F.[8]

In Subsections III A–III D, we restrict the treatment to isochronous spins. The Zeeman Liouvillian in Eq. (27) can then be dropped, because the $Q = 0$ block of $\mathbf{L}_{\mathrm{Z}}^{\mathrm{B}}$ is a null matrix. Explicit expressions for the elements of the supermatrices $\boldsymbol{\Delta}^{\alpha}$ and $\mathbf{R}^{\alpha}$ are derived in Appendix E.[8] In Sec. IV D and Appendix G,[8] we generalize the BWR treatment to include the effects of chemical shifts.

A. Exchange case *ISP–ISP*

In this case, $\mathbf{T}$ and $\mathbf{K}$ are identity matrices and there is no static dipole coupling, so Eqs. (26) and (27) yield

$$\widetilde{\mathbf{U}}^{\mathrm{BB}}(0) = \frac{\tau_{\mathrm{A}}}{P_{\mathrm{A}}}\left[\mathbf{1} - \mathbf{G}^{\mathrm{A}}(0)\right]^{-1} \tag{28}$$

and

$$\begin{aligned}\mathbf{G}^{\mathrm{A}}(0) &= \left\langle [\mathbf{1} + \mathbf{R}^{\alpha}\,\tau_{\mathrm{A}} + i\,\mathbf{L}_{\mathrm{Z}}^{\mathrm{A}}\,\tau_{\mathrm{A}}]^{-1} \right\rangle \\ &= (\mathbf{1} + i\,\mathbf{L}_{\mathrm{Z}}^{\mathrm{A}}\,\tau_{\mathrm{A}})^{-1} - (\mathbf{1} + i\,\mathbf{L}_{\mathrm{Z}}^{\mathrm{A}}\,\tau_{\mathrm{A}})^{-1} \\ &\quad \times \langle \mathbf{R}^{\alpha} \rangle\,\tau_{\mathrm{A}}\,(\mathbf{1} + i\,\mathbf{L}_{\mathrm{Z}}^{\mathrm{A}}\,\tau_{\mathrm{A}})^{-1},\end{aligned} \tag{29}$$

where, consistent with the MN approximation, we have expanded to second order in $\omega_{\mathrm{D}}\tau_{\mathrm{A}}$ (that is, to first order in $\|\mathbf{R}^{\alpha}\|\,\tau_{\mathrm{A}}$). In Eqs. (28) and (29), all matrices refer to the 19×19 $Q = 0$ block of the full 63×63 supermatrices. Because the $Q = 0$ block of $\mathbf{L}_{\mathrm{Z}}^{\mathrm{A}}$ is a null matrix, we obtain

$$\widetilde{\mathbf{U}}^{\mathrm{BB}}(0) = \frac{1}{P_{\mathrm{A}}}\langle \mathbf{R}^{\alpha} \rangle^{-1}. \tag{30}$$

The desired ILRR can now be obtained by inserting the required supermatrix elements from Eq. (30) into Eq. (23). For example,

$$\widehat{R}_{1,ISP}^{\mathrm{dil}} = P_{\mathrm{A}}\left[\frac{1}{3}\sum_{n=1}^{3}\sum_{p=1}^{3}\left(\langle \mathbf{R}^{\alpha} \rangle^{-1}\right)_{np}\right]^{-1}. \tag{31}$$

For clarity, the summand in Eq. (31) is the (np)-element of the inverse of the 19×19 $Q = 0$ block of the isotropically averaged relaxation supermatrix $\langle \mathbf{R}^{\alpha} \rangle$, given explicitly by Eq. (E.17).[8] Actually, since the relaxation supermatrix $\mathbf{R}^{\alpha}$ itself is block-diagonal with respect to the SIC parity of the basis operators (Appendix E[8]), we need only invert the 10×10 odd-parity $Q = 0$ block of $\langle \mathbf{R}^{\alpha} \rangle$ corresponding to the subspace spanned by the first ten basis operators in Table S1 A.[8] These ten spin modes comprise the three single-spin longitudinal

(L) magnetizations and seven three-spin zero-quantum coherences (ZQCs), so the 10×10 matrix can be further partitioned as

$$\langle \mathbf{R}^{\alpha} \rangle = \begin{bmatrix} \mathbf{R}_{\mathrm{L}} & \mathbf{R}_{\mathrm{L/ZQC}} \\ \mathbf{R}_{\mathrm{ZQC/L}} & \mathbf{R}_{\mathrm{ZQC}} \end{bmatrix}. \tag{32}$$

The 3×3 longitudinal block of the inverse $\langle \mathbf{R}^{\alpha} \rangle^{-1}$ in Eq. (31) can then be expressed as

$$[\langle \mathbf{R}^{\alpha} \rangle^{-1}]_{\mathrm{L}} = \left[\mathbf{R}_{\mathrm{L}} - \mathbf{R}_{\mathrm{L/ZQC}} \, \mathbf{R}_{\mathrm{ZQC}}^{-1} \, \mathbf{R}_{\mathrm{ZQC/L}} \right]^{-1}. \tag{33}$$

The elements of $\mathbf{R}_{\mathrm{L}}$ are auto-mode rates produced exclusively by self-correlations. In contrast, the elements of $\mathbf{R}_{\mathrm{L/ZQC}}$ and $\mathbf{R}_{\mathrm{ZQC/L}}$ are cross-mode rates produced exclusively by distinct correlations, corresponding to $X \neq Y$ in Eq. (E.17).[8] Because all relaxation rates are positive, it follows from Eqs. (31) and (33) that the distinct correlations make a negative contribution that reduces the ILRR: $\widehat{R}^{\mathrm{dil}}_{1,ISP} \leq \widehat{R}^{\mathrm{dil,self}}_{1,ISP}$. Relaxation coupling to the three-spin ZQCs occurs only in the *ISP–ISP* case, where the three spins exchange as an intact unit.

B. Exchange case *ISP–IS*

In this case, $\widetilde{\mathbf{U}}^{\mathrm{BB}}(0)$ in Eq. (27) is a 5×5 matrix in the subspace spanned by the first five basis operators (with $Q = 0$) in Table S2.[8] Since there is no static dipole coupling, the block-diagonality of $\mathbf{R}^{\alpha}$ with respect to SIC parity carries over to $\mathbf{G}^{\mathrm{A}}(0)$ and $\widetilde{\mathbf{U}}^{\mathrm{BB}}(0)$. To obtain the ILRR, we therefore need to consider only the 2×2 odd-parity $Q = 0$ subspace spanned by the first two basis operators $I_z/\sqrt{2}$ and $S_z/\sqrt{2}$, so that

$$\begin{aligned} \widetilde{\mathbf{U}}^{\mathrm{BB}}(0) &= \frac{\tau_{\mathrm{A}}}{P_{\mathrm{A}}} \begin{bmatrix} 1 - g_{11} & -g_{12} \\ -g_{21} & 1 - g_{22} \end{bmatrix}^{-1} \\ &= \frac{\tau_{\mathrm{A}}}{P_{\mathrm{A}}} \frac{1}{(1 - g_{11} - g_{22} + g_{11}g_{22} - g_{12}g_{21})} \\ &\quad \times \begin{bmatrix} 1 - g_{22} & g_{12} \\ g_{21} & 1 - g_{11} \end{bmatrix}, \end{aligned} \tag{34}$$

where, as before, $g_{np} \equiv (n|\mathbf{G}^{\mathrm{A}}(0)|p)$. The desired ILRR can now be obtained by inserting the required supermatrix elements from Eq. (34) into Eq. (22). For example,

$$\widehat{R}^{\mathrm{dil}}_{1,IS} = \frac{P_{\mathrm{A}}}{\tau_{\mathrm{A}}} \frac{2\,(1 - g_{11} - g_{22} + g_{11}g_{22} - g_{12}g_{21})}{(2 - g_{11} - g_{22} + g_{12} + g_{21})}. \tag{35}$$

Evaluating the four matrix elements g_{np} in Eq. (35), we obtain (Appendix F[8])

$$\widehat{R}^{\mathrm{dil}}_{1,IS} = P_{\mathrm{A}} \frac{2\,(\widetilde{R}_{II}\widetilde{R}_{SS} - \widetilde{R}_{IS}\widetilde{R}_{SI})}{(\widetilde{R}_{II} + \widetilde{R}_{SS} - \widetilde{R}_{IS} - \widetilde{R}_{SI})}, \tag{36}$$

where

$$\begin{bmatrix} \widetilde{R}_{II} & \widetilde{R}_{IS} \\ \widetilde{R}_{SI} & \widetilde{R}_{SS} \end{bmatrix} = \begin{bmatrix} \langle R^{II}_{zz} \rangle & \langle R^{IS}_{zz} \rangle \\ \langle R^{IS}_{zz} \rangle & \langle R^{SS}_{zz} \rangle \end{bmatrix} - \begin{bmatrix} \langle \Gamma_{II} \rangle & \langle \Gamma_{IS} \rangle \\ \langle \Gamma_{SI} \rangle & \langle \Gamma_{SS} \rangle \end{bmatrix}. \tag{37}$$

The elements of the last matrix are obtained by orientational averaging of the "cross relaxation" rates

$$\begin{aligned} \begin{bmatrix} \Gamma_{II} & \Gamma_{IS} \\ \Gamma_{SI} & \Gamma_{SS} \end{bmatrix} &= \begin{bmatrix} R^{IP}_{zz} & R^{IP}_{z+} & R^{IP}_{z-} \\ R^{SP}_{zz} & R^{SP}_{z+} & R^{SP}_{z-} \end{bmatrix} \\ &\quad \times \begin{bmatrix} R^{PP}_{zz} & R^{PP}_{z+} & R^{PP}_{z-} \\ R^{PP}_{+z} & (R^{PP}_{++} + i\,\omega_0) & R^{PP}_{+-} \\ R^{PP}_{-z} & R^{PP}_{-+} & (R^{PP}_{--} - i\,\omega_0) \end{bmatrix}^{-1} \\ &\quad \times \begin{bmatrix} R^{IP}_{zz} & R^{SP}_{zz} \\ (R^{IP}_{z+})^* & (R^{SP}_{z+})^* \\ (R^{IP}_{z-})^* & (R^{SP}_{z-})^* \end{bmatrix}, \end{aligned} \tag{38}$$

where ω_0 is the common Larmor frequency of the three isochronous spins in state A. The local relaxation rates that appear in Eq. (38) are given in explicit form in Eqs. (E.21)–(E.25).[8] They include cross-spin rates, such as R^{IP}_{zz}, as well as cross-mode rates, such as R^{PP}_{z+}. But because all these rates connect single-spin modes, they only involve dipolar self-correlations, as follows from the selection rule (E.15).

As shown in Appendix F,[8] the *ISP–IS* result in Eq. (36) reduces to the previously obtained[4,5] ILRR for the symmetric two-spin case *IS–IS* if spin *P* is removed and to the previously obtained[5] ILRR for the asymmetric two-spin case *IP–I* if spin *S* is removed.

In the secular approximation, valid for $\omega_0 \gg \omega_{\mathrm{D}}^2 \, \tau_{\mathrm{A}}$, all cross-mode rates vanish and Eqs. (36)–(38) yield (Appendix F[8])

$$\widehat{R}^{\mathrm{dil}}_{1,IS} = P_{\mathrm{A}} \frac{2\,(r_{II}\, r_{SS} - r_{IS}^2)}{(r_{II} + r_{SS} - 2\, r_{IS})}, \tag{39}$$

where

$$r_{II} = \langle R^{II}_{zz} \rangle - \left\langle \frac{(R^{IP}_{zz})^2}{R^{PP}_{zz}} \right\rangle, \tag{40a}$$

$$r_{SS} = \langle R^{SS}_{zz} \rangle - \left\langle \frac{(R^{SP}_{zz})^2}{R^{PP}_{zz}} \right\rangle, \tag{40b}$$

$$r_{IS} = \langle R^{IS}_{zz} \rangle - \left\langle \frac{R^{IP}_{zz}\, R^{SP}_{zz}}{R^{PP}_{zz}} \right\rangle. \tag{40c}$$

In the secular approximation, the ILRR is thus seen to be fully determined by the six unique longitudinal auto-mode rates.

C. Exchange case *ISP–I*

The dilute-regime ILRR for the *ISP–I* case, given by Eq. (24), only involves the element g_{11} of the supermatrix $\mathbf{G}^{\mathrm{A}}(0)$ defined by Eq. (26), where the supermatrix $\mathbf{\Delta}^{\alpha}$ associated with the static *SP* dipole coupling now must be reckoned with. Evaluating the element g_{11}, we find (Appendix F[8])

$$\widehat{R}^{\mathrm{dil}}_{1,I} = P_{\mathrm{A}} \left[\langle R^{II}_{zz} \rangle - \langle \Gamma^{II}_{zz} \rangle \right], \tag{41}$$

with the "cross relaxation" rate

$$\Gamma^{II}_{zz} \equiv \mathbf{R}^{\alpha}_{IS,IP} \begin{bmatrix} (\mathbf{R}^{\alpha}_{SS} + \mathbf{X}^{\alpha}_{SS} + i\,\omega_0\,\mathbf{Q}) & \mathbf{X}^{\alpha}_{SP} \\ \mathbf{X}^{\alpha}_{PS} & (\mathbf{R}^{\alpha}_{PP} + \mathbf{X}^{\alpha}_{PP} + i\,\omega_0\,\mathbf{Q}) \end{bmatrix}^{-1} \mathbf{R}^{\alpha\,\dagger}_{IS,IP}, \tag{42}$$

where $\mathbf{Q} = \mathrm{diag}(0,1,-1)$ and $\mathbf{R}^{\alpha}_{IS,IP} \equiv [\mathbf{R}^{\alpha}_{IS}\ \mathbf{R}^{\alpha}_{IP}]$. The elements of the 1×3 cross-spin relaxation matrices $\mathbf{R}^{\alpha}_{IS}$ and $\mathbf{R}^{\alpha}_{IP}$ are given in Eq. (E.25)[8] and the elements of the 3×3 auto-spin relaxation matrices $\mathbf{R}^{\alpha}_{SS}$ and $\mathbf{R}^{\alpha}_{PP}$ can be obtained from Eqs. (E.21)–(E.24).[8] All these rates connect single-spin modes and therefore only involve self-correlations.

The static SP dipole coupling affects the ILRR via the 3×3 matrices $\mathbf{X}^{\alpha}_{SS}$, $\mathbf{X}^{\alpha}_{SP}$, $\mathbf{X}^{\alpha}_{PS}$, and $\mathbf{X}^{\alpha}_{PP}$ in the single-spin S and P subspace. In Appendix F,[8] we show that

$$\begin{aligned} \mathbf{X}^{\alpha} &= \begin{bmatrix} \mathbf{X}^{\alpha}_{SS} & \mathbf{X}^{\alpha}_{SP} \\ \mathbf{X}^{\alpha}_{PS} & \mathbf{X}^{\alpha}_{PP} \end{bmatrix} \\ &= \begin{bmatrix} \boldsymbol{\Delta}^{\alpha}_{S,s0} \\ \boldsymbol{\Delta}^{\alpha}_{P,s0} \end{bmatrix} (\mathbf{R}^{\alpha}_{ss00} + i\,\omega_0\,\mathbf{Q}_{ss00})^{-1} \big[\, \boldsymbol{\Delta}^{\alpha\,\dagger}_{S,s0}\ \boldsymbol{\Delta}^{\alpha\,\dagger}_{P,s0} \,\big], \end{aligned} \tag{43}$$

where $\mathbf{Q}_{ss00} = \mathrm{diag}(0,0,0,1,1,-1,-1,2,-2)$. The elements of the 9×9 relaxation matrix $\mathbf{R}^{\alpha}_{ss00}$ in the two-spin-SP subspace, obtained from Eqs. (E.9) to (E.11),[8] involve IS and IP self-correlations as well as IS–IP distinct correlations. The elements of the 3×9 static dipolar Liouvillian matrices $\boldsymbol{\Delta}^{\alpha}_{S,s0}$ and $\boldsymbol{\Delta}^{\alpha}_{P,s0}$ can be obtained from Eq. (E.26).[8]

If we neglect the static SP dipole coupling, then Eq. (42) reduces to (Appendix F[8])

$$\begin{aligned} \Gamma^{II}_{zz} &= \mathbf{R}^{\alpha}_{IS}\,(\mathbf{R}^{\alpha}_{SS} + i\,\omega_0\,\mathbf{Q})^{-1}\,\mathbf{R}^{\alpha\,\dagger}_{IS} \\ &\quad + \mathbf{R}^{\alpha}_{IP}\,(\mathbf{R}^{\alpha}_{PP} + i\,\omega_0\,\mathbf{Q})^{-1}\,\mathbf{R}^{\alpha\,\dagger}_{IP}, \end{aligned} \tag{44}$$

showing, with Eq. (41), that the IS and IP dipole couplings contribute additively so that $\widehat{R}^{\mathrm{dil}}_{1,I}(ISP\text{–}I) = \widehat{R}^{\mathrm{dil}}_{1,I}(IS\text{–}I) + \widehat{R}^{\mathrm{dil}}_{1,I}(IP\text{–}I)$, with the two-spin ILRRs as given in Paper II. If spin P is located far away from spins I and S, so that both dipole couplings to spin P are negligibly weak, then the ISP–I result reduces further to the previously obtained[5] result (specialized to isochronous spins) for the asymmetric two-spin case IS–I.

If we (artificially) neglect cross-spin relaxation, so that $\mathbf{R}^{\alpha}_{IS} = \mathbf{R}^{\alpha}_{IP} = \mathbf{0}$, then Eqs. (41) and (42) yield

$$\begin{aligned} \widehat{R}^{\mathrm{dil}}_{1,I} &= P_{\mathrm{A}}\,\langle R^{II}_{zz}\rangle = \tfrac{2}{45}\,P_{\mathrm{A}}\,(\omega^2_{\mathrm{D},IS} + \omega^2_{\mathrm{D},IP}) \\ &\quad \times [\,j(0) + 3\,j(\omega_0) + 6\,j(2\,\omega_0)], \end{aligned} \tag{45}$$

where Eq. (E.20a)[8] was also used. This (unphysical) result shows that cross-spin relaxation is necessary for the ILRR to approach zero at high field.

In the secular approximation, valid when $\omega_0 \gg \omega^2_{\mathrm{D}}\tau_{\mathrm{A}}$ for the fluctuating IS and IP dipole couplings and $\omega_0 \gg \omega_{\mathrm{D}}$ for the static SP coupling, Eq. (42) reduces to (Appendix F[8])

$$\Gamma^{II}_{zz} = \frac{R^{SS}_{zz}\,(R^{IP}_{zz})^2 + R^{PP}_{zz}\,(R^{IS}_{zz})^2 + X(R^{IS}_{zz} + R^{IP}_{zz})^2}{R^{SS}_{zz}\,R^{PP}_{zz} + X(R^{SS}_{zz} + R^{PP}_{zz})}, \tag{46}$$

with

$$X \equiv \frac{2}{9}\big[\omega_{\mathrm{D},SP}\,D^2_{00}(\Omega_{SP})\big]^2\rho. \tag{47}$$

Here, ρ is the "33 element" (corresponding to basis operator B_{19} in Table S1 A)[8] of the inverse of the 3×3 $Q = 0$ block of $\mathbf{R}^{\alpha}$ in the two-spin-SP subspace. This result shows that, even in the secular approximation, the dipole couplings of the labile spin I with the two nonlabile spins S and P do not contribute independently to the ILRR if $\omega_{\mathrm{D},SP} \neq 0$.

D. Chemical shifts

The BWR results presented in Secs. III A–III C were derived under the assumption that the three spins are isochronous. In Appendix G,[8] we generalize the BWR treatment to include the effects of chemical shifts in the Zeeman Hamiltonians $H^{\mathrm{A}}_{\mathrm{Z}}$ and $H^{\mathrm{B}}_{\mathrm{Z}}$, as shown in Eq. (1). Whereas the SLE theory of Sec. II is valid for arbitrarily large chemical shifts (including heteronuclear spins), we restrict the generalized BWR treatment to homonuclear spins, so that $\delta \ll 1$. For example, proton shifts rarely exceed 10 ppm.

Chemical shift effects on the ILRR in the dilute regime are examined in detail in Appendix G.[8] One effect is to displace the primary and secondary dispersion steps to higher or lower frequency, but the relative displacement, of order δ, is negligible for homonuclear spins. For the asymmetric exchange cases ISP–IS and ISP–I, this is the only effect of chemical shifts in the MN regime. For the two-spin cases IS–IS and IS–I, this is also the only (negligibly small) effect of chemical shifts.[4,5]

In contrast, for the symmetric exchange case ISP–ISP, chemical shifts can significantly alter the ILRR dispersion profile even if $\delta \ll 1$. Formally, this effect can be described by replacing Eq. (33) with (Appendix G[8])

$$\begin{aligned} &[\langle \mathbf{R}^{\alpha}\rangle^{-1}]_{\mathrm{L}} \\ &\quad = \big[\mathbf{R}_{\mathrm{L}} - P_{\mathrm{A}}\,\mathbf{R}_{\mathrm{L/ZQC}}\,(P_{\mathrm{A}}\,\mathbf{R}_{\mathrm{ZQC}} + i\,\mathbf{W})^{-1}\,\mathbf{R}_{\mathrm{ZQC/L}}\big]^{-1}, \end{aligned} \tag{48}$$

where we have introduced the 7×7 frequency matrix

$$\mathbf{W} = \omega_0\,(P_{\mathrm{A}}\,\mathbf{D}_{\mathrm{A}} + P_{\mathrm{B}}\,\mathbf{D}_{\mathrm{B}})\,. \tag{49}$$

The elements of the matrix $\mathbf{D}_{\mathrm{A}}$ are linear combinations of the chemical shifts δ^{A}_S and δ^{A}_P, and similarly for $\mathbf{D}_{\mathrm{B}}$, as shown by Eqs. (G.4) and (G.5).[8]

This modification gives rise to a novel secondary dispersion step, not present for isochronous spins, centered at the nonsecular decoupling (NSD) frequency (Appendix G[8])

$$\omega_{\mathrm{NSD}} = \frac{P_{\mathrm{A}}\,\omega^2_{\mathrm{D}}\,\tau_{\mathrm{A}}}{P_{\mathrm{A}}\,\delta^{\mathrm{A}} + P_{\mathrm{B}}\,\delta^{\mathrm{B}}}, \tag{50}$$

where δ^{A} can be approximately identified as the largest of δ^{A}_S and δ^{A}_P, and similarly for δ^{B}. At low frequencies, such that $\omega_0 \ll \omega_{\mathrm{NSD}}$, chemical shifts have no effect on the ILRR. At $\omega_0 \approx \omega_{\mathrm{NSD}}$, there is an inverted secondary dispersion step as the (negative) contribution from distinct correlations in the L/ZQC cross-mode rates is partly lost. At higher frequencies, such that $\omega_0 \gg \omega_{\mathrm{NSD}}$, $\widehat{R}^{\mathrm{dil}}_{1,ISP}$ remains larger than for isochronous spins but it never exceeds the ILRR produced solely by self-correlations.

If chemical shifts are present only in state A, so that $\delta^{\mathrm{B}} = 0$, then Eq. (50) yields $\omega_{\mathrm{NSD}} = \omega^2_{\mathrm{D}}\,\tau_{\mathrm{A}}/\delta^{\mathrm{A}}$. This result

is also obtained for the special case $P_A = 1$, which has been discussed previously.[7] If the chemical shifts are the same in states A and B ($\delta^A = \delta^B \equiv \delta$), then Eq. (50) yields $\omega_{NSD} = P_A \omega_D^2 \tau_A/\delta$, so the secondary dispersion appears at a much lower frequency. In general, the chemical shift effect can be neglected if the secondary dispersion step occurs well above the primary dispersion, that is, if $\omega_{NSD} \gg 1/\tau_A$. As seen from Eq. (50), this is true if the chemical shifts in both states are sufficiently small that $|P_A \delta^A + P_B \delta^B| \ll P_A (\omega_D \tau_A)^2$.

IV. NUMERICAL RESULTS

In this section, we present numerical calculations that illustrate the theoretical results obtained in Secs. II and III. Since the prime application is water-^{1}H relaxation in tissue-like systems, we consider only homonuclear spins ($\kappa_S = \kappa_P = 1$) although the SLE theory in Sec. II can also handle heteronuclear spin systems. Moreover, in Secs. IV A–IV C, we assume that the spins are effectively isochronous, so that we can set $\delta_S = \delta_P = 0$ in both states A and B. This assumption is justified in Sec. IV D, where we show that the effect of chemical shifts is negligibly small in virtually all situations of practical interest.

In most calculations, the bound fraction of labile spin(s) is set to the experimentally relevant value of $P_A = 10^{-3}$, so we are in the dilute regime. Whereas the BWR theory of Sec. III is restricted to the dilute regime, the SLE theory of Sec. II is valid for arbitrary P_A, including the opposite limit of $P_A = 1$. In this limit, Eqs. (12b), (13), (14), and (D.15)[8] yield for the *ISP–ISP* case

$$\widehat{R}_{1,ISP} = 3\left\{\sum_{n=1}^{3}\sum_{p=1}^{3}\left(n\left|\left[\left\langle(\mathbf{1}/\tau_A + i\,\mathbf{L}_Z + i\,\mathbf{L}_D)^{-1}\right\rangle^{-1} - \mathbf{1}/\tau_A\right]^{-1}\right|p\right)\right\}^{-1}, \tag{51}$$

a result that we have used in a previous study.[7] In some calculations, we use $P_A = 10^{-4}$ to ensure that the BWR and SLE results agree to a high level of accuracy.

The calculation of the ILRR from SLE theory proceeds as follows. First, we construct the 63×63 supermatrix within square brackets in Eq. (14) from the Zeeman and dipolar Liouvillian supermatrices $\mathbf{L}_Z$ and $\mathbf{L}_D$ (Appendixes B and C[8]) and the exchange supermatrix $\mathbf{K}$ (Sec. II A). We then invert this matrix and compute the isotropic average over the Euler angles $\Omega^\alpha \equiv (\psi^\alpha, \vartheta^\alpha, \varphi^\alpha)$. For the angles ψ^α and ϑ^α, which determine the orientation of the internuclear vector $\boldsymbol{r}_{IS}^\alpha$, we use Lebedev quadrature with 350 points on the unit sphere.[15,16] For the angle φ^α, which determines the orientation of the nuclear plane about the $\boldsymbol{r}_{IS}^\alpha$ axis, we use a uniform grid with 30 points. From the $\mathbf{G}^A(0)$ supermatrix obtained in this way and the exchange matrix $\mathbf{T}$ (Sec. II A), we obtain $\widetilde{\mathbf{U}}^{BB}(0)$ from Eq. (12a). Finally, the ILRR in the dilute regime for the three exchange cases, $\widehat{R}_{1,I}^{dil}$, $\widehat{R}_{1,IS}^{dil}$, or $\widehat{R}_{1,ISP}^{dil}$, is calculated from Eqs. (24), (22b), or (23c), respectively. When using Eq. (24) for the *ISP–I* case, the ILRR is actually obtained directly from $\mathbf{G}^A(0)$, bypassing the calculation of $\widetilde{\mathbf{U}}^{BB}(0)$.

For the calculation of the ILRR from BWR theory, we use Eqs. (41)–(43) for the *ISP–I* case, Eqs. (36)–(38) for the *ISP–IS* case and Eqs. (31) and (33) for the *ISP–ISP* case, along with the required elements of the local relaxation supermatrix $\mathbf{R}^\alpha$ from Appendix E.[8] The isotropic orientational averages are computed in the same way as for the SLE theory. For all three exchange cases, we have confirmed that the BWR results coincide, to within numerical accuracy, with the SLE results in the MN regime.

A. Overview of dispersion profiles

To provide an overview of the longitudinal relaxation behavior of the three-spin system, we present in Fig. 2 the complete dispersion profiles of $\widehat{R}_{1,I}^{dil}(ISP\text{–}I)$, $\widehat{R}_{1,IS}^{dil}(ISP\text{–}IS)$, and $\widehat{R}_{1,ISP}^{dil}(ISP\text{–}ISP)$ at four values of the mean survival time τ_A, ranging from the MN regime with $\omega_D \tau_A = 0.01$ to the ultraslow-motion (USM) regime with $\omega_D \tau_A = 100$. These 12 profiles, all calculated from the SLE theory, are shown in the panels in left column of Fig. 2. Here, we assume an equilateral triangle geometry ($\beta_I = \beta_S = 60°$) so all three dipole couplings have the same magnitude, taken to be $\omega_D = 1 \times 10^5$ rad s^{-1}, which corresponds to an internuclear separation of $r_{IS} = 2.245$ Å for two protons. (Other internuclear geometries are considered in Sec. IV B.)

The panels in right column of Fig. 2 show the corresponding dispersion profiles for a two-spin (*IS*) system with the same values of ω_D and τ_A as in the left-hand panel. These profiles were computed from the two-spin dipolar EMOR theory presented in Papers I and II. The *IS–I* profile can also be obtained from the three-spin *ISP–I* result by setting β_P to a small value, which corresponds to locating spin *P* far away from spins *I* and *S*. Likewise, the *IS–IS* profile can be obtained from the three-spin *ISP–IS* result with small β_P. In both of these cases, the remote spin *P* is nonlabile.

In contrast, if we make the labile spin *P* remote in the *ISP–ISP* case, we obtain a situation where the ILRR is very small because the temporal decay of the observed total longitudinal magnetization of the three spins has an extended tail due to slow relaxation of the weakly dipole-coupled spin *P*. Because the magnetization decay is then strongly non-exponential, it is not adequately described by the ILRR. In any event, this "pathological" scenario is of little practical relevance, partly because of the special nature of the spin system and partly because of our neglect of scalar couplings, which would have a substantial effect in this particular case. This situation cannot occur when the exchanging species contains one (*ISP–I*) or two (*ISP–IS*)

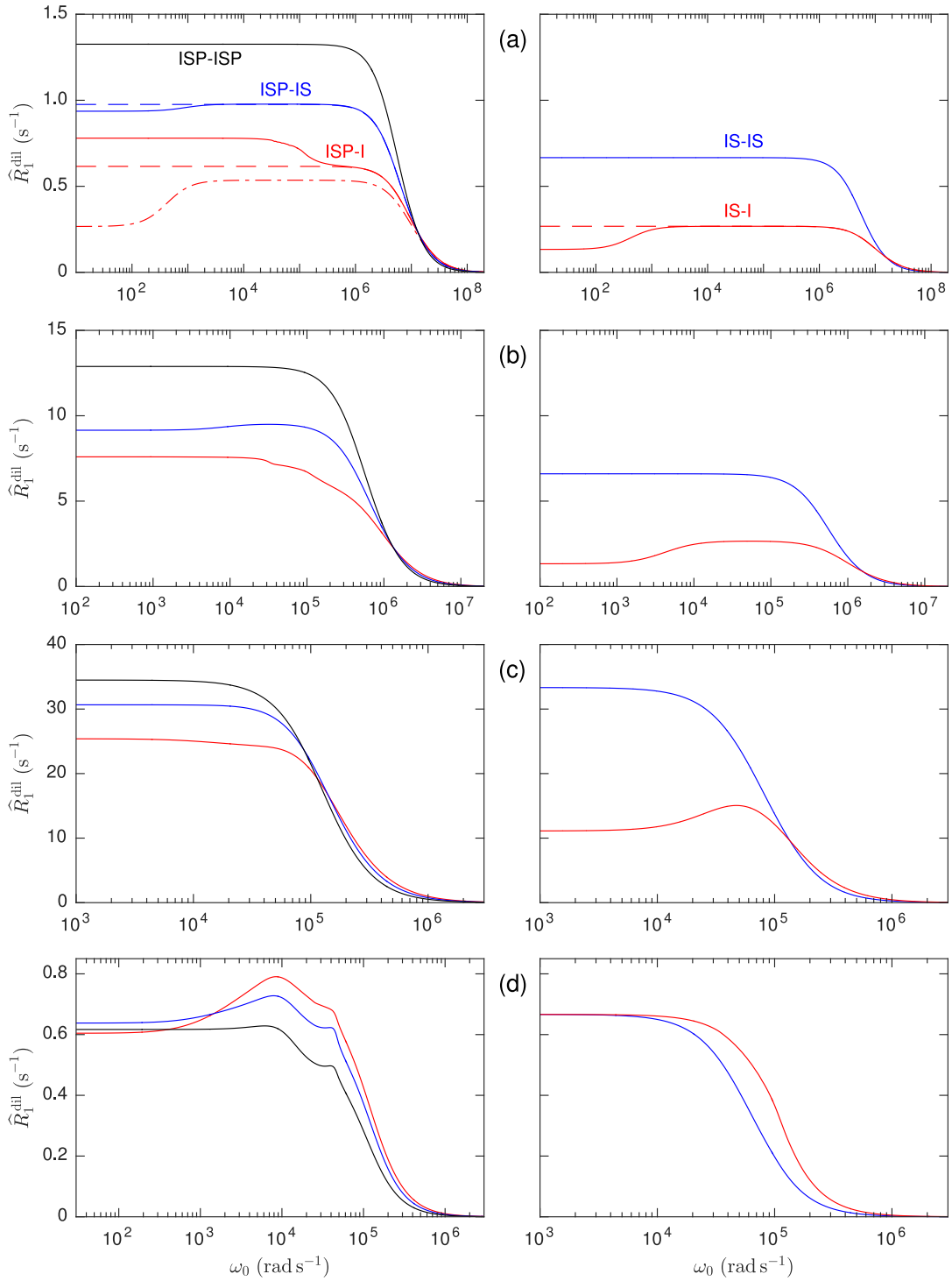

FIG. 2. ILRR dispersion profiles for the three-spin cases (left column) and for the two-spin cases (right column; same y-axis range as in the left column). Color coding of exchange cases as in top panels. Parameter values: $P_{\rm A} = 10^{-3}$, $\omega_{\rm D} = 10^5$ rad s^{-1}, $\beta_I = \beta_S = 60°$, and $\tau_{\rm A} = 10^{-7}$ s (a), 10^{-6} s (b), 10^{-5} s (c), or 10^{-3} s (d).

spins, which are the cases of primary interest for applications (see Sec. I). For those cases, as well as for the ISP–ISP case with magnetic equivalence (or, at least, three similar dipole couplings), we expect that the decay of the total observed longitudinal magnetization of the labile spin(s) is very nearly exponential in the dilute regime, as shown explicitly in Paper II for the two-spin IS–I case.

1. Motional-narrowing regime

In Fig. 2(a), with $\tau_{\rm A} = 100$ ns and $\omega_{\rm D}\tau_{\rm A} = 0.01$, we are squarely in the MN regime, where the BWR results of Sec. III apply. Let us first compare the symmetric exchange cases ISP–ISP and IS–IS, where the spin system exchanges as an intact unit. The IS–IS profile is given in

Paper I as

$$\widehat{R}^{\rm dil}_{1,IS}(IS\text{–}IS) = \frac{2}{3}\,P_{\rm A}\,\omega_{\rm D}^2\left[\frac{0.2\,\tau_{\rm A}}{1+(\omega_0\,\tau_{\rm A})^2}+\frac{0.8\,\tau_{\rm A}}{1+(2\,\omega_0\,\tau_{\rm A})^2}\right]. \tag{52}$$

In the three-spin system, each spin is involved in two equally strong dipole couplings, so one might expect $\widehat{R}^{\rm dil}_{1,ISP}(ISP\text{–}ISP)$ to be precisely a factor 2 larger than $\widehat{R}^{\rm dil}_{1,IS}(IS\text{–}IS)$. This is true as long as we only take self-correlations into account, that is, $\widehat{R}^{\rm dil,self}_{1,ISP}(ISP\text{–}ISP) = 2\,\widehat{R}^{\rm dil}_{1,IS}(IS\text{–}IS)$. However, correlations between distinct (albeit, here, equally strong) dipole couplings also contribute (negatively) to $\widehat{R}^{\rm dil}_{1,ISP}(ISP\text{–}ISP)$. This contribution happens to be quite small for the equilateral triangle geometry considered in Fig. 2, so $\widehat{R}^{\rm dil}_{1,ISP}(ISP\text{–}ISP)$ is merely 0.74% less than $2\,\widehat{R}^{\rm dil}_{1,IS}(IS\text{–}IS)$ in the extreme-narrowing (EN) regime. (Depending on ω_0, the relative difference varies between −0.6% and −0.8%, just as for spherical-top rotation in isotropic fluids.[7])

Consider now the asymmetric exchange cases $ISP\text{–}IS$ and $IS\text{–}I$, with one nonlabile spin. In the MN regime, which is also the fast-exchange regime for the EMOR model, relaxation rates that couple labile-spin modes are isotropically averaged, as in the first part of Eq. (37). In contrast, relaxation rates involving one or two nonlabile-spin modes are not exchange averaged, cf. Eq. (38). The local relaxation matrix (not exchange-averaged) has lower than axial symmetry and the Wigner-Eckart theorem does not forbid relaxation coupling of local spin modes with different quantum order Q, which we refer to as cross-mode relaxation.[5] If, as is the case here, the exchanging spin system contains one or two spins, the invariant odd-parity subspace only contains single-spin modes. The only available cross-mode relaxation channel is therefore between the longitudinal and transverse magnetizations of the same or different spins, at least one of which is nonlabile.[5]

Single-spin cross-mode relaxation is associated with nonsecular terms in the BWR master equation, that is, terms with $M' \neq -M$ in Eq. (E.4).[8] It is therefore eliminated by differential Larmor precession at higher frequencies, a phenomenon that we refer to as nonsecular decoupling. As a consequence, the EN regime is split into two subregimes:[5] the zero-field (ZF) regime with $\omega_0 \ll \omega_{\rm D}^2\,\tau_{\rm A}$, and the low-field (LF) regime with $\omega_{\rm D}^2\,\tau_{\rm A} \ll \omega_0 \ll 1/\tau_{\rm A}$. Single-spin cross-mode relaxation is only effective in the ZF regime, where it makes a negative contribution to the ILRR.[5] As a result, the dispersion profile exhibits an inverted secondary dispersion step at $\omega_0 \approx \omega_{\rm D}^2\,\tau_{\rm A}$, in addition to the primary dispersion step at $\omega_0 \approx 1/\tau_{\rm A}$. The dashed dispersion profiles in Fig. 2(a) were computed from the BWR results in the secular approximation, where cross-mode relaxation is neglected. The secular approximation is evidently not valid in the ZF regime. Comparing the $ISP\text{–}IS$ and $IS\text{–}I$ profiles in Fig. 2(a), we see that, while the secondary dispersion occurs at the same frequency, the step is much smaller for the $ISP\text{–}IS$ case (~4% versus a factor ~2).

In the two-spin IS system, the ILRR is reduced by a factor 5 in the ZF regime and by a factor ~2.5 in the LF regime when the S spin becomes nonlabile,[5] that is, going from $IS\text{–}IS$ to $IS\text{–}I$. In contrast, in the three-spin ISP system, the ILRR is only reduced by ~29% in the ZF regime and by ~26% in the LF regime when the P spin becomes nonlabile, that is, going from $ISP\text{–}ISP$ to $ISP\text{–}IS$. This difference reflects the fact that, for the three-spin system, the labile I and S spins are each involved in two dipole couplings, only one of which is fragmented by exchange.

Like the $ISP\text{–}IS$ profile, the $ISP\text{–}I$ profile in Fig. 2(a) exhibits a secondary dispersion in addition to the primary dispersion at $\omega_0 \approx 1/\tau_{\rm A}$. However, the secondary dispersion step now appears at $\omega_0 \approx \omega_{\rm D}$ (rather than at $\omega_0 \approx \omega_{\rm D}^2\,\tau_{\rm A}$) and it is not inverted. (The irregular "fine-structure" in the secondary dispersion step of the $ISP\text{–}I$ profiles in Figures 2(a) and 2(b) is a real feature — not a numerical imperfection.) The origin of the secondary dispersion step in the $ISP\text{–}I$ profile is the static dipole coupling between the nonlabile spins S and P. If we set $\omega_{{\rm D},SP} = 0$ without altering the other two (equal) dipole couplings, then this secondary dispersion step disappears and instead an inverted dispersion step at $\omega_0 \approx \omega_{\rm D}^2\,\tau_{\rm A}$ appears (the dashed-dotted curve in Fig. 2(a)). In fact, for $\omega_{{\rm D},SP} = 0$, we have $\widehat{R}^{\rm dil}_{1,I}(ISP\text{–}I) = 2\,\widehat{R}^{\rm dil}_{1,I}(IS\text{–}I)$, as noted in Sec. III C.

In Appendix H,[8] we examine in detail how the static dipole coupling removes the inverted secondary dispersion step at $\omega_0 \approx \omega_{\rm D}^2\,\tau_{\rm A}$ and instead produces a non-inverted secondary dispersion step at $\omega_0 \approx \omega_{\rm D}$. To characterize the strength of the static dipole coupling, we introduce the dimensionless parameter

$$\epsilon \equiv \frac{\omega_{{\rm D},SP}}{\omega_{{\rm D},I}^2\,\tau_{\rm A}}, \tag{53}$$

where $\omega_{{\rm D},I}^2 \equiv \omega_{{\rm D},IS}^2 + \omega_{{\rm D},IP}^2$. We refer to the static dipole coupling $\omega_{{\rm D},SP}$ as weak if $\epsilon \ll 1$ and as strong if $\epsilon \gg 1$. For the equilateral triangle geometry assumed in Fig. 2, where all three dipole couplings are equally strong, Eq. (53) implies that $\epsilon \gg 1$ in the MN regime ($\omega_{\rm D}\,\tau_{\rm A} \ll 1$). The weak coupling limit $\epsilon \ll 1$ is only relevant when one of the nonlabile spins is located far from the other two spins, in which case the $ISP\text{–}I$ case effectively reduces to the $IS\text{–}I$ case (Appendix H[8]).

The key to understanding the effect of the static dipole coupling is the singular nature of the matrix $\mathbf{X}$ in Eq. (43). Specifically, at all frequencies ω_0, $\mathbf{X}$ has one zero eigenvalue and the associated eigenvector defines a one-dimensional unitary subspace, even though $\mathbf{X}$ is Hermitian only for $\omega_0 = 0$ (Appendix H[8]). A weak static dipole coupling has no effect at all; the dispersion profile is the same as for $\omega_{{\rm D},SP} = 0$ (the dashed-dotted profile in Fig. 2(a)), with an inverted secondary dispersion at $\omega_0 \approx \omega_{\rm D}^2\,\tau_{\rm A}$, where single-spin cross-mode relaxation is abolished by nonsecular decoupling. A strong static dipole coupling projects the cross-spin and auto-spin relaxation matrices onto the unitary subspace associated with the zero eigenvalue (Appendix H[8]). As a result, the ZF regime is extended from $\omega_0 \approx \omega_{\rm D}^2\,\tau_{\rm A}$ to $\omega_0 \approx \omega_{{\rm D},SP}$, where a secondary dispersion step appears. Above this frequency, single-spin cross-mode relaxation is no longer effective and the secular approximation, Eq. (46), is valid (dashed profile in Fig. 2(a)). Single-spin cross-mode relaxation occurs throughout the extended ZF regime (up to $\omega_0 \approx \omega_{{\rm D},SP}$), but it is modified by the static dipole coupling. Above $\omega_0 \approx \omega_{{\rm D},SP}$, this modified single-spin cross-mode relaxation is abolished

by nonsecular decoupling, but this effect, which increases $\widehat{R}^{\rm dil}_{1,I}$, is overshadowed by the effects of nonsecular decoupling on the matrix $\mathbf{X}$ in Eq. (43), which decreases $\widehat{R}^{\rm dil}_{1,I}$, thus accounting for the non-inverted shape of the secondary dispersion step in the presence of a strong static dipole coupling. Nonsecular decoupling modifies $\mathbf{X}$ in two ways. First, it eliminates the nonsecular part of static dipole coupling, that is, terms with $M \neq 0$ in Eq. (E.8).[8] Second, it eliminates the nonsecular part of the two-spin relaxation matrix $\mathbf{R}^{\alpha}_{\rm ss00}$, corresponding to terms with $M' \neq -M$ in Eq. (E.4).[8] Note that, although relaxation coupling of two-spin modes with different quantum order Q is thus eliminated, cross-mode relaxation within the Q-blocks can still occur above the secondary dispersion ($\omega_0 > \omega_{{\rm D},SP}$). Note also that, whereas the strength of the static dipole coupling determines the frequency of the secondary dispersion step, it has no effect on $\widehat{R}^{\rm dil}_{1,I}$ in the ZF regime as long as the coupling is strong ($\epsilon \gg 1$).

2. Ultraslow-motion regime

Increasing $\tau_{\rm A}$, thereby moving from the MN regime to the USM regime, has two principal effects on the dispersion profile, as described in Papers I and II for the two-spin system. First, the position of the primary dispersion step at $\omega_0 \approx 1/\tau_{\rm A}$ is down-shifted in frequency until $\tau_{\rm A}$ becomes comparable to $1/\omega_{\rm D}$ (=10^{-5} s, here) and eventually stops at $\omega_0 \approx \omega_{\rm D}$ when the USM limit is reached. Second, the ILRR in the ZF regime first increases and then decreases, with a maximum near $\omega_{\rm D}\,\tau_{\rm A} \approx 1$. As seen from Figs. 2(a)-2(d), this is true for all three exchange cases. The continuous variation of $\widehat{R}^{\rm dil}_1(0)$ with $\tau_{\rm A}$ is shown in Fig. 3 for the five cases. For the two-spin cases, these curves are given by the analytical ZF results in Papers I and II,

$$\widehat{R}^{\rm dil}_{1,I}(0) = \frac{2}{3}\,P_{\rm A}\frac{\omega_{\rm D}^2\,\tau_{\rm A}}{[5+(\omega_{\rm D}\,\tau_{\rm A})^2]} \quad (IS\text{–}I), \tag{54a}$$

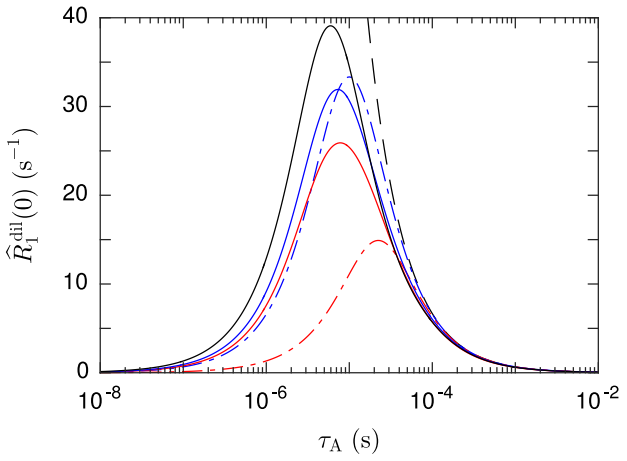

FIG. 3. Zero-field limit of the ILRR versus mean survival time for exchange case ISP–I (red solid curve), ISP–IS (blue solid curve), ISP–ISP (black solid curve), IS–I (red dashed-dotted curve), and IS–IS (blue dashed-dotted curve), computed from the SLE results of this work (solid curves) or from Eq. (54) (dashed-dotted curves). Parameter values: $P_{\rm A} = 10^{-3}$, $\omega_{\rm D}$ = 10^5 rad s^{-1}, and $\beta_I = \beta_S = 60°$. The black dashed curve is $(2/3)\,P_{\rm A}/\tau_{\rm A}$.

$$\widehat{R}^{\rm dil}_{1,IS}(0) = \frac{2}{3}\,P_{\rm A}\frac{\omega_{\rm D}^2\,\tau_{\rm A}}{[1+(\omega_{\rm D}\,\tau_{\rm A})^2]} \quad (IS\text{–}IS). \tag{54b}$$

For the three-spin cases, where simple analytical results are not available, the maximum occurs at $\tau_{\rm A}$ values slightly below $1/\omega_{\rm D}$. For the equilateral triangle geometry examined in Fig. 3, the ISP–IS curve happens to be close to the IS–IS curve, but for other internuclear geometries, the detailed shape, and even the rank order, of the three-spin curves can differ from that shown in Fig. 3. In the USM limit, $\omega_{\rm D}\,\tau_{\rm A} \gg 1$, the two-spin curves both reduce to $\widehat{R}^{\rm dil}_1(0) = (2/3)\,P_{\rm A}/\tau_{\rm A}$. In the same limit, the three-spin curves, while not far from this value, differ slightly, as seen in Fig. 2(d) for the equilateral triangle geometry. Also for other internuclear geometries, $\widehat{R}^{\rm dil}_1(\omega_0)$ is inversely proportional to $\tau_{\rm A}$ in the USM regime, so we can write $\widehat{R}^{\rm dil}_1(0) = (2/3)\,(P_{\rm A}/\tau_{\rm A})\,f(\beta_I,\beta_S)$, where $f(\beta_I,\beta_S)$ is a different function for each of the three cases. For $\beta_I = \beta_S = 60°$, $f \approx 0.907$, 0.957, and 0.925 for ISP–I, ISP–IS, and ISP–ISP, respectively.

Returning to the dispersion profiles in Fig. 2, we note that, once the USM limit is reached (as in Fig. 2(d)), $\widehat{R}^{\rm dil}_1(\omega_0)$ is inversely proportional to $\tau_{\rm A}$ over the whole frequency range and the shape and position of the dispersion profile no longer change as $\tau_{\rm A}$ is further increased. For the IS–IS case in the USM regime, we showed in Paper I that

$$\widehat{R}^{\rm dil}_{1,IS}(IS\text{–}IS) = \frac{2}{3}\,\frac{P_{\rm A}}{\tau_{\rm A}}\left[\frac{0.2}{1+(\omega_0/\omega_{\rm D})^2}+\frac{0.8}{1+(2\,\omega_0/\omega_{\rm D})^2}\right], \tag{55}$$

so the dispersion has the same "Lorentzian" shape as in the MN regime, but now with $1/\omega_{\rm D}$ playing the role of an apparent correlation time. In fact, Eq. (55) is obtained from Eq. (52) by substituting $1/\omega_{\rm D}$ for $\tau_{\rm A}$. For the other four cases, where analytical results are not available, the USM profiles are no longer "Lorentzian" but exhibit a "fine-structure" that is particularly striking for the three-spin cases, with two distinct maxima (or "bumps") for the equilateral triangle geometry (Fig. 2(d)).

B. Internuclear geometry

The ILRR depends on the fixed relative orientation of the internuclear vectors as well as on the length of those vectors, which determines the magnitude of the dipole couplings. In other words, the ILRR depends on the angles β_I and β_S (Fig. 1) directly via Eq. (4), as well as indirectly via Eq. (6). This is true for all three exchange cases. For the ISP–ISP case in the MN regime, Eq. (E.17)[8] shows that the direct dependence on these angles enters solely via the distinct correlations.

So far, we have examined the equilateral triangle geometry, where the three dipole couplings are of equal magnitude. To illustrate the effect of the internuclear geometry, we show in Fig. 4 the dispersion profiles of $\widehat{R}^{\rm dil}_{1,I}(ISP\text{–}I)$, $\widehat{R}^{\rm dil}_{1,IS}(ISP\text{–}IS)$, and $\widehat{R}^{\rm dil}_{1,ISP}(ISP\text{–}ISP)$ for five less symmetric nuclear configurations. For all these geometries, the I–S dipole coupling is taken to be the same, $\omega_{{\rm D},IS} = 1\times10^5$ rad s^{-1}. The other two dipole couplings are then determined by the angles β_I and β_S in Eq. (6). The examined internuclear geometries are drawn to scale in Fig. 4, where thick and dashed-dotted

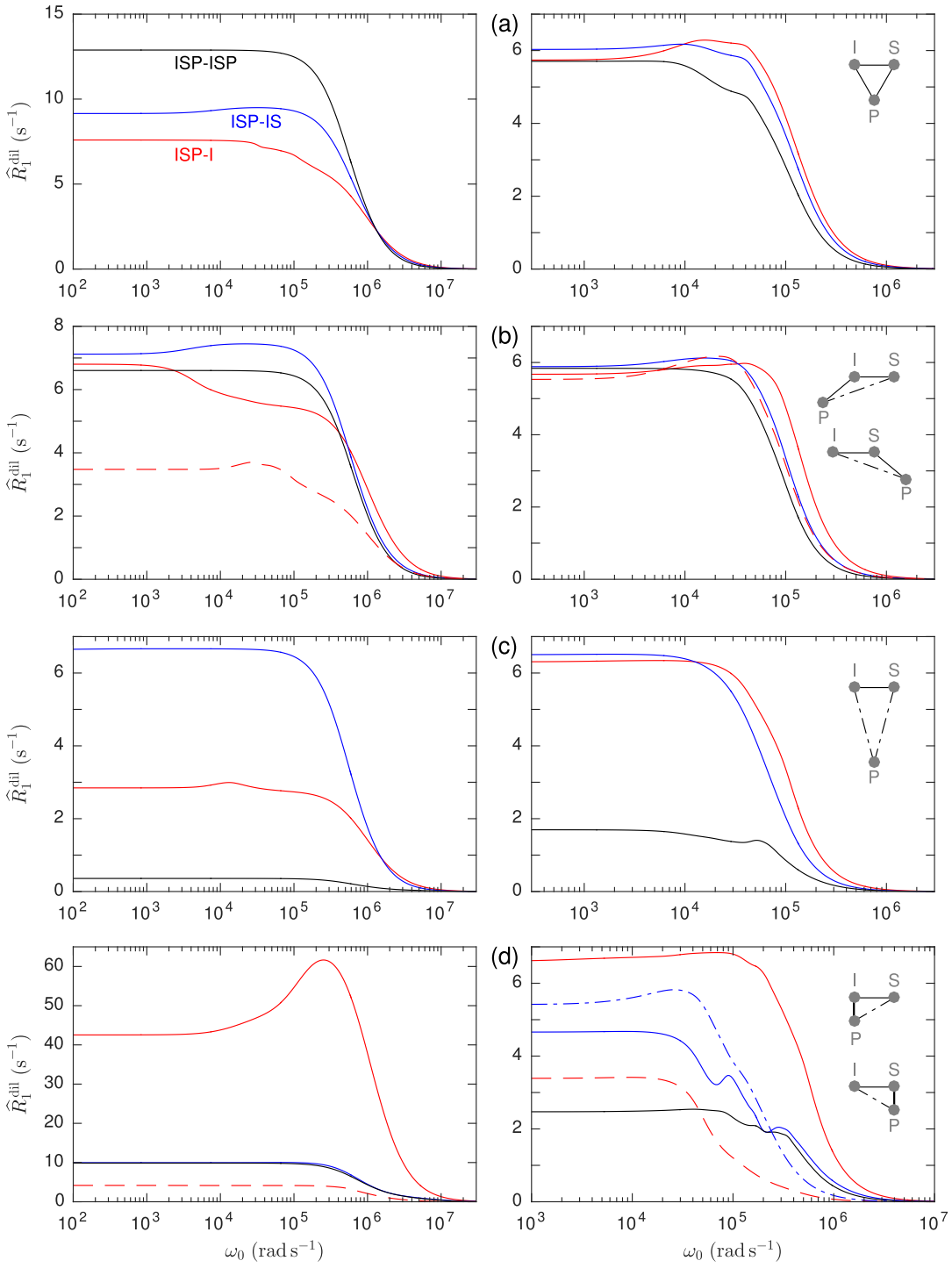

FIG. 4. ILRR dispersion profiles for the three-spin cases with different nuclear geometries as indicated to the right. Parameter values: $P_{\rm A} = 10^{-3}$, $\omega_{{\rm D},IS} = 10^5$ rad s^{-1}, and $\tau_{\rm A} = 10^{-6}$ s (left column) or 10^{-4} s (right column).

lines represent dipole couplings that are stronger or weaker, respectively, than $\omega_{{\rm D},IS}$. For reference, we show the equilateral triangle geometry ($\beta_I = \beta_S = 60°$) in Fig. 4(a). The other panels show the effect of weakening one (Fig. 4(b)) or two (Fig. 4(c)) dipole couplings, or making one coupling stronger and the other weaker (Fig. 4(d)). In Figs. 4(b) and 4(d), two geometries are included that differ by interchange of the I and S spins. Because of the nuclear permutation symmetry of the ILRR (Sec. II C), the $\widehat{R}^{\rm dil}_{1,IS}$ and $\widehat{R}^{\rm dil}_{1,ISP}$ profiles are unaffected by this permutation. For the permuted geometry (drawn below the original geometry in Fig. 4), we therefore display only the $\widehat{R}^{\rm dil}_{1,I}$ profile (dashed).

The mean survival time $\tau_{\rm A} = 1$ μs for the panels in the left column of Fig. 4, whereas $\tau_{\rm A} = 100$ μs for the panels in the right column. These $\tau_{\rm A}$ values are in the range typically found for internal water molecules and labile protons in globular

proteins.[17] Because $\omega_{D,IS}\,\tau_A = 0.1$ in the left column, these dispersion profiles can be rationalized almost quantitatively with the aid of BWR theory (Sec. III). On the other hand, since $\omega_{D,IS}\,\tau_A = 10$ in the right column, these dispersion profiles are nearly in the USM limit with respect to the I–S dipole coupling, but not always for the other dipole couplings.

We examine first how the dispersion profile is affected by internuclear geometry when $\tau_A = 1$ μs (left column of panels). Going from an equilateral triangle (Fig. 4(a)) to an isosceles triangle with $\beta_I = 140°$ and $\beta_S = 20°$ (solid curves in Fig. 4(b), corresponding to the uppermost geometry depicted on the right), so $\omega_{D,SP}$ is ~15% of $\omega_{D,IS} = \omega_{D,IP}$, we find that $\widehat{R}^{dil}_{1,ISP}(0)$ and $\widehat{R}^{dil}_{1,IS}(0)$ are reduced by factors of 0.51 and 0.78, whereas the dispersion shape is nearly unaffected. A twofold reduction of $\widehat{R}^{dil}_{1,ISP}$ is expected in the MN regime if distinct correlations can be neglected, so the three longitudinal magnetizations do not couple with the seven three-spin zero-quantum coherences in $\langle \mathbf{R}^\alpha \rangle$ of Eq. (32), and if $\omega_{D,SP} = 0$, so R^{SS}_{zz} and R^{PP}_{zz} are reduced by a factor 2 and $R^{SP}_{zz} = 0$ (Appendix E[8]).

In contrast, while $\widehat{R}^{dil}_{1,I}(0)$ is only reduced by a factor 0.90, the dispersion shape changes markedly when the static S–P coupling is weakened (Fig. 4(b)). In Fig. 4(a), the secondary dispersion step at $\omega_0 \approx \omega_{D,SP} = 10^5$ rad s^{-1} merges smoothly with the primary dispersion step at $\omega_0 \approx 1/\tau_A = 10^6$ rad s^{-1}. In Fig. 4(b), where $\omega_{D,SP} \approx 1.5 \times 10^4$ rad s^{-1}, the secondary dispersion is downshifted and reduced in magnitude, whereas the primary dispersion step is nearly unaffected since the dipole couplings involving the labile I spin are the same as in Fig. 4(a). Interchanging the I and S spins, so that $\beta_I = 20°$ and $\beta_S = 140°$, has no effect on the $\widehat{R}^{dil}_{1,ISP}$ and $\widehat{R}^{dil}_{1,IS}$ profiles (Sec. II C), but the $\widehat{R}^{dil}_{1,I}$ profile (dashed) changes qualitatively because now the weakened dipole coupling is not the static one.

Next, we consider the isosceles triangle geometry ($\beta_I = \beta_S = 75°$) in Fig. 4(c), where $\omega_{D,IP} = \omega_{D,SP}$ is ~14% of $\omega_{D,IS}$. The $\widehat{R}^{dil}_{1,ISP}(\omega_0)$ profile is strongly affected; relative to Fig. 4(a), $\widehat{R}^{dil}_{1,ISP}(0)$ is reduced by a factor 0.028, a much larger effect than the factor 1/3 expected (for the self-correlations) from removal of two out of three dipole couplings. As already noted, this large reduction of the ILRR is the result of a distinctly biphasic magnetization decay with very slow magnetization transfer from the weakly dipole-coupled spin P. In contrast, making the (nonlabile) P spin remote converts the ISP–IS case to the IS–IS case. Indeed, $\widehat{R}^{dil}_{1,IS}(ISP\text{–}IS)$ in Fig. 4(c) differs by only 0.8 % from $\widehat{R}^{dil}_{1,IS}(IS\text{–}IS)$ in Fig. 2(b). For the ISP–I case, the situation is more complex. Whereas $\widehat{R}^{dil}_{1,I}(ISP\text{–}I)$ closely follows $\widehat{R}^{dil}_{1,I}(IS\text{–}I)$ for $\omega_0 > 10^5$ rad s^{-1}, it does not exhibit the pronounced inverted dispersion step seen in Fig. 2(b). Instead, there is a small bump in the $\widehat{R}^{dil}_{1,I}$ profile due to two small overlapping secondary dispersion steps, one of which is inverted. For this geometry, $\epsilon \approx 1.4$ so the static dipole coupling is neither weak nor strong and the secondary dispersion steps appear at almost the same frequency $\omega_0 \approx \omega_{D,SP} \approx \omega^2_{D,I}\,\tau_A$.

Figure 4(d) shows the dispersion profiles for a right-angled triangle geometry with $\beta_I = 90°$ and $\beta_S = 30°$, making $\omega_{D,IP}$ larger by a factor 5.2 and $\omega_{D,SP}$ smaller by a factor 0.65 as compared to $\omega_{D,IS}$. The relaxation is now dominated by the strongest dipole coupling $\omega_{D,IP}$, which corresponds to a proton-proton separation of 1.3 Å (less than the smallest physically realized proton-proton separation of ~1.5 Å). In contrast to the equilateral triangle geometry in Fig. 4(a), distinct correlations now play an important role for the ISP–ISP profile, reducing $\widehat{R}^{dil}_{1,ISP}(0)$ by 40% in the BWR approximation and strongly coupling the longitudinal magnetizations to the three-spin zero-quantum coherences. As a result, even though the longitudinal auto-mode rates are now much larger (by a factor 14 for R^{II}_{zz} and R^{PP}_{zz} and by a factor 27 for R^{IP}_{zz}), $\widehat{R}^{dil}_{1,ISP}(0)$ is actually somewhat smaller than in Fig. 2(b). In addition, the primary dispersion is slightly upshifted and features a small high-frequency shoulder (hardly visible). In Fig. 4(d) (in contrast to Fig. 4(c)), the $\widehat{R}^{dil}_{1,IS}$ profile happens to be very similar to the $\widehat{R}^{dil}_{1,ISP}$ profile.

Consider now the $\widehat{R}^{dil}_{1,I}$ profiles in Fig. 4(d). The upper geometry corresponds to a weak static dipole coupling ($\epsilon \approx 0.23$), so we observe an inverted secondary dispersion step at $\omega_0 \approx \omega^2_{D,IS}\,\tau_A \approx 3 \times 10^5$ rad s^{-1}. The lower geometry corresponds to a strong static dipole coupling ($\epsilon \approx 36$), yielding a non-inverted secondary dispersion step at $\omega_0 \approx \omega_{D,SP} \approx 5 \times 10^5$ rad s^{-1}, which is hardly visible in Fig. 4(d) because it overlaps with the primary dispersion and because $\widehat{R}^{dil}_{1,I}$ is small (since the fluctuating dipole coupling $\omega_{D,IP}$ is 8-fold smaller than for the upper geometry).

We now consider the effect of internuclear geometry when $\tau_A = 100$ μs (right column of panels in Fig. 4). Since we are nearly in the USM limit, a further increase of τ_A hardly affects the shape of the dispersion profiles. Except for certain special cases (see below), the dispersion shape is much less sensitive to the internuclear geometry in the USM regime than in the MN regime. For example, $\widehat{R}^{dil}_1(0)$ differs by at most a few percent among the geometries in Figs. 4(a) and 4(b). This is also true for $\widehat{R}^{dil}_{1,IS}$ and $\widehat{R}^{dil}_{1,I}$ in Fig. 4(c), although the primary dispersions are slightly down-shifted in frequency as compared to Figs. 4(a) and 4(b). As for $\tau_A = 1$ μs, $\widehat{R}^{dil}_{1,ISP}$ in Fig. 4(c) is strongly suppressed because of slow magnetization transfer from the weakly coupled P spin. The dispersion profiles in Fig. 4(d) vary considerably in shape. The pronounced fine-structure in the $\widehat{R}^{dil}_{1,IS}$ profile (also present, albeit to lesser extent, in the $\widehat{R}^{dil}_{1,ISP}$ profile) is likely related to the (orientation-dependent) eigenfrequencies of the dipolar Liouvillian. If the unphysically strong I–P coupling is made slightly weaker by increasing β_S from 30 to 37°, whereby $\omega_{D,IP} = 2.34 \times 10^5$ rad s^{-1} corresponding to $r_{HH} = 1.69$ Å, the fine-structure almost disappears (blue dashed-dotted curve in Fig. 4(d)).

C. Odd spectral density function

With the exception of the longitudinal auto-mode rates, such as R^{SS}_{zz} and R^{SP}_{zz}, the local relaxation rates involve the odd-valued spectral density function (OSDF) $k(\omega) = \omega_0\,\tau_A\,j(\omega)$ as well as the usual even-valued spectral density function $j(\omega) = \tau_A/[1 + (\omega_0\,\tau_A)^2]$ (Appendix E[8]). We have recently shown that, contrary to conventional wisdom,[1] the OSDF can affect the longitudinal relaxation of a three-spin system

without full nuclear permutation symmetry.[7] It is therefore of some theoretical interest to examine the effect of the OSDF in the three EMOR cases: *ISP–I*, *ISP–IS*, and *ISP–ISP*. Because the spectral density function only appears in the BWR theory, this issue is only relevant in the MN regime.

Figure 5 shows the dispersion of $\widehat{R}^{\rm dil}_{1,ISP}(ISP\text{–}ISP)$ for an isosceles triangle geometry with $\beta_I = 110°$ and $\beta_S = 35°$. The profiles computed from the SLE and BWR theories coincide, as expected since $\omega_{{\rm D},IS}\,\tau_{\rm A} = \omega_{{\rm D},IP}\,\tau_{\rm A} = 0.01$ and $\omega_{{\rm D},SP}\,\tau_{\rm A} \approx 0.002$, so all three dipole couplings are in the MN regime. The upper panel of Fig. 5 shows that, for this internuclear geometry, removal of the OSDF decreases $\widehat{R}^{\rm dil}_{1,ISP}$ by up to 2.5%. Two conditions must be met for the OSDF to influence the longitudinal relaxation of a three-spin system.[7] First, the three spins must be geometrically or dynamically nonequivalent. The three spins are dynamically equivalent in the *ISP–ISP* EMOR model, but they are not geometrically equivalent for the geometry considered in Fig. 5. (The OSDF has no effect on $\widehat{R}^{\rm dil}_{1,ISP}$ for the equilateral geometry examined in Fig. 2.) Second, the OSDF can only have an effect in the dispersive regime, $0.1 \lesssim \omega_0\,\tau_{\rm A} \lesssim 10$, as is evident from Fig. 5. For $\widehat{R}^{\rm dil}_{1,ISP}$, which is governed by the 10×10 odd-parity zero-quantum block of the isotropically averaged relaxation supermatrix $\langle \mathbf{R}^{\alpha} \rangle$ in Eq. (31), the OSDF only appears in the cross-mode rates that couple the seven odd-rank modes with the three even-rank modes.[7] If the OSDF is neglected, it is therefore sufficient in Eq. (31) to invert the odd-rank 7×7 block. Moreover, because the coupling of the three longitudinal modes with the seven zero-quantum coherences is mediated entirely by distinct correlations, the OSDF can only affect $\widehat{R}^{\rm dil}_{1,ISP}$ via the distinct correlations.[7] For the geometry considered in Fig. 5, distinct correlations are seen to make a large (negative) contribution to $\widehat{R}^{\rm dil}_{1,ISP}$, thereby maximizing the OSDF effect.

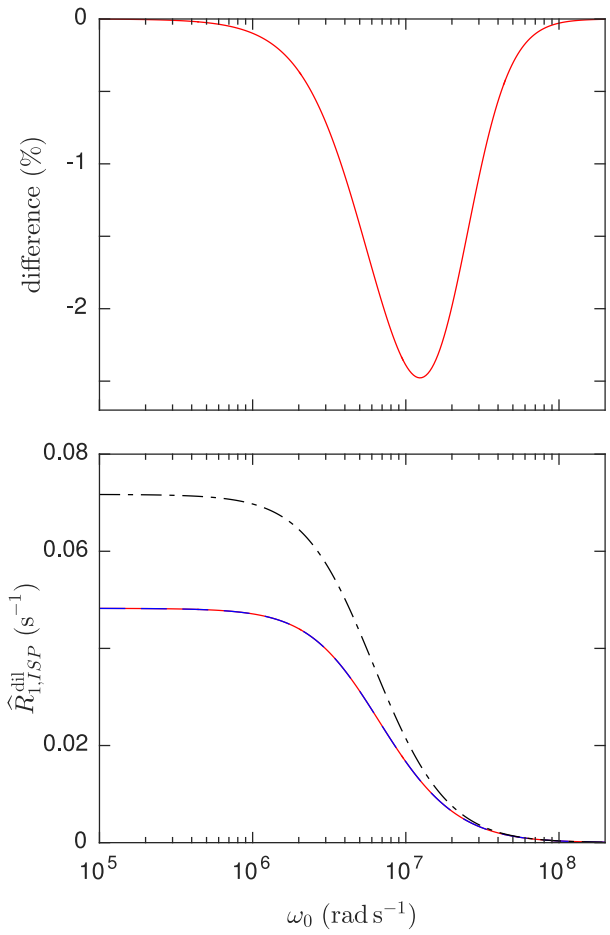

FIG. 5. Dispersion of $\widehat{R}^{\rm dil}_{1,ISP}(ISP\text{–}ISP)$ computed from the SLE theory (red solid curve), from the BWR theory (blue dashed), and from the BWR theory with only self-correlations included (black dashed-dotted). Parameter values: $P_{\rm A} = 10^{-4}$, $\tau_{\rm A} = 10^{-7}$ s, $\omega_{{\rm D},IS} = 10^5$ rad s^{-1}, $\beta_I = 110°$, and $\beta_S = 35°$. The upper panel shows the effect of removing the OSDF $k(\omega)$ as the relative difference $[\widehat{R}^{\rm dil}_{1,ISP}(k=0) - \widehat{R}^{\rm dil}_{1,ISP}(k\neq 0)]/\widehat{R}^{\rm dil}_{1,ISP}(k\neq 0)$, with both rates computed from the BWR theory.

For the *ISP–IS* case, the OSDF has no effect at all on $\widehat{R}^{\rm dil}_{1,IS}$. To demonstrate this, we first note that, if there is an OSDF effect, it must be fully manifested already in the secular approximation, valid for $\omega_0\,\tau_{\rm A} \gg (\omega_{\rm D}\,\tau_{\rm A})^2$. This follows because $(\omega_{\rm D}\,\tau_{\rm A})^2 \ll 1$ in the MN regime and $\omega_0\,\tau_{\rm A} \sim 1$ in the dispersive regime (see above). Any OSDF effect on $\widehat{R}^{\rm dil}_{1,IS}$ must therefore by contained in Eq. (39). As seen from Eq. (40), this expression only involves longitudinal auto-mode rates, which are unaffected by the OSDF (Appendix E[8]). Hence, the OSDF cannot affect $\widehat{R}^{\rm dil}_{1,IS}$, as we have also confirmed numerically.

For the *ISP–I* case, the same arguments imply that the OSDF can only affect $\widehat{R}^{\rm dil}_{1,I}$ via the "cross-relaxation" rate Γ^{II}_{zz} in Eq. (46). Since the longitudinal auto-mode rates are unaffected by the OSDF (Appendix E[8]), any OSDF effect must enter via the quantity X in Eq. (47), specifically via the relaxation rates in the 3×3 zero-quantum two-spin-SP relaxation matrix. Figure 6 shows the dispersion of $\widehat{R}^{\rm dil}_{1,I}$ for an equilateral triangle geometry. The profiles computed from the SLE and BWR theories coincide, as expected since $\omega_{\rm D}\,\tau_{\rm A} = 0.01$. As seen from the upper panel (red solid curve), omission of the OSDF increases $\widehat{R}^{\rm dil}_{1,I}$ in the dispersive regime, but only by a tiny amount (at most 14 ppm in this example). To demonstrate that this really is an OSDF effect, we multiplied $k(\omega)$ by a factor of 100. The effect of removing this artificially inflated OSDF (blue dashed-dotted curve in Fig. 6) is qualitatively the same, but more than three orders of magnitude larger than for the true OSDF. The opposite signs of the OSDF effects in Figs. 5 and 6 reflect their different origins: via cross-mode relaxation between odd-rank and even-rank zero-quantum modes for the *ISP–ISP* case, and via the static dipole coupling $\omega_{{\rm D},SP}$ and two-spin rates for the *ISP–I* case. We note also that the OSDF can influence $\widehat{R}^{\rm dil}_{1,I}$ even when the three spins are geometrically equivalent, because they are not dynamically equivalent in the *ISP–I* case.

D. Chemical shifts

For the ISP-ISP case and in the MN regime, chemical shifts increase the ILRR above the frequency, $\omega_{\rm NSD}$, where cross-mode relaxation is largely eliminated (Sec. III D). This behavior is illustrated in Fig. 7 for a nuclear configuration with $\beta_I = 90°$ and $\beta_S = 30°$. For the chosen parameter values, $\omega_{{\rm D},X}\,\tau_{\rm A} \lesssim 0.005$, so all three dipole couplings are in the MN regime. As expected, the profiles computed from

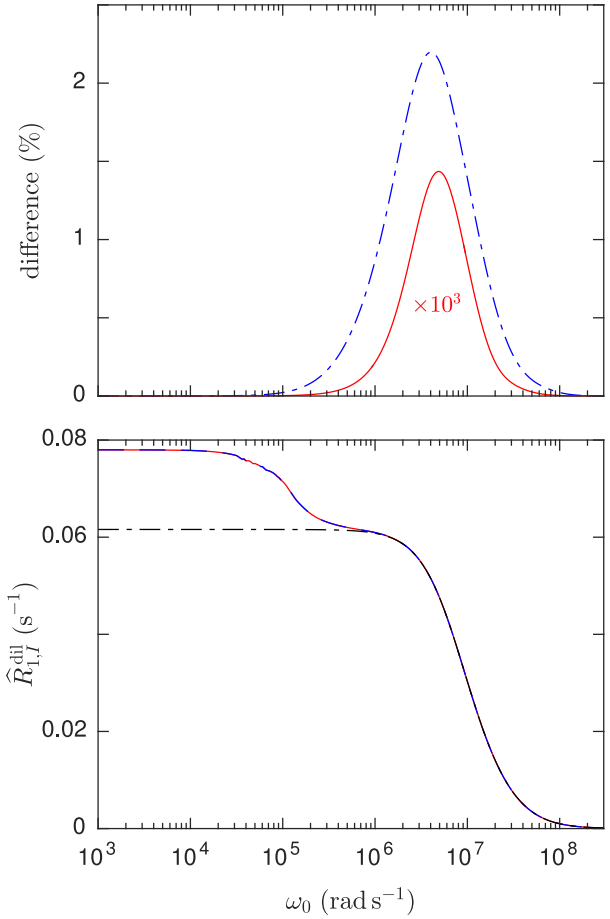

FIG. 6. Dispersion of $\widehat{R}^{\rm dil}_{1,I}(ISP\text{–}I)$ computed from the SLE theory (red solid curve), from the BWR theory (blue dashed), and from the BWR theory in the secular approximation (black dashed-dotted). Parameter values: $P_{\rm A}=10^{-4}$, $\tau_{\rm A}=10^{-7}$ s, $\omega_{\rm D}=10^5$ rad s^{-1}, and $\beta_I=\beta_S=60°$ (equilateral triangle). The upper panel shows the effect of removing the OSDF $k(\omega)$ as the relative difference $[\widehat{R}^{\rm dil}_{1,I}(k=0)-\widehat{R}^{\rm dil}_{1,I}(k\neq 0)]/\widehat{R}^{\rm dil}_{1,I}(k\neq 0)$, with both rates computed from the BWR theory in the secular approximation. The resulting curve (red solid) has been multiplied by a factor of 10^3. Also shown (blue dashed-dotted curve) is the percent relative difference $[\widehat{R}^{\rm dil}_{1,I}(k=0)-\widehat{R}^{\rm dil}_{1,I}(100\,k)]/\widehat{R}^{\rm dil}_{1,I}(100\,k)$, where $k(\omega)$ has been artificially multiplied by a factor of 100.

the generalized BWR theory (Sec. III D, Appendix G)[8] coincide with the profiles computed from the SLE theory, which incorporates the full effect of chemical shifts. For the internuclear geometry examined in Fig. 7, cross-mode relaxation is almost completely abolished even for modest shifts, so that, for $\omega_0 \gg \omega_{\rm NSD}$, $\widehat{R}^{\rm dil}_{1,ISP}$ nearly coincides with the ILRR $\widehat{R}^{\rm dil,self}_{1,ISP}$ induced solely by self-correlations.

This is true for most other geometries, but for the equilateral triangle geometry, chemical shifts only eliminate 60% of the cross-mode contribution to $\widehat{R}^{\rm dil}_{1,ISP}$. (Due to the small cross-mode contribution for that geometry, the shift effect is merely 0.4%, other parameters being the same as in Fig. 7.)

For the dispersion profile in Fig. 7 pertaining to equal shifts in states A and B, the secondary dispersion step exhibits two substeps, corresponding to NSD frequencies of $\sim 10^3$ and $\sim 2\times 10^4$ rad s^{-1}, as predicted by Eq. (50) for the I–S

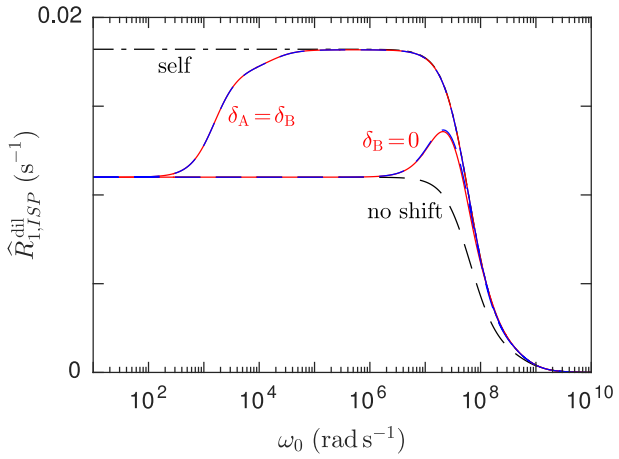

FIG. 7. Dispersion of $\widehat{R}^{\rm dil}_{1,ISP}(ISP\text{–}ISP)$ computed from the SLE theory (red solid curves), from the generalized BWR theory (blue dashed), and from the BWR theory without shifts (black dashed) and with only self-correlations (black dashed-dotted). Parameter values: $P_{\rm A}=10^{-4}$, $\tau_{\rm A}=10^{-8}$ s, $\omega_{{\rm D},IS}=10^5$ rad s^{-1}, $\beta_I=90°$, $\beta_S=30°$, $\delta_S=5$ ppm, and $\delta_P=10$ ppm. The superimposed SLE- and BWR-derived profiles were computed with the same shifts in states A and B ($\delta^{\rm A}=\delta^{\rm B}$) or with no shifts in state B ($\delta^{\rm B}=0$).

and I–P dipole couplings, respectively, adopted here. Also in accordance with Eq. (50), the secondary dispersion is upshifted by a factor $1/P_{\rm A}=10^4$ when the shifts are removed from state B (Fig. 7).

Within the MN regime, the chemical shift effect on the $\widehat{R}^{\rm dil}_{1,ISP}$ dispersion profile becomes negligibly small when $\omega_{\rm NSD}\,\tau_{\rm A}\gg 1$, or, for equal shifts in states A and B, when $\delta \ll P_{\rm A}\,(\omega_{\rm D}\,\tau_{\rm A})^2$ (Sec. III D). For $P_{\rm A}=10^{-3}$, $\omega_{\rm D}\approx 10^5$ rad s^{-1}, and chemical shifts of order 10 ppm, we thus expect the chemical shift effect to be negligible for $\tau_{\rm A}\gg 10^{-6}$ s. Although this prediction is strictly valid only within the MN regime, Fig. 8 shows that it is consistent with the (exact) SLE-based results.

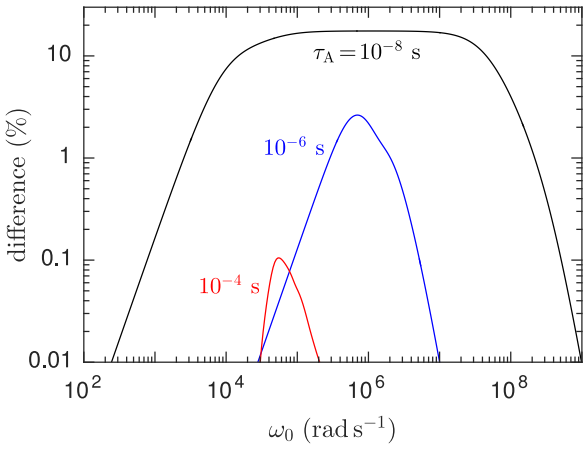

FIG. 8. Relative difference, $[\widehat{R}_{1,ISP}(\omega_0,\delta_S,\delta_P)-\widehat{R}_{1,ISP}(\omega_0,0,0)]/\widehat{R}_{1,ISP}(0,0,0)$, of the ISP–ISP ILRR with and without chemical shifts, computed from the SLE theory. Parameter values: $P_{\rm A}=10^{-3}$, $\omega_{{\rm D},IS}=10^5$ rad s^{-1}, $\beta_I=80°$, $\beta_S=40°$, $\delta_S=5$ ppm, $\delta_P=10$ ppm (same shifts in states A and B), and $\tau_{\rm A}=10^{-8}$ s, 10^{-6} s, or 10^{-4} s.

In Appendix G,[8] we show that chemical shifts have no significant effect for the asymmetric exchange cases ISP–IS and ISP–I as long as we are in the MN regime. Calculations based on the SLE theory confirm that this is true also outside the MN regime, the relative shift effect being less than 0.01% in all examined cases.

V. CONCLUSIONS

In Papers I and II, the general non-perturbative stochastic theory of longitudinal relaxation by the dipolar EMOR mechanism[5] was implemented for two-spin systems with symmetric (IS–IS) and asymmetric (IS–I) exchange, respectively. Here, we have implemented the theory for three-spin systems with symmetric (ISP–ISP) or asymmetric (ISP–IS and ISP–I) exchange. The theory is valid for homonuclear as well as heteronuclear spins and for any distribution of labile spins between the anisotropic (A) sites and the isotropic bulk (B) state. However, because water-proton relaxation in tissue-like systems is arguably the most important application of the dipolar EMOR theory, our theoretical analysis emphasizes homonuclear spin systems in the dilute regime ($P_\mathrm{A} \ll 1$). Within this realm, the three examined exchange cases might describe a protein-bound H_3O^+ ion (ISP–ISP), an internal H_2O molecule with a nearby nonlabile proton (ISP–IS), or a labile O–H or N–H proton with two nearby nonlabile protons (ISP–I).

A substantial part of the present study concerns the development of a perturbation (BWR) theory for the three-spin dipolar EMOR model. The semi-analytical results obtained for this limiting form of the general (SLE-based) theory reveal explicitly how the various features of the relaxation dispersion profile emerge from the interplay of the Larmor frequency (including chemical shifts), the static dipole coupling (in the ISP–I case), and specific elements of the local relaxation supermatrix, including cross-spin and cross-mode relaxation rates. Apart from the primary dispersion step at $\omega_0 \approx 1/\tau_\mathrm{A}$, three kinds of secondary dispersion step can appear. (1) For the ISP–IS case and the ISP–I case with a weak static dipole coupling, an inverted secondary dispersion appears at $\omega_0 \approx \omega_{\mathrm{D},I}^2\,\tau_\mathrm{A}$ because of nonsecular decoupling of longitudinal-transverse cross-mode relaxation. (2) For the ISP–I case with a strong static dipole coupling, a (non-inverted) secondary dispersion appears at $\omega_0 \approx \omega_{\mathrm{D},SP}$, primarily due to decoupling of the nonsecular parts of the static dipole coupling and the two-spin relaxation matrix. (3) For the ISP–ISP case, an inverted secondary dispersion step appears at $\omega_0 \approx \omega_\mathrm{D}^2\,\tau_\mathrm{A}/\delta^\mathrm{A}$ or $P_\mathrm{A}\,\omega_\mathrm{D}^2\,\tau_\mathrm{A}/\delta$ in the presence of chemical shifts.

Compared to our findings for the two-spin system in Papers I and II, the present analysis of the three-spin system has revealed several new phenomena or features:

- Longitudinal relaxation in the MN regime involves in addition to the usual single-spin modes I_z, S_z, and P_z, two-spin modes (ISP–I case), and three-spin modes (ISP–ISP case), and it can therefore not be described by extended Solomon equations.
- Correlations between distinct dipole couplings affect the longitudinal relaxation in the MN regime for the ISP–ISP case (via one-spin/three-spin and three-spin/three-spin rates) and for the ISP–I case (via two-spin/two-spin rates), but not for the ISP–IS case (which only involves one-spin/one-spin rates).
- The shape of the longitudinal relaxation dispersion profile depends on the relative orientation of the internuclear vectors, as well as on their lengths. For some internuclear geometries, the dispersion profile exhibits a fine-structure, particularly pronounced in the USM limit.
- For the ISP–I case, a strong static S–P dipole coupling gives rise to a secondary dispersion at $\omega_0 \approx \omega_{\mathrm{D},SP}$, while removing the inverted secondary dispersion seen at $\omega_0 \approx \omega_{\mathrm{D},I}^2\,\tau_\mathrm{A}$ with a weak (or absent) static dipole coupling. A strong static coupling thus extends the zero-field regime up to $\omega_0 \approx \omega_{\mathrm{D},SP}$.
- The longitudinal relaxation dispersion profile is significantly affected by chemical shifts only in the ISP–ISP case, where an inverted secondary dispersion step appears when the contribution from cross-mode relaxation is (partly) eliminated. Outside the MN regime, the chemical shift effect gradually disappears with increasing τ_A.
- In the region of the primary dispersion step in the MN regime, the OSDF can increase the ILRR by few percent for the ISP–ISP case and decrease it by a few ppm for the ISP–I case. The OSDF is manifested exclusively via distinct correlations and therefore has no effect for the ISP–IS case, which only involves self-correlations.

In a forthcoming final part of this series of papers, we will use the insights gained from our detailed studies of the two-spin and three-spin systems to formulate an approximate theory of longitudinal relaxation by the dipolar EMOR mechanism in multi-spin systems with one or two labile spins, which will then be applied to experimental ^{1}H relaxation data from aqueous protein gels.

ACKNOWLEDGMENTS

This work was financially supported by the Swedish Research Council.

[1]A. Abragam, *The Principles of Nuclear Magnetism* (Clarendon Press, Oxford, 1961).
[2]R. Kubo, J. Math. Phys. **4**, 174 (1963).
[3]R. Kubo, in *Advances in Chemical Physics*, edited by K. E. Shuler (Wiley, New York, 1969), Vol. 15, p. 101.
[4]Z. Chang and B. Halle, J. Chem. Phys. **139**, 144203 (2013), also referred to as Paper I.
[5]Z. Chang and B. Halle, J. Chem. Phys. **144**, 084202 (2016), also referred to as Paper II.
[6]N. R. Skrynnikov and R. R. Ernst, J. Magn. Reson. **137**, 276 (1999).
[7]Z. Chang and B. Halle, J. Chem. Phys. **143**, 234201 (2015).
[8]See supplementary material at http://dx.doi.org/10.1063/1.4955423 for tables of ISTO basis operators (Appendix A); Zeeman Liouvillian supermatrix elements (Appendix B); dipolar Liouvillian supermatrix elements (Appendix C); general ILRR expressions for all cases

(Appendix D); the local relaxation supermatrix in the MN regime (Appendix E); specific ILRR expressions for the the MN regime (Appendix F); chemical shift effects in the MN regime (Appendix G); and the effect of the static dipole coupling for the $ISP - I$ case in the MN regime (Appendix H).

[9]B. Halle, Magn. Reson. Med. **56**, 60 (2006).
[10]F. V. Chávez and B. Halle, Magn. Reson. Med. **56**, 73 (2006).
[11]E. P. Sunde and B. Halle, J. Am. Chem. Soc. **131**, 18214 (2009).
[12]D. M. Brink and G. R. Satchler, *Angular Momentum*, 3rd ed. (Clarendon Press, Oxford, 1994).
[13]N. C. Pyper, Mol. Phys. **21**, 1 (1971).
[14]S. Szymanski, A. M. Gryff-Keller, and G. Binsch, J. Magn. Reson. **68**, 399 (1986).
[15]V. I. Lebedev and D. N. Laikov, Dokl. Math. **59**, 477 (1999).
[16]X.-G. Wang and T. Carrington, J. Theor. Comput. Chem. **2**, 599 (2003).
[17]E. Persson and B. Halle, J. Am. Chem. Soc. **130**, 1774 (2008).

Supplemental Material

Nuclear magnetic relaxation by the dipolar EMOR mechanism: Three-spin systems

Zhiwei Chang and Bertil Halle
Division of Biophysical Chemistry, Department of Chemistry, Lund University, POB 124, SE-22100 Lund, Sweden

APPENDIX A: SPIN OPERATOR BASES

As a basis for three-spin Liouville space, we use the 64 irreducible spherical tensor operators (ISTOs) $T^K_Q(k_I k_S\{\bar{K}\}k_P)$, constructed by two consecutive couplings of the set of four orthonormal single-spin ISTOs for each spin, e.g.,

$$T^0_0(I) \,=\, \frac{1}{\sqrt{2}}\,E_I\,; \quad T^1_0(I) \,=\, \sqrt{2}\,I_z\,; \quad T^1_{\pm1}(I) \,=\, \mp\,I_\pm\,, \tag{A.1}$$

to obtain[1,2]

$$\begin{aligned} T^K_Q(k_I k_S\{\bar{K}\}k_P) \,=\, & (-1)^{k_I-k_S-k_P+\bar{K}+Q}\,(2K+1)^{1/2}(2\bar{K}+1)^{1/2} \\ & \times \sum_{\bar{Q}=-\bar{K}}^{\bar{K}} \sum_{q_I=-k_I}^{k_I} (-1)^{\bar{Q}} \begin{pmatrix} \bar{K} & k_P & K \\ \bar{Q} & Q-\bar{Q} & -Q \end{pmatrix} \begin{pmatrix} k_I & k_S & \bar{K} \\ q_I & \bar{Q}-q_I & -\bar{Q} \end{pmatrix} \\ & \times\, T^{k_I}_{q_I}(I)\, T^{k_S}_{\bar{Q}-q_I}(S)\, T^{k_P}_{Q-\bar{Q}}(P)\,, \end{aligned} \tag{A.2}$$

where $\bar{K}$ is the rank of the intermediate tensor operator obtained by first coupling spins I and S. Here, and in the following, the rank superscript is written in upper case for ISTOs that are normalized in three-spin Liouville space and in lower case for ISTOs that are normalized in single-spin Liouville space. The ISTOs $T^2_M(X)$ appearing in the dipolar Hamiltonian (3) belong to this basis set; e.g., $T^2_0(IS) = T^2_0(11\{2\}0) = (3I_zS_z - \boldsymbol{I}\cdot\boldsymbol{S})/\sqrt{3}$. The 63 basis operators (excluding the identity operator) listed in Tables S1 A – D are used to describe the three-spin system in state A and, in the symmetric case $ISP{-}ISP$, also in state B. For the asymmetric case $ISP{-}IS$, where state B only contains two spins, we use a basis comprising the 15 operators in Tables S1 A – D with $k_P = 0$. For convenience, these 15 operators are collected in Table S2. For the asymmetric case $ISP{-}I$, where state B only contains one spin, we use a basis comprising the 3 operators in Tables S1 A – C with $k_S = k_P = 0$. For convenience, these 3 operators are collected in Table S3. All the operators in Tables S1 – S3 are normalized in the same three-spin Liouville space. For example, $(B_1|B_1) = \frac{1}{2}\,(I_z|I_z) = \frac{1}{2}\,\mathrm{Tr}\{I_z^2\} = \frac{1}{2}\,\mathrm{Tr}_I\{I_z^2\} \times \mathrm{Tr}_S\{E_S\} \times \mathrm{Tr}_P\{E_P\} = \frac{1}{2} \times \frac{1}{2} \times 2 \times 2 = 1$.

TABLE S1 A. Spin basis operators $B_n = T_0^K(k_I k_S\{\bar{K}\}k_P)$ for three spins ISP.

n	K	k_I	k_S	k_P	$\bar{K}$	$\mathcal{W}^a$	$B_n^{b,c}$
1	1	1	0	0	1	$-$	$\frac{1}{\sqrt{2}}\, I_z$
2	1	0	1	0	1	$-$	$\frac{1}{\sqrt{2}}\, S_z$
3	1	0	0	1	0	$-$	$\frac{1}{\sqrt{2}}\, P_z$
4	1	1	1	1	0	$-$	$-\frac{2\sqrt{6}}{3}\, (\boldsymbol{I}\cdot\boldsymbol{S})\, P_z$
5	1	1	1	1	1	$-$	$\sqrt{2}\,[I_z(\boldsymbol{S}\cdot\boldsymbol{P}) - S_z(\boldsymbol{I}\cdot\boldsymbol{P})]$
6	1	1	1	1	2	$-$	$\frac{2}{\sqrt{30}}\,[2\, P_z(\boldsymbol{I}\cdot\boldsymbol{S}) - 3\, I_z(\boldsymbol{S}\cdot\boldsymbol{P}) - 3\, S_z(\boldsymbol{I}\cdot\boldsymbol{P})]$
7	3	1	1	1	2	$-$	$\frac{2}{\sqrt{5}}\,[5\, I_z S_z P_z - I_z(\boldsymbol{S}\cdot\boldsymbol{P}) - S_z(\boldsymbol{I}\cdot\boldsymbol{P}) - P_z(\boldsymbol{I}\cdot\boldsymbol{S})]$
8	0	1	1	1	1	$-$	$-i\,\frac{2}{\sqrt{3}}\,(\boldsymbol{I}\times\boldsymbol{S})\cdot\boldsymbol{P}$
9	2	1	1	1	1	$-$	$i\,\frac{2}{\sqrt{6}}\,(\boldsymbol{I}\times\boldsymbol{S})\cdot(3\, P_z\, \boldsymbol{e}_z - \boldsymbol{P})$
10	2	1	1	1	2	$-$	$i\,\sqrt{2}\,[I_z\,(\boldsymbol{S}\times\boldsymbol{P}) + S_z\,(\boldsymbol{I}\times\boldsymbol{P})]\cdot\boldsymbol{e}_z$
11	0	1	1	0	0	$+$	$-\frac{2}{\sqrt{6}}\, \boldsymbol{I}\cdot\boldsymbol{S}$
12	0	1	0	1	1	$+$	$-\frac{2}{\sqrt{6}}\, \boldsymbol{I}\cdot\boldsymbol{P}$
13	0	0	1	1	1	$+$	$-\frac{2}{\sqrt{6}}\, \boldsymbol{S}\cdot\boldsymbol{P}$
14	2	1	1	0	2	$+$	$\frac{1}{\sqrt{3}}\,[3\, I_z S_z - \boldsymbol{I}\cdot\boldsymbol{S}]$
15	2	1	0	1	1	$+$	$\frac{1}{\sqrt{3}}\,[3\, I_z P_z - \boldsymbol{I}\cdot\boldsymbol{P}]$
16	2	0	1	1	1	$+$	$\frac{1}{\sqrt{3}}\,[3\, S_z P_z - \boldsymbol{S}\cdot\boldsymbol{P}]$
17	1	1	1	0	1	$+$	$i\,(\boldsymbol{I}\times\boldsymbol{S})\cdot\boldsymbol{e}_z$
18	1	1	0	1	1	$+$	$i\,(\boldsymbol{I}\times\boldsymbol{P})\cdot\boldsymbol{e}_z$
19	1	0	1	1	1	$+$	$i\,(\boldsymbol{S}\times\boldsymbol{P})\cdot\boldsymbol{e}_z$

[a] Parity of B_n under spin inversion conjugation. [b] Identity operators have been omitted.

[c] $\boldsymbol{e}_z$ denotes the unit vector along the z axis.

TABLE S1 B. Spin basis operators $B_n = T_1^K(k_I k_S\{\bar{K}\}k_P)$ for three spins ISP.

n	K	k_I	k_S	k_P	$\bar{K}$	$\mathcal{W}^a$	B_n^b
20	1	1	0	0	1	−	$-\frac{1}{2}\,I_+$
21	1	0	1	0	1	−	$-\frac{1}{2}\,S_+$
22	1	0	0	1	0	−	$-\frac{1}{2}\,P_+$
23	1	1	1	1	0	−	$\frac{2}{\sqrt{3}}\,(\boldsymbol{I}\cdot\boldsymbol{S})\,P_+$
24	1	1	1	1	1	−	$(I_zS_+ - I_+S_z)\,P_z + \frac{1}{2}\,(I_-S_+ - I_+S_-)\,P_+$
25	1	1	1	1	2	−	$\frac{\sqrt{3}}{\sqrt{5}}\,[(I_zS_+ + I_+S_z)\,P_z + I_+S_+P_- - I_zS_zP_+ + \frac{1}{3}(\boldsymbol{I}\cdot\boldsymbol{S})\,P_+]$
26	2	1	1	1	1	−	$(I_zS_+ - I_+S_z)\,P_z - \frac{1}{2}\,(I_-S_+ - I_+S_-)\,P_+$
27	2	1	1	1	2	−	$\frac{\sqrt{3}}{6}\,[(4\,I_zS_z - I_+S_- - I_-S_+)\,P_+ + 2\,I_+S_+P_- - 2\,(I_zS_+ + I_+S_z)\,P_z]$
28	3	1	1	1	2	−	$-\frac{1}{\sqrt{15}}\,[(4\,I_zS_z - I_+S_- - I_-S_+)\,P_+ - I_+S_+P_- + 4\,(I_zS_+ + I_+S_z)\,P_z]$
29	1	1	1	0	1	+	$\frac{1}{\sqrt{2}}\,(I_zS_+ - I_+S_z)$
30	1	1	0	1	1	+	$\frac{1}{\sqrt{2}}\,(I_zP_+ - I_+P_z)$
31	1	0	1	1	1	+	$\frac{1}{\sqrt{2}}\,(S_zP_+ - S_+P_z)$
32	2	1	1	0	2	+	$-\frac{1}{\sqrt{2}}\,(I_zS_+ + I_+S_z)$
33	2	1	0	1	1	+	$-\frac{1}{\sqrt{2}}\,(I_zP_+ + I_+P_z)$
34	2	0	1	1	1	+	$-\frac{1}{\sqrt{2}}\,(S_zP_+ + S_+P_z)$

[a] Parity of B_n under spin inversion conjugation. [b] Identity operators have been omitted.

TABLE S1 C. Spin basis operators $B_n = T^K_{-1}(k_I k_S \{\bar{K}\} k_P)$ for three spins ISP.

n	K	k_I	k_S	k_P	$\bar{K}$	$\mathcal{W}^a$	B_n^b
35	1	1	0	0	1	$-$	$\frac{1}{2}\, I_-$
36	1	0	1	0	1	$-$	$\frac{1}{2}\, S_-$
37	1	0	0	1	0	$-$	$\frac{1}{2}\, P_-$
38	1	1	1	1	0	$-$	$-\frac{2}{\sqrt{3}}\, (\boldsymbol{I}\cdot\boldsymbol{S})\, P_-$
39	1	1	1	1	1	$-$	$-(I_z S_- - I_- S_z)\, P_z + \frac{1}{2}\, (I_- S_+ + I_+ S_-)\, P_-$
40	1	1	1	1	2	$-$	$-\frac{\sqrt{3}}{\sqrt{5}}\, [(I_z S_- + I_- S_z)\, P_z + I_- S_- P_+ - I_z S_z P_- + \frac{1}{3}(\boldsymbol{I}\cdot\boldsymbol{S})\, P_-]$
41	2	1	1	1	1	$-$	$(I_z S_- - I_- S_z)\, P_z + \frac{1}{2}\, (I_- S_+ - I_+ S_-)\, P_-$
42	2	1	1	1	2	$-$	$\frac{\sqrt{3}}{6}\, [(4\, I_z S_z - I_+ S_- - I_- S_+)\, P_- + 2\, I_- S_- P_+ - 2\, (I_z S_- + I_- S_z)\, P_z]$
43	3	1	1	1	2	$-$	$\frac{1}{\sqrt{15}}\, [(4\, I_z S_z - I_+ S_- - I_- S_+)\, P_- - I_- S_- P_+ + 4\, (I_z S_- + I_- S_z)\, P_z]$
44	1	1	1	0	1	$+$	$\frac{1}{\sqrt{2}}\, (I_z S_- - I_- S_z)$
45	1	1	0	1	1	$+$	$\frac{1}{\sqrt{2}}\, (I_z P_- - I_- P_z)$
46	1	0	1	1	1	$+$	$\frac{1}{\sqrt{2}}\, (S_z P_- - S_- P_z)$
47	2	1	1	0	2	$+$	$\frac{1}{\sqrt{2}}\, (I_z S_- + I_- S_z)$
48	2	1	0	1	1	$+$	$\frac{1}{\sqrt{2}}\, (I_z P_- + I_- P_z)$
49	2	0	1	1	1	$+$	$\frac{1}{\sqrt{2}}\, (S_z P_- + S_- P_z)$

[a] Parity of B_n under spin inversion conjugation. [b] Identity operators have been omitted.

TABLE S1 D. Spin basis operators $B_n = T^K_Q(k_I k_S\{\bar{K}\}k_P)$ with $Q = \pm 2$ or ± 3 for three spins ISP.

n	Q	K	k_I	k_S	k_P	$\bar{K}$	$\mathcal{W}^a$	B_n^b
50	2	2	1	1	1	1	$-$	$-(I_zS_+ - I_+S_z)\,P_+$
51	2	2	1	1	1	2	$-$	$\frac{1}{\sqrt{3}}\left[2\,I_+S_+P_z - (I_zS_+ + I_+S_z)\,P_+\right]$
52	2	3	1	1	1	2	$-$	$\frac{\sqrt{6}}{3}\left[I_+S_+P_z + (I_zS_+ + I_+S_z)\,P_+\right]$
53	2	2	1	1	0	2	$+$	$\frac{1}{\sqrt{2}}\,I_+S_+$
54	2	2	1	0	1	1	$+$	$\frac{1}{\sqrt{2}}\,I_+P_+$
55	2	2	0	1	1	1	$+$	$\frac{1}{\sqrt{2}}\,S_+P_+$
56	-2	2	1	1	1	1	$-$	$(I_zS_- - I_- + S_z)\,P_-$
57	-2	2	1	1	1	2	$-$	$-\frac{1}{\sqrt{3}}\left[2\,I_-S_-P_z - (I_zS_- + I_- + S_z)\,P_-\right]$
58	-2	3	1	1	1	2	$-$	$\frac{\sqrt{6}}{3}\left[I_-S_-P_z + (I_zS_- + I_-S_z)\,P_-\right]$
59	-2	2	1	1	0	2	$+$	$\frac{1}{\sqrt{2}}\,I_-S_-$
60	-2	2	1	0	1	1	$+$	$\frac{1}{\sqrt{2}}\,I_-P_-$
61	-2	2	0	1	1	1	$+$	$\frac{1}{\sqrt{2}}\,S_-P_-$
62	3	3	1	1	1	2	$-$	$-I_+S_+P_+$
63	-3	3	1	1	1	2	$-$	$I_-S_-P_-$

[a] Parity of B_n under spin inversion conjugation. [b] Identity operators have been omitted.

TABLE S2. Spin basis operators $B_n = T^K_Q(k_I k_S)$ for two spins IS.

n	Q	K	k_I	k_S	$\mathcal{W}^a$	B_n[b,c]
1	0	1	1	0	$-$	$\frac{1}{\sqrt{2}}\, I_z$
2	0	1	0	1	$-$	$\frac{1}{\sqrt{2}}\, S_z$
3	0	0	1	1	$+$	$-\frac{2}{\sqrt{6}}\, \boldsymbol{I}\cdot\boldsymbol{S}$
4	0	1	1	1	$+$	$i\,(\boldsymbol{I}\times\boldsymbol{S})\cdot\boldsymbol{e}_z$
5	0	2	1	1	$+$	$\frac{1}{\sqrt{3}}\,(3\, I_z\, S_z\, -\, \boldsymbol{I}\cdot\boldsymbol{S})$
6	1	1	1	0	$-$	$-\frac{1}{2}\, I_+$
7	1	1	0	1	$-$	$-\frac{1}{2}\, S_+$
8	1	1	1	1	$+$	$\frac{1}{\sqrt{2}}\,(I_z\, S_+ - I_+\, S_z)$
9	1	2	1	1	$+$	$-\frac{1}{\sqrt{2}}\,(I_z\, S_+ + I_+\, S_z)$
10	-1	1	1	0	$-$	$\frac{1}{2}\, I_-$
11	-1	1	0	1	$-$	$\frac{1}{2}\, S_-$
12	-1	1	1	1	$+$	$\frac{1}{\sqrt{2}}\,(I_z\, S_- - I_-\, S_z)$
13	-1	2	1	1	$+$	$\frac{1}{\sqrt{2}}\,(I_z\, S_- + I_-\, S_z)$
14	2	2	1	1	$+$	$\frac{1}{\sqrt{2}}\, I_+\, S_+$
15	-2	2	1	1	$+$	$\frac{1}{\sqrt{2}}\, I_-\, S_-$

[a] Parity of B_n under spin inversion conjugation. [b] Identity operators have been omitted.

[c] The operators B_n are normalized in the three-spin Liouville space.

TABLE S3. Spin basis operators $B_n = T^K_Q$ for a single spin I.

n	Q	K	B_n[a,b]
1	0	1	$\frac{1}{\sqrt{2}}\, I_z$
2	1	1	$-\frac{1}{2}\, I_+$
3	-1	1	$\frac{1}{2}\, I_-$

[a] Identity operators have been omitted.

[b] The operators B_n are normalized in the three-spin Liouville space.

APPENDIX B: ZEEMAN SUPERMATRIX

Here we calculate the supermatrix representation of the Zeeman Liouvillian $\mathcal{L}_{\mathrm{Z}} = [H_{\mathrm{Z}},\ ]$ in the ISTO basis of Table S1. To this end, we first consider the matrix representation of the superoperator $\mathcal{I}_z = [I_z,\ ]$, that is,

$$\begin{aligned}
&\left(T_Q^K(k_I k_S\{\bar{K}\}k_P)\,|\,\mathcal{I}_z\,|\,T_{Q'}^{K'}(k_I' k_S'\{\bar{K}'\}k_P')\right)\\
&=\sqrt{2}\left[\left(T_Q^K(k_I k_S\{\bar{K}\}k_P)\,|\,T_0^1(10(1)0)\,|\,T_{Q'}^{K'}(k_I' k_S'\{\bar{K}'\}k_P')\right)\right.\\
&\left.-\left(T_Q^K(k_I k_S\{\bar{K}\}k_P)\,|\,T_{Q'}^{K'}(k_I' k_S'\{\bar{K}'\}k_P')\,|\,T_0^1(10(1)0)\right)\right].
\end{aligned}\tag{B.1}$$

Regarding the coupled I and S spins as a composite system, we can write this as

$$\begin{aligned}
&\left(T_Q^K(k_I k_S\{\bar{K}\}k_P)\,|\,\mathcal{I}_z\,|\,T_{Q'}^{K'}(k_I' k_S'\{\bar{K}'\}k_P')\right)\\
&=\sqrt{2}\left[\left(T_Q^K(\bar{K}k_P)\,|\,T_0^1(10)\,|\,T_{Q'}^{K'}(\bar{K}'k_P')\right)-\left(T_Q^K(\bar{K}k_P)\,|\,T_{Q'}^{K'}(\bar{K}'k_P')\,|\,T_0^1(10)\right)\right].
\end{aligned}\tag{B.2}$$

According to the Wigner-Eckart theorem,[1]

$$\begin{aligned}
&\left(T_Q^K(\bar{K}k_P)\,|\,T_0^1(10)\,|\,T_{Q'}^{K'}(\bar{K}'k_P')\right)=\delta_{QQ'}\,(-1)^{K-Q}\begin{pmatrix}K & 1 & K'\\ -Q & 0 & Q\end{pmatrix}\\
&\times(2K+1)^{1/2}\left\langle T^K(\bar{K}k_P)\,||\,T^1(10)\,||\,T^{K'}(\bar{K}'k_P')\right\rangle,
\end{aligned}\tag{B.3}$$

and

$$\begin{aligned}
&\left(T_Q^K(\bar{K}k_P)\,|\,T_{Q'}^{K'}(\bar{K}'k_P')\,|\,T_0^1(10)\right)=\delta_{QQ'}\,(-1)^{K-Q}\begin{pmatrix}K & K' & 1\\ -Q & Q & 0\end{pmatrix}\\
&\times(2K+1)^{1/2}\left\langle T^K(\bar{K}k_P)\,||\,T^{K'}(\bar{K}'k_P')\,||\,T^1(10)\right\rangle.
\end{aligned}\tag{B.4}$$

The reduced supermatrix elements can be expressed as[1]

$$\begin{aligned}
&\left\langle T^K(\bar{K}k_P)\,||\,T^1(10)||\,T^{K'}(\bar{K}'k_P')\right\rangle=\left[3\,(2K'+1)\,(2\bar{K}+1)\,(2k_P+1)\right]^{1/2}\\
&\times\begin{Bmatrix}K & K' & 1\\ \bar{K} & \bar{K}' & 1\\ k_P & k_P' & 0\end{Bmatrix}\left\langle T^{\bar{K}}(k_I k_S)\,||\,T^1(10)\,||\,T^{\bar{K}'}(k_I' k_S')\right\rangle\left\langle k_P\,||\,T^0(P)\,||\,k_P'\right\rangle,
\end{aligned}\tag{B.5}$$

and

$$\begin{aligned}
&\left\langle T^K(\bar{K}k_P)\,||\,T^{K'}(\bar{K}'k_P')\,||\,T^1(10)\right\rangle=\left[3\,(2K'+1)\,(2\bar{K}+1)\,(2k_P+1)\right]^{1/2}\\
&\times\begin{Bmatrix}K & 1 & K'\\ \bar{K} & 1 & \bar{K}'\\ k_P & 0 & k_P'\end{Bmatrix}\left\langle T^{\bar{K}}(k_I k_S)\,||\,T^{\bar{K}'}(k_I' k_S')\,||\,T^1(10)\right\rangle\left\langle k_P\,||\,T^{k_P'}(P)\,||\,0\right\rangle.
\end{aligned}\tag{B.6}$$

Note that the argument (10) in $T^1(10)$ refers to $(\bar{K}k_P)$ in Eqs. (B.2) – (B.4) and on the left-hand side of Eqs. (B.5) and (B.6), but to $(k_I k_S)$ on the right-hand side of Eqs. (B.5) and (B.6).

The single-spin reduced supermatrix elements in Eqs. (B.5) and (B.6) can be expressed in terms of a $6j$ symbol as[1]

$$\begin{aligned}\left\langle k_P \,||\, T^0(P) \,||\, k'_P \right\rangle &= \left\langle k_P \,||\, T^{k'_P}(P) \,||\, 0 \right\rangle \\ &= (-1)^{k'_P+1} \, (2k'_P+1)^{1/2} \left\{ \begin{array}{ccc} k_P & k'_P & 0 \\ \frac{1}{2} & \frac{1}{2} & \frac{1}{2} \end{array} \right\} .\end{aligned} \tag{B.7}$$

The two-spin reduced supermatrix elements in Eqs. (B.5) and (B.6) can be expressed in terms of single-spin reduced supermatrix elements, as in Eqs. (B.5) and (B.6),

$$\begin{aligned}\left\langle T^{\bar{K}}(k_I k_S) \,||\, T^1(10) || \, T^{\bar{K}'}(k'_I k'_S) \right\rangle &= \left[3\,(2\bar{K}'+1)\,(2k_I+1)\,(2k_S+1)\right]^{1/2} \\ \times \left\{ \begin{array}{ccc} \bar{K} & \bar{K}' & 1 \\ k_I & k'_I & 1 \\ k_S & k'_S & 0 \end{array} \right\} &\left\langle k_I \,||\, T^1(I) \,||\, k'_I \right\rangle \left\langle k_S \,||\, T^0(S) \,||\, k'_S \right\rangle ,\end{aligned} \tag{B.8}$$

and

$$\begin{aligned}\left\langle T^{\bar{K}}(k_I k_S) \,||\, T^{\bar{K}'}(k'_I k'_S) \,||\, T^1(10) \right\rangle &= \left[3\,(2\bar{K}'+1)\,(2k_I+1)\,(2k_S+1)\right]^{1/2} \\ \times \left\{ \begin{array}{ccc} \bar{K} & 1 & \bar{K}' \\ k_I & 1 & k'_I \\ k_S & 0 & k'_S \end{array} \right\} &\left\langle k_I \,||\, T^{k'_I}(I) \,||\, 1 \right\rangle \left\langle k_S \,||\, T^{k'_S}(S) \,||\, 0 \right\rangle .\end{aligned} \tag{B.9}$$

The single-spin reduced supermatrix elements in Eqs. (B.8) and (B.9) can be expressed in terms of $6j$ symbols as

$$\begin{aligned}\left\langle k_I \,||\, T^1(I) \,||\, k'_I \right\rangle \left\langle k_S \,||\, T^0(S) \,||\, k'_S \right\rangle &= \left\langle k_I \,||\, T^{k'_I}(I) \,||\, 1 \right\rangle \left\langle k_S \,||\, T^{k'_S}(S) \,||\, 0 \right\rangle \\ = \; (-1)^{k'_I+k'_S+1} \, \left[3\,(2k'_I+1)(2k'_S+1)\right]^{1/2} &\left\{ \begin{array}{ccc} k_I & k'_I & 1 \\ \frac{1}{2} & \frac{1}{2} & \frac{1}{2} \end{array} \right\} \left\{ \begin{array}{ccc} k_S & k'_S & 0 \\ \frac{1}{2} & \frac{1}{2} & \frac{1}{2} \end{array} \right\} .\end{aligned} \tag{B.10}$$

Combining Eqs. (B.2) – (B.10) and using the symmetries of the Wigner $3j$, $6j$ and $9j$ symbols with respect to column permutations,[1] we find

$$\begin{aligned}\left(T^K_Q(k_I k_S\{\bar{K}\}k_P) \,|\, \mathcal{I}_z \,|\, T^{K'}_{Q'}(k'_I k'_S\{\bar{K}'\}k'_P) \right) &= \delta_{QQ'} \, (-1)^{K'-Q+1} \, \Delta \, W \\ \times \left(\begin{array}{ccc} K & K' & 1 \\ -Q & Q & 0 \end{array} \right) &\left\{ \begin{array}{ccc} k_I & k'_I & 1 \\ \frac{1}{2} & \frac{1}{2} & \frac{1}{2} \end{array} \right\} \left\{ \begin{array}{ccc} k_S & k'_S & 0 \\ \frac{1}{2} & \frac{1}{2} & \frac{1}{2} \end{array} \right\} \left\{ \begin{array}{ccc} k_P & k'_P & 0 \\ \frac{1}{2} & \frac{1}{2} & \frac{1}{2} \end{array} \right\} \\ \times \left\{ \begin{array}{ccc} \bar{K} & \bar{K}' & 1 \\ k_I & k'_I & 1 \\ k_S & k'_S & 0 \end{array} \right\} &\left\{ \begin{array}{ccc} K & K' & 1 \\ \bar{K} & \bar{K}' & 1 \\ k_P & k'_P & 0 \end{array} \right\} ,\end{aligned} \tag{B.11}$$

where

$$\Delta \;\equiv\; (-1)^{k_I+k_S+k_P} \;+\; (-1)^{k'_I+k'_S+k'_P} , \tag{B.12}$$

and

$$
\begin{aligned}
W \;\equiv\; & 3\,[6\,(2K+1)\,(2K'+1)\,(2\bar{K}+1)\,(2\bar{K}'+1) \\
& \times\,(2k_I+1)\,(2k'_I+1)\,(2k_S+1)\,(2k'_S+1)\,(2k_P+1)\,(2k'_P+1)]^{1/2}\,.
\end{aligned}
\tag{B.13}
$$

Using the identity, for integral a and b,[1]

$$
\left\{ \begin{array}{ccc} a & b & 0 \\ \frac{1}{2} & \frac{1}{2} & \frac{1}{2} \end{array} \right\} \;=\; \delta_{ab}\,\frac{(-1)^{a+1}}{[2\,(2a+1)]^{1/2}}\,, \tag{B.14}
$$

and noting that $k_I,\ k'_I = 0$ or 1, we see that

$$
\Delta \left\{ \begin{array}{ccc} k_S & k'_S & 0 \\ \frac{1}{2} & \frac{1}{2} & \frac{1}{2} \end{array} \right\} \left\{ \begin{array}{ccc} k_P & k'_P & 0 \\ \frac{1}{2} & \frac{1}{2} & \frac{1}{2} \end{array} \right\} \;=\; \delta_{k_I k'_I}\,\delta_{k_S k'_S}\,\delta_{k_P k'_P}\,\frac{(1-2k_I)}{[(2k_S+1)\,(2k_P+1)]^{1/2}}\,. \tag{B.15}
$$

Next, we rewrite the $9j$ symbols in Eq. (B.11) with the aid of the identity[1]

$$
\left\{ \begin{array}{ccc} a & b & c \\ d & e & c \\ g & h & 0 \end{array} \right\} \;=\; \delta_{gh}\,\frac{(-1)^{b+d+g+c}}{[(2c+1)\,(2g+1)]^{1/2}} \left\{ \begin{array}{ccc} a & b & c \\ e & d & g \end{array} \right\}. \tag{B.16}
$$

Combining Eqs. (B.11), (B.15) and (B.16), and noting that, since $k_I = 0$ or 1,

$$
\left\{ \begin{array}{ccc} k_I & k_I & 1 \\ \frac{1}{2} & \frac{1}{2} & \frac{1}{2} \end{array} \right\} \;=\; \delta_{k_I 1}\left(-\frac{1}{3}\right)\,, \tag{B.17}
$$

we obtain

$$
\begin{aligned}
& \Big(T^K_Q(k_I k_S\{\bar{K}\}k_P)\,|\,\mathcal{I}_z\,|\,T^{K'}_{Q'}(k'_I k'_S\{\bar{K}'\}k'_P)\Big) \;=\; \delta_{QQ'}\,\delta_{k_I k'_I}\,\delta_{k_S k'_S}\,\delta_{k_P k'_P}\,\delta_{k_I 1} \\
& \times (-1)^{\bar{K}+\bar{K}'+k_S+k_P-Q}\,[6\,(2K+1)\,(2K'+1)\,(2\bar{K}+1)\,(2\bar{K}'+1)]^{1/2} \\
& \times \left(\begin{array}{ccc} K & K' & 1 \\ -Q & Q & 0 \end{array} \right) \left\{ \begin{array}{ccc} K & K' & 1 \\ \bar{K}' & \bar{K} & k_P \end{array} \right\} \left\{ \begin{array}{ccc} \bar{K} & \bar{K}' & 1 \\ 1 & 1 & k_S \end{array} \right\}.
\end{aligned}
\tag{B.18}
$$

In the same way, we find

$$
\begin{aligned}
& \Big(T^K_Q(k_I k_S\{\bar{K}\}k_P)\,|\,\mathcal{S}_z\,|\,T^{K'}_{Q'}(k'_I k'_S\{\bar{K}'\}k'_P)\Big) \;=\; \delta_{QQ'}\,\delta_{k_I k'_I}\,\delta_{k_S k'_S}\,\delta_{k_P k'_P}\,\delta_{k_S 1} \\
& \times (-1)^{k_I+k_P-Q}\,[6\,(2K+1)\,(2K'+1)\,(2\bar{K}+1)\,(2\bar{K}'+1)]^{1/2} \\
& \times \left(\begin{array}{ccc} K & K' & 1 \\ -Q & Q & 0 \end{array} \right) \left\{ \begin{array}{ccc} K & K' & 1 \\ \bar{K}' & \bar{K} & k_P \end{array} \right\} \left\{ \begin{array}{ccc} \bar{K} & \bar{K}' & 1 \\ 1 & 1 & k_I \end{array} \right\},
\end{aligned}
\tag{B.19}
$$

and

$$
\begin{aligned}
& \Big(T^K_Q(k_I k_S\{\bar{K}\}k_P)\,|\,\mathcal{P}_z\,|\,T^{K'}_{Q'}(k'_I k'_S\{\bar{K}'\}k'_P)\Big) \;=\; \delta_{QQ'}\,\delta_{k_I k'_I}\,\delta_{k_S k'_S}\,\delta_{k_P k'_P}\,\delta_{k_P 1}\,\delta_{\bar{K}\bar{K}'} \\
& \times (-1)^{K+K'+k_I+k_S+1-Q}\,[6\,(2K+1)\,(2K'+1)\,(2\bar{K}+1)\,(2k_I+1)]^{1/2} \\
& \times \left(\begin{array}{ccc} K & K' & 1 \\ -Q & Q & 0 \end{array} \right) \left\{ \begin{array}{ccc} K & K' & 1 \\ 1 & 1 & \bar{K} \end{array} \right\} \left\{ \begin{array}{ccc} \bar{K} & \bar{K} & 0 \\ k_I & k_I & k_S \end{array} \right\}.
\end{aligned}
\tag{B.20}
$$

Using the identity[1]

$$\left\{ \begin{array}{ccc} \bar{K} & \bar{K} & 0 \\ k_I & k_I & k_S \end{array} \right\} \;=\; \frac{(-1)^{\bar{K}+k_I+k_S}}{[(2\bar{K}+1)\,(2k_I+1)]^{1/2}}\;, \tag{B.21}$$

we can also rewrite Eq. (B.20) as

$$\begin{aligned} &\left(T^K_Q(k_I k_S\{\bar{K}\}k_P)\,|\,\mathcal{P}_z\,|\,T^{K'}_{Q'}(k'_I k'_S\{\bar{K}'\}k'_P)\right) \;=\; \delta_{QQ'}\,\delta_{k_I k'_I}\,\delta_{k_S k'_S}\,\delta_{k_P k'_P}\,\delta_{k_P 1}\,\delta_{\bar{K}\bar{K}'} \\ &\times(-1)^{K+K'+\bar{K}+1-Q}\,[6\,(2K+1)\,(2K'+1)]^{1/2} \left(\begin{array}{ccc} K & K' & 1 \\ -Q & Q & 0 \end{array} \right) \left\{ \begin{array}{ccc} K & K' & 1 \\ 1 & 1 & \bar{K} \end{array} \right\}, \end{aligned} \tag{B.22}$$

which is independent of I and S except for the Kronecker deltas. Note that the supermatrix elements in Eqs. (B.18) and (B.19) are not simply related by an $I \leftrightarrow S$ interchange, because all basis operators are not invariant under this permutation.

According to Eq. (1), the Zeeman Liouvillian is

$$\mathcal{L}_{\rm Z} \;=\; \omega_I\,(\mathcal{I}_z + \mathcal{S}_z + \mathcal{P}_z) \;+\; \omega_I\,(\delta_S\,\mathcal{S}_z + \delta_P\,\mathcal{P}_z)\;. \tag{B.23}$$

The supermatrix representation of $\mathcal{I}_z + \mathcal{S}_z + \mathcal{P}_z$ is diagonal with the diagonal elements equal to Q, so

$$(n\,|\,\mathcal{L}_{\rm Z}\,|\,n') \;=\; \delta_{nn'}\,\omega_I\,Q \;+\; \omega_I\,[\delta_S\,(n\,|\,\mathcal{S}_z\,|\,n') + \delta_P\,(n\,|\,\mathcal{P}_z\,|\,n')]\;, \tag{B.24}$$

with the matrix elements $(n\,|\,\mathcal{S}_z\,|\,n')$ and $(n\,|\,\mathcal{P}_z\,|\,n')$ given by Eqs. (B.19) and (B.22), respectively. For isochronous spins, with $\delta_S = \delta_P = 0$ so that $\omega_I = \omega_S = \omega_P \equiv \omega_0$,

$$(n\,|\,\mathcal{L}_{\rm Z}\,|\,n') \;=\; \delta_{nn'}\,\omega_0\,Q\;. \tag{B.25}$$

APPENDIX C: DIPOLAR SUPERMATRIX

Here we calculate the supermatrix representation of the dipolar Liouvillian $\mathcal{L}^{\alpha}_{\mathrm{D}} = [H^{\alpha}_{\mathrm{D}},\ ]$ in the ISTO basis of Table S1. According to Eq. (3), the first part of the dipolar Liouvillian, corresponding to the I–S dipole coupling, is

$$\mathcal{L}^{\alpha}_{\mathrm{D},IS} \;=\; -\frac{2}{\sqrt{3}}\,\omega_{\mathrm{D},IS} \sum_{M=-2}^{2} \mathcal{T}^{2}_{M}(11\{2\}0)\; D^{2*}_{M0}(\Omega^{\alpha}_{IS})\,, \tag{C.1}$$

where $\mathcal{T}^{2}_{M} = [T^{2}_{M},\ ]$. We thus consider the matrix element

$$\begin{aligned}\big(n\,|\,\mathcal{T}^{2}_{M}(11\{2\}0)\,|\,n'\big) \;&=\; \Big(T^{K}_{Q}(k_I k_S\{\bar{K}\}k_P)\,|\,T^{2}_{M}(11\{2\}0)\,|\,T^{K'}_{Q'}(k'_I k'_S\{\bar{K}'\}k'_P)\Big)\\ &-\; \Big(T^{K}_{Q}(k_I k_S\{\bar{K}\}k_P)\,|\,T^{K'}_{Q'}(k'_I k'_S\{\bar{K}'\}k'_P)\,|\,T^{2}_{M}(11\{2\}0)\Big)\,.\end{aligned} \tag{C.2}$$

Regarding the coupled I and S spins as a composite system, we can write this as

$$\begin{aligned}\big(n\,|\,\mathcal{T}^{2}_{M}(11\{2\}0)\,|\,n'\big) \;&=\; \Big(T^{K}_{Q}(\bar{K}k_P)\,|\,T^{2}_{M}(20)\,|\,T^{K'}_{Q'}(\bar{K}'k'_P)\Big)\\ &-\; \Big(T^{K}_{Q}(\bar{K}k_P)\,|\,T^{K'}_{Q'}(\bar{K}'k'_P)\,|\,T^{2}_{M}(20)\Big)\,.\end{aligned} \tag{C.3}$$

According to the Wigner-Eckart theorem,[1]

$$\begin{aligned}&\Big(T^{K}_{Q}(\bar{K}k_P)\,|\,T^{2}_{M}(20)\,|\,T^{K'}_{Q'}(\bar{K}'k'_P)\Big) \;=\; \delta_{M,Q-Q'}(-1)^{K-Q}\,(2K+1)^{1/2}\\ &\times\begin{pmatrix} K & 2 & K'\\ -Q & Q-Q' & Q'\end{pmatrix}\Big\langle T^{K}(\bar{K}k_P)\,||\,T^{2}(20)\,||\,T^{K'}(\bar{K}'k'_P)\Big\rangle\,,\end{aligned} \tag{C.4}$$

and

$$\begin{aligned}&\Big(T^{K}_{Q}(\bar{K}k_P)\,|\,T^{K'}_{Q'}(\bar{K}'k'_P)\,|\,T^{2}_{M}(20)\Big) \;=\; \delta_{M,Q-Q'}(-1)^{K-Q}\,(2K+1)^{1/2}\\ &\times\begin{pmatrix} K & K' & 2\\ -Q & Q' & Q-Q'\end{pmatrix}\Big\langle T^{K}(\bar{K}k_P)\,||\,T^{K'}(\bar{K}'k'_P)\,||\,T^{2}(20)\Big\rangle\,.\end{aligned} \tag{C.5}$$

The reduced supermatrix elements can be expressed as[1]

$$\begin{aligned}&\Big\langle T^{K}(\bar{K}k_P)\,||\,T^{2}(20)\,||\,T^{K'}(\bar{K}'k'_P)\Big\rangle \;=\; [5\,(2K'+1)\,(2\bar{K}+1)\,(2k_P+1)]^{1/2}\\ &\times\begin{Bmatrix} K & K' & 2\\ \bar{K} & \bar{K}' & 2\\ k_P & k'_P & 0\end{Bmatrix}\Big\langle T^{\bar{K}}(k_I k_S)\,||\,T^{2}(11)\,||\,T^{\bar{K}'}(k'_I k'_S)\Big\rangle\,\big\langle k_P\,||\,T^{0}(P)\,||\,k'_P\big\rangle\,,\end{aligned} \tag{C.6}$$

and

$$\begin{aligned}&\Big\langle T^{K}(\bar{K}k_P)\,||\,T^{K'}(\bar{K}'k'_P)\,||\,T^{2}(20)\Big\rangle \;=\; [5\,(2K'+1)\,(2\bar{K}+1)\,(2k_P+1)]^{1/2}\\ &\times\begin{Bmatrix} K & 2 & K'\\ \bar{K} & 2 & \bar{K}'\\ k_P & 0 & k'_P\end{Bmatrix}\Big\langle T^{\bar{K}}(k_I k_S)\,||\,T^{\bar{K}'}(k'_I k'_S)\,||\,T^{2}(11)\Big\rangle\,\Big\langle k_P\,||\,T^{k'_P}(P)\,||\,0\Big\rangle\,.\end{aligned} \tag{C.7}$$

The single-spin reduced supermatrix elements in Eqs. (C.6) and (C.7) are given by Eq. (B.7), and the two-spin reduced supermatrix elements can be expressed in terms of single-spin reduced supermatrix elements as

$$\begin{aligned}\left\langle T^{\bar{K}}(k_I k_S) \,||\, T^2(11) \,||\, T^{\bar{K}'}(k'_I k'_S) \right\rangle \;&=\; \left[5\,(2\bar{K}'+1)\,(2k_I+1)\,(2k_S+1)\right]^{1/2} \\ \times \left\{ \begin{array}{ccc} \bar{K} & \bar{K}' & 2 \\ k_I & k'_I & 1 \\ k_S & k'_S & 1 \end{array} \right\} &\left\langle k_I \,||\, T^1(I) \,||\, k'_I \right\rangle \left\langle k_S \,||\, T^1(S) \,||\, k'_S \right\rangle \,,\end{aligned} \tag{C.8}$$

and

$$\begin{aligned}\left\langle T^{\bar{K}}(k_I k_S) \,||\, T^{\bar{K}'}(k'_I k'_S) \,||\, T^2(11) \right\rangle \;&=\; \left[5\,(2\bar{K}'+1)\,(2k_I+1)\,(2k_S+1)\right]^{1/2} \\ \times \left\{ \begin{array}{ccc} \bar{K} & 2 & \bar{K}' \\ k_I & 1 & k'_I \\ k_S & 1 & k'_S \end{array} \right\} &\left\langle k_I \,||\, T^{k'_I}(I) \,||\, 1 \right\rangle \left\langle k_S \,||\, T^{k'_S}(S) \,||\, 1 \right\rangle \,.\end{aligned} \tag{C.9}$$

The single-spin reduced supermatrix elements in Eqs. (C.8) and (C.9) can be expressed in terms of $6j$ symbols as

$$\begin{aligned}\left\langle k_I \,||\, T^1(I) \,||\, k'_I \right\rangle \left\langle k_S \,||\, T^1(S) \,||\, k'_S \right\rangle \;&=\; \left\langle k_I \,||\, T^{k'_I}(I) \,||\, 1 \right\rangle \left\langle k_S \,||\, T^{k'_S}(S) \,||\, 1 \right\rangle \\ =\; (-1)^{k'_I+k'_S}\, 3\left[(2k'_I+1)(2k'_S+1)\right]^{1/2} &\left\{ \begin{array}{ccc} k_I & k'_I & 1 \\ \frac{1}{2} & \frac{1}{2} & \frac{1}{2} \end{array} \right\} \left\{ \begin{array}{ccc} k_S & k'_S & 1 \\ \frac{1}{2} & \frac{1}{2} & \frac{1}{2} \end{array} \right\} .\end{aligned} \tag{C.10}$$

Combining Eqs. (C.2) – (C.10) and using the symmetries of the Wigner $3j$, $6j$ and $9j$ symbols with respect to column permutations,[1] we find

$$\begin{aligned}\left(n \,|\, \mathcal{T}^2_M(11\{2\}0) \,|\, n'\right) \;&=\; \delta_{M,Q-Q'}\,(-1)^{K'-Q}\left[(-1)^{k_I+k_S+k_P} - (-1)^{k'_I+k'_S+k'_P}\right] \\ \times 15\,\big[&(2K+1)\,(2K'+1)\,(2\bar{K}+1)\,(2\bar{K}'+1)\,(2k_I+1)\,(2k'_I+1)\,(2k_S+1)\,(2k'_S+1) \\ \times (2k_P+1)\,&(2k'_P+1)\big]^{1/2} \left(\begin{array}{ccc} K & K' & 2 \\ -Q & Q' & Q-Q' \end{array} \right) \left\{ \begin{array}{ccc} \bar{K} & \bar{K}' & 2 \\ k_I & k'_I & 1 \\ k_S & k'_S & 1 \end{array} \right\} \left\{ \begin{array}{ccc} K & K' & 2 \\ \bar{K} & \bar{K}' & 2 \\ k_P & k'_P & 0 \end{array} \right\} \\ \times \left\{ \begin{array}{ccc} k_I & k'_I & 1 \\ \frac{1}{2} & \frac{1}{2} & \frac{1}{2} \end{array} \right\} &\left\{ \begin{array}{ccc} k_S & k'_S & 1 \\ \frac{1}{2} & \frac{1}{2} & \frac{1}{2} \end{array} \right\} \left\{ \begin{array}{ccc} k_P & k'_P & 0 \\ \frac{1}{2} & \frac{1}{2} & \frac{1}{2} \end{array} \right\} .\end{aligned} \tag{C.11}$$

The last $6j$ symbol in Eq. (C.11) may be expressed with the aid of Eq. (B.14). For the second $9j$ symbol, Eq. (B.16) yields

$$\left\{ \begin{array}{ccc} K & K' & 2 \\ \bar{K} & \bar{K}' & 2 \\ k_P & k'_P & 0 \end{array} \right\} \;=\; \delta_{k_P k'_P}\, \frac{(-1)^{K'+\bar{K}+k_P}}{\left[5\,(2k_P+1)\right]^{1/2}} \left\{ \begin{array}{ccc} K & K' & 2 \\ \bar{K}' & \bar{K} & k_P \end{array} \right\} . \tag{C.12}$$

Combining Eqs. (C.11), (C.12) and (B.14) with Eq. (C.1) and noting that (since k_I, k'_I, k_S, $k'_S = 0$ or 1)

$$\Big[(-1)^{k_I+k_S} - (-1)^{k'_I+k'_S}\Big] \;=\; 2\left(\delta_{k_I k_S} - \delta_{k'_I k'_S}\right) , \tag{C.13}$$

we obtain

$$\begin{aligned}
&\left(n \,|\, \mathcal{L}^{\alpha}_{\mathrm{D},IS} \,|\, n'\right) \;=\; \left(\delta_{k_I k_S} - \delta_{k'_I k'_S}\right) \delta_{k_P k'_P}\, (-1)^{\bar{K}+k_P-Q}\, 2\sqrt{30}\, \omega_{\mathrm{D},IS}\, D^{2*}_{Q-Q',0}(\Omega^{\alpha}_{IS}) \\
&\times \Big[(2K+1)\,(2K'+1)\,(2\bar{K}+1)\,(2\bar{K}'+1)\,(2k_I+1)\,(2k'_I+1)\,(2k_S+1)\,(2k'_S+1)\Big]^{1/2} \\
&\times \begin{pmatrix} K & K' & 2 \\ -Q & Q' & Q-Q' \end{pmatrix} \begin{Bmatrix} k_I & k'_I & 1 \\ \frac{1}{2} & \frac{1}{2} & \frac{1}{2} \end{Bmatrix} \begin{Bmatrix} k_S & k'_S & 1 \\ \frac{1}{2} & \frac{1}{2} & \frac{1}{2} \end{Bmatrix} \begin{Bmatrix} K & K' & 2 \\ \bar{K}' & \bar{K} & k_P \end{Bmatrix} \begin{Bmatrix} \bar{K} & \bar{K}' & 2 \\ k_I & k'_I & 1 \\ k_S & k'_S & 1 \end{Bmatrix}
\end{aligned} \tag{C.14}$$

Since the first factor, $(\delta_{k_I k_S} - \delta_{k'_I k'_S})$, vanishes if $k_I = k'_I$ and $k_S = k'_S$, it follows that $\left(n \,|\, \mathcal{L}^{\alpha}_{\mathrm{D},IS} \,|\, n\right) = 0$, that is, only off-diagonal ($n \neq n'$) supermatrix elements can be nonzero. In the same way, we find

$$\begin{aligned}
&\left(n \,|\, \mathcal{L}^{\alpha}_{\mathrm{D},IP} \,|\, n'\right) \;=\; \left(\delta_{k_I k_P} - \delta_{k'_I k'_P}\right) \delta_{k_S k'_S}\, (-1)^{K'+\bar{K}'+k_I+k_S-Q+1}\, 2\sqrt{30}\, \omega_{\mathrm{D},IP}\, D^{2*}_{Q-Q',0}(\Omega^{\alpha}_{IP}) \\
&\times \Big[(2K+1)\,(2K'+1)\,(2\bar{K}+1)\,(2\bar{K}'+1)\,(2k_I+1)\,(2k'_I+1)\,(2k_P+1)\,(2k'_P+1)\Big]^{1/2} \\
&\times \begin{pmatrix} K & K' & 2 \\ -Q & Q' & Q-Q' \end{pmatrix} \begin{Bmatrix} k_I & k'_I & 1 \\ \frac{1}{2} & \frac{1}{2} & \frac{1}{2} \end{Bmatrix} \begin{Bmatrix} k_P & k'_P & 1 \\ \frac{1}{2} & \frac{1}{2} & \frac{1}{2} \end{Bmatrix} \begin{Bmatrix} \bar{K} & \bar{K}' & 1 \\ k'_I & k_I & k_S \end{Bmatrix} \begin{Bmatrix} K & K' & 2 \\ \bar{K} & \bar{K}' & 1 \\ k_P & k'_P & 1 \end{Bmatrix}
\end{aligned} \tag{C.15}$$

and

$$\begin{aligned}
&\left(n \,|\, \mathcal{L}^{\alpha}_{\mathrm{D},SP} \,|\, n'\right) \;=\; \left(\delta_{k_S k_P} - \delta_{k'_S k'_P}\right) \delta_{k_I k'_I}\, (-1)^{K'+\bar{K}+k_I+k'_S-Q+1}\, 2\sqrt{30}\, \omega_{\mathrm{D},SP}\, D^{2*}_{Q-Q',0}(\Omega^{\alpha}_{SP}) \\
&\times \Big[(2K+1)\,(2K'+1)\,(2\bar{K}+1)\,(2\bar{K}'+1)\,(2k_S+1)\,(2k'_S+1)\,(2k_P+1)\,(2k'_P+1)\Big]^{1/2} \\
&\times \begin{pmatrix} K & K' & 2 \\ -Q & Q' & Q-Q' \end{pmatrix} \begin{Bmatrix} k_S & k'_S & 1 \\ \frac{1}{2} & \frac{1}{2} & \frac{1}{2} \end{Bmatrix} \begin{Bmatrix} k_P & k'_P & 1 \\ \frac{1}{2} & \frac{1}{2} & \frac{1}{2} \end{Bmatrix} \begin{Bmatrix} \bar{K} & \bar{K}' & 1 \\ k'_S & k_S & k_I \end{Bmatrix} \begin{Bmatrix} K & K' & 2 \\ \bar{K} & \bar{K}' & 1 \\ k_P & k'_P & 1 \end{Bmatrix}
\end{aligned} \tag{C.16}$$

APPENDIX D: INTEGRAL RELAXATION RATE

Here we present explicit expressions, based on Eqs. (19) and (20), for the integral longitudinal relaxation rate in terms of the matrix elements $U_{np}^{\mathrm{XY}} \equiv (n|\widetilde{\mathbf{U}}^{\mathrm{XY}}(0)|p)$ and the relative magnetogyric ratios $\kappa_S \equiv \gamma_S/\gamma_I$ and $\kappa_P \equiv \gamma_P/\gamma_I$. Results are listed separately for the three exchange cases. Whereas Eqs. (21) – (24) of the main text are restricted to the dilute regime ($P_{\mathrm{A}} \ll 1$), the results given here are valid for arbitrary P_{A}. Excitation is either nonselective ('non'), meaning that all three spins are excited (as in a field-cycling experiment), or selective ('sel'), meaning that the labile spin(s) (present in both states) but not the nonlabile spin(s) (present only in state A) are excited.

1. Exchange case $ISP{-}I$

If only one of the three spins is observed, we have for the I-magnetization,

$$\widehat{R}_{1,I}^{\mathrm{non}} = [U_{11}^{\mathrm{BB}} + U_{11}^{\mathrm{BA}} + U_{11}^{\mathrm{AB}} + U_{11}^{\mathrm{AA}} + \kappa_S\,(U_{12}^{\mathrm{BA}} + U_{12}^{\mathrm{AA}}) + \kappa_P\,(U_{13}^{\mathrm{BA}} + U_{13}^{\mathrm{AA}})]^{-1}\,, \tag{D.1a}$$

$$\widehat{R}_{1,I}^{\mathrm{sel}} = [U_{11}^{\mathrm{BB}} + U_{11}^{\mathrm{BA}} + U_{11}^{\mathrm{AB}} + U_{11}^{\mathrm{AA}}]^{-1}\,, \tag{D.1b}$$

for the S-magnetization,

$$\widehat{R}_{1,S}^{\mathrm{non}} = \kappa_S\,P_{\mathrm{A}}\,[U_{21}^{\mathrm{AB}} + U_{21}^{\mathrm{AA}} + \kappa_S\,U_{22}^{\mathrm{AA}} + \kappa_P\,U_{23}^{\mathrm{AA}}]^{-1}\,, \tag{D.2}$$

and for the P-magnetization,

$$\widehat{R}_{1,P}^{\mathrm{non}} = \kappa_P\,P_{\mathrm{A}}\,[U_{31}^{\mathrm{AB}} + U_{31}^{\mathrm{AA}} + \kappa_S\,U_{32}^{\mathrm{AA}} + \kappa_P\,U_{33}^{\mathrm{AA}}]^{-1}\,. \tag{D.3}$$

If the combined magnetization of spins I and S is observed,

$$\begin{aligned}\widehat{R}_{1,IS}^{\mathrm{non}} = {} & (1 + \kappa_S\,P_{\mathrm{A}})\,[U_{11}^{\mathrm{BB}} + U_{11}^{\mathrm{BA}} + U_{11}^{\mathrm{AB}} + U_{21}^{\mathrm{AB}} + U_{11}^{\mathrm{AA}} + U_{21}^{\mathrm{AA}} \\ & + \kappa_S\,(U_{12}^{\mathrm{BA}} + U_{12}^{\mathrm{AA}} + U_{22}^{\mathrm{AA}}) + \kappa_P\,(U_{13}^{\mathrm{BA}} + U_{13}^{\mathrm{AA}} + U_{23}^{\mathrm{AA}})]^{-1}\,,\end{aligned} \tag{D.4a}$$

$$\widehat{R}_{1,IS}^{\mathrm{sel}} = [U_{11}^{\mathrm{BB}} + U_{11}^{\mathrm{BA}} + U_{11}^{\mathrm{AB}} + U_{21}^{\mathrm{AB}} + U_{11}^{\mathrm{AA}} + U_{21}^{\mathrm{AA}}]^{-1}\,. \tag{D.4b}$$

If the combined magnetization of all three spins is observed,

$$\begin{aligned}\widehat{R}_{1,ISP}^{\mathrm{non}} = {} & [1 + (\kappa_S + \kappa_P)\,P_{\mathrm{A}}]\,[U_{11}^{\mathrm{BB}} + U_{11}^{\mathrm{BA}} + U_{11}^{\mathrm{AB}} + U_{21}^{\mathrm{AB}} + U_{31}^{\mathrm{AB}} + U_{11}^{\mathrm{AA}} + U_{21}^{\mathrm{AA}} \\ & + U_{31}^{\mathrm{AA}} + \kappa_S\,(U_{12}^{\mathrm{BA}} + U_{12}^{\mathrm{AA}} + U_{22}^{\mathrm{AA}} + U_{32}^{\mathrm{AA}}) + \kappa_P\,(U_{13}^{\mathrm{BA}} + U_{13}^{\mathrm{AA}} + U_{23}^{\mathrm{AA}} + U_{33}^{\mathrm{AA}})]^{-1}\,,\end{aligned} \tag{D.5a}$$

$$\widehat{R}_{1,ISP}^{\mathrm{sel}} = [U_{11}^{\mathrm{BB}} + U_{11}^{\mathrm{BA}} + U_{11}^{\mathrm{AB}} + U_{21}^{\mathrm{AB}} + U_{31}^{\mathrm{AB}} + U_{11}^{\mathrm{AA}} + U_{21}^{\mathrm{AA}} + U_{31}^{\mathrm{AA}}]^{-1}\,. \tag{D.5b}$$

2. Exchange case $ISP{-}IS$

If only one of the three spins is observed, we have for the I-magnetization,

$$\begin{aligned}\widehat{R}_{1,I}^{\mathrm{non}} = {} & [U_{11}^{\mathrm{BB}} + U_{11}^{\mathrm{BA}} + U_{11}^{\mathrm{AB}} + U_{11}^{\mathrm{AA}} + \kappa_S\,(U_{12}^{\mathrm{BB}} + U_{12}^{\mathrm{BA}} + U_{12}^{\mathrm{AB}} + U_{12}^{\mathrm{AA}}) \\ & + \kappa_P\,(U_{13}^{\mathrm{BA}} + U_{13}^{\mathrm{AA}})]^{-1}\,,\end{aligned} \tag{D.6a}$$

$$\widehat{R}_{1,I}^{\mathrm{sel}} = [U_{11}^{\mathrm{BB}} + U_{11}^{\mathrm{BA}} + U_{11}^{\mathrm{AB}} + U_{11}^{\mathrm{AA}} + \kappa_S\,(U_{12}^{\mathrm{BB}} + U_{12}^{\mathrm{BA}} + U_{12}^{\mathrm{AB}} + U_{12}^{\mathrm{AA}})]^{-1}\,, \tag{D.6b}$$

for the S-magnetization,

$$\begin{aligned}\widehat{R}_{1,S}^{\text{non}} &= \kappa_S\,[U_{21}^{\text{BB}} + U_{21}^{\text{BA}} + U_{21}^{\text{AB}} + U_{21}^{\text{AA}} + \kappa_S\,(U_{22}^{\text{BB}} + U_{22}^{\text{BA}} + U_{22}^{\text{AB}} + U_{22}^{\text{AA}}) \\ &\quad + \kappa_P\,(U_{23}^{\text{BA}} + U_{23}^{\text{AA}})]^{-1}\,,\end{aligned} \tag{D.7a}$$

$$\widehat{R}_{1,S}^{\text{sel}} = \kappa_S\,[U_{21}^{\text{BB}} + U_{21}^{\text{BA}} + U_{21}^{\text{AB}} + U_{21}^{\text{AA}} + \kappa_S\,(U_{22}^{\text{BB}} + U_{22}^{\text{BA}} + U_{22}^{\text{AB}} + U_{22}^{\text{AA}})]^{-1}\,, \tag{D.7b}$$

and for the P-magnetization,

$$\widehat{R}_{1,P}^{\text{non}} = \kappa_P\,P_{\text{A}}\,[U_{31}^{\text{AB}} + U_{31}^{\text{AA}} + \kappa_S\,(U_{32}^{\text{AB}} + U_{32}^{\text{AA}}) + \kappa_P\,U_{33}^{\text{AA}}]^{-1}\,. \tag{D.8}$$

If the combined magnetization of spins I and S is observed,

$$\begin{aligned}\widehat{R}_{1,IS}^{\text{non}} &= (1+\kappa_S)\,[U_{11}^{\text{BB}} + U_{21}^{\text{BB}} + U_{11}^{\text{BA}} + U_{21}^{\text{BA}} + U_{11}^{\text{AB}} + U_{21}^{\text{AB}} + U_{11}^{\text{AA}} + U_{21}^{\text{AA}} \\ &\quad + \kappa_S\,(U_{12}^{\text{BB}} + U_{22}^{\text{BB}} + U_{12}^{\text{BA}} + U_{22}^{\text{BA}} + U_{12}^{\text{AB}} + U_{22}^{\text{AB}} + U_{12}^{\text{AA}} + U_{22}^{\text{AA}}) \\ &\quad + \kappa_P\,(U_{13}^{\text{BA}} + U_{23}^{\text{BA}} + U_{13}^{\text{AA}} + U_{23}^{\text{AA}})]^{-1}\,,\end{aligned} \tag{D.9a}$$

$$\begin{aligned}\widehat{R}_{1,IS}^{\text{sel}} &= (1+\kappa_S)\,[U_{11}^{\text{BB}} + U_{21}^{\text{BB}} + U_{11}^{\text{BA}} + U_{21}^{\text{BA}} + U_{11}^{\text{AB}} + U_{21}^{\text{AB}} + U_{11}^{\text{AA}} + U_{21}^{\text{AA}} \\ &\quad + \kappa_S\,(U_{12}^{\text{BB}} + U_{22}^{\text{BB}} + U_{12}^{\text{BA}} + U_{22}^{\text{BA}} + U_{12}^{\text{AB}} + U_{22}^{\text{AB}} + U_{12}^{\text{AA}} + U_{22}^{\text{AA}})]^{-1}\,.\end{aligned} \tag{D.9b}$$

If the combined magnetization of all three spins is observed,

$$\begin{aligned}\widehat{R}_{1,ISP}^{\text{non}} &= (1+\kappa_S+\kappa_P\,P_{\text{A}})\,[U_{11}^{\text{BB}} + U_{21}^{\text{BB}} + U_{11}^{\text{BA}} + U_{21}^{\text{BA}} + U_{11}^{\text{AB}} + U_{21}^{\text{AB}} + U_{31}^{\text{AB}} \\ &\quad + U_{11}^{\text{AA}} + U_{21}^{\text{AA}} + U_{31}^{\text{AA}} + \kappa_S\,(U_{12}^{\text{BB}} + U_{22}^{\text{BB}} + U_{12}^{\text{BA}} + U_{22}^{\text{BA}} + U_{12}^{\text{AB}} + U_{22}^{\text{AB}} + U_{32}^{\text{AB}} \\ &\quad + U_{12}^{\text{AA}} + U_{22}^{\text{AA}} + U_{32}^{\text{AA}}) + \kappa_P\,(U_{13}^{\text{BA}} + U_{23}^{\text{BA}} + U_{13}^{\text{AA}} + U_{23}^{\text{AA}} + U_{33}^{\text{AA}})]^{-1}\,,\end{aligned} \tag{D.10a}$$

$$\begin{aligned}\widehat{R}_{1,ISP}^{\text{sel}} &= (1+\kappa_S)\,[U_{11}^{\text{BB}} + U_{21}^{\text{BB}} + U_{11}^{\text{BA}} + U_{21}^{\text{BA}} + U_{11}^{\text{AB}} + U_{21}^{\text{AB}} + U_{31}^{\text{AB}} \\ &\quad + U_{11}^{\text{AA}} + U_{21}^{\text{AA}} + U_{31}^{\text{AA}} + \kappa_S\,(U_{12}^{\text{BB}} + U_{22}^{\text{BB}} + U_{12}^{\text{BA}} + U_{22}^{\text{BA}} \\ &\quad + U_{12}^{\text{AB}} + U_{22}^{\text{AB}} + U_{32}^{\text{AB}} + U_{12}^{\text{AA}} + U_{22}^{\text{AA}} + U_{32}^{\text{AA}})]^{-1}\,.\end{aligned} \tag{D.10b}$$

3. Exchange case $ISP{-}ISP$

If only one of the three spins is observed, we have for the I-magnetization,

$$\begin{aligned}\widehat{R}_{1,I}^{\rm non} \;=\; \widehat{R}_{1,I}^{\rm sel} \;=\; &[U_{11}^{\rm BB}+U_{11}^{\rm BA}+U_{11}^{\rm AB}+U_{11}^{\rm AA}\\ &+\kappa_S\,(U_{12}^{\rm BB}+U_{12}^{\rm BA}+U_{12}^{\rm AB}+U_{12}^{\rm AA})+\kappa_P\,(U_{13}^{\rm BB}+U_{13}^{\rm BA}+U_{13}^{\rm AB}+U_{13}^{\rm AA})]^{-1}\,,\end{aligned} \tag{D.11}$$

for the S-magnetization,

$$\begin{aligned}\widehat{R}_{1,S}^{\rm non} \;=\; \widehat{R}_{1,S}^{\rm sel} \;=\; &\kappa_S\,[U_{21}^{\rm BB}+U_{21}^{\rm BA}+U_{21}^{\rm AB}+U_{21}^{\rm AA}\\ &+\kappa_S\,(U_{22}^{\rm BB}+U_{22}^{\rm BA}+U_{22}^{\rm AB}+U_{22}^{\rm AA})+\kappa_P\,(U_{23}^{\rm BB}+U_{23}^{\rm BA}+U_{23}^{\rm BA}+U_{23}^{\rm AA})]^{-1}\,,\end{aligned} \tag{D.12}$$

and for the P-magnetization,

$$\begin{aligned}\widehat{R}_{1,P}^{\rm non} \;=\; \widehat{R}_{1,P}^{\rm sel} \;=\; &\kappa_P\,[U_{31}^{\rm BB}+U_{31}^{\rm BA}+U_{31}^{\rm AB}+U_{31}^{\rm AA}\\ &+\kappa_S\,(U_{32}^{\rm BB}+U_{32}^{\rm BA}+U_{32}^{\rm AB}+U_{32}^{\rm AA})+\kappa_P\,(U_{33}^{\rm BB}+U_{33}^{\rm BA}+U_{33}^{\rm BA}+U_{33}^{\rm AA})]^{-1}\,.\end{aligned} \tag{D.13}$$

If the combined magnetization of spins I and S is observed,

$$\begin{aligned}\widehat{R}_{1,IS}^{\rm non} \;=\; \widehat{R}_{1,IS}^{\rm sel} \;=\; &(1+\kappa_S)\,[U_{11}^{\rm BB}+U_{21}^{\rm BB}+U_{11}^{\rm BA}+U_{21}^{\rm BA}+U_{11}^{\rm AB}+U_{21}^{\rm AB}+U_{11}^{\rm AA}\\ &+U_{21}^{\rm AA}+\kappa_S\,(U_{12}^{\rm BB}+U_{22}^{\rm BB}+U_{12}^{\rm BA}+U_{22}^{\rm BA}+U_{12}^{\rm AB}+U_{22}^{\rm AB}+U_{12}^{\rm AA}+U_{22}^{\rm AA})\\ &+\kappa_P\,(U_{13}^{\rm BB}+U_{23}^{\rm BB}+U_{13}^{\rm BA}+U_{23}^{\rm BA}+U_{13}^{\rm AB}+U_{23}^{\rm AB}+U_{13}^{\rm AA}+U_{23}^{\rm AA})]^{-1}\,.\end{aligned} \tag{D.14}$$

If the combined magnetization of all three spins is observed,

$$\begin{aligned}\widehat{R}_{1,ISP}^{\rm non} \;=\; \widehat{R}_{1,ISP}^{\rm sel} \;=\; &(1+\kappa_S+\kappa_P)\,[U_{11}^{\rm BB}+U_{21}^{\rm BB}+U_{31}^{\rm BB}+U_{11}^{\rm BA}+U_{21}^{\rm BA}+U_{31}^{\rm BA}\\ &+U_{11}^{\rm AB}+U_{21}^{\rm AB}+U_{31}^{\rm AB}+U_{11}^{\rm AA}+U_{21}^{\rm AA}+U_{31}^{\rm AA}+\kappa_S\,(U_{12}^{\rm BB}+U_{22}^{\rm BB}+U_{32}^{\rm BB}+U_{12}^{\rm BA}\\ &+U_{22}^{\rm BA}+U_{32}^{\rm BA}+U_{12}^{\rm AB}+U_{22}^{\rm AB}+U_{32}^{\rm AB}+U_{12}^{\rm AA}+U_{22}^{\rm AA}+U_{32}^{\rm AA})+\kappa_P\,(U_{13}^{\rm BB}+U_{23}^{\rm BB}\\ &+U_{33}^{\rm BB}+U_{13}^{\rm BA}+U_{23}^{\rm BA}+U_{33}^{\rm BA}+U_{13}^{\rm AB}+U_{23}^{\rm AB}+U_{33}^{\rm AB}+U_{13}^{\rm AA}+U_{23}^{\rm AA}+U_{33}^{\rm AA})]^{-1}\,.\end{aligned} \tag{D.15}$$

4. Exchange case $ISP{-}I$ in the dilute regime

In the dilute regime ($P_{\rm A}\ll 1$), Eqs. (D.1), (D.4) and (D.5) reduce to

$$\widehat{R}_{1,I}^{\rm dil} \;=\; \widehat{R}_{1,IS}^{\rm dil} \;=\; \widehat{R}_{1,ISP}^{\rm dil} \;=\; \frac{1}{U_{11}^{\rm BB}}\,. \tag{D.16}$$

We shall now show that $U_{11}^{\rm BB}$ can be expressed in terms of the element $g_{11}\equiv(1|\mathbf{G}^{\rm A}(0)|1)$ of the supermatrix $\mathbf{G}^{\rm A}(0)$ in Eq. (14).

Combining Eqs. (12a) and (13) and the detailed balance relation $P_{\rm B}\tau_{\rm A}=P_{\rm A}\tau_{\rm B}$, we obtain

$$\widetilde{\mathbf{U}}^{\rm BB}(0) \;=\; \frac{P_{\rm B}^2\,\tau_{\rm A}}{P_{\rm A}}\left[\mathbf{1}^{\rm B}\;+\;i\,\mathbf{L}_{\rm Z}^{\rm B}\,\tau_{\rm B}-\mathbf{T}\,\mathbf{G}^{\rm A}(0)\,\mathbf{T}'\right]^{-1}\,. \tag{D.17}$$

Because the matrix $\mathbf{G}^{\rm A}(0)$ is isotropically averaged, it must reflect the axial symmetry in spin Liouville space. According to the Wigner-Eckart theorem,[1] $\mathbf{G}^{\rm A}(0)$ must then be

block-diagonal in the projection index Q of the ISTO basis (Table S1). Pre- and post-multiplication by the $ISP{-}I$ matrix $\mathbf{T}$ in Eq. (15) and its transpose picks out the first diagonal element in each of the first three blocks ($Q = 0, \pm 1$), that is,

$$\mathbf{T}\,\mathbf{G}^{\mathrm{A}}(0)\,\mathbf{T}' \;=\; \begin{bmatrix} g_{11} & 0 & 0 \\ 0 & g_{20,20} & 0 \\ 0 & 0 & g_{35,35} \end{bmatrix} . \tag{D.18}$$

Only spin I can access state B in the $ISP{-}I$ case, so the Zeeman Liouvillian supermatrix in the B-state basis is simply

$$\mathbf{L}_{\mathrm{Z}}^{\mathrm{B}} \;=\; \omega_I^{\mathrm{B}} \begin{bmatrix} 0 & 0 & 0 \\ 0 & 1 & 0 \\ 0 & 0 & -1 \end{bmatrix} . \tag{D.19}$$

Combination of Eqs. (D.17) – (D.19) yields

$$\widetilde{\mathbf{U}}^{\mathrm{BB}}(0) \;=\; \frac{P_{\mathrm{B}}^2\,\tau_{\mathrm{A}}}{P_{\mathrm{A}}} \begin{bmatrix} (1-g_{11})^{-1} & 0 & 0 \\ 0 & (1-g_{20,20}+i\,\omega_I^{\mathrm{B}}\tau_{\mathrm{B}})^{-1} & 0 \\ 0 & 0 & (1-g_{35,35}-i\,\omega_I^{\mathrm{B}}\tau_{\mathrm{B}})^{-1} \end{bmatrix} , \tag{D.20}$$

so that

$$U_{11}^{\mathrm{BB}} \;=\; \frac{P_{\mathrm{B}}^2\,\tau_{\mathrm{A}}}{P_{\mathrm{A}}(1-g_{11})} . \tag{D.21}$$

Finally, combination of Eqs. (D.16) and (D.21) yields for the dilute regime

$$\widehat{R}_{1,I}^{\mathrm{dil}} \;=\; \widehat{R}_{1,IS}^{\mathrm{dil}} \;=\; \widehat{R}_{1,ISP}^{\mathrm{dil}} \;=\; \frac{P_{\mathrm{A}}}{\tau_{\mathrm{A}}}\,(1-g_{11}) . \tag{D.22}$$

APPENDIX E: BWR RELAXATION THEORY

Here we obtain the elements of the orientation-dependent relaxation supermatrix $\mathbf{R}^{\alpha}$ in site α, starting from the Bloch-Wangsness-Redfield (BWR) master equation[4]

$$\frac{\mathrm{d}}{\mathrm{d}t}\,\widehat{\sigma}^{\alpha}(t) \;=\; -\,i\,\widehat{\Delta}^{\alpha}(t)\,\widehat{\sigma}^{\alpha}(t) \;-\; \int_{0}^{\infty}\mathrm{d}\tau\,\left\langle \widehat{\mathcal{L}}^{\alpha}_{\mathrm{D}}(t)\,\widehat{\mathcal{L}}^{\alpha}_{\mathrm{D}}(t-\tau)\right\rangle_{\alpha}\,\widehat{\sigma}^{\alpha}(t)\,, \tag{E.1}$$

where the angular brackets with subscript α denote an equilibrium ensemble average over the molecular degrees of freedom in site α. Further, $\widehat{\sigma}^{\alpha}(t) = \exp(i\,\mathcal{L}_{\mathrm{Z}}\,t)\,\sigma^{\alpha}(t)$ and $\widehat{\mathcal{L}}^{\alpha}_{\mathrm{D}}(t) = \exp(i\,\mathcal{L}_{\mathrm{Z}}\,t)\,\mathcal{L}^{\alpha}_{\mathrm{D}}(t)\,\exp(-i\,\mathcal{L}_{\mathrm{Z}}\,t)$ are the spin density operator and the dipolar Liouvillian for site α, both in the interaction representation. For exchange cases ISP–IS and ISP–ISP, all three dipole couplings fluctuate so $\mathcal{L}^{\alpha}_{\mathrm{D}}(t) = \mathcal{L}^{\alpha}_{\mathrm{D},IS}(t) + \mathcal{L}^{\alpha}_{\mathrm{D},IP}(t) + \mathcal{L}^{\alpha}_{\mathrm{D},SP}(t)$ and the first term in Eq. (E.1) is absent. For exchange case $ISP-I$, the SP dipole coupling is static so $\mathcal{L}^{\alpha}_{\mathrm{D}}(t) = \mathcal{L}^{\alpha}_{\mathrm{D},IS}(t) + \mathcal{L}^{\alpha}_{\mathrm{D},IP}(t)$ and, in the first term, $\widehat{\Delta}^{\alpha}(t) \equiv \widehat{\mathcal{L}}^{\alpha}_{\mathrm{D},SP}(t) = \exp(i\,\mathcal{L}_{\mathrm{Z}}\,t)\,\mathcal{L}^{\alpha}_{\mathrm{D},SP}\,\exp(-i\,\mathcal{L}_{\mathrm{Z}}\,t)$.

In a rigorous BWR treatment of the ISP–I case, the transformation to the interaction representation should involve the total static Liouvillian $\mathcal{L}_{\mathrm{Z}}+\mathcal{L}^{\alpha}_{\mathrm{D},SP}$. The first term in Eq. (E.1) would then be absent, but the ensuing analytical development would be complicated by the fact that the ISTOs T^{K}_{Q} are only eigenoperators of $\mathcal{L}_{\mathrm{Z}}$ (see below), not of the total static Liouvillian. The rigorous BWR treatment, which is valid without restrictions on the static dipole coupling $\omega_{\mathrm{D},SP}$, leads to spectral densities at frequencies that are linear combinations of ω_0 and $\omega_{\mathrm{D},SP}$. To avoid these complications, we pursue a restricted BWR treatment, valid for $\omega_{\mathrm{D},SP}\,\tau_{\mathrm{A}} \ll 1$, where we transform to an intermediate interaction representation as in Eq. (E.1). This additional restriction is unimportant, since, in practice, $\omega_{\mathrm{D},SP}$ cannot exceed 3×10^{5} rad s^{-1}, corresponding to the smallest physically realizable proton-proton separation of ~ 1.5 Å. If τ_{A} is so long that the condition $\omega_{\mathrm{D},SP}\,\tau_{\mathrm{A}} \ll 1$ is violated, then $\omega_{\mathrm{D},IS}$ and $\omega_{\mathrm{D},IP}$ must be $\ll 10^{5}$ rad s^{-1} in order not to violate the analogous (motional narrowing) conditions on these fluctuating dipole couplings. But for the dilute conditions ($P_{\mathrm{A}} \ll 1$) of primary interest, the ILRR is negligibly small if all dipole couplings involving the labile I spin are $\ll 10^{5}$ rad s^{-1}. In conclusion, Eq. (E.1) and the results that follow from it, is valid for all three exchange cases, provided that $\omega_{\mathrm{D},X}\,\tau_{\mathrm{A}} \ll 1$ for all three dipole couplings, regardless of whether they are static or fluctuating.

For simplicity, we assume that the spins are isochronous, that is, $\delta^{\mathrm{A}}_{S} = \delta^{\mathrm{A}}_{P} = 0$ in Eq. (1) so $\omega^{\mathrm{A}}_{I} = \omega^{\mathrm{A}}_{S} = \omega^{\mathrm{A}}_{P} \equiv \omega_0$. The ISTOs in Table S1 are then eigenoperators of the Zeeman Liouvillian,

$$\mathcal{L}_{\mathrm{Z}}\,T^{K}_{Q} \;=\; Q\,\omega_0\,T^{K}_{Q}\,, \tag{E.2}$$

so the interaction representation of the Liouvillian for dipole coupling X in site α becomes

$$\widehat{\mathcal{L}}^{\alpha}_{\mathrm{D},X}(t) \;=\; -\,\frac{2}{\sqrt{3}}\,\omega_{\mathrm{D},X}\sum_{M=-2}^{2}\exp(iM\omega_0 t)\,\mathcal{T}^{2}_{M}(X)\,D^{2*}_{M0}(\Omega^{\alpha}_{X})\,, \tag{E.3}$$

where $\mathcal{T}^2_M(X) \equiv [T^2_M(X), \ldots]$. Combination of Eqs. (E.1) and (E.3) yields for the EMOR model

$$\begin{aligned}\frac{\mathrm{d}}{\mathrm{d}t}\,\widehat{\sigma}^{\alpha}(t) \;=\; & i\,\frac{2}{\sqrt{3}}\,\omega_{\mathrm{D},SP}\sum_{M=-2}^{2}\exp(iM\omega_0 t)\,D^{2*}_{M0}(\Omega^{\alpha}_{SP})\,\mathcal{T}^2_M(SP)\,\widehat{\sigma}^{\alpha}(t) \\ & -\,\frac{4}{3}\sum_X\sum_Y\omega_{\mathrm{D},X}\,\omega_{\mathrm{D},Y}\sum_{M=-2}^{2}\sum_{M'=-2}^{2}\exp[i(M+M')\omega_0 t] \\ & \times\; F_{MM'}(\Omega^{\alpha}_X,\Omega^{\alpha}_Y)\,J(-M'\omega_0)\,\mathcal{T}^2_M(X)\,\mathcal{T}^2_{M'}(Y)\,\widehat{\sigma}^{\alpha}(t)\,.\end{aligned} \tag{E.4}$$

Here, we have introduced the angular functions

$$F_{MM'}(\Omega^{\alpha}_X,\Omega^{\alpha}_Y) \;\equiv\; D^{2*}_{M0}(\Omega^{\alpha}_X)\,D^{2*}_{M'0}(\Omega^{\alpha}_Y)\,, \tag{E.5}$$

with the Wigner functions for the three internuclear vectors given by Eq. (4), and the reduced spectral density function (SDF)

$$J(\omega) \;\equiv\; j(\omega) + i\,k(\omega) \;=\; \frac{\tau_{\mathrm{A}}}{1+(\omega\,\tau_{\mathrm{A}})^2}\,(1+i\,\omega\,\tau_{\mathrm{A}})\;. \tag{E.6}$$

Note that we retain the imaginary part, $k(\omega)$, of the SDF, which can have a small effect on the ILRR for exchange cases $ISP{-}ISP$ and $ISP{-}I$, but not for the $ISP{-}IS$ case (Sec. IV C). Because $k(-\omega) = -\,k(\omega)$, we refer to $k(\omega)$ as the odd SDF (OSDF).

Since we want to describe relaxation over the full frequency range, we shall not invoke the secular approximation to eliminate terms with oscillating factors in Eq. (E.4). Instead, we remove these factors by transforming the master equation (E.4) back to the Schrödinger representation. The supermatrix representation of the master equation in the space of the ISTO basis operators B_n of Table S1 then takes the form

$$\frac{\mathrm{d}}{\mathrm{d}t}\,\boldsymbol{\sigma}^{\alpha}(t) \;=\; -\,\big[\,i\,\mathbf{L}^{\mathrm{A}}_{\mathrm{Z}} + i\,\boldsymbol{\Delta}^{\alpha} + \mathbf{R}^{\alpha}\big]\,\boldsymbol{\sigma}^{\alpha}(t)\,, \tag{E.7}$$

where $\boldsymbol{\sigma}^{\alpha}(t)$ is a column vector of spin modes $\sigma^{\alpha}_n(t) = (B_n\,|\,\sigma^{\alpha}(t)) = \mathrm{Tr}\{B^{\dagger}_n\,\sigma^{\alpha}(t)\}$. In view of Eq. (E.4), the static dipolar Liouvillian supermatrix is

$$\boldsymbol{\Delta}^{\alpha} \;=\; -\,\frac{2}{\sqrt{3}}\,\omega_{\mathrm{D},SP}\sum_{M=-2}^{2}D^{2*}_{M0}(\Omega^{\alpha}_{SP})\,\mathbf{D}_M\,, \tag{E.8}$$

and the relaxation supermatrix is

$$\mathbf{R}^{\alpha} \;=\; \frac{4}{3}\sum_X\sum_Y\omega_{\mathrm{D},X}\,\omega_{\mathrm{D},Y}\sum_{M=-2}^{2}\sum_{M'=-2}^{2}F_{MM'}(\Omega^{\alpha}_X,\Omega^{\alpha}_Y)\,J(-M'\omega_0)\,\mathbf{C}^{XY}_{MM'}\,. \tag{E.9}$$

Note that, in the sums over dipole couplings, X and Y can be IS, IP or SP for exchange cases $ISP{-}IS$ and $ISP{-}ISP$ but only IS or IP for exchange case $ISP{-}I$, where the static SP coupling appears in $\boldsymbol{\Delta}^{\alpha}$. In Eqs. (E.8) and (E.9), we have defined the coefficient supermatrices $\mathbf{D}_M$ and $\mathbf{C}^{XY}_{MM'}$ with elements

$$D_{M,np} \;\equiv\; (n\,|\mathcal{T}^2_M(SP)|\,p) \;=\; \mathrm{Tr}\{B^{\dagger}_n\,[T^2_M(SP), B_p]\}\,, \tag{E.10}$$

and

$$C^{XY}_{MM',np} \equiv (n\,|\mathcal{T}^2_M(X)\,\mathcal{T}^2_{M'}(Y)|\,p) = \mathrm{Tr}\{[B^\dagger_n, T^2_M(X)]\,[T^2_{M'}(Y), B_p]\}\,. \tag{E.11}$$

According to Eq. (E.9), the relaxation supermatrix is determined by $3 \times 3 \times 5 \times 5 = 225$ coefficient supermatrices $\mathbf{C}^{XY}_{MM'}$, each with 63×63 elements. Fortunately, the computational task can be simplified considerably by making use of symmetry. First, we consider spin inversion conjugation (SIC) symmetry.[5–7] As indicated in Table S1, the ISTO basis operators have definite SIC parity (either odd or even). Furthermore, the relaxation superoperator $\mathcal{R}^\alpha$ has even SIC parity.[5–7] According to the basic orthogonality theorem of group theory,[8] the supermatrix $\mathbf{R}^\alpha$ in the ISTO basis can then have nonzero elements only between basis operators of the same parity. If we order the 63 basis operators so that the 36 odd operators (above the dashed lines in Table S1) precede the 27 even operators, then $\mathbf{R}^\alpha$ is block-diagonal,

$$\mathbf{R}^\alpha = \begin{bmatrix} \mathbf{R}^\alpha_{\mathrm{aa}} & \mathbf{0} \\ \mathbf{0} & \mathbf{R}^\alpha_{\mathrm{ss}} \end{bmatrix}, \tag{E.12}$$

where the subscripts indicate odd (or antisymmetric = a) and even (or symmetric = s) SIC parity. Conversely, the superoperator Δ^α has odd SIC parity and therefore has nonzero matrix elements between ISTO basis operators of different SIC parity. Consequently, the supermatrix $\mathbf{\Delta}^\alpha$ is anti-block-diagonal in the SIC-parity ordered ISTO basis,

$$\mathbf{\Delta}^\alpha = \begin{bmatrix} \mathbf{0} & \mathbf{\Delta}^\alpha_{\mathrm{as}} \\ \mathbf{\Delta}^\alpha_{\mathrm{sa}} & \mathbf{0} \end{bmatrix}. \tag{E.13}$$

If we are interested in relaxation of the longitudinal magnetization, described by the odd-parity operators I_z, S_z and P_z, it might seem that we only need to consider the odd relaxation matrix $\mathbf{R}^\alpha_{\mathrm{aa}}$. This is true for exchange cases ISP–IS and ISP–ISP. However, exchange case ISP–I also involves the static dipolar precession supermatrix $\mathbf{\Delta}^\alpha$, which couples the odd and even blocks, $\mathbf{R}^\alpha_{\mathrm{aa}}$ and $\mathbf{R}^\alpha_{\mathrm{ss}}$.

Several symmetry relations for the elements of the coefficient matrices $\mathbf{C}^{XY}_{MM'}$ can be derived from the defining relation (E.11). First, it can be shown that all elements of these matrices are real-valued.[5] Using this fact, the cyclic permutation invariance of the trace, and the identities $T^{2\,\dagger}_M = (-1)^M T^2_{-M}$ and $(AB)^\dagger = B^\dagger A^\dagger$, we find from Eq. (E.11) that

$$C^{YX}_{M'M,\,pn} = (-1)^{M+M'}\, C^{XY}_{-M,-M',\,np}\,. \tag{E.14}$$

Let a_α and b_β denote two of the nine single-spin operators with a, $b = I$, S or P and α, $\beta = z$, $+$ or $-$. Within this subspace,

$$C^{XY}_{MM',\,a_\alpha\,b_\beta} = \delta_{XY}\, C^{XX}_{MM',\,a_\alpha\,b_\beta}\,. \tag{E.15}$$

As a consequence of this selection rule, relaxation matrix elements $R^\alpha_{a_\alpha\,b_\beta}$ within the single-spin subspace only involve self-correlations ($X = Y$), that is, there is no contribution from

distinct correlations ($X \neq Y$). To establish this selection rule, we start from the defining Eq. (E.11): $C^{XY}_{MM',\,a_\alpha\,b_\beta} = \mathrm{Tr}\{[a^\dagger_\alpha,\, T^2_M(X)]\,[T^2_{M'}(Y),\, b_\beta]\}$. For both commutators to be nonzero, it is necessary that $a \in X$ and $b \in Y$. For example, if $X = IP$, then a_α must be an I-spin operator or a P-spin operator. The operators $T^2_M(X)$ are products of two single-spin operators (or sums of such products), one for each of the two spins associated with dipole coupling X. Therefore, each of the commutators is a product of two single-spin operators (or a sum of such products) associated with the two spins contained in X or Y, respectively. It then follows that, if $X \neq Y$, only two of the four operators in the trace belong to the same spin. In other words, two of the three spins are represented by only one operator in the trace. Since $\mathrm{Tr}_a\{a_\alpha\} = 0$, it follows that $C^{XY}_{MM',\,a_\alpha\,b_\beta} = 0$ if $X \neq Y$. On the other hand, if $X = Y$, the trace contains two operators associated with each of the two spins contained in X and it can therefore be nonzero.

In a similar way, one can show that $C^{XX}_{MM',\,a_\alpha\,n} = 0$ if a_α is a single-spin operator and n is a three-spin basis operator. In other words, the single-spin and three-spin subspaces are coupled in the relaxation matrix only via distinct correlations ($X \neq Y$).

The relaxation supermatrix $\mathbf{R}^\alpha$ depends on the site orientation Ω^α via the angular functions $F_{MM'}(\Omega^\alpha_X, \Omega^\alpha_Y)$. Recalling the orthogonality of the Wigner functions,[1] we obtain after averaging these functions over the isotropic distribution of site orientations,

$$\begin{aligned}
\langle F_{MM'} \rangle \;&=\; \sum_{N=-2}^{2} \left\langle D^{2\,*}_{M0}(\Omega^\alpha_X)\, D^{2\,*}_{M'N}(\Omega^\alpha_X) \right\rangle D^{2\,*}_{N0}(\Omega_{XY}) \\
&=\; (-1)^M \sum_{N=-2}^{2} \left[\frac{1}{8\pi^2} \int \mathrm{d}\Omega^\alpha_X\; D^2_{-M0}(\Omega^\alpha_X)\, D^{2\,*}_{M'N}(\Omega^\alpha_X) \right] D^{2\,*}_{N0}(\Omega_{XY}) \\
&=\; (-1)^M \sum_{N=-2}^{2} \delta_{M',-M}\, \delta_{N0}\, \frac{1}{5}\, D^{2\,*}_{N0}(\Omega_{XY}) \\
&=\; \delta_{M',-M}\, (-1)^M\, \frac{1}{5}\, P_2(\cos\beta_{XY})\,,
\end{aligned} \tag{E.16}$$

where β_{XY} is the fixed angle between internuclear vectors X and Y (in all sites α). Combination of Eqs. (E.9) and (E.16) yields for the isotropically averaged relaxation supermatrix,

$$\langle \mathbf{R}^\alpha \rangle \;=\; \frac{4}{15} \sum_X \sum_Y \omega_{\mathrm{D},X}\, \omega_{\mathrm{D},Y}\, P_2(\cos\beta_{XY}) \sum_{M=-2}^{2} (-1)^M J(M\,\omega_0)\, \mathbf{C}^{XY}_{M,-M}\,. \tag{E.17}$$

When expressed in the ISTO basis of Table S1, the isotropically averaged relaxation supermatrix $\langle \mathbf{R}^\alpha \rangle$ is block-diagonal in the projection index Q, in accordance with the Wigner-Eckart theorem.[1] Since $\mathbf{R}^\alpha$ is also block-diagonal with respect to SIC parity, as expressed by Eq. (E.12), it follows that the evolution of the longitudinal magnetization modes under the site-averaged relaxation supermatrix $\langle \mathbf{R}^\alpha \rangle$ can be fully described within the subspace of the ten odd-parity zero-quantum basis operators above the dashed line in Table S1A. We have previously[5] presented in explicit form the 18 unique coefficient matrices $\mathbf{C}^{XY}_{M,-M}$, then defined as $\mathbf{C}^{XY}_M \equiv (-1)^M\, \mathbf{C}^{XY}_{M,-M}$.

The secular approximation is valid in the frequency range $\omega_0 \gg \omega_{\mathrm{D}}^2\,\tau_{\mathrm{A}}$, where the rapidly oscillating complex exponentials in Eq. (E.4) effectively eliminate all terms except those with $M' = -M$. Consequently,

$$\mathbf{R}^{\alpha}_{\mathrm{sec}} \;=\; \frac{4}{3}\sum_{X}\sum_{Y}\omega_{\mathrm{D},X}\,\omega_{\mathrm{D},Y}\sum_{M=-2}^{2}F_{M,-M}(\Omega^{\alpha}_{X},\Omega^{\alpha}_{Y})\,J(M\,\omega_0)\,\mathbf{C}^{XY}_{M,-M}\,. \tag{E.18}$$

Comparison of Eqs. (E.17) and (E.18) shows that, with regard to rotational symmetry, secular truncation has the same effect as isotropic averaging: all the supermatrices $\mathbf{C}^{XY}_{M,-M}$, as well as $\mathbf{R}^{\alpha}_{\mathrm{sec}}$, are block-diagonal in Q. Furthermore, within the single-spin subspace, Eq. (E.15) yields

$$C^{XY}_{M,-M,\,a_\alpha\,b_\beta} \;=\; \delta_{XY}\,C^{XX}_{M,-M,\,a_\alpha\,b_\beta} \;=\; \delta_{XY}\,\delta_{\alpha\,\beta}\,C^{XX}_{M,-M,\,a_\alpha\,b_\alpha}\,. \tag{E.19}$$

As a consequence of this selection rule, the secular contributions to relaxation matrix elements in the single-spin subspace only involve auto-mode relaxation, that is, no cross-mode relaxation. To establish the second equality in Eq. (E.19), we start from the definition (E.11): $C^{XX}_{M,-M,\,a_\alpha\,b_\beta} = \mathrm{Tr}\{[a^{\dagger}_{\alpha},\,T^2_M(X)]\,[T^2_{-M}(X),\,b_\beta]\}$. For both commutators to be nonzero, it is necessary that $a, b \in X$. The trace then contains a product of two single-spin operators for each of the two spins associated with the dipole coupling X. Since the only non-vanishing traces of a product of two single-spin operators are $\mathrm{Tr}_a\{a_z^2\} = \frac{1}{2}$ and $\mathrm{Tr}_a\{a_{\pm}a_{\mp}\} = 1$, it follows that the total trace vanishes unless $\alpha = \beta$.

The elements of the relaxation supermatrix $\mathbf{R}^{\alpha}$ needed to calculate the ILRR can be obtained from Eqs. (E.9) and (E.11) or, in the case of isotropically averaged rates, from Eq. (E.17). In the following, we present explicit expressions for some of these rates. The isotropically averaged rates required in Eq. (31) for the $ISP{-}ISP$ case can be obtained from Eq. (E.17) and the coefficient matrices $\mathbf{C}^{XY}_{M,-M}$, which have been presented in explicit form.[5] In Eq. (37) for the $ISP{-}IS$ case, we need the isotropically averaged longitudinal auto-spin and cross-spin rates

$$\left\langle R^{II}_{zz}\right\rangle \;=\; \tfrac{2}{45}\,(\omega^2_{\mathrm{D},IS}+\omega^2_{\mathrm{D},IP})\,[j(0)+3\,j(\omega_0)+6\,j(2\,\omega_0)]\;, \tag{E.20a}$$

$$\left\langle R^{SS}_{zz}\right\rangle \;=\; \tfrac{2}{45}\,(\omega^2_{\mathrm{D},IS}+\omega^2_{\mathrm{D},SP})\,[j(0)+3\,j(\omega_0)+6\,j(2\,\omega_0)]\;, \tag{E.20b}$$

$$\left\langle R^{IS}_{zz}\right\rangle \;=\; \tfrac{2}{45}\,\omega^2_{\mathrm{D},IS}[-\,j(0)+6\,j(2\,\omega_0)]\,. \tag{E.20c}$$

In Eq. (41) for the $ISP{-}I$ case, we only need $\left\langle R^{II}_{zz}\right\rangle$, which is still given by Eq. (E20a).

The various local relaxation rates R^{α}_{np} appearing in Eqs. (38) and (42) are all in the single-spin subspace. The local auto-spin rates required for the $ISP{-}I$ case are

$$\mathbf{R}^{\alpha}_{SS} \;=\; \boldsymbol{\rho}^{IS}\,, \tag{E.21a}$$

$$\mathbf{R}^{\alpha}_{PP} \;=\; \boldsymbol{\rho}^{IP}\,, \tag{E.21b}$$

and for the $ISP{-}IS$ case

$$\mathbf{R}^{\alpha}_{PP} \;=\; \boldsymbol{\rho}^{IP}+\boldsymbol{\rho}^{SP}\,. \tag{E.22}$$

Here we have introduced the generic auto-spin relaxation matrix

$$\boldsymbol{\rho}^X \;=\; \left[\begin{array}{ccc} \rho^X_{zz} & \rho^X_{z+} & \rho^X_{z-} \\ \rho^X_{+z} & \rho^X_{++} & \rho^X_{+-} \\ \rho^X_{-z} & \rho^X_{-+} & \rho^X_{--} \end{array}\right] , \tag{E.23}$$

with the five unique rates

$$\rho^X_{zz} \;=\; \tfrac{4}{3}\,\omega^2_{\mathrm{D},X}\Big\{\tfrac{1}{6}\,F_{00}(X)\,j(0) - \tfrac{1}{2}\,F_{1-1}(X)\,j(\omega_0) + \,F_{2-2}(X)\,j(2\,\omega_0)\Big\} , \tag{E.24a}$$

$$\begin{aligned}\rho^X_{++} \;=\; (\rho^X_{--})^* \;=\; \tfrac{4}{3}\,\omega^2_{\mathrm{D},X}\Big\{&\tfrac{5}{12}\,F_{00}(X)\,j(0) \\ &- \tfrac{1}{4}\,F_{1-1}(X)\,\left[3\,j(\omega_0) + i\,k(\omega_0)\right] + \tfrac{1}{2}\,F_{2-2}(X)\,\left[j(2\,\omega_0) + i\,k(2\,\omega_0)\right]\Big\} ,\end{aligned} \tag{E.24b}$$

$$\begin{aligned}\rho^X_{z+} \;=\; -\,(\rho^X_{z-})^* \;=\; \tfrac{4}{3}\,\omega^2_{\mathrm{D},X}\Big\{&\tfrac{1}{4\sqrt{3}}\,F_{0-1}(X)\,\left[2\,j(0) - j(\omega_0) - i\,k(\omega_0)\right] \\ &- \tfrac{1}{\sqrt{8}}\,F_{-21}(X)\,\left[j(\omega_0) - i\,k(\omega_0)\right]\Big\} ,\end{aligned} \tag{E.24c}$$

$$\begin{aligned}\rho^X_{+z} \;=\; -\,(\rho^X_{-z})^* \;=\; \tfrac{4}{3}\,\omega^2_{\mathrm{D},X}\Big\{&\tfrac{1}{4\sqrt{3}}\,F_{01}(X)\,\left[j(0) - 2\,j(\omega_0) + i\,2\,k(\omega_0)\right] \\ &+ \tfrac{1}{\sqrt{8}}\,F_{-12}(X)\,\left[j(2\,\omega_0) - i\,k(2\,\omega_0)\right]\Big\} ,\end{aligned} \tag{E.24d}$$

$$\begin{aligned}\rho^X_{+-} \;=\; (\rho^X_{-+})^* \;=\; \tfrac{2}{3}\,\omega^2_{\mathrm{D},X}\Big\{&-\tfrac{1}{\sqrt{6}}\,F_{02}(X)\,\left[j(0) + j(2\,\omega_0) - i\,k(2\,\omega_0)\right] \\ &+ \,\tfrac{1}{2}\,F_{11}(X)\,\left[j(\omega_0) - i\,k(\omega_0)\right]\Big\} ,\end{aligned} \tag{E.24e}$$

where $F_{MM'}(X)$ is a short-hand notation for $F_{MM'}(\Omega^\alpha_X, \Omega^\alpha_X)$.

The required local cross-spin rates are contained in the row matrices $\mathbf{R}^\alpha_{IS}$ and $\mathbf{R}^\alpha_{IP}$ for the $ISP{-}I$ case, and in $\mathbf{R}^\alpha_{IP}$ and $\mathbf{R}^\alpha_{SP}$ for the $ISP{-}IS$ case. The three elements of these matrices are of the form,

$$R^X_{zz} \;=\; \tfrac{4}{3}\,\omega^2_{\mathrm{D},X}\left[-\tfrac{1}{6}\,F_{00}(X)\,j(0) + F_{2-2}(X)\,j(2\,\omega_0)\right] , \tag{E.25a}$$

$$\begin{aligned}R^X_{z+} \;=\; -\,(R^X_{z-})^* \;=\; \tfrac{4}{3}\,\omega^2_{\mathrm{D},X}\Big\{&\tfrac{1}{4\sqrt{3}}\,F_{0-1}(X)\,\left[j(0) + j(\omega_0) + i\,k(\omega_0)\right] \\ &- \,\tfrac{1}{\sqrt{8}}\,F_{1-2}(X)\,\left[j(\omega_0) + j(2\,\omega_0) - i\,k(\omega_0) + i\,k(2\,\omega_0)\right]\Big\} .\end{aligned} \tag{E.25b}$$

For isochronous spins, the cross-spin rates have the symmetry $\mathbf{R}^\alpha_{SI} = \mathbf{R}^\alpha_{IS}$ and similarly for the other two pairs. As can be seen, all the cross-mode rates involve both the even and odd parts of the SDF.

All of the local relaxation rates in Eqs. (E.20) – (E.25) connect single-spin modes and are therefore entirely produced by self-correlations. These rates fully determine the ILRR in the $ISP{-}IS$ case. For the other two exchange cases, the ILRR is also affected by distinct correlations via those elements in the 10×10 odd-parity $Q = 0$ block of $\langle \mathbf{R}^\alpha \rangle$ that involve at least one three-spin zero-quantum coherence ($ISP{-}ISP$ case) or via the elements of the 9×9 relaxation matrix $\mathbf{R}^\alpha_{\mathrm{ss}00}$ spanned by two-spin-SP operators ($ISP{-}I$ case). These rates can be calculated from Eqs. (E.17) and (E.9), respectively, but they are too numerous to list here.

The ILRR in the $ISP{-}I$ case also involves the static dipolar Liouvillian supermatrix $\mathbf{\Delta}^{\alpha}$ in Eq. (E.8) or, more precisely, the 3×9 submatrices connecting single-spin S or P modes with two-spin-SP modes. For example,

$$\mathbf{\Delta}^{\alpha}_{S,\mathrm{s0}} = \frac{\omega_{\mathrm{D},SP}}{\sqrt{6}} \times \begin{bmatrix} 0 & 0 & \frac{2}{\sqrt{3}}D_0 & D_1 & D_1 & D_{-1} & -D_{-1} & 2D_2 & -2D_{-2} \\ 0 & -\sqrt{3}D_{-1} & -D_{-1} & -\frac{1}{\sqrt{3}}D_0 & -\sqrt{3}D_0 & -\sqrt{2}D_{-2} & -\sqrt{2}D_{-2} & -\sqrt{2}D_1 & 0 \\ 0 & \sqrt{3}D_1 & -D_1 & -\sqrt{2}D_2 & \sqrt{2}D_2 & -\frac{1}{\sqrt{3}}D_0 & \sqrt{3}D_0 & 0 & \sqrt{2}D_{-1} \end{bmatrix}, \tag{E.26}$$

where $D_M \equiv D^2_{M0}(\Omega^{\alpha}_{SP})$, the complex conjugate of which is given by Eq. (4c). In Eq. (E.26), the basis ordering for the single-spin-S subspace is $\{S_z/\sqrt{2},\, -S_+/2,\, S_-/2\}$, while the two-spin-$SP$ operators are in the order in which they appear in Table S1, that is, {13, 16, 19, 31, 34, 46, 49, 55, 61}. The matrix $\mathbf{\Delta}^{\alpha}_{P,\mathrm{s0}}$ differs from $\mathbf{\Delta}^{\alpha}_{S,\mathrm{s0}}$ only in that the sign is reversed for all elements in columns 3, 4 and 6 (corresponding to the odd-rank basis operators 19, 31 and 46). Further, since the supermatrix $\mathbf{\Delta}^{\alpha}$ is Hermitian, it follows that $\mathbf{\Delta}^{\alpha}_{\mathrm{s0},S} = \mathbf{\Delta}^{\alpha\,\dagger}_{S,\mathrm{s0}}$.

APPENDIX F: INTEGRAL RELAXATION RATE IN THE MN REGIME

Here we present derivations of explicit expressions for the ILRR in the motional narrowing (MN) regime for exchange cases $ISP{-}IS$ and $ISP{-}I$. It is convenient to express $\mathbf{G}^{\mathrm{A}}(0)$ from Eq. (26) as

$$\mathbf{G}^{\mathrm{A}}(0) \;=\; \left\langle (\mathbf{\Lambda}^{\alpha})^{-1} \right\rangle \,, \tag{F.1}$$

with

$$\mathbf{\Lambda}^{\alpha} \;\equiv\; \mathbf{K} + \mathbf{R}^{\alpha}\,\tau_{\mathrm{A}} + i\,\mathbf{L}^{\mathrm{A}}_{\mathrm{Z}}\,\tau_{\mathrm{A}} + i\,\mathbf{\Delta}^{\alpha}\,\tau_{\mathrm{A}} \,, \tag{F.2}$$

where the last term appears only for exchange case $ISP{-}I$. We shall now use symmetry arguments and the MN condition $\omega_{\mathrm{D}}\,\tau_{\mathrm{A}} \ll 1$ to simplify the supermatrix $\mathbf{\Lambda}^{\alpha}$. Throughout Appendix F, we assume isochronous spins ($\delta^{\mathrm{A}}_S = \delta^{\mathrm{A}}_P = 0$), with $\omega^{\mathrm{A}}_I = \omega^{\mathrm{A}}_S = \omega^{\mathrm{A}}_P \equiv \omega_0$. In Appendix G, we generalize the treatment to include the effects of chemical shifts.

1. Exchange case $ISP{-}IS$

To obtain the four elements of $\mathbf{G}^{\mathrm{A}}(0)$ that appear in Eq. (35), we need only consider the 36×36 odd-parity block (Appendix E)

$$\mathbf{\Lambda}^{\alpha}_{\mathrm{aa}} \;=\; \mathbf{K}_{\mathrm{aa}} + \mathbf{R}^{\alpha}_{\mathrm{aa}}\tau_{\mathrm{A}} + i\,\mathbf{L}^{\mathrm{A}}_{\mathrm{Z,aa}}\,\tau_{\mathrm{A}} \,. \tag{F.3}$$

Before invoking the MN approximation, we reorder the 36 odd-parity basis operators so that the three operators (numbered 3, 22 and 37 in Table S1) that only involve spin P are at the end. With $\mathbf{K}_{\mathrm{aa}}$ from Eq. (18), we can then partition the supermatrices in Eq. (F.3) as

$$\mathbf{\Lambda}^{\alpha}_{\mathrm{aa}} \;=\; \begin{bmatrix} (\mathbf{1} + \mathbf{R}^{\alpha}_{11}\,\tau_{\mathrm{A}} + i\,\mathbf{L}^{\mathrm{A}}_{\mathrm{Z},11}\,\tau_{\mathrm{A}}) & \mathbf{R}^{\alpha}_{10}\,\tau_{\mathrm{A}} \\ \mathbf{R}^{\alpha}_{01}\,\tau_{\mathrm{A}} & (\mathbf{R}^{\alpha}_{00}\,\tau_{\mathrm{A}} + i\,\mathbf{L}^{\mathrm{A}}_{\mathrm{Z},00}\,\tau_{\mathrm{A}}) \end{bmatrix}, \tag{F.4}$$

where the subscripts indicate whether $K_{nn} = 1$ or 0. We need only consider the '11' block of the inverse $(\mathbf{\Lambda}^{\alpha}_{\mathrm{aa}})^{-1}$, which is

$$\begin{aligned} [(\mathbf{\Lambda}^{\alpha}_{\mathrm{aa}})^{-1}]_{11} \;&=\; \Big[\mathbf{1} + \mathbf{R}^{\alpha}_{11}\,\tau_{\mathrm{A}} + i\,\mathbf{L}^{\mathrm{A}}_{\mathrm{Z},11}\,\tau_{\mathrm{A}} \;-\; \mathbf{R}^{\alpha}_{10}\left(\mathbf{R}^{\alpha}_{00} + i\,\mathbf{L}^{\mathrm{A}}_{\mathrm{Z},00}\right)^{-1}\mathbf{R}^{\alpha}_{01}\,\tau_{\mathrm{A}}\Big]^{-1} \\ &=\; \mathbf{Z}^{-1} - \mathbf{Z}^{-1}\Big[\mathbf{R}^{\alpha}_{11} - \mathbf{R}^{\alpha}_{10}\left(\mathbf{R}^{\alpha}_{00} + i\,\mathbf{L}^{\mathrm{A}}_{\mathrm{Z},00}\right)^{-1}\mathbf{R}^{\alpha}_{01}\Big]\,\tau_{\mathrm{A}}\,\mathbf{Z}^{-1} \,, \end{aligned} \tag{F.5}$$

where, in the last step, we have expanded to second order in $\omega_{\mathrm{D}}\tau_{\mathrm{A}}$ (the MN approximation) and defined $\mathbf{Z} \equiv \mathbf{1} + i\,\mathbf{L}^{\mathrm{A}}_{\mathrm{Z},11}\,\tau_{\mathrm{A}}$. According to Eq. (F.1), isotropic averaging of this result yields the corresponding 33×33 block of $\mathbf{G}^{\mathrm{A}}(0)$. For the ILRR, we only need elements from the upper left 2×2 block of $\mathbf{G}^{\mathrm{A}}(0)$, corresponding to the basis operators $I_z/\sqrt{2}$ and $S_z/\sqrt{2}$. In this subspace $\mathbf{L}^{\mathrm{A}}_{\mathrm{Z}} = \mathbf{0}$, so Eq. (F.5) yields

$$\mathbf{G}^{\mathrm{A}}(0) \;=\; \mathbf{1} - \widetilde{\mathbf{R}}\,\tau_{\mathrm{A}} \,, \tag{F.6}$$

with

$$\widetilde{\mathbf{R}} \;\equiv\; \langle \mathbf{R}^{\alpha} \rangle - \langle \mathbf{\Gamma}^{\alpha} \rangle \,. \tag{F.7}$$

In the interest of notational economy, we do not explicitly indicate that all quantities in Eqs. (F.6) and (F.7) are 2×2 matrices in the subspace spanned by the basis operators $I_z/\sqrt{2}$ and $S_z/\sqrt{2}$. Combination of Eqs. (35) and (F.6) yields for the ILRR

$$\widehat{R}^{\,\mathrm{dil}}_{1,IS} \;=\; P_{\mathrm{A}}\,\frac{2\,(\widetilde{R}_{II}\widetilde{R}_{SS} - \widetilde{R}_{IS}\widetilde{R}_{SI})}{(\widetilde{R}_{II} + \widetilde{R}_{SS} - \widetilde{R}_{IS} - \widetilde{R}_{SI})}\,, \tag{F.8}$$

where the supermatrix $\widetilde{\mathbf{R}}$ is indexed by I and S rather than by the labels $n = 1$ and 2. The first part of $\widetilde{\mathbf{R}}$ is the isotropic orientational average of the longitudinal relaxation matrix

$$\mathbf{R}^{\alpha} \;=\; \begin{bmatrix} R^{II}_{zz} & R^{IS}_{zz} \\ R^{IS}_{zz} & R^{SS}_{zz} \end{bmatrix}\,. \tag{F.9}$$

The second part is the isotropic orientational average of the "cross relaxation" supermatrix

$$\mathbf{\Gamma}^{\alpha} \;\equiv\; \mathbf{R}^{\alpha}_{IP/SP}\,(\mathbf{R}^{\alpha}_{PP} + i\,\omega_0\,\mathbf{Q})^{-1}\,\mathbf{R}^{\alpha\,\dagger}_{IP/SP}\,, \tag{F.10}$$

where $\mathbf{Q} = \mathrm{diag}(0, 1, -1)$. Further, $\mathbf{R}^{\alpha\,\dagger}_{IP/SP}$ is the Hermitian conjugate (or conjugate transpose) of the rectangular relaxation matrix

$$\mathbf{R}^{\alpha}_{IP/SP} \;\equiv\; \begin{bmatrix} \mathbf{R}^{\alpha}_{IP} \\ \mathbf{R}^{\alpha}_{SP} \end{bmatrix} \;\equiv\; \begin{bmatrix} R^{IP}_{zz} & R^{IP}_{z+} & R^{IP}_{z-} \\ R^{SP}_{zz} & R^{SP}_{z+} & R^{SP}_{z-} \end{bmatrix}\,, \tag{F.11}$$

and

$$\mathbf{R}^{\alpha}_{PP} \;\equiv\; \begin{bmatrix} R^{PP}_{zz} & R^{PP}_{z+} & R^{PP}_{z-} \\ R^{PP}_{+z} & R^{PP}_{++} & R^{PP}_{+-} \\ R^{PP}_{-z} & R^{PP}_{-+} & R^{PP}_{--} \end{bmatrix}\,. \tag{F.12}$$

In Eqs. (F.9) and (F.10), we have made use of the following symmetry relations: $R^{SI}_{zz} = R^{IS}_{zz}$, $\mathbf{R}^{\alpha}_{PI} = \mathbf{R}^{\alpha}_{IP}$, $\mathbf{R}^{\alpha}_{PS} = \mathbf{R}^{\alpha}_{SP}$, $R^{IP}_{\pm z} = R^{IP\,*}_{z\pm}$ and $R^{SP}_{\pm z} = R^{SP\,*}_{z\pm}$. All these relations, except the first one, are only valid for isochronous spins. In contrast, $\widetilde{R}_{SI} \neq \widetilde{R}_{IS}$ in Eq. (F.8), because, as seen from Eqs. (E.22) – (E.24), $\mathbf{R}^{\alpha}_{PP}$ is not symmetric. The individual relaxation rates appearing in Eqs. (F.9), (F.11) and (F.12) are given in explicit form in Appendix E. All these rates connect single-spin modes and, according to the selection rule (E.15), they therefore only involve dipolar self-correlations. However, the ILRR is affected by cross-spin rates, such as R^{IS}_{zz}, as well as cross-mode rates, such as R^{PP}_{z+}.

In the absence of spin P, the ISP–IS results derived here must reduce to the previously obtained results for the symmetric two-spin case $IS-IS$. With $\omega_{\mathrm{D},IP} = \omega_{\mathrm{D},SP} = 0$, the "cross-relaxation" supermatrix in Eq. (F.10) vanishes so Eq. (F.7) reduces to $\widetilde{\mathbf{R}} = \langle \mathbf{R}^{\alpha} \rangle$. For isochronous spins $\langle R^{II}_{zz} \rangle = \langle R^{SS}_{zz} \rangle$ and $\langle R^{IS}_{zz} \rangle = \langle R^{SI}_{zz} \rangle$, so Eqs. (F.7) – (F.9) yield the expected[3,9] result

$$\widehat{R}^{\,\mathrm{dil}}_{1,IS} \;=\; P_{\mathrm{A}}\,\big[\langle R^{II}_{zz} \rangle + \langle R^{IS}_{zz} \rangle\big] \;=\; \frac{2}{15}\,P_{\mathrm{A}}\,\omega^2_{\mathrm{D},IS}\,[\,j(\omega_0) + 4\,j(2\,\omega_0)\,]\,, \tag{F.13}$$

where we have also used Eq. (E.20).

If spin S is removed, the $ISP{-}IS$ case degenerates into the asymmetric two-spin case $IP{-}I$. With $\omega_{\mathrm{D},IS} = \omega_{\mathrm{D},SP} = 0$, $R^{IS}_{zz} = R^{SI}_{zz} = R^{SS}_{zz} = 0$ in Eq. (F.9) and $\mathbf{R}^{\alpha}_{SP} = \mathbf{0}$ in Eq. (F.11). The only nonzero element of $\mathbf{G}^{\mathrm{A}}(0)$ is then

$$g_{11} \;=\; 1 - \left\langle R^{II}_{zz} \right\rangle \tau_{\mathrm{A}} + \left\langle \mathbf{R}^{\alpha}_{IP} \left(\mathbf{R}^{\alpha}_{PP} + i\,\omega_0\,\mathbf{Q}\right)^{-1} \mathbf{R}^{\alpha\,\dagger}_{IP} \right\rangle \tau_{\mathrm{A}} \,. \tag{F.14}$$

Replacing P by S to obtain the corresponding result for the previously treated $IS{-}I$ case and noting that, for this case, $\widehat{R}^{\mathrm{dil}}_{1,I} = (P_{\mathrm{A}}/\tau_{\mathrm{A}})\,(1 - g_{11})$, we recover the expected[9] result

$$\widehat{R}^{\mathrm{dil}}_{1,I} \;=\; P_{\mathrm{A}} \left[\left\langle R^{II}_{zz} \right\rangle - \left\langle \mathbf{R}^{\alpha}_{IS} \left(\mathbf{R}^{\alpha}_{SS} + i\,\omega_0\,\mathbf{Q}\right)^{-1} \mathbf{R}^{\alpha\,\dagger}_{IS} \right\rangle \right] . \tag{F.15}$$

The secular approximation is valid in the frequency range $\omega_0 \gg \omega_{\mathrm{D}}^2\,\tau_{\mathrm{A}}$, where the rapidly oscillating complex exponentials in Eq. (E.4) effectively eliminate all terms except those with $M' = -M$. The selection rule (E.19) then shows that all single-spin cross-mode rates vanish. As a result, Eqs. (F.7) – (F.12) yield

$$\widehat{R}^{\mathrm{dil}}_{1,IS} \;=\; P_{\mathrm{A}}\, \frac{2\,(r_{II}\,r_{SS} - r^2_{IS})}{(r_{II} + r_{SS} - 2\,r_{IS})} \,, \tag{F.16}$$

where

$$r_{II} \;=\; \left\langle R^{II}_{zz} \right\rangle \;-\; \left\langle \frac{(R^{IP}_{zz})^2}{R^{PP}_{zz}} \right\rangle \,, \tag{F.17a}$$

$$r_{IS} \;=\; \left\langle R^{IS}_{zz} \right\rangle \;-\; \left\langle \frac{R^{IP}_{zz}\,R^{SP}_{zz}}{R^{PP}_{zz}} \right\rangle \,, \tag{F.17b}$$

$$r_{SS} \;=\; \left\langle R^{SS}_{zz} \right\rangle \;-\; \left\langle \frac{(R^{SP}_{zz})^2}{R^{PP}_{zz}} \right\rangle \,. \tag{F.17c}$$

2. Exchange case $ISP{-}I$

If the basis is ordered with the 36 odd-parity operators before the 27 even operators, the supermatrices $\mathbf{L}^{\mathrm{A}}_{\mathrm{Z}}$ and $\mathbf{R}^{\alpha}$ are block-diagonal whereas $\mathbf{\Delta}^{\alpha}$ is anti-block-diagonal, as shown in Eqs. (E.12) and (E.13). Noting also that $\mathbf{K}$ is diagonal, we can partition $\mathbf{\Lambda}^{\alpha}$ in Eq. (F.2) as

$$\mathbf{\Lambda}^{\alpha} \;=\; \begin{bmatrix} (\mathbf{K}_{\mathrm{aa}} + \mathbf{R}^{\alpha}_{\mathrm{aa}}\,\tau_{\mathrm{A}} + i\,\mathbf{L}^{\mathrm{A}}_{\mathrm{Z,aa}}\,\tau_{\mathrm{A}}) & i\,\mathbf{\Delta}^{\alpha}_{\mathrm{as}}\,\tau_{\mathrm{A}} \\ i\,\mathbf{\Delta}^{\alpha}_{\mathrm{sa}}\,\tau_{\mathrm{A}} & (\mathbf{K}_{\mathrm{ss}} + \mathbf{R}^{\alpha}_{\mathrm{ss}}\,\tau_{\mathrm{A}} + i\,\mathbf{L}^{\mathrm{A}}_{\mathrm{Z,ss}}\,\tau_{\mathrm{A}}) \end{bmatrix} . \tag{F.18}$$

where the odd (or antisymmetric = a) and even (or symmetric = s) SIC parity is indicated by subscripts. The single-spin-I subspace is contained within the odd-parity subspace so we only need the 'aa' block of the inverse $(\mathbf{\Lambda}^{\alpha})^{-1}$, which is

$$(\mathbf{\Lambda}^{\alpha})^{-1}_{\mathrm{aa}} \;=\; \left[\mathbf{K}_{\mathrm{aa}} + (\mathbf{R}^{\alpha}_{\mathrm{aa}} + \mathbf{X}^{\alpha}_{\mathrm{aa}} + i\,\mathbf{L}^{\mathrm{A}}_{\mathrm{Z,aa}})\,\tau_{\mathrm{A}}\right]^{-1} \,, \tag{F.19}$$

with

$$\mathbf{X}^{\alpha}_{\mathrm{aa}} \;\equiv\; \mathbf{\Delta}^{\alpha}_{\mathrm{as}}\,(\mathbf{K}_{\mathrm{ss}} + \mathbf{R}^{\alpha}_{\mathrm{ss}}\,\tau_{\mathrm{A}} + i\,\mathbf{L}^{\mathrm{A}}_{\mathrm{Z,ss}}\,\tau_{\mathrm{A}})^{-1}\mathbf{\Delta}^{\alpha}_{\mathrm{sa}}\,\tau_{\mathrm{A}} \,. \tag{F.20}$$

We further partition the submatrices according to whether $K_{nn} = 1$ or 0. Ordering the basis so that, within the odd and even subspaces, basis operators with $K_{nn} = 1$ precede those with $K_{nn} = 0$, we have

$$\mathbf{K}_{\rm aa} \;=\; \left[\begin{array}{cc} \mathbf{1}_{\rm aa11} & \mathbf{0}_{\rm aa10} \\ \mathbf{0}_{\rm aa01} & \mathbf{0}_{\rm aa00} \end{array}\right] \qquad \text{and} \qquad \mathbf{K}_{\rm ss} \;=\; \left[\begin{array}{cc} \mathbf{1}_{\rm ss11} & \mathbf{0}_{\rm ss10} \\ \mathbf{0}_{\rm ss01} & \mathbf{0}_{\rm ss00} \end{array}\right] , \tag{F.21}$$

where the subscripts indicate the subspace. Since there are six single-spin S and P operators in the 'aa00' subspace and nine two-spin-SP operators in the 'ss00' subspace, it follows that $\mathbf{0}_{\rm aa00}$ is a 6×6 null matrix, while $\mathbf{0}_{\rm ss00}$ is a 9×9 null matrix. Furthermore, $\mathbf{1}_{\rm aa11}$ is a 30×30 identity matrix, while $\mathbf{1}_{\rm ss11}$ is a 18×18 identity matrix. We can thus partition the matrix to be inverted in Eq. (F.19) as

$$(\mathbf{\Lambda}^\alpha)^{-1}_{\rm aa} \;=\; \left[\begin{array}{cc} \mathbf{1}_{\rm aa11} + (\mathbf{R}^\alpha_{\rm aa11} + \mathbf{X}^\alpha_{\rm aa11} + i\,\mathbf{L}^{\rm A}_{\rm Z,aa11})\,\tau_{\rm A} & (\mathbf{R}^\alpha_{\rm aa10} + \mathbf{X}^\alpha_{\rm aa10})\,\tau_{\rm A} \\ (\mathbf{R}^\alpha_{\rm aa01} + \mathbf{X}^\alpha_{\rm aa01})\,\tau_{\rm A} & (\mathbf{R}^\alpha_{\rm aa00} + \mathbf{X}^\alpha_{\rm aa00} + i\,\mathbf{L}^{\rm A}_{\rm Z,aa00})\,\tau_{\rm A} \end{array}\right]^{-1} . \tag{F.22}$$

We only need the aa11 block of $(\mathbf{\Lambda}^\alpha)^{-1}_{\rm aa}$, which is

$$\begin{aligned} (\mathbf{\Lambda}^\alpha)^{-1}_{\rm aa11} \;=\; \Big[&\mathbf{1}_{\rm aa11} + (\mathbf{R}^\alpha_{\rm aa11} + \mathbf{X}^\alpha_{\rm aa11} + i\,\mathbf{L}^{\rm A}_{\rm Z,aa11})\,\tau_{\rm A} \\ &- (\mathbf{R}^\alpha_{\rm aa10} + \mathbf{X}^\alpha_{\rm aa10})\left(\mathbf{R}^\alpha_{\rm aa00} + \mathbf{X}^\alpha_{\rm aa00} + i\,\mathbf{L}^{\rm A}_{\rm Z,aa00}\right)^{-1}(\mathbf{R}^\alpha_{\rm aa01} + \mathbf{X}^\alpha_{\rm aa01})\,\tau_{\rm A}\Big]^{-1} . \end{aligned} \tag{F.23}$$

Expanding to second order in $\omega_{\rm D}\tau_{\rm A}$ (the MN approximation) and performing the isotropic orientational average, we obtain with Eq. (F.1)

$$\begin{aligned} \mathbf{G}^{\rm A}_{\rm aa11}(0) \;=\;& \mathbf{Z}^{-1} \;-\; \mathbf{Z}^{-1}\left[\langle\mathbf{R}^\alpha_{\rm aa11}\rangle + \langle\mathbf{X}^\alpha_{\rm aa11}\rangle\right]\tau_{\rm A}\,\mathbf{Z}^{-1} \\ &+\; \mathbf{Z}^{-1}\Big\langle(\mathbf{R}^\alpha_{\rm aa10} + \mathbf{X}^\alpha_{\rm aa10})\left(\mathbf{R}^\alpha_{\rm aa00} + \mathbf{X}^\alpha_{\rm aa00} + i\,\mathbf{L}^{\rm A}_{\rm Z,aa00}\right)^{-1}(\mathbf{R}^\alpha_{\rm aa01} + \mathbf{X}^\alpha_{\rm aa01})\Big\rangle\,\tau_{\rm A}\,\mathbf{Z}^{-1} , \end{aligned} \tag{F.24}$$

with $\mathbf{Z} \equiv \mathbf{1}_{\rm aa11} + i\,\mathbf{L}^{\rm A}_{\rm Z,aa11}\,\tau_{\rm A}$. The ILRR is determined by the single element $g_{11} = (1|\mathbf{G}^{\rm A}_{\rm aa11}(0)|1)$ of this 30×30 supermatrix, where $|1) = B_1 = I_z/\sqrt{2}$. For this element, two simplifications can be made in Eq. (F.24). First, because $(1|\mathbf{L}^{\rm A}_{\rm Z,aa11}|n) = (n|\mathbf{L}^{\rm A}_{\rm Z,aa11}|1) = 0$, it follows that $(1|\mathbf{Z}^{-1}|n) = (n|\mathbf{Z}^{-1}|1) = \delta_{n1}$. Second, because I_z commutes with $T^2_M(SP)$, it follows from Eq. (E.10) that $(1|\mathbf{\Delta}^\alpha_{\rm as}|n) = (n|\mathbf{\Delta}^\alpha_{\rm sa}|1) = 0$ and, in view of Eq. (F.20), that $(1|\mathbf{X}^\alpha_{\rm aa11}|1) = (1|\mathbf{X}^\alpha_{\rm aa10}|n) = (n|\mathbf{X}^\alpha_{\rm aa01}|1) = 0$. After these simplifications, Eq. (F.24) yields

$$g_{11} = 1 \;-\; \left[\left\langle R^{II}_{zz}\right\rangle - \left\langle\Gamma^{II}_{zz}\right\rangle\right]\tau_{\rm A} , \tag{F.25}$$

which is combined with Eq. (24) to yield

$$\widehat{R}^{\rm dil}_{1,I} \;=\; P_{\rm A}\left[\left\langle R^{II}_{zz}\right\rangle - \left\langle\Gamma^{II}_{zz}\right\rangle\right] . \tag{F.26}$$

Here, we have defined the "cross relaxation" rate

$$\begin{aligned} \Gamma^{II}_{zz} \;\equiv\;& (1|\mathbf{R}^\alpha_{\rm aa10}(\mathbf{R}^\alpha_{\rm aa00} + \mathbf{X}^\alpha_{\rm aa00} + i\,\mathbf{L}^{\rm A}_{\rm Z,aa00})^{-1}\mathbf{R}^\alpha_{\rm aa01}|1) \\ =\;& \mathbf{R}^\alpha_{IS,IP}\left[\begin{array}{cc} (\mathbf{R}^\alpha_{SS} + \mathbf{X}^\alpha_{SS} + i\,\omega_0\,\mathbf{Q}) & \mathbf{X}^\alpha_{SP} \\ \mathbf{X}^\alpha_{PS} & (\mathbf{R}^\alpha_{PP} + \mathbf{X}^\alpha_{PP} + i\,\omega_0\,\mathbf{Q}) \end{array}\right]^{-1}\mathbf{R}^{\alpha\,\dagger}_{IS,IP} , \end{aligned} \tag{F.27}$$

where $\mathbf{Q} = \mathrm{diag}(0, 1, -1)$ and we have noted that $\mathbf{R}^\alpha_{SP} = \mathbf{0}$ since the SP dipole coupling is static. Further, $\mathbf{R}^\alpha_{IS,IP} \equiv [\mathbf{R}^\alpha_{IS}\ \mathbf{R}^\alpha_{IP}]$ and $\mathbf{R}^\alpha_{IS}$, $\mathbf{R}^\alpha_{IP}$, $\mathbf{R}^\alpha_{SS}$ and $\mathbf{R}^\alpha_{PP}$ are defined in analogy with Eqs. (F.11) and (F.12). The individual relaxation rates appearing in these relaxation matrices are given in explicit form in Eqs. (E.21) – (E.25). All these rates connect single-spin modes and therefore, according to the selection rule Eq. (E.15), they only involve self-correlations.

The static SP dipole coupling affects the ILRR via the 3×3 blocks $\mathbf{X}^\alpha_{SS}$, $\mathbf{X}^\alpha_{SP}$, $\mathbf{X}^\alpha_{PS}$ and $\mathbf{X}^\alpha_{PP}$ of the 6×6 supermatrix $\mathbf{X}^\alpha_{\mathrm{aa00}}$ in the single-spin S and P subspace. According to Eq. (F.20), we have, for example,

$$\mathbf{X}^\alpha_{SP} \;=\; \mathbf{\Delta}^\alpha_{S,\mathrm{s}}\,(\mathbf{H}^\alpha_{\mathrm{ss}})^{-1}\mathbf{\Delta}^\alpha_{\mathrm{s},P}\,. \tag{F.28}$$

with $\mathbf{H}^\alpha_{\mathrm{ss}} \equiv \mathbf{K}_{\mathrm{ss}}/\tau_{\mathrm{A}} + \mathbf{R}^\alpha_{\mathrm{ss}} + i\,\mathbf{L}^{\mathrm{A}}_{\mathrm{Z,ss}}$. Note that subscript 's' refers to the symmetric subspace spanned by the 27 two-spin operators in Table S1, while subscript S refers to the single-spin-S subspace, spanned by $S_z/\sqrt{2}$, $-S_+/2$ and $S_-/2$. It follows from Eqs. (E.8) and (E.10) that the supermatrices $\mathbf{\Delta}^\alpha_{S,\mathrm{s}}$ and $\mathbf{\Delta}^\alpha_{\mathrm{s},P}$ have nonzero elements only within the 's0' subspace spanned by the nine two-spin-SP operators. Consequently,

$$\mathbf{X}^\alpha_{SP} \;=\; \mathbf{\Delta}^\alpha_{S,\mathrm{s0}}\,(\mathbf{H}^\alpha_{\mathrm{ss}})^{-1}_{00}\mathbf{\Delta}^\alpha_{\mathrm{s0},P}\,. \tag{F.29}$$

To obtain the quantity $(\mathbf{H}^\alpha_{\mathrm{ss}})^{-1}_{00}$, we partition $\mathbf{H}^\alpha_{\mathrm{ss}}$ in the same way as for $\mathbf{K}_{\mathrm{ss}}$ in Eq. (F.21),

$$\mathbf{H}^\alpha_{\mathrm{ss}} \;=\; \begin{bmatrix} (\mathbf{1}_{\mathrm{ss11}}/\tau_{\mathrm{A}} + \mathbf{R}^\alpha_{\mathrm{ss11}} + i\,\mathbf{L}^{\mathrm{A}}_{\mathrm{Z,ss11}}) & \mathbf{R}^\alpha_{\mathrm{ss10}} \\ \mathbf{R}^\alpha_{\mathrm{ss01}} & (\mathbf{R}^\alpha_{\mathrm{ss00}} + i\mathbf{L}^{\mathrm{A}}_{\mathrm{ss00}}) \end{bmatrix}. \tag{F.30}$$

The required block of the inverse $(\mathbf{H}^\alpha_{\mathrm{ss}})^{-1}$ is

$$\begin{aligned} (\mathbf{H}^\alpha_{\mathrm{ss}})^{-1}_{00} \;&=\; \Big[\mathbf{R}^\alpha_{\mathrm{ss00}} + i\,\mathbf{L}^{\mathrm{A}}_{\mathrm{ss00}} - \mathbf{R}^\alpha_{\mathrm{ss01}}\left(\mathbf{1}_{\mathrm{ss11}}/\tau_{\mathrm{A}} + \mathbf{R}^\alpha_{\mathrm{ss11}} + i\,\mathbf{L}^{\mathrm{A}}_{\mathrm{ss11}}\right)^{-1}\mathbf{R}^\alpha_{\mathrm{ss10}}\Big]^{-1} \\ &=\; \left(\mathbf{R}^\alpha_{\mathrm{ss00}} + i\,\mathbf{L}^{\mathrm{A}}_{\mathrm{ss00}}\right)^{-1}\,, \end{aligned} \tag{F.31}$$

where, in the last step, we have expanded to second order in $\omega_{\mathrm{D}}\tau_{\mathrm{A}}$ to be consistent with the MN approximation. Finally, combination of Eqs. (F.29) and (F.31) yields

$$\begin{bmatrix} \mathbf{X}^\alpha_{SS} & \mathbf{X}^\alpha_{SP} \\ \mathbf{X}^\alpha_{PS} & \mathbf{X}^\alpha_{PP} \end{bmatrix} \;=\; \mathbf{\Delta}^\alpha_{S/P,\mathrm{s0}}(\mathbf{R}^\alpha_{\mathrm{ss00}} + i\,\omega_0\,\mathbf{Q}_{\mathrm{ss00}})^{-1}\mathbf{\Delta}^{\alpha\,\dagger}_{S/P,\mathrm{s0}}\,, \tag{F.32}$$

where $\mathbf{Q}_{\mathrm{ss00}} = \mathrm{diag}(0, 0, 0, 1, 1, -1, -1, 2, -2)$, $\mathbf{\Delta}^\alpha_{S/P,\mathrm{s0}}$ is the 6×9 matrix

$$\mathbf{\Delta}^\alpha_{S/P,\mathrm{s0}} \;\equiv\; \begin{bmatrix} \mathbf{\Delta}^\alpha_{S,\mathrm{s0}} \\ \mathbf{\Delta}^\alpha_{P,\mathrm{s0}} \end{bmatrix}, \tag{F.33}$$

and $\mathbf{\Delta}^{\alpha\,\dagger}_{S/P,\mathrm{s0}}$ is its 9×6 Hermitian conjugate. This follows because the supermatrix $\mathbf{\Delta}^\alpha$ is Hermitian, so $\mathbf{\Delta}^\alpha_{\mathrm{s0},S} = \mathbf{\Delta}^{\alpha\,\dagger}_{S,\mathrm{s0}}$ and $\mathbf{\Delta}^\alpha_{\mathrm{s0},P} = \mathbf{\Delta}^{\alpha\,\dagger}_{P,\mathrm{s0}}$. The static dipolar Liouvillian submatrices $\mathbf{\Delta}^\alpha_{S,\mathrm{s0}}$ and $\mathbf{\Delta}^\alpha_{P,\mathrm{s0}}$ can be obtained from Eq. (E.26). The elements of the 9×9 relaxation

matrix $\mathbf{R}^{\alpha}_{\mathrm{ss00}}$, obtained from Eqs. (E.9) and (E.11), involve IS and IP self-correlations as well as IS–IP distinct correlations.

We now consider several special cases. If we neglect the static SP dipole coupling by setting $\omega_{\mathrm{D},SP} = 0$, then $\mathbf{\Delta}^{\alpha}_{\mathrm{as}} = \mathbf{\Delta}^{\alpha}_{\mathrm{sa}} = \mathbf{0}$ so the antisymmetric and symmetric blocks in Eq. (F.18) are decoupled and the relaxation behavior is fully described by the single-spin modes. Because now $\mathbf{X}^{\alpha}_{\mathrm{aa00}} = \mathbf{0}$, Eq. (F.27) yields

$$\Gamma^{II}_{zz} \;=\; \mathbf{R}^{\alpha}_{IS}\,(\mathbf{R}^{\alpha}_{SS} + i\,\omega_0\,\mathbf{Q})^{-1}\mathbf{R}^{\alpha\,\dagger}_{IS} \;+\; \mathbf{R}^{\alpha}_{IP}\,(\mathbf{R}^{\alpha}_{PP} + i\,\omega_0\,\mathbf{Q})^{-1}\mathbf{R}^{\alpha\,\dagger}_{IP}\,, \tag{F.34}$$

showing, with Eq. (F.26), that the IS and IP dipole couplings contribute additively to the ILRR $\widehat{R}^{\mathrm{dil}}_{1,I}$. If both dipole couplings to spin P are set to zero, then the ISP–I case must reduce to the asymmetric two-spin case IS–I. With $\omega_{\mathrm{D},IP} = 0$, the second term in Eq. (F.34) vanishes and what remains is, as in Eq. (F.15), the result obtained previously for the IS–I case, when specialized to isochronous spins.[9]

If we (artificially) neglect cross-spin relaxation, so that $\mathbf{R}^{\alpha}_{IS} = \mathbf{R}^{\alpha}_{IP} = \mathbf{0}$, then Eqs. (F.26) and (F.27) show that

$$\widehat{R}^{\mathrm{dil}}_{1,I} \;=\; P_{\mathrm{A}}\,\langle R^{II}_{zz}\rangle \;=\; \tfrac{2}{45}\,P_{\mathrm{A}}\,(\omega^2_{\mathrm{D},IS} + \omega^2_{\mathrm{D},IP})\,[\,j(0) + 3\,j(\omega_0) + 6\,j(2\,\omega_0)\,]\,, \tag{F.35}$$

where Eq. (E.20a) was also used. This (unphysical) result shows that cross-spin relaxation is necessary for the ILRR to approach zero at high field, as it must.

The secular approximation is valid in the frequency range $\omega_0 \gg \omega^2_{\mathrm{D}}\,\tau_{\mathrm{A}}$, where the rapidly oscillating complex exponentials in Eq. (E.4) effectively eliminate all terms except those with $M' = -M$. The selection rule (E.19) then shows that all single-spin cross-mode rates vanish. As a result, $\mathbf{R}^{\alpha}_{IS} = [R^{IS}_{zz},\, 0,\, 0]$ and similarly for $\mathbf{R}^{\alpha}_{IP}$ and Eq. (F.27) shows that Γ^{II}_{zz} is a sum of four terms, each being the product of two such longitudinal cross-spin rates and the zz component of the corresponding block inverse. Moreover, these inverses are trivial because all the 3×3 blocks in Eq. (F.27) are diagonal in the secular approximation. For $\mathbf{R}^{\alpha}_{SS}$ and $\mathbf{R}^{\alpha}_{PP}$, this follows from the vanishing of the cross-mode rates. For the four single-spin blocks of $\mathbf{X}^{\alpha}_{\mathrm{aa00}}$, the diagonality follows from Eq. (F.32), where now $\mathbf{R}^{\alpha}_{\mathrm{ss00}}$ is block-diagonal in Q (because $M' = -M$ in Eq. (E.4)) and $\mathbf{\Delta}^{\alpha}_{S,\mathrm{s0}}$ has only five nonzero elements, proportional to D_0 in Eq. (E.26). The latter simplification follows because the secular condition $\omega_0 \gg \omega_{\mathrm{D}}$ on the static SP coupling picks out the $M = 0$ term in Eq. (E.8). As a result of these simplifications in Eqs. (F.27) and (F.32), the "cross relaxation" rate in the secular approximation becomes

$$\Gamma^{II}_{zz} \;=\; \frac{R^{SS}_{zz}(R^{IP}_{zz})^2 + R^{PP}_{zz}(R^{IS}_{zz})^2 + X(R^{IS}_{zz} + R^{IP}_{zz})^2}{R^{SS}_{zz}\,R^{PP}_{zz} + X(R^{SS}_{zz} + R^{PP}_{zz})}\,. \tag{F.36}$$

Here, we have defined

$$X \;\equiv\; \frac{2}{9}\big[\omega_{\mathrm{D},SP}\,D^2_{00}(\Omega_{SP})\big]^2\rho\,, \tag{F.37}$$

where ρ is the '33' element (corresponding to basis operator B_{19} in Table S1A) of the inverse of the 3×3 $Q = 0$ block of $\mathbf{R}^{\alpha}_{\mathrm{ss00}}$.

APPENDIX G: CHEMICAL SHIFTS

Here we generalize the BWR treatment of Sec. III A – C and Appendix F by allowing the Larmor frequencies of the three homonuclear spins to differ, as in the Zeeman Hamiltonian of Eq. (1). In the BWR theory, the ILRR depends on the chemical shifts in two ways.

First, there is an implicit dependence on the chemical shifts via the local relaxation supermatrix $\mathbf{R}^\alpha$ in Eq. (26). This implicit shift effect essentially amounts to a replacement of ω_0 in the spectral densities by a linear combination of the unequal Larmor frequencies. The effect is therefore present in the frequency range ($\omega_0 \approx 1/\tau_\mathrm{A}$) of the primary dispersion, but not in the extreme-narrowing regime ($\omega_0\,\tau_\mathrm{A} \ll 1$). Chemical shifts displace the primary dispersion step along the frequency axis, but this displacement is of the same order as the chemical shifts themselves, so it is entirely negligible for homonuclear spins (with $\delta \lll 1$). In the generalized BWR treatment, we can therefore retain the isochronous $\mathbf{R}^\alpha$ derived in Appendix E.

Second, there is an explicit dependence on the chemical shifts via $\mathbf{L}_\mathrm{Z}^\mathrm{A}$ and $\mathbf{L}_\mathrm{Z}^\mathrm{B}$ in Eqs. (26) and (27), respectively. This explicit shift effect can be incorporated in the generalized BWR theory by using the non-isochronous Zeeman Liouvillians $\mathbf{L}_\mathrm{Z}^\mathrm{A}$ and $\mathbf{L}_\mathrm{Z}^\mathrm{B}$ derived in Appendix B. For the asymmetric exchange cases $ISP{-}IS$ and $ISP{-}I$, we find that the explicit shift effect amounts to displacements of the secondary dispersion steps of the same negligible order of magnitude as for the implicit shift effect on the primary dispersion step. In contrast, for the symmetric exchange case $ISP-ISP$, the explicit shift effect is of higher order, giving rise to a novel inverted secondary dispersion step.

In summary, for homonuclear spins within the MN regime, chemical shifts have a significant effect on the longitudinal relaxation dispersion profile only for the symmetric exchange case $ISP-ISP$. Under these conditions, the dispersion profiles computed from the generalized BWR theory developed here agree with the corresponding profiles obtained from the SLE theory, which rigorously incorporates all chemical shift effects. In Sec. IV D, we use the SLE theory to examine the effect of chemical shifts outside the MN regime.

1. Exchange case $ISP{-}ISP$

Combination of Eqs. (27) and (29), which are valid in the presence of chemical shifts, yields

$$\widetilde{\mathbf{U}}^{\mathrm{BB}}(0) \;=\; \frac{\tau_\mathrm{A}}{P_\mathrm{A}}\big[\,\mathbf{Z}_\mathrm{B} - \mathbf{Z}_\mathrm{A}^{-1} + \mathbf{Z}_\mathrm{A}^{-1}\,\langle\mathbf{R}^\alpha\rangle\,\tau_\mathrm{A}\,\mathbf{Z}_\mathrm{A}^{-1}\big]^{-1}\,, \tag{G.1}$$

where

$$\mathbf{Z}_\mathrm{A} \;\equiv\; \mathbf{1} + i\,\mathbf{L}_\mathrm{Z}^\mathrm{A}\,\tau_\mathrm{A}\,, \tag{G.2}$$

and similarly for $\mathbf{Z}_\mathrm{B}$. All matrices appearing in Eqs. (G.1) and (G.2) are block-diagonal with respect to the projection index Q and with respect to odd/even SIC parity. It is therefore sufficient to consider the 10×10 $Q = 0$ odd-parity block of these matrices. For isochronous spins, $\mathbf{L}_\mathrm{Z}^\mathrm{A} = \mathbf{L}_\mathrm{Z}^\mathrm{B} = \mathbf{0}$, so Eq. (G.1) reduces directly to Eq. (30).

According to Appendix B, the Zeeman Liouvillian in the presence of chemical shifts is

$$\mathbf{L}_{\mathrm{Z}}^{\mathrm{A}} \;=\; \omega_I^{\mathrm{A}} \begin{bmatrix} \mathbf{0} & \mathbf{0} \\ \mathbf{0} & \mathbf{D}_{\mathrm{A}} \end{bmatrix}, \tag{G.3}$$

where the upper left null matrix $\mathbf{0}$ is 3×3 and $\mathbf{D}_{\mathrm{A}}$ is the 7×7 matrix

$$\mathbf{D}_{\mathrm{A}} \;=\; \begin{bmatrix} \mathbf{0} & \boldsymbol{\delta}_{\mathrm{A}}' \\ \boldsymbol{\delta}_{\mathrm{A}} & \mathbf{0} \end{bmatrix}. \tag{G.4}$$

and where $\boldsymbol{\delta}_{\mathrm{A}}'$ is the transpose of

$$\boldsymbol{\delta}_{\mathrm{A}} \;=\; \begin{bmatrix} \frac{\sqrt{2}}{3}\,\delta_S^{\mathrm{A}} & \frac{1}{\sqrt{6}}\,(\delta_S^{\mathrm{A}} - 2\,\delta_P^{\mathrm{A}}) & -\frac{\sqrt{10}}{6}\,\delta_S^{\mathrm{A}} & 0 \\ -\frac{2}{3}\,\delta_S^{\mathrm{A}} & \frac{\sqrt{3}}{6}\,(\delta_S^{\mathrm{A}} - 2\,\delta_P^{\mathrm{A}}) & \frac{\sqrt{5}}{30}\,\delta_S^{\mathrm{A}} & -\frac{\sqrt{30}}{10}\,\delta_S^{\mathrm{A}} \\ 0 & -\frac{1}{2}\,\delta_S^{\mathrm{A}} & \frac{\sqrt{15}}{10}\,(\delta_S^{\mathrm{A}} - 2\,\delta_P^{\mathrm{A}}) & \frac{1}{\sqrt{10}}\,(\delta_S^{\mathrm{A}} - 2\,\delta_P^{\mathrm{A}}) \end{bmatrix}. \tag{G.5}$$

The supermatrix $\mathbf{L}_{\mathrm{Z}}^{\mathrm{B}}$ has a completely analogous form. In view of Eqs. (G.2) and (G.3),

$$\mathbf{Z}_{\mathrm{B}} \;=\; \begin{bmatrix} \mathbf{1} & \mathbf{0} \\ \mathbf{0} & \mathbf{Y}_{\mathrm{B}} \end{bmatrix} \qquad \text{and} \qquad \mathbf{Z}_{\mathrm{A}}^{-1} \;=\; \begin{bmatrix} \mathbf{1} & \mathbf{0} \\ \mathbf{0} & \mathbf{Y}_{\mathrm{A}}^{-1} \end{bmatrix}, \tag{G.6}$$

where

$$\mathbf{Y}_{\mathrm{A}} \;\equiv\; \mathbf{1} + i\,\omega_I^{\mathrm{A}}\,\tau_{\mathrm{A}}\,\mathbf{D}^{\mathrm{A}}, \tag{G.7}$$

and similarly for $\mathbf{Y}_{\mathrm{B}}$.

The orientationally averaged relaxation matrix $\langle \mathbf{R}^{\alpha} \rangle$ in Eq. (G.1) may be partitioned into a 3×3 longitudinal (L) block $\mathbf{R}_{\mathrm{L}}$, a 7×7 zero-quantum coherence (ZQC) block $\mathbf{R}_{\mathrm{ZQC}}$, and two rectangular cross-mode blocks $\mathbf{R}_{\mathrm{L/ZQC}}$ and $\mathbf{R}_{\mathrm{ZQC/L}}$,

$$\langle \mathbf{R}^{\alpha} \rangle \;=\; \begin{bmatrix} \mathbf{R}_{\mathrm{L}} & \mathbf{R}_{\mathrm{L/ZQC}} \\ \mathbf{R}_{\mathrm{ZQC/L}} & \mathbf{R}_{\mathrm{ZQC}} \end{bmatrix}. \tag{G.8}$$

Combination of Eqs. (G.1), (G.6), and (G.8) yields

$$\widetilde{\mathbf{U}}^{\mathrm{BB}}(0) \;=\; \frac{1}{P_{\mathrm{A}}} \begin{bmatrix} \mathbf{R}_{\mathrm{L}} & \mathbf{R}_{\mathrm{L/ZQC}}\,\mathbf{Y}_{\mathrm{A}}^{-1} \\ \mathbf{Y}_{\mathrm{A}}^{-1}\,\mathbf{R}_{\mathrm{ZQC/L}} & \mathbf{Y}_{\mathrm{A}}^{-1}\,\mathbf{R}_{\mathrm{ZQC}}\,\mathbf{Y}_{\mathrm{A}}^{-1} + (\mathbf{Y}_{\mathrm{B}} - \mathbf{Y}_{\mathrm{A}}^{-1})/\tau_{\mathrm{A}} \end{bmatrix}^{-1}. \tag{G.9}$$

We only need the 3×3 longitudinal block of $\widetilde{\mathbf{U}}^{\mathrm{BB}}(0)$, obtained from Eq. (G.9) as

$$\widetilde{\mathbf{U}}_{\mathrm{L}}^{\mathrm{BB}}(0) \;=\; \left[P_{\mathrm{A}}\,\mathbf{R}_{\mathrm{L}} - P_{\mathrm{A}}^2\,\mathbf{R}_{\mathrm{L/ZQC}}\,(P_{\mathrm{A}}\,\mathbf{R}_{\mathrm{ZQC}} + i\,\mathbf{W})^{-1}\,\mathbf{R}_{\mathrm{ZQC/L}}\right]^{-1}, \tag{G.10}$$

where we have defined the frequency shift matrix

$$\mathbf{W} \;\equiv\; -\,i\,\frac{P_{\mathrm{A}}}{\tau_{\mathrm{A}}}\,\mathbf{Y}_{\mathrm{A}}\,(\mathbf{Y}_{\mathrm{B}}\,\mathbf{Y}_{\mathrm{A}} - \mathbf{1}). \tag{G.11}$$

So far, no approximations have been introduced. To obtain a more transparent expression for $\mathbf{W}$, we note that $\epsilon \equiv \delta\,\omega_0\,\tau_{\mathrm{A}} \ll 1$ for homonuclear spins ($\delta \lll 1$) in the frequency range ($\omega_0\,\tau_{\mathrm{A}} \lesssim 10$) where longitudinal relaxation is effective. Here, δ is the largest of the

shifts δ_S and δ_P, and $\omega_0 \equiv \omega_I^{\mathrm{A}}$, which differs from ω_I^{B} by a negligible amount of order δ. To leading order in ϵ, we obtain from Eqs. (G.7) and (G.11),

$$\mathbf{W} \;=\; \omega_0 \left(P_{\mathrm{A}}\, \mathbf{D}_{\mathrm{A}} + P_{\mathrm{B}}\, \mathbf{D}_{\mathrm{B}}\right) . \tag{G.12}$$

To the same level approximation we can neglect the shift effect on the relaxation supermatrix $\langle \mathbf{R}^{\alpha} \rangle$ (see above), which can then be taken from Appendix E. We can now calculate $\widehat{R}_{1,ISP}^{\mathrm{dil}}$ by combing Eqs. (23c), (G.10), and (G.12), with $\mathbf{D}_{\mathrm{A}}$ and $\mathbf{D}_{\mathrm{B}}$ given by Eqs. (G.4) and (G.5).

In the absence of chemical shifts, $\mathbf{W} = \mathbf{0}$ so Eq. (G.10) reduces (after division by P_{A}) to Eq. (33). As discussed in Sec. III A, the second term in Eq. (G.10), or Eq. (33), represents the effect of cross-mode relaxation driven by distinct correlations, which reduces $\widehat{R}_{1,ISP}^{\mathrm{dil}}$ below the value $\widehat{R}_{1,ISP}^{\mathrm{dil,\,self}}$ that would prevail if only self-correlations were included. It then follows from Eq. (G.10) that chemical shifts suppress the effect of cross-mode relaxation (and distinct correlations), thereby increasing $\widehat{R}_{1,ISP}^{\mathrm{dil}}$. As shown in Sec. IV D, this suppression can be nearly complete, but it only sets in above a certain frequency (indeed, $\mathbf{W}$ vanishes in the ZF limit). By considering the order or magnitude of the terms in Eqs. (G.10) and (G.12), this nonsecular decoupling (NSD) frequency can be identified as

$$\omega_{\mathrm{NSD}} \;=\; \frac{P_{\mathrm{A}}\, \omega_{\mathrm{D}}^2\, \tau_{\mathrm{A}}}{P_{\mathrm{A}}\, \delta^{\mathrm{A}} + P_{\mathrm{B}}\, \delta^{\mathrm{B}}} . \tag{G.13}$$

We can now summarize the effect of chemical shifts on the dispersion profile $\widehat{R}_{1,ISP}^{\mathrm{dil}}(\omega_0)$. At low frequencies, such that $\omega_0 \ll \omega_{\mathrm{NSD}}$, there is no effect. At $\omega_0 \approx \omega_{\mathrm{NSD}}$, there is an inverted secondary dispersion step as the (negative) contribution from distinct correlations in the L/ZQC cross-mode rates is partly lost. At higher frequencies, such that $\omega_0 \gg \omega_{\mathrm{NSD}}$, $\widehat{R}_{1,ISP}^{\mathrm{dil}}$ remains larger than for isochronous spins but it never exceeds the ILRR $\widehat{R}_{1,ISP}^{\mathrm{dil,\,self}}$ produced by self-correlations alone.

2. Exchange case $ISP{-}IS$

Because $\mathbf{L}_{\mathrm{Z}}^{\mathrm{B}} = \mathbf{0}$ in the longitudinal two-spin subspace spanned by I_z and S_z, the arguments leading from Eq. (27) to Eq. (34) remain valid for non-isochronous spins. We therefore only need to calculate the corresponding 2×2 matrix $\mathbf{G}_{\mathrm{L}}^{\mathrm{A}}(0)$ in this longitudinal (L) subspace. Because also $\mathbf{L}_{\mathrm{Z},11}^{\mathrm{A}} = \mathbf{0}$ in this subspace, it follows that the development in Appendix F.1 remains valid, the only explicit effect of chemical shifts being the replacement of ω_0 with $\omega_0(1 + \delta_P^{\mathrm{A}})$ in Eq. (38). For isochronous spins, this explicit frequency dependence gives rise to an inverted secondary dispersion step at $\omega_0 \approx \omega_{\mathrm{D}}^2\, \tau_{\mathrm{A}}$, above which cross-mode relaxation no longer contributes to $\widehat{R}_{1,IS}^{\mathrm{dil}}$. The effect of the chemical shift (of the nonlabile spin P; the shift of spin S has no effect here) is thus to displace the position on the frequency axis of this secondary dispersion step by a relative amount of order δ_P^{A}, which is negligible for homonuclear spins. In fact, this explicit shift effect is of the same order as the implicit shift effect on the primary dispersion step (at $\omega_0 \approx 1/\tau_{\mathrm{A}}$) that

we neglect by retaining the isochronous relaxation supermatrix $\mathbf{R}^{\alpha}$ from Appendix E. In conclusion, for exchange case $ISP{-}IS$ the effects of chemical shifts are of higher order than for exchange case $ISP{-}ISP$ and can be neglected altogether for homonuclear spins.

3. Exchange case $ISP{-}I$

The development leading up to Eq. (41) remains valid in the presence of chemical shifts, because the 30×30 matrix $\mathbf{L}^{\mathrm{A}}_{\mathrm{Z,aa11}}$ is block-diagonal with the first scalar block (corresponding to basis operator I_z) equal to zero. The two explicit occurrences of the Larmor frequency in Eqs. (42) and (43) are associated with the two secondary dispersion steps related to cross-mode relaxation and to the static $S{-}P$ dipole coupling, respectively. The explicit shift effect in Eq. (42) amounts to replacement of ω_0 by $\omega_0(1+\delta^{\mathrm{A}}_S)$ in the SS block and by $\omega_0(1+\delta^{\mathrm{A}}_P)$ in the PP block. The explicit shift effect in Eq. (43) amounts to replacement of the diagonal 9×9 matrix $\mathbf{Q}_{\mathrm{ss00}}$ by the block-diagonal matrix

$$\mathbf{Q}_{\mathrm{ss00}} = \begin{bmatrix} \mathbf{Q}_0 & \mathbf{0} & \mathbf{0} & \mathbf{0} & \mathbf{0} \\ \mathbf{0} & \mathbf{Q}_1 & \mathbf{0} & \mathbf{0} & \mathbf{0} \\ \mathbf{0} & \mathbf{0} & \mathbf{Q}_{-1} & \mathbf{0} & \mathbf{0} \\ \mathbf{0} & \mathbf{0} & \mathbf{0} & Q_2 & 0 \\ \mathbf{0} & \mathbf{0} & \mathbf{0} & 0 & Q_{-2} \end{bmatrix} . \tag{G.14}$$

The diagonal blocks are

$$\mathbf{Q}_0 = \frac{1}{\sqrt{3}} \begin{bmatrix} 0 & 0 & \sqrt{2}\,\delta_- \\ 0 & 0 & \delta_- \\ \sqrt{2}\,\delta_- & \delta_- & 0 \end{bmatrix} , \tag{G.15a}$$

$$\mathbf{Q}_{\pm 1} = \frac{1}{2} \begin{bmatrix} \pm(2+\delta_+) & \delta_- \\ \delta_- & \pm(2+\delta_+) \end{bmatrix} , \tag{G.15b}$$

$$Q_{\pm 2} = \pm(2+\delta_+) , \tag{G.15c}$$

where $\delta_\pm \equiv \delta^{\mathrm{A}}_S \pm \delta^{\mathrm{A}}_P$.

The effect of chemical shifts is thus to displace the positions of the two secondary dispersion steps by relative amounts of order δ^{A}, which is of the same order as the neglected implicit shift effect on the primary dispersion step. In conclusion, for exchange case $ISP{-}I$, the effects of chemical shifts are of higher order than for exchange case $ISP{-}ISP$ and can be neglected altogether for homonuclear spins.

APPENDIX H: $ISP-I$ CASE IN THE MN REGIME: EFFECTS OF THE STATIC DIPOLE COUPLING

Here we examine in detail how the static dipole coupling $\omega_{\mathrm{D},SP}$ affects the MRD profile for the $ISP-I$ case in the dilute MN regime. According to Eq. (41), the ILRR of the labile I-spin is

$$\widehat{R}^{\mathrm{dil}}_{1,I}(\omega_0) \;=\; P_{\mathrm{A}}\left[\left\langle R^{II}_{zz}(\omega_0)\right\rangle - \left\langle \Gamma^{II}_{zz}(\omega_0)\right\rangle\right] \;. \tag{H.1}$$

with the isotropically averaged longitudinal auto-spin relaxation rate $\left\langle R^{II}_{zz}(\omega_0)\right\rangle$ as in Eq. (E.20a) and the "cross relaxation" rate $\Gamma^{II}_{zz}(\omega_0)$ as in Eq. (42), which we now express as

$$\Gamma^{II}_{zz}(\omega_0) \;=\; \boldsymbol{\sigma}\,\mathbf{V}^{-1}\,\boldsymbol{\sigma}^{\dagger}\,, \tag{H.2}$$

with the 1×6 cross-spin relaxation matrix $\boldsymbol{\sigma}$

$$\boldsymbol{\sigma} \;=\; \left[\boldsymbol{\sigma}^{IS}\;\boldsymbol{\sigma}^{IP}\right] \;=\; \left[\sigma^{IS}_{zz}\;\sigma^{IS}_{z+}\;\sigma^{IS}_{z-}\;\sigma^{IP}_{zz}\;\sigma^{IP}_{z+}\;\sigma^{IP}_{z-}\right] \;. \tag{H.3}$$

The elements of $\boldsymbol{\sigma}^{IS}$ and $\boldsymbol{\sigma}^{IP}$ are proportional to $\omega^2_{\mathrm{D},IS}\,\tau_{\mathrm{A}}$ and $\omega^2_{\mathrm{D},IP}\,\tau_{\mathrm{A}}$, respectively. The 6×6 matrix $\mathbf{V}$, the inverse of which appears in Eq. (H.2), is

$$\mathbf{V} \;=\; \mathbf{X} + \boldsymbol{\rho} + i\,\omega_0\,\mathbf{Q}_{11}\,, \tag{H.4}$$

where $\mathbf{Q}_{11} = \mathrm{diag}(0,\;1,\;-1,\;0,\;1,\;-1)$ and

$$\boldsymbol{\rho} \;=\; \begin{bmatrix} \boldsymbol{\rho}^{IS} & \mathbf{0} \\ \mathbf{0} & \boldsymbol{\rho}^{IP} \end{bmatrix} \;. \tag{H.5}$$

The elements of the 3×3 auto-S-spin and auto-P-spin relaxation matrices $\boldsymbol{\rho}^{IS}$ and $\boldsymbol{\rho}^{IP}$ are proportional to $\omega^2_{\mathrm{D},IS}\,\tau_{\mathrm{A}}$ and $\omega^2_{\mathrm{D},IP}\,\tau_{\mathrm{A}}$, respectively. The static dipole coupling $\omega_{\mathrm{D},SP}$ affects the ILRR exclusively via the 6×6 matrix $\mathbf{X}$, given by

$$\mathbf{X} \;=\; \boldsymbol{\Delta}\left(\mathbf{R}_{\mathrm{2spin}} + i\,\omega_0\,\mathbf{Q}_2\right)^{-1}\boldsymbol{\Delta}^{\dagger}\,, \tag{H.6}$$

where $\mathbf{Q}_2 = \mathrm{diag}(0,\;0,\;0,\;1,\;1,\;-1,\;-1,\;2,\;-2)$. The elements of the 9×9 relaxation matrix $\mathbf{R}_{\mathrm{2spin}}$ in the two-spin-SP subspace involve IS and IP self-correlations as well as IS–IP distinct correlations. The elements of the 6×9 static dipolar Liouvillian matrix $\boldsymbol{\Delta}$ are proportional to $\omega_{\mathrm{D},SP}$.

Figure S1a shows a typical $\widehat{R}^{\mathrm{dil}}_{1,I}(\omega_0)$ dispersion profile for the $ISP-I$ case in the MN regime and Fig. S1b shows the component parts $\left\langle R^{II}_{zz}(\omega_0)\right\rangle$ and $\left\langle \Gamma^{II}_{zz}(\omega_0)\right\rangle$ in units of $\omega^2_{\mathrm{D},I}\,\tau_{\mathrm{A}}$, where $\omega^2_{\mathrm{D},I} \equiv \omega^2_{\mathrm{D},IS} + \omega^2_{\mathrm{D},IP}$. If the static dipole coupling is artificially removed by setting $\omega_{\mathrm{D},SP} = 0$, then $\widehat{R}^{\mathrm{dil}}_{1,I}(\omega_0)$ is reduced at all frequencies. In other words, the effect of the static dipole coupling $\omega_{\mathrm{D},SP}$ is to speed up the longitudinal relaxation of the labile I spin. When $\omega_{\mathrm{D},SP} = 0$, the two fluctuating dipole couplings contribute additively so that

$\widehat{R}^{\mathrm{dil}}_{1,I} = \widehat{R}^{\mathrm{dil}}_{1,I}(IS{-}I) + \widehat{R}^{\mathrm{dil}}_{1,I}(IP{-}I)$, where $\widehat{R}^{\mathrm{dil}}_{1,I}(IS{-}I)$ is the ILRR for the two-spin $IS{-}I$ case.[9]

The $\widehat{R}^{\mathrm{dil}}_{1,I}(\omega_0)$ profile exhibits a primary dispersion step at $\omega_0 \approx 1/\tau_{\mathrm{A}}$, due mainly to the SDFs $j(\omega_0)$ and $j(2\,\omega_0)$ in $\big\langle R^{II}_{zz}(\omega_0)\big\rangle$. However, as seen from Fig. S1b, $\big\langle \Gamma^{II}_{zz}(\omega_0)\big\rangle$ also contributes to the primary dispersion step. In particular, it ensures that $\widehat{R}^{\mathrm{dil}}_{1,I}(\omega_0)$ approaches zero asymptotically. This happens because the contributions from the zero-frequency SDF to $\big\langle R^{II}_{zz}(\omega_0)\big\rangle$ and $\big\langle \Gamma^{II}_{zz}(\omega_0)\big\rangle$ cancel out, so that $\big\langle R^{II}_{zz}(\infty)\big\rangle = \big\langle \Gamma^{II}_{zz}(\infty)\big\rangle$.

In addition, $\big\langle \Gamma^{II}_{zz}(\omega_0)\big\rangle$ exhibits a secondary dispersion step at a lower frequency. In the absence of a static dipole coupling (or if $\omega_{\mathrm{D},SP}$ is "weak"), the secondary dispersion occurs at $\omega_0 \approx \omega^2_{\mathrm{D},I}\,\tau_{\mathrm{A}}$, which then defines the (upper) boundary of the zero-field (ZF) regime. In the ZF regime, I-spin relaxation is slowed down by longitudinal-transverse cross-mode relaxation, which is eliminated by nonsecular decoupling when $\omega_0 \gg \omega^2_{\mathrm{D},I}\,\tau_{\mathrm{A}}$. In the presence of a ("strong") static dipole coupling, this description is no longer valid. The secondary dispersion step at $\omega_0 \approx \omega^2_{\mathrm{D},I}\,\tau_{\mathrm{A}}$ then disappears and the ZF regime extends all the way up to $\omega_0 \approx \omega_{\mathrm{D},SP}$, where a new secondary dispersion step appears. Cross-mode relaxation occurs throughout this extended ZF regime, but it is modified by the static dipole coupling. Although relaxation in the ZF regime is modified by the static dipole coupling, it does not depend on the strength of this coupling as long as $\omega_{\mathrm{D},SP}$ is "strong" (in a sense to be defined). In this Appendix, we rationalize this rather intricate relaxation behavior.

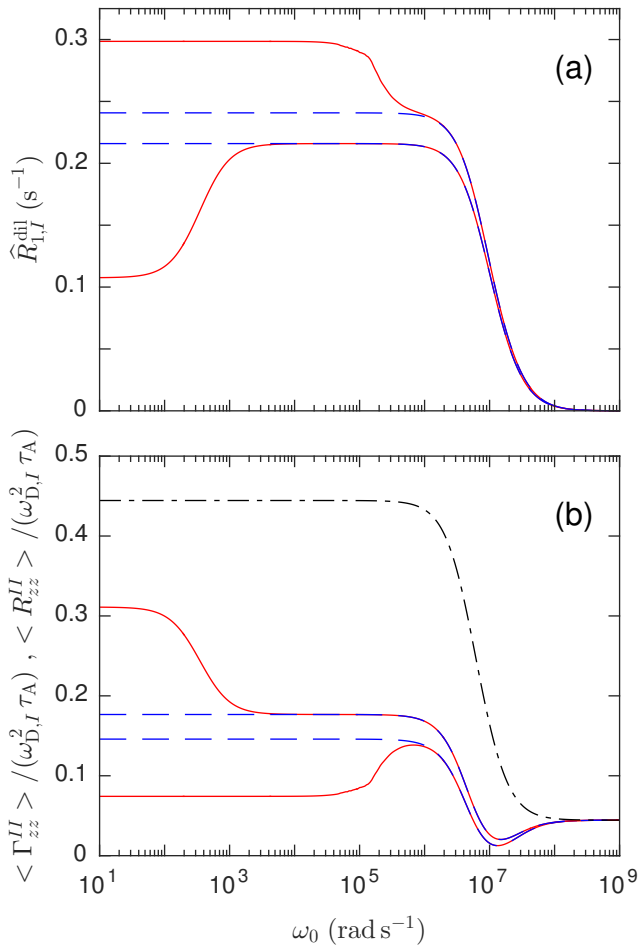

Figure S1: (**a**) Dispersion profile of $\widehat{R}^{\rm dil}_{1,I}(\omega_0)$ for the $ISP{-}I$ case in the MN regime with (upper red) and without (lower red) static dipole coupling, and in the secular approximation (blue dashed). (**b**) Dispersion profiles for $\left\langle R^{II}_{zz}(\omega_0)\right\rangle$ (black dash-dot) and $\left\langle \Gamma^{II}_{zz}(\omega_0)\right\rangle$, both normalized by $\omega^2_{{\rm D},I}\,\tau_{\rm A}$. $\left\langle \Gamma^{II}_{zz}(\omega_0)\right\rangle$ is shown with (lower red) and without (upper red) static dipole coupling and in the secular approximation (blue dashed). Parameter values: $P_{\rm A} = 10^{-3}$, $\tau_{\rm A} = 10^{-7}$ s, $\omega_{{\rm D},IS} = 1 \times 10^5$ rad s^{-1}, $\beta_I = 50°$, and $\beta_S = 70°$, yielding $\omega_{{\rm D},IP} = 0.7828 \times 10^5$ rad s^{-1} and $\omega_{{\rm D},SP} = 1.4449 \times 10^5$ rad s^{-1}.

1. Weak static dipole coupling

We characterize the strength of the static dipole coupling by the dimensionless parameter

$$\epsilon \;\equiv\; \frac{\omega_{\mathrm{D},SP}}{\omega_{\mathrm{D},I}^2\,\tau_\mathrm{A}}\,. \tag{H.7}$$

The static dipole coupling $\omega_{\mathrm{D},SP}$ is said to be weak if $\epsilon \ll 1$ and strong if $\epsilon \gg 1$. For the homonuclear $ISP{-}I$ case, the value of ϵ depends on the internuclear geometry (β_I and β_S) and on the MN parameter $\omega_{\mathrm{D},IS}\,\tau_\mathrm{A}$, which is $\ll 1$ in the MN regime. For an equilateral triangle, where all three couplings are equal, $\epsilon = 1/(2\,\omega_{\mathrm{D},IS}\,\tau_\mathrm{A})$, which is $\gg 1$ in the MN regime. If either of the nonlabile spins is remote from the other two spins, one of the fluctuating dipole couplings is much larger than the static one, so that $\epsilon \ll 1$. For example, if spin P is located far from spins I and S, the apex angle β_P is very small and $\epsilon = \beta_P^3/(\omega_{\mathrm{D},IS}\,\tau_\mathrm{A})$. But as long as all three dipole couplings are of comparable magnitude, $\epsilon \gg 1$ in the MN regime. In this subsection we set $\omega_{\mathrm{D},SP} = 0$, but the results are the same for a finite $\omega_{\mathrm{D},SP}$ as long as it is weak ($\epsilon \ll 1$). As seen from Fig. S2, the weak-coupling limit of $\big\langle \Gamma_{zz}^{II}(0)\big\rangle$ applies for $\epsilon \lesssim 0.1$, whereas the strong-coupling limit is a good approximation already for $\epsilon \gtrsim 2$.

If we set $\omega_{\mathrm{D},SP} = 0$ in Eq. (H.6), then $\mathbf{X} = \mathbf{0}$, so $\mathbf{V}$ in Eq. (H.4) is block-diagonal and Eqs. (H.2) – (H.5) yield

$$\big\langle \Gamma_{zz}^{II}(\omega_0)\big\rangle_0 \;=\; \big\langle \boldsymbol{\sigma}^{IS}\,(\boldsymbol{\rho}^{IS} + i\,\omega_0\,\mathbf{Q}_1)^{-1}\,\boldsymbol{\sigma}^{IS\,\dagger}\big\rangle + \big\langle \boldsymbol{\sigma}^{IP}\,(\boldsymbol{\rho}^{IP} + i\,\omega_0\,\mathbf{Q}_1)^{-1}\,\boldsymbol{\sigma}^{IP\,\dagger}\big\rangle\;, \tag{H.8}$$

where $\mathbf{Q}_1 = \mathrm{diag}(0,\ 1,\ -1)$ and the 0 subscript reminds us that $\omega_{\mathrm{D},SP} = 0$. As expected, this is the sum of the $\big\langle \Gamma_{zz}^{II}(\omega_0)\big\rangle$ expressions for the two-spin $IS{-}I$ and $IP{-}I$ cases.[9] To identify the frequency of the secondary dispersion step, we introduce dimensionless quantities (labeled by a tilde) by writing $\boldsymbol{\sigma}^{IS} = \omega_{\mathrm{D},IS}^2\,\tau_\mathrm{A}\,\widetilde{\boldsymbol{\sigma}}^{IS}$ and similarly for the other rates. Thus

$$\begin{aligned}\big\langle \Gamma_{zz}^{II}(\omega_0)\big\rangle_0 \;=\; &\omega_{\mathrm{D},IS}^2\,\tau_\mathrm{A}\left\langle \widetilde{\boldsymbol{\sigma}}^{IS}\left[\widetilde{\boldsymbol{\rho}}^{IS} + i\,\frac{\omega_0}{\omega_{\mathrm{D},IS}^2\,\tau_\mathrm{A}}\,\mathbf{Q}_1\right]^{-1}\widetilde{\boldsymbol{\sigma}}^{IS\,\dagger}\right\rangle \\ +\;&\omega_{\mathrm{D},IP}^2\,\tau_\mathrm{A}\left\langle \widetilde{\boldsymbol{\sigma}}^{IP}\left[\widetilde{\boldsymbol{\rho}}^{IP} + i\,\frac{\omega_0}{\omega_{\mathrm{D},IP}^2\,\tau_\mathrm{A}}\,\mathbf{Q}_1\right]^{-1}\widetilde{\boldsymbol{\sigma}}^{IP\,\dagger}\right\rangle .\end{aligned} \tag{H.9}$$

Well below the primary dispersion step, such that $\omega_0 \ll 1/\tau_\mathrm{A}$, the cross-spin and auto-spin rates in Eq. (H.9) are all frequency-independent, so any dependence of $\big\langle \Gamma_{zz}^{II}(\omega_0)\big\rangle_0$ on ω_0 in this regime must come from the explicit frequency factor in front of $\mathbf{Q}_1$.
Because the nonzero elements of $\widetilde{\boldsymbol{\rho}}^{IS}$, $\widetilde{\boldsymbol{\rho}}^{IP}$ and $\mathbf{Q}_1$ are of order 1, the secondary dispersion step should appear when the pre-factor in front of $\mathbf{Q}_1$ is of order 1, that is, at frequency $\omega_0 \approx \omega_{\mathrm{D},I}^2\,\tau_\mathrm{A}$. In the ZF regime, where $\omega_0 \ll \omega_{\mathrm{D},I}^2\,\tau_\mathrm{A}$, longitudinal-transverse cross-mode relaxation increases $\big\langle \Gamma_{zz}^{II}(\omega_0)\big\rangle_0$ to the value

$$\big\langle \Gamma_{zz}^{II}(0)\big\rangle_0 \;=\; \omega_{\mathrm{D},IS}^2\,\tau_\mathrm{A}\left\langle \widetilde{\boldsymbol{\sigma}}^{IS}\,(\widetilde{\boldsymbol{\rho}}^{IS})^{-1}\widetilde{\boldsymbol{\sigma}}^{IS\,\dagger}\right\rangle + \omega_{\mathrm{D},IP}^2\,\tau_\mathrm{A}\left\langle \widetilde{\boldsymbol{\sigma}}^{IP}\,(\widetilde{\boldsymbol{\rho}}^{IP})^{-1}\widetilde{\boldsymbol{\sigma}}^{IP\,\dagger}\right\rangle \;=\; \tfrac{14}{45}\,\omega_{\mathrm{D},I}^2\,\tau_\mathrm{A}\;, \tag{H.10}$$

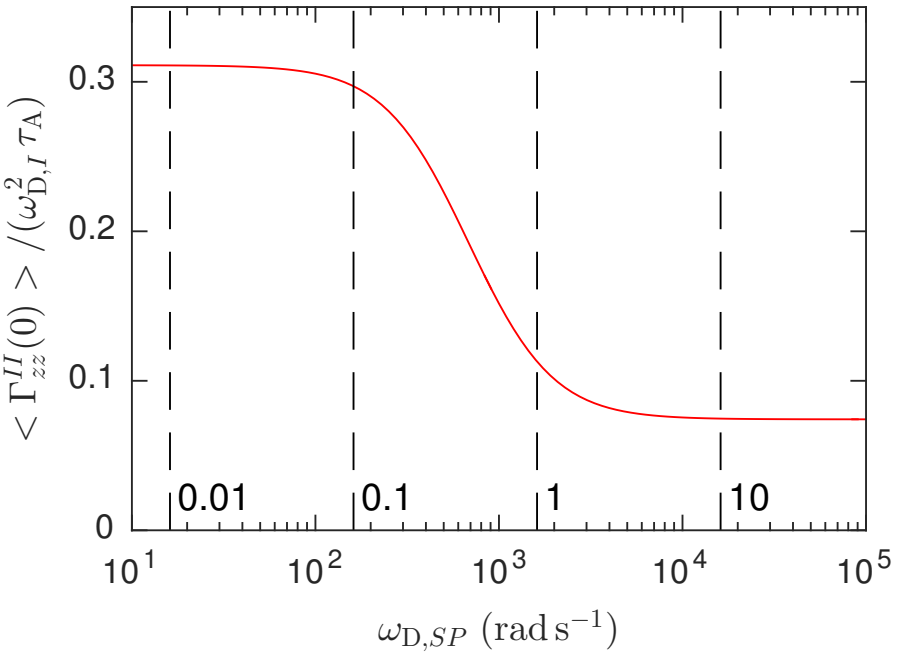

Figure S2: Variation of normalized $\left\langle \Gamma^{II}_{zz}(0) \right\rangle$ with $\omega_{\mathrm{D},SP}$ while all the other parameters are fixed at the values of Fig. S1.Vertical dashed lines correspond to indicated ϵ values.

where the last result has been derived before.[9] In the LF regime, where $\omega_0 \gg \omega^2_{\mathrm{D},I}\,\tau_{\mathrm{A}}$, nonsecular decoupling of cross-mode relaxation reduces $\left\langle \Gamma^{II}_{zz}(\omega_0) \right\rangle_0$ to

$$\left\langle \Gamma^{II}_{zz}(\omega_0) \right\rangle_0 \;=\; \gamma\,\omega^2_{\mathrm{D},I}\,\tau_{\mathrm{A}}\;, \tag{H.11}$$

where $\gamma = 4/9 - c = 0.17666\ldots$, as shown before.[9] This kind of secondary dispersion occurs only in spin systems with at least one nonlabile spin without strong static dipole couplings.

The secular approximation, which neglects longitudinal-transverse cross-mode relaxation, is justified at all frequencies such that $\omega_0 \gg \omega^2_{\mathrm{D},I}\,\tau_{\mathrm{A}}$, where Eq. (H.9) yields

$$\left\langle \Gamma^{II}_{zz}(\omega_0) \right\rangle_0^{\mathrm{sec}} \;=\; \omega^2_{\mathrm{D},I}\,\tau_{\mathrm{A}}\,\gamma(\omega_0\,\tau_{\mathrm{A}})\;, \tag{H.12}$$

where

$$\gamma(\omega_0\,\tau_{\mathrm{A}}) \;\equiv\; \left\langle \frac{(\widetilde{\sigma}^X_{zz})^2}{\widetilde{\rho}^X_{zz}} \right\rangle\;. \tag{H.13}$$

This result is valid at all frequencies above the secondary dispersion step, even in the primary dispersion step ($\omega_0 \approx 1/\tau_{\mathrm{A}}$), where the intrinsic rates $\widetilde{\sigma}^X_{zz}$ and $\widetilde{\rho}^X_{zz}$ are frequency-dependent. Note that $\gamma(\omega_0\,\tau_{\mathrm{A}})$ is independent of X. As shown above, $\gamma(0) = 0.17666\ldots$ and $\gamma(\infty) = 2/45 = 0.044444\ldots$ (cf. Fig. S1).

2. Strong static dipole coupling

Introducing dimensionless quantities through $\boldsymbol{\rho} = \omega_{\mathrm{D},I}^2\,\tau_\mathrm{A}\,\widetilde{\boldsymbol{\rho}}$ and $\mathbf{X} = [\omega_{\mathrm{D},SP}^2/(\omega_{\mathrm{D},I}^2\,\tau_\mathrm{A})]\,\widetilde{\mathbf{X}}$, we can write Eq. (H.4) as

$$\mathbf{V} \;=\; \omega_{\mathrm{D},I}^2\,\tau_\mathrm{A}\left[\epsilon^2\,\widetilde{\mathbf{X}} + \widetilde{\boldsymbol{\rho}} + i\,\frac{\omega_0}{\omega_{\mathrm{D},I}^2\,\tau_\mathrm{A}}\,\mathbf{Q}_{11}\right]\,, \tag{H.14}$$

with ϵ defined by Eq. (H.7). Similarly, with $\boldsymbol{\Delta} = \omega_{\mathrm{D},SP}\,\widetilde{\boldsymbol{\Delta}}$, Eq. (H.6) yields

$$\widetilde{\mathbf{X}} \;=\; \widetilde{\boldsymbol{\Delta}}\left(\widetilde{\mathbf{R}}_\mathrm{2spin} + i\,\frac{\omega_0}{\omega_{\mathrm{D},I}^2\,\tau_\mathrm{A}}\,\mathbf{Q}_2\right)^{-1}\widetilde{\boldsymbol{\Delta}}^\dagger\,. \tag{H.15}$$

In this subsection, we assume that the static dipole coupling is strong in the sense that $\epsilon \gg 1$.

2.1. Zero-field regime

In the extreme-narrowing regime, $\omega_0\,\tau_\mathrm{A} \ll 1$, the relaxation matrices $\boldsymbol{\rho}$ and $\mathbf{R}_\mathrm{2spin}$ are Hermitian. It follows, therefore, from Eqs. (H.14) and (H.15) that also the 6×6 matrices $\widetilde{\mathbf{X}}$ and $\mathbf{V}$ are Hermitian in the limit $\omega_0 = 0$. For $\epsilon \gg 1$, as assumed here, $\mathbf{V}$ is strongly dominated by the first term within square brackets in Eq. (H.14). All elements of $\mathbf{V}$ are therefore proportional to $\omega_{\mathrm{D},SP}^2$. Accordingly, one might expect $\mathbf{V}^{-1}$ and, by way of Eq. (H.2), $\big\langle\Gamma_{zz}^{II}(0)\big\rangle$, to be inversely proportional to $\omega_{\mathrm{D},SP}^2$. However, numerically we find that $\mathbf{V}^{-1}$ is independent of $\omega_{\mathrm{D},SP}$ when $\epsilon \gg 1$. This counter-intuitive behavior occurs because the matrix $\widetilde{\mathbf{X}}$ is singular, with one zero eigenvalue.

Let $\boldsymbol{\Lambda}$ be the diagonal eigenvalue matrix and $\mathbf{U}$ the unitary matrix ($\mathbf{U}^{-1} = \mathbf{U}^\dagger$) whose columns are the corresponding right eigenvectors of the Hermitian matrix $\widetilde{\mathbf{X}}$. Then

$$\widetilde{\mathbf{X}}\,\mathbf{U} \;=\; \mathbf{U}\,\boldsymbol{\Lambda}\,, \tag{H.16}$$

or

$$\widetilde{\mathbf{X}} \;=\; \mathbf{U}\,\boldsymbol{\Lambda}\,\mathbf{U}^\dagger\,. \tag{H.17}$$

Since $\widetilde{\mathbf{X}}$ is Hermitian, its eigenvalues are real. Numerical calculations confirm this and also show that the eigenvalues are non-negative and non-degenerate. Because of the normalization of $\widetilde{\mathbf{X}}$, the eigenvalues are independent of $\omega_{\mathrm{D},SP}$ and depend on the fluctuating dipole couplings only through their ratio $\omega_{\mathrm{D},IS}/\omega_{\mathrm{D},IP}$. Finally, the eigenvalues are independent of the site orientation Ω^α, but they do depend on the relative orientation of the dipole vectors as parametrized by β_I and β_S. For convenience, we order the eigenvalues in ascending order, so that $\lambda_1 = 0$. The other five eigenvalues are of order 1.

Combining Eq. (H.14) with $\omega_0 = 0$ and Eq. (H.17), we obtain

$$\mathbf{V} \;=\; \omega_{\mathrm{D},I}^2\,\tau_\mathrm{A}\,\mathbf{U}\,\mathbf{M}\,\mathbf{U}^\dagger\,, \tag{H.18}$$

and, since $\mathbf{V}^{-1} = \mathbf{V}^\dagger$,

$$\mathbf{V}^{-1} \;=\; \frac{1}{\omega_{\mathrm{D},I}^2\,\tau_\mathrm{A}}\,\mathbf{U}\,\mathbf{M}^{-1}\,\mathbf{U}^\dagger\,, \tag{H.19}$$

where

$$\mathbf{M} \equiv \epsilon^2 \mathbf{\Lambda} + \mathbf{U}^\dagger \widetilde{\boldsymbol{\rho}} \mathbf{U} . \tag{H.20}$$

We partition the 6×6 matrix $\mathbf{M}$ as

$$\mathbf{M} = \begin{bmatrix} M_{11} & \mathbf{M}_{1c} \\ \mathbf{M}_{c1} & \mathbf{M}_{cc} \end{bmatrix} , \tag{H.21}$$

where subscript c refers to the five-dimensional subspace spanned by eigenvectors $\mathbf{u}_2$ – $\mathbf{u}_6$. All nonzero elements of $\mathbf{M}$ are of order 1, except the diagonal elements of $\mathbf{M}_{cc}$, which are of order $\epsilon^2 \gg 1$. Consequently, all elements of $\mathbf{M}_{cc}^{-1}$ are $\ll 1$ and it follows from the standard expressions for the partitioned matrix inverse that all elements of $\mathbf{M}^{-1}$ are $\ll 1$, except $(\mathbf{M}^{-1})_{11} = 1/M_{11}$, which is of order 1. We thus obtain from Eq. (H.19),

$$\mathbf{V}^{-1} = \frac{\mathbf{u}_1 \, \mathbf{u}_1^\dagger}{\omega_{D,I}^2 \, \tau_A \, M_{11}} , \tag{H.22}$$

where $\mathbf{u}_1$ is the (column) eigenvector corresponding to the eigenvalue $\lambda_1 = 0$. According to Eq. (H.20),

$$M_{11} = \left(\mathbf{U}^\dagger \widetilde{\boldsymbol{\rho}} \, \mathbf{U} \right)_{11} = \mathbf{u}_1^\dagger \widetilde{\boldsymbol{\rho}} \, \mathbf{u}_1 . \tag{H.23}$$

Combining Eqs. (H.2), (H.22) and (H.23), and noting that $\boldsymbol{\sigma} \, \mathbf{u}_1 \, \mathbf{u}_1^\dagger \, \boldsymbol{\sigma}^\dagger = \boldsymbol{\sigma} \, \mathbf{u}_1 \, (\boldsymbol{\sigma} \, \mathbf{u}_1)^\dagger = |\boldsymbol{\sigma} \, \mathbf{u}_1|^2$, we obtain

$$\left\langle \Gamma_{zz}^{II}(0) \right\rangle = \left\langle \frac{|\boldsymbol{\sigma} \, \mathbf{u}_1|^2}{\mathbf{u}_1^\dagger \, \boldsymbol{\rho} \, \mathbf{u}_1} \right\rangle . \tag{H.24}$$

The components of the eigenvectors $\mathbf{u}_k$ refer to basis operators $\{S_z, \, S_+, \, S_-, \, P_z, \, P_+, \, P_-\}$ (disregarding normalization constants). The eigenvector $\mathbf{u}_1$ has the special form

$$\mathbf{u}_1 = \frac{1}{\sqrt{2}} \begin{bmatrix} \mathbf{u}_0 \\ \mathbf{u}_0 \end{bmatrix} , \tag{H.25}$$

where $\mathbf{u}_0$ is a 3×1 column vector and the numerical factor has been introduced to obtain the convenient normalization $\mathbf{u}_0^\dagger \, \mathbf{u}_0 = 1$. (Since $\mathbf{U}$ is unitary, it follows that $\mathbf{u}_1^\dagger \, \mathbf{u}_1 = 1$.) Making use of Eqs. (H.3), (H.11) and (H.25), we can now write Eq. (H.24) as

$$\left\langle \Gamma_{zz}^{II}(0) \right\rangle = \left\langle \frac{|(\boldsymbol{\sigma}^{IS} + \boldsymbol{\sigma}^{IP}) \, \mathbf{u}_0|^2}{\mathbf{u}_0^\dagger \, (\boldsymbol{\rho}^{IS} + \boldsymbol{\rho}^{IP}) \, \mathbf{u}_0} \right\rangle . \tag{H.26}$$

In Eq. (H.26), the eigenvector $\mathbf{u}_0$ has the effect of projecting the cross-spin and auto-spin relaxation matrices onto the stationary ($\lambda_1 = 0$) subspace: $\boldsymbol{\sigma}^{IS} \mathbf{u}_0 = \sigma_{zz}^{IS} \, u_{0,1} + \sigma_{z+}^{IS} \, u_{0,2} + \sigma_{z-}^{IS} \, u_{0,3}$ and $\mathbf{u}_0^\dagger \, \boldsymbol{\rho}^{IS} \mathbf{u}_0 = \sum_n \sum_p u_{0,n}^* u_{0,p} \, \rho_{np}^{IS}$. (For $\omega_0 = 0$, $\boldsymbol{\rho}^{IS}$ is Hermitian, ensuring that, for any orientation, $\mathbf{u}_0^\dagger \, \boldsymbol{\rho}^{IS} \mathbf{u}_0$, and thus $\Gamma_{zz}^{II}(0)$, is real-valued.) The eigenvector $\mathbf{u}_0$ is independent of $\omega_{D,SP}$, but it depends on the ratio $\omega_{D,IS}/\omega_{D,IP}$ and on the orientation Ω_{SP}^α of the static dipole vector. Consequently, while a strong static dipole coupling causes $\left\langle \Gamma_{zz}^{II}(0) \right\rangle$ in Eq. (H.26) to differ from $\left\langle \Gamma_{zz}^{II}(0) \right\rangle_0$ in Eq. (H.10), the actual value of $\left\langle \Gamma_{zz}^{II}(0) \right\rangle$ does not depend on $\omega_{D,SP}$ as long as this coupling is strong ($\epsilon \gg 1$). As we shall see, this behavior, illustrated for $\omega_0 = 0$ in Fig. S2, is actually observed throughout the ZF regime, that is, up to the secondary dispersion.

2.2. Secondary dispersion

For $\omega_0 > 0$, the explicit frequency term in Eq. (H.15) makes $\widetilde{\mathbf{X}}$ non-Hermitian. This follows by noting that the inverse of a Hermitian matrix is also Hermitian, so $\widetilde{\mathbf{X}}$ can be Hermitian only if $\{\widetilde{\mathbf{R}}_{2\text{spin}} + i\,[\omega_0/(\omega_{\text{D},I}^2\,\tau_\text{A})]\,\mathbf{Q}_2\}$ is Hermitian. But this cannot be true for $\omega_0 \neq 0$, because the diagonal elements of a Hermitian matrix must be real.

Because $\widetilde{\mathbf{X}}$ is no longer Hermitian, the eigenvector matrix $\mathbf{U}$ in Eq. (H.16) is not unitary so Eq. (H.17) must be replaced by

$$\widetilde{\mathbf{X}} \;=\; \mathbf{U}\,\mathbf{\Lambda}\,\mathbf{U}^{-1}\,. \tag{H.27}$$

In general, both the eigenvalues λ_k (as before, numbered in ascending order) and the eigenvectors $\mathbf{u}_k$ (the columns of $\mathbf{U}$) depend on the Larmor frequency ω_0. However, the singular eigenvalue $\lambda_1 = 0$ occurs for all frequencies ω_0 and the associated (orientation-dependent) eigenvector $\mathbf{u}_1$ is independent of ω_0, that is, it is the same as for $\omega_0 = 0$.

For $\omega_0 = 0$, when $\widetilde{\mathbf{X}}$ is Hermitian, all eigenvectors are orthonormal, $\mathbf{u}_k^\dagger\,\mathbf{u}_l = \delta_{kl}$. For $\omega_0 > 0$, when $\widetilde{\mathbf{X}}$ is non-Hermitian, the eigenvectors are still normalized, $\mathbf{u}_k^\dagger\,\mathbf{u}_k = 1$, but they are not orthogonal. The columns of $\mathbf{U}$ are still the eigenvectors $\mathbf{u}_k$, but the rows of $\mathbf{U}^{-1}$ are not equal to $\mathbf{u}_k^\dagger$. However, the eigenvector $\mathbf{u}_1$ corresponding to the eigenvalue $\lambda_1 = 0$ defines a one-dimensional unitary subspace, such that $\mathbf{u}_k^\dagger\,\mathbf{u}_1 = \mathbf{u}_1^\dagger\,\mathbf{u}_k = 0$ for all $k \neq 1$. With the chosen ordering, the first column of $\mathbf{U}$ is $\mathbf{u}_1$, while the first row of $\mathbf{U}^{-1}$ (or $\mathbf{U}^\dagger$) is $\mathbf{u}_1^\dagger$. Moreover, the half-eigenvector $\mathbf{u}_0$, defined by Eq. (H.25), has the property (for any ω_0 and any orientation)

$$|u_{0,2}| \;=\; |u_{0,3}|\,. \tag{H.28}$$

For $\omega_0 > 0$, we have in place of Eqs. (H.19) and (H.20)

$$\mathbf{V}^{-1} \;=\; \frac{1}{\omega_{\text{D},I}^2\,\tau_\text{A}}\,\mathbf{U}\,\mathbf{M}^{-1}\,\mathbf{U}^{-1}\,, \tag{H.29}$$

with

$$\mathbf{M} \;\equiv\; \epsilon^2\,\mathbf{\Lambda} + \mathbf{U}^{-1}\,\widetilde{\boldsymbol{\rho}}\,\mathbf{U} + i\,\frac{\omega_0}{\omega_{\text{D},I}^2\,\tau_\text{A}}\,\mathbf{U}^{-1}\,\mathbf{Q}_{11}\,\mathbf{U}\,. \tag{H.30}$$

We partition this $\mathbf{M}$ matrix as in Eq. (H.21), where now

$$M_{11} \;=\; \big(\mathbf{U}^{-1}\,\widetilde{\boldsymbol{\rho}}\,\mathbf{U}\big)_{11} + i\,\frac{\omega_0}{\omega_{\text{D},I}^2\,\tau_\text{A}}\,\big(\mathbf{U}^{-1}\,\mathbf{Q}_{11}\,\mathbf{U}\big)_{11} \;=\; \mathbf{u}_1^\dagger\widetilde{\boldsymbol{\rho}}\,\mathbf{u}_1\,, \tag{H.31}$$

where we have noted that Eq. (H.28) implies that

$$\big(\mathbf{U}^{-1}\,\mathbf{Q}_{11}\,\mathbf{U}\big)_{11} \;=\; 2\,\mathbf{u}_0^\dagger\begin{bmatrix} 0 & 0 & 0 \\ 0 & 1 & 0 \\ 0 & 0 & -1 \end{bmatrix}\mathbf{u}_0 \;=\; 2\,\big(|u_{0,2}|^2 - |u_{0,3}|^2\big) \;=\; 0\,. \tag{H.32}$$

Comparison of Eqs. (H.23) and (H.31) shows that M_{11} is independent of ω_0 throughout the extreme-narrowing regime, where $\omega_0 \ll 1/\tau_\text{A}$ so that $\boldsymbol{\rho}(\omega_0) = \boldsymbol{\rho}(0)$.

As long as the nonzero diagonal elements, $\epsilon^2\,\lambda_k$ for $k \geq 1$, in the first term of Eq. (H.30) are much larger than any elements in the other terms, the arguments presented below Eq. (H.21) hold and Eqs. (H.22), (H.24) and (H.26) remain valid also for $\omega_0 > 0$. To establish quantitatively the extent of the ZF regime in the presence of a static dipole coupling, we consider first the regime $\omega_0 \leq \omega_{\mathrm{D},I}^2\,\tau_\mathrm{A}$. According to Eq. (H.15), $\widetilde{\mathbf{X}}$ is then of order 1, as are the eigenvalues λ_k for $k \geq 1$. All matrix elements in the second and third terms of Eq. (H.30) are of order 1 or less, whereas $\epsilon^2\,\lambda_k \gg 1$ for $k \geq 1$ if the static dipole coupling is strong. The ZF result in Eq. (H.26) thus remains valid. In other words, a strong static dipole coupling abolishes the secondary dispersion at $\omega_0 \approx \omega_{\mathrm{D},I}^2\,\tau_\mathrm{A}$.

To find the upper limit of the ZF regime, we consider now the regime $\omega_0 \gg \omega_{\mathrm{D},I}^2\,\tau_\mathrm{A}$. According to Eq. (H.15), $\widetilde{\mathbf{X}}$ is then of order $\omega_{\mathrm{D},I}^2\,\tau_\mathrm{A}/\omega_0$, as are the eigenvalues λ_k for $k \geq 1$. The order of magnitude of $\epsilon^2\,\lambda_k$ for $k \geq 1$ is then $\omega_{\mathrm{D},SP}^2/[\omega_0\,\omega_{\mathrm{D},I}^2\,\tau_\mathrm{A}]$. With increasing Larmor frequency ω_0, the first term in Eq. (H.30) thus decreases, whereas the third term increases. The condition for dominance of the first term is

$$\omega_0 \;\ll\; \omega_{\mathrm{D},SP}\,, \tag{H.33}$$

which defines the ZF regime in the presence of a strong static dipole coupling.

Let us now summarize the frequency dependence of $\langle\Gamma_{zz}^{II}(\omega_0)\rangle$ below the primary dispersion at $\omega_0 \approx 1/\tau_\mathrm{A}$, as depicted in Fig. S1. For a weak ($\epsilon \ll 1$) static dipole coupling (or none), nonsecular decoupling of single-spin cross-mode relaxation occurs at $\omega_0 \approx \omega_{\mathrm{D},I}^2\,\tau_\mathrm{A}$, giving rise to a secondary dispersion near this frequency, where $\langle\Gamma_{zz}^{II}(\omega_0)\rangle$ drops to the secular-approximation value $\langle\Gamma_{zz}^{II}(\omega_0)\rangle_0^{\mathrm{sec}}$. In the presence of a strong ($\epsilon \gg 1$) static dipole coupling, there is no dispersion step at $\omega_0 \approx \omega_{\mathrm{D},I}^2\,\tau_\mathrm{A}$ and cross-mode relaxation remains effective also at $\omega_0 > \omega_{\mathrm{D},I}^2\,\tau_\mathrm{A}$, albeit modified by the static dipole coupling. Whereas for weak static dipole coupling the ZF regime extends up to $\omega_{\mathrm{D},I}^2\,\tau_\mathrm{A}$, for strong static dipole coupling it extends all the way up to $\omega_{\mathrm{D},SP}$. Now there is a secondary dispersion at $\omega_0 \approx \omega_{\mathrm{D},SP}$, where $\langle\Gamma_{zz}^{II}(\omega_0)\rangle$ increases to the secular-approximation value $\langle\Gamma_{zz}^{II}(\omega_0)\rangle^{\mathrm{sec}}$. This secondary dispersion is not caused by the SDFs, because we are still in the EN regime. Rather, it is caused by the explicit $\mathbf{Q}_{11}$ term in Eq. (H.14), which decreases $\langle\Gamma_{zz}^{II}(\omega_0)\rangle$, *and* by the explicit $\mathbf{Q}_2$ term in Eq. (H.15), which increases $\langle\Gamma_{zz}^{II}(\omega_0)\rangle$. As seen from Fig. S1, the latter effect dominates.

The secular approximation result in Eq. (46), which was derived under the assumption that $\omega_0 \gg \omega_{\mathrm{D},I}^2\,\tau_\mathrm{A}$ *and* $\omega_0 \gg \omega_{\mathrm{D},SP}$, is valid without restriction on $\omega_{\mathrm{D},SP}$. For weak static dipole coupling ($\epsilon \ll 1$), we can neglect the X terms in Eq. (46), which thereby reduces to Eq. (H.12). Conversely, for strong static dipole coupling ($\epsilon \gg 1$), the X terms dominate and Eq. (46) reduces to

$$\langle\Gamma_{zz}^{II}(\omega_0)\rangle^{\mathrm{sec}} \;=\; \left\langle \frac{(R_{zz}^{IS} + R_{zz}^{IP})^2}{(R_{zz}^{SS} + R_{zz}^{PP})} \right\rangle\,, \tag{H.34}$$

which is independent of $\omega_{\mathrm{D},SP}$. It can be shown that this result for $\langle\Gamma_{zz}^{II}(\omega_0)\rangle^{\mathrm{sec}}$ is smaller than the result $\langle\Gamma_{zz}^{II}(\omega_0)\rangle_0^{\mathrm{sec}}$ in Eq. (H.12), as is evident from Fig. S1.

The secular approximation simplifies the cross-spin relaxation matrix $\boldsymbol{\sigma}$ in Eq. (H.3), the auto-spin relaxation matrix $\boldsymbol{\rho}$ in Eq. (H.5), and the static dipole matrix $\mathbf{X}$ in Eq. (H.6). By applying the secular approximation selectively to these matrices, we find that, for strong static dipole coupling, the secular approximation acts mainly via $\mathbf{X}$, whereas, for weak static dipole coupling, the effect is on $\boldsymbol{\sigma}$ and $\boldsymbol{\rho}$ (since $\mathbf{X}$ is not involved). The different nonsecular decoupling effects for weak and strong dipole coupling explains why the $\widehat{R}_{1,I}^{\mathrm{dil}}(\omega_0)$ dispersion is inverted for weak but not for strong static dipole coupling (Fig. S1).

References

[1] D. M. Brink and G. R. Satchler, *Angular Momentum*, 3rd ed. (Clarendon Press, Oxford, 1994).

[2] K. Blum, *Density Matrix Theory and Applications*, 3rd ed. (Springer-Verlag, Berlin, 2012).

[3] Z. Chang and B. Halle, J. Chem. Phys. **139**, 144203 (2013).

[4] A. Abragam, *The Principles of Nuclear Magnetism* (Clarendon Press, Oxford, 1961).

[5] Z. Chang and B. Halle, J. Chem. Phys. **143**, 234201 (2015).

[6] N. C. Pyper, Mol. Phys. **21**, 1 (1971).

[7] S. Szymanski, A. M. Gryff-Keller and G. Binsch, J. Magn. Reson. **68**, 399 (1986).

[8] M. Tinkham, *Group Theory and Quantum Mechanics* (McGraw-Hill, New York, 1964).

[9] Z. Chang and B. Halle, J. Chem. Phys. **144**, 084202 (2016).

Paper IV

Nuclear magnetic relaxation by the dipolar EMOR mechanism: Multi-spin systems

Zhiwei Chang and Bertil Halle[a)]
Division of Biophysical Chemistry, Department of Chemistry, Lund University, POB 124, SE-22100 Lund, Sweden

(Dated: 9 May 2017)

In aqueous systems with immobilized macromolecules, including biological tissue, the longitudinal spin relaxation of water protons is primarily induced by exchange-mediated orientational randomization (EMOR) of intra- and intermolecular magnetic dipole-dipole couplings. Starting from the stochastic Liouville equation, we have previously developed a rigorous EMOR relaxation theory for dipole-coupled two-spin and three-spin systems. Here, we extend the stochastic Liouville theory to four-spin systems and use these exact results as a guide for constructing an approximate multi-spin theory, valid for spin systems of arbitrary size. This so-called GSRE theory includes the effects of longitudinal-transverse cross-mode relaxation, which gives rise to an inverted step in the relaxation dispersion profile, and coherent spin mode transfer among solid-like spins, which may be regarded as generalized spin diffusion. The GSRE theory is compared to an existing theory, based on the extended Solomon equations, which does not incorporate these phenomena. Relaxation dispersion profiles are computed from the GSRE theory for systems of up to 16 protons, taken from protein crystal structures. These profiles span the range from the motional narrowing limit, where coherent mode transfer plays a major role, to the ultra-slow motion limit, where the zero-field rate is closely related to the strong-collision limit of the dipolar relaxation rate. Although a quantitative analysis of experimental data is beyond the scope of this work, it is clear from the magnitude of the predicted relaxation rate and the shape of the relaxation dispersion profile that the dipolar EMOR mechanism is the principal cause of water-^{1}H low-field longitudinal relaxation in aqueous systems of immobilized macromolecules, including soft biological tissue. The relaxation theory developed here therefore provides a basis for molecular-level interpretation of endogenous soft-tissue image contrast obtained by the emerging low-field magnetic resonance imaging techniques.

PACS numbers: 76.60.Es, 82.56.Na, 87.64.kj, 87.61.Bj

I. INTRODUCTION

During the past two decades, a rigorous molecular theory has been developed for nuclear magnetic relaxation induced by exchange-modulated electric quadrupole[1–3] or magnetic dipole[4–7] couplings in aqueous systems with immobilized macromolecules. Such a theory is needed, for example, to interpret water ^{1}H or ^{2}H field-cycling (FC)[8–10] relaxation dispersion data in biophysical studies of water-protein interactions,[3,11–17] and to connect endogeneous soft-tissue image contrast to molecular-level phenomena in magnetic resonance imaging (MRI) analysis using emergent fast FC[18] or SQUID-detected[19] low-field MRI techniques. For biophysical applications, the ^{2}H nuclide is the NMR probe of choice on account of the more straight-forward analysis of relaxation data involving the single-spin quadrupolar mechanism. But medical MRI applications invariably utilize the ^{1}H resonance, thereby forcing us to confront the more challenging multi-spin dipolar relaxation problem.

The present work completes a series of four papers devoted to the theory of dipolar relaxation by the mechanism of exchange-mediated orientational randomization (EMOR). In the three preceding papers, here referred to as Paper I,[5] II[6] and III,[7] we treated two-spin and three-spin systems. Here, we make the leap to multi-spin systems, comprising one or two labile spins exchanging with an isotropic bulk phase and dipole-coupled to an arbitrary number of nonlabile spins in a solid-like environment.

In the EMOR mechanism, exchange plays a dual role: it transfers magnetization between the anisotropic macromolecular sites and the isotropic bulk phase and it drives relaxation by modulating the dipole couplings of the labile spin(s). The conventional Bloch-Wangsness-Redfield (BWR) perturbation theory of nuclear spin relaxation[20] therefore breaks down when, as is usually the case, fast-exchange conditions do not prevail. We have therefore developed a non-perturbative relaxation theory, based on the stochastic Liouville equation (SLE),[21,22] and valid without restrictions on exchange rate, dipole couplings and magnetic field strength.[5–7] To better understand the rich relaxation behavior exhibited by the dipolar EMOR model, we have also developed a perturbation theory, based on the stochastic Redfield equation (SRE), that is, the BWR master equation supplemented with exchange terms, which, however, is valid only in the restricted motional-narrowing (RMN) regime, where the exchange rate exceeds all (fluctuating and static) dipole couplings.

For larger spin systems, the SLE theory becomes computationally intractable. We therefore turn to the more

a)bertil.halle@bpc.lu.se

computationally efficient and physically transparent SRE theory, extending its validity beyond the RMN regime by certain physically inspired, but essentially ad hoc, modifications. These modifications were calibrated against the exact SLE solution of the EMOR model for four-spin systems, which is also presented here. The resulting generalized SRE (GSRE) theory, which is applicable in the full parameter space of the EMOR model, is then applied to spin systems comprising up to 16 protons extracted from crystal structures of two globular proteins. The GSRE theory is also compared to a previously proposed approximate theory,[4] based on the extended (by exchange terms) Solomon equations[23] (ESE). Unlike the GSRE and SLE theories, the ESE theory does not take into account longitudinal-transverse cross-mode relaxation or coherent transfer of magnetization (and higher spin modes) induced by the static dipole couplings.

The outline of this paper is as follows. In Sec. II, we briefly define the multi-spin dipolar EMOR model; more details can be found in Paper II. In Sec. III, we develop the analytical multi-spin SRE theory, making extensive use of symmetry selection rules, and, in Sec. IV, we rederive the multi-spin ESE theory, which, in the RMN regime, turns out to be a special case of the SRE theory. The exact solution of the SLE for four-spin systems, described in Sec. V, is used in Sec. VI to construct and assess the multi-spin GSRE theory for spin systems of increasing size. Finally, in Sec. VII, we discuss some limitations of the GSRE theory and how these can be overcome by suitable generalizations. The results presented in this paper are based on a substantial amount of analytical and numerical work, as reflected by the 14 appendices of the supplemental material.[24]

II. MODEL AND EXACT FORMAL RESULTS

A. Model definition

1. Spin system and EMOR mechanism

We consider an immobilized protein molecule containing one or two labile protons dipole-coupled to m nonlabile protein protons and exchanging with the protons in the surrounding bulk water phase. The case of a single labile proton, with spin I, might represent a hydroxyl or carboxyl proton in an amino acid side-chain. The case of two labile protons, with spins I and S, represents a water molecule transiently buried in a cavity inside the protein. For spins associated with nonlabile protons, we use the generic label P or lower-case Greek letters μ, ν, κ, λ, ...

To identify different spin systems and exchange cases, we use the notation '(spins in state A)–(spins in state B)', where state A comprises protons associated with the protein and state B includes the bulk water protons. The two generic multi-spin exchange cases treated here are thus denoted IP_m–I and ISP_m–IS. The two-spin cases IS–IS and IP–I were treated in Papers I and II, respectively, whereas the three-spin cases IP_2–I and ISP–IS (as well as ISP–ISP) were considered in Paper III. In the following, we present exact solutions for the four-spin cases IP_3–I and ISP_2–IS and approximate solutions for the generic multi-spin cases IP_m–I and ISP_m–IS without restriction on the number m of nonlabile protons.

The physical system that we have in mind is an aqueous protein gel or a soft biological tissue, where most or all protein molecules are effectively immobilized by chemical cross-links or non-covalent interactions. The system contains a large number of randomly oriented protein molecules, each of which is referred to as a site and identified by the generic label α. These sites, which make up state A, are identical in all respects except for their orientation (with respect to a lab-fixed frame), which conforms to an isotropic orientational distribution.

The labile protons undergo chemical or, in the case of internal water molecules, physical exchange with bulk water protons and their mean survival time in the A sites is denoted by $\tau_{\rm A}$. Detailed balance[25] then requires that $P_{\rm B}\,\tau_{\rm A} = P_{\rm A}\,\tau_{\rm B}$, where $P_{\rm A} = 1 - P_{\rm B}$ is the fraction of all labile protons (including bulk water) that, at any given time, reside in A sites. In practice,[4,12,15] $P_{\rm A} \ll 1$ and the following development will therefore focus on this dilute regime.

Exchange not only transfers magnetization between the A and B states and quenches multi-spin modes by fragmenting the spin system;[26] it is also the motion that induces spin relaxation by stochastically modulating all dipole couplings involving the labile spin(s) residing in A sites. In this dynamic model, which we refer to as exchange-mediated orientational randomization (EMOR), the orientation of all internuclear vectors involving the labile spin(s) is instantaneously randomized upon exchange. This simple model is justified if $\tau_{\rm A}$ is long compared to the time required for orientational randomization when the labile spin(s) has been transferred to state B. This is the case for chemical exchange of labile macromolecular protons with bulk water as well as for physical exchange of internal water molecules with bulk water.[5,27]

In the interest of clarity, we have here described the model in terms relevant for the most important applications. However, the theory developed in the following is more general. For example, the macromolecules need not be proteins, the bulk phase need not be water, and the spin-1/2 nuclei need not be protons.

2. Spin Hamiltonian

From an NMR point of view, the A state has the peculiar property of combining solid-like and liquid-like features. Whereas I–μ, S–μ and I–S dipole couplings are averaged to zero by exchange, thereby inducing spin-lattice relaxation, μ–ν dipole couplings are static and therefore induce coherent evolution of the spin system. The dipo-

lar spin Hamiltonian (in angular frequency units) for site α is

$$H^{\alpha}_{\mathrm{D},X} \;=\; -\,\frac{2}{\sqrt{6}}\sum_{X}\omega_{\mathrm{D},X}\sum_{M=-2}^{2}T^{2}_{M}(X)\,D^{2\,*}_{M0}(\Omega^{\alpha}_{X})\,, \quad (1)$$

where the first sum runs over all mutual dipole couplings among the $m+1$ or $m+2$ spins in site α. The irreducible spherical tensor operators (ISTOs) $T^{2}_{M}(X)$ are normalized in the two-spin Liouville space of the spins involved in dipole coupling X, as in Table S1 of Paper II. The argument of the rank-2 Wigner functions $D^{2}_{M0}(\Omega^{\alpha}_{X})$ are the Euler angles Ω^{α}_{X} that specify the orientation of the internuclear vector $\boldsymbol{r}_X$ in site α with respect to the lab-fixed frame.[28] As in papers I – III, we incorporate a factor 3/2 in the definition of the dipole coupling: $\omega_{\mathrm{D},X} \equiv (3/2)\,[\mu_0/(4\,\pi)]\,\gamma^2\,\hbar/r^{3}_{X}$.

As shown in Paper III, the effect of proton chemical shifts is negligibly small under the conditions of interest. The spins can therefore be taken to be isochronous, so the Zeeman spin Hamiltonian is the same in all sites,

$$H^{\alpha}_{Z} \;=\; \omega_0\Big[I_z + S_z + \sum_{\mu=1}^{m}P_{\mu,z}\Big]\,, \quad (2)$$

the S_z term being present only for the $ISP_m{-}IS$ case. The Zeeman Hamiltonian in state B is the same as in state A, but without the sum over nonlabile spins. We omit the rapidly fluctuating dipolar Hamiltonian in state B, which gives rise to a small and frequency-independent relaxation contribution that, if so desired, can be added to the final expression for the relaxation rate.[5]

B. Integral relaxation rate in the dilute regime

Our primary objective here is to calculate the frequency-dependent longitudinal relaxation rate, $R_1(\omega_0)$, of the abundant water proton spins. Under most conditions of interest, the system is in the dilute regime and relaxation is therefore strictly exponential. The so-called integral longitudinal relaxation rate (ILRR), $\widehat{R}^{\,\mathrm{dil}}_{1}(\omega_0)$, that is most readily obtained from theory,[1,6] is then identical to the observable $R_1(\omega_0)$. For this reason, and in the interest of notational economy, we shall omit the caret as well as the "dil" superscript (indicating dilute regime conditions) used in previous papers in this series. On the other hand, we will indicate with a subscript I or IS whether the relaxation rate pertains to the $IP_m{-}I$ or $ISP_m{-}IS$ case.

The general formalism for relaxation by the dipolar EMOR mechanism presented in Paper II is valid for arbitrarily large spin systems. The relaxation rate in the dilute regime and with observation of the labile spin(s), is given, for the two exchange cases considered here, by

$$R_{1,I} \;=\; \frac{P_{\mathrm{A}}}{\tau_{\mathrm{A}}\,U_{11}}\,, \quad (3a)$$

$$R_{1,IS} \;=\; \frac{2\,P_{\mathrm{A}}}{\tau_{\mathrm{A}}\,(U_{11}+U_{12}+U_{21}+U_{22})}\,, \quad (3b)$$

where $U_{np} \equiv (n|\mathbf{U}|p)$ is a Liouville-space supermatrix element of the superoperator $\mathbf{U}$ and the basis operators $B_n \equiv |n)$ are taken to be ordered so that $B_1 \sim I_z$ and $B_2 \sim S_z$. (The quantity here denoted by $\mathbf{U}$ corresponds to $P_{\mathrm{A}}/\tau_{\mathrm{A}}$ times the resolvent superoperator $\widetilde{\mathbf{U}}^{\mathrm{BB}}(s)$ at Laplace variable $s=0$, as defined in Paper II.) According to Paper II, in the dilute regime,

$$\mathbf{U} \;=\; \Big[\mathbf{1} \,+\, i\,\mathbf{L}_{\mathrm{Z}}\,\tau_{\mathrm{B}} \,-\, \mathbf{T}\,\mathbf{G}^{\mathrm{A}}\,\mathbf{T'}\Big]^{-1}\,, \quad (4)$$

where the exchange topology supermatrix $\mathbf{T}$ connects all B state basis operators (which only involve labile spins) with the corresponding operators in the larger A state basis, and $\mathbf{T'}$ is the transpose of $\mathbf{T}$. Furthermore,

$$\mathbf{G}^{\mathrm{A}} \;=\; \big\langle(\mathbf{\Lambda}^{\alpha})^{-1}\big\rangle\,, \quad (5)$$

where the angular brackets indicate an isotropic orientational average (over all sites) and the supermatrix $\mathbf{\Lambda}^{\alpha}$, associated with a particular site α, takes different forms depending on whether the subsequent theoretical development is based on the general stochastic Liouville equation (SLE) or its limiting form, the stochastic Redfield equation (SRE).[6,7] As seen from Eq. (3), for both exchange cases, the relaxation rate is strictly proportional to P_{A} in the dilute regime.

In the multi-spin SLE theory, valid in the full parameter space of the EMOR model, $\mathbf{\Lambda}^{\alpha}$ is given by[6]

$$\mathbf{\Lambda}^{\alpha} \;=\; \mathbf{K} + i\,\mathbf{L}^{\alpha}_{\mathrm{D}}\,\tau_{\mathrm{A}} + i\,\mathbf{L}_{\mathrm{Z}}\,\tau_{\mathrm{A}}\,, \quad (6)$$

where $\mathbf{L}^{\alpha}_{\mathrm{D}}$ and $\mathbf{L}_{\mathrm{Z}}$ are the Liouvillian supermatrices corresponding to the dipolar and Zeeman spin Hamiltonians in Eqs. (1) and (2), and the supermatrix $\mathbf{K}$ differs from the identity matrix only in that diagonal elements corresponding to basis operators that only involve nonlabile spins are zero. In the multi-spin SRE theory, valid in the restricted motional narrowing (RMN) regime, $\mathbf{\Lambda}^{\alpha}$ is instead given by[7]

$$\mathbf{\Lambda}^{\alpha} \;=\; \mathbf{K} + \mathbf{R}^{\alpha}\,\tau_{\mathrm{A}} + i\,\mathbf{\Delta}^{\alpha}\,\tau_{\mathrm{A}} + i\,\mathbf{L}_{\mathrm{Z}}\,\tau_{\mathrm{A}}\,, \quad (7)$$

featuring the relaxation supermatrix $\mathbf{R}^{\alpha}$ and the coherent mode transfer supermatrix $\mathbf{\Delta}^{\alpha}$, the explicit forms of which are given in Sec. III.A.

The supermatrix $\mathbf{G}^{\mathrm{A}}$ is isotropically averaged and therefore shares the cylindrical symmetry of the Zeeman Hamiltonian. The Wigner-Eckart theorem[29] then implies that $\mathbf{G}^{\mathrm{A}}$ is Q-block-diagonal in the ISTO basis for state A. The supermatrix $\mathbf{T}\,\mathbf{G}^{\mathrm{A}}\,\mathbf{T'}$ is therefore Q-block-diagonal in the B state basis, as is the Zeeman

Liouvillian supermatrix $\mathbf{L}_{\rm Z}$ in Eq. (4). Since the block structure is retained under matrix inversion, it follows from Eq. (4) that also $\mathbf{U}$ is Q-block-diagonal. As seen from Eq. (3), we only need elements from the $Q = 0$ block of $\mathbf{U}$, so we can disregard the other Q-blocks. For the $IP_m{-}I$ case, the $Q = 0$ block is one-dimensional and $[\mathbf{L}_{\rm Z}]_{Q=0} = L_{{\rm Z},11} = 0$. For the $ISP_m{-}IS$ case, the $Q = 0$ block is 5-dimensional, but, if the labile spins I and S are isochronous in state B, we have $[\mathbf{L}_{\rm Z}]_{Q=0} = \mathbf{0}$. For both exchange cases, $\mathbf{L}_{\rm Z}$ can therefore be omitted from Eq. (4), whereby

$$\mathbf{U}_{Q=0} \;=\; \Big[\mathbf{1} \;-\; \mathbf{T}_0\,\mathbf{G}^{\rm A}\,\mathbf{T}_0'\Big]^{-1}\;, \tag{8}$$

where $\mathbf{T}_0$ connects B state $Q = 0$ operators with the corresponding A state operators.

For exchange case $IP_m{-}I$,

$$T_{0,np} \;=\; \delta_{n1}\,\delta_{p1}\;, \tag{9}$$

so Eq. (8) yields

$$U_{11} \;=\; \frac{1}{(1-g_{11})}\;, \tag{10}$$

where $g_{np} = \equiv\; (n|\mathbf{G}^{\rm A}|p)$. Combination of Eqs. (3a) and (10) then yields

$$R_{1,I} \;=\; \frac{P_{\rm A}}{\tau_{\rm A}}\,(1-g_{11})\,. \tag{11}$$

This is an exact result for the multi-spin $IP_m{-}I$ case in the dilute regime.

For exchange case $ISP_m{-}IS$, the $Q = 0$ subspace is 5-dimensional. However, to an excellent approximation, we need only retain the 2×2 block of $\mathbf{G}^{\rm A}$ spanned by the first two basis operators B_1 and B_2, which have odd spin inversion conjugation parity.[30,31] As shown in Appendix A,[24] the relaxation rate then becomes

$$R_{1,IS} \;=\; \frac{P_{\rm A}}{\tau_{\rm A}}\,\frac{2\,(1-g_{11}-g_{22}+g_{11}g_{22}-g_{12}g_{21})}{(2-g_{11}-g_{22}+g_{12}+g_{21})}\;. \tag{12}$$

The test calculations reported in Appendix A[24] demonstrate that, in practice, this may be regarded as an exact result.

III. MULTI-SPIN SRE THEORY

A. Relaxation and coherent mode transfer

The starting point for the multi-spin SRE theory is the restricted BWR master equation, which we derive in Appendix B.[24] As shown in Paper II, this master equation leads to the exact results of Sec. II, notably Eqs. (5), (11) and (12) with $\mathbf{\Lambda}^\alpha$ given by Eq. (7). For isochronous spins, the relaxation supermatrix $\mathbf{R}^\alpha$ appearing in Eq. (7) is given explicitly by[7]

$$\begin{aligned}\mathbf{R}^\alpha \;&=\; \frac{2}{3}\sum_X\sum_Y \omega_{{\rm D},X}\,\omega_{{\rm D},Y} \\ &\times \sum_{M=-2}^{2}\sum_{M'=-2}^{2} F_{MM'}(\Omega_X^\alpha,\Omega_Y^\alpha)\,J(-M'\omega_0)\,\mathbf{C}_{MM'}^{XY}\;.\end{aligned} \tag{13}$$

The coherent mode transfer supermatrix $\mathbf{\Delta}^\alpha$, which is present for $m \geq 2$, is obtained as the obvious multi-spin generalization of the $ISP{-}I$ result given in Paper III,

$$\mathbf{\Delta}^\alpha \;=\; -\,\frac{2}{\sqrt{6}}\sum_X \omega_{{\rm D},X}\sum_{M=-2}^{2} D_{M0}^{2*}(\Omega_X^\alpha)\,\mathbf{D}_M^X\;. \tag{14}$$

In Eq. (13), X and Y refer to dipole couplings that involve at least one labile spin, so they are randomized by the exchange. In Eq. (14), X refers to static dipole couplings between pairs of nonlabile spins.

For the EMOR relaxation mechanism, the spectral density function (SDF) in Eq. (13) is of the form

$$J(n\,\omega_0) \;=\; \frac{\tau_{\rm A}}{1+(n\,\omega_0\,\tau_{\rm A})^2}\;. \tag{15}$$

As shown in Paper III, the odd SDF has no effect for the $ISP{-}IS$ case and a completely negligible effect for the $IP_2{-}I$ case. In Eq. (15), we therefore retain only the even part of the SDF.

The angular functions in Eq. (13) are defined as

$$\begin{aligned}F_{MM'}(\Omega_X^\alpha,\Omega_Y^\alpha) \;&\equiv\; D_{M0}^{2*}(\Omega_X^\alpha)\,D_{M'0}^{2*}(\Omega_Y^\alpha) \\ &=\; \exp[i(M\psi_X^\alpha + M'\psi_Y^\alpha)]\,d_{M0}^2(\vartheta_X^\alpha)\,d_{M'0}^2(\vartheta_Y^\alpha)\;.\end{aligned} \tag{16}$$

To compute the Wigner functions $D_{M0}^{2*}(\Omega_X^\alpha)$ in Eqs. (14) and (16), we need a convention for parametrizing the internuclear geometry. The Euler angles $\Omega_X^\alpha = (\psi_X^\alpha,\,\vartheta_X^\alpha,\,-)$ specify the orientation of the dipole vector $\boldsymbol{r}_X$ with respect to the lab-fixed frame. First, we need a convention for the direction of the dipole vector $\boldsymbol{r}_X$. For fluctuating dipole vectors, $\boldsymbol{r}_X$ is taken to point from the labile spin (I or S) to the nonlabile spin (μ) or, for the intramolecular water dipole coupling, from spin I to spin S. For static dipole couplings between nonlabile spins μ and ν, $\boldsymbol{r}_X$ is taken to point from μ to ν with $\mu < \nu$.

The total number of (static or fluctuating) dipole couplings is $m(m+1)/2$ for the $IP_m{-}I$ case and $1+m(m+3)/2$ for the $ISP_m - IS$ case. A description that, for each site α, specifies the two angles ψ_X^α and ϑ_X^α for each of those dipole couplings is redundant. To obtain a more parsimonious description, we perform the transformation from the lab-fixed frame L, with the $z_{\rm L}$ axis along the $\boldsymbol{B}_0$ field, to the dipole-fixed frame X, with the $z_{\rm X}$ axis along the dipole vector $\boldsymbol{r}_X$, via an intermediate site-fixed frame D. The first transformation step, which rotates the L frame into coincidence with the D frame of site α, is specified by the X-independent Euler angles $\Omega_{\rm LD}^\alpha = (\phi^\alpha,\,\theta^\alpha,\,\varphi^\alpha)$. The second transformation step is specified by the site-independent Euler angles

$\Omega_{\mathrm{DX}} = (\gamma_X, \beta_X, -)$, that is, the spherical polar angles that define the orientation of the dipole vector $\boldsymbol{r}_X$ with respect to the D frame. In terms of the two successive transformations L → D → X, the Wigner functions can be expressed as

$$\begin{aligned} D^{2\,*}_{M0}(\Omega^{\alpha}_{X}) \;&=\; \sum_{N=-2}^{2} D^{2\,*}_{MN}(\Omega^{\alpha}_{\mathrm{LD}})\, D^{2\,*}_{N0}(\Omega_{\mathrm{DX}}) \\ &=\; \exp(iM\phi^{\alpha}) \sum_{N=-2}^{2} d^{2}_{MN}(\theta^{\alpha})\, \exp[iN(\varphi^{\alpha}+\gamma_X)]\, d^{2}_{N0}(\beta_X)\,. \end{aligned} \tag{17}$$

In Appendix C,[24] we describe the conventions used to define the D frame and the Euler angles β_X and γ_X.

The isotropic orientational average in Eq. (5) involves the Euler angles $\Omega^{\alpha}_{\mathrm{LD}} = (\phi^{\alpha}, \theta^{\alpha}, \varphi^{\alpha})$. For the angles ϕ^{α} and θ^{α}, which determine the orientation of the z_{D} axis, we use Lebedev quadrature[32,33] with N_{L} points on the unit sphere. For the angle φ^{α}, which determines the orientation of the x_{D} and y_{D} axes, we use a uniform grid with N_{φ} points. Unless otherwise noted, we use $N_{\Omega} = N_{\mathrm{L}} \times N_{\varphi} = 14 \times 5 = 70$ Euler angle sets, but when extreme accuracy is desired we use $N_{\Omega} = 50 \times 15 = 750$ sets.

B. Symmetry rules

The real-valued elements of the coefficient supermatrices in Eqs. (13) and (14) are,[7]

$$C^{XY}_{MM',np} \;=\; \mathrm{Tr}\{[B_n^{\dagger}, T^{2}_{M}(X)]\,[T^{2}_{M'}(Y), B_p]\}\,, \tag{18}$$

$$\begin{aligned} D^{X}_{M,np} \;&=\; \mathrm{Tr}\{B_n^{\dagger}\,[T^{2}_{M}(X), B_p]\} \\ &=\; \mathrm{Tr}\{[B_n^{\dagger}, T^{2}_{M}(X)]\,B_p\}\,, \end{aligned} \tag{19}$$

where the last equality follows from the cyclic permutation invariance of the trace. Whereas the ISTOs $T^{2}_{M}(X)$ are normalized in the two-spin Liouville space corresponding to the two spins involved in the dipole coupling X, the basis operators B_n are normalized in the multi-spin Liouville space, that is, $\mathrm{Tr}\{B_n^{\dagger}\,B_p\} = \delta_{np}$ with the trace including all $m+1$ or $m+2$ spins. The numerical prefactors in Eqs. (13) and (14) are consistent with these conventions.

The coefficients $C^{XY}_{MM',np}$ and $D^{X}_{M,np}$ exhibit symmetries that allow us to formulate the SRE theory in a small part of the full $(4^{m+2}-1)$-dimensional spin Liouville space. The Liouville subspace notation used to describe these symmetries is defined in Appendix D.[24] For example, the subspaces $\mathbb{L}$ and $\mathbb{N}$ are spanned by basis operators involving only labile or nonlabile spins, respectively. The one- or two-dimensional subspace $\mathbb{LZ}$ is spanned by basis operators proportional to I_z or S_z, and the 27-dimensional subspace $\mathbb{N}_3(\mu\nu\kappa)$ is spanned by basis operators involving only the three indicated nonlabile spins. These subspaces may be further decomposed into subspaces spanned exclusively by basis operators with odd (antisymmetric = a) or even (symmetric = s) spin inversion conjugation (SIC) parity.[30,31] For example, $\mathbb{N} = \mathbb{NA} \oplus \mathbb{NS}$. The odd and even subspaces can then be decomposed into subspaces with basis operators involving a specific number of distinct spins, for example, $\mathbb{NA} = \mathbb{N}_1 \oplus \mathbb{N}_3 \oplus \mathbb{N}_5$ if $m = 6$.

By using the general properties of the commutator and trace operations, we can establish useful symmetry rules for the coefficients $C^{XY}_{MM',np}$ and $D^{X}_{M,np}$ in Eqs. (18) and (19). Here we merely state these rules; the proofs can be found in Appendix E.[24] The rules can be expressed most succinctly in terms of the relevant blocks of the supermatrices $\mathbf{C}^{XY}_{MM'}$ or $\mathbf{D}^{X}_{M}$.

Symmetry Rule I. Labile single-spin modes are relaxation-coupled to nonlabile single-spin modes but not to other nonlabile odd-parity modes, and the relaxation coupling only involves self-correlations.

$$\mathbf{C}^{XY}_{MM',\mathbb{L}_1\mathbb{N}_k} \;=\; \delta_{XY}\,\delta_{k1}\,\mathbf{C}^{XX}_{MM',\mathbb{L}_1\mathbb{N}_1}\,,\ (k = \text{odd})\,. \tag{20}$$

Symmetry Rule II. Relaxation does not couple nonlabile-spin modes involving different number of spins.

$$\mathbf{C}^{XY}_{MM',\mathbb{N}_k\mathbb{N}_l} \;=\; \delta_{kl}\,\mathbf{C}^{XY}_{MM',\mathbb{N}_k\mathbb{N}_k}\,. \tag{21}$$

Symmetry Rule III. Within the nonlabile k-spin subspace $\mathbb{N}_k$, relaxation only couples modes that involve the same set of k spins.

$$\begin{aligned} &\mathbf{C}^{XY}_{MM',\mathbb{N}_k(\mu\nu\kappa\lambda\cdots)\mathbb{N}_k(\mu'\nu'\kappa'\lambda'\cdots)} \;= \\ &\delta_{\mu\nu\kappa\lambda\cdots,\,\mu'\nu'\kappa'\lambda'\cdots}\,\mathbf{C}^{XY}_{MM',\mathbb{N}_k(\mu\nu\kappa\lambda\cdots)\mathbb{N}_k(\mu\nu\kappa\lambda\cdots)}\,. \end{aligned} \tag{22}$$

The supermatrices $\mathbf{C}^{XY}_{MM',\mathbb{N}_k\mathbb{N}_k}$ and $\mathbf{R}^{\alpha}_{\mathbb{N}_k\mathbb{N}_k}$ are therefore block-diagonal in spins ($k = 1$), spin pairs ($k = 2$), etc. Furthermore, relaxation coupling between single-spin modes only involves self-correlations.

Symmetry Rule IV. Relaxation supermatrix elements within the single-spin subspace only involve self-correlations.

$$C^{XY}_{MM',np} \;=\; \delta_{XY}\,C^{XX}_{MM',np}\,, \quad \text{if } n,\, p \in \mathbb{W}_1\,. \tag{23}$$

Symmetry Rule V. Coherent dipolar evolution does not couple directly to labile-spin modes.

$$\mathbf{D}^{X}_{M,\,\mathbb{LW}} \;=\; \mathbf{D}^{X}_{M,\,\mathbb{WL}} \;=\; \mathbf{0}\,. \tag{24}$$

Symmetry Rule VI. Coherent dipolar evolution does not couple nonlabile-spin modes with mixed modes.

$$\mathbf{D}^{X}_{M,\,\mathbb{NU}} \;=\; \mathbf{D}^{X}_{M,\,\mathbb{UN}} \;=\; 0\,. \tag{25}$$

Together, symmetry rules V and VI show that coherent dipolar evolution can only couple nonlabile-spin modes to other nonlabile-spin modes.

Symmetry Rule VII. Coherent dipolar evolution couples nonlabile single-spin modes with nonlabile two-spin modes, but not with any other nonlabile k-spin modes.

$$\mathbf{D}^X_{M,\,\mathbb{N}_1\mathbb{N}_k} \;=\; \delta_{k2}\,\mathbf{D}^X_{M,\,\mathbb{N}_1\mathbb{N}_2}\,. \tag{26}$$

Symmetry Rule VIII. Coherent dipolar evolution only couples nonlabile spin modes differing by one spin. Thus, for $k \geq 2$,

$$\mathbf{D}^X_{M,\,\mathbb{N}_k\mathbb{N}_l} \;=\; \delta_{l,k\pm1}\,\mathbf{D}^X_{M,\,\mathbb{N}_k\mathbb{N}_{k\pm1}}\,. \tag{27}$$

For $k = 1$, only the plus sign applies and Eq. (27) reduces to Eq. (26).

Symmetry Rule IX. Coherent dipolar evolution couples k-spin modes with $(k+1)$-spin modes only if k spins are shared between the modes. The mode coupling is induced by dipole couplings between the non-shared spin and each of the shared spins.

C. Integral relaxation rate

We have now defined all quantities in Eq. (7) that make up the supermatrix $\mathbf{\Lambda}^\alpha$, which must then be inverted and isotropically averaged to obtain the elements of the supermatrix $\mathbf{G}^{\rm A}$ in Eq. (5) needed to calculate the relaxation rate from Eq. (11) or (12). Even though the dimension of the supermatrix $\mathbf{\Lambda}^\alpha$ is prohibitively large for realistic spin systems, a computationally manageable theory can be obtained by using the SIC symmetry of the supermatrices $\mathbf{R}^\alpha$ and $\mathbf{\Delta}^\alpha$ and the symmetry rules in Sec. III.B. We shall thus generalize the three-spin treatment of Paper III to the multi-spin cases $IP_m - I$ and $ISP_m - IS$, without any limitation on the number m of nonlabile spins. This will be done exactly for $m \leq 3$, whereas, for $m \geq 4$, we neglect four-spin and higher spin modes. Here we only present an outline of the derivation of the multi-spin SRE theory; the full derivation can be found in Appendix F.[24]

Provided that the multi-spin ISTO basis for state A is ordered with the odd-parity operators before the even-parity operators, the SIC symmetry ensures that the relaxation supermatrix $\mathbf{R}^\alpha$ is block-diagonal whereas the coherent mode transfer supermatrix $\mathbf{\Delta}^\alpha$ is anti-block-diagonal. To make use of this symmetry, we partition $\mathbf{\Lambda}^\alpha$ into blocks associated with the anti-symmetric ($\mathbb{A}$) and symmetric ($\mathbb{S}$) subspaces. We only need the $\mathbb{AA}$ block of the inverse $(\mathbf{\Lambda}^\alpha)^{-1}$. Expanding this inverse to first order in $\mathbf{R}^\alpha\tau_{\rm A}$, that is, to second order in $\omega_{\rm D}\tau_{\rm A}$, consistent with our use of the RMN approximation in Eq. (13), and performing the isotropic average in Eq. (5), the relevant 1×1 ($IP_m - I$ case) or 2×2 ($ISP_m - IS$ case) block of the supermatrix $\mathbf{G}^{\rm A}$ can be expressed in terms of the auto-spin relaxation supermatrix $\mathbf{R}^\alpha_{\mathbb{LZ},\mathbb{LZ}}$ and the cross-relaxation supermatrix $\mathbf{\Gamma}^\alpha_{\mathbb{LZ},\mathbb{LZ}}$ for site α,

$$\mathbf{G}^{\rm A}_{\mathbb{LZ},\mathbb{LZ}} \;=\; \mathbf{1} \;-\; \left[\left\langle \mathbf{R}^\alpha_{\mathbb{LZ},\mathbb{LZ}}\right\rangle \;-\; \left\langle \mathbf{\Gamma}^\alpha_{\mathbb{LZ},\mathbb{LZ}}\right\rangle\right]\tau_{\rm A}\,. \tag{28}$$

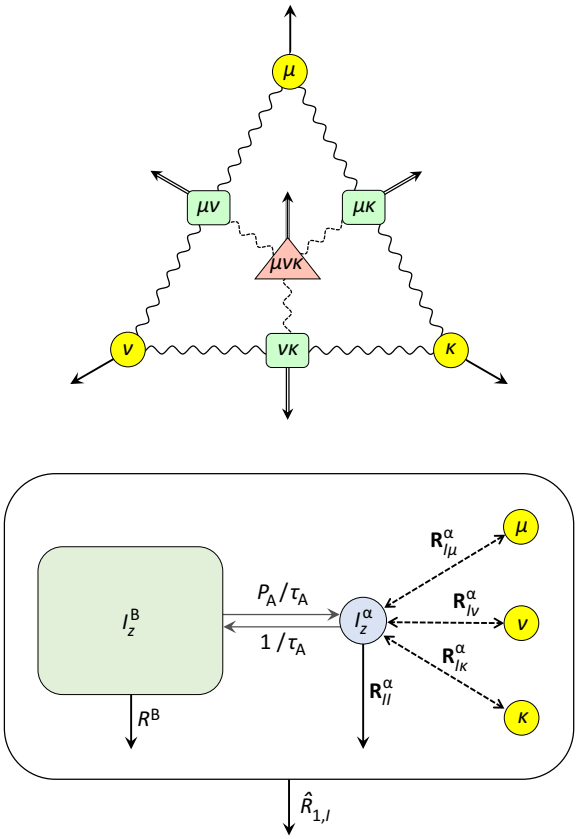

FIG. 1. Spin mode transfer pathways for the $IP_3 - I$ case, showing B $\leftrightarrow$ α exchange, auto-spin relaxation (solid arrows) and cross-spin relaxation (dashed arrows) in site α. In the upper part of the figure, wavy lines indicate coherent transfer of among the single-spin modes of the three nonlabile spins in site α via two-spin modes (solid) or via the three-spin mode (dashed), as well as auto-relaxation (arrows) of all these modes.

Using symmetry rules I and V, we obtain for the cross-relaxation supermatrix,

$$\mathbf{\Gamma}^\alpha_{\mathbb{LZ},\mathbb{LZ}} \;=\; \mathbf{R}^\alpha_{\mathbb{LZ},\mathbb{N}_1}\left(\mathbf{R}^\alpha_{\mathbb{N}_1\mathbb{N}_1} + \mathbf{X}^\alpha_{\mathbb{N}_1\mathbb{N}_1} - \mathbf{Y}^\alpha_{\mathbb{N}_1\mathbb{N}_1} + i\,\mathbf{L}_{\mathrm{Z},\,\mathbb{N}_1\mathbb{N}_1}\right)^{-1}\mathbf{R}^\alpha_{\mathbb{N}_1,\mathbb{LZ}}\,. \tag{29}$$

The supermatrices $\mathbf{X}^\alpha_{\mathbb{N}_1\mathbb{N}_1}$ and $\mathbf{Y}^\alpha_{\mathbb{N}_1\mathbb{N}_1}$ describe coherent transfer among single-spin modes associated with different nonlabile spins. This transfer proceeds via two-spin modes (described by $\mathbf{X}^\alpha_{\mathbb{N}_1\mathbb{N}_1}$) and also three-spin and higher (up to m-spin) modes (described by $\mathbf{Y}^\alpha_{\mathbb{N}_1\mathbb{N}_1}$), which simultaneously undergo relaxation induced by the fluctuating dipole couplings between the associated nonlabile spins and the labile spin(s).

The physical significance of the different parts of Eq. (29) may be appreciated with reference to Fig. 1, showing the pathways of dissipative (relaxation) and coherent (evolution under the static dipolar Hamiltonian) spin

mode transfers for the IP_3–I case. The 1×9 supermatrix $\mathbf{R}^{\alpha}_{\mathbb{LZ},\mathbb{N}_1}$ describes cross-spin relaxation between the labile spin I and the three nonlabile spins μ, ν and κ in site α, including cross-mode relaxation between longitudinal I_z magnetization and transverse nonlabile-spin magnetizations. These pathways are indicated by dashed arrows in the lower part of Fig. 1. The 9×9 supermatrix $\mathbf{R}^{\alpha}_{\mathbb{N}_1\mathbb{N}_1}$, which is block-diagonal in spin (with three 3×3 blocks along the diagonal), describes auto-spin relaxation of the single-nonlabile-spin modes (longitudinal and transverse magnetizations), as indicated by the three solid arrows pointing out from the corners of the triangle in the upper part of Fig. 1. The 9×9 supermatrix $\mathbf{X}^{\alpha}_{\mathbb{N}_1\mathbb{N}_1}$ describes the coherent interconversion of single-nonlabile-spin modes via two-spin modes, corresponding to two consecutive solid wavy lines in Fig. 1. Finally, the 9×9 supermatrix $\mathbf{Y}^{\alpha}_{\mathbb{N}_1\mathbb{N}_1}$ describes the coherent interconversion of single-nonlabile-spin modes via two-spin and three-spin modes, for example, $\mu\rightarrow\mu\kappa\rightarrow\mu\nu\kappa\rightarrow\nu\kappa\rightarrow\nu$, involving two solid and two dashed wavy lines in Fig. 1. Simultaneously, the two-spin and three-spin modes undergo relaxation, as indicated by the thicker arrows in Fig. 1.

Expressions for the $3m\times3m$ supermatrices $\mathbf{X}^{\alpha}_{\mathbb{N}_1\mathbb{N}_1}$ and $\mathbf{Y}^{\alpha}_{\mathbb{N}_1\mathbb{N}_1}$ in terms of the relevant blocks of the relaxation and coherent mode transfer supermatrices $\mathbf{R}^{\alpha}$ and $\mathbf{\Delta}^{\alpha}$ can be obtained by using the symmetry rules of Sec. III.B and expanding to second order in $\omega_{\mathrm{D}}\tau_{\mathrm{A}}$ (consistent with the RMN approximation). For $\mathbf{X}^{\alpha}_{\mathbb{N}_1\mathbb{N}_1}$, we thus obtain

$$\mathbf{X}^{\alpha}_{\mathbb{N}_1\mathbb{N}_1} \;=\; \mathbf{\Delta}^{\alpha}_{\mathbb{N}_1\mathbb{N}_2}\left(\mathbf{R}^{\alpha}_{\mathbb{N}_2\mathbb{N}_2}+i\,\mathbf{L}_{\mathrm{Z},\,\mathbb{N}_2\mathbb{N}_2}\right)^{-1}\mathbf{\Delta}^{\alpha}_{\mathbb{N}_2\mathbb{N}_1}\,. \qquad (30)$$

The supermatrix $\mathbf{Y}^{\alpha}_{\mathbb{N}_1\mathbb{N}_1}$ involves coherent spin mode pathways of the general form

$$1\rightarrow2\rightarrow3\rightarrow\{\mathrm{mixing\,of\,3-spin\,modes}\}\rightarrow3\rightarrow2\rightarrow1. \qquad (31)$$

The mixing of the three-spin modes involves modes from two-spin up to m-spin. To obtain a computationally tractable theory, we neglect k-spin modes with $k\geq4$. With this three-spin mode (3SM) approximation, we obtain

$$\begin{aligned}\mathbf{Y}^{\alpha}_{\mathbb{N}_1\mathbb{N}_1} \;=\; & \mathbf{\Delta}^{\alpha}_{\mathbb{N}_1\mathbb{N}_2}\left(\mathbf{R}^{\alpha}_{\mathbb{N}_2\mathbb{N}_2}+i\,\mathbf{L}_{\mathrm{Z},\,\mathbb{N}_2\mathbb{N}_2}\right)^{-1}\mathbf{\Delta}^{\alpha}_{\mathbb{N}_2\mathbb{N}_3}\times\\ & \left[\mathbf{R}^{\alpha}_{\mathbb{N}_3\mathbb{N}_3}+i\mathbf{L}_{\mathrm{Z},\mathbb{N}_3\mathbb{N}_3}+\mathbf{\Delta}^{\alpha}_{\mathbb{N}_3\mathbb{N}_2}\left(\mathbf{R}^{\alpha}_{\mathbb{N}_2\mathbb{N}_2}+i\mathbf{L}_{\mathrm{Z},\mathbb{N}_2\mathbb{N}_2}\right)^{-1}\mathbf{\Delta}^{\alpha}_{\mathbb{N}_2\mathbb{N}_3}\right]^{-1}\\ & \times\mathbf{\Delta}^{\alpha}_{\mathbb{N}_3\mathbb{N}_2}\left(\mathbf{R}^{\alpha}_{\mathbb{N}_2\mathbb{N}_2}+i\,\mathbf{L}_{\mathrm{Z},\,\mathbb{N}_2\mathbb{N}_2}\right)^{-1}\mathbf{\Delta}^{\alpha}_{\mathbb{N}_2\mathbb{N}_1}\,.\end{aligned} \qquad (32)$$

Expressions suitable for machine computation of the relaxation rates $R_{1,I}$ and $R_{1,IS}$ are presented in Appendix G.[24] These expressions are based on Eqs. (11), (12), (28) – (30) and (32), but also make use of special properties, such as block-diagonality and Hermiticity, of the relaxation and mode transfer supermatrices. As required, these expressions reduce to the results presented in Paper III for three-spin systems.

Explicit expressions for all relaxation supermatrices and coherent mode transfer supermatrices appearing in Eqs. (28) – (30) and (32) are given in Appendix H.[24] Whereas the single-spin mode relaxation supermatrices $\mathbf{R}^{\alpha}_{\mathbb{LZ},\mathbb{LZ}}$, $\mathbf{R}^{\alpha}_{\mathbb{LZ},\mathbb{N}_1}$ and $\mathbf{R}^{\alpha}_{\mathbb{N}_1\mathbb{N}_1}$ only involve self-correlations, that is, correlations of the dipole coupling between the same two spins at two different time points, the two-spin and three-spin mode relaxation supermatrices $\mathbf{R}^{\alpha}_{\mathbb{N}_2\mathbb{N}_2}$ and $\mathbf{R}^{\alpha}_{\mathbb{N}_3\mathbb{N}_3}$, appearing in Eqs. (30) and (32), also involve distinct correlations. Distinct correlations can be of two kinds: three-spin correlations, where one spin is shared between the two dipole couplings, and four-spin correlations, where four distinct spins are involved in the correlation. For the multi-spin EMOR cases considered here, a four-spin correlation must involve dipole couplings $X=I\mu$ and $Y=S\nu$. However, it follows from Eq. (18) that such correlations do not contribute. The multi-spin SRE theory thus only involves two-spin and three-spin correlations.

The theory simplifies considerably if all static dipole couplings between nonlabile spins are neglected. Then the coherent mode transfer supermatrices $\mathbf{\Delta}^{\alpha}_{\mathbb{N}_1\mathbb{N}_2}$ and $\mathbf{\Delta}^{\alpha}_{\mathbb{N}_2\mathbb{N}_3}$ vanish, so $\mathbf{X}^{\alpha}_{\mathbb{N}_1\mathbb{N}_1}=\mathbf{Y}^{\alpha}_{\mathbb{N}_1\mathbb{N}_1}=\mathbf{0}$. Computation of the cross-relaxation supermatrix $\mathbf{\Gamma}^{\alpha}_{\mathbb{LZ},\mathbb{LZ}}$ in Eq. (29) then only requires taking the inverse of the 3×3 blocks of the block-diagonal single-spin relaxation supermatrix $\mathbf{R}^{\alpha}_{\mathbb{N}_1\mathbb{N}_1}$.

IV. MULTI-SPIN ESE THEORY

A simpler and less rigorous theoretical approach to the multi-spin EMOR problem for the IP_m–I and ISP_m–IS cases has been described.[4] The starting point for that analysis was the multi-spin extended Solomon equations (ESE), describing the auto-spin and cross-spin relaxation of the longitudinal magnetizations of the labile and nonlabile spins and the exchange of the former between the anisotropic α sites and the isotropic B state. Being restricted to longitudinal magnetizations, the ESE theory cannot describe cross-mode relaxation and the inverted relaxation dispersion associated with it.[6,7] Moreover, because the orientation-dependent relaxation rates in the anisotropic α sites are replaced at the outset by isotropically averaged rates, the ESE theory disregards the dependence of the relaxation rate on the relative orientation of the dipole vectors, a dependence which, at least for small spin systems, is significant.[6,7] Finally, by neglecting static dipole couplings between nonlabile spins, the ESE theory omits all effects of coherent mode transfer.

On the other hand, the ESE theory is more general than the SRE theory because it does not assume fast exchange (that is, $\omega_{\mathrm{D}}\,\tau_{\mathrm{A}}$ need not be small), although it describes relaxation in the α sites with the aid of BWR theory (which presupposes that $\omega_{\mathrm{D}}\,\tau_{\mathrm{A}}\ll1$). The ESE theory is thus a hybrid approach, lacking internal consistency. Nevertheless, because the ESE theory is computationally expedient and at least approximately valid for arbitrarily slow exchange, it is of interest to compare it to the more rigorous, albeit more computationally de-

manding, theories developed here. Before doing so, we shall use the SRE framework established in Sec. III to re-derive the ESE theory. Apart from correcting a minor error in the original formulation,[4] this exercise allows us to precisely identify the approximations implicit in the ESE theory. The full derivation is relegated to Appendix I;[24] here we merely quote the final result.

According to the multi-spin ESE theory, the relaxation rate can be expressed on the familiar[34] dilute-regime form

$$R_1 \;=\; \frac{P_{\rm A}\,\tilde{r}}{1+\tilde{r}\,\tau_{\rm A}}\,, \qquad (33)$$

with the effective local longitudinal relaxation rate given by[4]

$$\tilde{r} \;=\; \frac{2}{15}\,\Omega_{\rm D}^2\big[J(\omega_0)+4\,J(2\,\omega_0)\big]\,, \qquad (34)$$

with the SDF as in Eq. (15). Equations (33) and (34) are valid for both exchange cases, but with different meanings for the effective, frequency-dependent, dipole coupling $\Omega_{\rm D}$. For the $IP_m{-}I$ case,

$$\Omega_{\rm D}^2 \;=\; \omega_{{\rm D},I}^2\left[\frac{2\,J(0)+3\,J(\omega_0)}{J(0)+3\,J(\omega_0)+6\,J(2\,\omega_0)}\right]\,, \qquad (35)$$

with the cumulative dipole coupling $\omega_{{\rm D},I}$ defined through

$$\omega_{{\rm D},I}^2 \;\equiv\; \sum_{\mu=1}^{m}\omega_{{\rm D},I\mu}^2\,. \qquad (36)$$

For the $ISP_m{-}IS$ case, $\Omega_{\rm D}$ has a more complicated form (Appendix I).

V. FOUR-SPIN SLE THEORY

The general theoretical framework for the exact multi-spin SLE theory, which is valid also outside the RMN regime, was established in Paper II. Unfortunately, implementation of the SLE theory is not practically feasible for large spin systems, because of the huge number of matrix elements that must be evaluated (by symbolic computer algebra) and because the required numerical computations (inversion of very large matrices at each of many Euler angle sets for each frequency point in the dispersion profile) become too time-consuming.

In Paper III, we implemented the SLE theory for the three-spin cases $IP_2{-}I$ and $ISP{-}IS$. Here, we describe the implementation of the SLE theory for the four-spin cases IP_3–I and ISP_2–IS. The motivation for this significant undertaking is to establish a benchmark and guide for the development of the more computationally efficient and physically transparent generalized multi-spin SRE theory described in Sec. VI. The three-spin cases are less suitable for this purpose, since they involve at most a single static dipole coupling. In contrast, the $IP_3{-}I$ case involves three static dipole couplings and it

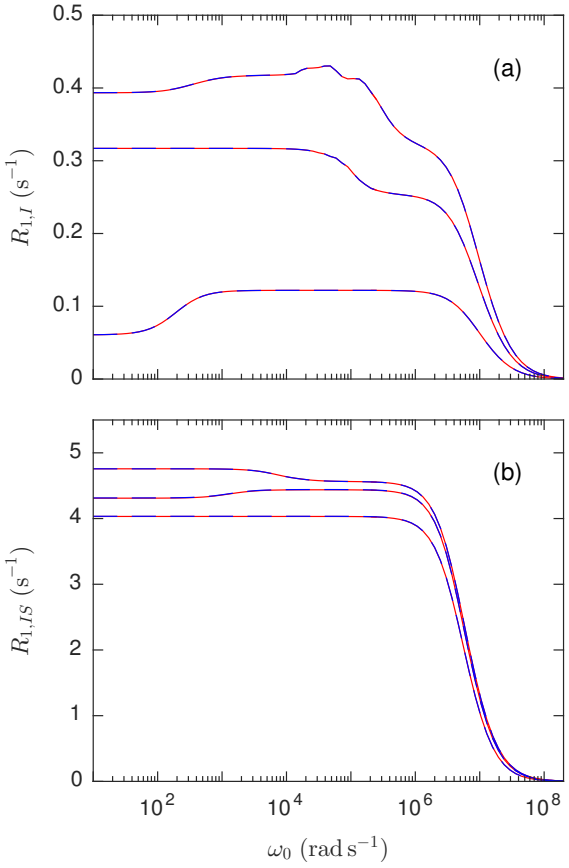

FIG. 2. (a) $R_{1,I}(\omega_0)$ dispersion profiles for the labile hydroxyl proton in Thr-22 (ubiquitin) coupled to $m = 1$, 2 or 3 nonlabile protons. (b) $R_{1,IS}(\omega_0)$ dispersion profiles for the protons of internal water W122 (BPTI), coupled to $m = 0$, 1 or 2 nonlabile protons. In both panels, m increases from the lower to the upper profile and the dispersion profiles were computed from SLE (red solid) and SRE (blue dash) theory with $\tau_{\rm A} = 10^{-7}$ s (in the RMN regime) and $N_\Omega = 750$.

can therefore be expected to capture the essential features of larger multi-spin systems. As an additional benefit, the four-spin SLE solution can be compared to the SRE solution in the RMN regime, where both theories are exact, thereby providing a valuable check on the considerable algebra and computer coding underlying these calculations.

The 256 ISTOs spanning the four-spin Liouville space were generated by symbolic computer algebra using three successive angular momentum couplings, as described in Appendix J.[24] A complete list of these basis operators can be found in Table S3.[24] The 65,025 elements of the supermatrix representation $\mathbf{L}_{\rm D}^{\alpha}$ in this basis of the dipolar Liouvillian corresponding to the dipolar Hamiltonian in Eq. (1) were generated as described in Appendix K,[24] again using symbolic computer algebra. The supermatrix representation $\mathbf{L}_{\rm Z}$ of the Zeeman Liouvillian corre-

sponding to the isochronous Zeeman Hamiltonian in Eq. (2) is diagonal in the ISTO basis, with elements $Q\,\omega_0$. The supermatrix $\mathbf{\Lambda}^{\alpha}$ is then computed from Eq. (6), numerically inverted and isotropically averaged to yield the supermatrix $\mathbf{G}^{\mathrm{A}}$ in Eq. (5). Finally, the relaxation rate is calculated from Eq. (11) or (12).

Several checks were performed on the four-spin SLE solution. First, we demonstrated that it agrees, to machine precision, with the previously presented two-spin[6] and three-spin[7] SLE solutions in the special cases where one or two nonlabile spins are located far away from the labile spin(s). Second, we demonstrated that the SLE and SRE theories agree, to machine precision, in the RMN regime, where both theories are exact. This agreement is shown in Fig. 2 for the $IP_m{-}I$ and $ISP_m{-}IS$ cases. Here, we also include the corresponding results for two-spin and three-spin systems to highlight the substantial qualitative differences in the shape of the dispersion profile as more nonlabile spins are incorporated in the spin system.

VI. MULTI-SPIN GSRE THEORY

In this section, we develop a generalized SRE (GSRE) theory that reduces to the SRE theory of Sec. III in the RMN regime, but also remains approximately valid outside the RMN regime, that is, for arbitrarily long τ_{A} values. We consider first the multi-spin case $IP_m{-}I$ for $m \geq 3$ and we then describe the few additional modifications needed for the $ISP_m{-}IS$ case.

The degree of success of the GSRE theory will be judged by comparison with results obtained from the exact SLE theory for the four-spin cases $IP_3 - I$ and $ISP_2 - IS$. These test calculations were performed on 25 four-proton fragments (20 side-chain hydroxyl or carboxyl protons and five internal water molecules) extracted from crystal structures of the globular proteins ubiquitin and BPTI, which have been studied extensively by water ^{1}H, ^{2}H and ^{17}O MRD.[3,35–38] The six dipole coupling constants $\omega_{\mathrm{D},X}$ for each of the 25 fragments are listed in Tables S4 and S5 of Appendix L.[24] The nuclear coordinates from these structures were also used to compute the Euler angles β_X and γ_X (Appendix C[24]). In Sec. VI.C, we use the GSRE theory to examine the scaling and convergence of the dispersion profile with increasing number m of nonlabile spins. For these calculations, we used protein fragments with up to $m = 15$ nonlabile protons, selected in order of increasing distance from the labile spin(s). All calculations reported in this paper use the experimentally relevant value $P_{\mathrm{A}} = 1 \times 10^{-3}$.[3,12] However, as seen from Eqs. (11) and (12), $R_1(\omega_0)$ is strictly proportional to P_{A}, so the value chosen is unimportant.

A. Exchange case $IP_m{-}I$

For the two-spin cases $IP{-}I$ and $IS{-}IS$,[5,6] the exact SLE theory leads to simple analytical results for the the zero-field (ZF) relaxation rate $R_{1,I}(0)$. For the $IS{-}IS$ case, this result suggests that the validity of the SRE theory can be extended beyond the MN regime simply by replacing the SDF with a generalized SDF (GSDF),

$$\widehat{J}(n\,\omega_0) \;=\; \frac{\tau_{\mathrm{A}}}{1 + (\omega_{\mathrm{D}}\,\tau_{\mathrm{A}})^2 + (n\,\omega_0\,\tau_{\mathrm{A}})^2}\,, \qquad (37)$$

where the caret distinguishes the GSDF from the regular SDF in Eq. (15). For the $IS - IS$ case, the resulting GSRE theory accurately reproduces the exact (SLE) dispersion profile $R_{1,I}(\omega_0)$ over the full τ_{A} range and it is exact in the MN and ZF regimes.[5] A similar GSDF accurately describe the exact $R_{1,I}(\omega_0)$ profile for the quadrupolar spin-1 EMOR case.[2] For the $IP{-}I$ case, the exact ZF rate $R_{1,I}(0)$ is reproduced with a GSDF of the same form, but with a factor 1/5 multiplying the $(\omega_{\mathrm{D}}\,\tau_{\mathrm{A}})^2$ term.[6] No attempt was made to reproduce the full dispersion profile with a GSRE theory for the $IP{-}I$ case, or for the three-spin cases treated in Paper III.

Although exact ZF results are not available for $IP_m{-}I$ cases with $m > 1$, physical considerations suggest a GSDF similar to that in Eq. (37), but with a different numerical coefficient in front of the $(\omega_{\mathrm{D}}\,\tau_{\mathrm{A}})^2$ term. Accordingly, we base the multi-spin GSRE theory on the GSDF

$$\widehat{J}(n\,\omega_0) \;\equiv\; \frac{\tau_{\mathrm{A}}}{1 \;+\; \zeta_I\,(\omega_{\mathrm{D},I}\,\tau_{\mathrm{A}})^2 \;+\; (n\,\omega_0\,\tau_{\mathrm{A}})^2}\,. \qquad (38)$$

To assess the accuracy of this ansatz, we first consider $R_{1,I}(0)$ for the $IP_m - I$ case without static dipole couplings (SDCs), which will be dealt with subsequently, whereby Eqs. (G.1) – (G.5) and (38) yield

$$R_{1,I}(0) \;=\; \frac{2}{15}\,\frac{P_{\mathrm{A}}}{\tau_{\mathrm{A}}}\,\frac{(\omega_{\mathrm{D},I}\,\tau_{\mathrm{A}})^2}{1 \;+\; \zeta_I\,(\omega_{\mathrm{D},I}\,\tau_{\mathrm{A}})^2}\,. \qquad (39)$$

Trial calculations of $R_{1,I}(0)$ for the IP_3–I case without SDCs show that the exact SLE result is reproduced to within a few percent over the full τ_{A} range (Fig. 3, and Figs. S2 and S3 of Appendix M[24]), provided that the coefficient ζ_I is allowed to vary from 1/3 near the MN regime to 2/15 in the ultraslow-motion (USM) regime, where $(\omega_{\mathrm{D},I}\,\tau_{\mathrm{A}})^2 \gg 1$, according to

$$\zeta_I \;\equiv\; \left[\frac{10 + \omega_{\mathrm{D},I}\,\tau_{\mathrm{A}}}{4 + \omega_{\mathrm{D},I}\,\tau_{\mathrm{A}}}\right]\frac{2}{15}\,. \qquad (40)$$

The ZF rate predicted by Eqs. (39) and (40) coincides with the exact SLE result, not only in the MN limit, but also in the USM limit, where

$$R_{1,I}(0) \;=\; \frac{P_{\mathrm{A}}}{\tau_{\mathrm{A}}}\,. \qquad (41)$$

This is a particularly simple instance of the exact result, $R_{1,I}(0) = C\,P_{\mathrm{A}}/\tau_{\mathrm{A}}$ with a numerical constant C of order

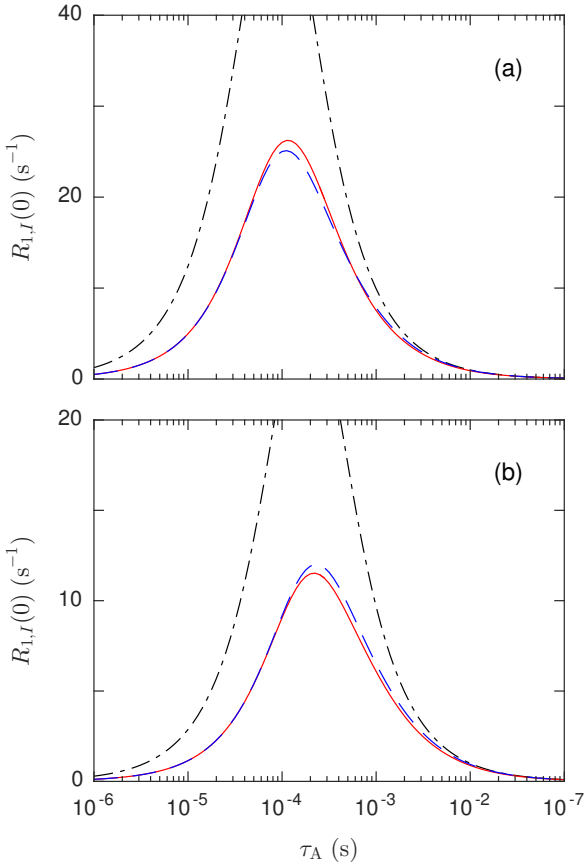

FIG. 3. $R_{1,I}(0)$ versus τ_A for the labile protons in Thr-7 (a) and Asp-39 (b) side-chains of ubiquitin coupled to three nonlabile protons without SDCs, computed from the SLE (red solid), GSRE (blue dash) and ESE (black dash-dot) theories.

unity, which holds generally for the dilute EMOR model in the USM limit. Importantly, this result is valid for the dipolar[5–7] EMOR model for any m and with or without SDCs, as well as for the quadrupolar[1,2] EMOR model. For the two-spin dipolar EMOR model (the $IP-I$ and $IS-IS$ cases) and for the isomorphic axially symmetric quadrupolar $I = 1$ case (or any integral I),[1,2] $C = 2/3$. In both of these cases, there are three ZF energy levels, two of which are degenerate. For the three-spin dipolar EMOR model (the IP_2–I and ISP–IS cases), C depends on the relative lengths and orientations of the dipole vectors. For the axially symmetric quadrupolar case with half-integral I, with $(2I-1)$ pairs of doubly degenerate energy levels, $C = 2/3-(2I+1)/[4I(I+1)]$, varying from $C = 2/5$ for $I = 3/2$ to $C = 2/3$ for $I \to \infty$.[1] For the four-spin dipolar EMOR model (the IP_3–I and ISP_2–IS cases), Eq. (41) is valid (that is, $C = 1$) regardless of the strengths and geometry of the dipole couplings. By adopting the GSDF defined by Eqs. (38) and (40), we ensure that the multi-spin GSRE theory reproduces the simple USM result in Eq. (41) for any m.

An intuitive understanding of Eq. (41) can be obtained from the classical vector picture. The labile spin (or an ensemble of such spins) precesses (uninterrupted for many periods in the USM regime) with frequency $\omega_{D,I}$ in the local magnetic field $\omega_{D,I}/\gamma_I$ produced by the m nonlabile spins in a particular site α, independent of the SDCs. A spin undergoing such local precession contributes a certain amount to the macroscopic longitudinal magnetization along any lab-fixed axis. After the spin leaves site α, it looses all correlation with the site orientation so that the next visited site can have any orientation drawn from an isotropic distribution. Consequently, the magnetization is randomized on the time scale τ_A and we can regard $1/\tau_A$ as the local relaxation rate in the ZF USM limit. Note that the SDCs play no role here, consistent with our SLE results. This local relaxation rate is closely related to the so-called dipolar relaxation rate, for which a semi-phenomenological "strong-collision" theory (invoking the spin temperature concept) yields $R_{1,D} = C_D/\tau_c$, where τ_c is the correlation time for some local rotational motion and the numerical coefficient C_D depends on what fraction of the dipolar energy is modulated by this motion.[39,40]

The USM result in Eq. (41) can also be obtained from the ESE theory by taking the slow-exchange limit of Eq. (33), since $\tilde{r}\,\tau_A \gg 1$ in the USM limit. This is true also if the local relaxation is induced by a different motion than exchange (as in the EMOR model). Making use of the detailed balance condition, Eq. (41) can also be expressed as $R_{1,I}(0) = 1/\tau_B$, implying that spin I is relaxed as soon as it reaches any A site. However, in contrast to the GSRE theory, the ESE theory grossly overestimates $R_{1,I}(0)$ at intermediate τ_A values, and it is not even correct in the MN limit (Figs. 3, S2 and S3).

We now consider the full dispersion profile $R_{1,I}(\omega_0)$, but still without SDCs. The GSRE theory is based on Eqs. (G.1) – (G.5) – but without the last two terms in Eq. (G.5), which vanish in the absence of SDCs – and the GSDF in Eq. (38) is used to calculate all relaxation supermatrix elements. This GSDF not only predicts $R_{1,I}(0)$ accurately; it also describes how the frequency of the primary dispersion varies from $\omega_0 \approx 1/\tau_A$ in the MN regime to $\omega_0 \approx \zeta_I^{1/2}\omega_{D,I}$ in the USM regime.

However, for $\omega_{D,I}\,\tau_A \gtrsim 1$, the GSRE profile also exhibits an inverted secondary dispersion step at $\omega_0 \approx 1/\tau_A$ that is not present in the exact SLE profile (see Figs. S4 – S7 of Appendix M[24]). The origin of this spurious GSRE dispersion is most readily appreciated in the USM regime. Well below the primary dispersion step, that is, for $\omega_0 \ll \omega_{D,I}$, the GSDF reduces to $\widehat{J}(n\,\omega_0) = \widehat{J}(0) = 15/(2\,\omega_{D,I}^2\,\tau_A)$ so the elements of the auto-spin relaxation matrix $\mathbf{R}^{\alpha}_{\mathbb{N}_1(\mu)\mathbb{N}_1(\mu)}$ in Eq. (G.5) are of order $1/\tau_A$. When $\omega_0 \gtrsim 1/\tau_A$ the term $i\,\omega_0\,\mathbf{Q}_1$ in Eq. (G.5) then cancels the off-diagonal cross-mode elements of $\mathbf{R}^{\alpha}_{\mathbb{N}_1(\mu)\mathbb{N}_1(\mu)}$, thus giving rise to the secondary dispersion step. To eliminate this spurious feature, we replace the Larmor frequency in the $i\,\omega_0\,\mathbf{Q}_1$ term of Eq. (G.5),

but not in the GSDF, by the renormalized frequency

$$\widehat{\omega}_0 \equiv \frac{\omega_0}{(1+2\,\omega_{\mathrm{D},I}\,\tau_\mathrm{A})}\,. \tag{42}$$

We refer to this modification of the SRE theory as suppression of nonsecular decoupling (SND).

As seen from Figs. S4 – S7, a GSRE theory that features the GSDF in Eq. (38) as well as the SND modification in Eq. (42) reproduces the exact SLE profile quite well also outside the MN regime. The numerical factor of 2 in Eq. (42) was not rigorously optimized, but without it the GSRE profiles for $\tau_\mathrm{A} = 10^{-4}$ s exhibit a small residual ND hump (more prominent for $m > 3$). In the USM limit ($\tau_\mathrm{A} = 10^{-2}$ s), the ZF regime extends all the way up to the primary dispersion in the GSRE profile, whereas the SLE profile exhibits some fine structure in the low-frequency (LF) regime ($1/\tau_\mathrm{A} \lesssim \omega_0 \lesssim \omega_{\mathrm{D},I}$). However, the difference between the two profiles is rather small (Figs. S6 and S7).

So far in this section, we have ignored the SDCs. What is their effect on the $R_{1,I}(\omega_0)$ profile? Judging from exact SLE calculations for the $IP_3{-}I$ case (Fig. S8), the SDCs greatly increase the ZF rate $R_{1,I}(0)$ in the RMN regime, but as τ_A becomes longer their effect is diminished and, as we have seen, in the USM limit they have no effect at all on $R_{1,I}(0)$. Moreover, the frequency of the primary dispersion is hardly affected by SDCs at any τ_A value (Fig. S8).

In contrast, the GSRE theory, as developed up to this point, predicts that the SDCs greatly increase $R_{1,I}(\omega_0)$ for all τ_A values, also in the USM regime (Fig. 4). The origin of this spurious effect is the assumption in the derivation of the SRE theory that, not only the fluctuating dipole couplings, but also the SDCs are "motionally narrowed" in the sense that $\omega_{\mathrm{D},\mu\nu}\,\tau_\mathrm{A} \ll 1$. Formally, the spurious $R_{1,I}(0)$ increase can be understood in terms of Eqs. (G.1) – (G.5). The ZF rate $R_{1,I}(0)$ can be increased by decreasing the cross-relaxation rate $\langle\Gamma^{II}_{zz}(0)\rangle$ in either of two ways: by increasing the nonlabile auto-spin relaxation rates or by increasing the rate of coherent mode transfer among the nonlabile spins, described by $\mathbf{R}^\alpha_{\mathbb{N}_1(\mu)\mathbb{N}_1(\mu)}$ and $[\mathbf{X}^\alpha_{\mathbb{N}_1(\mu)\mathbb{N}_1(\nu)} - \mathbf{Y}^\alpha_{\mathbb{N}_1(\mu)\mathbb{N}_1(\nu)}]$, respectively, in Eq. (G.5). These two phenomena are akin to incoherent and coherent spin decoupling, respectively. However, like the SRE theory itself, this picture is not valid outside the RMN regime. Indeed, according to the exact SLE theory, if the SDCs are artificially increased so that $\omega_{\mathrm{D},\mu\nu}\,\tau_\mathrm{A} \gg 1$, while keeping $\omega_{\mathrm{D},I}\,\tau_\mathrm{A} \ll 1$, then the SDCs actually decrease $R_{1,I}(\omega_0)$.

Outside the RMN regime, where $\omega_{\mathrm{D},\mu\nu}\,\tau_\mathrm{A} \gtrsim 1$, we must therefore introduce a SDC correction in the GSRE theory. The finding that the (true) SDC effect vanishes in the USM limit suggests a renormalization such that the individual SDCs vanish when $\omega_{\mathrm{D},\mu\nu}\,\tau_\mathrm{A} \gg 1$. Accordingly, we replace the SDCs appearing in the coherent mode transfer supermatrices $\mathbf{\Delta}^\alpha_{\mathbb{N}_1\mathbb{N}_2}$ and $\mathbf{\Delta}^\alpha_{\mathbb{N}_2\mathbb{N}_3}$ in Eqs. (30) and (32) of the GSRE theory by the renormalized SDCs,

$$\widehat{\omega}_{\mathrm{D},\mu\nu} \equiv \frac{\omega_{\mathrm{D},\mu\nu}}{(1+\frac{4}{3}\,\omega_{\mathrm{D},\mu\nu}\,\tau_\mathrm{A})^2}\,, \tag{43}$$

where the numerical coefficient was chosen to optimize the agreement with the exact SLE profiles for the $IP_3{-}I$ case. In addition, the SND correction in Eq. (42) is also applied to the $i\,\omega_0\,\mathbf{Q}_2$ and $i\,\mathbf{L}_{\mathrm{Z},\,\mathbb{N}_3\mathbb{N}_3}$ terms of Eqs. (G.6) – (G.9) to suppress nonsecular decoupling in the nonlabile two-spin mode and three-spin mode relaxation supermatrices. This additional SND correction has only a small effect for $m = 3$, but it is required for convergence of the dispersion profile with increasing m (Sec. VI.C).

As seen from Fig. 4 and Figs. S9 – S14 of Appendix M,[24] the GSRE theory, incorporating the renormalized quantities defined in Eqs. (38), (42) and (43), reproduces the exact $R_{1,I}(\omega_0)$ dispersion profile for the $IP_3{-}I$ case with good to excellent accuracy in the full parameter space of the EMOR model. In particular, the GSRE prediction of the $R_{1,I}(\omega_0)$ profile is virtually exact up to $\tau_\mathrm{A} \approx 10^{-6}$ s, $R_{1,I}(0)$ is exact in the USM limit, and the dispersion frequency is close to the exact one under all conditions.

B. Exchange case $ISP_m{-}IS$

The $ISP_m{-}IS$ case features three types of dipole coupling ($I{-}\mu$, $S{-}\mu$ and $I{-}S$) and two types of Euler angles ($\Omega_{I\mu}$ and $\Omega_{S\mu}$). It is therefore not possible to derive a simple result analogous to Eq. (39). Nevertheless, we postulate a GSDF analogous to that in Eq. (38), but accounting for the three different types of dipole coupling,

$$\widehat{J}(n\,\omega_0) = \frac{\tau_\mathrm{A}}{1+\zeta_{IS}(\omega_{\mathrm{D},IS}\tau_\mathrm{A})^2+\zeta_I(\omega_{\mathrm{D},I}\tau_\mathrm{A})^2+\zeta_S(\omega_{\mathrm{D},S}\tau_\mathrm{A})^2+(n\omega_0\tau_\mathrm{A})^2}\,. \tag{44}$$

The function ζ_I is given by Eq. (40) and ζ_S by the analogous expression with $\omega_{\mathrm{D},I}$ replaced by $\omega_{\mathrm{D},S}$. The function ζ_{IS} is taken to be of the same form, but with different numerical coefficients,

$$\zeta_{IS} = \left[\frac{10+\omega_{\mathrm{D},IS}\,\tau_\mathrm{A}}{5+\omega_{\mathrm{D},IS}\,\tau_\mathrm{A}}\right] 0.6425\,. \tag{45}$$

This choice of GSDF ensures that $R_{1,IS}(0) = P_\mathrm{A}/\tau_\mathrm{A}$ in the USM limit. In the (unrealistic) special case that $\omega_{\mathrm{D},IS} \gg (\omega_{\mathrm{D},I}, \omega_{\mathrm{D},S})$, the $ISP_2 - IS$ case reduces to the $IS{-}IS$ case, for which we have the exact ZF result $\zeta_{IS} = 1$, yielding the exact ZF USM result $R_{1,IS}(0) = (2/3)\,P_\mathrm{A}/\tau_\mathrm{A}$.[5] Even though the $I{-}S$ dipole coupling is dominant in the examined $ISP_2{-}IS$ cases (Table S4), the SLE theory yields $R_{1,IS}(0) = P_\mathrm{A}/\tau_\mathrm{A}$ exactly in the USM limit, just as for the $IP_3{-}I$ case. We assume that this result holds also for the $ISP_m{-}IS$ case with $m > 2$. To get the correct m-scaling in the GSRE theory, we

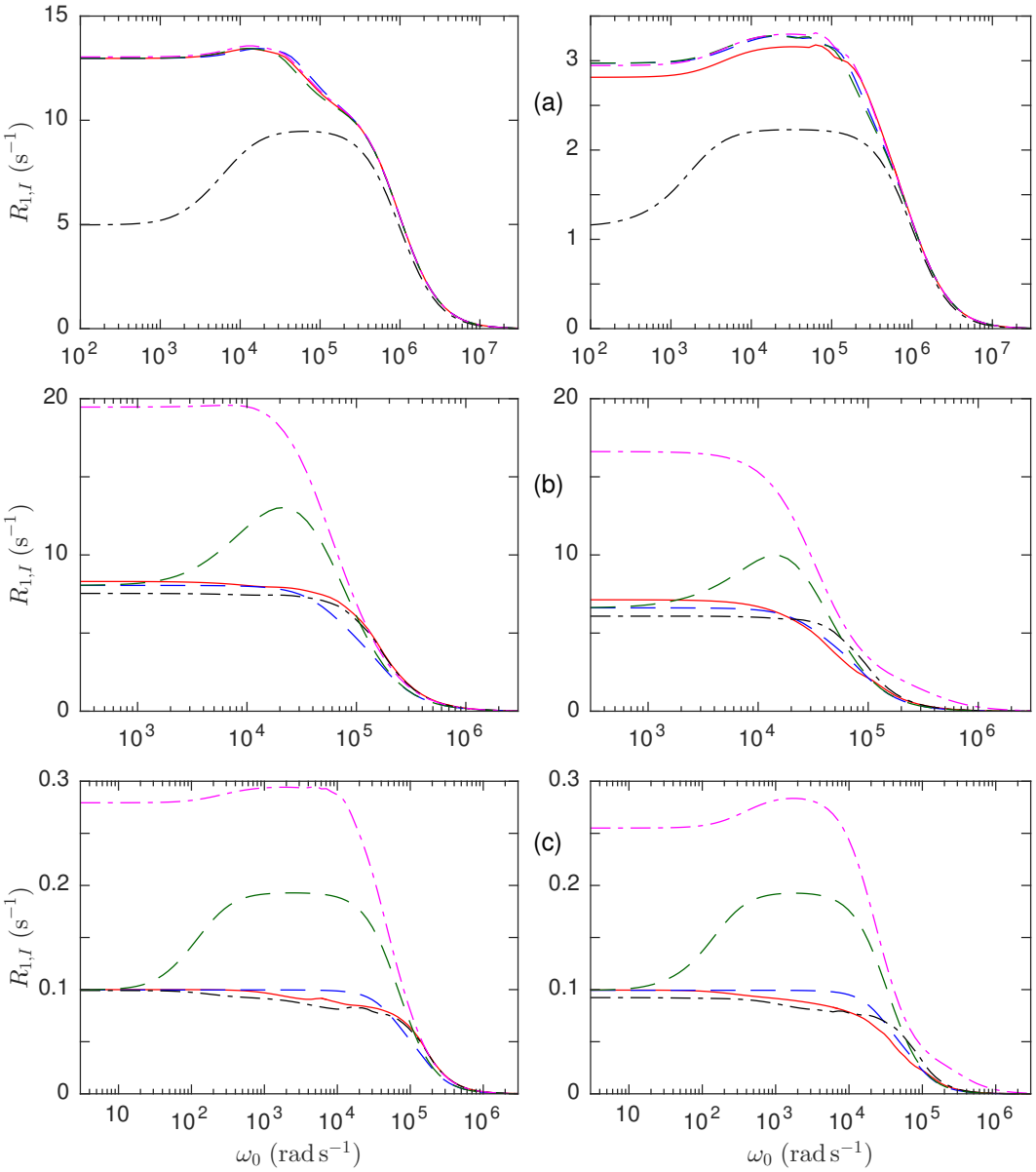

FIG. 4. $R_{1,I}(\omega_0)$ dispersion profiles with $\tau_A = 10^{-6}$ s (a), 10^{-4} s (b) and 10^{-2} s (c) for labile protons in Thr-7 (left column) and Asp-39 (right column) side-chains of ubiquitin coupled to three nonlabile protons, computed from the SLE theory with SDCs (red solid) and without SDCs (black dash-dot) and from the full GSRE theory (blue dash) and from GSRE theory without SND (green dash) or without SND and without SDC renormalization (magenta dash-dot).

must use a numerical coefficient in Eq. (45) that yields $R_{1,IS}(0) = P_A/\tau_A$. With the coefficient 0.6425 in Eq. (45), the GSRE theory for the $ISP_2{-}IS$ case reproduces this USM result to better than 0.5 % for all five internal water molecules.

As for the $IP_3 - I$ case, the GSRE theory for the $ISP_2 - IS$ case without SDC reproduces the exact SLE result for the ZF rate $R_{1,IS}(0)$ to within a few percent over the full τ_A range when Eqs. (44) and (45) are used for the GSDF (Fig. S15). In the MN regime, where the GSDF in Eq. (44) reduces to the regular SDF in Eq. (15), the (G)SRE profile agrees quantitatively with the SLE profile. This is true up to $\tau_A \approx 10^{-6}$ s (Fig. S16). The dispersion shape at $\tau_A = 10^{-6}$ s exhibits a small (because of the dominance of $\omega_{D,IS}$) inverted secondary dispersion at $\omega_0 \approx \omega_{D,I}^2\,\tau_A \approx \omega_{D,S}^2\,\tau_A$ (Fig. S16). The origin of this secondary dispersion step is nonsecular decoupling of longitudinal-transverse cross-mode relax-

ation in the nonlabile auto-spin relaxation supermatrix $\mathbf{R}^{\alpha}_{\mathbb{N}_1(\mu)\mathbb{N}_1(\mu)}(\omega_0)$, which does not involve $\omega_{\mathrm{D},IS}$, effected by the term $i\,\omega_0\,\mathbf{Q}_1$ in Eq. (G.5).

In the USM regime, the primary dispersion step in the SLE and GSRE profiles occurs at $\omega_0 \approx [0.6425\,\omega^2_{\mathrm{D},IS} + (2/15)(\omega^2_{\mathrm{D},I} + \omega^2_{\mathrm{D},S}]^{1/2}$, rather than at $\omega_0 \approx \omega_{\mathrm{D},I}$ (Fig. S17). However, the GSRE profile also exhibits a small inverted secondary dispersion step at $\omega_0 \approx 1/\tau_{\mathrm{A}}$ that is not present in the exact SLE profile (Fig. S17). To eliminate this spurious feature, we introduce a SND correction analogous to that in Eq. (42),

$$\widehat{\omega}_0 \;\equiv\; \frac{\omega_0}{[1 + 2\,(\omega^2_{\mathrm{D},IS} + \omega^2_{\mathrm{D},I} + \omega^2_{\mathrm{D},S})^{1/2}\,\tau_{\mathrm{A}}]}\,. \qquad (46)$$

As seen from Figs. S16 and S17, the GSRE profile based on the GSDF in Eq. (44) and the SND correction in Eq. (46) agrees rather well with the exact SLE profile without SDC, even though the fine structure in the USM regime is not captured by the GSRE theory.

For the five ISP_2-IS cases examined here, the single SDC is relatively weak (Table S4); it therefore has only a small effect on the dispersion profile, even in the RMN regime (Fig. S18). It may be noted that the fine structure seen in the USM regime (Fig. S18) is evidently not caused by the SDC. To approximately reproduce the SLE profiles in the presence of the SDC, we use Eq. (43) to renormalize the SDC. The ZF rate $R_{1,IS}(0)$ computed with the GSDF in Eq. (44) and renormalized SDC according to Eq. (43) agrees almost quantitatively with the exact (SLE) result (Fig. S19). Because of the dominant $\omega_{\mathrm{D},IS}$ coupling, the agreement is excellent also near the $R_{1,IS}(0)$ maximum. This is a welcome result since internal water molecules often have τ_{A} values in the range $10^{-6} - 10^{-5}$ s.[3,16,17] Similarly to the IP_3-I case, the GSRE theory is much more accurate than the ESE theory near the $R_{1,IS}(0)$ maximum.

Applying also the SND correction in Eq. (46) in all explicit Zeeman Liouvillians in Eqs. (G.5) – (G.9), as for the IP_3–I case, we find that the GSRE theory reproduces the exact $R_{1,IS}(\omega_0)$ dispersion profile for the ISP_2-IS case with excellent accuracy in the full parameter space of the EMOR model (Figs. S20 and S21).

C. Spin system scaling

Having calibrated the GSRE theory with the aid of exact SLE results for four-spin systems, we now examine the predictions of the GSRE theory for larger spin systems. We recall that the GSRE theory invokes the 3SM approximation for $m \geq 4$ (Sec. III.C). Specifically, we shall determine how, and at what rate, the dispersion profile converges as the number m of nonlabile spins increases. For the analysis of the IP_m-I case, we focus on the labile protons in the side-chains of Thr-7, Thr-22 and Asp-39 in ubiquitin (Table S5), successively adding nonlabile protons up to $m = 15$ in order of increasing

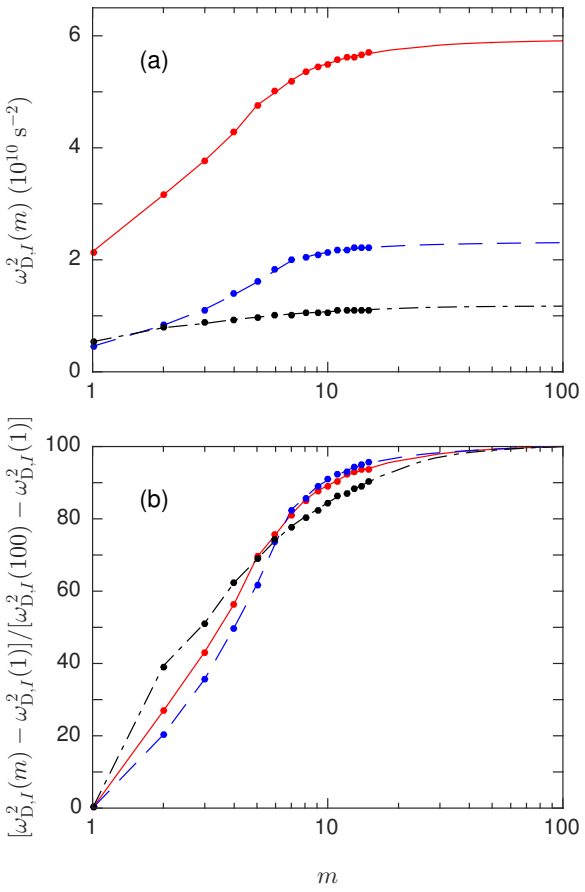

FIG. 5. (a) Cumulative labile-nonlabile dipole coupling squared, $\omega^2_{\mathrm{D},I}$, defined by Eq. (36), for the labile protons in Thr-7 (red, solid line), Thr-22 (blue, dash) and Asp-39 (black, dash-dot) of ubiquitin coupled to m nonlabile protons. (b) Fractional (in %) convergence to $m = 100$ of the normalized $\omega^2_{\mathrm{D},I}$.

distance from the labile proton. Figure 5 shows how the the cumulative dipole coupling squared, $\omega^2_{\mathrm{D},I}$, increases with m for these labile protons.

We first consider the ZF rate $R_{1,I}(0)$ (Fig. 6). At $\tau_{\mathrm{A}} = 10^{-6}$ s, we are near the RMN regime, where, in the absence of SDCs, Eq. (39) predicts that $R_{1,I}(0)$ scales with m as $\omega^2_{\mathrm{D},I}$, so, at $m = 15$, $R_{1,I}(0)$ has attained ~ 95 % of its converged value at $m = 100$ (as inferred from Fig. 5). In the presence of SDCs, $R_{1,I}(0)$ converges even faster, albeit less smoothly, coming within 5 % of convergence already at $m \approx 7$. At $\tau_{\mathrm{A}} = 10^{-4}$ s, we are approaching the USM limit, where $R_{1,I}(0) = P_{\mathrm{A}}/\tau_{\mathrm{A}} = 10\ \mathrm{s}^{-1}$. Among the three examined labile protons, Thr-7 has the largest cumulative dipole coupling (Fig. 5) and is therefore closest to the USM limit. In the absence of SDCs, $R_{1,I}(0)$ converges rapidly (~ 95 % convergence at $m = 6$) to a value ~ 20 % below the strict USM limit. In the presence of SDCs, $R_{1,I}(0)$ converges more slowly to

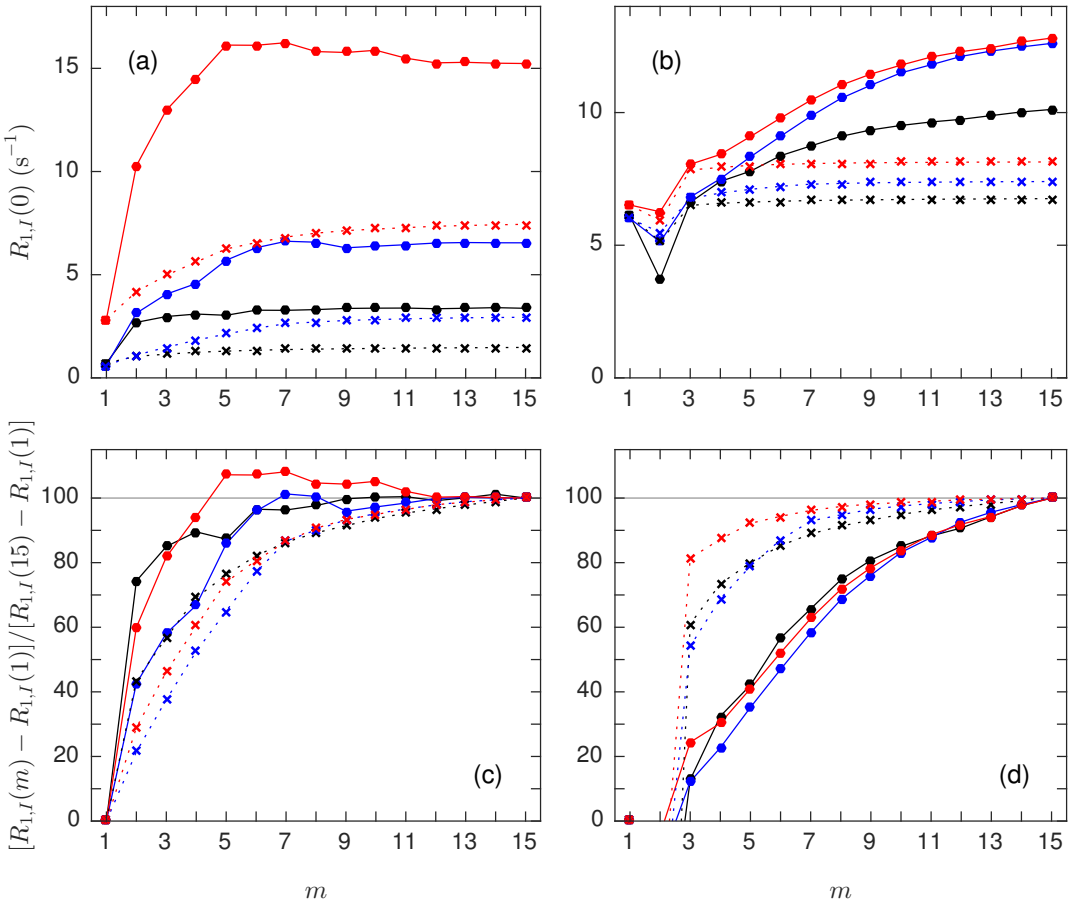

FIG. 6. Variation with m of the ZF rate $R_{1,I}(0)$ at $\tau_A = 10^{-6}$ s (a,c) and 10^{-4} s (b,d) for the labile protons in Thr-7 (red), Thr-22 (blue) and Asp-39 (black) of ubiquitin coupled to m nonlabile protons with (filled circles) or without (crosses) SDCs, computed from SLE theory for $m \leq 2$ and from GSRE theory for $m \geq 3$. (c,d) Fractional (in %) convergence to $m = 15$ of the normalized ZF rate.

a value ~ 30 % above the true USM limit. At $\tau_A = 10^{-4}$ s, the SDC effect is modest for $m = 3$ (Fig. 4), but, for larger m, the SDCs increase $R_{1,I}(0)$ substantially (Fig. 6).

We now consider the convergence with increasing m of the entire $R_{1,I}(\omega_0)$ dispersion profile (Fig. 7), focusing on the labile proton in Thr-22 (Figs. S22 – S27 of Appendix N[24] show similar results for Thr-7 and Asp-39). At $\tau_A = 10^{-6}$ s, two secondary dispersion steps are evident below the primary dispersion for all $m \geq 3$ and, in this frequency range, the profile becomes more smooth with increasing m (Fig. 7). Above the ZF regime, the profile scales approximately as $\omega_{D,I}^2$, as seen by normalizing $R_{1,I}(\omega_0)$ by $R_{1,I}^0(0) \equiv \frac{2}{15} P_A \omega_{D,I}^2 \tau_A$, which is the ZF rate in the MN regime in the absence of SDCs, as seen from Eq. (39). Whereas $R_{1,I}(0)$ converges at $m \approx 7$ (Fig. 6), the normalized rate $R_{1,I}(\omega_0)/R_{1,I}^0(0)$ above the ZF regime converges already at $m \approx 5$ (Fig. 7). At $\tau_A = 10^{-4}$ s, the profiles for $m \geq 3$ only exhibit the primary dispersion and, although the ZF rate $R_{1,I}(0)$ converges rather slowly (Fig. 6), the shape of the dispersion profile changes very little for $m \geq 4$ (Fig. 7). In fact, when normalized by the ZF rate, the profiles are virtually superimposed for $m \geq 4$ (Fig. 7). At $\tau_A = 10^{-2}$ s, in the USM regime, the ZF rate is independent of m, consistent with Eq. (41), and the primary dispersion frequency is essentially proportional to $\omega_{D,I}$ (Figs. S26 and S27), and therefore converges at modest m values (as can be inferred from Fig. 5).

As expected on account of the dominant intramolecular $I-S$ coupling (Appendix L), both the ZF rate $R_{1,IS}(0)$ and the shape of the $R_{1,IS}(\omega_0)$ dispersion profile converge faster with m for the ISP_m–IS case than for the IP_m–I case (Figs. S28 and S29).

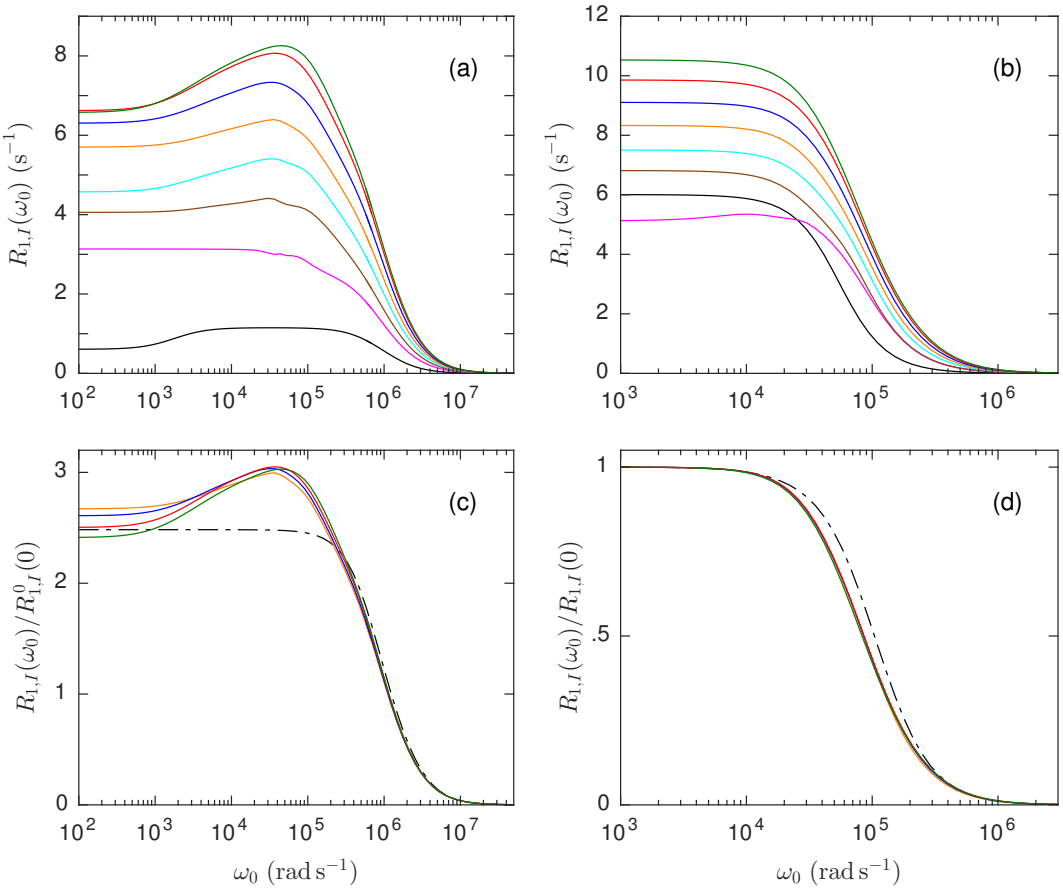

FIG. 7. (a,b) $R_{1,I}(\omega_0)$ dispersion profiles at $\tau_A = 10^{-6}$ s (a) and 10^{-4} s (b) for the labile proton in Thr-22 (ubiquitin) coupled to $m = 1$ (black), 2 (magenta), 3 (brown), 4 (cyan), 5 (orange), 6 (blue), 7 (red) or 8 (green) nonlabile protons, computed from SLE theory for $m \leq 2$ and from GSRE theory for $m \geq 3$. (c,d) Dispersion profiles with $R_{1,I}(\omega_0)$ normalized by the ZF MN/no SDC rate $R^0_{1,I}(0)$ (c) or by the ZF rate $R_{1,I}(0)$ (d), including profiles with $m = 5 - 8$ and the ESE profile with $m = 8$ (black, dash-dot).

VII. CONCLUDING REMARKS

This is the last one in a series of four papers developing the theory of longitudinal relaxation by the dipolar EMOR mechanism in systems comprising one or two spins exchanging with an isotropic bulk phase and dipole-coupled to a solid-like collection of m non-exchanging spins. The previous studies[5–7] provided exact solutions for two-spin and three-spin systems. Here, we have extended the exact theory to four spins, and presented an approximate treatment – the GSRE theory – applicable to arbitrarily large spin systems. For our Matlab implementation of the multi-spin GSRE theory, the computing time scales as m^9. Fortunately, the relaxation rate converges rapidly with m; in practice, it is rarely necessary to go beyond $m = 10$, corresponding to a distance of $3.5 - 4.5$ Å from the labile proton(s).

The multi-spin GSRE theory takes into account the transfer among the m nonlabile spins of magnetization, as well as of two-spin and three-spin modes, induced by the SDCs between these spins. This coherent process decisively influences the relaxation of the labile spin in the RMN regime, but the effect is attenuated as exchange becomes slower. In the more familiar so-called spin diffusion process, magnetization can be coherently transferred over large distances to a relaxation sink, which then drives the relaxation of the entire dipole-coupled spin system.[41] Spin diffusion from nonlabile to labile spins can greatly enhance the relaxation of the nonlabile spins, if their magnetization can be selectively detected. But when the magnetization of the labile spins is observed, as in a field-cycling experiment in the dilute regime, the magnetization starts at the relaxation sink (Fig. 1), so long-range transfer of magnetization (and higher spin modes) is unimportant. In the context of the EMOR mechanism, the labile spin is the relaxation sink.

Whereas we have obtained exact solutions for small spin systems, up to and including the IP_3–I and ISP_2–IS

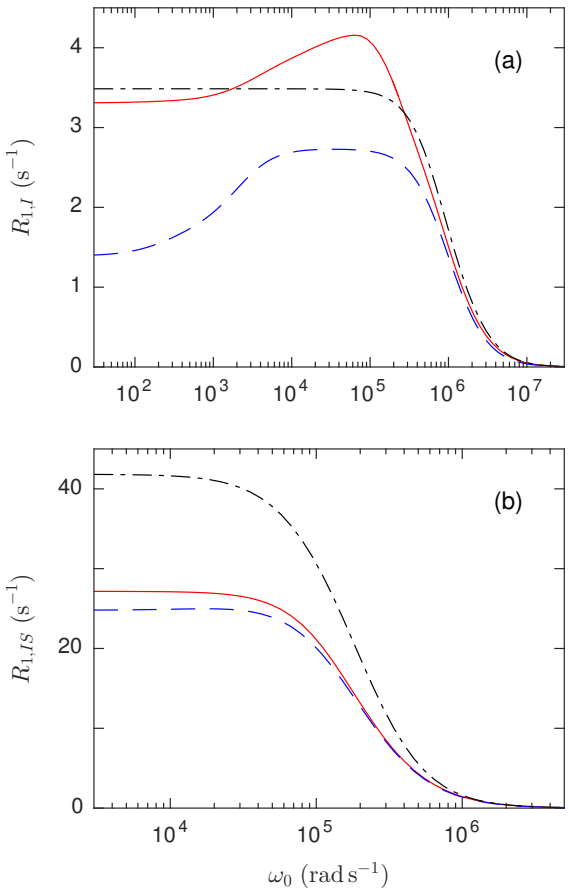

FIG. 8. (a) $R_{1,I}(\omega_0)$ dispersion profiles at $\tau_A = 10^{-6}$ s for the labile proton in Asp-39 (ubiquitin) coupled to eight nonlabile protons. (b) $R_{1,IS}(\omega_0)$ dispersion profiles at $\tau_A = 10^{-5}$ s for the labile protons in W122 (BPTI) coupled to seven nonlabile protons. The profiles were computed from the GSRE theory with (red solid) or without (blue dash) SDCs and from the ESE theory (black dash-dot).

cases, the multi-spin GSRE theory contains several approximations. The 3SM approximation neglects coherent transfer involving four-spin and higher modes and is therefore invoked only for $m \geq 4$. Given the limited range of coherent transfer in the EMOR context (see above) and the minor effect of SDCs outside the RMN regime, we do not expect the 3SM approximation to be a significant source of error. The GSRE theory was obtained by introducing three modifications designed to extend the validity of the SRE theory beyond the RMN regime: the GSDF and the renormalization of ω_0 and SDCs. Although inspired by theoretical considerations, these ad hoc modifications represent a trade-off between simplicity and accuracy. A more accurate GSRE theory could presumably be obtained at the expense of greater formal complexity. For example, to keep the theory simple, we have chosen to use a single GSDF, even though the multi-spin dipolar Hamiltonian has multiple eigenfrequencies. The non-axially-symmetric quadrupolar spin-1 EMOR theory involves three GSDFs, corresponding to the three NQR frequencies.[2] Since the dipolar Hamiltonian for a system of three or more spins also lacks axial symmetry, a GSRE theory featuring a single GSDF cannot be expected to achieve the same quantitative accuracy as for a two-spin system.[5]

Some time ago, one of us presented a more approximate relaxation theory for the dipolar EMOR mechanism in multi-spin systems in the dilute regime.[4] In Sec. IV, we re-derived this so-called ESE theory in a way that clearly identifies the approximations involved. Although less rigorous than the GSRE theory, the ESE theory is less computationally demanding. It is therefore of interest to directly compare the predictions of the ESE and GSRE theories. This is done in Fig. 8 for a labile carboxyl sidechain proton and for an internal water molecule. For each case, we have chosen an experimentally relevant τ_A value and included a sufficient number ($m = 7$ or 8) of nonlabile spins to approach convergence. For the carboxyl proton, the ESE profile differs surprisingly little from the GSRE profile, although the ESE theory fails to reproduce the low-field inverted dispersion step associated with nonsecular decoupling of longitudinal-transverse cross-mode relaxation. However, the near agreement in this case is largely a fortuitous result of error cancellation. Because the ESE theory does not include SDCs, it is more revealing to compare it with the GSRE profile calculated without SDCs. As seen from Fig. 8, the two theories then differ substantially. Also for the internal water case in Fig. 8, where SDCs play only a minor role, the ESE theory is seen to overestimate the relaxation rate significantly. The ESE theory was proposed with large spin systems in mind; for the two-spin and three-spin systems treated in Papers II and III, it is not a viable alternative.

There can be little doubt that the EMOR mechanism is the principal cause of water-^{1}H low-field longitudinal relaxation in aqueous systems of immobilized macromolecules, including soft biological tissue.[12–15] Nevertheless, the GSRE theory presented here ignores certain complications that should be addressed before the theory is used to quantitatively analyze experimental data. The two most obvious complications are as follows.

In the foregoing, we have tacitly assumed that the macromolecule is rigid, so exchange is the only motion capable of inducing spin relaxation. Conformational fluctuations tend to be fast (compared to τ_A) and, under typical conditions, their direct effect appears as an additive contribution to the labile-spin relaxation rate.[2,5] The only significant effect of internal motion on the EMOR contribution is that all dipole couplings are multiplied by orientational order parameters. For simplicity, this has not been done for the sample calculations reported here, except for the internal water molecules (Appendix L).

In the analyzed spin systems extracted from protein structures, all spins, except for the central labile spin(s), were treated as nonlabile, that is, non-exchanging. This

assumption is justified for most of the cases analyzed here, where the ten nearest protons are bound to carbon or amide nitrogens. However, to correctly describe special cases with two adjacent polar side-chains or a cluster of internal water molecules, the theory needs to be modified. This complication can be approximately handled by associating an effective mean survival time $\tau_{\mathrm{A},I\mu} = 1/(1/\tau_{\mathrm{A},I} + 1/\tau_{\mathrm{A},\mu})$ to each $I{-}\mu$ dipole coupling. This simple amendment might suffice for labile protons in side-chain hydroxyl or carboxyl groups, as considered here. For the three protons in the ammonium group of a lysine side-chain, a more rigorous analysis is warranted, explicitly incorporating all three labile spins in the dipolar Hamiltonian and in the exchange topology supermatrix. However, at neutral or acidic pH, nitrogen-bound protons tend to exchange too slowly to contribute significantly by the EMOR mechanism.[12,38] Barring such complications, the total water-^{1}H relaxation rate in the dilute regime can be obtained simple as a population-weighted sum over all individual labile protons and internal water molecules.[2,5]

ACKNOWLEDGMENTS

This work was financially supported by the Swedish Research Council.

[1]B. Halle, Progr. NMR Spectrosc. **28**, 137 (1996).
[2]T. Nilsson and B. Halle, J. Chem. Phys. **137**, 054503 (2012).
[3]E. Persson and B. Halle, J. Am. Chem. Soc. **130**, 1774 (2008).
[4]B. Halle, Magn. Reson. Med. **56**, 60 (2006).
[5]Z. Chang and B. Halle, J. Chem. Phys. **139**, 144203 (2013), also referred to as Paper I.
[6]Z. Chang and B. Halle, J. Chem. Phys. **144**, 084202 (2016), also referred to as Paper II.
[7]Z. Chang and B. Halle, J. Chem. Phys. **145**, 034202 (2016).
[8]F. Noack, Progr. NMR Spectrosc. **18**, 171 (1986).
[9]R. Kimmich and E. Anoardo, Progr. NMR Spectrosc. **44**, 257 (2004).
[10]G. Ferrante and S. Sykora, Adv. Inorg. Chem. **57**, 405 (2005).
[11]B. Halle and V. P. Denisov, Biophys. J. **69**, 242 (1995).
[12]F. V. Chávez and B. Halle, Magn. Reson. Med. **56**, 73 (2006).
[13]F. V. Chávez, E. Persson, and B. Halle, J. Am. Chem. Soc. **128**, 4902 (2006).
[14]F. V. Chávez, E. Hellstrand, and B. Halle, J. Phys. Chem. B **110**, 21551 (2006).
[15]E. P. Sunde and B. Halle, J. Am. Chem. Soc. **131**, 18214 (2009).
[16]S. Kaieda and B. Halle, J. Phys. Chem. B **117**, 14676 (2013).
[17]S. Kaieda and B. Halle, J. Phys. Chem. B **119**, 7957 (2015).
[18]D. J. Lurie, S. Aime, N. A. Baroni, S. Booth, L. M. Broche, C. H. Choi, S. Davies, G. R. Ismail, D. O. Hogain, and K. J. Pine, Compt. Rend. Phys. **11**, 136 (2010).
[19]M. Espy, A. Matlashov, and P. Volegov, J. Magn. Reson. **229**, 127 (2013).
[20]A. Abragam, *The Principles of Nuclear Magnetism* (Clarendon Press, Oxford, 1961).
[21]R. Kubo, J. Math. Phys. **4**, 174 (1963).
[22]R. Kubo, *Advances in Chemical Physics*, edited by K. E. Shuler, Vol. 15 (Wiley, New York, 1969) p. 101.
[23]I. Solomon, Phys. Rev. **99**, 559 (1955).
[24]See supplemental material at [URL to be inserted by AIP] for accuracy assessment of Eq. (12) (Appendix A); derivation of restricted BWR equation (Appendix B); Euler angle conventions (Appendix C); Liouville subspace notation (Appendix D); proofs of symmetry rules (Appendix E); derivation of multi-spin SRE theory (Appendix F); explicit SRE results (Appendix G); relaxation and mode transfer matrix elements (Appendix H); derivation of ESE theory (Appendix I); table of four-spin ISTO basis operators (Appendix J); Liouvillian supermatrix elements (Appendix K); protein spin systems (Appendix L); accuracy assessment of GSRE theory (Appendix M); and convergence of GSRE theory with spin system size (Appendix N).
[25]N. G. van Kampen, *Stochastic Processes in Physics and Chemistry*, 3rd ed. (North-Holland, Amsterdam, 2007).
[26]N. R. Skrynnikov and R. R. Ernst, J. Magn. Reson. **137**, 276 (1999).
[27]F. Persson and B. Halle, J. Am. Chem. Soc. **135**, 8735 (2013).
[28]D. M. Brink and G. R. Satchler, *Angular Momentum*, 3rd ed. (Clarendon Press, Oxford, 1994).
[29]M. Tinkham, *Group Theory and Quantum Mechanics* (McGraw-Hill, New York, 1964).
[30]N. C. Pyper, Mol. Phys. **21**, 1 (1971).
[31]S. Szymanski, A. M. Gryff-Keller, and G. Binsch, J. Magn. Reson. **68**, 399 (1986).
[32]V. I. Lebedev and D. N. Laikov, Dokl. Math. **59**, 477 (1999).
[33]X.-G. Wang and T. Carrington, J. Theor. Comput. Chem. **2**, 599 (2003).
[34]Z. Luz and S. Meiboom, J. Chem. Phys. **40**, 2686 (1964).
[35]V. P. Denisov and B. Halle, J. Mol. Biol. **245**, 682 (1995).
[36]V. P. Denisov and B. Halle, J. Mol. Biol. **245**, 698 (1995).
[37]V. P. Denisov, Peters, J., H. D. Hörlein, and B. Halle, Nat. Struct. Biol. **3**, 505 (1996).
[38]K. Venu, V. P. Denisov, and B. Halle, J. Am. Chem. Soc. **119**, 3122 (1997).
[39]C. P. Slichter and D. Ailion, Phys. Rev. **135**, A1099 (1964).
[40]D. C. Ailion, Advan. Magn. Reson. **5**, 177 (1971).
[41]T. T. P. Cheung, Phys. Rev. B **23**, 1404 (1981).

Supplemental Material

Nuclear magnetic relaxation by the dipolar EMOR mechanism: Multi-spin systems

Zhiwei Chang and Bertil Halle
Division of Biophysical Chemistry, Department of Chemistry, Lund University, POB 124, SE-22100 Lund, Sweden

APPENDIX A: ILRR FOR THE ISP_m-IS CASE

Here we derive and test an approximate formal expression for the ILRR valid for the exchange case ISP_m-IS. For this case, the exchange topology matrix is

$$T_{0,np} \;=\; \delta_{n1}\,\delta_{p1} + \delta_{n2}\,\delta_{p2} + \delta_{n3}\,\delta_{pq_3} + \delta_{n4}\,\delta_{pq_4} + \delta_{n5}\,\delta_{pq_5}\;, \tag{A.1}$$

where q_3, q_4 and q_5 are the sequence numbers in the A state multi-spin basis that correspond to basis operators 3, 4 and 5, respectively, in the B state two-spin basis, as defined in Table S2 of Paper III.[1] Combination of Eqs. (8) and (A.1) yields

$$\mathbf{U}_{Q=0} \;=\; \begin{bmatrix} 1-g_{11} & -g_{12} & -g_{1q_3} & -g_{1q_4} & -g_{1q_5} \\ -g_{21} & 1-g_{22} & -g_{2q_3} & -g_{2q_4} & -g_{2q_5} \\ -g_{q_3 1} & -g_{q_3 2} & 1-g_{q_3q_3} & -g_{q_3q_4} & -g_{q_3q_5} \\ -g_{q_4 1} & -g_{q_4 2} & -g_{q_4q_3} & 1-g_{q_4q_4} & -g_{q_4q_5} \\ -g_{q_5 1} & -g_{q_5 2} & -g_{q_5q_3} & -g_{q_5q_4} & 1-g_{q_5q_5} \end{bmatrix}^{-1} . \tag{A.2}$$

The five basis operators spanning the two-spin $Q = 0$ subspace are of two kinds: B_1 and B_2 are single-spin operators (proportional to I_z and S_z, respectively) with odd spin inversion conjugation (SIC) parity,[2,3] whereas B_{q_3}, B_{q_4} and B_{q_5} are two-spin operators (involving both I-spin and S-spin operators) with even SIC parity. The SIC symmetry of the basis operators can be used to establish selection rules for the matrix elements g_{np}, but only if the superoperator $\mathcal{G}^{\mathrm{A}}$ has definite SIC parity. In SLE theory this is not the case, because the superoperators $\mathcal{L}_{\mathrm{Z}}$ and $\mathcal{L}_{\mathrm{D}}^{\alpha}$ have different SIC parity. In terms of the supermatrices appearing in $\mathbf{\Lambda}^{\alpha}$ in Eq. (6), $\mathbf{L}_{\mathrm{Z}}$ is block-diagonal (or diagonal for isochronous spins) with respect to SIC parity whereas $\mathbf{L}_{\mathrm{D}}$ is anti-block-diagonal. Therefore, $\mathbf{G}^{\mathrm{A}}$ is neither block-diagonal nor anti-block-diagonal. In SRE theory, $\mathbf{\Lambda}^{\alpha}$ in Eq. (7) involves the supermatrices $\mathbf{R}^{\alpha}$ and $\mathbf{L}_{\mathrm{Z}}$, which are block-diagonal with respect to SIC parity, and (for $m \geq 2$) the supermatrix $\mathbf{\Delta}^{\alpha}$, which is anti-block-diagonal. Therefore, just as in SLE theory, $\mathbf{G}^{\mathrm{A}}$ is neither block-diagonal nor anti-block-diagonal. Consequently, the full 5×5 matrix in Eq. (A.2) must be retained in an exact (SLE or SRE) treatment of the exchange case ISP_m-IS.

In the absence of static dipole couplings, as for the three-spin $ISP-IS$ case, the SRE $\mathbf{\Lambda}^{\alpha}$ matrix in Eq. (7) only involves block-diagonal (or diagonal) matrices, so also $\mathbf{G}^{\mathrm{A}}$ is block-diagonal with respect to SIC parity. In the MN regime, where SRE and SLE are equivalent, also the SLE-derived $\mathbf{G}^{\mathrm{A}}$ must be block-diagonal with respect to SIC parity. However, outside the MN regime, the SLE-derived $\mathbf{G}^{\mathrm{A}}$ is no longer block-diagonal. Consequently, two conditions must be satisfied simultaneously for the mixed odd/even blocks in Eq. (A.2) to vanish: (1) there are no static dipole couplings, and (2) the fluctuating dipole couplings are in the MN regime ($\omega_{\mathrm{D}}\,\tau_{\mathrm{A}} \ll 1$).

In the zero-field (ZF) regime, the Wigner-Eckart theorem[4,5] implies that $\mathbf{G}^{\mathrm{A}}$ is block-diagonal in the rank index K, as well as in the projection index Q (see Paper II[6]). Apart from $B_1 \sim I_z$ and $B_2 \sim S_z$, only one more of the five $Q = 0$ two-spin basis operators are of rank $K = 1$, namely $B_4 \sim i\,(\boldsymbol{I} \times \boldsymbol{S}) \cdot \boldsymbol{e}_z$ (with basis ordering as in Table S2 of Paper III[1]). Consequently, in the ZF regime, Eq. (A.2) reduces to

$$\mathbf{U}_{Q=0,\,K=1} \;=\; \left[\begin{array}{ccc} 1-g_{11} & -g_{12} & -g_{14} \\ -g_{21} & 1-g_{22} & -g_{24} \\ -g_{41} & -g_{42} & 1-g_{44} \end{array}\right]^{-1} . \tag{A.3}$$

As we shall see, to a very good approximation, we can neglect the odd/even blocks in Eq. (A.2) so that $\mathbf{U}_{Q=0}$ becomes block-diagonal. In view of Eq. (3b), we only need to be concerned with the odd parity block,

$$\begin{aligned} \mathbf{U}_{Q=0,\,\mathrm{aa}} \;&=\; \left[\begin{array}{cc} 1-g_{11} & -g_{12} \\ -g_{21} & 1-g_{22} \end{array}\right]^{-1} \\ &=\; \frac{1}{(1-g_{11}-g_{22}+g_{11}g_{22}-g_{12}g_{21})} \left[\begin{array}{cc} 1-g_{22} & g_{12} \\ g_{21} & 1-g_{11} \end{array}\right] . \end{aligned} \tag{A.4}$$

Combination of Eqs. (3b) and (A.4) then yields

$$R_{1,IS} \;=\; \frac{P_{\mathrm{A}}}{\tau_{\mathrm{A}}}\,\frac{2\,(1-g_{11}-g_{22}+g_{11}g_{22}-g_{12}g_{21})}{(2-g_{11}-g_{22}+g_{12}+g_{21})} . \tag{A.5}$$

To assess the accuracy of this approximation, we use SLE theory for the $ISP_2{-}IS$ case to calculate $R_{1,IS}(\omega_0)$ approximately from Eq. (A.5) and exactly from Eqs. (3b) and (A.2). As seen from Fig. S1, Eq. (A.5) is virtually exact in the MN regime, where condition (2) is satisfied. In the slow-motion regime, the approximation causes a very slight upshift of the primary dispersion. Even for $\tau_{\mathrm{A}} = 10^{-5}$ s, the relative error is only ~ 0.01 % in the ZF regime, where Eq. (A.3) is valid.

For the $ISP{-}IS$ case, where condition (1) is satisfied automatically, we can examine the consequences of violating condition (2) by comparing the ILRR computed from the standard SLE theory, corresponding to the full 5×5 matrix in Eq. (1.11), with the ILRR computed from a modified SLE theory where only the 2×2 odd-parity block is retained in Eq. (1.11). Within the MN regime, of course, the two methods yield the same ILRR. Outside the MN regime they do differ, but not by more than a few % and typically by less than 1 % over the full parameter space.

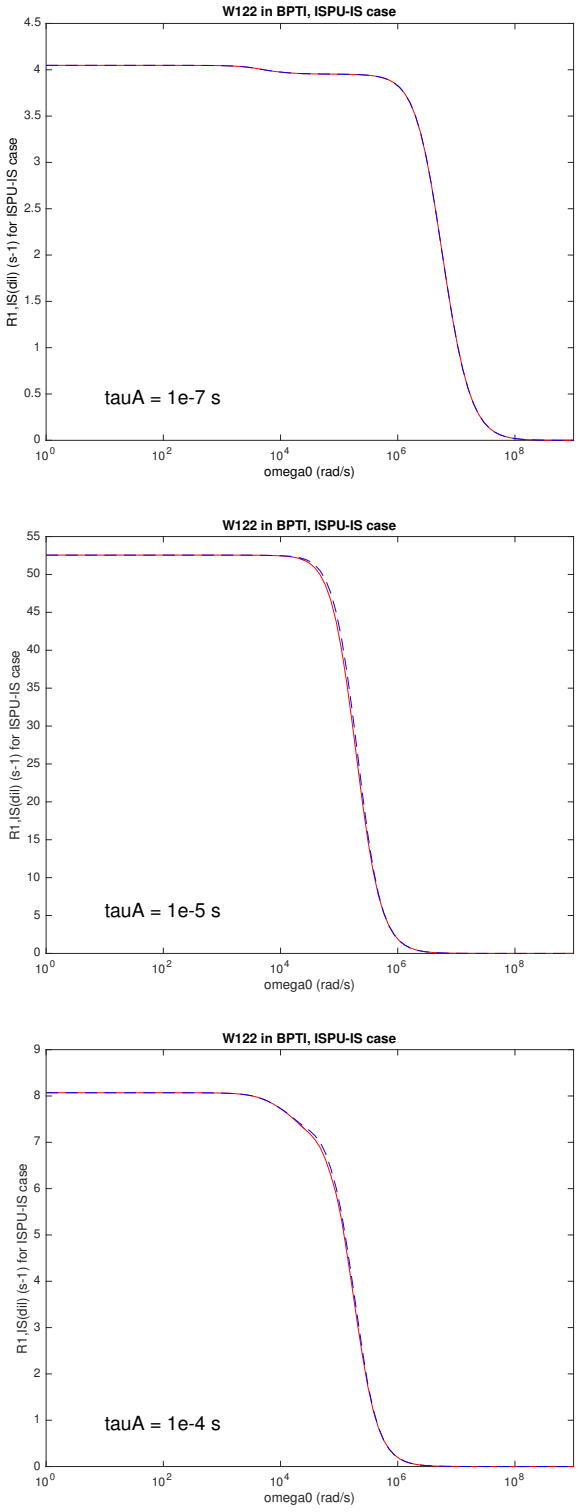

Figure S1: Dispersion of $R_{1,IS}(\omega_0)$ for the internal water molecule W122 coupled to two nonlabile protons in BPTI, computed from exact (red solid) SLE theory, Eqs. (3b) and (A.2), or from approximate (blue dash) SLE theory, Eq. (A.5), for $P_{\mathrm{A}} = 10^{-3}$ and different τ_{A} values. Isotropic averaging with $N_\Omega = 750$ points.

APPENDIX B: RESTRICTED BWR EQUATION

For completeness, we present here the derivation of the restricted BWR master equation, valid in the presence of static as well as fluctuating dipole couplings. This derivation closely follows the conventional one for the case with only fluctuating dipole couplings.[7] For clarity, we focus in this subsection on the exchange case $IP_m - I$. However, the final result is valid also for the exchange case $ISP_m - IS$.

For the exchange case $IP_m - I$, where the spin system comprises a labile spin I and m nonlabile spins, the mutual dipole couplings are of two kinds: static (between two nonlabile spins) and fluctuating (involving the labile spin I). For site α, the corresponding Liouvillians are denoted $\mathcal{L}^\alpha_{\mathrm{D},0}$ and $\mathcal{L}^\alpha_{\mathrm{D}}(t)$, respectively. In a semiclassical description, the stochastic time-dependence of the latter is associated with the exchange of the labile spin I between an anisotropic site α and an isotropic bulk state. In addition, the Zeeman Liouvillian $\mathcal{L}_{\mathrm{Z}}$ describes the interaction of the $m+1$ isochronous spins with an external magnetic field.

The evolution of the stochastic spin density operator for site α, $\rho^\alpha(t)$, under these Liouvillians is governed by the Liouville - von Neumann equation,[7]

$$\frac{\mathrm{d}}{\mathrm{d}t}\,\rho^\alpha(t) \;=\; -\,i\left[\mathcal{L}_{\mathrm{Z}} + \mathcal{L}^\alpha_{\mathrm{D},0} + \mathcal{L}^\alpha_{\mathrm{D}}(t)\right]\rho^\alpha(t)\,. \tag{B.1}$$

The BWR master equation is obtained from a perturbation expansion, truncated after second order in the small quantity $\omega_{\mathrm{D}}\,\tau_{\mathrm{A}}$. Here, ω_{D} is the typical magnitude of a fluctuating dipole coupling and τ_{A} is the correlation time. Before performing this expansion, we must remove the coherent time-dependence from the density operator by transforming to the interaction representation according to

$$\widehat{\rho}^\alpha(t) \;=\; \exp(i\,\mathcal{L}^\alpha_0\,t)\,\rho^\alpha(t)\,, \tag{B.2a}$$

$$\widehat{\mathcal{L}}^\alpha_{\mathrm{D},0}(t) \;=\; \exp(i\,\mathcal{L}^\alpha_0\,t)\,\mathcal{L}^\alpha_{\mathrm{D},0}\,\exp(-i\,\mathcal{L}^\alpha_0\,t)\,, \tag{B.2b}$$

$$\widehat{\mathcal{L}}^\alpha_{\mathrm{D}}(t) \;=\; \exp(i\,\mathcal{L}^\alpha_0\,t)\,\mathcal{L}^\alpha_{\mathrm{D}}(t)\,\exp(-i\,\mathcal{L}^\alpha_0\,t)\,, \tag{B.2c}$$

with

$$\mathcal{L}^\alpha_0 \;\equiv\; \mathcal{L}_{\mathrm{Z}} + \mathcal{L}^\alpha_{\mathrm{D},0}\,. \tag{B.3}$$

In this interaction picture, the Liouville - von Neumann equation (B.1) becomes

$$\frac{\mathrm{d}}{\mathrm{d}t}\,\widehat{\rho}^\alpha(t) \;=\; -\,i\,\widehat{\mathcal{L}}^\alpha_{\mathrm{D}}(t)\,\widehat{\rho}^\alpha(t)\,. \tag{B.4}$$

This differential equation is converted into an integral equation by a formal integration,

$$\widehat{\rho}^\alpha(t) \;=\; \widehat{\rho}^\alpha(0) \;-\; i\int_0^t \mathrm{d}t'\,\widehat{\mathcal{L}}^\alpha_{\mathrm{D}}(t')\,\widehat{\rho}^\alpha(t')\,, \tag{B.5}$$

which, when substituted into the right-hand side of Eq. (B.4), yields the exact result

$$\frac{\mathrm{d}}{\mathrm{d}t}\,\widehat{\rho}^\alpha(t) \;=\; -\,i\,\widehat{\mathcal{L}}^\alpha_{\mathrm{D}}(t)\,\widehat{\rho}^\alpha(0) \;-\; \int_0^t \mathrm{d}t'\,\widehat{\mathcal{L}}^\alpha_{\mathrm{D}}(t)\,\widehat{\mathcal{L}}^\alpha_{\mathrm{D}}(t')\,\widehat{\rho}^\alpha(t')\,. \tag{B.6}$$

The time dependence of the fluctuating dipolar Liouvillian, $\mathcal{L}_{\mathrm{D}}^{\alpha}(t)$, is stochastic. Therefore, the time dependence of the spin density operator, $\widehat{\rho}^{\alpha}(t)$, in Eq. (B.6) is also (partly) stochastic. The spin density operator related to the observable magnetization is obtained by taking an ensemble average,

$$\sigma^{\alpha}(t) \;\equiv\; \langle \rho^{\alpha}(t) \rangle \;. \tag{B.7}$$

The ensemble may be thought of as a collection of trajectories, in each of which the labile spin I exchanges (but at different time points) from site α, thereby randomizing all dipole couplings that it is involved in. Neither the Zeeman Liouvillian $\mathcal{L}_{\mathrm{Z}}$ nor the static dipolar Liouvillian $\mathcal{L}_{\mathrm{D},0}$ is affected by this ensemble averaging.

Taking the ensemble average of Eq. (B.6), we obtain

$$\frac{\mathrm{d}}{\mathrm{d}t}\,\widehat{\sigma}^{\alpha}(t) \;=\; -\,i\,\big\langle \widehat{\mathcal{L}}_{\mathrm{D}}^{\alpha}(t)\,\widehat{\rho}^{\alpha}(0) \big\rangle \;-\; \int_{0}^{t} \mathrm{d}t'\,\big\langle \widehat{\mathcal{L}}_{\mathrm{D}}^{\alpha}(t)\,\widehat{\mathcal{L}}_{\mathrm{D}}^{\alpha}(t')\,\widehat{\rho}^{\alpha}(t') \big\rangle \,. \tag{B.8}$$

Ensemble averaging does not affect the initial spin density operator so the average in the first term on the right-hand side of Eq. (B.8) can be written

$$\big\langle \widehat{\mathcal{L}}_{\mathrm{D}}^{\alpha}(t)\,\widehat{\rho}^{\alpha}(0) \big\rangle \;=\; \big\langle \widehat{\mathcal{L}}_{\mathrm{D}}^{\alpha}(t) \big\rangle\,\widehat{\sigma}^{\alpha}(0) \;=\; \exp(i\,\mathcal{L}_{0}^{\alpha}\,t)\,\big\langle \mathcal{L}_{\mathrm{D}}^{\alpha}(t) \big\rangle\,\exp(-i\,\mathcal{L}_{0}^{\alpha}\,t)\,\widehat{\sigma}^{\alpha}(0) \,, \tag{B.9}$$

where Eq. (B.2c) was used. The fluctuating dipolar Liouvillian is

$$\mathcal{L}_{\mathrm{D}}^{\alpha}(t) \;=\; -\,c \sum_{\mu=1}^{m} \omega_{\mathrm{D},I\mu} \sum_{M=-2}^{2} \mathcal{T}_{M}^{2}(I\mu)\,D_{M0}^{2*}(\Omega_{I\mu}^{\alpha}(t)) \,, \tag{B.10}$$

where c is a normalization constant. The ensemble average only involves the Wigner function, and

$$\big\langle D_{M0}^{2*}(\Omega_{I\mu}^{\alpha}(t)) \big\rangle \;=\; \int \mathrm{d}\Omega_{I\mu}^{\alpha}(t)\; f(\Omega_{I\mu}^{\alpha}(t)\,|\,\Omega_{I\mu}^{\alpha}(0))\; D_{M0}^{2*}(\Omega_{I\mu}^{\alpha}(t)) \,, \tag{B.11}$$

with the EMOR propagator

$$f(\Omega_{I\mu}^{\alpha}(t)\,|\,\Omega_{I\mu}^{\alpha}(0)) \;=\; \frac{1}{8\pi^2} \;+\; \left[\delta(\Omega_{I\mu}^{\alpha}(t) - \Omega_{I\mu}^{\alpha}(0)) \;-\; \frac{1}{8\pi^2}\right] \exp(-t/\tau_{\mathrm{A}}) \,, \tag{B.12}$$

where τ_{A} is the mean survival time of the labile spin I in site α. Consequently,

$$\big\langle D_{M0}^{2*}(\Omega_{I\mu}^{\alpha}(t)) \big\rangle \;=\; D_{M0}^{2*}(\Omega_{I\mu}^{\alpha}(0))\; \exp(-t/\tau_{\mathrm{A}}) \,. \tag{B.13}$$

Up to this point, the treatment is exact. We now introduce the motional narrowing (MN) approximation, stating that the time scale t for substantial variation in the observable of interest, that is, the longitudinal magnetization of the labile spin I, and the associated density matrix elements is much longer than the time scale τ_{A} of fluctuations in the dipole couplings of the labile spin. Several simplifications follow from this assumption. First, since the exponential factor in Eq. (B.13) is $\ll 1$ and, therefore, $\langle \mathcal{L}_{\mathrm{D}}^{\alpha}(t) \rangle \approx 0$,

we can drop the first term in Eq. (B.8). Physically, this simplification results from the orientation $\Omega^{\alpha}_{I\mu}(t)$ of the $I-\mu$ dipole couplings being completely randomized on the time scale $t \gg \tau_{\mathrm{A}}$.

As a second consequence of the MN approximation, the integrand in Eq. (B.8) can be simplified as

$$\begin{aligned} \left\langle \widehat{\mathcal{L}}^{\alpha}_{\mathrm{D}}(t)\, \widehat{\mathcal{L}}^{\alpha}_{\mathrm{D}}(t')\, \widehat{\rho}^{\alpha}(t') \right\rangle &= \left\langle \widehat{\mathcal{L}}^{\alpha}_{\mathrm{D}}(t)\, \widehat{\mathcal{L}}^{\alpha}_{\mathrm{D}}(t') \right\rangle \left\langle \widehat{\rho}^{\alpha}(t') \right\rangle \\ &= \left\langle \widehat{\mathcal{L}}^{\alpha}_{\mathrm{D}}(t)\, \widehat{\mathcal{L}}^{\alpha}_{\mathrm{D}}(t') \right\rangle \widehat{\sigma}^{\alpha}(t') \\ &= \left\langle \widehat{\mathcal{L}}^{\alpha}_{\mathrm{D}}(t)\, \widehat{\mathcal{L}}^{\alpha}_{\mathrm{D}}(t') \right\rangle \widehat{\sigma}^{\alpha}(t)\,. \end{aligned} \tag{B.14}$$

Inserting this expression in Eq. (B.8), changing integration variable according to $t' = t - \tau$, and extending the upper integration limit to ∞ (a third consequence of the MN approximation), we find

$$\frac{\mathrm{d}}{\mathrm{d}t}\, \widehat{\sigma}^{\alpha}(t) \;=\; -\int_0^{\infty} \mathrm{d}\tau\, \left\langle \widehat{\mathcal{L}}^{\alpha}_{\mathrm{D}}(t)\, \widehat{\mathcal{L}}^{\alpha}_{\mathrm{D}}(t-\tau) \right\rangle \widehat{\sigma}^{\alpha}(t)\,. \tag{B.15}$$

The master equation (B.15) in the interaction representation can be transformed back to the Schrödinger representation with the aid of Eq. (B.2), yielding

$$\frac{\mathrm{d}}{\mathrm{d}t}\, \sigma^{\alpha}(t) \;=\; -\,i\,\mathcal{L}^{\alpha}_{0}\, \sigma^{\alpha}(t) - \int_0^{\infty} \mathrm{d}\tau\, \left\langle \mathcal{L}^{\alpha}_{\mathrm{D}}(t)\, \exp(-i\mathcal{L}^{\alpha}_{0}\tau)\, \mathcal{L}^{\alpha}_{\mathrm{D}}(t-\tau)\, \exp(i\mathcal{L}^{\alpha}_{0}\tau) \right\rangle \sigma^{\alpha}(t)\,. \tag{B.16}$$

Finally, we make use of the stationarity of the stochastic process to set $t = 0$ in the time correlation function in the integrand, whereby

$$\frac{\mathrm{d}}{\mathrm{d}t}\, \sigma^{\alpha}(t) \;=\; -\,i\,\mathcal{L}^{\alpha}_{0}\, \sigma^{\alpha}(t) \;-\; \mathcal{R}^{\alpha}\, \sigma^{\alpha}(t)\,, \tag{B.17}$$

with

$$\mathcal{R}^{\alpha} \;\equiv\; \int_0^{\infty} \mathrm{d}\tau\, \left\langle \mathcal{L}^{\alpha}_{\mathrm{D}}(0)\, \widehat{\mathcal{L}}^{\alpha}_{\mathrm{D}}(-\tau) \right\rangle, \tag{B.18}$$

and

$$\begin{aligned} \widehat{\mathcal{L}}^{\alpha}_{\mathrm{D}}(-\tau) &= \exp(-i\,\mathcal{L}^{\alpha}_{0}\,\tau)\, \mathcal{L}^{\alpha}_{\mathrm{D}}(-\tau)\, \exp(i\,\mathcal{L}^{\alpha}_{0}\,\tau) \\ &= \exp[-i\,(\mathcal{L}_{\mathrm{Z}} + \mathcal{L}^{\alpha}_{\mathrm{D},0})\,\tau]\, \mathcal{L}^{\alpha}_{\mathrm{D}}(-\tau)\, \exp[i\,(\mathcal{L}_{\mathrm{Z}} + \mathcal{L}^{\alpha}_{\mathrm{D},0})\,\tau]\,. \end{aligned} \tag{B.19}$$

So far, we have only used the MN approximation, which is a condition on the dipole couplings with spin I: $\omega_{\mathrm{D},I\mu}\,\tau_{\mathrm{A}} \ll 1$. In the multi-spin SRE theory, we also impose a similar restriction on the static dipole couplings: $\omega_{\mathrm{D},\mu\nu}\,\tau_{\mathrm{A}} \ll 1$. As a consequence of the latter assumption, we can omit $\mathcal{L}^{\alpha}_{\mathrm{D},0}$ from Eq. (B.19) so that

$$\widehat{\mathcal{L}}^{\alpha}_{\mathrm{D}}(-\tau) \;=\; \exp[-i\,\mathcal{L}_{\mathrm{Z}}\,\tau]\, \mathcal{L}^{\alpha}_{\mathrm{D}}(-\tau)\, \exp[i\,\mathcal{L}_{\mathrm{Z}}\,\tau]\,. \tag{B.20}$$

This simplification is possible because the essential contribution to the integral in Eq. (B.18) comes from τ values on the order of τ_{A} or less, so that $\mathcal{L}^{\alpha}_{\mathrm{D},0}\,\tau \lesssim \mathcal{L}^{\alpha}_{\mathrm{D},0}\,\tau_{\mathrm{A}} \ll 1$. This argument only relies on the smallness of the numerical factor $\omega_{\mathrm{D},\mu\nu}\,\tau$ and is not invalidated

by the fact that $\mathcal{L}_{\rm Z}$ and $\mathcal{L}^{\alpha}_{{\rm D},0}$ do not commute. This can be shown explicitly by Taylor expanding the exponentials in Eq. (B.19).

The master equation (B.17) predicts that the density operator $\sigma^{\alpha}(t)$ evolves towards zero rather than towards the equilibrium density operator $\sigma^{\alpha}_{\rm eq}$. As usual, this deficiency is corrected by the ad hoc replacement of $\sigma^{\alpha}(t)$ by the difference $\Delta\sigma^{\alpha}(t) \equiv \sigma^{\alpha}(t) - \sigma^{\alpha}_{\rm eq}$ in the last (relaxation) term of Eq. (B.17):

$$\frac{\rm d}{{\rm d}t}\,\sigma^{\alpha}(t) \;=\; -\,i\,\mathcal{L}^{\alpha}_{0}\,\sigma^{\alpha}(t) \;-\; \mathcal{R}^{\alpha}\,\Delta\sigma^{\alpha}(t)\,. \tag{B.21}$$

Since $\sigma^{\alpha}_{\rm eq}$ is independent of time, we can replace $\sigma^{\alpha}(t)$ by $\Delta\sigma^{\alpha}(t)$ also on the left-hand side of Eq. (B.21). The same substitution can be made in the coherent term, because

$$\mathcal{L}^{\alpha}_{0}\,\sigma^{\alpha}_{\rm eq} \;=\; \frac{1}{Z}\,[H^{\alpha}_{0},\,\exp(-\beta\,H^{\alpha}_{0})] \;=\; 0\,, \tag{B.22}$$

where $\beta = 1/(k_{\rm B}T)$ and $Z = {\rm Tr}\{\exp(-\beta\,H^{\alpha}_{0})\}$ and last equality follows by Taylor expanding the exponential operator. We thus arrive at the restricted BWR master equation

$$\frac{\rm d}{{\rm d}t}\,\Delta\sigma^{\alpha}(t) \;=\; -\,i\,\mathcal{L}^{\alpha}_{0}\,\Delta\sigma^{\alpha}(t) \;-\; \mathcal{R}^{\alpha}\,\Delta\sigma^{\alpha}(t)\,. \tag{B.23}$$

APPENDIX C: EULER ANGLE CONVENTIONS

Here we delineate the conventions used to define the D frame and the Euler angles β_X and γ_X that specify the relative orientation of the dipole coupling vectors $\boldsymbol{r}_X$ in any A site.

For the $IP_m{-}I$ case, we first identify the nonlabile spin $\mu = 1$ nearest to spin I. The vector $\boldsymbol{r}^\alpha_{I1}$ from I to spin 1, and the corresponding unit vector $\boldsymbol{e}^\alpha_{I1} = \boldsymbol{r}^\alpha_{I1}/r^\alpha_{I1}$, defines the positive $z_{\rm D}$ axis, so that $\boldsymbol{e}^\alpha_{I1} = \boldsymbol{e}^\alpha_{z_{\rm D}}$ and $\beta_{I1} = 0$. For $m \geq 2$, we also identify the second-nearest nonlabile spin $\mu = 2$. The vector $\boldsymbol{r}^\alpha_{I2}$ from I to spin 2, and the corresponding unit vector $\boldsymbol{e}^\alpha_{I2} = \boldsymbol{r}^\alpha_{I2}/r^\alpha_{I2}$, is taken to lie in the $x^\alpha_{\rm D}{-}z^\alpha_{\rm D}$ half-plane with $x^\alpha_{\rm D} > 0$, so that $\boldsymbol{e}^\alpha_{I2} \cdot \boldsymbol{e}^\alpha_{x_{\rm D}} > 0$ and $\gamma_{I2} = 0$. For the m dipole vectors emanating from spin I, Eq. (17) then yields

$$D^{2*}_{M0}(\Omega^\alpha_{I1}) \;=\; \exp(iM\phi^\alpha)\, d^2_{M0}(\theta^\alpha)\,, \tag{C.1a}$$

$$D^{2*}_{M0}(\Omega^\alpha_{I2}) \;=\; \exp(iM\phi^\alpha) \sum_{N=-2}^{2} d^2_{MN}(\theta^\alpha) \exp(iN\varphi^\alpha)\, d^2_{N0}(\beta_{I2})\,, \tag{C.1b}$$

$$D^{2*}_{M0}(\Omega^\alpha_{I\mu}) \;=\; \exp(iM\phi^\alpha) \sum_{N=-2}^{2} d^2_{MN}(\theta^\alpha) \exp[iN(\varphi^\alpha + \gamma_{I\mu})]\, d^2_{N0}(\beta_{I\mu})\,, \tag{C.1c}$$

with $\mu = 3, \ldots, m$ in Eq. (C.1c). Furthermore,

$$\cos\beta_{I\mu} \;=\; \boldsymbol{e}^\alpha_{I\mu} \cdot \boldsymbol{e}^\alpha_{I1} \qquad (\mu = 2,\, 3,\, \ldots\,, m)\,, \tag{C.2}$$

which is independent of α. The range of $\beta_{I\mu}$ is $[0 - \pi]$.

For $\mu \geq 3$ we need the azimuthal angle $\gamma_{I\mu}$, which is also independent of α. This angle is uniquely defined by the two relations

$$\cos\gamma_{I\mu} \;=\; \frac{\boldsymbol{e}^\alpha_{I\mu} \cdot \boldsymbol{e}^\alpha_{x_{\rm D}}}{\sin\beta_{I\mu}}\,, \tag{C.3a}$$

$$\sin\gamma_{I\mu} \;=\; \frac{\boldsymbol{e}^\alpha_{I\mu} \cdot \boldsymbol{e}^\alpha_{y_{\rm D}}}{\sin\beta_{I\mu}}\,, \tag{C.3b}$$

where, in view of Eq. (C.2),

$$\sin\beta_{I\mu} \;=\; \left(1 - \cos^2\beta_{I\mu}\right)^{1/2} \;=\; \left[1 - (\boldsymbol{e}^\alpha_{I\mu} \cdot \boldsymbol{e}^\alpha_{I1})^2\right]^{1/2}\,. \tag{C.4}$$

The range of $\gamma_{I\mu}$ is $[0 - 2\pi]$, but Eq. (C.3a) cannot distinguish between $\gamma_{I\mu}$ and $2\pi - \gamma_{I\mu}$. Therefore, we first compute a provisional $\gamma'_{I\mu}$ in the range $[0 - \pi]$ from the inverse of Eq. (C.3a),

$$\gamma'_{I\mu} \;=\; \arccos\!\left(\frac{\boldsymbol{e}^\alpha_{I\mu} \cdot \boldsymbol{e}^\alpha_{x_{\rm D}}}{\sin\beta_{I\mu}}\right)\,. \tag{C.5}$$

Next, we use Eq. (C.3b) to compute $\sin\gamma_{I\mu}$. If $\sin\gamma_{I\mu} > 0$, then $\gamma_{I\mu} = \gamma'_{I\mu}$ (in the range $0 - \pi$). If $\sin\gamma_{I\mu} < 0$, then $\gamma_{I\mu} = 2\pi - \gamma'_{I\mu}$ (in the range $\pi - 2\pi$).

For $m \geq 2$, there are also dipole couplings between nonlabile spins. With the D frame defined as described above, Eq. (17) yields for these static dipole couplings

$$D^{2*}_{M0}(\Omega^\alpha_{12}) \;=\; \exp(iM\phi^\alpha) \sum_{N=-2}^{2} d^2_{MN}(\theta^\alpha) \exp(iN\varphi^\alpha)\, d^2_{N0}(\beta_{12})\,, \tag{C.6a}$$

$$D^{2*}_{M0}(\Omega^\alpha_{\mu\nu}) \;=\; \exp(iM\phi^\alpha) \sum_{N=-2}^{2} d^2_{MN}(\theta^\alpha) \exp[iN(\varphi^\alpha + \gamma_{\mu\nu})]\, d^2_{N0}(\beta_{\mu\nu})\,, \tag{C.6b}$$

where $\mu < \nu$ and $\mu\nu \neq 12$ in Eq. (C.6b). Because the spins I, 1 and 2 all lie in the $x^\alpha_{\rm D}$–$z^\alpha_{\rm D}$ plane, Eq. (C.5a) is of the same form as Eq. (C.1b) (that is, $\gamma_{I2} = \gamma_{12} = 0$). Let $\boldsymbol{r}^\alpha_{\mu\nu}$ be the vector from μ to ν with $\mu < \nu$ and let $\boldsymbol{e}^\alpha_{\mu\nu} = \boldsymbol{r}^\alpha_{\mu\nu}/r^\alpha_{\mu\nu}$ be the corresponding unit vector. In analogy with Eq. (C.2),

$$\cos\beta_{\mu\nu} \;=\; \boldsymbol{e}^\alpha_{\mu\nu} \cdot \boldsymbol{e}^\alpha_{I1}\,. \tag{C.7}$$

In analogy with Eq. (C.3), we have for $\mu\nu \neq 12$

$$\cos\gamma_{\mu\nu} \;=\; \frac{\boldsymbol{e}^\alpha_{\mu\nu} \cdot \boldsymbol{e}^\alpha_{x_{\rm D}}}{\sin\beta_{\mu\nu}}\,, \tag{C.8a}$$

$$\sin\gamma_{\mu\nu} \;=\; \frac{\boldsymbol{e}^\alpha_{\mu\nu} \cdot \boldsymbol{e}^\alpha_{y_{\rm D}}}{\sin\beta_{\mu\nu}}\,. \tag{C.8b}$$

To define the internuclear geometry of the IP_m spin system with $m \geq 2$, we need to specify $m(m+1)/2$ distances r_X and $m(m+1)-4$ internal angles (β_X, γ_X). For $m = 1$, only one distance (r_{IP}) and no angles are needed.

For the ISP_m–IS case, the vector $\boldsymbol{r}^\alpha_{IS}$ pointing from spin I to spin S in site α defines the positive $z^\alpha_{\rm D}$ axis, so that $\boldsymbol{e}^\alpha_{IS} = \boldsymbol{e}^\alpha_{z_{\rm D}}$ and $\beta_{IS} = 0$. The second vector needed to define the orientation of the D frame is taken to be $\boldsymbol{r}^\alpha_{I1}$ from spin I to the nearest nonlabile spin $\mu = 1$. This vector is taken to lie in the $x^\alpha_{\rm D} - z^\alpha_{\rm D}$ half-plane with $x^\alpha_{\rm D} > 0$, so that $\boldsymbol{e}^\alpha_{I1} \cdot \boldsymbol{e}^\alpha_{x_{\rm D}} > 0$ and $\gamma_{I1} = \gamma_{S1} = 0$. For the $2m$ dipole vectors emanating from spin I or spin S, Eq. (17) then yields

$$D^{2*}_{M0}(\Omega^\alpha_{IS}) \;=\; \exp(iM\phi^\alpha)\, d^2_{M0}(\theta^\alpha)\,, \tag{C.9a}$$

$$D^{2*}_{M0}(\Omega^\alpha_{I1}) \;=\; \exp(iM\phi^\alpha) \sum_{N=-2}^{2} d^2_{MN}(\theta^\alpha) \exp(iN\varphi^\alpha)\, d^2_{N0}(\beta_{I1})\,, \tag{C.9b}$$

$$D^{2*}_{M0}(\Omega^\alpha_{S1}) \;=\; \exp(iM\phi^\alpha) \sum_{N=-2}^{2} d^2_{MN}(\theta^\alpha) \exp(iN\varphi^\alpha)\, d^2_{N0}(\beta_{S1})\,, \tag{C.9c}$$

$$D^{2*}_{M0}(\Omega^\alpha_{I\mu}) \;=\; \exp(iM\phi^\alpha) \sum_{N=-2}^{2} d^2_{MN}(\theta^\alpha) \exp[iN(\varphi^\alpha + \gamma_{I\mu})]\, d^2_{N0}(\beta_{I\mu})\,, \tag{C.9d}$$

$$D^{2*}_{M0}(\Omega^\alpha_{S\mu}) \;=\; \exp(iM\phi^\alpha) \sum_{N=-2}^{2} d^2_{MN}(\theta^\alpha) \exp[iN(\varphi^\alpha + \gamma_{S\mu})]\, d^2_{N0}(\beta_{S\mu})\,, \tag{C.9e}$$

with $\mu = 2, \ldots, m$ in Eqs. (C.9d,e). In place of Eq. (C.2), we now have

$$\cos\beta_{I\mu} \;=\; \boldsymbol{e}^\alpha_{I\mu} \cdot \boldsymbol{e}^\alpha_{IS} \qquad (\mu = 1,\, 2,\, \ldots\,, m)\,, \tag{C.10a}$$

$$\cos\beta_{S\mu} \;=\; \boldsymbol{e}^\alpha_{S\mu} \cdot \boldsymbol{e}^\alpha_{IS} \qquad (\mu = 1,\, 2,\, \ldots\,, m)\,. \tag{C.10b}$$

The azimuthal angles $\gamma_{I\mu}$ and $\gamma_{S\mu}$ are obtained from Eqs. (C.3) and (C.5) and their S-spin analogs (with I replaced by S everywhere).

For the static dipole couplings between nonlabile spins (present when $m \geq 2$), Eq. (C.6b) applies for all $\mu\nu$ such that $\mu < \nu$ (including $\mu\nu = 12$, since the nonlabile spin $\mu = 2$ is now not in the $x^\alpha_{\rm D} - z^\alpha_{\rm D}$ plane),

$$D^{2*}_{M0}(\Omega^\alpha_{\mu\nu}) \;=\; \exp(iM\phi^\alpha) \sum_{N=-2}^{2} d^2_{MN}(\theta^\alpha) \exp[iN(\varphi^\alpha + \gamma_{\mu\nu})]\, d^2_{N0}(\beta_{\mu\nu})\,. \tag{C.11}$$

In place of Eq. (C.7), we have (for all $\mu\nu$)

$$\cos\beta_{\mu\nu} \;=\; \boldsymbol{e}^\alpha_{\mu\nu} \cdot \boldsymbol{e}^\alpha_{IS}\,, \tag{C.12}$$

and the azimuthal angle $\gamma_{\mu\nu}$ is obtained from Eqs. (C.8).

To define the internuclear geometry of the ISP_m spin system with $m \geq 1$, we need to specify $1 + m(m+3)/2$ distances r_X and $m(m+3) - 2$ internal angles (β_X, γ_X). For $m = 0$, only one distance (r_{IS}) and no angles are needed.

A slightly different convention was used for the three-spin system treated in Paper III,[1] where β_I and β_S were defined as the inner angles at spin I or S, respectively, in the triangle formed by the three spins I, S and P. For the $IP_2 - I$ case, the correspondence is $\beta_I = \beta_{I2}$ and $\beta_S = \pi - \beta_{12}$. For the $ISP - IS$ case, the correspondence is $\beta_I = \beta_{I1}$ and $\beta_S = \pi - \beta_{S1}$.

APPENDIX D: LIOUVILLE SUBSPACE NOTATION

Here we define the notation for the spin Liouville subspaces used in the derivation of the SRE theory. For the $IP_m{-}I$ and $ISP_m{-}IS$ cases, the full spin Liouville space $\mathbb{W}$ can be written as the direct sum $\mathbb{W} = \mathbb{L} \oplus \mathbb{N} \oplus \mathbb{U}$, where $\mathbb{L}$ is the subspace spanned by basis operators involving only labile spins (I, or I and S), $\mathbb{N}$ is the subspace spanned by basis operators involving only nonlabile spins, and $\mathbb{U}$ is the remaining subspace, spanned by basis operators involving both labile and nonlabile spins (at least one of each).

Each of these subspaces, as well as the full Liouville space, may also be decomposed into subspaces spanned exclusively by basis operators with odd (antisymmetric = a) or even (symmetric = s) spin inversion conjugation (SIC) parity, that is, involving single-spin operators associated with an odd or even number of distinct spins, respectively. For example, $\mathbb{W} = \mathbb{A} \oplus \mathbb{S}$ and $\mathbb{N} = \mathbb{NA} \oplus \mathbb{NS}$. The odd and even subspaces can be further decomposed into subspaces with basis operators involving a specific number of distinct spins. For example, if $m = 6$, then $\mathbb{NA} = \mathbb{N}_1 \oplus \mathbb{N}_3 \oplus \mathbb{N}_5 \equiv \mathbb{N}_1 \oplus \mathbb{NA}'$ and $\mathbb{NS} = \mathbb{N}_2 \oplus \mathbb{N}_4 \oplus \mathbb{N}_6 \equiv \mathbb{N}_2 \oplus \mathbb{NS}'$, where $\mathbb{NA}'$ is the subspace of odd nonlabile basis operators involving more than one spin and $\mathbb{NS}'$ is the subspace of even nonlabile basis operators involving more than two spins. These generic subspaces may be further decomposed into subspaces involving specific spins. For example, $\mathbb{L}_1 = \mathbb{L}_1(I) \oplus \mathbb{L}_1(S)$ (for the $ISP_m{-}IS$ case), or $\mathbb{N}_1 = \sum_{\mu=1}^{m} \mathbb{N}_1(\mu)$, or $\mathbb{N}_2 = \sum_{\mu,\nu} \mathbb{N}_2(\mu\nu)$, where the (direct) sum goes over all $m(m-1)/2$ distinct two-spin subspaces $\mathbb{N}_2(\mu\nu)$. Note that the order of the spins is irrelevant here: $\nu\mu$ and $\mu\nu$ refer to the same subspace.

For a spin system with m nonlabile spins, the number of distinct k-spin subspaces $\mathbb{N}_k(\mu\nu\kappa\cdots)$ is given by the binomial coefficient $m!/[(m-k)!\,k!]$, that is, the number of distinct ways of choosing a subset of k spins, irrespective of their order, from a set of m spins. Each distinct k-spin subspace $\mathbb{N}_k(\mu\nu\kappa\cdots)$ is spanned by 3^k basis operators, so it comprises 3^k k-spin modes. In other words, the dimension of $\mathbb{N}_k(\mu\nu\kappa\cdots)$ is 3^k. The dimension of the total k-spin subspace $\mathbb{N}_k$, comprising all distinct combinations of k spins, is $3^k\, m!/[(m-k)!\,k!]$. For $m = 3$, for example, there are three single-spin subspaces – $\mathbb{N}_1(\mu)$, $\mathbb{N}_1(\nu)$ and $\mathbb{N}_1(\kappa)$ – each of dimension 3, three two-spin subspaces – $\mathbb{N}_2(\mu\nu)$, $\mathbb{N}_2(\mu\kappa)$ and $\mathbb{N}_2(\nu\kappa)$ – each of dimension 9, and one three-spin subspace $\mathbb{N}_3(\mu\nu\kappa)$ of dimension 27.

The subscripts n and p denote basis operators B_n and B_p. To identify a basis operator belonging to a particular subspace, we give the subspace symbol as an argument. For example, the basis operator $n(\mathbb{L}_1)$ contains one single-spin operator associated with an unspecified labile spin, whereas $n(\mathbb{L}_1(I)) = n(I)$ is one of the three basis operators (proportional to I_z, I_+ or I_-) that span the I-spin Liouville space. The one- or two-dimensional subspace spanned by basis operators proportional to I_z or S_z is denoted by $\mathbb{LZ}$ and the associated basis operators are $n(\mathbb{LZ})$. Similarly, the basis operator $n(\mathbb{N}_1)$ contains one single-spin operator associated with an unspecified nonlabile spin, whereas $n(\mathbb{N}_1(\mu)) = n(\mu)$ is one of the three basis operators (proportional to μ_z, μ_+ or μ_-) that span the μ-spin Liouville space. Finally, the basis operator $n(\mathbb{N}_2)$ contains a product of

two single-spin operators (or a sum of such products), each associated with a different nonlabile spin, whereas $n(\mathbb{N}_2(\mu\nu)) = n(\mu\nu)$ is one of the nine basis operators that span the two-spin Liouville subspace associated with the specific nonlabile spins μ and ν (regardless of their order). The extension of these conventions to the nonlabile three-spin Liouville subspace $\mathbb{N}_3$ is obvious.

APPENDIX E: PROOFS OF SYMMETRY RULES

Employing the subspace notation defined in Appendix C, we shall now prove nine symmetry rules for the coefficients $C^{XY}_{MM',np}$ and $D^{X}_{M,np}$ in Eqs. (18) and (19). To do this, we shall make use of two general results. First, because two operators associated with different spins (such as I_z and μ_+) necessarily commute, it follows that the commutator of two operators, each of which is a product of single-spin operators associated with distinct spins, vanishes if the two product operators have no spin in common. Second, since $\mathrm{Tr}_I\{I_z\} = \mathrm{Tr}_I\{I_+\} = \mathrm{Tr}_I\{I_-\} = 0$, it follows that the multi-spin trace of a product operator, as in Eqs. (18) and (19), vanishes if the product operator contains at least one lone operator, that is, if any spin occurs only once in the product operator. Each symmetry rule will be derived from Eqs. (18) and (19) for basis operators B_n and B_p belonging to certain subspaces, but the symmetry rule will be expressed more succinctly in terms of the corresponding block of $\mathbf{C}^{XY}_{MM'}$ or $\mathbf{D}^{X}_{M}$.

Symmetry Rule I. Labile single-spin modes are relaxation-coupled to nonlabile single-spin modes but not to other nonlabile odd-parity modes (involving 3 or 5 or ... nonlabile spins) and the relaxation coupling only involves self-correlations.

$$\mathbf{C}^{XY}_{MM',\mathbb{L}_1\mathbb{N}_k} \;=\; \delta_{XY}\,\delta_{k1}\,\mathbf{C}^{XX}_{MM',\mathbb{L}_1\mathbb{N}_1} \quad , \qquad k = \text{odd}\;. \tag{E.1}$$

Proof. Assume that $B_n = n(\mathbb{L}_1) = n(I)$. For the other possibility, $B_n = n(S)$, the following arguments are the same except that I and S are interchanged everywhere. The first commutator in Eq. (18) then vanishes unless the dipole coupling X involves spin I, that is, if $X = I\mu$ or $X = IS$. Because $B_p = p(\mathbb{N}_k)$ only involves nonlabile-spin operators, the second commutator in Eq. (18) vanishes unless the dipole coupling Y involves one nonlabile spin, that is, if $Y = I\nu$ or $Y = S\nu$. To avoid having a lone I-spin or S-spin operator, which would cause the trace in Eq. (18) to vanish, we must have $X = I\mu$ and $Y = I\nu$. By assumption, B_p is a product of an odd number of single-spin operators associated with distinct nonlabile spins (or a sum of such products). If B_p involves 3 or more distinct nonlabile spins, the trace will vanish because its argument involves at least one lone nonlabile spin. For the trace to be nonzero, B_p must involve only one nonlabile spin, which must also occur in the dipole couplings X and Y. In other words, $X = Y = I\mu$ and $B_p = p(\mu)$. Q.E.D.

Symmetry Rule II. Relaxation does not couple nonlabile-spin modes involving different numbers of spins.

$$\mathbf{C}^{XY}_{MM',\mathbb{N}_k\mathbb{N}_l} \;=\; \delta_{kl}\,\mathbf{C}^{XY}_{MM',\mathbb{N}_k\mathbb{N}_k}\;. \tag{E.2}$$

Proof. Since B_n and B_p only involve nonlabile spins, the dipole couplings must be $X = I\mu$ and $Y = I\nu$ or $X = S\mu$ and $Y = S\nu$ and the nonlabile spins μ and ν must be contained in B_n and B_p, respectively. The trace over nonlabile spins then involves a product of k mutually distinct nonlabile-spin operators times a product of l mutually distinct nonlabile-spin operators. If $k \neq l$, at least one lone nonlabile-spin operator occurs, causing the trace to vanish. Q.E.D.

Symmetry Rule III. Within the nonlabile k-spin subspace $\mathbb{N}_k$, relaxation only couples modes that involve the same set of k spins.

$$\mathbf{C}^{XY}_{MM',\mathbb{N}_k(\mu\nu\kappa\lambda\cdots)\mathbb{N}_k(\mu'\nu'\kappa'\lambda'\cdots)} \;=\; \delta_{\mu\nu\kappa\lambda\cdots,\,\mu'\nu'\kappa'\lambda'\cdots}\,\mathbf{C}^{XY}_{MM',\mathbb{N}_k(\mu\nu\kappa\lambda\cdots)\mathbb{N}_k(\mu\nu\kappa\lambda\cdots)}\;. \tag{E.3}$$

The matrices $\mathbf{C}^{XY}_{MM',\mathbb{N}_k\mathbb{N}_k}$ and $\mathbf{R}^{\alpha}_{\mathbb{N}_k\mathbb{N}_k}$ are therefore block-diagonal in spins ($k = 1$), spin pairs ($k = 2$), etc. Furthermore, relaxation coupling between single-spin modes only involves self-correlations. Thus,

$$\mathbf{C}^{XY}_{MM',\mathbb{N}_1(\mu)\mathbb{N}_1(\mu')} \;=\; \delta_{XY}\,\delta_{\mu\mu'}\,\mathbf{C}^{XX}_{MM',\mathbb{N}_1(\mu)\mathbb{N}_1(\mu)}\;, \tag{E.4a}$$

$$\mathbf{C}^{XY}_{MM',\mathbb{N}_2(\mu\nu)\mathbb{N}_2(\mu'\nu')} \;=\; \delta_{\mu\nu,\mu'\nu'}\,\mathbf{C}^{XY}_{MM',\mathbb{N}_2(\mu\nu)\mathbb{N}_2(\mu\nu)}\;, \tag{E.4b}$$

$$\mathbf{C}^{XY}_{MM',\mathbb{N}_3(\mu\nu\kappa)\mathbb{N}_3(\mu'\nu'\kappa')} \;=\; \delta_{\mu\nu\kappa,\mu'\nu'\kappa'}\,\mathbf{C}^{XY}_{MM',\mathbb{N}_3(\mu\nu\kappa)\mathbb{N}_3(\mu\nu\kappa)}\;. \tag{E.4c}$$

Proof. For the trace to be nonzero, it is not only necessary that B_n and B_p involve the same *number* of nonlabile spins; actually, the *identity* of the nonlabile spins must be the same in B_n and B_p. Only then will all spins be pairwise matched so the trace can be nonzero. Moreover, for $k = 1$, the identifications $X = I\mu$ and $Y = I\mu'$, established in the proof of Eq. (E.2), imply when $\mu = \mu'$, as dictated by Eq. (E.4a), that $X = Y$, so only self-correlations contribute to $\mathbf{R}^{\alpha}_{\mathbb{N}_1\mathbb{N}_1}$. Q.E.D.

Symmetry Rule IV. Relaxation supermatrix elements within the single-spin subspace only involve self-correlations.

$$C^{XY}_{MM',np} \;=\; \delta_{XY}\,C^{XX}_{MM',np}\;, \quad \text{if } n,\, p \in \mathbb{W}_1\;. \tag{E.5}$$

Proof. According to Eq. (18), $C^{XY}_{MM',np}$ can be nonzero only if B_n and X share one spin (otherwise the first commutator vanishes) and if B_p and Y share one spin (otherwise the second commutator vanishes). The argument of the trace in Eq. (18) is then a product of four single-spin operators associated with the four spins that are involved in the two dipole couplings X and Y. Because the (partial) trace of a lone single-spin operator vanishes, the four operators must consist of two operators associated with one spin and two operators associated with another spin. Since a dipole coupling involves two different spins, it follows that $C^{XY}_{MM',np}$ can be nonzero only if $X = Y$. Q.E.D.

Symmetry Rule V. Coherent dipolar evolution does not couple directly to labile-spin modes.

$$\mathbf{D}^X_{M,\,\mathbb{LW}} \;=\; \mathbf{D}^X_{M,\,\mathbb{WL}} \;=\; \mathbf{0}\,. \tag{E.6}$$

Proof. Since $X = \mu\nu$, the commutator in Eq. (19) vanishes if either B_n or B_p only involves labile-spin operators. Q.E.D.

Symmetry Rule VI. Coherent dipolar evolution does not couple nonlabile-spin modes with mixed modes.

$$\mathbf{D}^X_{M,\,\mathbb{NU}} \;=\; \mathbf{D}^X_{M,\,\mathbb{UN}} \;=\; 0\,. \tag{E.7}$$

Together, symmetry rules V and VI show that coherent dipolar evolution can only couple nonlabile-spin modes to other nonlabile-spin modes.
Proof. The trace in Eq. (19) vanishes because it involves at least one lone labile-spin operator, contributed by the basis operator from the $\mathbb{U}$ subspace. Q.E.D.

Symmetry Rule VII. Coherent dipolar evolution couples nonlabile single-spin modes with nonlabile two-spin modes, but not with any other nonlabile k-spin modes.

$$\mathbf{D}^X_{M,\,\mathbb{N}_1\mathbb{N}_k} \;=\; \delta_{k2}\,\mathbf{D}^X_{M,\,\mathbb{N}_1\mathbb{N}_2}\,. \tag{E.8}$$

Proof. For $B_n = n(\mu)$ or $n(\nu)$ and $X = \mu\nu$, the commutator yields $\mu\nu$. The only way to match these two operators without introducing any new lone-spin operators is if B_p is a two-spin operator. In fact, it is necessary that $B_p = p(\mu\nu)$. Q.E.D.

Symmetry Rule VIII. Coherent dipolar evolution only couples nonlabile spin modes differing by one spin. Thus, for $k \geq 2$,

$$\mathbf{D}^X_{M,\,\mathbb{N}_k\mathbb{N}_l} \;=\; \delta_{l,k\pm1}\,\mathbf{D}^X_{M,\,\mathbb{N}_k\mathbb{N}_{k\pm1}}\,. \tag{E.9}$$

For $k = 1$, only the plus sign applies and Eq. (E.9) reduces to Eq. (E.8).
Proof. The commutator in the second form of Eq. (19) can be nonzero only if the basis operator $B_n = n(\mathbb{N}_k)$ involves either or both of the spins in the dipole coupling $X = \mu\nu$. In the former case, where $B_n = n(\mu\cdots)$ does not involve spin ν or $B_n = n(\nu\cdots)$ does not involve spin μ, the commutator yields $\mu\nu\cdots$. The trace in Eq. (19) can then be nonzero only if $B_p = p(\mu\nu\cdots)$, that is, if B_p contains the same spins as B_n plus the second spin (here, ν) involved in the dipole coupling X. Hence, $l = k + 1$. In the latter case, where $B_n = n(\mu\nu\cdots)$ involves both spins in X, the commutator yields products of $k+1$ operators associated with k spins, such as $\mu_a\mu_b\nu\cdots$ and $\mu\nu_a\nu_b\cdots$. Since one spin is represented by two operators, the trace in Eq. (19) can be nonzero only if $B_p = p(\mu\cdots)$ not involving spin ν or if $B_p = p(\nu\cdots)$ not involving spin μ, that is, if B_p contains the same spins as B_n except one of the spins involved in the dipole coupling X. Hence, $l = k - 1$. Q.E.D.

Symmetry Rule IX. Coherent dipolar evolution couples k-spin modes with $(k+1)$-spin modes only if k spins are shared between the modes. The mode coupling is induced by dipole couplings between the non-shared spin and each of the shared spins.

Proof. Implicit in the proofs of symmetry rules VII and VIII.

Special cases of symmetry rule IX are

$$\mathbf{D}^{X}_{M,\,\mathbb{N}_1(\kappa)\mathbb{N}_2(\mu\nu)} \;=\; \delta_{X,\mu\nu}\left[\delta_{\kappa\mu}\,\mathbf{D}^{\mu\nu}_{M,\,\mathbb{N}_1(\mu)\mathbb{N}_2(\mu\nu)} \;+\; \delta_{\kappa\nu}\,\mathbf{D}^{\mu\nu}_{M,\,\mathbb{N}_1(\nu)\mathbb{N}_2(\mu\nu)}\right]\,, \tag{E.10}$$

and

$$\begin{aligned}\mathbf{D}^{X}_{M,\,\mathbb{N}_2(\lambda\eta)\mathbb{N}_3(\mu\nu\kappa)} \;&=\delta_{\lambda\eta,\mu\nu}\left[\delta_{X,\mu\kappa}\,\mathbf{D}^{\mu\kappa}_{M,\,\mathbb{N}_2(\mu\nu)\mathbb{N}_3(\mu\nu\kappa)}+\delta_{X,\nu\kappa}\,\mathbf{D}^{\nu\kappa}_{M,\,\mathbb{N}_2(\mu\nu)\mathbb{N}_3(\mu\nu\kappa)}\right]\\ &+\delta_{\lambda\eta,\mu\kappa}\left[\delta_{X,\mu\nu}\,\mathbf{D}^{\mu\nu}_{M,\,\mathbb{N}_2(\mu\kappa)\mathbb{N}_3(\mu\nu\kappa)}+\delta_{X,\nu\kappa}\,\mathbf{D}^{\nu\kappa}_{M,\,\mathbb{N}_2(\mu\kappa)\mathbb{N}_3(\mu\nu\kappa)}\right]\\ &+\delta_{\lambda\eta,\nu\kappa}\left[\delta_{X,\mu\nu}\,\mathbf{D}^{\mu\nu}_{M,\,\mathbb{N}_2(\nu\kappa)\mathbb{N}_3(\mu\nu\kappa)}+\delta_{X,\mu\kappa}\,\mathbf{D}^{\mu\kappa}_{M,\,\mathbb{N}_2(\nu\kappa)\mathbb{N}_3(\mu\nu\kappa)}\right]\,.\end{aligned} \tag{E.11}$$

APPENDIX F: MULTI-SPIN SRE THEORY

Here we present the full derivation of the multi-spin SRE theory. Specifically, we obtain the supermatrix $\mathbf{G}^{\mathrm{A}}$, the elements of which determine the ILRR according to Eq. (11) or (12).

First, we exploit spin inversion conjugation (SIC) symmetry. If the $(4^{m+2}-1)$-dimensional multi-spin ISTO basis for state A is ordered with the odd-parity operators before the even-parity operators, the relaxation supermatrix $\mathbf{R}^{\alpha}$ is block-diagonal whereas the static dipole coupling supermatrix $\mathbf{\Delta}^{\alpha}$ is anti-block-diagonal. Furthermore, $\mathbf{K}$ and $\mathbf{L}_{\mathrm{Z}}$ (for isochronous spins) are diagonal. We can therefore partition $\mathbf{\Lambda}^{\alpha}$ in Eq. (7) into blocks associated with the anti-symmetric ($\mathbb{A}$) and symmetric ($\mathbb{S}$) subspaces:

$$\mathbf{\Lambda}^{\alpha} \;=\; \begin{bmatrix} (\mathbf{K}_{\mathbb{A}\mathbb{A}}+\mathbf{R}^{\alpha}_{\mathbb{A}\mathbb{A}}\,\tau_{\mathrm{A}}+i\,\mathbf{L}_{\mathrm{Z},\,\mathbb{A}\mathbb{A}}\,\tau_{\mathrm{A}}) & i\,\mathbf{\Delta}^{\alpha}_{\mathbb{A}\mathbb{S}}\,\tau_{\mathrm{A}} \\ i\,\mathbf{\Delta}^{\alpha}_{\mathbb{S}\mathbb{A}}\,\tau_{\mathrm{A}} & (\mathbf{K}_{\mathbb{S}\mathbb{S}}+\mathbf{R}^{\alpha}_{\mathbb{S}\mathbb{S}}\,\tau_{\mathrm{A}}+i\,\mathbf{L}_{\mathrm{Z},\,\mathbb{S}\mathbb{S}}\,\tau_{\mathrm{A}}) \end{bmatrix}\,. \tag{F.1}$$

To calculate the ILRR, we only need elements from the $\mathbb{A}\mathbb{A}$ block of the inverse $(\mathbf{\Lambda}^{\alpha})^{-1}$,

$$(\mathbf{\Lambda}^{\alpha})^{-1}_{\mathbb{A}\mathbb{A}} \;=\; [\mathbf{K}_{\mathbb{A}\mathbb{A}}+(\mathbf{R}^{\alpha}_{\mathbb{A}\mathbb{A}}+\mathbf{X}^{\alpha}_{\mathbb{A}\mathbb{A}}+i\,\mathbf{L}_{\mathrm{Z},\,\mathbb{A}\mathbb{A}})\,\tau_{\mathrm{A}}]^{-1}\,, \tag{F.2}$$

with

$$\mathbf{X}^{\alpha}_{\mathbb{A}\mathbb{A}} \;\equiv\; \mathbf{\Delta}^{\alpha}_{\mathbb{A}\mathbb{S}}\,(\mathbf{K}_{\mathbb{S}\mathbb{S}}/\tau_{\mathrm{A}}+\mathbf{R}^{\alpha}_{\mathbb{S}\mathbb{S}}+i\,\mathbf{L}_{\mathrm{Z},\,\mathbb{S}\mathbb{S}})^{-1}\mathbf{\Delta}^{\alpha}_{\mathbb{S}\mathbb{A}}\,. \tag{F.3}$$

We decompose the anti-symmetric subspace as $\mathbb{A}=\mathbb{L}'\mathbb{A}+\mathbb{N}\mathbb{A}$, where $\mathbb{L}'=\mathbb{L}+\mathbb{U}$. Noting that $\mathbf{K}_{\mathbb{N}\mathbb{A},\mathbb{N}\mathbb{A}}=\mathbf{0}$, we can partition Eq. (F.2) as

$$(\mathbf{\Lambda}^{\alpha})^{-1}_{\mathbb{A}\mathbb{A}}=\begin{bmatrix}\mathbf{1}_{\mathbb{L}'\mathbb{A},\mathbb{L}'\mathbb{A}}+(\mathbf{R}^{\alpha}_{\mathbb{L}'\mathbb{A},\mathbb{L}'\mathbb{A}}+\mathbf{X}^{\alpha}_{\mathbb{L}'\mathbb{A},\mathbb{L}'\mathbb{A}}+i\mathbf{L}_{\mathrm{Z},\mathbb{L}'\mathbb{A},\mathbb{L}'\mathbb{A}})\tau_{\mathrm{A}} & (\mathbf{R}^{\alpha}_{\mathbb{L}'\mathbb{A},\mathbb{N}\mathbb{A}}+\mathbf{X}^{\alpha}_{\mathbb{L}'\mathbb{A},\mathbb{N}\mathbb{A}})\tau_{\mathrm{A}} \\ (\mathbf{R}^{\alpha}_{\mathbb{N}\mathbb{A},\mathbb{L}'\mathbb{A}}+\mathbf{X}^{\alpha}_{\mathbb{N}\mathbb{A},\mathbb{L}'\mathbb{A}})\tau_{\mathrm{A}} & (\mathbf{R}^{\alpha}_{\mathbb{N}\mathbb{A},\mathbb{N}\mathbb{A}}+\mathbf{X}^{\alpha}_{\mathbb{N}\mathbb{A},\mathbb{N}\mathbb{A}}+i\mathbf{L}_{\mathrm{Z},\mathbb{N}\mathbb{A},\mathbb{N}\mathbb{A}})\tau_{\mathrm{A}}\end{bmatrix}^{-1}\,. \tag{F.4}$$

But we only need the $\mathbb{L}'\mathbb{A}, \mathbb{L}'\mathbb{A}$ block of $(\mathbf{\Lambda}^\alpha)^{-1}_{\mathbb{A}\mathbb{A}}$,

$$(\mathbf{\Lambda}^\alpha)^{-1}_{\mathbb{L}'\mathrm{A},\mathbb{L}'\mathrm{A}} \;=\; \Big[\mathbf{1}_{\mathbb{L}'\mathrm{A},\mathbb{L}'\mathrm{A}} + (\mathbf{R}^\alpha_{\mathbb{L}'\mathrm{A},\mathbb{L}'\mathrm{A}} + \mathbf{X}^\alpha_{\mathbb{L}'\mathrm{A},\mathbb{L}'\mathrm{A}} + i\,\mathbf{L}_{\mathrm{Z},\,\mathbb{L}'\mathrm{A},\mathbb{L}'\mathrm{A}})\,\tau_\mathrm{A} \\ -\; \big(\mathbf{R}^\alpha_{\mathbb{L}'\mathrm{A},\mathbb{N}\mathrm{A}} + \mathbf{X}^\alpha_{\mathbb{L}'\mathrm{A},\mathbb{N}\mathrm{A}}\big)\big(\mathbf{R}^\alpha_{\mathbb{N}\mathrm{A},\mathbb{N}\mathrm{A}} + \mathbf{X}^\alpha_{\mathbb{N}\mathrm{A},\mathbb{N}\mathrm{A}} + i\,\mathbf{L}_{\mathrm{Z},\,\mathbb{N}\mathrm{A},\mathbb{N}\mathrm{A}}\big)^{-1}\big(\mathbf{R}^\alpha_{\mathbb{N}\mathrm{A},\mathbb{L}'\mathrm{A}} + \mathbf{X}^\alpha_{\mathbb{N}\mathrm{A},\mathbb{L}'\mathrm{A}}\big)\,\tau_\mathrm{A}\Big]^{-1} . \tag{F.5}$$

This result is ill-suited for computations, because the $\mathbb{L}'\mathbb{A}$ subspace is very large for multi-spin systems. However, Eq. (F.5) can be simplified by implementing the RMN approximation. We thus expand the inverse in Eq. (F.5) to first order in $\mathbf{R}^\alpha\tau_\mathrm{A}$, that is, to second order in $\omega_\mathrm{D}\tau_\mathrm{A}$, consistent with our use in Eq. (13) of a relaxation supermatrix derived from BWR theory under the assumption that $(\omega_\mathrm{D}\tau_\mathrm{A})^2 \ll 1$ (for fluctuating and static dipole couplings). Performing also the isotropic orientational average, we then obtain from Eqs. (5) and (F.5),

$$\mathbf{G}^\mathrm{A}_{\mathbb{L}'\mathrm{A},\mathbb{L}'\mathrm{A}} \;=\; \mathbf{Z}^{-1} \;-\; \mathbf{Z}^{-1}\left[\big\langle\mathbf{R}^\alpha_{\mathbb{L}'\mathrm{A},\mathbb{L}'\mathrm{A}}\big\rangle + \big\langle\mathbf{X}^\alpha_{\mathbb{L}'\mathrm{A},\mathbb{L}'\mathrm{A}}\big\rangle\right]\tau_\mathrm{A}\,\mathbf{Z}^{-1} \\ +\,\mathbf{Z}^{-1}\Big\langle\big(\mathbf{R}^\alpha_{\mathbb{L}'\mathrm{A},\mathbb{N}\mathrm{A}} + \mathbf{X}^\alpha_{\mathbb{L}'\mathrm{A},\mathbb{N}\mathrm{A}}\big)\big(\mathbf{R}^\alpha_{\mathbb{N}\mathrm{A},\mathbb{N}\mathrm{A}} + \mathbf{X}^\alpha_{\mathbb{N}\mathrm{A},\mathbb{N}\mathrm{A}} + i\,\mathbf{L}_{\mathrm{Z},\,\mathbb{N}\mathrm{A},\mathbb{N}\mathrm{A}}\big)^{-1}\big(\mathbf{R}^\alpha_{\mathbb{N}\mathrm{A},\mathbb{L}'\mathrm{A}} + \mathbf{X}^\alpha_{\mathbb{N}\mathrm{A},\mathbb{L}'\mathrm{A}}\big)\Big\rangle\tau_\mathrm{A}\,\mathbf{Z}^{-1} , \tag{F.6}$$

where $\mathbf{Z} \equiv \mathbf{1}_{\mathbb{L}'\mathrm{A},\mathbb{L}'\mathrm{A}} + i\,\mathbf{L}_{\mathrm{Z},\,\mathbb{L}'\mathrm{A},\mathbb{L}'\mathrm{A}}\,\tau_\mathrm{A}$. The $\mathbb{L}'\mathbb{A}$ subspace comprises all odd-parity basis operators that contain at least one labile-spin operator (I or S). But to obtain the ILRR, we only need matrix elements of $\mathbf{G}^\mathrm{A}_{\mathbb{L}'\mathrm{A},\mathbb{L}'\mathrm{A}}$ in the $\mathbb{L}\mathbb{Z}$ subspace. In this subspace, $\mathbf{L}_\mathrm{Z} = \mathbf{0}$ so $\mathbf{Z} = \mathbf{1}$ and the 2×2 block $\mathbf{G}^\mathrm{A}_{\mathbb{L}\mathbb{Z},\mathbb{L}\mathbb{Z}}$ of $\mathbf{G}^\mathrm{A}_{\mathbb{L}'\mathrm{A},\mathbb{L}'\mathrm{A}}$ becomes

$$\mathbf{G}^\mathrm{A}_{\mathbb{L}\mathbb{Z},\mathbb{L}\mathbb{Z}} \;=\; \mathbf{1} \;-\; \big\langle\mathbf{R}^\alpha_{\mathbb{L}\mathbb{Z},\mathbb{L}\mathbb{Z}}\big\rangle\,\tau_\mathrm{A} \;-\; \big\langle\mathbf{X}^\alpha_{\mathbb{L}\mathbb{Z},\mathbb{L}\mathbb{Z}}\big\rangle\,\tau_\mathrm{A} \\ +\;\Big\langle\big(\mathbf{R}^\alpha_{\mathbb{L}\mathbb{Z},\mathbb{N}\mathrm{A}} + \mathbf{X}^\alpha_{\mathbb{L}\mathbb{Z},\mathbb{N}\mathrm{A}}\big)\big(\mathbf{R}^\alpha_{\mathbb{N}\mathrm{A},\mathbb{N}\mathrm{A}} + \mathbf{X}^\alpha_{\mathbb{N}\mathrm{A},\mathbb{N}\mathrm{A}} + i\,\mathbf{L}_{\mathrm{Z},\,\mathbb{N}\mathrm{A},\mathbb{N}\mathrm{A}}\big)^{-1}\big(\mathbf{R}^\alpha_{\mathbb{N}\mathrm{A},\mathbb{L}\mathbb{Z}} + \mathbf{X}^\alpha_{\mathbb{N}\mathrm{A},\mathbb{L}\mathbb{Z}}\big)\Big\rangle\,\tau_\mathrm{A} . \tag{F.7}$$

It follows from Eqs. (14), (25) and (F.3) that $\mathbf{X}^\alpha_{\mathbb{L}\mathbb{Z},\mathbb{L}\mathbb{Z}} = \mathbf{X}^\alpha_{\mathbb{L}\mathbb{Z},\mathbb{N}\mathrm{A}} = \mathbf{X}^\alpha_{\mathbb{N}\mathrm{A},\mathbb{L}\mathbb{Z}} = \mathbf{0}$, whereby Eq. (F.6) simplifies to

$$\mathbf{G}^\mathrm{A}_{\mathbb{L}\mathbb{Z},\mathbb{L}\mathbb{Z}} \;=\; \mathbf{1} \;-\; \big\langle\mathbf{R}^\alpha_{\mathbb{L}\mathbb{Z},\mathbb{L}\mathbb{Z}}\big\rangle\,\tau_\mathrm{A} \;+\; \big\langle\mathbf{\Gamma}^\alpha_{\mathbb{L}\mathbb{Z},\mathbb{L}\mathbb{Z}}\big\rangle\,\tau_\mathrm{A} , \tag{F.8}$$

where

$$\mathbf{\Gamma}^\alpha_{\mathbb{L}\mathbb{Z},\mathbb{L}\mathbb{Z}} \;\equiv\; \mathbf{R}^\alpha_{\mathbb{L}\mathbb{Z},\mathbb{N}\mathrm{A}}\big(\mathbf{R}^\alpha_{\mathbb{N}\mathrm{A},\mathbb{N}\mathrm{A}} + \mathbf{X}^\alpha_{\mathbb{N}\mathrm{A},\mathbb{N}\mathrm{A}} + i\,\mathbf{L}_{\mathrm{Z},\,\mathbb{N}\mathrm{A},\mathbb{N}\mathrm{A}}\big)^{-1}\mathbf{R}^\alpha_{\mathbb{N}\mathrm{A},\mathbb{L}\mathbb{Z}} . \tag{F.9}$$

According to Eqs. (13) and (20), $\mathbf{R}^\alpha_{\mathbb{L}\mathbb{Z},\mathbb{N}\mathrm{A}}$ is nonzero only in the nonlabile single-spin subspace $\mathbb{N}_1$, so Eq. (F.9) becomes

$$\mathbf{\Gamma}^\alpha_{\mathbb{L}\mathbb{Z},\mathbb{L}\mathbb{Z}} \;=\; \mathbf{R}^\alpha_{\mathbb{L}\mathbb{Z},\mathbb{N}_1}\big(\mathbf{R}^\alpha_{\mathbb{N}\mathrm{A},\mathbb{N}\mathrm{A}} + \mathbf{X}^\alpha_{\mathbb{N}\mathrm{A},\mathbb{N}\mathrm{A}} + i\,\mathbf{L}_{\mathrm{Z},\,\mathbb{N}\mathrm{A},\mathbb{N}\mathrm{A}}\big)^{-1}_{\mathbb{N}_1\mathbb{N}_1}\mathbf{R}^\alpha_{\mathbb{N}_1,\mathbb{L}\mathbb{Z}} . \tag{F.10}$$

Decomposing the $\mathbb{N}\mathbb{A}$ subspace as $\mathbb{N}_1 + \mathbb{N}\mathbb{A}'$, we can write the inverse in Eq. (F.10) as

$$\big(\mathbf{R}^\alpha_{\mathbb{N}\mathrm{A},\mathbb{N}\mathrm{A}} + \mathbf{X}^\alpha_{\mathbb{N}\mathrm{A},\mathbb{N}\mathrm{A}} + i\,\mathbf{L}_{\mathrm{Z},\,\mathbb{N}\mathrm{A},\mathbb{N}\mathrm{A}}\big)^{-1}_{\mathbb{N}_1\mathbb{N}_1} \;=\; \big(\mathbf{R}^\alpha_{\mathbb{N}_1\mathbb{N}_1} + \mathbf{X}^\alpha_{\mathbb{N}_1\mathbb{N}_1} + i\,\mathbf{L}_{\mathrm{Z},\,\mathbb{N}_1\mathbb{N}_1} - \mathbf{Y}^\alpha_{\mathbb{N}_1\mathbb{N}_1}\big)^{-1} , \tag{F.11}$$

where

$$\mathbf{Y}^\alpha_{\mathbb{N}_1\mathbb{N}_1} \;\equiv\; \big(\mathbf{R}^\alpha_{\mathbb{N}_1,\mathbb{N}\mathrm{A}'} + \mathbf{X}^\alpha_{\mathbb{N}_1,\mathbb{N}\mathrm{A}'}\big)\big(\mathbf{R}^\alpha_{\mathbb{N}\mathrm{A}',\mathbb{N}\mathrm{A}'} + \mathbf{X}^\alpha_{\mathbb{N}\mathrm{A}',\mathbb{N}\mathrm{A}'} + i\,\mathbf{L}_{\mathrm{Z},\,\mathbb{N}\mathrm{A}',\mathbb{N}\mathrm{A}'}\big)^{-1}\big(\mathbf{R}^\alpha_{\mathbb{N}\mathrm{A}',\mathbb{N}_1} + \mathbf{X}^\alpha_{\mathbb{N}\mathrm{A}',\mathbb{N}_1}\big) . \tag{F.12}$$

According to Eqs. (F.10) and (F.11),

$$\mathbf{\Gamma}^{\alpha}_{\mathbb{LZ},\mathbb{LZ}} \;=\; \mathbf{R}^{\alpha}_{\mathbb{LZ},\mathbb{N}_1}\left(\mathbf{R}^{\alpha}_{\mathbb{N}_1\mathbb{N}_1} + \mathbf{X}^{\alpha}_{\mathbb{N}_1\mathbb{N}_1} - \mathbf{Y}^{\alpha}_{\mathbb{N}_1\mathbb{N}_1} + i\,\mathbf{L}_{\mathrm{Z},\,\mathbb{N}_1\mathbb{N}_1}\right)^{-1}\mathbf{R}^{\alpha}_{\mathbb{N}_1,\mathbb{LZ}}\,. \tag{F.13}$$

We shall now use symmetry arguments and the RMN approximation to simplify the supermatrices $\mathbf{X}^{\alpha}_{\mathbb{N}_1\mathbb{N}_1}$ and $\mathbf{Y}^{\alpha}_{\mathbb{N}_1\mathbb{N}_1}$.

Unlike $\mathbf{R}^{\alpha}_{\mathbb{N}_1\mathbb{N}_1}$, the $3m\times 3m$ supermatrix $\mathbf{X}^{\alpha}_{\mathbb{N}_1\mathbb{N}_1}$ is *not* block-diagonal in spin. However, any one of the m^2 3×3 blocks $\mathbf{X}^{\alpha}_{\mathbb{N}_1(\mu)\mathbb{N}_1(\nu)}$, associated with spins μ and ν, can be expressed on a generic form involving matrix elements of the same form for all spins. To show this, we use Eq. (F.3) to write

$$\mathbf{X}^{\alpha}_{\mathbb{N}_1\mathbb{N}_1} \;=\; \mathbf{\Delta}^{\alpha}_{\mathbb{N}_1\mathbb{S}}\left[\frac{1}{\tau_{\mathrm{A}}}\,\mathbf{K}_{\mathbb{SS}} + \mathbf{R}^{\alpha}_{\mathbb{SS}} + i\,\mathbf{L}_{\mathrm{Z},\,\mathbb{SS}}\right]^{-1}\mathbf{\Delta}^{\alpha}_{\mathbb{SN}_1}\,, \tag{F.14}$$

We now decompose the symmetric subspace as $\mathbb{S} = \mathbb{L}'\mathbb{S} + \mathbb{NS}$, where $\mathbb{L}' = \mathbb{L} + \mathbb{U}$ as before. Noting that $\mathbf{K}_{\mathbb{NS},\mathbb{NS}} = \mathbf{0}$ and that, according to Eqs. (14), (25) and (26), $\mathbf{\Delta}^{\alpha}_{\mathbb{N}_1,\mathbb{L}'\mathbb{S}} = \mathbf{0}$, we obtain from Eq. (F.14),

$$\begin{aligned}\mathbf{X}^{\alpha}_{\mathbb{N}_1\mathbb{N}_1} \;&=\; \mathbf{\Delta}^{\alpha}_{\mathbb{N}_1,\mathbb{NS}}\Big[\mathbf{R}^{\alpha}_{\mathbb{NS},\mathbb{NS}} + i\,\mathbf{L}_{\mathrm{Z},\,\mathbb{NS},\mathbb{NS}} \\ &\qquad - \mathbf{R}^{\alpha}_{\mathbb{NS},\mathbb{L}'\mathbb{S}}\left(\mathbf{1}_{\mathbb{L}'\mathbb{S},\mathbb{L}'\mathbb{S}}/\tau_{\mathrm{A}} + \mathbf{R}^{\alpha}_{\mathbb{L}'\mathbb{S},\mathbb{L}'\mathbb{S}} + i\,\mathbf{L}_{\mathrm{Z},\,\mathbb{L}'\mathbb{S},\mathbb{L}'\mathbb{S}}\right)^{-1}\mathbf{R}^{\alpha}_{\mathbb{L}'\mathbb{S},\mathbb{NS}}\Big]^{-1}\mathbf{\Delta}^{\alpha}_{\mathbb{NS},\mathbb{N}_1} \\ &=\; \mathbf{\Delta}^{\alpha}_{\mathbb{N}_1,\mathbb{NS}}\left(\mathbf{R}^{\alpha}_{\mathbb{NS},\mathbb{NS}} + i\,\mathbf{L}_{\mathrm{Z},\,\mathbb{NS},\mathbb{NS}}\right)^{-1}\mathbf{\Delta}^{\alpha}_{\mathbb{NS},\mathbb{N}_1}\,,\end{aligned} \tag{F.15}$$

where, in the last step, we have expanded to second order in $\omega_{\mathrm{D}}\tau_{\mathrm{A}}$ (consistent with the RMN approximation). Decomposing the $\mathbb{NS}$ subspace further as $\mathbb{N}_2 + \mathbb{NS}'$, we can partition Eq. (F.15) as

$$\mathbf{X}^{\alpha}_{\mathbb{N}_1\mathbb{N}_1} = \begin{bmatrix}\mathbf{\Delta}^{\alpha}_{\mathbb{N}_1\mathbb{N}_2} & \mathbf{\Delta}^{\alpha}_{\mathbb{N}_1,\mathbb{NS}'}\end{bmatrix}\begin{bmatrix}\mathbf{R}^{\alpha}_{\mathbb{N}_2\mathbb{N}_2} + i\,\mathbf{L}_{\mathrm{Z},\,\mathbb{N}_2\mathbb{N}_2} & \mathbf{R}^{\alpha}_{\mathbb{N}_2,\mathbb{NS}'} \\ \mathbf{R}^{\alpha}_{\mathbb{NS}',\mathbb{N}_2} & \mathbf{R}^{\alpha}_{\mathbb{NS}',\mathbb{NS}'} + i\,\mathbf{L}_{\mathrm{Z},\,\mathbb{NS}',\mathbb{NS}'}\end{bmatrix}^{-1}\begin{bmatrix}\mathbf{\Delta}^{\alpha}_{\mathbb{N}_2\mathbb{N}_1} \\ \mathbf{\Delta}^{\alpha}_{\mathbb{NS}',\mathbb{N}_1}\end{bmatrix}. \tag{F.16}$$

But $\mathbf{R}^{\alpha}_{\mathbb{N}_2,\mathbb{NS}'} = \mathbf{0}$ according to Eqs. (13) and (21), and $\mathbf{\Delta}^{\alpha}_{\mathbb{N}_1,\mathbb{NS}'} = \mathbf{0}$ according to Eqs. (14) and (27). Consequently, Eq. (F.16) reduces to

$$\mathbf{X}^{\alpha}_{\mathbb{N}_1\mathbb{N}_1} \;=\; \mathbf{\Delta}^{\alpha}_{\mathbb{N}_1\mathbb{N}_2}\left(\mathbf{R}^{\alpha}_{\mathbb{N}_2\mathbb{N}_2} + i\,\mathbf{L}_{\mathrm{Z},\,\mathbb{N}_2\mathbb{N}_2}\right)^{-1}\mathbf{\Delta}^{\alpha}_{\mathbb{N}_2\mathbb{N}_1}\,. \tag{F.17}$$

The dimensions of the $\mathbb{N}_1$ and $\mathbb{N}_2$ subspaces are $3\,m$ and $9\,m\,(m-1)/2$, respectively. Consider the 3×3 block $\mathbf{X}^{\alpha}_{\mathbb{N}_1(\mu)\mathbb{N}_1(\nu)}$ associated with the nonlabile spins μ and ν. Block-wise matrix multiplication in Eq. (F.17) yields

$$\mathbf{X}^{\alpha}_{\mathbb{N}_1(\mu)\mathbb{N}_1(\nu)} \;=\; \sum_{(\kappa\lambda)}\sum_{(\kappa'\lambda')}\mathbf{\Delta}^{\alpha}_{\mathbb{N}_1(\mu)\mathbb{N}_2(\kappa\lambda)}\left(\mathbf{R}^{\alpha}_{\mathbb{N}_2\mathbb{N}_2} + i\,\mathbf{L}_{\mathrm{Z},\,\mathbb{N}_2\mathbb{N}_2}\right)^{-1}_{\mathbb{N}_2(\kappa\lambda)\mathbb{N}_2(\kappa'\lambda')}\mathbf{\Delta}^{\alpha}_{\mathbb{N}_2(\kappa'\lambda')\mathbb{N}_1(\nu)}\,, \tag{F.18}$$

where each sum runs over the $m\,(m-1)/2$ distinct two-spin subspaces associated with different pairs of nonlabile spins (without regard to order). According to Eqs. (13) and (23a), the two-spin relaxation supermatrix $\mathbf{R}^{\alpha}_{\mathbb{N}_2\mathbb{N}_2}$ is block-diagonal in spin pairs, so

$\mathbf{R}^{\alpha}_{\mathbb{N}_2(\kappa\lambda)\mathbb{N}_2(\kappa'\lambda')} = \delta_{\kappa\lambda,\kappa'\lambda'}\,\mathbf{R}^{\alpha}_{\mathbb{N}_2(\kappa\lambda)\mathbb{N}_2(\kappa\lambda)}$. Furthermore, $\mathbf{L}_{\mathrm{Z},\,\mathbb{N}_2(\kappa\lambda)\mathbb{N}_2(\kappa'\lambda')} = \delta_{\kappa\lambda,\kappa'\lambda'}\,\omega_0\,\mathbf{Q}_2$ and, if the two-spin basis operators are ordered as in Table S1 of Appendix H,

$$\mathbf{Q}_2 \;=\; \mathrm{diag}(0\;0\;0\;1\;1\;{-1}\;{-1}\;2\;{-2})\,. \tag{F.19}$$

Thus,

$$\mathbf{X}^{\alpha}_{\mathbb{N}_1(\mu)\mathbb{N}_1(\nu)} \;=\; \sum_{(\kappa\lambda)} \boldsymbol{\Delta}^{\alpha}_{\mathbb{N}_1(\mu)\mathbb{N}_2(\kappa\lambda)} \left(\mathbf{R}^{\alpha}_{\mathbb{N}_2(\kappa\lambda)\mathbb{N}_2(\kappa\lambda)} + i\,\omega_0\,\mathbf{Q}_2\right)^{-1} \boldsymbol{\Delta}^{\alpha}_{\mathbb{N}_2(\kappa\lambda)\mathbb{N}_1(\nu)}\,. \tag{F.20}$$

This result can be further simplified with the aid of Eqs. (14) and (E.10). For off-diagonal blocks $\mathbf{X}^{\alpha}_{\mathbb{N}_1(\mu)\mathbb{N}_1(\nu)}$ with $\mu \neq \nu$, the spin pair $\kappa\lambda$ must contain both μ and ν so the only term in the sum that survives is the one with $\kappa\lambda = \mu\nu$. For diagonal blocks $\mathbf{X}^{\alpha}_{\mathbb{N}_1(\mu)\mathbb{N}_1(\mu)}$, one spin in the pair $\kappa\lambda$ must be μ whereas the other spin in the pair can be any of the remaining $(m-1)$ spins (except μ). Thus,

$$\mathbf{X}^{\alpha}_{\mathbb{N}_1(\mu)\mathbb{N}_1(\nu)} \;=\; \boldsymbol{\Delta}^{\alpha}_{\mathbb{N}_1(\mu)\mathbb{N}_2(\mu\nu)} \left(\mathbf{R}^{\alpha}_{\mathbb{N}_2(\mu\nu)\mathbb{N}_2(\mu\nu)} + i\,\omega_0\,\mathbf{Q}_2\right)^{-1} \boldsymbol{\Delta}^{\alpha\,\dagger}_{\mathbb{N}_1(\nu)\mathbb{N}_2(\mu\nu)}\,, \tag{F.21a}$$

$$\mathbf{X}^{\alpha}_{\mathbb{N}_1(\mu)\mathbb{N}_1(\mu)} \;=\; {\sum_{\nu=1}^{m}}' \boldsymbol{\Delta}^{\alpha}_{\mathbb{N}_1(\mu)\mathbb{N}_2(\mu\nu)} \left(\mathbf{R}^{\alpha}_{\mathbb{N}_2(\mu\nu)\mathbb{N}_2(\mu\nu)} + i\,\omega_0\,\mathbf{Q}_2\right)^{-1} \boldsymbol{\Delta}^{\alpha\,\dagger}_{\mathbb{N}_1(\mu)\mathbb{N}_2(\mu\nu)}\,, \tag{F.21b}$$

where $\mu \neq \nu$ in both equations, as indicated by the prime in Eq. (F.21b). Here, we have also noted that $\boldsymbol{\Delta}^{\alpha}_{\mathbb{N}_2(\mu\nu)\mathbb{N}_1(\nu)} = \boldsymbol{\Delta}^{\alpha\,\dagger}_{\mathbb{N}_1(\nu)\mathbb{N}_2(\mu\nu)}$ since $\boldsymbol{\Delta}^{\alpha}$ in Eq. (14) is Hermitian.

Equation (F.21) shows that each of the m^2 3×3 blocks of the $3m\times 3m$ matrix $\mathbf{X}^{\alpha}_{\mathbb{N}_1\mathbb{N}_1}$ can be computed from the 3×9 matrices $\boldsymbol{\Delta}^{\alpha}_{\mathbb{N}_1(\mu)\mathbb{N}_2(\mu\nu)}$ and the 9×9 matrices $\mathbf{R}^{\alpha}_{\mathbb{N}_2(\mu\nu)\mathbb{N}_2(\mu\nu)}$. It follows from Eqs. (14) and (E.10) that $\boldsymbol{\Delta}^{\alpha}_{\mathbb{N}_1(\mu)\mathbb{N}_2(\mu\nu)}$ and $\boldsymbol{\Delta}^{\alpha}_{\mathbb{N}_1(\nu)\mathbb{N}_2(\mu\nu)}$ only involve the static dipole coupling $\omega_{\mathrm{D},\,\mu\nu}$ between nonlabile spins μ and ν. Thus, while the off-diagonal $(\mu \neq \nu)$ block $\mathbf{X}^{\alpha}_{\mathbb{N}_1(\mu)\mathbb{N}_1(\nu)}$ only involves $\omega_{\mathrm{D},\,\mu\nu}$, the diagonal block $\mathbf{X}^{\alpha}_{\mathbb{N}_1(\mu)\mathbb{N}_1(\mu)}$ involves all static dipole couplings with spin μ.

We now turn to the supermatrix $\mathbf{Y}^{\alpha}_{\mathbb{N}_1\mathbb{N}_1}$ in Eq. (F.12). It follows from Eqs. (13) and (20) that $\mathbf{R}^{\alpha}_{\mathbb{N}_1,\mathbb{N}\mathbb{A}'} = \mathbf{R}^{\alpha}_{\mathbb{N}\mathbb{A}',\mathbb{N}_1} = \mathbf{0}$, so Eq. (F.12) reduces to

$$\mathbf{Y}^{\alpha}_{\mathbb{N}_1\mathbb{N}_1} \;=\; \mathbf{X}^{\alpha}_{\mathbb{N}_1,\mathbb{N}\mathbb{A}'} \left(\mathbf{R}^{\alpha}_{\mathbb{N}\mathbb{A}',\mathbb{N}\mathbb{A}'} + \mathbf{X}^{\alpha}_{\mathbb{N}\mathbb{A}',\mathbb{N}\mathbb{A}'} + i\,\mathbf{L}_{\mathrm{Z},\,\mathbb{N}\mathbb{A}',\mathbb{N}\mathbb{A}'}\right)^{-1} \mathbf{X}^{\alpha}_{\mathbb{N}\mathbb{A}',\mathbb{N}_1}\,. \tag{F.22}$$

To simplify this expression, we examine the quantity $\mathbf{X}^{\alpha}_{\mathbb{N}_1,\mathbb{N}\mathbb{A}'}$, given by Eq. (F.3) as

$$\mathbf{X}^{\alpha}_{\mathbb{N}_1,\mathbb{N}\mathbb{A}'} \;=\; \boldsymbol{\Delta}^{\alpha}_{\mathbb{N}_1\mathbb{S}} \left(\mathbf{K}_{\mathbb{S}\mathbb{S}}/\tau_{\mathrm{A}} + \mathbf{R}^{\alpha}_{\mathbb{S}\mathbb{S}} + i\,\mathbf{L}_{\mathrm{Z},\,\mathbb{S}\mathbb{S}}\right)^{-1} \boldsymbol{\Delta}^{\alpha}_{\mathbb{S},\mathbb{N}\mathbb{A}'}\,. \tag{F.23}$$

According to Eqs. (14), (27) and (28),

$$\boldsymbol{\Delta}^{\alpha}_{\mathbb{N}_1\mathbb{S}} \;=\; \boldsymbol{\Delta}^{\alpha}_{\mathbb{N}_1\mathbb{N}_2}\,, \tag{F.24}$$

and

$$\boldsymbol{\Delta}^{\alpha}_{\mathbb{S},\mathbb{N}\mathbb{A}'} \;=\; \boldsymbol{\Delta}^{\alpha}_{\mathbb{N}_{2k},\mathbb{N}\mathbb{A}'} \;=\; \begin{cases} \boldsymbol{\Delta}^{\alpha}_{\mathbb{N}_2\mathbb{N}_3} & ,\quad \text{for } k=1 \\ \boldsymbol{\Delta}^{\alpha}_{\mathbb{N}_{2k}\mathbb{N}_{2k\pm1}} & ,\quad \text{for } k\geq 2 \end{cases}\,. \tag{F.25}$$

Combination of Eqs. (F.23) – (F.25) yields

$$\mathbf{X}^{\alpha}_{\mathbb{N}_1,\mathbb{N}\mathbb{A}'} \;=\; \boldsymbol{\Delta}^{\alpha}_{\mathbb{N}_1\mathbb{N}_2} \left[\sum_{k=1}^{\left[\frac{m-1}{2}\right]} \boldsymbol{\Xi}^{\alpha}_{\mathbb{N}_2\mathbb{N}_{2k}}\,\boldsymbol{\Delta}^{\alpha}_{\mathbb{N}_{2k}\mathbb{N}_{2k+1}} \;+\; \sum_{k=2}^{\left[\frac{m}{2}\right]} \boldsymbol{\Xi}^{\alpha}_{\mathbb{N}_2\mathbb{N}_{2k}}\,\boldsymbol{\Delta}^{\alpha}_{\mathbb{N}_{2k}\mathbb{N}_{2k-1}}\right]\,, \tag{F.26}$$

where the upper limit of the sums is the largest integer contained in $(m-1)/2$ or in $m/2$, respectively. Thus, for example,

$$\mathbf{X}^{\alpha}_{\mathbb{N}_1,\mathbb{N}\mathbb{A}'}(m=2) \;=\; 0\,, \tag{F.27a}$$

$$\mathbf{X}^{\alpha}_{\mathbb{N}_1,\mathbb{N}\mathbb{A}'}(m=3) \;=\; \mathbf{\Delta}^{\alpha}_{\mathbb{N}_1\mathbb{N}_2}\mathbf{\Xi}^{\alpha}_{\mathbb{N}_2\mathbb{N}_2}\mathbf{\Delta}^{\alpha}_{\mathbb{N}_2\mathbb{N}_3}\,, \tag{F.27b}$$

$$\mathbf{X}^{\alpha}_{\mathbb{N}_1,\mathbb{N}\mathbb{A}'}(m=4) \;=\; \mathbf{\Delta}^{\alpha}_{\mathbb{N}_1\mathbb{N}_2}\mathbf{\Xi}^{\alpha}_{\mathbb{N}_2\mathbb{N}_2}\mathbf{\Delta}^{\alpha}_{\mathbb{N}_2\mathbb{N}_3} + \mathbf{\Delta}^{\alpha}_{\mathbb{N}_1\mathbb{N}_2}\mathbf{\Xi}^{\alpha}_{\mathbb{N}_2\mathbb{N}_4}\mathbf{\Delta}^{\alpha}_{\mathbb{N}_4\mathbb{N}_5}\,, \tag{F.27c}$$

showing that $\mathbf{Y}^{\alpha}_{\mathbb{N}_1\mathbb{N}_1} = \mathbf{0}$ for the $IP_2{-}I$ and $ISP_2{-}IS$ cases. Furthermore,

$$\mathbf{\Xi}^{\alpha} \;\equiv\; \tau_{\mathrm{A}}\,(\mathbf{U}^{\alpha}_{\mathbb{S}\mathbb{S}})^{-1}\,, \tag{F.28}$$

$$\mathbf{U}^{\alpha}_{\mathbb{S}\mathbb{S}} \;\equiv\; \mathbf{K}_{\mathbb{S}\mathbb{S}} + \mathbf{R}^{\alpha}_{\mathbb{S}\mathbb{S}}\,\tau_{\mathrm{A}} + i\,\mathbf{L}_{\mathrm{Z},\mathbb{S}\mathbb{S}}\,\tau_{\mathrm{A}}\,. \tag{F.29}$$

We decompose the even-parity subspace as $\mathbb{S} = \mathbb{N}\mathbb{S} + \mathbb{L}'\mathbb{S}$, with $\mathbb{N}\mathbb{S} = \mathbb{N}_2 + \mathbb{N}_4 + \ldots$ comprising the even parity subspaces containing only nonlabile spins and the remaining subspace $\mathbb{L}'\mathbb{S} = \mathbb{L} + \mathbb{U}$ including even-parity mixed labile/nonlabile subspaces ($\mathbb{U}_2$, $\mathbb{U}_4$, etc) and, if the spin system contains two labile spins, also the labile two-spin subspace $\mathbb{L}_2$. Accordingly, we partition the supermatrix $\mathbf{U}^{\alpha}_{\mathbb{S}\mathbb{S}}$ in Eq. (F.29) as

$$\mathbf{U}^{\alpha}_{\mathbb{S}\mathbb{S}} \;=\; \begin{bmatrix} (\mathbf{R}^{\alpha}_{\mathbb{N}\mathbb{S},\mathbb{N}\mathbb{S}}\,\tau_{\mathrm{A}} + i\,\mathbf{L}_{\mathrm{Z},\mathbb{N}\mathbb{S},\mathbb{N}\mathbb{S}}\,\tau_{\mathrm{A}}) & \mathbf{R}^{\alpha}_{\mathbb{N}\mathbb{S},\mathbb{L}'\mathbb{S}}\,\tau_{\mathrm{A}} \\ \mathbf{R}^{\alpha}_{\mathbb{L}'\mathbb{S},\mathbb{N}\mathbb{S}}\,\tau_{\mathrm{A}} & (\mathbf{1} + \mathbf{R}^{\alpha}_{\mathbb{L}'\mathbb{S},\mathbb{L}'\mathbb{S}}\,\tau_{\mathrm{A}} + i\,\mathbf{L}_{\mathrm{Z},\mathbb{L}'\mathbb{S},\mathbb{L}'\mathbb{S}}\,\tau_{\mathrm{A}}) \end{bmatrix}. \tag{F.30}$$

The $(\mathbb{N}\mathbb{S},\mathbb{N}\mathbb{S})$ block of the inverse of this matrix is

$$\begin{aligned}(\mathbf{U}^{\alpha}_{\mathbb{S}\mathbb{S}})^{-1}_{\mathbb{N}\mathbb{S},\mathbb{N}\mathbb{S}} \;=\; \Big(&\mathbf{R}^{\alpha}_{\mathbb{N}\mathbb{S},\mathbb{N}\mathbb{S}}\,\tau_{\mathrm{A}} + i\,\mathbf{L}_{\mathrm{Z},\mathbb{N}\mathbb{S},\mathbb{N}\mathbb{S}}\,\tau_{\mathrm{A}} \\ &-\; \mathbf{R}^{\alpha}_{\mathbb{N}\mathbb{S},\mathbb{L}'\mathbb{S}}\,\tau_{\mathrm{A}}(\mathbf{1} + \mathbf{R}^{\alpha}_{\mathbb{L}'\mathbb{S},\mathbb{L}'\mathbb{S}}\,\tau_{\mathrm{A}} + i\,\mathbf{L}_{\mathrm{Z},\mathbb{L}'\mathbb{S},\mathbb{L}'\mathbb{S}}\,\tau_{\mathrm{A}})^{-1}\mathbf{R}^{\alpha}_{\mathbb{L}'\mathbb{S},\mathbb{N}\mathbb{S}}\,\tau_{\mathrm{A}}\Big)^{-1}\,.\end{aligned} \tag{F.31}$$

We now apply the MN approximation again by truncating the expansion of $(\mathbf{1}+\mathbf{R}^{\alpha}_{\mathbb{L}'\mathbb{S},\mathbb{L}'\mathbb{S}}\,\tau_{\mathrm{A}}+ i\,\mathbf{L}_{\mathrm{Z},\mathbb{L}'\mathbb{S},\mathbb{L}'\mathbb{S}}\,\tau_{\mathrm{A}})^{-1}$ after second order in $\omega_{\mathrm{D}}\tau_{\mathrm{A}}$,

$$(\mathbf{1} + \mathbf{R}^{\alpha}_{\mathbb{L}'\mathbb{S},\mathbb{L}'\mathbb{S}}\,\tau_{\mathrm{A}} + i\,\mathbf{L}_{\mathrm{Z},\mathbb{L}'\mathbb{S},\mathbb{L}'\mathbb{S}}\,\tau_{\mathrm{A}})^{-1} \;=\; \mathbf{Z} \;-\; \mathbf{Z}\,\mathbf{R}^{\alpha}_{\mathbb{L}'\mathbb{S},\mathbb{L}'\mathbb{S}}\,\tau_{\mathrm{A}}\,\mathbf{Z} \;+\; \mathcal{O}\left((\omega_{\mathrm{D}}\tau_{\mathrm{A}})^4\right)\,, \tag{F.32}$$

where $\mathbf{Z} \equiv (\mathbf{1} + i\,\mathbf{L}_{\mathrm{Z},\mathbb{L}'\mathbb{S},\mathbb{L}'\mathbb{S}}\,\tau_{\mathrm{A}})^{-1}$. Inserting this result into Eq. (F.31), we get

$$\begin{aligned}(\mathbf{U}^{\alpha}_{\mathbb{S}\mathbb{S}})^{-1}_{\mathbb{N}\mathbb{S},\mathbb{N}\mathbb{S}} \;=\; \Big(&\mathbf{R}^{\alpha}_{\mathbb{N}\mathbb{S},\mathbb{N}\mathbb{S}}\,\tau_{\mathrm{A}} + i\,\mathbf{L}_{\mathrm{Z},\mathbb{N}\mathbb{S},\mathbb{N}\mathbb{S}}\,\tau_{\mathrm{A}} \;-\; \mathbf{R}^{\alpha}_{\mathbb{N}\mathbb{S},\mathbb{L}'\mathbb{S}}\,\tau_{\mathrm{A}}\,\mathbf{Z}\,\mathbf{R}^{\alpha}_{\mathbb{L}'\mathbb{S},\mathbb{N}\mathbb{S}}\,\tau_{\mathrm{A}} \\ &-\; \mathbf{R}^{\alpha}_{\mathbb{N}\mathbb{S},\mathbb{L}'\mathbb{S}}\,\tau_{\mathrm{A}}\,\mathbf{Z}\,\mathbf{R}^{\alpha}_{\mathbb{L}'\mathbb{S},\mathbb{L}'\mathbb{S}}\,\tau_{\mathrm{A}}\,\mathbf{Z}\,\mathbf{R}^{\alpha}_{\mathbb{L}'\mathbb{S},\mathbb{N}\mathbb{S}}\,\tau_{\mathrm{A}}\Big)^{-1}\,.\end{aligned} \tag{F.33}$$

The last two terms are of order $(\omega_{\mathrm{D}}\tau_{\mathrm{A}})^4$ and $(\omega_{\mathrm{D}}\tau_{\mathrm{A}})^6$, respectively, and they can therefore be neglected in the MN regime. Consequently,

$$(\mathbf{U}^{\alpha}_{\mathbb{S}\mathbb{S}})^{-1}_{\mathbb{N}\mathbb{S},\mathbb{N}\mathbb{S}} \;=\; \left(\mathbf{R}^{\alpha}_{\mathbb{N}\mathbb{S},\mathbb{N}\mathbb{S}}\,\tau_{\mathrm{A}} + i\,\mathbf{L}_{\mathrm{Z},\mathbb{N}\mathbb{S},\mathbb{N}\mathbb{S}}\,\tau_{\mathrm{A}}\right)^{-1}\,. \tag{F.34}$$

According to Eqs. (13) and (21), the supermatrix $\mathbf{R}^{\alpha}_{\mathbb{N}\mathbb{S},\mathbb{N}\mathbb{S}}$ is block-diagonal with matrices $\mathbf{R}^{\alpha}_{\mathbb{N}_k\mathbb{N}_k}$ on the diagonal. Furthermore, $\mathbf{L}_{\mathrm{Z},\mathbb{N}\mathbb{S},\mathbb{N}\mathbb{S}}$ is purely diagonal. The matrix

$(\mathbf{U}^{\alpha}_{\mathbb{S}\mathbb{S}})^{-1}_{\mathbb{N}\mathbb{S},\mathbb{N}\mathbb{S}}$ is therefore also block-diagonal with diagonal blocks $(\mathbf{R}^{\alpha}_{\mathbb{N}_k\mathbb{N}_k}\tau_{\mathrm{A}} + i\,\mathbf{L}_{\mathrm{Z},\mathbb{N}_k\mathbb{N}_k}\tau_{\mathrm{A}})^{-1}$. Consequently,

$$\mathbf{\Xi}^{\alpha}_{\mathbb{N}_2\mathbb{N}_{2k}} \;=\; \tau_{\mathrm{A}}\,(\mathbf{U}^{\alpha}_{\mathbb{S}\mathbb{S}})^{-1}_{\mathbb{N}_2\mathbb{N}_{2k}} \;=\; \delta_{k1}\,\tau_{\mathrm{A}}\,(\mathbf{U}^{\alpha}_{\mathbb{S}\mathbb{S}})^{-1}_{\mathbb{N}_2\mathbb{N}_2} \;=\; \delta_{k1}\,(\mathbf{R}^{\alpha}_{\mathbb{N}_2\mathbb{N}_2} + i\,\mathbf{L}_{\mathrm{Z},\mathbb{N}_2\mathbb{N}_2})^{-1}\,, \tag{F.35}$$

which is substituted into Eq. (F.26) to give, for $k = 3,\,5,\,\ldots$,

$$\mathbf{X}^{\alpha}_{\mathbb{N}_1,\mathbb{N}_k} \;=\; \begin{cases} 0 \quad , & \text{if } m < 3 \\ \delta_{k3}\,\mathbf{\Delta}^{\alpha}_{\mathbb{N}_1\mathbb{N}_2}\,(\mathbf{R}^{\alpha}_{\mathbb{N}_2\mathbb{N}_2} + i\,\mathbf{L}_{\mathrm{Z},\mathbb{N}_2\mathbb{N}_2})^{-1}\mathbf{\Delta}^{\alpha}_{\mathbb{N}_2\mathbb{N}_3} \quad , & \text{if } m \geq 3\,. \end{cases} \tag{F.36}$$

Note that the second sum in Eq. (F.26), starting with $k = 2$, does not contribute to $\mathbf{X}^{\alpha}_{\mathbb{N}_1,\mathbb{N}_k}$. In the same way, we obtain, for $k = 3,\,5,\,\ldots$,

$$\mathbf{X}^{\alpha}_{\mathbb{N}_k,\mathbb{N}_1} \;=\; \begin{cases} 0 \quad , & \text{if } m < 3 \\ \delta_{k3}\,\mathbf{\Delta}^{\alpha}_{\mathbb{N}_3\mathbb{N}_2}\,(\mathbf{R}^{\alpha}_{\mathbb{N}_2\mathbb{N}_2} + i\,\mathbf{L}_{\mathrm{Z},\mathbb{N}_2\mathbb{N}_2})^{-1}\mathbf{\Delta}^{\alpha}_{\mathbb{N}_2\mathbb{N}_1} \quad , & \text{if } m \geq 3\,. \end{cases} \tag{F.37}$$

In view of Eqs. (F.36) and (F.37), it follows from Eq. (F.22) that $\mathbf{Y}^{\alpha}_{\mathbb{N}_1\mathbb{N}_1} = 0$ for $m < 3$ as already noted below Eq. (F.27), whereas, for $m \geq 3$,

$$\begin{aligned} \mathbf{Y}^{\alpha}_{\mathbb{N}_1\mathbb{N}_1} \;&=\; \mathbf{\Delta}^{\alpha}_{\mathbb{N}_1\mathbb{N}_2}\,(\mathbf{R}^{\alpha}_{\mathbb{N}_2\mathbb{N}_2} + i\,\mathbf{L}_{\mathrm{Z},\mathbb{N}_2\mathbb{N}_2})^{-1}\mathbf{\Delta}^{\alpha}_{\mathbb{N}_2\mathbb{N}_3} \\ &\times \big(\mathbf{R}^{\alpha}_{\mathbb{N}\mathbb{A}',\mathbb{N}\mathbb{A}'} + \mathbf{X}^{\alpha}_{\mathbb{N}\mathbb{A}',\mathbb{N}\mathbb{A}'} + i\,\mathbf{L}_{\mathrm{Z},\,\mathbb{N}\mathbb{A}',\mathbb{N}\mathbb{A}'}\big)^{-1}_{\mathbb{N}_3\mathbb{N}_3}\,\mathbf{\Delta}^{\alpha}_{\mathbb{N}_3\mathbb{N}_2}\,(\mathbf{R}^{\alpha}_{\mathbb{N}_2\mathbb{N}_2} + i\,\mathbf{L}_{\mathrm{Z},\mathbb{N}_2\mathbb{N}_2})^{-1}\mathbf{\Delta}^{\alpha}_{\mathbb{N}_2\mathbb{N}_1}\,. \end{aligned} \tag{F.38}$$

Now consider the matrix $\mathbf{M}^{\alpha}_{\mathbb{N}\mathbb{A}',\mathbb{N}\mathbb{A}'} \equiv \mathbf{R}^{\alpha}_{\mathbb{N}\mathbb{A}',\mathbb{N}\mathbb{A}'} + \mathbf{X}^{\alpha}_{\mathbb{N}\mathbb{A}',\mathbb{N}\mathbb{A}'} + i\,\mathbf{L}_{\mathrm{Z},\,\mathbb{N}\mathbb{A}',\mathbb{N}\mathbb{A}'}$. The Zeeman Liouvillian $\mathbf{L}_{\mathrm{Z},\,\mathbb{N}\mathbb{A}',\mathbb{N}\mathbb{A}'}$ is completely diagonal, whereas $\mathbf{R}^{\alpha}_{\mathbb{N}\mathbb{A}',\mathbb{N}\mathbb{A}'}$ is block-diagonal according to Eqs. (13) and (21). However, as we shall now show, $\mathbf{X}^{\alpha}_{\mathbb{N}\mathbb{A}',\mathbb{N}\mathbb{A}'}$ is *not* block-diagonal. In analogy with Eq. (F.23),

$$\mathbf{X}^{\alpha}_{\mathbb{N}\mathbb{A}',\mathbb{N}\mathbb{A}'} \;=\; \mathbf{\Delta}^{\alpha}_{\mathbb{N}\mathbb{A}',\mathbb{S}}\,(\mathbf{K}_{\mathbb{S}\mathbb{S}}/\tau_{\mathrm{A}} + \mathbf{R}^{\alpha}_{\mathbb{S}\mathbb{S}} + i\,\mathbf{L}_{\mathrm{Z},\,\mathbb{S}\mathbb{S}})^{-1}\mathbf{\Delta}^{\alpha}_{\mathbb{S},\mathbb{N}\mathbb{A}'}\,. \tag{F.39}$$

Using the selection rule for $\mathbf{\Delta}^{\alpha}_{\mathbb{S},\mathbb{N}\mathbb{A}'}$ in Eq. (F.25) and the corresponding relation for $\mathbf{\Delta}^{\alpha}_{\mathbb{N}\mathbb{A}',\mathbb{S}}$, we obtain for $m \geq 3$

$$\begin{aligned} \mathbf{X}^{\alpha}_{\mathbb{N}_{2k+1}\mathbb{N}_{2l+1}} \;&=\; \mathbf{\Delta}^{\alpha}_{\mathbb{N}_{2k+1}\mathbb{N}_{2k}}\Big[\mathbf{\Xi}^{\alpha}_{\mathbb{N}_{2k}\mathbb{N}_{2l}}\,\mathbf{\Delta}^{\alpha}_{\mathbb{N}_{2l}\mathbb{N}_{2l+1}} + \mathbf{\Xi}^{\alpha}_{\mathbb{N}_{2k}\mathbb{N}_{2l+2}}\,\mathbf{\Delta}^{\alpha}_{\mathbb{N}_{2l+2}\mathbb{N}_{2l+1}}\Big] \\ &\quad + \mathbf{\Delta}^{\alpha}_{\mathbb{N}_{2k+1}\mathbb{N}_{2k+2}}\Big[\mathbf{\Xi}^{\alpha}_{\mathbb{N}_{2k+2}\mathbb{N}_{2l}}\,\mathbf{\Delta}^{\alpha}_{\mathbb{N}_{2l}\mathbb{N}_{2l+1}} + \mathbf{\Xi}^{\alpha}_{\mathbb{N}_{2k+2}\mathbb{N}_{2l+2}}\,\mathbf{\Delta}^{\alpha}_{\mathbb{N}_{2l+2}\mathbb{N}_{2l+1}}\Big]\,, \end{aligned} \tag{F.40}$$

with $\mathbf{\Xi}^{\alpha}$ defined by Eqs. (F.28) and (F.29). It follows from Eqs. (F.30) – (F.35) that

$$\mathbf{\Xi}^{\alpha}_{\mathbb{N}_{2k}\mathbb{N}_{2l}} \;=\; \delta_{lk}\,\mathbf{\Xi}^{\alpha}_{\mathbb{N}_{2k}\mathbb{N}_{2k}} \;=\; \delta_{lk}\,(\mathbf{R}^{\alpha}_{\mathbb{N}_{2k}\mathbb{N}_{2k}} + i\,\mathbf{L}_{\mathrm{Z},\mathbb{N}_{2k}\mathbb{N}_{2k}})^{-1}\,, \tag{F.41}$$

which is combined with Eq. (F.40) to give

$$\begin{aligned} \mathbf{X}^{\alpha}_{\mathbb{N}_{2k+1}\mathbb{N}_{2l+1}} \;&=\; \delta_{lk}\Big[\mathbf{\Delta}^{\alpha}_{\mathbb{N}_{2k+1}\mathbb{N}_{2k}}\,\mathbf{\Xi}^{\alpha}_{\mathbb{N}_{2k}\mathbb{N}_{2k}}\,\mathbf{\Delta}^{\alpha}_{\mathbb{N}_{2k}\mathbb{N}_{2k+1}} + \mathbf{\Delta}^{\alpha}_{\mathbb{N}_{2k+1}\mathbb{N}_{2k+2}}\,\mathbf{\Xi}^{\alpha}_{\mathbb{N}_{2k+2}\mathbb{N}_{2k+2}}\,\mathbf{\Delta}^{\alpha}_{\mathbb{N}_{2k+2}\mathbb{N}_{2k+1}}\Big] \\ &+\; \delta_{l,k-1}\,\mathbf{\Delta}^{\alpha}_{\mathbb{N}_{2k+1}\mathbb{N}_{2k}}\,\mathbf{\Xi}^{\alpha}_{\mathbb{N}_{2k}\mathbb{N}_{2k}}\,\mathbf{\Delta}^{\alpha}_{\mathbb{N}_{2k}\mathbb{N}_{2k-1}} \;+\; \delta_{l,k+1}\,\mathbf{\Delta}^{\alpha}_{\mathbb{N}_{2k+1}\mathbb{N}_{2k+2}}\,\mathbf{\Xi}^{\alpha}_{\mathbb{N}_{2k+2}\mathbb{N}_{2k+2}}\,\mathbf{\Delta}^{\alpha}_{\mathbb{N}_{2k+2}\mathbb{N}_{2k+3}}\,. \end{aligned} \tag{F.42}$$

The supermatrix $\mathbf{X}^{\alpha}_{\mathbb{N}\mathbb{A}',\mathbb{N}\mathbb{A}'}$ thus has a block-tridiagonal structure, as does the supermatrix $\mathbf{M}^{\alpha}_{\mathbb{N}\mathbb{A}',\mathbb{N}\mathbb{A}'}$ in Eq. (F.38). To obtain the $\mathbb{N}_3\mathbb{N}_3$ block of the inverse $(\mathbf{M}^{\alpha}_{\mathbb{N}\mathbb{A}',\mathbb{N}\mathbb{A}'})^{-1}$ we must invert the full matrix (not just the diagonal blocks). The block-dimension of $\mathbf{M}^{\alpha}_{\mathbb{N}\mathbb{A}',\mathbb{N}\mathbb{A}'}$ is $[(m-1)/2]$, that is, the smallest integer contained in $(m-1)/2$. For $m=3$ or $m=4$, the supermatrix $\mathbf{M}^{\alpha}_{\mathbb{N}\mathbb{A}',\mathbb{N}\mathbb{A}'}$ thus contains a single block,

$$\mathbf{M}^{\alpha}_{\mathbb{N}\mathbb{A}',\mathbb{N}\mathbb{A}'} \;=\; \mathbf{M}^{\alpha}_{\mathbb{N}_3\mathbb{N}_3} \;=\; \mathbf{R}^{\alpha}_{\mathbb{N}_3\mathbb{N}_3} + \mathbf{X}^{\alpha}_{\mathbb{N}_3\mathbb{N}_3} + i\,\mathbf{L}_{\mathrm{Z},\,\mathbb{N}_3\mathbb{N}_3}\,, \quad \text{for} \quad m=3 \text{ or } 4\,, \tag{F.43}$$

with

$$\mathbf{X}^{\alpha}_{\mathbb{N}_3\mathbb{N}_3} \;=\; \begin{cases} \boldsymbol{\Delta}^{\alpha}_{\mathbb{N}_3\mathbb{N}_2}\,\boldsymbol{\Xi}^{\alpha}_{\mathbb{N}_2\mathbb{N}_2}\,\boldsymbol{\Delta}^{\alpha}_{\mathbb{N}_2\mathbb{N}_3}\,, & \text{for} \quad m=3 \\ \boldsymbol{\Delta}^{\alpha}_{\mathbb{N}_3\mathbb{N}_2}\,\boldsymbol{\Xi}^{\alpha}_{\mathbb{N}_2\mathbb{N}_2}\,\boldsymbol{\Delta}^{\alpha}_{\mathbb{N}_2\mathbb{N}_3} \;+\; \boldsymbol{\Delta}^{\alpha}_{\mathbb{N}_3\mathbb{N}_4}\,\boldsymbol{\Xi}^{\alpha}_{\mathbb{N}_4\mathbb{N}_4}\,\boldsymbol{\Delta}^{\alpha}_{\mathbb{N}_4\mathbb{N}_3}\,, & \text{for} \quad m=4 \end{cases}. \tag{F.44}$$

For $m=5$ or $m=6$, the supermatrix $\mathbf{M}^{\alpha}_{\mathbb{N}\mathbb{A}',\mathbb{N}\mathbb{A}'}$ has a 2×2 block structure,

$$\mathbf{M}^{\alpha}_{\mathbb{N}\mathbb{A}',\mathbb{N}\mathbb{A}'} \;=\; \begin{bmatrix} (\mathbf{R}^{\alpha}_{\mathbb{N}_3\mathbb{N}_3} + \mathbf{X}^{\alpha}_{\mathbb{N}_3\mathbb{N}_3} + i\,\mathbf{L}_{\mathrm{Z},\,\mathbb{N}_3\mathbb{N}_3}) & \mathbf{X}^{\alpha}_{\mathbb{N}_3\mathbb{N}_5} \\ \mathbf{X}^{\alpha}_{\mathbb{N}_5\mathbb{N}_3} & (\mathbf{R}^{\alpha}_{\mathbb{N}_5\mathbb{N}_5} + \mathbf{X}^{\alpha}_{\mathbb{N}_5\mathbb{N}_5} + i\,\mathbf{L}_{\mathrm{Z},\,\mathbb{N}_5\mathbb{N}_5}) \end{bmatrix}, \tag{F.45}$$

where $\mathbf{X}^{\alpha}_{\mathbb{N}_3\mathbb{N}_3}$ has the same form as for $m=4$ (this form is valid for all $m\geq 4$),

$$\mathbf{X}^{\alpha}_{\mathbb{N}_3\mathbb{N}_5} \;=\; \boldsymbol{\Delta}^{\alpha}_{\mathbb{N}_3\mathbb{N}_4}\,\boldsymbol{\Xi}^{\alpha}_{\mathbb{N}_4\mathbb{N}_4}\,\boldsymbol{\Delta}^{\alpha}_{\mathbb{N}_4\mathbb{N}_5}\,, \tag{F.46a}$$

$$\mathbf{X}^{\alpha}_{\mathbb{N}_5\mathbb{N}_3} \;=\; \boldsymbol{\Delta}^{\alpha}_{\mathbb{N}_5\mathbb{N}_4}\,\boldsymbol{\Xi}^{\alpha}_{\mathbb{N}_4\mathbb{N}_4}\,\boldsymbol{\Delta}^{\alpha}_{\mathbb{N}_4\mathbb{N}_3}\,, \tag{F.46b}$$

and

$$\mathbf{X}^{\alpha}_{\mathbb{N}_5\mathbb{N}_5} \;=\; \begin{cases} \boldsymbol{\Delta}^{\alpha}_{\mathbb{N}_5\mathbb{N}_4}\,\boldsymbol{\Xi}^{\alpha}_{\mathbb{N}_4\mathbb{N}_4}\,\boldsymbol{\Delta}^{\alpha}_{\mathbb{N}_4\mathbb{N}_5}\,, & \text{for} \quad m=5 \\ \boldsymbol{\Delta}^{\alpha}_{\mathbb{N}_5\mathbb{N}_4}\,\boldsymbol{\Xi}^{\alpha}_{\mathbb{N}_4\mathbb{N}_4}\,\boldsymbol{\Delta}^{\alpha}_{\mathbb{N}_4\mathbb{N}_5} \;+\; \boldsymbol{\Delta}^{\alpha}_{\mathbb{N}_5\mathbb{N}_6}\,\boldsymbol{\Xi}^{\alpha}_{\mathbb{N}_6\mathbb{N}_6}\,\boldsymbol{\Delta}^{\alpha}_{\mathbb{N}_6\mathbb{N}_5}\,, & \text{for} \quad m=6 \end{cases}. \tag{F.47}$$

For $m=5$ or $m=6$, the inverse of $\mathbf{M}^{\alpha}_{\mathbb{N}\mathbb{A}',\mathbb{N}\mathbb{A}'}$ in Eq. (F.38) is obtained from Eq. (F.45) as

$$(\mathbf{M}^{\alpha}_{\mathbb{N}\mathbb{A}',\mathbb{N}\mathbb{A}'})^{-1}_{\mathbb{N}_3\mathbb{N}_3} = \big[\mathbf{R}^{\alpha}_{\mathbb{N}_3\mathbb{N}_3} + \mathbf{X}^{\alpha}_{\mathbb{N}_3\mathbb{N}_3} + i\,\mathbf{L}_{\mathrm{Z},\,\mathbb{N}_3\mathbb{N}_3} - \mathbf{X}^{\alpha}_{\mathbb{N}_3\mathbb{N}_5}\,(\mathbf{R}^{\alpha}_{\mathbb{N}_5\mathbb{N}_5} + \mathbf{X}^{\alpha}_{\mathbb{N}_5\mathbb{N}_5} + i\,\mathbf{L}_{\mathrm{Z},\,\mathbb{N}_5\mathbb{N}_5})^{-1}\mathbf{X}^{\alpha}_{\mathbb{N}_5\mathbb{N}_3}\big]^{-1}. \tag{F.48}$$

For $m=2$, $\mathbf{Y}^{\alpha}_{\mathbb{N}_1\mathbb{N}_1} = \mathbf{0}$ since there are no nonlabile three-spin (or higher) modes. For $m=3$, Eqs. (F.38), (F.41) and (F.44) yield

$$\begin{aligned} \mathbf{Y}^{\alpha}_{\mathbb{N}_1\mathbb{N}_1}(m=3) \;=\; & \boldsymbol{\Delta}^{\alpha}_{\mathbb{N}_1\mathbb{N}_2}\,(\mathbf{R}^{\alpha}_{\mathbb{N}_2\mathbb{N}_2} + i\,\mathbf{L}_{\mathrm{Z},\,\mathbb{N}_2\mathbb{N}_2})^{-1}\boldsymbol{\Delta}^{\alpha}_{\mathbb{N}_2\mathbb{N}_3} \\ & \times \big[\mathbf{R}^{\alpha}_{\mathbb{N}_3\mathbb{N}_3} + i\,\mathbf{L}_{\mathrm{Z},\,\mathbb{N}_3\mathbb{N}_3} + \boldsymbol{\Delta}^{\alpha}_{\mathbb{N}_3\mathbb{N}_2}\,(\mathbf{R}^{\alpha}_{\mathbb{N}_2\mathbb{N}_2} + i\,\mathbf{L}_{\mathrm{Z},\,\mathbb{N}_2\mathbb{N}_2})^{-1}\boldsymbol{\Delta}^{\alpha}_{\mathbb{N}_2\mathbb{N}_3}\big]^{-1} \\ & \times \boldsymbol{\Delta}^{\alpha}_{\mathbb{N}_3\mathbb{N}_2}\,(\mathbf{R}^{\alpha}_{\mathbb{N}_2\mathbb{N}_2} + i\,\mathbf{L}_{\mathrm{Z},\,\mathbb{N}_2\mathbb{N}_2})^{-1}\boldsymbol{\Delta}^{\alpha}_{\mathbb{N}_2\mathbb{N}_1}\,. \end{aligned} \tag{F.49}$$

Similarly, we obtain for $m=4$,

$$\begin{aligned} \mathbf{Y}^{\alpha}_{\mathbb{N}_1\mathbb{N}_1}(m=4) \;=\; & \boldsymbol{\Delta}^{\alpha}_{\mathbb{N}_1\mathbb{N}_2}\,(\mathbf{R}^{\alpha}_{\mathbb{N}_2\mathbb{N}_2} + i\,\mathbf{L}_{\mathrm{Z},\,\mathbb{N}_2\mathbb{N}_2})^{-1}\boldsymbol{\Delta}^{\alpha}_{\mathbb{N}_2\mathbb{N}_3} \\ & \times \big[\mathbf{R}^{\alpha}_{\mathbb{N}_3\mathbb{N}_3} + i\,\mathbf{L}_{\mathrm{Z},\,\mathbb{N}_3\mathbb{N}_3} + \boldsymbol{\Delta}^{\alpha}_{\mathbb{N}_3\mathbb{N}_2}\,(\mathbf{R}^{\alpha}_{\mathbb{N}_2\mathbb{N}_2} + i\,\mathbf{L}_{\mathrm{Z},\,\mathbb{N}_2\mathbb{N}_2})^{-1}\boldsymbol{\Delta}^{\alpha}_{\mathbb{N}_2\mathbb{N}_3} \\ & + \boldsymbol{\Delta}^{\alpha}_{\mathbb{N}_3\mathbb{N}_4}\,(\mathbf{R}^{\alpha}_{\mathbb{N}_4\mathbb{N}_4} + i\,\mathbf{L}_{\mathrm{Z},\,\mathbb{N}_4\mathbb{N}_4})^{-1}\boldsymbol{\Delta}^{\alpha}_{\mathbb{N}_4\mathbb{N}_3}\big]^{-1} \\ & \times \boldsymbol{\Delta}^{\alpha}_{\mathbb{N}_3\mathbb{N}_2}\,(\mathbf{R}^{\alpha}_{\mathbb{N}_2\mathbb{N}_2} + i\,\mathbf{L}_{\mathrm{Z},\,\mathbb{N}_2\mathbb{N}_2})^{-1}\boldsymbol{\Delta}^{\alpha}_{\mathbb{N}_2\mathbb{N}_1}\,, \end{aligned} \tag{F.50}$$

and, using also Eq. (F.48), for $m = 5$,

$$\begin{aligned}
\mathbf{Y}^{\alpha}_{\mathbb{N}_1\mathbb{N}_1}(m=5) \;=\; & \boldsymbol{\Delta}^{\alpha}_{\mathbb{N}_1\mathbb{N}_2}\,(\mathbf{R}^{\alpha}_{\mathbb{N}_2\mathbb{N}_2} + i\,\mathbf{L}_{\mathrm{Z},\,\mathbb{N}_2\mathbb{N}_2})^{-1}\boldsymbol{\Delta}^{\alpha}_{\mathbb{N}_2\mathbb{N}_3} \\
& \times \Big\{\mathbf{R}^{\alpha}_{\mathbb{N}_3\mathbb{N}_3} + i\,\mathbf{L}_{\mathrm{Z},\,\mathbb{N}_3\mathbb{N}_3} + \boldsymbol{\Delta}^{\alpha}_{\mathbb{N}_3\mathbb{N}_2}\,(\mathbf{R}^{\alpha}_{\mathbb{N}_2\mathbb{N}_2} + i\,\mathbf{L}_{\mathrm{Z},\,\mathbb{N}_2\mathbb{N}_2})^{-1}\boldsymbol{\Delta}^{\alpha}_{\mathbb{N}_2\mathbb{N}_3} \\
& + \boldsymbol{\Delta}^{\alpha}_{\mathbb{N}_3\mathbb{N}_4}\,(\mathbf{R}^{\alpha}_{\mathbb{N}_4\mathbb{N}_4} + i\,\mathbf{L}_{\mathrm{Z},\,\mathbb{N}_4\mathbb{N}_4})^{-1}\boldsymbol{\Delta}^{\alpha}_{\mathbb{N}_4\mathbb{N}_3} \;-\; \boldsymbol{\Delta}^{\alpha}_{\mathbb{N}_3\mathbb{N}_4}\,(\mathbf{R}^{\alpha}_{\mathbb{N}_4\mathbb{N}_4} + i\,\mathbf{L}_{\mathrm{Z},\,\mathbb{N}_4\mathbb{N}_4})^{-1}\boldsymbol{\Delta}^{\alpha}_{\mathbb{N}_4\mathbb{N}_5} \\
& \times \big[\mathbf{R}^{\alpha}_{\mathbb{N}_5\mathbb{N}_5} + i\,\mathbf{L}_{\mathrm{Z},\,\mathbb{N}_5\mathbb{N}_5} + \boldsymbol{\Delta}^{\alpha}_{\mathbb{N}_5\mathbb{N}_4}\,(\mathbf{R}^{\alpha}_{\mathbb{N}_4\mathbb{N}_4} + i\,\mathbf{L}_{\mathrm{Z},\,\mathbb{N}_4\mathbb{N}_4})^{-1}\boldsymbol{\Delta}^{\alpha}_{\mathbb{N}_4\mathbb{N}_5}\big]^{-1} \\
& \times \boldsymbol{\Delta}^{\alpha}_{\mathbb{N}_5\mathbb{N}_4}\,(\mathbf{R}^{\alpha}_{\mathbb{N}_4\mathbb{N}_4} + i\,\mathbf{L}_{\mathrm{Z},\,\mathbb{N}_4\mathbb{N}_4})^{-1}\boldsymbol{\Delta}^{\alpha}_{\mathbb{N}_4\mathbb{N}_3}\Big\}^{-1}\boldsymbol{\Delta}^{\alpha}_{\mathbb{N}_3\mathbb{N}_2}\,(\mathbf{R}^{\alpha}_{\mathbb{N}_2\mathbb{N}_2} + i\,\mathbf{L}_{\mathrm{Z},\,\mathbb{N}_2\mathbb{N}_2})^{-1}\boldsymbol{\Delta}^{\alpha}_{\mathbb{N}_2\mathbb{N}_1}\,.
\end{aligned} \tag{F.51}$$

We now consider the individual 3×3 blocks $\mathbf{Y}^{\alpha}_{\mathbb{N}_1(\mu)\mathbb{N}_1(\nu)}$ of the $3m \times 3m$ supermatrix $\mathbf{Y}^{\alpha}_{\mathbb{N}_1\mathbb{N}_1}$ in Eq. (F.49). For $m = 3$, there are three single-spin modes (μ, ν and κ), three two-spin modes ($\mu\nu$, $\mu\kappa$ and $\nu\kappa$), and only one three-spin mode ($\mu\nu\kappa$). Performing the block-wise matrix multiplications in Eq. (F.49) and making use of the symmetry rules in Eqs. (E.4), (E.10) and (E.11), we obtain for $\mu \neq \nu$,

$$\begin{aligned}
\mathbf{Y}^{\alpha}_{\mathbb{N}_1(\mu)\mathbb{N}_1(\nu)}(m=3) \;=\; & \Big[\boldsymbol{\Delta}^{\alpha}_{\mathbb{N}_1(\mu)\mathbb{N}_2(\mu\nu)}\,(\mathbf{R}^{\alpha}_{\mathbb{N}_2(\mu\nu)\mathbb{N}_2(\mu\nu)} + i\,\omega_0\,\mathbf{Q}_2)^{-1}\boldsymbol{\Delta}^{\alpha}_{\mathbb{N}_2(\mu\nu)\mathbb{N}_3(\mu\nu\kappa)} \\
& \;+\; \boldsymbol{\Delta}^{\alpha}_{\mathbb{N}_1(\mu)\mathbb{N}_2(\mu\kappa)}\,(\mathbf{R}^{\alpha}_{\mathbb{N}_2(\mu\kappa)\mathbb{N}_2(\mu\kappa)} + i\,\omega_0\,\mathbf{Q}_2)^{-1}\boldsymbol{\Delta}^{\alpha}_{\mathbb{N}_2(\mu\kappa)\mathbb{N}_3(\mu\nu\kappa)}\Big] \\
& \times \Big[\mathbf{R}^{\alpha}_{\mathbb{N}_3(\mu\nu\kappa)\mathbb{N}_3(\mu\nu\kappa)} + i\,\omega_0\,\mathbf{Q}_3 + \mathbf{X}^{\alpha}_{\mathbb{N}_3(\mu\nu\kappa)\mathbb{N}_3(\mu\nu\kappa)}\Big]^{-1} \\
& \times \Big[\boldsymbol{\Delta}^{\alpha}_{\mathbb{N}_3(\mu\nu\kappa)\mathbb{N}_2(\mu\nu)}\,(\mathbf{R}^{\alpha}_{\mathbb{N}_2(\mu\nu)\mathbb{N}_2(\mu\nu)} + i\,\omega_0\,\mathbf{Q}_2)^{-1}\boldsymbol{\Delta}^{\alpha}_{\mathbb{N}_2(\mu\nu)\mathbb{N}_1(\nu)} \\
& \;+\; \boldsymbol{\Delta}^{\alpha}_{\mathbb{N}_3(\mu\nu\kappa)\mathbb{N}_2(\nu\kappa)}\,(\mathbf{R}^{\alpha}_{\mathbb{N}_2(\nu\kappa)\mathbb{N}_2(\nu\kappa)} + i\,\omega_0\,\mathbf{Q}_2)^{-1}\boldsymbol{\Delta}^{\alpha}_{\mathbb{N}_2(\nu\kappa)\mathbb{N}_1(\nu)}\Big]\,,
\end{aligned} \tag{F.52}$$

and for $\mu = \nu$,

$$\begin{aligned}
\mathbf{Y}^{\alpha}_{\mathbb{N}_1(\mu)\mathbb{N}_1(\mu)}(m=3) \;=\; & \Big[\boldsymbol{\Delta}^{\alpha}_{\mathbb{N}_1(\mu)\mathbb{N}_2(\mu\nu)}\,(\mathbf{R}^{\alpha}_{\mathbb{N}_2(\mu\nu)\mathbb{N}_2(\mu\nu)} + i\,\omega_0\,\mathbf{Q}_2)^{-1}\boldsymbol{\Delta}^{\alpha}_{\mathbb{N}_2(\mu\nu)\mathbb{N}_3(\mu\nu\kappa)} \\
& \;+\; \boldsymbol{\Delta}^{\alpha}_{\mathbb{N}_1(\mu)\mathbb{N}_2(\mu\kappa)}\,(\mathbf{R}^{\alpha}_{\mathbb{N}_2(\mu\kappa)\mathbb{N}_2(\mu\kappa)} + i\,\omega_0\,\mathbf{Q}_2)^{-1}\boldsymbol{\Delta}^{\alpha}_{\mathbb{N}_2(\mu\kappa)\mathbb{N}_3(\mu\nu\kappa)}\Big] \\
& \times \Big[\mathbf{R}^{\alpha}_{\mathbb{N}_3(\mu\nu\kappa)\mathbb{N}_3(\mu\nu\kappa)} + i\,\omega_0\,\mathbf{Q}_3 + \mathbf{X}^{\alpha}_{\mathbb{N}_3(\mu\nu\kappa)\mathbb{N}_3(\mu\nu\kappa)}\Big]^{-1} \\
& \times \Big[\boldsymbol{\Delta}^{\alpha}_{\mathbb{N}_3(\mu\nu\kappa)\mathbb{N}_2(\mu\nu)}\,(\mathbf{R}^{\alpha}_{\mathbb{N}_2(\mu\nu)\mathbb{N}_2(\mu\nu)} + i\,\omega_0\,\mathbf{Q}_2)^{-1}\boldsymbol{\Delta}^{\alpha}_{\mathbb{N}_2(\mu\nu)\mathbb{N}_1(\mu)} \\
& \;+\; \boldsymbol{\Delta}^{\alpha}_{\mathbb{N}_3(\mu\nu\kappa)\mathbb{N}_2(\mu\kappa)}\,(\mathbf{R}^{\alpha}_{\mathbb{N}_2(\mu\kappa)\mathbb{N}_2(\mu\kappa)} + i\,\omega_0\,\mathbf{Q}_2)^{-1}\boldsymbol{\Delta}^{\alpha}_{\mathbb{N}_2(\mu\kappa)\mathbb{N}_1(\mu)}\Big]\,.
\end{aligned} \tag{F.53}$$

The supermatrix $\mathbf{X}^{\alpha}_{\mathbb{N}_3(\mu\nu\kappa)\mathbb{N}_3(\mu\nu\kappa)}$ appearing in Eqs. (F.52) and (F.53) is given by

$$\begin{aligned}
\mathbf{X}^{\alpha}_{\mathbb{N}_3(\mu\nu\kappa)\mathbb{N}_3(\mu\nu\kappa)} \;=\; & \boldsymbol{\Delta}^{\alpha}_{\mathbb{N}_3(\mu\nu\kappa)\mathbb{N}_2(\mu\nu)}\,(\mathbf{R}^{\alpha}_{\mathbb{N}_2(\mu\nu)\mathbb{N}_2(\mu\nu)} + i\,\omega_0\,\mathbf{Q}_2)^{-1}\boldsymbol{\Delta}^{\alpha}_{\mathbb{N}_2(\mu\nu)\mathbb{N}_3(\mu\nu\kappa)} \\
& \;+\; \boldsymbol{\Delta}^{\alpha}_{\mathbb{N}_3(\mu\nu\kappa)\mathbb{N}_2(\mu\kappa)}\,(\mathbf{R}^{\alpha}_{\mathbb{N}_2(\mu\kappa)\mathbb{N}_2(\mu\kappa)} + i\,\omega_0\,\mathbf{Q}_2)^{-1}\boldsymbol{\Delta}^{\alpha}_{\mathbb{N}_2(\mu\kappa)\mathbb{N}_3(\mu\nu\kappa)} \\
& \;+\; \boldsymbol{\Delta}^{\alpha}_{\mathbb{N}_3(\mu\nu\kappa)\mathbb{N}_2(\nu\kappa)}\,(\mathbf{R}^{\alpha}_{\mathbb{N}_2(\nu\kappa)\mathbb{N}_2(\nu\kappa)} + i\,\omega_0\,\mathbf{Q}_2)^{-1}\boldsymbol{\Delta}^{\alpha}_{\mathbb{N}_2(\nu\kappa)\mathbb{N}_3(\mu\nu\kappa)}\,.
\end{aligned} \tag{F.54}$$

Here we have also introduced the 9×9 diagonal matrix $\mathbf{Q}_2$ from Eq. (F.19) and the analogous 27×27 matrix

$$\mathbf{Q}_3 \;=\; \mathrm{diag}(0\;0\;0\;0\;0\;0\;0\;1\;1\;1\;1\;1\;1\;{-1}\;{-1}\;{-1}\;{-1}\;{-1}\;{-1}\;2\;2\;2\;{-2}\;{-2}\;{-2}\;3\;{-3})\,, \tag{F.55}$$

provided the 27 three-spin basis operators are ordered according to Q index, as in Table S2 in Appendix H.

From the general result in Eq. (F.38), we see that, for any $m \geq 3$, the coherent spin mode pathways are of the general form

$$1 \;\to\; 2 \;\to\; 3 \;\to\; \{\text{mixing of } 3\text{−spin modes}\} \;\to\; 3 \;\to\; 2 \;\to\; 1\,. \tag{F.56}$$

The mixing of the three-spin modes is brought about the matrix

$$(\mathbf{M}^{\alpha}_{\mathbb{N}\mathbb{A}',\mathbb{N}\mathbb{A}'})^{-1}_{\mathbb{N}_3\mathbb{N}_3} \;=\; \big(\mathbf{R}^{\alpha}_{\mathbb{N}\mathbb{A}',\mathbb{N}\mathbb{A}'} + \mathbf{X}^{\alpha}_{\mathbb{N}\mathbb{A}',\mathbb{N}\mathbb{A}'} + i\,\mathbf{L}_{\mathrm{Z},\,\mathbb{N}\mathbb{A}',\mathbb{N}\mathbb{A}'}\big)^{-1}_{\mathbb{N}_3\mathbb{N}_3}\,. \tag{F.57}$$

The block-tridiagonal matrix $\mathbf{X}^{\alpha}_{\mathbb{N}\mathbb{A}',\mathbb{N}\mathbb{A}'}$ involves modes from two-spin up to m-spin. We now introduce the three-spin mode (3SM) approximation by neglecting k-spin modes with $k \geq 4$. The 3SM approximation is thus needed only for $m \geq 4$. The matrix $\mathbf{M}^{\alpha}_{\mathbb{N}\mathbb{A}',\mathbb{N}\mathbb{A}'}$ then contains only one block, so that

$$(\mathbf{M}^{\alpha}_{\mathbb{N}\mathbb{A}',\mathbb{N}\mathbb{A}'})^{-1}_{\mathbb{N}_3\mathbb{N}_3} \;=\; \big[\mathbf{R}^{\alpha}_{\mathbb{N}_3\mathbb{N}_3} + i\,\omega_0\,\mathbf{Q}_3 + \mathbf{\Delta}^{\alpha}_{\mathbb{N}_3\mathbb{N}_2}\,(\mathbf{R}^{\alpha}_{\mathbb{N}_2\mathbb{N}_2} + i\,\omega_0\,\mathbf{Q}_2)^{-1}\mathbf{\Delta}^{\alpha}_{\mathbb{N}_2\mathbb{N}_3}\big]^{-1}\,. \tag{F.58}$$

In the 3SM approximation, Eq. (F.49) applies also to $m > 3$,

$$\begin{aligned}\mathbf{Y}^{\alpha}_{\mathbb{N}_1\mathbb{N}_1}(m) \;&=\; \mathbf{\Delta}^{\alpha}_{\mathbb{N}_1\mathbb{N}_2}\,(\mathbf{R}^{\alpha}_{\mathbb{N}_2\mathbb{N}_2} + i\,\omega_0\,\mathbf{Q}_2)^{-1}\mathbf{\Delta}^{\alpha}_{\mathbb{N}_2\mathbb{N}_3} \\ &\quad\times\big[\mathbf{R}^{\alpha}_{\mathbb{N}_3\mathbb{N}_3} + i\,\omega_0\,\mathbf{Q}_3 + \mathbf{\Delta}^{\alpha}_{\mathbb{N}_3\mathbb{N}_2}\,(\mathbf{R}^{\alpha}_{\mathbb{N}_2\mathbb{N}_2} + i\,\omega_0\,\mathbf{Q}_2)^{-1}\mathbf{\Delta}^{\alpha}_{\mathbb{N}_2\mathbb{N}_3}\big]^{-1} \\ &\quad\times\mathbf{\Delta}^{\alpha}_{\mathbb{N}_3\mathbb{N}_2}\,(\mathbf{R}^{\alpha}_{\mathbb{N}_2\mathbb{N}_2} + i\,\omega_0\,\mathbf{Q}_2)^{-1}\mathbf{\Delta}^{\alpha}_{\mathbb{N}_2\mathbb{N}_1}\,.\end{aligned} \tag{F.59}$$

For a set of m spins, there are $m!/[(m-k)!\,k!]$ distinct k-spin subspaces $\mathbb{N}_k$, so the (approximate) generalizations of Eqs. (F.52) – (F.54) are as follows. For off-diagonal blocks ($\mu \neq \nu$),

$$\begin{aligned}\mathbf{Y}^{\alpha}_{\mathbb{N}_1(\mu)\mathbb{N}_1(\nu)}(m) \;&=\; \sum_{\kappa}{}' \sum_{\kappa'}{}' \sum_{\lambda}{}' \sum_{\lambda'}{}' \mathbf{\Delta}^{\alpha}_{\mathbb{N}_1(\mu)\mathbb{N}_2(\mu\kappa)}\,(\mathbf{R}^{\alpha}_{\mathbb{N}_2(\mu\kappa)\mathbb{N}_2(\mu\kappa)} + i\,\omega_0\,\mathbf{Q}_2)^{-1} \\ &\quad\times\mathbf{\Delta}^{\alpha}_{\mathbb{N}_2(\mu\kappa)\mathbb{N}_3(\mu\kappa\kappa')}\big[\mathbf{R}^{\alpha}_{\mathbb{N}_3\mathbb{N}_3} + \mathbf{X}^{\alpha}_{\mathbb{N}_3\mathbb{N}_3} + i\,\mathbf{L}_{\mathrm{Z},\,\mathbb{N}_3\mathbb{N}_3}\big]^{-1}_{\mathbb{N}_3(\mu\kappa\kappa')\mathbb{N}_3(\nu\lambda\lambda')} \\ &\quad\times\mathbf{\Delta}^{\alpha}_{\mathbb{N}_3(\nu\lambda\lambda')\mathbb{N}_2(\nu\lambda)}\,(\mathbf{R}^{\alpha}_{\mathbb{N}_2(\nu\lambda)\mathbb{N}_2(\nu\lambda)} + i\,\omega_0\,\mathbf{Q}_2)^{-1}\mathbf{\Delta}^{\alpha}_{\mathbb{N}_2(\nu\lambda)\mathbb{N}_1(\nu)}\,,\end{aligned} \tag{F.60}$$

where the primed sums over spins are restricted to ensure that a k-spin subspace contains k distinct spins. For diagonal blocks ($\mu = \nu$),

$$\begin{aligned}\mathbf{Y}^{\alpha}_{\mathbb{N}_1(\mu)\mathbb{N}_1(\mu)}(m) \;&=\; \sum_{\kappa}{}' \sum_{\kappa'}{}' \sum_{\lambda}{}' \sum_{\lambda'}{}' \mathbf{\Delta}^{\alpha}_{\mathbb{N}_1(\mu)\mathbb{N}_2(\mu\kappa)}\,(\mathbf{R}^{\alpha}_{\mathbb{N}_2(\mu\kappa)\mathbb{N}_2(\mu\kappa)} + i\,\omega_0\,\mathbf{Q}_2)^{-1} \\ &\quad\times\mathbf{\Delta}^{\alpha}_{\mathbb{N}_2(\mu\kappa)\mathbb{N}_3(\mu\kappa\kappa')}\big[\mathbf{R}^{\alpha}_{\mathbb{N}_3\mathbb{N}_3} + \mathbf{X}^{\alpha}_{\mathbb{N}_3\mathbb{N}_3} + i\,\mathbf{L}_{\mathrm{Z},\,\mathbb{N}_3\mathbb{N}_3}\big]^{-1}_{\mathbb{N}_3(\mu\kappa\kappa')\mathbb{N}_3(\mu\lambda\lambda')} \\ &\quad\times\mathbf{\Delta}^{\alpha}_{\mathbb{N}_3(\mu\lambda\lambda')\mathbb{N}_2(\mu\lambda)}\,(\mathbf{R}^{\alpha}_{\mathbb{N}_2(\mu\lambda)\mathbb{N}_2(\mu\lambda)} + i\,\omega_0\,\mathbf{Q}_2)^{-1}\mathbf{\Delta}^{\alpha}_{\mathbb{N}_2(\mu\lambda)\mathbb{N}_1(\mu)}\,.\end{aligned} \tag{F.61}$$

The supermatrix $\mathbf{R}^{\alpha}_{\mathbb{N}_3\mathbb{N}_3}$ is block-diagonal with $m(m-1)(m-2)/6$ blocks of dimension 27×27 on the diagonal. The supermatrix $\mathbf{X}^{\alpha}_{\mathbb{N}_3\mathbb{N}_3}$ is *not* block-diagonal and has $[m(m-$

$1)(m-2)/6]^2$ blocks of dimension 27×27 and of the general form

$$\begin{aligned}\mathbf{X}^{\alpha}_{\mathbb{N}_3(\mu\nu\kappa)\mathbb{N}_3(\mu'\nu'\kappa')} \;=\; & \delta_{\mu'\mu}\,\delta_{\nu'\nu}\,\mathbf{\Delta}^{\alpha}_{\mathbb{N}_3(\mu\nu\kappa)\mathbb{N}_2(\mu\nu)}\,(\mathbf{R}^{\alpha}_{\mathbb{N}_2(\mu\nu)\mathbb{N}_2(\mu\nu)} + i\,\omega_0\,\mathbf{Q}_2)^{-1}\mathbf{\Delta}^{\alpha}_{\mathbb{N}_2(\mu\nu)\mathbb{N}_3(\mu\nu\kappa')} \\ & +\; \delta_{\mu'\mu}\,\delta_{\kappa'\kappa}\,\mathbf{\Delta}^{\alpha}_{\mathbb{N}_3(\mu\nu\kappa)\mathbb{N}_2(\mu\kappa)}\,(\mathbf{R}^{\alpha}_{\mathbb{N}_2(\mu\kappa)\mathbb{N}_2(\mu\kappa)} + i\,\omega_0\,\mathbf{Q}_2)^{-1}\mathbf{\Delta}^{\alpha}_{\mathbb{N}_2(\mu\kappa)\mathbb{N}_3(\mu\nu'\kappa)} \\ & +\; \delta_{\nu'\nu}\,\delta_{\kappa'\kappa}\,\mathbf{\Delta}^{\alpha}_{\mathbb{N}_3(\mu\nu\kappa)\mathbb{N}_2(\nu\kappa)}\,(\mathbf{R}^{\alpha}_{\mathbb{N}_2(\nu\kappa)\mathbb{N}_2(\nu\kappa)} + i\,\omega_0\,\mathbf{Q}_2)^{-1}\mathbf{\Delta}^{\alpha}_{\mathbb{N}_2(\nu\kappa)\mathbb{N}_3(\mu'\nu\kappa)}\,. \end{aligned} \tag{F.62}$$

Equation (F.62) shows that the 27×27 blocks of $\mathbf{X}^{\alpha}_{\mathbb{N}_3\mathbb{N}_3}$ vanish unless the two involved three-spin subspaces have at least two spins in common. For the nonzero off-diagonal blocks, connecting distinct subspaces sharing exactly two spins, only one of the three terms in Eq. (F.62) contributes. For the diagonal blocks, where the two subspaces are identical (sharing all three spins), all three terms in Eq. (F.62) contribute.

The effect on the ILRR of coherent spin mode transfer induced by static dipole couplings can be identified by computing the ILRR from the multi-spin SRE theory with and without the $\mathbf{X}^{\alpha}_{\mathbb{N}_1\mathbb{N}_1}$ and $\mathbf{Y}^{\alpha}_{\mathbb{N}_1\mathbb{N}_1}$ supermatrices, which vanish in the absence of static dipole couplings. Omitting these supermatrices from Eq. (F.13), we obtain

$$\Gamma^{\alpha}_{np} \;=\; \sum_{\mu=1}^{m} \mathbf{R}^{\alpha}_{n,\mathbb{N}_1(\mu)}\,(\mathbf{R}^{\alpha}_{\mathbb{N}_1(\mu)\mathbb{N}_1(\mu)} + i\,\omega_0\,\mathbf{Q}_1)^{-1}\,\mathbf{R}^{\alpha}_{\mathbb{N}_1(\mu),p}\,. \tag{F.63}$$

The multi-spin SRE theory developed here reduces correctly to the results derived in Paper III for three-spin systems.[1] For the $ISP-IS$ case, there are no static dipole couplings, so Eq. (F.63) applies. Setting $m = 1$ and $\mathbb{N}_1(\mu) = P$, we find

$$\Gamma^{\alpha}_{np} \;=\; \mathbf{R}^{\alpha}_{nP}\,(\mathbf{R}^{\alpha}_{PP} + i\,\omega_0\,\mathbf{Q}_1)^{-1}\,\mathbf{R}^{\alpha}_{Pp}\,, \tag{F.64}$$

in agreement with Paper III.[1] For the IP_2-I case, $m = 2$ and $\mathbf{Y}^{\alpha}_{\mathbb{N}_1\mathbb{N}_1} = \mathbf{0}$. From Eq. (F.13), we then obtain, in agreement with Paper III,[1]

$$\Gamma^{\alpha}_{11} \;=\; \begin{bmatrix} \mathbf{R}^{\alpha}_{1S} & \mathbf{R}^{\alpha}_{1P} \end{bmatrix} \begin{bmatrix} (\mathbf{R}^{\alpha}_{SS} + \mathbf{X}^{\alpha}_{SS} + i\,\omega_0\,\mathbf{Q}_1) & \mathbf{X}^{\alpha}_{SP} \\ \mathbf{X}^{\alpha}_{PS} & (\mathbf{R}^{\alpha}_{PP} + \mathbf{X}^{\alpha}_{PP} + i\,\omega_0\,\mathbf{Q}_1) \end{bmatrix} \begin{bmatrix} \mathbf{R}^{\alpha}_{S1} \\ \mathbf{R}^{\alpha}_{P1} \end{bmatrix}. \tag{F.65}$$

APPENDIX G: EXPLICIT SRE RESULTS

In this Appendix, we summarize the steps involved in computing the ILRR from the multi-spin SRE theory in the 3SM approximation (only used for $m \geq 4$). In particular, we present explicit expressions for the special cases with $m = 1$, 2, 3 or 4, as well as general expressions, valid for any m, suitable for machine computation.

1. Exchange case $IP_m - I$

According to Eqs. (11) and (F.8), the ILRR for the $IP_m - I$ case is given exactly by

$$R_{1,I}(\omega_0) \;=\; P_{\rm A}\left[\left\langle R^{II}_{zz}(\omega_0)\right\rangle - \left\langle \Gamma^{II}_{zz}(\omega_0)\right\rangle\right] . \tag{G.1}$$

The auto-relaxation rate $\left\langle R^{II}_{zz}\right\rangle$ is obtained from Eqs. (H.5) and (H.7a) as

$$\left\langle R^{II}_{zz}(\omega_0)\right\rangle \;=\; \tfrac{2}{45}\,\omega^2_{{\rm D},I}\big[J(0) + 3\,J(\omega_0) + 6\,J(2\,\omega_0)\big] , \tag{G.2}$$

where the cumulative fluctuating dipole coupling $\omega_{{\rm D},I}$ is defined as

$$\omega_{{\rm D},I} \;\equiv\; \left[\sum_{\mu=1}^{m} \omega^2_{{\rm D},I\mu}\right]^{1/2} . \tag{G.3}$$

The cross-relaxation rate $\left\langle \Gamma^{II}_{zz}\right\rangle$ is obtained from Eqs. (F.13) and (H.13a) as

$$\begin{aligned} \left\langle \Gamma^{II}_{zz}(\omega_0)\right\rangle \;&=\; \left\langle \mathbf{R}^{\alpha}_{1,\mathbb{N}_1}\,(\mathbf{V}^{\alpha}_{\mathbb{N}_1\mathbb{N}_1})^{-1}\,\mathbf{R}^{\alpha}_{\mathbb{N}_1,1}\right\rangle \\ &=\; \sum_{\mu=1}^{m}\sum_{\nu=1}^{m}\left\langle \mathbf{R}^{\alpha}_{1,\mathbb{N}_1(\mu)}\,(\mathbf{V}^{\alpha}_{\mathbb{N}_1\mathbb{N}_1})^{-1}_{\mathbb{N}_1(\mu)\mathbb{N}_1(\nu)}\,\mathbf{R}^{\alpha\,\dagger}_{1,\mathbb{N}_1(\nu)}\right\rangle . \end{aligned} \tag{G.4}$$

The m 1×3 blocks $\mathbf{R}^{\alpha}_{1,\mathbb{N}_1(\mu)}$ of the $1\times 3m$ cross-spin relaxation matrix $\mathbf{R}^{\alpha}_{1,\mathbb{N}_1}$ have elements proportional to $\omega^2_{{\rm D},I\mu}\,\tau_{\rm A}$ given by Eqs. (H.11) and (H.12). The m^2 3×3 blocks $\mathbf{V}^{\alpha}_{\mathbb{N}_1(\mu)\mathbb{N}_1(\nu)}$ of the $3m\times 3m$ matrix $\mathbf{V}^{\alpha}_{\mathbb{N}_1\mathbb{N}_1}$ are given by

$$\mathbf{V}^{\alpha}_{\mathbb{N}_1(\mu)\mathbb{N}_1(\nu)} \;=\; \delta_{\mu\nu}\left(\mathbf{R}^{\alpha}_{\mathbb{N}_1(\mu)\mathbb{N}_1(\mu)} + i\,\omega_0\,\mathbf{Q}_1\right) \;+\; \mathbf{X}^{\alpha}_{\mathbb{N}_1(\mu)\mathbb{N}_1(\nu)} \;-\; \mathbf{Y}^{\alpha}_{\mathbb{N}_1(\mu)\mathbb{N}_1(\nu)} . \tag{G.5}$$

The 3×3 single-spin auto-relaxation matrix $\mathbf{R}^{\alpha}_{\mathbb{N}_1(\mu)\mathbb{N}_1(\mu)}$ has elements proportional to $\omega^2_{{\rm D},I\mu}\,\tau_{\rm A}$ given by Eqs. (H.10) and (H.14). The m^2 3×3 blocks $\mathbf{X}^{\alpha}_{\mathbb{N}_1(\mu)\mathbb{N}_1(\nu)}$ of the $3m\times 3m$ coherent transfer matrix $\mathbf{X}^{\alpha}_{\mathbb{N}_1\mathbb{N}_1}$ are obtained from Eq. (F.21), reproduced here for convenience:

$$\mathbf{X}^{\alpha}_{\mathbb{N}_1(\mu)\mathbb{N}_1(\nu)} \;=\; \mathbf{\Delta}^{\alpha}_{\mathbb{N}_1(\mu)\mathbb{N}_2(\mu\nu)}\left(\mathbf{R}^{\alpha}_{\mathbb{N}_2(\mu\nu)\mathbb{N}_2(\mu\nu)} + i\,\omega_0\,\mathbf{Q}_2\right)^{-1}\mathbf{\Delta}^{\alpha\,\dagger}_{\mathbb{N}_1(\nu)\mathbb{N}_2(\mu\nu)} , \tag{G.6a}$$

$$\mathbf{X}^{\alpha}_{\mathbb{N}_1(\mu)\mathbb{N}_1(\mu)} \;=\; {\sum_{\nu=1}^{m}}' \;\mathbf{\Delta}^{\alpha}_{\mathbb{N}_1(\mu)\mathbb{N}_2(\mu\nu)}\left(\mathbf{R}^{\alpha}_{\mathbb{N}_2(\mu\nu)\mathbb{N}_2(\mu\nu)} + i\,\omega_0\,\mathbf{Q}_2\right)^{-1}\mathbf{\Delta}^{\alpha\,\dagger}_{\mathbb{N}_1(\mu)\mathbb{N}_2(\mu\nu)} . \tag{G.6b}$$

The m^2 3×3 blocks $\mathbf{Y}^{\alpha}_{\mathbb{N}_1(\mu)\mathbb{N}_1(\nu)}$ of the $3m\times 3m$ coherent transfer matrix $\mathbf{Y}^{\alpha}_{\mathbb{N}_1\mathbb{N}_1}$ are obtained from Eqs. (F.60) and (F.61):

$$\begin{aligned}\mathbf{Y}^{\alpha}_{\mathbb{N}_1(\mu)\mathbb{N}_1(\nu)}(m) \;=\; &\sum_{\kappa}{}' \sum_{\kappa'}{}' \sum_{\lambda}{}' \sum_{\lambda'}{}' \boldsymbol{\Delta}^{\alpha}_{\mathbb{N}_1(\mu)\mathbb{N}_2(\mu\kappa)} \left(\mathbf{R}^{\alpha}_{\mathbb{N}_2(\mu\kappa)\mathbb{N}_2(\mu\kappa)} + i\,\omega_0\,\mathbf{Q}_2\right)^{-1} \\ &\times \boldsymbol{\Delta}^{\alpha}_{\mathbb{N}_2(\mu\kappa)\mathbb{N}_3(\mu\kappa\kappa')} \left[\mathbf{R}^{\alpha}_{\mathbb{N}_3\mathbb{N}_3} + \mathbf{X}^{\alpha}_{\mathbb{N}_3\mathbb{N}_3} + i\,\mathbf{L}_{\mathrm{Z},\,\mathbb{N}_3\mathbb{N}_3}\right]^{-1}_{\mathbb{N}_3(\mu\kappa\kappa')\mathbb{N}_3(\nu\lambda\lambda')} \\ &\times \boldsymbol{\Delta}^{\alpha}_{\mathbb{N}_3(\nu\lambda\lambda')\mathbb{N}_2(\nu\lambda)} \left(\mathbf{R}^{\alpha}_{\mathbb{N}_2(\nu\lambda)\mathbb{N}_2(\nu\lambda)} + i\,\omega_0\,\mathbf{Q}_2\right)^{-1} \boldsymbol{\Delta}^{\alpha}_{\mathbb{N}_2(\nu\lambda)\mathbb{N}_1(\nu)}\,,\end{aligned} \tag{G.7}$$

$$\begin{aligned}\mathbf{Y}^{\alpha}_{\mathbb{N}_1(\mu)\mathbb{N}_1(\mu)}(m) \;=\; &\sum_{\kappa}{}' \sum_{\kappa'}{}' \sum_{\lambda}{}' \sum_{\lambda'}{}' \boldsymbol{\Delta}^{\alpha}_{\mathbb{N}_1(\mu)\mathbb{N}_2(\mu\kappa)} \left(\mathbf{R}^{\alpha}_{\mathbb{N}_2(\mu\kappa)\mathbb{N}_2(\mu\kappa)} + i\,\omega_0\,\mathbf{Q}_2\right)^{-1} \\ &\times \boldsymbol{\Delta}^{\alpha}_{\mathbb{N}_2(\mu\kappa)\mathbb{N}_3(\mu\kappa\kappa')} \left[\mathbf{R}^{\alpha}_{\mathbb{N}_3\mathbb{N}_3} + \mathbf{X}^{\alpha}_{\mathbb{N}_3\mathbb{N}_3} + i\,\mathbf{L}_{\mathrm{Z},\,\mathbb{N}_3\mathbb{N}_3}\right]^{-1}_{\mathbb{N}_3(\mu\kappa\kappa')\mathbb{N}_3(\mu\lambda\lambda')} \\ &\times \boldsymbol{\Delta}^{\alpha}_{\mathbb{N}_3(\mu\lambda\lambda')\mathbb{N}_2(\mu\lambda)} \left(\mathbf{R}^{\alpha}_{\mathbb{N}_2(\mu\lambda)\mathbb{N}_2(\mu\lambda)} + i\,\omega_0\,\mathbf{Q}_2\right)^{-1} \boldsymbol{\Delta}^{\alpha}_{\mathbb{N}_2(\mu\lambda)\mathbb{N}_1(\mu)}\,.\end{aligned} \tag{G.8}$$

The $[m(m-1)(m-2)/6]^2$ 27×27 blocks of the $9m(m-1)(m-2)/2\times 9m(m-1)(m-2)/2$ supermatrix $\mathbf{X}^{\alpha}_{\mathbb{N}_3\mathbb{N}_3}$ are given by Eq. (F.62):

$$\begin{aligned}\mathbf{X}^{\alpha}_{\mathbb{N}_3(\mu\nu\kappa)\mathbb{N}_3(\mu'\nu'\kappa')}(m) \;=\; &\delta_{\mu'\mu}\,\delta_{\nu'\nu}\,\boldsymbol{\Delta}^{\alpha}_{\mathbb{N}_3(\mu\nu\kappa)\mathbb{N}_2(\mu\nu)} \left(\mathbf{R}^{\alpha}_{\mathbb{N}_2(\mu\nu)\mathbb{N}_2(\mu\nu)} + i\,\omega_0\,\mathbf{Q}_2\right)^{-1} \boldsymbol{\Delta}^{\alpha}_{\mathbb{N}_2(\mu\nu)\mathbb{N}_3(\mu\nu\kappa')} \\ &+\; \delta_{\mu'\mu}\,\delta_{\kappa'\kappa}\,\boldsymbol{\Delta}^{\alpha}_{\mathbb{N}_3(\mu\nu\kappa)\mathbb{N}_2(\mu\kappa)} \left(\mathbf{R}^{\alpha}_{\mathbb{N}_2(\mu\kappa)\mathbb{N}_2(\mu\kappa)} + i\,\omega_0\,\mathbf{Q}_2\right)^{-1} \boldsymbol{\Delta}^{\alpha}_{\mathbb{N}_2(\mu\kappa)\mathbb{N}_3(\mu\nu'\kappa)} \\ &+\; \delta_{\nu'\nu}\,\delta_{\kappa'\kappa}\,\boldsymbol{\Delta}^{\alpha}_{\mathbb{N}_3(\mu\nu\kappa)\mathbb{N}_2(\nu\kappa)} \left(\mathbf{R}^{\alpha}_{\mathbb{N}_2(\nu\kappa)\mathbb{N}_2(\nu\kappa)} + i\,\omega_0\,\mathbf{Q}_2\right)^{-1} \boldsymbol{\Delta}^{\alpha}_{\mathbb{N}_2(\nu\kappa)\mathbb{N}_3(\mu'\nu\kappa)}\,.\end{aligned} \tag{G.9}$$

The $m(m-1)/2$ 9×9 blocks $\mathbf{R}^{\alpha}_{\mathbb{N}_2(\mu\nu)\mathbb{N}_2(\mu\nu)}$ of the block-diagonal $9m(m-1)/2\times 9m(m-1)/2$ two-spin auto-relaxation matrix $\mathbf{R}^{\alpha}_{\mathbb{N}_2\mathbb{N}_2}$, appearing in Eqs. (G.6) – (G.9), have elements with terms proportional to $\omega^2_{\mathrm{D},I\mu}\,\tau_{\mathrm{A}}$, $\omega^2_{\mathrm{D},I\nu}\,\tau_{\mathrm{A}}$ and $\omega_{\mathrm{D},I\mu}\,\omega_{\mathrm{D},I\nu}\,\tau_{\mathrm{A}}$ and are given by Eqs. (H.15a) and (H.16) – (H.36) (and similar expressions).

The $m(m-1)(m-2)/6$ 27×27 blocks $\mathbf{R}^{\alpha}_{\mathbb{N}_3(\mu\nu\kappa)\mathbb{N}_3(\mu\nu\kappa)}$ of the block-diagonal $9m(m-1)(m-2)/2\times 9m(m-1)(m-2)/2$ three-spin auto-relaxation matrix $\mathbf{R}^{\alpha}_{\mathbb{N}_3\mathbb{N}_3}$, appearing in Eqs. (G.7) and (G.8), have elements with terms proportional to $\omega^2_{\mathrm{D},I\mu}\,\tau_{\mathrm{A}}$, $\omega^2_{\mathrm{D},I\nu}\,\tau_{\mathrm{A}}$, $\omega^2_{\mathrm{D},I\kappa}\,\tau_{\mathrm{A}}$, $\omega_{\mathrm{D},I\mu}\,\omega_{\mathrm{D},I\nu}\,\tau_{\mathrm{A}}$, $\omega_{\mathrm{D},I\mu}\,\omega_{\mathrm{D},I\kappa}\,\tau_{\mathrm{A}}$ and $\omega_{\mathrm{D},I\nu}\,\omega_{\mathrm{D},I\kappa}\,\tau_{\mathrm{A}}$, and are given by Eqs. (H.37a) and (H.38) – (H.44) (and similar expressions).

The $m^2(m-1)/2$ 3×9 blocks $\boldsymbol{\Delta}^{\alpha}_{\mathbb{N}_1(\mu)\mathbb{N}_2(\mu\nu)}$ of the $3m\times 9m(m-1)/2$ coherent 1-spin $\rightarrow$ 2-spin mode transfer supermatrix $\boldsymbol{\Delta}^{\alpha}_{\mathbb{N}_1\mathbb{N}_2}$, appearing in Eqs. (G.6) – (G.8), have elements proportional to $\omega_{\mathrm{D},\mu\nu}$ given by Eqs. (H.45) and (H.46). Actually, there are only $m(m-1)$ nonzero 3×9 blocks $\boldsymbol{\Delta}^{\alpha}_{\mathbb{N}_1(\mu)\mathbb{N}_2(\mu\nu)}$: for each of the $m(m-1)/2$ two-spin subspaces $\mathbb{N}_2(\mu\nu)$, these are the 3×9 matrices $\boldsymbol{\delta}^{\alpha}_{\mathbb{N}_1(\mu)\mathbb{N}_2(\mu\nu)}$ and $\boldsymbol{\delta}^{\alpha}_{\mathbb{N}_1(\nu)\mathbb{N}_2(\mu\nu)}$ in Eq. (H.45), with one spin shared between the single-spin and two-spin subspaces.

The $m^2(m-1)^2(m-2)/12$ 9×27 blocks $\boldsymbol{\Delta}^{\alpha}_{\mathbb{N}_2(\mu\nu)\mathbb{N}_3(\mu\nu\kappa)}$ of the $9m(m-1)/2\times 9m(m-1)(m-2)/2$ coherent 2-spin $\rightarrow$ 3-spin mode transfer supermatrix $\boldsymbol{\Delta}^{\alpha}_{\mathbb{N}_2\mathbb{N}_3}$, appearing in Eqs. (G.7) – (G.9), are each a sum of two 9×27 matrices proportional to $\omega_{\mathrm{D},\mu\kappa}$ and $\omega_{\mathrm{D},\nu\kappa}$, and given by Eqs. (H.47) and (H.48) (and similar expressions). Actually, there are only $m(m-1)(m-2)/2$ nonzero 9×27 blocks: for each of the $m(m-1)(m-2)/6$ three-spin subspaces $\mathbb{N}_3(\mu\nu\kappa)$, these are the three 9×27 matrices $\boldsymbol{\Delta}^{\alpha}_{\mathbb{N}_2(\mu\nu)\mathbb{N}_3(\mu\nu\kappa)}$, $\boldsymbol{\Delta}^{\alpha}_{\mathbb{N}_2(\mu\kappa)\mathbb{N}_3(\mu\nu\kappa)}$

and $\boldsymbol{\Delta}^{\alpha}_{\mathbb{N}_2(\nu\kappa)\mathbb{N}_3(\mu\nu\kappa)}$ with two spins shared between the two-spin and three-spin subspaces. According to Eq. (H.47), each of these matrices is a sum of two 9×27 matrices, such as $\boldsymbol{\delta}^{\alpha}_{\mathbb{N}_2(\mu\nu)\mathbb{N}_3(\mu\nu\kappa)}(\mu\kappa)$ and $\boldsymbol{\delta}^{\alpha}_{\mathbb{N}_2(\mu\nu)\mathbb{N}_3(\mu\nu\kappa)}(\nu\kappa)$. Altogether, $m(m-1)(m-2)/2$ such matrices must be computed.

Before considering the general case, we shall examine the special cases with $m = 1-4$. Here, we use subscript I for the labile spin (actually the I_z mode) and $\mu = 1, 2, \ldots, m$ for the nonlabile spins. (The lower-case Greek letters are generic nonlabile spin labels.)

For $m = 1$, there are no static dipole couplings, so $\mathbf{X}^{\alpha}_{\mathbb{N}_1\mathbb{N}_1} = \mathbf{Y}^{\alpha}_{\mathbb{N}_1\mathbb{N}_1} = \mathbf{0}$ and Eqs. (G.4) and (G.5) yield

$$\left\langle \Gamma^{II}_{zz}(\omega_0) \right\rangle \;=\; \left\langle \mathbf{R}^{\alpha}_{I,\,\mathbb{N}_1(1)} \left(\mathbf{R}^{\alpha}_{\mathbb{N}_1(1)\mathbb{N}_1(1)} + i\,\omega_0\,\mathbf{Q}_1 \right)^{-1} \mathbf{R}^{\alpha\,\dagger}_{I,\,\mathbb{N}_1(1)} \right\rangle \,, \tag{G.10}$$

consistent with Eq. (F.63) and the results of Paper II.[6]

For $m = 2$, there is a single static dipole coupling, so $\mathbf{Y}^{\alpha}_{\mathbb{N}_1\mathbb{N}_1} = \mathbf{0}$ and the sum in Eq. (G.6b) contains only one term. Equations (G.4) and (G.5) then agree with Eqs. (42) and (43) of Paper III,[1] with the four 3×3 blocks of $\mathbf{X}^{\alpha}_{\mathbb{N}_1\mathbb{N}_1}$ obtained from Eq. (G.6) as

$$\mathbf{X}^{\alpha}_{\mathbb{N}_1(1)\mathbb{N}_1(2)}(m=2) \;=\; \boldsymbol{\Delta}^{\alpha}_{\mathbb{N}_1(1)\mathbb{N}_2(12)} \left(\mathbf{R}^{\alpha}_{\mathbb{N}_2(12)\mathbb{N}_2(12)} + i\,\omega_0\,\mathbf{Q}_2 \right)^{-1} \boldsymbol{\Delta}^{\alpha\,\dagger}_{\mathbb{N}_1(2)\mathbb{N}_2(12)} \,, \tag{G.11a}$$

$$\mathbf{X}^{\alpha}_{\mathbb{N}_1(2)\mathbb{N}_1(1)}(m=2) \;=\; \boldsymbol{\Delta}^{\alpha}_{\mathbb{N}_1(2)\mathbb{N}_2(12)} \left(\mathbf{R}^{\alpha}_{\mathbb{N}_2(12)\mathbb{N}_2(12)} + i\,\omega_0\,\mathbf{Q}_2 \right)^{-1} \boldsymbol{\Delta}^{\alpha\,\dagger}_{\mathbb{N}_1(1)\mathbb{N}_2(12)} \,, \tag{G.11b}$$

$$\mathbf{X}^{\alpha}_{\mathbb{N}_1(1)\mathbb{N}_1(1)}(m=2) \;=\; \boldsymbol{\Delta}^{\alpha}_{\mathbb{N}_1(1)\mathbb{N}_2(12)} \left(\mathbf{R}^{\alpha}_{\mathbb{N}_2(12)\mathbb{N}_2(12)} + i\,\omega_0\,\mathbf{Q}_2 \right)^{-1} \boldsymbol{\Delta}^{\alpha\,\dagger}_{\mathbb{N}_1(1)\mathbb{N}_2(12)} \,, \tag{G.11c}$$

$$\mathbf{X}^{\alpha}_{\mathbb{N}_1(2)\mathbb{N}_1(2)}(m=2) \;=\; \boldsymbol{\Delta}^{\alpha}_{\mathbb{N}_1(2)\mathbb{N}_2(12)} \left(\mathbf{R}^{\alpha}_{\mathbb{N}_2(12)\mathbb{N}_2(12)} + i\,\omega_0\,\mathbf{Q}_2 \right)^{-1} \boldsymbol{\Delta}^{\alpha\,\dagger}_{\mathbb{N}_1(2)\mathbb{N}_2(12)} \,. \tag{G.11d}$$

For $m = 3$, there are three two-spin subspaces (12, 13 and 23) and one three-spin subspace (123). Equation (G.6a) then yields

$$\mathbf{X}^{\alpha}_{\mathbb{N}_1(1)\mathbb{N}_1(2)}(m=3) \;=\; \boldsymbol{\Delta}^{\alpha}_{\mathbb{N}_1(1)\mathbb{N}_2(12)} \left(\mathbf{R}^{\alpha}_{\mathbb{N}_2(12)\mathbb{N}_2(12)} + i\,\omega_0\,\mathbf{Q}_2 \right)^{-1} \boldsymbol{\Delta}^{\alpha\,\dagger}_{\mathbb{N}_1(2)\mathbb{N}_2(12)} \,, \tag{G.12a}$$

$$\mathbf{X}^{\alpha}_{\mathbb{N}_1(2)\mathbb{N}_1(1)}(m=3) \;=\; \boldsymbol{\Delta}^{\alpha}_{\mathbb{N}_1(2)\mathbb{N}_2(12)} \left(\mathbf{R}^{\alpha}_{\mathbb{N}_2(12)\mathbb{N}_2(12)} + i\,\omega_0\,\mathbf{Q}_2 \right)^{-1} \boldsymbol{\Delta}^{\alpha\,\dagger}_{\mathbb{N}_1(1)\mathbb{N}_2(12)} \,, \tag{G.12b}$$

$$\mathbf{X}^{\alpha}_{\mathbb{N}_1(1)\mathbb{N}_1(3)}(m=3) \;=\; \boldsymbol{\Delta}^{\alpha}_{\mathbb{N}_1(1)\mathbb{N}_2(13)} \left(\mathbf{R}^{\alpha}_{\mathbb{N}_2(13)\mathbb{N}_2(13)} + i\,\omega_0\,\mathbf{Q}_2 \right)^{-1} \boldsymbol{\Delta}^{\alpha\,\dagger}_{\mathbb{N}_1(3)\mathbb{N}_2(13)} \,, \tag{G.12c}$$

$$\mathbf{X}^{\alpha}_{\mathbb{N}_1(3)\mathbb{N}_1(1)}(m=3) \;=\; \boldsymbol{\Delta}^{\alpha}_{\mathbb{N}_1(3)\mathbb{N}_2(13)} \left(\mathbf{R}^{\alpha}_{\mathbb{N}_2(13)\mathbb{N}_2(13)} + i\,\omega_0\,\mathbf{Q}_2 \right)^{-1} \boldsymbol{\Delta}^{\alpha\,\dagger}_{\mathbb{N}_1(1)\mathbb{N}_2(13)} \,, \tag{G.12d}$$

$$\mathbf{X}^{\alpha}_{\mathbb{N}_1(2)\mathbb{N}_1(3)}(m=3) \;=\; \boldsymbol{\Delta}^{\alpha}_{\mathbb{N}_1(2)\mathbb{N}_2(23)} \left(\mathbf{R}^{\alpha}_{\mathbb{N}_2(23)\mathbb{N}_2(23)} + i\,\omega_0\,\mathbf{Q}_2 \right)^{-1} \boldsymbol{\Delta}^{\alpha\,\dagger}_{\mathbb{N}_1(3)\mathbb{N}_2(23)} \,, \tag{G.12e}$$

$$\mathbf{X}^{\alpha}_{\mathbb{N}_1(3)\mathbb{N}_1(2)}(m=3) \;=\; \boldsymbol{\Delta}^{\alpha}_{\mathbb{N}_1(3)\mathbb{N}_2(23)} \left(\mathbf{R}^{\alpha}_{\mathbb{N}_2(23)\mathbb{N}_2(23)} + i\,\omega_0\,\mathbf{Q}_2 \right)^{-1} \boldsymbol{\Delta}^{\alpha\,\dagger}_{\mathbb{N}_1(2)\mathbb{N}_2(23)} \,. \tag{G.12f}$$

According to Eqs. (H.45) and (H.46), $\boldsymbol{\Delta}^{\alpha}_{\mathbb{N}_1(2)\mathbb{N}_2(12)}$ differs from $\boldsymbol{\Delta}^{\alpha}_{\mathbb{N}_1(1)\mathbb{N}_2(12)}$ only by having reversed sign for the elements in columns 3, 4 and 6, whereas $\boldsymbol{\Delta}^{\alpha}_{\mathbb{N}_1(1)\mathbb{N}_2(13)}$ differs from $\boldsymbol{\Delta}^{\alpha}_{\mathbb{N}_1(1)\mathbb{N}_2(12)}$ only through the dipole coupling ($\omega_{\mathrm{D},13}$ versus $\omega_{\mathrm{D},12}$) and the Euler angles

(Ω_{13} versus Ω_{12}) in the Wigner functions $D_M = D^{2*}_{M0}(\Omega_X)$. From Eq. (G.6b) we obtain

$$\begin{aligned}\mathbf{X}^{\alpha}_{\mathbb{N}_1(1)\mathbb{N}_1(1)}(m=3) \;=\; & \boldsymbol{\Delta}^{\alpha}_{\mathbb{N}_1(1)\mathbb{N}_2(12)} \left(\mathbf{R}^{\alpha}_{\mathbb{N}_2(12)\mathbb{N}_2(12)} + i\,\omega_0\,\mathbf{Q}_2\right)^{-1} \boldsymbol{\Delta}^{\alpha\,\dagger}_{\mathbb{N}_1(1)\mathbb{N}_2(12)} \\ & +\; \boldsymbol{\Delta}^{\alpha}_{\mathbb{N}_1(1)\mathbb{N}_2(13)} \left(\mathbf{R}^{\alpha}_{\mathbb{N}_2(13)\mathbb{N}_2(13)} + i\,\omega_0\,\mathbf{Q}_2\right)^{-1} \boldsymbol{\Delta}^{\alpha\,\dagger}_{\mathbb{N}_1(1)\mathbb{N}_2(13)}\,,\end{aligned} \tag{G.13a}$$

$$\begin{aligned}\mathbf{X}^{\alpha}_{\mathbb{N}_1(2)\mathbb{N}_1(2)}(m=3) \;=\; & \boldsymbol{\Delta}^{\alpha}_{\mathbb{N}_1(2)\mathbb{N}_2(12)} \left(\mathbf{R}^{\alpha}_{\mathbb{N}_2(12)\mathbb{N}_2(12)} + i\,\omega_0\,\mathbf{Q}_2\right)^{-1} \boldsymbol{\Delta}^{\alpha\,\dagger}_{\mathbb{N}_1(2)\mathbb{N}_2(12)} \\ & +\; \boldsymbol{\Delta}^{\alpha}_{\mathbb{N}_1(2)\mathbb{N}_2(23)} \left(\mathbf{R}^{\alpha}_{\mathbb{N}_2(23)\mathbb{N}_2(23)} + i\,\omega_0\,\mathbf{Q}_2\right)^{-1} \boldsymbol{\Delta}^{\alpha\,\dagger}_{\mathbb{N}_1(2)\mathbb{N}_2(23)}\,,\end{aligned} \tag{G.13b}$$

$$\begin{aligned}\mathbf{X}^{\alpha}_{\mathbb{N}_1(3)\mathbb{N}_1(3)}(m=3) \;=\; & \boldsymbol{\Delta}^{\alpha}_{\mathbb{N}_1(3)\mathbb{N}_2(13)} \left(\mathbf{R}^{\alpha}_{\mathbb{N}_2(13)\mathbb{N}_2(13)} + i\,\omega_0\,\mathbf{Q}_2\right)^{-1} \boldsymbol{\Delta}^{\alpha\,\dagger}_{\mathbb{N}_1(3)\mathbb{N}_2(13)} \\ & +\; \boldsymbol{\Delta}^{\alpha}_{\mathbb{N}_1(3)\mathbb{N}_2(23)} \left(\mathbf{R}^{\alpha}_{\mathbb{N}_2(23)\mathbb{N}_2(23)} + i\,\omega_0\,\mathbf{Q}_2\right)^{-1} \boldsymbol{\Delta}^{\alpha\,\dagger}_{\mathbb{N}_1(3)\mathbb{N}_2(23)}\,.\end{aligned} \tag{G.13c}$$

Equation (G.7) yields for the off-diagonal blocks

$$\begin{aligned}\mathbf{Y}^{\alpha}_{\mathbb{N}_1(1)\mathbb{N}_1(2)}(m=3) \;=\; & \big[\boldsymbol{\Delta}^{\alpha}_{\mathbb{N}_1(1)\mathbb{N}_2(12)} \left(\mathbf{R}^{\alpha}_{\mathbb{N}_2(12)\mathbb{N}_2(12)} + i\,\omega_0\,\mathbf{Q}_2\right)^{-1} \boldsymbol{\Delta}^{\alpha}_{\mathbb{N}_2(12)\mathbb{N}_3(123)} \\ & + \boldsymbol{\Delta}^{\alpha}_{\mathbb{N}_1(1)\mathbb{N}_2(13)} \left(\mathbf{R}^{\alpha}_{\mathbb{N}_2(13)\mathbb{N}_2(13)} + i\,\omega_0\,\mathbf{Q}_2\right)^{-1} \boldsymbol{\Delta}^{\alpha}_{\mathbb{N}_2(13)\mathbb{N}_3(123)}\big] \\ & \times \left[\mathbf{R}^{\alpha}_{\mathbb{N}_3(123)\mathbb{N}_3(123)} + \mathbf{X}^{\alpha}_{\mathbb{N}_3(123)\mathbb{N}_3(123)} + i\,\omega_0\,\mathbf{Q}_3\right]^{-1} \\ & \big[\boldsymbol{\Delta}^{\alpha\,\dagger}_{\mathbb{N}_2(12)\mathbb{N}_3(123)} \left(\mathbf{R}^{\alpha}_{\mathbb{N}_2(12)\mathbb{N}_2(12)} + i\,\omega_0\,\mathbf{Q}_2\right)^{-1} \boldsymbol{\Delta}^{\alpha\,\dagger}_{\mathbb{N}_1(2)\mathbb{N}_2(12)} \\ & + \boldsymbol{\Delta}^{\alpha\,\dagger}_{\mathbb{N}_2(23)\mathbb{N}_3(123)} \left(\mathbf{R}^{\alpha}_{\mathbb{N}_2(23)\mathbb{N}_2(23)} + i\,\omega_0\,\mathbf{Q}_2\right)^{-1} \boldsymbol{\Delta}^{\alpha\,\dagger}_{\mathbb{N}_1(2)\mathbb{N}_2(23)}\big]\,,\end{aligned} \tag{G.14a}$$

$$\begin{aligned}\mathbf{Y}^{\alpha}_{\mathbb{N}_1(2)\mathbb{N}_1(1)}(m=3) \;=\; & \big[\boldsymbol{\Delta}^{\alpha}_{\mathbb{N}_1(2)\mathbb{N}_2(12)} \left(\mathbf{R}^{\alpha}_{\mathbb{N}_2(12)\mathbb{N}_2(12)} + i\,\omega_0\,\mathbf{Q}_2\right)^{-1} \boldsymbol{\Delta}^{\alpha}_{\mathbb{N}_2(12)\mathbb{N}_3(123)} \\ & + \boldsymbol{\Delta}^{\alpha}_{\mathbb{N}_1(2)\mathbb{N}_2(23)} \left(\mathbf{R}^{\alpha}_{\mathbb{N}_2(23)\mathbb{N}_2(23)} + i\,\omega_0\,\mathbf{Q}_2\right)^{-1} \boldsymbol{\Delta}^{\alpha}_{\mathbb{N}_2(23)\mathbb{N}_3(123)}\big] \\ & \times \left[\mathbf{R}^{\alpha}_{\mathbb{N}_3(123)\mathbb{N}_3(123)} + \mathbf{X}^{\alpha}_{\mathbb{N}_3(123)\mathbb{N}_3(123)} + i\,\omega_0\,\mathbf{Q}_3\right]^{-1} \\ & \big[\boldsymbol{\Delta}^{\alpha\,\dagger}_{\mathbb{N}_2(12)\mathbb{N}_3(123)} \left(\mathbf{R}^{\alpha}_{\mathbb{N}_2(12)\mathbb{N}_2(12)} + i\,\omega_0\,\mathbf{Q}_2\right)^{-1} \boldsymbol{\Delta}^{\alpha\,\dagger}_{\mathbb{N}_1(1)\mathbb{N}_2(12)} \\ & + \boldsymbol{\Delta}^{\alpha\,\dagger}_{\mathbb{N}_2(13)\mathbb{N}_3(123)} \left(\mathbf{R}^{\alpha}_{\mathbb{N}_2(13)\mathbb{N}_2(13)} + i\,\omega_0\,\mathbf{Q}_2\right)^{-1} \boldsymbol{\Delta}^{\alpha\,\dagger}_{\mathbb{N}_1(1)\mathbb{N}_2(13)}\big]\,,\end{aligned} \tag{G.14b}$$

$$\begin{aligned}\mathbf{Y}^{\alpha}_{\mathbb{N}_1(1)\mathbb{N}_1(3)}(m=3) \;=\; & \big[\boldsymbol{\Delta}^{\alpha}_{\mathbb{N}_1(1)\mathbb{N}_2(12)} \left(\mathbf{R}^{\alpha}_{\mathbb{N}_2(12)\mathbb{N}_2(12)} + i\,\omega_0\,\mathbf{Q}_2\right)^{-1} \boldsymbol{\Delta}^{\alpha}_{\mathbb{N}_2(12)\mathbb{N}_3(123)} \\ & + \boldsymbol{\Delta}^{\alpha}_{\mathbb{N}_1(1)\mathbb{N}_2(13)} \left(\mathbf{R}^{\alpha}_{\mathbb{N}_2(13)\mathbb{N}_2(13)} + i\,\omega_0\,\mathbf{Q}_2\right)^{-1} \boldsymbol{\Delta}^{\alpha}_{\mathbb{N}_2(13)\mathbb{N}_3(123)}\big] \\ & \times \left[\mathbf{R}^{\alpha}_{\mathbb{N}_3(123)\mathbb{N}_3(123)} + \mathbf{X}^{\alpha}_{\mathbb{N}_3(123)\mathbb{N}_3(123)} + i\,\omega_0\,\mathbf{Q}_3\right]^{-1} \\ & \big[\boldsymbol{\Delta}^{\alpha\,\dagger}_{\mathbb{N}_2(13)\mathbb{N}_3(123)} \left(\mathbf{R}^{\alpha}_{\mathbb{N}_2(13)\mathbb{N}_2(13)} + i\,\omega_0\,\mathbf{Q}_2\right)^{-1} \boldsymbol{\Delta}^{\alpha\,\dagger}_{\mathbb{N}_1(3)\mathbb{N}_2(13)} \\ & + \boldsymbol{\Delta}^{\alpha\,\dagger}_{\mathbb{N}_2(23)\mathbb{N}_3(123)} \left(\mathbf{R}^{\alpha}_{\mathbb{N}_2(23)\mathbb{N}_2(23)} + i\,\omega_0\,\mathbf{Q}_2\right)^{-1} \boldsymbol{\Delta}^{\alpha\,\dagger}_{\mathbb{N}_1(3)\mathbb{N}_2(23)}\big]\,,\end{aligned} \tag{G.14c}$$

$$\begin{aligned}\mathbf{Y}^{\alpha}_{\mathbb{N}_1(2)\mathbb{N}_1(3)}(m=3) \;=\; & \big[\boldsymbol{\Delta}^{\alpha}_{\mathbb{N}_1(2)\mathbb{N}_2(12)} \left(\mathbf{R}^{\alpha}_{\mathbb{N}_2(12)\mathbb{N}_2(12)} + i\,\omega_0\,\mathbf{Q}_2\right)^{-1} \boldsymbol{\Delta}^{\alpha}_{\mathbb{N}_2(12)\mathbb{N}_3(123)} \\ & + \boldsymbol{\Delta}^{\alpha}_{\mathbb{N}_1(2)\mathbb{N}_2(23)} \left(\mathbf{R}^{\alpha}_{\mathbb{N}_2(23)\mathbb{N}_2(23)} + i\,\omega_0\,\mathbf{Q}_2\right)^{-1} \boldsymbol{\Delta}^{\alpha}_{\mathbb{N}_2(23)\mathbb{N}_3(123)}\big] \\ & \times \left[\mathbf{R}^{\alpha}_{\mathbb{N}_3(123)\mathbb{N}_3(123)} + \mathbf{X}^{\alpha}_{\mathbb{N}_3(123)\mathbb{N}_3(123)} + i\,\omega_0\,\mathbf{Q}_3\right]^{-1} \\ & \big[\boldsymbol{\Delta}^{\alpha\,\dagger}_{\mathbb{N}_2(13)\mathbb{N}_3(123)} \left(\mathbf{R}^{\alpha}_{\mathbb{N}_2(13)\mathbb{N}_2(13)} + i\,\omega_0\,\mathbf{Q}_2\right)^{-1} \boldsymbol{\Delta}^{\alpha\,\dagger}_{\mathbb{N}_1(3)\mathbb{N}_2(13)} \\ & + \boldsymbol{\Delta}^{\alpha\,\dagger}_{\mathbb{N}_2(23)\mathbb{N}_3(123)} \left(\mathbf{R}^{\alpha}_{\mathbb{N}_2(23)\mathbb{N}_2(23)} + i\,\omega_0\,\mathbf{Q}_2\right)^{-1} \boldsymbol{\Delta}^{\alpha\,\dagger}_{\mathbb{N}_1(3)\mathbb{N}_2(23)}\big]\,,\end{aligned} \tag{G.14d}$$

where, to conserve space, we have omitted $\mathbf{Y}^{\alpha}_{\mathbb{N}_1(3)\mathbb{N}_1(1)}$ and $\mathbf{Y}^{\alpha}_{\mathbb{N}_1(3)\mathbb{N}_1(2)}$, since they are easily obtained by analogy with the expressions shown in Eq. (G.14).

Equation (G.8) yields for the diagonal blocks

$$\begin{aligned}
\mathbf{Y}^{\alpha}_{\mathbb{N}_1(1)\mathbb{N}_1(1)}(m=3) \;=\; & \big[\boldsymbol{\Delta}^{\alpha}_{\mathbb{N}_1(1)\mathbb{N}_2(12)}\,(\mathbf{R}^{\alpha}_{\mathbb{N}_2(12)\mathbb{N}_2(12)}+i\,\omega_0\,\mathbf{Q}_2)^{-1}\,\boldsymbol{\Delta}^{\alpha}_{\mathbb{N}_2(12)\mathbb{N}_3(123)} \\
& + \boldsymbol{\Delta}^{\alpha}_{\mathbb{N}_1(1)\mathbb{N}_2(13)}\,(\mathbf{R}^{\alpha}_{\mathbb{N}_2(13)\mathbb{N}_2(13)}+i\,\omega_0\,\mathbf{Q}_2)^{-1}\,\boldsymbol{\Delta}^{\alpha}_{\mathbb{N}_2(13)\mathbb{N}_3(123)}\big] \\
& \times \big[\mathbf{R}^{\alpha}_{\mathbb{N}_3(123)\mathbb{N}_3(123)}+\mathbf{X}^{\alpha}_{\mathbb{N}_3(123)\mathbb{N}_3(123)}+i\,\omega_0\,\mathbf{Q}_3\big]^{-1} \\
& \big[\boldsymbol{\Delta}^{\alpha\,\dagger}_{\mathbb{N}_2(12)\mathbb{N}_3(123)}\,(\mathbf{R}^{\alpha}_{\mathbb{N}_2(12)\mathbb{N}_2(12)}+i\,\omega_0\,\mathbf{Q}_2)^{-1}\boldsymbol{\Delta}^{\alpha\,\dagger}_{\mathbb{N}_1(1)\mathbb{N}_2(12)} \\
& + \boldsymbol{\Delta}^{\alpha\,\dagger}_{\mathbb{N}_2(13)\mathbb{N}_3(123)}\,(\mathbf{R}^{\alpha}_{\mathbb{N}_2(13)\mathbb{N}_2(13)}+i\,\omega_0\,\mathbf{Q}_2)^{-1}\boldsymbol{\Delta}^{\alpha\,\dagger}_{\mathbb{N}_1(1)\mathbb{N}_2(13)}\big]\,,
\end{aligned} \tag{G.15a}$$

$$\begin{aligned}
\mathbf{Y}^{\alpha}_{\mathbb{N}_1(2)\mathbb{N}_1(2)}(m=3) \;=\; & \big[\boldsymbol{\Delta}^{\alpha}_{\mathbb{N}_1(2)\mathbb{N}_2(12)}\,(\mathbf{R}^{\alpha}_{\mathbb{N}_2(12)\mathbb{N}_2(12)}+i\,\omega_0\,\mathbf{Q}_2)^{-1}\,\boldsymbol{\Delta}^{\alpha}_{\mathbb{N}_2(12)\mathbb{N}_3(123)} \\
& + \boldsymbol{\Delta}^{\alpha}_{\mathbb{N}_1(2)\mathbb{N}_2(23)}\,(\mathbf{R}^{\alpha}_{\mathbb{N}_2(23)\mathbb{N}_2(23)}+i\,\omega_0\,\mathbf{Q}_2)^{-1}\,\boldsymbol{\Delta}^{\alpha}_{\mathbb{N}_2(23)\mathbb{N}_3(123)}\big] \\
& \times \big[\mathbf{R}^{\alpha}_{\mathbb{N}_3(123)\mathbb{N}_3(123)}+\mathbf{X}^{\alpha}_{\mathbb{N}_3(123)\mathbb{N}_3(123)}+i\,\omega_0\,\mathbf{Q}_3\big]^{-1} \\
& \big[\boldsymbol{\Delta}^{\alpha\,\dagger}_{\mathbb{N}_2(12)\mathbb{N}_3(123)}\,(\mathbf{R}^{\alpha}_{\mathbb{N}_2(12)\mathbb{N}_2(12)}+i\,\omega_0\,\mathbf{Q}_2)^{-1}\boldsymbol{\Delta}^{\alpha\,\dagger}_{\mathbb{N}_1(2)\mathbb{N}_2(12)} \\
& + \boldsymbol{\Delta}^{\alpha\,\dagger}_{\mathbb{N}_2(23)\mathbb{N}_3(123)}\,(\mathbf{R}^{\alpha}_{\mathbb{N}_2(23)\mathbb{N}_2(23)}+i\,\omega_0\,\mathbf{Q}_2)^{-1}\boldsymbol{\Delta}^{\alpha\,\dagger}_{\mathbb{N}_1(2)\mathbb{N}_2(23)}\big]\,,
\end{aligned} \tag{G.15b}$$

$$\begin{aligned}
\mathbf{Y}^{\alpha}_{\mathbb{N}_1(3)\mathbb{N}_1(3)}(m=3) \;=\; & \big[\boldsymbol{\Delta}^{\alpha}_{\mathbb{N}_3(1)\mathbb{N}_2(13)}\,(\mathbf{R}^{\alpha}_{\mathbb{N}_2(13)\mathbb{N}_2(13)}+i\,\omega_0\,\mathbf{Q}_2)^{-1}\,\boldsymbol{\Delta}^{\alpha}_{\mathbb{N}_2(13)\mathbb{N}_3(123)} \\
& + \boldsymbol{\Delta}^{\alpha}_{\mathbb{N}_1(3)\mathbb{N}_2(23)}\,(\mathbf{R}^{\alpha}_{\mathbb{N}_2(23)\mathbb{N}_2(23)}+i\,\omega_0\,\mathbf{Q}_2)^{-1}\,\boldsymbol{\Delta}^{\alpha}_{\mathbb{N}_2(23)\mathbb{N}_3(123)}\big] \\
& \times \big[\mathbf{R}^{\alpha}_{\mathbb{N}_3(123)\mathbb{N}_3(123)}+\mathbf{X}^{\alpha}_{\mathbb{N}_3(123)\mathbb{N}_3(123)}+i\,\omega_0\,\mathbf{Q}_3\big]^{-1} \\
& \big[\boldsymbol{\Delta}^{\alpha\,\dagger}_{\mathbb{N}_2(13)\mathbb{N}_3(123)}\,(\mathbf{R}^{\alpha}_{\mathbb{N}_2(13)\mathbb{N}_2(13)}+i\,\omega_0\,\mathbf{Q}_2)^{-1}\boldsymbol{\Delta}^{\alpha\,\dagger}_{\mathbb{N}_1(3)\mathbb{N}_2(13)} \\
& + \boldsymbol{\Delta}^{\alpha\,\dagger}_{\mathbb{N}_2(23)\mathbb{N}_3(123)}\,(\mathbf{R}^{\alpha}_{\mathbb{N}_2(23)\mathbb{N}_2(23)}+i\,\omega_0\,\mathbf{Q}_2)^{-1}\boldsymbol{\Delta}^{\alpha\,\dagger}_{\mathbb{N}_1(3)\mathbb{N}_2(23)}\big]\,,
\end{aligned} \tag{G.15c}$$

Equation (G.9) yields for $m = 3$

$$\begin{aligned}
\mathbf{X}^{\alpha}_{\mathbb{N}_3(123)\mathbb{N}_3(123)}(m=3) \;=\; & \boldsymbol{\Delta}^{\alpha\,\dagger}_{\mathbb{N}_2(12)\mathbb{N}_3(123)}\,(\mathbf{R}^{\alpha}_{\mathbb{N}_2(12)\mathbb{N}_2(12)}+i\,\omega_0\,\mathbf{Q}_2)^{-1}\boldsymbol{\Delta}^{\alpha}_{\mathbb{N}_2(12)\mathbb{N}_3(123)} \\
& + \boldsymbol{\Delta}^{\alpha\,\dagger}_{\mathbb{N}_2(13)\mathbb{N}_3(123)}\,(\mathbf{R}^{\alpha}_{\mathbb{N}_2(13)\mathbb{N}_2(13)}+i\,\omega_0\,\mathbf{Q}_2)^{-1}\boldsymbol{\Delta}^{\alpha}_{\mathbb{N}_2(13)\mathbb{N}_3(123)} \\
& + \boldsymbol{\Delta}^{\alpha\,\dagger}_{\mathbb{N}_2(23)\mathbb{N}_3(123)}\,(\mathbf{R}^{\alpha}_{\mathbb{N}_2(23)\mathbb{N}_2(23)}+i\,\omega_0\,\mathbf{Q}_2)^{-1}\boldsymbol{\Delta}^{\alpha}_{\mathbb{N}_2(23)\mathbb{N}_3(123)}\,.
\end{aligned} \tag{G.16}$$

For $m = 4$, there are six two-spin subspaces (12, 13, 14, 23, 24 and 34) and four three-spin subspaces (123, 124, 134 and 234). Equation (G.6a) then yields for the off-diagonal blocks of $\mathbf{X}^{\alpha}_{\mathbb{N}_1\mathbb{N}_1}$

$$\mathbf{X}^{\alpha}_{\mathbb{N}_1(\mu)\mathbb{N}_1(\nu)}(m=4) \;=\; \mathbf{X}^{\alpha}_{\mathbb{N}_1(\mu)\mathbb{N}_1(\nu)}(m=3)\,, \quad \text{for } \mu,\nu \leq 3\,, \tag{G.17}$$

and, for the additional blocks involving spin 4,

$$\mathbf{X}^{\alpha}_{\mathbb{N}_1(1)\mathbb{N}_1(4)}(m=4) \;=\; \mathbf{\Delta}^{\alpha}_{\mathbb{N}_1(1)\mathbb{N}_2(14)} \left(\mathbf{R}^{\alpha}_{\mathbb{N}_2(14)\mathbb{N}_2(14)} + i\,\omega_0\,\mathbf{Q}_2\right)^{-1} \mathbf{\Delta}^{\alpha\,\dagger}_{\mathbb{N}_1(4)\mathbb{N}_2(14)}\,, \tag{G.18a}$$

$$\mathbf{X}^{\alpha}_{\mathbb{N}_1(4)\mathbb{N}_1(1)}(m=4) \;=\; \mathbf{\Delta}^{\alpha}_{\mathbb{N}_1(4)\mathbb{N}_2(14)} \left(\mathbf{R}^{\alpha}_{\mathbb{N}_2(14)\mathbb{N}_2(14)} + i\,\omega_0\,\mathbf{Q}_2\right)^{-1} \mathbf{\Delta}^{\alpha\,\dagger}_{\mathbb{N}_1(1)\mathbb{N}_2(14)}\,, \tag{G.18b}$$

$$\mathbf{X}^{\alpha}_{\mathbb{N}_1(2)\mathbb{N}_1(4)}(m=4) \;=\; \mathbf{\Delta}^{\alpha}_{\mathbb{N}_1(2)\mathbb{N}_2(24)} \left(\mathbf{R}^{\alpha}_{\mathbb{N}_2(24)\mathbb{N}_2(24)} + i\,\omega_0\,\mathbf{Q}_2\right)^{-1} \mathbf{\Delta}^{\alpha\,\dagger}_{\mathbb{N}_1(4)\mathbb{N}_2(24)}\,, \tag{G.18c}$$

$$\mathbf{X}^{\alpha}_{\mathbb{N}_1(4)\mathbb{N}_1(2)}(m=4) \;=\; \mathbf{\Delta}^{\alpha}_{\mathbb{N}_1(4)\mathbb{N}_2(24)} \left(\mathbf{R}^{\alpha}_{\mathbb{N}_2(24)\mathbb{N}_2(24)} + i\,\omega_0\,\mathbf{Q}_2\right)^{-1} \mathbf{\Delta}^{\alpha\,\dagger}_{\mathbb{N}_1(2)\mathbb{N}_2(24)}\,, \tag{G.18d}$$

$$\mathbf{X}^{\alpha}_{\mathbb{N}_1(3)\mathbb{N}_1(4)}(m=4) \;=\; \mathbf{\Delta}^{\alpha}_{\mathbb{N}_1(3)\mathbb{N}_2(34)} \left(\mathbf{R}^{\alpha}_{\mathbb{N}_2(34)\mathbb{N}_2(34)} + i\,\omega_0\,\mathbf{Q}_2\right)^{-1} \mathbf{\Delta}^{\alpha\,\dagger}_{\mathbb{N}_1(4)\mathbb{N}_2(34)}\,, \tag{G.18e}$$

$$\mathbf{X}^{\alpha}_{\mathbb{N}_1(4)\mathbb{N}_1(3)}(m=4) \;=\; \mathbf{\Delta}^{\alpha}_{\mathbb{N}_1(4)\mathbb{N}_2(34)} \left(\mathbf{R}^{\alpha}_{\mathbb{N}_2(34)\mathbb{N}_2(34)} + i\,\omega_0\,\mathbf{Q}_2\right)^{-1} \mathbf{\Delta}^{\alpha\,\dagger}_{\mathbb{N}_1(3)\mathbb{N}_2(34)}\,. \tag{G.18f}$$

Whereas the off-diagonal blocks of $\mathbf{X}^{\alpha}_{\mathbb{N}_1\mathbb{N}_1}$ always contain a single term, Eq. (G.6b) shows that the diagonal blocks contain three terms for $m = 4$,

$$\begin{aligned}
\mathbf{X}^{\alpha}_{\mathbb{N}_1(1)\mathbb{N}_1(1)}(m=4) \;=\;& \mathbf{\Delta}^{\alpha}_{\mathbb{N}_1(1)\mathbb{N}_2(12)} \left(\mathbf{R}^{\alpha}_{\mathbb{N}_2(12)\mathbb{N}_2(12)} + i\,\omega_0\,\mathbf{Q}_2\right)^{-1} \mathbf{\Delta}^{\alpha\,\dagger}_{\mathbb{N}_1(1)\mathbb{N}_2(12)} \\
&+\; \mathbf{\Delta}^{\alpha}_{\mathbb{N}_1(1)\mathbb{N}_2(13)} \left(\mathbf{R}^{\alpha}_{\mathbb{N}_2(13)\mathbb{N}_2(13)} + i\,\omega_0\,\mathbf{Q}_2\right)^{-1} \mathbf{\Delta}^{\alpha\,\dagger}_{\mathbb{N}_1(1)\mathbb{N}_2(13)} \\
&+\; \mathbf{\Delta}^{\alpha}_{\mathbb{N}_1(1)\mathbb{N}_2(14)} \left(\mathbf{R}^{\alpha}_{\mathbb{N}_2(14)\mathbb{N}_2(14)} + i\,\omega_0\,\mathbf{Q}_2\right)^{-1} \mathbf{\Delta}^{\alpha\,\dagger}_{\mathbb{N}_1(1)\mathbb{N}_2(14)}\,,
\end{aligned} \tag{G.19a}$$

$$\begin{aligned}
\mathbf{X}^{\alpha}_{\mathbb{N}_1(2)\mathbb{N}_1(2)}(m=4) \;=\;& \mathbf{\Delta}^{\alpha}_{\mathbb{N}_1(2)\mathbb{N}_2(12)} \left(\mathbf{R}^{\alpha}_{\mathbb{N}_2(12)\mathbb{N}_2(12)} + i\,\omega_0\,\mathbf{Q}_2\right)^{-1} \mathbf{\Delta}^{\alpha\,\dagger}_{\mathbb{N}_1(2)\mathbb{N}_2(12)} \\
&+\; \mathbf{\Delta}^{\alpha}_{\mathbb{N}_1(2)\mathbb{N}_2(23)} \left(\mathbf{R}^{\alpha}_{\mathbb{N}_2(23)\mathbb{N}_2(23)} + i\,\omega_0\,\mathbf{Q}_2\right)^{-1} \mathbf{\Delta}^{\alpha\,\dagger}_{\mathbb{N}_1(2)\mathbb{N}_2(23)} \\
&+\; \mathbf{\Delta}^{\alpha}_{\mathbb{N}_1(2)\mathbb{N}_2(24)} \left(\mathbf{R}^{\alpha}_{\mathbb{N}_2(24)\mathbb{N}_2(24)} + i\,\omega_0\,\mathbf{Q}_2\right)^{-1} \mathbf{\Delta}^{\alpha\,\dagger}_{\mathbb{N}_1(2)\mathbb{N}_2(24)}\,,
\end{aligned} \tag{G.19b}$$

$$\begin{aligned}
\mathbf{X}^{\alpha}_{\mathbb{N}_1(3)\mathbb{N}_1(3)}(m=4) \;=\;& \mathbf{\Delta}^{\alpha}_{\mathbb{N}_1(3)\mathbb{N}_2(13)} \left(\mathbf{R}^{\alpha}_{\mathbb{N}_2(13)\mathbb{N}_2(13)} + i\,\omega_0\,\mathbf{Q}_2\right)^{-1} \mathbf{\Delta}^{\alpha\,\dagger}_{\mathbb{N}_1(3)\mathbb{N}_2(13)} \\
&+\; \mathbf{\Delta}^{\alpha}_{\mathbb{N}_1(3)\mathbb{N}_2(23)} \left(\mathbf{R}^{\alpha}_{\mathbb{N}_2(23)\mathbb{N}_2(23)} + i\,\omega_0\,\mathbf{Q}_2\right)^{-1} \mathbf{\Delta}^{\alpha\,\dagger}_{\mathbb{N}_1(3)\mathbb{N}_2(23)} \\
&+\; \mathbf{\Delta}^{\alpha}_{\mathbb{N}_1(3)\mathbb{N}_2(34)} \left(\mathbf{R}^{\alpha}_{\mathbb{N}_2(34)\mathbb{N}_2(34)} + i\,\omega_0\,\mathbf{Q}_2\right)^{-1} \mathbf{\Delta}^{\alpha\,\dagger}_{\mathbb{N}_1(3)\mathbb{N}_2(34)}\,,
\end{aligned} \tag{G.19c}$$

$$\begin{aligned}
\mathbf{X}^{\alpha}_{\mathbb{N}_1(4)\mathbb{N}_1(4)}(m=4) \;=\;& \mathbf{\Delta}^{\alpha}_{\mathbb{N}_1(4)\mathbb{N}_2(14)} \left(\mathbf{R}^{\alpha}_{\mathbb{N}_2(14)\mathbb{N}_2(14)} + i\,\omega_0\,\mathbf{Q}_2\right)^{-1} \mathbf{\Delta}^{\alpha\,\dagger}_{\mathbb{N}_1(4)\mathbb{N}_2(14)} \\
&+\; \mathbf{\Delta}^{\alpha}_{\mathbb{N}_1(4)\mathbb{N}_2(24)} \left(\mathbf{R}^{\alpha}_{\mathbb{N}_2(24)\mathbb{N}_2(24)} + i\,\omega_0\,\mathbf{Q}_2\right)^{-1} \mathbf{\Delta}^{\alpha\,\dagger}_{\mathbb{N}_1(4)\mathbb{N}_2(24)} \\
&+\; \mathbf{\Delta}^{\alpha}_{\mathbb{N}_1(4)\mathbb{N}_2(34)} \left(\mathbf{R}^{\alpha}_{\mathbb{N}_2(34)\mathbb{N}_2(34)} + i\,\omega_0\,\mathbf{Q}_2\right)^{-1} \mathbf{\Delta}^{\alpha\,\dagger}_{\mathbb{N}_1(4)\mathbb{N}_2(34)}\,.
\end{aligned} \tag{G.19d}$$

For $m = 4$, Eq. (G.8) yields for the off-diagonal block with $\mu = 1$ and $\nu = 2$,

$$
\begin{aligned}
&\mathbf{Y}^{\alpha}_{\mathbb{N}_1(1)\mathbb{N}_1(2)}(m=4) \;= \\
&\big[\boldsymbol{\Delta}^{\alpha}_{\mathbb{N}_1(1)\mathbb{N}_2(12)}\,(\mathbf{R}^{\alpha}_{\mathbb{N}_2(12)\mathbb{N}_2(12)} + i\,\omega_0\,\mathbf{Q}_2)^{-1}\,\boldsymbol{\Delta}^{\alpha}_{\mathbb{N}_2(12)\mathbb{N}_3(123)} + \boldsymbol{\Delta}^{\alpha}_{\mathbb{N}_1(1)\mathbb{N}_2(13)}\,(\mathbf{R}^{\alpha}_{\mathbb{N}_2(13)\mathbb{N}_2(13)} + i\,\omega_0\,\mathbf{Q}_2)^{-1}\,\boldsymbol{\Delta}^{\alpha}_{\mathbb{N}_2(13)\mathbb{N}_3(123)}\big] \\
&\times \big[\mathbf{R}^{\alpha}_{\mathbb{N}_3\mathbb{N}_3} + \mathbf{X}^{\alpha}_{\mathbb{N}_3\mathbb{N}_3} + i\,\mathbf{L}_{\mathrm{Z},\,\mathbb{N}_3\mathbb{N}_3}\big]^{-1}_{\mathbb{N}_3(123)\mathbb{N}_3(123)} \\
&\big[\boldsymbol{\Delta}^{\alpha\,\dagger}_{\mathbb{N}_2(12)\mathbb{N}_3(123)}\,(\mathbf{R}^{\alpha}_{\mathbb{N}_2(12)\mathbb{N}_2(12)} + i\,\omega_0\,\mathbf{Q}_2)^{-1}\boldsymbol{\Delta}^{\alpha\,\dagger}_{\mathbb{N}_1(2)\mathbb{N}_2(12)} + \boldsymbol{\Delta}^{\alpha\,\dagger}_{\mathbb{N}_2(23)\mathbb{N}_3(123)}\,(\mathbf{R}^{\alpha}_{\mathbb{N}_2(23)\mathbb{N}_2(23)} + i\,\omega_0\,\mathbf{Q}_2)^{-1}\boldsymbol{\Delta}^{\alpha\,\dagger}_{\mathbb{N}_1(2)\mathbb{N}_2(23)}\big] \\
&+ \big[\boldsymbol{\Delta}^{\alpha}_{\mathbb{N}_1(1)\mathbb{N}_2(12)}\,(\mathbf{R}^{\alpha}_{\mathbb{N}_2(12)\mathbb{N}_2(12)} + i\,\omega_0\,\mathbf{Q}_2)^{-1}\,\boldsymbol{\Delta}^{\alpha}_{\mathbb{N}_2(12)\mathbb{N}_3(123)} + \boldsymbol{\Delta}^{\alpha}_{\mathbb{N}_1(1)\mathbb{N}_2(13)}\,(\mathbf{R}^{\alpha}_{\mathbb{N}_2(13)\mathbb{N}_2(13)} + i\,\omega_0\,\mathbf{Q}_2)^{-1}\,\boldsymbol{\Delta}^{\alpha}_{\mathbb{N}_2(13)\mathbb{N}_3(123)}\big] \\
&\times \big[\mathbf{R}^{\alpha}_{\mathbb{N}_3\mathbb{N}_3} + \mathbf{X}^{\alpha}_{\mathbb{N}_3\mathbb{N}_3} + i\,\mathbf{L}_{\mathrm{Z},\,\mathbb{N}_3\mathbb{N}_3}\big]^{-1}_{\mathbb{N}_3(123)\mathbb{N}_3(124)} \\
&\big[\boldsymbol{\Delta}^{\alpha\,\dagger}_{\mathbb{N}_2(12)\mathbb{N}_3(124)}\,(\mathbf{R}^{\alpha}_{\mathbb{N}_2(12)\mathbb{N}_2(12)} + i\,\omega_0\,\mathbf{Q}_2)^{-1}\boldsymbol{\Delta}^{\alpha\,\dagger}_{\mathbb{N}_1(2)\mathbb{N}_2(12)} + \boldsymbol{\Delta}^{\alpha\,\dagger}_{\mathbb{N}_2(24)\mathbb{N}_3(124)}\,(\mathbf{R}^{\alpha}_{\mathbb{N}_2(24)\mathbb{N}_2(24)} + i\,\omega_0\,\mathbf{Q}_2)^{-1}\boldsymbol{\Delta}^{\alpha\,\dagger}_{\mathbb{N}_1(2)\mathbb{N}_2(24)}\big] \\
&+ \big[\boldsymbol{\Delta}^{\alpha}_{\mathbb{N}_1(1)\mathbb{N}_2(12)}\,(\mathbf{R}^{\alpha}_{\mathbb{N}_2(12)\mathbb{N}_2(12)} + i\,\omega_0\,\mathbf{Q}_2)^{-1}\,\boldsymbol{\Delta}^{\alpha}_{\mathbb{N}_2(12)\mathbb{N}_3(123)} + \boldsymbol{\Delta}^{\alpha}_{\mathbb{N}_1(1)\mathbb{N}_2(13)}\,(\mathbf{R}^{\alpha}_{\mathbb{N}_2(13)\mathbb{N}_2(13)} + i\,\omega_0\,\mathbf{Q}_2)^{-1}\,\boldsymbol{\Delta}^{\alpha}_{\mathbb{N}_2(13)\mathbb{N}_3(123)}\big] \\
&\times \big[\mathbf{R}^{\alpha}_{\mathbb{N}_3\mathbb{N}_3} + \mathbf{X}^{\alpha}_{\mathbb{N}_3\mathbb{N}_3} + i\,\mathbf{L}_{\mathrm{Z},\,\mathbb{N}_3\mathbb{N}_3}\big]^{-1}_{\mathbb{N}_3(123)\mathbb{N}_3(234)} \\
&\big[\boldsymbol{\Delta}^{\alpha\,\dagger}_{\mathbb{N}_2(24)\mathbb{N}_3(234)}\,(\mathbf{R}^{\alpha}_{\mathbb{N}_2(24)\mathbb{N}_2(24)} + i\,\omega_0\,\mathbf{Q}_2)^{-1}\boldsymbol{\Delta}^{\alpha\,\dagger}_{\mathbb{N}_1(2)\mathbb{N}_2(24)} + \boldsymbol{\Delta}^{\alpha\,\dagger}_{\mathbb{N}_2(23)\mathbb{N}_3(234)}\,(\mathbf{R}^{\alpha}_{\mathbb{N}_2(23)\mathbb{N}_2(23)} + i\,\omega_0\,\mathbf{Q}_2)^{-1}\boldsymbol{\Delta}^{\alpha\,\dagger}_{\mathbb{N}_1(2)\mathbb{N}_2(23)}\big] \\
&+ \big[\boldsymbol{\Delta}^{\alpha}_{\mathbb{N}_1(1)\mathbb{N}_2(12)}\,(\mathbf{R}^{\alpha}_{\mathbb{N}_2(12)\mathbb{N}_2(12)} + i\,\omega_0\,\mathbf{Q}_2)^{-1}\,\boldsymbol{\Delta}^{\alpha}_{\mathbb{N}_2(12)\mathbb{N}_3(124)} + \boldsymbol{\Delta}^{\alpha}_{\mathbb{N}_1(1)\mathbb{N}_2(14)}\,(\mathbf{R}^{\alpha}_{\mathbb{N}_2(14)\mathbb{N}_2(14)} + i\,\omega_0\,\mathbf{Q}_2)^{-1}\,\boldsymbol{\Delta}^{\alpha}_{\mathbb{N}_2(14)\mathbb{N}_3(124)}\big] \\
&\times \big[\mathbf{R}^{\alpha}_{\mathbb{N}_3\mathbb{N}_3} + \mathbf{X}^{\alpha}_{\mathbb{N}_3\mathbb{N}_3} + i\,\mathbf{L}_{\mathrm{Z},\,\mathbb{N}_3\mathbb{N}_3}\big]^{-1}_{\mathbb{N}_3(124)\mathbb{N}_3(124)} \\
&\big[\boldsymbol{\Delta}^{\alpha\,\dagger}_{\mathbb{N}_2(12)\mathbb{N}_3(124)}\,(\mathbf{R}^{\alpha}_{\mathbb{N}_2(12)\mathbb{N}_2(12)} + i\,\omega_0\,\mathbf{Q}_2)^{-1}\boldsymbol{\Delta}^{\alpha\,\dagger}_{\mathbb{N}_1(2)\mathbb{N}_2(12)} + \boldsymbol{\Delta}^{\alpha\,\dagger}_{\mathbb{N}_2(24)\mathbb{N}_3(124)}\,(\mathbf{R}^{\alpha}_{\mathbb{N}_2(24)\mathbb{N}_2(24)} + i\,\omega_0\,\mathbf{Q}_2)^{-1}\boldsymbol{\Delta}^{\alpha\,\dagger}_{\mathbb{N}_1(2)\mathbb{N}_2(24)}\big] \\
&+ \big[\boldsymbol{\Delta}^{\alpha}_{\mathbb{N}_1(1)\mathbb{N}_2(12)}\,(\mathbf{R}^{\alpha}_{\mathbb{N}_2(12)\mathbb{N}_2(12)} + i\,\omega_0\,\mathbf{Q}_2)^{-1}\,\boldsymbol{\Delta}^{\alpha}_{\mathbb{N}_2(12)\mathbb{N}_3(124)} + \boldsymbol{\Delta}^{\alpha}_{\mathbb{N}_1(1)\mathbb{N}_2(14)}\,(\mathbf{R}^{\alpha}_{\mathbb{N}_2(14)\mathbb{N}_2(14)} + i\,\omega_0\,\mathbf{Q}_2)^{-1}\,\boldsymbol{\Delta}^{\alpha}_{\mathbb{N}_2(14)\mathbb{N}_3(124)}\big] \\
&\times \big[\mathbf{R}^{\alpha}_{\mathbb{N}_3\mathbb{N}_3} + \mathbf{X}^{\alpha}_{\mathbb{N}_3\mathbb{N}_3} + i\,\mathbf{L}_{\mathrm{Z},\,\mathbb{N}_3\mathbb{N}_3}\big]^{-1}_{\mathbb{N}_3(124)\mathbb{N}_3(123)} \\
&\big[\boldsymbol{\Delta}^{\alpha\,\dagger}_{\mathbb{N}_2(12)\mathbb{N}_3(123)}\,(\mathbf{R}^{\alpha}_{\mathbb{N}_2(12)\mathbb{N}_2(12)} + i\,\omega_0\,\mathbf{Q}_2)^{-1}\boldsymbol{\Delta}^{\alpha\,\dagger}_{\mathbb{N}_1(2)\mathbb{N}_2(12)} + \boldsymbol{\Delta}^{\alpha\,\dagger}_{\mathbb{N}_2(23)\mathbb{N}_3(123)}\,(\mathbf{R}^{\alpha}_{\mathbb{N}_2(23)\mathbb{N}_2(23)} + i\,\omega_0\,\mathbf{Q}_2)^{-1}\boldsymbol{\Delta}^{\alpha\,\dagger}_{\mathbb{N}_1(2)\mathbb{N}_2(23)}\big] \\
&+ \big[\boldsymbol{\Delta}^{\alpha}_{\mathbb{N}_1(1)\mathbb{N}_2(12)}\,(\mathbf{R}^{\alpha}_{\mathbb{N}_2(12)\mathbb{N}_2(12)} + i\,\omega_0\,\mathbf{Q}_2)^{-1}\,\boldsymbol{\Delta}^{\alpha}_{\mathbb{N}_2(12)\mathbb{N}_3(124)} + \boldsymbol{\Delta}^{\alpha}_{\mathbb{N}_1(1)\mathbb{N}_2(14)}\,(\mathbf{R}^{\alpha}_{\mathbb{N}_2(14)\mathbb{N}_2(14)} + i\,\omega_0\,\mathbf{Q}_2)^{-1}\,\boldsymbol{\Delta}^{\alpha}_{\mathbb{N}_2(14)\mathbb{N}_3(124)}\big] \\
&\times \big[\mathbf{R}^{\alpha}_{\mathbb{N}_3\mathbb{N}_3} + \mathbf{X}^{\alpha}_{\mathbb{N}_3\mathbb{N}_3} + i\,\mathbf{L}_{\mathrm{Z},\,\mathbb{N}_3\mathbb{N}_3}\big]^{-1}_{\mathbb{N}_3(124)\mathbb{N}_3(234)} \\
&\big[\boldsymbol{\Delta}^{\alpha\,\dagger}_{\mathbb{N}_2(24)\mathbb{N}_3(234)}\,(\mathbf{R}^{\alpha}_{\mathbb{N}_2(24)\mathbb{N}_2(24)} + i\,\omega_0\,\mathbf{Q}_2)^{-1}\boldsymbol{\Delta}^{\alpha\,\dagger}_{\mathbb{N}_1(2)\mathbb{N}_2(24)} + \boldsymbol{\Delta}^{\alpha\,\dagger}_{\mathbb{N}_2(23)\mathbb{N}_3(234)}\,(\mathbf{R}^{\alpha}_{\mathbb{N}_2(23)\mathbb{N}_2(23)} + i\,\omega_0\,\mathbf{Q}_2)^{-1}\boldsymbol{\Delta}^{\alpha\,\dagger}_{\mathbb{N}_1(2)\mathbb{N}_2(23)}\big] \\
&+ \big[\boldsymbol{\Delta}^{\alpha}_{\mathbb{N}_1(1)\mathbb{N}_2(13)}\,(\mathbf{R}^{\alpha}_{\mathbb{N}_2(13)\mathbb{N}_2(13)} + i\,\omega_0\,\mathbf{Q}_2)^{-1}\,\boldsymbol{\Delta}^{\alpha}_{\mathbb{N}_2(13)\mathbb{N}_3(134)} + \boldsymbol{\Delta}^{\alpha}_{\mathbb{N}_1(1)\mathbb{N}_2(14)}\,(\mathbf{R}^{\alpha}_{\mathbb{N}_2(14)\mathbb{N}_2(14)} + i\,\omega_0\,\mathbf{Q}_2)^{-1}\,\boldsymbol{\Delta}^{\alpha}_{\mathbb{N}_2(14)\mathbb{N}_3(134)}\big] \\
&\times \big[\mathbf{R}^{\alpha}_{\mathbb{N}_3\mathbb{N}_3} + \mathbf{X}^{\alpha}_{\mathbb{N}_3\mathbb{N}_3} + i\,\mathbf{L}_{\mathrm{Z},\,\mathbb{N}_3\mathbb{N}_3}\big]^{-1}_{\mathbb{N}_3(134)\mathbb{N}_3(123)} \\
&\big[\boldsymbol{\Delta}^{\alpha\,\dagger}_{\mathbb{N}_2(23)\mathbb{N}_3(123)}\,(\mathbf{R}^{\alpha}_{\mathbb{N}_2(23)\mathbb{N}_2(23)} + i\,\omega_0\,\mathbf{Q}_2)^{-1}\boldsymbol{\Delta}^{\alpha\,\dagger}_{\mathbb{N}_1(2)\mathbb{N}_2(23)} + \boldsymbol{\Delta}^{\alpha\,\dagger}_{\mathbb{N}_2(12)\mathbb{N}_3(123)}\,(\mathbf{R}^{\alpha}_{\mathbb{N}_2(12)\mathbb{N}_2(12)} + i\,\omega_0\,\mathbf{Q}_2)^{-1}\boldsymbol{\Delta}^{\alpha\,\dagger}_{\mathbb{N}_1(2)\mathbb{N}_2(12)}\big] \\
&+ \big[\boldsymbol{\Delta}^{\alpha}_{\mathbb{N}_1(1)\mathbb{N}_2(13)}\,(\mathbf{R}^{\alpha}_{\mathbb{N}_2(13)\mathbb{N}_2(13)} + i\,\omega_0\,\mathbf{Q}_2)^{-1}\,\boldsymbol{\Delta}^{\alpha}_{\mathbb{N}_2(13)\mathbb{N}_3(134)} + \boldsymbol{\Delta}^{\alpha}_{\mathbb{N}_1(1)\mathbb{N}_2(14)}\,(\mathbf{R}^{\alpha}_{\mathbb{N}_2(14)\mathbb{N}_2(14)} + i\,\omega_0\,\mathbf{Q}_2)^{-1}\,\boldsymbol{\Delta}^{\alpha}_{\mathbb{N}_2(14)\mathbb{N}_3(134)}\big] \\
&\times \big[\mathbf{R}^{\alpha}_{\mathbb{N}_3\mathbb{N}_3} + \mathbf{X}^{\alpha}_{\mathbb{N}_3\mathbb{N}_3} + i\,\mathbf{L}_{\mathrm{Z},\,\mathbb{N}_3\mathbb{N}_3}\big]^{-1}_{\mathbb{N}_3(134)\mathbb{N}_3(124)} \\
&\big[\boldsymbol{\Delta}^{\alpha\,\dagger}_{\mathbb{N}_2(14)\mathbb{N}_3(124)}\,(\mathbf{R}^{\alpha}_{\mathbb{N}_2(14)\mathbb{N}_2(14)} + i\,\omega_0\,\mathbf{Q}_2)^{-1}\boldsymbol{\Delta}^{\alpha\,\dagger}_{\mathbb{N}_1(2)\mathbb{N}_2(14)} + \boldsymbol{\Delta}^{\alpha\,\dagger}_{\mathbb{N}_2(12)\mathbb{N}_3(124)}\,(\mathbf{R}^{\alpha}_{\mathbb{N}_2(12)\mathbb{N}_2(12)} + i\,\omega_0\,\mathbf{Q}_2)^{-1}\boldsymbol{\Delta}^{\alpha\,\dagger}_{\mathbb{N}_1(2)\mathbb{N}_2(12)}\big] \\
&+ \big[\boldsymbol{\Delta}^{\alpha}_{\mathbb{N}_1(1)\mathbb{N}_2(13)}\,(\mathbf{R}^{\alpha}_{\mathbb{N}_2(13)\mathbb{N}_2(13)} + i\,\omega_0\,\mathbf{Q}_2)^{-1}\,\boldsymbol{\Delta}^{\alpha}_{\mathbb{N}_2(13)\mathbb{N}_3(134)} + \boldsymbol{\Delta}^{\alpha}_{\mathbb{N}_1(1)\mathbb{N}_2(14)}\,(\mathbf{R}^{\alpha}_{\mathbb{N}_2(14)\mathbb{N}_2(14)} + i\,\omega_0\,\mathbf{Q}_2)^{-1}\,\boldsymbol{\Delta}^{\alpha}_{\mathbb{N}_2(14)\mathbb{N}_3(134)}\big] \\
&\times \big[\mathbf{R}^{\alpha}_{\mathbb{N}_3\mathbb{N}_3} + \mathbf{X}^{\alpha}_{\mathbb{N}_3\mathbb{N}_3} + i\,\mathbf{L}_{\mathrm{Z},\,\mathbb{N}_3\mathbb{N}_3}\big]^{-1}_{\mathbb{N}_3(134)\mathbb{N}_3(234)} \\
&\big[\boldsymbol{\Delta}^{\alpha\,\dagger}_{\mathbb{N}_2(24)\mathbb{N}_3(234)}\,(\mathbf{R}^{\alpha}_{\mathbb{N}_2(24)\mathbb{N}_2(24)} + i\,\omega_0\,\mathbf{Q}_2)^{-1}\boldsymbol{\Delta}^{\alpha\,\dagger}_{\mathbb{N}_1(2)\mathbb{N}_2(24)} + \boldsymbol{\Delta}^{\alpha\,\dagger}_{\mathbb{N}_2(23)\mathbb{N}_3(234)}\,(\mathbf{R}^{\alpha}_{\mathbb{N}_2(23)\mathbb{N}_2(23)} + i\,\omega_0\,\mathbf{Q}_2)^{-1}\boldsymbol{\Delta}^{\alpha\,\dagger}_{\mathbb{N}_1(2)\mathbb{N}_2(23)}\big]\,.
\end{aligned}
\tag{G.20}
$$

For $m = 4$, Eq. (G.8) yields for the diagonal block with $\mu = 1$ and $\nu = 1$,

$$
\begin{aligned}
&\mathbf{Y}^{\alpha}_{\mathbb{N}_1(1)\mathbb{N}_1(1)}(m=4) \;= \\
&\big[\boldsymbol{\Delta}^{\alpha}_{\mathbb{N}_1(1)\mathbb{N}_2(12)}\,(\mathbf{R}^{\alpha}_{\mathbb{N}_2(12)\mathbb{N}_2(12)} + i\,\omega_0\,\mathbf{Q}_2)^{-1}\,\boldsymbol{\Delta}^{\alpha}_{\mathbb{N}_2(12)\mathbb{N}_3(123)} + \boldsymbol{\Delta}^{\alpha}_{\mathbb{N}_1(1)\mathbb{N}_2(13)}\,(\mathbf{R}^{\alpha}_{\mathbb{N}_2(13)\mathbb{N}_2(13)} + i\,\omega_0\,\mathbf{Q}_2)^{-1}\,\boldsymbol{\Delta}^{\alpha}_{\mathbb{N}_2(13)\mathbb{N}_3(123)}\big] \\
&\times \big[\mathbf{R}^{\alpha}_{\mathbb{N}_3\mathbb{N}_3} + \mathbf{X}^{\alpha}_{\mathbb{N}_3\mathbb{N}_3} + i\,\mathbf{L}_{\mathrm{Z},\,\mathbb{N}_3\mathbb{N}_3}\big]^{-1}_{\mathbb{N}_3(123)\mathbb{N}_3(123)} \\
&\big[\boldsymbol{\Delta}^{\alpha\,\dagger}_{\mathbb{N}_2(12)\mathbb{N}_3(123)}\,(\mathbf{R}^{\alpha}_{\mathbb{N}_2(12)\mathbb{N}_2(12)} + i\,\omega_0\,\mathbf{Q}_2)^{-1}\boldsymbol{\Delta}^{\alpha\,\dagger}_{\mathbb{N}_1(1)\mathbb{N}_2(12)} + \boldsymbol{\Delta}^{\alpha\,\dagger}_{\mathbb{N}_2(13)\mathbb{N}_3(123)}\,(\mathbf{R}^{\alpha}_{\mathbb{N}_2(13)\mathbb{N}_2(13)} + i\,\omega_0\,\mathbf{Q}_2)^{-1}\boldsymbol{\Delta}^{\alpha\,\dagger}_{\mathbb{N}_1(1)\mathbb{N}_2(13)}\big] \\
&+ \big[\boldsymbol{\Delta}^{\alpha}_{\mathbb{N}_1(1)\mathbb{N}_2(12)}\,(\mathbf{R}^{\alpha}_{\mathbb{N}_2(12)\mathbb{N}_2(12)} + i\,\omega_0\,\mathbf{Q}_2)^{-1}\,\boldsymbol{\Delta}^{\alpha}_{\mathbb{N}_2(12)\mathbb{N}_3(124)} + \boldsymbol{\Delta}^{\alpha}_{\mathbb{N}_1(1)\mathbb{N}_2(14)}\,(\mathbf{R}^{\alpha}_{\mathbb{N}_2(14)\mathbb{N}_2(14)} + i\,\omega_0\,\mathbf{Q}_2)^{-1}\,\boldsymbol{\Delta}^{\alpha}_{\mathbb{N}_2(14)\mathbb{N}_3(124)}\big] \\
&\times \big[\mathbf{R}^{\alpha}_{\mathbb{N}_3\mathbb{N}_3} + \mathbf{X}^{\alpha}_{\mathbb{N}_3\mathbb{N}_3} + i\,\mathbf{L}_{\mathrm{Z},\,\mathbb{N}_3\mathbb{N}_3}\big]^{-1}_{\mathbb{N}_3(124)\mathbb{N}_3(123)} \\
&\big[\boldsymbol{\Delta}^{\alpha\,\dagger}_{\mathbb{N}_2(12)\mathbb{N}_3(123)}\,(\mathbf{R}^{\alpha}_{\mathbb{N}_2(12)\mathbb{N}_2(12)} + i\,\omega_0\,\mathbf{Q}_2)^{-1}\boldsymbol{\Delta}^{\alpha\,\dagger}_{\mathbb{N}_1(1)\mathbb{N}_2(12)} + \boldsymbol{\Delta}^{\alpha\,\dagger}_{\mathbb{N}_2(13)\mathbb{N}_3(123)}\,(\mathbf{R}^{\alpha}_{\mathbb{N}_2(13)\mathbb{N}_2(13)} + i\,\omega_0\,\mathbf{Q}_2)^{-1}\boldsymbol{\Delta}^{\alpha\,\dagger}_{\mathbb{N}_1(1)\mathbb{N}_2(13)}\big] \\
&+ \big[\boldsymbol{\Delta}^{\alpha}_{\mathbb{N}_1(1)\mathbb{N}_2(12)}\,(\mathbf{R}^{\alpha}_{\mathbb{N}_2(12)\mathbb{N}_2(12)} + i\,\omega_0\,\mathbf{Q}_2)^{-1}\,\boldsymbol{\Delta}^{\alpha}_{\mathbb{N}_2(12)\mathbb{N}_3(123)} + \boldsymbol{\Delta}^{\alpha}_{\mathbb{N}_1(1)\mathbb{N}_2(13)}\,(\mathbf{R}^{\alpha}_{\mathbb{N}_2(13)\mathbb{N}_2(13)} + i\,\omega_0\,\mathbf{Q}_2)^{-1}\,\boldsymbol{\Delta}^{\alpha}_{\mathbb{N}_2(13)\mathbb{N}_3(123)}\big] \\
&\times \big[\mathbf{R}^{\alpha}_{\mathbb{N}_3\mathbb{N}_3} + \mathbf{X}^{\alpha}_{\mathbb{N}_3\mathbb{N}_3} + i\,\mathbf{L}_{\mathrm{Z},\,\mathbb{N}_3\mathbb{N}_3}\big]^{-1}_{\mathbb{N}_3(123)\mathbb{N}_3(124)} \\
&\big[\boldsymbol{\Delta}^{\alpha\,\dagger}_{\mathbb{N}_2(12)\mathbb{N}_3(124)}\,(\mathbf{R}^{\alpha}_{\mathbb{N}_2(12)\mathbb{N}_2(12)} + i\,\omega_0\,\mathbf{Q}_2)^{-1}\boldsymbol{\Delta}^{\alpha\,\dagger}_{\mathbb{N}_1(1)\mathbb{N}_2(12)} + \boldsymbol{\Delta}^{\alpha\,\dagger}_{\mathbb{N}_2(14)\mathbb{N}_3(124)}\,(\mathbf{R}^{\alpha}_{\mathbb{N}_2(14)\mathbb{N}_2(14)} + i\,\omega_0\,\mathbf{Q}_2)^{-1}\boldsymbol{\Delta}^{\alpha\,\dagger}_{\mathbb{N}_1(1)\mathbb{N}_2(14)}\big] \\
&+ \big[\boldsymbol{\Delta}^{\alpha}_{\mathbb{N}_1(1)\mathbb{N}_2(12)}\,(\mathbf{R}^{\alpha}_{\mathbb{N}_2(12)\mathbb{N}_2(12)} + i\,\omega_0\,\mathbf{Q}_2)^{-1}\,\boldsymbol{\Delta}^{\alpha}_{\mathbb{N}_2(12)\mathbb{N}_3(124)} + \boldsymbol{\Delta}^{\alpha}_{\mathbb{N}_1(1)\mathbb{N}_2(14)}\,(\mathbf{R}^{\alpha}_{\mathbb{N}_2(14)\mathbb{N}_2(14)} + i\,\omega_0\,\mathbf{Q}_2)^{-1}\,\boldsymbol{\Delta}^{\alpha}_{\mathbb{N}_2(14)\mathbb{N}_3(124)}\big] \\
&\times \big[\mathbf{R}^{\alpha}_{\mathbb{N}_3\mathbb{N}_3} + \mathbf{X}^{\alpha}_{\mathbb{N}_3\mathbb{N}_3} + i\,\mathbf{L}_{\mathrm{Z},\,\mathbb{N}_3\mathbb{N}_3}\big]^{-1}_{\mathbb{N}_3(124)\mathbb{N}_3(124)} \\
&\big[\boldsymbol{\Delta}^{\alpha\,\dagger}_{\mathbb{N}_2(12)\mathbb{N}_3(124)}\,(\mathbf{R}^{\alpha}_{\mathbb{N}_2(12)\mathbb{N}_2(12)} + i\,\omega_0\,\mathbf{Q}_2)^{-1}\boldsymbol{\Delta}^{\alpha\,\dagger}_{\mathbb{N}_1(1)\mathbb{N}_2(12)} + \boldsymbol{\Delta}^{\alpha\,\dagger}_{\mathbb{N}_2(14)\mathbb{N}_3(124)}\,(\mathbf{R}^{\alpha}_{\mathbb{N}_2(14)\mathbb{N}_2(14)} + i\,\omega_0\,\mathbf{Q}_2)^{-1}\boldsymbol{\Delta}^{\alpha\,\dagger}_{\mathbb{N}_1(1)\mathbb{N}_2(14)}\big] \\
&+ \big[\boldsymbol{\Delta}^{\alpha}_{\mathbb{N}_1(1)\mathbb{N}_2(12)}\,(\mathbf{R}^{\alpha}_{\mathbb{N}_2(12)\mathbb{N}_2(12)} + i\,\omega_0\,\mathbf{Q}_2)^{-1}\,\boldsymbol{\Delta}^{\alpha}_{\mathbb{N}_2(12)\mathbb{N}_3(123)} + \boldsymbol{\Delta}^{\alpha}_{\mathbb{N}_1(1)\mathbb{N}_2(13)}\,(\mathbf{R}^{\alpha}_{\mathbb{N}_2(13)\mathbb{N}_2(13)} + i\,\omega_0\,\mathbf{Q}_2)^{-1}\,\boldsymbol{\Delta}^{\alpha}_{\mathbb{N}_2(13)\mathbb{N}_3(123)}\big] \\
&\times \big[\mathbf{R}^{\alpha}_{\mathbb{N}_3\mathbb{N}_3} + \mathbf{X}^{\alpha}_{\mathbb{N}_3\mathbb{N}_3} + i\,\mathbf{L}_{\mathrm{Z},\,\mathbb{N}_3\mathbb{N}_3}\big]^{-1}_{\mathbb{N}_3(123)\mathbb{N}_3(134)} \\
&\big[\boldsymbol{\Delta}^{\alpha\,\dagger}_{\mathbb{N}_2(13)\mathbb{N}_3(134)}\,(\mathbf{R}^{\alpha}_{\mathbb{N}_2(13)\mathbb{N}_2(13)} + i\,\omega_0\,\mathbf{Q}_2)^{-1}\boldsymbol{\Delta}^{\alpha\,\dagger}_{\mathbb{N}_1(1)\mathbb{N}_2(13)} + \boldsymbol{\Delta}^{\alpha\,\dagger}_{\mathbb{N}_2(14)\mathbb{N}_3(134)}\,(\mathbf{R}^{\alpha}_{\mathbb{N}_2(14)\mathbb{N}_2(14)} + i\,\omega_0\,\mathbf{Q}_2)^{-1}\boldsymbol{\Delta}^{\alpha\,\dagger}_{\mathbb{N}_1(1)\mathbb{N}_2(14)}\big] \\
&+ \big[\boldsymbol{\Delta}^{\alpha}_{\mathbb{N}_1(1)\mathbb{N}_2(13)}\,(\mathbf{R}^{\alpha}_{\mathbb{N}_2(13)\mathbb{N}_2(13)} + i\,\omega_0\,\mathbf{Q}_2)^{-1}\,\boldsymbol{\Delta}^{\alpha}_{\mathbb{N}_2(13)\mathbb{N}_3(134)} + \boldsymbol{\Delta}^{\alpha}_{\mathbb{N}_1(1)\mathbb{N}_2(14)}\,(\mathbf{R}^{\alpha}_{\mathbb{N}_2(14)\mathbb{N}_2(14)} + i\,\omega_0\,\mathbf{Q}_2)^{-1}\,\boldsymbol{\Delta}^{\alpha}_{\mathbb{N}_2(14)\mathbb{N}_3(134)}\big] \\
&\times \big[\mathbf{R}^{\alpha}_{\mathbb{N}_3\mathbb{N}_3} + \mathbf{X}^{\alpha}_{\mathbb{N}_3\mathbb{N}_3} + i\,\mathbf{L}_{\mathrm{Z},\,\mathbb{N}_3\mathbb{N}_3}\big]^{-1}_{\mathbb{N}_3(134)\mathbb{N}_3(123)} \\
&\big[\boldsymbol{\Delta}^{\alpha\,\dagger}_{\mathbb{N}_2(12)\mathbb{N}_3(123)}\,(\mathbf{R}^{\alpha}_{\mathbb{N}_2(12)\mathbb{N}_2(12)} + i\,\omega_0\,\mathbf{Q}_2)^{-1}\boldsymbol{\Delta}^{\alpha\,\dagger}_{\mathbb{N}_1(1)\mathbb{N}_2(12)} + \boldsymbol{\Delta}^{\alpha\,\dagger}_{\mathbb{N}_2(13)\mathbb{N}_3(123)}\,(\mathbf{R}^{\alpha}_{\mathbb{N}_2(13)\mathbb{N}_2(13)} + i\,\omega_0\,\mathbf{Q}_2)^{-1}\boldsymbol{\Delta}^{\alpha\,\dagger}_{\mathbb{N}_1(1)\mathbb{N}_2(13)}\big] \\
&+ \big[\boldsymbol{\Delta}^{\alpha}_{\mathbb{N}_1(1)\mathbb{N}_2(12)}\,(\mathbf{R}^{\alpha}_{\mathbb{N}_2(12)\mathbb{N}_2(12)} + i\,\omega_0\,\mathbf{Q}_2)^{-1}\,\boldsymbol{\Delta}^{\alpha}_{\mathbb{N}_2(12)\mathbb{N}_3(124)} + \boldsymbol{\Delta}^{\alpha}_{\mathbb{N}_1(1)\mathbb{N}_2(14)}\,(\mathbf{R}^{\alpha}_{\mathbb{N}_2(14)\mathbb{N}_2(14)} + i\,\omega_0\,\mathbf{Q}_2)^{-1}\,\boldsymbol{\Delta}^{\alpha}_{\mathbb{N}_2(14)\mathbb{N}_3(124)}\big] \\
&\times \big[\mathbf{R}^{\alpha}_{\mathbb{N}_3\mathbb{N}_3} + \mathbf{X}^{\alpha}_{\mathbb{N}_3\mathbb{N}_3} + i\,\mathbf{L}_{\mathrm{Z},\,\mathbb{N}_3\mathbb{N}_3}\big]^{-1}_{\mathbb{N}_3(124)\mathbb{N}_3(134)} \\
&\big[\boldsymbol{\Delta}^{\alpha\,\dagger}_{\mathbb{N}_2(13)\mathbb{N}_3(134)}\,(\mathbf{R}^{\alpha}_{\mathbb{N}_2(13)\mathbb{N}_2(13)} + i\,\omega_0\,\mathbf{Q}_2)^{-1}\boldsymbol{\Delta}^{\alpha\,\dagger}_{\mathbb{N}_1(1)\mathbb{N}_2(13)} + \boldsymbol{\Delta}^{\alpha\,\dagger}_{\mathbb{N}_2(14)\mathbb{N}_3(134)}\,(\mathbf{R}^{\alpha}_{\mathbb{N}_2(14)\mathbb{N}_2(14)} + i\,\omega_0\,\mathbf{Q}_2)^{-1}\boldsymbol{\Delta}^{\alpha\,\dagger}_{\mathbb{N}_1(1)\mathbb{N}_2(14)}\big] \\
&+ \big[\boldsymbol{\Delta}^{\alpha}_{\mathbb{N}_1(1)\mathbb{N}_2(13)}\,(\mathbf{R}^{\alpha}_{\mathbb{N}_2(13)\mathbb{N}_2(13)} + i\,\omega_0\,\mathbf{Q}_2)^{-1}\,\boldsymbol{\Delta}^{\alpha}_{\mathbb{N}_2(13)\mathbb{N}_3(134)} + \boldsymbol{\Delta}^{\alpha}_{\mathbb{N}_1(1)\mathbb{N}_2(14)}\,(\mathbf{R}^{\alpha}_{\mathbb{N}_2(14)\mathbb{N}_2(14)} + i\,\omega_0\,\mathbf{Q}_2)^{-1}\,\boldsymbol{\Delta}^{\alpha}_{\mathbb{N}_2(14)\mathbb{N}_3(134)}\big] \\
&\times \big[\mathbf{R}^{\alpha}_{\mathbb{N}_3\mathbb{N}_3} + \mathbf{X}^{\alpha}_{\mathbb{N}_3\mathbb{N}_3} + i\,\mathbf{L}_{\mathrm{Z},\,\mathbb{N}_3\mathbb{N}_3}\big]^{-1}_{\mathbb{N}_3(134)\mathbb{N}_3(124)} \\
&\big[\boldsymbol{\Delta}^{\alpha\,\dagger}_{\mathbb{N}_2(14)\mathbb{N}_3(124)}\,(\mathbf{R}^{\alpha}_{\mathbb{N}_2(14)\mathbb{N}_2(14)} + i\,\omega_0\,\mathbf{Q}_2)^{-1}\boldsymbol{\Delta}^{\alpha\,\dagger}_{\mathbb{N}_1(1)\mathbb{N}_2(14)} + \boldsymbol{\Delta}^{\alpha\,\dagger}_{\mathbb{N}_2(12)\mathbb{N}_3(124)}\,(\mathbf{R}^{\alpha}_{\mathbb{N}_2(12)\mathbb{N}_2(12)} + i\,\omega_0\,\mathbf{Q}_2)^{-1}\boldsymbol{\Delta}^{\alpha\,\dagger}_{\mathbb{N}_1(1)\mathbb{N}_2(12)}\big] \\
&+ \big[\boldsymbol{\Delta}^{\alpha}_{\mathbb{N}_1(1)\mathbb{N}_2(13)}\,(\mathbf{R}^{\alpha}_{\mathbb{N}_2(13)\mathbb{N}_2(13)} + i\,\omega_0\,\mathbf{Q}_2)^{-1}\,\boldsymbol{\Delta}^{\alpha}_{\mathbb{N}_2(13)\mathbb{N}_3(134)} + \boldsymbol{\Delta}^{\alpha}_{\mathbb{N}_1(1)\mathbb{N}_2(14)}\,(\mathbf{R}^{\alpha}_{\mathbb{N}_2(14)\mathbb{N}_2(14)} + i\,\omega_0\,\mathbf{Q}_2)^{-1}\,\boldsymbol{\Delta}^{\alpha}_{\mathbb{N}_2(14)\mathbb{N}_3(134)}\big] \\
&\times \big[\mathbf{R}^{\alpha}_{\mathbb{N}_3\mathbb{N}_3} + \mathbf{X}^{\alpha}_{\mathbb{N}_3\mathbb{N}_3} + i\,\mathbf{L}_{\mathrm{Z},\,\mathbb{N}_3\mathbb{N}_3}\big]^{-1}_{\mathbb{N}_3(134)\mathbb{N}_3(134)} \\
&\big[\boldsymbol{\Delta}^{\alpha\,\dagger}_{\mathbb{N}_2(14)\mathbb{N}_3(134)}\,(\mathbf{R}^{\alpha}_{\mathbb{N}_2(14)\mathbb{N}_2(14)} + i\,\omega_0\,\mathbf{Q}_2)^{-1}\boldsymbol{\Delta}^{\alpha\,\dagger}_{\mathbb{N}_1(1)\mathbb{N}_2(14)} + \boldsymbol{\Delta}^{\alpha\,\dagger}_{\mathbb{N}_2(13)\mathbb{N}_3(134)}\,(\mathbf{R}^{\alpha}_{\mathbb{N}_2(13)\mathbb{N}_2(13)} + i\,\omega_0\,\mathbf{Q}_2)^{-1}\boldsymbol{\Delta}^{\alpha\,\dagger}_{\mathbb{N}_1(1)\mathbb{N}_2(13)}\big]\,.
\end{aligned}
\tag{G.21}
$$

For $m = 3$, with a single three-spin subspace, the supermatrix $\mathbf{X}^{\alpha}_{\mathbb{N}_3\mathbb{N}_3}$ consists of a single 27×27 block. For $m = 4$, with four three-spin subspaces, $\mathbf{X}^{\alpha}_{\mathbb{N}_3\mathbb{N}_3}$ has $4^2 = 16$ blocks given by Eq. (G.9). Each of the four diagonal blocks contains three terms, corresponding to the three two-spin subspaces contained in each three-spin subspace,

$$\begin{aligned}
\mathbf{X}^{\alpha}_{\mathbb{N}_3(123)\mathbb{N}_3(123)}(m=4) \;=\; & \boldsymbol{\Delta}^{\alpha\,\dagger}_{\mathbb{N}_2(12)\mathbb{N}_3(123)} \left(\mathbf{R}^{\alpha}_{\mathbb{N}_2(12)\mathbb{N}_2(12)} + i\,\omega_0\,\mathbf{Q}_2\right)^{-1} \boldsymbol{\Delta}^{\alpha}_{\mathbb{N}_2(12)\mathbb{N}_3(123)} \\
& + \boldsymbol{\Delta}^{\alpha\,\dagger}_{\mathbb{N}_2(13)\mathbb{N}_3(123)} \left(\mathbf{R}^{\alpha}_{\mathbb{N}_2(13)\mathbb{N}_2(13)} + i\,\omega_0\,\mathbf{Q}_2\right)^{-1} \boldsymbol{\Delta}^{\alpha}_{\mathbb{N}_2(13)\mathbb{N}_3(123)} \\
& + \boldsymbol{\Delta}^{\alpha\,\dagger}_{\mathbb{N}_2(23)\mathbb{N}_3(123)} \left(\mathbf{R}^{\alpha}_{\mathbb{N}_2(23)\mathbb{N}_2(23)} + i\,\omega_0\,\mathbf{Q}_2\right)^{-1} \boldsymbol{\Delta}^{\alpha}_{\mathbb{N}_2(23)\mathbb{N}_3(123)} \,, \qquad \text{(G.22a)} \\
\mathbf{X}^{\alpha}_{\mathbb{N}_3(124)\mathbb{N}_3(124)}(m=4) \;=\; & \boldsymbol{\Delta}^{\alpha\,\dagger}_{\mathbb{N}_2(12)\mathbb{N}_3(124)} \left(\mathbf{R}^{\alpha}_{\mathbb{N}_2(12)\mathbb{N}_2(12)} + i\,\omega_0\,\mathbf{Q}_2\right)^{-1} \boldsymbol{\Delta}^{\alpha}_{\mathbb{N}_2(12)\mathbb{N}_3(124)} \\
& + \boldsymbol{\Delta}^{\alpha\,\dagger}_{\mathbb{N}_2(14)\mathbb{N}_3(124)} \left(\mathbf{R}^{\alpha}_{\mathbb{N}_2(14)\mathbb{N}_2(14)} + i\,\omega_0\,\mathbf{Q}_2\right)^{-1} \boldsymbol{\Delta}^{\alpha}_{\mathbb{N}_2(14)\mathbb{N}_3(124)} \\
& + \boldsymbol{\Delta}^{\alpha\,\dagger}_{\mathbb{N}_2(24)\mathbb{N}_3(124)} \left(\mathbf{R}^{\alpha}_{\mathbb{N}_2(24)\mathbb{N}_2(24)} + i\,\omega_0\,\mathbf{Q}_2\right)^{-1} \boldsymbol{\Delta}^{\alpha}_{\mathbb{N}_2(24)\mathbb{N}_3(124)} \,, \qquad \text{(G.22b)} \\
\mathbf{X}^{\alpha}_{\mathbb{N}_3(134)\mathbb{N}_3(134)}(m=4) \;=\; & \boldsymbol{\Delta}^{\alpha\,\dagger}_{\mathbb{N}_2(13)\mathbb{N}_3(134)} \left(\mathbf{R}^{\alpha}_{\mathbb{N}_2(13)\mathbb{N}_2(13)} + i\,\omega_0\,\mathbf{Q}_2\right)^{-1} \boldsymbol{\Delta}^{\alpha}_{\mathbb{N}_2(13)\mathbb{N}_3(134)} \\
& + \boldsymbol{\Delta}^{\alpha\,\dagger}_{\mathbb{N}_2(14)\mathbb{N}_3(134)} \left(\mathbf{R}^{\alpha}_{\mathbb{N}_2(14)\mathbb{N}_2(14)} + i\,\omega_0\,\mathbf{Q}_2\right)^{-1} \boldsymbol{\Delta}^{\alpha}_{\mathbb{N}_2(14)\mathbb{N}_3(134)} \\
& + \boldsymbol{\Delta}^{\alpha\,\dagger}_{\mathbb{N}_2(34)\mathbb{N}_3(134)} \left(\mathbf{R}^{\alpha}_{\mathbb{N}_2(34)\mathbb{N}_2(34)} + i\,\omega_0\,\mathbf{Q}_2\right)^{-1} \boldsymbol{\Delta}^{\alpha}_{\mathbb{N}_2(34)\mathbb{N}_3(134)} \,, \qquad \text{(G.22c)} \\
\mathbf{X}^{\alpha}_{\mathbb{N}_3(234)\mathbb{N}_3(234)}(m=4) \;=\; & \boldsymbol{\Delta}^{\alpha\,\dagger}_{\mathbb{N}_2(23)\mathbb{N}_3(234)} \left(\mathbf{R}^{\alpha}_{\mathbb{N}_2(23)\mathbb{N}_2(23)} + i\,\omega_0\,\mathbf{Q}_2\right)^{-1} \boldsymbol{\Delta}^{\alpha}_{\mathbb{N}_2(23)\mathbb{N}_3(234)} \\
& + \boldsymbol{\Delta}^{\alpha\,\dagger}_{\mathbb{N}_2(24)\mathbb{N}_3(234)} \left(\mathbf{R}^{\alpha}_{\mathbb{N}_2(24)\mathbb{N}_2(24)} + i\,\omega_0\,\mathbf{Q}_2\right)^{-1} \boldsymbol{\Delta}^{\alpha}_{\mathbb{N}_2(24)\mathbb{N}_3(234)} \\
& + \boldsymbol{\Delta}^{\alpha\,\dagger}_{\mathbb{N}_2(34)\mathbb{N}_3(234)} \left(\mathbf{R}^{\alpha}_{\mathbb{N}_2(34)\mathbb{N}_2(34)} + i\,\omega_0\,\mathbf{Q}_2\right)^{-1} \boldsymbol{\Delta}^{\alpha}_{\mathbb{N}_2(34)\mathbb{N}_3(234)} \,. \qquad \text{(G.22d)}
\end{aligned}$$

For the off-diagonal blocks, only one of the three terms in Eq. (G.9) contributes, because there can only be one two-spin subspace contained in each of two different three-spin subspaces (which must share two spins). Some of the 12 off-diagonal blocks for $m = 4$ are (the others are readily obtained by analogy),

$$\begin{aligned}
\mathbf{X}^{\alpha}_{\mathbb{N}_3(123)\mathbb{N}_3(124)}(m=4) \;=\; & \boldsymbol{\Delta}^{\alpha\,\dagger}_{\mathbb{N}_2(12)\mathbb{N}_3(123)} \left(\mathbf{R}^{\alpha}_{\mathbb{N}_2(12)\mathbb{N}_2(12)} + i\,\omega_0\,\mathbf{Q}_2\right)^{-1} \boldsymbol{\Delta}^{\alpha}_{\mathbb{N}_2(12)\mathbb{N}_3(124)} \,, \qquad \text{(G.23a)} \\
\mathbf{X}^{\alpha}_{\mathbb{N}_3(124)\mathbb{N}_3(123)}(m=4) \;=\; & \boldsymbol{\Delta}^{\alpha\,\dagger}_{\mathbb{N}_2(12)\mathbb{N}_3(124)} \left(\mathbf{R}^{\alpha}_{\mathbb{N}_2(12)\mathbb{N}_2(12)} + i\,\omega_0\,\mathbf{Q}_2\right)^{-1} \boldsymbol{\Delta}^{\alpha}_{\mathbb{N}_2(12)\mathbb{N}_3(123)} \,, \qquad \text{(G.23b)} \\
\mathbf{X}^{\alpha}_{\mathbb{N}_3(123)\mathbb{N}_3(134)}(m=4) \;=\; & \boldsymbol{\Delta}^{\alpha\,\dagger}_{\mathbb{N}_2(13)\mathbb{N}_3(123)} \left(\mathbf{R}^{\alpha}_{\mathbb{N}_2(13)\mathbb{N}_2(13)} + i\,\omega_0\,\mathbf{Q}_2\right)^{-1} \boldsymbol{\Delta}^{\alpha}_{\mathbb{N}_2(13)\mathbb{N}_3(134)} \,, \qquad \text{(G.23c)} \\
\mathbf{X}^{\alpha}_{\mathbb{N}_3(123)\mathbb{N}_3(234)}(m=4) \;=\; & \boldsymbol{\Delta}^{\alpha\,\dagger}_{\mathbb{N}_2(23)\mathbb{N}_3(123)} \left(\mathbf{R}^{\alpha}_{\mathbb{N}_2(23)\mathbb{N}_2(23)} + i\,\omega_0\,\mathbf{Q}_2\right)^{-1} \boldsymbol{\Delta}^{\alpha}_{\mathbb{N}_2(23)\mathbb{N}_3(234)} \,, \qquad \text{(G.23d)} \\
\mathbf{X}^{\alpha}_{\mathbb{N}_3(234)\mathbb{N}_3(124)}(m=4) \;=\; & \boldsymbol{\Delta}^{\alpha\,\dagger}_{\mathbb{N}_2(24)\mathbb{N}_3(234)} \left(\mathbf{R}^{\alpha}_{\mathbb{N}_2(24)\mathbb{N}_2(24)} + i\,\omega_0\,\mathbf{Q}_2\right)^{-1} \boldsymbol{\Delta}^{\alpha}_{\mathbb{N}_2(24)\mathbb{N}_3(124)} \,. \qquad \text{(G.23e)}
\end{aligned}$$

We now consider the general case, with $m \geq 3$. The ILRR for the $IP_m{-}I$ case is given by Eqs. (G.1) – (G.5). In Eq. (G.4), we need to invert the $3m \times 3m$ matrix $\mathbf{V}^{\alpha}_{\mathbb{N}_1\mathbb{N}_1}$, the constituent 3×3 blocks of which are given by Eq. (G.5). To obtain $\mathbf{V}^{\alpha}_{\mathbb{N}_1\mathbb{N}_1}$, we need to calculate m diagonal blocks $\mathbf{R}^{\alpha}_{\mathbb{N}_1(\mu)\mathbb{N}_1(\mu)}$, m^2 blocks $\mathbf{X}^{\alpha}_{\mathbb{N}_1(\mu)\mathbb{N}_1(\nu)}$, and m^2 blocks $\mathbf{Y}^{\alpha}_{\mathbb{N}_1(\mu)\mathbb{N}_1(\nu)}$. The matrices $\mathbf{X}^{\alpha}_{\mathbb{N}_1\mathbb{N}_1}$ and $\mathbf{Y}^{\alpha}_{\mathbb{N}_1\mathbb{N}_1}$ are neither symmetric, nor Hermitian.

According to Eq. (G.6a), the off-diagonal ($\mu \neq \nu$) 3×3 blocks $\mathbf{X}^{\alpha}_{\mathbb{N}_1(\mu)\mathbb{N}_1(\nu)}$ contain a single term, which involves the two-spin subspace $\mathbb{N}_2(\mu\nu)$. The diagonal blocks $\mathbf{X}^{\alpha}_{\mathbb{N}_1(\mu)\mathbb{N}_1(\mu)}$

contain $m-1$ terms, corresponding to the two-spin subspaces involving spin μ and one of the remaining $m-1$ spins. We can thus express Eq. (G.6b) as

$$\mathbf{X}^{\alpha}_{\mathbb{N}_1(\mu)\mathbb{N}_1(\mu)} \;=\; \sum_{\mathbf{a}_\mu=1}^{m-1} \mathbf{\Delta}^{\alpha}_{\mathbb{N}_1(\mu)\mathbb{N}_2(\mathbf{a}_\mu)} \big(\mathbf{R}^{\alpha}_{\mathbb{N}_2(\mathbf{a}_\mu)\mathbb{N}_2(\mathbf{a}_\mu)} + i\,\omega_0\,\mathbf{Q}_2\big)^{-1} \mathbf{\Delta}^{\alpha\,\dagger}_{\mathbb{N}_1(\mu)\mathbb{N}_2(\mathbf{a}_\mu)} \,, \tag{G.24}$$

where $\mathbb{N}_2(\mathbf{a}_\mu)$ denotes one of the $m-1$ two-spin subspaces that includes spin μ.

The 3×3 blocks $\mathbf{Y}^{\alpha}_{\mathbb{N}_1(\mu)\mathbb{N}_1(\nu)}$ are given by Eqs. (G.7) – (G.9). Equations (G.7) and (G.8) may be expressed concisely as

$$\mathbf{Y}^{\alpha}_{\mathbb{N}_1(\mu)\mathbb{N}_1(\nu)} \;=\; \sum_{\mathbf{A}_\mu=1}^{\mathcal{N}(m)} \sum_{\mathbf{A}_\nu=1}^{\mathcal{N}(m)} \nabla^{\alpha}_{\mathbb{N}_1(\mu)\mathbb{N}_3(\mathbf{A}_\mu)} \mathbf{\Xi}^{\alpha}_{\mathbb{N}_3(\mathbf{A}_\mu)\mathbb{N}_3(\mathbf{A}_\nu)} \overline{\nabla}^{\alpha}_{\mathbb{N}_3(\mathbf{A}_\nu)\mathbb{N}_1(\nu)} \,, \tag{G.25}$$

where $\mathbb{N}_3(\mathbf{A}_\mu)$ denotes one of the $\mathcal{N}(m) = (m-1)(m-2)/2$ three-spin subspaces that includes spin μ. For example, for $m=5$ the six subspaces that include spin 3 are 123, 134, 135, 234, 235 and 345. Note that the ordering of the spins is irrelevant here; we consistently use ascending order. Note also that some subspaces may occur in both sets $\{\mathbb{N}_3(\mathbf{A}_\mu)\}$ and $\{\mathbb{N}_3(\mathbf{A}_\nu)\}$. For example, for $m=4$ the three-spin subspaces that include spin 1 are 123, 124 and 134, whereas those including spin 2 are 123, 124 and 234.

Equation (G.25) is valid for diagonal ($\mu=\nu$) as well as for off-diagonal ($\mu\neq\nu$) blocks. In either case, $\mathbf{Y}^{\alpha}_{\mathbb{N}_1(\mu)\mathbb{N}_1(\nu)}$ is composed of $[\mathcal{N}(m)]^2 = (m-1)^2(m-2)^2/4$ terms. Three new quantities are introduced in Eq. (G.25). The 3×27 matrix $\nabla^{\alpha}_{\mathbb{N}_1(\mu)\mathbb{N}_3(\mathbf{A}_\mu)}$ and the 27×3 matrix $\overline{\nabla}^{\alpha}_{\mathbb{N}_3(\mathbf{A}_\mu)\mathbb{N}_1(\mu)}$ are defined as

$$\nabla^{\alpha}_{\mathbb{N}_1(\mu)\mathbb{N}_3(\mathbf{A}_\mu)} \;=\; \sum_{\mathbf{b}_\mu=1}^{2} \mathbf{\Delta}^{\alpha}_{\mathbb{N}_1(\mu)\mathbb{N}_2(\mathbf{b}_\mu)} \big(\mathbf{R}^{\alpha}_{\mathbb{N}_2(\mathbf{b}_\mu)\mathbb{N}_2(\mathbf{b}_\mu)} + i\,\omega_0\,\mathbf{Q}_2\big)^{-1} \mathbf{\Delta}^{\alpha}_{\mathbb{N}_2(\mathbf{b}_\mu)\mathbb{N}_3(\mathbf{A}_\mu)} \,, \tag{G.26a}$$

$$\overline{\nabla}^{\alpha}_{\mathbb{N}_3(\mathbf{A}_\mu)\mathbb{N}_1(\mu)} \;=\; \sum_{\mathbf{b}_\mu=1}^{2} \mathbf{\Delta}^{\alpha\,\dagger}_{\mathbb{N}_2(\mathbf{b}_\mu)\mathbb{N}_3(\mathbf{A}_\mu)} \big(\mathbf{R}^{\alpha}_{\mathbb{N}_2(\mathbf{b}_\mu)\mathbb{N}_2(\mathbf{b}_\mu)} + i\,\omega_0\,\mathbf{Q}_2\big)^{-1} \mathbf{\Delta}^{\alpha\,\dagger}_{\mathbb{N}_1(\mu)\mathbb{N}_2(\mathbf{b}_\mu)} \,, \tag{G.26b}$$

where $\mathbb{N}_2(\mathbf{b}_\mu)$ denotes one of the two two-spin subspaces that contain spin μ and one of the other spins in the three-spin subspace $\mathbb{N}_3(\mathbf{A}_\mu)$.

The $9m(m-1)(m-2)/2 \times 9m(m-1)(m-2)/2$ matrix $\mathbf{\Xi}^{\alpha}_{\mathbb{N}_3\mathbb{N}_3}$, whose 27×27 blocks $\mathbf{\Xi}^{\alpha}_{\mathbb{N}_3(\mathbf{A}_\mu)\mathbb{N}_3(\mathbf{A}_\nu)}$ appear in Eq. (G.25), is defined as

$$\mathbf{\Xi}^{\alpha}_{\mathbb{N}_3\mathbb{N}_3} \;=\; \big(\mathbf{R}^{\alpha}_{\mathbb{N}_3\mathbb{N}_3} + \mathbf{X}^{\alpha}_{\mathbb{N}_3\mathbb{N}_3} + i\,\mathbf{L}_{\mathrm{Z},\,\mathbb{N}_3\mathbb{N}_3}\big)^{-1} \,. \tag{G.27}$$

This matrix inversion is the most computationally demanding step in the multi-spin SRE-3SM theory. For $m=3$, 4, 5 and 6, the dimension of this matrix is 27, 108, 270 and 540, respectively. For large m, the dimension grows as m^3. The three-spin-mode relaxation supermatrix $\mathbf{R}^{\alpha}_{\mathbb{N}_3\mathbb{N}_3}$ is block-diagonal, with the 27×27 blocks computed as described in Appendix H. The three-spin Zeeman supermatrix $\mathbf{L}_{\mathrm{Z},\,\mathbb{N}_3\mathbb{N}_3}$ is also block-diagonal, and all the blocks are equal to $\omega_0\,\mathbf{Q}_3$, with the 27×27 diagonal matrix $\mathbf{Q}_3$ given by Eq. (F.55) if the three-spin basis operators are ordered as in Table S2 of Appendix H.

The 27×27 blocks of the $3 \to 2 \to 3$-spin mode transfer matrix $\mathbf{X}^{\alpha}_{\mathbb{N}_3\mathbb{N}_3}$ are given by Eq. (G.9). The off-diagonal blocks may be expressed as

$$\mathbf{X}^{\alpha}_{\mathbb{N}_3(\mathbf{A})\mathbb{N}_3(\mathbf{B})} \;=\; \delta_{\mathbf{c}(\mathbf{A}),\mathbf{c}(\mathbf{B})}\, \mathbf{\Delta}^{\alpha\,\dagger}_{\mathbb{N}_2(\mathbf{c})\mathbb{N}_3(\mathbf{A})}\, (\mathbf{R}^{\alpha}_{\mathbb{N}_2(\mathbf{c})\mathbb{N}_2(\mathbf{c})} + i\,\omega_0\,\mathbf{Q}_2)^{-1} \mathbf{\Delta}^{\alpha}_{\mathbb{N}_2(\mathbf{c})\mathbb{N}_3(\mathbf{B})}\,, \tag{G.28}$$

where $\mathbb{N}_3(\mathbf{A})$ and $\mathbb{N}_3(\mathbf{B})$ are two different three-spin subspaces. The delta function $\delta_{\mathbf{c}(\mathbf{A}),\mathbf{c}(\mathbf{B})}$ signifies that $\mathbf{X}^{\alpha}_{\mathbb{N}_3(\mathbf{A})\mathbb{N}_3(\mathbf{B})}$ vanishes unless these subspaces share two spins, in which case the two-spin subspace $\mathbb{N}_2(\mathbf{c})$ comprises the two shared spins. For a given three-spin subspace $\mathbb{N}_3(\mathbf{A})$, how many *other* three-spin subspaces $\mathbb{N}_3(\mathbf{B})$ share exactly two spins with $\mathbb{N}_3(\mathbf{A})$? The three-spin subspace $\mathbb{N}_3(\mathbf{A})$ contains three pairs, for each of which we can form another three-spin subspace $\mathbb{N}_3(\mathbf{B})$ in $m-3$ ways, corresponding to having any of the $m-3$ spins not present in $\mathbb{N}_3(\mathbf{A})$ as the third spin in $\mathbb{N}_3(\mathbf{B})$. Consequently, among the $m(m-1)(m-2)/6$ three-spin subspaces, $3(m-3)$ share two spins with another subspace. Of the total number $[m(m-1)(m-2)/6]^2 - m(m-1)(m-2)/6$ off-diagonal blocks, only $3(m-3) \times m(m-1)(m-2)/6 = m(m-1)(m-2)(m-3)/2$ are nonzero. For $m = 4$, all 12 off-diagonal blocks are nonzero. However, for $m = 10$, only 2520 of the 14280 off-diagonal blocks are nonzero (~ 18 %). The supermatrix $\mathbf{X}^{\alpha}_{\mathbb{N}_3\mathbb{N}_3}$ is thus rather sparse for large m.

According to Eq. (G.9), the diagonal blocks of $\mathbf{X}^{\alpha}_{\mathbb{N}_3\mathbb{N}_3}$ contain three terms,

$$\mathbf{X}^{\alpha}_{\mathbb{N}_3(\mathbf{A})\mathbb{N}_3(\mathbf{A})} \;=\; \sum_{\mathbf{c}=1}^{3} \mathbf{\Delta}^{\alpha\,\dagger}_{\mathbb{N}_2(\mathbf{c})\mathbb{N}_3(\mathbf{A})}\, (\mathbf{R}^{\alpha}_{\mathbb{N}_2(\mathbf{c})\mathbb{N}_2(\mathbf{c})} + i\,\omega_0\,\mathbf{Q}_2)^{-1} \mathbf{\Delta}^{\alpha}_{\mathbb{N}_2(\mathbf{c})\mathbb{N}_3(\mathbf{A})}\,, \tag{G.29}$$

where $\mathbf{c}$ denotes one of the three pairs contained in $\mathbf{A}$.

2. Exchange case $ISP_m{-}IS$

According to Eqs. (12) and (31), the ILRR for the $ISP_m{-}IS$ case is given by

$$R_{1,IS}(\omega_0) \;=\; 2\,P_{\mathrm{A}}\, \frac{\big\langle \widetilde{R}^{II}_{zz}(\omega_0)\big\rangle \big\langle \widetilde{R}^{SS}_{zz}(\omega_0)\big\rangle - \big\langle \widetilde{R}^{IS}_{zz}(\omega_0)\big\rangle \big\langle \widetilde{R}^{SI}_{zz}(\omega_0)\big\rangle}{\big\langle \widetilde{R}^{II}_{zz}(\omega_0)\big\rangle + \big\langle \widetilde{R}^{SS}_{zz}(\omega_0)\big\rangle - \big\langle \widetilde{R}^{IS}_{zz}(\omega_0)\big\rangle - \big\langle \widetilde{R}^{SI}_{zz}(\omega_0)\big\rangle}\,, \tag{G.30}$$

with

$$\big\langle \widetilde{R}^{II}_{zz}(\omega_0)\big\rangle \;\equiv\; \big\langle R^{II}_{zz}(\omega_0)\big\rangle - \big\langle \Gamma^{II}_{zz}(\omega_0)\big\rangle\,, \tag{G.31a}$$

$$\big\langle \widetilde{R}^{SS}_{zz}(\omega_0)\big\rangle \;\equiv\; \big\langle R^{SS}_{zz}(\omega_0)\big\rangle - \big\langle \Gamma^{SS}_{zz}(\omega_0)\big\rangle\,, \tag{G.31b}$$

$$\big\langle \widetilde{R}^{IS}_{zz}(\omega_0)\big\rangle \;\equiv\; \big\langle R^{IS}_{zz}(\omega_0)\big\rangle - \big\langle \Gamma^{IS}_{zz}(\omega_0)\big\rangle\,. \tag{G.31c}$$

$$\big\langle \widetilde{R}^{SI}_{zz}(\omega_0)\big\rangle \;\equiv\; \big\langle R^{SI}_{zz}(\omega_0)\big\rangle - \big\langle \Gamma^{SI}_{zz}(\omega_0)\big\rangle\,. \tag{G.31d}$$

The longitudinal auto-mode rates are obtained from Eqs. (H.6), (H.7), and (G.3) (along with the analogous expression for $\omega_{\mathrm{D},S}^2$) as

$$\big\langle R_{zz}^{II}(\omega_0)\big\rangle \;=\; \tfrac{2}{45}\big(\omega_{\mathrm{D},IS}^2+\omega_{\mathrm{D},I}^2\big)\big[J(0)+3\,J(\omega_0)+6\,J(2\,\omega_0)\big]\;, \tag{G.32a}$$

$$\big\langle R_{zz}^{SS}(\omega_0)\big\rangle \;=\; \tfrac{2}{45}\big(\omega_{\mathrm{D},IS}^2+\omega_{\mathrm{D},S}^2\big)\big[J(0)+3\,J(\omega_0)+6\,J(2\,\omega_0)\big]\;, \tag{G.32b}$$

$$\big\langle R_{zz}^{IS}(\omega_0)\big\rangle \;=\; \big\langle R_{zz}^{SI}(\omega_0)\big\rangle \;=\; \tfrac{2}{45}\,\omega_{\mathrm{D},IS}^2\big[-J(0)+6\,J(2\,\omega_0)\big]\;. \tag{G.32c}$$

The cross-relaxation rates are obtained from Eqs. (32) and (H.13) as

$$\big\langle \Gamma_{zz}^{II}(\omega_0)\big\rangle \;=\; \sum_{\mu=1}^{m}\sum_{\nu=1}^{m}\Big\langle \mathbf{R}_{I,\mathbb{N}_1(\mu)}^{\alpha}\,(\mathbf{V}_{\mathbb{N}_1\mathbb{N}_1}^{\alpha})_{\mathbb{N}_1(\mu)\mathbb{N}_1(\nu)}^{-1}\,\mathbf{R}_{I,\mathbb{N}_1(\nu)}^{\alpha\,\dagger}\Big\rangle\;, \tag{G.33a}$$

$$\big\langle \Gamma_{zz}^{SS}(\omega_0)\big\rangle \;=\; \sum_{\mu=1}^{m}\sum_{\nu=1}^{m}\Big\langle \mathbf{R}_{S,\mathbb{N}_1(\mu)}^{\alpha}\,(\mathbf{V}_{\mathbb{N}_1\mathbb{N}_1}^{\alpha})_{\mathbb{N}_1(\mu)\mathbb{N}_1(\nu)}^{-1}\,\mathbf{R}_{S,\mathbb{N}_1(\nu)}^{\alpha\,\dagger}\Big\rangle\;, \tag{G.33b}$$

$$\big\langle \Gamma_{zz}^{IS}(\omega_0)\big\rangle \;=\; \sum_{\mu=1}^{m}\sum_{\nu=1}^{m}\Big\langle \mathbf{R}_{I,\mathbb{N}_1(\mu)}^{\alpha}\,(\mathbf{V}_{\mathbb{N}_1\mathbb{N}_1}^{\alpha})_{\mathbb{N}_1(\mu)\mathbb{N}_1(\nu)}^{-1}\,\mathbf{R}_{S,\mathbb{N}_1(\nu)}^{\alpha\,\dagger}\Big\rangle\;, \tag{G.33c}$$

$$\big\langle \Gamma_{zz}^{SI}(\omega_0)\big\rangle \;=\; \sum_{\mu=1}^{m}\sum_{\nu=1}^{m}\Big\langle \mathbf{R}_{S,\mathbb{N}_1(\mu)}^{\alpha}\,(\mathbf{V}_{\mathbb{N}_1\mathbb{N}_1}^{\alpha})_{\mathbb{N}_1(\mu)\mathbb{N}_1(\nu)}^{-1}\,\mathbf{R}_{I,\mathbb{N}_1(\nu)}^{\alpha\,\dagger}\Big\rangle\;. \tag{G.33d}$$

The m 1×3 blocks $\mathbf{R}_{I,\mathbb{N}_1(\mu)}^{\alpha}$ and $\mathbf{R}_{S,\mathbb{N}_1(\mu)}^{\alpha}$ of the $2\times3m$ cross-spin relaxation matrix $\mathbf{R}_{\mathbb{LZ},\mathbb{N}_1}^{\alpha}$ have elements proportional to $\omega_{\mathrm{D},I\mu}^2\,\tau_{\mathrm{A}}$ and $\omega_{\mathrm{D},S\mu}^2\,\tau_{\mathrm{A}}$, respectively, given by Eqs. (H.11) and (H.12).

The m^2 3×3 blocks $\mathbf{V}_{\mathbb{N}_1(\mu)\mathbb{N}_1(\nu)}^{\alpha}$ of the $3m\times3m$ matrix $\mathbf{V}_{\mathbb{N}_1\mathbb{N}_1}^{\alpha}$ are given by Eq. (G.5), as for the IP_m–I case. The longitudinal auto-mode rates in Eq. (G.32) depend on the dipole coupling $\omega_{\mathrm{D},IS}$ between the two labile spins, but the quantities $\mathbf{R}_{\mathbb{N}_1(\mu)\mathbb{N}_1(\mu)}^{\alpha}$, $\mathbf{X}_{\mathbb{N}_1(\mu)\mathbb{N}_1(\nu)}^{\alpha}$ and $\mathbf{Y}_{\mathbb{N}_1(\mu)\mathbb{N}_1(\nu)}^{\alpha}$ appearing in $\mathbf{V}_{\mathbb{N}_1(\mu)\mathbb{N}_1(\nu)}^{\alpha}$ do not involve $\omega_{\mathrm{D},IS}$.

The elements of the 3×3 single-spin auto-relaxation matrix $\mathbf{R}_{\mathbb{N}_1(\mu)\mathbb{N}_1(\mu)}^{\alpha}$, given by Eqs. (H.10) and (H.14b), have one term proportional to $\omega_{\mathrm{D},I\mu}^2\,\tau_{\mathrm{A}}$ involving angular functions $F_{MM'}(\Omega_{I\mu})$ and another term proportional to $\omega_{\mathrm{D},S\mu}^2\,\tau_{\mathrm{A}}$ involving $F_{MM'}(\Omega_{S\mu})$.

The m^2 3×3 blocks $\mathbf{X}_{\mathbb{N}_1(\mu)\mathbb{N}_1(\nu)}^{\alpha}$ of the $3m\times3m$ coherent transfer matrix $\mathbf{X}_{\mathbb{N}_1\mathbb{N}_1}^{\alpha}$ are given by Eq. (G.6), and the m^2 3×3 blocks $\mathbf{Y}_{\mathbb{N}_1(\mu)\mathbb{N}_1(\nu)}^{\alpha}$ of the $3m\times3m$ coherent transfer matrix $\mathbf{Y}_{\mathbb{N}_1\mathbb{N}_1}^{\alpha}$ are obtained Eqs. (G.7) – (G.9). These expressions apply to both the exchange cases IP_m-I and ISP_m-IS. The only difference between these two cases for the quantities appearing in the expressions for $\mathbf{X}_{\mathbb{N}_1\mathbb{N}_1}^{\alpha}$ and $\mathbf{Y}_{\mathbb{N}_1\mathbb{N}_1}^{\alpha}$ is that the two-spin auto-relaxation matrix $\mathbf{R}_{\mathbb{N}_2\mathbb{N}_2}^{\alpha}$, given by Eq. (H.15b), and the three-spin auto-relaxation matrix $\mathbf{R}_{\mathbb{N}_3\mathbb{N}_3}^{\alpha}$, given by Eq. (H.37b), now involve $S-\mu$ as well as $I-\mu$ dipole couplings. The 1-spin $\rightarrow$ 2-spin mode and 2-spin $\rightarrow$ 3-spin mode coherent transfer matrices $\mathbf{\Delta}_{\mathbb{N}_1\mathbb{N}_2}^{\alpha}$ and $\mathbf{\Delta}_{\mathbb{N}_2\mathbb{N}_3}^{\alpha}$ only involve dipole couplings between nonlabile spins, and are therefore the same for the two exchange cases.

Before considering the general case, we shall examine the special cases with $m = 0-4$. For $m = 0$, that is, the symmetric exchange case $IS-IS$, there are no nonlabile spins so the cross-relaxation rates in Eq. (G.31) vanish and the longitudinal auto-mode rates are given by Eq. (G.32) with $\omega_{\mathrm{D},I} = \omega_{\mathrm{D},S} = 0$.

For $m = 1$, that is, the exchange case $ISP-IS$, there are no static dipole couplings, so $\mathbf{X}^{\alpha}_{\mathbb{N}_1\mathbb{N}_1} = \mathbf{Y}^{\alpha}_{\mathbb{N}_1\mathbb{N}_1} = \mathbf{0}$ and Eqs. (G.5) and (G.33) yield

$$\left\langle \Gamma^{II}_{zz}(\omega_0) \right\rangle = \left\langle \mathbf{R}^{\alpha}_{I,\mathbb{N}_1(1)} \left(\mathbf{R}^{\alpha}_{\mathbb{N}_1(1)\mathbb{N}_1(1)} + i\,\omega_0\,\mathbf{Q}_1 \right)^{-1} \mathbf{R}^{\alpha\,\dagger}_{I,\mathbb{N}_1(1)} \right\rangle , \tag{G.34a}$$

$$\left\langle \Gamma^{SS}_{zz}(\omega_0) \right\rangle = \left\langle \mathbf{R}^{\alpha}_{S,\mathbb{N}_1(1)} \left(\mathbf{R}^{\alpha}_{\mathbb{N}_1(1)\mathbb{N}_1(1)} + i\,\omega_0\,\mathbf{Q}_1 \right)^{-1} \mathbf{R}^{\alpha\,\dagger}_{S,\mathbb{N}_1(1)} \right\rangle , \tag{G.34b}$$

$$\left\langle \Gamma^{IS}_{zz}(\omega_0) \right\rangle = \left\langle \mathbf{R}^{\alpha}_{I,\mathbb{N}_1(1)} \left(\mathbf{R}^{\alpha}_{\mathbb{N}_1(1)\mathbb{N}_1(1)} + i\,\omega_0\,\mathbf{Q}_1 \right)^{-1} \mathbf{R}^{\alpha\,\dagger}_{S,\mathbb{N}_1(1)} \right\rangle , \tag{G.34c}$$

$$\left\langle \Gamma^{SI}_{zz}(\omega_0) \right\rangle = \left\langle \mathbf{R}^{\alpha}_{S,\mathbb{N}_1(1)} \left(\mathbf{R}^{\alpha}_{\mathbb{N}_1(1)\mathbb{N}_1(1)} + i\,\omega_0\,\mathbf{Q}_1 \right)^{-1} \mathbf{R}^{\alpha\,\dagger}_{I,\mathbb{N}_1(1)} \right\rangle . \tag{G.34d}$$

For $m = 2$, that is, the exchange case ISP_2–IS, there is a single static dipole coupling, so $\mathbf{Y}^{\alpha}_{\mathbb{N}_1\mathbb{N}_1} = \mathbf{0}$ and the four 3×3 blocks of $\mathbf{X}^{\alpha}_{\mathbb{N}_1\mathbb{N}_1}$ are given by Eq. (G.11), the only difference form the IP_2-I case being that the two-spin relaxation matrix $\mathbf{R}^{\alpha}_{\mathbb{N}_2(12)\mathbb{N}_2(12)}$ now involves $S-\mu$ as well as $I-\mu$ dipole couplings.

For $m = 3$ and $m = 4$, that is, the exchange cases ISP_3-IS and ISP_4-IS, $\mathbf{X}^{\alpha}_{\mathbb{N}_1\mathbb{N}_1}$ and $\mathbf{Y}^{\alpha}_{\mathbb{N}_1\mathbb{N}_1}$ are given by the expressions in Eqs. (G.12) – (G.23), the only difference form the IP_3-I and IP_4-I cases being that the two-spin and three-spin relaxation matrices $\mathbf{R}^{\alpha}_{\mathbb{N}_2\mathbb{N}_2}$ and $\mathbf{R}^{\alpha}_{\mathbb{N}_3\mathbb{N}_3}$ now involves $S-\mu$ as well as $I-\mu$ dipole couplings.

In the general case, with $m \geq 3$, the expressions for $\mathbf{X}^{\alpha}_{\mathbb{N}_1(\mu)\mathbb{N}_1(\nu)}$ and $\mathbf{Y}^{\alpha}_{\mathbb{N}_1(\mu)\mathbb{N}_1(\nu)}$ in Eqs. (G.24) – (G.29) are valid for the ISP_m-IS case as well as for the IP_m-I case. Again, the only difference is that the two-spin and three-spin auto-relaxation matrices $\mathbf{R}^{\alpha}_{\mathbb{N}_2\mathbb{N}_2}$ and $\mathbf{R}^{\alpha}_{\mathbb{N}_3\mathbb{N}_3}$ now involve $S-\mu$ as well as $I-\mu$ dipole couplings.

APPENDIX H: $\mathbf{R}^\alpha$ AND $\mathbf{\Delta}^\alpha$ MATRIX ELEMENTS

1. Relaxation of single-spin modes

In this Appendix, we specify in explicit form all the matrix elements required in the multi-spin SRE theory, beginning with relaxation matrix elements between single-spin basis operators. According to Eq. (24), such matrix elements only involve self-correlations, that is, $X = Y$ in Eq. (13). It also follows from Eq. (18) that for auto-spin rates, where n and p refer to the same (labile or nonlabile) spin, all (exchange-modulated) dipole couplings involving that spin contribute to the rate. Conversely, for cross-spin rates, where n and p refer to distinct (labile or nonlabile) spins, only the dipole coupling between those two spins contributes to the rate.

Since single-spin relaxation matrices only involve self-correlations, the angular functions appearing in Eq. (13) and defined in Eq. (16) take the simpler form

$$F_{MM'}(X) \;=\; D^{2*}_{M0}(\Omega^\alpha_X)\, D^{2*}_{M'0}(\Omega^\alpha_X) \;=\; \exp[i(M+M')\psi^\alpha_X]\, d^2_{M0}(\vartheta^\alpha_X)\, d^2_{M'0}(\vartheta^\alpha_X)\,. \tag{H.1}$$

Noting that $d^2_{-M0}(\beta) = (-1)^M d^2_{M0}(\beta)$, we obtain the symmetry relations

$$F_{MM'}(X) \;=\; F_{M'M}(X) \;=\; (-1)^{M+M'} F^*_{-M-M'}(X)\,. \tag{H.2}$$

We consider first the isotropically averaged relaxation matrix in the labile single-spin longitudinal subspace $\mathbb{LZ}$, which appears in Eq. (31),

$$\left\langle \mathbf{R}^\alpha_{\mathbb{LZ},\mathbb{LZ}} \right\rangle \;=\; \left[\begin{array}{cc} \left\langle R^{II}_{zz}\right\rangle & \left\langle R^{IS}_{zz}\right\rangle \\ \left\langle R^{SI}_{zz}\right\rangle & \left\langle R^{SS}_{zz}\right\rangle \end{array}\right]. \tag{H.3}$$

This 2×2 matrix is relevant for the $ISP_m{-}IS$ case, whereas only the element $\left\langle R^{II}_{zz}\right\rangle$ is needed for the $IP_m{-}I$ case. These matrix elements are obtained by combining Eq. (13), symmetry rule (24), and the Wigner function orthogonality relation

$$\langle F_{MM'}(X)\rangle \;=\; \delta_{M',-M}\,(-1)^M\,\frac{1}{5}\,. \tag{H.4}$$

For the $IP_m{-}I$ case, we thus obtain

$$\left\langle R^{II}_{zz}\right\rangle \;=\; \sum_{\mu=1}^{m} \left\langle \rho^{I\mu}_{zz}\right\rangle\,, \tag{H.5}$$

and for the $ISP_m{-}IS$ case

$$\left\langle R^{II}_{zz}\right\rangle \;=\; \left\langle \rho^{IS}_{zz}\right\rangle + \sum_{\mu=1}^{m} \left\langle \rho^{I\mu}_{zz}\right\rangle\,, \tag{H.6a}$$

$$\left\langle R^{SS}_{zz}\right\rangle \;=\; \left\langle \rho^{IS}_{zz}\right\rangle + \sum_{\mu=1}^{m} \left\langle \rho^{S\mu}_{zz}\right\rangle\,, \tag{H.6b}$$

$$\left\langle R^{IS}_{zz}\right\rangle \;=\; \left\langle R^{SI}_{zz}\right\rangle \;=\; \left\langle \sigma^{IS}_{zz}\right\rangle\,. \tag{H.6c}$$

Here we have introduced the generic isotropically averaged longitudinal auto-spin and cross-spin relaxation rates associated with dipole coupling X,

$$\left\langle \rho_{zz}^{X} \right\rangle \;=\; \tfrac{2}{45}\,\omega_{\mathrm{D},X}^{2}\big[J(0)+3\,J(\omega_0)+6\,J(2\,\omega_0)\big]\,, \tag{H.7a}$$

$$\left\langle \sigma_{zz}^{X} \right\rangle \;=\; \tfrac{2}{45}\,\omega_{\mathrm{D},X}^{2}\big[-J(0)+6\,J(2\,\omega_0)\big]\,, \tag{H.7b}$$

with the SDF $J(n\,\omega_0)$ given by Eq. (15).

Next, we consider orientation-dependent local relaxation matrices in single-spin subspaces. These can all be expressed in terms of the generic auto-spin relaxation matrix associated with the dipole coupling X

$$\boldsymbol{\rho}^{X} \;=\; \begin{bmatrix} \rho_{zz}^{X} & \rho_{z+}^{X} & \rho_{z-}^{X} \\ \rho_{+z}^{X} & \rho_{++}^{X} & \rho_{+-}^{X} \\ \rho_{-z}^{X} & \rho_{-+}^{X} & \rho_{--}^{X} \end{bmatrix}\,, \tag{H.8}$$

and the generic cross-spin relaxation matrix associated with the dipole coupling X

$$\boldsymbol{\sigma}^{X} \;=\; \begin{bmatrix} \sigma_{zz}^{X} & \sigma_{z+}^{X} & \sigma_{z-}^{X} \\ \sigma_{+z}^{X} & \sigma_{++}^{X} & \sigma_{+-}^{X} \\ \sigma_{-z}^{X} & \sigma_{-+}^{X} & \sigma_{--}^{X} \end{bmatrix} \;=\; \boldsymbol{\sigma}^{X\,\dagger}\,. \tag{H.9}$$

A comment about indexing is in order here. In single-spin mode relaxation matrix elements, such as R_{zz}^{IS} or $R_{+z}^{\nu S}$, the left (row) basis operator is indicated by the left superscript and subscript, and the right (column) basis operator is indicated by the right superscript and subscript. In generic auto-spin and cross-spin rates, such as $\rho_{z-}^{I\mu}$ or $\sigma_{+z}^{S\nu}$, the subscripts are the same as in the corresponding relaxation matrix element (indicating row and column position in the matrix), but the superscript now refers to a dipole coupling X. For cross-spin rates, X involves the same two spins as the left and right basis vectors, but for auto-spin rates this is not always the case since several dipole couplings may contribute to a given auto-spin rate. In the generic rates, where the superscript refers to a dipole coupling X, the order of the two spins is irrelevant and we use the order corresponding to the convention adopted for the direction of the dipole vectors (Appendix C).

In terms of the angular functions in Eq. (H.1) and the SDF in Eq. (15), the elements of the generic auto-spin relaxation matrix are obtained from Eqs. (13) and (18) as

$$\rho^X_{zz} \;=\; \tfrac{2}{9}\,\omega^2_{\mathrm{D},X}\big\{F_{00}(X)\,J(0) - 3\,F_{1-1}(X)\,J(\omega_0) + 6\,F_{2-2}(X)\,J(2\omega_0)\big\}\,, \tag{H.10a}$$

$$\rho^X_{\pm\pm} \;=\; \tfrac{1}{9}\,\omega^2_{\mathrm{D},X}\big\{5\,F_{00}(X)\,J(0) - 9\,F_{1-1}(X)\,J(\omega_0) + 6\,F_{2-2}(X)\,J(2\omega_0)\big\}\,, \tag{H.10b}$$

$$\rho^X_{z+} \;=\; \tfrac{\sqrt{3}}{9}\,\omega^2_{\mathrm{D},X}\big\{F_{0-1}(X)\,[2\,J(0) - J(\omega_0)] - \sqrt{6}\,F_{1-2}(X)\,J(\omega_0)\big\}\,, \tag{H.10c}$$

$$\rho^X_{z-} \;=\; -\,(\rho^X_{z+})^*\,, \tag{H.10d}$$

$$\rho^X_{+z} \;=\; \tfrac{\sqrt{3}}{9}\,\omega^2_{\mathrm{D},X}\big\{F_{01}(X)\,[J(0) - 2\,J(\omega_0)] + \sqrt{6}\,F_{-12}(X)\,J(2\omega_0)\big\}\,, \tag{H.10e}$$

$$\rho^X_{-z} \;=\; -\,(\rho^X_{+z})^*\,, \tag{H.10f}$$

$$\rho^X_{+-} \;=\; \tfrac{1}{9}\,\omega^2_{\mathrm{D},X}\big\{-\sqrt{6}\,F_{02}(X)\,[J(0) + J(2\omega_0)] + 3\,F_{11}(X)\,J(\omega_0)\big\}\,, \tag{H.10g}$$

$$\rho^X_{-+} \;=\; (\rho^X_{+-})^*\,. \tag{H.10h}$$

Similarly, the elements of the generic cross-spin relaxation matrix are obtained as

$$\sigma^X_{zz} \;=\; \tfrac{2}{9}\,\omega^2_{\mathrm{D},X}\big\{-F_{00}(X)\,J(0) + 6\,F_{2-2}(X)\,J(2\omega_0)\big\}\,, \tag{H.11a}$$

$$\sigma^X_{\pm\pm} \;=\; \tfrac{2}{9}\,\omega^2_{\mathrm{D},X}\big\{2\,F_{00}(X)\,J(0) - 3\,F_{1-1}(X)\,J(\omega_0)\big\}\,, \tag{H.11b}$$

$$\sigma^X_{z+} \;=\; \tfrac{\sqrt{3}}{9}\,\omega^2_{\mathrm{D},X}\big\{F_{0-1}(X)\,[J(0) + J(\omega_0)] - \sqrt{6}\,F_{1-2}(X)\,[J(\omega_0) + J(2\omega_0)]\big\}\,, \tag{H.11c}$$

$$\sigma^X_{z-} \;=\; -\,(\sigma^X_{z+})^*\,, \tag{H.11d}$$

$$\sigma^X_{+z} \;=\; (\sigma^X_{z+})^* \;=\; -\,\sigma^X_{z-}\,, \tag{H.11e}$$

$$\sigma^X_{-z} \;=\; (\sigma^X_{z-})^* \;=\; -\,\sigma^X_{z+}\,, \tag{H.11f}$$

$$\sigma^X_{+-} \;=\; \tfrac{\sqrt{6}}{9}\,\omega^2_{\mathrm{D},X}\big\{-2\,F_{02}(X)\,[J(0) + J(2\omega_0)] + \sqrt{6}\,F_{11}(X)\,J(\omega_0)\big\}\,, \tag{H.11g}$$

$$\sigma^X_{-+} \;=\; (\sigma^X_{+-})^*\,. \tag{H.11h}$$

As indicated in Eqs. (H.9) and (H.11), the generic cross-spin relaxation matrix $\boldsymbol{\sigma}^X$ is Hermitian. The generic auto-spin relaxation matrix $\boldsymbol{\rho}^X$ is Hermitian only at $\omega_0 = 0$.

The 1×3 cross-spin matrices $\mathbf{R}^{\alpha}_{n,\mathbb{N}_1(\mu)}$, which constitute the blocks of the $3 \times 3m$ supermatrix $\mathbf{R}^{\alpha}_{\mathbb{L}\mathbb{Z},\mathbb{N}_1}$ in Eq. (32), correspond to the first row of the cross-spin relaxation matrix $\boldsymbol{\sigma}^X$ in Eq. (H.9), that is,

$$\mathbf{R}^{\alpha}_{1,\mathbb{N}_1(\mu)} \;=\; \big[R^{I\mu}_{zz}\;\; R^{I\mu}_{z+}\;\; R^{I\mu}_{z-}\big] \;=\; \big[\sigma^{I\mu}_{zz}\;\; \sigma^{I\mu}_{z+}\;\; \sigma^{I\mu}_{z-}\big]\,, \tag{H.12a}$$

$$\mathbf{R}^{\alpha}_{2,\mathbb{N}_1(\mu)} \;=\; \big[R^{S\mu}_{zz}\;\; R^{S\mu}_{z+}\;\; R^{S\mu}_{z-}\big] \;=\; \big[\sigma^{S\mu}_{zz}\;\; \sigma^{S\mu}_{z+}\;\; \sigma^{S\mu}_{z-}\big]\,. \tag{H.12b}$$

Similarly, the 3×1 cross-spin matrices $\mathbf{R}^{\alpha}_{\mathbb{N}_1(\nu),p}$ correspond to the first column of the cross-spin relaxation matrix $\boldsymbol{\sigma}^X$ in Eq. (H.9), that is,

$$\mathbf{R}^{\alpha}_{\mathbb{N}_1(\nu),1} \;=\; \begin{bmatrix} R^{\nu I}_{zz} \\ R^{\nu I}_{+z} \\ R^{\nu I}_{-z} \end{bmatrix} \;=\; \begin{bmatrix} \sigma^{I\nu}_{zz} \\ \sigma^{I\nu}_{+z} \\ \sigma^{I\nu}_{-z} \end{bmatrix} \;=\; \mathbf{R}^{\alpha\,\dagger}_{1,\mathbb{N}_1(\nu)}\,, \tag{H.13a}$$

$$\mathbf{R}^{\alpha}_{\mathbb{N}_1(\nu),2} \;=\; \begin{bmatrix} R^{\nu S}_{zz} \\ R^{\nu S}_{+z} \\ R^{\nu S}_{-z} \end{bmatrix} \;=\; \begin{bmatrix} \sigma^{S\nu}_{zz} \\ \sigma^{S\nu}_{+z} \\ \sigma^{S\nu}_{-z} \end{bmatrix} \;=\; \mathbf{R}^{\alpha\,\dagger}_{2,\mathbb{N}_1(\nu)}\,. \tag{H.13b}$$

The 3×3 nonlabile single-spin auto-relaxation matrices $\mathbf{R}^{\alpha}_{\mathbb{N}_1(\mu)\mathbb{N}_1(\mu)}$, which constitute the blocks of the $3m \times 3m$ supermatrix $\mathbf{R}^{\alpha}_{\mathbb{N}_1,\mathbb{N}_1}$ in Eq. (32), are obtained from the generic relaxation matrices as

$$\mathbf{R}^{\alpha}_{\mathbb{N}_1(\mu)\mathbb{N}_1(\mu)} \;=\; \boldsymbol{\rho}^{I\mu} \qquad (IP_m{-}I \text{ case})\,, \tag{H.14a}$$

$$\mathbf{R}^{\alpha}_{\mathbb{N}_1(\mu)\mathbb{N}_1(\mu)} \;=\; \boldsymbol{\rho}^{I\mu} + \boldsymbol{\rho}^{S\mu} \qquad (ISP_m{-}IS \text{ case})\,. \tag{H.14b}$$

TABLE S1. Basis operators for the $\mathbb{N}_2(\mu\nu)$ subspace for spins μ and ν.

n	Q	K	$\mathcal{P}$ [a]	B_n [b]
1	0	0	+	$-\frac{2}{\sqrt{3}}\,\boldsymbol{\mu}\cdot\boldsymbol{\nu}$
2	0	2	+	$\frac{2}{\sqrt{6}}\,(3\,\mu_z\,\nu_z \;-\; \boldsymbol{\mu}\cdot\boldsymbol{\nu})$
3	0	1	−	$i\,\sqrt{2}\,(\boldsymbol{\mu}\times\boldsymbol{\nu})\cdot\boldsymbol{e}_z$
4	1	1	−	$\mu_z\,\nu_+ - \mu_+\,\nu_z$
5	1	2	+	$-\,(\mu_z\,\nu_+ + \mu_+\,\nu_z)$
6	−1	1	−	$\mu_z\,\nu_- - \mu_-\,\nu_z$
7	−1	2	+	$\mu_z\,\nu_- + \mu_-\,\nu_z$
8	2	2	+	$\mu_+\,\nu_+$
9	−2	2	+	$\mu_-\,\nu_-$

[a] Parity of B_n under spin permutation $\mu \leftrightarrow \nu$.
[b] The basis operators B_n are normalized in the two-spin $(\mu\nu)$ Liouville space.

2. Relaxation of two-spin modes

The 9×9 nonlabile two-spin relaxation matrices $\mathbf{R}^{\alpha}_{\mathbb{N}_2(\mu\nu)\mathbb{N}_2(\mu\nu)}$ appearing in Eq. (F.21) can be expressed as

$$\mathbf{R}^{\alpha}_{\mathbb{N}_2(\mu\nu)\mathbb{N}_2(\mu\nu)} = \boldsymbol{\rho}^{I\mu,\,I\nu} \qquad (IP_m{-}I \text{ case}) , \tag{H.15a}$$

$$\mathbf{R}^{\alpha}_{\mathbb{N}_2(\mu\nu)\mathbb{N}_2(\mu\nu)} = \boldsymbol{\rho}^{I\mu,\,I\nu} + \boldsymbol{\rho}^{S\mu,\,S\nu} \qquad (ISP_m{-}IS \text{ case}) . \tag{H.15b}$$

The elements ρ^{XY}_{np} of the 9×9 two-spin relaxation matrix $\boldsymbol{\rho}^{XY}$ are all auto-(spin pair) rates, and either auto-mode ($n = p$) or cross-mode ($n \neq p$) rates. The nine two-spin modes are ordered as in Table S1. As noted in Sec. III.C of the main text, terms like $\boldsymbol{\rho}^{I\mu,\,S\nu}$, which involve four-spin correlations, do not appear in the SRE theory.

Because the two-spin modes involve two different nonlabile spins (μ and ν), the two-spin rates involve two different dipole couplings ($X = I\mu$ and $Y = I\nu$) for a given labile spin. In general, the two-spin rates therefore have contributions from self-correlations (s) as well as from distinct correlations (d), corresponding to the diagonal ($X = Y$) and off-diagonal ($X \neq Y$) terms, respectively, in the double sum of Eq. (13). Accordingly, we decompose the two-spin rates as

$$\rho^{XY}_{np} = \rho^{\mathrm{s}}_{np}(X) + \rho^{\mathrm{s}}_{np}(Y) + \rho^{\mathrm{d}}_{np}(XY) , \tag{H.16}$$

where $\rho^{\mathrm{d}}_{np}(XY)$ is the sum of the two terms in Eq. (13) that differ by $X \leftrightarrow Y$ interchange. Consequently, the ordering of X and Y in $\rho^{\mathrm{d}}_{np}(XY)$ is irrelevant.

Within the Q-blocks (where $Q_n = Q_p$; see Table S1), ρ^{XY}_{np} only has contributions from $M' = -M$ terms in Eq. (13). The Q-blocks are Hermitian, so $\rho^{XY}_{pn} = (\rho^{XY}_{np})^*$, implying that ρ^{XY}_{nn} is real. The quantities $\rho^{\mathrm{s}}_{nn}(X)$ and $\rho^{\mathrm{s}}_{nn}(Y)$ are identical, except for the $X \leftrightarrow Y$ interchange. This is also true for off-diagonal elements $\rho^{\mathrm{s}}_{np}(X)$ and $\rho^{\mathrm{s}}_{np}(Y)$ if the basis operators B_n and B_p have the same parity under spin permutation (Table S1). If the parity is different, $\rho^{\mathrm{s}}_{np}(X)$ and $\rho^{\mathrm{s}}_{np}(Y)$ differ in sign (apart from the $X \leftrightarrow Y$ interchange). Off-diagonal elements ρ^{XY}_{np} within the Q-blocks are real if B_n and B_p have the same spin permutation parity, and complex (for $np = 45$ and 67) or purely imaginary (for $np = 13$ and 23) otherwise. From Table S1, it is seen that basis operators with odd rank have odd parity under spin permutation.

The generic two-spin rates within the 3×3 $Q = 0$ block are obtained from Eqs. (13) and (18) as

$$\rho^{\mathrm{s}}_{11}(X) = \tfrac{4}{9}\,\omega^2_{\mathrm{D},X}\big\{F_{00}(X)\,J(0) - 2\,F_{1-1}(X)\,J(\omega_0) + 2\,F_{2-2}(X)\,J(2\omega_0)\big\} , \tag{H.17a}$$

$$\begin{aligned}\rho^{\mathrm{d}}_{11}(XY) = \tfrac{8}{9}\,\omega_{\mathrm{D},X}\,\omega_{\mathrm{D},Y}\big\{ &- F_{00}(X,Y)\,J(0) + 2\,\mathrm{Re}[F_{1-1}(X,Y)]\,J(\omega_0) \\ &- 2\,\mathrm{Re}[F_{2-2}(X,Y)]\,J(2\omega_0)\big\} ,\end{aligned} \tag{H.17b}$$

$$\rho^{\mathrm{s}}_{22}(X) = \tfrac{1}{9}\,\omega^2_{\mathrm{D},X}\big\{3\,F_{00}(X)\,J(0) - 7\,F_{1-1}(X)\,J(\omega_0) + 10\,F_{2-2}(X)\,J(2\omega_0)\big\} , \tag{H.18a}$$

$$\rho^{\mathrm{d}}_{22}(XY) = \tfrac{4}{9}\,\omega_{\mathrm{D},X}\,\omega_{\mathrm{D},Y}\big\{ - \mathrm{Re}[F_{1-1}(X,Y)]\,J(\omega_0) + 4\,\mathrm{Re}[F_{2-2}(X,Y)]\,J(2\omega_0)\big\} , \tag{H.18b}$$

$$\rho^{\rm s}_{33}(X) \;=\; \tfrac{1}{9}\,\omega_{{\rm D},X}^2\big\{5\,F_{00}(X)\,J(0) - 9\,F_{1-1}(X)\,J(\omega_0) + 6\,F_{2-2}(X)\,J(2\omega_0)\big\}\,, \tag{H.19a}$$
$$\rho^{\rm d}_{33}(XY) \;=\; \tfrac{4}{9}\,\omega_{{\rm D},X}\,\omega_{{\rm D},Y}\big\{-2\,F_{00}(X,Y)\,J(0) + 3\,{\rm Re}[F_{1-1}(X,Y)]\,J(\omega_0)\big\}\,, \tag{H.19b}$$

$$\rho^{\rm s}_{12}(X) \;=\; \tfrac{\sqrt{2}}{9}\,\omega_{{\rm D},X}^2\big\{F_{00}(X)\,J(0) - F_{1-1}(X)\,J(\omega_0) - 2\,F_{2-2}(X)\,J(2\omega_0)\big\}\,, \tag{H.20a}$$
$$\begin{aligned}\rho^{\rm d}_{12}(XY) \;=\; \tfrac{\sqrt{2}}{9}\,\omega_{{\rm D},X}\,\omega_{{\rm D},Y}\big\{&-2\,F_{00}(X,Y)\,J(0) + {\rm Re}[F_{1-1}(X,Y)]\,J(\omega_0)\\ &+ 2\,{\rm Re}[F_{2-2}(X,Y)]\,J(2\omega_0)\big\}\,,\end{aligned} \tag{H.20b}$$

$$\rho^{\rm s}_{13}(X) \;=\; 0\,, \tag{H.21a}$$
$$\rho^{\rm d}_{13}(XY) \;=\; i\,\tfrac{2\sqrt{6}}{9}\,\omega_{{\rm D},X}\,\omega_{{\rm D},Y}\big\{-{\rm Im}[F_{1-1}(X,Y)]\,J(\omega_0) + 2\,{\rm Im}[F_{2-2}(X,Y)]\,J(2\omega_0)\big\}\,, \tag{H.21b}$$

$$\rho^{\rm s}_{23}(X) \;=\; 0\,, \tag{H.22a}$$
$$\rho^{\rm d}_{23}(XY) \;=\; i\,\tfrac{4\sqrt{3}}{9}\,\omega_{{\rm D},X}\,\omega_{{\rm D},Y}\big\{{\rm Im}[F_{1-1}(X,Y)]\,J(\omega_0) - 2\,{\rm Im}[F_{2-2}(X,Y)]\,J(2\omega_0)\big\}\,. \tag{H.22b}$$

It may be noted that Eq. (16) implies that ${\rm Re}[F_{M-M}(X,Y)] = {\rm Re}[F_{M-M}(Y,X)]$, whereas ${\rm Im}[F_{M-M}(X,Y)] = -{\rm Im}[F_{M-M}(Y,X)]$.

For the 2×2 $Q=1$ and $Q=-1$ blocks, we obtain in the same way

$$\rho^{\rm s}_{44}(X) \;=\; \tfrac{1}{18}\,\omega_{{\rm D},X}^2\big\{7\,F_{00}(X)\,J(0) - 15\,F_{1-1}(X)\,J(\omega_0) + 18\,F_{2-2}(X)\,J(2\omega_0)\big\}\,, \tag{H.23a}$$
$$\begin{aligned}\rho^{\rm d}_{44}(XY) \;=\; \tfrac{2}{9}\,\omega_{{\rm D},X}\,\omega_{{\rm D},Y}\big\{&-F_{00}(X,Y)\,J(0) + 3\,{\rm Re}[F_{1-1}(X,Y)]\,J(\omega_0)\\ &- 6\,{\rm Re}[F_{2-2}(X,Y)]\,J(2\omega_0)\big\}\,,\end{aligned} \tag{H.23b}$$

$$\rho^{\rm s}_{55}(X) \;=\; \rho^{\rm s}_{44}(X)\,, \tag{H.24a}$$
$$\rho^{\rm d}_{55}(XY) \;=\; -\,\rho^{\rm d}_{44}(XY)\,, \tag{H.24b}$$

$$\rho^{\rm s}_{45}(X) \;=\; \tfrac{1}{6}\,\omega_{{\rm D},X}^2\big\{F_{00}(X)\,J(0) - F_{1-1}(X)\,J(\omega_0) - 2\,F_{2-2}(X)\,J(2\omega_0)\big\}\,, \tag{H.25a}$$
$$\rho^{\rm s}_{45}(Y) \;=\; -\,\tfrac{1}{6}\,\omega_{{\rm D},Y}^2\big\{F_{00}(Y)\,J(0) - F_{1-1}(Y)\,J(\omega_0) - 2\,F_{2-2}(Y)\,J(2\omega_0)\big\}\,, \tag{H.25b}$$
$$\rho^{\rm d}_{45}(XY) \;=\; i\,\tfrac{2}{3}\,\omega_{{\rm D},X}\,\omega_{{\rm D},Y}\big\{-{\rm Im}[F_{1-1}(X,Y)]\,J(\omega_0) + 2\,{\rm Im}[F_{2-2}(X,Y)]\,J(2\omega_0)\big\}\,, \tag{H.25c}$$

$$\rho^{\rm s}_{66}(X) \;=\; \rho^{\rm s}_{44}(X)\,, \tag{H.26a}$$
$$\rho^{\rm d}_{66}(XY) \;=\; \rho^{\rm d}_{44}(XY)\,, \tag{H.26b}$$

$$\rho^{\rm s}_{77}(X) \;=\; \rho^{\rm s}_{55}(X)\,, \tag{H.27a}$$
$$\rho^{\rm d}_{77}(XY) \;=\; \rho^{\rm d}_{55}(XY)\,, \tag{H.27b}$$

$$\rho^{\rm s}_{67}(X) \;=\; -\,\rho^{\rm s}_{45}(X)\,, \tag{H.28a}$$
$$\rho^{\rm s}_{67}(Y) \;=\; -\,\rho^{\rm s}_{45}(Y)\,, \tag{H.28b}$$
$$\rho^{\rm d}_{67}(XY) \;=\; \rho^{\rm d}_{45}(XY)\,. \tag{H.28c}$$

Finally, for the $Q = \pm 2$ rates, we obtain

$$\rho^{\rm s}_{88}(X) \;=\; \tfrac{1}{9}\,\omega^2_{{\rm D},X}\big\{5\,F_{00}(X)\,J(0) - 9\,F_{1-1}(X)\,J(\omega_0) + 6\,F_{2-2}(X)\,J(2\omega_0)\big\}\,, \tag{H.29a}$$

$$\rho^{\rm d}_{88}(XY) \;=\; \tfrac{4}{9}\,\omega_{{\rm D},X}\,\omega_{{\rm D},Y}\big\{2\,F_{00}(X,Y)\,J(0) - 3\,{\rm Re}[F_{1-1}(X,Y)]\,J(\omega_0)\big\}\,, \tag{H.29b}$$

$$\rho^{\rm s}_{99}(X) \;=\; \rho^{\rm s}_{88}(X)\,, \tag{H.30a}$$

$$\rho^{\rm d}_{99}(XY) \;=\; \rho^{\rm d}_{88}(XY)\,. \tag{H.30b}$$

Outside the Q-blocks, the Wigner-Eckart theorem requires that $\rho^{XY}_{np} = 0$ whenever $|Q_n - Q_p| > 2$, the rank of the ISTO $T^2_M(X)$ in the dipole coupling. With the basis ordering of Table S1, the ten vanishing elements are $np = 49$, 94, 59, 95, 68, 86, 78, 87, 89, and 98. The remaining $81 - 19 - 10 = 52$ nonzero off-Q elements have a more complicated structure since it is now the $M' \neq -M$ terms in Eq. (13) that contribute. Also, there is no simple relation between ρ^{XY}_{np} and ρ^{XY}_{pn}. As examples, we show only four of the 52 off-Q elements. First, for $np = 14$ or 41, with one basis operator from the $Q = 0$ subspace and the other from the $Q = 1$ subspace, we obtain from Eqs. (13) and (18),

$$\rho^{\rm s}_{14}(X) \;=\; \tfrac{1}{18}\,\omega^2_{{\rm D},X}\big\{-3\sqrt{2}\,F_{0-1}(X)\,[J(0) - J(\omega_0)] + 2\sqrt{3}\,F_{1-2}(X)\,[J(\omega_0) - J(2\omega_0)]\big\}\,, \tag{H.31a}$$

$$\rho^{\rm s}_{14}(Y) \;=\; -\tfrac{1}{18}\,\omega^2_{{\rm D},Y}\big\{-3\sqrt{2}\,F_{0-1}(Y)\,[J(0) - J(\omega_0)] + 2\sqrt{3}\,F_{1-2}(Y)\,[J(\omega_0) - J(2\omega_0)]\big\}\,, \tag{H.31b}$$

$$\begin{aligned}\rho^{\rm d}_{14}(XY) \;=\; \tfrac{1}{18}\,\omega_{{\rm D},X}\,\omega_{{\rm D},Y}\big\{&3\sqrt{2}\,[F_{0-1}(X,Y) - F_{-10}(X,Y)]\,[J(0) + J(\omega_0)] \\ &- 2\sqrt{3}\,[F_{1-2}(X,Y) - F_{-21}(X,Y)]\,[J(\omega_0) + J(2\omega_0)]\big\}\,,\end{aligned} \tag{H.31c}$$

and

$$\rho^{\rm s}_{41}(X) \;=\; \tfrac{1}{18}\,\omega^2_{{\rm D},X}\big\{-3\sqrt{2}\,F_{01}(X)\,[J(0) - J(\omega_0)] + 2\sqrt{3}\,F_{-12}(X)\,[J(\omega_0) - J(2\omega_0)]\big\}\,, \tag{H.32a}$$

$$\rho^{\rm s}_{41}(Y) \;=\; -\tfrac{1}{18}\,\omega^2_{{\rm D},X}\big\{-3\sqrt{2}\,F_{01}(X)\,[J(0) - J(\omega_0)] + 2\sqrt{3}\,F_{-12}(X)\,[J(\omega_0) - J(2\omega_0)]\big\}\,, \tag{H.32b}$$

$$\begin{aligned}\rho^{\rm d}_{41}(XY) \;=\; -\tfrac{1}{18}\,\omega_{{\rm D},X}\,\omega_{{\rm D},Y}\big\{&3\sqrt{2}\,[F_{01}(X,Y) - F_{10}(X,Y)]\,[J(0) + J(\omega_0)] \\ &- 2\sqrt{3}\,[F_{-12}(X,Y) - F_{2-1}(X,Y)]\,[J(\omega_0) + J(2\omega_0)]\big\}\,,\end{aligned} \tag{H.32c}$$

In view of Eq. (H.2), it follows from Eqs. (H.31) and (H.32) that

$$\rho^{\rm s}_{41}(X) \;=\; -\,[\rho^{\rm s}_{14}(X)]^*\,, \tag{H.33a}$$

$$\rho^{\rm d}_{41}(XY) \;=\; [\rho^{\rm d}_{14}(XY)]^*\,. \tag{H.33b}$$

Similarly, we obtain for $np = 58$ or 85, with one basis operator from the $Q = 1$ subspace and the other from the $Q = 2$ subspace,

$$\rho^{\mathrm{s}}_{58}(X) \;=\; \tfrac{1}{18}\,\omega^2_{\mathrm{D},X}\big\{\sqrt{6}\,F_{0-1}(X)\,[2\,J(0) - J(\omega_0)] - 6\,F_{1-2}(X)\,J(\omega_0)\big\}\,, \tag{H.34a}$$

$$\begin{aligned}\rho^{\mathrm{d}}_{58}(XY) \;=\; \tfrac{1}{18}\,\omega_{\mathrm{D},X}\,\omega_{\mathrm{D},Y}\big\{&\sqrt{6}\,[F_{0-1}(X,Y) + F_{-10}(X,Y)]\,[J(0) + J(\omega_0)] \\ &- 6\,[F_{1-2}(X,Y) + F_{-21}(X,Y)]\,[J(\omega_0) + J(2\omega_0)]\big\}\,,\end{aligned} \tag{H.34b}$$

and

$$\rho^{\mathrm{s}}_{85}(X) \;=\; \tfrac{1}{18}\,\omega^2_{\mathrm{D},X}\big\{\sqrt{6}\,F_{01}(X)\,[J(0) - 2\,J(\omega_0)] + 6\,F_{-12}(X)\,J(2\omega_0)\big\}\,, \tag{H.35a}$$

$$\begin{aligned}\rho^{\mathrm{d}}_{85}(XY) \;=\; -\,\tfrac{1}{18}\,\omega_{\mathrm{D},X}\,\omega_{\mathrm{D},Y}\big\{&\sqrt{6}\,[F_{01}(X,Y) + F_{10}(X,Y)]\,[J(0) + J(\omega_0)] \\ &- 6\,[F_{-12}(X,Y) + F_{2-1}(X,Y)]\,[J(\omega_0) + J(2\omega_0)]\big\}\,.\end{aligned} \tag{H.35b}$$

As in Eq. (H.33b), we have $\rho^{\mathrm{d}}_{85}(XY) = [\rho^{\mathrm{d}}_{58}(XY)]^*$, but, unlike Eq. (H.33a), there is no simple relation between $\rho^{\mathrm{s}}_{85}(X)$ and $\rho^{\mathrm{s}}_{58}(X)$. For basis operators B_5 and B_8, which both have even parity under spin permutation (Table S1), $\rho^{\mathrm{s}}_{58}(Y) = \rho^{\mathrm{s}}_{58}(X \to Y)$. In contrast, for basis operators B_1 and B_4, which have different spin permutation parity, $\rho^{\mathrm{s}}_{14}(Y) = -\,\rho^{\mathrm{s}}_{14}(X \to Y)$, as seen from Eq. (H.31b).

Finally, we note that, apart from a normalization factor, the self-correlated two-spin rates in Eqs. (H.34a) and (H.35a) are identical to the single-spin cross-mode rates in Eq. (H.10) that involve the same single-spin operators (μ_z and μ_+),

$$\rho^{\mathrm{s}}_{58}(X) \;=\; \tfrac{1}{\sqrt{2}}\,\rho^X_{z+}\,, \tag{H.36a}$$

$$\rho^{\mathrm{s}}_{85}(X) \;=\; \tfrac{1}{\sqrt{2}}\,\rho^X_{+z}\,. \tag{H.36b}$$

3. Relaxation of three-spin modes

The 27×27 nonlabile three-spin relaxation matrices $\mathbf{R}^{\alpha}_{\mathbb{N}_3(\mu\nu\kappa)\mathbb{N}_3(\mu\nu\kappa)}$ in the block-diagonal supermatrices $\mathbf{R}^{\alpha}_{\mathbb{N}_3\mathbb{N}_3}$ appearing in Eqs. (F.60) and (F.61) can be expressed as

$$\mathbf{R}^{\alpha}_{\mathbb{N}_3(\mu\nu\kappa)\mathbb{N}_3(\mu\nu\kappa)} \;=\; \boldsymbol{\rho}^{I\mu,\,I\nu,\,I\kappa} \qquad (IP_m{-}I\,\text{case})\,, \tag{H.37a}$$

$$\mathbf{R}^{\alpha}_{\mathbb{N}_3(\mu\nu\kappa)\mathbb{N}_3(\mu\nu\kappa)} \;=\; \boldsymbol{\rho}^{I\mu,\,I\nu,\,I\kappa} + \boldsymbol{\rho}^{S\mu,\,S\nu,\,S\kappa} \qquad (ISP_m{-}IS\,\text{case})\,. \tag{H.37b}$$

The elements ρ^{XYZ}_{np} of the 27×27 three-spin relaxation matrix $\boldsymbol{\rho}^{XYZ}$ are all auto-(spin triplet) rates, and either auto-mode ($n = p$) or cross-mode ($n \neq p$) rates. The 27 three-spin modes are ordered as in Table S2.

Because the three-spin modes involve three different nonlabile spins (μ, ν and κ), the three-spin rates involve three different dipole couplings ($X = I\mu$, $Y = I\nu$ and $Z = I\kappa$) for a given labile spin. In general, the three-spin rates therefore have contributions from self-correlations (s) as well as from distinct correlations (d), corresponding to diagonal

and off-diagonal terms, respectively, in the double sum of Eq. (13). Accordingly, we decompose the three-spin rates as

$$\rho_{np}^{XYZ} \;=\; \rho_{np}^{\mathrm{s}}(X) + \rho_{np}^{\mathrm{s}}(Y) + \rho_{np}^{\mathrm{s}}(Z) + \rho_{np}^{\mathrm{d}}(XY) + \rho_{np}^{\mathrm{d}}(XZ) + \rho_{np}^{\mathrm{d}}(YZ)\,. \tag{H.38}$$

where, for example, $\rho_{np}^{\mathrm{d}}(XY)$ is the sum of the two terms in Eq. (13) that differ by $X \leftrightarrow Y$ interchange.

TABLE S2. Basis operators for the $\mathbb{N}_3(\mu\nu\kappa)$ subspace for spins μ, ν and κ.

n	Q	K	$\mathcal{P}_{\mu\nu}$ [a]	B_n [c]
1	0	0	$-$ [b]	$\frac{1}{\sqrt{3}}[\mu_z(\nu_+\kappa_- - \nu_-\kappa_+) + \nu_z(\mu_-\kappa_+ - \mu_+\kappa_-) + \kappa_z(\mu_+\nu_- - \mu_-\nu_+)]$
2	0	1	$+$	$-\frac{2}{\sqrt{6}}\,\kappa_z(\mu_+\nu_- + \mu_-\nu_+ + 2\mu_z\nu_z)$
3	0	1	$-$	$\frac{1}{\sqrt{2}}[\mu_z(\nu_+\kappa_- + \nu_-\kappa_+) - \nu_z(\mu_-\kappa_+ + \mu_+\kappa_-)]$
4	0	1	$+$	$-\frac{1}{\sqrt{30}}[3\mu_z(\nu_+\kappa_- + \nu_-\kappa_+) + 3\nu_z(\mu_+\kappa_- + \mu_-\kappa_+) - 2\kappa_z(\mu_+\nu_- + \mu_-\nu_+) + 8\mu_z\nu_z\kappa_z]$
5	0	2	$-$	$\frac{1}{\sqrt{6}}[\mu_z(\nu_+\kappa_- - \nu_-\kappa_+) + \nu_z(\mu_-\kappa_+ - \mu_+\kappa_-) - 2\kappa_z(\mu_+\nu_- - \mu_-\nu_+)]$
6	0	2	$+$	$\frac{1}{\sqrt{2}}[\mu_z(\nu_-\kappa_+ - \nu_+\kappa_-) + \nu_z(\mu_-\kappa_+ - \mu_+\kappa_-)]$
7	0	3	$+$ [b]	$-\frac{1}{\sqrt{5}}[\mu_z(\nu_+\kappa_- + \nu_-\kappa_+) + \nu_z(\mu_-\kappa_+ + \mu_+\kappa_-) + \kappa_z(\mu_+\nu_- + \mu_-\nu_+) - 4\mu_z\nu_z\kappa_z]$
8	1	1	$+$	$\frac{1}{\sqrt{3}}\,\kappa_+(\mu_+\nu_- + \mu_-\nu_+ + 2\mu_z\nu_z)$
9	1	1	$-$	$\frac{1}{2}\,[\kappa_+(\mu_-\nu_+ - \mu_+\nu_-) + 2\kappa_z(\mu_z\nu_+ - \mu_+\nu_z)]$
10	1	1	$+$	$\frac{1}{\sqrt{60}}\,[\kappa_+(\mu_+\nu_- + \mu_-\nu_+) + 6\mu_+\nu_+\kappa_- + 6\kappa_z(\mu_z\nu_+ + \mu_+\nu_z) - 4\mu_z\nu_z\kappa_+]$
11	1	2	$-$	$\frac{1}{2}\,[\kappa_+(\mu_+\nu_- - \mu_-\nu_+) + 2\kappa_z(\mu_z\nu_+ - \mu_+\nu_z)]$
12	1	2	$+$	$-\frac{1}{2\sqrt{3}}\,[\kappa_+(\mu_+\nu_- + \mu_-\nu_+ - 4\mu_z\nu_z) + 2\kappa_z(\mu_z\nu_+ + \mu_+\nu_z) - 2\mu_+\nu_+\kappa_-]$
13	1	3	$+$ [b]	$\frac{1}{\sqrt{15}}\,[\mu_-\nu_+\kappa_+ + \mu_+\nu_-\kappa_+ + \mu_+\nu_+\kappa_-) - 4(\mu_+\nu_z\kappa_z + \mu_z\nu_+\kappa_z + \mu_z\nu_z\kappa_+)]$
14	-1	1	$+$	$-\frac{1}{\sqrt{3}}\,\kappa_-(\mu_+\nu_- + \mu_-\nu_+ + 2\mu_z\nu_z)$
15	-1	1	$-$	$\frac{1}{2}\,[\kappa_-(\mu_-\nu_+ - \mu_+\nu_-) - 2\kappa_z(\mu_z\nu_- - \mu_-\nu_z)]$
16	-1	1	$+$	$-\frac{1}{\sqrt{60}}\,[\kappa_-(\mu_+\nu_- + \mu_-\nu_+) + 6\mu_-\nu_-\kappa_+ + 6\kappa_z(\mu_z\nu_- + \mu_-\nu_z) - 4\mu_z\nu_z\kappa_-]$
17	-1	2	$-$	$\frac{1}{2}\,[-\kappa_-(\mu_+\nu_- - \mu_-\nu_+) + 2\kappa_z(\mu_z\nu_- - \mu_-\nu_z)]$
18	-1	2	$+$	$-\frac{1}{2\sqrt{3}}\,[\kappa_-(\mu_+\nu_- + \mu_-\nu_+ - 4\mu_z\nu_z) + 2\kappa_z(\mu_z\nu_- + \mu_+\nu_z) - 2\mu_-\nu_-\kappa_+]$
19	-1	3	$+$ [b]	$-\frac{1}{\sqrt{15}}\,[\mu_+\nu_-\kappa_- + \mu_-\nu_+\kappa_- + \mu_-\nu_-\kappa_+) - 4(\mu_-\nu_z\kappa_z + \mu_z\nu_-\kappa_z + \mu_z\nu_z\kappa_-)]$
20	2	2	$-$	$\kappa_+(\mu_+\nu_z - \mu_z\nu_+)$
21	2	2	$+$	$-\frac{1}{\sqrt{3}}\,[\kappa_+(\mu_+\nu_z + \mu_z\nu_+) - 2\mu_+\nu_+\kappa_z]$
22	2	3	$+$ [b]	$\frac{2}{\sqrt{6}}\,(\mu_z\nu_+\kappa_+ + \mu_+\nu_z\kappa_+ + \mu_+\nu_+\kappa_z)$
23	-2	2	$-$	$\kappa_-(\mu_z\nu_- - \mu_-\nu_z)$
24	-2	2	$+$	$\frac{1}{\sqrt{3}}\,[\kappa_-(\mu_-\nu_z + \mu_z\nu_-) - 2\mu_-\nu_-\kappa_z]$
25	-2	3	$+$ [b]	$\frac{2}{\sqrt{6}}\,(\mu_z\nu_-\kappa_- + \mu_-\nu_z\kappa_- + \mu_-\nu_-\kappa_z)$
26	3	3	$+$ [b]	$-\mu_+\nu_+\kappa_+$
27	-3	3	$+$ [b]	$\mu_-\nu_-\kappa_-$

[a] Parity of B_n under spin permutation $\mu \leftrightarrow \nu$.

[b] These basis operators have full spin permutation symmetry.

[c] The basis operators B_n are normalized in the three-spin ($\mu\nu\kappa$) Liouville space.

The generic three-spin relaxation matrix $\boldsymbol{\rho}^{XYZ}$ contains $27^2 = 729$ elements. Among these, 141 elements are within the Q-blocks (where $Q_n = Q_p$; see Table S2). Outside the Q-blocks, the Wigner-Eckart theorem requires that $\rho_{np}^{XY} = 0$ whenever $|Q_n - Q_p| > 2$. Consequently, there are 156 vanishing elements and $729 - 141 - 156 = 432$ nonzero elements outside the Q-blocks.

The sequential coupling scheme used to construct the basis operators does not, in general, produce operators with definite parity under spin permutation. While all our basis operators have definite (odd or even) parity under $\mu \leftrightarrow \nu$ interchange (see Tables S1 and S2), definite permutation parity involving other spins is only present in special cases. Among the 27 three-spin basis operators in Table S2, only eight have definite parity under all possible spin permutations: B_1 is odd whereas B_7, B_{13}, B_{19}, B_{22}, B_{25}, B_{26} and B_{27} are even. Because our three-spin basis is not fully symmetry-adapted, the relations found among the elements of $\boldsymbol{\rho}^{XY}$ only apply to $\rho_{np}^{\mathrm{s}}(X)$, $\rho_{np}^{\mathrm{s}}(Y)$ and $\rho_{np}^{\mathrm{d}}(XY)$, but not in general to $\rho_{np}^{\mathrm{s}}(Z)$, $\rho_{np}^{\mathrm{d}}(XZ)$ and $\rho_{np}^{\mathrm{d}}(YZ)$, where the dipole coupling $Z = I\kappa$ involves spin κ.

To illustrate these considerations, we shall examine a few elements of the three-spin relaxation matrix $\boldsymbol{\rho}^{XYZ}$, calculated from Eqs. (13) and (18). Consider first matrix elements between fully permutation symmetric (odd or even) basis operators,

$$\rho_{11}^{\mathrm{s}}(X) = \tfrac{4}{9}\,\omega_{\mathrm{D},X}^2\big\{F_{00}(X)\,J(0) - 2\,F_{1-1}(X)\,J(\omega_0) + 2\,F_{2-2}(X)\,J(2\omega_0)\big\}\,, \tag{H.39a}$$

$$\begin{aligned}\rho_{11}^{\mathrm{d}}(XY) = \tfrac{4}{9}\,\omega_{\mathrm{D},X}\,\omega_{\mathrm{D},Y}\big\{ &- F_{00}(X,Y)\,J(0) + 2\,\mathrm{Re}[F_{1-1}(X,Y)]\,J(\omega_0)\\ &- 2\,\mathrm{Re}[F_{2-2}(X,Y)]\,J(2\omega_0)\big\}\,,\end{aligned} \tag{H.39b}$$

$$\rho_{77}^{\mathrm{s}}(X) = \tfrac{4}{45}\,\omega_{\mathrm{D},X}^2\big\{4\,F_{00}(X)\,J(0) - 9\,F_{1-1}(X)\,J(\omega_0) + 12\,F_{2-2}(X)\,J(2\omega_0)\big\}\,, \tag{H.40a}$$

$$\begin{aligned}\rho_{77}^{\mathrm{d}}(XY) = \tfrac{4}{45}\,\omega_{\mathrm{D},X}\,\omega_{\mathrm{D},Y}\big\{&F_{00}(X,Y)\,J(0) - 6\,\mathrm{Re}[F_{1-1}(X,Y)]\,J(\omega_0)\\ &+ 18\,\mathrm{Re}[F_{2-2}(X,Y)]\,J(2\omega_0)\big\}\,,\end{aligned} \tag{H.40b}$$

$$\rho_{27,27}^{\mathrm{s}}(X) = \tfrac{1}{9}\,\omega_{\mathrm{D},X}^2\big\{5\,F_{00}(X)\,J(0) - 9\,F_{1-1}(X)\,J(\omega_0) + 6\,F_{2-2}(X)\,J(2\omega_0)\big\}\,, \tag{H.41a}$$

$$\rho_{27,27}^{\mathrm{d}}(XY) = -\tfrac{4}{9}\,\omega_{\mathrm{D},X}\,\omega_{\mathrm{D},Y}\big\{-2\,F_{00}(X,Y)\,J(0) + 3\,\mathrm{Re}[F_{1-1}(X,Y)]\,J(\omega_0)\big\}\,. \tag{H.41b}$$

In addition $\rho_{26,26}^{XYZ} = \rho_{27,27}^{XYZ}$. For these four diagonal elements between fully permutation invariant basis operators,

$$\rho_{nn}^{\mathrm{s}}(Y) = \rho_{nn}^{\mathrm{s}}(X \to Y)\,, \tag{H.42a}$$

$$\rho_{nn}^{\mathrm{s}}(Z) = \rho_{nn}^{\mathrm{s}}(X \to Z)\,, \tag{H.42b}$$

$$\rho_{nn}^{\mathrm{d}}(XZ) = \rho_{nn}^{\mathrm{d}}(XY \to XZ)\,, \tag{H.42c}$$

$$\rho_{nn}^{\mathrm{d}}(YZ) = \rho_{nn}^{\mathrm{d}}(XY \to YZ)\,. \tag{H.42d}$$

As anticipated, these diagonal elements are real, and there is complete symmetry among the dipole couplings X, Y and Z.

In contrast, consider two diagonal matrix elements involving basis operators that only have $\mu \leftrightarrow \nu$ symmetry,

$$\rho^{\mathrm{s}}_{22}(X) = \tfrac{4}{9}\,\omega^2_{\mathrm{D},X}\big\{F_{00}(X)\,J(0) - 2\,F_{1-1}(X)\,J(\omega_0) + 2\,F_{2-2}(X)\,J(2\omega_0)\big\}\,, \tag{H.43a}$$

$$\rho^{\mathrm{s}}_{22}(Y) = \rho^{\mathrm{s}}_{22}(X \to Y)\,, \tag{H.43b}$$

$$\rho^{\mathrm{s}}_{22}(Z) = \tfrac{2}{9}\,\omega^2_{\mathrm{D},Z}\big\{F_{00}(Z)\,J(0) - 3\,F_{1-1}(Z)\,J(\omega_0) + 6\,F_{2-2}(Z)\,J(2\omega_0)\big\}\,, \tag{H.43c}$$

$$\begin{aligned}\rho^{\mathrm{d}}_{22}(XY) = -\tfrac{8}{9}\,\omega_{\mathrm{D},X}\,\omega_{\mathrm{D},Y}\big\{&F_{00}(X,Y)\,J(0) - 2\,\mathrm{Re}[F_{1-1}(X,Y)]\,J(\omega_0)\\ &+ 2\,\mathrm{Re}[F_{2-2}(X,Y)]\,J(2\omega_0)\big\}\,,\end{aligned} \tag{H.43d}$$

$$\rho^{\mathrm{d}}_{22}(XZ) = 0\,, \tag{H.43e}$$

$$\rho^{\mathrm{d}}_{22}(YZ) = 0\,, \tag{H.43f}$$

$$\begin{aligned}\rho^{\mathrm{s}}_{66}(X) = \tfrac{1}{18}\,\omega^2_{\mathrm{D},X}\big\{&7\,F_{00}(X)\,J(0) - 15\,F_{1-1}(X)\,J(\omega_0)\\ &+ 18\,F_{2-2}(X)\,J(2\omega_0)\big\}\,,\end{aligned} \tag{H.44a}$$

$$\rho^{\mathrm{s}}_{66}(Y) = \rho^{\mathrm{s}}_{66}(X \to Y)\,,$$

$$\rho^{\mathrm{s}}_{66}(Z) = \tfrac{1}{9}\,\omega^2_{\mathrm{D},Z}\big\{5\,F_{00}(Z)\,J(0) - 9\,F_{1-1}(Z)\,J(\omega_0) + 6\,F_{2-2}(Z)\,J(2\omega_0)\big\}\,, \tag{H.44b}$$

$$\begin{aligned}\rho^{\mathrm{d}}_{66}(XY) = \tfrac{2}{9}\,\omega_{\mathrm{D},X}\,\omega_{\mathrm{D},Y}\big\{&F_{00}(X,Y)\,J(0) - 3\,\mathrm{Re}[F_{1-1}(X,Y)]\,J(\omega_0)\\ &+ 6\,\mathrm{Re}[F_{2-2}(X,Y)]\,J(2\omega_0)\big\}\,,\end{aligned} \tag{H.44c}$$

$$\rho^{\mathrm{d}}_{66}(XZ) = \tfrac{2}{9}\,\omega_{\mathrm{D},X}\,\omega_{\mathrm{D},Z}\big\{-2\,F_{00}(X,Z)\,J(0) + 3\,\mathrm{Re}[F_{1-1}(X,Z)]\,J(\omega_0)\big\}\,, \tag{H.44d}$$

$$\rho^{\mathrm{d}}_{66}(YZ) = \rho^{\mathrm{d}}_{66}(XZ \to YZ)\,. \tag{H.44e}$$

Also these diagonal elements are real, but now the components involving dipole coupling Z deviate from those involving only X and Y. Although all diagonal elements ρ^{XYZ}_{nn} are real, the Q-blocks of $\boldsymbol{\rho}^{XYZ}$ are *not* Hermitian.

4. Coherent spin mode transfer

The coherent spin mode transfer supermatrices $\boldsymbol{\Delta}^{\alpha}_{\mathbb{N}_1\mathbb{N}_2}$ and $\boldsymbol{\Delta}^{\alpha}_{\mathbb{N}_2\mathbb{N}_3}$ describe, respectively, coherent transfer between single-spin and two-spin modes and between two-spin and three-spin modes. The former enters into $\mathbf{X}^{\alpha}_{\mathbb{N}_1(\mu)\mathbb{N}_1(\nu)}$ in Eq. (F.21) and into $\mathbf{Y}^{\alpha}_{\mathbb{N}_1(\mu)\mathbb{N}_1(\nu)}$ in Eqs. (F.60) and (F.61). The two distinct generic matrices are expressed as

$$\boldsymbol{\Delta}^{\alpha}_{\mathbb{N}_1(\mu)\mathbb{N}_2(\mu\nu)} = -\frac{\omega_{\mathrm{D},\mu\nu}}{3\sqrt{2}}\,\boldsymbol{\delta}^{\alpha}_{\mathbb{N}_1(\mu)\mathbb{N}_2(\mu\nu)}\,, \tag{H.45a}$$

$$\boldsymbol{\Delta}^{\alpha}_{\mathbb{N}_1(\nu)\mathbb{N}_2(\mu\nu)} = -\frac{\omega_{\mathrm{D},\mu\nu}}{3\sqrt{2}}\,\boldsymbol{\delta}^{\alpha}_{\mathbb{N}_1(\nu)\mathbb{N}_2(\mu\nu)}\,, \tag{H.45b}$$

With the single-spin basis ordered as $\{\mu_z\,,\,\mu_+\,,\,\mu_-\}$ and the two-spin basis ordered as in Table S1, Eqs. (14) and (19) yield for the dimensionless 3×9 matrix $\boldsymbol{\delta}^{\alpha}_{\mathbb{N}_1(\mu)\mathbb{N}_2(\mu\nu)}$,

$\boldsymbol{\delta}^{\alpha}_{\mathbb{N}_1(\mu)\mathbb{N}_2(\mu\nu)} \;=$

$$\left[\begin{array}{ccccccccc}
1(+) & 2(+) & 3(-) & 4(-) & 5(+) & 6(-) & 7(+) & 8(+) & 9(+) \\ \hline
0 & 0 & -2D_0 & \sqrt{3}D_{-1} & \sqrt{3}D_{-1} & \sqrt{3}D_1 & -\sqrt{3}D_1 & -2\sqrt{3}D_{-2} & 2\sqrt{3}D_2 \\
0 & -3D_1 & -\sqrt{3}D_1 & D_0 & 3D_0 & \sqrt{6}D_2 & \sqrt{6}D_2 & -\sqrt{6}D_{-1} & \mathbf{0} \\
0 & 3D_{-1} & -\sqrt{3}D_{-1} & \sqrt{6}D_{-2} & -\sqrt{6}D_{-2} & D_0 & -3D_0 & \mathbf{0} & \sqrt{6}D_1
\end{array}\right], \tag{H.46}$$

where $D_M \equiv D^{2*}_{M0}(\Omega^{\alpha}_{\mu\nu})$, as given by Eq. (C.6) or (C.11), with the internuclear vector pointing from spin μ to spin ν and $\mu<\nu$. The two-spin basis operators are defined as in Table S1, again assuming that $\mu<\nu$. The Wigner-Eckart theorem requires that $\delta^{\alpha}_{np}=0$ whenever $|Q_n-Q_p|>2$, the rank of the ISTO $T^2_M(X)$ in Eq. (19). The two elements that vanish for this reason are shown in boldface in Eq. (H.46).

The matrix $\boldsymbol{\delta}^{\alpha}_{\mathbb{N}_1(\nu)\mathbb{N}_2(\mu\nu)}$ is identical to $\boldsymbol{\delta}^{\alpha}_{\mathbb{N}_1(\mu)\mathbb{N}_2(\mu\nu)}$ in Eq. (H.46), except for a sign reversal of all elements that involve a two-spin mode with odd permutation parity (and odd rank K). The parity is given in Table S1 and it is also reproduced on the line above the matrix in Eq. (H.46), showing that elements in columns 3, 4 and 6 are sign inverted in $\boldsymbol{\delta}^{\alpha}_{\mathbb{N}_1(\nu)\mathbb{N}_2(\mu\nu)}$.

The two-spin to three-spin transfer matrices enter into $\mathbf{Y}^{\alpha}_{\mathbb{N}_1(\mu)\mathbb{N}_1(\nu)}$ directly in Eqs. (F.60) and (F.61) and via $\mathbf{X}^{\alpha}_{\mathbb{N}_3\mathbb{N}_3}$ in Eq. (F.62). The three distinct transfer matrices can be expressed in terms of six generic matrices as

$$\boldsymbol{\Delta}^{\alpha}_{\mathbb{N}_2(\mu\nu)\mathbb{N}_3(\mu\nu\kappa)} \;=\; \omega_{\mathrm{D},\mu\kappa}\,\boldsymbol{\delta}^{\alpha}_{\mathbb{N}_2(\mu\nu)\mathbb{N}_3(\mu\nu\kappa)}(\mu\kappa) + \omega_{\mathrm{D},\nu\kappa}\,\boldsymbol{\delta}^{\alpha}_{\mathbb{N}_2(\mu\nu)\mathbb{N}_3(\mu\nu\kappa)}(\nu\kappa)\,, \tag{H.47a}$$

$$\boldsymbol{\Delta}^{\alpha}_{\mathbb{N}_2(\mu\kappa)\mathbb{N}_3(\mu\nu\kappa)} \;=\; \omega_{\mathrm{D},\mu\nu}\,\boldsymbol{\delta}^{\alpha}_{\mathbb{N}_2(\mu\kappa)\mathbb{N}_3(\mu\nu\kappa)}(\mu\nu) + \omega_{\mathrm{D},\nu\kappa}\,\boldsymbol{\delta}^{\alpha}_{\mathbb{N}_2(\mu\kappa)\mathbb{N}_3(\mu\nu\kappa)}(\nu\kappa)\,, \tag{H.47b}$$

$$\boldsymbol{\Delta}^{\alpha}_{\mathbb{N}_2(\nu\kappa)\mathbb{N}_3(\mu\nu\kappa)} \;=\; \omega_{\mathrm{D},\mu\nu}\,\boldsymbol{\delta}^{\alpha}_{\mathbb{N}_2(\nu\kappa)\mathbb{N}_3(\mu\nu\kappa)}(\mu\nu) + \omega_{\mathrm{D},\mu\kappa}\,\boldsymbol{\delta}^{\alpha}_{\mathbb{N}_2(\nu\kappa)\mathbb{N}_3(\mu\nu\kappa)}(\mu\kappa)\,. \tag{H.47c}$$

With the two-spin basis ordered as in Table S1 and the three-spin basis as in Table S2, Eqs. (14) and (19) yield the result in Eq. (H.48) for the dimensionless 9×27 matrix $\boldsymbol{\delta}^{\alpha}_{\mathbb{N}_2(\mu\nu)\mathbb{N}_3(\mu\nu\kappa)}(\mu\kappa)$ with $D_M \equiv D^{2*}_{M0}(\Omega^{\alpha}_{\mu\kappa})$, as given by Eq. (C.6) or (C.11). In Eq. (H.48), the numbering of the two-spin and three-spin basis operators is given to the left of and above the matrix, along with the $\mu\leftrightarrow\nu$ permutation parity. The Wigner-Eckart theorem requires that $\delta^{\alpha}_{np}=0$ whenever $|Q_n-Q_p|>2$, the rank of the ISTO $T^2_M(X)$ in Eq. (19). The 42 elements that vanish for this reason are shown in boldface in Eq. (H.48).

The matrix $\boldsymbol{\delta}^{\alpha}_{\mathbb{N}_2(\mu\nu)\mathbb{N}_3(\mu\nu\kappa)}(\nu\kappa)$ in Eq. (H.47a) is identical to $\boldsymbol{\delta}^{\alpha}_{\mathbb{N}_2(\mu\nu)\mathbb{N}_3(\mu\nu\kappa)}(\mu\kappa)$, except for a sign reversal of all elements that connect two-spin and three spin modes with different $\mu\leftrightarrow\nu$ permutation parity. (Also the Euler angles are $\Omega^{\alpha}_{\nu\kappa}$ instead of $\Omega^{\alpha}_{\mu\kappa}$.) The other four generic matrices in Eq. (H.47) are similar to the one shown in Eq. (H.48). However, the identity (apart from a sign reversal when the basis operators have different parity) of the pair of matrices applies to Eqs. (H.47b) and (H.47c) only for the eight columns associated with three-spin operators with full permutation symmetry (Table S2).

$\boldsymbol{\delta}^{\alpha}_{\mathbb{N}_2(\mu\nu)\mathbb{N}_3(\mu\nu\kappa)}(\mu\kappa) \;=$

	1(−)	2(+)	3(−)	4(+)	5(−)	6(+)	7(+)	8(+)	9(−)
1(+)	0	0	0	0	$-\frac{2}{3}D_0$	0	0	0	0
2(+)	$\frac{1}{3}D_0$	0	0	0	$-\frac{\sqrt{2}}{6}D_0$	$\frac{\sqrt{6}}{6}D_0$	0	0	$-\frac{\sqrt{2}}{4}D_{-1}$
3(−)	0	$-\frac{2\sqrt{6}}{9}D_0$	$\frac{\sqrt{2}}{6}D_0$	$\frac{\sqrt{30}}{90}D_0$	0	0	$-\frac{\sqrt{5}}{5}D_0$	$\frac{\sqrt{2}}{3}D_{-1}$	$-\frac{\sqrt{6}}{12}D_{-1}$
4(−)	0	$-\frac{\sqrt{2}}{3}D_1$	$\frac{\sqrt{6}}{12}D_1$	$\frac{\sqrt{10}}{60}D_1$	$\frac{\sqrt{2}}{4}D_1$	$\frac{\sqrt{6}}{12}D_1$	$\frac{\sqrt{15}}{15}D_1$	$\frac{\sqrt{6}}{9}D_0$	$-\frac{\sqrt{2}}{12}D_0$
5(+)	$\frac{1}{3}D_1$	0	$\frac{\sqrt{6}}{12}D_1$	$-\frac{\sqrt{10}}{20}D_1$	$-\frac{\sqrt{2}}{12}D_1$	$\frac{\sqrt{6}}{12}D_1$	$\frac{2\sqrt{15}}{15}D_1$	0	$-\frac{\sqrt{2}}{4}D_0$
6(−)	0	$-\frac{\sqrt{2}}{3}D_{-1}$	$\frac{\sqrt{6}}{12}D_{-1}$	$\frac{\sqrt{10}}{60}D_{-1}$	$-\frac{\sqrt{2}}{4}D_{-1}$	$-\frac{\sqrt{6}}{12}D_{-1}$	$\frac{\sqrt{15}}{15}D_{-1}$	$\frac{2}{3}D_{-2}$	$-\frac{\sqrt{3}}{6}D_{-2}$
7(+)	$\frac{1}{3}D_{-1}$	0	$-\frac{\sqrt{6}}{12}D_{-1}$	$\frac{\sqrt{10}}{20}D_{-1}$	$-\frac{\sqrt{2}}{12}D_{-1}$	$\frac{\sqrt{6}}{12}D_{-1}$	$-\frac{2\sqrt{15}}{15}D_{-1}$	0	$-\frac{\sqrt{3}}{6}D_{-2}$
8(+)	$\frac{1}{3}D_2$	0	$\frac{\sqrt{6}}{6}D_2$	$-\frac{\sqrt{10}}{10}D_2$	$\frac{\sqrt{2}}{6}D_2$	$-\frac{\sqrt{6}}{6}D_2$	$-\frac{\sqrt{15}}{15}D_2$	0	$-\frac{\sqrt{3}}{6}D_1$
9(+)	$\frac{1}{3}D_{-2}$	0	$-\frac{\sqrt{6}}{6}D_{-2}$	$\frac{\sqrt{10}}{10}D_{-2}$	$\frac{\sqrt{2}}{6}D_{-2}$	$-\frac{\sqrt{6}}{6}D_{-2}$	$\frac{\sqrt{15}}{15}D_{-2}$	$\mathbf{0}$	$\mathbf{0}$

	10(+)	11(−)	12(+)	13(+)	14(+)	15(−)	16(+)	17(−)	18(+)
1(+)	0	$\frac{2}{3}D_{-1}$	0	0	0	0	0	$\frac{2}{3}D_1$	0
2(+)	$\frac{\sqrt{30}}{20}D_{-1}$	$\frac{\sqrt{2}}{12}D_{-1}$	$-\frac{\sqrt{6}}{12}D_{-1}$	$-\frac{\sqrt{30}}{15}D_{-1}$	0	$\frac{\sqrt{2}}{4}D_1$	$-\frac{\sqrt{30}}{20}D_1$	$\frac{\sqrt{2}}{12}D_1$	$-\frac{\sqrt{6}}{12}D_1$
3(−)	$-\frac{\sqrt{10}}{60}D_{-1}$	$-\frac{\sqrt{6}}{12}D_{-1}$	$-\frac{\sqrt{2}}{12}D_{-1}$	$\frac{2\sqrt{10}}{15}D_{-1}$	$\frac{\sqrt{2}}{3}D_1$	$-\frac{\sqrt{6}}{12}D_1$	$-\frac{\sqrt{10}}{60}D_1$	$\frac{\sqrt{6}}{12}D_1$	$\frac{\sqrt{2}}{12}D_1$
4(−)	$-\frac{\sqrt{30}}{180}D_0$	$-\frac{\sqrt{2}}{4}D_0$	$-\frac{\sqrt{6}}{12}D_0$	$-\frac{\sqrt{30}}{15}D_0$	$\frac{2}{3}D_2$	$-\frac{\sqrt{3}}{6}D_2$	$-\frac{\sqrt{5}}{30}D_2$	$-\frac{\sqrt{3}}{6}D_2$	$-\frac{1}{6}D_2$
5(+)	$\frac{\sqrt{30}}{20}D_0$	$-\frac{\sqrt{2}}{12}D_0$	$\frac{\sqrt{6}}{12}D_0$	$-\frac{\sqrt{30}}{15}D_0$	0	$\frac{\sqrt{3}}{6}D_2$	$-\frac{\sqrt{5}}{10}D_2$	$\frac{\sqrt{3}}{6}D_2$	$-\frac{1}{2}D_2$
6(−)	$-\frac{\sqrt{5}}{30}D_{-2}$	$\frac{\sqrt{3}}{6}D_{-2}$	$\frac{1}{6}D_{-2}$	$-\frac{\sqrt{5}}{15}D_{-2}$	$\frac{\sqrt{6}}{9}D_0$	$-\frac{\sqrt{2}}{12}D_0$	$-\frac{\sqrt{30}}{180}D_0$	$\frac{\sqrt{2}}{4}D_0$	$\frac{\sqrt{6}}{12}D_0$
7(+)	$\frac{\sqrt{5}}{10}D_{-2}$	$\frac{\sqrt{3}}{6}D_{-2}$	$-\frac{1}{2}D_{-2}$	$\frac{\sqrt{5}}{5}D_{-2}$	0	$\frac{\sqrt{2}}{4}D_0$	$-\frac{\sqrt{30}}{20}D_0$	$-\frac{\sqrt{2}}{12}D_0$	$\frac{\sqrt{6}}{12}D_0$
8(+)	$\frac{\sqrt{5}}{10}D_1$	$-\frac{\sqrt{3}}{6}D_1$	$\frac{1}{2}D_1$	$\frac{\sqrt{5}}{5}D_1$	$\mathbf{0}$	$\mathbf{0}$	$\mathbf{0}$	$\mathbf{0}$	$\mathbf{0}$
9(+)	$\mathbf{0}$	$\mathbf{0}$	$\mathbf{0}$	$\mathbf{0}$	0	$\frac{\sqrt{3}}{6}D_{-1}$	$-\frac{\sqrt{5}}{10}D_{-1}$	$-\frac{\sqrt{3}}{6}D_{-1}$	$\frac{1}{2}D_{-1}$

	19(+)	20(−)	21(+)	22(+)	23(−)	24(+)	25(+)	26(+)	27(+)
1(+)	0	$-\frac{2}{3}D_{-2}$	0	0	$-\frac{2}{3}D_2$	0	0	$\mathbf{0}$	$\mathbf{0}$
2(+)	$\frac{\sqrt{30}}{15}D_1$	$\frac{\sqrt{2}}{6}D_{-2}$	$-\frac{\sqrt{6}}{6}D_{-2}$	$\frac{\sqrt{3}}{3}D_{-2}$	$\frac{\sqrt{2}}{6}D_2$	$-\frac{\sqrt{6}}{6}D_2$	$-\frac{\sqrt{3}}{3}D_2$	$\mathbf{0}$	$\mathbf{0}$
3(−)	$\frac{2\sqrt{10}}{15}D_1$	$\frac{\sqrt{6}}{6}D_{-2}$	$\frac{\sqrt{2}}{6}D_{-2}$	$-\frac{1}{3}D_{-2}$	$-\frac{\sqrt{6}}{6}D_2$	$-\frac{\sqrt{2}}{6}D_2$	$-\frac{1}{3}D_2$	$\mathbf{0}$	$\mathbf{0}$
4(−)	$-\frac{\sqrt{5}}{15}D_2$	$\frac{\sqrt{3}}{6}D_{-1}$	$\frac{1}{6}D_{-1}$	$\frac{\sqrt{2}}{3}D_{-1}$	$\mathbf{0}$	$\mathbf{0}$	$\mathbf{0}$	$-\frac{\sqrt{3}}{3}D_{-2}$	$\mathbf{0}$
5(+)	$-\frac{\sqrt{5}}{5}D_2$	$\frac{\sqrt{3}}{6}D_{-1}$	$-\frac{1}{2}D_{-1}$	0	$\mathbf{0}$	$\mathbf{0}$	$\mathbf{0}$	$\frac{\sqrt{3}}{3}D_{-2}$	$\mathbf{0}$
6(−)	$-\frac{\sqrt{30}}{15}D_0$	$\mathbf{0}$	$\mathbf{0}$	$\mathbf{0}$	$-\frac{\sqrt{3}}{6}D_1$	$-\frac{1}{6}D_1$	$\frac{\sqrt{2}}{3}D_1$	$\mathbf{0}$	$-\frac{\sqrt{3}}{3}D_2$
7(+)	$\frac{\sqrt{30}}{15}D_0$	$\mathbf{0}$	$\mathbf{0}$	$\mathbf{0}$	$\frac{\sqrt{3}}{6}D_1$	$-\frac{1}{2}D_1$	0	$\mathbf{0}$	$-\frac{\sqrt{3}}{3}D_2$
8(+)	$\mathbf{0}$	$\frac{\sqrt{2}}{6}D_0$	$-\frac{\sqrt{6}}{6}D_0$	$-\frac{\sqrt{3}}{3}D_0$	0	0	0	$\frac{\sqrt{3}}{3}D_{-1}$	0
9(+)	$-\frac{\sqrt{5}}{5}D_{-1}$	0	0	0	$\frac{\sqrt{2}}{6}D_0$	$-\frac{\sqrt{6}}{6}D_0$	$\frac{\sqrt{3}}{3}D_0$	0	$-\frac{\sqrt{3}}{3}D_1$

(H.48)

APPENDIX I: MULTI-SPIN ESE THEORY

In this Appendix, we use the SRE framework and well-defined approximations to derive the multi-spin ESE theory for the $IP_m - I$ and $ISP_m - IS$ cases. Our starting point is the multi-spin SRE framework as defined by Eqs. (5), (7), (11) – (19) of the main text. The RMN condition $\omega_D \tau_A \ll 1$ will not be assumed except in so far that the relaxation supermatrix in Eq. (13) is based on BWR theory. Specifically, we will not implement the RMN approximation via series expansions, as we did in the derivation of $\mathbf{G}^A_{\mathbb{LZ},\mathbb{LZ}}$ in Eqs. (31) – (35) (see Appendix F).

1. Single-spin mode truncation

The first approximation required to obtain the ESE theory is the single-spin mode (1SM) approximation, where all couplings between single-spin modes and multi-spin modes are neglected so the theory can be developed within a single-spin Liouville subspace of dimension $(3m + 3)$ for the $IP_m - I$ case and $(3m + 6)$ for the $ISP_m - IS$ case. Within the SLE framework, the 1SM is not a viable approach, because $\mathbf{L}^\alpha_D = \mathbf{0}$ in the single-spin subspace. This follows because all single-spin operators have odd SIC parity, but $\mathbf{L}^\alpha_D$ has nonzero matrix elements only between odd and even basis operators.

The single-spin Liouville subspace can be partitioned into a $(3\,m)$-dimensional nonlabile single-spin subspace $\mathbb{N}_1$ and a 3-dimensional (for exchange case $IP_m - I$) or 6-dimensional (for exchange case $ISP_m - IS$) labile single-spin subspace $\mathbb{L}_1$. Two consequences of the rather drastic 1SM approximation can be noted immediately. First, because labile two-spin operators are omitted, only the 2×2 single-spin block of the 5×5 matrix in Eq. (A.2) remains, so Eq. (12) is obtained without further approximation. Second, because all single-spin operators have odd SIC parity, $\mathbf{\Delta}^\alpha$, which is anti-block-diagonal with respect to SIC parity, can be omitted from Eq. (7). The ESE theory, being based on the 1SM approximation, therefore cannot describe the secondary dispersion step at $\omega_0 \approx \omega_D$ or any other effects of the static dipole couplings.

Partitioning the supermatrix $\mathbf{\Lambda}^\alpha$ in Eq. (7) (without $\mathbf{\Delta}^\alpha$) into $\mathbb{L}_1$ and $\mathbb{N}_1$ subspaces, and noting that $\mathbf{K}_{\mathbb{L}_1\mathbb{L}_1} = \mathbf{1}$ and $\mathbf{K}_{\mathbb{N}_1\mathbb{N}_1} = \mathbf{0}$, we obtain

$$\mathbf{\Lambda}^\alpha \;=\; \begin{bmatrix} (\mathbf{1} + \mathbf{R}^\alpha_{\mathbb{L}_1\mathbb{L}_1}\,\tau_A + i\,\mathbf{L}_{Z,\mathbb{L}_1\mathbb{L}_1}\,\tau_A & \mathbf{R}^\alpha_{\mathbb{L}_1\mathbb{N}_1}\,\tau_A \\ \mathbf{R}^\alpha_{\mathbb{N}_1\mathbb{L}_1}\,\tau_A & (\mathbf{R}^\alpha_{\mathbb{N}_1\mathbb{N}_1}\,\tau_A + i\,\mathbf{L}_{Z,\mathbb{N}_1\mathbb{N}_1}\,\tau_A) \end{bmatrix}. \tag{I.1}$$

We need only the $\mathbb{L}_1\mathbb{L}_1$ block of the inverse $(\mathbf{\Lambda}^\alpha)^{-1}$,

$$[(\mathbf{\Lambda}^\alpha)^{-1}]_{\mathbb{L}_1\mathbb{L}_1} = \Big[\mathbf{1} + \mathbf{R}^\alpha_{\mathbb{L}_1\mathbb{L}_1}\,\tau_A + i\,\mathbf{L}_{Z,\mathbb{L}_1\mathbb{L}_1}\,\tau_A \;-\; \mathbf{R}^\alpha_{\mathbb{L}_1\mathbb{N}_1}\left(\mathbf{R}^\alpha_{\mathbb{N}_1\mathbb{N}_1} + i\,\mathbf{L}_{Z,\mathbb{N}_1\mathbb{N}_1}\right)^{-1}\mathbf{R}^\alpha_{\mathbb{N}_1\mathbb{L}_1}\,\tau_A\Big]^{-1}. \tag{I.2}$$

According Eq. (23a), $\mathbf{R}^\alpha_{\mathbb{N}_1\mathbb{N}_1}$ is block-diagonal in spin, with one 3×3 block for each of the m nonlabile spins, provided that the basis operators of the $\mathbb{N}_1$ subspace are grouped by spin. Moreover, $\mathbf{R}^\alpha_{\mathbb{N}_1\mathbb{N}_1}$ only involves self-correlations. If all spins are isochronous, Eq.

(I.2) can therefore be expressed entirely in terms of 3×3 matrices as

$$[(\mathbf{\Lambda}^{\alpha})^{-1}]_{\mathbb{L}_1\mathbb{L}_1} \;=\; \Big[\mathbf{1} + \widetilde{\mathbf{R}}^{\,\alpha}_{\mathbb{I}\mathbb{I}}\,\tau_{\mathrm{A}} + i\,\omega_0\tau_{\mathrm{A}}\mathbf{Q}_1\Big]^{-1}\,, \quad (IP_m{-}I \text{ case}) \tag{I.3}$$

$$[(\mathbf{\Lambda}^{\alpha})^{-1}]_{\mathbb{L}_1\mathbb{L}_1} = \begin{bmatrix} (\mathbf{1} + \widetilde{\mathbf{R}}^{\,\alpha}_{\mathbb{I}\mathbb{I}}\,\tau_{\mathrm{A}} + i\,\omega_0\tau_{\mathrm{A}}\mathbf{Q}_1) & \widetilde{\mathbf{R}}^{\,\alpha}_{\mathbb{I}\mathbb{S}}\,\tau_{\mathrm{A}} \\ \widetilde{\mathbf{R}}^{\,\alpha}_{\mathbb{S}\mathbb{I}}\,\tau_{\mathrm{A}} & (\mathbf{1} + \widetilde{\mathbf{R}}^{\,\alpha}_{\mathbb{S}\mathbb{S}}\,\tau_{\mathrm{A}} + i\,\omega_0\tau_{\mathrm{A}}\mathbf{Q}_1) \end{bmatrix}^{-1}, \quad (ISP_m{-}IS \text{ case}) \tag{I.4}$$

where $\mathbf{Q}_1 = \mathrm{diag}(0, 1, -1)$. Here, we also use the short-hand notation $\mathbb{I} \equiv \mathbb{L}_1(I)$ and $\mathbb{S} \equiv \mathbb{L}_1(S)$ for the 3-dimensional labile single-spin subspaces. Furthermore,

$$\widetilde{\mathbf{R}}^{\,\alpha}_{\mathbb{I}\mathbb{I}} \;\equiv\; \mathbf{R}^{\alpha}_{\mathbb{I}\mathbb{I}} - \mathbf{\Gamma}^{\alpha}_{\mathbb{I}\mathbb{I}}\,, \tag{I.5a}$$

$$\widetilde{\mathbf{R}}^{\,\alpha}_{\mathbb{I}\mathbb{S}} \;\equiv\; \mathbf{R}^{\alpha}_{\mathbb{I}\mathbb{S}} - \mathbf{\Gamma}^{\alpha}_{\mathbb{I}\mathbb{S}}\,, \tag{I.5b}$$

$$\widetilde{\mathbf{R}}^{\,\alpha}_{\mathbb{S}\mathbb{I}} \;\equiv\; \mathbf{R}^{\alpha}_{\mathbb{S}\mathbb{I}} - \mathbf{\Gamma}^{\alpha}_{\mathbb{S}\mathbb{I}}\,, \tag{I.5c}$$

$$\widetilde{\mathbf{R}}^{\,\alpha}_{\mathbb{S}\mathbb{S}} \;\equiv\; \mathbf{R}^{\alpha}_{\mathbb{S}\mathbb{S}} - \mathbf{\Gamma}^{\alpha}_{\mathbb{S}\mathbb{S}}\,, \tag{I.5d}$$

$$\mathbf{\Gamma}^{\alpha}_{\mathbb{I}\mathbb{I}} \;\equiv\; \sum_{\mu=1}^{m} \mathbf{R}^{\alpha}_{\mathbb{I}\mathbb{N}_1(\mu)} \left[\mathbf{R}^{\alpha}_{\mathbb{N}_1(\mu)\mathbb{N}_1(\mu)} + i\,\omega_0\,\mathbf{Q}_1\right]^{-1} \mathbf{R}^{\alpha}_{\mathbb{N}_1(\mu)\mathbb{I}}\,, \tag{I.6a}$$

$$\mathbf{\Gamma}^{\alpha}_{\mathbb{I}\mathbb{S}} \;\equiv\; \sum_{\mu=1}^{m} \mathbf{R}^{\alpha}_{\mathbb{I}\mathbb{N}_1(\mu)} \left[\mathbf{R}^{\alpha}_{\mathbb{N}_1(\mu)\mathbb{N}_1(\mu)} + i\,\omega_0\,\mathbf{Q}_1\right]^{-1} \mathbf{R}^{\alpha}_{\mathbb{N}_1(\mu)\mathbb{S}}\,, \tag{I.6b}$$

$$\mathbf{\Gamma}^{\alpha}_{\mathbb{S}\mathbb{I}} \;\equiv\; \sum_{\mu=1}^{m} \mathbf{R}^{\alpha}_{\mathbb{S}\mathbb{N}_1(\mu)} \left[\mathbf{R}^{\alpha}_{\mathbb{N}_1(\mu)\mathbb{N}_1(\mu)} + i\,\omega_0\,\mathbf{Q}_1\right]^{-1} \mathbf{R}^{\alpha}_{\mathbb{N}_1(\mu)\mathbb{I}}\,, \tag{I.6c}$$

$$\mathbf{\Gamma}^{\alpha}_{\mathbb{S}\mathbb{S}} \;\equiv\; \sum_{\mu=1}^{m} \mathbf{R}^{\alpha}_{\mathbb{S}\mathbb{N}_1(\mu)} \left[\mathbf{R}^{\alpha}_{\mathbb{N}_1(\mu)\mathbb{N}_1(\mu)} + i\,\omega_0\,\mathbf{Q}_1\right]^{-1} \mathbf{R}^{\alpha}_{\mathbb{N}_1(\mu)\mathbb{S}}\,, \tag{I.6d}$$

where the sums run over the m nonlabile spins μ.

The 3×3 relaxation matrices appearing in Eqs. (I.5) and (I.6) can be expressed in terms of the generic auto-spin and cross-spin relaxation matrices in Eqs. (H.8) and (H.9). For the cross-spin matrices, we thus have $\mathbf{R}^{\alpha}_{\mathbb{I}\mathbb{S}} = \mathbf{R}^{\alpha}_{\mathbb{S}\mathbb{I}} = \boldsymbol{\sigma}^{IS}$, $\mathbf{R}^{\alpha}_{\mathbb{I}\mathbb{N}_1(\mu)} = \mathbf{R}^{\alpha\,\dagger}_{\mathbb{N}_1(\mu)\mathbb{I}} = \boldsymbol{\sigma}^{I\mu}$, and $\mathbf{R}^{\alpha}_{\mathbb{S}\mathbb{N}_1(\mu)} = \mathbf{R}^{\alpha\,\dagger}_{\mathbb{N}_1(\mu)\mathbb{S}} = \boldsymbol{\sigma}^{S\mu}$. The nonlabile auto-spin matrix $\mathbf{R}^{\alpha}_{\mathbb{N}_1(\mu)\mathbb{N}_1(\mu)}$ is given by Eq. (H.14). In analogy with Eqs. (H.5) and (H.6), the labile auto-spin matrices are for the $IP_m{-}I$ case,

$$\mathbf{R}^{\alpha}_{\mathbb{I}\mathbb{I}} \;=\; \sum_{\mu=1}^{m} \boldsymbol{\rho}^{I\mu}\,, \tag{I.7}$$

and for the $ISP_m{-}IS$ case,

$$\mathbf{R}^{\alpha}_{\mathbb{I}\mathbb{I}} \;=\; \boldsymbol{\rho}^{IS} \;+\; \sum_{\mu=1}^{m} \boldsymbol{\rho}^{I\mu}\,, \tag{I.8a}$$

$$\mathbf{R}^{\alpha}_{\mathbb{S}\mathbb{S}} \;=\; \boldsymbol{\rho}^{IS} \;+\; \sum_{\mu=1}^{m} \boldsymbol{\rho}^{S\mu}\,. \tag{I.8b}$$

The calculation of the ILRR in the 1SM approximation involves the following steps. Given ω_0, τ_A, and the internuclear geometry, which defines the dipole couplings $\omega_{D,X}$ and the Euler angles $\Omega_{DX} = (\gamma_X, \beta_X, -)$, we compute the SDF $J(n\,\omega_0)$ from Eq. (15) and the angular functions $F_{MM'}(X)$ from the expressions in Appendix C. These are then substituted into Eqs. (H.10), (H.11), (H.14), (I.7), and (I.8) to obtain the relevant auto-spin and cross-spin relaxation matrices. Combining these matrices with Eqs. (I.3) – (I.6), we obtain the 3×3 ($IP_m{-}I$ case) or 6×6 ($ISP_m{-}IS$ case) matrix $[(\mathbf{\Lambda}^\alpha)^{-1}]_{\mathbb{L}_1\mathbb{L}_1}$, the relevant elements of which are then isotropically averaged, as in Eq. (5), to obtain the matrix elements g_{np} required to calculate the ILRR from Eq. (11) or (12). With the single-spin basis ordered by spin type (first spin I and then spin S for the $ISP_m{-}IS$ case), the matrix elements needed in Eq. (12) are $g_{11} = (1|\mathbf{G}^{A}_{\mathbb{L}_1\mathbb{L}_1}(0)|1)$, $g_{12} = (1|\mathbf{G}^{A}_{\mathbb{L}_1\mathbb{L}_1}(0)|4)$, $g_{21} = (4|\mathbf{G}^{A}_{\mathbb{L}_1\mathbb{L}_1}(0)|1)$, and $g_{22} = (4|\mathbf{G}^{A}_{\mathbb{L}_1\mathbb{L}_1}(0)|4)$. Note that the $\mathbb{L}_1$ subspace contains all three components of the labile spin operators, whereas the longitudinal $\mathbb{LZ}$ subspace only contains the z component.

For the three-spin case $ISP{-}IS$ in the MN regime, there are no static dipole couplings and the ILRR only involves single-spin modes. In the MN regime, the 1SM approximation is therefore exact for the $ISP{-}IS$ case. In contrast, for $m \geq 2$, including the $IP_2{-}I$ case, the 1SM approximation is not exact even in the MN regime.

2. Isotropic pre-averaging

The second approximation required to obtain the ESE theory amounts to replacing all local relaxation rates by their isotropic orientational averages, rather than performing this average at the end, as in Eq. (5). Averaging the angular functions as in Eq. (H.4), we find that Eq. (13) in the single-spin subspace (so that $X = Y$) reduces to

$$\left\langle \mathbf{R}^\alpha \right\rangle \;=\; \frac{2}{15} \sum_X \omega_{D,X}^2 \sum_{M=-2}^{2} (-1)^M J(M\omega_0)\, \mathbf{C}^{XX}_{M,-M}\,. \tag{I.9}$$

Let a_α and b_β denote two single-spin operators, with a, $b = I$, S or μ and α, $\beta = z$, $+$ or $-$. Within the single-spin subspace, Eq. (18) yields for the coefficients with $M' = -M$,

$$C^{XX}_{M,-M,\,a_\alpha\,b_\beta} \;=\; \delta_{\alpha\,\beta}\, C^{XX}_{M,-M,\,a_\alpha\,b_\alpha}\,, \tag{I.10}$$

the proof of which is the same as for the three-spin system (see Appendix E of Paper III[1]). As a consequence of the symmetry rules in Eqs. (24) and (I.10), all cross-mode rates vanish, so that all averaged 3×3 relaxation matrices are diagonal.

For the $IP_m{-}I$ case, Eqs. (5), (11) and (I.3) now yield

$$R_{1,I} \;=\; \frac{P_A\, \tilde{r}_{II}}{1 + \tilde{r}_{II}\, \tau_A}\,. \tag{I.11}$$

Similarly, for the $ISP_m{-}IS$ case, Eqs. (5) and (I.4) yield

$$g_{11} \;=\; \frac{(1+\tilde{r}_{SS}\,\tau_{\rm A})}{\rho_{\rm iso}}\,, \tag{I.12a}$$

$$g_{22} \;=\; \frac{(1+\tilde{r}_{II}\,\tau_{\rm A})}{\rho_{\rm iso}}\,, \tag{I.12b}$$

$$g_{12} \;=\; g_{21} \;=\; -\frac{\tilde{r}_{IS}\,\tau_{\rm A}}{\rho_{\rm iso}}\,, \tag{I.12c}$$

with

$$\rho_{\rm iso} \;\equiv\; 1+\left[\tilde{r}_{II}+\tilde{r}_{SS}\right]\tau_{\rm A}+\left[\tilde{r}_{II}\,\tilde{r}_{SS}-\tilde{r}_{IS}^{\,2}\right]\tau_{\rm A}^{2}\,. \tag{I.13}$$

Combination of Eqs. (12), (I.12), and (I.13) yields a result of the same form as Eq. (I.11),

$$R_{1,IS} \;=\; \frac{P_{\rm A}\,\tilde{r}}{1+\tilde{r}\,\tau_{\rm A}}\,, \tag{I.14}$$

with the effective local relaxation rate $\tilde{r}$ now given by

$$\tilde{r} \;\equiv\; \frac{2\,(\tilde{r}_{II}\,\tilde{r}_{SS}-\tilde{r}_{IS}^{\,2})}{(\tilde{r}_{II}+\tilde{r}_{SS}-2\,\tilde{r}_{IS})}\,. \tag{I.15}$$

The effective longitudinal auto-mode rates appearing in Eqs. (I.11) – (I.15) are

$$\tilde{r}_{II} \;=\; \left\langle R_{zz}^{II}\right\rangle-\sum_{\mu=1}^{m}\frac{\left\langle R_{zz}^{I\mu}\right\rangle^{2}}{\left\langle R_{zz}^{\mu\mu}\right\rangle}\,, \tag{I.16a}$$

$$\tilde{r}_{SS} \;=\; \left\langle R_{zz}^{SS}\right\rangle-\sum_{\mu=1}^{m}\frac{\left\langle R_{zz}^{S\mu}\right\rangle^{2}}{\left\langle R_{zz}^{\mu\mu}\right\rangle}\,, \tag{I.16b}$$

$$\tilde{r}_{IS} \;=\; \tilde{r}_{SI} \;=\; \left\langle R_{zz}^{IS}\right\rangle-\sum_{\mu=1}^{m}\frac{\left\langle R_{zz}^{I\mu}\right\rangle\left\langle R_{zz}^{S\mu}\right\rangle}{\left\langle R_{zz}^{\mu\mu}\right\rangle}\,. \tag{I.16c}$$

With the aid of Eqs. (H.5), (H.7), (H.12) and (H.14), the effective rate in Eq. (I.16a) can be expressed, for the $IP_m{-}I$ case, as

$$\tilde{r}_{II} \;=\; \sum_{\mu=1}^{m}\left[\left\langle\rho_{zz}^{I\mu}\right\rangle+\left\langle\sigma_{zz}^{I\mu}\right\rangle\right]H(\omega_0\tau_{\rm A}) \;=\; \frac{2}{15}\,\omega_{{\rm D},I}^{2}\left[J(\omega_0)+4\,J(2\,\omega_0)\right]H(\omega_0\tau_{\rm A})\,, \tag{I.17}$$

with the cumulative dipole coupling $\omega_{{\rm D},I}$ defined in Eq. (39), and

$$H(\omega_0\tau_{\rm A}) \;\equiv\; \frac{\left\langle\rho_{zz}^{I\mu}\right\rangle-\left\langle\sigma_{zz}^{I\mu}\right\rangle}{\left\langle\rho_{zz}^{I\mu}\right\rangle} \;=\; \frac{2\,J(0)+3\,J(\omega_0)}{J(0)+3\,J(\omega_0)+6\,J(2\,\omega_0)}\,. \tag{I.18}$$

As seen from Eqs. (15) and (I.18), the function $H(\omega_0\tau_{\rm A})$ increases monotonically from $1/2$ to 2 as $\omega_0\,\tau_{\rm A}$ goes from 0 to ∞. Consequently, $\tilde{r}_{II}$ in Eq. (I.17) approaches zero asymptotically, as befits a longitudinal relaxation rate.

For the $ISP_m - IS$ case, we use Eqs. (H.6), (H.7), (H.12), and (H.14) to express the effective rates in Eq. (I.16) as

$$\begin{aligned}\tilde{r}_{II} \;=\; & \tfrac{2}{45}\,(\omega_{\mathrm{D},IS}^2 + \Omega_{\mathrm{D},IS}^2)\big[J(0) + 3J(\omega_0) + 6J(2\,\omega_0)\big] \\ & +\; \tfrac{2}{15}\,\Omega_{\mathrm{D},II}^2 \frac{\big[J(\omega_0) + 4J(2\,\omega_0)\big]\big[2J(0) + 3J(\omega_0)\big]}{\big[J(0) + 3J(\omega_0) + 6J(2\,\omega_0)\big]}\,,\end{aligned} \tag{I.19a}$$

$$\begin{aligned}\tilde{r}_{SS} \;=\; & \tfrac{2}{45}\,(\omega_{\mathrm{D},IS}^2 + \Omega_{\mathrm{D},IS}^2)\big[J(0) + 3J(\omega_0) + 6J(2\,\omega_0)\big] \\ & +\; \tfrac{2}{15}\,\Omega_{\mathrm{D},SS}^2 \frac{\big[J(\omega_0) + 4J(2\,\omega_0)\big]\big[2J(0) + 3J(\omega_0)\big]}{\big[J(0) + 3J(\omega_0) + 6J(2\,\omega_0)\big]}\,,\end{aligned} \tag{I.19b}$$

$$\tilde{r}_{IS} \;=\; \tfrac{2}{45}\,\omega_{\mathrm{D},IS}^2\big[6J(2\,\omega_0) - J(0)\big] \;-\; \tfrac{2}{45}\,\Omega_{\mathrm{D},IS}^2\,\frac{\big[6J(2\,\omega_0) - J(0)\big]^2}{\big[J(0) + 3J(\omega_0) + 6J(2\,\omega_0)\big]}\,, \tag{I.19c}$$

where we have defined

$$\Omega_{\mathrm{D},II}^2 \;\equiv\; \sum_{\mu=1}^{m} \frac{\omega_{\mathrm{D},I\mu}^4}{\omega_{\mathrm{D},I\mu}^2 + \omega_{\mathrm{D},S\mu}^2}\,, \tag{I.20a}$$

$$\Omega_{\mathrm{D},SS}^2 \;\equiv\; \sum_{\mu=1}^{m} \frac{\omega_{\mathrm{D},S\mu}^4}{\omega_{\mathrm{D},I\mu}^2 + \omega_{\mathrm{D},S\mu}^2}\,, \tag{I.20b}$$

$$\Omega_{\mathrm{D},IS}^2 \;\equiv\; \sum_{\mu=1}^{m} \frac{\omega_{\mathrm{D},I\mu}^2\,\omega_{\mathrm{D},S\mu}^2}{\omega_{\mathrm{D},I\mu}^2 + \omega_{\mathrm{D},S\mu}^2}\,. \tag{I.20c}$$

We note that

$$\Omega_{\mathrm{D},II}^2 + \Omega_{\mathrm{D},SS}^2 + 2\,\Omega_{\mathrm{D},IS}^2 \;=\; \omega_{\mathrm{D},I}^2 + \omega_{\mathrm{D},S}^2\,, \tag{I.21}$$

with $\omega_{\mathrm{D},I}$ defined by Eq. (39) and $\omega_{\mathrm{D},S}$ analogously.

Substituting from Eq. (I.19), we can express the effective rate in Eq. (I.15) on the same form as in Eq. (I.17),

$$\tilde{r} \;=\; \frac{2}{15}\,\big[\Omega_{\mathrm{D}}(\omega_0\tau_{\mathrm{A}})\big]^2\big[J(\omega_0) + 4\,J(2\,\omega_0)\big]\,, \tag{I.22}$$

where the effective dipole coupling $\Omega_{\mathrm{D}}(\omega_0\tau_{\mathrm{A}})$ depends on $\omega_0\,\tau_{\mathrm{A}}$. The full expression for $\Omega_{\mathrm{D}}(\omega_0\tau_{\mathrm{A}})$ is lengthy, but in the absence of dipole couplings to nonlabile spins it reduces to $\omega_{\mathrm{D},IS}$, as expected. The limits of the full expression for $\Omega_{\mathrm{D}}(\omega_0\tau_{\mathrm{A}})$ are

$$[\Omega_{\mathrm{D}}(0)]^2 \;=\; \frac{4\,(\omega_{\mathrm{D},IS}^2 + \Omega_{\mathrm{D},IS}^2)\,(\omega_{\mathrm{D},IS}^2 + \omega_{\mathrm{D},I}^2 + \omega_{\mathrm{D},S}^2) + 3\,(\Omega_{\mathrm{D},II}^2\Omega_{\mathrm{D},SS}^2 - \Omega_{\mathrm{D},IS}^4)}{3\,(\omega_{\mathrm{D},IS}^2 + \omega_{\mathrm{D},I}^2 + \omega_{\mathrm{D},S}^2) + \omega_{\mathrm{D},IS}^2 + 4\,\Omega_{\mathrm{D},IS}^2}\,, \tag{I.23a}$$

$$[\Omega_{\mathrm{D}}(\infty)]^2 \;=\; \omega_{\mathrm{D},IS}^2 + \omega_{\mathrm{D},I}^2 + \omega_{\mathrm{D},S}^2\,. \tag{I.23b}$$

It is clear, therefore, that $\tilde{r}$ approaches zero asymptotically, as expected.

The multi-spin ESE theory developed here is equivalent to the theory previously obtained from the extended Solomon equations.[8] For the $IP_m - I$ case, the result in Eqs. (I.11) and (I.17) is essentially identical to the result in Eqs. [18] and [23] of the 2006 paper. The only (and trivial) difference is that, in the 2006 paper, we added the bulk relaxation rate and allowed for internal motions by multiplying all dipole couplings with orientational order parameters. For the $ISP_m - IS$ case, the 2006 paper suggests that, in Eq. (I.22),

$$[\Omega_{\rm D}(\omega_0\tau_{\rm A})]^2 \;=\; \omega_{{\rm D},IS}^2 + \frac{1}{2}\big[\omega_{{\rm D},I}^2 + \omega_{{\rm D},S}^2\big] H(\omega_0\tau_{\rm A})\;. \tag{I.24}$$

This is *not* the correct result for the model considered in the 2006 paper (and here). However, as seen from Eq. (I.23), it agrees with the correct result in the limit $\omega_0\,\tau_{\rm A} \to \infty$. Equation (I.24) is also exact for the special case of equilateral triangle geometry, where $\Omega_{\rm D}^2(0) = (3/2)\,\omega_{\rm D}^2$ and $\Omega_{\rm D}^2(\infty) = 3\,\omega_{\rm D}^2$. Furthermore, in the USM limit, both the 2006 theory and the present corrected ESE theory correctly yield $R_{1,I}(0) = R_{1,IS}(0) = P_{\rm A}/\tau_{\rm A}$. However, for both exchange cases, neither the 2006 theory nor the present corrected ESE theory is correct in the MN regime, since isotropic pre-averaging eliminates cross-mode relaxation.

APPENDIX J: FOUR-SPIN OPERATOR BASIS

As a basis for four-spin Liouville space, we use the $2^8 = 256$ irreducible spherical tensor operators (ISTOs) $T^K_Q\big(\,[k_I k_S\,(\bar{K})\,k_P]\,\{\bar{\bar{K}}\}k_U\big)$, constructed by three consecutive couplings of the set of four orthonormal single-spin ISTOs for each spin, e.g.,

$$T^0_0(I) \;=\; \frac{1}{\sqrt{2}}\,E_I\;; \quad T^1_0(I) \;=\; \sqrt{2}\,I_z\;; \quad T^1_{\pm 1}(I) \;=\; \mp\, I_\pm\;, \tag{J.1}$$

to obtain[4,9]

$$\begin{aligned}
&T^K_Q\big(\,[k_I k_S\,(\bar{K})\,k_P]\,\{\bar{\bar{K}}\}k_U\big) \\
&= (-1)^{k_I-k_S-k_P-k_U+\bar{K}+\bar{\bar{K}}+Q}\,(2K+1)^{1/2}(2\bar{K}+1)^{1/2}(2\bar{\bar{K}}+1)^{1/2} \\
&\times \sum_{\bar{Q}=-\bar{\bar{K}}}^{\bar{\bar{K}}}\sum_{\bar{Q}=-\bar{K}}^{\bar{K}}\sum_{q_I=-k_I}^{k_I}
\begin{pmatrix} \bar{\bar{K}} & k_U & K \\ \bar{\bar{Q}} & Q-\bar{\bar{Q}} & -Q \end{pmatrix}
\begin{pmatrix} \bar{K} & k_P & \bar{\bar{K}} \\ \bar{Q} & \bar{\bar{Q}}-\bar{Q} & -\bar{\bar{Q}} \end{pmatrix}
\begin{pmatrix} k_I & k_S & \bar{K} \\ q_I & \bar{Q}-q_I & -\bar{Q} \end{pmatrix} \\
&\times\; T^{k_I}_{q_I}(I)\;T^{k_S}_{\bar{Q}-q_I}(S)\;T^{k_P}_{\bar{\bar{Q}}-\bar{Q}}(P)\;T^{k_U}_{Q-\bar{\bar{Q}}}(U)\,,
\end{aligned} \tag{J.2}$$

where $\bar{K}$ and $\bar{\bar{K}}$ are the ranks of the intermediate tensor operators obtained by first coupling spins I and S and then spin P. In This Appendix, the fourth spin is denoted U. Here, and in the following, the rank superscript is written in upper case for ISTOs that are normalized in three-spin Liouville space and in lower case for ISTOs that are normalized in single-spin Liouville space. The explicit forms of the 255 basis operators (excluding the identity operator) are listed in Table S3, ordered first by increasing projection index Q and then by increasing rank K. Note that the operators corresponding to the longitudinal magnetization of the I and S spins have sequence numbers 14 and 15 in Table S3, whereas they are assigned sequence numbers 1 and 2 elsewhere.

All the operators in Table S3 are normalized in the same four-spin Liouville space, in the sense

$$\begin{aligned}
&\Big(T^K_Q\big(\,[k_I k_S\,(\bar{K})\,k_P]\,\{\bar{\bar{K}}\}k_U\big)\,|\,T^{K'}_{Q'}\big(\,[k'_I k'_S\,(\bar{K}')\,k'_P]\,\{\bar{\bar{K}}'\}k'_U\big)\Big) \\
&\qquad =\; \delta_{KK'}\,\delta_{QQ'}\,\delta_{\bar{\bar{K}}\bar{\bar{K}}'}\,\delta_{\bar{K}\bar{K}'}\,\delta_{k_I k'_I}\,\delta_{k_S k'_S}\,\delta_{k_P k'_P}\delta_{k_U k'_U}\;.
\end{aligned} \tag{J.3}$$

TABLE S3: Basis operators $B_n = T_Q^K\big(\left[k_I k_S\left(\bar{K}\right) k_P\right]\{\bar{\bar{K}}\}k_U\big)$ for four spins $ISPU$.

n	$T_Q^K\big(\left[k_I k_S\left(\bar{K}\right) k_P\right]\{\bar{\bar{K}}\}k_U\big)$	B_n
001	$T_0^0([11(0)0]\{0\}0)$	$-\frac{1}{2\sqrt{3}}(I_-S_+ + I_+S_- + 2I_zS_z)$
002	$T_0^0([10(1)1]\{0\}0)$	$-\frac{1}{2\sqrt{3}}(I_-P_+ + I_+P_- + 2I_zP_z)$
003	$T_0^0([01(1)1]\{0\}0)$	$-\frac{1}{2\sqrt{3}}(P_-S_+ + P_+S_- + 2P_zS_z)$
004	$T_0^0([11(1)1]\{0\}0)$	$\frac{I_-P_+S_z - I_-P_zS_+ - I_+P_-S_z + I_+P_zS_- + I_zP_-S_+ - I_zP_+S_-}{\sqrt{6}}$
005	$T_0^0([10(1)0]\{1\}1)$	$-\frac{1}{2\sqrt{3}}(I_-U_+ + I_+U_- + 2I_zU_z)$
006	$T_0^0([01(1)0]\{1\}1)$	$-\frac{1}{2\sqrt{3}}(S_-U_+ + S_+U_- + 2S_zU_z)$
007	$T_0^0([11(1)0]\{1\}1)$	$\frac{-I_-S_+U_z + I_-S_zU_+ + I_+S_-U_z - I_+S_zU_- - I_zS_-U_+ + I_zS_+U_-}{\sqrt{6}}$
008	$T_0^0([00(0)1]\{1\}1)$	$-\frac{1}{2\sqrt{3}}(P_-U_+ + P_+U_- + 2P_zU_z)$
009	$T_0^0([10(1)1]\{1\}1)$	$\frac{-I_-P_+U_z + I_-P_zU_+ + I_+P_-U_z - I_+P_zU_- - I_zP_-U_+ + I_zP_+U_-}{\sqrt{6}}$
010	$T_0^0([01(1)1]\{1\}1)$	$\frac{P_-S_+U_z - P_-S_zU_+ - P_+S_-U_z + P_+S_zU_- + P_zS_-U_+ - P_zS_+U_-}{\sqrt{6}}$
011	$T_0^0([11(0)1]\{1\}1)$	$\frac{1}{3}(I_-S_+ + I_+S_- + 2I_zS_z)(P_-U_+ + P_+U_- + 2P_zU_z)$
012	$T_0^0([11(1)1]\{1\}1)$	$\frac{I_-(-P_-S_+U_+ + P_+S_+U_- + 2P_+S_zU_z - 2P_zS_zU_+)}{2\sqrt{3}}$ $+\frac{I_+(P_-S_-U_+ + 2P_-S_zU_z - P_+S_-U_- - 2P_zS_zU_-)}{2\sqrt{3}}$ $+\frac{2I_z(-P_-S_+U_z - P_+S_-U_z + P_zS_-U_+ + P_zS_+U_-)}{2\sqrt{3}}$
013	$T_0^0([11(2)1]\{1\}1)$	$\frac{I_-(P_-S_+U_+ + 6P_+S_-U_+ + P_+S_+U_- + 6P_+S_zU_z - 4P_zS_+U_z + 6P_zS_zU_+)}{6\sqrt{5}}$ $+\frac{I_+(P_-S_-U_+ + 6P_-S_+U_- + 6P_-S_zU_z + P_+S_-U_- - 4P_zS_-U_z + 6P_zS_zU_-)}{6\sqrt{5}}$ $+\frac{2I_z(3P_-S_+U_z - 2P_-S_zU_+ + 3P_+S_-U_z - 2P_+S_zU_- + 3P_zS_-U_+ + 3P_zS_+U_- + 8P_zS_zU_z)}{6\sqrt{5}}$
014	$T_0^1([10(1)0]\{1\}0)$	$\frac{1}{2}I_z$
015	$T_0^1([01(1)0]\{1\}0)$	$\frac{1}{2}S_z$
016	$T_0^1([11(1)0]\{1\}0)$	$\frac{I_-S_+ - I_+S_-}{2\sqrt{2}}$
017	$T_0^1([00(0)1]\{1\}0)$	$\frac{1}{2}P_z$
018	$T_0^1([10(1)1]\{1\}0)$	$\frac{I_-P_+ - I_+P_-}{2\sqrt{2}}$
019	$T_0^1([01(1)1]\{1\}0)$	$\frac{P_+S_- - P_-S_+}{2\sqrt{2}}$
020	$T_0^1([11(0)1]\{1\}0)$	$-\frac{P_z(I_-S_+ + I_+S_- + 2I_zS_z)}{\sqrt{3}}$
021	$T_0^1([11(1)1]\{1\}0)$	$\frac{1}{2}[I_z(P_-S_+ + P_+S_-) - S_z(I_-P_+ + I_+P_-)]$
022	$T_0^1([11(2)1]\{1\}0)$	$-\frac{(3I_-P_+S_z - 2I_-P_zS_+ + 3I_+P_-S_z - 2I_+P_zS_- + I_z(3P_-S_+ + 3P_+S_- + 8P_zS_z))}{2\sqrt{15}}$
023	$T_0^1([00(0)0]\{0\}1)$	$\frac{1}{2}U_z$
024	$T_0^1([11(0)0]\{0\}1)$	$-\frac{U_z(I_-S_+ + I_+S_- + 2I_zS_z)}{\sqrt{3}}$
025	$T_0^1([10(1)1]\{0\}1)$	$-\frac{U_z(I_-P_+ + I_+P_- + 2I_zP_z)}{\sqrt{3}}$
026	$T_0^1([01(1)1]\{0\}1)$	$-\frac{U_z(P_-S_+ + P_+S_- + 2P_zS_z)}{\sqrt{3}}$
027	$T_0^1([11(1)1]\{0\}1)$	$\sqrt{\frac{2}{3}}U_z(I_-P_+S_z - I_-P_zS_+ - I_+P_-S_z$ $+I_+P_zS_- + I_zP_-S_+ - I_zP_+S_-)$
028	$T_0^1([10(1)0]\{1\}1)$	$\frac{I_-U_+ - I_+U_-}{2\sqrt{2}}$
029	$T_0^1([01(1)0]\{1\}1)$	$\frac{S_-U_+ - S_+U_-}{2\sqrt{2}}$

030	$T_0^1([11(1)0]\{1\}1)$	$\frac{1}{2}[I_z(S_-U_+ + S_+U_-) - S_z(I_-U_+ + I_+U_-)]$
031	$T_0^1([00(0)1]\{1\}1)$	$\frac{P_-U_+ - P_+U_-}{2\sqrt{2}}$
032	$T_0^1([10(1)1]\{1\}1)$	$\frac{1}{2}[I_z(P_-U_+ + P_+U_-) - P_z(I_-U_+ + I_+U_-)]$
033	$T_0^1([01(1)1]\{1\}1)$	$\frac{1}{2}[S_z(P_-U_+ + P_+U_-) - P_z(S_-U_+ + S_+U_-)]$
034	$T_0^1([11(0)1]\{1\}1)$	$\frac{(P_+U_- - P_-U_+)(I_-S_+ + I_+S_- + 2I_zS_z)}{\sqrt{6}}$
035	$T_0^1([11(1)1]\{1\}1)$	$\frac{I_-(P_-S_+U_+ + P_+S_+U_- + 2P_zS_zU_+) - I_+(P_-S_-U_+ + P_+S_-U_- + 2P_zS_zU_-)}{2\sqrt{2}}$
		$+ \frac{2I_zP_z(S_+U_- - S_-U_+)}{2\sqrt{2}}$
036	$T_0^1([11(2)1]\{1\}1)$	$\frac{I_-(-P_-S_+U_+ - 6P_+S_-U_+ + P_+S_+U_- - 6P_zS_zU_+)}{2\sqrt{30}}$
		$+ \frac{I_+(-P_-S_-U_+ + 6P_-S_+U_- + P_+S_-U_- + 6P_zS_zU_-)}{2\sqrt{30}}$
		$+ \frac{2I_z(2P_-S_zU_+ - 2P_+S_zU_- - 3P_zS_-U_+ + 3P_zS_+U_-)}{2\sqrt{30}}$
037	$T_0^1([11(2)0]\{2\}1)$	$-\frac{[-2I_-S_+U_z + 3I_-S_zU_+ - 2I_+S_-U_z + 3I_+S_zU_- + I_z(3S_-U_+ + 3S_+U_- + 8S_zU_z)]}{2\sqrt{15}}$
038	$T_0^1([10(1)1]\{2\}1)$	$-\frac{[-2I_-P_+U_z + 3I_-P_zU_+ - 2I_+P_-U_z + 3I_+P_zU_- + I_z(3P_-U_+ + 3P_+U_- + 8P_zU_z)]}{2\sqrt{15}}$
039	$T_0^1([01(1)1]\{2\}1)$	$-\frac{[-2P_-S_+U_z + 3P_-S_zU_+ - 2P_+S_-U_z + 3P_+S_zU_- + P_z(3S_-U_+ + 3S_+U_- + 8S_zU_z)]}{2\sqrt{15}}$
040	$T_0^1([11(1)1]\{2\}1)$	$\frac{-I_-(3P_-S_+U_+ + 3P_+S_+U_- + 4P_+S_zU_z + 8P_zS_+U_z - 6P_zS_zU_+)}{2\sqrt{30}}$
		$+ \frac{I_+(3P_-S_-U_+ + 4P_-S_zU_z + 3P_+S_-U_- + 8P_zS_-U_z - 6P_zS_zU_-)}{2\sqrt{30}}$
		$+ \frac{2I_z(-2P_-S_+U_z + 2P_+S_-U_z - 3P_zS_-U_+ + 3P_zS_+U_-)}{2\sqrt{30}}$
041	$T_0^1([11(2)1]\{2\}1)$	$\frac{I_-(U_+(P_-S_+ + 2P_zS_z) - P_+(2S_-U_+ + S_+U_- + 4S_zU_z))}{2\sqrt{10}}$
		$+ \frac{I_+(P_-S_-U_+ + 2P_-S_+U_- + 4P_-S_zU_z - P_+S_-U_- - 2P_zS_zU_-)}{2\sqrt{10}}$
		$+ \frac{2I_z(2P_-S_+U_z - 2P_-S_zU_+ - 2P_+S_-U_z + 2P_+S_zU_- + P_zS_-U_+ - P_zS_+U_-)}{2\sqrt{10}}$
042	$T_0^2([11(2)0]\{2\}0)$	$-\frac{(I_-S_+ + I_+S_- - 4I_zS_z)}{2\sqrt{6}}$
043	$T_0^2([10(1)1]\{2\}0)$	$-\frac{(I_-P_+ + I_+P_- - 4I_zP_z)}{2\sqrt{6}}$
044	$T_0^2([01(1)1]\{2\}0)$	$-\frac{(P_-S_+ + P_+S_- - 4P_zS_z)}{2\sqrt{6}}$
045	$T_0^2([11(1)1]\{2\}0)$	$\frac{(I_-P_+S_z + 2I_-P_zS_+ - I_+P_-S_z - 2I_+P_zS_- + I_zP_-S_+ - I_zP_+S_-)}{2\sqrt{3}}$
046	$T_0^2([11(2)1]\{2\}0)$	$\frac{1}{2}(I_-P_+S_z - I_+P_-S_z - I_zP_-S_+ + I_zP_+S_-)$
047	$T_0^2([10(1)0]\{1\}1)$	$-\frac{(I_-U_+ + I_+U_- - 4I_zU_z)}{2\sqrt{6}}$
048	$T_0^2([01(1)0]\{1\}1)$	$-\frac{(S_-U_+ + S_+U_- - 4S_zU_z)}{2\sqrt{6}}$
049	$T_0^2([11(1)0]\{1\}1)$	$\frac{2I_-S_+U_z + I_-S_zU_+ - 2I_+S_-U_z - I_+S_zU_- - I_zS_-U_+ + I_zS_+U_-}{2\sqrt{3}}$
050	$T_0^2([00(0)1]\{1\}1)$	$-\frac{(P_-U_+ + P_+U_- - 4P_zU_z)}{2\sqrt{6}}$
051	$T_0^2([10(1)1]\{1\}1)$	$\frac{2I_-P_+U_z + I_-P_zU_+ - 2I_+P_-U_z - I_+P_zU_- - I_zP_-U_+ + I_zP_+U_-}{2\sqrt{3}}$
052	$T_0^2([01(1)1]\{1\}1)$	$\frac{-2P_-S_+U_z - P_-S_zU_+ + 2P_+S_-U_z + P_+S_zU_- + P_zS_-U_+ - P_zS_+U_-}{2\sqrt{3}}$
053	$T_0^2([11(0)1]\{1\}1)$	$\frac{(I_-S_+ + I_+S_- + 2I_zS_z)(P_-U_+ + P_+U_- - 4P_zU_z)}{3\sqrt{2}}$
054	$T_0^2([11(1)1]\{1\}1)$	$\frac{I_-(-P_-S_+U_+ + P_+S_+U_- - 4P_+S_zU_z - 2P_zS_zU_+)}{2\sqrt{6}}$
		$- \frac{I_+(-P_-S_-U_+ + 4P_-S_zU_z + P_+S_-U_- + 2P_zS_zU_-)}{2\sqrt{6}}$
		$+ \frac{2I_z(2P_-S_+U_z + 2P_+S_-U_z + P_zS_-U_+ + P_zS_+U_-)}{2\sqrt{6}}$
055	$T_0^2([11(2)1]\{1\}1)$	$\frac{I_-(P_-S_+U_+ + 6P_+S_-U_+ + P_+S_+U_- - 12P_+S_zU_z + 8P_zS_+U_z + 6P_zS_zU_+)}{6\sqrt{10}}$
		$+ \frac{I_+(P_-S_-U_+ + 6P_-S_+U_- - 12P_-S_zU_z + P_+S_-U_- + 8P_zS_-U_z + 6P_zS_zU_-)}{6\sqrt{10}}$
		$- \frac{2I_z(6P_-S_+U_z + 2P_-S_zU_+ + 6P_+S_-U_z + 2P_+S_zU_- - 3P_zS_-U_+ - 3P_zS_+U_- + 16P_zS_zU_z)}{6\sqrt{10}}$

056	$T_0^2([11(2)0]\{2\}1)$	$\frac{1}{2}(I_-S_zU_+ - I_+S_zU_- + I_zS_-U_+ - I_zS_+U_-)$
057	$T_0^2([10(1)1]\{2\}1)$	$\frac{1}{2}(I_-P_zU_+ - I_+P_zU_- + I_zP_-U_+ - I_zP_+U_-)$
058	$T_0^2([01(1)1]\{2\}1)$	$\frac{1}{2}(P_-S_zU_+ - P_+S_zU_- + P_zS_-U_+ - P_zS_+U_-)$
059	$T_0^2([11(1)1]\{2\}1)$	$\frac{I_-(P_-S_+U_+ - P_+S_+U_- - 2P_zS_zU_+) + I_+(-P_-S_-U_+ + P_+S_-U_- - 2P_zS_zU_-)}{2\sqrt{2}}$ $+\frac{2I_zP_z(S_-U_+ + S_+U_-)}{2\sqrt{2}}$
060	$T_0^2([11(2)1]\{2\}1)$	$-\frac{I_-(P_-S_+U_+ - 2P_+S_-U_+ + P_+S_+U_- + 2P_zS_zU_+)}{2\sqrt{6}}$ $+\frac{I_+(P_-S_-U_+ - 2P_-S_+U_- + P_+S_-U_- + 2P_zS_zU_-)}{2\sqrt{6}}$ $+\frac{2I_z(-2P_-S_zU_+ - 2P_+S_zU_- + P_zS_-U_+ + P_zS_+U_-)}{2\sqrt{6}}$
061	$T_0^2([11(2)1]\{3\}1)$	$\sqrt{\frac{2}{105}}\Big[I_-(P_-S_+U_+ + P_+(S_-U_+ + S_+U_- + 3S_zU_z) + 3P_zS_+U_z - 4P_zS_zU_+)$ $-I_z\big[-3P_-S_+U_z + 4P_-S_zU_+ - 3P_+S_-U_z + 4P_+S_zU_-$ $+4P_z(S_-U_+ + S_+U_- + 3S_zU_z)\big]$ $+ I_+(P_-S_-U_+ + P_-S_+U_- + 3P_-S_zU_z + P_+S_-U_- + 3P_zS_-U_z - 4P_zS_zU_-)\Big]$
062	$T_0^3([11(2)1]\{3\}0)$	$-\frac{(I_-P_+S_z + I_-P_zS_+ + I_+P_-S_z + I_+P_zS_- + I_z(P_-S_+ + P_+S_- - 4P_zS_z))}{\sqrt{10}}$
063	$T_0^3([11(2)0]\{2\}1)$	$-\frac{(I_-S_+U_z + I_-S_zU_+ + I_+S_-U_z + I_+S_zU_- + I_z(S_-U_+ + S_+U_- - 4S_zU_z))}{\sqrt{10}}$
064	$T_0^3([10(1)1]\{2\}1)$	$-\frac{(I_-P_+U_z + I_-P_zU_+ + I_+P_-U_z + I_+P_zU_- + I_z(P_-U_+ + P_+U_- - 4P_zU_z))}{\sqrt{10}}$
065	$T_0^3([01(1)1]\{2\}1)$	$-\frac{(P_-S_+U_z + P_-S_zU_+ + P_+S_-U_z + P_+S_zU_- + P_z(S_-U_+ + S_+U_- - 4S_zU_z))}{\sqrt{10}}$
066	$T_0^3([11(1)1]\{2\}1)$	$\frac{I_-(-P_-S_+U_+ - P_+S_+U_- + 2P_+S_zU_z + 4P_zS_+U_z + 2P_zS_zU_+)}{2\sqrt{5}}$ $+\frac{I_+(P_-S_-U_+ - 2P_-S_zU_z + P_+S_-U_- - 4P_zS_-U_z - 2P_zS_zU_-)}{2\sqrt{5}}$ $+\frac{2I_z(P_-S_+U_z - P_+S_-U_z - P_zS_-U_+ + P_zS_+U_-)}{2\sqrt{5}}$
067	$T_0^3([11(2)1]\{2\}1)$	$\frac{I_-(P_-S_+U_+ - 2P_+S_-U_+ - P_+S_+U_- + 6P_+S_zU_z + 2P_zS_zU_+)}{2\sqrt{15}}$ $+\frac{I_+(P_-S_-U_+ + 2P_-S_+U_- - 6P_-S_zU_z - P_+S_-U_- - 2P_zS_zU_-)}{2\sqrt{15}}$ $+\frac{2I_z(-3P_-S_+U_z - 2P_-S_zU_+ + 3P_+S_-U_z + 2P_+S_zU_- + P_zS_-U_+ - P_zS_+U_-)}{2\sqrt{15}}$
068	$T_0^3([11(2)1]\{3\}1)$	$\frac{I_-(-P_-S_+U_+ - P_+S_-U_+ + P_+S_+U_- + 4P_zS_zU_+)}{\sqrt{30}}$ $+\frac{I_+(-P_-S_-U_+ + P_-S_+U_- + P_+S_-U_- - 4P_zS_zU_-)}{\sqrt{30}}$ $+\frac{4I_z(P_-S_zU_+ - P_+S_zU_- + P_zS_-U_+ - P_zS_+U_-)}{\sqrt{30}}$
069	$T_0^4([11(2)1]\{3\}1)$	$\frac{I_-(P_-S_+U_+ + P_+(S_-U_+ + S_+U_- - 4S_zU_z) - 4P_z(S_+U_z + S_zU_+))}{\sqrt{70}}$ $+\frac{I_+(P_-(S_-U_+ + S_+U_- - 4S_zU_z) + P_+S_-U_- - 4P_z(S_-U_z + S_zU_-))}{\sqrt{70}}$ $-\frac{4I_z(P_-S_+U_z + P_-S_zU_+ + P_+S_-U_z + P_+S_zU_- + P_z(S_-U_+ + S_+U_- - 4S_zU_z))}{\sqrt{70}}$

070	$T_1^1([10(1)0]\{1\}0)$	$-\frac{I_+}{2\sqrt{2}}$
071	$T_1^1([01(1)0]\{1\}0)$	$-\frac{S_+}{2\sqrt{2}}$
072	$T_1^1([11(1)0]\{1\}0)$	$\frac{1}{2}(I_zS_+ - I_+S_z)$
073	$T_1^1([00(0)1]\{1\}0)$	$-\frac{P_+}{2\sqrt{2}}$
074	$T_1^1([10(1)1]\{1\}0)$	$\frac{1}{2}(I_zP_+ - I_+P_z)$
075	$T_1^1([01(1)1]\{1\}0)$	$\frac{1}{2}(P_+S_z - P_zS_+)$
076	$T_1^1([11(0)1]\{1\}0)$	$\frac{P_+(I_-S_+ + I_+S_- + 2I_zS_z)}{\sqrt{6}}$
077	$T_1^1([11(1)1]\{1\}0)$	$\frac{I_-P_+S_+ - I_+P_+S_- - 2I_+P_zS_z + 2I_zP_zS_+}{2\sqrt{2}}$

078	$T_1^1([11(2)1]\{1\}0)$	$\frac{[I_-P_+S_+ + I_+(6P_-S_+ + P_+S_- + 6P_zS_z) - 4I_zP_+S_z + 6I_zP_zS_+]}{2\sqrt{30}}$
079	$T_1^1([00(0)0]\{0\}1)$	$-\frac{U_+}{2\sqrt{2}}$
080	$T_1^1([11(0)0]\{0\}1)$	$\frac{U_+(I_-S_+ + I_+S_- + 2I_zS_z)}{\sqrt{6}}$
081	$T_1^1([10(1)1]\{0\}1)$	$\frac{U_+(I_-P_+ + I_+P_- + 2I_zP_z)}{\sqrt{6}}$
082	$T_1^1([01(1)1]\{0\}1)$	$\frac{U_+(P_-S_+ + P_+S_- + 2P_zS_z)}{\sqrt{6}}$
083	$T_1^1([11(1)1]\{0\}1)$	$\frac{U_+(-I_-P_+S_z + I_-P_zS_+ + I_+P_-S_z - I_+P_zS_- - I_zP_-S_+ + I_zP_+S_-)}{\sqrt{3}}$
084	$T_1^1([10(1)0]\{1\}1)$	$\frac{1}{2}(I_zU_+ - I_+U_z)$
085	$T_1^1([01(1)0]\{1\}1)$	$\frac{1}{2}(S_zU_+ - S_+U_z)$
086	$T_1^1([11(1)0]\{1\}1)$	$\frac{I_-S_+U_+ - I_+S_-U_+ - 2I_+S_zU_z + 2I_zS_+U_z}{2\sqrt{2}}$
087	$T_1^1([00(0)1]\{1\}1)$	$\frac{1}{2}(P_zU_+ - P_+U_z)$
088	$T_1^1([10(1)1]\{1\}1)$	$\frac{I_-P_+U_+ - I_+P_-U_+ - 2I_+P_zU_z + 2I_zP_+U_z}{2\sqrt{2}}$
089	$T_1^1([01(1)1]\{1\}1)$	$\frac{-P_-S_+U_+ + P_+S_-U_+ + 2P_+S_zU_z - 2P_zS_+U_z}{2\sqrt{2}}$
090	$T_1^1([11(0)1]\{1\}1)$	$-\frac{(P_zU_+ - P_+U_z)(I_-S_+ + I_+S_- + 2I_zS_z)}{\sqrt{3}}$
091	$T_1^1([11(1)1]\{1\}1)$	$\frac{1}{2}\big[I_-P_+(S_+U_z - S_zU_+) - I_+(P_-S_zU_+ + P_+S_-U_z + 2P_zS_zU_z)$ $+I_z(P_-S_+U_+ + P_+S_-U_+ + 2P_zS_+U_z)\big]$
092	$T_1^1([11(2)1]\{1\}1)$	$\frac{I_-(P_+S_+U_z - 3P_+S_zU_+ + 2P_zS_+U_+)}{2\sqrt{15}}$ $+\frac{I_+(6P_-S_+U_z - 3P_-S_zU_+ + P_+S_-U_z + 2P_zS_-U_+ + 6P_zS_zU_z)}{2\sqrt{15}}$ $-\frac{I_z(3P_-S_+U_+ + 3P_+S_-U_+ + 4P_+S_zU_z - 6P_zS_+U_z + 8P_zS_zU_+)}{2\sqrt{15}}$
093	$T_1^1([11(2)0]\{2\}1)$	$\frac{I_-S_+U_+ + I_+(S_-U_+ + 6S_+U_- + 6S_zU_z) + 6I_zS_+U_z - 4I_zS_zU_+}{2\sqrt{30}}$
094	$T_1^1([10(1)1]\{2\}1)$	$\frac{I_-P_+U_+ + I_+(P_-U_+ + 6P_+U_- + 6P_zU_z) + 6I_zP_+U_z - 4I_zP_zU_+}{2\sqrt{30}}$
095	$T_1^1([01(1)1]\{2\}1)$	$\frac{P_-S_+U_+ + P_+(S_-U_+ + 6S_+U_- + 6S_zU_z) + 6P_zS_+U_z - 4P_zS_zU_+}{2\sqrt{30}}$
096	$T_1^1([11(1)1]\{2\}1)$	$\frac{-I_-(-3P_+S_+U_z + P_+S_zU_+ + 2P_zS_+U_+)}{2\sqrt{15}}$ $+\frac{I_+(P_-S_zU_+ - 3P_+S_-U_z + 6P_+S_zU_- + 2P_zS_-U_+ + 6P_zS_zU_z)}{2\sqrt{15}}$ $+\frac{I_z(P_-S_+U_+ - P_+S_-U_+ + 6P_+S_+U_- + 6P_zS_+U_z)}{2\sqrt{15}}$
097	$T_1^1([11(2)1]\{2\}1)$	$\frac{I_-P_+(S_+U_z - S_zU_+)}{2\sqrt{5}}$ $+\frac{I_+(-2P_-S_+U_z + P_-S_zU_+ + P_+S_-U_z - 2P_+S_zU_- + 4P_zS_+U_- + 2P_zS_zU_z)}{2\sqrt{5}}$ $+\frac{I_z[S_+(P_-U_+ + 2P_zU_z) - P_+(S_-U_+ + 2S_+U_- + 4S_zU_z)]}{2\sqrt{5}}$
098	$T_1^2([11(2)0]\{2\}0)$	$-\frac{1}{2}(I_+S_z + I_zS_+)$
099	$T_1^2([10(1)1]\{2\}0)$	$-\frac{1}{2}(I_+P_z + I_zP_+)$
100	$T_1^2([01(1)1]\{2\}0)$	$-\frac{1}{2}(P_+S_z + P_zS_+)$
101	$T_1^2([11(1)1]\{2\}0)$	$\frac{-I_-P_+S_+ + I_+P_+S_- - 2I_+P_zS_z + 2I_zP_zS_+}{2\sqrt{2}}$
102	$T_1^2([11(2)1]\{2\}0)$	$-\frac{[I_-P_+S_+ + I_+(-2P_-S_+ + P_+S_- + 2P_zS_z) - 4I_zP_+S_z + 2I_zP_zS_+]}{2\sqrt{6}}$
103	$T_1^2([10(1)0]\{1\}1)$	$-\frac{1}{2}(I_+U_z + I_zU_+)$
104	$T_1^2([01(1)0]\{1\}1)$	$-\frac{1}{2}(S_+U_z + S_zU_+)$
105	$T_1^2([11(1)0]\{1\}1)$	$\frac{-I_-S_+U_+ + I_+S_-U_+ - 2I_+S_zU_z + 2I_zS_+U_z}{2\sqrt{2}}$
106	$T_1^2([00(0)1]\{1\}1)$	$-\frac{1}{2}(P_+U_z + P_zU_+)$
107	$T_1^2([10(1)1]\{1\}1)$	$\frac{-I_-P_+U_+ + I_+P_-U_+ - 2I_+P_zU_z + 2I_zP_+U_z}{2\sqrt{2}}$

108	$T_1^2([01(1)1]\{1\}1)$	$\frac{P_-S_+U_+ - P_+S_-U_+ + 2P_+S_zU_z - 2P_zS_+U_z}{2\sqrt{2}}$
109	$T_1^2([11(0)1]\{1\}1)$	$\frac{(P_+U_z + P_zU_+)(I_-S_+ + I_+S_- + 2I_zS_z)}{\sqrt{3}}$
110	$T_1^2([11(1)1]\{1\}1)$	$\frac{1}{2}\big[I_-P_+(S_+U_z + S_zU_+) + I_+(P_-S_zU_+ - P_+S_-U_z - 2P_zS_zU_z)$ $-I_z(P_-S_+U_+ + P_+S_-U_+ - 2P_zS_+U_z)\big]$
111	$T_1^2([11(2)1]\{1\}1)$	$\frac{I_-(P_+S_+U_z + 3P_+S_zU_+ - 2P_zS_+U_+)}{2\sqrt{15}}$ $+\frac{I_+(6P_-S_+U_z + 3P_-S_zU_+ + P_+S_-U_z - 2P_zS_-U_+ + 6P_zS_zU_z)}{2\sqrt{15}}$ $+\frac{I_z(3P_-S_+U_+ + 3P_+S_-U_+ - 4P_+S_zU_z + 6P_zS_+U_z + 8P_zS_zU_+)}{2\sqrt{15}}$
112	$T_1^2([11(2)0]\{2\}1)$	$-\frac{[I_-S_+U_+ + I_+(S_-U_+ - 2S_+U_- + 2S_zU_z) + 2I_zS_+U_z - 4I_zS_zU_+]}{2\sqrt{6}}$
113	$T_1^2([10(1)1]\{2\}1)$	$-\frac{[I_-P_+U_+ + I_+(P_-U_+ - 2P_+U_- + 2P_zU_z) + 2I_zP_+U_z - 4I_zP_zU_+]}{2\sqrt{6}}$
114	$T_1^2([01(1)1]\{2\}1)$	$-\frac{[P_-S_+U_+ + P_+(S_-U_+ - 2S_+U_- + 2S_zU_z) + 2P_zS_+U_z - 4P_zS_zU_+]}{2\sqrt{6}}$
115	$T_1^2([11(1)1]\{2\}1)$	$\frac{I_-(-P_+S_+U_z + P_+S_zU_+ + 2P_zS_+U_+)}{2\sqrt{3}}$ $+\frac{I_+(-P_-S_zU_+ + P_+S_-U_z + 2P_+S_zU_- - 2P_zS_-U_+ - 2P_zS_zU_z)}{2\sqrt{3}}$ $+\frac{I_z(P_-S_+U_+ - P_+S_-U_+ - 2P_+S_+U_- + 2P_zS_+U_z)}{2\sqrt{3}}$
116	$T_1^2([11(2)1]\{2\}1)$	$\frac{1}{6}\big[I_-P_+(3S_zU_+ - S_+U_z) + I_+(2P_-S_+U_z - 3P_-S_zU_+ - P_+S_-U_z$ $-2P_+S_zU_- + 4P_zS_+U_- - 2P_zS_zU_z) + I_z(-3P_-S_+U_+ + 3P_+S_-U_+$ $-2P_+S_+U_- + 4P_+S_zU_z - 2P_zS_+U_z)\big]$
117	$T_1^2([11(2)1]\{3\}1)$	$\frac{I_-(-4P_+S_+U_z + 3P_+S_zU_+ + 3P_zS_+U_+)}{3\sqrt{35}}$ $+\frac{I_+(-4P_-S_+U_z + 3P_-S_zU_+ - 4P_+S_-U_z + 10P_+S_zU_- + 3P_zS_-U_+ + 10P_zS_+U_- + 16P_zS_zU_z)}{3\sqrt{35}}$ $+\frac{I_z(3P_-S_+U_+ + P_+(3S_-U_+ + 10S_+U_- + 16S_zU_z) + 16P_zS_+U_z - 12P_zS_zU_+)}{3\sqrt{35}}$
118	$T_1^3([11(2)1]\{3\}0)$	$\frac{[I_-P_+S_+ + I_+(P_-S_+ + P_+S_- - 4P_zS_z) - 4I_z(P_+S_z + P_zS_+)]}{\sqrt{30}}$
119	$T_1^3([11(2)0]\{2\}1)$	$\frac{[I_-S_+U_+ + I_+(S_-U_+ + S_+U_- - 4S_zU_z) - 4I_z(S_+U_z + S_zU_+)]}{\sqrt{30}}$
120	$T_1^3([10(1)1]\{2\}1)$	$\frac{[I_-P_+U_+ + I_+(P_-U_+ + P_+U_- - 4P_zU_z) - 4I_z(P_+U_z + P_zU_+)]}{\sqrt{30}}$
121	$T_1^3([01(1)1]\{2\}1)$	$\frac{[P_-S_+U_+ + P_+(S_-U_+ + S_+U_- - 4S_zU_z) - 4P_z(S_+U_z + S_zU_+)]}{\sqrt{30}}$
122	$T_1^3([11(1)1]\{2\}1)$	$\frac{-I_-(2P_+S_+U_z + P_+S_zU_+ + 2P_zS_+U_+)}{\sqrt{15}}$ $+\frac{I_+(P_-S_zU_+ + 2P_+S_-U_z + P_+S_zU_- + 2P_zS_-U_+ - 4P_zS_zU_z)}{\sqrt{15}}$ $+\frac{I_z(-P_-S_+U_+ + P_+S_-U_+ - P_+S_+U_- + 4P_zS_+U_z)}{\sqrt{15}}$
123	$T_1^3([11(2)1]\{2\}1)$	$-\frac{I_-P_+(2S_+U_z + 3S_zU_+)}{3\sqrt{5}}$ $-\frac{I_+(-4P_-S_+U_z - 3P_-S_zU_+ + 2P_+S_-U_z + P_+S_zU_- - 2P_zS_+U_- + 4P_zS_zU_z)}{3\sqrt{5}}$ $-\frac{I_z(-3P_-S_+U_+ + P_+(3S_-U_+ + S_+U_- - 8S_zU_z) + 4P_zS_+U_z)}{3\sqrt{5}}$
124	$T_1^3([11(2)1]\{3\}1)$	$\frac{I_-(P_+S_+U_z - 3P_+S_zU_+ - 3P_zS_+U_+)}{3\sqrt{10}}$ $+\frac{I_+(P_-S_+U_z - 3P_-S_zU_+ + P_+S_-U_z + 5P_+S_zU_- - 3P_zS_-U_+ + 5P_zS_+U_- - 4P_zS_zU_z)}{3\sqrt{10}}$ $-\frac{I_z(3P_-S_+U_+ + P_+(3S_-U_+ - 5S_+U_- + 4S_zU_z) + 4P_zS_+U_z - 12P_zS_zU_+)}{3\sqrt{10}}$
125	$T_1^4([11(2)1]\{3\}1)$	$\frac{I_-(P_+S_+U_z + P_+S_zU_+ + P_zS_+U_+)}{\sqrt{14}}$ $+\frac{I_+(P_-S_+U_z + P_-S_zU_+ + P_+S_-U_z + P_+S_zU_- + P_z(S_-U_+ + S_+U_- - 4S_zU_z))}{\sqrt{14}}$ $+\frac{I_z(P_-S_+U_+ + P_+(S_-U_+ + S_+U_- - 4S_zU_z) - 4P_z(S_+U_z + S_zU_+))}{\sqrt{14}}$
126	$T_{-1}^1([10(1)0]\{1\}0)$	$\frac{I_-}{2\sqrt{2}}$
127	$T_{-1}^1([01(1)0]\{1\}0)$	$\frac{S_-}{2\sqrt{2}}$

128	$T^1_{-1}([11(1)0]\{1\}0)$	$\frac{1}{2}(I_zS_- - I_-S_z)$
129	$T^1_{-1}([00(0)1]\{1\}0)$	$\frac{P_-}{2\sqrt{2}}$
130	$T^1_{-1}([10(1)1]\{1\}0)$	$\frac{1}{2}(I_zP_- - I_-P_z)$
131	$T^1_{-1}([01(1)1]\{1\}0)$	$\frac{1}{2}(P_-S_z - P_zS_-)$
132	$T^1_{-1}([11(0)1]\{1\}0)$	$-\frac{P_-(I_-S_+ + I_+S_- + 2I_zS_z)}{\sqrt{6}}$
133	$T^1_{-1}([11(1)1]\{1\}0)$	$\frac{I_-P_-S_+ + 2I_-P_zS_z - I_+P_-S_- - 2I_zP_zS_-}{2\sqrt{2}}$
134	$T^1_{-1}([11(2)1]\{1\}0)$	$-\frac{[I_-(P_-S_+ + 6P_+S_- + 6P_zS_z) + I_+P_-S_- - 4I_zP_-S_z + 6I_zP_zS_-]}{2\sqrt{30}}$
135	$T^1_{-1}([00(0)0]\{0\}1)$	$\frac{U_-}{2\sqrt{2}}$
136	$T^1_{-1}([11(0)0]\{0\}1)$	$-\frac{U_-(I_-S_+ + I_+S_- + 2I_zS_z)}{\sqrt{6}}$
137	$T^1_{-1}([10(1)1]\{0\}1)$	$-\frac{U_-(I_-P_+ + I_+P_- + 2I_zP_z)}{\sqrt{6}}$
138	$T^1_{-1}([01(1)1]\{0\}1)$	$-\frac{U_-(P_-S_+ + P_+S_- + 2P_zS_z)}{\sqrt{6}}$
139	$T^1_{-1}([11(1)1]\{0\}1)$	$\frac{U_-(I_-P_+S_z - I_-P_zS_+ - I_+P_-S_z + I_+P_zS_- + I_zP_-S_+ - I_zP_+S_-)}{\sqrt{3}}$
140	$T^1_{-1}([10(1)0]\{1\}1)$	$\frac{1}{2}(I_zU_- - I_-U_z)$
141	$T^1_{-1}([01(1)0]\{1\}1)$	$\frac{1}{2}(S_zU_- - S_-U_z)$
142	$T^1_{-1}([11(1)0]\{1\}1)$	$\frac{I_-S_+U_- + 2I_-S_zU_z - I_+S_-U_- - 2I_zS_-U_z}{2\sqrt{2}}$
143	$T^1_{-1}([00(0)1]\{1\}1)$	$\frac{1}{2}(P_zU_- - P_-U_z)$
144	$T^1_{-1}([10(1)1]\{1\}1)$	$\frac{I_-P_+U_- + 2I_-P_zU_z - I_+P_-U_- - 2I_zP_-U_z}{2\sqrt{2}}$
145	$T^1_{-1}([01(1)1]\{1\}1)$	$\frac{-P_-(S_+U_- + 2S_zU_z) + P_+S_-U_- + 2P_zS_-U_z}{2\sqrt{2}}$
146	$T^1_{-1}([11(0)1]\{1\}1)$	$-\frac{(P_zU_- - P_-U_z)(I_-S_+ + I_+S_- + 2I_zS_z)}{\sqrt{3}}$
147	$T^1_{-1}([11(1)1]\{1\}1)$	$\frac{1}{2}\big[-I_-(P_-S_+U_z + P_+S_zU_- + 2P_zS_zU_z) + I_+P_-(S_-U_z - S_zU_-) + I_z(P_-S_+U_- + P_+S_-U_- + 2P_zS_-U_z)\big]$
148	$T^1_{-1}([11(2)1]\{1\}1)$	$\frac{I_-(P_-S_+U_z + 6P_+S_-U_z - 3P_+S_zU_- + 2P_zS_+U_- + 6P_zS_zU_z)}{2\sqrt{15}} + \frac{I_+(P_-S_-U_z - 3P_-S_zU_- + 2P_zS_-U_-)}{2\sqrt{15}} - \frac{I_z(3P_-S_+U_- + 4P_-S_zU_z + 3P_+S_-U_- - 6P_zS_-U_z + 8P_zS_zU_-)}{2\sqrt{15}}$
149	$T^1_{-1}([11(2)0]\{2\}1)$	$-\frac{[I_-(6S_-U_+ + S_+U_- + 6S_zU_z) + I_+S_-U_- + 6I_zS_-U_z - 4I_zS_zU_-]}{2\sqrt{30}}$
150	$T^1_{-1}([10(1)1]\{2\}1)$	$-\frac{[I_-(6P_-U_+ + P_+U_- + 6P_zU_z) + I_+P_-U_- + 6I_zP_-U_z - 4I_zP_zU_-]}{2\sqrt{30}}$
151	$T^1_{-1}([01(1)1]\{2\}1)$	$-\frac{[P_-(6S_-U_+ + S_+U_- + 6S_zU_z) + P_+S_-U_- + 6P_zS_-U_z - 4P_zS_zU_-]}{2\sqrt{30}}$
152	$T^1_{-1}([11(1)1]\{2\}1)$	$\frac{I_-(-3P_-S_+U_z + 6P_-S_zU_+ + P_+S_zU_- + 2P_zS_+U_- + 6P_zS_zU_z)}{2\sqrt{15}} - \frac{I_+(-3P_-S_-U_z + P_-S_zU_- + 2P_zS_-U_-)}{2\sqrt{15}} - \frac{I_z(6P_-S_-U_+ - P_-S_+U_- + P_+S_-U_- + 6P_zS_-U_z)}{2\sqrt{15}}$
153	$T^1_{-1}([11(2)1]\{2\}1)$	$\frac{I_-(P_-S_+U_z - 2P_-S_zU_+ - 2P_+S_-U_z + P_+S_zU_- + 4P_zS_-U_+ + 2P_zS_zU_z)}{2\sqrt{5}} + \frac{I_+P_-(S_-U_z - S_zU_-)}{2\sqrt{5}} + \frac{I_z(-P_-(2S_-U_+ + S_+U_- + 4S_zU_z) + P_+S_-U_- + 2P_zS_-U_z)}{2\sqrt{5}}$
154	$T^2_{-1}([11(2)0]\{2\}0)$	$\frac{1}{2}(I_-S_z + I_zS_-)$
155	$T^2_{-1}([10(1)1]\{2\}0)$	$\frac{1}{2}(I_-P_z + I_zP_-)$
156	$T^2_{-1}([01(1)1]\{2\}0)$	$\frac{1}{2}(P_-S_z + P_zS_-)$
157	$T^2_{-1}([11(1)1]\{2\}0)$	$\frac{I_-P_-S_+ - 2I_-P_zS_z - I_+P_-S_- + 2I_zP_zS_-}{2\sqrt{2}}$

158	$T^2_{-1}([11(2)1]\{2\}0)$	$-\frac{(I_-P_-S_+-2I_-P_+S_-+2I_-P_zS_z+I_+P_-S_--4I_zP_-S_z+2I_zP_zS_-)}{2\sqrt{6}}$
159	$T^2_{-1}([10(1)0]\{1\}1)$	$\frac{1}{2}(I_-U_z+I_zU_-)$
160	$T^2_{-1}([01(1)0]\{1\}1)$	$\frac{1}{2}(S_-U_z+S_zU_-)$
161	$T^2_{-1}([11(1)0]\{1\}1)$	$\frac{I_-S_+U_--2I_-S_zU_z-I_+S_-U_-+2I_zS_-U_z}{2\sqrt{2}}$
162	$T^2_{-1}([00(0)1]\{1\}1)$	$\frac{1}{2}(P_-U_z+P_zU_-)$
163	$T^2_{-1}([10(1)1]\{1\}1)$	$\frac{I_-P_+U_--2I_-P_zU_z-I_+P_-U_-+2I_zP_-U_z}{2\sqrt{2}}$
164	$T^2_{-1}([01(1)1]\{1\}1)$	$\frac{-P_-S_+U_-+2P_-S_zU_z+P_+S_-U_--2P_zS_-U_z}{2\sqrt{2}}$
165	$T^2_{-1}([11(0)1]\{1\}1)$	$-\frac{(P_-U_z+P_zU_-)(I_-S_++I_+S_-+2I_zS_z)}{\sqrt{3}}$
166	$T^2_{-1}([11(1)1]\{1\}1)$	$\frac{1}{2}\big[I_-(P_-S_+U_z-P_+S_zU_-+2P_zS_zU_z)-I_+P_-(S_-U_z+S_zU_-)$ $+I_z(P_-S_+U_-+P_+S_-U_--2P_zS_-U_z)\big]$
167	$T^2_{-1}([11(2)1]\{1\}1)$	$-\frac{I_-(P_-S_+U_z+6P_+S_-U_z+3P_+S_zU_--2P_zS_+U_-+6P_zS_zU_z)}{2\sqrt{15}}$ $-\frac{I_+(P_-S_-U_z+3P_-S_zU_--2P_zS_-U_-)}{2\sqrt{15}}$ $-\frac{I_z(3P_-S_+U_--4P_-S_zU_z+3P_+S_-U_-+6P_zS_-U_z+8P_zS_zU_-)}{2\sqrt{15}}$
168	$T^2_{-1}([11(2)0]\{2\}1)$	$-\frac{[I_-(-2S_-U_++S_+U_-+2S_zU_z)+I_+S_-U_-+2I_zS_-U_z-4I_zS_zU_-]}{2\sqrt{6}}$
169	$T^2_{-1}([10(1)1]\{2\}1)$	$-\frac{[I_-(-2P_-U_++P_+U_-+2P_zU_z)+I_+P_-U_-+2I_zP_-U_z-4I_zP_zU_-]}{2\sqrt{6}}$
170	$T^2_{-1}([01(1)1]\{2\}1)$	$-\frac{[P_-(-2S_-U_++S_+U_-+2S_zU_z)+P_+S_-U_-+2P_zS_-U_z-4P_zS_zU_-]}{2\sqrt{6}}$
171	$T^2_{-1}([11(1)1]\{2\}1)$	$\frac{I_-(-P_-S_+U_z-2P_-S_zU_++P_+S_zU_-+2P_zS_+U_-+2P_zS_zU_z)}{2\sqrt{3}}$ $+\frac{I_+(P_-S_-U_z-P_-S_zU_--2P_zS_-U_-)}{2\sqrt{3}}$ $+\frac{I_z(2P_-S_-U_++P_-S_+U_--P_+S_-U_--2P_zS_-U_z)}{2\sqrt{3}}$
172	$T^2_{-1}([11(2)1]\{2\}1)$	$\frac{1}{6}\big[I_-(P_-S_+U_z+2P_-S_zU_+-2P_+S_-U_z+3P_+S_zU_--4P_zS_-U_+$ $+2P_zS_zU_z)+I_+P_-(S_-U_z-3S_zU_-)+I_z(2P_-S_-U_+-3P_-S_+U_-$ $-4P_-S_zU_z+3P_+S_-U_-+2P_zS_-U_z)\big]$
173	$T^2_{-1}([11(2)1]\{3\}1)$	$-\frac{I_-(-4P_-S_+U_z+10P_-S_zU_+-4P_+S_-U_z+3P_+S_zU_-+10P_zS_-U_++3P_zS_+U_-+16P_zS_zU_z)}{3\sqrt{35}}$ $-\frac{I_+(-4P_-S_-U_z+3P_-S_zU_-+3P_zS_-U_-)}{3\sqrt{35}}$ $-\frac{I_z(10P_-S_-U_++3P_-S_+U_-+16P_-S_zU_z+3P_+S_-U_-+16P_zS_-U_z-12P_zS_zU_-)}{3\sqrt{35}}$
174	$T^3_{-1}([11(2)1]\{3\}0)$	$-\frac{[I_-(P_-S_++P_+S_--4P_zS_z)+I_+P_-S_--4I_z(P_-S_z+P_zS_-)]}{\sqrt{30}}$
175	$T^3_{-1}([11(2)0]\{2\}1)$	$-\frac{[I_-(S_-U_++S_+U_--4S_zU_z)+I_+S_-U_--4I_z(S_-U_z+S_zU_-)]}{\sqrt{30}}$
176	$T^3_{-1}([10(1)1]\{2\}1)$	$-\frac{[I_-(P_-U_++P_+U_--4P_zU_z)+I_+P_-U_--4I_z(P_-U_z+P_zU_-)]}{\sqrt{30}}$
177	$T^3_{-1}([01(1)1]\{2\}1)$	$-\frac{[P_-(S_-U_++S_+U_--4S_zU_z)+P_+S_-U_--4P_z(S_-U_z+S_zU_-)]}{\sqrt{30}}$
178	$T^3_{-1}([11(1)1]\{2\}1)$	$\frac{I_-(2P_-S_+U_z+P_-S_zU_++P_+S_zU_-+2P_zS_+U_--4P_zS_zU_z)}{\sqrt{15}}$ $-\frac{I_+(2P_-S_-U_z+P_-S_zU_-+2P_zS_-U_-)}{\sqrt{15}}$ $+\frac{I_z(-P_-S_-U_++P_-S_+U_--P_+S_-U_-+4P_zS_-U_z)}{\sqrt{15}}$
179	$T^3_{-1}([11(2)1]\{2\}1)$	$\frac{I_-(-2P_-S_+U_z-P_-S_zU_++4P_+S_-U_z+3P_+S_zU_-+2P_zS_-U_+-4P_zS_zU_z)}{3\sqrt{5}}$ $-\frac{I_+P_-(2S_-U_z+3S_zU_-)}{3\sqrt{5}}$ $+\frac{I_z(-P_-S_-U_+-3P_-S_+U_-+8P_-S_zU_z+3P_+S_-U_--4P_zS_-U_z)}{3\sqrt{5}}$
180	$T^3_{-1}([11(2)1]\{3\}1)$	$\frac{I_-(P_-S_+U_z+5P_-S_zU_++P_+S_-U_z-3P_+S_zU_-+5P_zS_-U_+-3P_zS_+U_--4P_zS_zU_z)}{3\sqrt{10}}$

		$+\frac{I_+(P_-S_-U_z-3P_-S_zU_--3P_zS_-U_-)}{3\sqrt{10}}$
		$-\frac{I_z(-5P_-S_-U_++3P_-S_+U_-+4P_-S_zU_z+3P_+S_-U_-+4P_zS_-U_z-12P_zS_zU_-)}{3\sqrt{10}}$
181	$T^4_{-1}([11(2)1]\{3\}1)$	$-\frac{I_-[P_-S_+U_z+P_-S_zU_++P_+S_-U_z+P_+S_zU_-+P_z(S_-U_++S_+U_--4S_zU_z)]}{\sqrt{14}}$
		$-\frac{I_+(P_-S_-U_z+P_-S_zU_-+P_zS_-U_-)}{\sqrt{14}}$
		$-\frac{I_z[P_-(S_-U_++S_+U_--4S_zU_z)+P_+S_-U_--4P_z(S_-U_z+S_zU_-)]}{\sqrt{14}}$
182	$T^2_2([11(2)0]\{2\}0)$	$\frac{1}{2}I_+S_+$
183	$T^2_2([10(1)1]\{2\}0)$	$\frac{1}{2}I_+P_+$
184	$T^2_2([01(1)1]\{2\}0)$	$\frac{1}{2}P_+S_+$
185	$T^2_2([11(1)1]\{2\}0)$	$\frac{P_+(I_+S_z-I_zS_+)}{\sqrt{2}}$
186	$T^2_2([11(2)1]\{2\}0)$	$-\frac{(I_+P_+S_z-2I_+P_zS_++I_zP_+S_+)}{\sqrt{6}}$
187	$T^2_2([10(1)0]\{1\}1)$	$\frac{1}{2}I_+U_+$
188	$T^2_2([01(1)0]\{1\}1)$	$\frac{1}{2}S_+U_+$
189	$T^2_2([11(1)0]\{1\}1)$	$\frac{U_+(I_+S_z-I_zS_+)}{\sqrt{2}}$
190	$T^2_2([00(0)1]\{1\}1)$	$\frac{1}{2}P_+U_+$
191	$T^2_2([10(1)1]\{1\}1)$	$\frac{U_+(I_+P_z-I_zP_+)}{\sqrt{2}}$
192	$T^2_2([01(1)1]\{1\}1)$	$\frac{U_+(P_zS_+-P_+S_z)}{\sqrt{2}}$
193	$T^2_2([11(0)1]\{1\}1)$	$-\frac{P_+U_+(I_-S_++I_+S_-+2I_zS_z)}{\sqrt{3}}$
194	$T^2_2([11(1)1]\{1\}1)$	$\frac{1}{2}U_+(-I_-P_+S_+ + I_+P_+S_- + 2I_+P_zS_z - 2I_zP_zS_+)$
195	$T^2_2([11(2)1]\{1\}1)$	$-\frac{U_+(I_-P_+S_++I_+(6P_-S_++P_+S_-+6P_zS_z)-4I_zP_+S_z+6I_zP_zS_+)}{2\sqrt{15}}$
196	$T^2_2([11(2)0]\{2\}1)$	$-\frac{(-2I_+S_+U_z+I_+S_zU_++I_zS_+U_+)}{\sqrt{6}}$
197	$T^2_2([10(1)1]\{2\}1)$	$-\frac{(-2I_+P_+U_z+I_+P_zU_++I_zP_+U_+)}{\sqrt{6}}$
198	$T^2_2([01(1)1]\{2\}1)$	$-\frac{(-2P_+S_+U_z+P_+S_zU_++P_zS_+U_+)}{\sqrt{6}}$
199	$T^2_2([11(1)1]\{2\}1)$	$\frac{I_+(P_+S_-U_++4P_+S_zU_z-2P_zS_zU_+)-S_+(I_-P_+U_++4I_zP_+U_z-2I_zP_zU_+)}{2\sqrt{3}}$
200	$T^2_2([11(2)1]\{2\}1)$	$\frac{1}{6}\big[-I_-P_+S_+U_+ - I_+(-2P_-S_+U_+ + P_+S_-U_+ + 4P_+S_zU_z$ $-8P_zS_+U_z + 2P_zS_zU_+) - 2I_z(2P_+S_+U_z - 2P_+S_zU_+ + P_zS_+U_+)\big]$
201	$T^2_2([11(2)1]\{3\}1)$	$-\frac{I_-P_+S_+U_++I_+(P_-S_+U_++P_+(S_-U_++15S_+U_-+10S_zU_z)+10P_zS_+U_z-4P_zS_zU_+)}{3\sqrt{35}}$
		$+\frac{2I_z(-5P_+S_+U_z+2P_+S_zU_++2P_zS_+U_+)}{3\sqrt{35}}$
202	$T^3_2([11(2)1]\{3\}0)$	$\frac{I_+P_+S_z+I_+P_zS_++I_zP_+S_+}{\sqrt{3}}$
203	$T^3_2([11(2)0]\{2\}1)$	$\frac{I_+S_+U_z+I_+S_zU_++I_zS_+U_+}{\sqrt{3}}$
204	$T^3_2([10(1)1]\{2\}1)$	$\frac{I_+P_+U_z+I_+P_zU_++I_zP_+U_+}{\sqrt{3}}$
205	$T^3_2([01(1)1]\{2\}1)$	$\frac{P_+S_+U_z+P_+S_zU_++P_zS_+U_+}{\sqrt{3}}$
206	$T^3_2([11(1)1]\{2\}1)$	$\frac{S_+[I_-P_+U_+-2I_z(P_+U_z+P_zU_+)]+I_+(-P_+S_-U_++2P_+S_zU_z+2P_zS_zU_+)}{\sqrt{6}}$
207	$T^3_2([11(2)1]\{2\}1)$	$\frac{I_-P_+S_+U_++I_+(-2P_-S_+U_++P_+S_-U_+-2P_+S_zU_z+4P_zS_+U_z+2P_zS_zU_+)}{3\sqrt{2}}$
		$+\frac{2I_z(-P_+S_+U_z-2P_+S_zU_++P_zS_+U_+)}{3\sqrt{2}}$
208	$T^3_2([11(2)1]\{3\}1)$	$\frac{1}{6}\big[I_-P_+S_+U_+ + I_+(P_-S_+U_+ + P_+(S_-U_+ - 3S_+U_- + 4S_zU_z)$ $+4P_zS_+U_z - 4P_zS_zU_+) - 4I_z(-P_+S_+U_z + P_+S_zU_+ + P_zS_+U_+)\big]$
209	$T^4_2([11(2)1]\{3\}1)$	$-\frac{I_-P_+S_+U_++I_+(P_-S_+U_++P_+(S_-U_++S_+U_--4S_zU_z)-4P_z(S_+U_z+S_zU_+))}{2\sqrt{7}}$

		$+\frac{4I_z(P_+S_+U_z+P_+S_zU_++P_zS_+U_+)}{2\sqrt{7}}$
210	$T^2_{-2}([11(2)0]\{2\}0)$	$\frac{1}{2}I_-S_-$
211	$T^2_{-2}([10(1)1]\{2\}0)$	$\frac{1}{2}I_-P_-$
212	$T^2_{-2}([01(1)1]\{2\}0)$	$\frac{1}{2}P_-S_-$
213	$T^2_{-2}([11(1)1]\{2\}0)$	$\frac{P_-(I_zS_--I_-S_z)}{\sqrt{2}}$
214	$T^2_{-2}([11(2)1]\{2\}0)$	$\frac{I_-P_-S_z-2I_-P_zS_-+I_zP_-S_-}{\sqrt{6}}$
215	$T^2_{-2}([10(1)0]\{1\}1)$	$\frac{1}{2}I_-U_-$
216	$T^2_{-2}([01(1)0]\{1\}1)$	$\frac{1}{2}S_-U_-$
217	$T^2_{-2}([11(1)0]\{1\}1)$	$\frac{U_-(I_zS_--I_-S_z)}{\sqrt{2}}$
218	$T^2_{-2}([00(0)1]\{1\}1)$	$\frac{1}{2}P_-U_-$
219	$T^2_{-2}([10(1)1]\{1\}1)$	$\frac{U_-(I_zP_--I_-P_z)}{\sqrt{2}}$
220	$T^2_{-2}([01(1)1]\{1\}1)$	$\frac{U_-(P_-S_z-P_zS_-)}{\sqrt{2}}$
221	$T^2_{-2}([11(0)1]\{1\}1)$	$-\frac{P_-U_-(I_-S_++I_+S_-+2I_zS_z)}{\sqrt{3}}$
222	$T^2_{-2}([11(1)1]\{1\}1)$	$\frac{1}{2}U_-(I_-P_-S_+ + 2I_-P_zS_z - I_+P_-S_- - 2I_zP_zS_-)$
223	$T^2_{-2}([11(2)1]\{1\}1)$	$-\frac{U_-(I_-(P_-S_++6P_+S_-+6P_zS_z)+I_+P_-S_--4I_zP_-S_z+6I_zP_zS_-)}{2\sqrt{15}}$
224	$T^2_{-2}([11(2)0]\{2\}1)$	$\frac{-2I_-S_-U_z+I_-S_zU_-+I_zS_-U_-}{\sqrt{6}}$
225	$T^2_{-2}([10(1)1]\{2\}1)$	$\frac{-2I_-P_-U_z+I_-P_zU_-+I_zP_-U_-}{\sqrt{6}}$
226	$T^2_{-2}([01(1)1]\{2\}1)$	$\frac{-2P_-S_-U_z+P_-S_zU_-+P_zS_-U_-}{\sqrt{6}}$
227	$T^2_{-2}([11(1)1]\{2\}1)$	$\frac{I_-(P_-S_+U_-+4P_-S_zU_z-2P_zS_zU_-)-I_+P_-S_-U_-+2I_zS_-(P_zU_--2P_-U_z)}{2\sqrt{3}}$
228	$T^2_{-2}([11(2)1]\{2\}1)$	$\frac{1}{6}\big[I_-(-P_-S_+U_- - 4P_-S_zU_z + 2P_+S_-U_- + 8P_zS_-U_z - 2P_zS_zU_-)$
		$-I_+P_-S_-U_- - 2I_z(2P_-S_-U_z - 2P_-S_zU_- + P_zS_-U_-)\big]$
229	$T^2_{-2}([11(2)1]\{3\}1)$	$-\frac{I_-(15P_-S_-U_++P_-S_+U_-+10P_-S_zU_z+P_+S_-U_-+10P_zS_-U_z-4P_zS_zU_-)+I_+P_-S_-U_-}{3\sqrt{35}}$
		$+\frac{I_-(2I_z(-5P_-S_-U_z+2P_-S_zU_-+2P_zS_-U_-)}{3\sqrt{35}}$
230	$T^3_{-2}([11(2)1]\{3\}0)$	$\frac{I_-P_-S_z+I_-P_zS_-+I_zP_-S_-}{\sqrt{3}}$
231	$T^3_{-2}([11(2)0]\{2\}1)$	$\frac{I_-S_-U_z+I_-S_zU_-+I_zS_-U_-}{\sqrt{3}}$
232	$T^3_{-2}([10(1)1]\{2\}1)$	$\frac{I_-P_-U_z+I_-P_zU_-+I_zP_-U_-}{\sqrt{3}}$
233	$T^3_{-2}([01(1)1]\{2\}1)$	$\frac{P_-S_-U_z+P_-S_zU_-+P_zS_-U_-}{\sqrt{3}}$
234	$T^3_{-2}([11(1)1]\{2\}1)$	$\frac{I_-(P_-S_+U_--2P_-S_zU_z-2P_zS_zU_-)-I_+P_-S_-U_-+2I_zS_-(P_-U_z+P_zU_-)}{\sqrt{6}}$
235	$T^3_{-2}([11(2)1]\{2\}1)$	$-\frac{I_-(P_-S_+U_--2P_-S_zU_z-2P_+S_-U_-+4P_zS_-U_z+2P_zS_zU_-)+I_+P_-S_-U_-}{3\sqrt{2}}$
		$-\frac{2I_z(-P_-S_-U_z-2P_-S_zU_-+P_zS_-U_-)}{3\sqrt{2}}$
236	$T^3_{-2}([11(2)1]\{3\}1)$	$\frac{1}{6}\big[-I_-(-3P_-S_-U_+ + P_-S_+U_- + 4P_-S_zU_z + P_+S_-U_- + 4P_zS_-U_z$
		$-4P_zS_zU_-) - I_+P_-S_-U_- + 4I_z(-P_-S_-U_z + P_-S_zU_- + P_zS_-U_-)\big]$
237	$T^4_{-2}([11(2)1]\{3\}1)$	$-\frac{I_-(P_-(S_-U_++S_+U_--4S_zU_z)+P_+S_-U_--4P_z(S_-U_z+S_zU_-))+I_+P_-S_-U_-}{2\sqrt{7}}$
		$+\frac{4I_z(P_-S_-U_z+P_-S_zU_-+P_zS_-U_-)}{2\sqrt{7}}$
238	$T^3_3([11(2)1]\{3\}0)$	$-\frac{I_+P_+S_+}{\sqrt{2}}$
239	$T^3_3([11(2)0]\{2\}1)$	$-\frac{I_+S_+U_+}{\sqrt{2}}$

240	$T^3_3([10(1)1]\{2\}1)$	$-\frac{I_+P_+U_+}{\sqrt{2}}$
241	$T^3_3([01(1)1]\{2\}1)$	$-\frac{P_+S_+U_+}{\sqrt{2}}$
242	$T^3_3([11(1)1]\{2\}1)$	$P_+U_+(I_zS_+ - I_+S_z)$
243	$T^3_3([11(2)1]\{2\}1)$	$\frac{U_+(I_+P_+S_z - 2I_+P_zS_+ + I_zP_+S_+)}{\sqrt{3}}$
244	$T^3_3([11(2)1]\{3\}1)$	$\frac{I_+(-3P_+S_+U_z + P_+S_zU_+ + P_zS_+U_+) + I_zP_+S_+U_+}{\sqrt{6}}$
245	$T^4_3([11(2)1]\{3\}1)$	$-\frac{I_+(P_+S_+U_z + P_+S_zU_+ + P_zS_+U_+) + I_zP_+S_+U_+}{\sqrt{2}}$
246	$T^3_{-3}([11(2)1]\{3\}0)$	$\frac{I_-P_-S_-}{\sqrt{2}}$
247	$T^3_{-3}([11(2)0]\{2\}1)$	$\frac{I_-S_-U_-}{\sqrt{2}}$
248	$T^3_{-3}([10(1)1]\{2\}1)$	$\frac{I_-P_-U_-}{\sqrt{2}}$
249	$T^3_{-3}([01(1)1]\{2\}1)$	$\frac{P_-S_-U_-}{\sqrt{2}}$
250	$T^3_{-3}([11(1)1]\{2\}1)$	$P_-U_-(I_zS_- - I_-S_z)$
251	$T^3_{-3}([11(2)1]\{2\}1)$	$\frac{U_-(I_-P_-S_z - 2I_-P_zS_- + I_zP_-S_-)}{\sqrt{3}}$
252	$T^3_{-3}([11(2)1]\{3\}1)$	$\frac{I_-(-3P_-S_-U_z + P_-S_zU_- + P_zS_-U_-) + I_zP_-S_-U_-}{\sqrt{6}}$
253	$T^4_{-3}([11(2)1]\{3\}1)$	$\frac{I_-(P_-S_-U_z + P_-S_zU_- + P_zS_-U_-) + I_zP_-S_-U_-}{\sqrt{2}}$
254	$T^4_4([11(2)1]\{3\}1)$	$I_+P_+S_+U_+$
255	$T^4_{-4}([11(2)1]\{3\}1)$	$I_-P_-S_-U_-$

APPENDIX K: LIOUVILLIAN SUPERMATRICES

Here we calculate the supermatrix representation of the Zeeman Liouvillian $\mathcal{L}_{\rm Z} = [H_{\rm Z}, \,]$ and the dipolar Liouvillian $\mathcal{L}^\alpha_{\rm D} = [H^\alpha_{\rm D}, \,]$, with the Hamiltonians given by Eqs. (1) and (2), in the four-spin ISTO basis of Table S3. For isochronous spins, the Zeeman Liouvillian is diagonal and

$$(n \,|\, \mathcal{L}_{\rm Z} \,|\, n') \;=\; \delta_{nn'}\, \omega_0\, Q\,. \tag{K.1}$$

Similar manipulations as in the three-spin case (see Paper III[1]) yields for the six terms in the dipolar Liouvillian, with the Wigner functions $D^{2\,*}_{Q-Q',0}(\Omega^\alpha_X)$ given by the expressions in Appendix C,

$$
\begin{aligned}
&\Big(T^{K}_{Q}\big(\,[k_I k_S(\bar{K})k_P]\,\{\bar{\bar{K}}\}k_U\big)\,|\,\mathcal{L}^{\alpha}_{\mathrm{D},IS}\,|\,T^{K'}_{Q'}\big(\,[k'_I k'_S(\bar{K}')k'_P]\,\{\bar{\bar{K}}'\}k'_U\big)\Big)\\
&=\omega_{\mathrm{D},IS}\,D^{2*}_{Q-Q',0}(\Omega^{\alpha}_{IS})\,(-1)^{K'-Q}\,\delta_{k_P k'_P}\delta_{k_U k'_U}\left[(-1)^{k_I+k_S+k_P+k_U}-(-1)^{k'_I+k'_S+k'_P+k'_U}\right]\\
&\quad\times 10\sqrt{3}\left[(2K+1)(2K'+1)(2\bar{K}+1)(2\bar{K}'+1)(2\bar{\bar{K}}+1)(2\bar{\bar{K}}'+1)\right.\\
&\quad\left.(2k_I+1)(2k'_I+1)(2k_S+1)(2k'_S+1)(2k_P+1)(2k'_P+1)(2k_U+1)(2k'_U+1)\right]^{1/2}\\
&\quad\times\begin{pmatrix} K & K' & 2\\ -Q & Q' & Q-Q'\end{pmatrix}\begin{Bmatrix} K & K' & 2\\ \bar{\bar{K}} & \bar{\bar{K}}' & 2\\ k_U & k'_U & 0\end{Bmatrix}\begin{Bmatrix} \bar{\bar{K}} & \bar{\bar{K}}' & 2\\ \bar{K} & \bar{K}' & 2\\ k_P & k'_P & 0\end{Bmatrix}\begin{Bmatrix} \bar{K} & \bar{K}' & 2\\ k_I & k'_I & 1\\ k_S & k'_S & 1\end{Bmatrix}\\
&\quad\times\begin{Bmatrix} k_I & k'_I & 1\\ \frac{1}{2} & \frac{1}{2} & \frac{1}{2}\end{Bmatrix}\begin{Bmatrix} k_S & k'_S & 1\\ \frac{1}{2} & \frac{1}{2} & \frac{1}{2}\end{Bmatrix}\begin{Bmatrix} k_P & k'_P & 0\\ \frac{1}{2} & \frac{1}{2} & \frac{1}{2}\end{Bmatrix}\begin{Bmatrix} k_U & k'_U & 0\\ \frac{1}{2} & \frac{1}{2} & \frac{1}{2}\end{Bmatrix},
\end{aligned}
\tag{K.2}
$$

$$
\begin{aligned}
&\Big(T^{K}_{Q}\big(\,[k_I k_S(\bar{K})k_P]\,\{\bar{\bar{K}}\}k_U\big)\,|\,\mathcal{L}^{\alpha}_{\mathrm{D},IP}\,|\,T^{K'}_{Q'}\big(\,[k'_I k'_S(\bar{K}')k'_P]\,\{\bar{\bar{K}}'\}k'_U\big)\Big)\\
&=\omega_{\mathrm{D},IP}\,D^{2*}_{Q-Q',0}(\Omega^{\alpha}_{IP})\,(-1)^{K'-Q}\,\delta_{k_S k'_S}\delta_{k_U k'_U}\left[(-1)^{k_I+k_S+k_P+k_U}-(-1)^{k'_I+k'_S+k'_P+k'_U}\right]\\
&\quad\times 30\sqrt{2}\left[(2K+1)(2K'+1)(2\bar{K}+1)(2\bar{K}'+1)(2\bar{\bar{K}}+1)(2\bar{\bar{K}}'+1)\right.\\
&\quad\left.(2k_I+1)(2k'_I+1)(2k_S+1)(2k'_S+1)(2k_P+1)(2k'_P+1)(2k_U+1)(2k'_U+1)\right]^{1/2}\\
&\quad\times\begin{pmatrix} K & K' & 2\\ -Q & Q' & Q-Q'\end{pmatrix}\begin{Bmatrix} K & K' & 2\\ \bar{\bar{K}} & \bar{\bar{K}}' & 2\\ k_U & k'_U & 0\end{Bmatrix}\begin{Bmatrix} \bar{\bar{K}} & \bar{\bar{K}}' & 2\\ \bar{K} & \bar{K}' & 1\\ k_P & k'_P & 1\end{Bmatrix}\begin{Bmatrix} \bar{K} & \bar{K}' & 1\\ k_I & k'_I & 1\\ k_S & k'_S & 0\end{Bmatrix}\\
&\quad\times\begin{Bmatrix} k_I & k'_I & 1\\ \frac{1}{2} & \frac{1}{2} & \frac{1}{2}\end{Bmatrix}\begin{Bmatrix} k_S & k'_S & 0\\ \frac{1}{2} & \frac{1}{2} & \frac{1}{2}\end{Bmatrix}\begin{Bmatrix} k_P & k'_P & 1\\ \frac{1}{2} & \frac{1}{2} & \frac{1}{2}\end{Bmatrix}\begin{Bmatrix} k_U & k'_U & 0\\ \frac{1}{2} & \frac{1}{2} & \frac{1}{2}\end{Bmatrix},
\end{aligned}
\tag{K.3}
$$

$$
\begin{aligned}
&\Big(T^{K}_{Q}\big(\,[k_I k_S(\bar{K})k_P]\,\{\bar{\bar{K}}\}k_U\big)\,|\,\mathcal{L}^{\alpha}_{\mathrm{D},IU}\,|\,T^{K'}_{Q'}\big(\,[k'_I k'_S(\bar{K}')k'_P]\,\{\bar{\bar{K}}'\}k'_U\big)\Big)\\
&=\omega_{\mathrm{D},IU}\,D^{2*}_{Q-Q',0}(\Omega^{\alpha}_{IU})\,(-1)^{K'-Q}\,\delta_{k_S k'_S}\delta_{k_P k'_P}\left[(-1)^{k_I+k_S+k_P+k_U}-(-1)^{k'_I+k'_S+k'_P+k'_U}\right]\\
&\quad\times 6\sqrt{30}\left[(2K+1)(2K'+1)(2\bar{K}+1)(2\bar{K}'+1)(2\bar{\bar{K}}+1)(2\bar{\bar{K}}'+1)\right.\\
&\quad\left.(2k_I+1)(2k'_I+1)(2k_S+1)(2k'_S+1)(2k_P+1)(2k'_P+1)(2k_U+1)(2k'_U+1)\right]^{1/2}\\
&\quad\times\begin{pmatrix} K & K' & 2\\ -Q & Q' & Q-Q'\end{pmatrix}\begin{Bmatrix} K & K' & 2\\ \bar{\bar{K}} & \bar{\bar{K}}' & 1\\ k_U & k'_U & 1\end{Bmatrix}\begin{Bmatrix} \bar{\bar{K}} & \bar{\bar{K}}' & 1\\ \bar{K} & \bar{K}' & 1\\ k_P & k'_P & 0\end{Bmatrix}\begin{Bmatrix} \bar{K} & \bar{K}' & 1\\ k_I & k'_I & 1\\ k_S & k'_S & 0\end{Bmatrix}\\
&\quad\times\begin{Bmatrix} k_I & k'_I & 1\\ \frac{1}{2} & \frac{1}{2} & \frac{1}{2}\end{Bmatrix}\begin{Bmatrix} k_S & k'_S & 0\\ \frac{1}{2} & \frac{1}{2} & \frac{1}{2}\end{Bmatrix}\begin{Bmatrix} k_P & k'_P & 0\\ \frac{1}{2} & \frac{1}{2} & \frac{1}{2}\end{Bmatrix}\begin{Bmatrix} k_U & k'_U & 1\\ \frac{1}{2} & \frac{1}{2} & \frac{1}{2}\end{Bmatrix},
\end{aligned}
\tag{K.4}
$$

$$
\begin{aligned}
&\Big(T^{K}_{Q}\big(\,[k_I k_S(\bar{K})k_P]\,\{\bar{\bar{K}}\}k_U\big)|\,\mathcal{L}^{\alpha}_{\mathrm{D},SP}\,|\,T^{K'}_{Q'}\big(\,[k'_I k'_S(\bar{K}')k'_P]\,\{\bar{\bar{K}}'\}k'_U\big)\Big)\\
&=\omega_{\mathrm{D},SP}\,D^{2\,*}_{Q-Q',0}(\Omega^{\alpha}_{SP})\,(-1)^{K'-Q}\,\delta_{k_I k'_I}\delta_{k_U k'_U}\Big[(-1)^{k_I+k_S+k_P+k_U}-(-1)^{k'_I+k'_S+k'_P+k'_U}\Big]\\
&\quad\times 30\sqrt{2}\,\big[(2K+1)(2K'+1)(2\bar{K}+1)(2\bar{K}'+1)(2\bar{\bar{K}}+1)(2\bar{\bar{K}}'+1)\\
&\quad(2k_I+1)(2k'_I+1)(2k_S+1)(2k'_S+1)(2k_P+1)(2k'_P+1)(2k_U+1)(2k'_U+1)\big]^{1/2}\\
&\quad\times\begin{pmatrix} K & K' & 2\\ -Q & Q' & Q-Q'\end{pmatrix}\begin{Bmatrix} K & K' & 2\\ \bar{\bar{K}} & \bar{\bar{K}}' & 2\\ k_U & k'_U & 0\end{Bmatrix}\begin{Bmatrix} \bar{\bar{K}} & \bar{\bar{K}}' & 2\\ \bar{K} & \bar{K}' & 1\\ k_P & k'_P & 1\end{Bmatrix}\begin{Bmatrix} \bar{K} & \bar{K}' & 1\\ k_I & k'_I & 0\\ k_S & k'_S & 1\end{Bmatrix}\\
&\quad\times\begin{Bmatrix} k_I & k'_I & 0\\ \frac{1}{2} & \frac{1}{2} & \frac{1}{2}\end{Bmatrix}\begin{Bmatrix} k_S & k'_S & 1\\ \frac{1}{2} & \frac{1}{2} & \frac{1}{2}\end{Bmatrix}\begin{Bmatrix} k_P & k'_P & 1\\ \frac{1}{2} & \frac{1}{2} & \frac{1}{2}\end{Bmatrix}\begin{Bmatrix} k_U & k'_U & 0\\ \frac{1}{2} & \frac{1}{2} & \frac{1}{2}\end{Bmatrix},
\end{aligned}
\tag{K.5}
$$

$$
\begin{aligned}
&\Big(T^{K}_{Q}\big(\,[k_I k_S(\bar{K})k_P]\,\{\bar{\bar{K}}\}k_U\big)|\,\mathcal{L}^{\alpha}_{\mathrm{D},SU}\,|\,T^{K'}_{Q'}\big(\,[k'_I k'_S(\bar{K}')k'_P]\,\{\bar{\bar{K}}'\}k'_U\big)\Big)\\
&=\omega_{\mathrm{D},SU}\,D^{2\,*}_{Q-Q',0}(\Omega^{\alpha}_{SU})\,(-1)^{K'-Q}\,\delta_{k_I k'_I}\delta_{k_P k'_P}\Big[(-1)^{k_I+k_S+k_P+k_U}-(-1)^{k'_I+k'_S+k'_P+k'_U}\Big]\\
&\quad\times 6\sqrt{30}\,\big[(2K+1)(2K'+1)(2\bar{K}+1)(2\bar{K}'+1)(2\bar{\bar{K}}+1)(2\bar{\bar{K}}'+1)\\
&\quad(2k_I+1)(2k'_I+1)(2k_S+1)(2k'_S+1)(2k_P+1)(2k'_P+1)(2k_U+1)(2k'_U+1)\big]^{1/2}\\
&\quad\times\begin{pmatrix} K & K' & 2\\ -Q & Q' & Q-Q'\end{pmatrix}\begin{Bmatrix} K & K' & 2\\ \bar{\bar{K}} & \bar{\bar{K}}' & 2\\ k_U & k'_U & 1\end{Bmatrix}\begin{Bmatrix} \bar{\bar{K}} & \bar{\bar{K}}' & 1\\ \bar{K} & \bar{K}' & 1\\ k_P & k'_P & 0\end{Bmatrix}\begin{Bmatrix} \bar{K} & \bar{K}' & 1\\ k_I & k'_I & 0\\ k_S & k'_S & 1\end{Bmatrix}\\
&\quad\times\begin{Bmatrix} k_I & k'_I & 0\\ \frac{1}{2} & \frac{1}{2} & \frac{1}{2}\end{Bmatrix}\begin{Bmatrix} k_S & k'_S & 1\\ \frac{1}{2} & \frac{1}{2} & \frac{1}{2}\end{Bmatrix}\begin{Bmatrix} k_P & k'_P & 0\\ \frac{1}{2} & \frac{1}{2} & \frac{1}{2}\end{Bmatrix}\begin{Bmatrix} k_U & k'_U & 1\\ \frac{1}{2} & \frac{1}{2} & \frac{1}{2}\end{Bmatrix},
\end{aligned}
\tag{K.6}
$$

$$
\begin{aligned}
&\Big(T^{K}_{Q}\big(\,[k_I k_S(\bar{K})k_P]\,\{\bar{\bar{K}}\}k_U\big)|\,\mathcal{L}^{\alpha}_{\mathrm{D},PU}\,|\,T^{K'}_{Q'}\big(\,[k'_I k'_S(\bar{K}')k'_P]\,\{\bar{\bar{K}}'\}k'_U\big)\Big)\\
&=\omega_{\mathrm{D},PU}\,D^{2\,*}_{Q-Q',0}(\Omega^{\alpha}_{PU})\,(-1)^{K'-Q}\,\delta_{k_I k'_I}\delta_{k_S k'_S}\Big[(-1)^{k_I+k_S+k_P+k_U}-(-1)^{k'_I+k'_S+k'_P+k'_U}\Big]\\
&\quad\times 6\sqrt{10}\,\big[(2K+1)(2K'+1)(2\bar{K}+1)(2\bar{K}'+1)(2\bar{\bar{K}}+1)(2\bar{\bar{K}}'+1)\\
&\quad(2k_I+1)(2k'_I+1)(2k_S+1)(2k'_S+1)(2k_P+1)(2k'_P+1)(2k_U+1)(2k'_U+1)\big]^{1/2}\\
&\quad\times\begin{pmatrix} K & K' & 2\\ -Q & Q' & Q-Q'\end{pmatrix}\begin{Bmatrix} K & K' & 2\\ \bar{\bar{K}} & \bar{\bar{K}}' & 1\\ k_U & k'_U & 1\end{Bmatrix}\begin{Bmatrix} \bar{\bar{K}} & \bar{\bar{K}}' & 1\\ \bar{K} & \bar{K}' & 0\\ k_P & k'_P & 1\end{Bmatrix}\begin{Bmatrix} \bar{K} & \bar{K}' & 0\\ k_I & k'_I & 0\\ k_S & k'_S & 0\end{Bmatrix}\\
&\quad\times\begin{Bmatrix} k_I & k'_I & 0\\ \frac{1}{2} & \frac{1}{2} & \frac{1}{2}\end{Bmatrix}\begin{Bmatrix} k_S & k'_S & 0\\ \frac{1}{2} & \frac{1}{2} & \frac{1}{2}\end{Bmatrix}\begin{Bmatrix} k_P & k'_P & 1\\ \frac{1}{2} & \frac{1}{2} & \frac{1}{2}\end{Bmatrix}\begin{Bmatrix} k_U & k'_U & 1\\ \frac{1}{2} & \frac{1}{2} & \frac{1}{2}\end{Bmatrix}.
\end{aligned}
\tag{K.7}
$$

APPENDIX L: PROTEIN SPIN SYSTEMS

All SLE and GSRE calculations reported here pertain to protein-derived fragments of proton spins, with m nonlabile protons and one labile side-chain proton ($IP_m{-}I$ case) or one internal water molecule ($ISP_m{-}IS$ case). The nuclear coordinates were extracted either from the BPTI crystal structure 5PTI (A conformer) or from the ubiquitin crystal structure 1UBQ (H atoms added with WHATIF). Proton dipole coupling constants were obtained from the internuclear separation r_X as $\omega_{\mathrm{D},X}\,(\mathrm{rad\ s^{-1}}) = (3/2)\,[\mu_0/(4\pi)]\,\gamma^2\,\hbar/r_X^3 = 1.132 \times 10^6\,[r_X(\text{Å})]^{-3}$.

For the $IP_m{-}I$ case, the labile proton I was chosen as one of 25 hydroxyl or carboxyl protons in the serine, threonine, tyrosine, aspartic acid or glutamic acid side-chains of ubiquitin (Table S5). No order parameters were used.

For the $ISP_m - IS$ case, the labile protons I and S were identified with the H_2O protons of five internal water molecules in BPTI (W111, W112, W113 and W122) and ubiquitin (W128). The intramolecular $I{-}S$ dipole coupling was set to $\omega_{\mathrm{D},IS} = 2.46 \times 10^5$ rad $\mathrm{s^{-1}}$. This value was estimated from the experimental H–H separation in liquid water, $r_{IS} = 1.545$ Å, and a typical orientational order parameter of 0.8 for the I–S vector.[10,11]

For each fragment, all protons except the selected labile ones were regarded as nonlabile. Dipole couplings for the four-spin systems used to calibrate the approximate GSRE theory against the exact SLE theory are listed in Tables S4 and S5.

TABLE S4. Dipole couplings (10^5 rad $\mathrm{s^{-1}}$) for four-spin systems with an internal water molecule (protons I, S) and two nonlabile protons (μ, ν) in BPTI and ubiquitin.

spin I	$\omega_{\mathrm{D},I\mu}$	$\omega_{\mathrm{D},I\nu}$	$\omega_{\mathrm{D},I}$ [a]	$\omega_{\mathrm{D},S\mu}$	$\omega_{\mathrm{D},S\nu}$	$\omega_{\mathrm{D},S}$ [a]	$\omega_{\mathrm{D},\mu\nu}$
W111	0.54	0.82	0.98	1.28	0.54	1.39	0.30
W112	1.04	1.24	1.62	1.06	0.53	1.18	0.58
W113	0.73	1.06	1.29	0.84	0.27	0.88	0.20
W122	0.81	0.57	0.99	1.56	0.75	1.73	0.14
W128	0.59	0.52	0.78	1.31	0.74	1.50	0.18

[a] Defined as in Eq. (39).

TABLE S5. Dipole couplings (10^5 rad s^{-1}) for four-spin systems in ubiquitin with a labile hydroxyl or carboxyl side-chain proton (I) and three nonlabile protons (μ, ν, κ).

spin I	$\omega_{\mathrm{D},I\mu}$	$\omega_{\mathrm{D},I\nu}$	$\omega_{\mathrm{D},I\kappa}$	$\omega_{\mathrm{D},I}$ [a]	$\omega_{\mathrm{D},\mu\nu}$	$\omega_{\mathrm{D},\mu\kappa}$	$\omega_{\mathrm{D},\nu\kappa}$	$\omega_{\mathrm{D},P}$ [a]
Ser-20	0.98	0.57	0.57	1.27	2.60	0.43	0.27	2.65
Ser-57	1.02	0.99	0.55	1.53	0.21	2.60	0.23	2.62
Ser-65	0.79	0.79	0.75	1.34	0.18	0.95	0.11	0.97
Thr-7	1.46	1.01	0.78	1.94	0.24	0.67	0.17	0.73
Thr-9	1.46	0.70	0.70	1.76	0.32	0.49	1.46	1.58
Thr-12	0.69	0.64	0.53	1.08	0.81	2.60	0.46	2.76
Thr-14	0.90	0.33	0.28	1.00	0.81	0.23	0.21	0.87
Thr-22	0.67	0.61	0.53	1.06	0.81	2.60	0.45	2.76
Thr-55	0.99	0.97	0.88	1.64	0.29	0.15	0.22	0.40
Thr-66	0.72	0.59	0.39	1.01	0.83	0.45	2.60	2.77
Tyr-59	1.42	1.06	0.66	1.89	1.00	0.14	0.22	1.03
Asp-21	1.12	0.53	0.42	1.31	0.92	0.14	0.34	0.99
Asp-32	0.29	0.18	0.17	0.38	2.60	0.48	0.68	2.73
Asp-39	0.73	0.50	0.27	0.93	1.99	2.60	0.32	3.29
Asp-52	0.68	0.29	0.24	0.78	0.81	0.09	0.06	0.82
Asp-58	0.30	0.22	0.21	0.43	0.16	0.80	0.09	0.82
Glu-16	0.24	0.23	0.21	0.39	0.92	0.48	2.60	2.80
Glu-24	0.31	0.19	0.19	0.41	0.91	2.60	0.48	2.80
Glu-51	0.54	0.21	0.20	0.62	0.64	2.60	0.51	2.73
Glu-64	0.58	0.30	0.28	0.71	0.11	0.64	0.26	0.70

[a] Defined as in Eq. (39).

APPENDIX M: ACCURACY OF GSRE THEORY

In this Appendix, we compare the results of GSRE and SLE calculations on the four-spin systems listed in Tables S4 and S5 (Appendix L) to assess the accuracy of the GSRE theory for the $IP_3{-}I$ and $ISP_2{-}IS$ cases. We also include results from the ESE theory.

1. Exchange case $IP_3{-}I$

Figures S2 and S3 show that, for the 20 four-spin systems in Table S5 without SDCs, the simple GSRE result for $R_{1,I}(0)$, based on Eqs. (42) and (43), remains very close to the exact $R_{1,I}(0)$ computed from SLE theory over the full τ_A range. While the GSRE result is exact in the MN and USM limits, it remains highly accurate also at intermediate τ_A values. For example, at $\tau_A = 10^{-5}$ s, the GSRE result is off by less than 2.5 % in 16 out of 20 cases. In contrast, the ESE theory yields a much too large $R_{1,I}(0)$ near the maximum and is not even correct in the MN limit.

Figures S4 – S7 show that, for the 20 four-spin systems in Table S5 without SDCs, a GSRE theory that incorporates the GSDF in Eq. (41) as well as the SND correction in Eq. (45) removes the spurious secondary dispersion (evident in the green profiles, without SND correction) and brings the GSRE theory into good agreement with the exact SLE theory over the full frequency range and for all τ_A values. It may be noted that, even though $\omega_{D,I}\,\tau_A \approx 400$ at $\tau_A = 10^{-2}$ s for the labile protons with smallest $\omega_{D,I}$ (most Asp and Glu residues), the SLE profiles are not fully in the USM limit, where $R_{1,I}(0) = P_A/\tau_A$. In contrast, the GSRE profiles are in this limit, and therefore have a slightly larger $R_{1,I}(0)$. For $\tau_A = 10^{-2}$ s, the ESE profile nearly coincides with the GSRE profile, although the primary dispersion is slightly upshifted and closer to the SLE profile.

The exact SLE dispersion profiles in Fig. S8, for the four-spin systems of Thr-7 and Asp-39 (Table S5), demonstrate how the effect of the SDCs is diminished as τ_A becomes longer.

Figures S9 – S14 show that, for the 20 four-spin systems in Table S5, a GSRE theory that incorporates the GSDF in Eq. (41) as well as the SND correction in Eq. (45) and the SDC renormalization in Eq. (46), provides a good to excellent approximation to the exact SLE $R_{1,I}(\omega_0)$ dispersion profile in the full parameter space of the EMOR model. These figures also show the corresponding ESE profiles.

For $\tau_A = 10^{-6}$ s (Figs. S9 and S10), the GSRE theory, unlike the ESE theory, reproduces the hump in the profile, including its fine structure, and accurately describes the primary dispersion step. On the other hand, $R_{1,I}(0)$ is too large by typically 5 – 7 % for those spin systems that include a strong SDC (2.6×10^5 rad s^{-1}, for two protons in a CH_2 or CH_3 group). This discrepancy is a result of insufficient renormalization of these strong SDCs. By using a different functional form in Eq. (46), better agreement between the GSRE and SLE profiles at $\tau_A = 10^{-6}$ s can be achieved. However, the agreement will then deteriorate somewhat for τ_A values above the $R_{1,I}(0)$ maximum, which is the τ_A

range for most labile protons near neutral pH. Moreover, the renormalization function in Eq. (46) predicts that $\widehat{\omega}_{\mathrm{D},\mu\nu} \to 0$ when $\omega_{\mathrm{D},\mu\nu} \to \infty$, thus ensuring that $R_{1,I}(0) = P_\mathrm{A}/\tau_\mathrm{A}$ for any $m \geq 3$. Without the square in the denominator of eq. (46), $\widehat{\omega}_{\mathrm{D},\mu\nu}$ tends to a finite value when $\omega_{\mathrm{D},\mu\nu} \to \infty$ so the coherent mode transfer matrices $\mathbf{X}_{\mathbb{N}_1\mathbb{N}_1}$ and $\mathbf{Y}_{\mathbb{N}_1\mathbb{N}_1}$ do not vanish and $R_{1,I}(0)$ increases with m in the USM limit, contrary to expectation.

For $\tau_\mathrm{A} = 10^{-4}$ s (Figs. S11 and S12), the GSRE theory predicts a too small $R_{1,I}(0)$ for most residues, by as much as 10 – 15 % in some cases. However, the ESE theory overestimates $R_{1,I}(0)$ even more. As for $\tau_\mathrm{A} = 10^{-6}$ s, the GSRE theory accurately predicts the primary dispersion frequency. At $\tau_\mathrm{A} = 10^{-5}$ s, the GSRE theory substantially overestimates $R_{1,I}(0)$ for some residues, but it is still much better than the ESE theory.

For $\tau_\mathrm{A} = 10^{-2}$ s (Figs. S13 and S14), in the USM regime, all three theories predict that $R_{1,I}(0) = P_\mathrm{A}/\tau_\mathrm{A}$ or very nearly so. The SLE profile exhibits a depression with fine structure in the LF regime, features that are not captured by the approximate theories. In most cases, at least the high-frequency part of the primary dispersion is accurately described by the approximate theories.

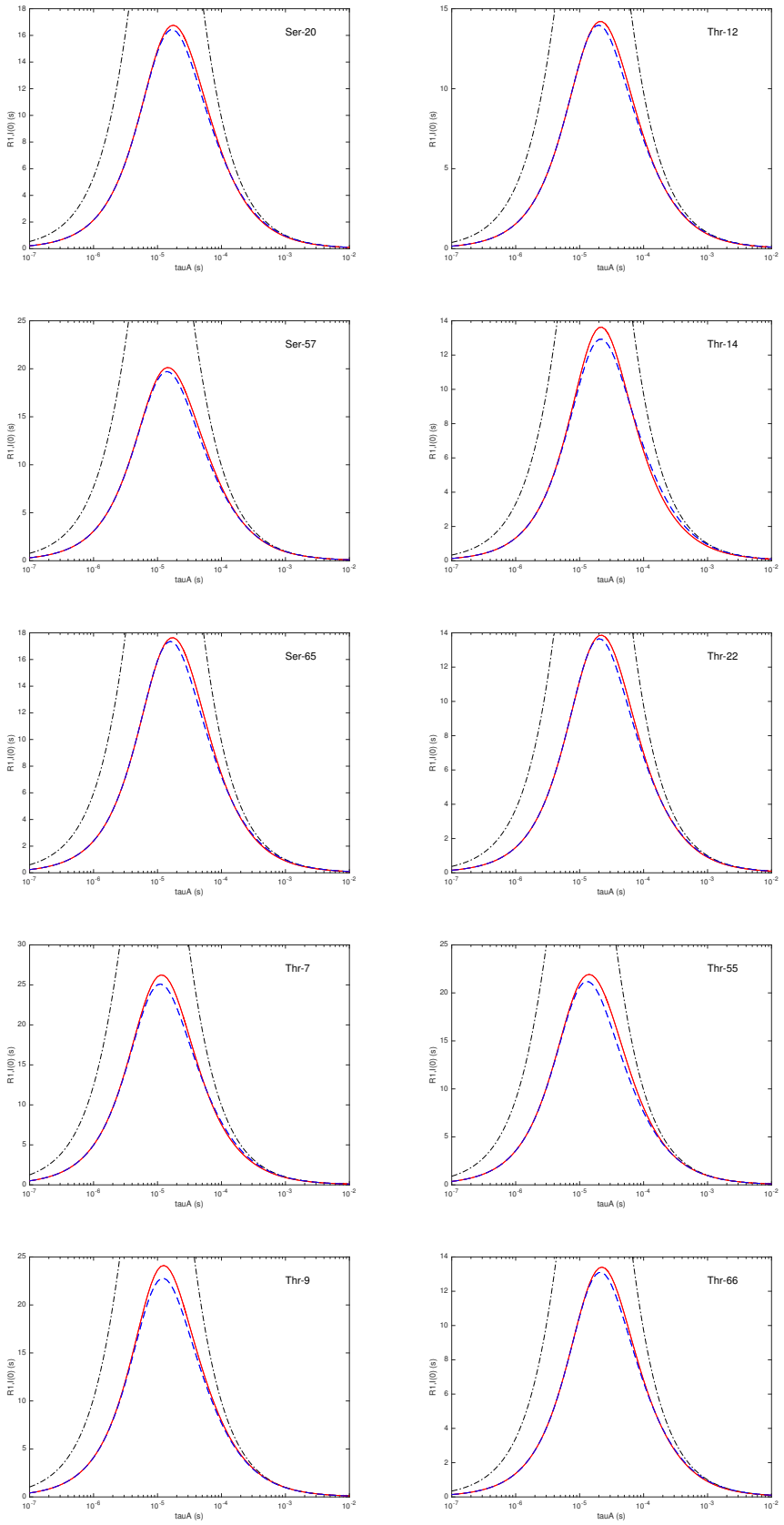

Figure S2: $R_{1,I}(0)$ versus τ_{A} for labile protons in Ser and Thr side-chains in ubiquitin coupled to three nonlabile protons without SDCs, computed from the SLE (red solid), GSRE (blue dash) and ESE (black dash-dot) theories.

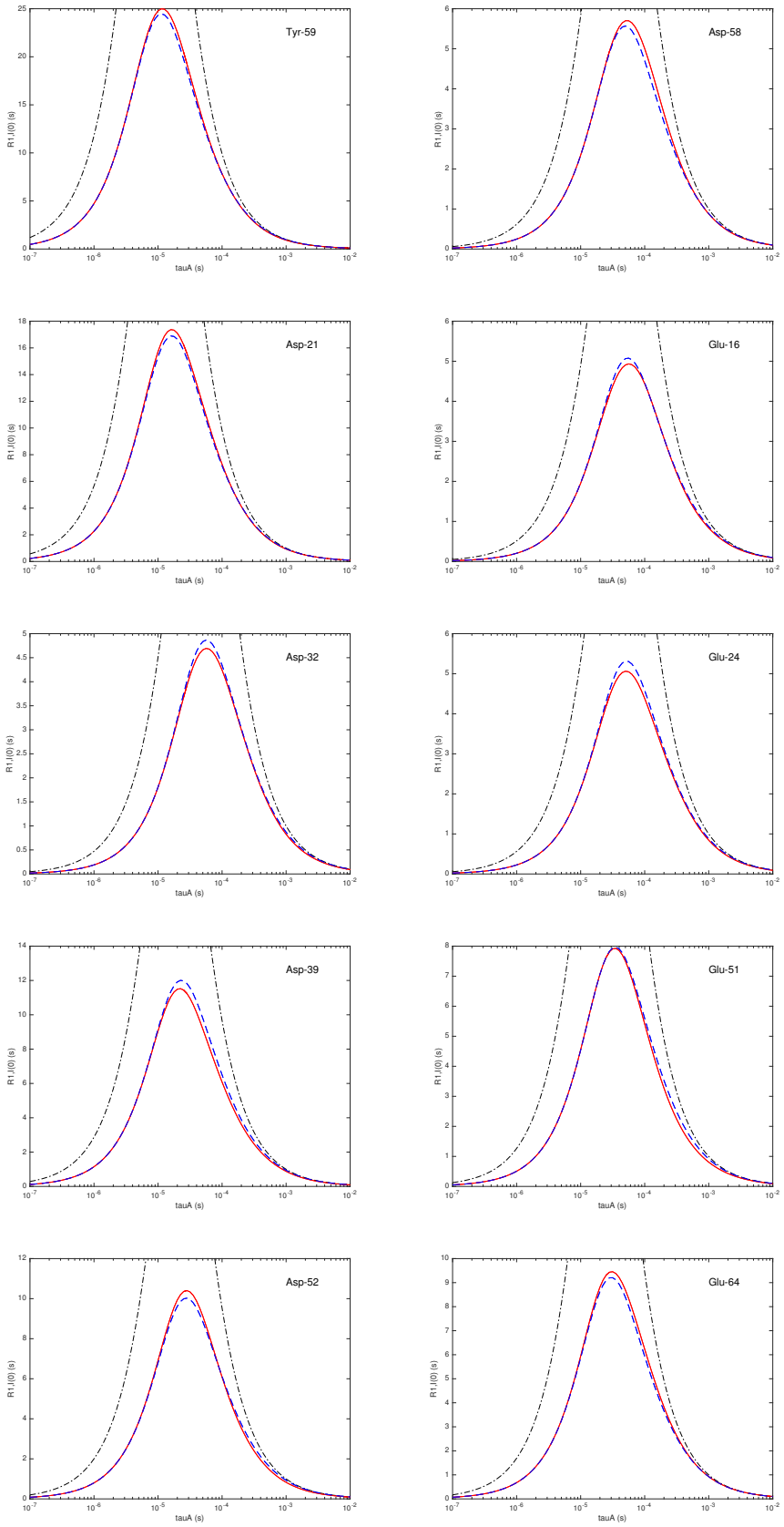

Figure S3: $R_{1,I}(0)$ versus τ_{A} for labile protons in Tyr, Asp and Glu side-chains in ubiquitin coupled to three nonlabile protons without SDCs, computed from the SLE (red solid), GSRE (blue dash) and ESE (black dash-dot) theories.

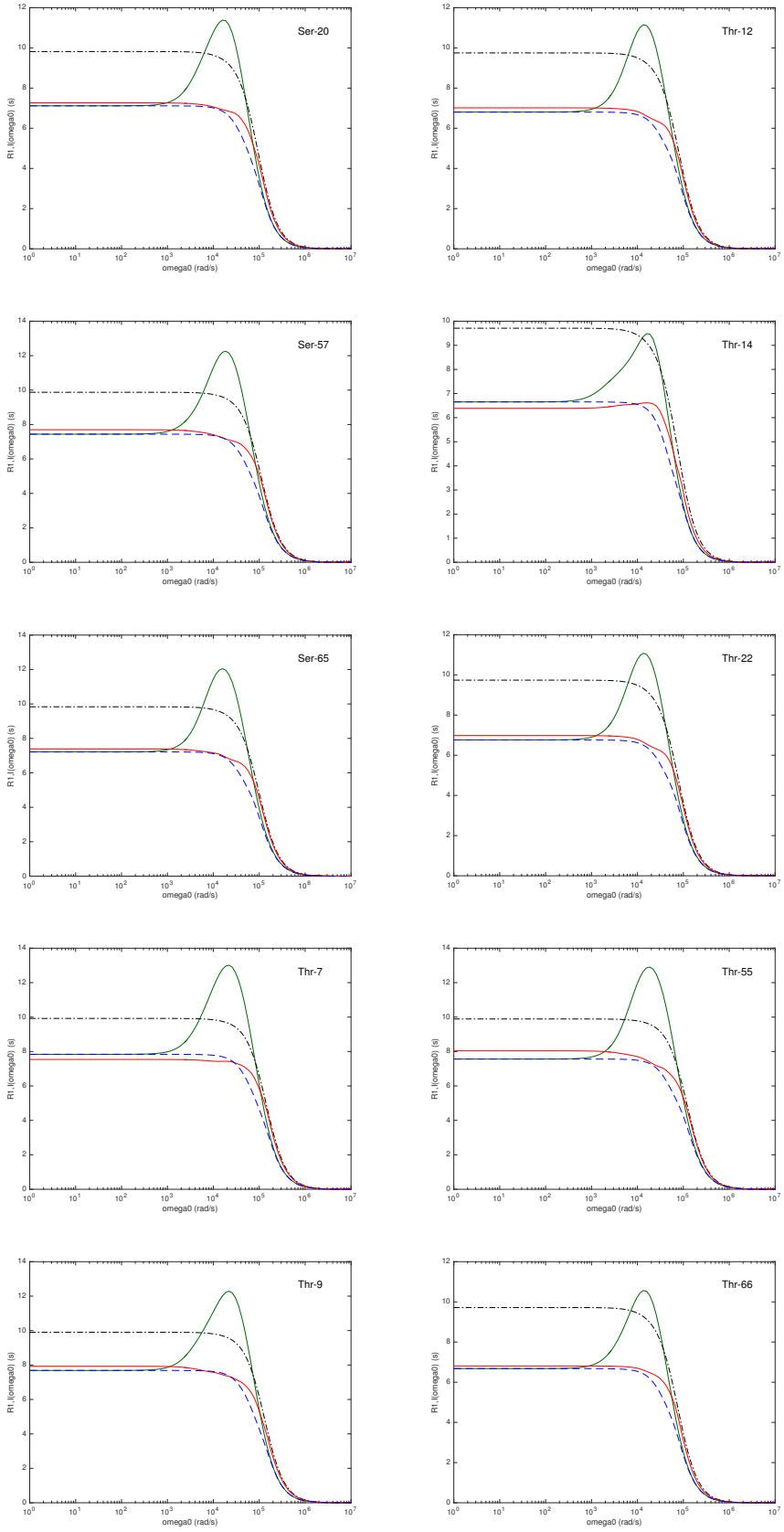

Figure S4: $R_{1,I}(\omega_0)$ dispersion with $\tau_A = 10^{-4}$ s for labile protons in Ser and Thr side-chains in ubiquitin coupled to three nonlabile protons without SDCs, computed from the SLE (red solid), GSRE without SND (green solid), GSRE with SND (blue dash) and ESE (black dash-dot) theories.

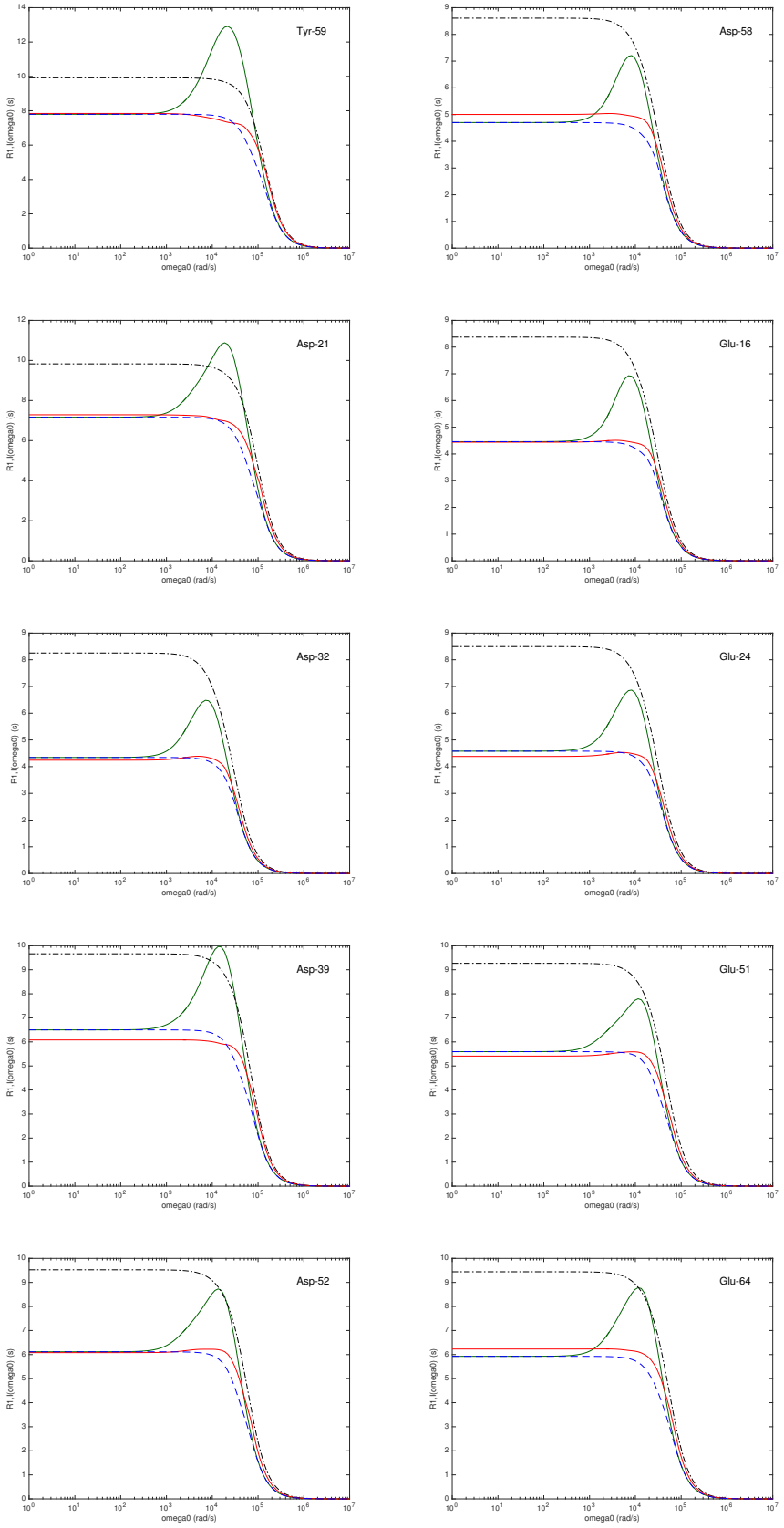

Figure S5: $R_{1,I}(\omega_0)$ dispersion with $\tau_A = 10^{-4}$ s for labile protons in Tyr, Asp and Glu side-chains in ubiquitin coupled to three nonlabile protons without SDCs, computed from the SLE (red solid), GSRE without SND (green solid), GSRE with SND (blue dash) and ESE (black dash-dot) theories.

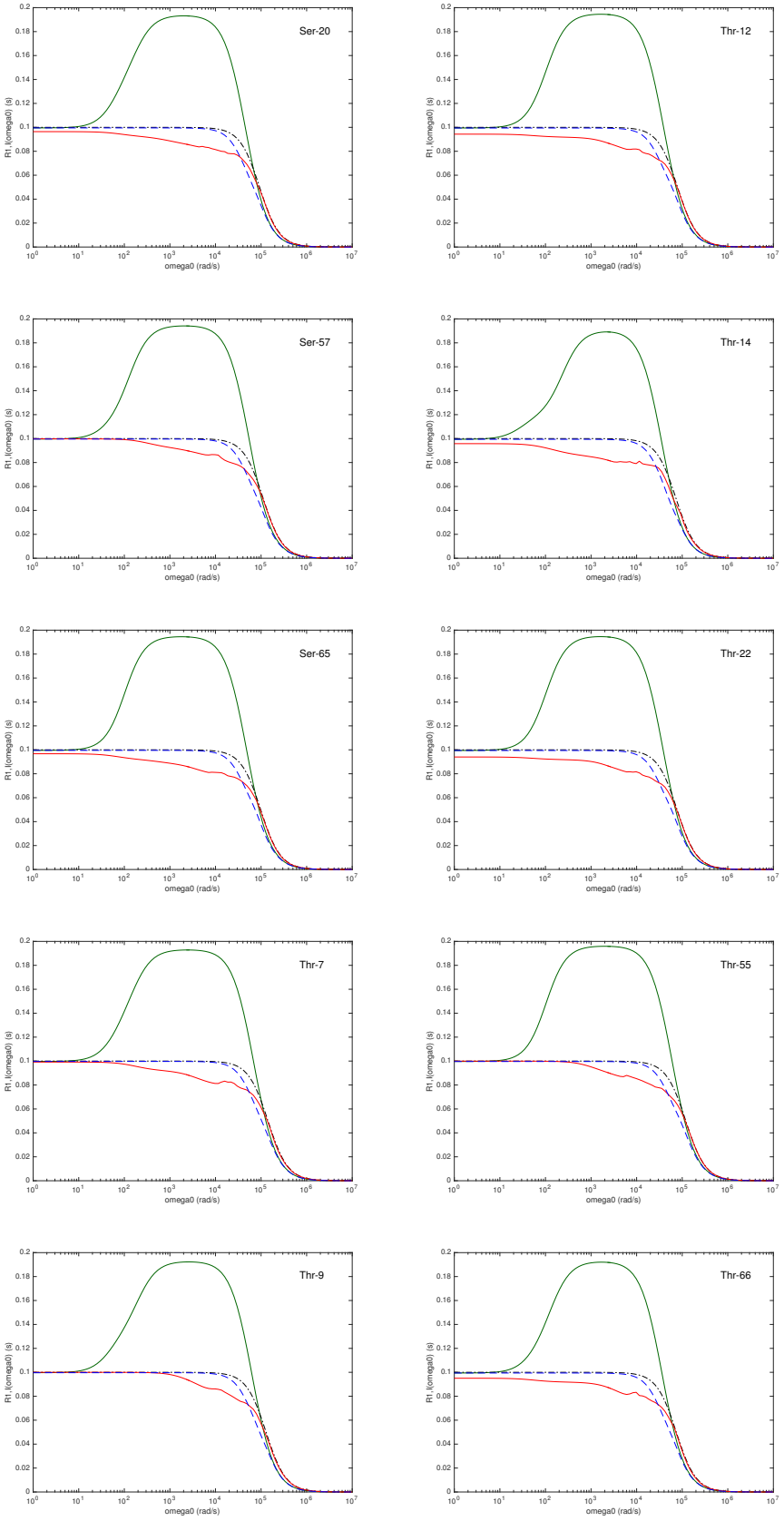

Figure S6: $R_{1,I}(\omega_0)$ dispersion with $\tau_A = 10^{-2}$ s for labile protons in Ser and Thr side-chains in ubiquitin coupled to three nonlabile protons without SDCs, computed from the SLE (red solid), GSRE without SND (green solid), GSRE with SND (blue dash) and ESE (black dash-dot) theories.

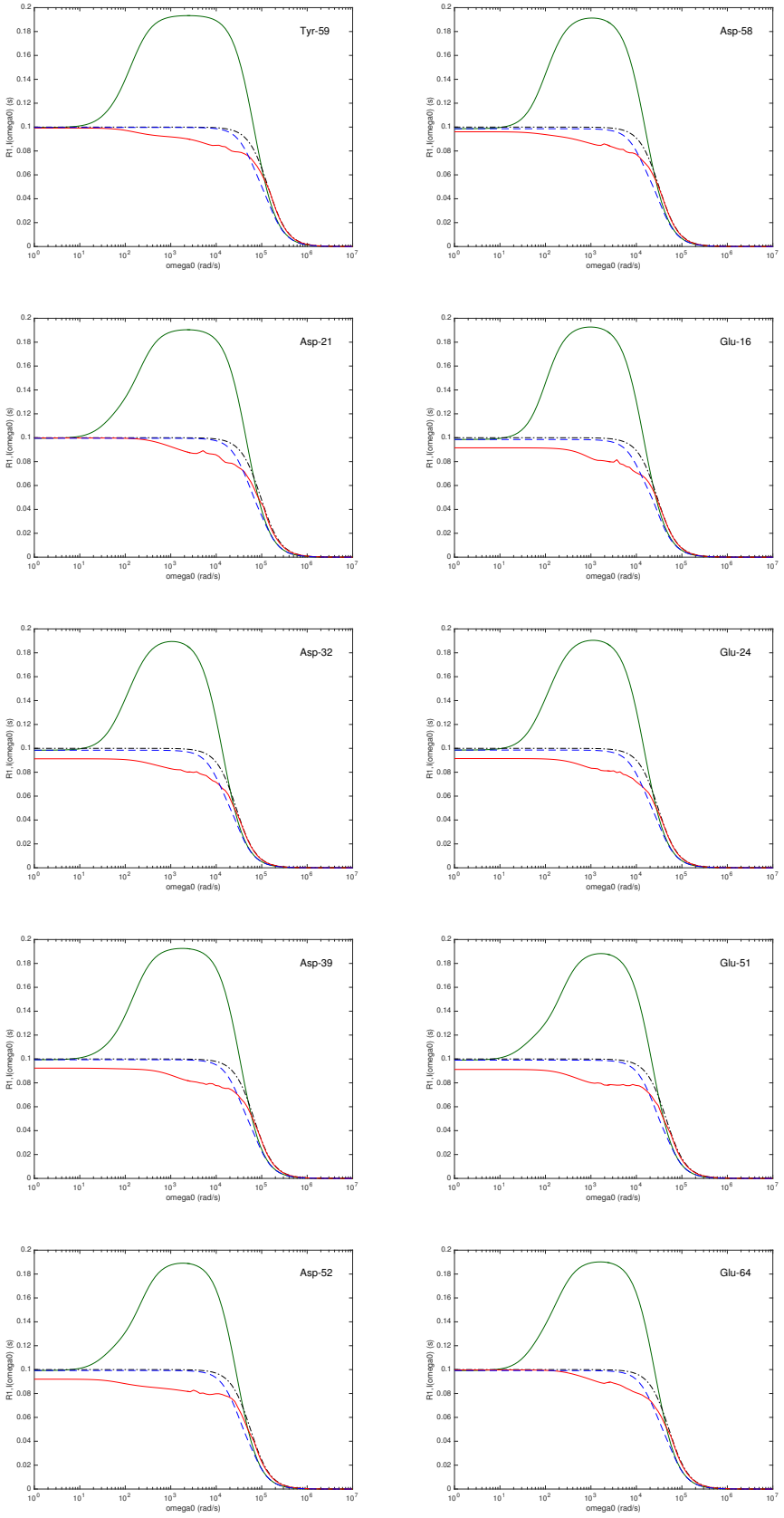

Figure S7: $R_{1,I}(\omega_0)$ dispersion with $\tau_A = 10^{-2}$ s for labile protons in Tyr, Asp and Glu side-chains in ubiquitin coupled to three nonlabile protons without SDCs, computed from the SLE (red solid), GSRE without SND (green solid), GSRE with SND (blue dash) and ESE (black dash-dot) theories.

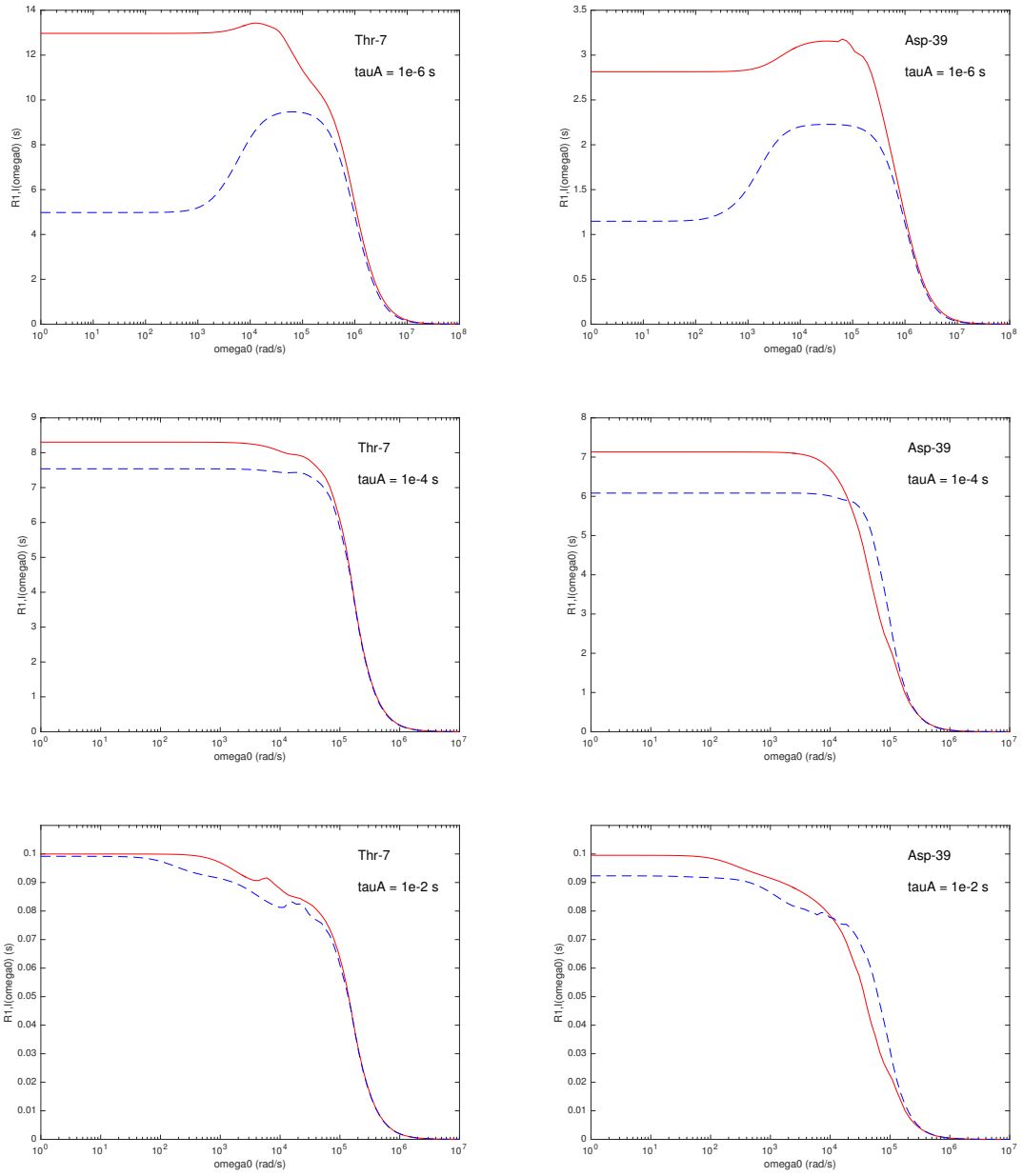

Figure S8: $R_{1,I}(\omega_0)$ dispersion with $\tau_A = 10^{-6}$ s (top row), 10^{-4} s (middle row) and 10^{-2} s (bottom row) for labile protons in Thr-7 (left column) and Asp-39 (right column) side-chains in ubiquitin coupled to three nonlabile protons, computed from the SLE theory with SDCs (red solid) and without SDCs (blue dash).

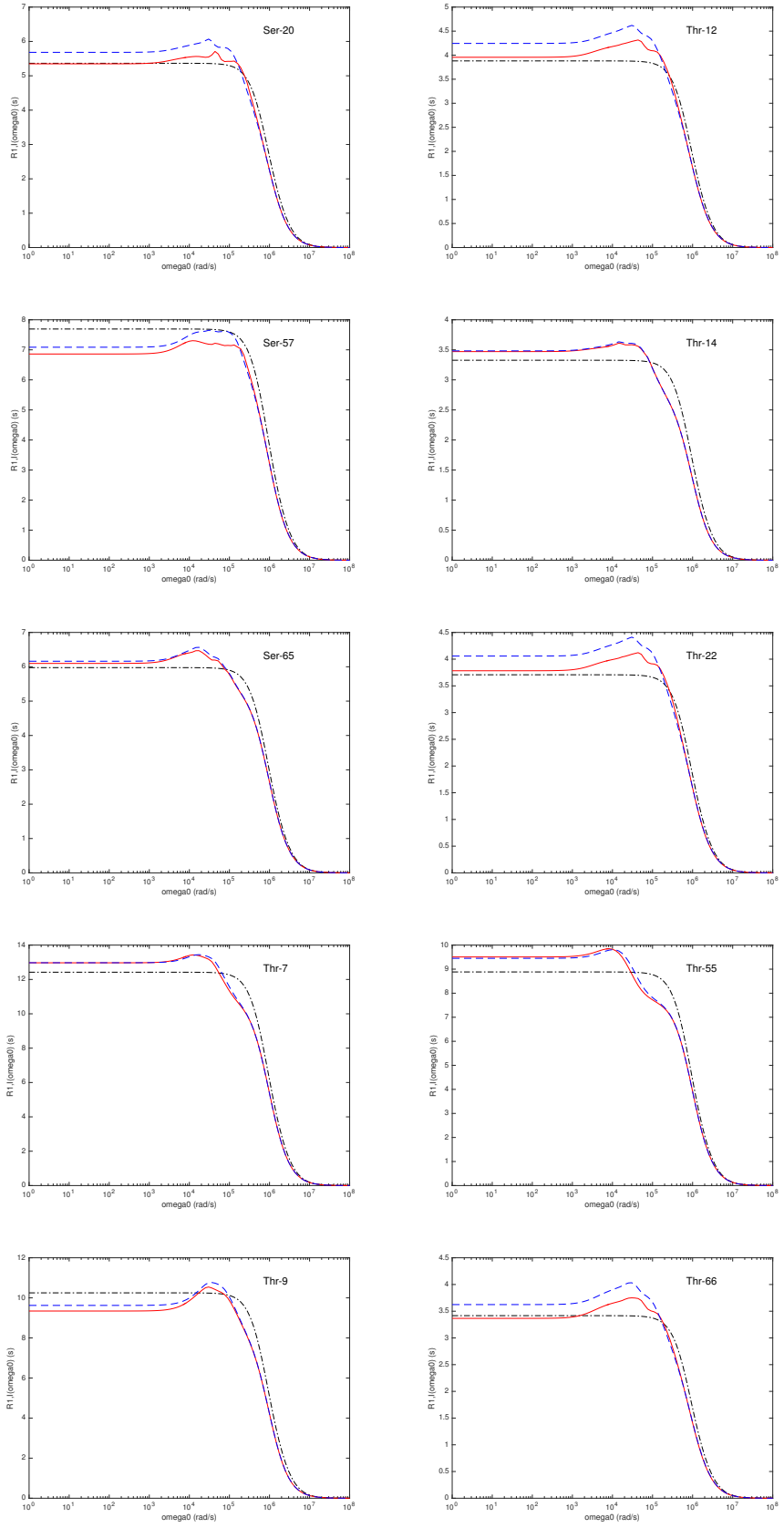

Figure S9: $R_{1,I}(\omega_0)$ dispersion with $\tau_A = 10^{-6}$ s for labile protons in Ser and Thr side-chains in ubiquitin coupled to three nonlabile protons with SDCs, computed from the SLE (red solid), GSRE (blue dash) and ESE (black dash-dot) theories.

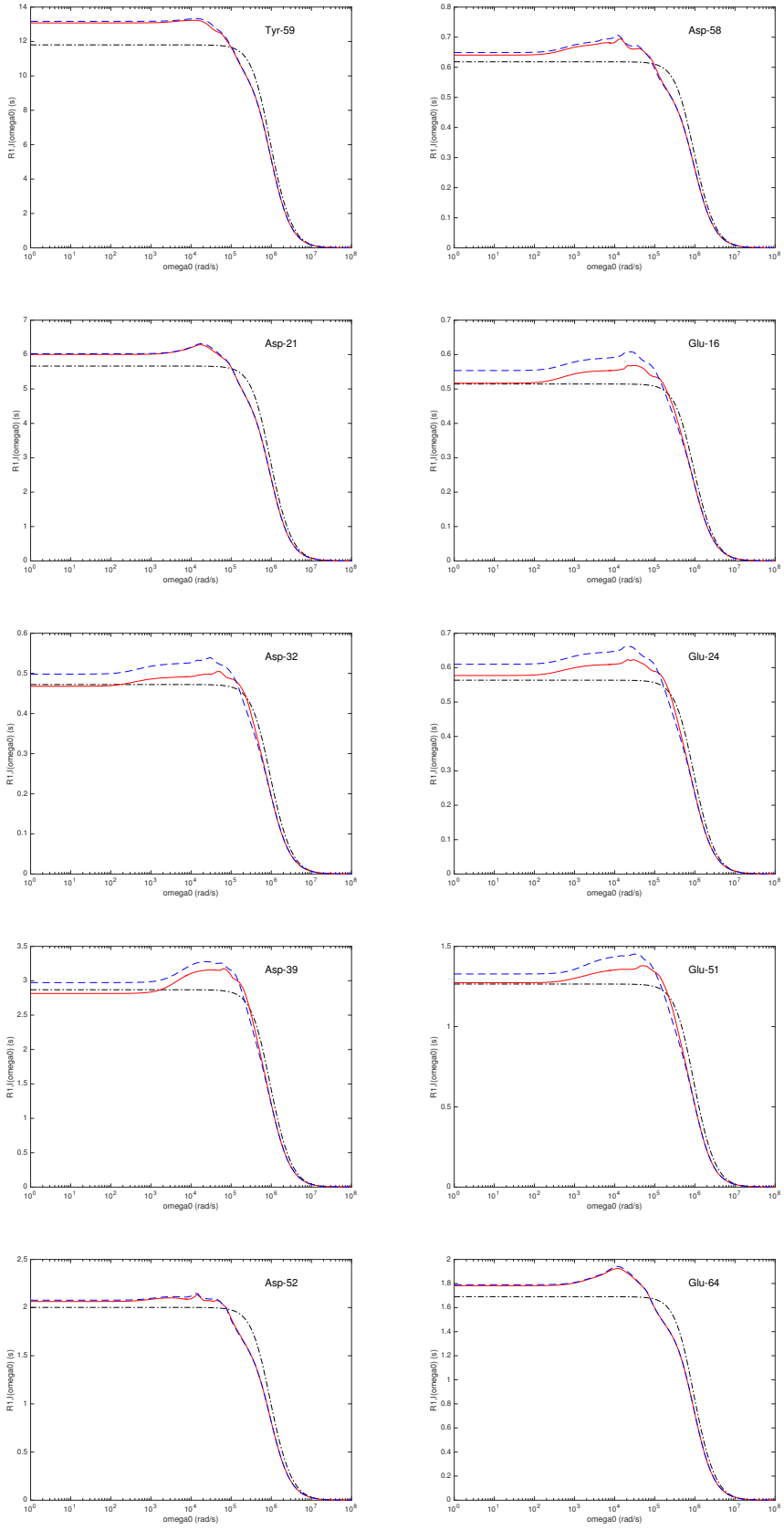

Figure S10: $R_{1,I}(\omega_0)$ dispersion with $\tau_A = 10^{-6}$ s for labile protons in Tyr, Asp and Glu side-chains in ubiquitin coupled to three nonlabile protons with SDCs, computed from the SLE (red solid), GSRE (blue dash) and ESE (black dash-dot) theories.

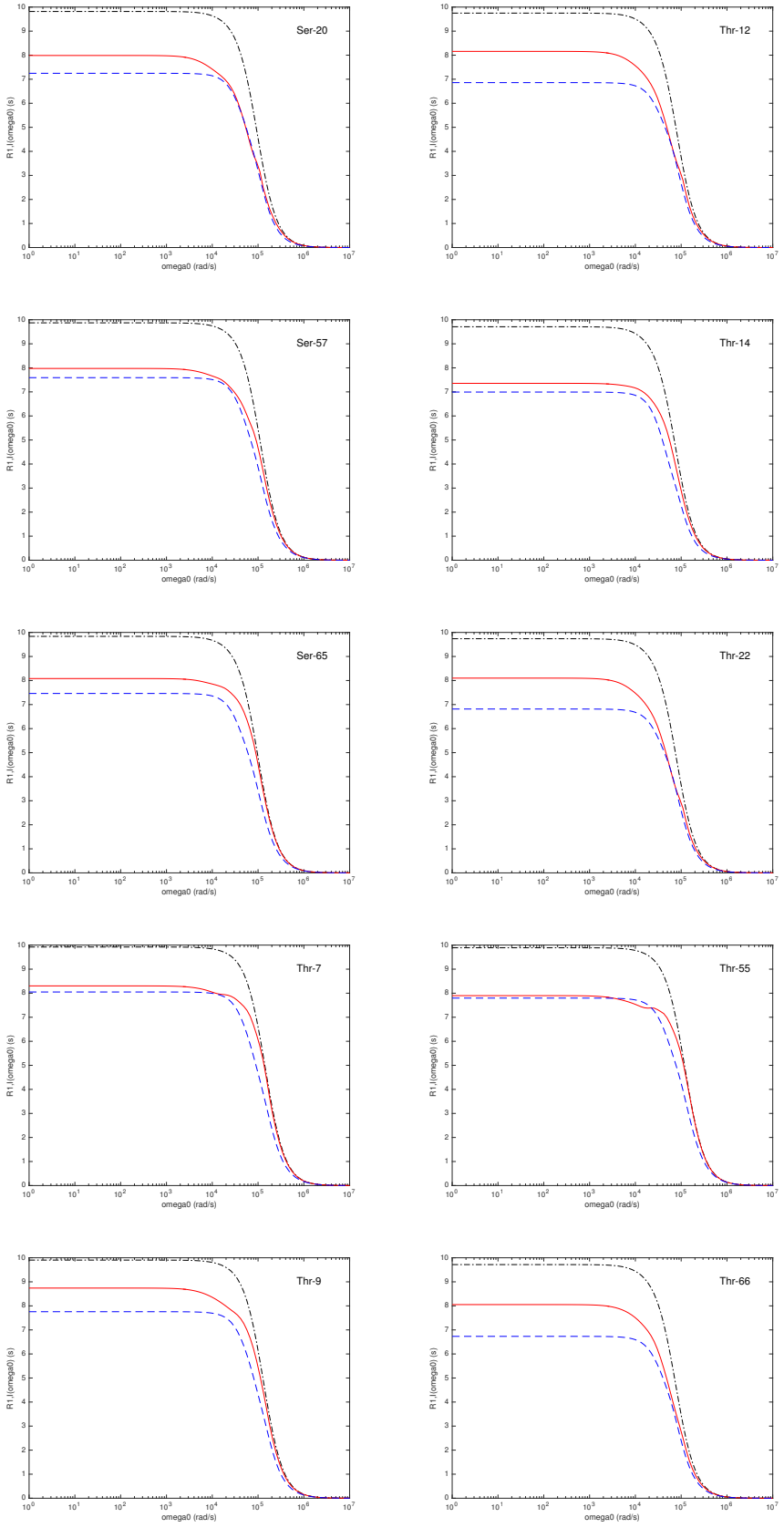

Figure S11: $R_{1,I}(\omega_0)$ dispersion with $\tau_A = 10^{-4}$ s for labile protons in Ser and Thr side-chains in ubiquitin coupled to three nonlabile protons with SDCs, computed from the SLE (red solid), GSRE (blue dash) and ESE (black dash-dot) theories.

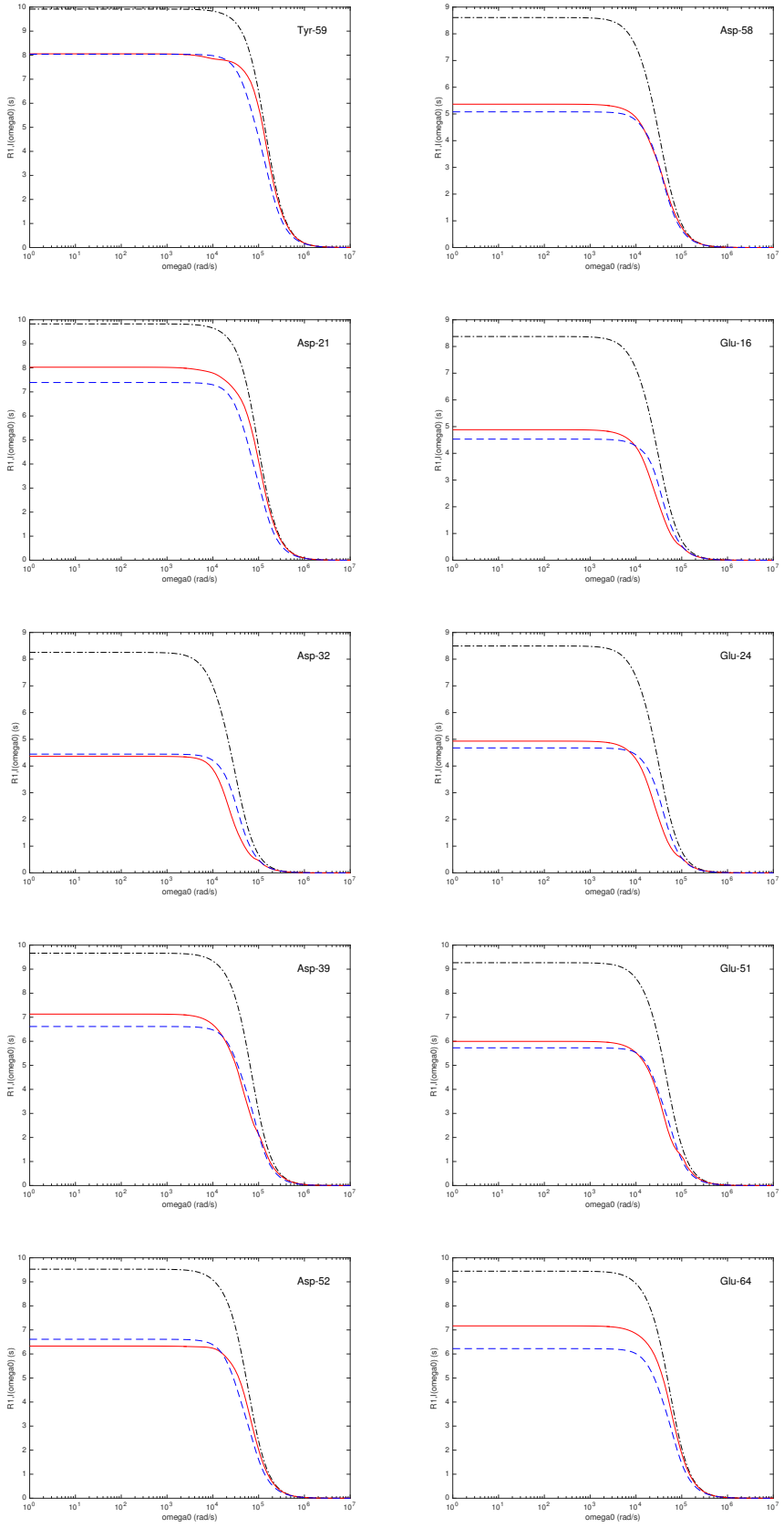

Figure S12: $R_{1,I}(\omega_0)$ dispersion with $\tau_A = 10^{-4}$ s for labile protons in Tyr, Asp and Glu side-chains in ubiquitin coupled to three nonlabile protons with SDCs, computed from the SLE (red solid), GSRE (blue dash) and ESE (black dash-dot) theories.

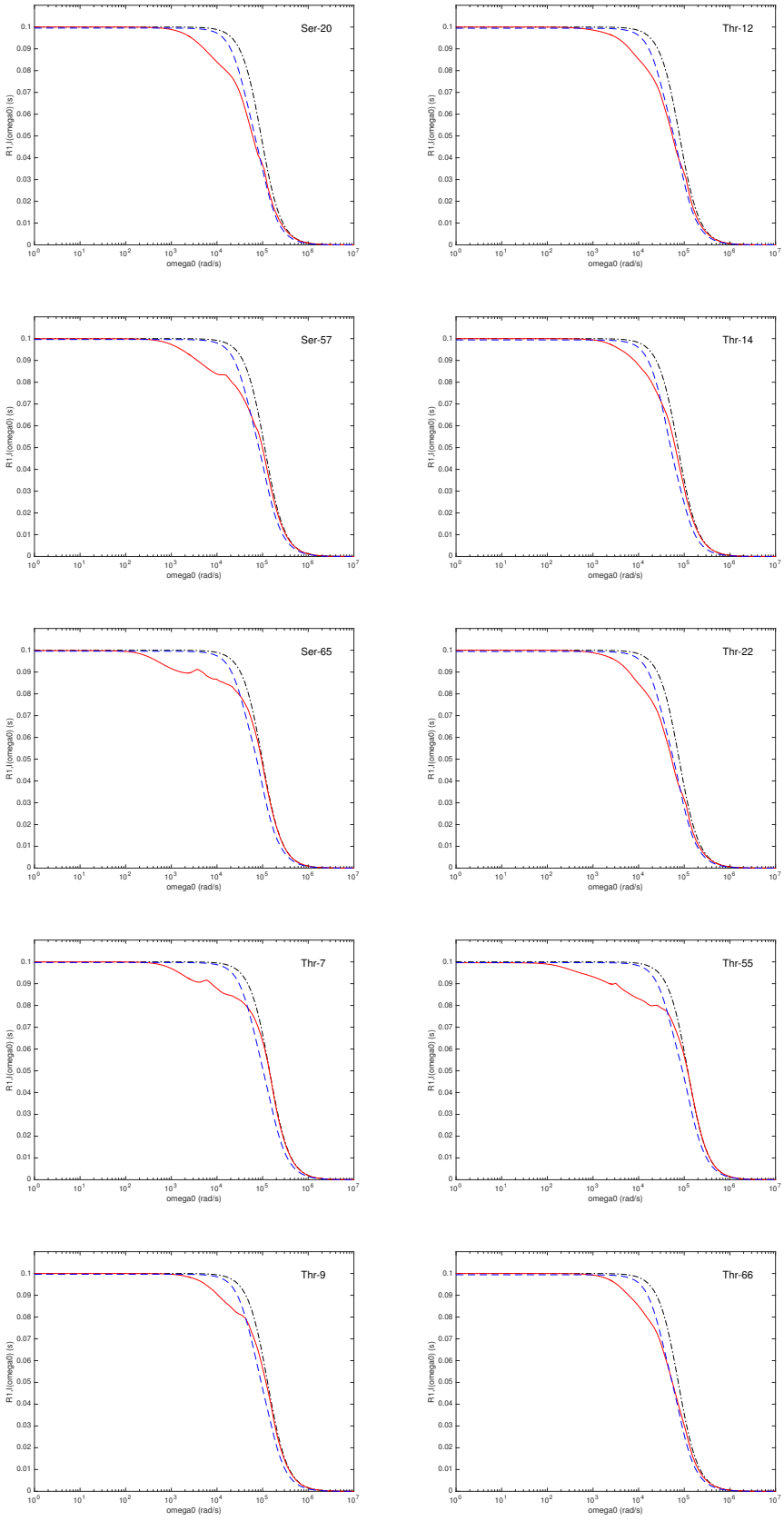

Figure S13: $R_{1,I}(\omega_0)$ dispersion with $\tau_A = 10^{-2}$ s for labile protons in Ser and Thr sidechains in ubiquitin coupled to three nonlabile protons with SDCs, computed from the SLE (red solid), GSRE (blue dash) and ESE (black dash-dot) theories.

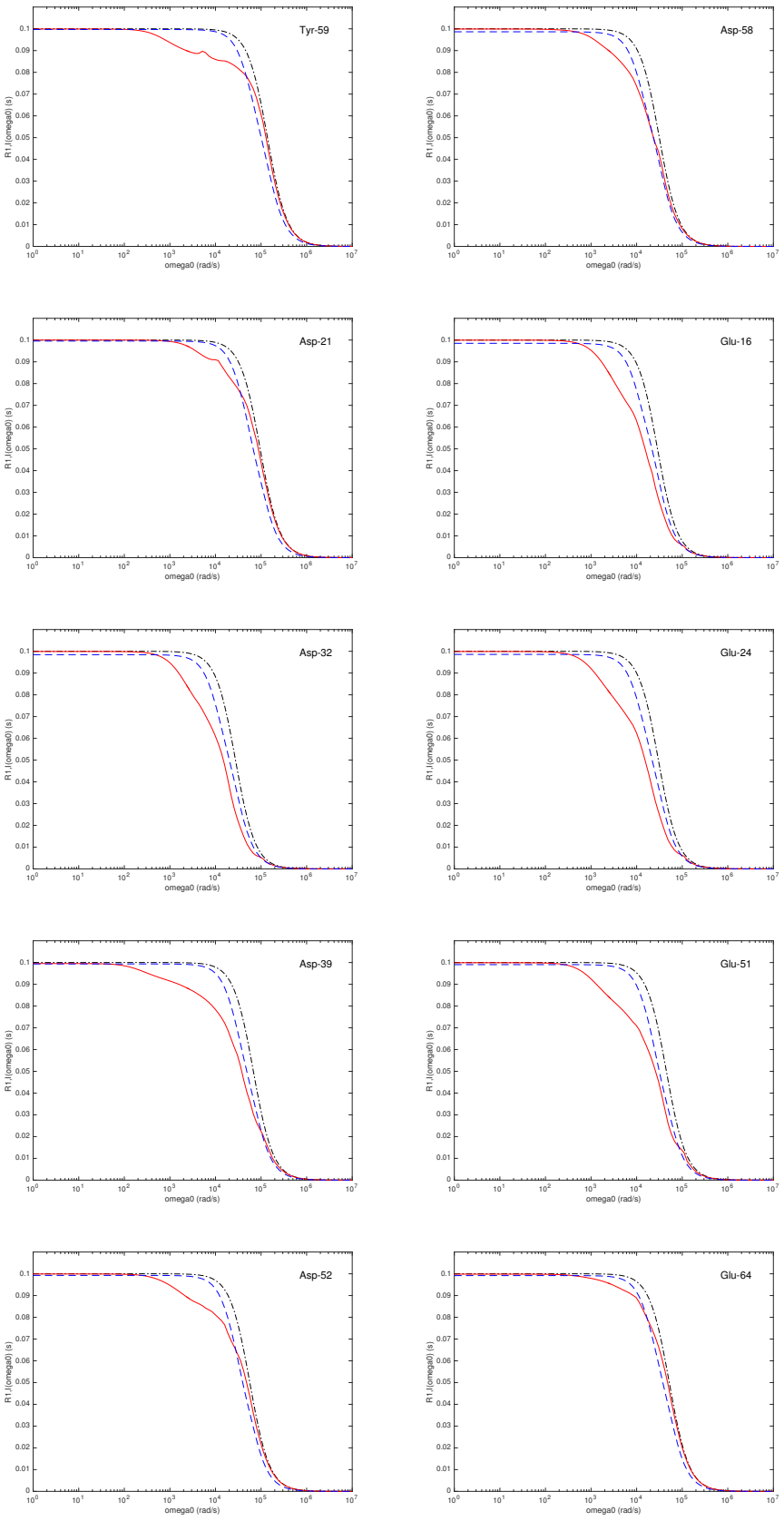

Figure S14: $R_{1,I}(\omega_0)$ dispersion with $\tau_A = 10^{-2}$ s for labile protons in Tyr, Asp and Glu side-chains in ubiquitin coupled to three nonlabile protons with SDCs, computed from the SLE (red solid), GSRE (blue dash) and ESE (black dash-dot) theories.

2. Exchange case $ISP_2{-}IS$

Figure S15 shows that, for the five four-spin systems in Table S4 without SDC, the ZF rate $R_{1,IS}(0)$ computed from the GSRE theory based on the GSDF in Eq. (47) remains very close to the exact $R_{1,IS}(0)$ computed from SLE theory. This is true over the full range of τ_A values, from the MN regime to the USM regime. While the GSRE theory is exact in the MN and USM limits, it remains highly accurate even for $\tau_A = 10^{-5}$ s, erring by at most 2.1 %.

Figures S16 and S17 show that, for the five four-spin systems in Table S4 without SDC, a GSRE theory that incorporates the GSDF in Eq. (47) as well as the SND correction in Eq. (49) removes the spurious secondary dispersion (evident in the green profiles, without SND correction) and brings the GSRE theory into good agreement with the exact SLE theory over the full frequency range and for all τ_A values.

The exact SLE dispersion profiles in Fig. S18, for the internal water molecules W111 and W113 in BPTI coupled to two nonlabile protons, demonstrate the small effect of the SDC for the $ISP_2{-}IS$ case with a dominant $I{-}S$ coupling.

Figure S19 shows that the ZF rate $R_{1,IS}(0)$ computed with the GSDF in Eq. (47) and the renormalized SDC in Eq. (46) almost coincides with the exact (SLE) result, which is not the case for the ESE theory. For $\tau_A = 10^{-6}$ s, the GSRE theory errs by at most 0.2 % for the five cases. Although not evident from Fig. S19, the GSRE theory is also highly accurate in the USM regime; for $\tau_A = 10^{-2}$ s the GSRE theory errs by at most 0.7 % for the five cases.

Figures S20 and S21 show $R_{1,IS}(\omega_0)$ dispersion profiles for $\tau_A = 10^{-6}$, 10^{-5}, 10^{-4} and 10^{-2} s, comparing the predictions of the approximate GSRE and ESE theories with the exact SLE theory. For $\tau_A = 10^{-6}$ s, the GSRE theory is nearly exact and, unlike the ESE theory, it reproduces the tiny hump in the profile for W128. For $\tau_A = 10^{-5}$ s, the GSRE theory remains highly accurate, although the primary dispersion step is slightly stretched to low field. For $\tau_A = 10^{-4}$ s, the picture is much the same as for $\tau_A = 10^{-5}$ s, although the difference between the GSRE and ESE theories is not so large. For $\tau_A = 10^{-2}$ s, in the USM regime, all three theories predict that $R_{1,I}(0) = P_A/\tau_A$ or very nearly so. The SLE profile exhibits a depression with fine structure in the LF regime, features that are not captured by the approximate theories.

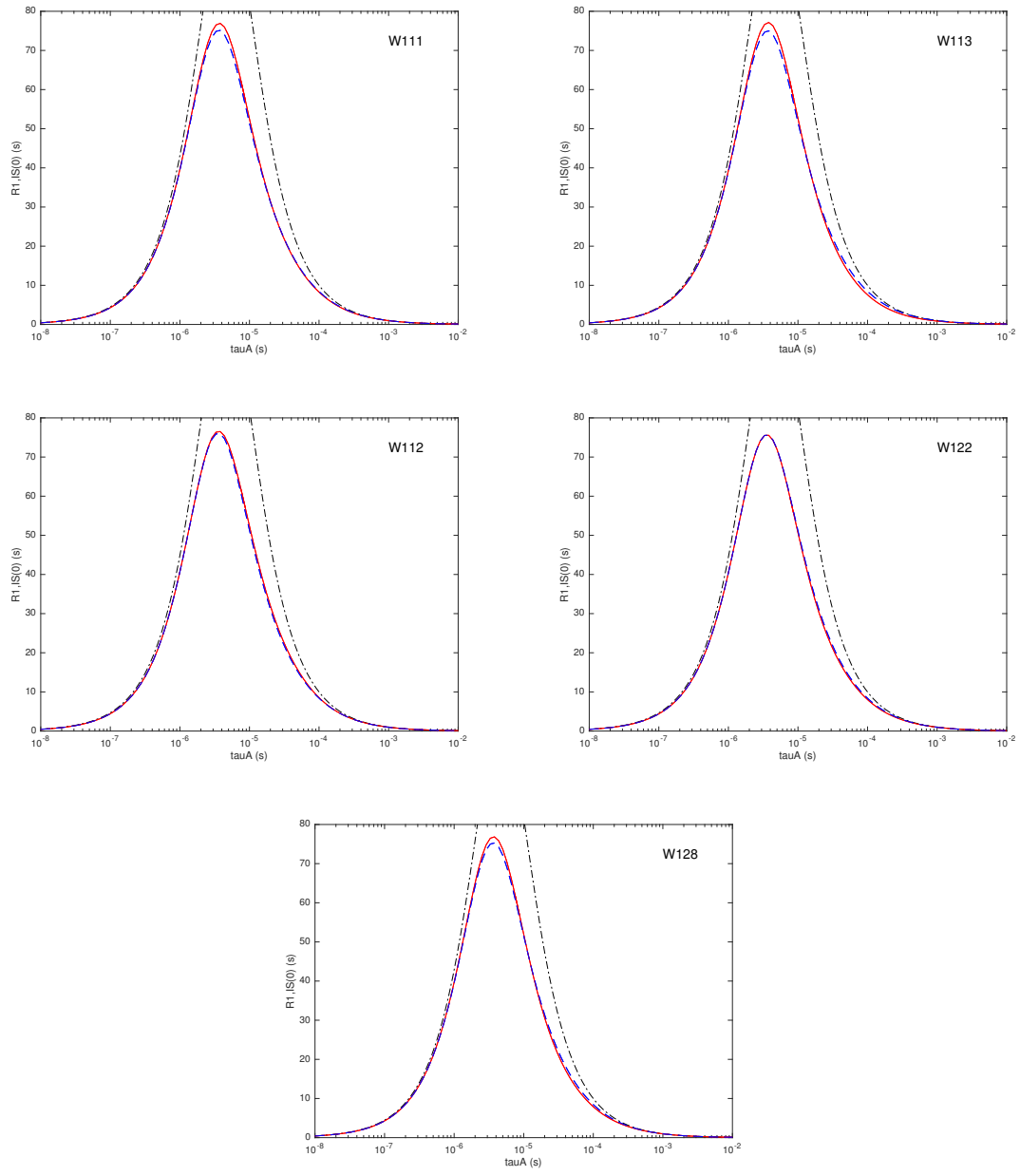

Figure S15: ZF rate $R_{1,IS}(0)$ versus τ_{A} for internal-water protons in BPTI and ubiquitin coupled to two nonlabile protons without SDC, computed from the SLE (red solid), GSRE (blue dash) and ESE (black dash-dot) theories.

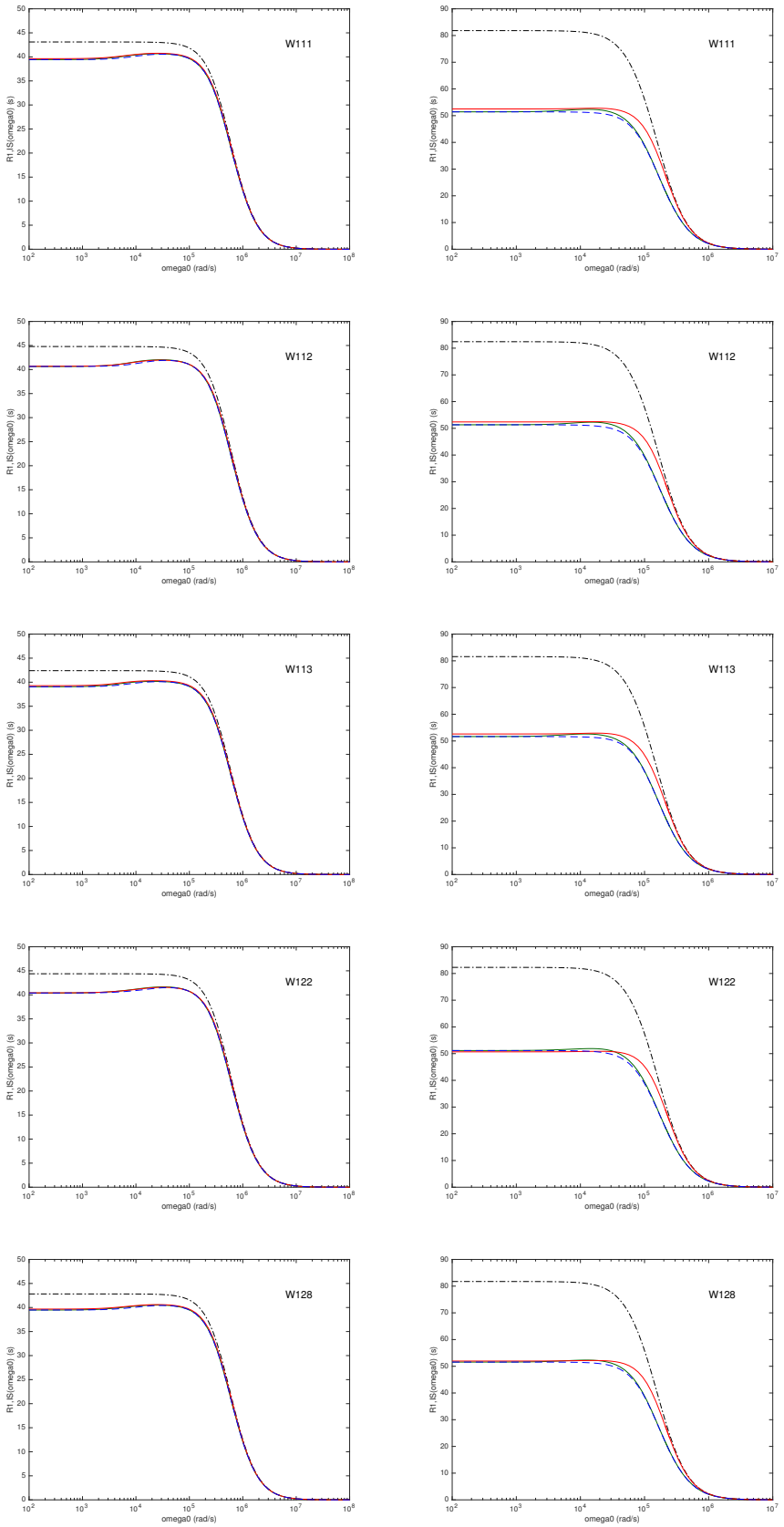

Figure S16: $R_{1,IS}(\omega_0)$ dispersion with $\tau_A = 10^{-6}$ s (left column) or 10^{-5} s (right column) for internal-water protons in BPTI and ubiquitin coupled to two nonlabile protons without SDC, computed from the SLE (red solid), GSRE without SND (green solid), GSRE with SND (blue dash) and ESE (black dash-dot) theories.

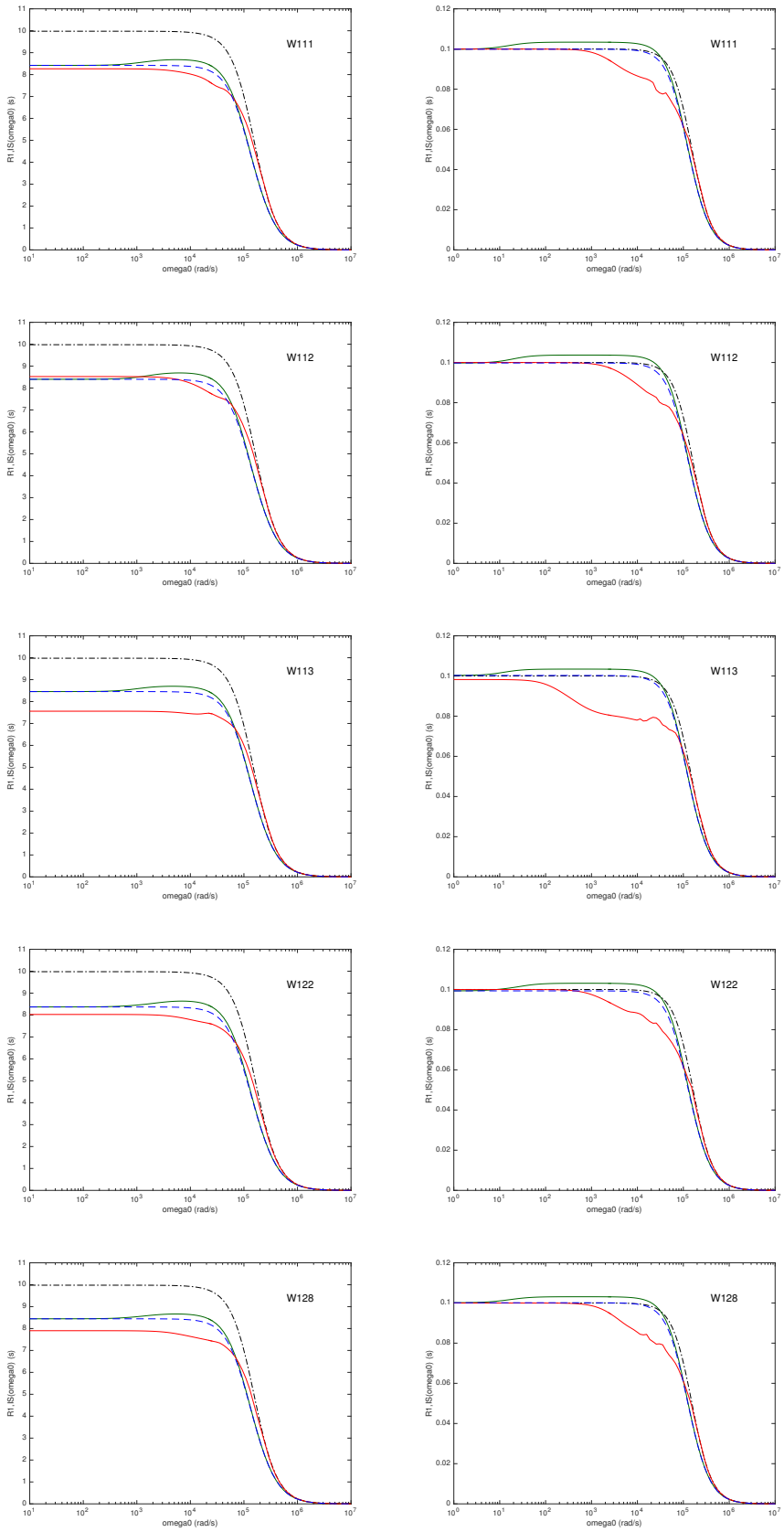

Figure S17: $R_{1,IS}(\omega_0)$ dispersion with $\tau_A = 10^{-4}$ s (left column) or 10^{-2} s (right column) for internal-water protons in BPTI and ubiquitin coupled to two nonlabile protons without SDC, computed from the SLE (red solid), GSRE without SND (green solid), GSRE with SND (blue dash) and ESE (black dash-dot) theories.

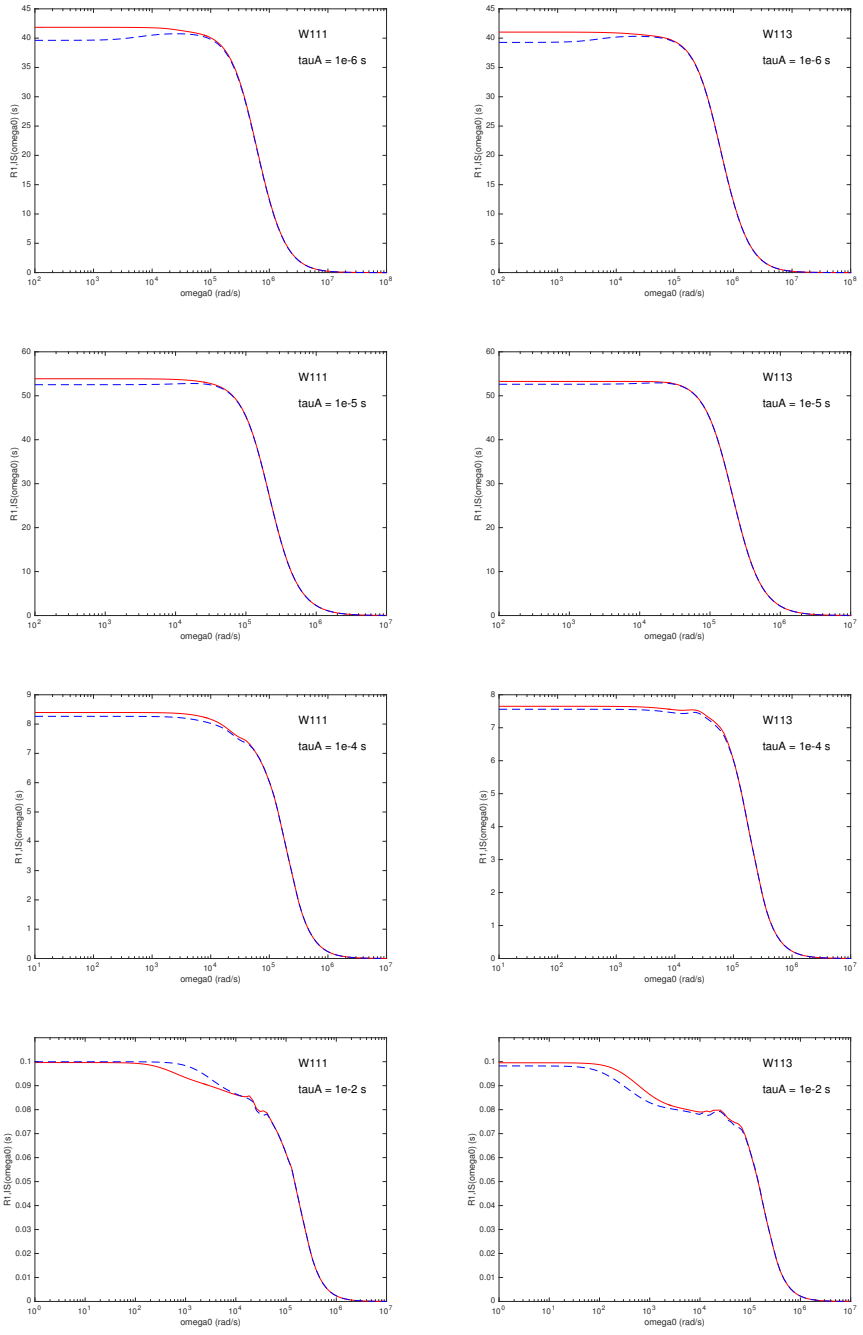

Figure S18: $R_{1,IS}(\omega_0)$ dispersion with $\tau_A = 10^{-6}$ s (top row), 10^{-5} s, 10^{-4} s or 10^{-2} s (bottom row) for internal water molecules W111 (left column) and W113 (right column) in BPTI coupled to two nonlabile protons, computed from SLE theory with SDC (red solid) and without SDC (blue dash).

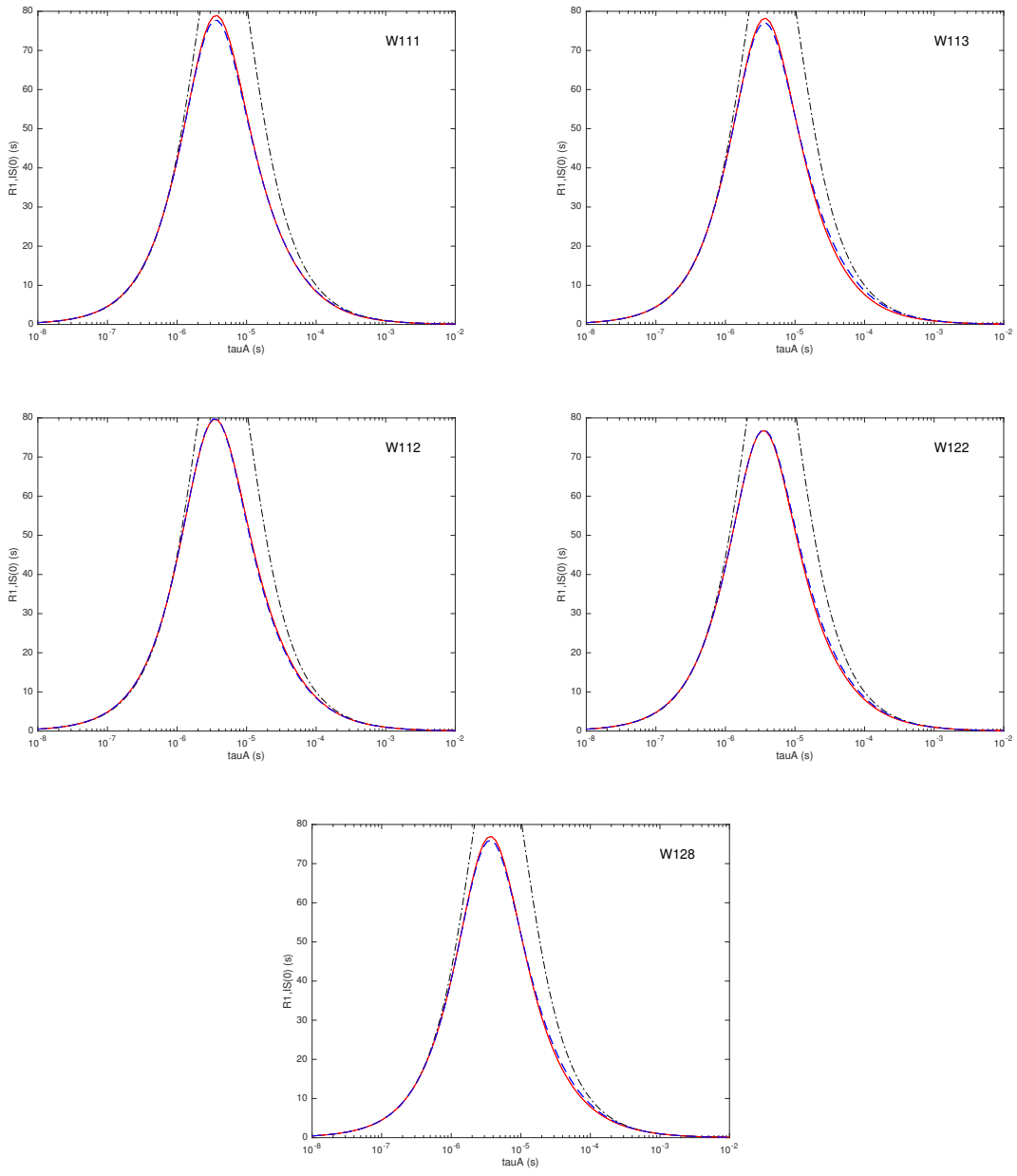

Figure S19: $R_{1,IS}(0)$ versus τ_{A} for internal-water protons in BPTI and ubiquitin coupled to two nonlabile protons, computed from the SLE (red solid), GSRE (blue dash) and ESE (black dash-dot) theories.

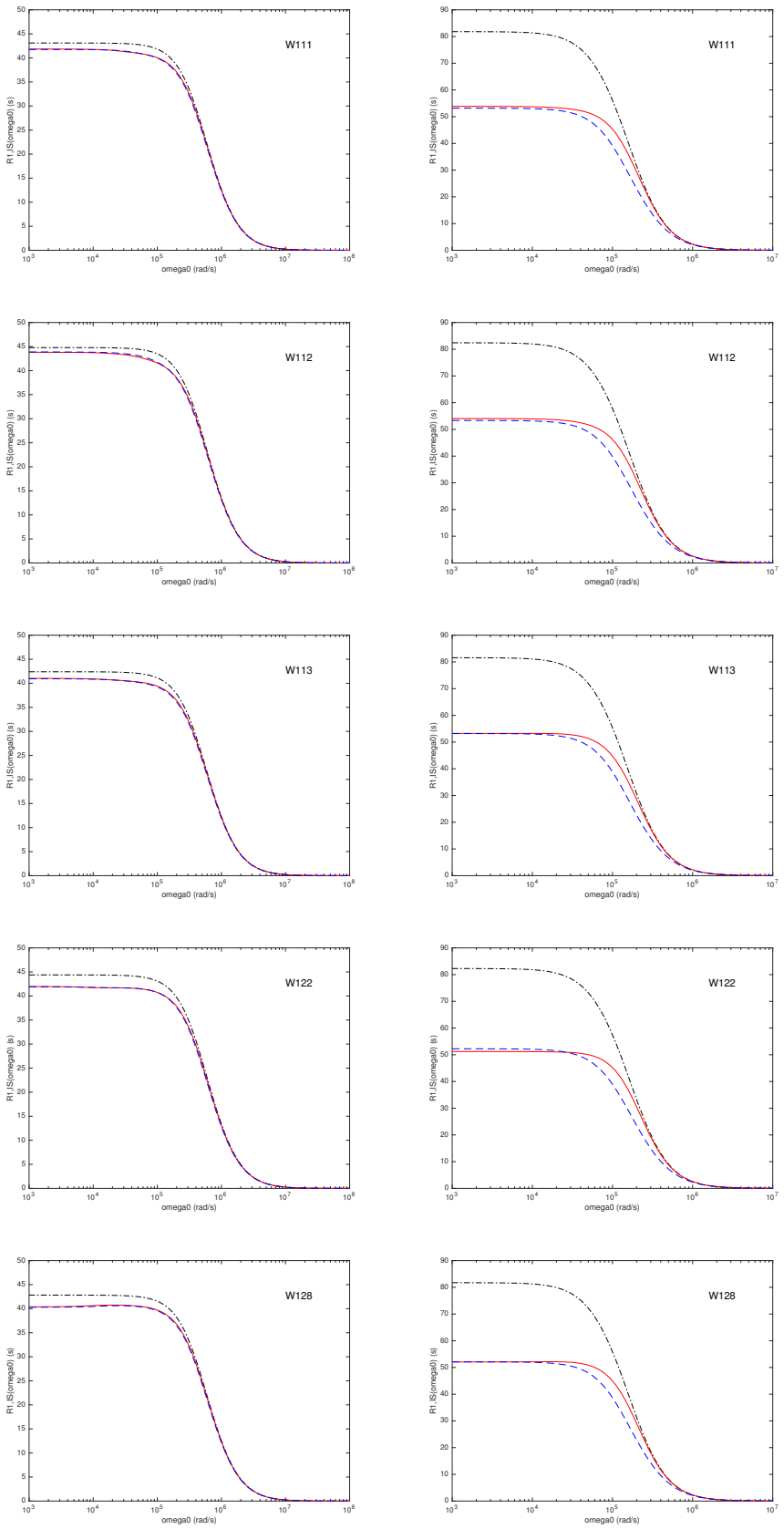

Figure S20: $R_{1,IS}(\omega_0)$ dispersion with $\tau_A = 10^{-6}$ s (left column) or 10^{-5} s (right column) for internal-water protons in BPTI and ubiquitin coupled to two nonlabile protons, computed from the SLE (red solid), GSRE (blue dash) and ESE (black dash-dot) theories.

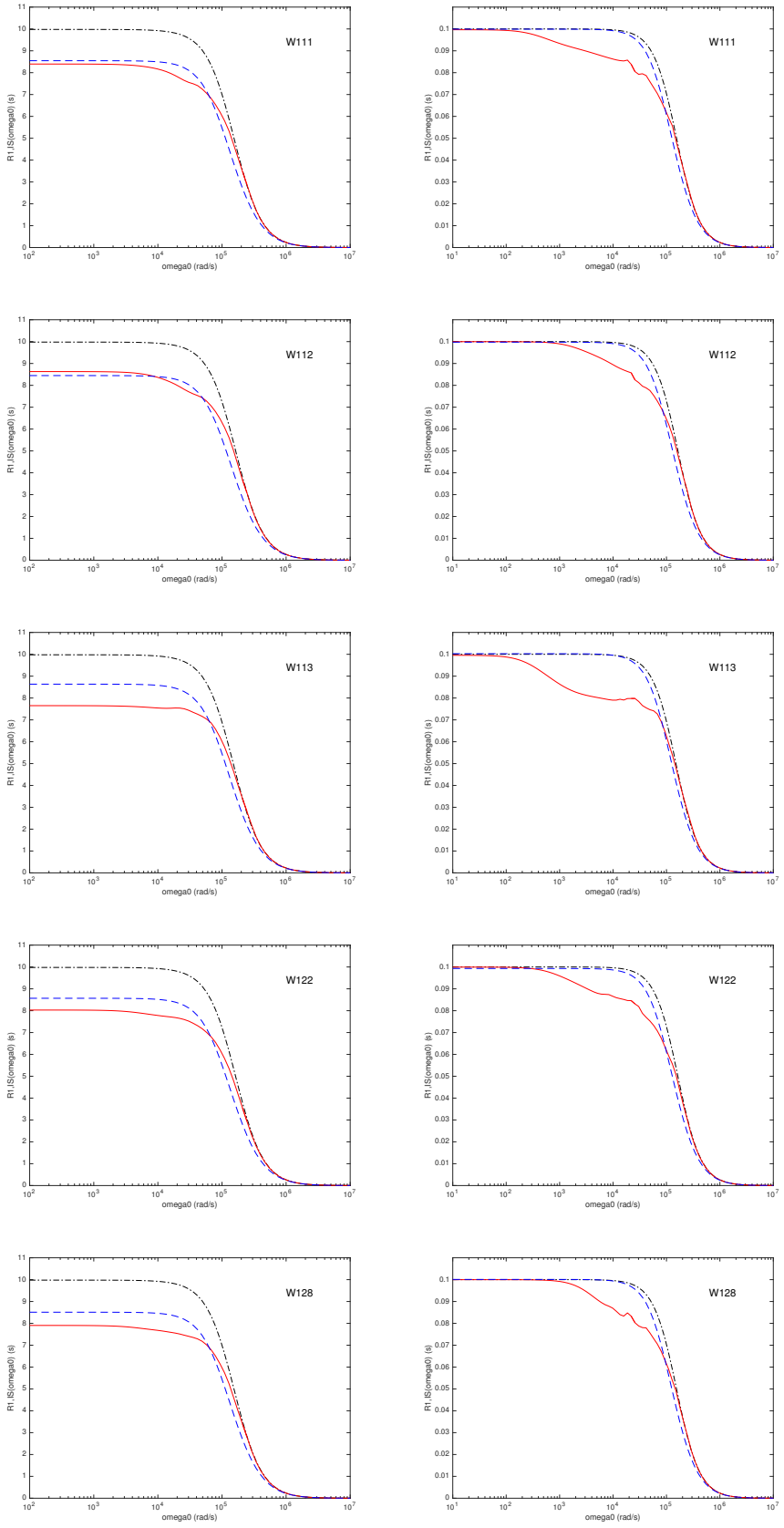

Figure S21: $R_{1,IS}(\omega_0)$ dispersion with $\tau_A = 10^{-4}$ s (left column) or 10^{-2} s (right column) for internal-water protons in BPTI and ubiquitin coupled to two nonlabile protons, computed from the SLE (red solid), GSRE (blue dash) and ESE (black dash-dot) theories.

APPENDIX N: GSRE THEORY FOR LARGER m

In this Appendix, we present dispersion profiles, computed from the multi-spin GSRE theory, for some of the labile protons and internal water molecules listed in Tables S4 and S5 (Appendix L), but now coupled with up to eight nonlabile protons. We also include results from the ESE theory.

1. Exchange case $IP_m - I$

The following figures show $R_{1,I}(\omega_0)$ dispersion profiles for the labile protons in Thr-7, Thr-22 and Asp-39 in ubiquitin coupled to $m = 1 - 8$ nonlabile protons and at $\tau_A = 10^{-6}$ s (Figs. S22 and S23), 10^{-4} s (Figs. S24 and S25) and 10^{-2} s (Figs. S26 and S27). The profiles were computed with the SLE theory for $m = 1$ and 2 and with the GSRE theory for $m = 3 - 8$. The ESE profile for $m = 8$ is also included. In Fig. S23, the profiles at $\tau_A = 10^{-6}$ s are shown normalized by $P_A\,\omega_{D,I}^2\,\tau_A$. In Figs. 25 and 27, the profiles at $\tau_A = 10^{-4}$ and 10^{-2} s are shown normalized by the corresponding ZF rate $R_{1,I}(0)$.

2. Exchange case $ISP_m - IS$

Figure S28 shows the relative fast convergence with m of the ZF rate $R_{1,IS}(0)$ for the $ISP_m - IS$ case with $m = 0 - 12$, and Fig. S29 shows the similarly fast convergence of the shape of the $R_{1,IS}(\omega_0)$ dispersion profile for $m = 0 - 7$. In both figures, we use the internal water W122 in BPTI as an example. The other four internal water molecule in Table S4 give rise to similar results.

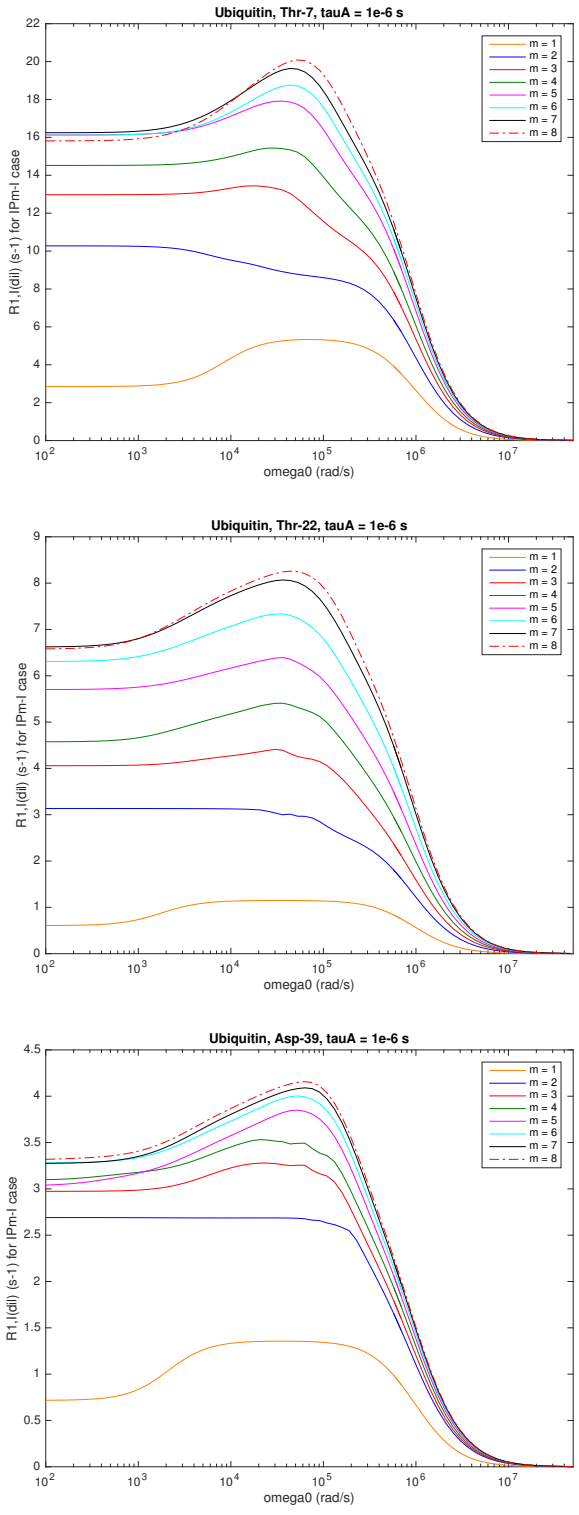

Figure S22: Dispersion profiles, $R_{1,I}(\omega_0)$, with $\tau_A = 10^{-6}$ s for the labile protons in Thr-7 (top), Thr-22 (middle) and Asp-39 (bottom) in ubiquitin coupled to $m = 1 - 8$ nonlabile protons, computed from SLE ($m = 1$ and 2) or GSRE ($m = 3 - 8$) theory.

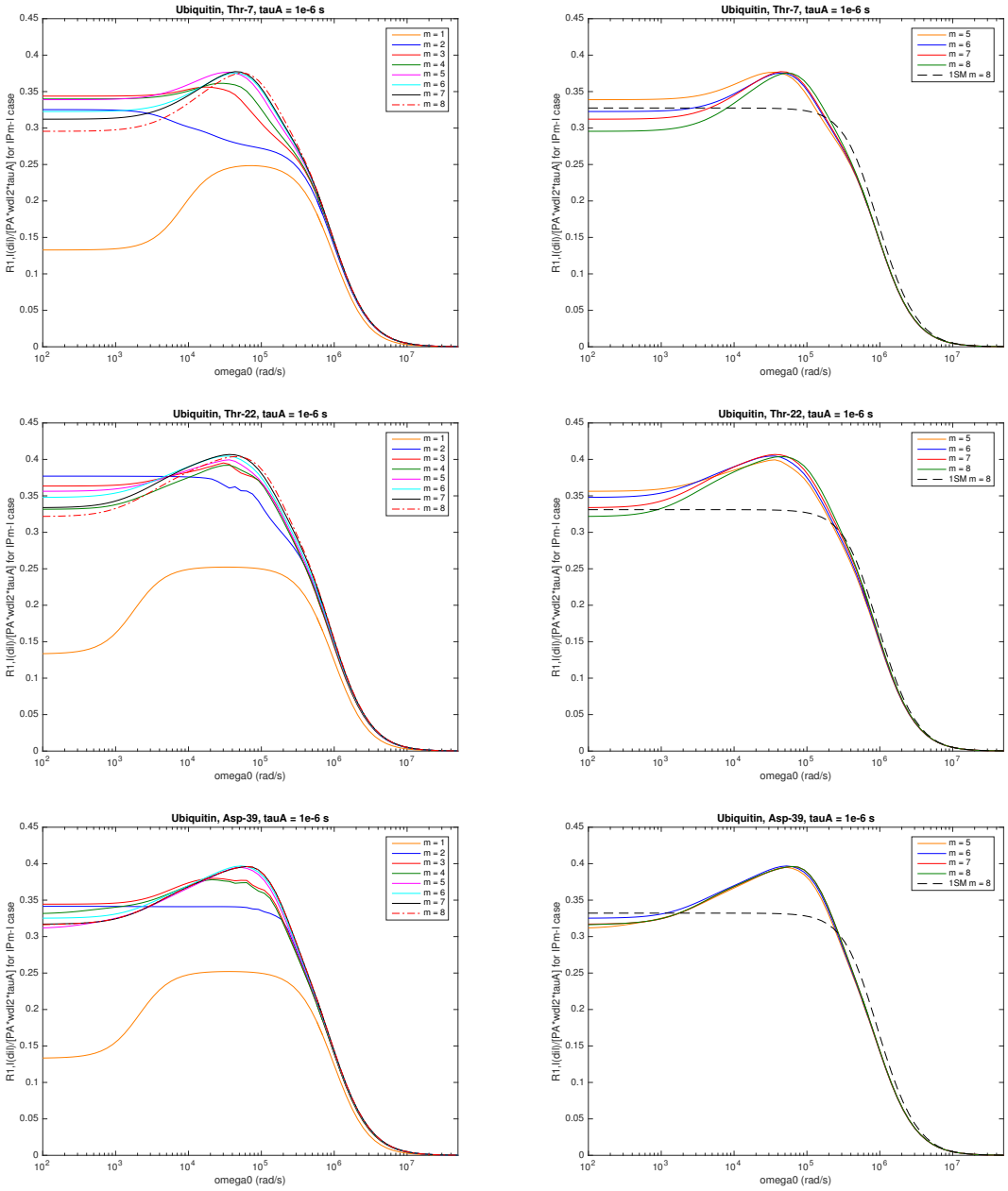

Figure S23: Scaled dispersion profiles, $R_{1,I}(\omega_0)/[P_\mathrm{A}\,\omega_{\mathrm{D},I}^2\,\tau_\mathrm{A}]$, with $\tau_\mathrm{A} = 10^{-6}$ s for the labile protons in Thr-7 (top), Thr-22 (middle) and Asp-39 (bottom) in ubiquitin coupled to $m = 1-8$ nonlabile protons (left column), computed from SLE ($m = 1$ and 2) or GSRE ($m = 3-8$) theory. The right column shows the GSRE profiles for $m = 5-8$ together with the ESE profile for $m = 8$ (dashed).

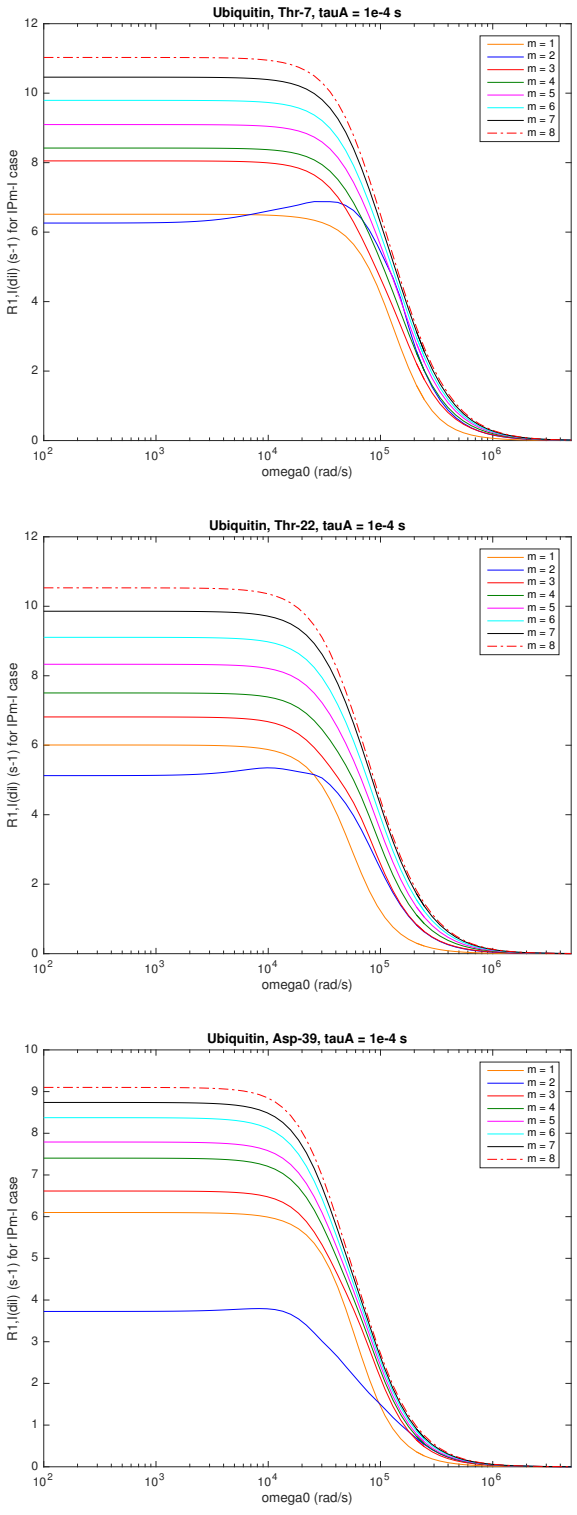

Figure S24: Dispersion profiles, $R_{1,I}(\omega_0)$, with $\tau_A = 10^{-4}$ s for the labile protons in Thr-7 (top), Thr-22 (middle) and Asp-39 (bottom) in ubiquitin coupled to $m = 1 - 8$ nonlabile protons, computed from SLE ($m = 1$ and 2) or GSRE ($m = 3 - 8$) theory.

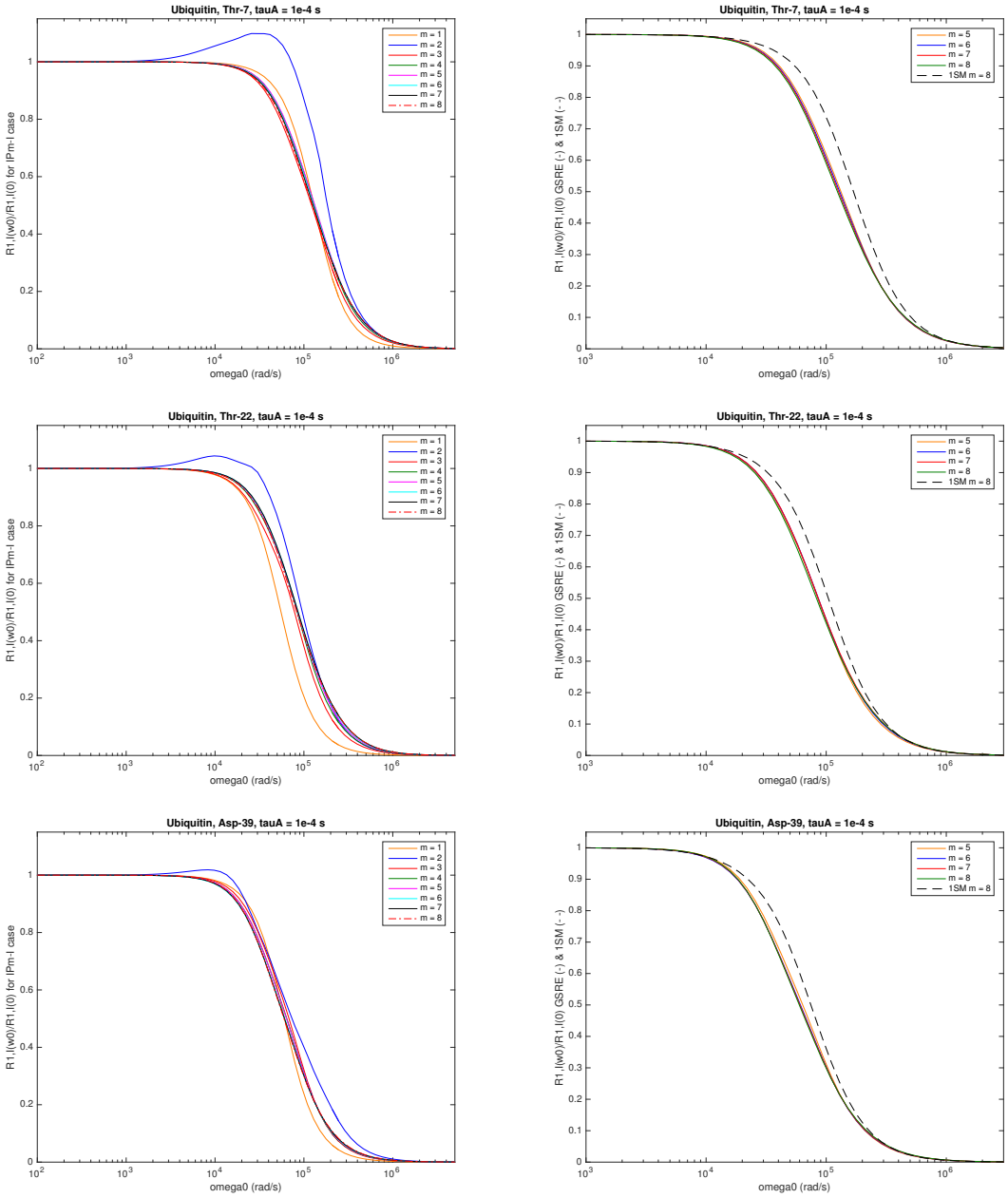

Figure S25: Normalized dispersion profiles, $R_{1,I}(\omega_0)/R_{1,I}(0)$, with $\tau_A = 10^{-4}$ s for the labile protons in Thr-7 (top), Thr-22 (middle) and Asp-39 (bottom) in ubiquitin coupled to $m = 1 - 8$ nonlabile protons (left column), computed from SLE ($m = 1$ and 2) or GSRE ($m = 3 - 8$) theory. The right column shows the GSRE profiles for $m = 5 - 8$ together with the ESE profile for $m = 8$ (dashed).

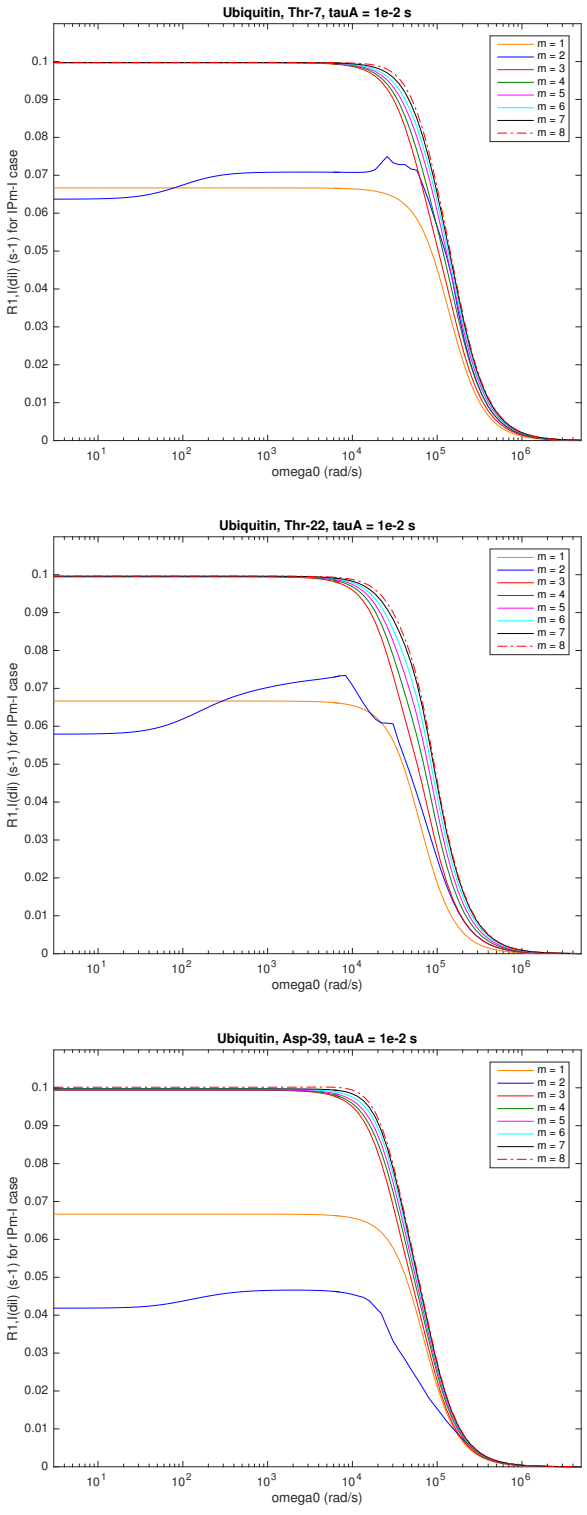

Figure S26: Dispersion profiles, $R_{1,I}(\omega_0)$, with $\tau_{\rm A} = 10^{-2}$ s for the labile protons in Thr-7 (top), Thr-22 (middle) and Asp-39 (bottom) in ubiquitin coupled to $m = 1 - 8$ nonlabile protons, computed from SLE ($m = 1$ and 2) or GSRE ($m = 3 - 8$) theory.

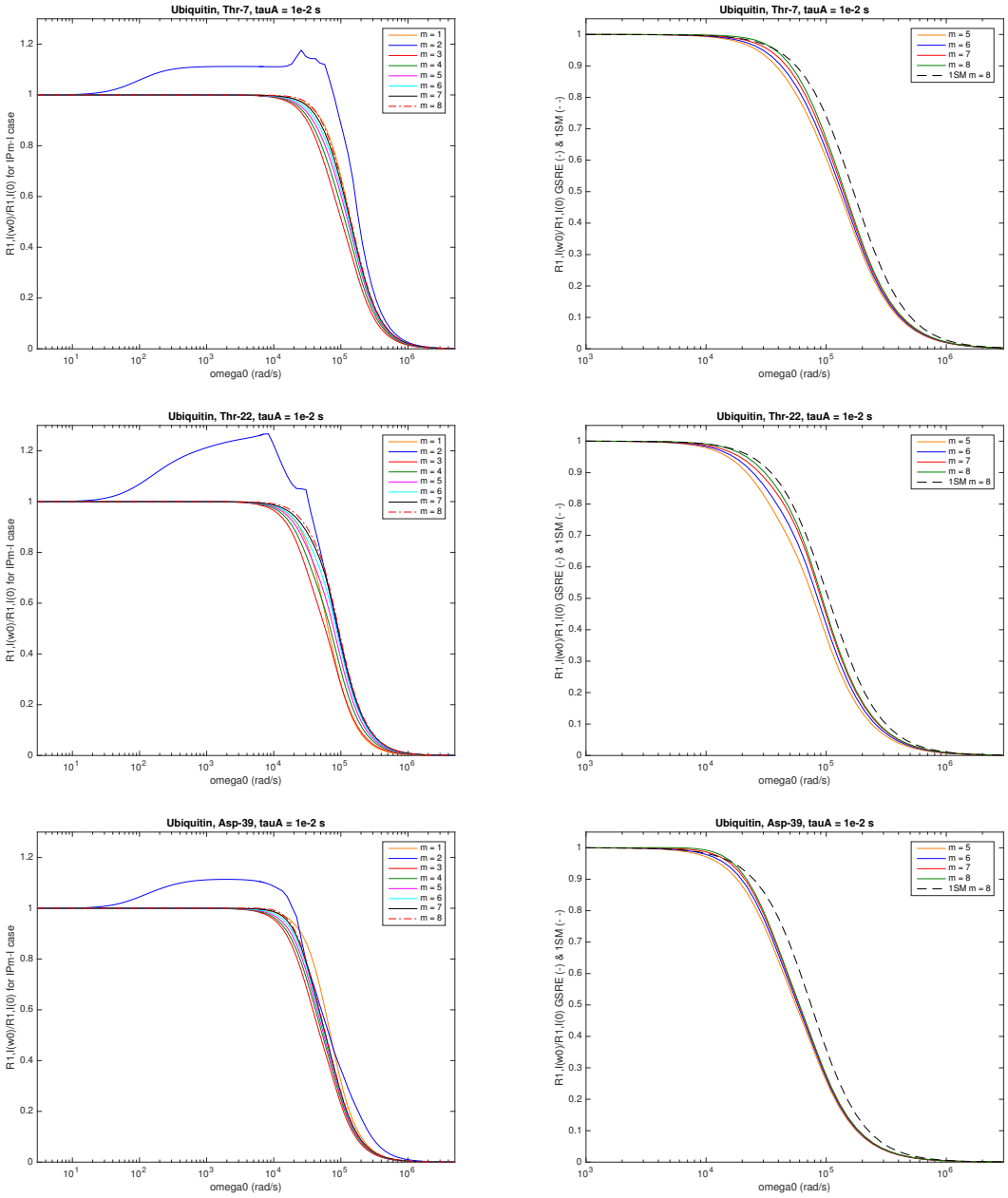

Figure S27: Normalized dispersion profiles, $R_{1,I}(\omega_0)/R_{1,I}(0)$, with $\tau_A = 10^{-2}$ s for the labile protons in Thr-7 (top), Thr-22 (middle) and Asp-39 (bottom) in ubiquitin coupled to $m = 1 - 8$ nonlabile protons (left column), computed from SLE ($m = 1$ and 2) or GSRE ($m = 3 - 8$) theory. The right column shows the GSRE profiles for $m = 5 - 8$ together with the ESE profile for $m = 8$ (dashed).

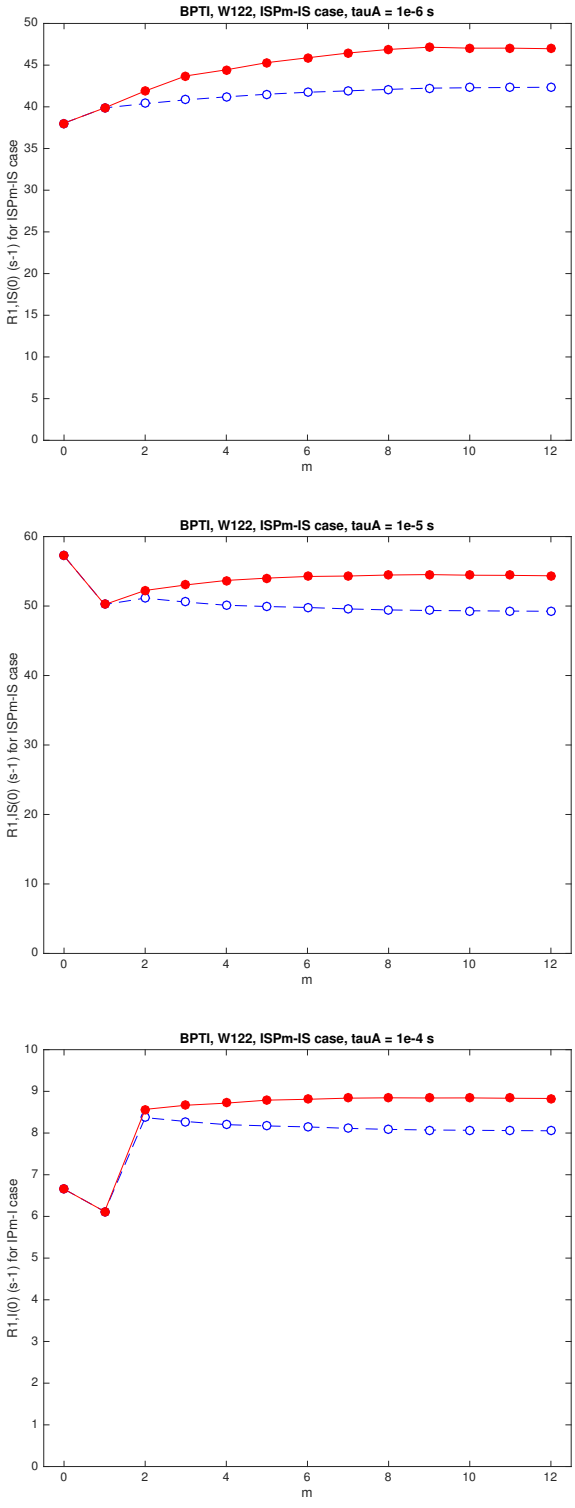

Figure S28: Variation with m of $R_{1,IS}(0)$ at $\tau_{\mathrm{A}} = 10^{-6}$ s (top), 10^{-5} s (middle) and 10^{-4} s (bottom) for W122 in BPTI coupled to $m = 0-12$ nonlabile protons with (filled symbols) or without (open symbols) SDCs, computed from SLE theory for $m \leq 1$ and from GSRE theory for $m \geq 2$.

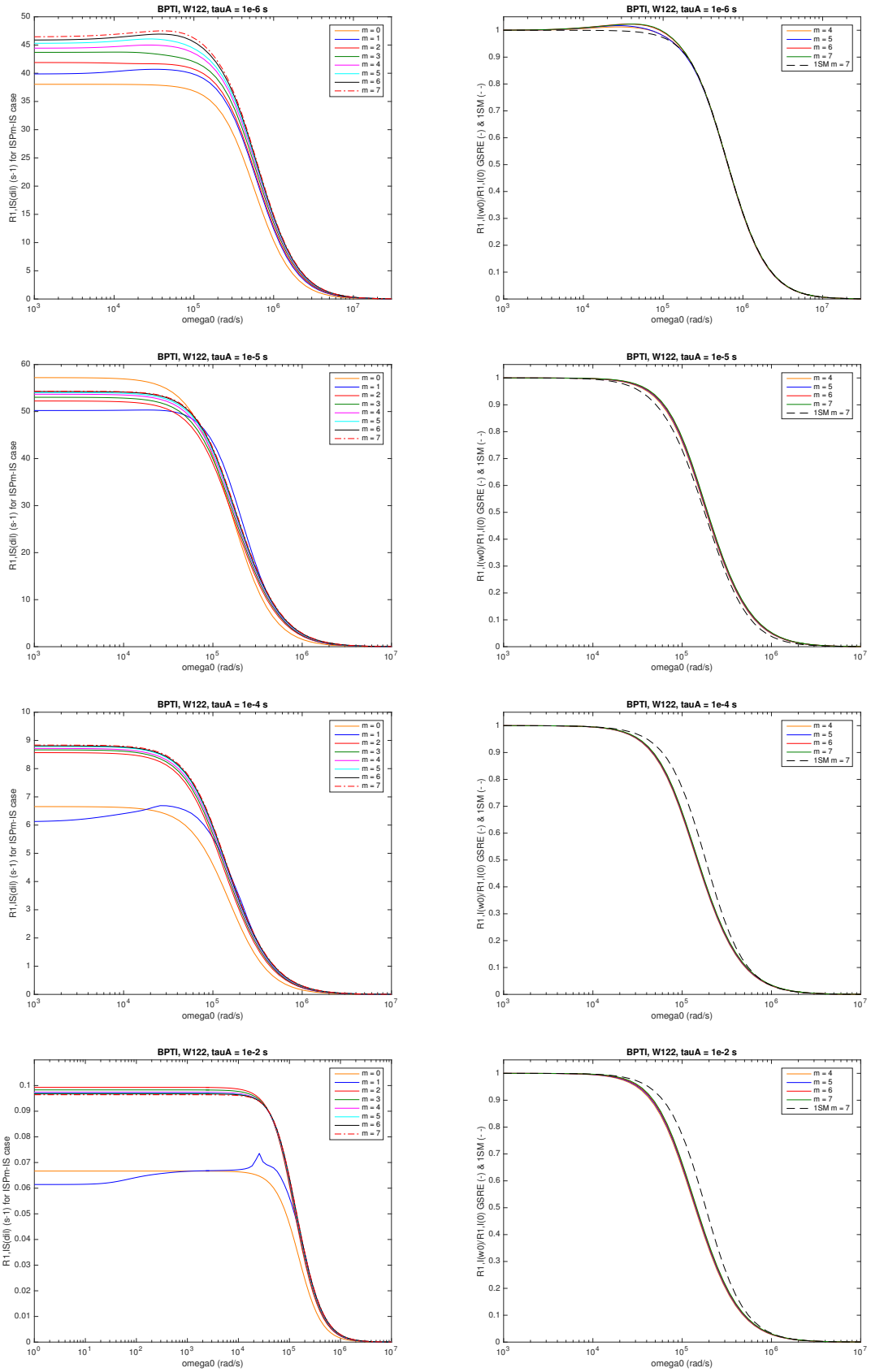

Figure S29: Dispersion profiles $R_{1,IS}(\omega_0)$ for W122 in BPTI coupled to $m = 0-7$ nonlabile protons at $\tau_A = 10^{-6}$ (top), 10^{-5}, 10^{-4} and 10^{-2} s (bottom), computed from SLE ($m = 0$ and 1) or GSRE ($m = 2-7$) theory. The right column shows profiles normalized by $R_{1,IS}(0)$ for $m = 4-7$ together with the ESE profile for $m = 7$ (dashed).

References

[1] Z. Chang and B. Halle, J. Chem. Phys. **145**, 034202 (2016).

[2] N. C. Pyper, Mol. Phys. **21**, 1 (1971).

[3] S. Szymanski, A. M. Gryff-Keller and G. Binsch, J. Magn. Reson. **68**, 399 (1986).

[4] D. M. Brink and G. R. Satchler, *Angular Momentum*, 3rd ed. (Clarendon Press, Oxford, 1994).

[5] M. Tinkham, *Group Theory and Quantum Mechanics* (McGraw-Hill, New York, 1964).

[6] Z. Chang and B. Halle, J. Chem. Phys. **144**, 084202 (2016).

[7] A. Abragam, *The Principles of Nuclear Magnetism* (Clarendon Press, Oxford, 1961).

[8] B. Halle, Magn. Reson. Med. **56**, 60 (2006).

[9] K. Blum, *Density Matrix Theory and Applications*, 3rd ed. (Springer-Verlag, Berlin, 2012).

[10] V. P. Denisov, B. Halle, J. Peters and H. D. Hörlein, Biochemistry **34**, 9046 (1995).

[11] E. Persson and B. Halle, J. Am. Chem. Soc. **130**, 1774 (2008).

Paper V

THE JOURNAL OF CHEMICAL PHYSICS **143**, 234201 (2015)

Longitudinal relaxation in dipole-coupled homonuclear three-spin systems: Distinct correlations and odd spectral densities

Zhiwei Chang and Bertil Halle[a)]
Department of Chemistry, Division of Biophysical Chemistry, Lund University, P.O. Box 124, SE-22100 Lund, Sweden

(Received 19 October 2015; accepted 24 November 2015; published online 16 December 2015)

A system of three dipole-coupled spins exhibits a surprisingly intricate relaxation behavior. Following Hubbard's pioneering 1958 study, many authors have investigated different aspects of this problem. Nevertheless, on revisiting this classic relaxation problem, we obtain several new results, some of which are at variance with conventional wisdom. Most notably from a fundamental point of view, we find that the odd-valued spectral density function influences longitudinal relaxation. We also show that the effective longitudinal relaxation rate for a non-isochronous three-spin system can exhibit an unusual inverted dispersion step. To clarify these and other issues, we present a comprehensive theoretical treatment of longitudinal relaxation in a three-spin system of arbitrary geometry and with arbitrary rotational dynamics. By using the Liouville-space formulation of Bloch-Wangsness-Redfield theory and a basis of irreducible spherical tensor operators, we show that the number of relaxation components in the different cases can be deduced from symmetry arguments. For the isochronous case, we present the relaxation matrix in analytical form, whereas, for the non-isochronous case, we employ a computationally efficient approach based on the stochastic Liouville equation. [http://dx.doi.org/10.1063/1.4937377]

I. INTRODUCTION

A few years after Solomon's seminal analysis of dipolar cross relaxation in two-spin systems,[1] Hubbard investigated longitudinal relaxation in systems of three or four dipole-coupled spins.[2] In multi-spin systems, correlations between distinct dipole couplings (usually referred to as cross correlations) come into play, and Hubbard showed that their effect is to make the relaxation of the total longitudinal magnetization in the extreme-narrowing (EN) regime weakly bi-exponential and slightly slower.[2] Subsequent studies[3–10] confirmed Hubbard's results and extended them to non-EN conditions, where longitudinal relaxation is tri-exponential, and to anisotropic rotation models, where distinct correlations can have a more pronounced effect.

All of these studies considered a system of three geometrically equivalent spins, located at the vertices of an equilateral triangle, as in the widely occurring $-CH_3$ and $-NH_3$ groups. Relatively little attention has been devoted to less symmetric nuclear geometries, where the three dipole couplings differ in magnitude. The first attempt in this direction, pertaining to three isochronous spins at the vertices of an isosceles triangle, predicted that longitudinal relaxation in the EN regime involves seven exponentials.[11] However, as noted by several authors, a correct treatment of this case yields four-exponential longitudinal relaxation in the EN regime.[12–15] In two rarely cited papers,[12,13] Schneider examined the relaxation (also outside the EN regime) of three isochronous spins at the vertices of equilateral, isosceles, and right-angled triangles. In contrast to all other authors, he retained the odd-valued spectral density function (OSDF) and showed that it influences longitudinal relaxation in the dispersive regime when at least two of the three dipole couplings differ in magnitude.[12,13] To our knowledge, this is the only explicit demonstration in the literature that the OSDF affects relaxation. Although the effect is numerically small for the isotropic rotation model considered by Schneider, it is of fundamental theoretical interest, not least because of the widespread belief that the OSDF or, equivalently, the imaginary part of the spectral density function, only gives rise to coherent evolution.[16–23]

For example, Abragam[16] dismisses the OSDF with the following assertion: "*It can be shown that the imaginary term results in a very small shift in the energy levels of the system which can be included in a redefined unperturbed Hamiltonian and thus dropped from the relaxation equation.*" It is true that the imaginary part of the relaxation superoperator $\mathcal{R}$, associated with the OSDF, can be expressed as a commutator superoperator, $-i\,\mathrm{Im}\{\mathcal{R}\} = -i\,[H', \ldots]$, just like the Liouvillian associated with the time-independent spin Hamiltonian.[22,24] (Karthik and Kumar,[22] following Jeener,[18] refer instead to the anti-Hermitian part of $\mathcal{R}$, but for all cases considered here this is identical to the imaginary part of $\mathcal{R}$.) It is also true that if there were no other terms in the equation of motion, the total evolution superoperator would be unitary (since H' is Hermitian), resulting in purely coherent evolution without dissipation. However, in the presence of the real part of $\mathcal{R}$, we (and Schneider[12,13]) find that the imaginary part of $\mathcal{R}$ does affect (longitudinal) relaxation, in addition

a)bertil.halle@bpc.lu.se

to its well-known coherent effect of inducing a second-order dynamic frequency shift.[16,22,25–27]

Consistent with these results, Pfeifer argued in general terms that the OSDF can affect relaxation outside the EN regime, except when the relaxation function is strictly exponential so that a unique relaxation time can be defined.[28] However, this general conclusion must be amended in at least two respects. First, for the isochronous three-spin system, both cross relaxation between nonequivalent spins (with different dipole couplings) and correlations between distinct dipole couplings (equal or unequal in magnitude) can give rise to multi-exponential relaxation. The relaxation effect of the OSDF is only associated with the latter type of non-exponentiality. Second, the relaxation effect of the OSDF vanishes when the relaxation superoperator is invariant under permutation of all spins. Such invariance requires both geometric and dynamic equivalence, as for three spins at the vertices of an equilateral triangle undergoing spherical-top rotational diffusion. For lower geometric or dynamic symmetry, longitudinal relaxation is affected by the OSDF.

To clarify the subtle and sometimes misunderstood manifestations of distinct correlations, cross relaxation (in the Solomon sense), and the OSDF in multi-spin systems, we present here a comprehensive analysis of longitudinal dipolar relaxation in a three-spin system. Using the Liouville space formulation of Bloch-Wangsness-Redfield (BWR) theory[15,29] with a basis of irreducible spherical tensor operators to exploit inherent symmetries, we obtain in analytical closed form the 10×10 relaxation supermatrix that governs the longitudinal relaxation of three isochronous spins with arbitrary nuclear geometry and without restrictions on the motional model (as long as the bath is isotropic). Depending on the number of unequal dipole couplings (one, two, or three), on the dynamic symmetry, and on the Larmor frequency, the relaxation of the total longitudinal magnetization involves between two and ten exponential components. In practice, it is often useful to characterize longitudinal relaxation by a single effective rate[4] $\widehat{R}_1$, which we refer to as the integral relaxation rate. To illustrate the full range of relaxation behavior, we compute the relaxation dispersion profile $\widehat{R}_1(\omega_0)$ for several cases of interest, including two anisotropic rotation models. While the emphasis is on the isochronous three-spin system, we also examine the effect of different chemical shifts for the three nuclei. We find that chemical shifts can give rise to an unusual inverted step in the dispersion profile, resulting from symmetry-breaking nonsecular decoupling that principally affects distinct correlations. We establish the range of validity of the isochronous relaxation theory and we show that the effect of chemical shifts on longitudinal relaxation is always negligible outside the motional-narrowing (MN) regime.

This paper is organized as follows. In Sec. II, starting from the BWR master equation, we develop the theory of longitudinal relaxation in an isochronous three-spin system of arbitrary geometry and without restrictions on the motional model other than the overall isotropy of the molecular system. In Sec. III, we specialize to isotropic motions and investigate, for each of the three geometric cases (with one, two, or three distinct dipole couplings), the eigenmode rates and weights and the integral relaxation rate over the full frequency range. We also examine the time dependence of the longitudinal magnetization. In Sec. IV, we explore two anisotropic motional models: axial internal rotation superimposed on spherical-top rotation and symmetric-top rotation with arbitrary orientation of the rotational diffusion tensor. In Sec. V, we use the stochastic Liouville equation to examine the effect of chemical shifts on the longitudinal relaxation behavior, finding an unusual inverted relaxation dispersion at the nonsecular decoupling frequency. Finally, in Sec. VI, we summarize the principal results of this work.

II. RELAXATION THEORY

A. Liouville space formulation of BWR theory

We consider three isochronous spin–1/2 nuclei, labeled I, S, and P, subject to Zeeman and mutual intramolecular dipole couplings. If we neglect scalar couplings, the static Hamiltonian is

$$H_{\rm Z} = \omega_0 (I_z + S_z + P_z), \tag{1}$$

where ω_0 is the common Larmor frequency. In Sec. V, we consider the more general case where the three nuclei have different Larmor frequencies.

The fluctuating dipolar Hamiltonian, with vanishing ensemble average, is

$$H_{\rm D}(t) = H_{{\rm D},IS}(t) + H_{{\rm D},IP}(t) + H_{{\rm D},SP}(t), \tag{2}$$

with (X denotes either of the three spin pairs IS, IP, or SP)

$$H_{{\rm D},X}(t) = -\frac{2}{\sqrt{3}}\,\omega_{{\rm D},X} \sum_{M=-2}^{2} T^2_M(X)\, D^{2\,*}_{M0}(\Omega_X(t)). \tag{3}$$

Here, the $T^2_M(X)$ are orthonormal three-spin irreducible spherical tensor operators (Sec. II C), the $D^2_{M0}(\Omega_X)$ are rank-2 Wigner functions,[30] $\Omega_X(t) \equiv (\theta_X(t), \varphi_X(t))$ are the fluctuating spherical polar angles that specify the orientation of the internuclear vector $\boldsymbol{r}_X$ with respect to the lab-fixed frame, and the dipole coupling frequency is defined as $\omega_{{\rm D},X} \equiv (3/2)(\mu_0/4\pi)\,\gamma^2\,\hbar/r^3_X$. Since the geometric arrangement of the three nuclei is arbitrary, the three dipole couplings may differ in magnitude.

We start from the semi-classical BWR master equation[16]

$$\frac{\rm d}{{\rm d}t}\,\widehat{\sigma}(t) = -\int_0^\infty {\rm d}\tau\, \left\langle \widehat{\mathcal{L}}_{\rm D}(t)\, \widehat{\mathcal{L}}_{\rm D}(t-\tau) \right\rangle \widehat{\sigma}(t), \tag{4}$$

where $\widehat{\sigma}(t) = \exp(i\,\mathcal{L}_{\rm Z}\,t)\,\sigma(t)$ and $\widehat{\mathcal{L}}_{\rm D}(t) = \exp(i\,\mathcal{L}_{\rm Z}\,t)\,\mathcal{L}_{\rm D}(t)\,\exp(-i\,\mathcal{L}_{\rm Z}\,t)$ are, respectively, the density operator (relative to its equilibrium value) and the dipolar Liouvillian in the interaction representation, and the Liouvillians are the usual derivation superoperators $\mathcal{L}_{\rm Z} \equiv [H_Z, \ldots]$ and $\mathcal{L}_{\rm D}(t) \equiv [H_D(t), \ldots]$. The angular brackets denote an equilibrium ensemble average over the molecular degrees of freedom (the so-called "lattice" or "bath").

The set of three-spin irreducible spherical tensor operators T^K_Q, to which the $T^2_M(X)$ in Eq. (3) belong, are eigenoperators

of the Zeeman Liouvillian (Sec. II C),

$$\mathcal{L}_Z T_Q^K = Q\,\omega_0 T_Q^K. \tag{5}$$

The BWR equation (4) can therefore be expressed, in the Schrödinger representation, as

$$\frac{\mathrm{d}}{\mathrm{d}t}\,\sigma(t) = -i\,\mathcal{L}_Z\,\sigma(t) - \mathcal{R}\,\sigma(t). \tag{6}$$

The relaxation superoperator is given by

$$\mathcal{R} = \frac{4}{3}\sum_X\sum_Y \omega_{\mathrm{D},X}\,\omega_{\mathrm{D},Y}\sum_{M=-2}^{2}\sum_{M'=-2}^{2}\int_0^\infty \mathrm{d}\tau\,\exp(iM'\omega_0\tau) \times G_{MM'}^{XY}(\tau)\,\mathcal{T}_M^2(X)\,\mathcal{T}_{M'}^{2\,\dagger}(Y), \tag{7}$$

where the superscript † signifies the adjoint (Hermitian conjugate) and we have introduced the superoperators $\mathcal{T}_M^2(X) \equiv [T_M^2(X), \ldots]$.

The time correlation functions in Eq. (7) are defined as

$$G_{MM'}^{XY}(\tau) \equiv \left\langle D_{M0}^{2\,*}(\Omega_X(0))\,D_{M'0}^2(\Omega_Y(\tau))\right\rangle, \tag{8}$$

where the angles $\Omega_X(\tau)$ are modelled as a stationary random process. We assume that the bath is isotropic, meaning that Ω_X is uniformly distributed, and that, as a result of molecular motions, this distribution is sampled by each spin-bearing molecule on a time scale that is short compared to $1/\omega_{\mathrm{D},X}$. The propagator $P(\Omega_Y,\tau \mid \Omega_X,0)$ is then rotationally invariant so that time correlation functions involving Wigner functions, which transform according to the irreducible representations of the rotation group, obey the symmetry selection rule[31]

$$\begin{aligned} G_{MM'}^{XY}(\tau) &= \delta_{MM'}\langle P_2(\cos\theta_X(0))\,P_2(\cos\theta_Y(\tau))\rangle \\ &\equiv \delta_{MM'}\,G_{XY}(\tau), \end{aligned} \tag{9}$$

which evidently is a real-valued quantity. Combination of Eqs. (7) and (9) yields

$$\mathcal{R} = \sum_X\sum_Y\sum_{M=-2}^{2} J_{XY}(M\omega_0)\,C_M^{XY}, \tag{10}$$

where we have introduced the superoperators

$$C_M^{XY} \equiv \mathcal{T}_M^2(X)\,\mathcal{T}_M^{2\,\dagger}(Y) = (-1)^M\mathcal{T}_M^2(X)\,\mathcal{T}_{-M}^2(Y), \tag{11}$$

and the complex-valued spectral density functions

$$\begin{aligned} J_{XY}(\omega) &\equiv \frac{4}{3}\,\omega_{\mathrm{D},X}\,\omega_{\mathrm{D},Y}\left[\int_0^\infty \mathrm{d}\tau\,\cos(\omega\,\tau)\,G_{XY}(\tau) + i\int_0^\infty \mathrm{d}\tau\,\sin(\omega\,\tau)\,G_{XY}(\tau)\right] \\ &\equiv j_{XY}(\omega) + i\,k_{XY}(\omega). \end{aligned} \tag{12}$$

Clearly, the real and imaginary parts of $J_{XY}(\omega)$ are even and odd functions of frequency, respectively: $j_{XY}(-\omega) = j_{XY}(\omega)$ and $k_{XY}(-\omega) = -k_{XY}(\omega)$. We refer to these parts as the even spectral density function (ESDF) and the OSDF. The complex-valued spectral density functions have the general properties,

$$J_{XY}^*(\omega) = J_{XY}(-\omega), \tag{13a}$$

$$J_{YX}(\omega) = J_{XY}(\omega). \tag{13b}$$

The second relation follows from Eq. (12) and the equality $G_{YX}(\tau) = G_{XY}(\tau)$, which in turn follows from Eq. (9) and the assumption that the stationary process obeys the principle of detailed balance, which ensures that the propagator is invariant under time reversal. Throughout Sec. II, we place no further restrictions on the time correlation functions $G_{XY}(\tau)$. Specific motional models will be introduced in Secs. III and IV, where we also present numerical results.

Although we have not yet specified the motional model, it is convenient to loosely define a correlation time τ_c as the time scale for the essential decay of the time correlation functions $G_{XY}(\tau)$. This allows us to distinguish three frequency regimes: the EN regime ($\omega_0\tau_c \ll 1$), the dispersive regime ($\omega_0\tau_c \sim 1$), and the adiabatic regime ($\omega_0\tau_c \gg 1$). There are no fixed and universal demarcation lines between these regimes. For example, the value of $\omega_0\tau_c$ below which relaxation can be considered to be independent of ω_0 depends on the chosen (geometric and dynamic) model and on the desired accuracy. For some purposes, it is more appropriate to refer to the zero-field limit rather than to the EN regime.

The foregoing results are well-known; their derivation is sketched here merely to establish our notation and to exhibit the underlying assumptions.

B. Spin inversion and conjugation symmetries of the relaxation superoperator

The density operator must remain Hermitian at all times[32] so the two operators on the right-hand side of Eq. (6) must also be Hermitian.[29] In other words, physical consistency demands that $(\mathcal{L}_Z\,\sigma)^\dagger = -\mathcal{L}_Z\,\sigma$ and $(\mathcal{R}\,\sigma)^\dagger = \mathcal{R}\,\sigma$. The first of these identities is readily verified by noting that $(\mathcal{L}_Z\,\sigma)^\dagger = [H_Z,\sigma]^\dagger = -[H_Z^\dagger,\sigma^\dagger] = -[H_Z,\sigma]$ since both H_Z and σ are Hermitian. To prove the second identity, we use Eq. (13a) and note that $(C_M^{XY}\,\sigma)^\dagger = C_{-M}^{XY}\,\sigma$ by virtue of Eq. (11). To complete the proof, we substitute these results into the expression for $(\mathcal{R}\,\sigma)^\dagger$ obtained from Eq. (10) and then interchange M and $-M$ in the symmetric sum.

The general physical requirement that the operator $\mathcal{R}\sigma$ is Hermitian does not imply that the relaxation superoperator $\mathcal{R}$ itself is Hermitian. Since $(\mathcal{S}\,\mathcal{T})^\dagger = \mathcal{T}^\dagger\mathcal{S}^\dagger$ for arbitrary superoperators $\mathcal{S}$ and $\mathcal{T}$,[18] Eq. (11) yields $C_M^{XY\,\dagger} = C_M^{YX}$. Inserting this result into the adjoint of Eq. (10), interchanging

the dummy variables X and Y, and using Eq. (13b), we find

$$\mathcal{R}^\dagger = \sum_X \sum_Y \sum_{M=-2}^{2} J^*_{XY}(M\omega_0)\, C^{XY}_M. \tag{14}$$

In view of Eq. (12), this result shows that the relaxation superoperator is the sum of Hermitian and anti-Hermitian parts. The Hermitian part is the real part of $\mathcal{R}$, associated with the ESDF, $j_{XY}(M\omega_0)$. The anti-Hermitian part is i times the imaginary part of $\mathcal{R}$, associated with the OSDF, $k_{XY}(M\omega_0)$. Therefore, $\mathcal{R}$ is Hermitian only in the EN regime, where $k_{XY}(\omega) \ll j_{XY}(\omega)$, and in the adiabatic regime, where $j_{XY}(\omega), k_{XY}(\omega) \ll j_{XY}(0)$.

We now consider the effect on $\mathcal{R}$ of spin inversion, spin conjugation, and spin inversion conjugation.[15,29] The superoperators, collectively denoted by $\mathcal{X}$, associated with each of these symmetry operations are unitary and self-inverse,[29] and, for our three-spin system, they can be factorized as

$$\mathcal{X} = \mathcal{X}^\dagger = \mathcal{X}^{-1} = \mathcal{X}_I\, \mathcal{X}_S\, \mathcal{X}_P. \tag{15}$$

The spin inversion superoperator acting on I-spin operators is defined as[15,29]

$$\mathcal{Y}_I \equiv \exp(i\,\pi\, \mathcal{I}_y), \tag{16}$$

with $\mathcal{I}_y = [I_y, \ldots]$, so it transforms the spherical spin operators according to Table I. The spin conjugation superoperator is usually defined in terms of its action on the shift operators,[15,29]

$$\mathcal{V}_I\ |Im\rangle\langle In| \equiv (|Im\rangle\langle In|)^\dagger = |In\rangle\langle Im|\,, \tag{17}$$

and the spin inversion conjugation operation is simply the combination of the first two operations, $\mathcal{W} = \mathcal{V}\mathcal{Y} = \mathcal{Y}\mathcal{V}$.[15,29] The transformation rules in the last two columns in the upper part of Table I are readily obtained from these definitions.

TABLE I. Spin inversion and conjugation symmetries of operators and superoperators.

Operator	Transformed operator		
I_α	$\mathcal{Y}_I\, I_\alpha$	$\mathcal{V}_I\, I_\alpha$	$\mathcal{W}_I\, I_\alpha$
I_z	$-I_z$	I_z	$-I_z$
I_+	$-I_-$	I_-	$-I_+$
I_-	$-I_+$	I_+	$-I_-$
Superoperator	**Transformed superoperator**		
$\mathcal{S}$	$\mathcal{Y}\,\mathcal{S}\,\mathcal{Y}$	$\mathcal{V}\,\mathcal{S}\,\mathcal{V}$	$\mathcal{W}\,\mathcal{S}\,\mathcal{W}$
$\mathcal{T}^2_M$	$(-1)^M \mathcal{T}^2_{-M}$	$(-1)^M \mathcal{T}^2_{-M}$	$\mathcal{T}^2_M$
C^{XY}_M	C^{XY}_{-M}	C^{XY}_{-M}	C^{XY}_M
$\mathcal{R}$	$\mathcal{R}^\dagger$	$\mathcal{R}^\dagger$	$\mathcal{R}$

To establish the behavior of the relaxation superoperator $\mathcal{R}$ under these symmetry operations, we first use the explicit form of the operators $T^2_M(X)$ and the transformation rules for single-spin operators in the upper part of Table I to obtain the rules on the fourth row of the table. The rules for the superoperator C^{XY}_M, shown in the next row, are then obtained with the aid of Eq. (11). Finally, we use Eqs. (10), (13a), and (14) to obtain the transformation rules for $\mathcal{R}$ in the last row of Table I. We thus find that the relaxation superoperator is invariant under spin inversion conjugation, whereas it is invariant under spin inversion and spin conjugation separately only in the EN and adiabatic regimes, where the OSDF can be neglected.

C. Spin operator basis and spin modes

As a basis for three-spin Liouville space, we use the 64 irreducible spherical tensor operators (ISTOs) $T^K_Q(k_I k_S\{\bar{K}\}k_P)$, constructed by two consecutive couplings of the set of four orthonormal single-spin ISTOs for each spin, e.g.,

$$T^0_0(I) = \frac{1}{\sqrt{2}}\, E_I, \quad T^1_0(I) = \sqrt{2}\, I_z, \quad T^1_{\pm 1}(I) = \mp I_\pm, \tag{18}$$

to obtain[30,32]

$$T^K_Q(k_I k_S\{\bar{K}\}k_P) = (-1)^{k_I - k_S - k_P + \bar{K} + Q}\,(2K+1)^{1/2}(2\bar{K}+1)^{1/2} \times \sum_{\bar{Q}=-\bar{K}}^{\bar{K}} \sum_{q_I=-k_I}^{k_I} (-1)^{\bar{Q}} \begin{pmatrix} \bar{K} & k_P & K \\ \bar{Q} & Q-\bar{Q} & -Q \end{pmatrix} \begin{pmatrix} k_I & k_S & \bar{K} \\ q_I & \bar{Q}-q_I & -\bar{Q} \end{pmatrix} T^{k_I}_{q_I}(I)\, T^{k_S}_{\bar{Q}-q_I}(S)\, T^{k_P}_{Q-\bar{Q}}(P), \tag{19}$$

where $\bar{K}$ is the rank of the intermediate tensor operator obtained by first coupling spins I and S. Here, and in the following, the rank and projection indices are written in upper case for three-spin ISTOs and in lower case for single-spin ISTOs. The ISTOs $T^2_M(X)$ appearing in dipolar Hamiltonian (3) belong to this basis set, e.g., $T^2_0(IS) = T^2_0(11\{2\}0) = (3I_zS_z - \boldsymbol{I}\cdot\boldsymbol{S})/\sqrt{3}$, and Eq. (5) follows directly from Eq. (19) and the fundamental commutation relation[30] $[I_z, T^{k_I}_{q_I}(I)] = q_I\, T^{k_I}_{q_I}(I)$.

The main virtue of the ISTO basis is that the $2K+1$ operators T^K_Q of a given rank K transform according to the irreducible representation $\mathcal{D}^K$ of the three-dimensional rotation group,[30,33] leading to selection rules for the relaxation supermatrix (Sec. II D 2) that greatly simplify the relaxation problem. In addition, some of the ISTOs have well-defined parity under spin inversion, spin conjugation, and spin inversion conjugation, leading to additional selection rules (Sec. II D 3). Applying the transformation rules in the upper

part of Table I to Eqs. (18) and (19) and using the symmetry properties of the $3j$ symbol,[30] we find

$$\mathcal{Y}\, T_Q^K = (-1)^{Q+K}\, T_{-Q}^K, \tag{20a}$$

$$\mathcal{V}\, T_Q^K = T_Q^{K\,\dagger} = (-1)^{Q+K+N_s}\, T_{-Q}^K, \tag{20b}$$

$$\mathcal{W}\, T_Q^K = (-1)^{N_s}\, T_Q^K, \tag{20c}$$

where $N_s = k_I + k_S + k_P$ is the number of single-spin operators (not counting identity operators) involved in the basis operator. Equation (20b) is the generalization to three-spin ISTOs of the familiar conjugation relation, $T_q^{k\,\dagger} = (-1)^q\, T_{-q}^k$, for single-spin ISTOs.[30,33] As seen from Eq. (20c), all 64 basis operators have definite parity with respect to spin inversion conjugation, being odd (anti-symmetric) if they involve one or three spins and even (symmetric) if they involve two spins. In the following, we refer to basis operators that are odd or even under spin inversion conjugation as OSIC or ESIC operators, respectively. In contrast, only the 20 zero-quantum ($Q = 0$) ISTOs have definite parity under spin inversion and spin conjugation. Equation (20a) shows that these basis operators are either even (for even rank K) or odd (for odd K) under spin inversion, and Eq. (20b) shows that they are either Hermitian (for even $K + N_s$) or anti-Hermitian (odd $K + N_s$).

As we shall see in Sec. II D, the symmetry properties of the ISTO basis operators under rotation and spin inversion conjugation ensure that longitudinal relaxation in the three-spin system can be described, for arbitrary nuclear geometry, in the subspace of the ten zero-quantum OSIC operators listed in Table II. (The identity operator also belongs to this category, but it can be omitted on physical grounds.) Based on their parity with respect to $\mathcal{Y}$ and $\mathcal{V}$, these ten operators fall in two groups: seven Hermitian operators with odd rank K and three anti-Hermitian operators with even rank.

For convenience, we index the basis by a single number n, denoting the basis operators by B_n. The basis operators obtained from Eq. (19) are orthonormal in the sense,

$$(B_n|B_p) \equiv \mathrm{Tr}\{B_n^\dagger B_p\} = \delta_{np}. \tag{21}$$

Because the basis is complete, we can expand the density operator in spin modes (sometimes called state multipoles),[32] defined as $\sigma_n \equiv (B_n|\,\sigma)$. Using Eqs. (5), (6), and (21), we find that the zero-quantum spin modes obey the BWR master equation

$$\frac{\mathrm{d}}{\mathrm{d}t}\sigma_n(t) = -\sum_p R_{np}\,\sigma_p(t), \tag{22}$$

since the coherent term $-i\,Q(n)\,\omega_0\,\sigma_n(t)$ vanishes for $Q = 0$. The relaxation supermatrix elements are obtained from Eq. (10) as

$$R_{np} \equiv (B_n|\mathcal{R}|B_p) = \sum_X \sum_Y \sum_{M=-2}^{2} C_{M,np}^{XY}\, J_{XY}(M\omega_0), \tag{23}$$

with the coefficients $C_{M,np}^{XY} \equiv (B_n|C_M^{XY}|B_p)$.

D. Symmetry properties of the relaxation supermatrix in the ISTO basis

1. Transposition and complex conjugation

According to Eq. (11), the coefficients in Eq. (23) are given by

$$\begin{aligned} C_{M,np}^{XY} &= \mathrm{Tr}\left\{B_n^\dagger\, \mathcal{T}_M^2(X)\, \mathcal{T}_M^2(Y)^\dagger B_p\right\} \\ &= -\mathrm{Tr}\left\{\left(\mathcal{T}_M^2(X)\, B_n^\dagger\right)\left(\mathcal{T}_M^2(Y)^\dagger B_p\right)\right\}, \end{aligned} \tag{24}$$

where the last form results from the cyclic permutation invariance of the trace. As shown in Appendix A of the supplementary material,[34] all matrix elements $C_{M,np}^{XY}$ are real-valued in the ISTO basis. It then follows from Eqs. (12) and (23) that the real part of the relaxation supermatrix is associated with the ESDF and the imaginary part with the OSDF. While this correspondence was established for the relaxation superoperator in Sec. II B, it is not true for the relaxation supermatrix in any basis. Indeed, in a basis of Hermitian operators, the relaxation supermatrix is real even though the spectral density is complex.[29]

TABLE II. The zero-quantum OSIC basis operators $T_0^K(k_I k_S\{\bar{K}\}k_P)$.

n	K	k_I	k_S	k_P	$\bar{K}$	$\mathcal{Y}$[a]	$\mathcal{V}$[b]	B_n[c,d]
1	1	1	0	0	1	−	+	$\frac{1}{\sqrt{2}}\, I_z$
2	1	0	1	0	1	−	+	$\frac{1}{\sqrt{2}}\, S_z$
3	1	0	0	1	0	−	+	$\frac{1}{\sqrt{2}}\, P_z$
4	1	1	1	1	0	−	+	$-\frac{2\sqrt{6}}{3}\,(\boldsymbol{I}\cdot\boldsymbol{S})\, P_z$
5	1	1	1	1	1	−	+	$\sqrt{2}[I_z(\boldsymbol{S}\cdot\boldsymbol{P}) - S_z(\boldsymbol{I}\cdot\boldsymbol{P})]$
6	1	1	1	1	2	−	+	$\frac{2}{\sqrt{30}}[2\, P_z(\boldsymbol{I}\cdot\boldsymbol{S}) - 3\, I_z(\boldsymbol{S}\cdot\boldsymbol{P}) - 3\, S_z(\boldsymbol{I}\cdot\boldsymbol{P})]$
7	3	1	1	1	2	−	+	$\frac{2}{\sqrt{5}}[5\, I_z S_z P_z - I_z(\boldsymbol{S}\cdot\boldsymbol{P}) - S_z(\boldsymbol{I}\cdot\boldsymbol{P}) - P_z(\boldsymbol{I}\cdot\boldsymbol{S})]$
8	0	1	1	1	1	+	−	$-i\,\frac{2}{\sqrt{3}}\,(\boldsymbol{I}\times\boldsymbol{S})\cdot\boldsymbol{P}$
9	2	1	1	1	1	+	−	$i\,\frac{2}{\sqrt{6}}\,(\boldsymbol{I}\times\boldsymbol{S})\cdot(3\, P_z\, \boldsymbol{e}_z - \boldsymbol{P})$
10	2	1	1	1	2	+	−	$i\,\sqrt{2}[I_z\,(\boldsymbol{S}\times\boldsymbol{P}) + S_z\,(\boldsymbol{I}\times\boldsymbol{P})]\cdot\boldsymbol{e}_z$

[a] Parity under spin inversion.
[b] Parity under spin conjugation.
[c] Identity operators have been omitted.
[d] $\boldsymbol{e}_z$ denotes the unit vector along the z axis.

Noting that $C^{XY}_{M,np}$ is real, we can use Eq. (24) to show that

$$C^{XY}_{M,np} = (C^{XY}_{M,np})^* = \mathrm{Tr}\{(B_n^\dagger \mathcal{T}^2_M(X)\,\mathcal{T}^2_M(Y)^\dagger B_p)^\dagger\}$$
$$= \mathrm{Tr}\{B_p^\dagger \mathcal{T}^2_M(Y)\,\mathcal{T}^2_M(X)^\dagger B_n\} = C^{YX}_{M,pn}. \quad (25)$$

By interchanging the dummy variables X and Y in Eq. (23) and using Eqs. (13b) and (25), we obtain

$$R_{np} = R_{pn}, \quad (26)$$

showing that (both the real and imaginary parts of) the relaxation supermatrix is symmetric in the ISTO basis.

Another symmetry property of the relaxation supermatrix in the ISTO basis can be demonstrated by first using Eqs. (10)–(13) to show that $(\mathcal{R}\,A)^\dagger = \mathcal{R}\,A^\dagger$ for an arbitrary operator A and then using this result and the cyclic permutation invariance of the trace in the definition of the supermatrix element as follows:

$$R^*_{np} = \mathrm{Tr}\{(B_n^\dagger \mathcal{R}\,B_p)^\dagger\} = \mathrm{Tr}\{(\mathcal{R}\,B_p)^\dagger B_n\}$$
$$= \mathrm{Tr}\{\mathcal{R}\,B_p^\dagger B_n\} = \mathrm{Tr}\{B_n\,\mathcal{R}\,B_p^\dagger\} = R_{\underline{n}\underline{p}}, \quad (27)$$

where the underlined subscript $\underline{n}$ denotes the adjoint basis operator $B_n^\dagger$. This relation is particularly useful in the zero-quantum subspace, for which Eq. (20b) shows that the basis operators are either Hermitian or anti-Hermitian. It then follows from Eq. (27) that relaxation supermatrix elements connecting two Hermitian or two anti-Hermitian basis operators are real ($R^*_{np} = R_{np}$), whereas matrix elements connecting basis operators of different conjugation parity are imaginary ($R^*_{np} = -R_{np}$). Since $J_{XY}(M\omega_0)$ is the only complex-valued quantity in Eq. (23), it is clear that the OSDF has the effect of coupling odd-rank (Hermitian) and even-rank (anti-Hermitian) spin modes.

2. Rotational symmetry

Because the superoperator $\mathcal{R}$ is ensemble averaged over the isotropic molecular system, it must exhibit the cylindrical symmetry of the spin system in the external magnetic field. According to the Wigner-Eckart theorem,[15,29,30,32,33] the relaxation supermatrix in the ISTO basis must therefore be block-diagonal in the projection index Q,

$$R_{n(Q)p(Q')} = \delta_{QQ'}\,R_{n(Q)p(Q)}. \quad (28)$$

The evolution of the longitudinal magnetization modes $\sigma_1(t)$, $\sigma_2(t)$, and $\sigma_3(t)$ (Table II) can, therefore, be fully described within the subspace of the 19 zero-quantum operators (omitting the identity operator). In the EN regime, where the Zeeman Hamiltonian may be neglected, the relaxation superoperator $\mathcal{R}$ becomes fully rotationally invariant. The Wigner-Eckart theorem then implies that the relaxation supermatrix in the ISTO basis is block-diagonal not only in the projection index Q but also in the rank index K,[15,29]

$$R_{n(KQ)p(K'Q')} = \delta_{KK'}\,\delta_{QQ'}\,R_{n(KQ)p(KQ)} \quad (\omega_0\,\tau_c \ll 1). \quad (29)$$

In the EN regime, rotational symmetry thus reduces the invariant subspace to the nine rank-1 zero-quantum basis operators.

3. Spin inversion conjugation symmetry

As seen from Table I and Eq. (20c), the relaxation superoperator is invariant and the ISTO basis operators have definite parity under spin inversion conjugation. According to the basic orthogonality theorem of group theory,[15,33] of which the Wigner-Eckart theorem is a special case, the relaxation supermatrix in the ISTO basis can, therefore, have nonzero elements only between basis operators of the same parity (that is, belonging to the same irreducible representation of the symmetry group). Among the 19 zero-quantum operators, 10 are OSIC (including the ones representing the longitudinal magnetizations) and 9 are ESIC. Longitudinal relaxation in a three-spin system can, therefore, be fully described within the subspace of the ten zero-quantum OSIC operators in Table II, corresponding to the three longitudinal magnetizations and seven zero-quantum coherences (ZQCs).

Since N_s is odd for these ten basis operators, Eq. (20b) shows that the seven odd-rank operators are Hermitian, whereas the three even-rank operators are anti-Hermitian, as can be verified from Table II. In view of Eq. (27), it then follows that the 10×10 relaxation supermatrix that governs longitudinal relaxation has 7×7 and 3×3 real symmetric blocks along the diagonal (Fig. 1, top left). The elements in these two blocks are linear combinations of some or all of the ESDFs $j_{XY}(0)$, $j_{XY}(\omega_0)$, and $j_{XY}(2\omega_0)$. The seven odd-rank spin modes are coupled to the three even-rank modes via the purely imaginary "off-diagonal" 7×3 and 3×7 blocks (Fig. 1, top left). The elements of these blocks are linear combinations of the OSDFs $k_{XY}(\omega_0)$ and $k_{XY}(2\omega_0)$. In other words, the only effect of the OSDFs is to couple odd-rank and even-rank spin modes; they have no effect on the odd-rank and even-rank blocks. If the OSDF is neglected, this coupling disappears and the longitudinal relaxation is then fully described by the real symmetric 7×7 block associated with the odd-rank basis

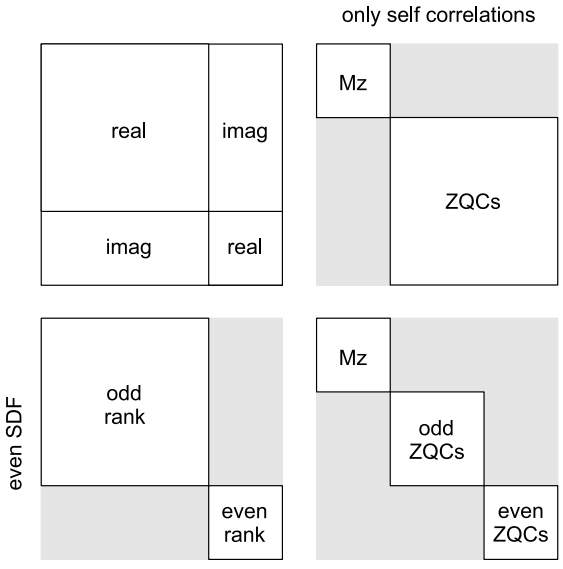

FIG. 1. Schematic representation of the 10×10 relaxation supermatrix in the zero-quantum OSIC subspace, comprising three longitudinal modes (Mz) and seven ZQCs. The effects of removing distinct correlations and/or the OSDF are shown by shading supermatrix elements that then become identically zero.

operators (Fig. 1, bottom left). This is the case in the EN regime, where, in addition, selection rule (29) holds so that only the six rank-1 modes of this subspace can couple.

To compute the relevant 10×10 block of the relaxation supermatrix from Eq. (23), we need 45 $\mathbf{C}_M^{XY}$ matrices. On account of symmetry relations (25) and

$$C_{-M,np}^{XY} = (-1)^{K(n)+K(p)} C_{M,np}^{XY}, \tag{30}$$

which follows from Eqs. (13) and (27) and is valid only in the zero-quantum subspace, there are only 18 unique $\mathbf{C}_M^{XY}$ matrices to compute. The details of this straight-forward but tedious task can be found in Appendix A of the supplementary material.[34] By combining these matrices, given in exact analytical form in Appendix A,[34] with Eqs. (22) and (23), the longitudinal relaxation behavior is readily calculated for any geometrical arrangement of the three spins and for any motional model.

4. Nuclear permutation symmetry

In the context of spin relaxation, nuclear permutation symmetry refers to the spectral density functions.[15,29] For dipolar relaxation in an isochronous multi-spin system, the relaxation superoperator $\mathcal{R}$ is invariant under permutation (or interchange) of two nuclei if these nuclei are related by a symmetry operation of the molecular point group (geometric symmetry) and if the dipole couplings between each of these nuclei and any other nucleus are modulated in the same way by the molecular motion (dynamic symmetry). These two requirements can be concisely expressed in terms of the spectral density functions $J_{XY}(\omega)$. For our three-spin system, $\mathcal{R}$ is invariant under $I \leftrightarrow S$ interchange if $J_{IP,IP}(\omega) = J_{SP,SP}(\omega)$ and $J_{IS,IP}(\omega) = J_{IS,SP}(\omega)$. Similarly, $\mathcal{R}$ is invariant under permutations of all three nuclei if $J_{IS,IS}(\omega) = J_{IP,IP}(\omega) = J_{SP,SP}(\omega)$ and $J_{IS,IP}(\omega) = J_{IS,SP}(\omega) = J_{IP,SP}(\omega)$.

We shall use the conventional spin system notation, normally based on the static spin Hamiltonian, to label the three possible types of geometric symmetry or equivalence. In the A_3 system, the three nuclei reside at the vertices of an equilateral triangle and are therefore geometrically equivalent. In the A_2A' system, the nuclei define an isosceles triangle. If spin P is at the apex, then spins I and S are geometrically equivalent. Finally, in the $AA'A''$ system, all three internuclear vectors have different lengths so there is no geometrical equivalence.

For isotropic dynamic models (Sec. III), such as spherical-top rotational diffusion, all dipole couplings are modulated in the same way (full dynamic symmetry). Geometric equivalence then implies nuclear permutation symmetry. For anisotropic rotation models, the lower dynamic symmetry may reduce or abolish the nuclear permutation symmetry even though geometric symmetry is present (Sec. IV).

For the isotropic dynamic model considered in Sec. III, the relaxation superoperator is thus invariant under permutation of geometrically equivalent nuclei. For the A_3 and A_2A' systems, the relaxation supermatrix, therefore, becomes block-diagonal in a basis of operators that have definite parity under permutation of equivalent nuclei.[17,29] The ISTO basis operators in Table II are constructed by first coupling spins I and S and then coupling the resultant to spin P (Sec. II C). Accordingly, they have definite parity under interchange of spins I and S, but not under permutations of all three spins. This basis is, therefore, adapted to the geometric symmetry of the A_2A' system (with spin P at the apex), but not to the higher symmetry of the A_3 system.

E. Self- and distinct correlations

A relaxation supermatrix element R_{np} with $n \neq p$ describes cross relaxation between spin modes n and p. For example, n and p might be the longitudinal magnetizations of two different spins (as in the two-spin Solomon equations[1]), or they might represent a longitudinal magnetization and a ZQC. Both auto-relaxation rates R_{nn} and cross relaxation rates R_{np} $(n \neq p)$ may have contributions from self-correlations (terms with $X = Y$) and from distinct correlations (terms with $X \neq Y$). In the literature, these contributions are usually referred to as auto- and cross correlations, but we prefer the descriptors "self" and "distinct" to distinguish them from "auto-mode" and "cross-mode" relaxation. Note that the term "distinct" here refers to the spin pairs X and Y rather than to the dipole couplings $\omega_{D,X}$ and $\omega_{D,Y}$, which may or may not be distinct.

The role of self- and distinct correlations is illuminated by the selection rules (derived in Appendix B[34])

$$C_{M,np}^{XX} = 0, \qquad \text{for } n = 1\text{–}3 \text{ and } p = 4\text{–}10, \tag{31a}$$

$$C_{M,np}^{XY} = \delta_{XY} C_{M,np}^{XX}, \qquad \text{for } n,p = 1\text{–}3, \tag{31b}$$

where the indices n and p refer to the basis operator ordering in Table II. The first rule shows that cross relaxation between longitudinal magnetization modes (n = 1–3) and ZQCs (p = 4–10) is induced entirely by distinct correlations. The second rule shows that cross relaxation among the longitudinal magnetization modes (in the A_2A' and $AA'A''$ systems) is induced entirely by self-correlations.

If distinct correlations are omitted, the relaxation behavior simplifies considerably (Fig. 1). According to selection rule (31a), the self-matrices $\mathbf{C}_M^{XX}$ are block-diagonal, with a 3×3 longitudinal magnetization block and a 7×7 ZQC block (Fig. 1, top right). The longitudinal self-relaxation is, therefore, fully determined by the 3×3 block, for which Eq. (30) yields $\mathbf{C}_{-M}^{XX} = \mathbf{C}_M^{XX}$. We then obtain from Eqs. (12), (13), and (23)

$$\mathbf{R}^{\text{self}} = \sum_X \sum_{M=0}^{2} (2 - \delta_{M0})\, \mathbf{C}_M^{XX}\, j_{XX}(M\omega_0), \tag{32}$$

where the matrices refer to the 3×3 longitudinal magnetization block. In the absence of distinct correlations, longitudinal relaxation is thus at most tri-exponential and the OSDF has no effect. In other words, the OSDF affects longitudinal relaxation only via distinct correlations, consistent with our earlier conclusion (Sec. II D 3) that the OSDF only affects cross relaxation between odd-rank and even-rank spin modes. Neglect of the OSDF does abolish the cross relaxation (induced by self-correlations) between odd-rank and even-rank ZQCs (Fig. 1, bottom right), but this decoupling within the ZQC manifold does not impact on the longitudinal

magnetizations, which are decoupled from the ZQCs in the absence of distinct correlations.

Substituting the $\mathbf{C}_M^{XX}$ matrices from Appendix A[34] into Eq. (32), we find

$$\mathbf{R}^{\text{self}} = \frac{1}{6}\begin{bmatrix} (j_{IS}^{\text{a}} + j_{IP}^{\text{a}}) & j_{IS}^{\text{c}} & j_{IP}^{\text{c}} \\ j_{IS}^{\text{c}} & (j_{IS}^{\text{a}} + j_{SP}^{\text{a}}) & j_{SP}^{\text{c}} \\ j_{IP}^{\text{c}} & j_{SP}^{\text{c}} & (j_{IP}^{\text{a}} + j_{SP}^{\text{a}}) \end{bmatrix}, \tag{33}$$

with the familiar auto- and cross relaxation combinations of (self) spectral densities[16]

$$j_X^{\text{a}} \equiv j_{XX}(0) + 3\, j_{XX}(\omega_0) + 6\, j_{XX}(2\omega_0), \tag{34a}$$

$$j_X^{\text{c}} \equiv 6\, j_{XX}(2\omega_0) - j_{XX}(0). \tag{34b}$$

F. Eigenmode decomposition

The time evolution of the total longitudinal magnetization, $\sigma_z \equiv \sigma_1 + \sigma_2 + \sigma_3$, after a nonselective excitation, with $\sigma_n(0) = \delta_{n1} + \delta_{n2} + \delta_{n3}$, may be decomposed into eigenmode contributions as

$$\frac{\sigma_z(t)}{\sigma_z(0)} = \sum_{k=1}^{10} C_k \exp(-\Lambda_k\, t). \tag{35}$$

The normalized mode amplitudes or weights, some of which may be zero for symmetry reasons, are given by

$$C_k = \frac{1}{3}(V_{1k} + V_{2k} + V_{3k})^2. \tag{36}$$

The eigenvalues Λ_k and eigenvectors $\{V_{nk},\ n = 1,2,\ldots,10\}$ are obtained by diagonalizing the symmetric 10×10 relaxation matrix by the similarity transformation

$$\mathbf{\Lambda} = \widetilde{\mathbf{V}}\mathbf{R}\mathbf{V}, \tag{37}$$

where $\widetilde{\mathbf{V}}$ is the transpose of the complex orthogonal matrix $\mathbf{V}$. Note that the defining relation, $\widetilde{\mathbf{V}} = \mathbf{V}^{-1}$, for an orthogonal matrix is the same whether $\mathbf{V}$ has real or complex elements.[35] In both cases, the columns (eigenvectors) $\mathbf{v}_k$ of $\mathbf{V}$ are orthonormal in the sense $\widetilde{\mathbf{v}}_k\, \mathbf{v}_l = \delta_{kl}$, which differs from the normal (Hermitian) inner product $\widetilde{\mathbf{v}}_k^*\, \mathbf{v}_l$ in a complex vector space. If the OSDF is neglected, as allowed in the EN and adiabatic regimes, the relaxation matrix $\mathbf{R}$ is real symmetric (Sec. II D 1) so the eigenvalues Λ_k are real.[35] In general, however, the spectral density is complex and $\mathbf{R}$ is complex symmetric. A sufficient condition for a complex symmetric matrix to be diagonalizable by a complex orthogonal similarity transformation is that all its eigenvalues are distinct,[35] which is the case whenever $\mathbf{R}$ is complex. (Degenerate eigenvalues do occur in the EN and adiabatic regimes, where $\mathbf{R}$ is real, and at all frequencies for the A_3 system with isotropic motion (Sec. III) since nuclear permutation symmetry then cancels the effect of the OSDF. Because a real symmetric matrix is always diagonalizable,[35] these degeneracies do not pose a problem. Furthermore, in all cases, eigenvalues with nonzero weights C_k are distinct.) In the dispersive regime, $\mathbf{R}$ can have up to three complex-conjugate pairs of eigenvalues, $\Lambda_k = \lambda_k \pm i\, \mu_k$, and associated weights, $C_k = a_k \pm i\, b_k$. The remaining eigenvalues and weights are real. By combining any complex-conjugate pairs, we can express the evolution function in terms of real quantities,

$$\frac{\sigma_z(t)}{\sigma_z(0)} = \sum_{k=1}^{N_\lambda} c_k(t)\, \exp(-\lambda_k\, t), \tag{38}$$

where $N_\lambda \le 10$ is the number of exponential components with nonzero weight. For real eigenvalues $c_k = C_k = a_k$, whereas complex-conjugate eigenvalue pairs have oscillating weights: $c_k(t) = 2\,[a_k \cos(\mu_k t) + b_k \sin(\mu_k t)]$. Whereas λ_k is always positive, a_k, b_k, and μ_k may have either sign. Thus, although Eq. (38) implies that the initial weights $c_k(0)$ sum up to 1, some of them may be negative.

The number, N_λ, of exponential components in Eq. (38) cannot exceed the dimension of the invariant subspace to which the longitudinal magnetizations belong. In Table III, we give N_λ for the different nuclear geometries and frequency regimes, with and without distinct correlations. Here, we have assumed an isotropic motion (Sec. III), so nuclear permutation symmetry is governed solely by geometry (Sec. II D 4). For anisotropic motions, N_λ can be larger (Sec. IV). In the absence of distinct correlations, $N_\lambda \le 3$ (Sec. II E), also for anisotropic motions. For self-relaxation induced by isotropic motions, N_λ equals the number of distinct dipole couplings. For isotropic motions, the OSDF only affects the longitudinal relaxation in the dispersive regime and then only for the less symmetric geometries A_2A' and $AA'A''$. If the OSDF is neglected, $N_\lambda = 5$ and 7, respectively, for these cases. When the OSDF is included, one (A_2A') or one — three ($AA'A''$) complex-conjugate eigenvalues occur, which split into two real eigenvalues in certain frequency ranges, thereby increasing the number of exponential components by one for the A_2A' system and by one, two, or three for the $AA'A''$ system. But these bifurcating eigenmodes have very small weights.

For the A_3 system with isotropic motion, the relaxation superoperator is invariant under permutation of the three geometrically and dynamically equivalent nuclei. Because only three orthonormal odd-rank modes exhibit this invariance (Sec. III B), $N_\lambda = 3$ in the dispersive regime. In the EN regime, selection rule (29) forbids coupling to the rank-3 mode (Sec. III B) so $N_\lambda = 2$. For A_3 case, the deviation from single-exponential relaxation is entirely due to motional correlations between dipole couplings of distinct spin pairs (with one shared spin).

TABLE III. Number, N_λ, of exponential components in different frequency regimes for longitudinal relaxation in a three-spin system with isotropic motion.

		Frequency regime		
Correlations	Geometry	EN	Dispersive	Adiabatic
All	$AA'A''$	4	7–10[a]	2
All	A_2A'	4	5–6[a]	2
All	A_3	2	3	2
Self	$AA'A''$	2	3	1
Self	A_2A'	2	2	1
Self	A_3	1	1	1

[a]See text.

In contrast, for the A_2A' and $AA'A''$ systems, multi-exponential relaxation is caused both by distinct correlations and by cross relaxation between the longitudinal modes of nonequivalent spins. For the A_2A' system, there are five odd-rank and one even-rank mode with $I \leftrightarrow S$ interchange symmetry (Sec. III C), so $N_\lambda = 6$ in the dispersive regime. If the OSDF is neglected, $N_\lambda = 5$ since coupling between odd-rank and even-rank modes is then no longer allowed (Sec. II D). However, also with a complex spectral density, $N_\lambda = 5$ in a limited frequency range where two distinct real eigenvalues merge into a complex conjugate pair. In the EN regime, where selection rule (29) only allows couplings within the rank-1 subspace, two of the modes are decoupled so that $N_\lambda = 4$. The reduction of the invariant spin operator subspace, and thus of N_λ, as the various symmetries are taken into account is presented in graphical form in Fig. 2, which contains most of the information from Table III. Like Table III, Fig. 2 only applies to the case of isotropic motion, which yields the maximum nuclear permutation symmetry.

G. Integral and initial relaxation rates

If the longitudinal relaxation does not deviate strongly from a single exponential, it can be characterized, with little loss of information, by a single effective rate, defined as

$$\widehat{R}_1 \equiv \left[\int_0^\infty \mathrm{d}t \frac{\sigma_z(t)}{\sigma_z(0)}\right]^{-1}. \tag{39}$$

Even when relaxation is markedly multi-exponential, this integral longitudinal relaxation rate may be useful (at the expense of some information loss) since it can be measured and computed under all conditions. By integrating the matrix form of BWR master equation (28) and applying the nonselective initial condition, we find

$$\widehat{R}_1 = \left[\frac{1}{3}\sum_{n=1}^{3}\sum_{p=1}^{3}(\mathbf{R}^{-1})_{np}\right]^{-1}. \tag{40}$$

Alternatively, we can insert the eigenmode expansion (35) into Eq. (39) to obtain

$$\widehat{R}_1 = \left[\sum_{k=1}^{N}\frac{C_k}{\Lambda_k}\right]^{-1} = \left[\sum_{k=1}^{N_\lambda}\frac{c'_k}{\lambda_k}\right]^{-1}, \tag{41}$$

where $c'_k = C_k = a_k$ for real eigenvalues, whereas $c'_k = 2\,\lambda_k\,(a_k\,\lambda_k + b_k\,\mu_k)/(\lambda_k^2 + \mu_k^2)$ for complex-conjugate eigenvalue pairs. Consequently, $\widehat{R}_1$ is always real. The real weights c'_k sum up to 1, but some of them may be negative.

The initial longitudinal relaxation rate is defined as

$$R_1^0 \equiv -\frac{\mathrm{d}}{\mathrm{d}t}\left[\frac{\sigma_z(t)}{\sigma_z(0)}\right]\Big|_{t=0}. \tag{42}$$

By setting $t = 0$ in BWR master equation (22) and applying the nonselective initial condition, we find

$$R_1^0 = \frac{1}{3}\sum_{n=1}^{3}\sum_{p=1}^{3}R_{np} = \frac{1}{3}\sum_{n=1}^{3}\sum_{p=1}^{3}R_{np}^{\mathrm{self}}, \tag{43}$$

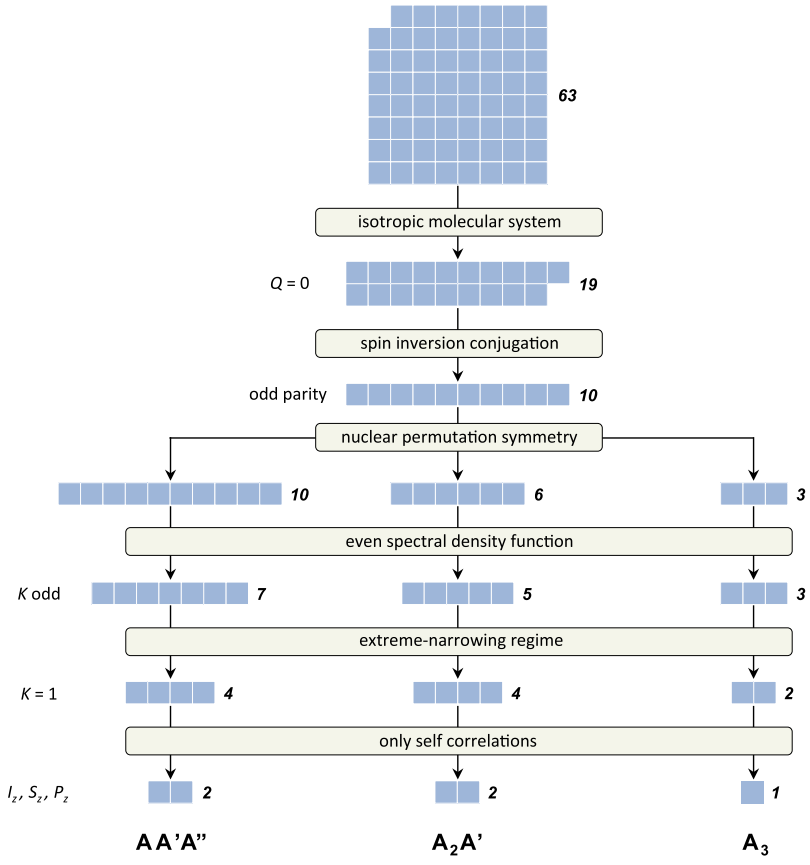

FIG. 2. Reduction of the spin operator subspace required to describe longitudinal relaxation in three-spin systems with isotropic motion. To the right of each operator block is given the number of basis operators that exhibit all the symmetries that follow from the properties listed above it. This is also the maximum number of exponential components in the relaxation function.

where the last form follows from Eqs. (23) and (31b). The initial rate is thus unaffected by distinct correlations (and the OSDF). Combining this result with Eqs. (33) and (34), we obtain

$$R_1^0 = \frac{2}{3}\left(R_1^{IS} + R_1^{IP} + R_1^{SP}\right), \tag{44}$$

where R_1^{IS} is the relaxation rate for the isolated two-spin IS system[1]

$$R_1^{IS} = \frac{1}{2}\left[\, j_{IS,IS}(\omega_0) + 4\, j_{IS,IS}(2\omega_0)\,\right]. \tag{45}$$

The initial rate may thus be regarded as the average two-spin rate, obtained by taking the arithmetic average of the relaxation rates for three isolated two-spin systems and then multiplying by 2 since, in the three-spin system, each spin is dipole-coupled to two other spins.

Although the initial rate R_1^0 is unaffected by distinct correlations, it differs, in general, from the integral self-relaxation rate $\widehat{R}_1^{\rm self}$, obtained by substituting $\mathbf{R}^{\rm self}$ from Eq. (33) into Eq. (40). In contrast to the initial rate, $\widehat{R}_1^{\rm self}$ generally involves the zero-frequency spectral densities, $j_{XX}(0)$. Only for the A_3 system with motional models that do not violate the dynamic equivalence of the three spins is $\widehat{R}_1^{\rm self} = R_1^0$ (Secs. III B and IV).

III. LONGITUDINAL RELAXATION BY ISOTROPIC MOTIONS

In this section, we illustrate the theory developed in Sec. II by quantitatively examining the longitudinal relaxation behavior for the A_3, A_2A', and $AA'A''$ spin systems in the special case where the dipole couplings are modulated by an isotropic motion. (Anisotropic motions are considered in Sec. IV.) If the motion is isotropic in the molecular frame, the time correlation functions $G_{XY}(\tau)$ defined in Eq. (9) take the simple exponential form

$$G_{XY}(\tau) = \frac{1}{5}\, P_2(\cos\beta_{XY})\, \exp(-\tau/\tau_{\rm c}), \tag{46}$$

where β_{XY} is the fixed angle between internuclear vectors X and Y, that is, $\cos\beta_{XY} = (\boldsymbol{r}_X \cdot \boldsymbol{r}_Y)/(r_X\, r_Y)$. This form is valid for the spherical-top rotational diffusion model and for the strong-collision model, with the correlation time $\tau_{\rm c}$ being the rotational correlation time, $(6\, D_{\rm R})^{-1}$, or the mean survival time, respectively. The spectral density function in Eq. (12) can then be factorized as

$$J_{XY}(\omega) = D_{XY}\, J(\omega), \tag{47}$$

with the real-valued geometric factor

$$D_{XY} \equiv \frac{4}{3}\,\omega_{{\rm D},X}\,\omega_{{\rm D},Y}\, G_{XY}(0) = \frac{4}{15}\,\omega_{{\rm D},X}\,\omega_{{\rm D},Y}\, P_2(\cos\beta_{XY}), \tag{48}$$

and the complex-valued reduced spectral density function

$$J(\omega) \equiv j(\omega) + ik(\omega) \equiv \int_0^\infty {\rm d}\tau\, \exp(i\,\omega\tau)\, \frac{G_{XY}(\tau)}{G_{XY}(0)} = \frac{\tau_{\rm c}}{1 + (\omega\tau_{\rm c})^2}\,(1 + i\,\omega\tau_{\rm c})\,. \tag{49}$$

In Sec. III A, we examine the deviation from single-exponential relaxation and in Subsections III B–III D, we present the complete frequency dependence (dispersion) of the integral relaxation rate $\widehat{R}_1$, the integral self-relaxation rate $\widehat{R}_1^{\rm self}$, and the initial rate R_1^0, as well as of the eigenmode rates λ_k and weights c_k, for the three spin systems. We also examine the effect of the OSDF. The numerical results were computed from the 10×10 relaxation matrix defined by Eqs. (23) and (47)–(49) and the $\mathbf{C}_M^{XY}$ matrices in Appendix A.[34] All relaxation rates are presented in reduced form, in units of $\omega_{{\rm D},IS}^2\,\tau_{\rm c}$ versus the reduced frequency $\omega_0\,\tau_{\rm c}$. As geometric parameters, we use the interior angles of the triangle, denoted by β_I, β_S, and β_P. We thus specify $\beta_P = \beta_{IP,SP}$ for the A_2A' system, and $\beta_I = \beta_{IS,IP}$ and $\beta_S = \pi - \beta_{IS,SP}$ for the $AA'A''$ system. The remaining dipole couplings are then, for the A_2A' system,

$$\omega_{{\rm D},IP} = \omega_{{\rm D},SP} = 8\,\sin^3(\beta_P/2)\;\omega_{{\rm D},IS}, \tag{50}$$

and for the $AA'A''$ system,

$$\omega_{{\rm D},IP} = \left[\frac{\sin(\beta_I + \beta_S)}{\sin\beta_S}\right]^3 \omega_{{\rm D},IS}, \tag{51a}$$

$$\omega_{{\rm D},SP} = \left[\frac{\sin(\beta_I + \beta_S)}{\sin\beta_I}\right]^3 \omega_{{\rm D},IS}. \tag{51b}$$

A. Non-exponential relaxation

To examine the deviation from single-exponential relaxation of the normalized longitudinal non-equilibrium magnetization, $\sigma_z(t)/\sigma_z(0)$, we compare the multi-exponential decay obtained from eigenmode expansion (38) with the single-exponential decay $\exp(-\widehat{R}_1\, t)$, with the integral longitudinal relaxation rate $\widehat{R}_1$ obtained from Eq. (40) or (41). We define a deviation function as $\delta(t) \equiv \exp(-\widehat{R}_1\, t) - \Sigma_k\, c_k(t)\exp(-\lambda_k t)$.

As noted many years ago,[2,4] the deviation from single-exponential relaxation is insignificant for the A_3 spin system with isotropic motion. The largest deviation, with $\delta_{\rm max} = 0.002$, is found in the EN regime. Such small deviations are certainly beyond experimental detection. For the A_2A' spin system, the deviation from single-exponential relaxation is more pronounced, as shown in Fig. 3 for $\beta_P = 120°$. Again, the deviation is larger in the EN regime ($\delta_{\rm max} = 0.13$) than in the dispersive regime ($\delta_{\rm max} = 0.05$ at $\omega_0\,\tau_{\rm c} = 1$). If the OSDF is omitted, the deviations become slightly larger ($\delta_{\rm max} = 0.14$ and 0.06, respectively). The largest deviations are seen for the $AA'A''$ spin system, as illustrated in Fig. 4 for a geometry with $\beta_I = 80°$ and $\beta_S = 40°$. Here, the maximum deviation $\delta_{\rm max}$ is 0.23 in the EN regime and 0.16 at $\omega_0\,\tau_{\rm c} = 1$.

In all cases, the initial decay is faster for $\sigma_z(t)/\sigma_z(0)$ than for the exponential function $\exp(-\widehat{R}_1\, t)$. In other words, the calculations show that $R_1^0 > \widehat{R}_1$. Since distinct correlations affect $\widehat{R}_1$ but not R_1^0 (Sec. II G), this observation is consistent with a slowing down of longitudinal relaxation by distinct correlations, as can be demonstrated in a general way for the A_3 system with isotropic motion.[4] As seen from Eq. (39), the areas under the two decay curves shown in each panel of Figs. 3 and 4 are equal by definition. Therefore, $\sigma_z(t)/\sigma_z(0)$

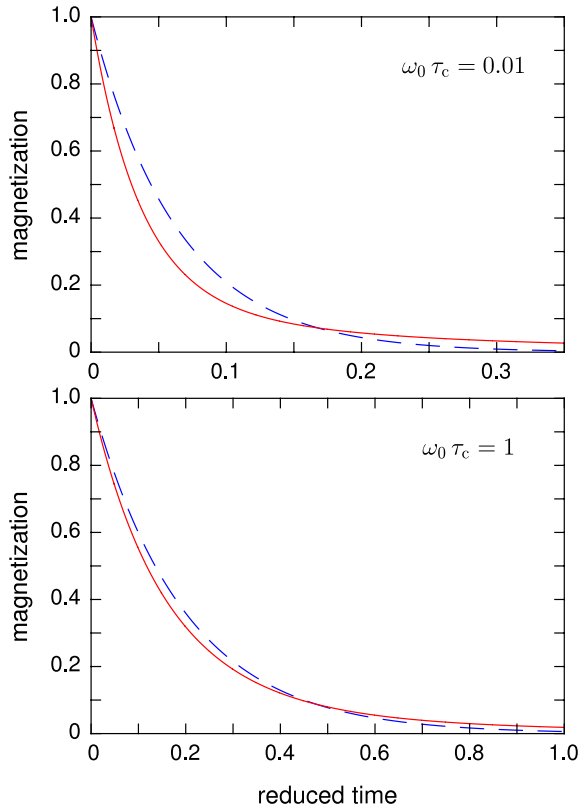

FIG. 3. Decay of the longitudinal magnetization, $\sigma_z(t)/\sigma_z(0)$, versus reduced time, $t\times\omega^2_{D,IS}\tau_c$, for the A_2A' spin system with $\beta_P = 120°$ and isotropic motion. The multi-exponential decay obtained from Eq. (38) (solid curve) is compared with the single-exponential decay $\exp(-\widehat{R}_1\,t)$ (dashed curve).

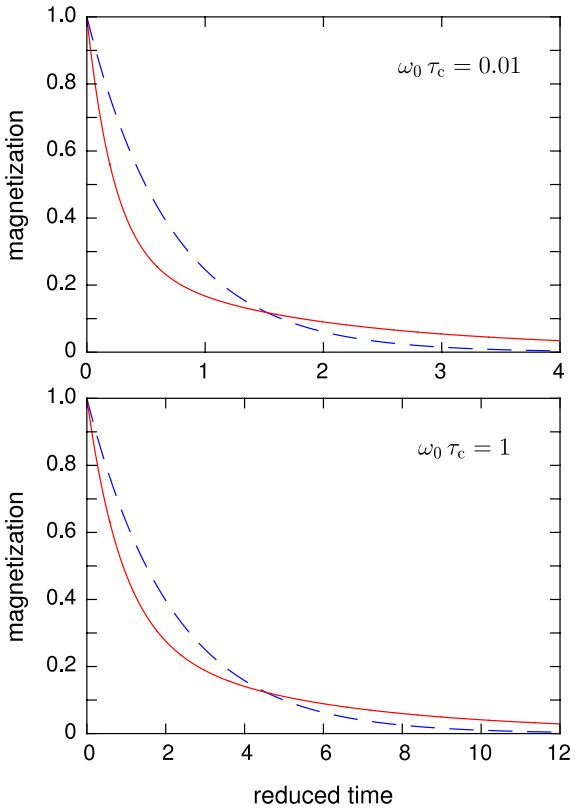

FIG. 4. Decay of the longitudinal magnetization, $\sigma_z(t)/\sigma_z(0)$, versus reduced time, $t\times\omega^2_{D,IS}\tau_c$, for the $AA'A''$ spin system with $\beta_I = 80°$ and $\beta_S = 40°$ and isotropic motion. The multi-exponential decay obtained from Eq. (38) (solid curve) is compared with the single-exponential decay $\exp(-\widehat{R}_1\,t)$ (dashed curve).

must decay more slowly than $\exp(-\widehat{R}_1\,t)$ at longer times, leading to a crossover (Figs. 3 and 4). An exponential fit to the multi-exponential decay is, therefore, likely to yield an effective rate that is close to the integral rate $\widehat{R}_1$. However, if the deviation from single-exponential relaxation is substantial, it may be better to determine the integral rate directly from the experimental data.

B. Relaxation dispersion in the A_3 system

For the A_3 spin system, the three nuclei are geometrically equivalent and if the motion is isotropic, as assumed in this section, the relaxation superoperator is invariant under permutation of all three nuclei (Sec. II D 4). The spin operator basis in Table II is not fully symmetry-adapted for this case, because we have broken the nuclear permutation symmetry by first coupling spins I and S and then coupling their resultant to spin P (Sec. II C). However, the ten basis operators in Table II can be transformed into a fully symmetry-adapted basis comprising three operators that are even and seven that are odd under permutations of the three nuclei. In this basis, the relaxation supermatrix is block-diagonal and longitudinal relaxation is fully described within the even subspace, spanned by the following fully symmetry-adapted orthonormal basis operators (distinguished by an overbar from the operators in Table II),[17]

$$\bar{B}_1 = \frac{1}{\sqrt{3}}\,(B_1 + B_2 + B_3) = \frac{1}{\sqrt{6}}\,[I_z + S_z + P_z]\,, \tag{52a}$$

$$\bar{B}_2 = -\frac{1}{3}\left(\sqrt{5}\,B_4 + 2\,B_6\right) = \frac{\sqrt{8}}{\sqrt{15}}\,[I_z(\boldsymbol{S}\cdot\boldsymbol{P}) + S_z(\boldsymbol{I}\cdot\boldsymbol{P}) + P_z(\boldsymbol{I}\cdot\boldsymbol{S})]\,, \tag{52b}$$

$$\bar{B}_3 = B_7 = \frac{2}{\sqrt{5}}\,[5\,I_zS_zP_z - I_z(\boldsymbol{S}\cdot\boldsymbol{P}) - S_z(\boldsymbol{I}\cdot\boldsymbol{P}) - P_z(\boldsymbol{I}\cdot\boldsymbol{S})]\,. \tag{52c}$$

Consequently, longitudinal relaxation in the A_3 system is in general tri-exponential. However, in the EN regime, selection rule (29) ensures that the rank-1 modes $\bar{\sigma}_1$ and $\bar{\sigma}_2$ do not couple to the rank-3 ZQC $\bar{\sigma}_3$ (Table II). Therefore, longitudinal relaxation is bi-exponential in the EN regime.

Since all three operators in Eq. (52) are of odd rank, Eq. (30) shows that $\bar{\mathbf{C}}^{XY}_{-M} = \bar{\mathbf{C}}^{XY}_{M}$ in the fully symmetry-adapted basis. It then follows from Eq. (23), which is valid for any orthonormal basis, and Eqs. (12) and (13a), which yield $J_{XY}(M\omega_0) + J_{XY}(-M\omega_0) = 2\,j_{XY}(M\omega_0)$, that the OSDF does not affect longitudinal relaxation in the A_3 system with isotropic motion. (As we shall see in Sec. IV B, this is not always true if the motion is anisotropic.) The three eigenvalues Λ_k of $\mathbf{R}$ (and of $\bar{\mathbf{R}}$) and the associated weights C_k are, therefore, real. From Eqs. (23), (30), (47)–(49), and (52) and the $\mathbf{C}^{XY}_M$

matrices in Appendix A,[34] we obtain the relaxation matrix $\bar{\mathbf{R}}$ in the fully symmetry-adapted basis (Appendix C[34]), in full agreement with the results presented by Werbelow and Grant.[17]

Figure 5 shows the eigenmode rates λ_k and the corresponding nonzero weights c_k (=a_k) in Eq. (38), obtained by diagonalizing the relaxation matrix $\mathbf{R}$ as in Eq. (37). Here, and in the following, the eigenmodes are numbered in order of decreasing absolute real weight $|\mathrm{Re}\{C_k\}|$ at $\omega_0\tau_c = 1$. The rank order of the three eigenvalues is independent of frequency, but λ_1 exhibits avoided crossings with λ_3 and λ_2 at $\omega_0\tau_c \approx 0.28$ and 1.09, respectively, where the weights of the corresponding eigenmodes are equal. Each eigenmode is a linear combination of the longitudinal magnetization mode $\bar{\sigma}_1$ and the ZQCs $\bar{\sigma}_2$ and $\bar{\sigma}_3$, but the dominant eigenmode (different in each frequency regime) is essentially a $\bar{\sigma}_1$ mode.

To reconcile the very nearly exponential longitudinal relaxation in the A_3 system (Sec. III A) with the distinctly different eigenvalues in Fig. 5, the following observations can be made. In the EN regime, one eigenmode, which is essentially a longitudinal mode, dominates strongly ($c_3 = 0.9908$). In the dispersive regime, two eigenmodes have equal weight (close to 0.5) at the avoided-crossing frequencies, but then the corresponding eigenvalues are nearly equal so the longitudinal relaxation remains almost exponential. One eigenvalue has a high-frequency plateau, $\lambda_3 = (9/20)\,\omega_{D,IS}^2\,\tau_c$ for $\omega_0\tau_c \gg 1$, but the corresponding weight is effectively zero in the adiabatic regime. The weight of the minor adiabatic eigenmode is not negligible ($c_1 = 0.0412$) but λ_1 is close to λ_2 for $\omega_0\tau_c > 1$, so, again, the deviation from exponential longitudinal relaxation is insignificant.

The dipolar relaxation of the total magnetization of two isochronous spins–1/2 is isomorphic with the quadrupolar relaxation of a single spin-1. However, because of the occurrence of distinct correlations, this isomorphism does not carry over to three or more spins. The longitudinal relaxation of a single quadrupolar spin-3/2 is bi-exponential in the dispersive regime and exponential in the EN regime,[36] and the relaxation rates only involve the spectral densities $j(\omega_0)$ and $j(2\omega_0)$. In contrast, the total longitudinal magnetization of three equivalent spins–1/2 relaxes tri-exponentially in the dispersive regime and bi-exponentially in the extreme-narrowing regime (Table III, Fig. 5). Moreover, the component rates also depend on the zero-frequency spectral density $j(0)$. Inserting the inverse of $\bar{\mathbf{R}}$ into Eq. (40), we find, for the integral relaxation rate,

$$\widehat{R}_1 = \frac{9}{10}\omega_D^2 \frac{j_0(63\,j_1 + 256\,j_2) + 18\,j_1^2 + 110\,j_1\,j_2 + 128\,j_2^2}{216\,j_0 + 63\,j_1 + 112\,j_2}, \tag{53}$$

where we have used the short-hand notation $j_M \equiv j(M\omega_0)$. Although $\widehat{R}_1$ depends on j_0, this is not a linear dependence that would give rise to a high-frequency plateau in the dispersion profile $\widehat{R}_1(\omega_0)$. The j_0 dependence derives from the auto- and cross relaxation rates of the ZQCs $\bar{\sigma}_2$ and $\bar{\sigma}_3$, which couple to the longitudinal mode $\bar{\sigma}_1$ via cross relaxation rates (produced

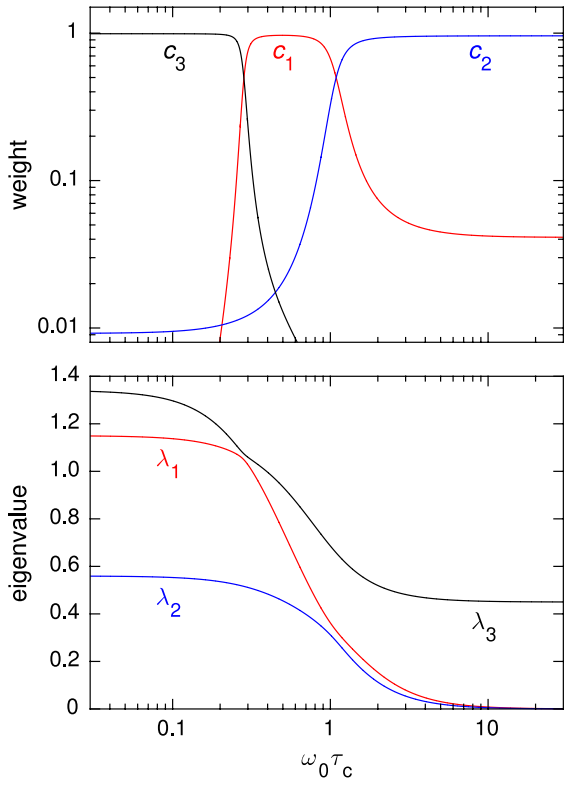

FIG. 5. Eigenmode rates λ_k (in units of $\omega_D^2\,\tau_c$) and weights c_k for the A_3 spin system with isotropic motion versus the reduced Larmor frequency $\omega_0\tau_c$.

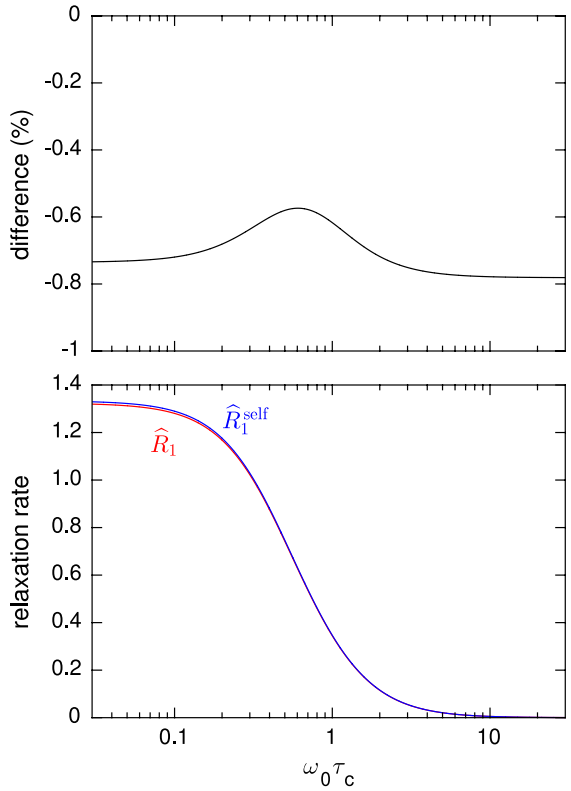

FIG. 6. Dispersion of the integral relaxation rate $\widehat{R}_1$ and its self-correlation part $\widehat{R}_1^{\mathrm{self}}$ (both in units of $\omega_D^2\,\tau_c$) for the A_3 spin system with isotropic motion. The upper panel shows the relative difference between the two rates.

by distinct correlations) that go to zero at high frequencies since they do not involve j_0 (Appendix C[34]).[17] This is seen by rearranging Eq. (53) into

$$\widehat{R}_1 = \frac{4}{15}\omega_D^2\,(\,j_1 + 4\,j_2 - \delta\,)\,, \tag{54}$$

and noting that $\delta = j_1/64$ when $\omega_0\tau_c \gg 1$. Therefore, at high frequencies, $\widehat{R}_1$ does not exhibit a plateau but goes to zero as ω_0^{-2} and is then numerically very close to $R_1^0 = \widehat{R}_1^{\rm self} = (4/15)\,\omega_D^2\,(j_1 + 4\,j_2)$. This behavior is evident from Fig. 6, which also shows that the distinct correlations slow down the longitudinal relaxation by at most 0.8%.

C. Relaxation dispersion in the A_2A' system

The ISTO basis in Table II allows us to directly exploit the $I \leftrightarrow S$ interchange symmetry of the A_2A' system with spin P at the apex and with isotropic motion (Sec. II D 4). Forming the symmetric magnetization mode $\sigma_{IS} = (\sigma_1 + \sigma_2)/\sqrt{2}$, we see from Table II that five of the remaining spin modes are even (invariant) under $I \leftrightarrow S$ interchange, while three modes ($n = 5$, 8, and 9) are odd. Longitudinal relaxation in the A_2A' system can, therefore, be fully described within the invariant subspace of the six even basis operators. In the EN regime, the interchange symmetric operators B_7 and B_{10} with rank $K > 1$ can be omitted on account of selection rule (29), leaving an invariant subspace spanned by four fully symmetry-adapted basis operators. In other words, longitudinal relaxation in the A_2A' system with isotropic motion involves (at most) six exponential components in the dispersive regime, but only four components in the EN regime (Table III).

Figure 7 shows, for an A_2A' system with $\beta_P = 120°$, the six eigenmode rates λ_k and the corresponding nonzero weights c_k for the four eigenvalues that remain real at all frequencies. Each of these four eigenvalues exhibit one avoided crossing and the corresponding eigenmodes are each dominant in some frequency range (Fig. 7). In contrast to the A_3 system, the OSDF now affects longitudinal relaxation in the dispersive regime, where the real eigenvalues λ_4 and λ_5 coalesce to a complex conjugate pair at $\omega_0\tau_c \approx 0.80$ and then split up again at $\omega_0\tau_c \approx 2.70$. These two eigenmodes have significant but not dominant weights, e.g., $c_4 + c_5 = 0.06$ at $\omega_0\tau_c = 0.7$ and $c_{4,5}(0) = 0.12$ at $\omega_0\tau_c = 0.9$. We also note that the two eigenmodes (c_3 and c_1) that have nonzero weights in the adiabatic regime correspond to eigenvalues without a high-frequency plateau (due to j_0). If the OSDF is discarded, the eigenvalues λ_1, λ_3, and λ_6 and the corresponding weights are hardly affected, but the complex conjugate eigenvalues $\lambda_{4,5}$ and the real eigenvalue λ_2 are now replaced by two real eigenvalues with an avoided crossing. (Note that Fig. 7 shows a crossing for the real parts of these eigenvalues; the complex eigenvalues are distinct at all frequencies.) The number of exponential components in the dispersive regime is thus five without the OSDF, but five or six (depending on frequency) when the OSDF is included. In the EN regime (where the

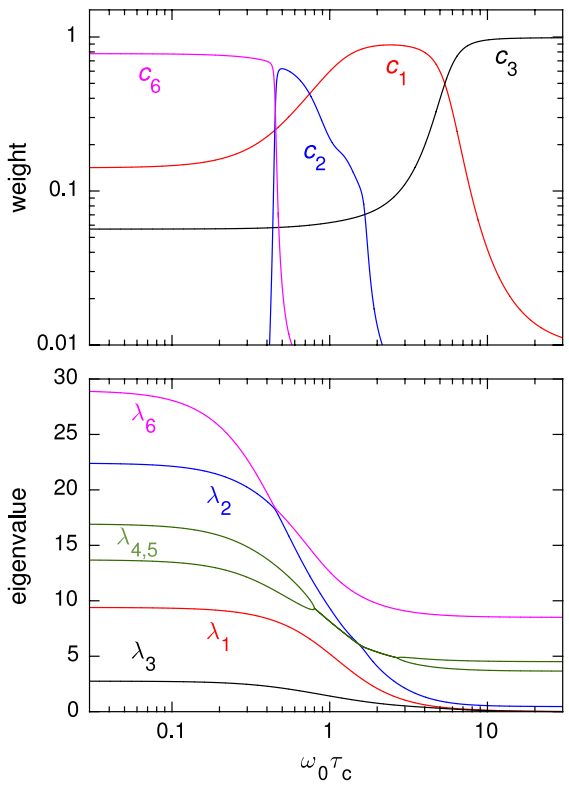

FIG. 7. Eigenmode rates λ_k (in units of $\omega_{D,IS}^2\tau_c$) and weights c_k for an A_2A' spin system with $\beta_P = 120°$ and isotropic motion versus the reduced Larmor frequency $\omega_0\tau_c$.

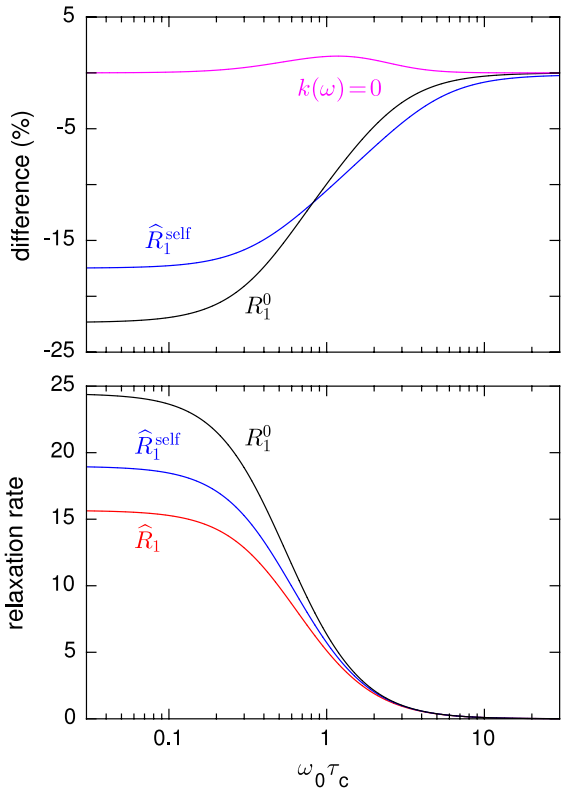

FIG. 8. Dispersion of the integral relaxation rate $\widehat{R}_1$, its self-correlation part $\widehat{R}_1^{\rm self}$, and the initial relaxation rate R_1^0 (all three in units of $\omega_{D,IS}^2\tau_c$) for an A_2A' spin system with $\beta_P = 120°$ and isotropic motion. The upper panel shows the relative differences between $\widehat{R}_1$ and $\widehat{R}_1^{\rm self}$ (blue), between $\widehat{R}_1^{\rm self}$ and R_1^0 (black), and between $\widehat{R}_1$ with and without the OSDF (magenta).

OSDF is negligible), there are four components: c_6, c_1, c_3 (shown in Fig. 7), and c_5 (corresponding to the larger of the two bifurcated eigenvalues; $c_4 = 0$ in the EN regime).

The only previous theoretical study of relaxation in the A_2A' system over the full frequency range is that of Schneider, who also included the OSDF.[13] Comparing our numerical results for C_k and Λ_k with those tabulated by Schneider, we find agreement to the last quoted decimal in the EN and adiabatic regimes and essential agreement (nearly always to the second decimal place in C_k and to the first decimal place in Λ_k) in the dispersive regime.

Figure 8 shows the dispersion profiles of the total ($\widehat{R}_1$) and self-($\widehat{R}_1^{\rm self}$) integral relaxation rates and of the initial relaxation rate (R_1^0). As compared to the A_3 system, distinct correlations have a much larger effect in the A_2A' system, reducing $\widehat{R}_1$ by as much as 36% (in the EN regime) as compared to R_1^0, which is unaffected by distinct correlations (Sec. II G). Unlike in the A_3 system, $\widehat{R}_1^{\rm self}$ is not identical to R_1^0, being 17.5% smaller in the EN regime. Figure 8 also shows that the OSDF increases $\widehat{R}_1$ by up to 1.5% in the dispersive regime. The maximum OSDF effect for the A_2A' system, 2.6%, is found for $\beta_P = 108°$.

D. Relaxation dispersion in the AA′A″ system

As expected, the most complicated relaxation behavior is obtained when all three dipole couplings are distinct so there is no nuclear permutation symmetry at all. Then, all ten spin modes in Table II contribute and longitudinal relaxation can, in principle, involve up to ten exponential components. In the EN regime, there can be at most six components since selection rule (29) restricts the invariant subspace to the six rank-1 modes (Table II). We illustrate the generic AA′A″ relaxation behavior with results for a specific nuclear geometry with $\beta_I = 80°$ and $\beta_S = 40°$ (and thus $\beta_P = 60°$).

As for the A_2A' system, four eigenvalues (λ_1–λ_4) are real at all frequencies (Fig. 9, bottom). However, there are now three complex-conjugate pairs of eigenvalues (Fig. 9, top). Two of them bifurcate at both low and high frequencies but further away from $\omega_0\tau_c = 1$ than for the A_2A' system ($\lambda_{5,6}$ bifurcates at $\omega_0\tau_c = 0.0783$ and 5.94, $\lambda_{7,8}$ at $\omega_0\tau_c = 0.0493$ and 18.8), whereas the third complex-conjugate eigenvalue ($\lambda_{9,10}$) only bifurcates in the adiabatic regime (at $\omega_0\tau_c = 62.4$), where this mode has vanishingly small weight. The weights of the four real eigenmodes are shown in two formats in Fig. 10. These four modes contribute in the EN and dispersive regimes, but only the two modes that lack a high-frequency eigenvalue plateau (Fig. 9) contribute in the adiabatic regime. In the EN regime, the two additional modes c_7 and c_8 have negligibly small weights that decrease gradually to zero as the zero-field limit is approached. Hence, Table III and Fig. 2 quote $N_\lambda = 4$ (rather than 6) for the AA′A″ system in the EN regime.

In the frequency range $0.0783 < \omega_0\tau_c < 5.94$, where there are three complex-conjugate eigenvalues, longitudinal relaxation involves seven exponential components. The

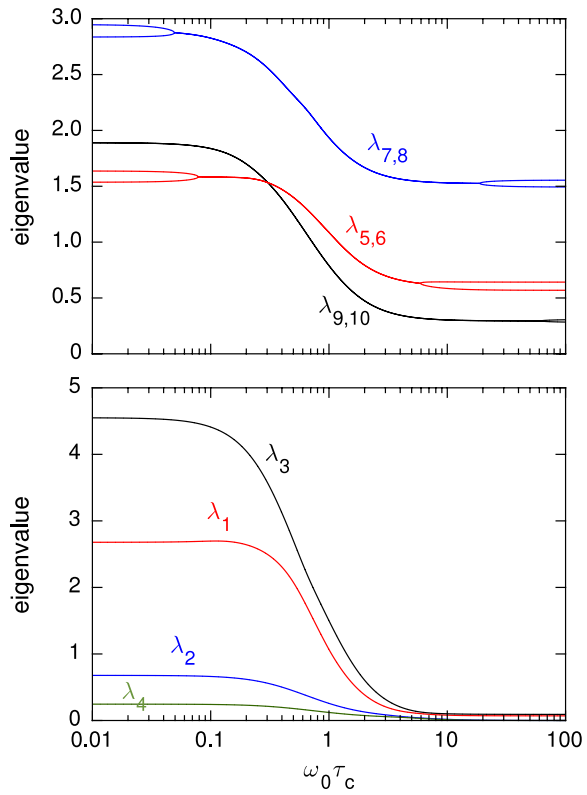

FIG. 9. Eigenmode rates λ_k (in units of $\omega_{D,IS}^2\tau_c$) for an AA′A″ spin system with $\beta_I = 80°$ and $\beta_S = 40°$ and isotropic motion versus the reduced Larmor frequency $\omega_0\tau_c$. Shown in separate panels are the four major real eigenvalues (bottom) and three minor complex conjugate eigenvalues (top).

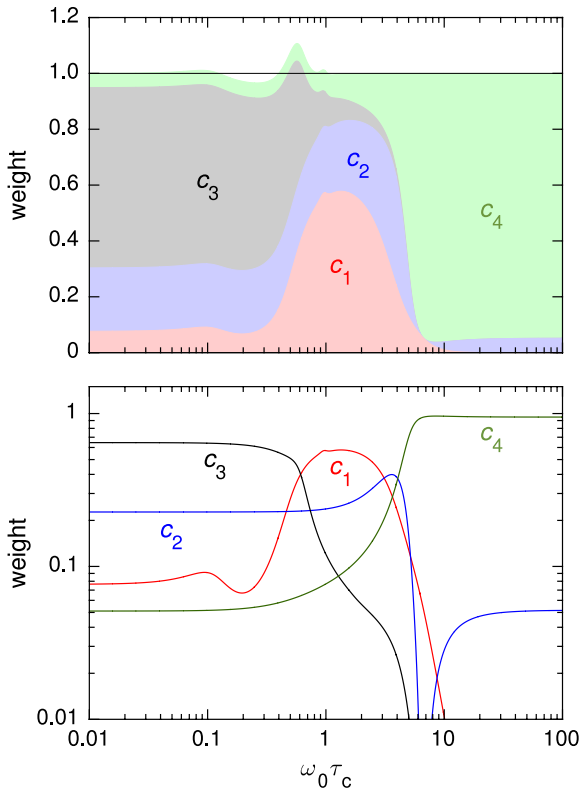

FIG. 10. Eigenmode weights c_k for an AA′A″ spin system with $\beta_I = 80°$ and $\beta_S = 40°$ and isotropic motion versus the reduced Larmor frequency $\omega_0\tau_c$. Only the four major eigenmodes with real weights and real eigenvalues are shown. In the top panel, the cumulative weights are shown on a linear scale so the colored areas correspond to the relative mode contributions.

influence of the three complex-conjugate modes is the largest at $\omega_0\tau_c = 0.57$, where their combined weight is −0.11. Accordingly, the sum of the four real mode weights is 1.11 at this frequency (Fig. 10, top). Outside this frequency range, one or more eigenvalues has bifurcated, so the relaxation function contains eight, nine, or ten exponential components, but the combined weight of modes c_5–c_{10} then never deviates by more than −0.01 from zero (Fig. 10, top). If the OSDF is omitted, there are seven distinct real eigenvalues which maintain their rank order at all frequencies and exhibit six avoided crossings. The relaxation function then contains seven components in the dispersive regime and four in the EN regime.

Figure 11 shows the dispersion profiles of the total ($\widehat{R}_1$) and self-($\widehat{R}_1^{\rm self}$) integral relaxation rates and of the initial relaxation rate (R_1^0). Distinct correlations have an even larger effect than for the A_2A' system, reducing $\widehat{R}_1$ by as much as 58% (in the EN regime) as compared to R_1^0. The OSDF increases $\widehat{R}_1$ by at most 0.29% in the dispersive regime. Other $AA'A''$ geometries yield larger OSDF effects, which, however, do not exceed the A_2A' maximum of 2.6%.

IV. ANISOTROPIC MOTIONS

The analysis in Sec. III was restricted to the simplest possible time correlation function, with the single-exponential form of Eq. (46). However, the relaxation theory in Sec. II is valid for any motional model as long as the bath is isotropic. Replacing Eq. (46) by an anisotropic motional model will obviously affect the results of Sec. III in a quantitative way. More importantly, if the dynamic symmetry is broken (Sec. II D 4), the relaxation behavior may also be altered qualitatively. For the A_3 and A_2A' systems, where nuclear permutation symmetry reduces the invariant subspace in the case of isotropic motion (Fig. 2), anisotropic motions may introduce additional relaxation components and can enhance the influence of the OSDF on longitudinal relaxation, also in the A_3 system. In the following, we examine two anisotropic motional models, one of which breaks the dynamic symmetry and one which does not.

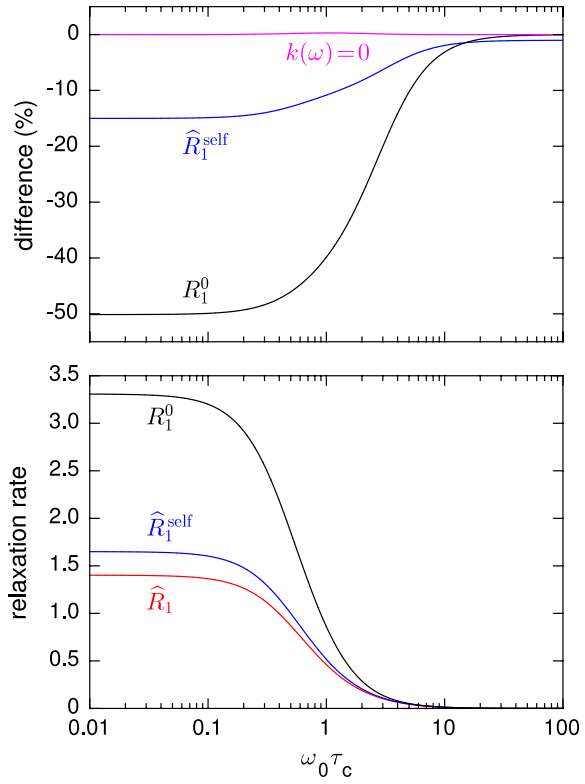

FIG. 11. Dispersion of the integral relaxation rate $\widehat{R}_1$, its self-correlation part $\widehat{R}_1^{\rm self}$, and the initial relaxation rate R_1^0 (all three in units of $\omega_{D,IS}^2\tau_c$) for an $AA'A''$ spin system with $\beta_I = 80°$ and $\beta_S = 40°$ and isotropic motion. The upper panel shows the relative differences between $\widehat{R}_1$ and $\widehat{R}_1^{\rm self}$ (blue), between $\widehat{R}_1^{\rm self}$ and R_1^0 (black), and between $\widehat{R}_1$ with and without the OSDF (magenta).

A. Axial internal rotation

First, we consider the situation where, in addition to spherical-top rotational diffusion (as in Sec. III), there is a statistically independent internal rotational diffusion of the spin system about an axis perpendicular to the nuclear plane. In the A_3 case, this model might represent a spherical macromolecule with a methyl group that rotates freely about its threefold axis. As shown in Appendix D,[34] the time correlation function for this model is

$$G_{XY}(\tau) = \frac{1}{20}\exp(-\tau/\tau_{\rm R})\,[1 + 3\,\cos(2\beta_{XY})\exp(-\tau/\tau_{\rm int})]\,, \tag{55}$$

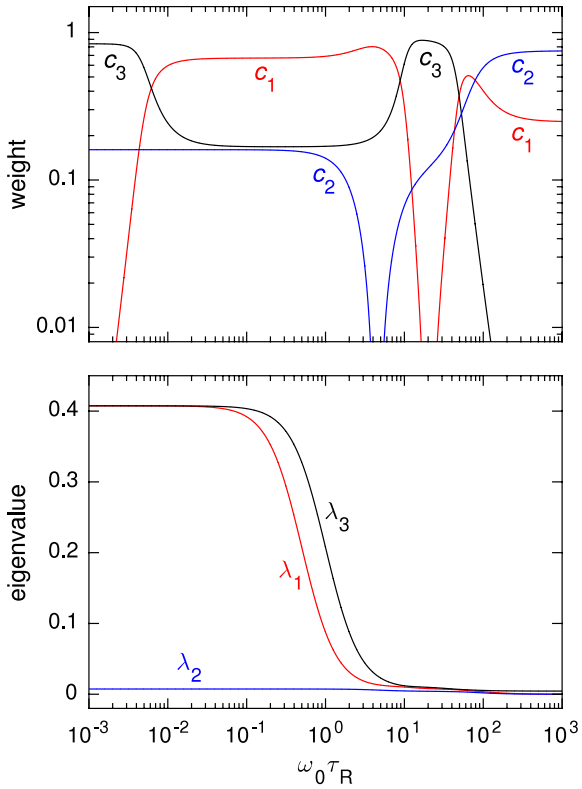

FIG. 12. Eigenmode rates λ_k (in units of $\omega_D^2\tau_R$) and weights c_k versus the reduced Larmor frequency $\omega_0\tau_R$ for the A_3 spin system modulated by spherical-top tumbling and internal rotation with $\tau_R = 100\,\tau_{\rm int}$.

with $\tau_R = 1/(6\,D_R)$ and $\tau_{int} = 1/(4\,D_{int})$. The spectral density functions now cannot be split into geometric and purely dynamic factors, as in Eq. (47). Instead, we obtain from Eqs. (12) and (55)

$$J_{XY}(\omega) = \frac{1}{15}\,\omega_{D,X}\,\omega_{D,Y}\,[J_R(\omega) + 3\,\cos(2\beta_{XY})\,J_{int}(\omega)]\,, \tag{56}$$

where $J_R(\omega)$ and $J_{int}(\omega)$ are given by Eq. (49) with τ_c replaced by τ_R or $(1/\tau_R + 1/\tau_{int})^{-1}$, respectively.

For the A_3 system, all dipole vectors are affected in the same way by the internal rotation so the nuclear permutation symmetry is not affected. Formally, this conclusion follows by noting that the factor within square brackets in Eq. (56) is the same for all self correlations, since $\beta_{XX} = 0$, and for all distinct correlations, since $\cos(2\,\beta_{XY}) = -1/2$ for $\beta_{XY} = 60°$ or 120°. For the A_2A' system, the internal rotation does not affect the dynamic symmetry of the two geometrically equivalent nuclei I and S, as seen by noting that $\cos(2\beta_{IS,SP}) = \cos[2(\pi - \beta_S)] = \cos(2\beta_S) = \cos(2\beta_I) = \cos(2\beta_{IS,IP})$ so that $J_{IS,IP}(\omega) = J_{IS,SP}(\omega)$. Consequently, internal rotation about an axis perpendicular to the nuclear plane does not affect the nuclear permutation symmetry for any of the three spin systems.

Even though internal rotation does not alter the relaxation behavior qualitatively, it can have substantial quantitative effects. For example, Fig. 12 shows the three eigenvalues and associated nonzero weights for the A_3 system when $\tau_R = 100\,\tau_{int}$, as might be the case for a methyl group in a macromolecule. (Here, we depart from our eigenmode numbering convention in order to maintain correspondence with the case of isotropic motion.) As in the isotropic case (Fig. 5), $\lambda_2 < \lambda_1 < \lambda_3$ at all frequencies, although the two avoided crossings are not evident on the scale of Fig. 12. However, as compared to the isotropic case, the boundaries of the EN and adiabatic regimes, where the relaxation function changes from tri-exponential to bi-exponential, move out to much lower and higher frequencies, respectively. Whereas in the isotropic case each eigenmode dominates in one frequency regime, now two of the modes dominate in two separate frequency intervals (Fig. 12). Moreover, the weight of eigenmode c_2 vanishes "accidentally" at two frequencies ($\omega_0\,\tau_c \approx 4.50$ and 20.31), where relaxation becomes bi-exponential. Except at these frequencies, longitudinal relaxation becomes much more non-exponential than in the isotropic case (Fig. 13). For example, $\delta_{max} = 0.27$ at $\omega_0\,\tau_c = 1$ as compared to 0.0014 in the isotropic case. We note also that the tabular results reported by Schneider[13] for the A_3 system and the spectral density function in Eq. (56) agree quantitatively with our calculations.

Because the internal rotation is two orders of magnitude faster than the overall tumbling, the relaxation dispersion exhibits two well-resolved steps (Fig. 14). The retarding effect of distinct correlations is modest for the high-frequency internal-rotation step (−5.4% at $\omega_0\,\tau_c = 10$) but very large for the low-frequency tumbling step (a factor 8 at $\omega_0\,\tau_c = 0.01$). For the A_3 system $\widehat{R}_1^{self} = R_1^0$, as for isotropic rotation (Sec. II G), but for the axial rotation model $\widehat{R}_1^{self} = (\omega_D^2/15)\,[j_R(\omega_0) + 4\,j_R(2\omega_0) + 3\,j_{int}(\omega_0) + 12\,j_{int}(2\omega_0)]$.

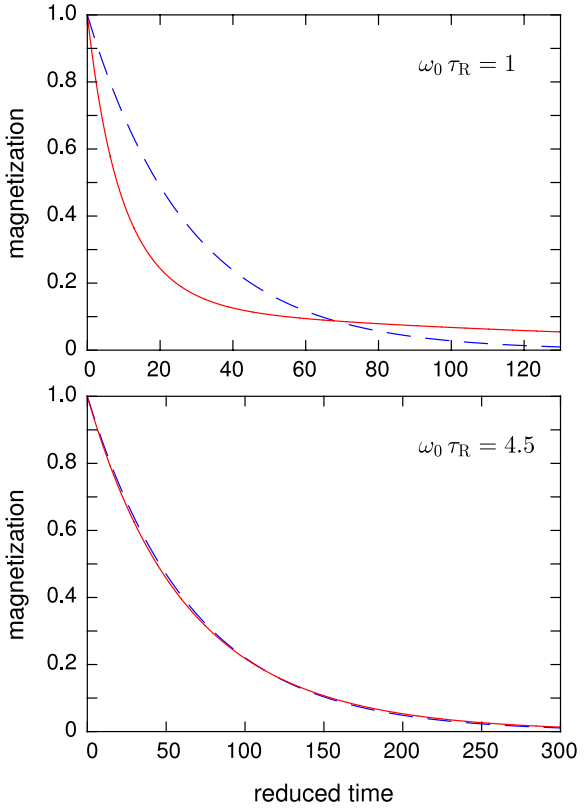

FIG. 13. Decay of the longitudinal magnetization, $\sigma_z(t)/\sigma_z(0)$, versus reduced time, $t \times \omega_D^2\,\tau_R$, for the A_3 spin system modulated by spherical-top tumbling and internal rotation with $\tau_R = 100\,\tau_{int}$. The multi-exponential decay obtained from Eq. (38) (solid curve) is compared with the single-exponential decay $\exp(-\widehat{R}_1\,t)$ (dashed curve).

B. Symmetric-top tumbling

The simplest motional model that breaks the nuclear permutation symmetry in the A_3 and A_2A' systems is rigid-

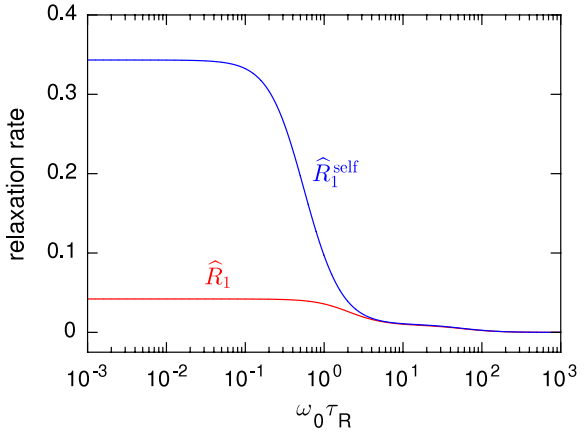

FIG. 14. Dispersion of the integral relaxation rate $\widehat{R}_1$ and its self-correlation part $\widehat{R}_1^{self}$ (both in units of $\omega_D^2\,\tau_R$) for the A_3 spin system modulated by spherical-top tumbling and internal rotation with $\tau_R = 100\,\tau_{int}$.

body symmetric-top rotational diffusion. Remarkably, this simple model, with arbitrary orientation of the principal axis of the rotational diffusion tensor with respect to the nuclear plane, does not seem to have been investigated even for the A_3 system. For the A_3 system, Hubbard examined the special case where the principal rotation axis is perpendicular to the nuclear plane,[6] in which case the three spins are "scrambled" as in the axial rotation model considered in Sec. IV A. The nuclear permutation symmetry is therefore not broken. Hubbard,[7] and later Werbelow and Marshall,[8] also considered, for the A_3 system, a principal rotation axis with arbitrary orientation, but only in the simultaneous presence of internal rotation about an axis perpendicular to the nuclear plane. Because of the internal motion, the three spins are again "scrambled," so the nuclear permutation symmetry is unaffected and the relaxation function has at most three components.[7] Even if the rate of internal rotation is set to zero, these results do not reduce to the results for rigid-body symmetric-top rotation, because rotational symmetry about an axis perpendicular to the nuclear plane has been imposed in the derivation.

We show in Appendix E[34] that, for the rigid-body symmetric-top rotational diffusion model, the spectral density function in Eq. (12) is a sum of three terms of the same type as in Eq. (47),

$$J_{XY}(\omega) = \sum_{N=0}^{2} D_{XY,N}\, J_N(\omega), \tag{57}$$

with the real-valued geometric coefficients $D_{XY,N}$ given in Eq. (E.7) of the supplementary material.[34] The complex-valued spectral densities $J_N(\omega)$ are given by Eq. (49), but with the correlation times[37]

$$\tau_N = \frac{\tau_0}{1 + N^2(\gamma - 1)/6}, \tag{58}$$

where $\tau_0 \equiv 1/(6\, D_{\mathrm{R},\perp})$ and $\gamma \equiv D_{\mathrm{R},\parallel}/D_{\mathrm{R},\perp}$. Rather than pursuing the general case, we shall illustrate the relaxation behavior for symmetric-top rotation by examining two special cases of the model.

If the principal axis of the rotational diffusion tensor is perpendicular to the nuclear plane, Eq. (57) reduces to (Appendix E[34])

$$J_{XY}(\omega) = \frac{1}{15}\, \omega_{\mathrm{D},X}\, \omega_{\mathrm{D},Y}\, [J_0(\omega) + 3\, \cos(2\beta_{XY})\, J_2(\omega)], \tag{59}$$

as previously shown by Hubbard.[6] This result differs from Eq. (56) only in the interpretation of the correlation times. Consequently, the relaxation behavior is qualitatively the same as for the internal rotation model in Sec. IV A. In particular, symmetric-top rotational diffusion with the principal axis perpendicular to the nuclear plane does not break the nuclear permutation symmetry in the A_3 and A_2A' systems. In the EN regime, the self and distinct spectral densities for the A_3 system are obtained from Eq. (59) as

$$J_{XX}(\omega) = \frac{2}{15}\, \omega_{\mathrm{D}}^2\, \tau_0 \left(\frac{2\, D_{\mathrm{R},\parallel} + 5\, D_{\mathrm{R},\perp}}{2\, D_{\mathrm{R},\parallel} + D_{\mathrm{R},\perp}} \right), \tag{60a}$$

$$J_{XY}(\omega) = \frac{1}{30}\, \omega_{\mathrm{D}}^2\, \tau_0 \left(\frac{4\, D_{\mathrm{R},\parallel} - 7\, D_{\mathrm{R},\perp}}{2\, D_{\mathrm{R},\parallel} + D_{\mathrm{R},\perp}} \right). \tag{60b}$$

In the special event that $D_{\mathrm{R},\perp} = (4/7)\, D_{\mathrm{R},\parallel}$, the distinct spectral density thus vanishes, making longitudinal relaxation single-exponential, as first noted by Hubbard.[6]

To illustrate the full scope of anisotropic rotation effects, we consider the case where the principal axis of the rotational diffusion tensor lies in the nuclear plane. For this model, Eq. (57) yields (Appendix E[34])

$$J_{XY}(\omega) = \frac{4}{15}\, \omega_{\mathrm{D},X}\, \omega_{\mathrm{D},Y} \sum_{N=0}^{2} (2 - \delta_{N0})\, d^2_{N0}(\widetilde{\alpha}_X)\, d^2_{N0}(\widetilde{\alpha}_Y)\, J_N(\omega). \tag{61}$$

Here, $\widetilde{\alpha}_X \equiv \alpha_X + \theta$, where α_X specifies the orientation of the internuclear vector $\boldsymbol{r}_X$ relative to $\boldsymbol{r}_{IS}$ (so $\alpha_{IS} = 0$, $\alpha_{IP} = \beta_I$, and $\alpha_{SP} = \pi - \beta_S$) and θ specifies the orientation of the principal rotation axis (also relative to $\boldsymbol{r}_{IS}$).

Because of its lower dynamic symmetry, this model alters the nuclear permutation symmetry for the A_3 and A_2A' systems (Sec. II D 4). However, if the principal rotation axis is either parallel with or perpendicular to the internuclear vector $\boldsymbol{r}_{IS}$, that is, if $\theta = 0$ or $\pi/2$, the $I \leftrightarrow S$ interchange symmetry is not affected. For any other orientation θ, the $I \leftrightarrow S$ interchange symmetry is broken. As a result, the A_2A' system with symmetric-top rotation behaves qualitatively as the $AA'A''$ system with spherical-top rotation. For the A_2A' system, the number of relaxation components in the dispersive regime therefore increases from 5–6 for spherical-top rotation to 7–10 for symmetric-top rotation (Table III).

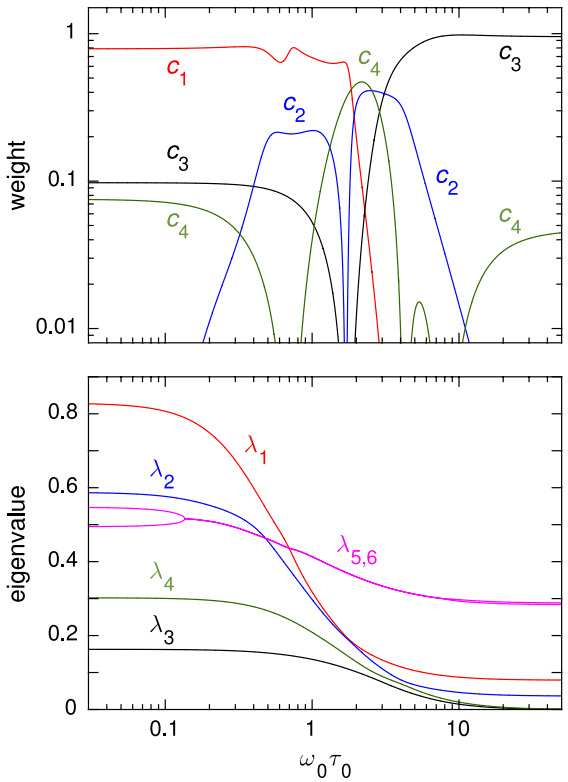

FIG. 15. Eigenmode rates λ_k (in units of $\omega_{\mathrm{D}}^2\tau_0$) and weights c_k versus the reduced Larmor frequency $\omega_0\tau_0$ for the A_3 spin system modulated by symmetric-top rotational diffusion with $\gamma = 10$ and the principal rotation axis in the nuclear plane.

For the A_3 system, symmetric-top rotation with $\theta = 0$ or $\pi/2$ leaves only $I \leftrightarrow S$ interchange symmetry, so the A_3 system with symmetric-top rotation behaves qualitatively as the A_2A' system with spherical-top rotation. Indeed, Eq. (61) yields for $\theta = 0$,

$$J_{IS,IS}(\omega) = \frac{4}{15}\,\omega_D^2\,J_0(\omega), \tag{62a}$$

$$J_{IP,IP}(\omega) = J_{SP,SP}(\omega) = \frac{1}{240}\,\omega_D^2\,[J_0(\omega) + 36\,J_1(\omega) + 27\,J_2(\omega)], \tag{62b}$$

$$J_{IS,IP}(\omega) = J_{IS,SP}(\omega) = -\frac{1}{30}\,\omega_D^2\,J_0(\omega), \tag{62c}$$

$$J_{IP,SP}(\omega) = \frac{1}{240}\,\omega_D^2\,[J_0(\omega) - 36\,J_1(\omega) + 27\,J_2(\omega)]\,, \tag{62d}$$

and for $\theta = \pi/2$,

$$J_{IS,IS}(\omega) = \frac{1}{15}\,\omega_D^2\,[J_0(\omega) + 3\,J_2(\omega)]\,, \tag{63a}$$

$$J_{IP,IP}(\omega) = J_{SP,SP}(\omega) = \frac{1}{240}\,\omega_D^2\,[25\,J_0(\omega) + 36\,J_1(\omega) + 3\,J_2(\omega)], \tag{63b}$$

$$J_{IS,IP}(\omega) = J_{IS,SP}(\omega) = -\frac{1}{60}\,\omega_D^2\,[5\,J_0(\omega) - 3\,J_2(\omega)]\,, \tag{63c}$$

$$J_{IP,SP}(\omega) = \frac{1}{240}\,\omega_D^2\,[25\,J_0(\omega) - 36\,J_1(\omega) + 3\,J_2(\omega)]\,. \tag{63d}$$

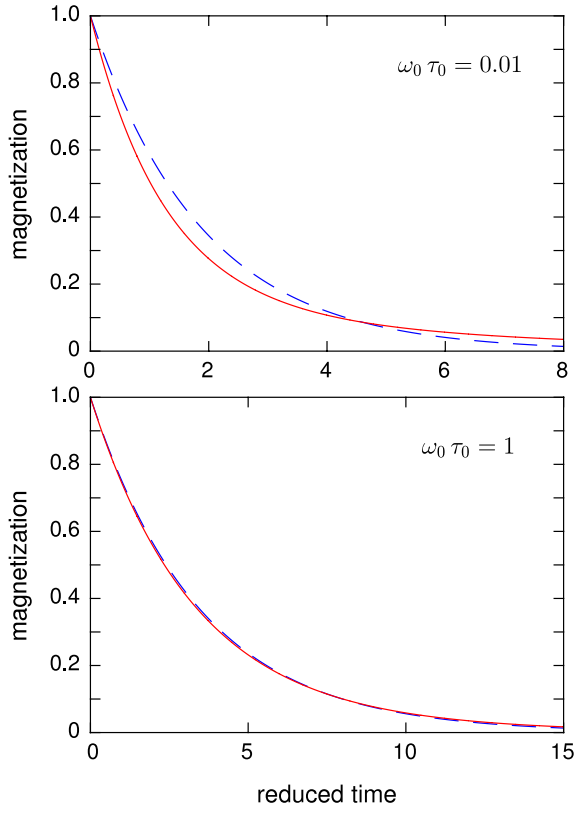

FIG. 16. Decay of the longitudinal magnetization, $\sigma_z(t)/\sigma_z(0)$, versus reduced time, $t \times \omega_D^2\,\tau_0$, for the A_3 spin system modulated by symmetric-top rotational diffusion with $\gamma = 10$ and the principal rotation axis in the nuclear plane. The multi-exponential decay obtained from Eq. (38) (solid curve) is compared with the single-exponential decay $\exp(-\widehat{R}_1\,t)$ (dashed curve).

These results show that, for $\theta = 0$ or $\pi/2$, the A_3 system does not have full nuclear permutation symmetry, but only $I \leftrightarrow S$ interchange symmetry (Sec. II D 4), like the A_2A' system with isotropic motion. This symmetry breaking has two important consequences. First, the number of relaxation components increases from 2 to 4 in the EN regime and from 3 to 5 or 6 in the dispersive regime (Table III). Second, the OSDF now affects longitudinal relaxation also in the A_3 system.

For the A_2A' system, the orientations $\theta = 0$ and $\pi/2$ yield the same number of relaxation components (the same as for isotropic motion), but the eigenmode rates (and the integral relaxation rate) are quantitatively different for the two orientations. For the A_3 system, on the other hand, these two orientations yield quantitatively the same relaxation behavior. This is not obvious from the spectral densities in Eqs. (62) and (63), which, although the same in the EN regime, differ in general. In fact, the A_3 relaxation behavior is quantitatively the same for any orientation θ of the principal diffusion axis in the nuclear plane. For the A_3 system, the relaxation supermatrix $\mathbf{R}(\theta)$ is related to $\mathbf{R}(0)$ by a similarity transformation so the eigenvalue spectrum is independent of θ.[35] (However, this is not true for $\mathbf{R}^{\rm self}(\theta)$.) Although the eigenvectors depend on θ, the component weights C_k in Eq. (36) do not. In other words, a less symmetrical orientation of the diffusion axis not only does not lead to further symmetry breaking (and additional relaxation components), but it has no effect at all. Even out-of-plane orientations do not alter the qualitative relaxation behavior further (as long as the diffusion axis is not perpendicular to the nuclear plane; see above), although there are quantitative changes.

To illustrate these results quantitatively, we consider the A_3 system with rotational anisotropy $\gamma = 10$. The relaxation rates λ_k and weights c_k of the six contributing eigenmodes are shown in Fig. 15. The two eigenvalues with the smallest weight, $\lambda_{5,6}$, form a complex conjugate pair in the dispersive regime, which splits up into two real eigenvalues in the EN and adiabatic regimes. In the EN regime, four components make significant contributions (the fourth one, not shown in

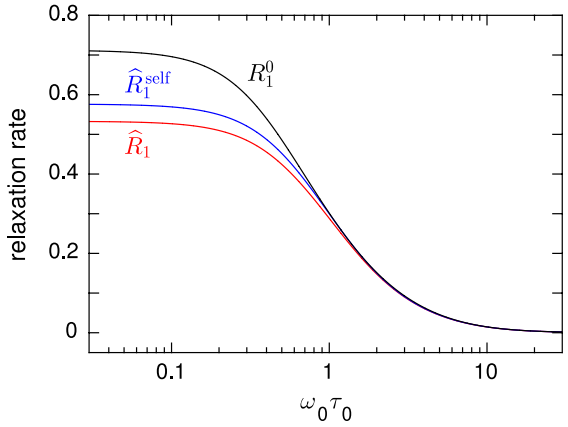

FIG. 17. Dispersion of the integral relaxation rate $\widehat{R}_1$, its self-correlation part $\widehat{R}_1^{\rm self}$, and the initial relaxation rate R_1^0 (all three in units of $\omega_D^2\,\tau_0$) for the A_3 spin system modulated by symmetric-top rotational diffusion with $\gamma = 10$ and the principal rotation axis along the *IS* internuclear vector.

Fig. 15, is $c_5 = 0.038$), as compared to only two components for isotropic rotation (Fig. 5, Table III). As a result, the relaxation function is markedly non-exponential (Fig. 16) with $\delta_{\max} = 0.082$ as compared to 0.002 in the isotropic case. In the dispersive regime, there are five relaxation components (Fig. 15), as compared to three in the isotropic case (Fig. 5, Table III). However, because the four major (real) eigenvalues are of similar magnitude (Fig. 15), relaxation is nearly exponential (Fig. 16) with $\delta_{\max} = 0.008$ at $\omega_0 \tau_0 = 1$. Distinct correlations now have a substantial effect (Fig. 17), reducing $\widehat{R}_1$ by up to 25%, as compared to 0.8% in the isotropic case (Fig. 6). Despite the large rotational anisotropy ($\gamma = 10$) used here, the dispersion shape is only slightly more extended than expected for a single correlation time because the dispersion profiles of the three spectral density functions $J_N(\omega)$ in Eq. (61) overlap. The OSDF increases $\widehat{R}_1$ by at most 0.02% in the dispersive regime, but this effect becomes more pronounced for larger rotational anisotropy. For example, for $\gamma = 200$, the OSDF increases $\widehat{R}_1$ by up to 1.9% for the A_3 system and by up to 22.5% for the A_2A' system with $\beta_P = 103°$ and $\theta = 7°$. For still larger γ, the OSDF effect increases further.

V. NON-ISOCHRONOUS SPINS

For the sake of simplicity and clarity, we assumed at the outset that the three spins are isochronous. We now remove this restriction, replacing the Zeeman Hamiltonian in Eq. (1) by

$$\begin{aligned} H_Z &= \omega_I I_z + \omega_S S_z + \omega_P P_z \\ &= \omega_0 [I_z + (1+\delta_S) S_z + (1+\delta_P) P_z], \end{aligned} \tag{64}$$

with the "chemical shifts" defined with reference to spin I so $\delta_I = 0$ and $\delta_X \equiv (\omega_X - \omega_I)/\omega_I$ for $X = S$ or P. The analytical complexity of the non-isochronous three-spin BWR theory can be avoided by realizing that, within the MN regime ($\omega_D \tau_c \ll 1$), the spherical-top rotational diffusion and strong-collision models produce the same relaxation behavior. This must be so because both models yield the time correlation function in Eq. (46), albeit with different interpretations of the correlation time. Moreover, for the strong-collision model, the orientational part of the stochastic Liouville equation (SLE) can be solved analytically, thereby allowing the integral relaxation rate to be obtained with modest computational effort.[38]

By a straight-forward extension of the two-spin SLE theory,[38] we can, in full analogy with Eq. (40), compute the integral relaxation rate as

$$\widehat{R}_1^{\rm SLE} = \left[\frac{1}{3} \sum_{n=1}^{3} \sum_{p=1}^{3} (\mathbf{R}_{\rm SLE}^{-1})_{np} \right]^{-1}, \tag{65}$$

where $\mathbf{R}_{\rm SLE}$ is the supermatrix representation of the relaxation superoperator

$$\mathcal{R}_{\rm SLE} = \left\langle \left(\tau_c^{-1} \mathcal{E} + i \mathcal{L}_Z + i \mathcal{L}_D \right)^{-1} \right\rangle^{-1} - \tau_c^{-1} \mathcal{E}. \tag{66}$$

Here, $\mathcal{E}$ is the identity superoperator, $\mathcal{L}_Z$ and $\mathcal{L}_D$ are the Liouvillians corresponding to the Hamiltonians in Eqs. (64) and (2), respectively, and the angular brackets signify an isotropic orientational average. As a bonus, the SLE theory is valid also outside the MN regime, although the strong collision and spherical-top rotational diffusion models are then no longer equivalent. Because the relaxation superoperator $\mathcal{R}_{\rm SLE}$ is isotropically averaged, it must reflect the cylindrical symmetry of the spin system. Consequently, selection rule (28) applies so we only need to retain the 19×19 zero-quantum block of $\mathbf{R}_{\rm SLE}$ (Sec. II D 2). This is true also outside the MN regime. Within the MN regime, the relaxation supermatrix $\mathbf{R}_{\rm SLE}$ must be identical to the supermatrix $\mathbf{R}_{\rm BWR}$ that would be obtained from the non-isochronous BWR theory, although this is not obvious from the corresponding superoperators. Furthermore, because chemical shifts can only break nuclear permutation symmetry, the non-isochronous BWR relaxation superoperator $\mathcal{R}_{\rm BWR}$ is still invariant under spin inversion conjugation. Therefore, within the MN regime, we need only consider the 10×10 block of $\mathbf{R}_{\rm SLE}$, corresponding to the invariant subspace spanned by the basis operators in Table II.

Before examining the effect of chemical shifts, we shall use the SLE theory to check our conclusion, based on BWR theory, that the OSDF affects longitudinal relaxation.

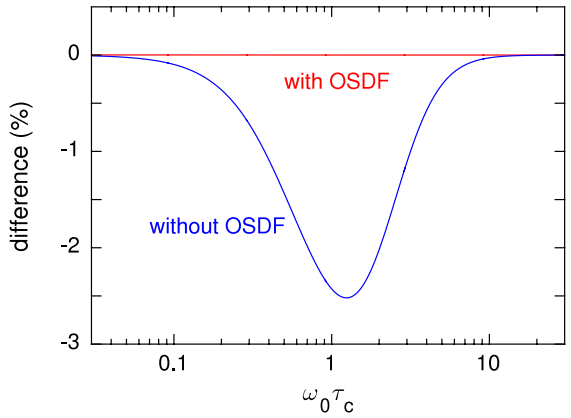

FIG. 18. Relative difference $(\widehat{R}_1^{\rm BWR} - \widehat{R}_1^{\rm SLE})/\widehat{R}_1^{\rm SLE}$ of integral relaxation rates computed with BWR and SLE theories, the former with or without inclusion of the OSDF, for an isochronous A_2A' system with $\beta_P = 108°$, $\omega_{D,IS} = 10^4$ rad s^{-1}, $\tau_c = 10^{-7}$ s, and isotropic motion.

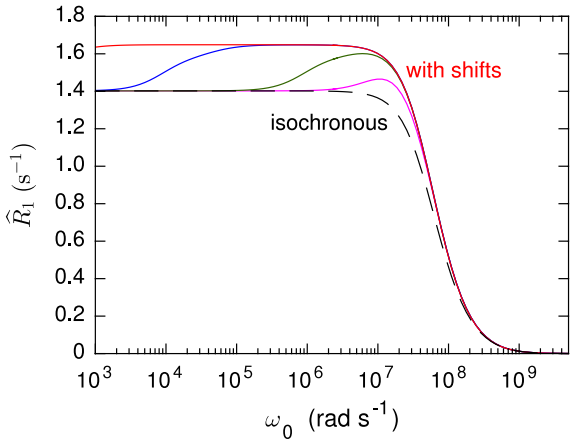

FIG. 19. Dispersion of the integral relaxation rate $\widehat{R}_1$ for isochronous (dashed) or chemically shifted (solid curves) AA′A″ systems with $\beta_I = 80°$ and $\beta_S = 40°$ and isotropic motion. Parameter values: $\omega_{D,IS} = 10^4$ rad s^{-1}, $\tau_c = 10^{-8}$ s, $\delta_P = 2\,\delta_S = 10^4$, 100, 1, and 0.1 ppm (from left to right).

If this is true, then $\widehat{R}_1^{\rm SLE}$ computed from Eqs. (65) and (66), which implicitly incorporate any effect of the OSDF, should agree with $\widehat{R}_1^{\rm BWR}$ computed with the aid of Eqs. (23) and (47)–(49) provided that the imaginary part of $J(\omega)$ is included. As seen from Fig. 18, this prediction is confirmed quantitatively. Because $\omega_{{\rm D},IS}\,\tau_{\rm c} = 10^{-3}$ in this calculation, the relative difference between $\widehat{R}_1^{\rm BWR}$ and $\widehat{R}_1^{\rm SLE}$ due to the MN approximation is less than 0.001%.

Using the SLE computational scheme, Eqs. (65) and (66), but with parameter values in the MN regime ($\omega_{{\rm D},IS}\,\tau_{\rm c} = 10^{-4}$), we now examine the effect on the integral relaxation dispersion $\widehat{R}_1(\omega_0)$ of chemical shifts of different magnitudes. We set $\delta_P = 2\,\delta_S$ so that all three spins have different Larmor frequencies and we let δ_P vary from 0.1 to 1000 ppm (^{1}H shifts rarely exceed 10 ppm). The results in Fig. 19 show that chemical shifts increase $\widehat{R}_1$ by up to 17.6% for an AA′A″ system with $\beta_I = 80°$ and $\beta_S = 40°$. Figure 20 shows how the shift effect depends on the nuclear geometry. For the A_3 geometry, the maximum effect is only 0.42% for $\delta_S = 5$ ppm and $\delta_P = 10$ ppm, but for the A_2A' and AA′A″ systems the maximum shift effect is larger (19.4% and 17.4%, respectively) and depends on the triangle angles. (We still use the spin system notation solely to indicate geometric symmetry.)

For non-isochronous spins, the relaxation dispersion profiles are non-monotonic (Fig. 19). This unusual feature appears because not all of the ISTOs $T_M^2(X)$ in the dipolar Hamiltonian (3) are eigenoperators of the Zeeman Liouvillian corresponding to Eq. (64). For homonuclear spins (so that $\delta_S, \delta_P \ll 1$), the only effect of this complication is that each of the superoperators C_M^{XY} in Eq. (11) becomes a (double) sum of superoperators (derived from eigenoperators of $\mathcal{L}_{\rm Z}$) multiplied by oscillating factors $\exp(i\,\omega_{MNN'}^{XY}\,t)$ with frequencies $\omega_{MNN'}^{XY}$ that are linear combinations of the shifts δ_S and δ_P. If this frequency, of order $\delta\,\omega_0$, is much larger than the corresponding "partial relaxation rate," of order $\omega_{\rm D}^2\,\tau_{\rm c}$, then the modulated term is effectively cancelled and only terms with $\omega_{MNN'}^{XY} = 0$ survive. The Larmor frequency where this "nonsecular decoupling" (NSD) sets in is thus given by

$$\omega_{\rm NSD} \approx \frac{\omega_{\rm D}^2\,\tau_{\rm c}}{\delta}, \tag{67}$$

where $\omega_{\rm D}$ and δ characterize the magnitudes of the dipole couplings and shifts, respectively. For example, for $\omega_{\rm D} = 10^4$ rad s^{-1}, $\tau_{\rm c} = 10^{-8}$ s, and $\delta_P = 100$ ppm, Eq. (67) yields $\omega_{\rm NSD} = 10^4$ rad s^{-1} (Fig. 19).

For a given pair of dipole couplings X and Y, C_M^{XY} is a sum of 14 terms. In the general case, where $\delta_S \neq \delta_P$, the number of terms for which $\omega_{MNN'}^{XY} = 0$ is six for self-correlations ($X = Y$) but only two for distinct correlations ($X \neq Y$). The NSD thus mainly suppresses distinct correlations, which tend to slow down relaxation, so an "inverted dispersion," where $\widehat{R}_1$ increases with frequency, appears at $\omega_0 \approx \omega_{\rm NSD}$ (Fig. 19). The greater susceptibility of distinct correlations to NSD also explains the very small chemical-shift effect on the A_3 system (Fig. 20), where $\widehat{R}_1$ is only marginally influenced by distinct correlations (Fig. 6).

According to Eq. (67), the NSD frequency increases linearly with the correlation time. When $\tau_{\rm c}$ is so long that $\omega_{\rm NSD}$ approaches the main dispersion at $\omega_0 \approx 1/\tau_{\rm c}$, the chemical-shift effect is diminished (Fig. 21) and when $\omega_{\rm NSD}$ is far above the main dispersion, so that $\delta \ll (\omega_{\rm D}\,\tau_{\rm c})^2$, chemical shifts do not affect longitudinal relaxation. Outside the MN regime, where $\omega_{\rm D}\,\tau_{\rm c} \gtrsim 1$, chemical shifts can therefore safely be ignored when considering the longitudinal relaxation of homonuclear spin systems.

Also in the presence of chemical shifts, the relaxation supermatrix is symmetric ($R_{pn} = R_{np}$) and the odd-rank (n = 1–7) and even-rank (n = 8–10) blocks are real-valued while the mixed odd-even blocks are pure imaginary (Fig. 1). However, the imaginary supermatrix elements are now caused by chemical shifts as well as by the OSDF. In fact, the chemical shifts only affect the imaginary elements. Specifically, they affect the coupling between odd-rank ZQCs (n = 4–7) and even-rank ZQCs (n = 8–10). In the isochronous A_2A' system, the $I \leftrightarrow S$ interchange symmetry prohibits coupling between the symmetric ZQCs σ_4, σ_6, and σ_7 and the anti-symmetric

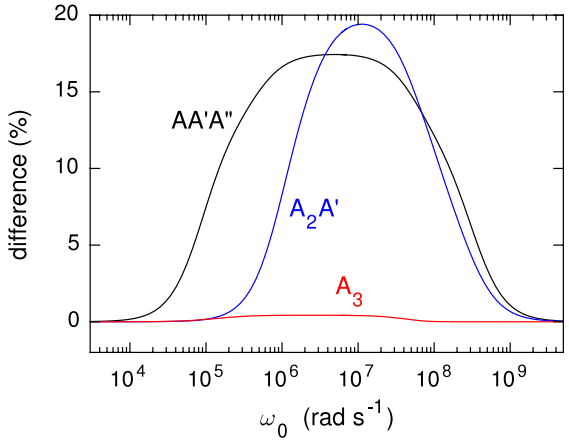

FIG. 20. Relative difference $[\widehat{R}_1(\delta_S,\delta_P) - \widehat{R}_1(0,0)]/\widehat{R}_1(0,0)$ of integral relaxation rates with and without chemical shifts for the A_3, A_2A', and AA′A″ systems with isotropic motion. Parameter values: $\omega_{{\rm D},IS} = 10^4$ rad s^{-1}, $\tau_{\rm c} = 10^{-8}$ s, $\delta_S = 5$ ppm, $\delta_P = 10$ ppm, $\beta_P = 120°$ (A_2A' system), and $\beta_I = 80°$, $\beta_S = 40°$ (AA′A″ system).

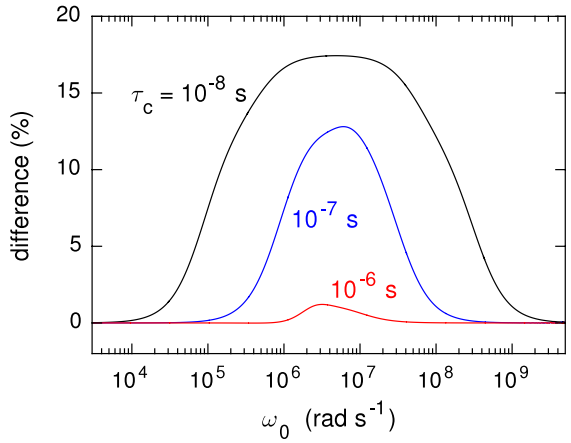

FIG. 21. Relative difference $[\widehat{R}_1(\delta_S,\delta_P) - \widehat{R}_1(0,0)]/\widehat{R}_1(0,0)$ of integral relaxation rates with and without chemical shifts for the AA′A″ system with $\beta_I = 80°$, $\beta_S = 40°$, and isotropic motion. Parameter values: $\omega_{{\rm D},IS} = 10^4$ rad s^{-1}, $\delta_S = 5$ ppm, $\delta_P = 10$ ppm, and $\tau_{\rm c}$ as indicated.

ZQCs σ_8 and σ_9. In the presence of chemical shifts, the $I \leftrightarrow S$ interchange symmetry is broken above the NSD frequency, leading to mixing of these modes. Just like anisotropic rotation (Sec. IV B), chemical shifts make the A_2A' system behave qualitatively as an $AA'A''$ system, with up to ten relaxation components in the dispersive regime. Presumably, the OSDF affects longitudinal relaxation also in the A_3 system with isotropic motion if the nuclear permutation symmetry is broken by chemical shifts. However, without actually solving the non-isochronous BWR problem, we cannot demonstrate this particular OSDF effect, which is likely to be small. For the A_2A' and $AA'A''$ systems, on the other hand, our calculations show that the combined effect on $\widehat{R}_1$ of typical proton chemical shifts (of order 1 ppm) and the OSDF is 1–2 orders of magnitude larger than the effect of the chemical shifts alone.

VI. CONCLUSIONS

We have revisited the problem of longitudinal relaxation in a dipole-coupled homonuclear three-spin system, first addressed by Hubbard in 1958.[2] Nearly all subsequent studies of this problem have been concerned with the special, but important, case of three geometrically equivalent, isochronous spins. In contrast, our treatment is valid for arbitrary geometry. By formulating the BWR theory in Liouville space and making full use of symmetry, we establish the number of exponential relaxation components for all nuclear geometries and for isotropic as well as anisotropic motions. We characterize the relaxation behavior with an eigenmode expansion and with the integral relaxation rate, both of which are examined over the full frequency range. We also investigate the effect of chemical shifts on the integral relaxation rate by means of the stochastic Liouville equation. This is a computationally efficient approach because the orientational part of the stochastic Liouville equation can be solved analytically for the strong-collision model, which is equivalent to the spherical-top rotational diffusion model in the motional-narrowing regime.

The main results of this study are as follows.

(1) Using an irreducible spherical tensor operator basis, we show that longitudinal relaxation in a three-spin system interacting with an isotropic bath can be fully described within an invariant subspace spanned by ten zero-quantum operators that, like the relaxation superoperator, are invariant under spin inversion conjugation. These basis operators correspond to the three longitudinal magnetizations and seven zero-quantum coherences. The 10×10 relaxation supermatrix, valid for arbitrary nuclear geometry and motional model, is obtained in analytical form.

(2) Contrary to conventional wisdom,[16–23] we find that the odd spectral density contributes, via distinct correlations, to longitudinal relaxation in the dispersive regime if the three spins are geometrically or dynamically nonequivalent. For the A_2A' and $AA'A''$ geometries with dynamically equivalent spins, we reproduce the results of Schneider,[13] but we also find that the odd spectral density influences longitudinal relaxation for the A_3 system in the presence of symmetry-breaking motions. For strong rotational anisotropy, the OSDF can enhance the integral relaxation rate by more than 25%.

(3) The symmetric-top rotational diffusion model with arbitrary orientation of the principal rotation axis has not previously been investigated for multi-spin systems. For this model, we find that longitudinal relaxation in the A_3 geometry involves up to six exponential components. In contrast, previous studies of the A_3 geometry, restricted to motional models that do not break the nuclear permutation symmetry, have found at most three relaxation components.[17]

(4) Chemical shifts break the nuclear permutation symmetry, thereby increasing the number of relaxation components. An inverted relaxation dispersion step is predicted at the frequency where the differential precession rate matches the relaxation rate. Above this frequency, nonsecular decoupling preferentially eliminates contributions from distinct correlations, thereby increasing the integral relaxation rate. The effect of chemical shifts disappears when the nonsecular decoupling frequency exceeds the main dispersion frequency, as is always the case for homonuclear spin systems outside the motional-narrowing regime.

ACKNOWLEDGMENTS

We thank Larry Werbelow and Rafael Brüschweiler for discussion and the Swedish Research Council for financial support.

[1] I. Solomon, Phys. Rev. **99**, 559 (1955).
[2] P. S. Hubbard, Phys. Rev. **109**, 1153 (1958).
[3] P. M. Richards, Phys. Rev. **132**, 27 (1963).
[4] L. K. Runnels, Phys. Rev. **134**, A28 (1964).
[5] R. L. Hilt and P. S. Hubbard, Phys. Rev. **134**, A392 (1964).
[6] P. S. Hubbard, J. Chem. Phys. **51**, 1647 (1969).
[7] P. S. Hubbard, J. Chem. Phys. **52**, 563 (1970).
[8] L. G. Werbelow and A. G. Marshall, J. Magn. Reson. **11**, 299 (1973).
[9] G. B. Matson, J. Chem. Phys. **65**, 4147 (1976).
[10] L. G. Werbelow, D. M. Grant, E. P. Black, and J. M. Courtieu, J. Chem. Phys. **69**, 2407 (1978).
[11] G. W. Kattawar and M. Eisner, Phys. Rev. **126**, 1054 (1962).
[12] H. Schneider, Ann. Phys. **13**, 313 (1964).
[13] H. Schneider, Ann. Phys. **16**, 135 (1965).
[14] M. D. Zeidler, Ber. Bunsenges. Phys. Chem. **72**, 481 (1968).
[15] N. C. Pyper, Mol. Phys. **21**, 1 (1971).
[16] A. Abragam, *The Principles of Nuclear Magnetism* (Clarendon Press, Oxford, 1961), p. 279.
[17] L. G. Werbelow and D. M. Grant, Adv. Magn. Reson. **9**, 189 (1977).
[18] J. Jeener, Adv. Magn. Reson. **10**, 1 (1982).
[19] R. R. Ernst, G. Bodenhausen, and A. Wokaun, *Principles of Nuclear Magnetic Resonance in One and Two Dimensions* (Clarendon Press, Oxford, 1987), p. 51.
[20] C. P. Slichter, *Principles of Magnetic Resonance* (Springer-Verlag, Berlin, 1990), p. 203.
[21] A. Kumar, C. R. Rani Grace, and P. K. Madhu, Prog. Nucl. Magn. Reson. Spectrosc. **37**, 191 (2000).
[22] G. Karthik and A. Kumar, J. Chem. Phys. **113**, 7131 (2000).
[23] M. Goldman, J. Magn. Reson. **149**, 160 (2001).
[24] R. Brüschweiler, J. Chem. Phys. **105**, 6164 (1996).
[25] G. K. Fraenkel, J. Chem. Phys. **42**, 4275 (1965).
[26] L. G. Werbelow, A. Thevand, and G. Pouzard, J. Chem. Soc., Faraday Trans. 2 **75**, 971 (1979).
[27] L. G. Werbelow, in *Encyclopedia of Nuclear Magnetic Resonance*, edited by D. M. Grant and R. K. Harris (Wiley, Chichester, 1996), p. 1776.
[28] H. Pfeifer, Ann. Phys. **13**, 174 (1964).
[29] S. Szymanski, A. M. Gryff-Keller, and G. Binsch, J. Magn. Reson. **68**, 399 (1986).

[30]D. M. Brink and G. R. Satchler, *Angular Momentum*, 3rd ed. (Clarendon Press, Oxford, 1994).
[31]P. S. Hubbard, Phys. Rev. **180**, 319 (1969).
[32]K. Blum, *Density Matrix Theory and Applications*, 3rd ed. (Springer-Verlag, Berlin, 2012).
[33]M. Tinkham, *Group Theory and Quantum Mechanics* (McGraw-Hill, New York, 1964).
[34]See supplementary material at http://dx.doi.org/10.1063/1.4937377 for derivation, properties, and explicit form of the $\mathbf{C}_M^{XY}$ matrices (Appendix A); derivation of selection rules for the $\mathbf{C}_M^{XY}$ matrices (Appendix B); derivation of the relaxation supermatrix for the A_3 system (Appendix C); and derivation of spectral density functions for models of axial internal rotation (Appendix D) and symmetric-top rotation (Appendix E).
[35]R. A. Horn and C. R. Johnson, *Matrix Analysis* (Cambridge University Press, New York, 1985).
[36]P. S. Hubbard, J. Chem. Phys. **53**, 985 (1970).
[37]L. D. Favro, Phys. Rev. **119**, 53 (1960).
[38]Z. Chang and B. Halle, J. Chem. Phys. **139**, 144203 (2013).

Supplemental Material

Longitudinal relaxation in dipole-coupled homonuclear three-spin systems: Distinct correlations and odd spectral densities

Zhiwei Chang and Bertil Halle
Division of Biophysical Chemistry, Department of Chemistry, Lund University, POB 124, SE-22100 Lund, Sweden

APPENDIX A: THE $\mathbf{C}_M^{XY}$ MATRICES

Here we show how to evaluate the coefficient matrices $\mathbf{C}_M^{XY}$ that, together with Eqs. (12) and (23), define the relaxation supermatrix in the ISTO basis. We prove that these matrices are real-valued and we present in explicit form the 10×10 $\mathbf{C}_M^{XY}$ matrices needed to describe longitudinal relaxation in a three-spin system.

Our starting point is Eq. (24), we may be expressed as

$$C_{M,np}^{XY} \;=\; \mathrm{Tr}\big\{\big[T_Q^K(k_Ik_S\{\bar{K}\}k_P)^\dagger, T_M^2(l_Il_S\{\bar{L}\}l_P)\big]\big[T_M^2(l_I'l_S'\{\bar{L}'\}l_P')^\dagger, T_{Q'}^{K'}(k_I'k_S'\{\bar{K}'\}k_P')\big]\big\}\,. \tag{A.1}$$

Using Eq. (19) and the single-spin ISTO conjugation relation[1] $T_q^{k\,\dagger} = (-1)^q\, T_{-q}^k$, we obtain for the first commutator in Eq. (A.1),

$$\begin{aligned}
&\big[T_Q^K(k_Ik_S\{\bar{K}\}k_P)^\dagger,\, T_M^2(l_Il_S\{\bar{L}\}l_P)\big] \\
&=\; (-1)^{k_I-k_S-k_P+\bar{K}+l_I-l_S-l_P+\bar{L}+M}\,\sqrt{5}\,[(2K+1)(2\bar{K}+1)(2\bar{L}+1)]^{1/2} \\
&\times \sum_{\bar{Q}=-\bar{K}}^{\bar{K}}\sum_{q_I=-k_I}^{k_I}(-1)^{\bar{Q}}\begin{pmatrix} \bar{K} & k_P & K \\ \bar{Q} & Q-\bar{Q} & -Q\end{pmatrix}\begin{pmatrix} k_I & k_S & \bar{K} \\ q_I & \bar{Q}-q_I & -\bar{Q}\end{pmatrix} \\
&\times \sum_{\bar{M}=-\bar{L}}^{\bar{L}}\sum_{r_I=-l_I}^{l_I}(-1)^{\bar{M}}\begin{pmatrix} \bar{L} & l_P & 2 \\ \bar{M} & M-\bar{M} & -M\end{pmatrix}\begin{pmatrix} l_I & l_S & \bar{L} \\ r_I & \bar{M}-r_I & -\bar{M}\end{pmatrix} C_1\,,
\end{aligned} \tag{A.2}$$

with

$$\begin{aligned}
C_1 \;&\equiv\; \big[T_{-q_I}^{k_I}(I)\,T_{q_I-\bar{Q}}^{k_S}(S)\,T_{\bar{Q}-Q}^{k_P}(P),\, T_{r_I}^{l_I}(I)\,T_{\bar{M}-r_I}^{l_S}(S)\,T_{M-\bar{M}}^{l_P}(P)\big] \\
&=\; \big[T_{-q_I}^{k_I}(I),\, T_{r_I}^{l_I}(I)\big]T_{\bar{M}-r_I}^{l_S}(S)\,T_{q_I-\bar{Q}}^{k_S}(S)\,T_{M-\bar{M}}^{l_P}(P)\,T_{\bar{Q}-Q}^{k_P}(P) \\
&+\; T_{-q_I}^{k_I}(I)\,T_{r_I}^{l_I}(I)\big[T_{q_I-\bar{Q}}^{k_S}(S),\, T_{\bar{M}-r_I}^{l_S}(S)\big]T_{M-\bar{M}}^{l_P}(P)\,T_{\bar{Q}-Q}^{k_P}(P) \\
&+\; T_{-q_I}^{k_I}(I)\,T_{r_I}^{l_I}(I)\,T_{q_I-\bar{Q}}^{k_S}(S)\,T_{\bar{M}-r_I}^{l_S}(S)\big[T_{\bar{Q}-Q}^{k_P}(P),\, T_{M-\bar{M}}^{l_P}(P)\big]\,.
\end{aligned} \tag{A.3}$$

Using the general expression for single-spin ISTO commutators[2] and noting that, for spins-1/2, the tensor rank must be 0 or 1, we find

$$\big[T_q^k,\, T_m^l\big] \;=\; \delta_{k1}\,\delta_{l1}\,\psi(q,m)\,\sqrt{2}\,T_{q+m}^1\,, \tag{A.4}$$

where we have defined the sign function (equal to 0, +1 or −1)

$$\psi(q,m) \;\equiv\; (1-\delta_{qm})\,[(1-\delta_{m0})\,\mathrm{sgn}(m) \;-\; \delta_{m0}\,\mathrm{sgn}(q)]\,. \tag{A.5}$$

Combination of Eqs. (A.2) –(A.4) yields

$$\big[T_Q^K(k_Ik_S\{\bar{K}\}k_P)^\dagger,\, T_M^2(l_Il_S\{\bar{L}\}l_P)\big] \;=\; A_I + A_S + A_P\,, \tag{A.6}$$

where

$$
\begin{aligned}
A_I \;=\; & \delta_{k_I,1}\,\delta_{l_I,1}\,(-1)^{\bar{K}+\bar{L}+M-k_S-k_P-l_S-l_P}\,\sqrt{10}\,[(2K+1)(2\bar{K}+1)(2\bar{L}+1)]^{1/2} \\
& \times \sum_{\bar{Q}=-\bar{K}}^{\bar{K}} \sum_{q_I=-1}^{1} (-1)^{\bar{Q}} \begin{pmatrix} \bar{K} & k_P & K \\ \bar{Q} & Q-\bar{Q} & -Q \end{pmatrix} \begin{pmatrix} 1 & k_S & \bar{K} \\ q_I & \bar{Q}-q_I & -\bar{Q} \end{pmatrix} \\
& \times \sum_{\bar{M}=-\bar{L}}^{\bar{L}} \sum_{r_I=-1}^{1} (-1)^{\bar{M}} \begin{pmatrix} \bar{L} & l_P & 2 \\ \bar{M} & M-\bar{M} & -M \end{pmatrix} \begin{pmatrix} 1 & l_S & \bar{L} \\ r_I & \bar{M}-r_I & -\bar{M} \end{pmatrix} \\
& \times \psi(-q_I, r_I)\, T^1_{r_I-q_I}(I)\, T^{l_S}_{\bar{M}-r_I}(S)\, T^{k_S}_{q_I-\bar{Q}}(S)\, T^{l_P}_{M-\bar{M}}(P)\, T^{k_P}_{\bar{Q}-Q}(P)\,,
\end{aligned}
\tag{A.7}
$$

$$
\begin{aligned}
A_S \;=\; & \delta_{k_S,1}\,\delta_{l_S,1}\,(-1)^{\bar{K}+\bar{L}+M+k_I-k_P+l_I-l_P}\,\sqrt{10}\,[(2K+1)(2\bar{K}+1)(2\bar{L}+1)]^{1/2} \\
& \times \sum_{\bar{Q}=-\bar{K}}^{\bar{K}} \sum_{q_I=-k_I}^{k_I} (-1)^{\bar{Q}} \begin{pmatrix} \bar{K} & k_P & K \\ \bar{Q} & Q-\bar{Q} & -Q \end{pmatrix} \begin{pmatrix} k_I & 1 & \bar{K} \\ q_I & \bar{Q}-q_I & -\bar{Q} \end{pmatrix} \\
& \times \sum_{\bar{M}=-\bar{L}}^{\bar{L}} \sum_{r_I=-l_I}^{l_I} (-1)^{\bar{M}} \begin{pmatrix} \bar{L} & l_P & 2 \\ \bar{M} & M-\bar{M} & -M \end{pmatrix} \begin{pmatrix} l_I & 1 & \bar{L} \\ r_I & \bar{M}-r_I & -\bar{M} \end{pmatrix} \\
& \times \psi(q_I-\bar{Q}, \bar{M}-r_I)\, T^{k_I}_{-q_I}(I)\, T^{l_I}_{r_I}(I)\, T^1_{q_I-r_I-\bar{Q}+\bar{M}}(S)\, T^{l_P}_{M-\bar{M}}(P)\, T^{k_P}_{\bar{Q}-Q}(P)\,,
\end{aligned}
\tag{A.8}
$$

$$
\begin{aligned}
A_P \;=\; & \delta_{k_P,1}\,\delta_{l_P,1}\,(-1)^{\bar{K}+\bar{L}+M+k_I-k_S+l_I-l_S}\,\sqrt{10}\,[(2K+1)(2\bar{K}+1)(2\bar{L}+1)]^{1/2} \\
& \times \sum_{\bar{Q}=-\bar{K}}^{\bar{K}} \sum_{q_I=-k_I}^{k_I} (-1)^{\bar{Q}} \begin{pmatrix} \bar{K} & 1 & K \\ \bar{Q} & Q-\bar{Q} & -Q \end{pmatrix} \begin{pmatrix} k_I & k_S & \bar{K} \\ q_I & \bar{Q}-q_I & -\bar{Q} \end{pmatrix} \\
& \times \sum_{\bar{M}=-\bar{L}}^{\bar{L}} \sum_{r_I=-l_I}^{l_I} (-1)^{\bar{M}} \begin{pmatrix} \bar{L} & 1 & 2 \\ \bar{M} & M-\bar{M} & -M \end{pmatrix} \begin{pmatrix} l_I & l_S & \bar{L} \\ r_I & \bar{M}-r_I & -\bar{M} \end{pmatrix} \\
& \times \psi(\bar{Q}-Q, M-\bar{M})\, T^{k_I}_{-q_I}(I)\, T^{l_I}_{r_I}(I)\, T^{k_S}_{q_I-\bar{Q}}(S)\, T^{l_S}_{\bar{M}-r_I}(S)\, T^1_{\bar{Q}-\bar{M}-Q+M}(P)\,.
\end{aligned}
\tag{A.9}
$$

In the same way, we obtain for the second commutator in Eq. (A.1),

$$
\begin{aligned}
& \big[T^2_M(l'_I l'_S\{\bar{L}'\}l'_P)^\dagger,\, T^{K'}_{Q'}(k'_I k'_S\{\bar{K}'\}k'_P)\big] \\
& \;=\; \big[T^{K'}_{Q'}(k'_I k'_S\{\bar{K}'\}k'_P)^\dagger,\, T^2_M(l'_I l'_S\{\bar{L}'\}l'_P)\big]^\dagger \;=\; A'_I + A'_S + A'_P\,.
\end{aligned}
\tag{A.10}
$$

A comparison of Eqs. (A.6) and (A.10) shows that A'_I, A'_S and A'_P can be obtained from A_I, A_S and A_P in Eqs. (A.7) – (A.9) by adding a prime to all quantum numbers except M and taking the adjoint of all five single-spin ISTOs (remembering to invert their order). Combination of Eqs. (A.1), (A.6) and (A.10) yields

$$
\begin{aligned}
C^{XY}_{M,np} \;=\; & \mathrm{Tr}\{A_I A'_I\} \;+\; \mathrm{Tr}\{A_I A'_S\} \;+\; \mathrm{Tr}\{A_I A'_P\} \\
& +\; \mathrm{Tr}\{A_S A'_I\} \;+\; \mathrm{Tr}\{A_S A'_S\} \;+\; \mathrm{Tr}\{A_S A'_P\} \\
& +\; \mathrm{Tr}\{A_P A'_I\} \;+\; \mathrm{Tr}\{A_P A'_S\} \;+\; \mathrm{Tr}\{A_P A'_P\}\,.
\end{aligned}
\tag{A.11}
$$

Substitution from Eqs. (A.7) – (A.9) and the analogous expressions for the primed quantities shows that the traces factorize into partial traces over products of two, three or four single-spin ISTOs. The first of these is simply

$$\mathrm{Tr}\{T^k_q\, T^{k'}_{q'}\} \;=\; \delta_{kk'}\,\delta_{q,-q'}\,(-1)^q\,, \tag{A.12}$$

as follows from the orthonormality (21) of the single-spin ISTOs. The trace over a product of three single-spin-1/2 ISTOs is given by[2]

$$\begin{aligned}\mathrm{Tr}\{T^k_q\, T^{k'}_{q'}\, T^{k''}_{q''}\} \;&=\; \delta_{q'',-q-q'}\,(-1)^{k+k'+k''+1}\\ &\times\,[(2k+1)(2k'+1)(2k''+1)]^{1/2}\begin{pmatrix} k & k' & k'' \\ q & q' & -q-q' \end{pmatrix}\begin{Bmatrix} k & k' & k'' \\ \frac{1}{2} & \frac{1}{2} & \frac{1}{2} \end{Bmatrix}\,,\end{aligned} \tag{A.13}$$

and the trace over a product of four single-spin-1/2 ISTOs is given by[2]

$$\begin{aligned}\mathrm{Tr}\{T^k_q\, T^{k'}_{q'}\, T^{k''}_{q''}\, T^{k'''}_{q'''}\} \;&=\; \delta_{q+q',-q''-q'''}\,(-1)^{k+k'+k''+k'''+q+q'}\\ &\times\,[(2k+1)(2k'+1)(2k''+1)(2k'''+1)]^{1/2}\\ &\times\sum_{\lambda=0}^{1}(2\lambda+1)\begin{pmatrix} k & k' & \lambda \\ q & q' & -q-q' \end{pmatrix}\begin{pmatrix} \lambda & k'' & k''' \\ -q''-q''' & q'' & q''' \end{pmatrix}\\ &\times\begin{Bmatrix} k & k' & \lambda \\ \frac{1}{2} & \frac{1}{2} & \frac{1}{2} \end{Bmatrix}\begin{Bmatrix} \lambda & k'' & k''' \\ \frac{1}{2} & \frac{1}{2} & \frac{1}{2} \end{Bmatrix}\,,\end{aligned} \tag{A.14}$$

where the summation range, $\lambda = 0,\, 1$, follows from the triangular conditions on the $6j$

symbols.[1] We can now evaluate the nine traces in Eq. (A.11). For example,

$$
\begin{aligned}
&\mathrm{Tr}\{A_I A'_S\} \;=\; \delta_{QQ'}\,\delta_{k_I,1}\,\delta_{l_I,1}\,\delta_{k'_S,1}\,\delta_{l'_S,1}\,(-1)^{\bar{K}+\bar{K}'+\bar{L}+\bar{L}'+M} \\
&\times 30\,[(2K+1)(2K'+1)(2\bar{K}+1)(2\bar{K}'+1)(2\bar{L}+1)(2\bar{L}'+1)]^{1/2} \\
&\times [(2k'_I+1)(2l'_I+1)(2k_S+1)(2l_S+1)(2k_P+1)(2k'_P+1)(2l_P+1)(2l'_P+1)]^{1/2} \\
&\times \sum_{\bar{Q}=-\bar{K}}^{\bar{K}} \sum_{q_I=-1}^{1} \begin{pmatrix} \bar{K} & k_P & K \\ \bar{Q} & Q-\bar{Q} & -Q \end{pmatrix} \begin{pmatrix} 1 & k_S & \bar{K} \\ q_I & \bar{Q}-q_I & -\bar{Q} \end{pmatrix} \\
&\times \sum_{\bar{Q}'=-\bar{K}'}^{\bar{K}'} \sum_{q'_I=-k'_I}^{k'_I} (-1)^{\bar{Q}'} \begin{pmatrix} \bar{K}' & k'_P & K' \\ \bar{Q}' & Q-\bar{Q}' & -Q \end{pmatrix} \begin{pmatrix} k'_I & 1 & \bar{K}' \\ q'_I & \bar{Q}'-q'_I & -\bar{Q}' \end{pmatrix} \\
&\times \sum_{\bar{M}=-\bar{L}}^{\bar{L}} \sum_{r_I=-1}^{1} \begin{pmatrix} \bar{L} & l_P & 2 \\ \bar{M} & M-\bar{M} & -M \end{pmatrix} \begin{pmatrix} 1 & l_S & \bar{L} \\ r_I & \bar{M}-r_I & -\bar{M} \end{pmatrix} \\
&\times \sum_{\bar{M}'=-\bar{L}'}^{\bar{L}'} \sum_{r'_I=-l'_I}^{l'_I} (-1)^{\bar{M}'} \begin{pmatrix} \bar{L}' & l'_P & 2 \\ \bar{M}' & M-\bar{M}' & -M \end{pmatrix} \begin{pmatrix} l'_I & 1 & \bar{L}' \\ r'_I & \bar{M}'-r'_I & -\bar{M}' \end{pmatrix} \qquad \text{(A.15)} \\
&\times \psi(-q_I, r_I)\,\psi(q'_I-\bar{Q}', \bar{M}'-r'_I)\,\delta_{r_I-q_I,r'_I-q'_I}\,\delta_{\bar{M}-\bar{Q},\bar{M}'-\bar{Q}'} \\
&\times \begin{pmatrix} l_S & k_S & 1 \\ \bar{M}-r_I & q_I-\bar{Q} & r_I-q_I+\bar{Q}-\bar{M} \end{pmatrix} \begin{pmatrix} 1 & l'_I & k'_I \\ r'_I-q'_I & -r'_I & q'_I \end{pmatrix} \\
&\times \begin{Bmatrix} l_S & k_S & 1 \\ \frac{1}{2} & \frac{1}{2} & \frac{1}{2} \end{Bmatrix} \begin{Bmatrix} 1 & l'_I & k'_I \\ \frac{1}{2} & \frac{1}{2} & \frac{1}{2} \end{Bmatrix} \\
&\times \sum_{\lambda=0}^{1} (2\lambda+1) \begin{pmatrix} l_P & k_P & \lambda \\ M-\bar{M} & \bar{Q}-Q & \bar{M}-M+Q-\bar{Q} \end{pmatrix} \\
&\times \begin{pmatrix} \lambda & k'_P & l'_P \\ M-\bar{M}'+\bar{Q}'-Q & Q-\bar{Q}' & \bar{M}'-M \end{pmatrix} \begin{Bmatrix} l_P & k_P & \lambda \\ \frac{1}{2} & \frac{1}{2} & \frac{1}{2} \end{Bmatrix} \begin{Bmatrix} \lambda & k'_P & l'_P \\ \frac{1}{2} & \frac{1}{2} & \frac{1}{2} \end{Bmatrix} .
\end{aligned}
$$

and similar expressions for the other eight traces.

It is evident from these expressions that all the coefficients $C^{XY}_{M,np}$ are real-valued. This may be shown without evaluating the traces by the following arguments. According to Eqs. (A.6) – (A.9) and (A.11), $C^{XY}_{M,np}$ can be expressed as a linear combination, with real-valued coefficients, of products $Z_I Z_S Z_P$ of single-spin traces of the form

$$
Z_I \;=\; \mathrm{Tr}_I\big\{T^{k_1}_{q_1}(I)\,T^{k_2}_{q_2}(I)\,\cdots\,T^{k_n}_{q_n}(I)\big\}\;, \qquad \text{(A.16)}
$$

with $n = 2$, 3 or 4. Evaluating the traces in the angular momentum eigenbasis and noting that[3]

$$
\big\langle I\,m\,|T^k_q(I)|I\,m'\big\rangle \;=\; (-1)^{I-m}(2k+1)^{1/2} \begin{pmatrix} I & k & I \\ -m & q & m' \end{pmatrix}\;, \qquad \text{(A.17)}
$$

is a real-valued quantity, it follows that all matrix elements $C^{XY}_{M,np}$ are real-valued in the ISTO basis.

From the foregoing expressions, we can obtain the 45 different 63×63 matrices $\mathbf{C}^{XY}_{M}$. Because of symmetry relations (Sect. II D), we only need to compute 18 of these 45 matrices. Moreover, to describe longitudinal relaxation, we only need the first 10×10 block of $\mathbf{C}^{XY}_{M}$, corresponding to the ten zero-quantum ($Q = 0$) basis operators (Table II) with odd spin inversion conjugation parity (Sect. II D). These 18 submatrices are given in Eqs. (A.18) – (A.35) with the spin pairs (X and Y) indexed as follows: $1 = IS$, $2 = IP$ and $3 = SP$.

$$\mathbf{C}_0^{11} = \frac{1}{12}\begin{bmatrix} 2 & -2 & 0 & 0 & 0 & 0 & 0 & 0 & 0 & 0 \\ -2 & 2 & 0 & 0 & 0 & 0 & 0 & 0 & 0 & 0 \\ 0 & 0 & 0 & 0 & 0 & 0 & 0 & 0 & 0 & 0 \\ 0 & 0 & 0 & 0 & 0 & 0 & 0 & 0 & 0 & 0 \\ 0 & 0 & 0 & 0 & 1 & 0 & 0 & 0 & 0 & 0 \\ 0 & 0 & 0 & 0 & 0 & 27/5 & 9\sqrt{6}/5 & 0 & 0 & 0 \\ 0 & 0 & 0 & 0 & 0 & 9\sqrt{6}/5 & 18/5 & 0 & 0 & 0 \\ 0 & 0 & 0 & 0 & 0 & 0 & 0 & 2 & -\sqrt{2} & 0 \\ 0 & 0 & 0 & 0 & 0 & 0 & 0 & -\sqrt{2} & 3 & 0 \\ 0 & 0 & 0 & 0 & 0 & 0 & 0 & 0 & 0 & 9 \end{bmatrix} \tag{A.18}$$

$$\mathbf{C}_0^{22} = \frac{1}{12}\begin{bmatrix} 2 & 0 & -2 & 0 & 0 & 0 & 0 & 0 & 0 & 0 \\ 0 & 0 & 0 & 0 & 0 & 0 & 0 & 0 & 0 & 0 \\ -2 & 0 & 2 & 0 & 0 & 0 & 0 & 0 & 0 & 0 \\ 0 & 0 & 0 & 10/3 & -4\sqrt{3}/3 & 2\sqrt{5}/15 & 3\sqrt{30}/5 & 0 & 0 & 0 \\ 0 & 0 & 0 & -4\sqrt{3}/3 & 5/2 & -7\sqrt{15}/30 & -9\sqrt{10}/10 & 0 & 0 & 0 \\ 0 & 0 & 0 & 2\sqrt{5}/15 & -7\sqrt{15}/30 & 17/30 & 3\sqrt{6}/10 & 0 & 0 & 0 \\ 0 & 0 & 0 & 3\sqrt{30}/5 & -9\sqrt{10}/10 & 3\sqrt{6}/10 & 18/5 & 0 & 0 & 0 \\ 0 & 0 & 0 & 0 & 0 & 0 & 0 & 2 & \sqrt{2}/2 & \sqrt{6}/2 \\ 0 & 0 & 0 & 0 & 0 & 0 & 0 & \sqrt{2}/2 & 15/2 & -3\sqrt{3}/2 \\ 0 & 0 & 0 & 0 & 0 & 0 & 0 & \sqrt{6}/2 & -3\sqrt{3}/2 & 9/2 \end{bmatrix} \tag{A.19}$$

$$\mathbf{C}_0^{33} = \frac{1}{12}\begin{bmatrix} 0 & 0 & 0 & 0 & 0 & 0 & 0 & 0 & 0 & 0 \\ 0 & 2 & -2 & 0 & 0 & 0 & 0 & 0 & 0 & 0 \\ 0 & -2 & 2 & 0 & 0 & 0 & 0 & 0 & 0 & 0 \\ 0 & 0 & 0 & 10/3 & 4\sqrt{3}/3 & 2\sqrt{5}/15 & 3\sqrt{30}/5 & 0 & 0 & 0 \\ 0 & 0 & 0 & 4\sqrt{3}/3 & 5/2 & 7\sqrt{15}/30 & 9\sqrt{10}/10 & 0 & 0 & 0 \\ 0 & 0 & 0 & 2\sqrt{5}/15 & 7\sqrt{15}/30 & 17/30 & 3\sqrt{6}/10 & 0 & 0 & 0 \\ 0 & 0 & 0 & 3\sqrt{30}/5 & 9\sqrt{10}/10 & 3\sqrt{6}/10 & 18/5 & 0 & 0 & 0 \\ 0 & 0 & 0 & 0 & 0 & 0 & 0 & 2 & \sqrt{2}/2 & -\sqrt{6}/2 \\ 0 & 0 & 0 & 0 & 0 & 0 & 0 & \sqrt{2}/2 & 15/2 & 3\sqrt{3}/2 \\ 0 & 0 & 0 & 0 & 0 & 0 & 0 & -\sqrt{6}/2 & 3\sqrt{3}/2 & 9/2 \end{bmatrix} \tag{A.20}$$

$$\mathbf{C}_0^{12} = \frac{1}{12}\begin{bmatrix} 0 & 0 & 0 & -4\sqrt{3}/3 & 1 & \sqrt{15}/15 & -3\sqrt{10}/5 & 0 & 0 & 0 \\ 0 & 0 & 0 & 4\sqrt{3}/3 & -1 & -\sqrt{15}/15 & 3\sqrt{10}/5 & 0 & 0 & 0 \\ 0 & 0 & 0 & 0 & 0 & 0 & 0 & 0 & 0 & 0 \\ 0 & 0 & 0 & 0 & 0 & 0 & 0 & 0 & 0 & 0 \\ -1 & 0 & 1 & \sqrt{3}/3 & -1 & 2\sqrt{15}/15 & 3\sqrt{10}/10 & 0 & 0 & 0 \\ -3\sqrt{15}/5 & 0 & 3\sqrt{15}/5 & -3\sqrt{5}/5 & 3\sqrt{15}/5 & -6/5 & -9\sqrt{6}/10 & 0 & 0 & 0 \\ -3\sqrt{10}/5 & 0 & 3\sqrt{10}/5 & -\sqrt{30}/5 & 3\sqrt{10}/5 & -2\sqrt{6}/5 & -9/5 & 0 & 0 & 0 \\ 0 & 0 & 0 & 0 & 0 & 0 & 0 & -1 & -\sqrt{2} & 0 \\ 0 & 0 & 0 & 0 & 0 & 0 & 0 & \sqrt{2}/2 & 0 & \sqrt{3} \\ 0 & 0 & 0 & 0 & 0 & 0 & 0 & \sqrt{6}/2 & 2\sqrt{3} & -3 \end{bmatrix} \tag{A.21}$$

$$\mathbf{C}_0^{13} = \frac{1}{12}\begin{bmatrix} 0 & 0 & 0 & 4\sqrt{3}/3 & 1 & -\sqrt{15}/15 & 3\sqrt{10}/5 & 0 & 0 & 0 \\ 0 & 0 & 0 & -4\sqrt{3}/3 & -1 & \sqrt{15}/15 & -3\sqrt{10}/5 & 0 & 0 & 0 \\ 0 & 0 & 0 & 0 & 0 & 0 & 0 & 0 & 0 & 0 \\ 0 & 0 & 0 & 0 & 0 & 0 & 0 & 0 & 0 & 0 \\ 0 & 1 & -1 & -\sqrt{3}/3 & -1 & -2\sqrt{15}/15 & -3\sqrt{10}/10 & 0 & 0 & 0 \\ 0 & -3\sqrt{15}/5 & 3\sqrt{15}/5 & -3\sqrt{5}/5 & -3\sqrt{15}/5 & -6/5 & -9\sqrt{6}/10 & 0 & 0 & 0 \\ 0 & -3\sqrt{10}/5 & 3\sqrt{10}/5 & -\sqrt{30}/5 & -3\sqrt{10}/5 & -2\sqrt{6}/5 & -9/5 & 0 & 0 & 0 \\ 0 & 0 & 0 & 0 & 0 & 0 & 0 & -1 & -\sqrt{2} & 0 \\ 0 & 0 & 0 & 0 & 0 & 0 & 0 & \sqrt{2}/2 & 0 & -\sqrt{3} \\ 0 & 0 & 0 & 0 & 0 & 0 & 0 & -\sqrt{6}/2 & -2\sqrt{3} & -3 \end{bmatrix} \tag{A.22}$$

$$\mathbf{C}_0^{23} = \frac{1}{12}\begin{bmatrix} 0 & 0 & 0 & 2\sqrt{3}/3 & 2 & 4\sqrt{15}/15 & 3\sqrt{10}/5 & 0 & 0 & 0 \\ 0 & 0 & 0 & 0 & 0 & 0 & 0 & 0 & 0 & 0 \\ 0 & 0 & 0 & -2\sqrt{3}/3 & -2 & -4\sqrt{15}/15 & -3\sqrt{10}/5 & 0 & 0 & 0 \\ 0 & 2\sqrt{3}/3 & -2\sqrt{3}/3 & -8/3 & -2\sqrt{3}/3 & 2\sqrt{5}/15 & -2\sqrt{30}/5 & 0 & 0 & 0 \\ 0 & -2 & 2 & 2\sqrt{3}/3 & 1/2 & -\sqrt{15}/30 & 3\sqrt{10}/10 & 0 & 0 & 0 \\ 0 & 4\sqrt{15}/15 & -4\sqrt{15}/15 & 2\sqrt{5}/15 & \sqrt{15}/30 & -1/30 & \sqrt{6}/10 & 0 & 0 & 0 \\ 0 & 3\sqrt{10}/5 & -3\sqrt{10}/5 & -2\sqrt{30}/5 & -3\sqrt{10}/10 & \sqrt{6}/10 & -9/5 & 0 & 0 & 0 \\ 0 & 0 & 0 & 0 & 0 & 0 & 0 & -1 & \sqrt{2}/2 & \sqrt{6}/2 \\ 0 & 0 & 0 & 0 & 0 & 0 & 0 & \sqrt{2}/2 & -9/2 & -\sqrt{3}/2 \\ 0 & 0 & 0 & 0 & 0 & 0 & 0 & -\sqrt{6}/2 & \sqrt{3}/2 & 3/2 \end{bmatrix} \tag{A.23}$$

$$\mathbf{C}_1^{11} = \frac{1}{12}\begin{bmatrix} 3 & 0 & 0 & 0 & 0 & 0 & 0 & 0 & 0 & 0 \\ 0 & 3 & 0 & 0 & 0 & 0 & 0 & 0 & 0 & 0 \\ 0 & 0 & 0 & 0 & 0 & 0 & 0 & 0 & 0 & 0 \\ 0 & 0 & 0 & 0 & 0 & 0 & 0 & 0 & 0 & 0 \\ 0 & 0 & 0 & 0 & 3/2 & 0 & 0 & \sqrt{6}/2 & \sqrt{3}/2 & 0 \\ 0 & 0 & 0 & 0 & 0 & 9/2 & -3\sqrt{6}/2 & 0 & 0 & 3\sqrt{15}/10 \\ 0 & 0 & 0 & 0 & 0 & -3\sqrt{6}/2 & 6 & 0 & 0 & 3\sqrt{10}/10 \\ 0 & 0 & 0 & 0 & \sqrt{6}/2 & 0 & 0 & 2 & -\sqrt{2}/2 & 0 \\ 0 & 0 & 0 & 0 & \sqrt{3}/2 & 0 & 0 & -\sqrt{2}/2 & 5/2 & 0 \\ 0 & 0 & 0 & 0 & 0 & 3\sqrt{15}/10 & 3\sqrt{10}/10 & 0 & 0 & 3/2 \end{bmatrix} \tag{A.24}$$

$$\mathbf{C}_1^{22} = \frac{1}{12}\begin{bmatrix} 3 & 0 & 0 & 0 & 0 & 0 & 0 & 0 & 0 & 0 \\ 0 & 0 & 0 & 0 & 0 & 0 & 0 & 0 & 0 & 0 \\ 0 & 0 & 3 & 0 & 0 & 0 & 0 & 0 & 0 & 0 \\ 0 & 0 & 0 & 3 & -\sqrt{3} & 0 & -\sqrt{30}/2 & -\sqrt{2}/2 & 1 & 0 \\ 0 & 0 & 0 & -\sqrt{3} & 9/4 & -\sqrt{15}/4 & 3\sqrt{10}/4 & -\sqrt{6}/4 & -\sqrt{3}/4 & 3/4 \\ 0 & 0 & 0 & 0 & -\sqrt{15}/4 & 3/4 & -\sqrt{6}/4 & \sqrt{10}/4 & -\sqrt{5}/20 & -3\sqrt{15}/20 \\ 0 & 0 & 0 & -\sqrt{30}/2 & 3\sqrt{10}/4 & -\sqrt{6}/4 & 6 & 0 & 3\sqrt{30}/20 & -3\sqrt{10}/20 \\ 0 & 0 & 0 & -\sqrt{2}/2 & -\sqrt{6}/4 & \sqrt{10}/4 & 0 & 2 & \sqrt{2}/4 & \sqrt{6}/4 \\ 0 & 0 & 0 & 1 & -\sqrt{3}/4 & -\sqrt{5}/20 & 3\sqrt{30}/20 & \sqrt{2}/4 & 7/4 & \sqrt{3}/4 \\ 0 & 0 & 0 & 0 & 3/4 & -3\sqrt{15}/20 & -3\sqrt{10}/20 & \sqrt{6}/4 & \sqrt{3}/4 & 9/4 \end{bmatrix} \tag{A.25}$$

$$\mathbf{C}_1^{33} = \frac{1}{12}\begin{bmatrix} 0 & 0 & 0 & 0 & 0 & 0 & 0 & 0 & 0 & 0 \\ 0 & 3 & 0 & 0 & 0 & 0 & 0 & 0 & 0 & 0 \\ 0 & 0 & 3 & 0 & 0 & 0 & 0 & 0 & 0 & 0 \\ 0 & 0 & 0 & 3 & \sqrt{3} & 0 & -\sqrt{30}/2 & \sqrt{2}/2 & -1 & 0 \\ 0 & 0 & 0 & \sqrt{3} & 9/4 & \sqrt{15}/4 & -3\sqrt{10}/4 & -\sqrt{6}/4 & -\sqrt{3}/4 & -3/4 \\ 0 & 0 & 0 & 0 & \sqrt{15}/4 & 3/4 & -\sqrt{6}/4 & -\sqrt{10}/4 & \sqrt{5}/20 & -3\sqrt{15}/20 \\ 0 & 0 & 0 & -\sqrt{30}/2 & -3\sqrt{10}/4 & -\sqrt{6}/4 & 6 & 0 & -3\sqrt{30}/20 & -3\sqrt{10}/20 \\ 0 & 0 & 0 & \sqrt{2}/2 & -\sqrt{6}/4 & -\sqrt{10}/4 & 0 & 2 & \sqrt{2}/4 & -\sqrt{6}/4 \\ 0 & 0 & 0 & -1 & -\sqrt{3}/4 & \sqrt{5}/20 & -3\sqrt{30}/20 & \sqrt{2}/4 & 7/4 & -\sqrt{3}/4 \\ 0 & 0 & 0 & 0 & -3/4 & -3\sqrt{15}/20 & -3\sqrt{10}/20 & -\sqrt{6}/4 & -\sqrt{3}/4 & 9/4 \end{bmatrix} \tag{A.26}$$

$$\mathbf{C}_1^{12} = \frac{1}{12}\begin{bmatrix} 0 & 0 & 0 & -\sqrt{3} & 3/2 & -\sqrt{15}/10 & 9\sqrt{10}/10 & -\sqrt{6}/2 & -\sqrt{3}/2 & -3/2 \\ 0 & 0 & 0 & \sqrt{3} & 0 & -\sqrt{15}/5 & 3\sqrt{10}/10 & -\sqrt{6}/2 & \sqrt{3} & 0 \\ 0 & 0 & 0 & 0 & 0 & 0 & 0 & 0 & 0 & 0 \\ 0 & 0 & 0 & 0 & 0 & 0 & 0 & 0 & 0 & 0 \\ 0 & 0 & 3/2 & \sqrt{3}/2 & -3/4 & \sqrt{15}/20 & -9\sqrt{10}/20 & -\sqrt{6}/4 & -\sqrt{3}/4 & -3/4 \\ -3\sqrt{15}/5 & 0 & 3\sqrt{15}/10 & -3\sqrt{5}/10 & 9\sqrt{15}/20 & -21/20 & 3\sqrt{6}/20 & -3\sqrt{10}/20 & -3\sqrt{5}/20 & 9\sqrt{15}/20 \\ 9\sqrt{10}/10 & 0 & 3\sqrt{10}/10 & -\sqrt{30}/10 & -3\sqrt{10}/10 & 2\sqrt{6}/5 & 9/5 & 2\sqrt{15}/5 & \sqrt{30}/5 & -3\sqrt{10}/10 \\ \sqrt{6}/2 & 0 & \sqrt{6}/2 & \sqrt{2}/2 & 0 & -\sqrt{10}/10 & -2\sqrt{15}/5 & -1 & -\sqrt{2}/2 & 0 \\ -\sqrt{3} & 0 & \sqrt{3}/2 & 1/2 & -3\sqrt{3}/4 & 7\sqrt{5}/20 & -\sqrt{30}/20 & \sqrt{2}/4 & 1/4 & -3\sqrt{3}/4 \\ 0 & 0 & 3/2 & -\sqrt{3}/2 & 3/4 & -\sqrt{15}/20 & 9\sqrt{10}/20 & \sqrt{6}/4 & \sqrt{3}/4 & 3/4 \end{bmatrix} \tag{A.27}$$

$$\mathbf{C}_1^{13} = \frac{1}{12}\begin{bmatrix} 0 & 0 & 0 & \sqrt{3} & 0 & -\sqrt{15}/5 & 3\sqrt{10}/10 & \sqrt{6}/2 & -\sqrt{3} & 0 \\ 0 & 0 & 0 & -\sqrt{3} & -3/2 & -\sqrt{15}/10 & 9\sqrt{10}/10 & \sqrt{6}/2 & \sqrt{3}/2 & -3/2 \\ 0 & 0 & 0 & 0 & 0 & 0 & 0 & 0 & 0 & 0 \\ 0 & 0 & 0 & 0 & 0 & 0 & 0 & 0 & 0 & 0 \\ 0 & 0 & -3/2 & -\sqrt{3}/2 & -3/4 & -\sqrt{15}/20 & 9\sqrt{10}/20 & -\sqrt{6}/4 & -\sqrt{3}/4 & 3/4 \\ 0 & -3\sqrt{15}/5 & 3\sqrt{15}/10 & -3\sqrt{5}/10 & -9\sqrt{15}/20 & -21/20 & 3\sqrt{6}/20 & 3\sqrt{10}/20 & 3\sqrt{5}/20 & 9\sqrt{15}/20 \\ 0 & 9\sqrt{10}/10 & 3\sqrt{10}/10 & -\sqrt{30}/10 & 3\sqrt{10}/10 & 2\sqrt{6}/5 & 9/5 & -2\sqrt{15}/5 & -\sqrt{30}/5 & -3\sqrt{10}/10 \\ 0 & -\sqrt{6}/2 & -\sqrt{6}/2 & -\sqrt{2}/2 & 0 & \sqrt{10}/10 & 2\sqrt{15}/5 & -1 & -\sqrt{2}/2 & 0 \\ 0 & \sqrt{3} & -\sqrt{3}/2 & -1/2 & -3\sqrt{3}/4 & -7\sqrt{5}/20 & \sqrt{30}/20 & \sqrt{2}/4 & 1/4 & 3\sqrt{3}/4 \\ 0 & 0 & 3/2 & -\sqrt{3}/2 & -3/4 & -\sqrt{15}/20 & 9\sqrt{10}/20 & -\sqrt{6}/4 & -\sqrt{3}/4 & 3/4 \end{bmatrix} \tag{A.28}$$

$$\mathbf{C}_1^{23} = \frac{1}{12}\begin{bmatrix} 0 & 0 & 0 & 0 & 3/2 & 3\sqrt{15}/10 & 3\sqrt{10}/10 & -\sqrt{6}/2 & -\sqrt{3}/2 & -3/2 \\ 0 & 0 & 0 & 0 & 0 & 0 & 0 & 0 & 0 & 0 \\ 0 & 0 & 0 & -\sqrt{3} & -3/2 & -\sqrt{15}/10 & 9\sqrt{10}/10 & -\sqrt{6}/2 & -\sqrt{3}/2 & 3/2 \\ 0 & 0 & -\sqrt{3} & -2 & -\sqrt{3}/2 & \sqrt{5}/10 & \sqrt{30}/5 & 0 & 3/2 & -\sqrt{3}/2 \\ 0 & -3/2 & 3/2 & \sqrt{3}/2 & 0 & -\sqrt{15}/10 & 3\sqrt{10}/20 & \sqrt{6}/4 & -\sqrt{3}/2 & 0 \\ 0 & 3\sqrt{15}/10 & -\sqrt{15}/10 & \sqrt{5}/10 & \sqrt{15}/10 & 1/5 & -7\sqrt{6}/20 & -3\sqrt{10}/20 & 0 & \sqrt{15}/10 \\ 0 & 3\sqrt{10}/10 & 9\sqrt{10}/10 & \sqrt{30}/5 & -3\sqrt{10}/20 & -7\sqrt{6}/20 & 9/5 & 2\sqrt{15}/5 & -\sqrt{30}/4 & -3\sqrt{10}/20 \\ 0 & \sqrt{6}/2 & \sqrt{6}/2 & 0 & \sqrt{6}/4 & 3\sqrt{10}/20 & -2\sqrt{15}/5 & -1 & \sqrt{2}/4 & \sqrt{6}/4 \\ 0 & \sqrt{3}/2 & \sqrt{3}/2 & -3/2 & -\sqrt{3}/2 & 0 & \sqrt{30}/4 & \sqrt{2}/4 & 1 & -\sqrt{3}/2 \\ 0 & -3/2 & 3/2 & -\sqrt{3}/2 & 0 & \sqrt{15}/10 & -3\sqrt{10}/20 & -\sqrt{6}/4 & \sqrt{3}/2 & 0 \end{bmatrix} \tag{A.29}$$

$$\mathbf{C}_2^{11} = \frac{1}{12}\begin{bmatrix} 6 & 6 & 0 & 0 & 0 & 0 & 0 & 0 & 0 & 0 \\ 6 & 6 & 0 & 0 & 0 & 0 & 0 & 0 & 0 & 0 \\ 0 & 0 & 0 & 0 & 0 & 0 & 0 & 0 & 0 & 0 \\ 0 & 0 & 0 & 0 & 0 & 0 & 0 & 0 & 0 & 0 \\ 0 & 0 & 0 & 0 & 3 & 0 & 0 & \sqrt{6} & \sqrt{3} & 0 \\ 0 & 0 & 0 & 0 & 0 & 9/5 & 3\sqrt{6}/5 & 0 & 0 & 3\sqrt{15}/5 \\ 0 & 0 & 0 & 0 & 0 & 3\sqrt{6}/5 & 6/5 & 0 & 0 & 3\sqrt{10}/5 \\ 0 & 0 & 0 & 0 & \sqrt{6} & 0 & 0 & 2 & \sqrt{2} & 0 \\ 0 & 0 & 0 & 0 & \sqrt{3} & 0 & 0 & \sqrt{2} & 1 & 0 \\ 0 & 0 & 0 & 0 & 0 & 3\sqrt{15}/5 & 3\sqrt{10}/5 & 0 & 0 & 3 \end{bmatrix} \tag{A.30}$$

$$\mathbf{C}_2^{22} = \frac{1}{12}\begin{bmatrix} 6 & 0 & 6 & 0 & 0 & 0 & 0 & 0 & 0 & 0 \\ 0 & 0 & 0 & 0 & 0 & 0 & 0 & 0 & 0 & 0 \\ 6 & 0 & 6 & 0 & 0 & 0 & 0 & 0 & 0 & 0 \\ 0 & 0 & 0 & 2 & 0 & -2\sqrt{5}/5 & \sqrt{30}/5 & -\sqrt{2} & 2 & 0 \\ 0 & 0 & 0 & 0 & 3/2 & -3\sqrt{15}/10 & -3\sqrt{10}/10 & -\sqrt{6}/2 & -\sqrt{3}/2 & 3/2 \\ 0 & 0 & 0 & -2\sqrt{5}/5 & -3\sqrt{15}/10 & 13/10 & \sqrt{6}/10 & \sqrt{10}/2 & -\sqrt{5}/10 & -3\sqrt{15}/10 \\ 0 & 0 & 0 & \sqrt{30}/5 & -3\sqrt{10}/10 & \sqrt{6}/10 & 6/5 & 0 & 3\sqrt{30}/10 & -3\sqrt{10}/10 \\ 0 & 0 & 0 & -\sqrt{2} & -\sqrt{6}/2 & \sqrt{10}/2 & 0 & 2 & -\sqrt{2}/2 & -\sqrt{6}/2 \\ 0 & 0 & 0 & 2 & -\sqrt{3}/2 & -\sqrt{5}/10 & 3\sqrt{30}/10 & -\sqrt{2}/2 & 5/2 & -\sqrt{3}/2 \\ 0 & 0 & 0 & 0 & 3/2 & -3\sqrt{15}/10 & -3\sqrt{10}/10 & -\sqrt{6}/2 & -\sqrt{3}/2 & 3/2 \end{bmatrix} \tag{A.31}$$

$$\mathbf{C}_2^{33} = \frac{1}{12}\begin{bmatrix} 0 & 0 & 0 & 0 & 0 & 0 & 0 & 0 & 0 & 0 \\ 0 & 6 & 6 & 0 & 0 & 0 & 0 & 0 & 0 & 0 \\ 0 & 6 & 6 & 0 & 0 & 0 & 0 & 0 & 0 & 0 \\ 0 & 0 & 0 & 2 & 0 & -2\sqrt{5}/5 & \sqrt{30}/5 & \sqrt{2} & -2 & 0 \\ 0 & 0 & 0 & 0 & 3/2 & 3\sqrt{15}/10 & 3\sqrt{10}/10 & -\sqrt{6}/2 & -\sqrt{3}/2 & -3/2 \\ 0 & 0 & 0 & -2\sqrt{5}/5 & 3\sqrt{15}/10 & 13/10 & \sqrt{6}/10 & -\sqrt{10}/2 & \sqrt{5}/10 & -3\sqrt{15}/10 \\ 0 & 0 & 0 & \sqrt{30}/5 & 3\sqrt{10}/10 & \sqrt{6}/10 & 6/5 & 0 & -3\sqrt{30}/10 & -3\sqrt{10}/10 \\ 0 & 0 & 0 & \sqrt{2} & -\sqrt{6}/2 & -\sqrt{10}/2 & 0 & 2 & -\sqrt{2}/2 & \sqrt{6}/2 \\ 0 & 0 & 0 & -2 & -\sqrt{3}/2 & \sqrt{5}/10 & -3\sqrt{30}/10 & -\sqrt{2}/2 & 5/2 & \sqrt{3}/2 \\ 0 & 0 & 0 & 0 & -3/2 & -3\sqrt{15}/10 & -3\sqrt{10}/10 & \sqrt{6}/2 & \sqrt{3}/2 & 3/2 \end{bmatrix} \tag{A.32}$$

$$\mathbf{C}_2^{12} = \frac{1}{12}\begin{bmatrix} 0 & 0 & 0 & 0 & 3 & -3\sqrt{15}/5 & -3\sqrt{10}/5 & -\sqrt{6} & -\sqrt{3} & 3 \\ 0 & 0 & 0 & 0 & 3 & -3\sqrt{15}/5 & -3\sqrt{10}/5 & -\sqrt{6} & -\sqrt{3} & 3 \\ 0 & 0 & 0 & 0 & 0 & 0 & 0 & 0 & 0 & 0 \\ 0 & 0 & 0 & 0 & 0 & 0 & 0 & 0 & 0 & 0 \\ 3 & 0 & 3 & \sqrt{3} & 0 & -\sqrt{15}/5 & 3\sqrt{10}/10 & -\sqrt{6}/2 & \sqrt{3} & 0 \\ -3\sqrt{15}/5 & 0 & -3\sqrt{15}/5 & 3\sqrt{5}/5 & 0 & -3/5 & 3\sqrt{6}/10 & -3\sqrt{10}/10 & 3\sqrt{5}/5 & 0 \\ -3\sqrt{10}/5 & 0 & -3\sqrt{10}/5 & \sqrt{30}/5 & 0 & -\sqrt{6}/5 & 3/5 & -\sqrt{15}/5 & \sqrt{30}/5 & 0 \\ \sqrt{6} & 0 & \sqrt{6} & \sqrt{2} & 0 & -\sqrt{10}/5 & \sqrt{15}/5 & -1 & \sqrt{2} & 0 \\ \sqrt{3} & 0 & \sqrt{3} & 1 & 0 & -\sqrt{5}/5 & \sqrt{30}/10 & -\sqrt{2}/2 & 1 & 0 \\ -3 & 0 & -3 & \sqrt{3} & 0 & -\sqrt{15}/5 & 3\sqrt{10}/10 & -\sqrt{6}/2 & \sqrt{3} & 0 \end{bmatrix} \tag{A.33}$$

$$\mathbf{C}_2^{13} = \frac{1}{12}\begin{bmatrix} 0 & 0 & 0 & 0 & -3 & -3\sqrt{15}/5 & -3\sqrt{10}/5 & \sqrt{6} & \sqrt{3} & 3 \\ 0 & 0 & 0 & 0 & -3 & -3\sqrt{15}/5 & -3\sqrt{10}/5 & \sqrt{6} & \sqrt{3} & 3 \\ 0 & 0 & 0 & 0 & 0 & 0 & 0 & 0 & 0 & 0 \\ 0 & 0 & 0 & 0 & 0 & 0 & 0 & 0 & 0 & 0 \\ 0 & -3 & -3 & -\sqrt{3} & 0 & \sqrt{15}/5 & -3\sqrt{10}/10 & -\sqrt{6}/2 & \sqrt{3} & 0 \\ 0 & -3\sqrt{15}/5 & -3\sqrt{15}/5 & 3\sqrt{5}/5 & 0 & -3/5 & 3\sqrt{6}/10 & 3\sqrt{10}/10 & -3\sqrt{5}/5 & 0 \\ 0 & -3\sqrt{10}/5 & -3\sqrt{10}/5 & \sqrt{30}/5 & 0 & -\sqrt{6}/5 & 3/5 & \sqrt{15}/5 & -\sqrt{30}/5 & 0 \\ 0 & -\sqrt{6} & -\sqrt{6} & -\sqrt{2} & 0 & \sqrt{10}/5 & -\sqrt{15}/5 & -1 & \sqrt{2} & 0 \\ 0 & -\sqrt{3} & -\sqrt{3} & -1 & 0 & \sqrt{5}/5 & -\sqrt{30}/10 & -\sqrt{2}/2 & 1 & 0 \\ 0 & -3 & -3 & \sqrt{3} & 0 & -\sqrt{15}/5 & 3\sqrt{10}/10 & \sqrt{6}/2 & -\sqrt{3} & 0 \end{bmatrix} \tag{A.34}$$

$$\mathbf{C}_2^{23} = \frac{1}{12}\begin{bmatrix} 0 & 0 & 0 & -2\sqrt{3} & 0 & 2\sqrt{15}/5 & -3\sqrt{10}/5 & -\sqrt{6} & 2\sqrt{3} & 0 \\ 0 & 0 & 0 & 0 & 0 & 0 & 0 & 0 & 0 & 0 \\ 0 & 0 & 0 & -2\sqrt{3} & 0 & 2\sqrt{15}/5 & -3\sqrt{10}/5 & -\sqrt{6} & 2\sqrt{3} & 0 \\ 0 & -2\sqrt{3} & -2\sqrt{3} & 0 & 0 & 0 & 0 & 0 & 0 & 0 \\ 0 & 0 & 0 & 0 & -3/2 & -3\sqrt{15}/10 & -3\sqrt{10}/10 & \sqrt{6}/2 & \sqrt{3}/2 & 3/2 \\ 0 & 2\sqrt{15}/5 & 2\sqrt{15}/5 & 0 & 3\sqrt{15}/10 & 9/10 & 3\sqrt{6}/10 & -3\sqrt{10}/10 & -3\sqrt{5}/10 & -3\sqrt{15}/10 \\ 0 & -3\sqrt{10}/5 & -3\sqrt{10}/5 & 0 & 3\sqrt{10}/10 & 3\sqrt{6}/10 & 3/5 & -\sqrt{15}/5 & -\sqrt{30}/10 & -3\sqrt{10}/10 \\ 0 & \sqrt{6} & \sqrt{6} & 0 & \sqrt{6}/2 & 3\sqrt{10}/10 & \sqrt{15}/5 & -1 & -\sqrt{2}/2 & -\sqrt{6}/2 \\ 0 & -2\sqrt{3} & -2\sqrt{3} & 0 & \sqrt{3}/2 & 3\sqrt{5}/10 & \sqrt{30}/10 & -\sqrt{2}/2 & -1/2 & -\sqrt{3}/2 \\ 0 & 0 & 0 & 0 & -3/2 & -3\sqrt{15}/10 & -3\sqrt{10}/10 & \sqrt{6}/2 & \sqrt{3}/2 & 3/2 \end{bmatrix} \tag{A.35}$$

APPENDIX B: SELECTION RULES

Here we derive the two selection rules

$$C^{XX}_{M,np} \;=\; 0\,, \qquad \text{for } \; n = 1-3 \text{ and } p = 4-10\,, \tag{B.1a}$$

$$C^{XY}_{M,np} \;=\; \delta_{XY}\, C^{XX}_{M,np}\,, \qquad \text{for } \; n,p = 1-3\,, \tag{B.1b}$$

where the indices refer to the basis operator ordering in Table II. From the explicit matrices in Eqs. (A.18) – (A.35), it can be verified that these rules are obeyed.

Both selection rules can be derived from the second form of Eq. (24),

$$C^{XY}_{M,np} \;=\; -\,\mathrm{Tr}\left\{\left(\mathcal{T}^2_M(X)\,B^\dagger_n\right)\left(\mathcal{T}^2_M(Y)^\dagger B_p\right)\right\}\,. \tag{B.2}$$

In both selection rules, B_n is a single-spin longitudinal basis operator. The first commutator in Eq. (B.2) is then either zero or a sum of products of two single-spin operators associated with each of the two spins involved in the dipole coupling X.

In rule (B.1a), B_p is a three-spin ZQC operator and $Y = X$. The second commutator then yields a sum of products of 4 single-spin operators, one of which is not associated with X. The product of the two commutators is therefore a sum of terms, each of which contains only one single-spin operator for the spin that does not belong to X. Equation (B.1a) then follows by noting that the (partial) trace of a single-spin operator is zero, e.g., $\mathrm{Tr}_I\{I_z\} = \mathrm{Tr}_I\{I_\pm\} = 0$.

In the selection rule (B.1b), B_p is a single-spin longitudinal basis operator, like B_n. If $Y \neq X$, the second commutator is then either zero or a sum of products of two single-spin operators associated with each of the two spins involved in the dipole coupling Y. Since the distinct dipole couplings X and Y share one spin, it follows that the product of the two commutators is a sum of terms, each of which contains only one single-spin operator for each of the two spins that are not shared by X and Y. Since the partial trace of each of these two operators is zero, Eq. (B.1b) follows.

APPENDIX C: A_3 RELAXATION SUPERMATRIX

For convenience, we reproduce here the known[4] relaxation supermatrix $\bar{\mathbf{R}}$ for the A_3 spin system in the fully symmetry-adapted basis in Eq. (52). By making use of Eqs. (23), (30) and (47) – (49), we obtain

$$\bar{\mathbf{R}} \;=\; \frac{4}{15}\,\omega_{\mathrm{D}}^2 \sum_{M=0}^{2} (2-\delta_{M0})\,\bar{\mathbf{C}}_M\, j(M\omega_0)\,, \tag{C.1}$$

where

$$\bar{\mathbf{C}}_M \;\equiv\; \sum_X \left(\bar{\mathbf{C}}_M^{XX} \;-\; \frac{1}{8} \sum_{Y\neq X} \bar{\mathbf{C}}_M^{XY} \right). \tag{C.2}$$

The fully symmetry-adapted basis operators in Eq. (52) are linear combinations of the basis operators in Table II,

$$\bar{B}_\alpha \;=\; \sum_n U_{\alpha n}\, B_n\,, \tag{C.3}$$

where the coefficients $U_{\alpha n}$ are given in Eq. (52). Consequently,

$$\bar{C}_{M,\alpha\beta}^{XY} \;=\; \sum_n \sum_p U_{\alpha n}\, U_{\beta n}\, C_{M,np}^{XY}\,. \tag{C.4}$$

Using Eqs. (C.2), (C.4) and the $\mathbf{C}_M^{XY}$ matrices in Appendix A, we find

$$\bar{\mathbf{C}}_0 \;=\; \frac{1}{80} \begin{bmatrix} 0 & 0 & 0 \\ 0 & 54 & -27\sqrt{6} \\ 0 & -27\sqrt{6} & 81 \end{bmatrix}, \tag{C.5a}$$

$$\bar{\mathbf{C}}_1 \;=\; \frac{1}{80} \begin{bmatrix} 80 & -2\sqrt{5} & -4\sqrt{30} \\ -2\sqrt{5} & 88 & 41\sqrt{6} \\ -4\sqrt{30} & 41\sqrt{6} & 222 \end{bmatrix}, \tag{C.5b}$$

$$\bar{\mathbf{C}}_2 \;=\; \frac{1}{80} \begin{bmatrix} 320 & -8\sqrt{5} & 4\sqrt{30} \\ -8\sqrt{5} & 28 & -14\sqrt{6} \\ 4\sqrt{30} & -14\sqrt{6} & 42 \end{bmatrix}. \tag{C.5c}$$

Substitution of these matrices into Eq. (C.1) yields the relaxation matrix $\bar{\mathbf{R}}$. Like $\mathbf{R}$, it is a symmetric matrix and the six unique elements are

$$\bar{R}_{11} = \frac{4}{15}\,\omega_{\mathrm{D}}^2\,(\,j_1 + 4\,j_2\,)\;, \tag{C.6a}$$

$$\bar{R}_{22} = \frac{1}{150}\,\omega_{\mathrm{D}}^2\,(\,27\,j_0 + 44\,j_1 + 14\,j_2\,)\;, \tag{C.6b}$$

$$\bar{R}_{33} = \frac{1}{100}\,\omega_{\mathrm{D}}^2\,(\,27\,j_0 + 74\,j_1 + 14\,j_2\,)\;, \tag{C.6c}$$

$$\bar{R}_{12} = -\frac{\sqrt{5}}{150}\,\omega_{\mathrm{D}}^2\,(\,j_1 + 4\,j_2\,)\;, \tag{C.6d}$$

$$\bar{R}_{13} = -\frac{\sqrt{30}}{75}\,\omega_{\mathrm{D}}^2\,(\,j_1 - j_2\,)\;, \tag{C.6e}$$

$$\bar{R}_{23} = -\frac{\sqrt{6}}{300}\,\omega_{\mathrm{D}}^2\,(\,27\,j_0 - 41\,j_1 + 14\,j_2\,)\;. \tag{C.6f}$$

These results agree fully with Eq. (5.5) in the review by Werbelow and Grant.[4]

APPENDIX D: AXIAL INTERNAL ROTATION

Here we derive the spectral density function $J_{XY}(\omega)$, defined by Eqs. (9) and (12), for a model with rotational diffusion about an axis perpendicular to the nuclear plane superimposed on spherical-top rotational diffusion of the nuclear plane.

Transforming from the lab frame (with the $z_{\rm L}$ axis along the $\boldsymbol{B}_0$ field) to the internuclear frame (with the z_X axis along the internuclear vector $\boldsymbol{r}_X$) via the axial internal-motion frame (with the $z_{\rm A}$ axis perpendicular to the nuclear plane), we have[1]

$$P_2(\cos\theta_X) \;=\; \sum_{N=-2}^{2} D^{2*}_{0N}(\Omega_{\rm LA})\, D^{2}_{N0}(\Omega_{\rm AX})\,. \tag{D.1}$$

Inserting this expression into Eq. (9) and assuming that the two motions are statistically independent, we obtain

$$G_{XY}(\tau) \;=\; \sum_{N=-2}^{2}\sum_{N'=-2}^{2} \left\langle D^{2}_{0N}(\Omega_{\rm LA}(0))\, D^{2*}_{0N'}(\Omega_{\rm LA}(\tau))\right\rangle \left\langle D^{2*}_{N0}(\Omega_{\rm AX}(0))\, D^{2}_{N'0}(\Omega_{\rm AY}(\tau))\right\rangle\,. \tag{D.2}$$

For spherical-top rotational diffusion,

$$\left\langle D^{2}_{0N}(\Omega_{\rm LA}(0))\, D^{2*}_{0N'}(\Omega_{\rm LA}(\tau))\right\rangle \;=\; \delta_{NN'}\,\frac{1}{5}\,\exp(-\tau/\tau_{\rm R})\,, \tag{D.3}$$

with the rotational correlation time $\tau_{\rm R} \equiv 1/(6\,D_{\rm R})$. Combination of Eqs. (D.2) and (D.3) yields

$$G_{XY}(\tau) \;=\; \frac{1}{5}\,\exp(-\tau/\tau_{\rm R})\, G^{XY}_{\rm int}(\tau)\,, \tag{D.4}$$

with the internal-motion time correlation function

$$G^{XY}_{\rm int}(\tau) \;\equiv\; \sum_{N=-2}^{2} \left\langle D^{2*}_{N0}(\Omega_{\rm AX}(0))\, D^{2}_{N0}(\Omega_{\rm AY}(\tau))\right\rangle\,. \tag{D.5}$$

Since the $z_{\rm A}$ axis perpendicular to the nuclear plane,

$$G^{XY}_{\rm int}(\tau) \;=\; \sum_{N=-2}^{2} [d^{2}_{N0}(\pi/2)]^2\, \langle\exp\{iN[\alpha_X(0)-\alpha_Y(\tau)]\}\rangle\,. \tag{D.6}$$

Introducing the fixed angle, $\beta_{XY} \equiv \alpha_X(\tau) - \alpha_Y(\tau)$, between internuclear vectors $\boldsymbol{r}_X$ and $\boldsymbol{r}_Y$ and noting that the angular displacement $\phi(\tau) \equiv \alpha_X(\tau) - \alpha_X(0)$ is the same for all three internuclear vectors, we can write Eq. (D.6) as

$$G^{XY}_{\rm int}(\tau) \;=\; \sum_{N=-2}^{2} [d^{2}_{N0}(\pi/2)]^2\, \exp(iN\beta_{XY})\, \langle\exp[-iN\phi(\tau)]\rangle\,. \tag{D.7}$$

For one-dimensional rotational diffusion,

$$\langle\exp[-iN\phi(\tau)]\rangle \;=\; \exp(-N^2 D_{\rm int}\tau)\,. \tag{D.8}$$

Inserting this result and evaluating the reduced Wigner functions in Eq. (D.7), we obtain

$$G_{\rm int}^{XY}(\tau) \;=\; \frac{1}{4} \;+\; \frac{3}{4}\,\cos(2\beta_{XY})\,\exp(-\tau/\tau_{\rm int})\,, \tag{D.9}$$

with $\tau_{\rm int} \equiv 1/(4\,D_{\rm int})$.

The desired spectral density function is now obtained by combining Eqs. (12), (D.4) and (D.9), with the result

$$J_{XY}(\omega) \;=\; \frac{1}{15}\,\omega_{{\rm D},X}\,\omega_{{\rm D},Y}[J_{\rm R}(\omega) + 3\,\cos(2\beta_{XY})\,J_{\rm int}(\omega)]\;, \tag{D.10}$$

with

$$J_{\rm R}(\omega) \;\equiv\; \frac{\tau_{\rm R}}{1+(\omega\tau_{\rm R})^2}\,(1+i\,\omega\tau_{\rm R})\;, \tag{D.11}$$

and

$$J_{\rm int}(\omega) \;\equiv\; \frac{\tau_{\rm R,int}}{1+(\omega\tau_{\rm R,int})^2}\,(1+i\,\omega\tau_{\rm R,int})\;, \tag{D.12}$$

where

$$\tau_{\rm R,int} \;\equiv\; \frac{\tau_{\rm R}\,\tau_{\rm int}}{\tau_{\rm R}+\tau_{\rm int}}\,. \tag{D.13}$$

In the absence of internal rotation, $D_{\rm int} = 0$ so that $J_{\rm int}(\omega) = J_{\rm R}(\omega)$ and, since $1 + 3\,\cos(2\beta_{XY}) = 4\,P_2(\cos\beta_{XY})$, Eq. (D.10) reduces to the result in Eqs. (47) – (49).

APPENDIX E: SYMMETRIC-TOP ROTATION

Here we derive the spectral density function $J_{XY}(\omega)$, defined by Eqs. (9) and (12), for the symmetric-top rotational diffusion model.

We now transform from the lab frame (with the z_{L} axis along the $\boldsymbol{B}_0$ field) to the internuclear frame (with the z_X axis along the internuclear vector $\boldsymbol{r}_X$) via two intermediate frames: the rotation frame (with the z_{R} axis along the principal axis of the rotational diffusion tensor) and the axial frame (with the z_{A} axis perpendicular to the nuclear plane). We then have[1]

$$P_2(\cos\theta_X) \;=\; \sum_{N=-2}^{2}\sum_{P=-2}^{2} D^{2*}_{0N}(\Omega_{\mathrm{LR}})\, D^{2*}_{NP}(\Omega_{\mathrm{RA}})\, D^{2}_{P0}(\Omega_{\mathrm{AX}})\,. \tag{E.1}$$

Inserting this expression into Eq. (9), we obtain

$$\begin{aligned} G_{XY}(\tau) \;=\; & \sum_{N=-2}^{2}\sum_{N'=-2}^{2}\sum_{P=-2}^{2}\sum_{P'=-2}^{2} \left\langle D^{2}_{0N}(\Omega_{\mathrm{LR}}(0))\, D^{2*}_{0N'}(\Omega_{\mathrm{LR}}(\tau))\right\rangle \\ & \times\; D^{2}_{NP}(\Omega_{\mathrm{RA}})\, D^{2*}_{N'P'}(\Omega_{\mathrm{RA}})\, D^{2*}_{P0}(\Omega_{\mathrm{AX}})\, D^{2}_{P'0}(\Omega_{\mathrm{AY}})\,, \end{aligned} \tag{E.2}$$

where Euler angles without argument are time-independent. For symmetric-top rotational diffusion,

$$\left\langle D^{2}_{0N}(\Omega_{\mathrm{LR}}(0))\, D^{2*}_{0N'}(\Omega_{\mathrm{LR}}(\tau))\right\rangle \;=\; \delta_{NN'}\,\frac{1}{5}\,\exp(-\tau/\tau_N)\,, \tag{E.3}$$

with the correlation times τ_N as given by Eq. (58). Combining Eqs. (E.2) and (E.3) and noting that $\tau_{-N}=\tau_N$, $d^2_{-N,-P}(\beta)=(-1)^{P-N}\,d^2_{NP}(\beta)$ and $\beta_{\mathrm{AX}}=\pi/2$, we obtain

$$G_{XY}(\tau) \;=\; \frac{1}{20}\sum_{N=0}^{2}(2-\delta_{N0})\,H_{XY,N}\,\exp(-\tau/\tau_N)\,, \tag{E.4}$$

with the real-valued, time-independent, geometric coefficients given by

$$\begin{aligned} H_{XY,N} \;\equiv\; & \left[d^2_{N0}(\vartheta)\right]^2 \\ & -\;\sqrt{6}\,d^2_{N0}(\vartheta)\left[d^2_{N2}(\vartheta)+d^2_{N-2}(\vartheta)\right]\cos(\widehat{\alpha}_X-\widehat{\alpha}_Y)\,\cos(\widehat{\alpha}_X+\widehat{\alpha}_Y) \\ & +\;\frac{3}{2}\left\{\left[d^2_{N2}(\vartheta)\right]^2+\left[d^2_{N-2}(\vartheta)\right]^2\right\}\cos[2(\widehat{\alpha}_X-\widehat{\alpha}_Y)] \\ & +\;3\,d^2_{N2}(\vartheta)\,d^2_{N-2}(\vartheta)\,\cos[2(\widehat{\alpha}_X+\widehat{\alpha}_Y)]\,. \end{aligned} \tag{E.5}$$

Here, $\vartheta\equiv\beta_{\mathrm{RA}}$ is the angle between the principal rotation axis z_{R} and the nuclear plane normal z_{A}. Furthermore, $\widehat{\alpha}_X\equiv\alpha_X-\gamma_{\mathrm{A}}$, where γ_{A} is the azimuthal angle of z_{A} in the R frame and α_X is the azimuthal angle of $\boldsymbol{r}_X$ in the A frame.

The desired spectral density function is now obtained by combining Eqs. (12) and (E.4), with the result

$$J_{XY}(\omega) \;=\; \sum_{N=0}^{2} D_{XY,N}\,J_N(\omega)\,, \tag{E.6}$$

with

$$D_{XY,N} \;\equiv\; \frac{1}{15}\,\omega_{\mathrm{D},X}\,\omega_{\mathrm{D},Y}\,(2-\delta_{N0})\,H_{XY,N}\;, \tag{E.7}$$

and

$$J_N(\omega) \;\equiv\; \frac{\tau_N}{1+(\omega\tau_N)^2}\,(1+i\,\omega\tau_N)\;. \tag{E.8}$$

For the special case where the principal rotation axis z_{R} is perpendicular to the nuclear plane, we have $\vartheta = 0$. Since $d^2_{NP}(0) = \delta_{NP}$, Eq. (E.5) then reduces to

$$H_{XY,N} \;=\; \delta_{N0} \;+\; (\delta_{N2}+\delta_{N-2})\cos(2\,\beta_{XY})\,, \tag{E.9}$$

where we have also noted that $\beta_{XY} \equiv \alpha_X - \alpha_Y = \widehat{\alpha}_X - \widehat{\alpha}_Y$. Combination of Eqs. (E.6), (E.7) and (E.9) then yields

$$J_{XY}(\omega) \;=\; \frac{1}{15}\,\omega_{\mathrm{D},X}\,\omega_{\mathrm{D},Y}[J_0(\omega) + 3\,\cos(2\beta_{XY})\,J_2(\omega)]\;, \tag{E.10}$$

which is of the same form as Eq. (D.10) for the axial rotation model.

For the special case where the principal rotation axis z_{R} lies in the nuclear plane making an angle θ with the x_{A} axis, we have $\vartheta = \pi/2$ and $\gamma_{\mathrm{A}} = \pi - \theta$. Substituting these angles in Eq. (E.5) and using Eqs. (E.6) and (E.7), we find

$$J_{XY}(\omega) \;=\; \frac{4}{15}\,\omega_{\mathrm{D},X}\,\omega_{\mathrm{D},Y}\sum_{N=0}^{2}(2-\delta_{N0})\,d^2_{N0}(\widetilde{\alpha}_X)\,d^2_{N0}(\widetilde{\alpha}_Y)\,J_N(\omega)\,, \tag{E.11}$$

with $\widetilde{\alpha}_X \equiv \alpha_X + \theta$. Because of the uniaxial symmetry of the rotational diffusion tensor, we can, without loss of generality, take the x_{A} axis to coincide with the $\boldsymbol{r}_{IS}$ vector. Then $\alpha_{IS} = 0$, $\alpha_{IP} = \beta_I$, $\alpha_{SP} = \pi - \beta_S$ and θ specifies the orientation of the principal rotation axis in the nuclear plane relative to $\boldsymbol{r}_{IS}$.

References

[1] D. M. Brink and G. R. Satchler, *Angular Momentum*, 3rd ed. (Clarendon Press, Oxford, 1994).

[2] R. D. Nielsen and B. H. Robinson, Concepts Magn. Reson. **28A**, 270 (2006).

[3] K. Blum, *Density Matrix Theory and Applications*, 3rd ed. (Springer-Verlag, Berlin, 2012).

[4] L. G. Werbelow and D. M. Grant, Advan. Magn. Reson. **9**, 189 (1977).